protein structure and molecular enzymology

Book No. 2

Cub-H05433-2-25707

②

SAMPLE COPY

for additional information contact:

ALLIED/ELSEVIER JOURNALS
MARKETING GROUP
30, WEST COTT ROAD, Ph: 82468
MADRAS - 600 014./
750, MOUNT ROAD,
MADRAS - 600 002.

40 YEARS OF BBA !

PUBLICATION SCHEDULE FOR 1987

BBA is published according to a volume-numbering scheme that embraces all sections of the journal In addition, each regular section has its own sequential volume-numbering system, running parallel to the overall BBA scheme, as set out below
Full subscription: 42 volumes plus Cumulative Index 1986

	BIO-ENERGETICS 6 volumes [a]	BIO-MEMBRANES 11 volumes [b]	GENE STRUCTURE AND EXPRESSION 3 volumes	PROTEIN STRUCTURE AND MOLECULAR ENZYMOLOGY 6 volumes	LIPIDS AND LIPID METABOLISM 6 volumes	GENERAL SUBJECTS 4 volumes	MOLECULAR CELL RESEARCH 5 volumes	BBA REVIEW SECTIONS 3 volumes
Jan	890-1 = B80-1	896-1 = M145-1 896-2 = M145-2		911-1 = P39-1 911-2 = P39-2	917-1 = L82-1 917-2 = L82-2	923-1 = G126-1	927-1 = C17-1	BBA REVIEWS ON BIOENERGETICS
Feb	890-2 = B80-2 890-3 = B80-3	897-1 = M146-1 897-2 = M146-2	908-1 = N17-1	911-3 = P39-3	917-3 = L82-3	923-2 = G126-2	927-2 = C17-2	895-1 = BR15-1
March	891-1 = B81-1	897-3 = M146-3 898-1 = M147-1	908-2 = N17-2	912-1 = P40-1 912-2 = P40-2	918-1 = L83-1 918-2 = L83-2	923-3 = G126-3	927-3 = C17-3 928-1 = C18-1	895-2 = BR15-2 895-3 = BR15-3
April	891-2 = B81-2	898-2 = M147-2 898-3 = M147-3	908-3 = N17-3	912-3 = P40-3	918-3 = L83-3	924-1 = G127-1	928-2 = C18-2	
May	891-3 = B81-3	899-1 = M148-1 899-2 = M148-2		913-1 = P41-1 913-2 = P41-2	919-1 = L84-1 919-2 = L84-2	924-2 = G127-2	928-3 = C18-3	BBA REVIEWS ON BIOMEMBRANES
June	892-1 = B82-1 892-2 = B82-2	900-1 = M149-1 900-2 = M149-2	909-1 = N18-1	913-3 = P41-3	919-3 = L84-3	924-3 = G127-3	929-1 = C19-1 929-2 = C19-2	906-1 = MR16-1 906-2 = MR16-2
July	892-3 = B82-3	901-1 = M150-1 901-2 = M150-2	909-2 = N18-2	914-1 = P42-1 914-2 = P42-2	920-1 = L85-1 920-2 = L85-2	925-1 = G128-1	929-3 = C19-3	906-3 = MR16-3
Aug	893-1 = B83-1	902-1 = M151-1 902-2 = M151-2	909-3 = N18-3	914-3 = P42-3	920-3 = L85-3	925-2 = G128-2	930-1 = C20-1	BBA REVIEWS ON CANCER
Sept	893-2 = B83-2	902-3 = M151-3 903-1 = M152-1	910-1 = N19-1	915-1 = P43-1 915-2 = P43-2	921-1 = L86-1 921-2 = L86-2	925-3 = G128-3	930-2 = C20-2	907-1 = CR14-1 907-2 = CR14-2
Oct	893-3 = B83-3 894-1 = B84-1	903-2 = M152-2 903-3 = M152-3	910-2 = N19-2	915-3 = P43-3	921-3 = L86-3	926-1 = G129-1	930-3 = C20-3 931-1 = C21-1	907-3 = CR14-3
Nov	894-2 = B84-2	904-1 = M153-1 904-2 = M153-2		916-1 = P44-1 916-2 = P44-2	922-1 = L87-1 922-2 = L87-2	926-2 = G129-2	931-2 = C21-2	
Dec	894-3 = B84-3	905-1 = M154-1 905-2 = M154-2	910-3 = N19-3	916-3 = P44-3	922-3 = L87-3	926-3 = G129-3	931-3 = C21-3	

[a] This includes BBA Reviews on Bioenergetics, Vol 895 [b] This includes BBA Reviews on Biomembranes, Vol 906

Authors should submit their manuscripts (four copies) for publication in BIOCHIMICA ET BIOPHYSICA ACTA by sending them one of the Managing Editors

Dr P Borst, c/o BBA Editorial Secretariat, P.O Box 1345, 1000 BH Amsterdam, The Netherlands
Dr P Cohen, Department of Biochemistry, Medical Sciences Institute, University of Dundee, Dundee, DD1 4HN, U K
Dr. K van Dam, c/o BBA Editorial Secretariat, P O Box 1345, 1000 BH Amsterdam, The Netherlands
Dr L L M van Deenen, c/o BBA Editorial Secretariat, P O Box 1345, 1000 BH Amsterdam, The Netherlands
Dr E P Kennedy, c/o BBA Editorial Secretariat (Boston), Box C 9123, Brookline, MA 02146, U S.A
Dr G K Radda, Department of Biochemistry, University of Oxford, South Parks Road, Oxford, OX1 3QU, U K

Detailed information for contributors may be found in Biochim Biophys Acta 715 (1982) 1–23, also published as the 1982 edition c the booklet
INFORMATION FOR CONTRIBUTORS TO BIOCHIMICA ET BIOPHYSICA ACTA
which is available free of charge from the BBA Editorial Secretariat

P25 707

Subscription information

1987 BBA Protein Structure & Molecular Enzymology, Volumes 911–916 (6 volumes in 18 issues), Dfl 1470 (US$ 592 75) + Dfl 15 (US$ 60 50) postage, packaging and handling Total price Dfl 1620 (US$ 653.25).
1987 BBA full subscription, Volumes 890–931 (42 volumes in 120 issues), Dfl 7812 (US$ 3150 00) + Dfl 1050 (US$ 423.50) postag packaging and handling Total price Dfl 8862 (US$ 3573 50)
The Dutch guilder price is definitive. The U S dollar price is subject to exchange-rate fluctuations and is given only as a guid Journals are sent by surface delivery to all countries, except the following countries where SAL air delivery (Surface Airlifted Ma is ensured. U S.A , Canada, Japan, Australia, New Zealand, P R China, India, Israel, South Africa, Malaysia, Singapore, Sou Korea, Taiwan, Pakistan, Hong Kong, Brazil, Argentina, Mexico, Thailand Airmail rates for other countries are available on reque Subscription orders can be entered only by calendar year (Jan - Dec) and should be sent to Elsevier Science Publishers, Journ Department, P O. Box 211, 1000 AE Amsterdam, The Netherlands, Telex 18582 ESPA NL, or to your usual subscription age Claims for missing issues should be made within 3 months of publication, otherwise they cannot be honoured free of charge T Publisher reserves the right to issue additional volumes during the course of the year Such volumes will be invoiced befo publication and delivered after receipt of payment
In the U S A and Canada for further information contact Elsevier Science Publishers, Journal Information Center, 52 Vanderb Avenue, New York, NY 10017, U S A , Tel (212) 370-5520

Biochimica et Biophysica Acta

BIOCHIMICA ET BIOPHYSICA ACTA

MANAGING EDITORS

L.L.M. van Deenen (Utrecht)
(Chairman)
P. Borst (Amsterdam)
P. Cohen (Dundee)
E.P. Kennedy (Boston, MA)
G.K. Radda (Oxford)
K. van Dam (Amsterdam)

HONORARY MANAGING EDITOR

E.C. Slater (Southampton)

EDITORS

H.R.V. Arnstein (London)
J. Barber (London)
I. Björkhem (Huddinge)
B. Borgström (Lund)
J. Brachet (Brussels)
J. Bremer (Oslo)
R. Burgess (Madison, WI)
E. Carafoli (Zürich)
J.E. Cleaver (San Francisco, CA)
C. Crane-Robinson (Portsmouth)
J.W. Daly (Bethesda, MD)
E.A. Dawidowicz (Boston, MA)
B. de Kruijff (Utrecht)
J.G. Demaille (Montpellier)
J.J.H.H.M. de Pont (Nijmegen)
B. Deuticke (Aachen)
K.T. Douglas (Colchester)
S. Ebashi (Tokyo)
L. Ernster (Stockholm)
S. Ferguson (Birmingham)
I. Fridovich (Durham)
F. Gibson (Canberra)
W.B. Gratzer (London)
M. Hamberg (Stockholm)
T.E. Hardingham (London)
J.L. Harwood (Cardiff)
E. Heinz (Dortmund)
E.J.M. Helmreich (Würzburg)
F. Hofmann (Homburg)
M.D. Houslay (Glasgow)
R.C. Hughes (London)
J.B. Jackson (Birmingham)
P. Jollès (Paris)
P.L. Jørgensen (Århus)
Y. Kagawa (Tochigi)
K.-A. Karlsson (Gothenburg)
M. Kates (Ottawa)
J. Kay (Cardiff)
Y. Kaziro (Tokyo)
R. Kinne (Dortmund)
C. Klee (Bethesda, MD)
A. Kleinzeller (Philadelphia, PA)
P. Läuger (Constance)
A.G. Lee (Southampton)
D.M. Lee (Oklahoma City, OK)
F. Maley (Albany, NY)
D. Marsh (Göttingen)
V. Massey (Ann Arbor, MI)
D.J. Morré (West Lafayette, IN)
J.F. Morrison (Canberra)
L.E. Mortensen (Athens, GA)
G. Nelsestuen (St. Paul, MN)
D.G. Nicholls (Dundee)
Y. Nishizuka (Kobe)
R.C. Nordlie (Grand Forks, ND)
S. Numa (Kyoto)
C. Pace-Asciak (Toronto)
P.G.W. Plagemann (Minneapolis, MN)
I. Ragan (Harlow)
P. Randle (Oxford)
A. Razin (Jerusalem)
A.M. Scanu (Chicago, IL)
H.J. Schatzmann (Bern)
G.L. Scherphof (Groningen)
J. Seelig (Basel)
N. Sharon (Rehovot)
G.G. Shipley (Boston, MA)
D. Shugar (Warsaw)
W.D. Stein (Jerusalem)
J.M. Tager (Amsterdam)
T. Taniguchi (Tokyo)
J.P. Thornber (Los Angeles, CA)
I. Tinoco (Berkeley, CA)
K.F. Tipton (Dublin)
I.P. Trayer (Birmingham)
I. Trowbridge (San Diego, CA)
C.L. Tsou (Beijing)
D.E. Vance (Edmonton)
H.J. van Gorkom (Leiden)
T. Vänngård (Gothenburg)
A. Watts (Oxford)
C. Weissmann (Zürich)
R.J.P. Williams (Oxford)
R.G. Williamson (London)
C. Wraight (Urbana, IL)
K. Wüthrich (Zürich)
R.F.A. Zwaal (Maastricht)

ELSEVIER SCIENCE PUBLISHERS B.V.
AMSTERDAM

BIOCHIMICA ET BIOPHYSICA ACTA

INTERNATIONAL JOURNAL OF BIOCHEMISTRY AND BIOPHYSICS

protein structure and molecular enzymology

911 (1987)
(P39)

ELSEVIER SCIENCE PUBLISHERS B.V.
AMSTERDAM

PUBLICATION SCHEDULE FOR 1987

BBA is published according to a volume-numbering scheme that embraces all sections of the journal In addition, each regular section has its own sequential volume-numbering system, running parallel to the overall BBA scheme, as set out below
Full subscription· 42 volumes plus Cumulative Index 1986

	BIO-ENERGETICS 6 volumes [a]	BIO-MEMBRANES 11 volumes [b]	GENE STRUCTURE AND EXPRESSION 3 volumes	PROTEIN STRUCTURE AND MOLECULAR ENZYMOLOGY 6 volumes	LIPIDS AND LIPID METABOLISM 6 volumes	GENERAL SUBJECTS 4 volumes	MOLECULAR CELL RESEARCH 5 volumes	BBA REVIEW SECTIONS 3 volumes
Jan	890-1 = B80-1	896-1 = M145-1 896-2 = M145-2	908-1 = N17-1	911-1 = P39-1 911-2 = P39-2	917-1 = L82-1 917-2 = L82-2	923-1 = G126-1	927-1 = C17-1	BBA REVIEWS ON BIOENERGETICS
Feb	890-2 = B80-2 890-3 = B80-3	897-1 = M146-1 897-2 = M146-2		911-3 = P39-3	917-3 = L82-3	923-2 = G126-2	927-2 = C17-2	895-1 = BR15-1
March	891-1 = B81-1	897-3 = M146-3 898-1 = M147-1	908-2 = N17-2	912-1 = P40-1 912-2 = P40-2	918-1 = L83-1 918-2 = L83-2	923-3 = G126-3	927-3 = C17-3 928-1 = C18-1	895-2 = BR15-2 895-3 = BR15-3
April	891-2 = B81-2	898-2 = M147-2 898-3 = M147-3	908-3 = N17-3	912-3 = P40-3	918-3 = L83-3	924-1 = G127-1	928-2 = C18-2	
May	891-3 = B81-3	899-1 = M148-1 899-2 = M148-2		913-1 = P41-1 913-2 = P41-2	919-1 = L84-1 919-2 = L84-2	924-2 = G127-2	928-3 = C18-3	BBA REVIEWS ON BIOMEMBRANES
June	892-1 = B82-1 892-2 = B82-2	900-1 = M149-1 900-2 = M149-2	909-1 = N18-1	913-3 = P41-3	919-3 = L84-3	924-3 = G127-3	929-1 = C19-1 929-2 = C19-2	906-1 = MR16-1 906-2 = MR16-2
July	892-3 = B82-3	901-1 = M150-1 901-2 = M150-2	909-2 = N18-2	914-1 = P42-1 914-2 = P42-2	920-1 = L85-1 920-2 = L85-2	925-1 = G128-1	929-3 = C19-3	906-3 = MR16-3
Aug	893-1 = B83-1	902-1 = M151-1 902-2 = M151-2	909-3 = N18-3	914-3 = P42-3	920-3 = L85-3	925-2 = G128-2	930-1 = C20-1	BBA REVIEWS ON CANCER
Sept	893-2 = B83-2	902-3 = M151-3 903-1 = M152-1	910-1 = N19-1	915-1 = P43-1 915-2 = P43-2	921-1 = L86-1 921-2 = L86-2	925-3 = G128-3	930-2 = C20-2	907-1 = CR14-1 907-2 = CR14-2
Oct	893-3 = B83-3	903-2 = M152-2 903-3 = M152-3	910-2 = N19-2	915-3 = P43-3	921-3 = L86-3	926-1 = G129-1	930-3 = C20-3	907-3 = CR14-3
Nov	894-1 = B84-1 894-2 = B84-2	904-1 = M153-1 904-2 = M153-2		916-1 = P44-1 916-2 = P44-2	922-1 = L87-1 922-2 = L87-2	926-2 = G129-2	931-1 = C21-1 931-2 = C21-2	
Dec	894-3 = B84-3	905-1 = M154-1 905-2 = M154-2	910-3 = N19-3	916-3 = P44-3	922-3 = L87-3	926-3 = G129-3	931-3 = C21-3	

[a] This includes BBA Reviews on Bioenergetics, Vol 895 [b] This includes BBA Reviews on Biomembranes, Vol 906

© 1987, Elsevier Science Publishers B V (Biomedical Division)

All rights reserved No part of this publication may be reproduced, stored in a retrieval system, or transmitted, in any form or by any means, electronic, mechanical, photocopying, recording or otherwise without the prior written permission of the publisher, Elsevier Science Publishers B V (Biomedical Division), P O. Box 1527, 1000 BM Amsterdam, The Netherlands Submission of a paper to this journal entails the author's irrevocable and exclusive authorization of the publisher to collect any sums or considerations for copying or reproduction payable by third parties (as mentioned in article 17 paragraph 2 of the Dutch Copyright Act of 1912 and in the Royal Decree of June 20, 1974 (S. 351) pursuant to article 16b of the Dutch Copyright Act of 1912) and/or to act in or out of Court in connection therewith.

Special regulations for readers in the U S A This journal has been registered with the Copyright Clearance Center, Inc Consent is given for copying of articles for personal or internal use, or for the personal use of specific clients This consent is given on the condition that the copier pays through the Center the per-copy fee stated in the code on the first page of each article for copying beyond that permitted by Sections 107 or 108 of the U S. Copyright Law The appropriate fee should be forwarded with a copy of the first page of the article to the Copyright Clearance Center, Inc , 27 Congress Street, Salem, MA 01970, U S A If no code appears in an article, the author has not given broad consent to copy and permission to copy must be obtained directly from the author. All articles published prior to 1980 may be copied for a per-copy fee of US$ 2.25, also payable through the Center This consent does not extend to other kinds of copying, such as for general distribution, resale, advertising and promotion purposes, or for creating new collective works Special written permission must be obtained from the publisher for such copying

Special regulations for authors Upon acceptance of an article by the journal, the author(s) will be asked to transfer copyright of the article to the publisher This transfer will ensure the widest possible dissemination of information.

Printed in The Netherlands

Biochimica et Biophysica Acta: 40 years on

Professor H.G.K. Westenbrink

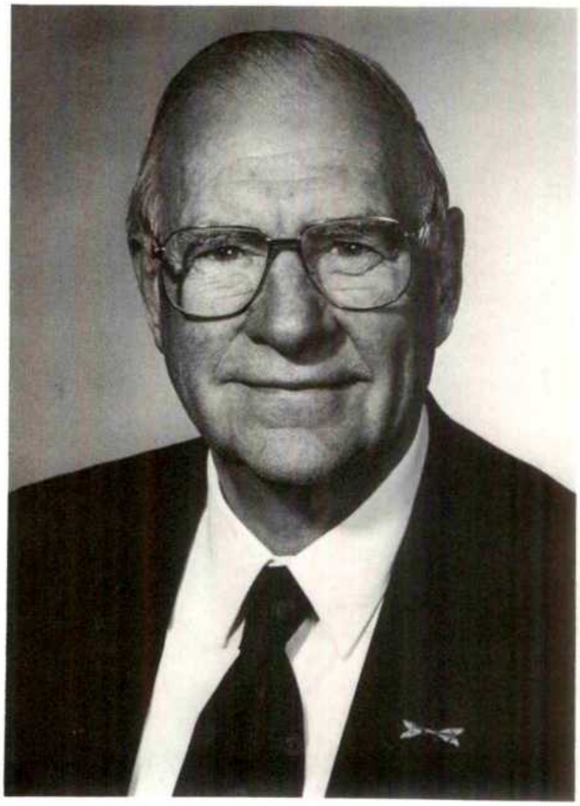

Professor E.C. Slater

Biochimica et Biophysica Acta, the first truly international journal in the field of biochemistry and biophysics, and now undoubtedly one of the largest, is celebrating its 40th anniversary with this issue.

The journal was founded in 1947 by Professor H.G.K. Westenbrink, who remained Managing Editor of the journal until 1964. He was succeeded by Professor E.C. Slater, who was able to fulfil this function until his recent retirement as Chairman of the Board of Managing Editors. Professor Slater was encouraged to write a history of BBA, recalling its remarkably rapid growth and some of the intricacies involved in the journal's birth and early development [1].

On the auspicious occasion of the journal's 40th birthday, the Publisher would like to take the opportunity of thanking all those who have played an active role in the journal's development, and looks forward to further stimulating developments over subsequent decades.

The photograph of E.C. Slater is reproduced by permission of Godfrey Argent, U.K., photographers.

[1] *Biochimica et Biophysica Acta: The Story of a Biochemical Journal* by E.C. Slater (1986) Elsevier Science Publishers, ISBN 0-444-80769-1; Price Dfl.75.00.

Biochimica et Biophysica Acta 911 (1987) 1–10
Elsevier

BBA 32594

A covalent complex between horse heart cytochrome *c* and yeast cytochrome *c* peroxidase: kinetic properties

James E. Erman [a], Kil Lyong Kim [a], Lidia B. Vitello [a], Susan J. Moench [b] and James D. Satterlee [b]

Departments of Chemistry, [a] Northern Illinois University, DeKalb, IL and [b] University of New Mexico, Albuquerque, NM (U.S.A.)

(Received 23 June 1986)
(Revised manuscript received 24 September 1986)

Key words: Cytochrome *c*, Cytochrome *c* peroxidase; Enzyme-substrate complex: (Horse, Yeast)

The kinetic properties of a 1:1 covalent complex between horse-heart cytochrome *c* and yeast cytochrome *c* peroxidase (ferrocytochrome-*c*:hydrogen-peroxide oxidoreductase, EC 1.11.1.5) have been investigated by transient-state and steady-state kinetic techniques. Evidence for heterogeneity in the complex is presented. About 50% of the complex reacts with hydrogen peroxide with a rate 20–40% faster than that of native enzyme; 20% of the complex exists in a conformation which does not react with hydrogen peroxide but converts to the reactive form at a rate of 20 ± 5 s^{-1}; 30% of the complex does not react with hydrogen peroxide to form the oxidized enzyme intermediate, cytochrome *c* peroxidase Compound I. Intramolecular electron transfer between covalently bound ferrocytochrome *c* and an oxidized site in cytochrome *c* peroxidase Compound I is too fast to measure, but a lower limit of 600 s^{-1} can be estimated at 5°C in a 10 mM potassium phosphate buffer at pH 7.5. Free ferrocytochrome *c* reduces cytochrome *c* peroxidase Compound I covalently bound to ferricytochrome *c* at a rate 10^{-4} to 10^{-5}-times slower than for free Compound I. The transient-state ferrocytochrome *c* reduction rates of Compound I covalently linked to ferricytochrome *c* are about 70-times too slow to account for the steady-state catalytic properties of the 1:1 covalent complex. This indicates that hydrogen peroxide can interact with the 1:1 complex at sites other than the heme of cytochrome *c* peroxidase, generating additional species capable of oxidizing free ferrocytochrome *c*.

Introduction

Yeast cytochrome *c* peroxidase (ferrocytochrome-*c*:hydrogen-peroxide oxidoreductase, EC 1.11.1.5; CcP) catalyzes the oxidation of ferrocytochrome *c* (C^{2+}) by hydrogen peroxide according to Eqn. 1:

$$2C^{2+} + H_2O_2 \xrightarrow[CcP]{} 2C^{3+} + 2H_2O \quad (1)$$

Steady-state kinetic studies with both cytochrome *c* and non-physiological reductants indicate that initial velocity rate expressions contain second-order reductant concentration terms [1–4]. The steady-state kinetics have been interpreted based on one [2] and two [1] binding sites for cytochrome *c*, and no binding sites for the non-physiological reductants [3]. In order to explore the

---

Abbreviations; EDC, 1-ethyl-3-(3-dimethylaminopropyl)carbodiimide, SDS, sodium dodecyl sulfate, CcP, cytochrome *c* peroxidase; C^{2+}, ferrocytochrome *c*; C^{3+}, ferricytochrome *c*

Correspondence. Dr. J.E. Erman, Department of Chemistry, Northern Illinois University, DeKalb, IL 60115, U.S.A.

0167-4838/87/$03 50 © 1987 Elsevier Science Publishers B.V (Biomedical Division)

question of interaction sites between cytochrome *c* peroxidase and cytochrome *c* we have synthesized the 1 : 1 covalent complex between horse-heart cytochrome *c* and cytochrome *c* peroxidase according to the procedure of Waldmeyer and Bosshard [5,6] using EDC. The results of a detailed investigation of the kinetic properties of this covalent complex are presented in this report.

Experimental procedures

Cytochrome *c* peroxidase was purified from commercial baker's yeast (Red Star) and crystallized by modifications [7] of the procedure of Yonetani and co-workers [8,9]. The purity index (ratio of absorbance at 408 nm to that at 280 nm) was 1.2 or greater for all preparations used in this study. Cytochrome *c* (horse heart, type VI) was purchased from Sigma and used without further purification. Cytochrome *c* and cytochrome *c* peroxidase were crosslinked by the method of Waldmeyer et al. [5,6] with minor modifications. A detailed description of the crosslinking reaction under a variety of conditions and an extensive characterization of the products of the reaction will be described elsewhere (Moench, S.J., Satterlee, J.D. and Erman, J.E., unpublished data). The 1 : 1 cytochrome *c*-cytochrome *c* peroxidase covalent complex was the major product under all conditions explored. Minor products included dimers and trimers of cytochrome *c* peroxidase, 1 : 2 and 2 : 1 cytochrome *c*-cytochrome *c* peroxidase complexes and other high-molecular-weight aggregates with molecular weights greater than 70 000. The 1 : 1 covalent complex of cytochrome *c* and cytochrome *c* peroxidase was isolated from the reaction mixture using a combination of gel-filtration and ion-exchange chromatography. The purity of the 1 : 1 covalent complex used in this study was estimated by SDS-polyacrylamide gel electrophoresis and more than 98% of the sample migrated as a single band with a molecular weight of 46 000. The SDS-polyacrylamide gel electrophoresis experiments can clearly resolve the 1 : 1 covalent complex (46 500) from cytochrome *c* peroxidase (34 000) and the 2 : 1 covalent complex (59 000). Possible contaminants which might not be resolved would be cytochrome trimers (37 500) or tetramers (50 000). However, control experiments using EDC and cytochrome *c* alone showed very little cytochrome *c* dimer and no detectable amounts of larger cytochrome *c* polymers under our crosslinking conditions. In addition, the ultraviolet/visible spectrum was identical to the sum of the cytochrome *c* peroxidase and cytochrome *c* spectra and integration of the heme methyl groups in the NMR spectrum gave a 1 : 1 stoichiometry, indicating there was no significant contamination by cytochrome *c* polymers.

The chemical reactions of the 1 : 1 covalent complex were investigated at pH 7.5 in potassium phosphate buffers ranging in ionic strength between 10 and 25 mM. The kinetic studies were carried out using either a Cary 219 UV/VIS spectrophotometer or a Durrum-Gibson stopped-flow spectrophotometer, depending upon the rates of the various reactions. Both instruments were thermostatically controlled to within ±1 deg C and the reactions were studied at temperatures between 5 and 25°C.

Results and Discussion

Titration with hydrogen peroxide

The ferricytochrome *c*-cytochrome *c* peroxidase complex was titrated with hydrogen peroxide along with the native enzyme. The results are shown in Fig. 1. Only 70 ± 4% of cytochrome *c* peroxidase in the covalent complex reacts with hydrogen peroxide to form the oxidized intermediate, Compound I. That portion of the covalently linked enzyme which does react with hydrogen peroxide has essentially the same changes in absorptivity upon reaction with hydrogen peroxide as the native enzyme, 42 $mM^{-1} \cdot cm^{-1}$ and 44 $mM^{-1} \cdot cm^{-1}$ at 424 nm, respectively.

The titration of the 1 : 1 covalent complex between cytochrome *c* and cytochrome *c* peroxidase with hydrogen peroxide indicates that this preparation is heterogeneous. Waldmeyer and Bosshard [5] have shown that there is heterogeneity in the crosslinked product, with some of the complexes having one crosslink and some two. In addition to promoting amide bond formation between carboxylate and amino groups, the EDC reaction has been shown to convert carboxylic acid groups to *N*-acylurea derivatives in the ab-

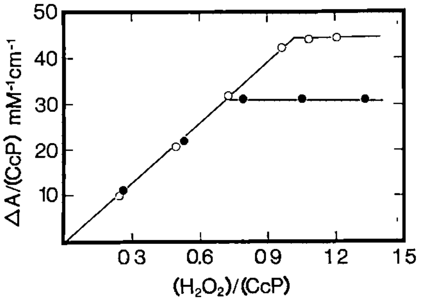

Fig. 1 Hydrogen peroxide titration of native cytochrome *c* peroxidase (○) and the 1:1 ferricytochrome *c*-cytochrome *c* peroxidase covalent complex (●) Compound I formation was observed at 424 nm Experimental conditions: pH 7.5, 10 mM potassium phosphate buffer, 25°C.

sence of nucleophiles [10]. Using carbon-14-labelled glycine ethyl ester as a nucleophile, Waldmeyer et al. [7] have shown that about five residues of glycine were incorporated into cytochrome *c* peroxidase under conditions comparable to those used for preparation of the cytochrome *c*-cytochrome *c* peroxidase crosslinked product. This is a minimum estimate of the number of modified carboxyl groups, since *N*-acylurea derivatives can also be formed in the presence of glycine ethyl ester [7,10]. Trace labelling experiments indicate that essentially all of the carboxyl groups on cytochrome *c* peroxidase can potentially be modified, but that five groups have significantly higher reactivity in the native enzyme when compared to the denatured enzyme [11]. Heterogeneity in carboxyl group modification on both the crosslinked cytochrome *c* and cytochrome *c* peroxidase moities probably exists.

The question of why 30% of the crosslinked product does not react with hydrogen peroxide is interesting. There is strong evidence [5,7,11] that the crosslinked cytochrome *c* occupies the binding site proposed by Poulos and Kraut [12] and this does not block the putative hydrogen peroxide access channel to the heme. Based upon the ultraviolet visible absorption and NMR spectroscopy, there is no evidence for gross conformational changes such as denaturation in the crosslinked product [5]. However, the NMR spectrum of the complex (Satterlee, J.D., unpublished observation) does reveal one significant difference. The resonance due to the methyl group at position 1 on the heme in cytochrome *c* peroxidase is split in the covalent complex, suggesting a localized environmental perturbation in the vicinity of this group. Modification of Asp-146 may be responsible for the perturbation of heme methyl 1, since this is the closest carboxylate group. Modification at other sites could also be responsible for the loss of reactivity toward hydrogen peroxide, including Asp-235, which hydrogen bonds to the proximal histidine (His-175) and is thought to be involved in determination of the redox potential of the heme [13,14]. Modification of Asp-235 would appear to be less likely than Asp-146 under the mild crosslinking conditions used in these experiments, since Asp-235 is a buried residue involved in hydrogen bonding with His-175 and Trp-191 while Asp-146 is surface accessible. The reaction between hydrogen peroxide and cytochrome *c* peroxidase depends upon a pH-dependent conformational change in solution [15,16]. It is possible that carboxyl group modification and crosslinking with cytochrome *c* can lock 30% of the enzyme in the unreactive conformation. Future experiments are planned for identification of the EDC-modified carboxyl groups and these should help in determining the reasons for the 30% loss of hydrogen peroxide reactivity.

Rate of the hydrogen peroxide reaction

Stopped-flow kinetic studies of the rate of the hydrogen peroxide reaction with the reactive 70% of the crosslinked cytochrome *c* peroxidase were carried out at 5°C. The rates were determined under pseudo-first order conditions using 0.3 μM enzyme and 3–9 μM hydrogen peroxide. The reaction between hydrogen peroxide and the ferricytochrome *c*-cytochrome *c* peroxidase complex is biphasic when monitored at 424 nm. The fast phase accounted for about 70–80% of the reaction, was dependent upon hydrogen peroxide concentration and gave a bimolecular rate constant of $(4.5 \pm 0.6) \cdot 10^7\ M^{-1} \cdot s^{-1}$ (Table I). The slower phase was independent of the hydrogen peroxide and gave a rate constant of $23 \pm 4\ s^{-1}$. Under the same experimental conditions the native enzyme reacts with hydrogen peroxide in a monophasic process with a bimolecular rate constant of $(3.2 \pm 0.4) \cdot 10^7\ M^{-1} \cdot s^{-1}$.

The simplest explanation for the kinetic behav-

TABLE I

REACTION RATE CONSTANTS FOR THE CYTOCHROME *c*-CYTOCHROME *c* PEROXIDASE COVALENT COMPLEX

All reactions were determined in 10 mM potassium phosphate buffer (pH 7.5)

Reaction	Temperature (°C)	Rate constant	Rate 1 : 1 complex/free reactant
C^{3+}-CcP + H_2O_2 → C^{3+}-CcP·I	5	$(4.5 \pm 0.6) \cdot 10^7\ M^{-1} \cdot s^{-1}$	1.4 ± 0.3
(biphasic)		$23 \pm 4\ s^{-1}$	–
C^{2+}-CcP + H_2O_2 → C^{2+}-CcP·I	5	$(3.7 \pm 0.5) \cdot 10^7\ M^{-1} \cdot s^{-1}$	1.2 ± 0.2
(biphasic)		$17 \pm 3\ s^{-1}$	–
C^{2+}-CcP·I → C^{3+}-CcP·II	5	$> 600\ s^{-1}$	?
C^{3+}-CcP·I + $2C^{2+}$ → C^{3+}-CcP + $2C^{3+}$	20	$(3.8 \pm 0.4) \cdot 10^3\ M^{-1}\ s^{-1}$	$1 \cdot 10^{-4}$
(biphasic)		$(9.8 \pm 0.4) \cdot 10^2\ M^{-1} \cdot s^{-1}$	$2 \cdot 10^{-5}$
C^{3+}-CcP·I → C^{3+}-CcP_{ox}	20	$(3.6 \pm 0.4) \cdot 10^{-5}\ s^{-1}$	0.4
C^{3+}-CcP + ascorbate → C^{2+}-CcP + dehydroascorbate	20	$3.8 \pm 0.4\ M^{-1}\ s^{-1}$	0.029 ± 0.006

ior of the covalently linked enzyme is that the enzyme can exist in two conformations, one of which reacts rapidly with hydrogen peroxide, and a second which is unreactive toward hydrogen peroxide but can be converted to the reactive form at a rate of 23 s^{-1}. The titration and kinetic data provide evidence for three forms of the covalently linked enzyme. About 50% is in a form which reacts with hydrogen peroxide at a rate 40% faster than the native enzyme; 20% of the enzyme is in an unreactive conformation but converts to the reactive form at a rate of 23 s^{-1}; 30% of the enzyme is in a nonreactive form and cannot be converted to a reactive species.

Ascorbate can reduce the ferricytochrome *c* in the 1 : 1 covalent complex to the ferrous state (see below) and we have also investigated the reaction of hydrogen peroxide with the ferrocytochrome *c*-cytochrome *c* peroxidase complex. Two redox reactions are expected. Hydrogen peroxide will convert cytochrome *c* peroxidase to an oxidized intermediate, Compound I, which is two equivalents above the native ferric state. The covalently linked ferrocytochrome *c* should reduce Compound I to Compound II, a second enzyme intermediate oxidized one equivalent above the native ferric state. In this second reaction the covalently linked ferrocytochrome *c* will be oxidized to ferricytochrome *c*. By using appropriate wavelengths, the redox changes of the individual components can be determined. The oxidation of cytochrome *c* peroxidase to its oxidized intermediates was followed at 408 and 432 nm, isobestic points between ferro- and ferricytochrome *c*. The oxidation of ferro- to ferricytochrome *c* was observed at 412 nm, the isobestic point between the native enzyme and Compound I. The isobestic points were experimentally determined on the stopped-flow instrument used in this study and are within 2 nm of literature values [17,18].

Two reactions were observed at 432 nm for the reaction between hydrogen peroxide and cytochrome *c* peroxidase covalently bonded to ferrocytochrome *c*. The fast phase, which accounted for about 80% of the reaction, was dependent upon the hydrogen peroxide concentration, Fig. 2, and gave a bimolecular rate constant of (3.7 ± 0.5)

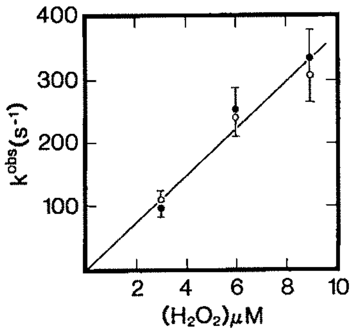

Fig. 2 Pseudo-first-order rate constant for the oxidation of the ferrocytochrome *c*-cytochrome *c* peroxidase covalent complex as a function of hydrogen peroxide concentration. Formation of the oxidized cytochrome *c* peroxidase intermediates were followed at 408 and 432 nm (●) and the oxidation of the covalently linked ferrocytochrome *c* was followed at 412 nm (○). Experimental conditions: pH 7.5, 10 mM potassium buffer, 5°C.

$\cdot 10^7\ M^{-1} \cdot s^{-1}$. The slow phase was independent of hydrogen peroxide and had a rate constant of $17 \pm 3\ s^{-1}$. At 408 nm, the total absorbance change for the reaction is much smaller than at 432 nm, and the slow phase was obscured by instrumental noise. The fast phase gave results comparable to those at 432 nm. Both the second-order and first-order rate constants, as well as the reaction amplitudes, are similar to those observed for the reaction between hydrogen peroxide and the ferricytochrome *c*-cytochrome *c* peroxidase covalent complex. The interpretation of these results is the same as described above.

Those forms of the covalent complex which react with hydrogen peroxide react at a slightly faster rate than the native enzyme. Although the rate between the ferrocytochrome *c*-cytochrome *c* peroxidase complex and hydrogen peroxide is within experimental error of the rate for the reaction of hydrogen peroxide and the native enzyme when considering the day-to-day reproducibility of the data, the rate for the covalent complex is systematically faster when comparing data obtained on the same day using the same stock hydrogen peroxide solutions. The small increase in the rate of the reaction between hydrogen peroxide and the covalent complex does appear to be real.

The rate increase is not due to complex formation per se, since there was about a 15% decrease in the rate of the hydrogen peroxide reaction in the noncovalent ferricytochrome *c*-cytochrome *c* peroxidase complex at pH 6.0 [25]. The increase is more likely an effect of the EDC modification of cytochrome *c* peroxidase. One general effect of EDC modification would be to decrease the net negative charge on cytochrome *c* peroxidase at pH 7.5. This could have an effect by stabilizing the transition state. Poulos and Kraut [26] have suggested that the rate-limiting event in the reaction between hydrogen peroxide and cytochrome *c* peroxidase is the heterolytic cleavage of the oxygen-oxygen bond of peroxide and that the transition state involves a negative charge on the oxygen which eventually dissociates as water in the reaction. A nearby positively charged arginine, Arg-48, is thought to stabilize this transition state, allowing the rapid reaction between cytochrome *c* peroxidase and hydrogen peroxide. EDC modification could provide an additional stabilization of the transition state by decreasing the net negative charge on the protein or by neutralizing a nearby carboxylate such as Asp-146. An increase of 40% in the reaction rate would require less than a 200 calorie decrease in the activation energy at 5 °C.

Internal electron transfer

Oxidation of covalently bound ferrocytochrome *c* was monitored at 412 nm during the reaction of hydrogen peroxide with the ferrocytochrome *c*-cytochrome *c* peroxidase complex. A fast reaction, dependent upon the hydrogen peroxide concentration, was observed and the pseudo-first-order rate constants are shown in Fig. 2. The total absorbance change for the ferro/ferricytochrome *c* reaction is small at this wavelength. There is an indication that a slow reaction also occurs but its amplitude is so small that quantitative results could not be obtained. This slow phase is probably related to the slow, hydrogen-peroxide-independent rate observed when monitoring changes in the peroxidase absorbance.

Within experimental error, the rate of oxidation of the covalently bound ferrocytochrome *c* is identical with the rate of oxidation of cytochrome *c* peroxidase by hydrogen peroxide (Fig. 2). This indicates that the reaction between enzyme and hydrogen peroxide is rate-limiting and that the electron transfer between covalently bound ferrocytochrome *c* and one of the oxidized sites in the enzyme is significantly faster. The simplest mechanism is explain the results is shown in Eqn. 2.

$$C^{2+}\text{-CcP} \xrightarrow{k_1[H_2O_2]} C^{2+}\text{-CcP}\cdot\text{I} \xrightarrow{k_2} C^{3+}\text{-CcP}\cdot\text{II} \tag{2}$$

If k_2 is much faster than $k_1[H_2O_2]$ then the intermediate can be considered to be in a steady state during the reaction and the observed rate constant for the oxidation of ferro- to ferricytochrome *c* is given by Eqn. 3, where k^{obs} is the observed rate at 412 nm.

$$k^{obs} = \frac{k_1 k_2 [H_2O_2]}{k_1[H_2O_2] + k_2} \tag{3}$$

In theory, the rate of the first reaction in Eqn. 2 can be increased by increasing the hydrogen peroxide concentration until $k_1[H_2O_2]$ is larger than

k_2. In that case the conversion of the enzyme to Compound I would be observed prior to the oxidation of ferrocytochrome *c*. In practice, the mixing time of our stopped-flow apparatus (3.7 ms) limits the maximum rate that can be observed. Hydrogen peroxide concentrations up to 30 μM were investigated, but at concentrations above about 12 μM the amplitude of the fast reaction was too small to measure accurately. At 30 μM hydrogen peroxide, the fast phase of the reaction could not be detected at any wavelength monitored. These data can be used to determine a minimum value for k_2. At 8.95 μM hydrogen peroxide, the observed rate of ferrocytochrome *c* oxidation was 305 ± 40 s^{-1}, which is identical, within experimental error, with the rate of the hydrogen peroxide–cytochrome *c* peroxidase reaction, the rate-limiting step. The value of k_2 must be significantly larger than 305 s^{-1}. A conservative lower limit can be estimated from a consideration of the mixing time of the flow system and the sensitivity of the optical detection system. We would be able to detect the absorbance changes if the rate were slow enough to allow the last 10% of the reaction to be observed under our experimental conditions. This gives a minimum estimate of 600 s^{-1} for k_2 and this value is included in Table I. In a recent report [19], Hazzard and Tollin, using laser flash photolysis of flavins to reduce ferricytochrome *c* in the presence of cytochrome *c* peroxidase Compound I, observed a one-electron intramolecular electron transfer between cytochrome *c* and the oxidized enzyme with a rate of 750 s^{-1}. The reaction was observed at room temperature, pH 7, using potassium phosphate buffer with an ionic strength of 8 mM.

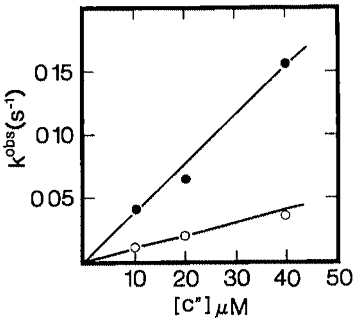

Fig. 3 Pseudo-first order rate constants for the reduction of the ferricytochrome *c*-cytochrome *c* peroxidase compound I covalent complex by free ferrocytochrome *c* The reaction was biphasic at 424 nm and the rate constants for the fast (●) and slow (○) component are shown Experimental conditions: pH 7.5, 10 mM potassium phosphate, 20 °C

Reduction of the ferricytochrome c-cytochrome c peroxidase compound I covalent complex by free ferrocytochrome c

It was found that free ferrocytochrome *c* could reduce cytochrome c peroxidase Compound I covalently linked to ferricytochrome *c*. The reaction was biphasic, with both phases dependent upon the free ferrocytochrome *c* concentration as shown in Fig. 3. The bimolecular rate constants derived from the data at 20 °C are given in Table I. These bimolecular rate constants are 10^{-4} to 10^{-5}-times smaller than those for the reduction of free Compound I, as estimated from the initial slope of the steady-state velocity as a function of ferrocytochrome *c* concentration, which is $0.5 \cdot 10^8$ to $1 \cdot 10^8$ $M^{-1} \cdot s^{-1}$ depending upon the empirical equation used to fit the steady-state data (see below). These data are consistent with the conclusion that the primary cytochrome *c* interaction site is blocked in the covalent complex but also provides evidence that there may be other sites of interaction between the enzyme and cytochrome *c* which can participate in electron transfer reactions, although at a significantly slower rate. There is no evidence of complex formation at these secondary sites, since the rate constants are strictly bimolecular up to 40 μM cytochrome *c*. However, these data provide minimum values for the cytochrome *c* affinity and electron transfer rates at these secondary sites, since it is likely that the carboxyl groups on the enzyme involved in any secondary site interaction could have been modified by the EDC reaction.

It is also possible that the slow reduction of Compound I covalently linked to ferricytochrome *c* by free ferrocytochrome *c* could occur via the primary interaction site. Evidence has been presented that the crosslinking is heterogeneous and it is possible that the crosslinked cytochrome *c* could move in such a way that free ferrocytochrome *c* could interact with the primary binding site. If this occurred at a rate of 10^{-4}- to 10^{-5}-times the normal rate of interaction, it could provide another explanation for the observed slow reduction rate of Compound I in the covalent complex.

Since the reduction of covalently bound Compound I by free ferrocytochrome *c* is so slow, the rate of the endogeneous reduction of the oxidized sites in covalently bound Compound I (CcP · I) was determined to differentiate the endogeneous decay from reduction by ferrocytochrome *c*. The endogeneous reduction rate of covalently bound Compound I is $3.6 \cdot 10^{-5}$ s^{-1} (Table I) and is about 2.5-times more stable than free Compound I at 25°C [20].

Ascorbate reducibility of free and covalently bound ferricytochrome c

The reduction rate of both free and covalently bound ferricytochrome *c* by ascorbate was determined. Ascorbate concentrations between 0.2 and 2 mM were used and the bimolecular reduction rate constant for the covalent complex is given in Table I. Under the conditions of these experiments, the ferricytochrome in the covalent complex is reduced 34-times more slowly than free cytochrome *c* by ascorbate. Waldmeyer and Bosshard [5] report that, at pH 5, the rate of ascorbate reducibility of ferricytochrome *c* in the covalent complex is reduced by factors of 9 and 16 at 200 and 10 mM ionic strength, respectively.

Catalytic properties of the covalent complex

Initial velocities for the steady-state oxidation of ferrocytochrome *c* by hydrogen peroxide as catalyzed by native cytochrome *c* peroxidase and by the 1 : 1 ferricytochrome *c*-cytochrome *c* peroxidase covalent complex were determined at constant hydrogen peroxide concentrations (200 μM) and varying ferrocytochrome *c* concentration (0.6 to 104 μM). Eadie-Hofstee plots of the data are shown in Fig. 4 for catalysis by the native enzyme and Fig. 5 for catalysis by the covalent complex. The data for the native enzyme include four experiments performed over the period of 1 year using two different enzyme preparations and three different lots of cytochrome *c*. The average coefficient of variation for the four data sets is 10%. The data from two experiments with the same sample of covalent complex are shown in Fig. 5 and have an average coefficient of variation of 14%.

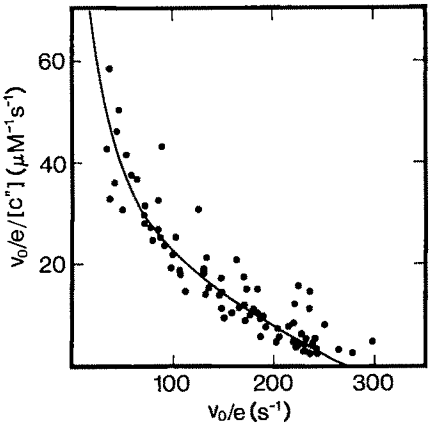

Fig. 4. Eadie-Hofstee plots for the steady-state hydrogen peroxide oxidation of ferrocytochrome *c* as catalyzed by cytochrome *c* peroxidase. Experimental conditions: pH 7.5, 4 2 mM potassium phosphate buffer, 25°C, 200 μM hydrogen peroxide, ferrocytochrome *c* 0.6 to 104 μM. The solid line was calculated using Eqn 4 in the text.

The Eadie-Hofstee plots are not linear, suggesting that higher-order terms in cytochrome *c* are required to fit the data. The empirical equation shown in Eqn. 4 was used for a weighted non-linear least-squares regression analysis of the data.

$$\frac{v_0}{e} = \frac{P(1)[C^{2+}] + P(2)[C^{2+}]^2}{1 + P(3)[C^{2+}] + P(4)[C^{2+}]^2} \tag{4}$$

$P(1)$–$P(4)$ are empirical parameters adjusted to minimize the weighted sum of squared residuals. Since the coefficient of variation was essentially independent of the value of the velocity, weights proportional to the inverse of the square of the observed velocities were used. A three-parameter fit to the data could also be used by setting $P(4)$ equal to zero in Eqn. 4. The results of the analysis are given in Table II.

For the covalent complex, the three-parameter equation is sufficient to account for the data. Addition of a fourth parameter does not lead to an improvement in the fit. The weighted residuals correspond to an average coefficient of variation between calculated and experimental values of 17%, which is similar to the value of 14% calculated between experimental data sets. There is no apparent systematic variation in the residuals with either cytochrome *c* concentration or the velocity. The solid line in Fig. 5 was calculated from Eqn. 4 using the parameters shown in Table II.

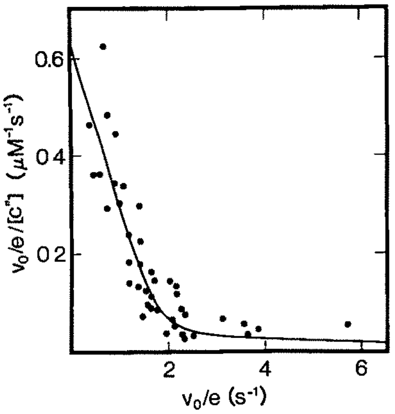

Fig. 5. Eadie-Hofstee plots for the steady-state hydrogen peroxide oxidation of ferrocytochrome *c* as catalyzed by the 1 : 1 ferricytochrome *c*-cytochrome *c* peroxidase covalent complex. Experimental conditions are identical to those in Fig. 4. The solid line was calculated according to Eqn. 4 in the text.

Applications of the *F*-test [21] to discriminate between the three and four-parameter fit to the steady-state data of the native enzyme indicates that the four-parameter equation gives a statistically better fit at the 99% confidence level. The weighted residuals for the four-parameter equation correspond to an average coefficient of variation of 10.5% compared to 11.5% for the three-parameter equation. There were no apparent systematic variations in the residuals for either the three-parameter or four-parameter equation. The solid line in Fig. 4 was calculated using the four-parameter equation and the parameter values given in Table II.

The steady-state mechanism for catalysis by the native enzyme has not been established. Non-linear Eadie-Hofstee plots were first observed by Margoliash and co-workers [1]. They suggested there were two catalytically active binding sites for cytochrome *c* on the enzyme and presented gel filtration studies indicating greater than 1 : 1 complex formation between cytochrome *c* and cytochrome *c* peroxidase. Nicholls and Mochan [22] and Kang and Erman [2] have pointed out that random addition of the two substrates, hydrogen peroxide and ferrocytochrome *c*, can lead to non-linear Eadie-Hofstee plots. However, at saturating concentrations of hydrogen peroxide, such as used in this study, the Eadie-Hofstee plots should become linear. Yandell and Yonetani [3] have observed non-linear Eadie-Hofstee plots for oxidation of transition metal complexes. There is no evidence that the transition metal complexes bind to the enzyme and Yandell and Yonetani have proposed a mechanism involving only bimolecular

TABLE II

STEADY-STATE PARAMETERS FOR THE CYTOCHROME *c* PEROXIDASE AND THE CYTOCHROME *c*-CYTOCHROME *c* PEROXIDASE COVALENT COMPLEX CATALYZED OXIDATION OF FERROCYTOCHROME *c* BY HYDROGEN PEROXIDE

All reactions were carried out at 25°C, pH 7.5, in 4.2 mM potassium phosphate buffer. The hydrogen peroxide concentration was constant at 200 μM and ferrocytochrome *c* varied between 0.6 and 104 μM. The experimental data were analyzed by non-linear least-squares regression using the empirical equation:

$$\frac{v_0}{e}=\frac{P(1)[C^{2+}]+P(2)[C^{2+}]^2}{1+P(3)[c^{2+}]+P(4)[C^{2+}]^2}$$

P(4) was either set equal to zero or allowed to vary to generate a three-parameter or four-parameter equation.

Catalyst	$P(1)$ ($\mu M^{-1} \cdot s^{-1}$)	$P(2)$ ($\mu M^{-2} \cdot s^{-1}$)	$P(3)$ (μM^{-1})	$P(4)$ (μM^{-2})	$\Sigma\delta^2$	*n*
CcP						
3-param eqn	46.7 ±130	0.116 ± 0.041	0.220±0.019	–	11272	85
4-param eqn.	105 ±100	83 ±167	3.14 ±5.64	0.312±0.633	9406	85
C^{3+}-CcP						
3-param. eqn	0.635± 0.075	0.00528± 0.00208	0.362±0.071	–	1.17	41
4-param. eqn.	0.635± 0.089	0.00528± 0.0123	0.362±0.114	$<10^{-23}$	1.17	41

electron transfer steps between the enzyme and the non-physiological reductants. At low reductant concentration there is a rate-limiting electron transfer within the enzyme, but this step can be bypassed at high substrate concentration. Erman and Vitello [7] have investigated the binding of ferricytochrome *c* and cytochrome *c* peroxidase using the perturbation of the absorption spectrum upon complex formation. They observed only 1 : 1 complex formation.

It was initially thought that investigating the catalytic properties of 1 : 1 covalent complex could provide information about the catalytic activity of a second site. However, the EDC method of forming the covalent complex is not a good method for investigating the properties of a second site because of the possibility of carboxyl group modification to *N*-acylurea derivatives. We cannot eliminate the possibility that carboxyl groups on the peroxidase, which would most likely be involved in the binding of cytochrome *c* at the secondary site, are modified. Such modification would lead to reduced interaction at the secondary site.

One very intriguing feature of the catalytic properties of the 1 : 1 covalent complex is that the rate of reduction of ferricytochrome *c*-cytochrome *c* peroxidase Compound I by free ferrocytochrome *c* (Table I) cannot explain the catalytic turnover rate. Assuming only the following reactions occur

$$\mathrm{C^{3+}\text{-}CcP + H_2O_2 \xrightarrow{k_1} C^{3+}\text{-}CcP\ I} \tag{5}$$

$$\mathrm{C^{3+}\text{-}CcP\cdot I + C^{2+} \xrightarrow{k_2} C^{3+}\text{-}CcP\cdot II + C^{3+}} \tag{6}$$

$$\mathrm{C^{3+}\text{-}CcP\ II + C^{2+} \xrightarrow{k_3} C^{3+}\text{-}CcP + C^{3+}} \tag{7}$$

and that the two last steps are strictly bimolecular up to 100 μM ferrocytochrome *c*, the steady-state velocity is given by Eqn. 8.

$$\frac{v_0}{e} = \frac{k_1 k_2 k_3 (\mathrm{H_2O_2})(\mathrm{C^{2+}})}{k_1(k_2 + k_3)(\mathrm{H_2O_2}) + k_2 k_3 (\mathrm{C^{2+}})} \tag{8}$$

This equation predicts a linear Eadie-Hofstee plot with cytochrome *c* the variable substrate. In addition the value of v_0/e at 200 μM hydrogen peroxide and 100 μM ferrocytochrome *c* calculated from Eqn. 8 and the values for k_1, k_2 and k_3 from Table I is 0.078 $\mathrm{s^{-1}}$ whereas the observed value is 5.7 $\mathrm{s^{-1}}$. Clearly, during the steady-state turnover, a species capable of oxidizing ferrocytochrome *c* at a significantly faster rate than $\mathrm{C^{3+}}$-CcP · I or $\mathrm{C^{3+}}$-CcP · II is generated. This same phenomenon has been observed with the oxidation of ferrocyanide [23,24]. The steady-state oxidation of ferrocyanide is faster than predicted from the rate of ferrocyanide oxidation by cytochrome *c* peroxidase Compounds I and II as measured by single turnover kinetics. This suggests that under multiple turnover conditions, in the presence of excess hydrogen peroxide, hydrogen peroxide can interact with the enzyme to generate intermediates other than Compound I, and that these intermediates, in turn, are capable of oxidizing ferrocytochrome *c* and nonphysiological substrates such as ferrocyanide.

There is evidence that excess hydrogen peroxide can react with CcP Compound I to form additional oxidized species. Small changes in the ultraviolet visible spectrum of cytochrome *c* peroxidase Compound I develop with time in the presence of excess hydrogen peroxide [27]. The EPR spectrum of Compound I is altered in the presence of excess hydrogen peroxide. The sharp central signal observed at a *g* value of 2.004 at 77 K increases in amplitude by a factor of 4 to 5 in the presence of a 2- to 4-fold molar excess of peroxide, although the integrated intensity only corresponds to about a 10% increase in spin concentration (Yonetani, T. and Erman, J.E., unpublished observations). The broad 'wings' on the EPR signal observed at 77 K, which accounts for most of the spin concentration in the Compound I EPR spectrum [28], does not change in the presence of excess peroxide (Yonetani, T. and Erman, J.E., unpublished observations). This 'excess' free-radical signal complicates the search for the free-radical site in Compound I and it is becoming more evident that there may be multiple sites in CcP capable of undergoing one-electron oxidation to free-radical states [28].

We can speculate on the nature of 'excess' free radical. At pH 4.5, one of the major products of Compound I decay is a cytochrome *c* peroxidase dimer formed through a dityrosine crosslink [29].

Dityrosine can be formed via radical-radical condensation reactions and we suggest that the 'excess' free radical may be due to tyrosine oxidation. The 'excess' radicals, whatever their identity, are probably responsible for the observed catalysis of the ferricytochrome *c*-cytochrome *c* peroxidase covalent complex under steady-state conditions. A 10% 'excess' free-radical concentration would be sufficient to account for the observed catalytic rate of the cytochrome *c*-cytochrome *c* peroxidase covalent complex if the 'excess' radicals had intrinsic reactivities of about 20% that of Compound I toward ferrocytochrome *c*.

Finally, we can also conclude that the electron transfer rate between ferrocytochrome *c* and Compound I is not rate-limiting in the steady-state catalysis by the native enzyme. The maximum turnover rate for the enzyme is 266 s^{-1} (Fig. 4), while the electron transfer rate between ferrocytochrome *c* and Compound I in the covalent complex is too fast to measure but has a lower limit of 600 s^{-1} (Table I). Possible rate-limiting steps in the steady-state catalytic process could be product dissociation, electron transfer between ferrocytochrome *c* and Compound II, or an internal electron transfer step between the radical and Fe(IV) sites as suggested by Yandell and Yonetani [3].

Acknowledgements

This work was supported, in part, by grants from the National Science Foundation (PCM-DMB-8403353 and CHE-8201374, J.D.S.) and the USPHS through Grant RR07176 awarded by the Biomedical Research Support Grant Program, Division of Research Resources, NIH. J.D.S. is a Fellow of the Alfred P. Sloan Foundation and support from this Foundation is gratefully acknowledged.

References

1 Kang, C.H , Ferguson-Miller, S and Margoliash, E. (1977) J Biol Chem 252, 919–926
2 Kang, D S. and Erman, J.E. (1982) J Biol. Chem 257, 12775–12779
3 Yandell, J.K. and Yonetani, T. (1983) Biochim. Biophys Acta 748, 263–270
4 Kang, C.H., Brautigan, D.L., Osheroff, N and Margoliash, E (1978) J Biol Chem 253, 6502–6510
5 Waldmeyer, B , and Bosshard, H.R. (1985) J Biol. Chem. 260, 5184–5190
6 Waldmeyer, B., Bechtold, R., Bosshard, H R. and Poulos, T.L. (1982) J. Biol. Chem 257, 6073–6076
7 Erman, J E. and Vitello, L.B (1980) J Biol. Chem. 255, 6224–6227
8 Yonetani, T. and Ray, G S (1965) J. Biol. Chem. 240, 4503–4508
9 Yonetani, T., Chance, B and Kajiwara, S (1966) J Biol Chem 241, 2981–2982
10 Timkovich, R. (1977) Anal Biochem 79, 135–143
11 Bechtold, R. and Bosshard, H.R. (1985) J Biol Chem 260, 5191–5200
12 Poulos, T.L. and Kraut, J (1980) J. Biol. Chem. 255, 10322–10330
13 Poulos, T.L and Finzel, B.C. (1984) Peptide Protein Rev 4, 115–171
14 Finzel, B.C., Poulos, T L and Kraut, J. (1984) J Biol. Chem 259, 13027–13036
15 Satterlee, J D. and Erman, J E (1980) Arch. Biochem. Biophys 202, 608–616
16 Loo, S and Erman, J E (1975) Biochemistry 14, 3467–3470
17 Margoliash, E. and Frohwirt, N (1959) Biochem. J. 71, 570–572
18 Yonetani, T. (1965) J. Biol. Chem. 240, 4509–4514
19 Hazzard, J T and Tollin, G. (1986) Biophys. J 49, 540a
20 Erman, J E. and Yonetani, T. (1975) Biochim Biophys Acta 393, 350–357
21 Burguillo, F J., Wright, A.J and Bardsley, W G (1983) Biochem. J 211, 23–34
22 Nicholls, P. and Mochan, E (1971) Biochem J. 121, 55–67
23 Jordi, H.C and Erman, J.E (1974) Biochemistry 13, 3734–3741
24 Jordi, H C. and Erman, J.E (1974) Biochemistry 13, 3741–3745
25 Hoth, L R and Erman, J.E. (1984) Biochim. Biophys. Acta 788, 151–153
26 Poulos, T L. and Kraut, J (1980) J Biol. Chem 255, 8199–8205
27 Erman, J E. and Yonetani, T (1975) Biochim. Biophys Acta 393, 343–349
28 Hori, H and Yonetani, T. (1985) J. Biol Chem. 260, 349–355
29 Spangler, B D. and Erman, J.E (1986) Biochim Biophys Acta 872, 155–157

Biochimica et Biophysica Acta 911 (1987) 11–18
Elsevier

BBA 32651

Spectroscopic studies on the structural organization of the lectin discoidin I: homologies with fibronectin

Alfonso Valencia [a], Amparo Cano [a], Rafael Caballero [b] and Angel Pestaña [a]

[a] *Departamento de Bioquímica e Instituto de Investigaciones Biomédicas del CSIC, Universidad Autonoma Madrid, Madrid and* [b] *Departamento de Bioquímica, Facultad de Ciencias, Universidad Complutense, Madrid (Spain)*

(Received 15 July 1986)

Key words: Circular dichroism; Fluorescence spectroscopy; Secondary structure; Discoidin I, Fibronectin; (*D. discoideum*)

The structure of the lectin discoidin I has been studied by circular dichroism and fluorescence spectroscopy. A positive ellipticity band at 224 nm is detected in the CD spectrum of discoidin I. The fluorescence spectra show a defined shoulder at 325 nm that through acrylamide quenching has been associated with a displaced tryptophan residue partly buried in the discoidin I molecule. This tryptophan could also be responsible for the 224 nm positive band of the CD spectrum. These spectroscopic characteristics of discoidin I indicate the existence of structural homologies with fibronectin, where the optical activity of aromatic chromophores has been associated with the positive ellipticity band at 227 nm. The CD adjust parameters and theoretical secondary structure predictions show that discoidin I is a molecule with a low content of α-helix and β-strand and high content of β-turn structures, similar to other lectins.

Introduction

The cellular slime mold *Dictyostelium discoideum* synthesizes two β-galactosidase-binding lectins, discoidin I and II, as it differentiates from vegetative cells to multicellular aggregates [1]. Discoidin I is an *N*-acetylgalactosamine-binding lectin whose native state has been described as a tetramer [2]. A number of reports have shown indirect evidence for the involvement of discoidin I in the aggregation process of this organism [3–5]. Our previous work strongly supports a direct role for discoidin I in intercellular adhesion and morphogenesis, as univalent anti-discoidin I blocks these processes [6].

Discoidin I has also been involved in cell-substratum attachment and ordered cell migration by a mechanism related to that found in fibronectin-mediated cell adhesion in higher organisms [7]. A 67 kDa glycoprotein has recently been reported as a putative receptor for the cell-binding site of discoidin I [8]. Whereas the nature of the carbohydrate-containing receptors is unclear [5,9], both the cell-binding activity and carbohydrate-binding functions of discoidin I appear to be distinct [7]. These recent data suggest that discoidin I might be organized in a multifunctional structure with different binding activities (cell-surface, sugars) located on discrete domains, as has been previously established for fibronectin [10].

A recent report [11] has shown that the chick embryo 14 kDa lectin presents several amino-acid regions homologous to those in discoidin I, including the supposed cell-binding sequence. These similarities suggest that lectins can possess bio-

---

Correspondence: Dr. A. Cano, Departamento de Bioquímica e Instituto de Investigaciones Biomédicas del CSIC, Facultad de Medicina, U.A.M., Arzobispo Morcillo, 4, 28029 Madrid, Spain

0167-4838/87/$03.50 © 1987 Elsevier Science Publishers B.V. (Biomedical Division)

logical functions similar to those related to cellular interactions in higher organisms.

In order to investigate the structural organization of discoidin I and its possible relationship with that of fibronectin we have undertaken a series of spectroscopic studies, circular dichroism (CD) and fluorescence, on this lectin. Both techniques are very useful for evaluating the secondary and tertiary structure of proteins and have been extensively applied to fibronectin in the past years [12,13].

In this report we present evidence of structural homologies between discoidin I and fibronectin. In analogy with fibronectin [12,13], the discoidin I CD spectrum shows very low ellipticity values and exhibits a positive band around 224 nm. A similar positive band at 227 nm has been detected in the fibronectin CD spectrum and has been associated with the optical activity of tyrosine side-chains located in a specific environment [14]. The fluorescence studies on discoidin I presented here indicate the existence of at least one tryptophan residue partly buried in the discoidin I molecule which could be responsible for the positive ellipticity band detected in the CD spectrum. These results are discussed in the light of the secondary structure prediction data and of the possible implications for the biological role of this lectin.

Materials and Methods

Discoidin I purification

Discoidin I was purified from *Dictyostelium discoideum,* axenic strain AX-2, developed over a period of 9 h in shaken suspension, by affinity chromatography on Sepharose 6B as described [6]. The purity of the discoidin I preparation was assessed by sodium dodecyl sulphate (SDS) polyacrylamide gel electrophoresis [15]. For all spectroscopic studies, discoidin I was used in a buffer comprising 0.01 M Tris/0.075 M NaCl (pH 7.3) (Tris-Na buffer).

Circular dichroism spectroscopy

Circular dichroism (CD) spectra were recorded on a Marck III dicrograph (Jobin-Yvon). For spectra in the far ultraviolet region (200–250 nm), 0.05 cm optical path cells were used. The sensitivity of the instrument was set at $2 \cdot 10^{-6}\ \Delta A \cdot \text{mm}^{-1}$. Samples were prepared at a concentration of 0.3 mg/ml in Tris-Na buffer. When indicated, sugars or SDS were added using solutions 10–200-times more concentrated than the final desired concentration. Results are expressed as molar ellipticities in deg · cm^2 · (dmol of residue)$^{-1}$. The samples exhibit no turbidity, as hown by their negligible absorbance at 350 and 310 nm. The spectra represented in Fig. 1 are the average of more than four independent measurements obtained with different discoidin I samples over a wide range of time. Standard deviations were less than 150 molar ellipticity for 224 nm.

Fluorescence measurements

Fluorescence spectra were taken in a Perkin-Elmer NPF-44E spectrophotometer. Fluorescence was measured at right angles. The entrance slit of the excitation monochromator was 2.0 nm and the exit slit was adjusted to 1.0 nm. The analog electrical outputs were processed in a microcomputer. For the emission spectra the voltage of the photomultiplier was adjusted to 700 V and the sensitivity of the photometer to 10 or 30 nm, depending of the fluorescence of the sample. The scan speed was set at 60 mm/min. Two excitation wavelength were used: 275 and 295 nm. Discoidin I samples were prepared in a concentration range 1/10 of those used for CD spectra. When indicated, acrylamide was added to discoidin I preparations from concentrated solutions of the final one (100–200 times). The basal line was obtained at different acrylamide concentrations and subtracted from the experimental spectra. The spectra were also corrected for the acrylamide absorbance, which has a molar extinction coefficient of 0.23 $\text{M}^{-1} \cdot \text{cm}^{-1}$ at 295 nm [16].

Other analytical procedures

Analytical centrifugation of discoidin I samples (1 mg/ml) in the presence or absence of 0.5 M galactose in Tris-Na buffer was carried out in a Beckman Analytical Ultracentrifuge model E at 60000 rpm at 20 °C. The migration of the protein was followed by Schlieren optics.

Protein concentration of discoidin I samples was determined by the procedure of Bradford [17] using bovine serum albumin as standard and from amino-acid analysis when fine adjustment were needed. The amino-acid analyses were performed in a Durrum D-500 amino-acid analyzer. Hydrolysis of protein was carried out at 150°C in constant-boiling HCl containing 0.1% phenol in evacuated sealed tubes for 24 h.

Results

Analytical centrifugation

Analytical sedimentation analysis of our discoidin I preparation was a prerequisite for the spectroscopic studies because it has been previously reported that this protein (from NC-4 strain) has a non-quantitatively determined tendency to aggregate in the absence of sugars [2]. Discoidin I was purified from the AX-2 strain and equivalent aliquots were subjected to analytical centrifugtion in the presence or absence of 0.5 M galactose as described in Materials and Methods. Under both conditions a single symmetrical boundary was observed with sedimentation coefficients of 4.2 and 4.9 S in the presence and absence of galactose, respectively. Both coefficients are in agreement with the native structure of a tetramer of about 30 kDa monomers previously described [2]. The lower sedimentation coefficient found in the presence of sugar can not be explained by changes in the aggregation state of discoidin I and probably reflects the higher viscosity of the 0.5 M galactose buffer. Moreover, we have analysed our discoidin I preparations by native gel electrophoresis and we do not find any qualitative difference in tetramer structure in the absence or presence of various sugar concentrations (results not shown).

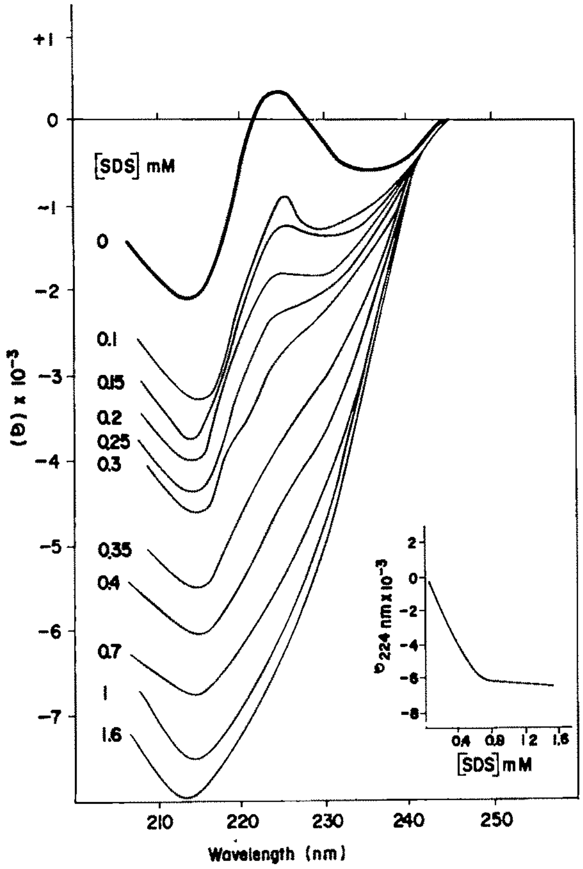

Fig. 1. Circular dichroism spectra (far ultraviolet) of discoidin I, alone (▬▬) and in the presence of increasing SDS concentrations (———) Actual concentrations of protein were estimated by amino-acid analysis, as described in Materials and Methods The final SDS concentration reached in each sample is shown next to its spectrum. Inset. Variation of the ellipticity, θ, monitored at 224 nm with increasing SDS concentration

Circular dichroism studies

The CD spectrum of discoidin I in the wavelength range normally used for studies on peptide-chain conformation (210–240 nm) is shown in Fig. 1. The spectrum shows two minima at around 215 and 237 nm and a maximum at around 224 nm and is of very low intensity in comparison with CD spectra of typical globular proteins. The discoidin I CD spectrum closely resembles that previously described for fibronectin [12–14]. In particular, the existence of the positive band at 224 nm in discoidin I is reminiscent of that found in fibronectin at 227 nm. Similar CD spectra have been observed with different discoidin I preparations and in the presence of different sugars (galactose, *N*-acetylgalactosamine, *N*-acetylglucosamine).

The weak ellipticity of the peptide group detected in discoidin I spectra suggest that there can be few groups in organized α-helical or β-structures. In order to evaluate the presence of other kinds of interaction as well as the conformational dynamics of the putative structured regions we have investigated the effect of SDS on discoidin I spectrum. This anionic detergent is able to induce conformational alterations in many proteins by changing their α-helix and β-structure content at the expense of the tertiary structure [18,19]. The main action of SDS seems to be mediated through a screening effect on positively charged regions eliminating repulsive forces which would prevent ordered α- and β-structure folding [20].

As can be seen in Fig. 1, addition of 0.25 mM SDS to discoidin I leads to the disappearance of the 224 nm positive ellipticity band on the CD spectrum and increasing SDS concentrations progressively decrease the polarization of the protein, giving rise subsequently to higher negative ellipticity values between 240 and 210 nm. The change in 224 nm ellipticity is dependent on SDS concentration, with a half-maximum change at about 0.4 mM SDS (see inset in Fig. 1).

The fit of 240 and 215 nm data of discoidin I CD spectra to the parameters of Chang et al. [21] for the α-helix, β-structure and random coils is very poor (r.m.s., 29.9), as has also been found for fibronectin [22]. Within these limitations it can clearly be observed that increasing concentrations of SDS progressively induce α-helix conformation with concomitant disappearance of β-turn structures and random coils (Table I). This result indicates that there are no impediments to the formation of secondary structures imposed by the amino-acid sequence of the polypeptide chain.

TABLE I

CHANGES IN SECONDARY STRUCTURE INDUCED BY SDS

CD adjustment parameters from Chang et al [21]

[SDS] (mM)	α-helix	β-strand	β-turn	Random
0	12 2	12.7	40 1	33 0
0.25	18 5	12.1	38 04	31.4
0.70	19 5	11.3	34 0	35.2
3.65	39 2	8 7	30 5	21 6
Sec str. pred. [a]	11 5	25 7	32.8	30.0

[a] Secondary structure prediction following Chou and Fasman [26,27].

Fluorescence studies

It has been reported that a positive ellipticity band observed between 225 and 230 nm for a number of proteins may arise from the optical activity of aromatic chromophores [23]. The whole CD spectrum of discoidin I resembles more closely that of tryptophan residues (positive band between 215 and 240 nm) than that of tyrosine residues (positive ellipticities between 200 and 240 nm).

In order to evaluate the contribution of aromatic chromophores to discoidin I structure, we have studied the fluorescence properties of the protein. Fig. 2A shows the fluorescence emission spectra of discoidin I at 275 and 295 nm excitation wavelengths. Both spectra present a maximum at around 340 nm and a shoulder at 325 nm. The 295 nm spectrum corresponds mainly to a tryptophan spectrum and the 325 nm shoulder is better defined

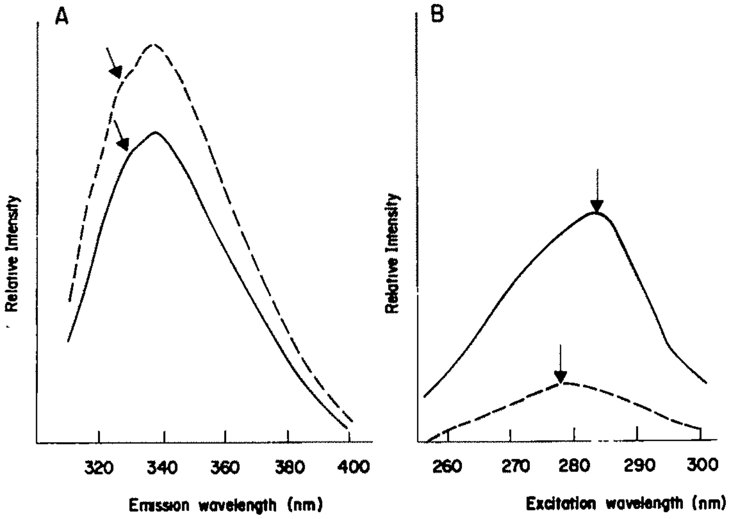

Fig 2 Intrinsic fluorescence spectra of discoidin I. In panel A the emission spectra obtained by excitation at 275 (— — —) and 295 nm (———) are represented; the shoulder around 325 nm is shown with arrows. In panel B the excitation spectra, obtained by emission monitored at 340 (———) and 300 nm (— — —) are represented; the positions of the maxima are shown with arrows.

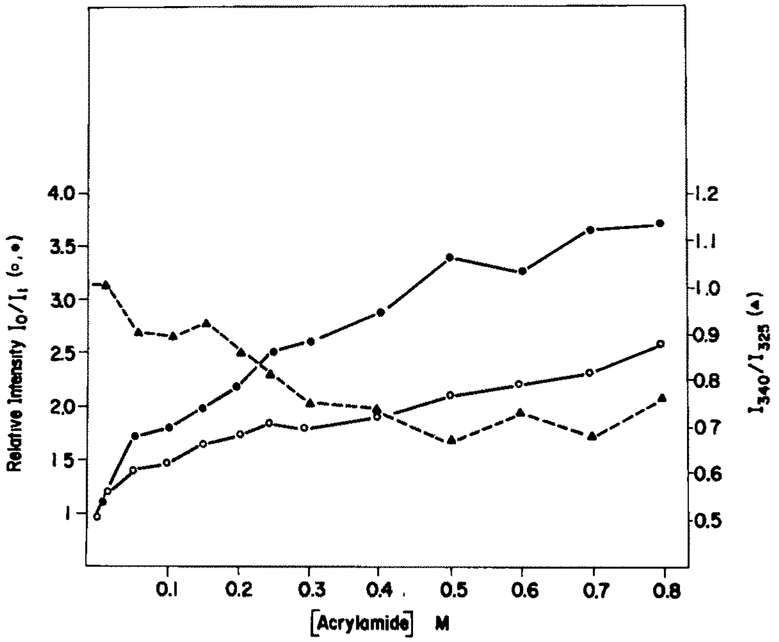

Fig 3 Stern-Volmer plot (I_o/I_i) of the acrylamide quenching of discoidin I fluorescence emission for 340 nm (●) and 325 nm (○) (295 nm excitation wavelength) The ratio I_{340}/I_{325} is also represented (▲)

than in the 275 nm spectrum. The excitation spectra of discoidin I obtained by monitoring the fluorescence emission at 300 and 340 nm are shown in Fig. 2B. For the 340 nm emission the excitation maximum is found around 285 nm, as could be expected for the high tryptophan content of discoidin I (5 residues per monomer). For the 300 nm emission the excitation maximum is displaced towards 278 nm, indicating a significant contribution from the tyrosine residues (11 per monomer).

The 325 nm emission shoulder, observed at 295 nm excitation wavelength, can be due to the emission of internal tryptophan residues in discoidin I molecule, as has been suggested to account for such displaced fluorescence in other proteins [24]. In order to test this possibility we investigated the exposure of different fluorophores on discoidin I, monitoring the quenching efficiency of acrylamide on the fluorescence emissions of the molecule. Acrylamide has been reported to be very sensitive to the degree of exposure of tryptophan residues in proteins [16].

Fig. 3 shows the fluorescence emissions of discoidin I at 340 and 325 nm in the presence of acrylamide as a Stern-Volmer plot (I_0/I_1). As can be seen, a rapid quenching of both fluorescence emissions is observed at low concentrations of acrylamide, followed by a much slower but progressive decrease with increasing acrylamide concentrations (without reaching saturation). The higher quenching constant component of the plot is associated with the more exposed tryptophan residues on the molecule being easily accessible to acrylamide, whereas the second component can be associated with the more internal tryptophans less accessible to acrylamide quenching [16]. As can be deduced from the 340/325 nm emission ratio (shown also in Fig. 3), the 340 nm emission decreases much faster and in higher proportion in the presence of acrylamide than does the 325 nm emission. A 3-fold reduction in the 340 nm emission and a 2-fold reduction in the 325 nm emission is reached at 0.8 M acrylamide.

These results support the hypothesis that the 325 nm emission shoulder is associated to at least one tryptophan residue located in an average environment less polar than the others and therefore partly buried in the discoidin I molecule.

Secondary structure prediction

We have made a theoretical secondary structure prediction for the discoidin I monomer, according to the amino-acid sequence decuced from discoidin I cloned genes [25], by the method of Chou and Fasman [26,27]. A schematic representation of the secondary stucture model obtained is shown in Fig. 4. The values for secondary structure content of discoidin I obtained by this method are: 11.5% α-helix, 25.7% β-structure, 32.8% β-turns and 30% random coils (Table I). The data for β-strand differ by a factor of 2 from those obtained by CD adjust parameters (12.7%). We have already mentioned the poor fit of discoidin I CD data to the theoretical parameters established for secondary structures (see above). These differences suggest that, like fibronectin, discoidin I is a protein with low β-structure content in its native configuration. The model presented in Fig. 4 also predicts the hydrophobicity [28] of the discoidin I monomer. As can be observed, the cell-binding sequence (Gly-Arg-Gly-Asp) previously reported to be in a β-turn [7], is located in a clearly exposed region of the molecule. From a comparative analysis of the α-helix potentials of the sequence, five positively charged regions have been detected, mainly located in the C-terminal region, which could be candidates for the adoption of α-helical structure, under the influence of SDS.

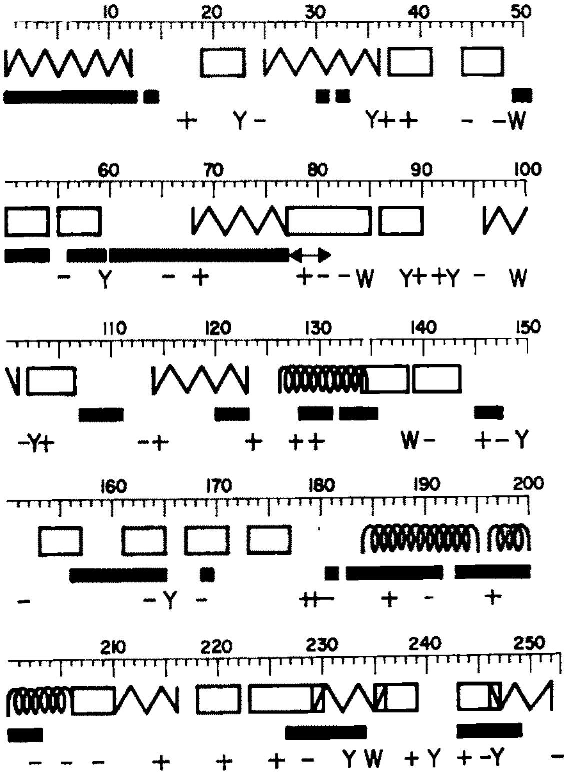

Fig 4 Secondary structure prediction of the discoidin I monomer The results obtained with the Chou and Fasman method [26,27] are represented (∿∿∿ α-helix, ⋀⋀⋀ β-strand, ▭ β-turn). ▬, Hydrophobicity prediction, obtained with the Kyte and Doolittle parameters [28] The positions of the charged aminoacids (+, −), and that of the fluorophores (Y, tyrosine and W, tryptophan) are represented The localization of the sequence (Gly-Arg-Gly-Asp) homologous to the fibronectin cell-attachment sequence is also given (◀—▶)

Discussion

The recent suggestion that discoidin I might be involved in the cell substratum attachment of *Dictyostelium discoideum* cells by a mechanism similar to that found in fibronectin-mediated cell adhesion of vertebrate cells [7] raises the question of the structural organization of this lectin and its possible homologies with that of fibronectin. Several meaningful structural traits of fibronectin have been described in the past years through studies on the spectroscopic properties of this protein [12–14]. We have used a similar approach for discoidin I in order to gain information about its structure.

The studies on CD spectra of discoidin I reported in this paper show that this lectin presents structrual homologies with fibronectin. As with fibronectin, the low intensity of discoidin I CD spectra indicates that this protein should present a low level of secondary structure. More significant is the detection of a 224 nm positive ellipticity band which resembles that at 227 nm found in fibronectin, suggesting a contribution to aromatic chromophores on the C.D. behavior of the discoidin I molecule. The optical activity of tyrosine side-chains has been reported to be responsible for the 227 nm positive band detected in the CD spectra of fibronectin [14]. The CD spectrum of discoidin I resembles more closely that of tryptophan residues than that of tyrosine between 210 and 240 nm [29]. Nonetheless, the maximum observed for discoidin I is displaced towards 224 nm relative to tryptophan (228 nm). The fluorescence studies reported here clearly support the existence of at least one displaced tryptophan residue partly buried in a more hydrophobic environment in the discoidin I molecule. From the model of discoidin I presented in Fig. 4 it can be observed that two out of five tryptophan residues of the monomer are located in a hydrophobic environment (Trp-50 and -236). One of both residues could be responsible for the characteristic 224 nm positive ellipticity band of the CD spectrum as well as for the 325 nm emission shoulder detect in the fluorescence spectra.

The displacement of the positive band at 224 nm in discoidin I could be explained by a high contribution of β-turns in this molecule [29]. In fact, from the CD data adjusted to the parameters of Chang et al. [21] and from the theoretical prediction of Chou and Fasman [26,27], discoidin I shows a high content of β-turns (see Table I). When the secondary structure estimation is done following the method of Garnier [30], 35% of β-turn structures is also obtained. These values are also in agreement with those recently reported by Ohyama et al. [11] and taken together strongly support a high β-turn content for discoidin I. In this context it is also worthy of mention that the lectin concanavalin A is one of the typical β-proteins (50% β-strand and 25% β-turn), with very little α-helical structure [29]. The results discussed here for discoidin I together with those recently reported for the 14 kDa chick embryo lectin [11] support the notion that, in general, lectins may possess similar structures with low α-helical and high β-structures (β-strand and/or β-turn) organization.

In the case of discoidin I, the results obtained in the presence of SDS point out that the amino-acid sequence of this lectin has a higher potential for α-helical conformation (up to 39.2%), suggesting the existence of structural constraints imposed by the tertiary structure of the protein. This behavior closely resembles that previously reported for fibronectin when treated with SDS, where a 20% of α-helix conformation is induced by low concentrations of the detergent [22]. In spite of the higher complexity of fibronectin molecule (dimer of 440 kDa) compared to that of discoidin I (tetramer of 120 kDa) the similarities in their spectroscopic properties tempt us to speculate about the existence of general structural homologies in both proteins. At least for the cell-binding sequence, the secondary structure predictive methods show that the specific peptide is located in a β-turn of an exposed region both in discoidin I (this work) and in fibronectin [31].

On the other hand, the significant contribution of aromatic chromophores to the optical activity of both proteins strengthens these homologies further than those arising from amino-acid sequencing and raises the question of the possible involvement of those chromophores in the biological function of cell-attachment proposed to be shared by both molecules [7]. This implication remains to be investigated in the future.

Regarding the sugar-binding activity of discoidin I, the fact that CD spectra do not change in the presence of various sugars indicates that no major changes in the overall secondary structure of discoidin I are induced by the binding of these ligands. On the other hand, the fluorescence studies show that the 325 nm shoulder arising from a displaced tryptophan residue is also observed in the presence of different concentrations of sugar ligands (galactose, *N*-acetylgalactosamine, *N*-acetylglucosamine; results not shown). The shoulder is more apparent in the presence of low concentrations of *N*-acetylgalactosamine (10^{-3} M) than with similar concentrations of less specific sugars. Even when the differences between sugars are apparent (about 5%) the whole difference compared to control is rather small (2–3%). This low variation does not allow an accurate quantification of the different emissions with the various sugars. Nonetheless, the better definition of the shoulder with a lower concentration of *N*-acetylgalactosamine indicates that some specific environmental changes in tryptophan residues are induced by the binding of this specific sugar ligand to discoidin I. More work should be done on this aspect in order to determine the role of this fluorophore in the sugar-binding function and how (if at all) it can influence the cell-binding activity.

Given the structural homologies between discoidin I and fibronectin reported here, it would be of interest to extend this kind of study to other lectins such as the 14 kDa chick embryo lectin, in order to explore further the possible structural and functional homologies between lectins and fibronectin and to gain a deeper insight into the biological function of these molecules.

Acknowledgements

The CD and fluorescence spectra have been produced in the Departamento de Bioquímica, Facultad de Ciencias, Universidad Complutense, Madrid, Spain. We are very grateful to Dr. F. Montero for the use of facilities and for his important contribution, as well as that of Dr. F. Morán, in the interpretation of results and reading the manuscript. We also appreciate the collaboration of Dr. P. Usobiaga in the analytical centrifugation analysis. This work has been done with the support of the CAICYT, CSIC project 151. A.V. is supported by the CAICYT, R.C. by a grant from the PFPI.

References

1 Frazier, W, Rosen, S D, Reitherman, R.W and Barondes, S H (1975) J Biol Chem 250, 7712–7721

2 Simpson, D L, Rosen, S.D. and Barondes, S H (1974) Biochemistry 13, 3487–3493

3 Rosen, S., Kafka, S, Simpson, D. and Barondes, S H (1973) Proc. Natl. Acad. Sci. USA 70, 2554–2557

4 Ray, J, Shinnick, T and Lerner, R (1979) Nature 279, 215–221

5 Ray, J and Lerner, R (1979) Cell 28, 91–98

6 Cano, A and Pestaña, A (1984) J Cell. Biochem 25, 31–43

7 Springer, W R, Cooper, D.N W and Barondes, S H (1984) Cell 39, 557–564

8 Gabius, H J, Spronger, W.R. and Barondes, S H (1985) Cell 42, 449–456

9 Cooper, D N, Lee, S C and Barondes, S H. (1983) J Biol. Chem 258, 8745–8750

10 Hynes, R.O and Yamada, K.M (1982) J Cell Biol 955, 369–377

11 Ohyama, Y., Hirabayashi, J, Oda, Y, Ohno, S.A., Kawasaki, H., Suzuki, K. and Kasai, K (1986) Biochem. Biophys. Res Commun 134, 51–56

12 Alexander, S S, Jr, Colonna, G, Yamada, K.M., Pastan, I and Edelhoch, H (1978) J Biol Chem 253, 5820–5824

13 Koteliansky, V.E., Glukova, M.A., Bejanian, M V., Smirnov, V N, Filimonov, V.V., Zalite, O M and Venyaminov, S V. (1981) Eur J. Biochem. 119, 619–624

14 Welsh, E J, Frangou, S.A, Morris, E R and Rees, D A (1983) Biopolymers 22, 821–831

15 Laemmli, U K (1970) Nature 277, 680–685

16 Eftink, M R and Ghiron, C A (1976) Biochemistry 15, 672–680

17 Bradford, M.M (1976) Anal Biochem 72, 248–254

18 Jirgensons, B (1976) Biochim Biophys. Acta 434, 58–68

19 Wu, C S, Ideda, K. and Yang, J T. (1981) Biochemistry 20, 566–570

20 Wu, C.S. and Yang, J.T (1980) Biochemistry 19, 2117–2122

21 Chang, C.T., Wu, C.S and Yang, J T. (1978) Anal. Biochem. 91, 13–31

22 Colonna, G., Alexander, S S Jr., Yamada, K M., Pastan, I. and Edelhoch, H (1978) J. Biol Chem 253, 7787–7790

23 Woody, R.W. (1978) Biopolymers 17, 1451–1467

24 Lakowicz, J.R. (1983) in Principles of Fluorescence Spectroscopy, Plenum Press, New York

25 Poole, S., Firtel, R A, Lamar, E. and Rowekamp, W (1981) J Mol. Biol 153, 273–289

26 Chou, P Y and Fasman, G D (1974) Biochemistry 13, 222–245

27 Chou, P.Y and Fasman, G D (1979) Biophys. J 26, 367–383

28 Kyte, J and Doolittle, R F (1982) J Mol. Biol 157, 105–132

29 Brahms, S and Brahms, J (1980) J Mol Biol 138, 149–178

30 Garnier, J., Osguthorpe, D J. and Robson, B. (1978) J. Mol Biol. 120, 97–120

31 Pierschbacher, M.D and Ruoslahti, E. (1984) Nature 309, 30–33

Biochimica et Biophysica Acta 911 (1987) 19–24
Elsevier

BBA 32689

Conformational and activity changes during guanidine denaturation of D-glyceraldehyde-3-phosphate dehydrogenase

Gui-Fu Xie and Chen-Lu Tsou

Institute of Biophysics, Academia Sinica, Beijing (China)

(Received 3 October 1986)

Key words: Glyceraldehyde-3-phosphate dehydrogenase inactivation; Protein denaturation, Active site probe

Changes in intrinsic protein fluorescence of lobster muscle D-glyceraldehyde-3-phosphate dehydrogenase (D-glyceraldehyde-3-phosphate : NAD$^+$ oxidoreductase (phosphorylating), EC 1.2.1.12) have been compared with inactivation of the enzyme during denaturation in guanidine solutions. The holoenzyme is completely inactivated at guanidine concentrations less than 0.5 M and this is accompanied by a red shift of the emission maximum at 335 nm and a marked decrease in intensity of the intrinsic fluorescence. At 0.5 M guanidine, the inactivation is a slow process, with a first-order rate constant of $2.4 \cdot 10^{-3}$ s^{-1}. A further red shift in the emission maximum and a decrease in intensity occur at guanidine concentrations higher than 1.5 M. The emission peak at 410 nm of the fluorescent NAD derivative introduced at the active site of this enzyme (Tsou, C.L. et al. (1983) Biochem. Soc. Trans. 11, 425–429) shows both a red shift and a marked decrease in intensity at the same guanidine concentration required to bring about the inactivation and the initial changes in the intrinsic fluorescence of the holoenzyme. It appears that treatment by low guanidine concentrations leads to both complete inactivation and perturbation of the active site conformation and that a tryptophan residue is situated at or near the active site.

Introduction

The effects of structural changes on the activity of enzymes have been extensively studied in the literature. However, previous authors have largely concentrated on the effect of chemical modification of the primary structures [1–4]. On the other hand, although the importance of conformational integrity for the activity of an enzyme is generally recognized and the folding and unfolding of protein molecules under different conditions have been extensively studied [5–8], relatively few attempts have been made to correlate the conformational changes of an enzyme to changes in its catalytic activity. In this laboratory, the conformational changes of creatine kinase (EC 2.7.3.2) during guanidine or urea denaturation at different concentrations have been followed by changes in ultraviolet absorbance, fluorescence and CD as well as by exposure of buried SH groups. At low guanidine or urea concentrations, the activity of creatine kinase is seriously affected without any detectable change in conformation [9–11]. It has been suggested that the active site of creatine kinase is situated in a limited region of the molecule which is more sensitive to guanidine or urea than the enzyme as a whole. A slight perturbance to the correct spatial geometry of the functional groups responsible for the catalytic mechanism destroys its activity before any gross conformational changes can be detected. A probe introduced at the active site would be useful in revealing conformation changes at this region as com-

---

Correspondence: Dr C.-L. Tsou, Institute of Biophysics, Academia Sinica, Beijing 100080, China

0167-4838/87/$03.50 © 1987 Elsevier Science Publishers B.V. (Biomedical Division)

pared to the molecule as a whole.

We have previously reported that by ultraviolet irradiation of active site carboxymethylated glyceraldehyde-3-phosphate dehydrogenase (D-glyceraldehyde-3-phosphate : NAD$^+$ oxidoreductase (phosphorylating), EC 1.2.1.12) a fluorescent derivative of NAD is formed covalently linked to the enzyme presumably at its active site [12–16]. This fluorescent NAD derivative has now been employed as a probe to study the conformational changes at the active site during guanidine denaturation of this enzyme. It is shown that the same low concentration of guanidine leads to the complete inactivation of the holoenzyme and affects markedly both the intrinsic fluorescence of the enzyme at 335 nm and the fluorescent properties of this covalent NAD derivative.

Materials and Methods

Lobster muscle D-glyceraldehyde-3-phosphate dehydrogenase, recrystallized three times, was prepared by the method of Allison and Kaplan [17] from the tail muscle of *Palinurus versicolor* with a specific activity of about 60000. The molar absorption coefficient used for concentration determination and the method of activity assay were as given by Allison and Kaplan [17]. Guanidine used was a local guaranteed reagent and the absorbance at 250 nm of a 6 M solution was less than 0.05.

The removal of tightly bound NAD$^+$, carboxymethylation at the active-site SH groups as well as preparation of the enzyme with the covalently linked fluorescent NAD derivative were essentially as described for the rabbit muscle [13] and the *Stearothermophilus* enzymes [18]. The holoenzyme (0.2 mM) was treated with 6 mM iodoacetate, for 10 min at 0°C, resulting in an inactivation of approximately 98%. The solution was then passed through a Sephadex G-50 column to remove the excess iodoacetate. Determination with 3,5′-dithiobis(2-nitrobenzoic acid) showed that only the active site SH group per each subunit has been modified. The carboxymethylated enzyme, 30 μM, in 0.1 M phosphate buffer (pH 7.0) containing 0.6 mM NAD$^+$ in a 3 ml cuvette was placed about 8 cm before an 150 W xenon lamp and irradiated for 20 min. The solution was occasionally stirred and cooled with an electric fan during irradiation.

During denaturation the enzyme (final concentration, 0.3 μM) was dissolved in 0.1 M phosphate buffer at pH 7.0 containing 1 mM EDTA and guanidine at the desired concentration. The solutions were allowed to stand at room temperature, usually around 20°C, for 24 h for the reaction to reach completion as indicated by no further activity or fluorescence changes. The enzyme was completely stable in the absence of the denaturant under similar conditions. Aliquots were then taken for activity and fluorescence measurements. The lobster muscle enzyme was found to be poorly soluble in guanidine solutions of concentrations around 1 M and this prevents the measurements of the conformational changes of the enzyme by methods which would require higher enzyme concentrations such as CD or ultraviolet difference spectra measurements. At 0.3 μM, the enzyme is soluble throughout the concentration range of guanidine solutions employed.

Absorbance and fluorescence measurements were carried out with a Cary 219 spectrophotometer and a Hitachi MPF-4 spectrofluorometer, respectively, both maintained at 25°C.

Results

Fluorescence and activity changes of the holoenzyme in guanidine solutions of different concentrations

Changes in the fluorescence emission spectra of the holo- and apo-D-glyceraldehyde-3-phosphate dehydrogenase after denaturation in guanidine solutions of increasing concentrations for 24 h are shown in Fig. 1. Both the decrease in emission intensity and the red shift of the emission maximum occur in two stages, as can be seen from Fig. 2. At guanidine concentrations less than 0.1 M, very little, if any, fluorescence change can be observed for the holoenzyme. A marked decrease in emission intensity takes place at about 0.2–0.4 M guanidine together with a slight red shift of the emission maximum from 335 to 339 nm. Further changes in the fluorescence properties occur at guanidine concentrations between 1.5 and 2.0 M with a slight decrease in emission intensity but a marked red shift of the emission maximum from 342 to 357 nm. The extents of inactivation in

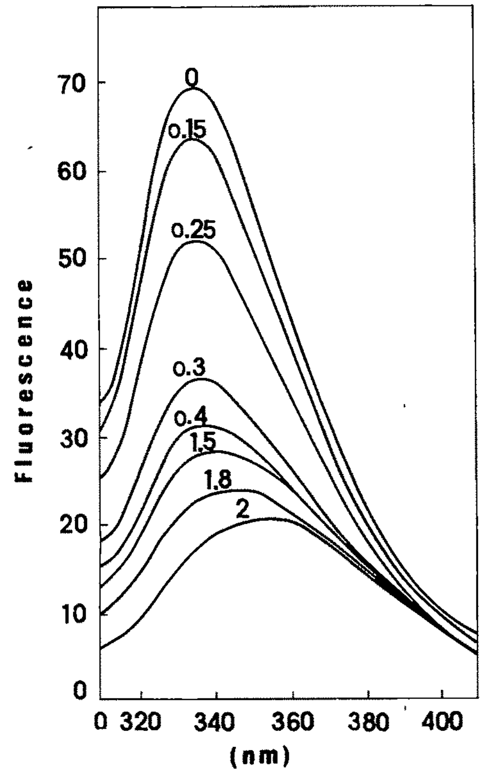

Fig. 1. Fluorescence emission spectra of the holoenzyme in guanidine solutions of different concentrations The lobster enzyme (0 3 μM) was dissolved in 0 1 M phosphate buffer at pH 7.0 containing 1 mM EDTA and guanidine at the desired concentration. The solutions were allowed to stand at room temperature usually around 20 °C for 24 h for the denaturation to reach completion before fluorescence measurements with an excitation wavelength of 295 nm. Numbers on each curve denote guanidine molar concentrations

guanidine solutions are also recorded in Fig. 2 and; as can be clearly seen, coincide almost exactly with the extents of fluorescence changes in the initial stage. The enzyme is completely inactivated by incubation with 0.4 M guanidine for 24 h, whereas control samples without guanidine show complete activity.

Fluorescence and activity changes of the apoenzyme in guanidine solutions of different concentrations

Similar results have been obtained with the apoenzyme (Fig. 3) except that the initial drop in emission intensity, the red shift of the emission maximum as well as the inactivation take place at lower guanidine concentrations than in the case of the holoenzyme. Whereas there is very little change in 0.1 M guanidine for the holoenzyme, marked changes have been observed for the apoenzyme. This is doubtless due to the protective effects of NAD$^+$ at the active site. Again, the change in activity coincides almost exactly with changes in fluorescence properties.

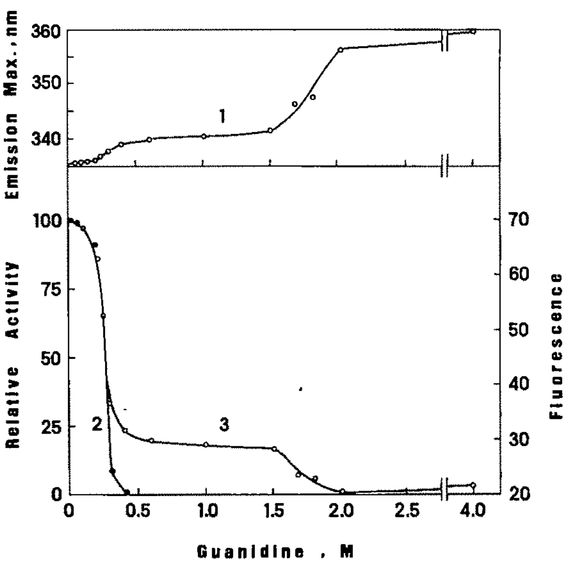

Fig 2. Fluorescence and activity changes of the holoenzyme in guanidine solutions of different concentrations. Conditions were as for Fig. 1 except that at the end of the incubation, aliquots were then taken for activity measurements The enzyme was stable under the above conditions in the absence of guanidine Curves 1–3 represent respectively the effects of guanidine on emission maximum, relative activity (left ordinate) and emission intensity (right ordinate)

A similar two-stage change in both the fluorescence intensity and emission maximum has been observed for the enzyme carboxymethylated at its active-site SH groups (data not shown).

Changes in fluorescence properties of the enzyme carrying the fluorescent NAD derivative in guanidine solutions of different concentrations

It has been shown in this laboratory that the ultraviolet irradiation of the active site carboxymethylated enzyme produces a fluorescent NAD derivative covalently linked to the enzyme with a fluorescence emission maximum at 410 nm [13] and that the emission intensity of this fluorescent NAD derivative decreases during the gradual unfolding of the enzyme molecule by sodium dode-

P 25707

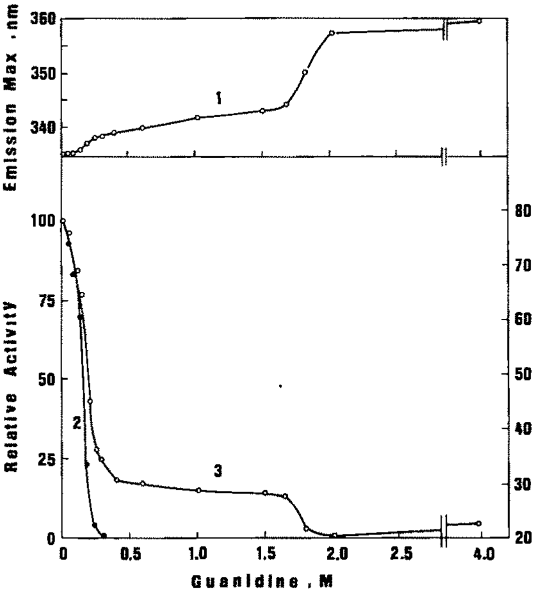

Fig. 3 Fluorescence and activity changes of the apoenzyme in guanidine solutions of different concentrations Conditions were as for Fig 2 except that the apoenzyme with an A_{280}/A_{260} of 1.90 was employed. Curves 1–3 represent respectively the effects of guanidine on emission maximum, relative activity (left ordinate) and emission intensity (right ordinate)

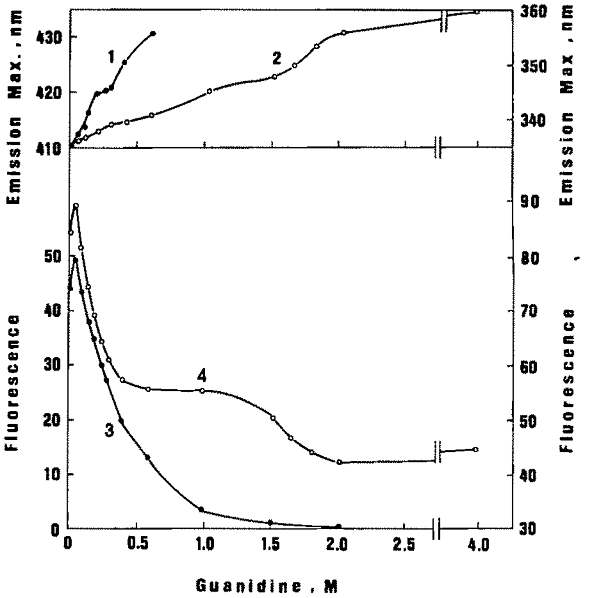

Fig 4. Changes in fluorescence properties of the enzyme carrying the fluorescent NAD derivative in guanidine solutions of different concentrations. Conditions were as for Fig 2 except that the enzyme carrying the fluorescent NAD derivative was employed. For the measurements of the fluorescence at 410 nm, an excitation wavelength of 325 nm was used Curves 1–4 represent respectively the effects of guanidine on emission maxima of the fluorescent derivative (left ordinate) and the intrinsic fluorescence (right ordinate), emission intensities of the fluorescent derivative (left ordinate) and the intrinsic fluorescence (right ordinate).

cylsulfate of increasing concentrations [14]. denaturation by guanidine produces decreases in emission intensities of both the intrinsic protein fluorescence as well as the fluorescence at 410 nm of this modified enzyme carrying the fluorescent NAD derivative together with marked red shifts of the respective emission maxima, as summarized in Fig. 4. The effect of guanidine solutions of different concentrations on the intrinsic protein fluorescence of the enzyme carrying the fluorescent NAD derivative is closely similar to those for the holo- and apo-enzymes, indicating again that no gross conformational changes has occurred during the formation of this fluorescent derivative [15].

It is to be noted that the greater part of the decrease in the fluorescence at 410 nm takes place at guanidine concentrations less than 0.5 M, largely in coincidence with the initial stage of the intrinsic fluorescence changes of the native as well as the enzyme carrying the fluorescent derivative. As this NAD derivative is formed in situ at the active site of this enzyme, it appears that the fluorescence change at low guanidine concentrations results from the unfolding of the active site region of the enzyme molecule. It is also to be noted that at a guanidine concentration of 0.05 M, both the intensity of the fluorescence of the enzyme protein and that of the NAD derivative increase slightly. This will be discussed in a later section.

Course of inactivation in guanidine solutions

The course of inactivation of the holoenzyme in 0.5 M guanidine, as shown in Fig. 5, is a fairly slow first-order process with a rate constant of $2.4 \cdot 10^{-3}$ s^{-1}. The conformational changes as indicated by changes in the intrinsic fluorescence properties of the enzyme produced by such a low guanidine concentration is likewise a slow first-order reaction and a semilogarithmic plot gives a rate constant very similar to that for the inactivation reaction.

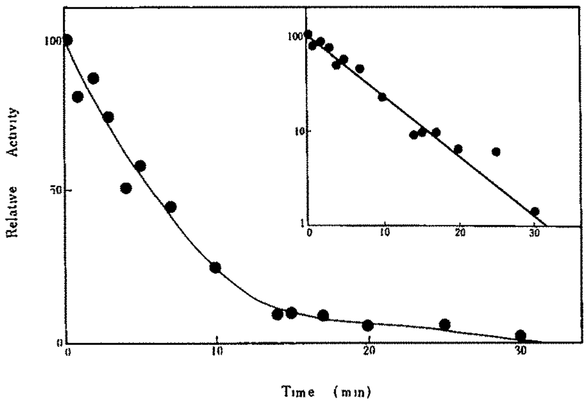

Fig. 5 The course of inactivation in 0.5 M guanidine. The holoenzyme, 0.3 μM, was incubated with 0.5 M guanidine in 0.1 M phosphate buffer at pH 7.0 containing 1 mM EDTA at 25°C and aliquots were taken at different time intervals for activity assay. The inset shows a semilogarithmic plot of the results obtained.

Discussion

In previous publications [9–11] the activity and conformation changes of creatine kinase during unfolding of the molecule in guanidine and urea solutions have been studied and it has been shown that at low guanidine or urea concentrations, the activity of creatine kinase is seriously affected without any gross conformational change which can be detected by the physicochemical methods employed. It is suggested that the active site of this enzyme is situated in a limited region of the molecule which is more fragile to conformational disturbances in the denaturation process [11]. It has now been shown that the inactivation of lobster muscle D-glyceraldehyde-3-phosphate dehydrogenase, also occurs at low guanidine concentrations. That such low concentrations of guanidine does produce conformational changes at the active site has now been demonstrated for glyceraldehyde-3-phosphate dehydrogenase by the changes in emission properties of the fluorescent NAD derivative introduced at the active site by ultraviolet irradiation of the carboxymethylated enzyme in the presence of NAD [12]. It is to be noted, however, that complete exposure of this fluorescent NAD derivative requires a slightly higher guanidine concentration. It is known that exposure of the fluorescent NAD derivative by SDS denaturation of this enzyme also leads to decrease in emission intensity and red shift of the emission maximum [14].

The inactivation of glyceraldehyde-3-phosphate dehydrogenase is accompanied by marked intrinsic fluorescence changes at the same range of guanidine concentrations, presumably due to environmental changes of a tryptophan residue at or near the active site. Radiationless energy transfer between tryptophan residue(s) of the enzyme and the fluorescent NAD derivative has been shown previously [15]. A disruption of the conformational integrity at the active site and therefore the spatial arrangement between the substituted nicotinamide ring of the fluorescent NAD derivative and the indole ring of tryptophan at or near the active site could lead to the increase in emission intensity of the intrinsic fluorescence of the enzyme carrying the fluorescent NAD derivative, as shown in Fig. 4. It is interesting to note that the activity of the enzyme is affected at such low concentration of guanidine which also affects the energy transfer. Although the effect of guanidine on the conformational integrity of the native enzyme may or may not be identical to that of the enzyme carrying the fluorescent NAD derivative, it is to be noted that the courses of changes in the fluorescence properties with increasing guanidine concentrations are closely similar. On the other hand, it has been shown previously by CD measurements that no gross conformational change has occurred during the introduction of a fluorescent NAD derivative at the active site [16].

Heilmann and Pfleiderer have provided evidence to show that Trp-193 is essential for the activity of this dehydrogenase from yeast [19]. It is also known that Trp-193 of the lobster enzyme is situated not very far from the active site [20]. However, this tryptophan residue is not conserved in the sequences of the enzymes isolated from thermophilic bacteria [21]. On the other hand, quantitative studies on the energy transfer between tryptophan and the fluorescent NAD derivatives have shown that, for both the muscle [15] and the bacterial enzymes [18], at least one of the tryptophan residues is situated much closer to the nicotinamide ring than indicated from X-ray crystallographic results. The results obtained in the present study show the concomitant exposure of the tryptophan residue near the active site and the inactivation of the enzyme and this is suggestive that a tryptophan residue could play a role in the catalytic mechanism of this enzyme. Whether this involves subtle conformational arrangements so as to favor substrate binding or the chemical aspects of hydride transfer would require further investigation.

References

1 Thomas, J O. (1974) in Companion to Biochemistry (Bull, A.T., Lagnado, J.R , Thomas, J.O. and Tipton, K.F., eds.), pp. 87–138, Longman Green, London

2 Sigman, D.S. and Mooser, G (1975) Annu. Rev. Biochem 44, 889–931

3 Brocklehurst, K. (1979) Int. J. Biochem. 10, 259–274

4 Lundbladd, R.L. (1984) Chemical Reagents for Protein Modification, Vol. 1, pp. 1–23, CRC Press, Boca Raton

5 Jaenicke, R. (1982) Biophys. Struct Mech. 8, 231–256

6 Kim, P.S. and Baldwin, R.L. (1982) Annu. Rev. Biochem. 51, 459–489

7 Creighton, T.E. (1984) Adv. Biophys. 18, 1–20

8 Grossman, S H. (1984) Biochim. Biophys. Acta 785, 61–67

9 Yao, Q.Z., Tian, M and Tsou, C.L. (1984) Biochemistry 23, 2740–2744

10 Yao, Q Z , Zhou, H.M., Hou, L.X. and Tsou, C L (1982) Sci. Sin. 25B, 1296–1302

11 Yao, Q.Z., Tian, M and Tsou, C L (1985) Sci. Sin 28B, 484–493

12 Tsou, C.L , Xu, G.Q , Zhou, J M. and Zhao, K.Y. (1983) Biochem. Soc Trans 11, 425–429

13 Ho, Y.S., Lian, Y.N , Chiang, S.H and Tsou, C.L. (1979) Sci. Sin 22, 207–221

14 Tsou, C L., Zhao, K Y and Ho, Y S. (1979) Sci. Sin. 22, 693–704

15 Ho, Y.S. and Tsou, C.L (1979) Sci. Sin. 22, 478–489

16 Lian, Y.N. and Tsou, C L (1981) Sci. Sin 24, 1146–1153

17 Allison, W S. and Kaplan, N.O. (1964) J Biol Chem 239, 2140–2152

18 Ho, Y S., Liang, S.J. and Tsou, C.L. (1980) Biochim. Biophys Acta 613, 249–255

19 Heilmann, H.D. and Pfleiderer, G (1975) Biochim. Biophys Acra 384, 331–341

20 Moras, D., Olsen, K.W., Sabesen, M.N., Buehner, M., Ford, G.C and Rossmann, M.G. (1975) J Biol. Chem. 250, 9137–9162

21 Hocking, J.D. and Harris, J.I. (1980) Eur J. Biochem. 108, 567–579

Biochimica et Biophysica Acta 911 (1987) 25–36
Elsevier

BBA 32595

Conformation similarities of the globular and tailed forms of acetylcholinesterase from *Torpedo californica*

Chuen-Shang C. Wu, Lydia Gan and Jen Tsi Yang

Cardiovascular Research Institute, University of California, San Francisco, CA (U.S.A.)

(Received 30 June 1986)

Key words Acetylcholinesterase; Enzyme conformation, Protein conformation; Circular dichroism

The conformation of the globular dimer (G_2), the tailed asymmetric dodecamer (A_{12}, also containing some tailed octamer A_8) and the globular tetramer (G_4, prepared by removing the collagen-like tail from A_{12}) of acetylcholinesterase (acetylcholine acetylhydrolase, EC 3.1.1.7) was studied by circular dichroism (CD) in the ultraviolet region. The G_2 and G_4 forms had similar conformation with about 40% α-helix, 35% β-sheets and 4% β-turns; the tailed form had a lower helicity (about 34%) and β-form (about 25%) content probably because of the presence of the tail whose CD spectrum resembles that of an unordered form, but it had about the same amount of β-turns as the other two forms. All three forms also had similar CD spectra in the near-ultraviolet region due to their non-peptide chromophores. The pH, thermal and urea denaturation of the three acetylcholinesterase forms was also similar to each other. The pH-dependency of both the enzymatic activity and CD intensity of the three forms showed bell-shaped curves with a plateau at pH 7–8. The activity was completely lost at pH below 5 or above 10, but the corresponding CD spectra retained 70–80% of the original magnitudes. Thermal denaturation of the three forms at pH 7.5 showed a conformational transition and loss of activity between 30 and 40°C, but the CD intensity of the helical band at 222 nm was reduced by only 20–30%. Urea denaturation of the three forms began at 1 M urea; it was protein concentration- and time-dependent. Again, the activity disappeared faster than the decreasing CD intensity. Thus, the overall conformation of the three acetylcholinesterase forms appears to be relatively stable, but their active site is easily perturbed by changing the environment. The loss of activity correlated well with the disapperance of the CD band of tryptophan(s) in the near-ultraviolet region, suggesting that the Trp residue(s) might be at or near the active center of the enzyme.

Introduction

Polymorphism of acetylcholinesterase (acetylcholine acetylhydrolase, EC 3.1.1.7) in vertebrate tissues has been a subject of extensive study. The multiple molecular forms were identified not by differences in electrical charges like many other isozymes but by differences in sedimentation velocity in sucrose density gradient centrifugation. The most abundant source of synaptic acetylcholinesterase is the electric organs of electric eel and ray. The enzyme from these sources has been isolated and studied extensively [1–4]. The majority of acetylcholinesterase from these sources is the asymmetric or tailed dodecamer A_{12} in the

---

Abbreviations: $C_{12}E_7$, dodecylheptaoxyethylene ether; $C_{12}E_{11.2}$, dodecylpolyoxyethylene ether, with an average oxyethylene chain length of 11.2; CD, circular dichroism.

Correspondence: Dr. C.-S.C. Wu, Cardiovascular Research Institute, University of California, San Francisco, CA 94143, U.S.A.

0167-4838/87/$03.50 © 1987 Elsevier Science Publishers B.V (Biomedical Division)

basal lamina of the extracellular matrix. It has a sedimentation coefficient of 17–18 S and consists of 12 globular catalytic subunits (each subunit has an M_r of about 70 000), which form three tetramers and are linked by disulfide bonds to three collagen-like tails (each strand has an M_r of 55 000). For *Torpedo californica*, a non-catalytic subunit with an M_r of 100 000 was also identified in the asymmetric enzyme [4]. The extracted asymmetric acetylcholinesterase is heterogeneous; it also contains about 25% of asymmetric octamer A_8 (13 S) and a trace mount of asymmetric tetramer A_4 (8 S), which has 8 and 4 catalytic subunits, respectively. All these forms can be converted to a globular catalytic tetramer G_4, (11 S) by proteolytic enzymes such as trypsin, papain or collagenase. The other species of acetylcholinesterase in the electric fish is the globular dimer G_2 (6 S) on the outer surface of the synaptic cell membrane which can be further classified into low-salt-soluble G_2 and detergent-soluble G_2. Both G_2's are hydrophobic but they have some structural differences [5]. Differences between G_2 and the catalytic subunits of A_{12} have also been reported [3,6].

Schumacher et al. [7] have recently determined the amino-acid sequence of the G_4 form of acetylcholinesterase from the corresponding sequence of cDNA. The exact homology or differences among these molecular forms can be identified when the sequences of globular G_2 (both low salt-soluble and detergent soluble) become available in the near future.

In this paper we compared the CD spectra of the tailed and the low-salt-soluble globular acetylcholinesterase. These two acetylcholinesterase forms appeared to have slightly different spectra, but they had essentially the same conformation when the collagen-tail of the tailed acetylcholinesterase was removed by proteolysis. All three acetylcholinesterase forms behaved similarly toward denaturation by acid, alkali, heat or urea. In all cases acetylcholinesterase was irreversibly denatured, but the overall conformation of the enzymes appeared to be relatively stable, even though their enzymatic activities were completely lost under various denaturing conditions.

This work was first presented at the Annual Meeting of the American Society of Biological Chemists, Washington, DC [34,35].

Materials and Methods

Materials

Liquid-nitrogen-frozen electroplax of *Torpedo californica* was obtained from Marinus, Westchester, CA. 9-Chloroacridine and 1,3-diaminopropane were respectively from American Scientific Products and Aldrich. ϵ-Aminocaproic acid, Triton X-100, aprotinin, decamethonium bromide and Sepharose CL-4B were from Sigma. Cholic acid from Sigma was recrystallized from ethanol. Nonionic detergents $C_{12}E_7$ and $C_{12}E_{11\ 2}$ were from Nikkol and KaoAtlas, both of Japan. A calibrated protein standard, plasma gamma globulin was from Bio-Rad Laboratories.

The acridine resin, 9-(ϵ-aminocaproyl-γ-aminopropylamino)acridinium-Sepharose, was synthesized by the method of Rosenberry and Richardson [1]. The amount of bound ligand, as measured by absorbance at 412 nm, was about 1 μmol acridine per ml packed resin.

Buffers used for extractions were: buffer 1, 0.1 M NaCl/10 mM Tris-HCl (pH 7.5); buffer 2, 2 M $MgCl_2$/10 mM Tris-HCl (pH 7.5); buffer 3, 1 M NaCl/40 mM $MgCl_2$/10 mM Tris-HCl (pH 7.5).

Methods

Extraction and purification of acetylcholinesterase. Both G_2 and tailed acetylcholinesterase were extracted by the methods of Lee et al. [4,8] except that the volume of the buffer and the time and speed of centrifugation were changed slightly. In addition, the filtration step for the tailed acetylcholinesterase after dialysis was omitted and substituted with centrifugation for 30 min at 45 000 rpm in a Beckman 45 Ti rotor. The G_4 form was extracted according to the method of Taylor et al. [9].

All three acetylcholinesterases were purified on acridine resin columns (1.5 × 20 cm) equilibrated with respective buffers: buffer 1 plus 1% of either Triton X-100 or $C_{12}E_{11.2}$ for G_2, buffer 1 plus 40 mM $MgCl_2$ for G_4 and buffer 3 for the tailed enzyme. The enzyme fractions which were eluted with 25 mM decamethonium bromide were pooled and dialyzed to remove decamethonium bromide. Triton X-100 in the solution of G_2 was removed by treatment with Bio-Beads SM-2 (0.3 g beads per ml of acetylcholinesterase solution) and replaced with another non-ionic detergent $C_{12}E_7$ (10 mM). When Triton X-100 was substituted with $C_{12}E_{11\,2}$ in the affinity column of G_2, the Bio-Beads SM-2 step was eliminated. The purified enzymes were stored at −70°C. For CD measurements, the enzymes were further dialyzed against 40 mM sodium pyrophosphate (pH 7.5) to remove excess salts. Both Triton X-100 and chloride ions absorb far-ultraviolet wavelengths and are undesirable for CD studies.

Protein and enzyme assays. Protein concentrations were determined by the Lowry method with γ-globulin as a standard (the standard curve for γ-globulin was very close to that of acetylcholinesterase calibrated by amino-acid analysis). For routine measurement of acetylcholinesterase activities, the method of Ellman et al. [10] was employed. The enzyme reaction was measured at room temperature either by monitoring the change in optical absorbance at 412 nm with the aid of a recorder attached to a Zeiss spectrophotometer or by stopping the enzyme reaction after 5 min with 1% SDS and measuring the developed color afterwards. The assay medium contained 2.5 ml of 0.1 M sodium phosphate, 5 mM $MgCl_2$ (pH 7.5), 100 μl of 10 mM 5,5′-dithiobis(2-nitrobenzoic acid), 20 μl of 75 mM acetylthiocholine and 10 μl of appropriately diluted acetylcholinesterase. For activities at different pH levels and temperatures, the pH-stat method was used on a Radiometer PHM 84 pH meter equipped with TTT-80 Titrator and ABU Autoburet. The assay mixture contained 5 ml of 0.1 M NaCl, 5 mM $MgCl_2$, 50 μl of 15 mg/ml acetylcholine chloride and 10 μl of acetylcholinesterase. The reaction mixture was maintained at a constant temperature in a water-circulating cell connected to a Hakke water bath. Nitrogen was purged over the solution to minimize the effect of CO_2 in the air. Acetic acid liberated by the enzymatic reaction was titrated with 0.01 M NaOH to a prefixed end-point pH. For pH-dependent activity studies, the decreased ionization of acetic acid at low pH and increased deprotonation of the choline group at high pH may slightly affect the NaOH consumption, but such corrections were neglected.

SDS-polyacrylamide gel electrophoresis. Slab SDS-polyacrylamide gel electrophoresis was performed in 1 mm-thick gels containing 3–12% linear gradient of polyacrylamide in a Bio-Rad Protean II unit. The acetylcholinesterase samples were prepared by adding SDS to 1% and dialyzed against 25 mM Tris-HCl (pH 7.5) to remove excess salts before mixing with the sample buffer. Bio-Rad high-molecular-weight and Pharmacia low-molecular-weight standards were used as the molecular-weight markers.

Sucrose density gradient centrifugation. A linear density gradient of sucrose (5–25% w/v) containing buffer 1 or 3 was made in 40-ml tubes for the SW 28 rotor. The solutions were stored at 4°C overnight before layering 50-200 μl of acetylcholinesterase on top of the gradient. The contents were centrifuged in a Beckman LB 55M centrifuge at 28000 rpm and 4°C for 26 h. Fractions were collected from the bottom and analyzed for acetylcholinesterase activities. *E. coli* β-galactosidase (16 S) and bovine catalase (11.4 S) were used as the S-value markers. The two proteins were assayed, respectively, by the method of Craven et al. [11] and Beers and Sizer [12].

Amino-acid analysis. Amino-acid compositions were determined after the proteins had been hydrolyzed in 6 M HCl for 24 h on a Beckman 6300 amino-acid analyzer at the Department of Biochemistry and Biophysics, University of California at Davis.

CD spectra. CD was measured on a JASCO J-500A spectropolarimeter equipped with a DP-500 for data acquisition and an IBM personal computer for data analysis. Temperature of the protein solution was maintained by a jacketed aluminum cell holder connected to a Hakke constant-temperature water bath. Optical activity is expressed as mean residue ellipticity, $[\theta]$, in deg · cm^2/dmol, which is calculated according to the equation:

$$[\theta] = (d \cdot s\ M_0)/(c \cdot l)$$

where M_0 denotes mean residue weight, d observed ellipticity (the displacement in cm from the baseline), s sensitivity in mdeg/cm, c protein concentration in mg/ml, and l the cell pathlength in mm. The CD data were analyzed by the methods of Chang et al. [13] using the reference spectra obtained from 15 proteins of known structure.

For pH studies, buffers of constant ionic strength containing glycine (pH 2–3.5, 9.5–12), acetate (pH 4–5.5) and phosphate (pH 6–7.5) [14] were used. Appropriate amounts of the pH 7.5 and pH 10 buffers were mixed to cover the pH range of 8–10 (veronal buffer (pH 8–0.5) was not used because it absorbs in the far-ultraviolet region). To save the proteins and to overcome the buffering capacity of pyrophosphate in the acetylcholinesterase stock solution, 1 part of acetylcholinesterase and 10 parts of the buffer were mixed and the pH of the mixture was rechecked. For urea denaturation studies, a constant amount of acetylcholinesterase solution was mixed with an appropriate amount of 10 M urea solution and water to final urea concentrations of 1–8 M.

Results

Homogeniety of acetylcholinesterase preparations

All three forms of acetylcholinesterase were purified by acridine-Sepharose affinity column and their homogeniety was checked by the sucrose density gradient centrifugation in the presence of Triton X-100. In general, G_2 was quite homogeneous. but G_4 and A_{12} were somewhat contaminated by other acetylcholinesterase forms. The contaminants in G_4 were probably undigested A_{12} (17 S) and partially digested A_4 (8 S), whereas high-molecular-weight aggregates and a trace amount of G_2 may be present in the tailed enzyme. No attempt was made to separate A_8 from A_{12}; they were grouped as the tailed acetylcholinesterase.

SDS-polyacrylamide gel electrophoresis

The subunit structure of acetylcholinesterase was studied by SDS-polyacrylamide gel electrophoresis in the absence and presence of the reducing agent, dithiothreitol. The electrophoretic patterns were similar to those of the published results [1,4,8]. In the absence of dithiothreitol, G_2 showed a major and a minor bands with M_r of 120000 and 67000, respectively. The M_r 120000 band was reduced to M_r 67000 with dithiothreitol. G_4 showed bands with M_r of 69000, 120000, 215000 and multiples of higher-molecular-weight aggregates without reduction. On addition of dithiothreitol all became the 69000 band. Both with and without dithiothreitol, G_4 also showed a sharp band of 18000, probably a product of the proteolysis during preparation, and a faint 95000 band. The tailed acetylcholinesterase existed as a mixture of high-molecular-weight aggregates, dimer, and monomer without dithiothreitol and reduced to the monomer and a collagen band of 55000 with dithiothreitol. Lee et al. [4] reported that the noncatalytic M_r 100000 component was released upon reduction of the tailed acetylcholinesterase; this component may correspond to our 95000 band. However, we also found this band in samples stored in 1% SDS for a prolonged time without reduction.

Amino-acid compositions

Although the G_2 form of acetylcholinesterase is found in the synaptic membrane and the G_4 form derived from the tailed acetylcholinesterase in the extracellular matrix, the amino-acid composition of the two proteins was very similar, one to the other (Table I) and to that reported previously for G_2 from the same species [8] and for G_4 from

TABLE I

AMINO-ACID COMPOSITIONS OF ACETYLCHOLINESTERASES FROM *TORPEDO CALIFORNICA*

The numbers are expressed in mol% and calculated on the basis of analyzed amino-acid residues. Cysteine and tryptophan residues were found in the amino-acid sequence but are excluded from the table for the sake of comparison.

Residue	G_2	G_4	G_4 [a]
Asx	11.79	11.59	11.63
Thr	4.75	4.46	4.36
Ser	8.78	8.10	8.55
Glx	9.45	10.85	10.54
Pro	6.45	6.28	5.82
Gly	8.60	8.60	8.00
Ala	5.15	4.86	4.55
Val	6.91	6.41	7.27
Met	1.18	1.61	3.09
Ile	3.53	3.61	4.00
Leu	9.52	9.32	9.09
Try	4.37	3.98	3.45
Phe	6.96	6.88	6.55
His	2.99	3.54	3.27
Lys	4.97	4.99	4.91
Arg	4.63	4.91	4.91

[a] Calculated from sequence

another species [1]. The mol% of each amino acid for G_4 was very close to that calculated from the sequence data (exclusing Cys and Trp) of Schumacher et al. [7]. Our low value of Met may be due to partial destruction during hydrolysis. Lee et al. [8] reported that the hydrophobic gloular dimer contained more hydrophobic amino acids than the catalytic subunits of the asymmetric acetylcholinesterase, but our results showed no significant differences between these two forms of acetylcholinesterase.

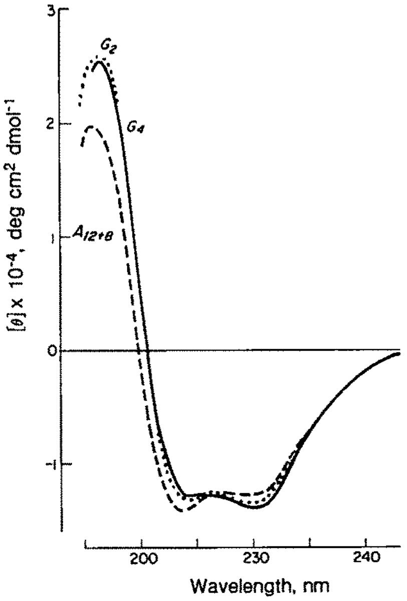

Fig. 1. CD spectra of acetylcholinesterase in the far-ultraviolet region at 4°C. Symbols: ·····, G_2; ———, G_4; — — —, A_{12+8}. Solutions: 0.1–0 4 mg/ml in 40 mM sodium pyrophosphate (pH 7.5) (The G_2 solution also contained 10 mM dodecylheptaoxyethylene ether ($C_{12}E_7$)). Cells: 0.1–2 mm pathlength.

CD spectra in the far-ultraviolet region

The far-UV CD spectra reflect the secondary structure (α-helix, β-sheets and β-turns) of proteins. Each curve for the three forms of acetylcholinesterase in Fig. 1 represented the average of at least three preparations of freshly prepared samples. The spectrum for G_2 and G_4 overlapped each other within experimental errors. The magnitude of the positive band at 193 nm and the double minimum at 208 and 222 nm suggest the presence of a moderate amount of α-helix. As in the spectra of all-α proteins, such as myoglobin and cytochrome *c*, the ellipticity at 208 nm was smaller than that at 222 nm. However, the analysis of CD spectra revealed a considerable amount of β-structure in both proteins (Table II). The helical and the β-form contents were higher than those obtained by Manavalan et al. [15] for G_2 and G_4 from the same tissue source, but the β-turn content was lower for our preparations. The spectrum of the tailed acetylcholinesterase (Fig. 1) was slightly different from those of G_2 and G_4 in that the ellipticity at 193 nm was smaller, but that at 208 nm was larger than the ellipticities of G_2 and G_4. The CD analysis showed slightly reduced contents of the helical and β-form (Table II). This is probably due to the presence of the collagen-like tail, which has a spectrum similar to that of an unordered polypeptide [16]. With the tail removed,

TABLE II

CONFORMATIONAL PARAMETERS OF ACETYLCHOLINESTERASE (AChE) FROM *TORPEDO CALIFORNICA*

Based on the method of Chang et al. [13].

AChE	f_H	f_β	f_t	f_R	Ref.
G_2	0.40	0.35	0.04	0.21	this work
	0.31	0.23 [a]	0.18	0.26	Ref 15
G_4	0.40	0.35	0.04	0 21	this work
	0.33	0.23 [a]	0.17	0 28	Ref. 15
A_{12+8}	0.34	0 25	0 06	0 35	this work
Sequence prediction					
G_4	0.33	0.33	0.25	0.08	Chou-Fasman
	0.32	0.34	0.13	0.21	Garnier et al.

[a] Combined fractions of parallel and antiparallel β-structure.

the catalytic tetramer G_4 had essentially the same conformation as that of G_2. Thus, the catalytic subunits of the hydrophobic dimer and the asymmetric acetylcholinesterase appeared to have a similar secondary structure. The conformation of acetylcholinesterase was also predicted by the sequence method of Chou and Fasman [17] and that of Garnier et al. [18]. The results (Table II) were close to those of CD analysis.

CD spectra in the near-ultraviolet region

The near-ultraviolet CD spectra often reveal differences in tertiary and quaternary structures and the microenvironment of aromatic residues. The near-ultraviolet CD spectra of acetylcholinesterase (Fig. 2) were very sensitive to changes in environment and to the freshness of the proteins. The ellipticities varied by more than 50% in some cases. Each curve for the three forms of acetylcholineterase represented the average of two or three most fresh preparations. The variations in ellipticities among these preparations were less than 5% for the presented data. All three forms of acetylcholinesterase had very similar profiles; the bands for Phe at 262 and 268 nm, Tyr at 276 and 282 nm and Trp at 289 and 295 nm can be clearly identified. However, certain features seemed to be specific for each type of acetylcholinesterase. For instance, for G_2 the ellipticity at 291 nm was usually near zero, and the bands at 268 and 295 nm were larger than those at 276 and 289 nm, respectively. For G_4, the ellipticity at 289 nm was usually greater than that at 295 nm and the spectrum was more or less symmetrical for the 275 nm band. For A_{12+8}, the trough at 275 nm never exceeded 100 deg cm^2/dmol. The contributions of the disulfide bonds in these acetylcholinesterases to the near ultraviolet spectra were not known, but the decrease in magnitude of the Trp bands correlated well with the disappearance of the enzymatic activity (not shown).

pH denaturation

The pH-dependency of the enzymatic activities of acetylcholinesterase was studied by the pH-stat method between pH 5 and 10. The activity was optimal over a narrow range of pH 7 to 8 and fell steeply on both sides of the neutral pH (Fig. 3). It was completely abolished at pH 5 and 10. The activity-pH curves for the three forms of acetylcholinesterase overlapped each other within experimental errors. A similar curve for a mixture of G_2 and the tailed form of acetylcholinesterase from *Torpedo marmorata* under comparable conditions was reported by Hofer et al. [19], who further stated that the addition of $MgCl_2$ and $CaCl_2$ as well as NaCl increased the activity of acetylcholinesterase. A similar salt effect was also found with our acetylcholinesterase preparations.

The far-ultraviolet CD spectra of the three forms of acetylcholinesterase at pH 2, 7, and 12

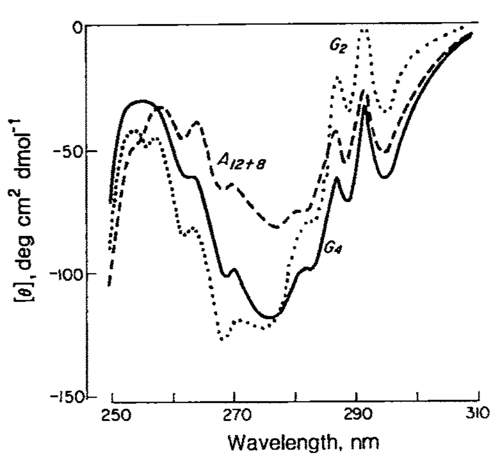

Fig. 2 CD spectra of acetylcholinesterase in the near-ultraviolet region at 4°C. Symbols and solutions: same as in Fig 1. Cells: 10–20 mm pathlength

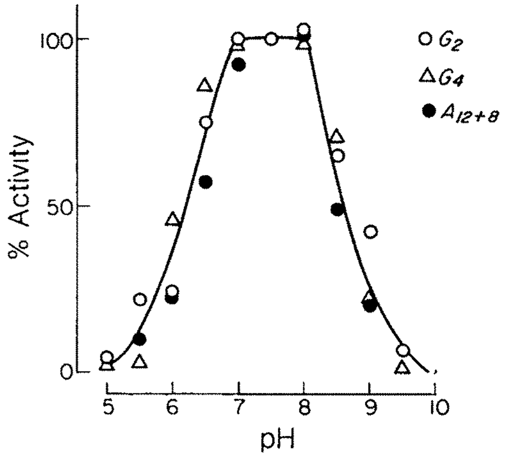

Fig. 3. Effect of pH on the enzymatic activity of acetylcholinesterase at 20°C The activities were normalized to those at pH 7.5

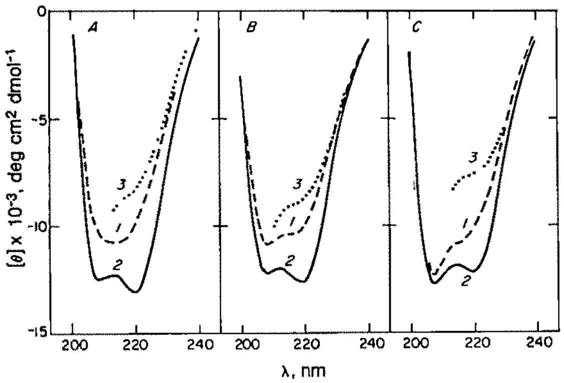

Fig. 4. Effect of pH on the CD spectra of acetylcholinesterase in the far-ultraviolet region at 20°C. The solutions were kept at room temperature for 30 min before measurements (A) G_2 (27 μg/ml); (B) G_4 (16 μg/ml); (C) A_{12+8} (22 μg/ml). Curves: (1) pH 2; (2) pH 7; (3) pH 12.

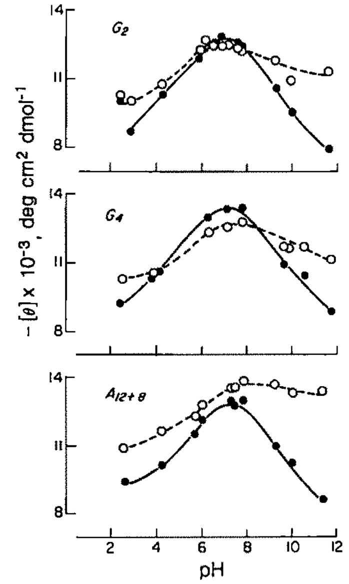

Fig. 5. Plots of mean residue ellipticity vs pH for acetylcholinesterase at 20°C. Symbols: ○, at 208 nm, ●, at 222 nm. G_2, 27 μg/ml; G_4, 16 μg/ml; A_{12+8}, 14 μg/ml. The readings became constant in about 30 min

(Fig. 4) showed a double minimum at neutral pH, which is typical of the presence of a helical conformation, but at either acidic or alkaline pH, the proteins appeared to be less ordered as reflected by smaller CD magnitudes. The CD spectra at pH 12 were limited to above 210 nm because of excessive noise at lower wavelengths. Judged from the CD magnitudes, the denaturation of the enzyme was more extensive at pH 12 than at pH 2. The G_2 form at pH 2 showed a broad minimum around 215 nm, suggesting the presence of a β-form-like conformation probably due to aggregation of the protein.

Acid and alkaline denaturation of the three forms of acetylcholineterase was followed by their mean residue ellipticities at 208 and 222 nm, which represent the two helical bands (Fig. 5). All of them showed a bell-shaped curve with an optimal pH around neutral. The magnitude of the ellipticities gradually reduced at acidic and alkaline pH. In general, $-[\theta]_{222}$ decreased more than $[\theta]_{208}$, but a considerable amount of ellipticities remained even at the extreme pH, suggesting that the proteins were not extensively unfolded.

The effect of pH on the CD spectra of acetylcholinesterase in the near-UV region was represented by the G_2 form (Fig. 6). At pH 2 most of the bands of aromatic side chains disappeared and the ellipticities became positive between 255 to 280 nm (curve 1). At pH 10 the spectrum showed a broad negative band without the fine structure of individual bands (curve 2). Notable was the Trp band at 295 nm, which had disappeared completely. The spectral changes with pH in both far- and near-ultraviolet regions were irreversible; that is, adjusting the pH back to neutral

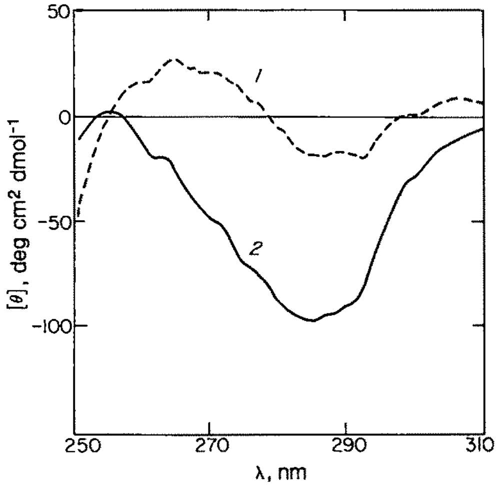

Fig. 6. CD spectra of acetylcholinesterase in the near-ultraviolet region at 20°C. Curves: (1) pH 2; (2) pH 10 Protein concentration: 0.26 mg/ml

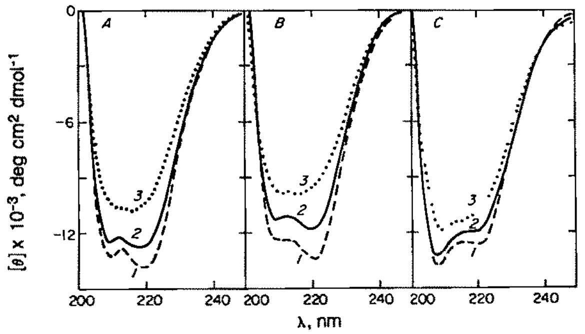

Fig. 7 Effect of temperature on the CD spectra of acetylcholinesterase in 40 mM sodium pyrophosphate at pH 7 5. (A) G_2 (0.26 mg/ml); (B) G_4 (0 26 mg/ml), (C) A_{12+8} (0.12 mg/ml). Curves. (1) 20 °C; (2) 30 °C; (3) 40 °C. The readings became stabilized after 30 min at each temperature

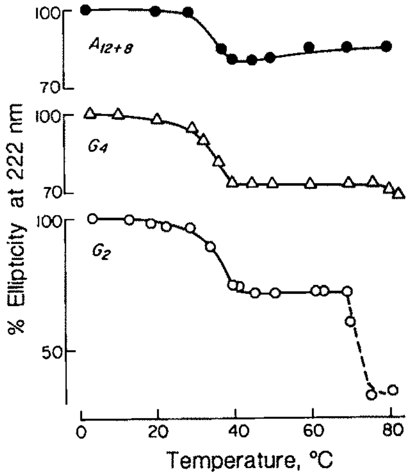

Fig. 8 Thermal denaturation of acetylcholinesterase in 40 mM sodium pyrophosphate at pH 7 5 G_2: 0.56 mg/ml plus 10 mM dodecylheptaoxyethylene ether, G_4: 0.24 mg/ml; A_{12+8}: 0.23 mg/ml. The ellipticities normalized to those at 4 °C were considered final when they were constant over a period of 20 min. The broken line in the G_2 curve indicates precipitation

could not restore the original spectrum at neutral pH.

Thermal denaturation

The magnitudes of the CD spectra in the far-ultraviolet region of G_2, G_4 and A_{12+8} at pH 7.5 decreased with increasing temperature from 20 °C to 40 °C (Fig. 7). G_2 and G_4 appeared to be denatured slightly more than A_{12+8} at 40 °C. Plot of $[\theta]_{222}$ vs. temperature indicated a conformational transition between 30° and 40 °C for all three forms (Fig. 8). The magnitude of the ellipticities at 40 °C was about 70–80% of that at 4 °C; the plateau remained unchanged up to 70 °C, above which G_2, but not G_4 and A_{12+8}, began to precipitate. A quick scan of the far-ultraviolet spectra of the three forms at 70 °C revealed no further change in conformation above 40 °C. While the change in CD magnitude with temperature was relatively small, the corresponding enzymatic activity dropped steeply above 30 °C and reached zero at 40 °C (not shown).

The effect of temperature on the CD spectra of acetylcholinesterase in the near-ultraviolet region was represented by the G_2 form (Fig. 9). As in the case of pH effect (Fig. 6), the fine structure of the CD spectra due to Trp, Tyr and Phe that were present at 4 °C or 20 °C became less defined at 30 °C (curve 1) and the overall ellipticites between 250 and 310 nm decreased slightly in magnitude. At 35 °C (curve 2), the Trp band at 295 nm dropped to zero and the magnitude of all other bands was about one half of those at 4 °C or 20 °C. At 40 °C (curve 3), all CD bands were converted into a slightly positive broad spectrum. Thus, the change in CD of aromatic groups appeared to parallel the loss of enzymatic activity.

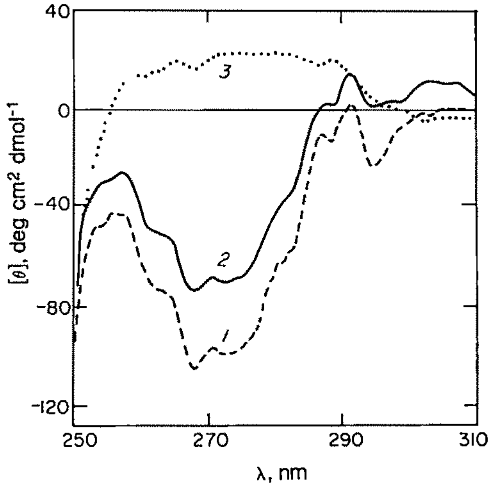

Fig 9 CD spectra of the globular dimer of acetylcholinesterase in the near-ultraviolet region at pH 7.5. Curves: (1) 30 °C; (2) 35 °C; (3) 40 °C. Protein concentration: 0.23 mg/ml in 40 mM sodium pyrophosphate plus 10 mM dodecylheptaoxyethylene ether (pH 7 5).

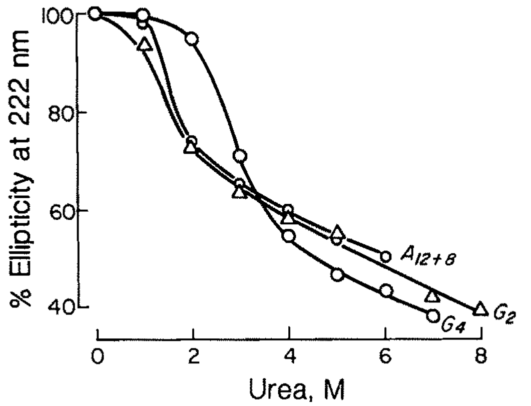

Fig 10. Urea denaturation of acetylcholinesterase in 20 mM sodium phosphate at pH 7.5 and 25°C. The urea solutions of the enzymes (11–18 μg/ml) were incubated at room temperature for about 2 h before measurements.

Urea denaturation

The unfolding of acetylcholinesterase in urea solution was monitored by the spectral change at 222 nm. Fig. 10 shows that all three forms began to unfold even at 1 M urea and the ellipticities at 222 nm reduced sharply up to 3 M urea, followed by a gradual decrease at higher urea concentrations. The initial phase of denaturation was both protein concentration- and time-dependent. For instance, in 1 M urea, $[\theta]_{222}$ (in deg · cm^2/dmol) of the G_4 form at 0.01 mg/ml was −10000 at 10 min and −7900 after 24 h. This dependency of protein concentration can also be shown by enzymatic activity. In 1 M urea the activity of G_4 at 15 μg/ml decreased by 64% after 30 min and 95% after 24 h, but that at 150 μg/ml decreased only 36% and 43%, respectively. At 3 M urea, the ellipticities fell to about 70% of that without urea (Fig. 10), but the enzymatic activity was lost completely regardless of the protein concentration. Attempt to renature the urea-denatured acetylcholinesterase either through dialysis or by dilution was unsuccessful. The CD spectra did not reverse to those of the native acetylcholinesterase and the enzymatic activity remained zero after the removal of urea. SDS-polyacrylamide gel electrophoretic analysis revealed that the protein was highly aggregated in the absence of dithiothreitol, but was reduced to the monomer in the presence of dithiothreitol. A control sample without urea treatment also showed the same degree of aggregation without dithiothreitol, but it retained the enzymatic activity as well as the CD spectra.

Discussion

The catalytic properties, polymorphism and histochemical localization of acetylcholinesterase in tissues of many animal species have been studied extensively (for review, see Ref. 20). The difference in molecular forms apparently determine their cellular localization, and hence their action in cholinergic neurotransmission, but the physiological importance of the requirement for the multiple forms of acetylcholinesterase is not understood. Accumulating evidence suggests that the three major acetylcholinesterase forms found in *Torpedo* [21–23] are not from the same origin; the dimeric acetylcholinesterase is neither the precursor nor the breakdown product of the asymmetric acetylcholinesterase. This evidence is: (1) The globular dimer has a higher content of hydrophobic amino acids than the tailed acetylcholinesterase and they have different peptide maps after trypsin, chymotrypsin and cyanogen bromide fragmentation [8]. (2) The globular dimer and the tailed acetylcholinesterase are antigenically distinct. One line of monoclonal antibody raised against the mixture of the two acetylcholinesterase forms showed a 100-fold greater affinity for the globular dimer than for the tailed acetylcholinesterase [6]. (3) The subunit molecular weights of low-salt-soluble (M_r 76000), detergent-soluble (M_r 69000) and high-salt-soluble acetylcholinesterase (M_r 72000) in *T. marmorata* are different. These isozymes exhibited different susceptibilities toward pronase [5]. (4) The molecular weight of the hydrophobic dimer is independent of the acrylamide concentration in SDS-polyacrylamide gel electrophoresis, but that of the non-reduced dimer from the tailed acetylcholinesterase decreased with increasing acrylamide concentration [8].

In spite of these dissimilarities, our CD studies could not reveal any difference in the secondary structure between G_2 and G_4; the far-ultraviolet spectra are similar in magnitude and the calculated fractions of helix, β-form, and β-turn were the same. Manavalan et al. [15] reported that the CD spectra of 11 S (G_4) and 5.6 S (G_2) acetylcholinesterase were similar to each other, but the analysis of the secondary structure revealed 4% greater antiparallel β-sheets for the 5.6 S enzyme which was outside of their experimental error. However, our experience indicated that variations of 4% between preparations were not uncommon. The collagen-like tail constitutes about 17% (by weight) of the A_{12} molecule, since it consists of twelve M_r 68 000 globular subunits and three 55 000 tails. The CD spectra of the collagen-like tail is similar to that of an unordered form [16]. Thus, the ordered conformation in A_{12} is expected to be smaller than that in G_4. The calculated f_H, f_β, f_t and f_R of A_{12} from those of G_4 were 0.33, 0.29, 0.03 and 0.34, respectively, which were close to the experimental values for A_{12} in Table II.

All current CD analysis of protein conformation are empirical and there is no guarantee that the estimated conformation of an unknown protein will always be correct. At present the estimate of α-helix can be viewed with some confidence, but the estimates of the β-sheets and β-turns still seem to be uncertain. The prediction of the secondary structure from the primary structure is also empirical. Thus, the estimates of α-helix based on CD and those from the sequence methods in Table II must be regarded as remarkably close to each other, even though such agreement can still be fortuitous. Our f_β from CD analysis was close to the predicted value, but that of f_H and f_t were slightly off; the reverse was true for the CD estimates of Manavalan et al. [15]. The CD spectra in the near-ultraviolet region for the three forms of acetylcholinesterase showed some minor differences, but the overall feature of the spectra is the same. This suggests that the microenvironment of the aromatic side-chains of these acetylcholinesterase forms may be slightly different from one another, but the overall tertiary structure is similar.

Further studies revealed that the three forms of acetylcholinesterase have about the same stability against unfolding and inactivation by acid, alkali, high temperature or urea. The pH-ellipticity curve can often reveal differences in the ionizable side groups that are responsible for the stability of proteins, and thermal unfolding of proteins is a sensitive method for detecting isozymes and variations in primary structures of proteins [24,25]. Although there were differences in peptide mapping of the G_2 and G_4 acetylcholinesterase [8], no variations in pH-dependency, thermostability, or urea denaturation pattern of these acetylcholinesterase could be detected. One possibility is that the sequence difference may be in the portion that was not unfolded by the purturbants, or that it may be located at either the C- or the N-terminal segment that did not affect the overall conformation of the enzyme molecule. Futerman et al. [26] found that one or more molecules of phosphatidylinositol was covalently attached to the detergent-soluble acetylcholinesterase of *T. californica*. This lipid moiety may be responsible for anchoring the enzyme on the plasma membrane and can be removed by treatment with phospholipase C or proteinase K. More recently, Rosenberry and coworkers [27–29] found covalently attached fatty acids in the form of glycolipid at the C-terminus of the erythrocyte acetylcholinesterase which can be cleaved by papain digestion. Because of its hydrophobic nature [8], the low-salt-soluble G_2 probably also contains such a hydrophobic patch which may be responsible for differences in antigenicity and peptide maps when compared with the G_4 acetylcholinesterase [6]. This hydrophobic patch probably did not affect the over-all conformation of the acetylcholinesterase because of its size and location. At present CD can only give macroscopic information on the overall conformation of macromolecules. Minor substitutions in the primary structure or variations in the relative orientation of side-chains on the surface of protein molecules may not be detected.

Denaturation studies revealed several important facts about acetylcholinesterase. First, the three forms of acetylcholinesterase completely lost their enzymatic activities at a moderate pH (below 5 or above 10) and a moderate temperature (above 40°C). However, the enzyme retained more than 70% of their secondary structure under the same conditions. Our sequence prediction suggests that the Ser residue in the binding site of acetylcholinesterase is in a β-turn between two β-strands. This β-turn may be extruded on the surface of the molecule and be easily disturbed. The fact that acetylcholinesterase can bind many structurally different ligands and is easily inactivated also supports our contention that the active site may be exposed. The conformational stability as reflected by the retention of the double minimum of the CD spectra at pH 2 and 12 or at 30 and 40°C (Figs. 4 and 7) may well be due to the presence of disulfide bonds in the enzyme [30].

Second, the decrease in the CD magnitude around 295 nm due to Trp residue(s) corresponded well with the loss of the enzymatic activity of the three acetylcholinesterase forms, suggesting that the Trp residue(s) may be close to the active center of the enzyme. The same conclusion was reached by Mooser et al. [31] and Shinitzky et al. [32] from their fluorescence studies. Of the 17 Trp residues in acetylcholinesterase, none is sequentially close to the active Ser residue [7]. Therefore, the tertiary folding of the polypeptide chain must play an important role in the active-center integrity of acetylcholinesterase.

Third, urea unfolded acetylcholinesterase more extensively than either at an extreme pH or at a high temperature. Like guanidine-HCl [33], urea denaturation showed two different stages with increasing urea concentration. In the first stage the unfolding of the acetylcholinesterase molecule was steep (Fig. 10) and was accompanied by a total loss of the enzymatic activity. This unfolding may correspond to that induced by pH or thermal denaturation. In the second stage the unfolding was slower and may involve muti-state intermediates. The unfolded acetylcholinesterase could not be renatured either through dialysis or by dilution of the urea-enzyme mixture. On the other hand, Ahmad [33] reported a complete recovery of both CD and absorption properties, but not the enzymatic activity, of the 11 S acetylcholinesterase after guanidine-HCl denaturation. He also found that the renatured protein was highly aggregated to form high molecular weight species. The facility of acetylcholinesterase to aggregate was attributed to the collagen tail of the asymmetric form or the hydrophobic surface of the globular dimer form. Our SDS-gel electrophoretic study indicated that the G_4 form also aggregated on storage (without affecting the enzymatic activity), but can be dissociated by a reducing agent such as dithiothreitol. A sulfhydryl group located near the active center of the enzyme [30] may be very reactive and partially responsible for the observed aggregation. However, the irreversible inactivation of acetylcholinesterase after exposure to urea was not caused by aggregation because aggregated acetylcholinesterase did not lose its enzymatic activity. More likely, the inactivation was due to partial unfolding near the active site as shown by the CD spectra of the renatured acetylcholinesterase.

In conclusion, all three acetylcholinesterases have a similar conformation and behave similarly toward pH, thermal and urea denaturation. It is catalytically unstable, but conformationally stable.

Acknowledgments

We thank Professor P. Taylor for showing us the purification method of acetylcholinesterase and Ms. Mary Hirsch for her excellent technical assistance. This work was supported in part by the US Army Medical Research and Development Command, Contract No. DAMD17-85-5048 and by the US Public Health Service Grant No. GM-10880-26. The views, opinions and finding contained in this report are those of the authors and should not be construed as an official Department of the Army (U.S.A.) position, policy or decision unless so designated by other documentation.

References

1 Rosenberry, T.L. and Richardson, J.M (1977) Biochemistry 16, 3550–3558

2 Anglister, L. and Silman, I. (1978) J Mol. Biol 125, 293–311

3 Lee, S L and Taylor, P (1982) J Biol Chem. 257, 12292–12301

4 Lee, S L., Heinemann, S. and Taylor, P (1982) J. Biol Chem 257, 12283–12291

5 Witzemann, V. and Boustead, C. (1983) EMBO J. 2, 873–878

6 Doctor, B.P., Camp, S., Gentry, M.K., Taylor, S S and Taylor, P. (1983) Proc Natl Acad Aci. USA 80, 5767–5771

7 Schumacher, M , Camp, S., Maulet, Y , Newton, M , MacPhee-Quigley, K., Taylor, S S , Friedman, T and Taylor, P (1986) Nature 319, 407–409

8 Lee, S.L., Camp, S.J. and Taylor, P (1982) J. Biol Chem 257, 12302–12309

9 Taylor, P , Jones, J.W. and Jacobs, N M (1974) Mol Pharmacol. 10, 78–92

10 Ellman, G L., Courtney, K.D., Andres, V , Jr and Featherstone, R M. (1961) Biochem. Pharmacol 7, 88–95

11 Craven, G.R , Steers, E., Jr. and Anfinsen, C.B. (1965) J. Biol. Chem 240, 2468–2477

12 Beers, R F., Jr and Sizer, I.W. (1952) J. Biol Chem. 195, 133–140

13 Chang, C.T., Wu, C.-S C. and Yang, J.T. (1978) Anal. Biochem 91, 13–31
14 Miller, G.L. and Golden, R.H (1950) Arch. Biochem 29, 420–423
15 Manavalan, P , Taylor, P. and Johnson, W C , Jr (1985) Biochim Biophys. Acta 829, 365–370
16 Mays, C. and Rosenberry, T.L. (1981) Biochemistry 20, 2810–2817
17 Chou, P. and Fasman, G.D. (1974) Biochemistry 13, 222–245
18 Garnier, J., Osgutherpe, D.J. and Robson, B (1978) J. Mol. Biol 120, 97–120
19 Hofer, P , Fringele, U.P. and Hopff, W.H (1984) Biochemistry 23, 2730–2734
20 Massoulie, J. and Bon, S. (1982) Annu Rev. Neurosci 5. 57–106
21 Witzemann, V (1980) Neurosci Lett 20, 277–282
22 Bon, S. and Massoulie, J. (1980) Proc. Natl. Acad Sci. USA 77, 4464–4468
23 Viratelle, O.M and Bernhard, S.A. (1980) Biochemistry 19, 4999–5007
24 Chang, K., Williamson, J.R. and Zarkowsky, H S. (1979) J Clin Invest. 64, 326–328
25 Paigen, K. (1971) in Enzyme Synthesis and Degradation in Mammalian Systems (Recheigl, M., Jr., ed.), pp. 1–46, University Park Press, Baltimore
26 Futerman, A.M., Fionini, R.M., Roth, E., Low, M.G. and Silman, I (1985) Biochem. J. 226, 369–377
27 Kim, B.H. and Rosenberry, T.L. (1985) Biochemistry 24, 3586–3592
28 Roberts, W.L. and Rosenberry, T.L. (1985) Biochem Biophys. Res. Commun. 133, 621–627
29 Roberts, W.L. and Rosenberry, T.L (1986) Fed. Proc. 45, 1816
30 MacPhee-Quigley, K., Vedvick, T., Taylor, P and Taylor, S. (1986) Fed. Proc. 45, 1848
31 Mooser, G., Schulman, H. and Sigman, D.S (1972) Biochemistry 11, 1595–1602
32 Shinitzky, M., Dudai, Y and Silman, I. (1973) FEBS Lett 30, 125–128
33 Ahmad, F (1981) Can. J. Biochem 59, 551–555
34 Wu, C.-S.C., Hirsch, M and Yang, J.T (1986) Fed. Proc 45, 1545
35 Gan, L , Wu, C -S.C and Yang, J.T. (1986) Fed Proc. 45, 1545

Biochimica et Biophysica Acta 911 (1987) 37–44
Elsevier

BBA 32596

Spectroscopic properties of spinach catalase

Masakazu Hirasawa, Kevin A. Gray, Robert W. Shaw and David B. Knaff

Department of Chemistry and Biochemistry, Texas Tech University, Lubbock, TX 79409 (U.S.A.)

(Received 15 May 1986)

Key words: Catalase; Spectral property; Protoheme; Novel heme; (Spinach)

Spinach catalase (hydrogen-peroxide: hydrogen-peroxide oxidoreductase, EC 1.11.1.6) has been purified to homogeneity. The purified enzyme has a specific activity of 25 000 units per mg protein. The presence of 2-mercaptoethanol and phenylmethylsulfonyl fluoride (PMSF) were required for high yields of the enzyme. The molecular weight of the enzyme was estimated to be 125 000 by gel filtration. Subunit analysis by polyacrylamide gel electrophoresis in the presence of sodium dodecyl sulfate revealed a single peptide with M_r 55 000. The enzyme, which exhibits optical absorbance maxima at 279, 403, 542, 592 and 723 nm and shoulders at 290, 500 and 630 nm, contains 2 mol iron per mol protein. One of the two irons can be attributed to protoheme, while the other iron appears to be present in a novel heme. The oxidized catalase exhibited two sets of high-spin, ferriheme EPR signals.

Introduction

Many hemoproteins are red, but recently some unusual green hemoproteins have been isolated from a variety of sources [1–3]. These include peroxidase found in bovine spleen [3], which has an optical spectrum similar to that of myeloperoxidase of polymorphonuclear leukocytes and a catalase found in *Neurospora crassa* [1]. Catalases (hydrogen-peroxide: hydrogen peroxide oxidoreductase, EC 1.11.1.6), catalyzing the decomposition of H_2O_2 to H_2O and O_2, have been purified and characterized from plants, bacteria and from mammalian liver and blood. The molecular weights of these catalases, usually composed of four identical subunits, are all close to 240 000. The erythrocyte enzyme has been shown to contain 4 mol of protoheme per mole of enzyme as its sole prosthetic groups [4]. Preparations of the liver enzyme contain three protohemes and one verdoheme [5], although it appears likely that the verdoheme is a degradation product [6]. The *N. crassa* catalase has a ferric dihydroporphyrin prosthetic group [7]. While there have been several reports on the existence of higher plant catalases [8–13], probably located in the chloroplasts [8], few details are available concerning the composition or ligand-binding properties of these plant enzymes. We have developed a procedure for isolating a previously undetected, green catalase from spinach leaves and obtained the enzyme in pure form. This spinach catalase has been characterized in terms of its subunit and prosthetic group content and compared with other green hemoproteins.

Materials and Methods

Fresh leaves of spinach (*Spinacia oleracea*), grown during the 1985 growing season, were used as the starting material for the enzyme purifica-

---

Abbreviation: PMSF, phenylmethylsulfonyl fluoride.

Correspondence: Dr. D.B. Knaff, Department of Chemistry and Biochemistry, Texas Tech University, Lubbock, TX 79409, U.S.A.

0167-4838/87/$03.50 © 1987 Elsevier Science Publishers B.V. (Biomedical Division)

tion. All chemicals used were of the highest purity commercially available. DEAE-cellulose (DE-52) was obtained from Whatman Ltd., Ultrogel AcA 34 was obtained from LKB Produkter AB, PMSF from Sigma Chemical Co. and SDS-polyacrylamide gel electrophoresis molecular weight standards were obtained from Bio-Rad. Spinach ferredoxin was prepared by the method of Tagawa and Arnon [14] ($A_{422}:A_{277}=0.45$) and stored in 30 mM Tris-HCl buffer (pH 8.0) at liquid N_2 temperature until used.

Catalase activity was assayed at 20°C, essentially as described by Beer and Sizer [15]. The reaction mixture contained, in a total volume of 1.5 ml, 60 mM H_2O_2 and 50 mM potassium phosphate buffer (pH 6.0). The reaction was initiated by the addition of enzyme and the change in absorbance at 240 nm monitored with an Aminco DW-2a Spectrophotometer. One unit of activity is defined as 1 μmol of H_2O_2 decomposed per min. Protein concentration was determined by the method of Bradford [16], using bovine serum albumin as a standard. Protoheme was determined spectrophotometrically by the method of Takahashi and Morita [17]. The iron content of the enzyme was determined with *o*-phenanthroline according to Massey [18], except that 1 M HCl in acetone replaced trichloroacetic acid for the iron extraction. Ferric ammonium sulfate and spinach ferredoxin were used as standards.

Absorbance spectra were measured at ambient temperature with a Perkin-Elmer Lambda 5 Spectrophotometer. Electron paramagnetic resonance spectra were recorded with a Varian E-109 spectrometer interfaced with a Varian/Hewlett-Packard E-935 Data Acquisition system. Temperature was maintained using a modified Air Products Model LTD-3-110 flexible helium transfer line and a temperature controller of our own design. Sample temperatures were measured by use of a chromel vs. gold + 0.07 atom% iron thermocouple positioned just below the sample. Microwave frequency and magnetic field strength were measured using a EIP Microwave, Inc. Model 331 Autohet microwave frequency counter, and Varian E-500 NMR Gaussmeter, respectively.

All steps in the purification procedure were carried out at 0–4°C.

Step I. Preparation of the acetone powder. 500 g of spinach leaves were homogenized for 2 min in a Waring Blendor in 500 ml of 50 mM potassium phosphate buffer (pH 7.5)/12.5 mM 2-mercaptoethanol/200 mM NaCl/1 mM EDTA/1 mM PMSF. The homogenate was filtered through cheesecloth. To this crude homogenate was added cold acetone (−20°C), and the protein precipitating between 35 and 75% acetone (v/v) was collected by centrifugation at 10000 × *g* for 5 min. The precipitate from 50 kg of spinach was suspended in 1000 ml of 50 mM potassium phosphate buffer (pH 7.5)/200 mM NaCl/12.5 mM 2-mercaptoethanol/1 mM PMSF. The sample was dialyzed in Spectra/Por 1 dialysis tubing for 48 h against 30 liters of the same buffer with six changes of dialysis buffer. After dialysis, insoluble material was removed by centrifugation.

Step II. DEAE-cellulose column chromatography. The sample was redialyzed against 50 mM potassium phosphate buffer (pH 7.5)/50 mM NaCl/12.5 mM 2-mercaptoethanol and applied to a DEAE-cellulose column (8 × 90 cm) previously equilibrated with the same buffer. The green fractions were collected and concentrated by precipitation with 70% saturated ammonium sulfate. The precipitated catalase was dissolved in a minimum volume of 50 mM potassium phosphate buffer (pH 7.5)/200 mM NaCl/12.5 mM 2-mercaptoethanol and dialyzed against the same buffer.

Step III. Ultrogel AcA chromatography. 35 ml aliquots of the dialyzed enzyme were applied to an Ultrogel AcA 34 column (4 × 90 cm) that had been previously equilibrated with the dialyzing buffer. Those fractions exhibiting high specific activity in the catalase assay were combined, concentrated by ammonium sulfate precipitation as above and dialyzed against 50 mM Tris-HCl (pH 7.5)/12.5 mM 2-mercaptoethanol.

Step IV. Additional chromatography. The dialyzed solution was passed through a DEAE-cellulose column (4 × 70 cm) that had been previously equilibrated with dialyzing buffer. Elution was performed and fractions with high specific catalase activity concentrated as in step II. The sample was dialyzed, applied to an Ultrogel AcA 34 column (2 × 100 cm) equilibrated with the dialyzing buffer and chromatography conducted as in step III. The high specific catalase activity fractions were combined and concentrated by membrane filtration with an Amicon PM-10 membrane (molecular weight exclusion limit: 10000).

Results

Typical results from a purification using 50 kg of spinach leaves are summarized in Table I. The final catalase preparation obtained with the present purification protocol showed a specific activity approx. 35-times higher than that reported by Gregory [10] for spinach catalase. The overall yield of pure enzyme was 45%. High ionic strength and the presence of 2-mercaptoethanol and PMSF were necessary in order to obtain such high yields. For example, if PMSF was omitted from the initial extraction medium, an overall yield of only 1% was obtained. No additional protection was obtained by including PMSF in the subsequent chromatography steps. Omission of 2-mercaptoethanol from all buffers used during the extraction and purification steps had no effect on the absorbance spectrum of the purified enzyme but reduced the overall yield approx. 5-fold. Eliminating NaCl from the extraction buffer had no effect on the absorbance spectrum or catalytic activity of the purified catalase but also significantly reduced its yield. The purified enzyme showed a single protein band upon electrophoresis on a 7.5% polyacrylamide gel at pH 8.3 using the method of Davis [19]. The pH optimum of the purified enzyme's catalase activity was 6.0, with little activity detected above pH 9.0 or below pH 4.5. Fig. 1 shows the effect of varying $[H_2O_2]$ concentration on the rate of the catalase-catalyzed reaction. This data did not give a good fit to the Michaelis-Menten equation and a Hill plot [20] showed a Hill coefficient of 2.3 (data not shown), indicating the possibility of positive cooperativity. The enzyme was inhibited by cyanide (complete inhibition at 1.7 μM KCN), azide (complete inhibition at 33 μM NaN_3), formate (93% inhibition at 6.7 mM NaOOCH) and fluoride (83% inhibition at 33 mM NaF).

The molecular weight of the spinach catalase under non-denaturing conditions was determined to be 125000 by gel-filtration on an Ultrogel AcA 34 column, using a modification of the method of Andrews [21]. The enzyme exhibited a single protein band, after SDS-polyacrylamide gel electrophoresis and staining with Coomassie brilliant blue, corresponding to a molecular weight [22] of 55000. As the molecular weight of the native enzyme appears to be near 125000, it is likely that the enzyme consists of two subunits that are either identical or of very similar molecular weight. The molecular weight value determined for the native enzyme in this study is considerably lower than the $M_r = 300000$ value reported for spinach catalase by Gregory [10]. The results of chemical analyses of three different catalase preparations showed the presence of 2 mol (2.04 ± 0.12) of total iron per mo of enzyme. (Extraction of iron from spinach catalase proved to be quite difficult. Even upon addition of 20% (w/v) trichloroacetic acid, very little iron was released (0.20 ± 0.03 mol per enzyme molecule). However, as described in materials and Methods, 1 M HCl in acetone was able to completely extract the iron.) Analysis for metals other than Fe was not performed. Pyridine hemochromogen analysis indicated the presence of 1 mol (0.96 ± 0.06) of protoheme per mol of catalase.

The absorbance spectrum of the native enzyme in the oxidized state is shown in Fig. 2. Maxima

TABLE I

SUMMARY OF THE PURIFICATION OF CATALASE FROM 50 kg OF SPINACH LEAVES

Fractions	Total protein (mg)	Volume (ml)	Total activity (units × 10^{-3})	Specific activity (units/mg protein)	$A_{403}:A_{279}$	Yield (%)
Acetone (35–75%)	30446	1725	16914	556	–	100
1st DEAE-cellulose	11160	360	15136	1356	–	90
1st Ultrogel AcA 34	1285	50	13531	10527	0 4	80
2nd DEAE-cellulose	696	20	10994	15790	0 6	65
2nd Ultrogel AcA 34	304	5	7611	25004	0.95	45

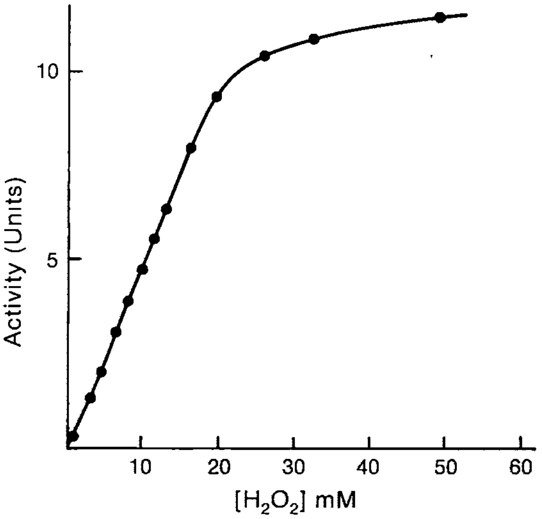

Fig 1 Effect of H_2O_2 concentration on spinach catalase. The enzyme assay was conducted as described in the Materials and methods section except that [H_2O_2] was varied as indicated on the abscissa

were found at 279, 403, 542, 592 and 723 nm with shoulders at 290, 500 and 630 nm. The ratios of the absorbance at 403 to 279 nm and 592 to 403 nm were 0.95 and 0.25, respectively. This spectrum differs from those reported by Galston et al. [9] and Gregory [10] for spinach catalase, Yamaguchi and Nishiyama [13] for pumpkin catalase or Esaka and Asahi [11] for sweet potato catalase, but is very similar to that reported by Jacob and Orme-Johnson [1] for *Neurospora crassa* catalase. Prolonged exposure of the enzyme to 1 mM H_2O_2 had no effect on the visible absorbance spectrum, iron and protoheme content or specific activity of the enzyme. Treatment of the native enzyme with sodium dihtionite did not cause any spectral changes, a result which is characteristic of other catalases [1,23]. It should be noted (see below) that sodium dithionite is apparently able to reduce the enzyme in very basic solution (pH ≈ 13.5).

From the spectral properties of the enzyme and the chemical composition data, it appeared likely that the enzyme contained a second heme species in addition to protoheme. Evidence supporting this possibility was obtained during pyridine hemochromogen analysis of the enzyme for protoheme. As can be seen in Fig. 3, addition of dithionite to spinach catalase dissolved in pyridine/NaOH resulted in the appearance of absorbance bands at 608 and 658 nm in addition to that at 557 nm due to protoheme [17]. In an attempt to characterize their chemical nature further, the heme prosthetic groups of spinach catalase were extracted by treatment of enzyme with 9 vol. of acetone containing 0.1 M HCl at 0°C. After centrifugation to remove denatured protein, the supernatant was concentrated under a stream of N_2 in the dark. On addition of pyridine/NaOH to the extract and reduction with sodium dithionite, absorbance maxima to 420, 480, 524, 557

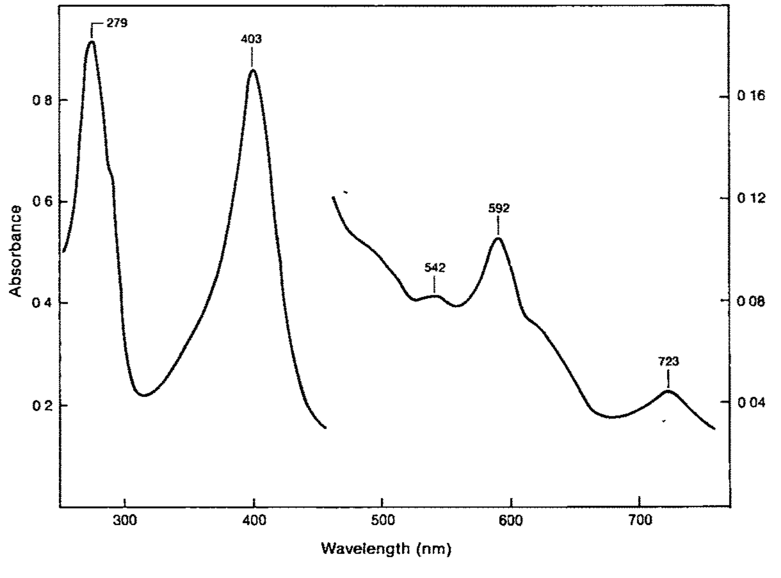

Fig. 2. Absorbance spectrum of spinach catalase The sample cuvette contained 10 μM enzyme in 50 mM Tris-HCl buffer (pH 7.5) and the reference cuvette contained only buffer.

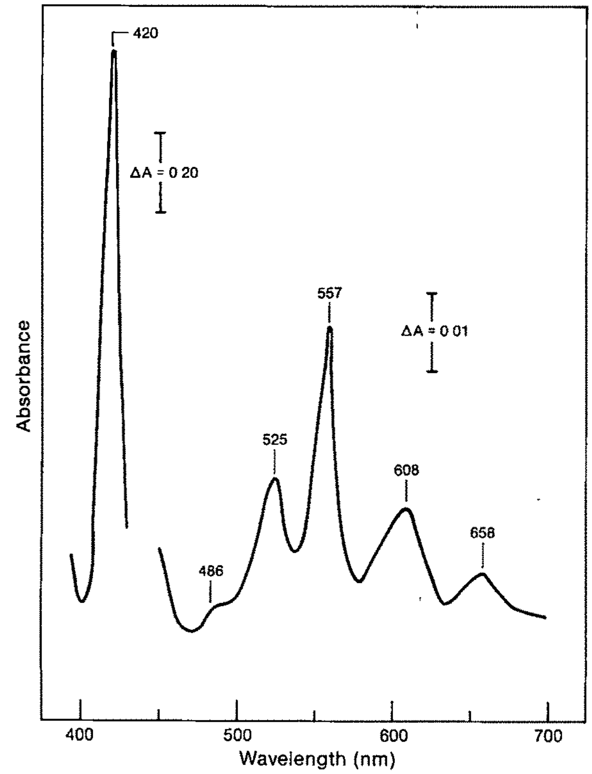

Fig 3. Difference spectrum of the pyridine hemochromogen derivative of spinach catalase. The sample and reference cuvettes contained 10 μM enzyme in 25% (v/v) pyridine/0.25 M NaOH. After an absorbance baseline was recorded, a few crystals of sodium dithionite were added to the sample cuvette and the difference spectrum measured.

and 612 nm with a shoulder at 650 nm were observed (data not shown). If protoheme were the only component present, only maxima at 420, 524 and 557 nm would be expected [17]. No contributions from heme *a*, heme *d* or siroheme were detected. The possible presence of a second heme, chemically distinct from protoheme, in spinach catalase was also supported by the spectral characteristics of the enzyme-CO adduct in alkaline solution. The absorbance difference spectrum of the enzyme-CO complex in 0.25 M NaOH solution with sodium dithionite present to reduce the enzyme is shown in Fig. 4. The difference spectrum exhibits absorbance maxima at 426, 572 and 624 nm and minima at 404, 504, 596 and 650 nm. The maximum at 572 nm can be attributed to the CO-adduct of protoheme [24], while the maximum

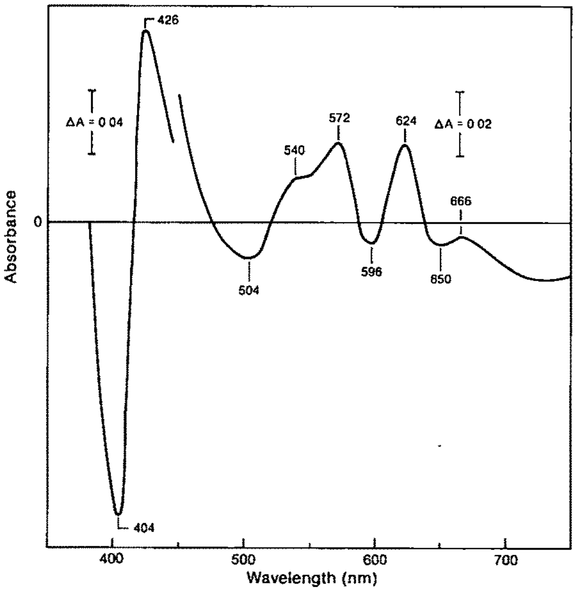

Fig. 4. CO-difference spectrum of spinach catalase in alkaline solution. A 10 μM enzyme solution in 0.25 M NaOH in a Thunberg cuvette was reduced with sodium dithionite and exposed to CO for 15 min. The difference spectrum was recorded using a reference cuvette containing an identical reduced enzyme sample that had not been exposed to CO.

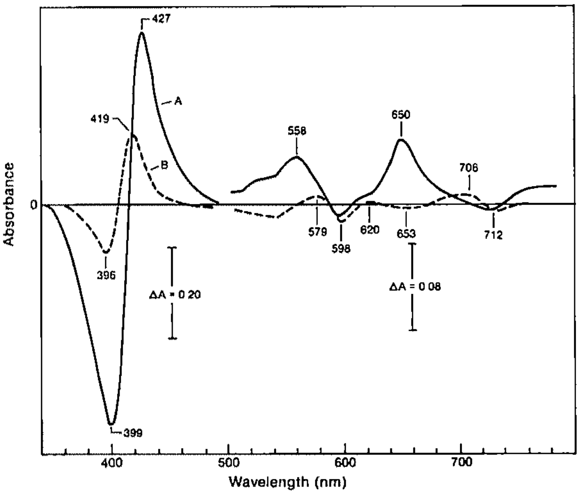

Fig. 5. Difference spectra of spinach catalase complexes with cyanide and azide. The sample cuvette contained 10 μM spinach catalase in 50 mM Tris-HCl buffer (pH 7.5) plus either 0.1 mM KCN (A) or 0.1 mM NaN_3 (B). The reference cuvette contained an identical enzyme solution but neither KCN nor NaN_3. In spectrum A, the absorbance scale was altered for wavelengths above 500 nm In spectrum B, the same absorbance scale was used throughout.

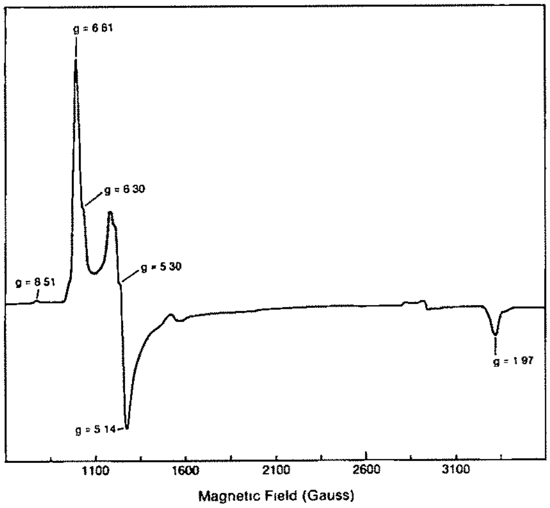

Fig 6. EPR spectrum of spinach catalase. The sample contained 1 mM catalase in 50 mM Tris-HCl (pH 7.5) EPR conditions: Microwave frequency, 9.152 GHz; Modulation frequency, 100 kHz; Modulation amplitude, 8 G; Temperature, 13 K

at 624 nm is similar to that reported for verdoheme [5,24].

Fig. 5A and B show the difference spectra resulting from formation of complexes between the oxidized enzyme and cyanide or azide, respectively. The addition of cyanide to the enzyme resulted in a shift in the Soret absorbance maximum from 403 to 421 nm, the disappearance of the peaks at 592 and 723 nm and the appearance of peaks at 572 and 665 nm. These spectral changes are similar to those reported for *N. crassa* catalase [7]. Addition of azide shifted the Soret band maximum from 403 to 406 nm, caused shifts in other maxima from 592 to 587 nm and from 723 to 710 nm and resulted in the disappearance of the peak at 540 nm.

EPR analysis of the oxidized spinach catalase supports the presence of two different heme groups in the enzyme. The data (Fig. 6), obtained at pH 7.5, indicate the presence of two overlapping sets of rhombic, high-spin ferriheme signals. Spinach catalase also showed weak low-spin heme signals with apparent g values of 2.33, 2.24 and 1.78. In addition, a minor component at $g = 8.51$, similar to that previously reported for other catalases [25], was detected. Addition of sodium dithionite caused no changes in the EPR spectrum of the enzyme at pH 7.5 (data not shown), consistent with optical data indicating that dithionite does not reduce the enzyme at this pH.

Discussion

Although catalase has been known to be present in spinach leaves for some time [9,10] and has been prepared in crystalline form, relatively few details were available concerning its ligand-binding properties or the nature of its prosthetic groups. We have therefore undertaken to establish the molecular properties of spinach catalase. To accomplish this purpose, it was necessary to develop an improved purification protocol for the enzyme. As the inclusion of PMSF in the extraction medium proved essential for achieving high yields of spinach catalase, it would appear that the enzyme is particularly susceptible to attack by proteinase(s). PMSF has also been reported to protect the *N. crassa* catalase against proteolysis [1]. In the present study, it was also shown that the presence of 2-mercaptoethanol is essential for high yields of spinach catalase. The molecular weight (125 000) and the optical absorbance spectrum of the spinach catalase described in this report are quire different from those reported [9,10] for the tetrameric ($M_r \approx 300\,000$) catalase that contains protoheme as its sole heme prosthetic group. It may be possible that spinach leaves contain more than one catalase. In fact, during some preparations we have detected a catalase with spectral properties similar to those previously described in addition to the green catalase. The green catalase described in this work may have escaped detection in the earlier work, in which neither proteinase inhibitors nor 2-mercaptoethanol were used, because it was lost to proteolysis during the isolation and purification [9,10].

The spinach catalase described in this work, although having a considerably lower molecular weight than that reported for other catalases, does resemble other catalases from mammalian, plant and bacterial sources in subunit molecular weight and the presence of protoheme as a prosthetic group [1,2,4,10–13,22,23,26–31]. However, our spectral data and pyridine hemochromogen analyses clearly indicate the presence, in spinach catalase, of an additional iron-containing prosthetic group that differs from protoheme. The observation of two sets of high-spin ferriheme signals in the EPR spectrum of the oxidized enzyme (Fig. 6) and the Hill coefficient of 2.3 calculated from kinetic data, while not proving the existence of two chemically different heme groups in the enzyme, are consistent with the presence of two heme groups.

Some spectral properties of spinach catalase suggested that the second heme might be verdoheme or a related compound. Lemberg and Legge [5] assigned the absorbance band at 630 nm in the spectrum of the CO complex of horse liver catalase in 0.25 M NaOH to verdoheme and the spectrum of the spinach catalase-CO complex in strongly alkaline solution contains a similar feature (Fig. 4). However, Lemberg [24] has shown that the pyridine hemochromogen of verdoheme has an absorbance maximum at 662 nm, while that of spinach catalase is at 608 nm (Fig. 3). It is difficult to reconcile this discrepancy with the presence of verdoheme in spinach catalase. It should also be pointed out that the spinach catalase characterized in this work shows considerable spectral resemblance to the *N. crassa* catalase, an enzyme that contains an iron-dihydroporphyrin (iron-chlorin) prosthetic group [1,7]. The pyridine hemochromogen of the *N. crassa* enzyme [1] exhibits an absorbance maximum at 602 nm, similar to that at 608 nm observed with the spinach enzyme (Fig. 3). However, no spectral feature at 658 nm, observed with spinach catalase (Fig. 3), was seen with the pyridine hemochromogen of *N. crassa* enzyme.

It has been reported that the verdoheme found in liver catalase is an artifact arising from the oxidation of the enzyme's normal protoheme prosthetic group [6]. A similar situation may exist with respect to the novel heme present in spinach catalase. This possibility merits particular attention because of the use of 2-mercaptoethanol in our purification protocol, since verdoheme can result from the coupled oxidation of protoheme and an added reductant by O_2 [6]. However, we have found that catalase prepared in the absence of 2-mercapto-ethanol has the same absorbance spectrum shown in Fig. 3. It has also been proposed [6] that the verdoheme of hepatic catalase may arise from the oxidation of protoheme by H_2O_2. However, the constant stoichiometry of 1.0 mol of novel heme per mol of enzyme observed in three different enzyme preparations and the fact that prolonged exposure of the catalase to H_2O_2 altered neither the absorbance spectrum nor the protoheme content of the enzyme argue against the novel heme's arising from the degradation of protoheme by H_2O_2. While it is certainly possible that the novel heme may arise from an extremely rapid, undetected degradation process, it is also possible that the spinach catalase characterized in this work may contain, as a natural constituent, a novel heme in addition to protoheme. Further chemical characterization studies of the second heme are clearly required before its identity can be definitively established. Such studies, and studies on the relationship between this catalase and the previously characterized spinach catalase, are currently underway in our laboratory.

Acknowledgements

We are grateful to Prof. Shigeo Horie of the Department of Biochemistry, School of Medicine, Kitasato University and Prof. Graham Palmer of the Department of Biochemistry, Rice University for valuable discussions. We are also grateful to Mr. J. Milton Boyer and R. Max Wynn for assistance with the enzyme purification. This work was supported by grants (to D.B.K.) from the U.S. Department of Agriculture (85-CRCR-1-1574) and the National Science Foundation (PCM-8408564 and (to R.W.S.) PCM-8119188).

References

1 Jacob, G.S and Orme-Johnson, W.H (1979) Biochemistry 18, 2967–2975

2 DeFilippi, L J. and Hultquist, D E. (1978) J. Biol Chem. 253, 2946–2953

3 Davis, J C and Averill, B A. (1981) J. Biol. Chem. 256, 5992–5996

4 Schonbaum, G R and Chance, B. (1976) in The Enzymes (Boyer, P D., ed.), pp. 363–408, Academic Press, New York

5 Lemberg, R. and Legge, J W. (1943) Biochem. J 37, 117–127

6 O'Carra, P (1975) in Porphyrins and Metalloporphyrins (Smith, K.M , ed), pp 123–153, Elsevier Scientific Publishing Co , Amsterdam

7 Jacob, G.S and Orme-Johnson, W H. (1979) Biochemistry 18, 2975–2980

8 Neish, A C. (1939) Biochem. J. 33, 330–337

9 Galston, A.W., Bonnichsen, R.K and Arnon, D I. (1951) Acta Chem. Scand. 5, 781–790

10 Gregory, R.P.F. (1968) Biochim. Biophys Acta 159, 429–439
11 Esaka, M. and Asahi, T. (1982) Plant Cell Physiol. 23, 315–322
12 Lamb, J E., Riezman, H. and Becker, W M. (1978) Plant Physiol. 62, 754–760
13 Yamaguchi, J. and Nishiyama, M (1984) Physiology 74, 261–267
14 Tagawa, K. and Arnon, D I. (1962) Nature 195, 537–543
15 Beer, R.F., Jr. and Sizer, I.W (1952) J. Biol. Chem 195, 133–140
16 Bradford, M.M. (1976) Anal Biochem. 72, 248–254
17 Takahashi, S. and Morita, S. (1981) J. Biochem. 89, 1513–1519
18 Massey, V. (1957) J. Biol. Chem. 229, 763–770.
19 Davis, B.J. (1964) Ann. NY Acad Sci. 121, 404–429
20 Hammes, G.G. (1982) Enzyme Catalysis and Regulation, pp. 165–166, Academic Press, New York
21 Andrews, P (1965) Biochem. J. 96, 595–606
22 Weber, K. and Osborn, M (1969) J. Biol. Chem 244, 4406–4412
23 Deisseroth, A. and Dounce, A.L (1970) Physiol. Rev. 50, 319–379
24 Lemberg, R. (1935) Biochem. J 29, 1322–1336
25 Blumberg, W E and Peisach, J (1973) in Oxidases and Related Redox Systems (King, T.E, Mason, H.S. and Morrison, M., eds.), pp. 299–310, University Park Press, Baltimore
26 Williams-Smith, D.L. and Patel, K. (1975) Biochim. Biophys. Acta 405, 243–252.
27 Palcic, M.M. and Dunford, H.B. (1980) J. Biol. Chem. 255, 6128–6132
28 Aebi, H., Wyss, S.R., Scherz, B. and Skvaril, F. (1974) Eur J. Biochem 48, 137–147
29 Nicholls, P. and Schonbaum, G.R. (1963) in The Enzymes (Boyer, P D., Lardy, H. and Myrbäck, K., eds.), Vol 8, pp. 147–225, Academic Press, New York
30 Keilin, D and Hartree, E.F. (1937) Proc. R. Soc. Ser. B 121, 173–191
31 Kajiyoshi, M and Anan, F K (1977) J. Biochem. 81, 1319–1325

Biochimica et Biophysica Acta 911 (1987) 45–52
Elsevier

BBA 32690

Functional differentiation of amphiphilic helices of the apolipoproteins by hydrophobic moment analysis

Hans De Loof [a], Maryvonne Rosseneu [a], Robert Brasseur [b]
and Jean-Marie Ruysschaert [b]

[a] Department of Clinical Biochemistry, A.Z. St-Jan, 8000 Brugge (Belgium)
and [b] Laboratory of Macromolecules at Interfaces, Free University Brussels, 1050 Brussels (Belgium)

(Received 4 August 1986)

Key words: Amphiphilic helix; Apolipoprotein, Hydrophobic moment

The amphiphilic character of different plasma apolipoproteins was investigated by a combination of established hydrophobicity analysis methods. These methods proved to be powerful in the detection of amphiphilic phospholipid-binding domains. Within this class of lipid-binding domains, lecithin–cholesterol acyltransferase activating and non-activating helices could be differentiated by calculating hydrophobic moments at different angles. We conclude that the hydrophobic characteristics of the different helices determined the mode of lipid binding and the substrate properties of these phospholipid-protein complexes for the lecithin–cholesterol acyltransferase reaction.

Introduction

Amphiphilic segments have been detected in the secondary structure of many proteins [1] and this feature seems to be clearly present in the plasma apolipoproteins [2]. These soluble plasma proteins, most of which have been sequenced, have several functions such as transport of lipids in the form of lipoproteins, the activation of lipolytic enzymes and the interaction with cellular receptors (for reviews, see Refs. 3 and 4).

The amphiphilicity of a protein segment can be expressed in terms of its hydrophobic moment as proposed by Eisenberg and co-workers [5–7]. This parameter can yield information about the protein secondary structure or can be used to classify helices into several groups such as membrane-spanning, surface-seeking and globular helices [5]. We have recently applied this type of analysis to predict recepetor-binding domains in the apolipoprotein E protein and their complementary domains of the LDL apolipoprotein (B-E) receptor [8].

Each of the plasma apolipoproteins contains several amphiphilic helices, to which lipid-binding and other physiological functions, such as enzyme activation, have been attributed (for reviews see Refs. 4 and 9). There is, however, no theoretical method available to distinguish between the different helical segments in apolipoproteins or to assign specific functions to some of them. The purpose of this work was to calculate the hydrophobic moment of several protein segments in apolipoproteins and to propose a differentiation between such helical segments, in relationship to their activation properties for the enzyme lecithin–cholesterol acyltransferase (phosphatidylcholine:sterol *O*-acyltransferase, EC 2.3.1.43).

The validity of this theoretical approach will be established through a comparison of the predicted

---

Correspondence: Dr. H. De Loof, Department of Clinical Biochemistry, A.Z. St-Jan, 8000 Brugge, Belgium.

0167-4838/87/$03.50 © 1987 Elsevier Science Publishers B.V. (Biomedical Division)

domains with those identified experimentally using either native apolipoproteins, apolipoprotein fragments, or synthetic model peptides.

During the preparation of this manuscript a similar methodology was used by Von Heijne [10] for the characterization of structural features of mitochondrial targeting sequences and of the lipid binding events during the membrane translocation of these sequences.

Methods

The hydrophobic moment of a protein segment was calculated according to the procedure of Eisenberg et al. [5] using the following equation (Eqn. 1).

$$\mu_{\mathrm{H}}=\left\{\left(\sum_{i}^{i+n-1} H_i \sin(\delta_i)\right)^2+\left(\sum_{i}^{i+n-1} H_i \cos(\delta_i)\right)^2\right\}^{1/2} \qquad (1)$$

where μ_{H} is the hydrophobic moment calculated at an angle δ, H_i is the hydrophobicity of residue i and n is the total segment-length used in the calculations. As the hydrophobic moment is a function of the periodicity in the protein structure, this parameter was calculated assuming different values for the angle δ at which the side chains emerge from the backbone, when the periodic segment is viewed down its axis. By varying δ, the secondary structure of the segment in question can be thoroughly investigated. This angle can assume any value from 0°, for a helix with an infinite repeat, to 180° for a straight segment of beta-sheet structure. For an alpha helix this angle is 100°, while for an average strand of beta structure it is expected to be in the range 160° to 180°, not exactly 180° because of the tendency of this kind of structure to twist [11]. This can be visualized in a plot of the hydrophobic moment of the periodic segment as a function of the angle used for the calculations [4].

An additional method was proposed by Finer-Moore and Stroud [12], in which hydrophobic moments were calculated, at all angles, for a window moving through the amino acid sequence. A slightly modified version of this method was programmed using Eqn. 1. These results were plotted as a function of the midpoint of the segment used in the calculation. Moreover we developed an additional procedure consisting in the averaging of the calculations made on the moving window. The average of the hydrophobic moments of the consecutive segments was plotted as a function of the angle used for the calculation of the hydrophobic moment.

Most hydrophobicity analysis calculations are carried out using an arbitrary segment length [5,13,14]. We selected the segment length by calculating the values of the following equation (Eqn. 2), a clear indicator of the autocorrelation and repetitivity of the sequences.

$$A=\frac{\displaystyle\sum_{i=1}^{i=m-n+1}\left|\frac{\displaystyle\sum_{i}^{i+n-1} H_i}{n}-\frac{\displaystyle\sum_{i+1}^{i+n} H_i}{n}\right|}{m-n} \qquad (2)$$

H_i is the hydrophobicity of residue i, n is the segment length and m is the total sequence length. These data were compared to those obtained from 100 random permutations of the same sequence in order to calculate an S.D. factor [15]. This value corresponds to the number of standard deviations from the actual value to the mean of the random permutations.

The frequently used normalized 'consensus' hydrophobicity scale, developed by Eisenberg [6], was used in all calculations. Therefore hydrophobicity values are expressed in arbitrary units, and hydrophobic moments are plotted on an arbitrary scale in Figs. 3–7.

Results

Selection of the most adequate segment length

The S.D. factors obtained for different apolipoproteins with different segment lengths are shown in Fig. 1. Two distinct minima of the S.D. factor were obtained for segment lengths of 11 and 22 residues. These minima together with those detected at 4, 7, 14 and 18 residues reflect the high alpha-helix content of these apolipoproteins, in agreement with circular dichroism measurements and the Chou and Fasman analysis [4,16]. As a highly negative S.D. value is the reflection of lower noise in the hydrophobicity plots and in view of the importance of the 11 residue-long

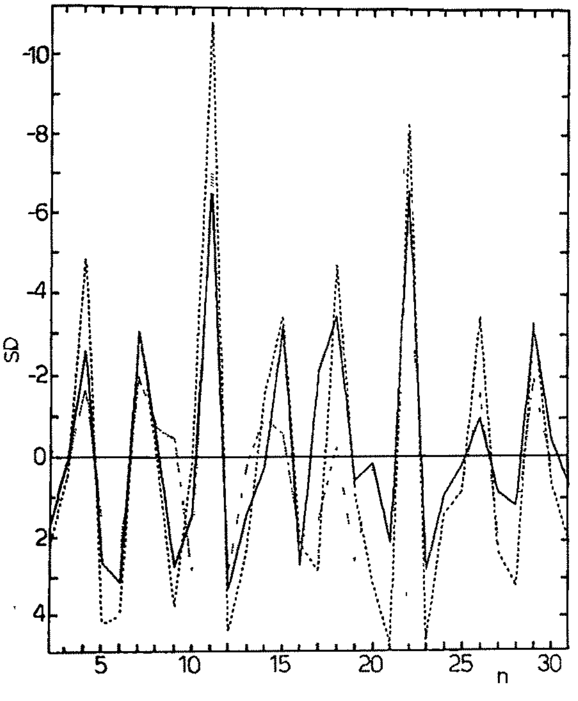

Fig. 1. S.D values of the results obtained with Eqn 2 compared to the values obtained by compiling a distribution of results of 100 random permutations of the same sequences [15]. An S.D. value of -6, for example, corresponds to a probability of random occurrence of $1\cdot10^{-9}$, based on a normal distribution. Values for apolipoproteins A-I (————), E (···· ·), and A-IV (— — —) are shown for a segment length of 2 to 31 residues. (Sequences are taken from Refs. 3 and 18.)

repeats present in nearly all apolipoproteins [17–21] we used an 11-residue segment length in all calculations.

Lipid-binding properties of apolipoproteins

The method described above could easily be applied to the detection of amphiphilic helices within the apolipoprotein sequences. As these amphiphilic helices are supposed to be involved in lipid-binding, we compared the results of the modified Finer-Moore plots to the experimental data reported in the literature [4,9].

An example of such a plot is shown in Fig. 2A for apolipoprotein A-II. The existence of two lipid-binding domains in apolipoprotein A-II was documented from experiments with synthetic peptides [4,9,22]. One domain is located in the NH_2-terminal region, around residues 12–31, while the second domain encompassing residues 50–58 lies in the COOH-terminal region of the protein. The modified Finer-Moore plot for apolipoprotein A-II shows two pronounced maxima at an angle of 100°, which match exactly the two lipid-binding domains detected experimentally. It is striking that these two regions contain only one distinct maximum around 100°, to the exclusion of any other angle.

A plot of the hydrophobic moment at 100° versus the mean hydrophobicity for all apolipoprotein A-II segments is shown in Fig. 3. This classical Eisenberg [5] plot is characterized by the appearance of a cluster of several helices with a high hydrophobic moment and a relatively high mean hydrophobicity value, which correspond to the helices responsible for phospholipid binding. According to their relative position on this plot and the nomenclature used by Eisenberg et al. [5] these helices should be classified as 'surface-seeking' helices.

Some of these features were also shared by the hydrophobicity profiles of other small apolipoproteins in which phospholipid-binding domains have been identified experimentally. There is evidence that residues 45–55 of apolipoprotein C-II are involved in phospholipid binding and activation of lipoprotein lipase at high phospholipid packing [4,9,23,24]. On the modified Finer-Moore plot (Fig. 2B) this region shows a maximum around 100°. In another small apolipoprotein, C-I, residues 16–32 have been implicated in phospholipid binding [4,9] and the hydrophobicity profile of this protein domain shows again a maximum at an angle of 100° (Fig. 2C).

Activation properties of apolipoproteins for the lecithin–cholesterol acyltransferase enzyme

Lecithin–cholesterol acyltransferase (EC 2.3.1.43) is the enzyme responsible for cholesterol esterification in serum (for a review see Ref. 25). High-density lipoproteins (HDL) are its natural substrate, and several HDL apolipoproteins have activator properties towards this enzyme, though each of them to a different extent [26,27]. Human apolipoprotein A-I is the most efficient activator, followed by apolipoproteins A-IV, C-I and E [26–30]. Apolipoproteins C-II and C-III are only minor activators, whereas apolipoprotein A-II does

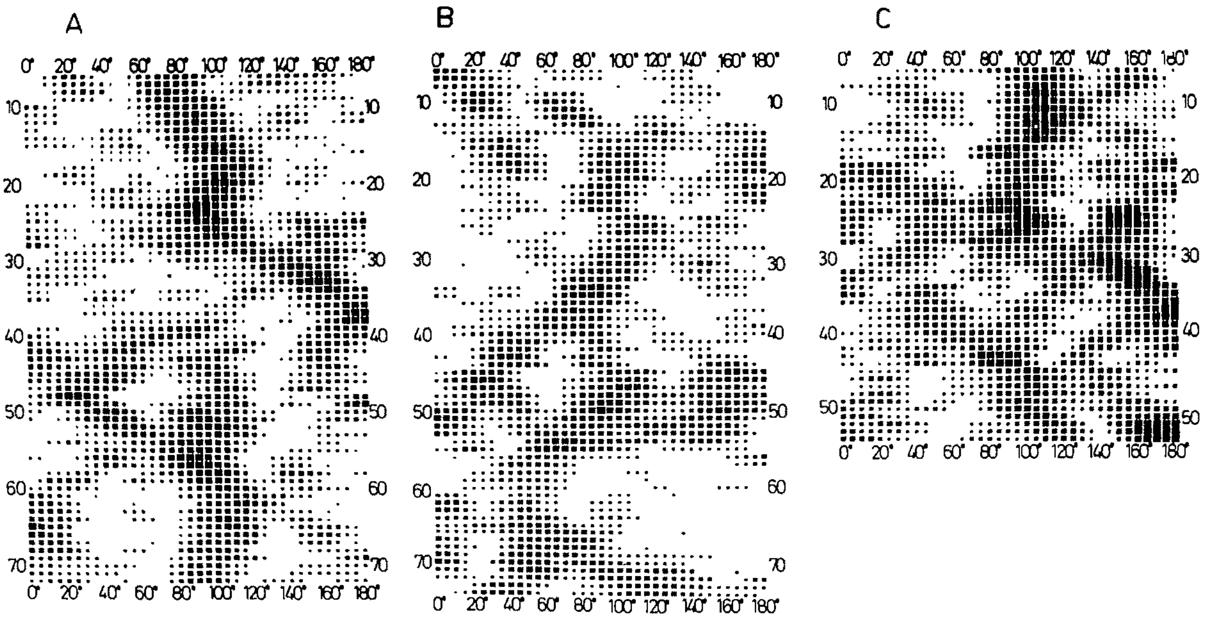

Fig 2 Modified Finer-Moore plot of human apolipoproteins A-II (A), C-II (B) and C-I (C) The increasing dot size corresponds to increasing values of the hydrophobic moment These hydrophobic moments are plotted for different angles (x-axis) as a function of the midpoint of the segments used (y-axis) (Sequences are taken from Ref 3.)

not activate the enzyme, but rather inhibits the effect of A-I [27–29]. The enzyme activation seems partially species-dependent, as apolipoprotein A-IV appears to be a very important activator in vivo in the rat [31]. According to a recent report [32], rat apolipoprotein A-I is a less potent activator than human A-I in vitro, for both the human and the rat enzyme.

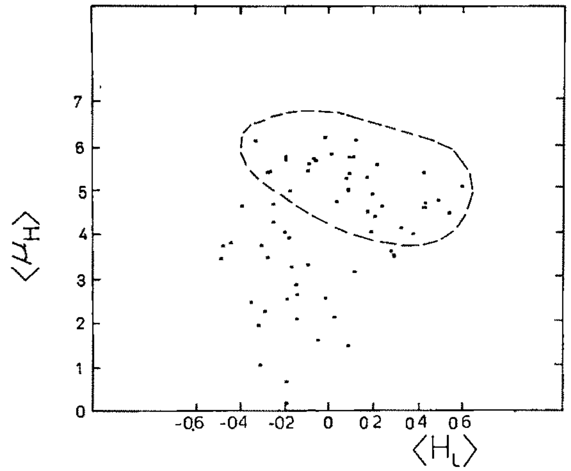

Fig 3. Eisenberg [5] plot for apolipoprotein A-II. All segments identified as being involved in lipid binding are situated within the encircled region, a region that, according to Eisenberg, contains the surface-seeking helices.

Enzyme activation was demonstrated in vitro, with both apolipoprotein fragments and synthetic peptides. These peptides were either identical to apolipoprotein segments or designed to form amphiphilic helical structures [4,9]. The structural requirements for lecithin–cholesterol acyltransferase activation have not been clearly defined yet. A correlation between the experimental data available and the hydrophobicity analysis of these sequences was sought.

A plot of the average of all hydrophobic moments per 11-residue segments of the polypeptide is shown in Fig. 4 for human apolipoproteins A-I, A-II and A-IV. All three proteins bind phospholipids to form complexes [35,36] and have a pronounced maximum at an angle of about 100°, corresponding to an amphiphilic helical structure, as described above for apolipoprotein A-II. However, in the plots of human apolipoproteins A-I and A-IV, a second maximum of similar magnitude appears at an angle of 160–170°. Although

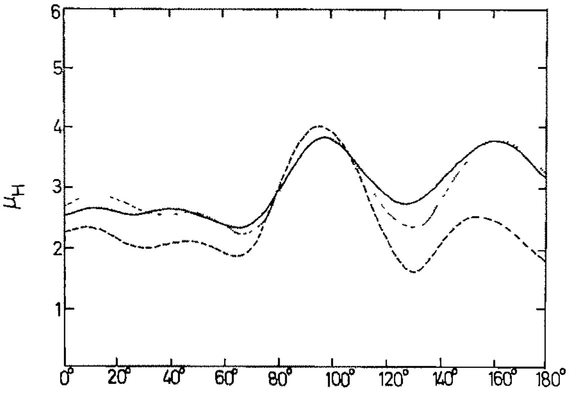

Fig. 4. Average of the modified Finer-Moore hydrophobicity plot [11] for human apolipoproteins A-I (————), A-II (— — —) and A-IV (· ·· ·). The human sequences are taken from Refs 3 and 18.

such a maximum is mostly related to amphiphilic beta-sheet structures, Eisenberg et al. [7] have already noted the appearance of extra peaks, besides the one at 100°, in the profiles of some helices. It is important to note that in apolipoprotein A-II, which has no activator properties, this extra peak is very weak, while the peak at 100° is realtively more important.

A detailed analysis of the hydrophobic moment along the human apolipoprotein A-I sequence further confirmed the relationship between hydrophobicity profiles and lecithin–cholesterol acyltransferase activation properties. Using synthetic lipid-binding peptides, Sparrow and Gotto [4] reported a negligible lecithin–cholesterol acyltransferase activation by the COOH-terminal fragments of apolipoprotein A-I compared to fragments situated between residue 145–185. The average hydrophobicity profiles of these fragments are shown in Fig. 5. These sequences are much shorter and consequently they have a more detailed pattern. The absence of a maximum around 160° for the non-activating compared to the activating peptides is, however, very clear. It is interesting to note that an increase of the activator capacity is accompanied by a concomitant increase of the maximum at 160–170°.

A decreased maximum at 160–170° and an increased maximum at 100° corresponding to a different activator capacity [32] was also observed in a comparison of four repetitive segments of

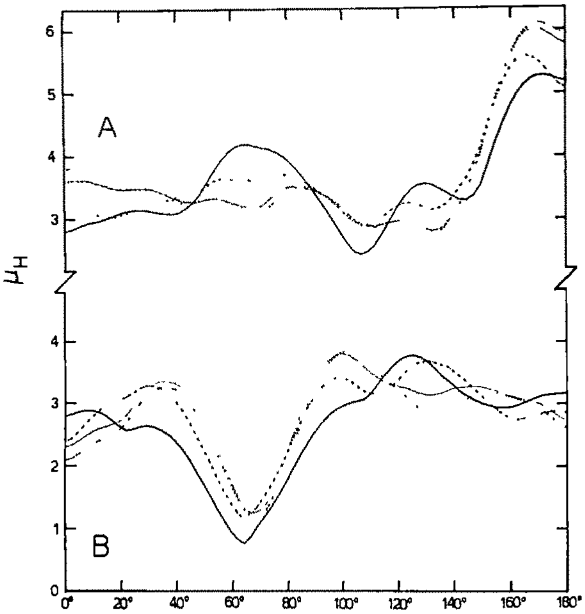

Fig. 5. Hydrophobicity profile (as in Fig 4.) for different lipid-binding synthetic fragments of apolipoproteins A-I, described by Sparrow and Gotto [4]. (A) Four lecithin–cholesterol acyltransferase-activating peptides: 145–185 (— — —), 148–185 (· · · · · ·), 152–185 (— · — · —), 157–185 (————) with respectively 24%, 19%, 6% and 8% of the activating capacity of apolipoprotein A-I. (B) Lipid-binding non-activating peptides situated at the COOH-terminal end of apolipoprotein A-I: 197–245 (————), 204–245 (- - - - - – -), 213–245 (· · · · ·), 220–245 (— · — · —).

human apolipoprotein A-I (Fig. 6A), located between residues 99 and 187, with the corresponding residues in the rat apolipoprotein A-I sequence. The available experimental data [4,9,34,37] together with the detailed hydrophobicity analysis of apolipoprotein A-I therefore suggest that the activator properties are located in four repetitive helical segments between residues 99 and 187.

The same calculations were also carried out for the apolipoprotein C sequences (Fig. 6B). In apolipoprotein C-I, a long-known activator of lecithin–cholesterol acyltransferase [26], the maximum at 160° is similar to that in apolipoprotein A-I, whereas it is virtually absent in C-II and C-III, which are less potent lecithin–cholesterol acyltransferase activators. The hydrophobicity profile of apolipoprotein E also shows a maximum at an angle between 160° and 180°, in accordance with the recently reported [29,30] activator proper-

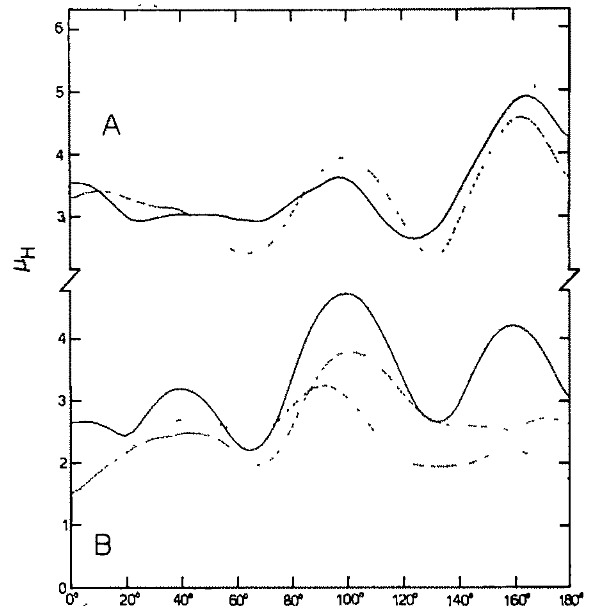

Fig 6 (A) Hydrophobicity profile (as in Fig. 4.) of four 22-residue-long repeats (residues 99–187) of human apolipoprotein A-I (—————) and the corresponding region of rat apolipoprotein A-I (- - - - - -). The sequence of rat A-I is taken from Ref. 19. (B) Hydrophobicity profile (as in Fig. 4) for apolipoproteins C-I (—————), C-II (- - - - - -) and C-III (· · · · ·) Sequences are taken from Ref. 3

ties of apolipoprotein E (data not shown).

An additional test of our theoretical approach lies in an analysis of the synthetic 'model' peptides designed for their lipid-binding properties, and which also have the ability to activate lecithin–cholesterol acyltransferase. The hydrophobicity profiles of two such peptides, LAP-20 described by Pownall et al. [33], and the one described by Yokoyama et al. [38], are shown in Fig. 7A together with the profile of a 20-residue-long segment of apolipoprotein A-II (residues 51–70) located in a lipid-binding domain. An Edmundson wheel representation [1] of these peptides and the 20-residue-long segment of apolipoprotein A-II (residues 51–70) are given in Fig. 8.

Although the hydrophobicity profiles of the two model peptides have peaks of different magnitude, their overall shape is the same and both show the appearance of a peak at 160°. In contrast, the lipid-binding segment of apolipoprotein A-II lacks the peak around 160°. Extra peaks in

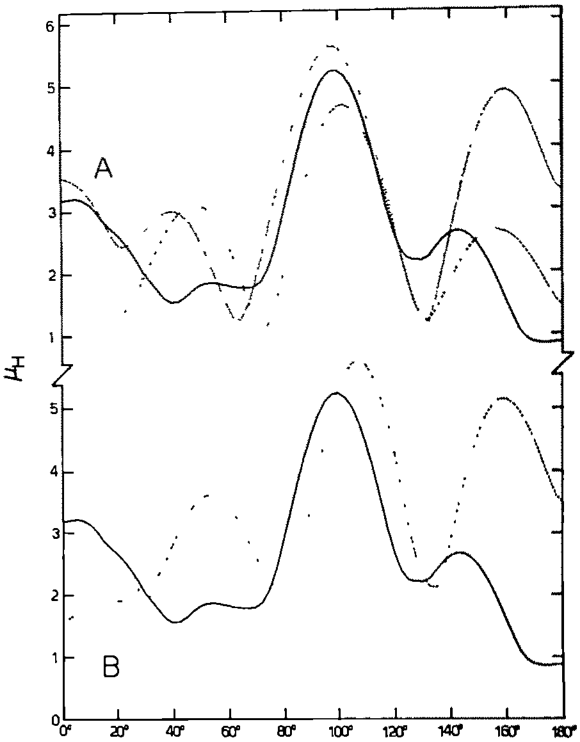

Fig. 7. A. Hydrophobicity profile (as in Fig 4) of two synthetic lipid-binding peptides: LAP-20 (- - - - - -) described by Pownall et al. [33], and the docosapeptide described by Yokoyama et al. [38] (· · · · ·), together with a lipid-binding domain of apolipoprotein A-II (—————) (residues 51–70) B. Example of the effect of residue modification on the hydrophobicity profiles: lipid-binding domain of apolipoprotein A-II (residues 51–70) (—————) and modified (as shown in Fig. 8) (— — —)

addition to the one at 100° were also observed, in isolated helical fragments, by Eisenberg et al. [7], who did not provide a clear interpretation of this phenomenon. We observed that strongly hydrophilic residues, at the edges of the apolar face of the helix, and less polar residues, in the hydrophilic side of the helix, affect the balance between the hydrophilic and hydrophobic sides of the amphiphilic helices and generate the extra peak around 160°. Such residues in apolipoprotein A-I for example are Lys-133 and -140 and Ala-124, -154 and -176, respectively. Recently the experimental modification of lysine residues of apolipoprotein A-I has been shown to affect the lecithin–cholesterol acyltransferase activation properties of this protein [39]. The importance of the hydro-

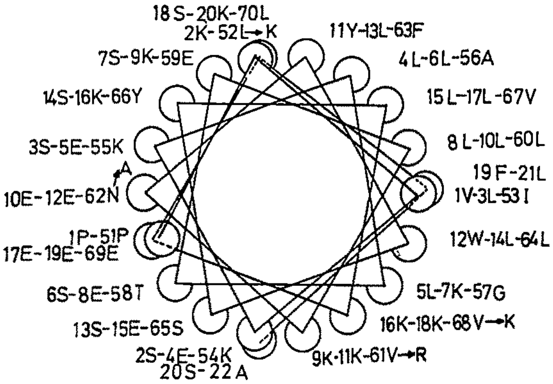

Fig. 8. Edmundson wheel representation [1] of the three amphiphilic peptides described in the text. The helices are superimposed on each other in order to orient their hydrophobic surfaces toward the same side of the figure. The numbering of the peptides is in the following order· LAP-20 described by Pownall et al. [33]; the peptide described by Yokoyama et al. [38] and in last position the apolipoprotein A-II segment (residues 51–70) with its modifications as indicated by arrows. The NH_2-terminal ends of the peptides are shown as closed circles The LAP-20 peptide begins at the left side of the figure, the other two begin at the right side of the figure. Amino acids are shown in the single letter code which translates to the three letter code as follows: A, Ala; C, Cys, D, Asp; E, Glu; F, Phe; G, Gly, H, His; I, Ile; K, Lys; L, Leu; M, Met; N, Asn; P, Pro; Q, Gln; R, Arg; S, Ser; T, Thr; V, Val; W, Trp; Y, Tyr

philic residues at the boundary of the hydrophobic side of the helix and of less-polar residues in the hydrophilic part of the helix can also be demonstrated by making changes in the segment (residues 51 to 70) of the non-activating apolipoprotein A-II. An example of such changes is shown in Fig. 8 and the effects of these changes on the hydrophobicity profile are shown in Fig. 7B. For example, the Leu → Lys substitution at position 52 and the Val-61 → Arg, Asn-62 → Ala, Val-68 → Lys substitutions are able to transform the pattern of a lipid-binding fragment into the pattern of a lecithin–cholesterol acyltransferase-activating fragment such as LAP-20.

Discussion

In this paper we applied hydrophobic moment calculations to detect lipid-binding fragments in apolipoproteins and proposed a new theoretical approach to differentiate between helical segments of apolipoproteins. We have shown that the analysis of the helical hydrophobic moment and the calculation of the hydrophobic moment at various angles can lead to the recognition of different types of helices and to a better understanding of the correlation between structure and function of these protein domains.

Segments with a high helical hydrophobic moment and a single maximum at 100° in the modified Finer-Moore plot were present in apolipoprotein A-II, corresponding to the experimentally identified lipid-binding domains of this protein. Experimentally determined lipid-binding domains could also be localized, by the hydrophobicity analysis in the sequences of apolipoproteins C-II and C-I.

In other apolipoproteins, human and rat A-I, as well as in C-I, A-IV and E, there is a maximum at 100° and an extra maximum at 160° in the hydrophobicity profiles. Moreover there was a clear relationship between the intensity of the peaks around 100° and 160° and the relative degree of lecithin–cholesterol acyltransferase activation of the different proteins and peptides. This correlation also holds for apolipoprotein A-I of different species, such as human and rat.

The appearance of two peaks in the hydrophobicity profiles of synthetic model peptides also correlates with their lipid-binding and lecithin–cholesterol acyltransferase activation properties. Previous reports attempted to define the requirements necessary for lipid binding, based on the calculation of the mean hydrophobicity [9]. Although such calculations can yield interesting information they are critically dependent on the hydrophobicity scale used, and do not allow a clear classification, differentiation or delimitation of the different domains.

Our results suggest that amphiphilic lipid-binding helices in apolipoproteins can be separated into two types: helices whose hydrophobicity profile has one maximum at 100° and helices whose hydrophobicity periodicity shows a second maximum around 160°. The former helices would be essential for lipid binding, and the presence of two such domains in apolipoprotein A-II accounts for the special lipid-binding properties of this protein [40]. The other helices play an important role in the activation of lecithin–cholesterol acyltransferase. Specific lipid-binding optimizes the substrate enzyme interactions.

In a way, our findings quantify the proposal of Fukushima et al. [34] in which the 'depth' of penetration of the amphiphilic helices into the phospholipid bilayer is an important factor in lecithin–cholesterol acyltransferase activation. The balance between the hydrophilic and hydrophobic sides of the helices has a strong influence on the hydrophobicity profiles and the lecithin–cholesterol acyltransferase-activating properties. These characteristics of the helical structure might affect the phospholipid-apolipoprotein association and in turn modulate the substrate properties of the complex.

Acknowledgement

H.D.L. is a recipient of an "Instituut tot aanmoediging van het wetenschappelijk onderzoek in Nijverheid en Landbouw" fellowship.

References

1 Schiffer, M. and Edmundson, A B (1967) Biophys. J. 7, 121–135

2 Segrest, J.P., Jackson, R L., Morrisett, J.D. and Gotto, A.M., Jr. (1974) FEBS Lett. 38, 247–253

3 Mahley, R W , Innerarity, T.L., Rall, C.R. and Weisgraber, K.H (1984) J. Lipid Res 25, 1277–1294

4 Sparrow, J T. and Gotto, A M , Jr (1981) Crit. Rev Biochem. 12, 87–107

5 Eisenberg, D., Weiss, R.M and Terwilliger, T.C. (1982) Nature 299, 371–374

6 Eisenberg, D. (1984) Annu Rev Biochem. 53, 595–623

7 Eisenberg, D., Weiss, R.M. and Terwilliger, T.C (1984) Proc Natl Acad. Sci. USA 81, 140–144

8 De Loof, H , Rosseneu, M., Brasseur, R. and Ruysschaert, J M (1986) Proc Natl Acad. Sci USA 83, 2295–2299

9 Sparrow, J T and Gotto, A.M., Jr. (1980) Ann. N.Y. Acad Sci. 348, 187–209

10 Von Heijne, G. (1986) EMBO J. 5, 1335–1332

11 Schultz, G.E. and Schirmer, R H (1984) Principles of Protein Structure, Springer, New York

12 Finer-Moore, J. and Stroud, R.M. (1984) Proc. Natl. Acad Sci. USA 81, 155–159

13 Rose, G.D. (1978) Nature (London) 272, 586–590

14 Kyte, J. and Doolittle, R F. (1982) J. Mol. Biol 157, 105–132

15 Dayhoff, M.O., Barker, W.C and Hunt, L T (1983) Methods Enzymol. 91, 524–545

16 Chou, P.Y. and Fasman, G.D. (1974) Annu. Rev. Biochem. 47, 251, 1978

17 Barker, W.C. and Dayhoff, M. (1977) Comp. Biochem Physiol B.57, 309–315

18 Elshourbagy, N.A., Walker, D W., Boguski, M.S., Gordon, J.I. and Taylor, J.M. (1986) J. Biol Chem. 261, 1998–2002

19 Boguski, M S , Elshourbagy, N., Taylor, J M and Gordon, J.I (1984) Proc. Natl. Acad. Sci USA 81, 5021–5025

20 Boguski, M.S., Elshourbagy, N., Taylor, J.M and Gordon, J I. (1984) Methods Enzymol 128, 753–773

21 Luo, C -C., Li, W H., Moore, M.N. and Chan, L. (1986) J. Mol Biol. 167, 325–340

22 Mao, S.J T., Jackson, R.L , Gotto, A.M., Jr and Sparrow J.T. (1981) Biochemistry 20, 1676–1680

23 Smith, L.C., Voyta, J C , Catapano, A L., Kinnunen, P.K.J , Gotto, A.M., Jr. and Sparrow, J.T. (1980) Ann. N.Y Acad Sci. 348, 213–223

24 Vainio, P., Virtanen, J.A , Kinnunen, P.K.J., Voyta, J.C., Smith, L.C., Gotto, A.M., Jr., Sparrow, J.T., Pattus, F and Verger, R (1983) Biochemistry 22, 2270–2275

25 Marcel, Y L. (1982) Adv. Lipid Res. 19, 85–136

26 Soutar, A.K , Garner, C W., Baker, H.N., Sparrow, J.T , Jackson, R.L., Gotto, A.M., Jr. and Smith, L.C. (1975) Biochemistry 14, 3057–3064

27 Jonas, A., Sweeny, S A and Herbert, P N (1984) J. Biol Chem. 259, 6369–6375

28 Steinmetz, A. and Utermann, G (1985) J. Biol. Chem. 260, 2258–2264

29 Zorich, N., Jonas, A and Pownall, H J. (1985) J. Biol. Chem 260, 8831–8837

30 Chen, C H and Albers, J.J (1985) Biochim Biophys. Acta 836, 279–285

31 DeLamatre, J.G., Hoffmeier, C A., Lacko, A G and Roheim, P.S (1983) J. Lipid Res 24, 1578–1584

32 Pownall, H J , Pao, Q. and Massey, J.B. (1985) Biochim. Biophys Acta 833, 456–462

33 Pownall, H J., Hu, A., Gotto, A.M., Jr., Albers, J J. and Sparrow, J.T (1980) Proc. Natl. Acad. Sci. USA 77, 3154–3158

34 Fukushima, D., Yokoyama, S , Kroon, D J , Kezdy, F.J. and Kaiser, E T. (1980) J. Biol Chem. 255, 10651–10657

35 Scanu, A M., Edelstein, C. and Shen, B. (1982) in Lipid-Protein Interactions (Jost, P C., and Griffith, O.H., eds.), Vol. 1, pp. 259–316, Wiley, New York

36 Rifici, V.A., Eder, H.A. and Swaney, J.B. (1985) Biochim Biphys Acta 834, 205–214

37 Segrest, J.P., Brouillette, C.G., Chung, B.H , Schmidt, C F , Gawish, A. and Anantharamaiah, G.M (1985) Arteriosclerosis 5, 546a

38 Yokoyama, S., Fukushima, D., Kupferberg, J.P , Kezdy, F.J and Kaiser, E.T. (1980) J. Biol Chem. 255, 7333–7339

39 Jonas, A., Covinsky, K.E. and Sweeny, S A. (1985) Biochemistry 24, 3508–3513

40 Van Tornout, P., Caster, H., Lievens, M.J., Rosseneu, M and Assmann, G. (1981) Biochim Biophys. Acta 663, 630–636

Biochimica et Biophysica Acta 911 (1987) 53–58
Elsevier

BBA 32677

The association reaction of yeast alcohol dehydrogenase with coenzyme is partly diffusion-controlled in solvents of increased viscosity

Brian B. Hasinoff, Richard Dreher and John P. Davey

Department of Chemistry and Faculty of Medicine, Memorial University of Newfoundland, St John's, Newfoundland (Canada)

(Received 4 July 1986)

Key words: Alcohol dehydrogenase kinetics, Diffusion control; NADH; Coenzyme association

The steady-state kinetics of the yeast and liver alcohol dehydrogenase catalyzed reduction of aldehydes were examined in solvent mixtures of increased viscosity. This was done to investigate the effects of diffusion control on the fast association of NADH with the enzymes. Both glycerol and sucrose were unsatisfactory as viscosogens, as they inhibited the enzyme, but poly(ethylene glycol)/water mixtures were satisfactory. The 5-fold faster reaction of yeast alcohol dehydrogenase with NADH is partly diffusion controlled, whereas the slower liver alcohol dehydrogenase reaction showed no diffusion effects. These results are consistent with a yeast alcohol dehydrogenase active site that has relatively little steric hindrance to NADH binding. It is estimated that contributions to this association reaction from diffusion control and chemical activation control are equal at a solvent viscosity of 10 cP. Thus, under physiological conditions of increased viscosity the NADH association may be significantly affected by diffusion effects. In order to estimate accurately the maximum diffusion-controlled rate constant from diffusion theory, the diffusion coefficients of NADH were measured in poly(ethylene glycol)/water mixtures and were found to vary inversely as the solvent viscosity raised to the power of 0.5. The non-Stokesian behaviour of molecules as large as NADH in polymer/water mixtures may be a serious limitation to the routine use of poly(ethylene glycol) as a viscosogen for diffusion studies.

Introduction

Enzymes are remarkable in that their association reactions with their substrates are often very fast. They are so fast that their rates of reaction can be partly limited by diffusion of reactants towards one another. Since the diffusion-controlled rate of reaction is an upper rate limit, the degree to which it is achieved is some measure of the evolutionary development of the enzyme. Under physiological conditions of higher viscosity the importance of the diffusion of the reactants is increased.

Alcohol dehydrogenases [1–9] catalyze the reduction of aldehydes and the oxidation of alcohols using the coenzymes NADH and NAD^+ respectively. The association reaction of NADH with yeast alcohol dehydrogenase

$$E + NADH \xrightarrow{k_1} E \cdot NADH$$

measured by the steady-state method is fast and gives $k_1 = 40\ \mu M^{-1} \cdot s^{-1}$ [1]. The horse-liver alcohol dehydrogenase reaction is slower, with $k_1 = 10\ \mu M^{-1} \cdot s^{-1}$ as measured by both steady-state [3] and stopped-flow [4,5] methods. These rates

---

Correspondence: Dr. B.B. Hasinoff, Department of Chemistry and Faculty of Medicine, Memorial University of Newfoundland, St. John's, Newfoundland, Canada, A1B 3X7.

0167-4838/87/$03.50 © 1987 Elsevier Science Publishers B.V. (Biomedical Division)

are so fast that they may be influenced by diffusion of the reactants towards one another [10].

The basis for the theory of diffusion-controlled reactions is the classical Smoluchowski equation [10,11]

$$k_D = 4\pi NDR/1000 \quad (1)$$

where k_D ($M^{-1} \cdot s^{-1}$) is the diffusion-controlled rate constant for non-interacting spheres reacting on every collision, N is Avogadro's Number, D ($cm^2 \cdot s^{-1}$) is the sum of the diffusion coefficients of the reacting species and R (cm) is the encounter distance, often taken as the sum of the radii of the two reacting molecules. The effect of diffusion control on enzyme reactions has been recently reviewed [10]. Since the active site on an enzyme may be but a small fraction of the total surface area of the protein, the diffusion-controlled rate of an enzyme reaction may be substantially reduced over that given by Eqn. 1. Hence Eqn. 1 may be modified by inclusion of an experimentally determinable factor, f, that might include steric, interaction and probability factors

$$k_D = f4\pi NDR/1000 \quad (2)$$

More generally, if a reaction is not 100% diffusion-controlled and is affected simultaneously by normal chemical activation and by diffusion control [10]

$$k^{-1} = k_C^{-1} + k_D^{-1} \quad (3)$$

where k is the experimentally observed second order rate constant and k_C is the chemical activation rate constant. Substitution of Eqn. 2 in Eqn. 3 predicts that k^{-1} is a linear function of D^{-1}. Since D may be decreased by increasing the solvent viscosity the decrease in k with increasing solvent viscosity allows an experimental determination of f. The importance of diffusion control has been shown for the reactions of carbonic anhydrase [12], Mb [13,14], the separated chains of Hb [15], β-lactamase [16] and acetylcholinesterase [17].

Experimental procedures

Materials

Yeast alcohol dehydrogenase (Sigma) and horse-liver alcohol dehydrogenase (Sigma) were dissolved in ionic strength 0.1 M Na_2HPO_4-NaH_2PO_4 buffer and centrifuged. To stabilize the yeast alcohol dehydrogenase stock solutions EDTA (0.3 mM) and either cysteine or glutathione (0.5 mM) were added. The protein concentrations were measured from A at 280 nm [9] and the active site concentrations by fluorescence titration [18] with NADH in the presence of 0.5 M acetamide for yeast alcohol dehydrogenase and in the presence of 0.1 M isobutyramide for liver alcohol dehydrogenase [19,20]. For yeast alcohol dehydrogenase 45% or 1.8 (out of a maximum of 4) of the active sites per molecule were titrated compared to 2.4 found in Ref. 18. For liver alcohol dehydrogenase 42% or 0.8 (out of a maximum of 2) active sites per molecule were titrated.

Solutions of the viscosogen poly(ethylene glycol) 6000 (Baker, M_r 6000–7500) were prepared by weight (up to 11.8% (w/v) poly(ethylene glycol), about 20 mM polymer). This water-soluble polymer is large enough that it would not be expected to fit into the dehydrogenase active site. The enzymes were stable in these solutions for times much longer than were necessary for rate measurements. Both glycerol and sucrose solutions were also tried as viscosogens, but were unsatisfactory as they both weakly inhibited liver alcohol dehydrogenase ($K_i \approx 1$ M).

The enzyme kinetics were studied in ionic strength 0.1 NaH_2PO_4-Na_2HPO_4 (liver alcohol dehydrogenase at pH 7.0, yeast alcohol dehydrogenase at pH 6.9) buffer. NADH (Sigma) solutions in pH 7.0 phosphate buffer were prepared fresh just before use and were assayed spectrophotometrically at 340 nm using ε 6.15 $mM^{-1} \cdot cm^{-1}$ and $\Delta\varepsilon$ 6.05 $mM^{-1} \cdot cm^{-1}$ for conversion to NAD^+. The reactions measured were the yeast alcohol dehydrogenase catalyzed reduction of acetaldehyde by NADH and the liver alcohol dehydrogenase catalyzed reduction of butyraldehyde by NADH. Acetaldehyde and butyraldehyde were freshly distilled and their aqueous solutions were prepared fresh daily and were 40 mM and 1 mM, respectively, in their reaction mixtures. The NADH concentration was varied typically from 20 to 900 μM.

Apparatus and methods

The enzyme catalyzed reaction of NADH with the aldehyde was followed at 340 nm on a Shimadzu 260 spectrophotometer. The reaction was initiated by injecting a small volume of aqueous stock enzyme solution into the motor-stirred 1 cm reaction cell at 25°C. Initial velocity, v, measurements were computed from first-derivative time-course records extrapolated back to zero time. The velocities were corrected for the slow loss of activity of the stock enzyme solution over time. Usually 8–10 initial velocity measurements were made and analyzed in Lineweaver-Burk plots by weighted (assuming 2% error in v) linear least-squares analyses. The least-squares-determined errors on the slopes averaged 2.2% and on the intercepts 1.5%.

The viscosities of the reaction mixtures were measured on a calibrated thermostatically controlled Wells-Brookfield cone-plate microviscometer to about 1% and ranged from 0.9 to 6.3 cP (1 cP = 1 centipoise = 1 mPa · s). The diffusion coefficients of NADH in poly(ethylene glycol)/water mixtures were measured by the Taylor dispersion technique [21,22]. A small sample (5 μl) of NADH solution was injected into the solvent as it was pumped down a thermostatically controlled 30.5 m long stainless steel capillary tube. The broadened eluted peak was recorded by the spectrophotometer as it passed through a 1 cm flow-through cell. The diffusion coefficient was calculated from $D = 2310 \cdot r_c^2 \cdot t_r / W_{1/2}^2$ where r_c (cm) is the capillary radius, t_r (s) the residence time of solute in the tube and $W_{1/2}$ (s) is the width at half-height of the eluted peak [21,22]. Values of log (D_{NADH}) in aqueous and poly(ethylene glycol)/water buffers are plotted vs. log η in Fig. 1.

Results and Discussion

Diffusion coefficient of NADH

The Stokes-Einstein equation

$$D = kT/(6\pi r\eta) \tag{4}$$

where k is Boltzmann's constant, r is the effective molecular radius and η the solvent viscosity, is often used to predict D. However, the failure of Eqn. 4 for small solute molecules is well known [12,13,21–23] and is a serious limitation on its use in Eqn. 2 [12,13]. However, the striking empirical correlation [21,22]

$$D = A/\eta^p \tag{5}$$

has been found where A and p are constants. The viscosity exponent p depends upon the solute size and has a value of 1 or less. Linear least-squares fits to the logarithmic form of Eqn. 5 plotted in Fig. 1 gives for NADH, $p = 0.474 \pm 0.003$ and $A = (3.73 \pm 0.02) \cdot 10^{-6}$ cm$^2 \cdot$ s^{-1}. Failure of Eqn. 4 is particularly acute in polymer/water mixtures. For Na$^+$ in poly(ethylene glycol)/water, $p = 0.16$ was observed [23]. The validity of Eqn. 5 for the much larger yeast alcohol dehydrogenase and liver alcohol dehydrogenase molecules in poly(ethylene glycol)/water mixtures was not tested, but it was for the smaller horse-heart cytochrome c (M_r 12500) in a related study and yielded a value of $p = 0.97 \pm 0.03$. Thus it appears that failure of Eqn. 4 occurs when the solute size is small relative to solvent size. The non-Stokesian behaviour of a relatively large substrate molecule like NADH in poly(ethylene glycol)/water solutions is a serious limitation to the routine use of the solvent viscosity in Eqn. 4 to predict the diffusion coefficients used in Eqn. 2.

Effect of increased viscosity in poly(ethylene glycol)/water on the kinetics

The effect on the yeast alcohol dehydrogenase kinetics of increasing the viscosity of the solvent with poly(ethylene glycol) is shown in Fig. 2. The kinetics of aldehyde (Ald) reduction by NADH

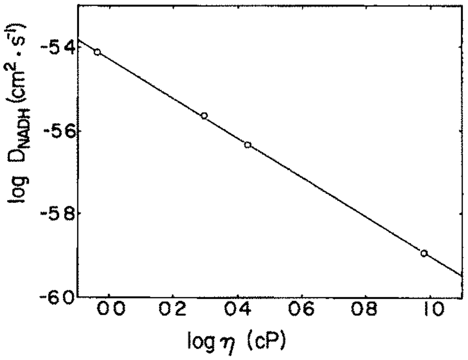

Fig 1 Plot of log D_{NADH} vs log η for poly(ethylene glycol)/water mixtures at 25°C in pH 7.0, 0.1 M ionic strength phosphate buffer A weighted linear least-squares fit yields from the slope the viscosity exponent p = .47 in Eqn. 5.

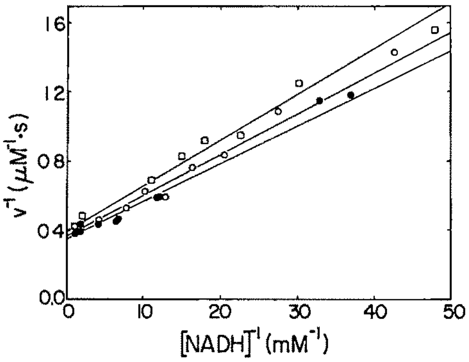

Fig. 2. Lineweaver-Burk plots for the yeast alcohol dehydrogenase-catalyzed reduction of acetaldehyde by NADH in 0, 8.0 and 10.8% g/100 ml (●, ○, □) poly(ethylene glycol)/water, respectively. The enzyme concentration refers to a 955 pM active site basis and [acetaldehyde] = 40 mM. The lines are weighted linear least-squares calculated.

are given by the Dalziel relationship [1,2,7,18]:

$$\frac{[E]_0}{v} = \phi_0 = \frac{\phi_1}{[NADH]} + \frac{\phi_2}{[Ald]} + \frac{\phi_{12}}{[NADH][Ald]} \tag{6}$$

The relationship of ϕ_2 to ϕ_0 and ϕ_{12} to ϕ_2 is such that at high [Ald] and under conditions where [Ald] $\gg$ [NADH] Eqn. 6 reduces to

$$\frac{[E]_0}{v} = \phi_0 + \frac{\phi_1}{[NADH]} \tag{7}$$

and allows a measure of ϕ_1 and ϕ_0 without the necessity of using secondary plots. Under the conditions of the yeast alcohol dehydrogenase study with [acetaldehyde] = 40 mM, the ϕ_{12} term is but 0.3% of the ϕ_1 term and the ϕ_2 term is 2.3% of the ϕ_0 term [1]. Eqn. 7 is still valid at high acetaldehyde concentrations as the K_m^{NADH} (ϕ_1/ϕ_0) of 73 μM from [1] agrees well with our value of 65 μM. Also our value of ϕ_0 which depends upon an absolute determination of $[E]_0$ agreed within 18% of that previously found [2]. In the case of liver alcohol dehydrogenase with [butyraldehyde] = 1 mM the ϕ_{12} is just 0.04% of the ϕ_1 term and the ϕ_2 term is 2.3% of the ϕ_0 term [3,7].

The yeast alcohol dehydrogenase [1,2,7] and liver alcohol dehydrogenase [3,7] catalyzed reduction of aldehyde is usually interpreted in terms of compulsory ordered binding. NADH is the substrate that binds first and it is then followed by the aldehyde. For both yeast alcohol dehydrogenase and liver alcohol dehydrogenase the relationship among the rate constants in the compulsory ordered mechanism is such that $\phi_1^{-1} = k_1$. This result has been confirmed by direct stopped-flow measurement of k_1 for liver alcohol dehydrogenase [4,5]. Substituting k_1 for the k of Eqn. 2 in Eqn. 3 gives

$$k_1^{-1} = k_C^{-1} + (f4\pi NDR/1000)^{-1} \tag{8}$$

Thus plots of k_1^{-1} vs. D^{-1} (Fig. 3 yield from the slopes experimental values of f (Table I). The S.D.s on the k_1^{-1} parameters obtained from the weighted linear least-squares analyses of the double-reciprocal plots were used as weights in the analyses of the data of Fig. 3. The S.D.s of these slopes and intercepts were used to calculate the error limits shown in Table I. R was calculated from $R = r_E + r_{NADH}$. The value of r (yeast alcohol dehydrogenase) = 45.6 Å was estimated from Eqn. 4 with D (yeast alcohol dehydrogenase) = $4.70 \cdot 10^{-7}$ cm$^2 \cdot$ s^{-1} [9]. Similarly with D (liver alcohol dehydrogenase) = $5.95 \cdot 10^{-7}$ cm$^2 \cdot$ s^{-1}, r (liver alcohol dehydrogenase) = 36.0 Å. Eqn. 4 was also used to calculate r_{NADH} = 6.1 Å from the

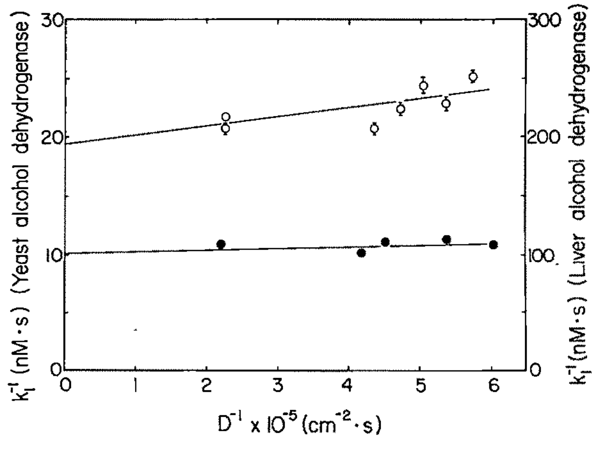

Fig. 3. Plot of k_1^{-1} vs. D^{-1} for yeast alcohol dehydrogenase (○, left scale) and liver alcohol dehydrogenase (●, right scale) in poly(ethylene glycol)/water mixtures of increased viscosity. The straight lines are weighted linear least-squares calculated. The slopes yield the steric factor, f, in Eqn. 8 and the intercepts yield the chemical activation rate constant, k_C. The error bars are the S.D.s used in the analysis and were obtained from weighted linear least-squares analyses of the type carried out on the data of Fig. 2.

TABLE I

RATE CONSTANTS, DIFFUSION CONTROL PARAMETERS AND STERIC FACTORS FOR THE REACTION OF ALCOHOL DEHYDROGENASES WITH NADH

All parameters are on a per active site basis The S.D.s are fitting errors only from weighted linear least-squares analyses.

Description/model	Parameter	Reaction	
		yeast alcohol dehydrogenase	liver alcohol dehydrogenase
Chemical activation [a]	k_C ($\mu M^{-1} \cdot s^{-1}$)	52 ±3	9.9 ±0.3
Steric factor	f (exp)	0.033±0.005	0.025±0.013
Half-cone solid angle [b]	θ (°)	48	–

[a] From intercepts of Fig 3 at $D^{-1} = 0$ ($\eta = 0$ cP).

[b] Calculated from the Schurr-Schmitz model [25] using the experimental f above.

measured value of $D_{NADH} = 3.9 \cdot 10^{-6}$ cm$^2 \cdot$ s^{-1} in aqueous buffer at 25°C. Values of D_E in poly(ethylene glycol)/water were calculated from Eqn. 4 using r (yeast alcohol dehydrogenase) = 45.6 Å and r (liver alcohol dehydrogenase) = 36.0 Å. D_{NADH} was obtained from Fig. 1. Thus D was calculated from $D = D_E + D_{NADH}$. The slope of the plot of Fig. 3 shows a statistically significant dependence on D^{-1} in the case of yeast alcohol dehydrogenase (±15% error) but not for liver alcohol dehydrogenase. Since the value of f for liver alcohol dehydrogenase is zero within 2 S.D.s no meaningful estimate of f is obtained for this enzyme. Thus only the faster yeast alcohol dehydrogenase reaction shows the influence of diffusion control. In aqueous buffer at 25°C, Eqn. 2 yields, with the experimental value of $f = 0.033$, $k_D = 0.033 \cdot 1.7 \cdot 10^{10}$ M$^{-1} \cdot$ s^{-1} = $5.6 \cdot 10^8$ M$^{-1} \cdot$ s^{-1}. Provided both reactants obey the Stokes-Einstein expression, it can be shown from Eqn. 8 that contributions from chemical activation control and diffusion control are equal at about a viscosity of 10 cP. Measurements of the viscosity of the cytoplasm of the cell range from 2 to 70 cP depending upon the cell and the experimental method [24]. Thus under physiological conditions of increased viscosity the reaction of NADH with yeast alcohol dehydrogenase may be significantly influenced by diffusion control. It should be noted that if an enzyme reaction is significantly affected by diffusion control, evolutionary changes that increase the chemical activation rate constant will have only marginal effects on the observed association rate constant. On this basis, yeast alcohol dehydrogenase is a highly evolved enzyme.

Diffusion models

The diffusion of a reactant to a sterically hindered site on an enzyme is predicted to result in a significant reduction in the diffusion-controlled rate constant [10]. The simple surface reactivity model assumes that a fraction of the surface area of the enzyme, σ_E, is reactive [13,15]. This model does have the advantage, however, that it contains no adjustable parameters. Estimating σ_E from the ratio of the cross-sectional area of the substrate molecule to the total surface area of the enzyme gives $\sigma_E = \pi r_{NADH}^2 / 4\pi r_E^2$. Assuming half the NADH molecule is reactive ($\sigma_{NADH} = 1/2$) the value of f can be calculated from $f = \sigma_E \cdot \sigma_{NADH}$. On this basis the calculated f of 0.002 does not compare well with the experimental f value of 0.033. The reason for this poor agreement may be, as has been pointed out [10], that diffusion is really a volume-filling process and thus f should be proportional to sin θ rather than sin$^2\theta$ [10], where θ is the half-cone angle subtended by a circular reactive patch on the enzyme surface.

The more sophisticated Schurr and Schmitz solid angle model [25] considers both translational and rotational diffusion of the reactants and gives $f = (1 - \cos\theta)\theta r_E/(r_E + r_{NADH})$ where θ is the minimum half-cone angle (in rads) necessary for reaction at a hemispherical target. Thus, using the experimentally determined value of f, the half-cone angle, θ, can be calculated. This model is

TABLE II

A COMPARISON OF SOME PROTEIN REACTIONS THAT ARE INFLUENCED BY DIFFUSION CONTROL

Reaction	Experimental f [a]	Half-cone solid angle, θ (°) [b]	Ref.
Ferric cytochrome $c + e^-_{aq}$	0.40	114	14
Ferric myoglobin $+ e^-_{aq}$	0.17	86	14
Yeast alcohol dehydrogenase + NADH	0.033	48	this work
Carbonic anhydrase + CO_2	0.0135	40	12
Carbonic anhydrase + HCO_3^-	0.005	25	12
α-Haemoglobin chain + CO	0.003	23	15
β-Haemoglobin chain + CO	0.002	22	15
Myoglobin + CO	0.001	18	13

[a] In the equation $k_D = f4NDR/1000$ (Eqn. 2).

[b] Calculated from the experimental f [25]

useful because it allows a comparison to be made between proteins and substrates of different sizes (Table II). From Table II the reaction of yeast alcohol dehydrogenase with NADH has a minimum angle of entry, θ, exceeded only by the reaction of hydrated electrons with haem proteins in which tunnelling or two-dimensional surface diffusion processes [14] may be involved. On this basis the comparatively large value of θ for yeast alcohol dehydrogenase indicates a relatively unrestricted entrance to the active site. The large unrestricted angle of entry may be partly explained by the fact that yeast alcohol dehydrogenase is a two-substate enzyme. Thus the yeast alcohol dehydrogenase active site must be large enough to accommodate both NADH and an aldehyde. Since NADH binds first, the active site that NADH 'sees' when it binds is free of the second substrate and is thus relatively unhindered in its open conformation [26]. Evidence for a relatively unrestricted coenzyme binding site also comes from the observation [26] that the hydrophobic cavity for the adenine ring is larger than required. Thus this cavity can also accommodate a variety of inhibitors.

Acknowledgments

The financial support of the Natural Sciences and Engineering Research Council of Canada is gratefully acknowledged.

References

1 Dickinson, F.M. and Monger, G.P. (1973) Biochem. J. 131, 261–270

2 Dickenson, C.J. and Dickinson, F.M. (1975) Biochem. J 147, 303–311

3 Dalziel, K. and Dickinson, F.M. (1966) Biochem. J 100, 34–46

4 Shore, J.D. and Gutfreund, H (1970) Biochemistry 9, 4655–4659

5 Anderson, P., Kvassman, J., Oldén, B. and Pettersson, G. (1984) Eur. J. Biochem. 159, 519–527

6 Klinman, J P. (1981) Critical Rev. Biochem. 10, 39–78

7 Dalziel, K. (1975) in The Enzymes (Boyer, P.D., ed.), 3rd Edn , Vol. 11A, pp. 1–60, Academic Press, New York

8 Brändén, C.-I., Jörnvall, H., Eklund, H. and Furugren, B. (1975) in The Enzymes (Boyer, P D., ed), 3rd Edn., Vol. 11A, pp. 103–190, Academic Press, New York

9 Sund, H. and Theorell, H. (1963) in The Enzymes (Boyer, P.D., Lardy, H., Myrback, K., eds), 2nd Edn , Vol. 7, pp. 25–83, Academic Press, New York

10 Berg, O G. and Von Hippel, P.H. (1985) Annu. Rev. Biophys · Biophys. Chem. 14, 131–160

11 Von Smoluchowski, M. (1917) Z Phys. Chem. Stoechiom. Verwandlschaftsl. 92, 129–168

12 Hasinoff, B.B. (1984) Arch. Biochem. Biophys. 233, 676–681

13 Hasinoff, B.B. and Chishti, S.B. (1982) Biochemistry 21, 4275–4278

14 Hasinoff, B.B , Licht, A. and Pecht, I. (1984) Biochim. Biophys. Acta 767, 627–634

15 Hasinoff, B.B. and Chishti, S.B (1983) Biochemistry 22, 58–61

16 Hardy, L.W. and Kirsch, J.F. (1984) Biochemistry 23, 1275–1282

17 Bazelyansky, M., Robey, E. and Kirsch, J.F. (1986) Biochemistry 25, 125–130

18 Dickinson, F.M. (1970) Biochem. J. 120, 821–830

19 Theorell, H and McKinley-McKee, J.S. (1961) Acta Chem Scand. 15, 1811–1833

20 Yonetani, T. and Theorell, H. (1962) Arch. Biochem. Biophys. 99, 433–446

21 Evans, D.F., Tominaga, T. and Chan, C (1979) J. Soln. Chem. 8, 461–478

22 Evans, D.F., Tominaga, T. and Davis, H.T. (1981) J. Chem. Phys. 74, 1298–1305

23 Phillips, H.O., Marcinkowsky, A.E., Sachs, S B. and Kraus, K.A (1977) J. Phys Chem. 81, 679–682

24 Wojcieszyn, J.W., Schlegel, R.A., Wu, F.-S. and Jacobson, K.A (1981) P.N.A.S. U.S.A. 78, 4407–4410

25 Schurr, J.M. and Schmitz, K.S. (1976) J. Phys Chem. 80, 1934–1936

26 Brändén, C.-I. and Eklund, H. (1980) in Dehydrogenases Requiring Nicotinamide Coenzymes (Jeffery, J., ed), pp 40–84, Birkhäuser Verlag, Basel

Biochimica et Biophysica Acta 911 (1987) 59–65
Elsevier

BBA 32688

Oxidation reaction of human oxyhemoglobin with nitrite: a reexamination

Carla Spagnuolo [a], Paola Rinelli [a], Massimiliano Coletta [a], Emilia Chiancone [a] and Franca Ascoli [b]

[a] *CNR Center of Molecular Biology, Department of Biochemical Sciences, University 'La Sapienza', Rome and*
[b] *Department of Experimental Medicine and Biochemical Sciences, University 'Tor Vergata', Rome (Italy)*

(Received 5 August 1986)

Key words: Oxyhemoglobin oxidation, Nitrite; Oxidation mechanism

The oxidation reaction of human oxyhemoglobin with nitrite is complex and is characterized by a lag period followed by an autocatalytic phase. On the basis of contradictory experimental results, in order to describe the time-course of the reaction, two different mechanisms have been proposed, involving either hydrogen peroxide or the superoxide anion as reaction intermediates. This paper reports a careful reinvestigation of this reaction carried out as a function of reagent concentration, buffer composition, presence of enzymatic scavengers of oxygen radicals or of other compounds which may affect the intermediate steps of the reaction. The results obtained show that: (i) hydrogen peroxide can be definitely identified as the reaction intermediate, in agreement with the mechanism proposed by Kosaka et al. (Biochim. Biophys. Acta 702 (1982) 237–241); (ii) the reaction time-course depends in a different way on the concentrations of hemoglobin and nitrite, a finding that cannot be explained on the basis of this mechanism. A more complex reaction scheme is proposed, that provides a satisfactory description in quantitative terms for all the available experimental data.

Introduction

Conversion of human oxy- to methemoglobin may be easily obtained by addition of oxidizing agents, such as ferricyanide or nitrite. The interest in this latter reagent resides mainly in its ability to penetrate into the erythrocyte, thus allowing the study of methemoglobin generated in situ. Methemoglobin is always present in the blood in small amounts (about 3%) and its level is maintained constant by the methemoglobin reductase system, but increases in a variety of pathological conditions; indeed, the side-products which accompany hemoglobin oxidation, such as hydrogen peroxide, or the oxidizing agents which can produce methemoglobin, such as oxygen radicals generated endogenously or derived from exogenous sources, may be involved in a number of diseases [1].

The oxidation of human oxyhemoglobin with ferricyanide has been well characterized both at equilibrium and kinetically and has been described in terms of a displacement reaction, on the assumption that the bound oxygen and ferricyanide compete for the same site. The stoichiometry is simple: oxidation of oxyhemoglobin requires one equivalent of oxidant per heme iron and the half-time of the reaction depends on the concentration of the reagents as expected for a second-order process [2].

In contrast, the oxidation reaction of oxyhemoglobin by nitrite is complex and the reaction kinetics is characterized by a lag period followed by an autocatalytic phase [3–8]. While the overall

---

Correspondence: Dr. C Spagnuolo, Department of Biochemical Sciences, University 'La Sapienza', Piazzale Aldo Moro 5, 00173 Roma, Italy

0167-4838/87/$03.50 © 1987 Elsevier Science Publishers B V. (Biomedical Division)

stoichiometry has been well established [9], two different mechanisms involving peroxide or superoxide anions as reaction intermediates have been proposed by Kosaka et al. [8] and Tomoda et al. [7], respectively, on the basis of conflicting results concerning the effect of superoxide dismutase and of catalase on the time-course of the reaction. Later, Kosaka et al. [10] established that superoxide anion is generated in the presence of Bistris, but not of phosphate buffer, and confirmed that peroxide is the 'natural' reaction intermediate.

In the framework of a comparative study concerning the oxidation reaction of molluscan hemoglobins, where the sixth ligand of the ferric iron is contributed by the protein [11], the kinetics of the reaction of human oxyhemoglobin with nitrite under a variety of carefully controlled conditions have been reexamined. In particular the overall rate constant was found not to depend in a simple way on the concentration of the two reagents, nitrite and oxyhemoglobin, in contrast to the reaction scheme proposed by Kosaka et al. [8]. On this basis, the oxidation reaction has been investigated as a function of several factors: reagent concentration, presence of superoxide dismutase and catalase, addition of other compounds, such as methemoglobin or cyanide, that should affect the different steps of the reaction according to Kosaka et al. [8]. A more complex mechanism of the oxidation reaction is proposed that provides a satisfactory description in quantitative terms for both the time-course of the reaction and its disparate dependence on the concentration of oxyhemoglobin and nitrite.

Materials and Methods

Human hemoglobin was prepared from fresh blood and stripped of organic and inorganic ions as previously reported [12]. The protein was then freed from catalase and superoxide dismutase by treatment with cellulose DEAE-52 in batch. The resin was equilibrated with 1.5 mM phosphate buffer at pH 6.8 and mixed with the hemoglobin solution dialysed against the same buffer (4 vol. of protein solution per volume of swollen resin), and was stirred gently for 30 min. Under these conditions both catalase and superoxide dismutase are bound to the resin. The supernatant obtained after centrifugation at 1500 rpm for 10 min, contains pure oxyhemoglobin (HbO_2) as indicated by measurements of the catalase and superoxide dismutase activity (see below).

Methemoglobin (Hb^{3+}) was prepared by treating oxyhemoglobin with 5 equivalents of $K_3Fe(CN)_6$ at 25°C for 30 min; the excess of oxidant was removed by gel-filtration on a Sephadex G-25 column.

The concentration of oxyhemoglobin was determined using its molar extinction coefficient (on a heme basis) in phosphate buffer (pH 7.0) at 577 nm ($\epsilon = 14600\ M^{-1} \cdot cm^{-1}$). The concentration of methemoglobin was determined on the basis of the molar extinction coefficient of the deoxy-derivative, obtained by addition of dithionite ($\epsilon = 12000\ M^{-1} \cdot cm^{-1}$ at 555 nm, phosphate buffer at pH 7.0).

Catalase was obtained from Sigma Chemical Co. The catalase assay was performed according to Lück [13]. One unit of catalase activity is defined as the amount of enzyme which decomposes 1.0 μmol of H_2O_2 per min at a starting H_2O_2 concentration of 0.02 M in 0.05 M phosphate buffer at pH 7.0 and 25°C.

Superoxide dismutase was prepared from bovine red cells and was assayed by observing the inhibition of the autoxidation of epinephrine at alkaline pH, according to Misra and Fridovich [14]. One unit of enzymatic activity is defined as the amount of enzyme (usually about 100 ng) which inhibits the reaction by 50%.

Potassium nitrite and hydrogen peroxide solutions were prepared in water just before use. The latter reagent was diluted from a titrated stock (Merck).

The oxidation reactions were initiated by the addition of nitrite to the oxyhemoglobin solution in the desired buffer in thermostatically controlled cuvettes (25°C); the reagents were added to the reaction mixture just before the oxidant, unless otherwise stated. The majority of experiments was performed at pH 7.0 in phosphate buffer of $I = 0.1$ M; alternatively, 0.1 M Tris-HCl or 0.1 M Tris-HCl, containing $1 \cdot 10^{-4}$ or $5 \cdot 10^{-4}$ M inositol hexakisphosphate at the same pH, was used. Methemoglobin formation was followed at a constant wavelength (577 nm) as a function of time.

Spectrophotometric experiments were carried out with a Cary 219 spectrophotometer; a Radiometer pH M 64 was used for the pH measurements.

The time-course of the reaction was fitted to the reaction schemes using a Runge Kutta simulation kinetic program run on a PDP 11/23 computer (Digital Equipment).

Results

The effect of several experimental variables (concentration of the reagents, buffer composition, addition of catalase, superoxide dismutase, hydrogen peroxide, methemoglobin and cyanide) on both the lag period and the autocatalytic phase of the reaction has been examined in phosphate buffer at pH 7.0, unless otherwise stated. The maximum nitrite concentration used in all the experiments was $5 \cdot 10^{-4}$ M in order to minimize the formation of the methemoglobin-nitrite complex whose affinity constant is 340 M^{-1} at pH 7.0 at 25°C [9].

Effect of oxyhemoglobin and nitrite concentration

At a constant concentration of oxyhemoglobin ($1 \cdot 10^{-4}$ M) an increase of the concentration of nitrite (from $2 \cdot 10^{-4}$ to $5 \cdot 10^{-4}$ M) results in a shortening of the lag period, and in a steeper autocatalytic phase (Fig. 1A). On the other hand, variations in protein concentration over the range $(0.12–2.5) \cdot 10^{-4}$ M at a constant concentration of nitrite ($5 \cdot 10^{-4}$ M) lead to smaller changes in the half-time of the reaction (Fig. 1B).

Effect of catalase, hydrogen peroxide and superoxide dismutase

The relevance of hydrogen peroxide in the reaction mechanism was checked in experiments performed in the presence of catalase at a constant protein concentration of $1 \cdot 10^{-4}$ M. When catalase (1800 U) is added before the oxidant, the time-course of the reaction is affected in a different way depending on nitrite concentration (Fig. 2A). Thus there is a very marked increase in the lag phase at a nitrite concentration of $2 \cdot 10^{-4}$ M, but the effect becomes less evident at higher oxidant concentrations ($(3–5) \cdot 10^{-4}$ M). Under the latter conditions a prolongation of the lag phase can be observed only if the amount of catalase is increased 4- to 5-fold (data not shown). In a further set of experiments catalase (1800 U) was added to the reaction mixture (HbO_2 $1 \cdot 10^{-4}$ M, nitrite $2 \cdot 10^{-4}$ M) after the oxidant; a retarding effect is present only when the addition is made during the lag phase (Fig. 2B).

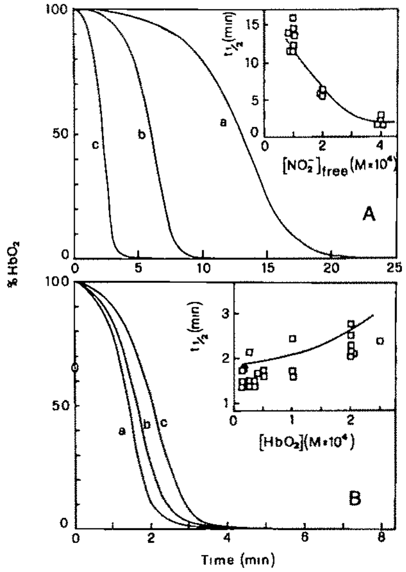

Fig. 1. Effect of nitrite (A) and protein (B) concentration on the time-course of HbO_2 oxidation by nitrite Phosphate buffer, $I = 0.1$ M, pH 7.0. (A) HbO_2, $1 \cdot 10^{-4}$ M; nitrite, $2 \cdot 10^{-4}$ M (a), $3 \cdot 10^{-4}$ M (b), $5 \cdot 10^{-4}$ M (c) (B) Nitrite, $5 \cdot 10^{-4}$ M; HbO_2, $2.5 \cdot 10^{-5}$ M (a), $1 \cdot 10^{-4}$ M (b), $2 \cdot 10^{-4}$ M (c). Insets: half-time of the reaction as a function of free nitrite (A) or of HbO_2 (B) concentration. The experimental points were obtained with different hemoglobin preparations; the curves are theoretical ones calculated on the basis of the proposed reaction scheme (see text) The values of the apparent rate constants used are: $8 \cdot 10^{-4}$ s^{-1} (reaction (9)), 240 $M^{-1} \cdot s^{-1}$ (reaction (10)), 300 $M^{-1} \cdot s^{-1}$ (reaction (3)), 4 $M^{-1} \cdot s^{-1}$ (reaction (4)), $8 \cdot 10^{5}$ M^{-1} s^{-1} (reaction (5)), $8 \cdot 10^{-4}$ s^{-1} (reaction (7))

The involvement of hydrogen peroxide is apparent also in experiments in which substoichiometric amounts of this compound were added to the oxyhemoglobin solution just before the addition of nitrite. Hydrogen peroxide affects mainly the lag period, in agreement with previous data [6,10,15] and the effect depends on both hydrogen peroxide and nitrite concentration (Fig. 3A, B). Under the conditions used, the amount of oxyhemoglobin oxidized by hydrogen peroxide in the absence of nitrite is negligible, as already described in Ref. 6.

The presence of superoxide dismutase (1200 U)

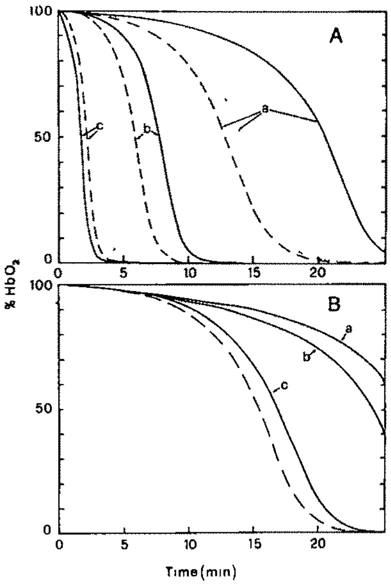

Fig. 2 Effect of catalase and superoxide dismutase on the time-course of HbO$_2$ oxidation by nitrite HbO$_2$ $1\cdot 10^{-4}$ M, phosphate buffer $I = 0.1$ M, pH 7.0. (A) nitrite, $2\cdot10^{-4}$ M (a), $3\cdot10^{-4}$ M (b), $5\cdot10^{-4}$ M (c); control (------), plus catalase, 1800 U (———); plus superoxide dismutase, 1200 U (····). (B) Nitrite, $2\cdot10^{-4}$ M Control (------) Addition of catalase (1800 U): at zero time (a), at 5 min (b) and at 15 min (c)

does not affect the time-course of the oxidation reaction significantly (Fig. 2A), as expected on the basis of published data in phosphate buffer [10].

Effect of methemoglobin and cyanide

In view of the proposed involvement of methemoglobin in the onset of the autocatalytic phase [8], methemoglobin was added to the reaction mixture before nitrite (HbO$_2$ $1\cdot10^{-4}$ M; nitrite $2\cdot10^{-4}$ M; met-Hb $1\cdot10^{-4}$ M). Under these conditions, addition of methemoglobin induces a shortening of the lag period, but leaves the second phase essentially unaffected (Fig. 4A). At higher nitrite concentrations ($5\cdot10^{-4}$ M), no effect of methemoglobin is detectable (data not shown).

In another set of experiments, cyanide, at concentrations ranging from $2\cdot10^{-4}$ to $2\cdot10^{-3}$ M was added to oxyhemoglobin solutions ($1\cdot10^{-4}$ M) before nitrite ($2\cdot10^{-4}$ M). Fig. 4B shows that the half-time of the reaction increases with increase in cyanide concentration, in agreement with previous data [8].

Lastly H$_2$O$_2$ (0.1 and 0.2 equiv./heme) and methemoglobin ($1\cdot10^{-4}$ M) were both added to oxyhemoglobin ($1\cdot10^{-4}$ M) before nitrite ($2\cdot10^{-4}$ M) in order to establish whether their effect on the lag phase is additive. The additional presence of methemoglobin results in a further shortening of the lag period with respect to that produced by hydrogen peroxide alone (Fig. 3B).

Effect of buffer composition

The effect of buffer composition on both the lag and the autocatalytic phase was studied in parallel experiments carried out in Tris-HCl and phosphate buffers. In addition the influence of

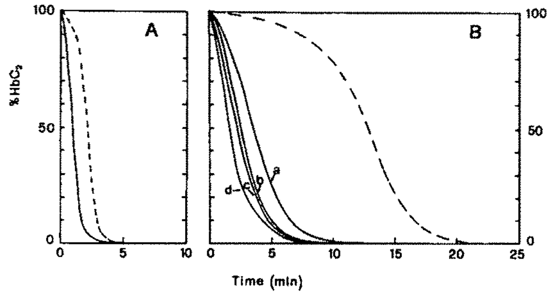

Fig 3 Effect of hydrogen peroxide and methemoglobin addition on the time-course of HbO$_2$ oxidation by nitrite. Phosphate buffer, $I = 0.1$ M, pH 7.0. HbO$_2$, $1\cdot10^{-4}$ M. (A) Nitrite, $5\cdot10^{-4}$ M without (------) and with (———) H$_2$O$_2$, $1\cdot 10^{-5}$ M (B) Nitrite, $2\cdot10^{-4}$ M; control (------); plus H$_2$O$_2$, $1\cdot10^{-5}$ M (a), $2\cdot10^{-5}$ M (b); plus met-Hb, $1\cdot10^{-4}$ M and H$_2$O$_2$, $1\cdot10^{-5}$ M (c); plus met-Hb, $1\cdot 10^{-4}$ M and H$_2$O$_2$, $2\cdot10^{-5}$ M (d).

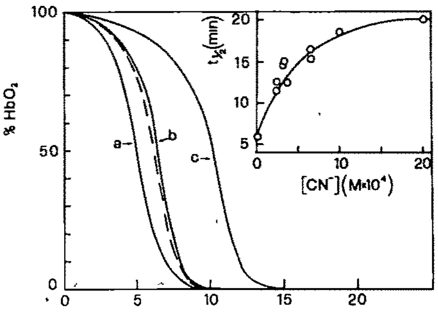

Fig. 4. Effect of methemoglobin or cyanide addition on the time-course of HbO$_2$ oxidation by nitrite Phosphate buffer, $I = 0.1$ M, pH 7.0. HbO$_2$, $1\cdot10^{-4}$ M; nitrite, $2\cdot10^{-4}$ M; control (------); plus met-Hb, $1\cdot10^{-4}$ M (a); plus cyanide, $2.5\cdot10^{-4}$ M (b) and $2\cdot 10^{-3}$ M (c) Inset: half-time of the reaction as a function of cyanide concentration

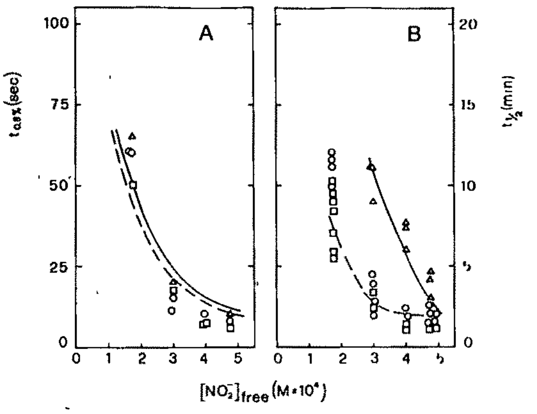

Fig 5. Effect of buffer composition on the initial velocity (A) and on the half-time (B) of the HbO_2 oxidation by nitrite. Buffers: phosphate, $I = 0.1$ M, pH 7.0 (○); Tris-HCl, 0 1 M, pH 7.0 without (□), and with $1 \cdot 10^{-4}$ M or $5 \cdot 10^{-4}$ M inositol hexakisphosphate (△). The experimental points were obtained at HbO_2 concentrations ranging from $1.2 \cdot 10^{-5}$ M and $2 \cdot 10^{-4}$ M. The curves are theoretical ones calculated on the basis of the proposed reaction scheme (see text) for the data measured in the absence (------) and in the presence (———) of inositol hexakisphosphate For (------) the values of the apparent rate constants are given in Fig. 1; for (———) the values used are: $5.5 \cdot 10^{-4}$ s^{-1} (reaction (9)), 275 $M^{-1} \cdot s^{-1}$ (reaction (10)), 275 M^{-1} s^{-1} (reaction (3)), 0.55 $M^{-1} \cdot s^{-1}$ (reaction (4)), $5.5 \cdot 10^3$ $M^{-1} \cdot s^{-1}$ (reaction (5)), $5.5 \cdot 10^{-4}$ s^{-1} (reaction (7))

inositol hexakisphosphate was investigated, since this allosteric effector is known to shift the conformational equilibrium towards the T-state in met-, but not in oxyhemoglobin [17]. Fig. 5 shows the dependence of the initial velocity (expressed as $t_{0.5\%}$) and of the overall rate (expressed as $t_{1/2}$) on nitrite concentration in the different buffer systems. While the values of $t_{0.5\%}$ are essentially unaffected by buffer composition, the $t_{1/2}$ values are significantly higher in the presence of initial hexakisphosphate, in agreement with earlier observation of Tomoda and Yoneyama [18].

Discussion

The stoichiometry of the overall oxidation reaction of human hemoglobin by nitrite has been definitively established [9] and can be described as follows:

$$4HbO_2 + 4NO_2^- + 4H^+ \rightarrow 4Hb^{3+} + 4NO_3^- + O_2 + 2H_2O \quad (1)$$

On the other hand, despite numerous studies, the reaction mechanism has not been fully elucidated. Thus, contradictory results concerning the nature of the intermediates formed during the lag phase have led to the proposal of two different mechanisms based on the involvement of superoxide or peroxide anions, respectively. Tomoda et al. [7] claimed that superoxide anion ($O_2^{\cdot -}$) is formed during the lag period, since they observed that in Bistris buffer superoxide dismutase induced a lengthening of the lag phase and that catalase had almost no effect on the time-course of the reaction.

A quite different mechanism has been proposed by Kosaka et al. [8] who observed that, in phosphate buffer, the time-course of the reaction is not affected by superoxide dismutase or other $O_2^{\cdot -}$ scavengers, and that catalase did prolong the lag phase. Hence, in their scheme hydrogen peroxide is generated during the lag phase concomitantly with methemoglobin and $NO_2^{\cdot}$:

$$3HbO_2 + 3NO_2^- + 6H^+ \rightarrow 3Hb^{3+} + 3NO_2^{\cdot} + 3H_2O_2 \quad (2)$$

Subsequently methemoglobin and hydrogen peroxide give rise to an EPR-detectable ferryl hemoglobin radical:

$$3Hb^{3+} + 3H_2O_2 \rightarrow 3Hb^{\cdot 4+} + 3H_2O \quad (3)$$

This reaction provides the basis for the autocatalytic phase which comprises several steps involving ferryl hemoglobin and nitrite:

$$3Hb^{\cdot 4+} + 3NO_2^- + 3H^+ \rightarrow 3Hb^{4+} + 3NO_2^{\cdot} \quad (4)$$

$$3Hb^{4+} + 3NO_2^- + 3H^+ \rightarrow 3Hb^{3+} + 3NO_2^{\cdot} + 3H_2O \quad (5)$$

$$HbO_2 + NO_2^{\cdot} \rightarrow Hb^{3+} + O_2 + NO_2^- \quad (6)$$

The chain termination reaction is represented by:

$$8NO_2^{\cdot} + 4H_2O \rightarrow 4NO_2^- + 4NO_3^- + 8H^+ \quad (7)$$

In a later paper, Kosaka and Tyuma [10] explained the different effect of superoxide dismutase in phosphate and Bistris buffer as due to the generation of superoxide anion upon reduction of O_2 by a radical derived from Bistris. However, these Authors did not provide an explanation for the conflicting results concerning the effect of catalase described in Refs. 7 and 8. The data of Fig. 2, obtained with oxyhemoglobin carefully freed from both catalase and superoxide dismutase, focus on this particular point. The effect of catalase (1800 U) appears to depend on the concentration of nitrite. Thus, at the low nitrite concentrations ($(2–3) \cdot 10^{-4}$ M) used by Kosaka et al. [8], there is a lengthening of the lag phase; on the other hand, at a nitrite concentration of $5 \cdot 10^{-4}$ M, there is a negligible effect of the enzyme, as found by Tomoda et al. [7]. At this latter concentration a significant prolongation of the lag phase may be obtained if the catalase concentration is increased about 4–5-fold. Therefore, the present data explain the contradictory results just mentioned [7,8] in terms of a competition between catalase and methemoglobin for H_2O_2. On this basis, the availability of the latter compound for the formation of the ferryl radical (reaction (3)) involved in the autocatalytic phase, depends on the experimental conditions, i.e., on the relative concentrations of oxyhemoglobin and catalase.

The effect of catalase and the composite experimental findings obtained upon addition of methemoglobin (Fig. 4) and of substoichiometric amounts of H_2O_2 (Fig. 3), which shorten the lag phase, and of cyanide, which lengthens the lag phase (Fig. 4), agree qualitatively with the expectations based on reactions (2) and (3) and on the subsequent steps of the oxidation mechanism proposed by Kosaka et al. [8].

However, from a quantitative viewpoint, the present findings on the effect of exogenous methemoglobin and hydrogen peroxide cannot be explained in terms of the above-mentioned scheme. Thus, in contrast to the prediction of reactions (2) and (3), the lag phase is shortened much less by addition of 1 equiv./heme of methemoglobin than by that of 0.1 equiv./heme of hydrogen peroxide. Moreover, the reaction scheme requires the time-course to depend in a similar way on the concentrations of the two reagents, oxyhemoglobin and nitrite. In contrast, the overall reaction velocity does not vary as expected as a function of the concentration of oxyhemoglobin.

Additional steps have to be introduced to account for these experimental findings. In particular, the observed dependence of the overall reaction rate on the concentration of oxyhemoglobin implies that this species is not oxidized directly. It may be envisaged that nitrite displaces the bound dioxygen giving rise to $HbNO_2^-$ that is in fast equilibrium with oxyhemoglobin. $HbNO_2^-$ could behave as an activated species which may be readily oxidized and may also act as the catalyst for the oxidation of nitrite to $NO_2^{\bullet}$. The latter reaction occurs concomitantly with the reduction of dioxygen to hydrogen peroxide. As to the nature of the oxidant, recent experimental evidence points to the direct involvement of $NO_2^{\bullet}$, since amines, which are known to react with $NO_2^{\bullet}$ to yield nitrosamines, inhibit the oxidation reaction [19]. In particular, among the primary amines, the most powerful inhibitors are represented by the least basic ones (e.g., aniline) which are known to form nitrosamines most rapidly [20]. According to this view, in the presence of amines the overall rate of the oxidation reaction is determined mainly by their interaction with $NO_2^{\bullet}$ rather than by their inhibition of the peroxide compound formation as proposed by Kosaka and Uozumi [19].

On the basis of these considerations, the initial steps of the oxidation reaction can be described as

$$4HbO_2 + 4NO_2^- \leftrightarrows 4HbNO_2^- + 4O_2 \tag{8}$$

$$3HbNO_2^- + 3O_2 + 6NO_2^- + 6H^+ \rightarrow 3HbNO_2^- + 6NO_2^{\bullet} + 3H_2O_2 \tag{9}$$

$$4HbNO_2^- + 4NO_2^{\bullet} \rightarrow 4Hb^{3+} + 8NO_2^- \tag{10}$$

These steps substitute reactions (2) and (6) in the scheme of Kosaka et al. [8] reported above. With an appropriate choice of constants (see insets of Figs. 1 and 6), the proposed scheme describes the observed dependence of the reaction time-course on the concentrations of both nitrite and oxyhemoglobin. It may be noticed that the rate constant of reaction (3) used in the simulation procedure corresponds closely to the value determined experimentally for the reaction of metmyoglobin with hydrogen peroxide [21].

Lastly the effect of inositol hexakisphosphate on the oxidation reaction deserves a comment. The data summarized in Fig. 5 clearly show that inositol hexakisphosphate influences mainly the autocatalytic phase in line: (i) with the knowledge that this allosteric effector shifts significantly the conformational equilibrium in the case of met-

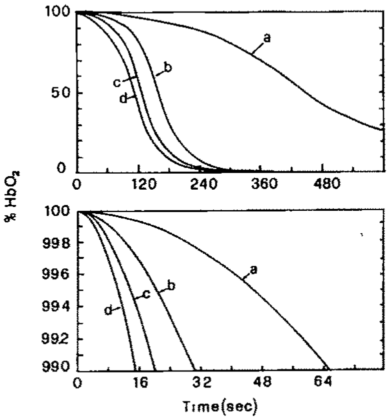

Fig 6. Time-course of the oxidation reaction of HbO_2 by nitrite in phosphate buffer simulated according to the proposed scheme (see text) For the values of the rate constants used, see Fig 1. (a) HbO_2, 0 25·10^{-4} M, nitrite, 2·10^{-4} M; (b) HbO_2, 2·10^{-4} M, nitrite 5·10^{-4} M; (c) HbO_2, 1·10^{-4} M, nitrite, 5 10^{-4} M, (d). HbO_2, 0.25·10^{-4} M, nitrite 5·10^{-4} M. Note that the lower panel expands the origin region of the upper panel.

and not of oxyhemoglobin [17] and (ii) with the involvement of methemoglobin in the autocatalysis. In turn, the data indicate that methemoglobin in the T-state is endowed with a decreased reactivity. The theoretical curves shown in Fig. 5, which describe the dependence of the initial velocity and of the half-time of the oxidation reaction as a function of nitrite concentration in the presence of inositol hexakisphosphate, were obtained by decreasing the rates of reactions (4) and (5) as indicated in the figure legend.

In conclusion, the present data demonstrate that the complex oxidation mechanism of oxyhemoglobin by nitrite results in a disparate dependence of the overall rate of the reaction on the concentration of the reagents; they confirm also that H_2O_2 is the reaction intermediate and suggest that the only oxidant in the reaction is $NO_2^{\cdot}$. Moreover, they provide an explanation for the conflicting literature data concerning the effect of catalase on the time-course of the reaction.

References

1 Kiese, M. (1974) Methemoglobinemia: A Comprehensive Treatise, CRC Press, Cleveland
2 Antonini, E., Brunori, M. and Wyman, J (1965) Biochemistry 4, 545–551
3 Jung, F and Remmer, H. (1949) Arch Exp Pathol Pharmakol 206, 459–474
4 Rodkey, F.L (1976) Clin Chem 22, 1986–1990
5 Wallace, W.J and Caughey, W.S. (1975) Biochem. Biophys Res Commun. 62, 561–567
6 Doyle, M.P, Pickering, R A., Dykstra, R.L., Nelson, C L and Boyer, R F. (1982) Biochem. Biophys. Res Commun. 105, 127–132
7 Tomoda, A., Tsuji, A and Yoneyama, Y (1981) Biochem J. 193, 167–179
8 Kosaka, H., Imaizumi, K and Tyuma, I (1982) Biochim Biophys Acta 702, 237–241
9 Kosaka, H, Imaizumi, K., Imai, K and Tyuma, I (1979) Biochim Biophys. Acta 581, 184–188
10 Kosaka, H and Tyuma, I. (1982) Biochim Biophys. Acta 709, 187–193
11 Spagnuolo, C., Ascoli, F., Chiancone, E., Vecchini, P and Antonini, E. (1983) J. Mol. Biol 164, 627–644
12 Berger, R.Z., Carpenter, L., Everse, J and Kaplan, J.L (1973) Anal. Lett. 6, 125–129
13 Luck, H. (1963) in Methods of Enzymatic Analysis (Bergmeyer, H U., ed.), pp. 885–888, Academic Press, New York
14 Misra, H.P. and Fridovich, I. (1972) J. Biol. Chem 247, 3170–3175
15 Jung, F. and Kahl, R. (1967) Acta Biol Med. Ger 19, 853–868
16 Eyer, P., Hertle, H, Kiese, M. and Klein, G. (1975) Mol Pharmacol. 11, 326–334
17 Perutz, M F, Fersht, A.R., Simon, S R. and Roberts, C K (1974) Biochemistry 13, 2174–2186
18 Tomoda, A. and Yoneyama, Y. (1979) Experientia 35, 15–16
19 Kosaka, H. and Uozumi, M (1986) Biochim. Biophys. Acta 871, 14–18
20 Challis, B.C. (1981) in Safety Evaluation of Nitrosatable Drugs and Chemicals (Gibson, G.G and Ioannides, C, eds.), pp 16–55, Taylor and Francis, London
21 Yonetani, T. and Schleyer, H (1967) J Biol. Chem. 242, 1974–1979

Biochimica et Biophysica Acta 911 (1987) 66–70
Elsevier

BBA 32687

Comparison of the kinetic behavior of human and bovine proteins in the heparin-catalyzed antithrombin III / thrombin reaction

Mark T. Cunningham and Gary L. Nelsestuen

Department of Biochemistry, University of Minnesota, St. Paul, MN (U.S.A.)

(Received 8 April 1986)
(Revised manuscript received 30 September 1986)

Key words: Thrombin; Heparin; Antithrombin III; Proteinase inhibitor; (Human, Bovine)

Significant differences between saturation kinetic properties of heparin-stimulated reactions between thrombin and antithrombin III from human and bovine species were observed. In both systems, the apparent K_m for antithrombin III was higher than the K_D for antithrombin III-heparin interaction, monitored by intrinsic protein fluorescence change. The K_m for thrombin and k_{cat} were much higher for proteins of the human species than the bovine species. The apparent K_m for one human protein was dependent on the concentration of the other human protein, indicating interaction of the binding events. The reaction product formed from the bovine proteins was a potent inhibitor of the reaction but the product from the human proteins was a poor inhibitor. The major differences between the two species appeared to be related to interaction of thrombin or thrombin derivatives with heparin or heparin-antithrombin III complexes.

Introduction

The heparin-catalyzed reaction between antithrombin III and certain proteinases is an unusual event where a polysaccharide can be viewed as the catalyst of a reaction between an enzyme and an irreversible inhibitor of that enzyme. Modelling this reaction by standard saturation kinetic analysis appears possible, with the proteins occupying the role of the substrates and the polysaccharide assuming the role of the enzyme [1,2]. Some striking properties found for proteins from the bovine species, such as an extremely low K_m for thrombin (under 2 nM) and a low k_{cat} (about 0.3 s^{-1}) [1,2], have not been observed for human proteins, where K_m values have varied from 7 nM to as high as 4 μM [3–9]. Various studies have estimated a k_{cat} for the human proteins of about 50 to 800 min^{-1} [3–9]. Perhaps these variations arise from differences in assay methods or conditions. The studies reported below utilize similar conditions and methods to compare reactions of the human and bovine proteins. The results indicate major differences between the kinetic properties for proteins from these two species. The results show that detailed cross-species comparisons of kinetic properties are not appropriate. Coordinate study of these two systems may provide a basis for comparisons and determination of the range of heparin function.

Materials and Methods

Bovine α-thrombin and bovine antithrombin III were isolated and assayed as previously described [1]. Human thrombin was purchased from the Sigma Chemical Co., and was reported to be over 80% pure by gel electrophoresis with a specific

---

Abbreviation TLCK, *N*-α-*p*-tosyl-L-lysine chloromethyl ketone.

Correspondence: M.T Cunningham, Department of Biochemistry, University of Minnesota, 1479 Gortner Avenue, St. Paul, MN 55108, U.S.A.

0167-4838/87/$03.50 © 1987 Elsevier Science Publishers B.V (Biomedical Division)

activity of 3000 NIH units/mg. Highly purified human antithrombin III was a gift from the American Red Cross, and was further purified by gel-filtration chromatography on a Bio-Gel A-0.5 m column before use.

Active-site-blocked thrombins (bovine and human) were prepared by incubating the purified proteases with 1 mM TLCK (Sigma) in a buffer of 0.1 M Tris (pH 8.4)/0.1 M NaCl/0.1% poly(ethylene glycol) 6000 (Sigma) at 25°C for 24 h. This was followed by dialysis in the same buffer to remove unreacted TLCK. No amidolytic activity could be detected after this reaction time.

Bovine and human antithrombin III-thrombin complexes (product) were prepared by incubating antithrombin III and thrombin in a 2 : 1 (antithrombin III : thrombin) molar ratio at 25°C until less than 2% of the original thrombin activity remained. The final product concentration was assumed to be equal to the total thrombin concentration in the reaction mixture. Extinction coefficients ($E_{1\%,280\mathrm{nm}}$) for determining protein concentrations were 19.5 for thrombin [10] and 6.1 for antithrombin III [11].

Porcine mucosal heparin was donated by Riker Laboratories, 3M Company (Northridge, CA), with a reported specific activity of 161 units/mg. This unfractionated heparin was used in all antithrombin III/thrombin reactions. The molar concentration of heparin was determined by titrating the heparin-induced fluorescence change of antithrombin III by the method of Nordenmann and Bjork [12], assuming that heparin bound to antithrombin III in a 1 : 1 molar ratio.

The antithrombin III/thrombin reaction was performed by adding thrombin to a mixture of antithrombin III and heparin (or antithrombin III, inhibitor, and heparin) in 0.05 M Tris (pH 8.4)/0.1 M NaCl/0.1% poly(ethylene glycol) 8000 at 25°C. At timed intervals, a solution of Polybrene was added to the reaction mixture (1.0 mg/ml final concentration) to quench the heparin-catalyzed reaction. The remaining thrombin concentration was determined by adding the chromogenic substrate S-2288, *H*-D-isoleucyl-L-prolyl-L-arginine *p*-nitroanilide dihydrochloride (Helena Laboratories), to the quenched reaction mixture (the final concentration of S-2288 was 100 μM), followed by continuously recording the absorbance of the mixture at 405 nm. The concentration of thrombin was determined from the velocity of *p*-nitroaniline ($E_{405\mathrm{nm}} = 1.06 \cdot 10^4$ $\mathrm{M}^{-1} \cdot \mathrm{cm}^{-1}$) liberation from S-2288. The k_{cat} values for thrombin acting on S-2288 were 100 s^{-1} and 54 s^{-1} at 25°C for the bovine and human protein, respectively.

The initial velocity of the heparin-catalyzed antithrombin III/thrombin reaction (in the presence and absence of inhibitor) was estimated from thrombin activity vs. time plots. Between 20% and 30% of the total thrombin was inactivated in the time required to get accurate initial velocities and the velocities are therefore approximate initial velocities. All velocities were corrected for the heparin-independent reaction. The error bars shown in the text figures represent the standard deviation of 3–6 velocity measurements. The data points without error bars had negligible error.

Results

The apparent K_m for human antithrombin III was dependent on the thrombin concentration (Fig. 1A). A 5-fold increase in thrombin concentration caused a 2.3-fold increase in the apparent K_m for antithrombin III and a 3-fold increase in the apparent $V_{\max}$. This result indicated that antithrombin III and thrombin binding to heparin were interrelated. At 120 nM antithrombin III, the apparent K_m for thrombin was 21 nM (Fig. 1B).

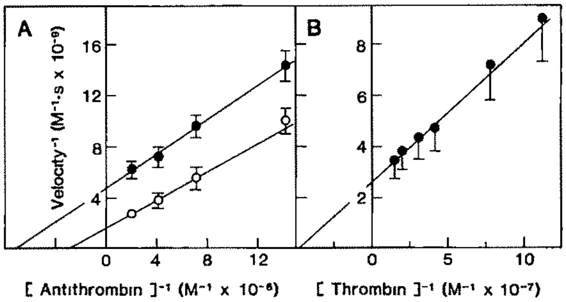

Fig 1 Double-reciprocal plot of the initial velocities of the heparin catalyzed human antithrombin III/thrombin reaction In part A, heparin (0.92 nM) was incubated with varying amounts of antithrombin III at 23°C, and the reaction was started by adding 5 nM (●) or 25 nM (○) thrombin In part B heparin (1 0 nM) and human antithrombin III (120 nM) were incubated at 25°C. The reaction was started by adding varying amounts of thrombin.

For the bovine proteins, the heparin-dependent reaction was saturated with respect to thrombin at the accessible thrombin concentrations (Ref. 1 and Fig. 2) and active site blocked thrombin was a potent reaction inhibitor. Additional thrombin overcame the inhibition by TLCK-thrombin (Fig. 2) suggestive of competitive inhibition by TLCK-thrombin. However, in both the presence and absence of the inhibitor, high thrombin concentrations inhibited the reaction. This behavior prevented more thorough analysis of the inhibitory properties of TLCK-thrombin.

Inhibition of the reactions by TLCK-thrombin was observed for proteins of both species (Fig. 3). The inhibition characteristics were different for the two systems. For the bovine proteins, relative inhibition was greater at high antithrombin III concentrations, while inhibition of the human protein reaction was best observed at low antithrombin III concentrations. Unfortunately, accurate kinetic studies could not be conducted at higher inhibitor concentrations because the reaction velocity of the heparin-independent reaction became a major portion of the total reaction velocity. Therefore, inhibition constants for the interaction between TLCK-thrombin and the heparin-antithrombin III complex could not be rigorously determined.

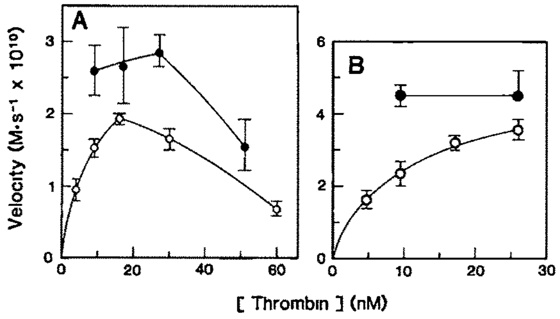

Fig 2. Inhibition of the heparin-catalyzed bovine antithrombin III/thrombin reaction by TLCK-thrombin (part A) or by reaction product (part B). Heparin (6.0 nM) and antithrombin III (60 nM) were incubated at 25°C in the absence (●) or presence of 40 nM (○) TLCK-thrombin The reaction was initiated by adding varying amounts of thrombin. Similar velocities were obtained if antithrombin III was added last or if thrombin plus TLCK-thrombin were added last. In part B, heparin (6.0 nM) and antithrombin III (120 nM) were incubated at 25°C in the absence (●) or presence of 20 nM (○) product. The reaction was started by adding varying amounts of thrombin.

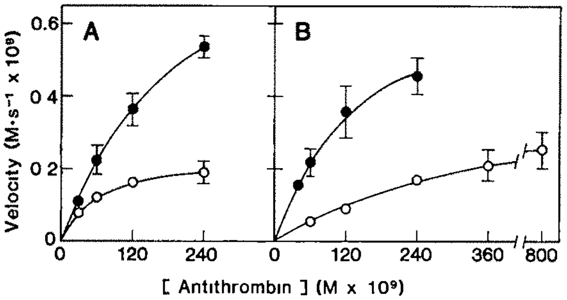

Fig. 3. Inhibition of the heparin-catalyzed antithrombin III/thrombin reactions by TLCK thrombin. In part A heparin (6.0 nM) and varying amounts of bovine antithrombin III were incubated at 25°C in the absence (●) or presence of 36 nM (○) bovine TLCK-thrombin The reaction was started by adding 9.6 nM bovine thrombin. In part B heparin (1.0 nM) and varying amounts of human antithrombin III were incubated at 25°C in the absence (●) or presence (○) of 100 nM human TLCK-thrombin. The reaction was started by adding 24 nM human thrombin

Like TLCK-thrombin, the product of reaction between the bovine proteins was a potent inhibitor (Fig. 2B). Evidence indicating that the product undergoes self-association and aggregation with heparin [14,15] makes it difficult to establish which product species was the true inhibitor.

The reaction product of the human proteins was a poor inhibitor of the reaction. Only 26% of the initial velocity was inhibited at 1 nM heparin, 120 nM antithrombin III, 11 nM thrombin and 240 nM product preparation (25°C). In contrast, the bovine reaction product caused 50% inhibition at a concentration of 20 nM (Fig. 2B).

Discussion

These studies have identified significant species differences between the human and bovine antithrombin III/thrombin proteins in reaction with heparin. In the bovine system the K_m for thrombin was low (under 2 nM estimate), the k_{cat} was also low (0.16 s^{-1}) [1,2] and the K_m for antithrombin III was 150–250 nM [1,2,16]. For the human proteins, the apparent K_m for thrombin and the apparent k_{cat} were much higher. These latter observations agree qualitatively with other studies utilizing the human proteins [3–8]. In our study, the apparent K_m value for one protein varied with the concentration of the second protein. Several previous studies on the human proteins assumed non-interacting binding but did not test this assumption [3–6]. Estimations of the true K_m and k_{cat} values (i.e., the K_m and k_{cat} value at saturating fixed substrate) were not made for the human proteins in our studies due to limitations in the substrate concentrations available to the experimental approach used. However, the results indicated that the true K_m for human antithrombin III was greater than 300 nM.

The K_m is greater than the K_D for the antithrombin III-heparin binding that produces the antithrombin III fluorescence enhancement. The latter is about 30 nM under the conditions of this experiment [3] and this is similar to values for the bovine protein [1,2]. One explanation for this result that has been presented for reactions of the bovine proteins is that k_{cat}/K_m is a diffusionally controlled parameter [1,2]. Alternatively, it is possible that the antithrombin III-heparin binding event monitored by fluorescence change does not correspond to the substrate addition step in the kinetic reaction. Results supporting the latter conclusion have been presented by Evington et al. [8]. In fact, two lines of evidence indicate the spectroscopically silent addition of a second antithrombin III molecule to the antithrombin III-heparin complex [8,14,15].

Evington et al. [8] have recently provided a two-substrate kinetic analysis of this reaction using human proteins. Fluorescent-labeled protein was used to observe product formation. The K_m for antithrombin III was high (0.5–2 μM), which agreed qualitatively with our result at high thrombin concentration. However, Evington et al. [8] did not observe interactive binding events for thrombin and antithrombin; the K_m for antithrombin was independent of the thrombin concentration. This contrasted with our result. In addition, the K_m for antithrombin obtained by Evington et al. [8] was much higher than the apparent K_m values for antithrombin obtained in several previous studies (refs. 3–6, $K_m = 0.03–0.2$ μM). These latter values are similar to our data obtained at low thrombin concentrations. In fact, there may be a general correlation between the observed K_m for antithrombin and the thrombin concentration used in the analysis. However, such an explanation is not sufficient, since apparent k_{cat} values in the different studies are relatively constant at about 1 to 5 s^{-1}, despite very different antithrombin concentrations used; the studies giving higher K_m values for antithrombin [8] would predict much lower apparent k_{cat} values at the 0.03–0.2 μM antithrombin concentrations used in the other studies [3–6]. The differences may arise from artifacts associated with the use of different techniques or from concentration-dependent changes in kinetic mechanism. Protein concentrations used to obtain the very different results did not overlap. High thrombin concentrations (over 50 nM) provided a high K_m for antithrombin and noninteractive sites [8] while low thrombin concentrations (2–25 nM) gave low K_m values for antithrombin [3–6]. Unfortunately, the protein concentrations used may be limited by the methodologies and direct comparison of different techniques at the same protein concentrations may pose acute difficulties.

Similar problems arise in comparison of the observed K_m for human thrombin. One set of observations, obtained with two-stage assay methods and with single, relatively low antithrombin concentrations, gave apparent K_m values of 7–25 nM [3–6]. Other values using alternative assay methods and different conditions including a higher range of protein concentrations, gave K_m values for thrombin of 0.2–2 μM [8] and 4 μM [9]. Once again, these differences could be due to the assay procedure or to concentration-dependent changes in kinetic mechanism. Further studies are needed to determine the basis for these different values and kinetic properties.

Overall, this study showed surprising differences in the manner in which proteins of two species interact kinetically with porcine heparin. While other sources for these differences such as purification methodologies cannot be ruled out, high protein purity makes such explanations seem unlikely. All of the major species differences (substrate inhibition, K_m for thrombin, inhibition by product) involve thrombin or thrombin conjugates. Direct molecular weight studies also showed substantial species differences in the manner of interaction of thrombin conjugates with heparin [14,15]. The kinetic results could therefore be related to species differences in the thrombin-heparin interaction involving thrombin from the two species. In all cases, the bovine protein would have substantially tighter interaction. These differences may serve a valuable function and continued evaluation of both species may allow more in-depth understanding of heparin function.

Acknowledgement

This work was supported in part by grant number HL26989 from the National Institutes of Health.

References

1 Pletcher, C H. and Nelsestuen, G L. (1982) J. Biol. Chem 257, 5342–5345
2 Pletcher, C.H. and Nelsestuen, G.L (1983) J Biol Chem 258, 1086–1091
3 Griffith, M.J. (1983) Proc. Natl Acad Sci. USA 80, 5460–5464
4 Scully, M.F. and Kakkar, V.V. (1984) Biochem. J. 218, 657–665
5 Griffith, M.J. (1982) J. Biol. Chem. 257, 13899–13922
6 Griffith, M.J. (1982) J. Biol. Chem. 257, 7360–7365
7 Hoylaerts, M., Owen, M G. and Collen, D. (1984) J Biol Chem. 254, 5670–5677
8 Evington, J.R.N., Feldman, P A , Luscombe, M and Holbrook, J.J. (1986) Biochim. Biophys. Acta 870, 92–101
9 Olson, S.T. and Shore, J D. (1982) J. Biol Chem. 257, 14891–14895
10 Mann, K.G (1976) Methods Enzymol. 45, 123–156
11 Miller-Andersson, M , Borg, H and Andersson, L.-O (1974) Thromb. Res. 5, 439–452
12 Nordenmann, B and Bjor, I. (1978) Biochemistry 17, 3339–3344
13 Segel, I.H (1975) Enzyme Kinetics, John Wiley & Sons, New York
14 Pletcher, C., Cunningham, M. and Nelsestuen, G (1985) Fed. Proc. 44, 1071
15 Pletcher, C., Cunningham, M and Nelsestuen, G L. (1986) J. Biol. Chem. 261, 4143–4147
16 Pletcher, C.H., Cunningham, M. and Nelsestuen, G. (1985) Biochim Biophys. Acta 838, 106–113

Biochimica et Biophysica Acta 911 (1987) 71–80
Elsevier

BBA 32597

The electronic and magnetic properties of rubredoxin: a low-temperature magnetic circular dichroism study

Deborah E. Bennett and Michael K. Johnson

Department of Chemistry, Louisiana State University, Baton Rouge, LA 70803 (U.S.A.)

(Received 5 June 1986)

Key words: Metalloprotein; Charge transfer; Magnetic circular dichroism;
Low temperature; Rubredoxin; Fe-S cluster

Oxidized rubredoxin from *Clostridium pasteurianum* has been investigated by magnetic circular dichroism (MCD) spectroscopy over the temperature range 1.5 to 150 K and at magnetic fields between 0 and 4.5 tesla. The results show that studies of the temperature and field dependence of MCD transitions afford insight into the polarization of electronic transitions for ground states with large *g*-value anisotropy, in addition to estimates of ground-state *g* values and zero-field splitting parameters. In agreement with the assignment made by Eaton and Lovenberg (Eaton, W.A. and Lovenberg, W. (1973) in Iron-Sulfur Proteins, Vol. II (Lovenberg, W., ed.), pp. 131–162, Academic Press, New York), the ultraviolet-visible spectrum of oxidized rubredoxin is assigned to two S → Fe(III) charge transfer transitions (both $^6A_1 \rightarrow {}^6T_2$ under tetrahedral symmetry), each spanning a range of 650–430 nm and 430–330 nm, respectively. The observed splitting in each of these transitions is attributed to a predominant axial distortion in the excited state resulting in effective D_{2d} symmetry.

Introduction

Over the past decade, low-temperature magnetic circular dichroism (MCD) spectroscopy has emerged as a valuable method for investigating the electronic and magnetic properties of paramagnetic transition metal centers in metalloproteins [1,2]. In addition to its well-established role in assigning electronic transitions, the technique has been shown to be effective in determining electronic ground-state parameters for paramagnetic chromophores by detailed studies of the magnetic field and temperature dependence of discrete MCD transitions. The type of ground state information that is available includes spin state, effective *g* values, zero-field splitting parameters, and magnetic coupling constants (for examples see Refs. 3–9). Thus MCD magnetization data afford an important link between optical and EPR spectroscopy and a means of selectively investigating the magnetic properties of individual metal centers in a multicenter enzyme or protein. Moreover, the technique is particularly useful for investigating paramagnetic centers that are EPR-silent due to zero-field splittings (e.g. reduced [3Fe-xS] clusters [5]) or magnetic interaction between metal centers (e.g. the magnetically coupled heme and Cu centers in cytochrome *c* oxidase [6]).

The form of the MCD magnetization curve originating from an isolated Kramers doublet ground state depends on both the effective ground state *g* values and the polarization of the electronic transition [3,10]. The majority of the studies reported thus far have simplified the data analysis

---

Abbreviations: MCD, magnetic circular dichroism; EXAFS, extended X-ray absorption fine structure.

Correspondence: Dr. M.K. Johnson, Department of Chemistry, University of Georgia, Athens, GA 30602, U.S.A.

0167-4838/87/$03.50 © 1987 Elsevier Science Publishers B.V. (Biomedical Division)

by focusing on two special cases: chromophores with $S = 1/2$ ground states exhibiting small g-value anisotropy and chromophores in which all electronic transitions are of similar polarization. In the former case, the MCD magnetization data will be almost independent of the polarization of the transition [4]. The latter case is well illustrated by hemes where *xy*-polarized π–π^* transitions from the porphyrin dominate the UV-visible MCD spectrum [3]. To date no experimental studies have examined the change in MCD magnetization data as a function of the polarization of electronic transitions originating from a ground-state doublet with large g-value anisotropy. Such ground-state doublets are commonly encountered with transition metal centers which have $S > 1/2$ and significant zero field splitting. The ability to analyse MCD magnetization data from these types of ground state will be particularly important in investigating the electronic and magnetic properties of a range of novel biological iron-sulfur clusters, e.g. P and M clusters in nitrogenase ($S = 5/2$ and $3/2$, respectively [7,11,12]), reduced [3Fe-xS] clusters ($S = 2$ (Refs. 5, 13 and the following paper [37])), reduced [4Fe-4S] clusters in nitrogenase Fe-protein ($S = 1/2$ or $3/2$ depending on solvent medium [14]), and in amidotransferase ($S > 1/2$ [15]).

In this and the following paper, we report and analyse MCD magnetization data for oxidized rubredoxin from *Clostridium pasteurianum* ($S = 5/2$) and reduced [3Fe-xS] clusters ($S = 2$) in *Azotobacter vinelandii* and *Thermus thermophilus* ferredoxins. The data illustrate how MCD magnetization data can be dramatically affected by the polarization of the electronic transition. Indeed MCD magnetization curves are shown to provide an effective method for estimating the polarization of electronic transitions even though the sample molecules are randomly orientated in a frozen glass.

Rubredoxin was chosen for investigation, since it is one of the best-characterized of all metalloproteins and therefore provides a suitable sample for assessing the validity of the data analysis. The structure in the ground state has been studied by X-ray crystallography to a resolution of 1.2 Å [16,17], as well as by EXAFS [18] and resonance Raman spectroscopy [19–22]. Electronic ground-state parameters have been determined by EPR and Mössbauer spectroscopies [23–28] and the UV-visible spectrum has been assigned by polarized single-crystal studies [29] as well as CD [29,30] and MCD [29,31] investigations. In agreement with the polarized single-crystal absorption studies, analysis of MCD magnetization data reported here reveals distinct differences in the polarizations of the electronic transitions. The polarizations of the individual transitions are shown to be consistent with spectral assignments based on effective D_{2d} symmetry. Estimates of the axial zero-field splitting parameter, *D*, were obtained by detailed studies of the temperature dependence at small applied fields. The values are compared with those from EPR and Mössbauer spectroscopies.

Materials and Methods

Materials. C. pasteurianum (ATCC 6013) was grown as previously described [32] and harvested in late log phase using a continuous-flow RC-5B Sorvall centrifuge. Rubredoxin was isolated according to the method described by Lovenberg [33] and the concentration was determined from the molar extinction coefficient at 380 nm ($\varepsilon_{380} = 10\,700\ \mathrm{M}^{-1} \cdot \mathrm{cm}^{-1}$). Samples for spectroscopic studies were in aqueous 0.15 M Tris-HCl buffer, pH 7.4, and contained 50% v/v ethylene glycol, which facilitates the formation of optical-quality glasses on freezing.

Instrumentation. Absorption spectra were recorded on a Cary 219 spectrophotometer in 1 mm quartz cuvettes. MCD spectra were measured with a JASCO J500C spectropolarimeter fitted with an Oxford Instruments SM3 superconducting solenoid capable of generating magnetic fields up to 5 T and sample temperatures down to 1.5 K. Further experimental details, including sample temperature measurement and control and magnetic field calibration, have been given elsewhere [34]. MCD spectra, corrected for natural CD, are expressed as $\Delta\varepsilon$, which is the difference in the absorption coefficients for left and right circularly polarized light in units of $\mathrm{mM}^{-1} \cdot \mathrm{cm}^{-1}$. The magnetic fields are indicated in the figure legends.

EPR spectra were recorded on a Varian E-line X-band spectrometer interfaced to an Apple IIc microcomputer and fitted with an Air Products Helitrans low-temperature cryostat.

Theoretical analysis of magnetization data

The algebraic expression used in determining theoretical MCD magnetization data for a randomly orientated paramagnetic chromophore exhibiting axial symmetry is

$$\frac{\Delta\varepsilon}{K} = m_{xy}^2 \left\{ \int_0^{\frac{\pi}{2}} \frac{\cos^2\theta \sin\theta}{\Gamma} g_{\parallel} \tanh\left(\frac{\Gamma\beta B}{2kT}\right) \cdot d\theta - \sqrt{2}\,\frac{m_z}{m_{xy}} \int_0^{\frac{\pi}{2}} \frac{\sin^3\theta}{\Gamma} g_{\perp} \tanh\left(\frac{\Gamma\beta B}{2kT}\right) \cdot d\theta \right\} \qquad (1)$$

where $\Delta\varepsilon$ is the temperature-dependent MCD intensity after correcting for any temperature independent contributions, K is a collection of physical constants, θ is the angle between the molecular z axis and the direction of the applied field, m_z and m_{xy} are the transition dipole moments for the molecular z and xy polarized transitions, respectively, and $\Gamma = (g_{\parallel}^2 \cos^2\theta + g_{\perp}^2 \sin^2\theta)^{1/2}$. All other symbols have their usual meaning. This expression is derived from Eqn. 17 of Schatz et al. [10] and is applicable to a $1/2 \rightarrow 1/2$ electronic transition with axial symmetry. Clearly Eqn. 1 is the sum of two terms, the first of which is the contribution from the xy-polarized component and the second is the contribution from the z-polarized component. Since the sample consists of an assembly of molecules in a frozen glass, it is necessary to average over all angles by integration. This integration cannot be performed analytically but may be readily accomplished numerically using a microcomputer.

By inspection of Eqn. 1, it is apparent that magnetization data for an axial chromophore can vary as a function of the wavelength of measurement as a result of varying amounts of z- and xy-polarized transitions. However, there are three special cases where the form of the magnetization data will be independent of the wavelength of measurement. The first case is where the electronic spectrum is dominated by transitions of a particular polarization, e.g. xy-polarized transitions from the porphyrin in hemes. In this instance the second term in Eqn. 1 can be neglected. The second case is an isotropic doublet ground state, i.e. $g_{\parallel} = g_{\perp} = g$, in which case Eqn. 1 simplifies to a simple tanh function:

$$\frac{\Delta\varepsilon}{K} = \tfrac{1}{3} m_{xy}^2 \left(1 - 2\sqrt{2}\,\frac{m_z}{m_{xy}}\right) \tanh\left(\frac{g\beta B}{2kT}\right) \qquad (2)$$

The polarization ratio, m_z/m_{xy}, attenuates the MCD intensity but leaves the form of the magnetization curve unaltered. Eqn. 2 is applicable for analysing magnetization data from $S = 1/2$ ground states with small g-value anisotropy. The third case is a ground-state doublet with $g_{\parallel} \neq 0$ and $g_{\perp} = 0$. Such a ground-state double can arise as a result of axial zero-field splitting of non-Kramers ground states with $S > 0$. In this case Eqn. 1 reduces to

$$\frac{\Delta\varepsilon}{K} = m_{xy}^2 \int_0^{\frac{\pi}{2}} \cos\theta \sin\theta \cdot \tanh\left(g_{\parallel} \frac{\beta B \cos\theta}{2kI}\right) \cdot \mathrm{d}\theta \qquad (3)$$

As expected, when $g_{\perp} = 0$ all temperature-dependent MCD transitions from the ground state become xy-polarized and magnetization data should be invariant as a function of wavelength.

Eqns. 1, 2 and 3 are only rigorously valid for analysing MCD magnetization curves from paramagnetic chromophores with isolated $S = 1/2$ ground states. Paramagnetic transition metal centers with $S > 1/2$ are frequently subject to significant zero-field splitting which gives rise to low-lying excited states that can be thermally populated over the temperature range of the experiment. Such a situation is usually apparent by the non-coincidence or 'nesting' of magnetization curves measured at different temperatures [2]. Complete analysis of magnetization data for any $S > 1/2$ system has yet to be reported. It presents a complex theoretical problem which will require inclusion of field-induced mixing of zero-field components and many additional parameters, e.g. axial and rhombic zero-field splitting parameters and effective principal g values for each doublet. Here we will only attempt preliminary analysis of the data by fitting the magnetization data at the lowest temperature, so that only the lowest doublet is significantly populated. Eqn. 1 can then be used to estimate effective g values and the polarization of the transitions from the lowest doublet. The assumptions implicit in this analysis should

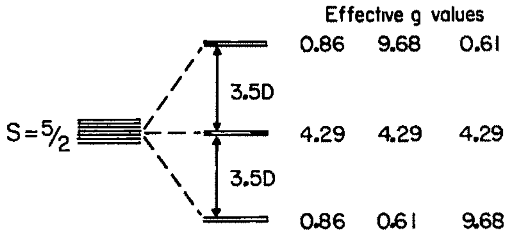

Fig. 1. Zero-field splitting of an $S = 5/2$ ground state with pure rhombic symmetry, $E/D = 1/3$

be emphasized. First, we are approximating the ground state to axial symmetry and assuming axial polarization of electronic transitions. Second, we are ignoring field-induced mixing of zero-field components. This assumption is only valid if the Zeeman splitting, $g_0\beta B$, where g_0 is the g value in the Zeeman term of the spin Hamiltonian, is much less than the zero-field splitting. Third, we are assuming that only the lowest doublet is populated at 1.5 K, the lowest temperature available in the present study. The latter two assumptions can be experimentally tested by assessing the magnitude of the zero-field splitting by measuring the temperature dependence of MCD transitions at small magnetic fields [8].

It is of interest to evaluate Eqn. 1 for parameters that are relevant to the analysis of data for oxidized rubredoxin. Oxidized rubredoxin is in the high-spin ferric state ($3d^5$, $S = 5/2$), with the ground state being $^6A_1$. This state can be mixed by spin-orbit coupling with excited ligand field states, such as $^4T_1$, thereby splitting the degenerate spin sextet into three Kramers doublet zero-field components. This lifting of the ground-state spin degeneracy is described by the axial and rhombic zero-field splitting parameters, D and E, respectively, in the electronic spin Hamiltonian, H_e:

$$H_e = g_0\beta \boldsymbol{B}\cdot\boldsymbol{S} + D(S_z^2 - S(S+1)/3) + E(S_x^2 - S_y^2) \qquad (4)$$

Analysis of the low-temperature EPR spectra of

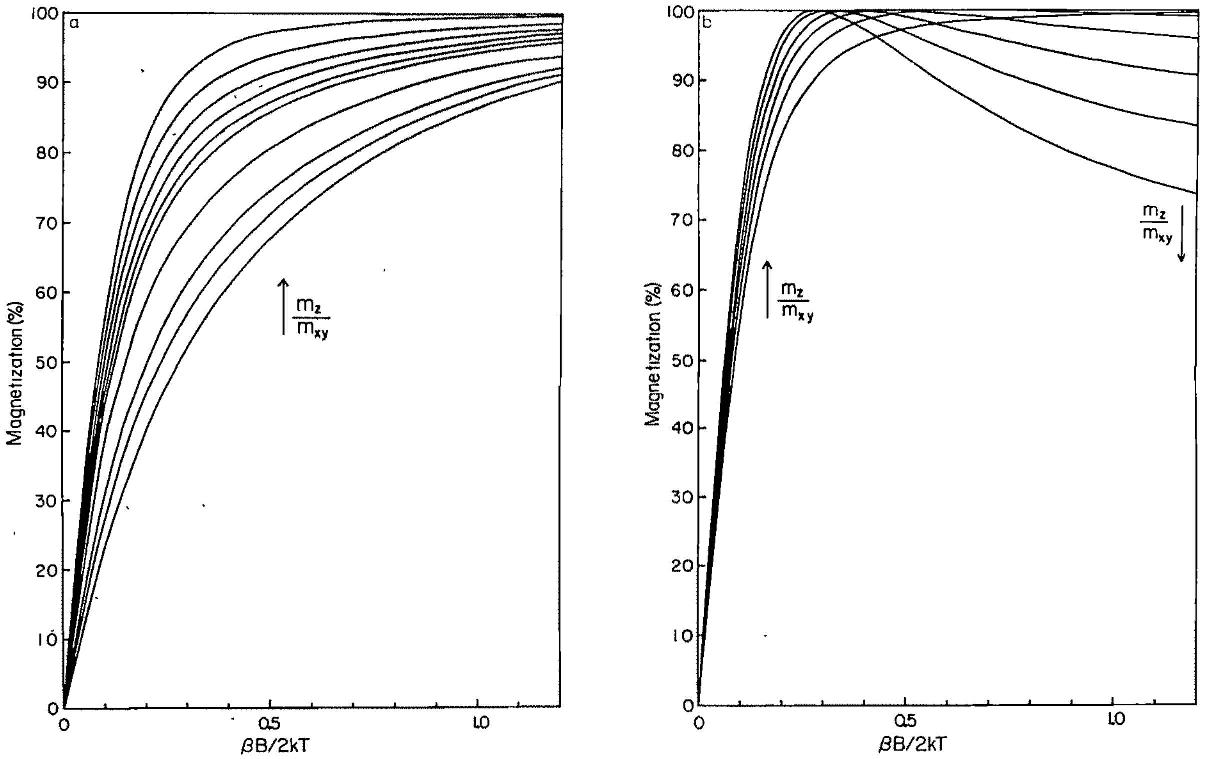

Fig. 2 Theoretical MCD magnetization data Theoretical data calculated using equation 1, with $g_{\parallel} = 9.68$ and $g_{\perp} = 0.75$. (a) $m_z/m_{xy} = 0, -0.2, -0.4, -0.6, -0.8, -1.0, -2.0, -5.0, -10.0$, and -100.0. (b) $m_z/m_{xy} = 0, 0.2, 0.4, 0.6, 0.8$, and 1.0

a range of rubredoxins from a variety of bacteria indicates that the ground state has almost completely rhombic symmetry ($E/D = 1/3$) [23–25]. For completely rhombic symmetry, the ground state is split into three Kramers doublets that are equally separated in energy by an amount $(4\sqrt{7}/3)D$. Principal g values for each of these doublets are given in Fig. 1. The g-value anisotropy of the lowest doublet ($g_1 = 9.68$, $g_2 = 0.86$, $g_3 = 0.61$) can be considered as axial to a good approximation by averaging g_2 and g_3 to give $g_\perp$ ($g_\perp = [(g_2^2 + g_3^2)/2]^{1/2}$) and equating $g_\parallel$ with g_1. Single-crystal polarized absorption studies [29] and previous low-temperature MCD investigations [31] concur in attributing the dominant splitting in the UV-visible absorption bands to predominantly axial distortion in the excited charge transfer state. Hence the assumption of axial polarized transitions appears to be valid to a first approximation. Bearing in mind these approximations, theoretical MCD magnetization curves for the lowest zero-field component in rubredoxin are shown in Fig. 2 for polarization ratios, m_z/m_{xy}, varying between $+1$ and -100. Since we have no knowledge of the absolute sign of the polarization ratio for a particular MCD transition, it is necessary to consider both positive and negative values. The data are plotted in terms of percentage magnetization (MCD intensity as a percentage of the maximum intensity), since we are generally unable to evaluate the transition dipole moments and hence predict the absolute intensity of MCD transitions.

Fig. 2 clearly demonstrates that MCD magnetization data for ground states with large g-value anisotropy are critically dependent on the polarization of the electronic transition. When the z-polarized and xy-polarized components have the opposite sign, i.e., $m_z/m_{xy} < 0$, Fig. 2(a), the initial slope of the magnetization curve decreases as the relative amount of the z-polarized component increases. In contrast, when the z-polarized and xy-polarized components have the same sign, i.e. $m_z/m_{xy} > 0$, Fig. 2(b), the unusual situation arises whereby the magnetization curve reaches a maximum and then decreases with increasing $\beta B/2kT$. Such a situation has been experimentally observed for the reduced [3Fe-xS] cluster in *Azotobacter vinelandii* ferredoxin I (see the following paper [37]).

Results

Fig. 3 shows the room-temperature absorption spectrum and MCD spectra recorded at 1.55, 4.22, 7.2, 11.0 and 20.0 K and 4.5 tesla for oxidized rubredoxin from *C. pasteurianum*. Six temperature-dependent MCD bands (C-terms) are resolved in the wavelength region 330–650 nm. MCD magnetization data were collected at the peak maxima of each MCD transition at temperatures between 1.55 and 140 K and magnetic fields between 0 and 4.5 tesla. Magnetization plots at 400, 466, 501 and 555 nm are shown in Fig. 4. The magnetization plots at 344 and 370 nm (not shown) closely resemble those at 555 and 501 nm, respectively. The presence of low-lying zero-field components that become thermally populated with increasing temperature is indicated by the nesting of the magnetization data which is apparent at all wavelengths investigated. The pronounced differences in the magnetization plots as a function of wavelength are attributed to differences in the polarization of the electronic transitions.

To proceed further in analysing the magnetiza-

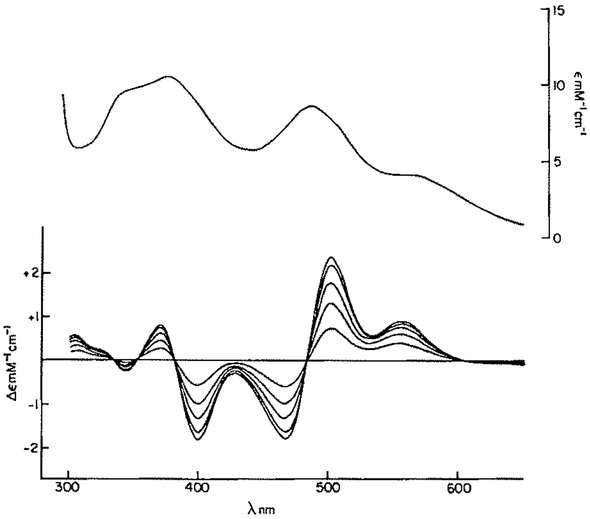

Fig. 3. Low-temperature MCD and room-temperature absorption spectra of oxidized *C. pasteurianum* rubredoxin. Sample concentration was 0.034 mM, in 0.15 M Tris-HCl buffer, pH 7.4, containing 50% v/v ethylene glycol. Upper spectrum, room-temperature absorption. Lower spectrum: MCD recorded at 1.55, 4.22, 7.2, 11.0 and 20.0 K (intensity of all transitions increasing with decreasing temperature) at a magnetic field of 4.5 tesla, pathlength = 0.169 cm.

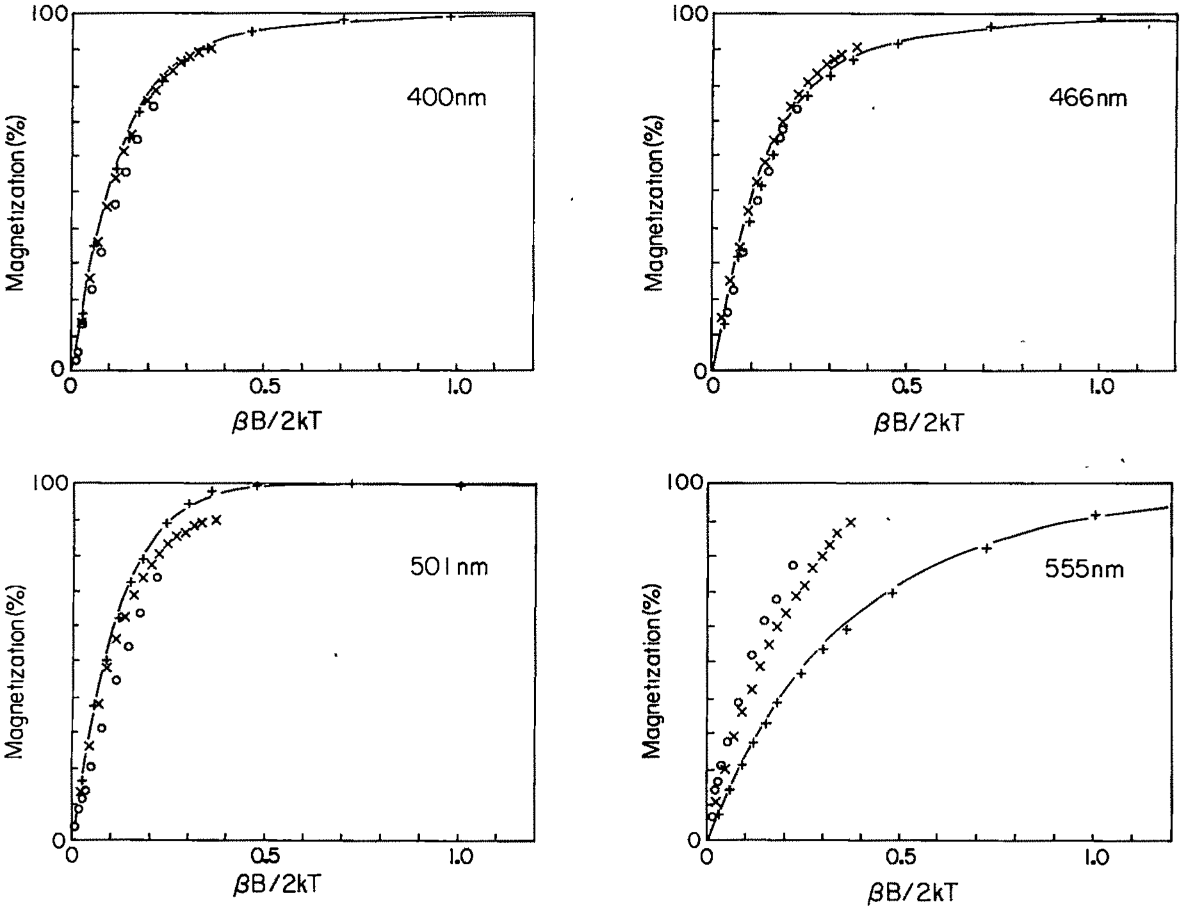

Fig 4. MCD magnetization data for oxidized *C. pasteurianum* rubredoxin Sample as used in Fig 2. Wavelengths as indicated on figure. 1.55 K (+) and 4.22 K (×) at magnetic fields between 0 and 4.5 tesla, various temperatures between 7.2 and 140 K at 4.5 tesla (O). Solid lines indicate theoretical fits to the data at 1.55 K, $g_{\parallel} = 9.4$ and $g_{\perp} = 1.07$, $m_z/m_{xy} = -100.0$ (at 555 nm), 0.1 (at 501 nm), −0.3 (466 nm), and −0.1 (at 400 nm).

tion data, we require effective g values for the lowest doublet and an estimation of the magnitude of the zero-field splitting. To this end, EPR spectra for the samples of oxidized rubredoxin used in the MCD investigations were recorded in the temperature range 8 to 70 K. The spectra consist of a resonance at $g = 9.4$ (observable only up to 15 K) from the lowest doublet and a broad resonance with maxima, cross-over, and minima at $g = 4.7$, 4.3 and 4.0 from the middle doublet (data not shown). The spectra are identical to those previously reported for oxidized rubredoxin from *C. pasteurianum* [26,35], showing that the presence of ethylene glycol does not alter the ground-state properties. The EPR spectrum is also very similar to that of the oxidized rubredoxin from *Pseudomonas oleovorans*, for which the high-field components of the lowest doublet are also observable at $g = 1.22$ and 0.90 [23]. Using the effective g values of the lower and middle doublets, a value of $E/D = 0.28$ was inferred, and from the temperature dependence of the relative intensity of the signals from the two doublets, a value of $D = 1.76$ cm^{-1} was calculated. For oxidized rubredoxin from *C. pasteurianum*, where the high-field resonances from the lowest doublet have not been observed, Shultz [26] determined $E/D = 0.25$ and $D = 1.4$ cm^{-1} from EPR simulations which allowed for contributions from g-strain to the linewidth. Therefore, from the available EPR data, we conclude that only the lowest doublet will be significantly populated at 1.55 K and that it should

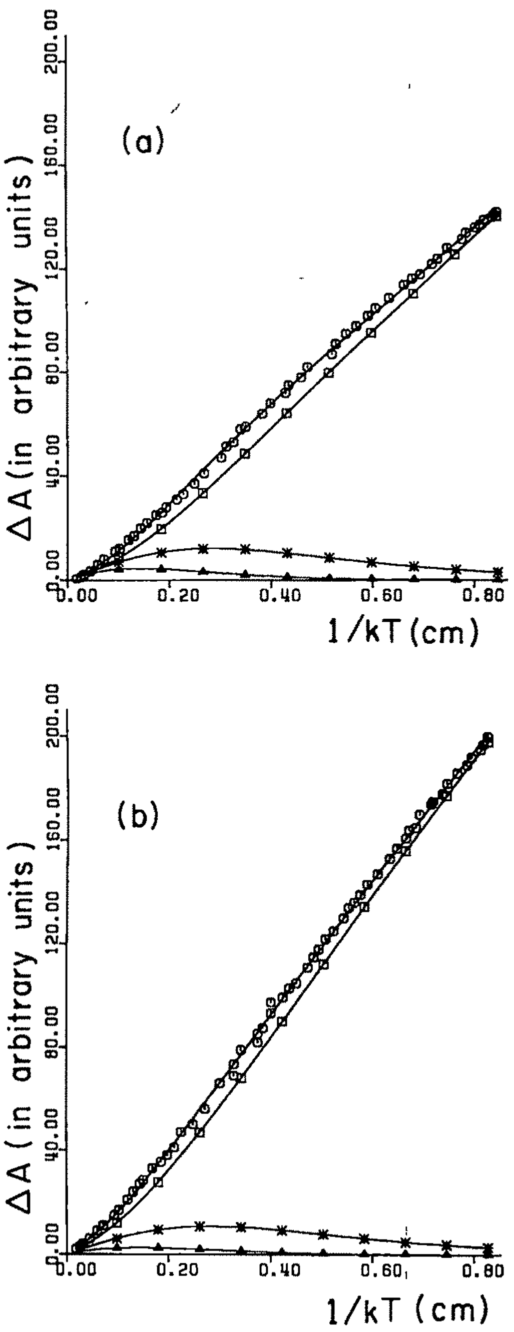

Fig. 5. MCD temperature dependence of oxidized rubredoxin Magnetic field = 0.24 tesla. (a) 400 nm, (b) 501 nm. Circles are experimental data Solid lines are the best fit to the data and the individual contributions from each of the three doublets (□, ★ and △ indicate contributions from lowest, middle and upper doublets, respectively) Individual contributions are plotted as positive quantities irrespective of the sign of c Parameters used in best fits: (a) $D = 1.4$ cm^{-1}, $c_1 = 711$, $c_2 = 950$, $c_3 = -939$; (b) $D = 1.4$ cm^{-1}, $c_1 = 1029$, $c_2 = 839$, $c_3 = -528$ (c values are in arbitrary units and indicate only the relative values of the C-terms)

be possible to fit the magnetization data at this temperature to Eqn. 1, using $g_{\parallel} = 9.4$ and $g_{\perp} = 1.07$, to obtain estimates of the polarization ratio, m_z/m_{xy}. Fig. 4 shows that this is indeed the case. The best fits are shown by solid lines and the corresponding values of m_z/m_{xy} are given in the figure caption. Clearly the transitions at 370, 501, 466 and 400 nm are all predominantly xy-polarized, since the absolute value of the polarization ratio does not exceed 0.3 in any instance. In contrast, the transitions at 344 and 555 nm are almost exclusively z-polarized. The data shown in Fig. 4 serve to illustrate that the form of the magnetization data from an $S > 1/2$ ground state can be dramatically affected by the polarization of the transition and that great care must be exercised in using MCD magnetization to determine the ground-state spin of an unknown sample.

Since the transitions at 501 and 400 nm were found to be almost exclusively xy-polarized, detailed studies of the temperature dependence (1.7 to 100 K) of the MCD intensity at these wavelengths were carried out to determine the magnitude of the axial zero-field splitting parameter, D (see Fig. 5). Our analysis closely follows that described by Browett et al. [8] for the $S = 5/2$ ground state of a high-spin iron porphyrin complex. In the Curie law limit (i.e. when the MCD intensity is a linear function of B/T), the MCD intensity, ΔA, can be expressed as a sum of contributions from the C-terms originating from each doublet:

$$\Delta A = \left\{ \sum_{i=1}^{3} \frac{c_i}{kT}\alpha_i + d \right\} B \qquad (5)$$

where c_i and α_i are the C-term contributions and the fractional populations of the ith doublet, respectively, and d is the diamagnetic, temperature-independent contribution from A- and B-terms. Assuming completely rhombic ground-state symmetry, i.e. $E/D = 0.33$ (see Fig. 1), the fractional populations of the three doublets are given by:

$$\alpha_1 = 1/(1+e^{-3.5D/kT}+e^{-7.0D/kT})$$
$$\alpha_2 = e^{-3.5D/kT}/(1+e^{-3.5D/kT}+e^{-7.0D/kT}) \qquad (6)$$
$$\alpha_3 = e^{-7.0D/kT}/(1+e^{-3.5D/kT}+e^{-7.0D/kT})$$

Studies of the MCD intensity at magnetic fields of 4.5 tesla and temperatures up to 150 K indicate that diamagnetic contributions are negligible compared to the paramagnetic contributions and thus d can be ignored in Eqn. 5. A magnetic field of 0.24 tesla was chosen for the study of the temperature dependence, since the MCD intensity at both wavelengths was observed to be linear as a function of applied magnetic field up to 0.4 tesla at 1.7 K. The experimental data were fit to Eqn. 5 using non-linear least-squares with c_1, c_2, c_3 and D as parameters. Our best fits to the experimental data and the contributions from the three ground-state doublets are shown in Fig. 5. At both wavelengths optimal fits were obtained for $D = 1.4$ cm^{-1}. However, the theoretical curves are not particularly sensitive to the values of D and satisfactory fits that are within the experimental uncertainty of the data points are possible with values ranging from 1.0 to 2.0 cm^{-1}.

Discussion

The low-temperature MCD spectra and magnetization data reported in this work are consistent with the analysis of the optical spectrum made by Eaton and Lovenberg on the basis of polarized single-crystal absorption and room-temperature MCD studies [29]. The visible spectrum in the region 330 to 650 nm was assigned to two allowed S → Fe(III) charge transfer transitions, being $^6A_1 \rightarrow {}^6T_2$ of tetrahedral parentage, each spanning a range 650–430 nm and 430–330 nm. The assignment of a $^6A_1 \rightarrow {}^6T_2$ transition to the bands in the region 430–330 nm was questioned by Rivoal et al. [31], since four temperature-dependent transitions were resolved in this region of the low-temperature MCD spectrum. However, we have been unable to observe the shoulder to the low-wavelength side of the negative MCD band at 400 nm that was reported by these workers. It seems likely that this additional band may be attributed to the glass sample cell, since subsequent low-temperature MCD investigations by the same group reported a negative, temperature-dependent MCD band centered at 375 nm that originated from glass [36].

Eaton and Lovenberg attributed the observed splitting in each of the two charge transfer transitions to a predominant axial distortion in the excited state resulting in effective D_{2d} symmetry [29]. Low-temperature MCD studies confirmed that this splitting is primarily due to a static distortion rather than spin-orbit coupling in the excited state [31]. Based on differences in polarization and the form of the MCD spectrum, the visible absorption bands centered at 382 and 495 nm were assigned to $^6A_1 \rightarrow {}^6E$ and those at 347 and 565 nm to $^6A_1 \rightarrow {}^6B_2$ under D_{2d} symmetry. Each of the two $^6A_1 \rightarrow {}^6E$ transitions appears in the low-temperature MCD spectrum as two overlapping C-terms of opposite sign. This occurs quite generally in systems with orbitally non-degenerate, spin-degenerate ground states when the transition is to an orbitally degenerate, spin-degenerate excited state that is split by spin-orbit coupling. As predicted for this assignment, polarized single-crystal absorption measurements showed markedly different polarization ratios, with respect to the crystallographic axes, for each of the components of the parent transitions. The MCD magnetization data reported here enable estimates to be made of the polarization ratios in terms of their molecular axes rather than the crystallographic axes. The results are entirely consistent with the above assignments. From symmetry considerations the $^6A_1 \rightarrow {}^6B_2$ transitions that exhibit MCD maxima at 344 and 555 nm would be expected to be z-polarized, whereas the $^6A_1 \rightarrow {}^6E$ transitions that exhibit MCD maxima at 370, 400, 466 and 501 nm would be expected to be xy-polarized, under D_{2d} symmetry.

It should be emphasized that D_{2d} is the effective optical symmetry of the chromophore. For the excited states, the form of the optical spectrum does indicate that the axial distortion far outweighs any rhombic component [29,31]. However, based on the currently available EPR (see above), resonance Raman [22], and X-ray crystallographic [16,17] data, the ground-state geometry must be lower than D_{2d}.

For transitions of unique polarization, MCD spectroscopy offers an independent means of assessing the magnitude of the zero-field splittings for magnetically dilute chromophores which is not sensitive to relaxation effects. In the case of rubredoxin, the temperature dependence of the MCD intensity was not particularly sensitive to the value of the axial zero-field splitting parameter, *D*. Nevertheless, the range of values that are consistent with the observed temperature dependence, $1\ \text{cm}^{-1} < D < 2\ \text{cm}^{-1}$, does encompass the values derived from both EPR and Mössbauer investigations for *C. pasteurianum* rubredoxin, $D = 1.4$ to $1.74\ \text{cm}^{-1}$ [25,26]. There are currently very few examples of the use of variable-temperature MCD spectroscopy to determine zero-field splitting parameters. The present work illustrates that reliable, albeit approximate, values can be obtained provided some knowledge of the polarization of the transitions is available. This method of determining zero-field parameters is particularly useful for investigating EPR-silent, non-Kramers ground states (e.g. reduced [3Fe-xS] clusters; see the following paper [37]).

In summary, the results presented here provide experimental evidence that MCD magnetization data are critically dependent on the polarization of an electronic transition from a ground state with large *g*-value anisotropy. Furthermore, analysis of the data affords insight into the molecular transition polarization for chromophores with axial symmetry. The technique is likely to become increasingly important for establishing ground-state parameters, as well as assigning the nature and polarization of electronic transitions in metalloproteins.

Acknowledgements

This work was supported by grants from the National Institutes of Health (GM-33806), the National Science Foundation (DMB 86-03546), Research corporation, and the American Chemical Society Petroleum Research Fund.

References

1 Dooley, D M. and Dawson, J H (1984) Coord Chem Rev 60, 1–66

2 Johnson, M.K, Robinson, A.E. and Thomson, A J (1982) in Iron-Sulfur Proteins (Spiro, T G, ed.), pp 367–406, John Wiley and Sons, New York

3 Thomson, A.J and Johnson, M.K. (1980) Biochem J. 191, 411–420

4 Johnson, M.K., Thomson, A.J, Robinson, A E, Rao, K K and Hall, D.O. (1981) Biochim. Biophys. Acta 667, 433–451

5 Thomson, A.J., Robinson, A.E., Johnson, M.K., Moura, J.J.G, Moura, I., Xavier, A.V. and LeGall, J (1981) Biochim. Biophys. Acta 670, 93–100

6 Thomson, A.J., Johnson, M K, Greenwood, C. and Gooding, P.E (1981) Biochem J 193, 687–697

7 Johnson, M.K., Robinson, A.E., Thomson, A.J. and Smith, B.E. (1981) Biochim. Biophys. Acta 671, 61–70

8 Browett, W.R, Fucaloro, A F., Morgan, T.V. and Stephens, P.J (1983) J Am. Chem. Soc. 105, 1868–1872

9 Whittaker, J W. and Solomon, E I. (1986) J. Am Chem. Soc 108, 835–836

10 Schatz, P.N., Mowery, R.L. and Krausz, E.R (1978) Mol. Phys. 35, 1537–1557

11 Zimmerman, R., Münck, E, Brill, W.J., Shah, V.K, Henzl, J., Rawlings, J. and Orme-Johnson, W.H (1978) Biochim. Biophys Acta 537, 185–207

12 Smith, J.P., Emptage, M.H and Orme-Johnson, W.J. (1982) J. Biol. Chem 257, 2310–2313

13 Johnson, M.K., Thomson, A.J., Richards, A.J.M, Peterson, J., Robinson, A E, Ramsay, R.R. and Singer, T.P (1984) J Biol. Chem. 259, 2274–2282

14 Lindahl, P A., Day, E.P., Kent, T A., Orme-Johnson, W.H and Münck, E. (1985) J Biol. Chem. 260, 11160–11173

15 Vollmer, S.J., Switzer, R.L. and Debrunner, P.G (1983) J. Biol. Chem. 258, 14284–14293

16 Watenpaugh, K D., Sieker, L.C. and Jensen, L.H (1979) J. Mol. Biol. 131, 509–522

17 Watenpaugh, K.D., Sieker, L.C and Jensen, L H. (1980) J Mol. Biol. 138, 615–633

18 Shulman, R.G., Eisenberger, P., Teo, B.K, Kincaid, B.M. and Brown, G S. (1978) J. Mol. Biol. 124, 305–321

19 Long, T.V and Loehr, T.M. (1970) J. Am. Chem. Soc. 92, 6384–6386

20 Long, T.V., Loehr, T M., Allkins, J.R. and Lovenberg, W. (1971) J. Am Chem. Soc. 93, 1809–1811

21 Yachandra, V.K., Hare, J, Moura, I. and Spiro, T.G. (1983) J. Am Chem. Soc. 105, 6455–6461

22 Czernuszewicz, R.S., LeGall, J., Moura, I. and Spiro, T.G (1986) Inorg Chem. 25, 696–700

23 Peisach, J., Blumberg, W.E, Lode, E.T. and Coon, M J. (1971) J. Biol. Chem. 246, 5877–5881

24 Blumberg, W.E. and Peisach, J. (1979) Ann N.Y. Acad. Sci 222, 539–560

25 Debrunner, P G., Münck, E, Que, L. and Schulz, C.E (1977) in Iron-Sulfur Proteins, Vol. III (Lovenberg, W., ed.), pp. 381–417, Academic Press, New York

26 Schulz, C.E. (1979) PhD Thesis, University of Illinois at Urbana-Champaign

27 Phillips, W.D, Poe, M, Weiher, J F., McDonald, C.C. and Lovenberg, W. (1970) Nature 227, 574–578

28 Rao, K.K, Evans, M C W., Cammack, R., Hall, D.O.,

Thompson, C.L., Jackson, P.J. and Johnson, C.E. (1972) Biochem J. 129, 1063–1068

29 Eaton, W.A. and Lovenberg, W. (1973) in Iron-Sulfur Proteins, Vol. II (Lovenberg, W., ed.), pp 131–162, Academic Press, New York

30 Eaton, W.A. and Lovenberg, W. (1970) J Am Chem Soc 92, 7195–7198

31 Rivoal, J.C., Briat, B., Cammack, R., Hall, D.O., Rao, K.K., Douglas, I.N. and Thomson, A.J. (1977) Biochim. Biophys Acta 493, 122–131

32 Rabinowitz, J (1971) Methods Enzymol 24, 431–446

33 Lovenberg, W. (1971) Methods Enzymol. 24, 477–480

34 Johnson, M.K., Morningstar, J.E., Bennett, D.E., Ackrell, B.A.C. and Kearney, E.B (1985) J Biol Chem 260, 7368–7378

35 Lode, E.T. and Coon, M.J. (1971) J Biol Chem 246, 791–802

36 Thomson, A.J., Brittain, T., Greenwood, C. and Springall, J.P (1977) Biochem. J 165, 327–336

37 Johnson, M.K., Bennett, D.E., Fee, J.A. and Sweeney, W.V (1987) Biochim Biophys Acta 911, 81–94

Biochimica et Biophysica Acta 911 (1987) 81–94
Elsevier

BBA 32598

Spectroscopic studies of the seven-iron-containing ferredoxins from *Azotobacter vinelandii* and *Thermus thermophilus*

Michael K. Johnson [a], Deborah E. Bennett [a], James A. Fee [b] and William V. Sweeney [c]

[a] *Department of Chemistry, Louisiana State University, Baton Rouge, LA 70803 (U.S.A.),* [b] *Division of Isotope and Nuclear Chemistry, Los Alamos National Laboratory, University of California, Los Alamos, NM 87545 (U.S A.) and* [c] *Department of Chemistry, Hunter College, City University of New York, NY 10021 (U.S.A.)*

(Received 5 June 1986)

Key words: Iron-sulfur protein; Fe-S cluster structure; Magnetic circular dichroism; EPR; Ferredoxin

The seven-iron-containing ferredoxins from *Azotobacter vinelandii* and *Thermus thermophilus* have been investigated by low-temperature magnetic circular dichroism (MCD) and electron paramagnetic resonance (EPR) spectroscopies and room temperature ultraviolet-visible absorption spectroscopy. The results confirm the presence of one trinuclear and one tetranuclear iron-sulfur cluster in both ferredoxins and facilitate comparison of the electronic and magnetic properties of the oxidized and reduced [3Fe-*x*S] clusters. MCD magnetization data are consistent with an $S = 2$ ground state for both reduced [3Fe-*x*S] clusters, but indicate differences in the rhombicity of the zero-field splittings. The data permit rationalization of the absence of a $\Delta M = 4$ EPR transition for the reduced [3Fe-*x*S] cluster in *A. vinelandii* ferredoxin I. Spectroscopic studies of anaerobically isolated *A. vinelandii* ferredoxin I do not support the hypothesis that the [3Fe-*x*S] cluster arises as a result of aerial oxidative damage to a [4Fe-4S] cluster during isolation. The possibility that two distinct forms of [3Fe-*x*S] clusters can exist in *A. vinelandii* ferredoxin I was investigated by spectroscopic studies as a function of pH. The results reveal two distinct and interconvertible forms of the reduced [3Fe-*x*S] cluster, but do not permit rationalization of the inconsistencies in the structural data that have been reported for the oxidized clusters.

Introduction

The ferredoxins (Fd) that have been isolated from the nitrogen-fixing bacterium *Azotobacter vinelandii* [1,2] and the thermophilic bacterium *Thermus thermophilus* [3,4] are currently the best-characterized examples of 7Fe-containing iron-sulfur proteins. The structure of *A. vinelandii* FdI (using the nomenclature of Yoch and Arnon [2]) has been determined to a resolution of 2 Å [5,6] and Mössbauer, EPR and resonance Raman spectroscopies [7–9] indicate analogous iron-sulfur cluster compositions for the aerobically isolated proteins, i.e. one 3Fe-containing cluster and one cubane-type [4Fe-4S] center.

The structure of the 3Fe-containing cluster in these ferredoxins is still controversial despite the X-ray crystallographic data for *A. vinelandii* FdI. The X-ray structure determination indicates an approximately planar [3Fe-3S] core, with Fe–Fe distances close to 4.1 Å. Approximate tetrahedral

---

Abbreviations: Fd, ferredoxin; EXAFS, extended X-ray absorption fine structure; MCD, magnetic circular dichroism

Correspondence: Dr. M.K. Johnson, Department of Chemistry, University of Georgia, Athens, GA 30602, U.S A

0167-4838/87/$03.50 © 1987 Elsevier Science Publishers B.V. (Biomedical Division)

coordination about each Fe is completed by 5 cysteine residues and one other ligand, possibly H_2O. In contrast, EXAFS data for the 3Fe clusters in *Desulfovibrio gigas* FdII [10], aconitase [11] and in [4Fe-4S]-cluster-depleted *A. vinelandii* FdI [12] indicate Fe–Fe distances of approximately 2.7 Å. Moreover, resonance Raman studies of the oxidized 3Fe clusters in *A. vinelandii* FdI, *T. thermophilus* Fd, *D. gigas* FdII and aconitase [9,13], as well as analytical data for *D. gigas* FdII and aconitase [11], indicate a cluster of stoichiometric [3Fe-4S] with a structure based on that of a cubane cluster minus one Fe. In view of the current uncertainty in the structure, we will refer to these centers as [3Fe-xS] clusters where $x = 3$ or 4.

As judged by the currently available Mössbauer, EPR and resonance Raman data [7–9], the [3Fe-xS] clusters in *A. vinelandii* FdI and *T. thermophilus* Fd appear to be very similar in terms of their structural, magnetic and electronic properties. The observed difference in their redox potentials (−250 mV for *T. thermophilus* Fd [3] and −420 mV for *A. vinelandii* FdI [2,14]) is, therefore, most probably attributable to differences in protein environment. Stephens et al. have recently reported that reconstitution of *A. vinelandii* FdI apoprotein with Fe(II) and sulfide results in the formation of an 8Fe Fd containing two $[4Fe\text{-}4S]^{2+,1+}$ clusters [15], and that dithionite reduction of the aerobically isolated protein at pH 9.0 results in conversion of the [3Fe-xS] cluster to a $[4Fe\text{-}4S]^{1+}$ cluster [16]. These results raise the possibility that the [3Fe-xS] clusters in *A. vinelandii* FdI and *T. thermophilus* Fd may be artifacts, produced by oxidative degradation of a [4Fe-4S] cluster during purification [15,16].

The $[4Fe\text{-}4S]^{n+}$ centers in both Fds are now believed to be of the low-potential type, cycling between the $n = 2+$ and $1+$ redox states [8,16,17]. In *T. thermophilus* Fd the [4Fe-4S] cluster has a redox potential of −530 mV [3]. This cluster can be reduced with dithionite to give a complex EPR signal with $g_{av} = 1.94$ that has been attributed to the $S = 1/2$ $[4Fe\text{-}4S]^{1+}$ interacting via weak spin-spin interaction with the $S = 2$ reduced [3Fe-xS] cluster [18]. Since a similar EPR signal is not observed on dithionite reduction of *A. vinelandii* Fd I at neutral pH, the midpoint potential of the [4Fe-4S] cluster must be lower than −530 mV in this Fd [16,17]. Recently, Stephens et al. have reported a $g_{av} = 1.94$ EPR signal from the reduced [4Fe-4S] cluster in *A. vinelandii* FdI in samples reduced by dithionite at pH 9.0 (16). Unfortunately this treatment also results in partial destruction of the constituent iron-sulfur clusters. The [4Fe-4S] clusters in these ferredoxins also differ in their reaction with oxidizing agents such as ferricyanide. For *A. vinelandii* FdI, ferricyanide treatment is reported to result in a novel three-electron oxidation of the $[4Fe\text{-}4S]^{2+}$ cluster, leading to the formation of an EPR-active radical species, most probably a cysteinyldisulfide radical [17]. Prolonged incubation with ferricyanide (> 3-fold stoichiometric excess) causes selective oxidative destruction of the [4Fe-4S] cluster [19]. In contrast, *T. thermophilus* Fd is reported to be very resistant to oxidative degradation [3,20]. Proton NMR studies of samples of dithionite-reduced *T. thermophilus* Fd after treatment with excess solid ferricyanide have been interpreted in terms of conversion of the $[4Fe\text{-}4S]^{2+}$ cluster to a [3Fe-xS] cluster [20].

We report here a comparative study of the oxidized and reduced iron-sulfur centers in *A. vinelandii* FdI and *T. thermophilus* Fd using low-temperature magnetic circular dichroism (MCD) and EPR, and room-temperature UV-visible absorption spectroscopies. The results confirm the currently accepted iron-sulfur cluster composition of both ferredoxins and facilitate a critical comparison of the spectroscopic and electronic ground-state properties of the [3Fe-xS] clusters. MCD magnetization studies of the reduced [3Fe-xS] clusters indicate $S = 2$ ground states in both ferredoxins, and reveal differences in the zero-field splittings that permit rationalization of EPR data. We also report spectroscopic studies of anaerobically isolated *A. vinelandii* FdI and of the aerobically isolated ferredoxins as a function of pH. The results provide additional information concerning the possibility of cluster conversion during aerobic isolation and address the question of whether more than one type of [3Fe-xS] cluster can exist in the same polypeptide under different conditions.

Materials and Methods

Materials. A. vinelandii FdI and *T. thermophilus* Fd were isolated and purified by the published procedures [8,21]. Samples used in this work had 400/280 nm absorbance ratios of 0.62 and 0.57 for *T. thermophilus* Fd and *A. vinelandii* FdI, respectively. *A. vinelandii* Fd was also purified anaerobically by an analogous procedure, using degassed buffers, with all operations being performed inside a Vacuum Atmospheres glove box under argon (< 1 ppm O_2). The sample concentrations used in quantifying both the EPR and the MCD spectra were based on the published molar extinction coefficients for the ferredoxins as isolated: $\varepsilon_{400} = 28\,140$ $M^{-1} \cdot cm^{-1}$ for *T. thermophilus* Fd [8] and $\varepsilon_{400} = 29\,800$ $M^{-1} \cdot cm^{-1}$ for *A. vinelandii* FdI [17]. Samples for spectroscopic studies were in buffer solutions (see figure legends for details), and contained 50% v/v ethylene glycol, which facilitates the formation of optical-quality glasses on freezing. All dithionite reductions were carried out anaerobically in a glove box and the pH of the samples was measured after addition of both dithionite and ethylene glycol.

Instrumentation. Absorption spectra were recorded on a Cary 219 spectrophotometer in 1 mm quartz cuvettes. MCD spectra were measured with a Jasco J500C spectropolarimeter fitted with an Oxford Instruments SM3 superconducting solenoid capable of generating magnetic fields up to 5 T and sample temperatures down to 1.5 K. Further experimental details, including sample temperature measurement and control, and magnetic field calibration, have been described elsewhere [22]. MCD spectra, corrected for natural CD, are expressed as $\Delta\varepsilon$, which is the difference in the absorption coefficients for left and right circularly polarized light in units of $M^{-1} \cdot cm^{-1}$. The magnetic fields and sample temperatures are indicated in the figure legends. EPR spectra were recorded on a Varian E-line X-band spectrometer interfaced to an Apple IIc microcomputer and fitted with an Air Products Helitrans low-temperature cryostat. The spectra were quantified by double integration according to the published procedures [23] using 1 mM metmyoglobin cyanide as standard. Care was taken to ensure that both sample and standard were under non-saturating conditions for all spin quantitations.

Results

Fig. 1 shows the room-temperature absorption spectra for the samples of *T. thermophilus* Fd and *A. vinelandii* FdI used in the EPR and MCD

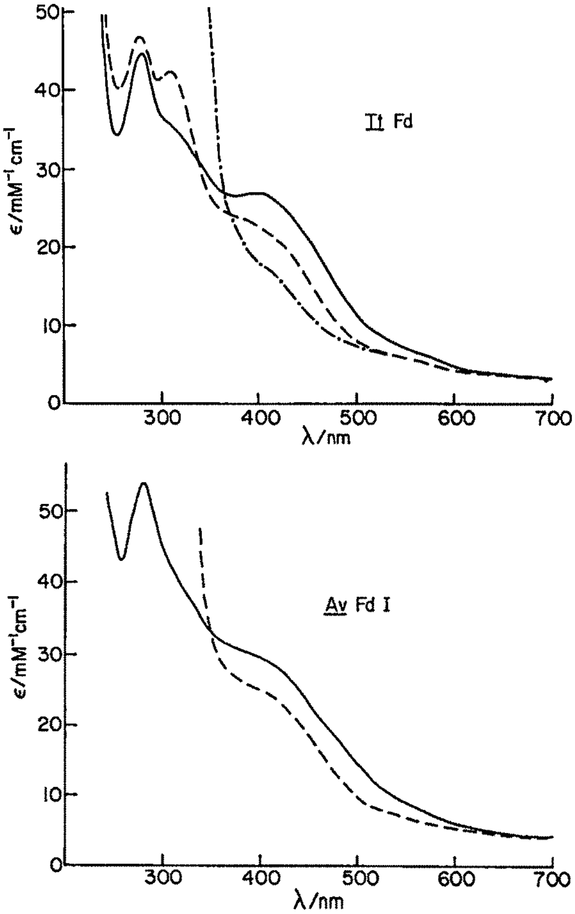

Fig. 1 Room-temperature UV-visible absorption spectra of *T thermophilus* Fd and *A. vinelandii* FdI. Upper panel *T. thermophilus* Fd as isolated (———), partially reduced (— — —), and fully reduced (·—·—·) in 100 mM potassium phosphate buffer, pH 7.8, with 50% v/v ethylene glycol. Partial reduction was accomplished by anaerobic addition of a 10-fold excess of sodium dithionite to sample containing ethylene glycol. Complete reduction was accomplished by anaerobic addition of excess solid sodium dithionite to sample prior to anaerobic addition of ethylene glycol Sample concentration was 0.306 mM for as isolated and partially reduced, and 0 215 mM for fully reduced Lower panel: *A vinelandii* FdI as isolated (———), and partially reduced (— — —) in 100 mM Tris-HCl buffer, pH 7.8, with 50% v/v ethylene glycol Partial reduction was accomplished by anaerobic addition of a 10-fold excess of sodium dithionite to sample containing ethylene glycol. Sample concentration was 0.181 mM.

investigations. Depending on the conditions of reduction by dithionite, two stable reduced states were obtainable for *T. thermophilus* Fd. Anaerobic addition of dithionite (up to a 100-fold excess) to samples containing 50% v/v ethylene glycol resulted in a stable, partially reduced sample ($A_{red}/A_{ox} = 0.84$ at 400 nm), whereas addition of dithionite (> 4-fold excess) prior to addition of ethylene glycol resulted in a more reduced sample ($A_{red}/A_{ox} = 0.69$ at 400 nm). The absorption changes are consistent with those attributed to the partially reduced (reduced [3Fe-*x*S], $[4Fe\text{-}4S]^{2+}$) and fully reduced (reduced [3Fe-*x*S], $[4Fe\text{-}4S]^{1+}$) Fd by Hille et al. [8], in a combined optical/EPR reductive titration with dithionite. This method of producing a stable one-electron-reduced state offers a considerable simplification compared to reduction by NADPH in the presence of a catalytic amount of ferredoxin:NADP$^+$ reductase [8]. In contrast, dithionite reduction of *A. vinelandii* FdI at pH 7.8, in the presence or absence of ethylene glycol, invariably produced the partially reduced (reduced [3Fe-*x*S], $[4Fe\text{-}4S]^{2+}$) sample ($A_{red}/A_{ox} = 0.84$ at 400 nm), irrespective of the excess of dithionite. This is consistent with a redox potential of < -600 mV for the [4Fe-4S] cluster in *A. vinelandii* FdI [16,17].

EPR and MCD studies of T. thermophilus Fd and A. vinelandii FdI, as isolated and after treatment with ferricyanide

EPR spectra of *T. thermophilus* Fd and *A. vinelandii* FdI, recorded at 11 K, are shown in Fig. 2. While the signal from *T. thermophilus* exhibits greater anisotropy, both EPR spectra are characteristic of oxidized [3Fe-*x*S] clusters, i.e. a sharp peak at $g = 2.02$ and a relatively structureless, broad feature to higher field [24]. The forms of the EPR spectra were invariant as a function of pH over the range 6.3 to 8.5. Power saturation studies indicate that the cluster in *A. vinelandii* FdI has slower spin relaxation, but relative to other types of iron-sulfur cluster they both exhibit rapid relaxation, being observed only at temperatures below 30 K. At 12 K, the EPR signals begin to saturate at microwave powers greater than 2 mW and 10 mW for *A. vinelandii* FdI and *T. thermophilus* Fd, respectively.

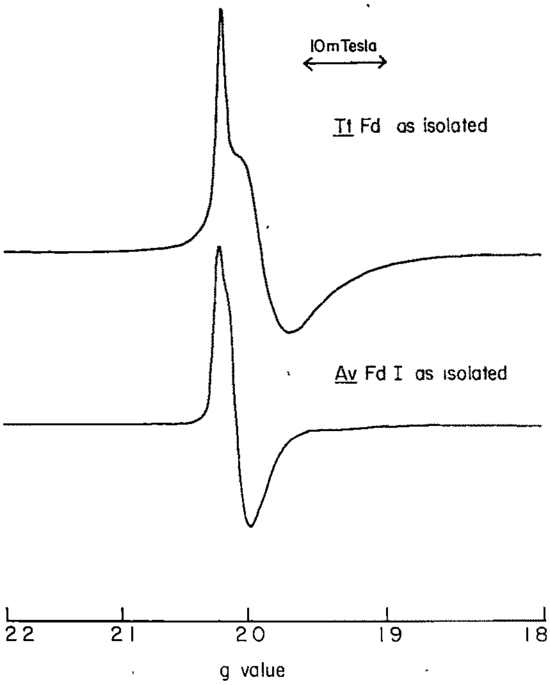

Fig. 2. X-band EPR spectra of *T. thermophilus* Fd and *A. vinelandii* FdI, as isolated. Samples were identical to those used in Fig. 1. Temperature 11 K, microwave power 1 mW, modulation amplitude 0.63 mT, microwave frequency 9.017 GHz

Quantitation of the EPR signals in Fig. 2 affords 0.7 ± 0.1 spin/molecule for *A. vinelandii* FdI and 1.0 ± 0.1 spin/molecule for *T. thermophilus* Fd. Anaerobically isolated *A. vinelandii* FdI exhibited an EPR signal identical to that of the aerobically isolated protein, except for a slightly higher spin quantitation. We conclude that both proteins contain approximately one [3Fe-*x*S] cluster and that this cluster is not generated by aerial oxidative damage during isolation.

Fig. 3 shows the low-temperature MCD spectra of the as-isolated ferredoxins at temperatures between 1.55 K and 16.5 K and at a magnetic field of 4.5 T. The spectrum of *A. vinelandii* FdI is identical to that reported previously by Morgan et al. [17]. No change in the MCD spectra of either ferredoxin was observed over the pH range 6.3 to 8.5. The complexity of the low-temperature MCD spectra contrast sharply with the broad featureless absorption spectra, and serve to indicate the multiplicity of electronic excited states. Although assignment of the low-temperature MCD spectra has yet to be achieved for any iron-sulfur cluster,

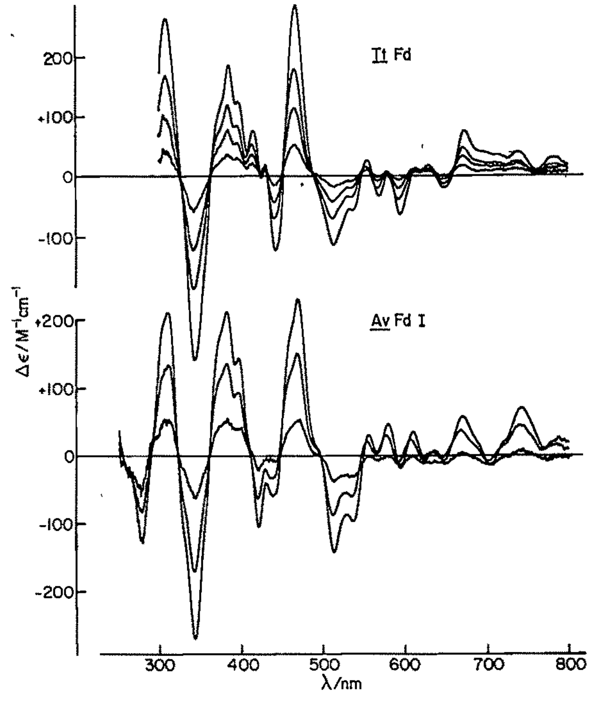

Fig. 3. Low-temperature MCD spectra of *T. thermophilus* Fd and *A. vinelandii* FdI, as isolated. Samples were identical to those used in Fig. 1. Upper panel: as-isolated *T. thermophilus* Fd, temperatures 1.55 K, 4.22 K, 9.0 K and 16.5 K, pathlength 0.163 cm, magnetic field 4.5 T. Lower panel: as-isolated *A. vinelandii* FdI, temperatures 1.55 K, 4.22 K and 14.7 K, pathlength 0.156 cm, magnetic field 4.5 T. MCD intensity at all wavelengths increases with decreasing temperature for both samples.

the spectra are useful as fingerprints of cluster type. As illustrated by Fig. 3, below 550 nm all oxidized [3Fe-xS] clusters characterized thus far have a similar pattern of MCD transitions that are attributable to S → Fe(III) charge transfer bands. Other examples include aconitase [25], *Azotobacter chroococcum* Fd [25], *D. gigas* FdII [26], *D. gigas* hydrogenase [27], *E. coli* nitrate reductase [28] and fumarate reductase [29], and ferricyanide-treated *Clostridium pasteurianum* Fd [30].

All the MCD transitions exhibited by as-isolated *A. vinelandii* FdI and *T. thermophilus* Fd show pronounced temperature dependence which is indicative of a paramagnetic, spin-degenerate ground state. To determine the nature of the ground state, magnetization curves were constructed [31] at wavelengths corresponding to each of the major bands in the spectrum. The plots at all wavelengths were identical within experimental error and representative data are shown in Fig. 4. All the experimental points lie on the same curve irrespective of the temperature of measurement, showing that the ground state is an isolated Kramers doublet and that no excited states are thermally accessible over the temperature range of the experiment. Since the experimental data are well fit by theoretical curves constructed for $g_{\text{isotropic}} = 2.01$, we conclude that all transitions are originating from the $S = 1/2$ ground state that is

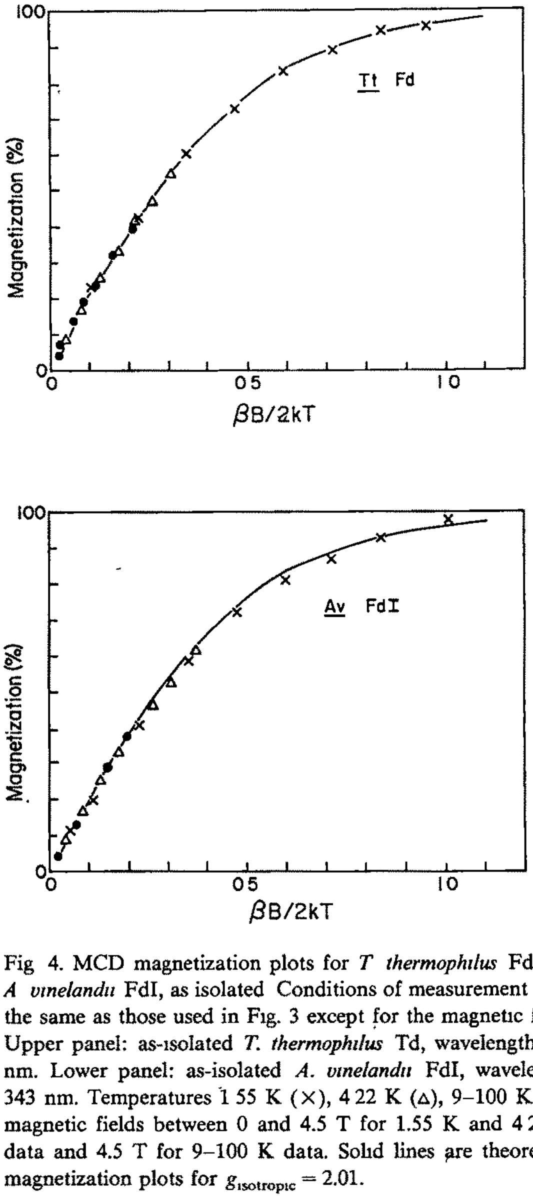

Fig. 4. MCD magnetization plots for *T. thermophilus* Fd and *A. vinelandii* FdI, as isolated. Conditions of measurement were the same as those used in Fig. 3 except for the magnetic field. Upper panel: as-isolated *T. thermophilus* Td, wavelength 343 nm. Lower panel: as-isolated *A. vinelandii* FdI, wavelength 343 nm. Temperatures 1.55 K (×), 4.22 K (△), 9–100 K (●); magnetic fields between 0 and 4.5 T for 1.55 K and 4.22 K data and 4.5 T for 9–100 K data. Solid lines are theoretical magnetization plots for $g_{\text{isotropic}} = 2.01$.

responsible for the EPR signal. This conclusion is in accord with the observation that the intensities of the MCD signals of these two ferredoxins, normalized for differences in concentration, pathlength and depolarization of the light beam, correlate well with the observed EPR spin quantitations.

The effect of ferricyanide on the UV-visible CD, MCD and EPR spectral properties of *A. vinelandii* FdI have been extensively investigated by Stephens et al. [12,17,19], and these experiments were not repeated in the present work. In contrast to *A. vinelandii* FdI, but in accord with previous spectroscopic studies [3,20], *T. thermophilus* Fd was found to be extremely resistant to ferricyanide oxidation. The EPR and MCD properties of *T. thermophilus* Fd were found to be unchanged after a 2-h incubation at room temperature with a 5-fold stoichiometric excess of ferricyanide.

EPR and MCD studies of partially reduced A. vinelandii FdI and T. thermophilus Fd

Anaerobic reduction of *A. vinelandii* FdI and *T. thermophilus* Fd with a 10-fold excess of dithionite, at pH 7.8 and in the presence of 50% ethylene glycol, results in almost complete loss of the $g = 2.02$ EPR signal ($< 2\%$ of original intensity) in both cases. No additional EPR signals were apparent for the reduced sample of *A. vinelandii* FdI. In contrast, an extremely broad and weak signal appears at low field in the X-band EPR spectrum of reduced *T. thermophilus* Fd (data not shown). The resultant spectrum was identical to that reported previously by Hagen et al. [18] for the one-electron-reduced ferredoxin, and is attributed to a $\Delta M = 4$ transition between the $M_s = \pm 2$ components of the $S = 2$ ground state of the reduced [3Fe-*x*S] cluster [18].

Low-temperature MCD spectra at temperatures between 1.57 K and 24.5 K and a magnetic field of 4.5 T for the partially reduced (reduced [3Fe-*x*S], $[4Fe\text{-}4S]^{2+}$) ferredoxins at pH 7.8 are shown in Fig. 5. As is the case for the as-isolated proteins, the $[4Fe\text{-}4S]^{2+}$ clusters are diamagnetic at low temperature and thus do not contribute to the temperature dependence of the MCD spectra. The MCD spectra, therefore, originate almost exclusively from the paramagnetic reduced [3Fe-*x*S] clusters. The forms of the MCD spectra are remarkably similar to each other and to those of other reduced [3Fe-*x*S] clusters (e.g. in *D. gigas* FdII [26,32], *A. chroococcum* Fd [32], aconitase [25], mammalian succinate dehydrogenase [22], *D. gigas* hydrogenase [27], *E. coli* fumarate reductase [29] and nitrate reductase [28]). Moreover, the intensities of the low-temperature MCD spectra together with the absence of EPR signals attributable to $[4Fe\text{-}4S]^{1+}$ clusters are consistent with reduction of the [3Fe-*x*S] centers occurring without any cluster conversion to yield [4Fe-4S] centers. The observed difference in the [3Fe-*x*S] content of the ferredoxins, as indicated by the spin quantitations of the as isolated samples, is mirrored by the MCD intensities of the reduced [3Fe-*x*S] clusters.

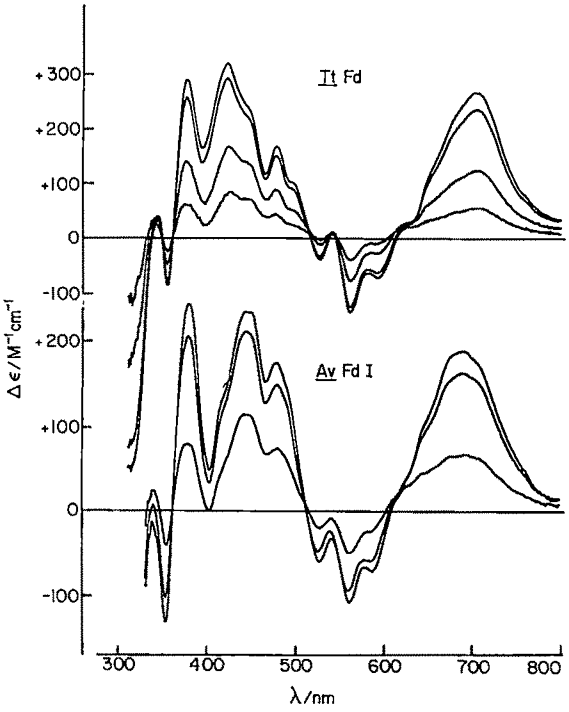

Fig. 5 Low-temperature MCD spectra of partially reduced *T. thermophilus* Fd and *A. vinelandii* FdI. Samples were identical to those used in Fig. 1. Upper panel: partially reduced *T. thermophilus* Fd, temperatures 1.57 K, 4.22 K, 10.9 K and 24.5 K, pathlength 0.158 cm, magnetic field 4.5 K. Lower panel: partially reduced *A. vinelandii* FdI, temperatures 1.60 K, 4.22 K and 15.3 K, pathlength 0.164 cm, magnetic field 4.5 T. MCD intensity at all wavelengths increases with decreasing temperature for both samples.

In an attempt to probe the electronic ground-

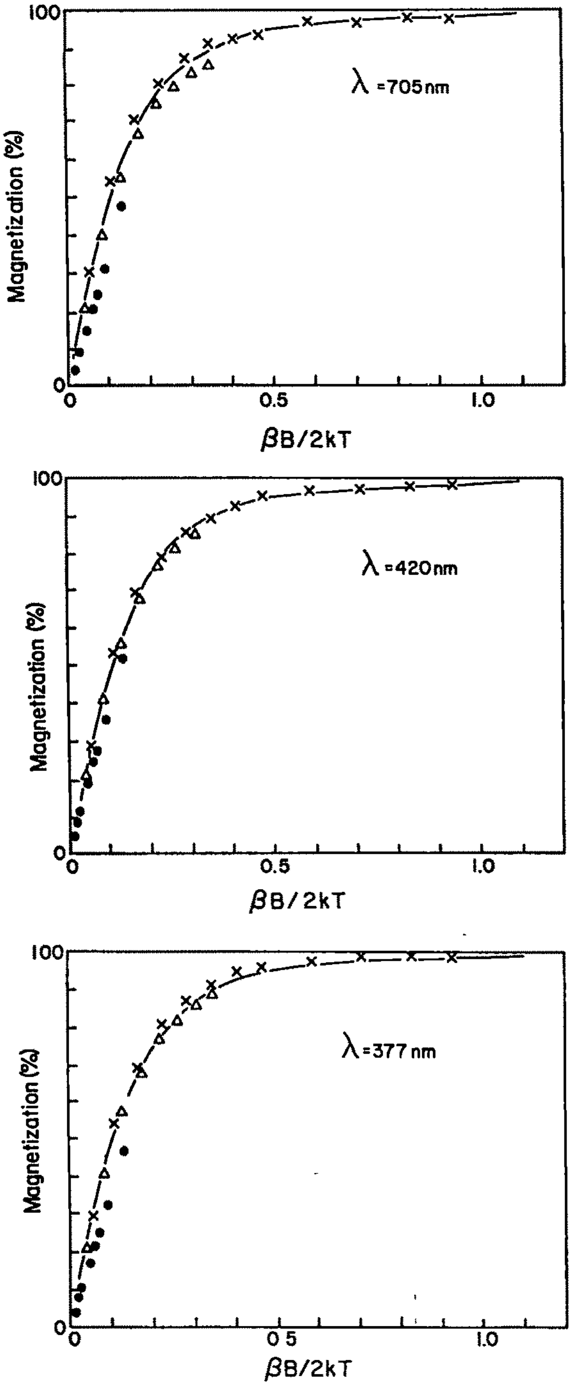

Fig. 6. MCD magnetization plots for partially reduced *T. thermophilus* Fd Conditions of measurement were the same as those used in Fig 5, except for temperatures and magnetic fields. Wavelengths 705 nm, 420 nm and 377 nm; temperatures 1.57 K (×), 4.22 (△), 9–100 K (●); magnetic fields between 0 and 4.5 T for 1.57 K and 4 22 K data, and 4.5 T for 9–100 K data. Solid lines are the theoretical magnetization curves for $g_{\parallel} = 8.0$ and $g_{\perp} = 0$.

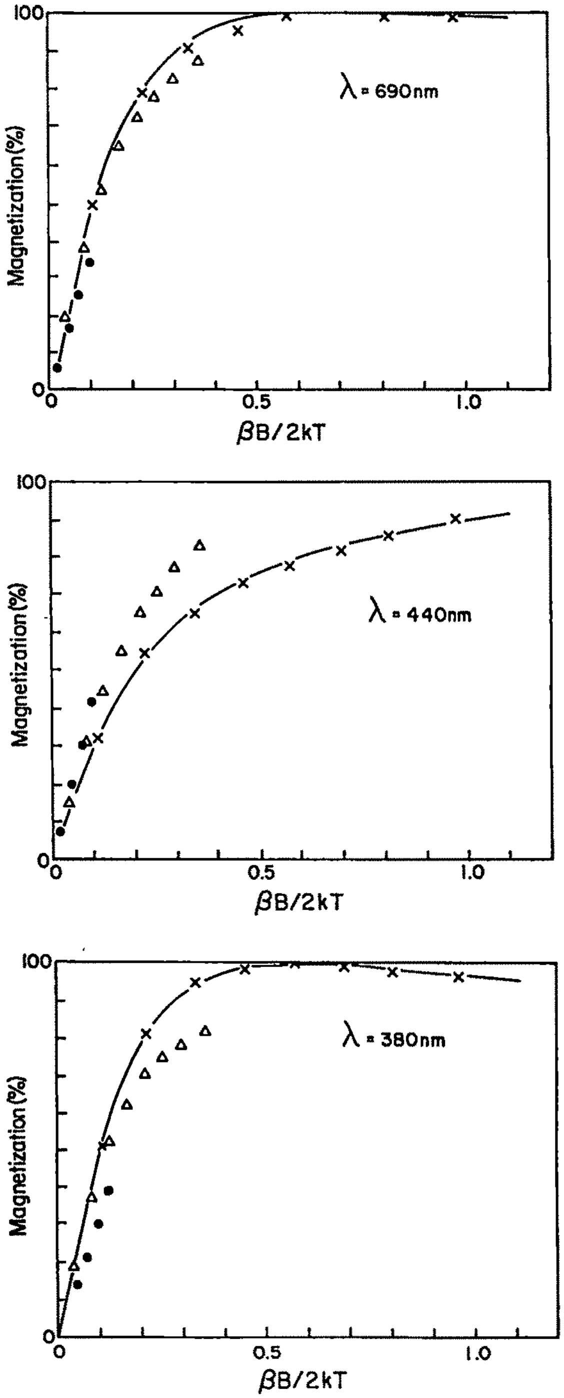

Fig. 7. MCD magnetization plots for partially reduced *A. vinelandii* FdI. Conditions of measurement were the same as those used in Fig 5, except for temperatures and magnetic fields Wavelengths 690 nm, 440 nm and 380 nm; temperatures 1.60 K (×), 4.22 K (△), 10–100 K (●); magnetic fields between 0 and 4.5 T for the 1.60 K and 4.22 K data, and 4.5 T for 10–100 K data. Solid lines are theoretical magnetization curves for $g_{\parallel} = 6.5$ and $g_{\perp} = 0.6$ with $m_z/m_{xy} = 0.35$ (690 nm), -1.4 (440 nm), and 0.5 (380 nm).

state properties of the reduced [3Fe-*x*S] clusters, MCD magnetization data were recorded for the partially reduced ferredoxins at the peak maxima of each of the major bands. Magnetization data for partially reduced *T. thermophilus* Fd recorded at 705 nm, 420 nm and 377 nm are shown in Fig. 6 and equivalent data for partially reduced *A. vinelandii* FdI recorded at 690 nm, 440 nm and 380 nm are shown in Fig. 7. The non-coincidence or 'nesting' of the magnetization curves measured at different temperatures that is observed at all wavelengths for both samples is indicative of a ground state with $S > 1/2$ with significant zero-field splitting such that low-lying energy levels can become thermally populated over the temperature range of the experiment. The pronounced differences in the MCD magnetization data shown in Figs. 6 and 7 suggest substantial differences in the ground-state zero-field splitting of the two reduced [3Fe-*x*S] clusters.

We have undertaken a preliminary analysis of the magnetization data by fitting only the lowest-temperature data to theoretical expressions derived for an $S = 1/2$ doublet and ignoring field-induced mixing of zero-field components. The limitations of this procedure and the nature of the theoretical expressions are discussed in more detail in the preceding paper [39].

The magnetization data for partially reduced *T. thermophilus* Fd do not exhibit wavelength dependence, indicating that all transitions are of similar polarization. Moreover the lowest-temperature data (1.57 K) are well fit by theoretical data for a ground-state doublet with effective g values of $g_{\parallel} = 8.0$ and $g_{\perp} = 0.0$. These are the predicted effective g values for an $M_s = \pm 2$ doublet originating from an $S = 2$ ground state with purely axial zero-field splitting [33]. The magnetization data for the reduced [3Fe-*x*S] cluster in *T. thermophilus* Fd can, therefore, be interpreted in terms of an $S = 2$ ground state with axial zero-field splitting such that an $M_s = \pm 2$ doublet is lowest in energy, $D < 0$, with the $M_s = \pm 1$ doublet not significantly populated at 1.57 K. Such an energy level scheme is depicted in Fig. 8. Since $g_{\perp} = 0.0$, all temperature-dependent MCD transitions from the ground state become *xy*-polarized and the resultant magnetization data should be invariant as a function of wavelength.

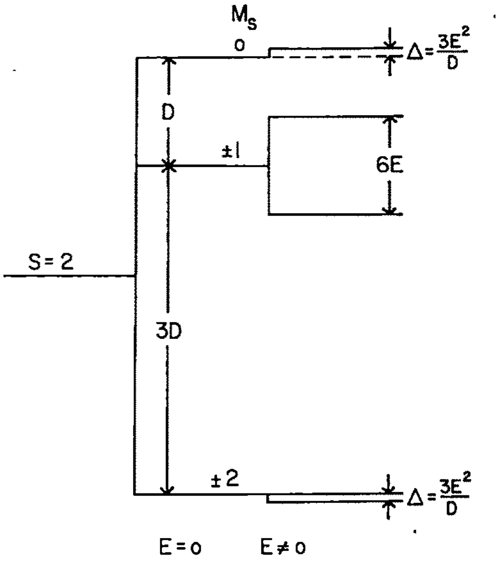

Fig 8 Zero-field splitting of an $S = 2$ ground state with axial ($D \neq 0$ and $E = 0$) and rhombic ($D \neq 0$ and $E \neq 0$) symmetry and $D < 0$. The energy levels for the rhombic case are drawn to scale for $E = 0.3\ \text{cm}^{-1}$ and $D = -2.0\ \text{cm}^{-1}$

In contrast, the magnetization data for the reduced [3Fe-*x*S] cluster in partially-reduced *A. vinelandii* FdI at the lowest temperature, 1.60 K, exhibit a pronounced wavelength-dependence. The magnetization behavior at 690 nm and 380 nm, in which the data at the lowest temperature rise to a maximum and then decrease with increasing magnetic field, is unique among metal centers investigated thus far. Provided only one paramagnetic chromophore is present, the magnetization data shown in Fig. 7 can only arise as a result of differences in the polarization of electronic transitions from a ground state with large g-value anisotropy. This phenomenon is well illustrated by oxidized rubredoxin (see preceding paper [39]). In the case of an $S = 2$ ground state, z-polarized transitions from the $M_s = \pm 2$ doublet are possible if $g_{\perp} \neq 0$, and this situation arises if the zero-field splitting is not completely axial, $E \neq 0$. The effect of a rhombic zero-field splitting is to remove the degeneracy of the $M_s = \pm 2$ and ± 1 doublets [33]; see Fig. 8. Full analysis of the magnetization data shown in Fig. 7, taking into account field-induced mixing, has not yet been attempted. It presents a complex theoretical problem, since the mixing must be averaged over all angles and will require inclusion of numerous parameters. For the present we have confined our analysis to fitting the lowest-temperature data using Eqn. 1 of the preceding paper. As shown in Fig. 7, satisfactory fits are possible at all three wavelengths for the same effective g values, $g_{\parallel} = 6.5$ and $g_{\perp} = 0.6$, if the polarization ratios for transitions from the lowest doublet are allowed to vary so that the bands at 690 nm and 380 nm have predominant xy-polarization ($m_z/m_{xy} = 0.35$ and 0.5, respectively), whereas the band at 440 nm has a large z-polarized contribution ($m_z/m_{xy} = -1.4$). This fit is not unique and is shown purely for illustrative purposes to demonstrate how such magnetization data could arise.

Detailed studies of the temperature dependence of the MCD signals over the temperature range 4.2 to 100 K were performed to determine the magnitude of the axial zero-field splitting parameter, D, for the reduced [3Fe-xS] clusters; see Fig. 9. Data for partially reduced *T. thermophilus* Fd were collected at 705 nm and 420 nm, and for partially reduced *A. vinelandii* FdI at 690 nm. The latter wavelength was chosen, since analysis of the data requires unique polarization of the electronic transition, and magnetization studies indicate predominant xy-polarization at this wavelength. At 4.2 K, the MCD intensity at these wavelengths was found to be linear as a function of magnetic field for fields up to and including those used in this investigation, 0.6 T for *T. thermophilus* Fd and 0.5 T for *A. vinelandii* FdI. Our analysis of the data closely follows that described by Browett et al. [34] and assumes that the zero-field splitting is axial with $D < 0$ (see Fig. 8) so that the $M_s = \pm 2$ and ± 1 levels are both doublets.

In the Curie law limit (i.e. when the MCD intensity is a linear function of B/T), the MCD intensity, ΔA, can be expressed as a sum of contributions from the C-terms originating from each of the three zero-field components of the ground state:

$$\Delta A = \left\{ \sum_{i=1}^{3} \frac{c_i}{kT} \alpha_i + d \right\} B \qquad (1)$$

where c_i and α_i are the C-term contributions and the fractional populations of the ith levels, respectively, and d is the diamagnetic temperature-independent contribution from A- and B-terms. For completely axial zero-field splitting, $D < 0$ and $E = 0$, see Fig. 8, the fractional populations of each of the three levels are given by:

$$\begin{aligned} \alpha_1 &= 2/(2+2e^{-3D/kT}+e^{-4D/kT}) \\ \alpha_2 &= 2e^{-3D/kT}/(2+2e^{-3D/kT}+e^{-4D/kT}) \\ \alpha_3 &= e^{-4D/kT}/(2+2e^{-3D/kT}+e^{-4D/kT}) \end{aligned} \qquad (2)$$

Studies of the MCD spectra of both samples at a magnetic field of 4.5 T and at temperatures up to 150 K (data not shown) indicate that diamagnetic

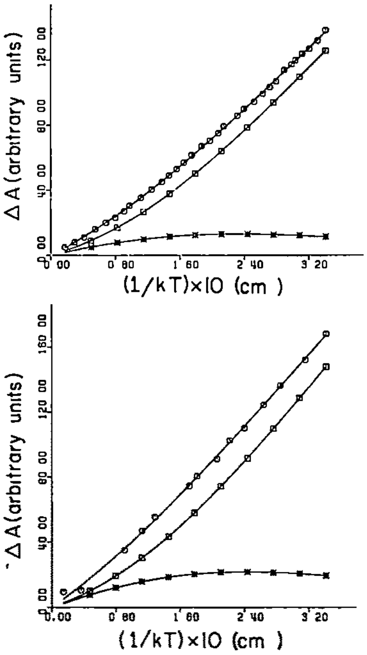

Fig. 9 MCD temperature dependence of partially reduced *T. thermophilus* Fd and *A vinelandii* FdI. Circles are experimental data, and the solid lines are the best fit to the data and the contributions to the total intensity from the $M_s = \pm 1$ (★) and $M_s = \pm 2$ (□) doublets. Upper panel: partially reduced *T. thermophilus* Fd, 0.40 mM in 100 mM potassium phosphate buffer with 50% ethylene glycol, pH 7.8 Reduced by anaerobic addition of a 10-fold excess of sodium dithionite. Wavelength 705 nm, magnetic field 0.60 T, temperatures 4.22 K to 100 K Parameters used in best fit: $D = -2.1$ cm^{-1}, $c_1 = 1831$, $c_2 = 1395$. Lower panel: partially reduced *A. vinelandii* FdI, 0.19 mM in 100 mM Taps with 50% ethylene glycol, pH 8.5 Reduced by anaerobic addition of a 10-fold excess of sodium dithionite Wavelength 690 nm, magnetic field 0.50 T, temperatures 4.22 K to 100 K. Parameters used in best fit: $D = -2.0$ cm^{-1}, $c_1 = 1042$, $c_2 = 1058$ c values are in arbitrary units and indicate only the relative values of the C-terms from the two doublets.

contributions are negligible compared to the paramagnetic contributions and thus d can be ignored in Eqn. 1. The experimental data were fit to Eqn. 1 using non-linear least-squares regression with c_1, c_2 and D as parameters. Since the upper level is a singlet, c_3 was set to zero. Values of $D = -2.1$ cm^{-1} and -2.3 cm^{-1} gave the best fits to the experimental data at 705 nm and 420 nm, respectively, for *T. thermophilus* Fd, and $D = -2.0$ cm^{-1} gave the best fit to the experimental data at 690 nm for *A. vinelandii* FdI. The experimental data and the theoretical data based on the best fit parameters, together with the contributions from each of the two ground-state doublets, are shown in Fig. 9. In an attempt to estimate the uncertainty in D, the experimental data were fit allowing only c_1 and c_2 to vary, for a wide range of fixed values of D (-0.5 to -10 cm^{-1}). For partially reduced *T. thermophilus* Fd, satisfactory fits (i.e. within the experimental uncertainty of the data points) were possible at both 420 nm and 705 nm with values of D between -1.2 cm^{-1} and -3.2 cm^{-1}. Values of D between -1.0 cm^{-1} and -4.0 cm^{-1} afforded satisfactory fits to the data for partially reduced *A. vinelandii* FdI.

The low-temperature MCD spectrum of partially reduced *T. thermophilus* Fd was unaffected by pH over the range investigated, pH 6.3 to 8.5. In contrast, the low-temperature MCD spectrum of partially reduced *A. vinelandii* FdI has pronounced pH-dependence; see Fig. 10. The spectra recorded at pH 6.3 are distinctly different from those at pH 7.8 and 8.3 and the low-pH and high-pH spectra are reversibly interconvertible. EPR spectra recorded for samples at pH 6.3 indicate that the [3Fe-xS] cluster is only 70% reduced. This is presumably a consequence of the lower reduction potential of dithionite at the lower pH. Computer subtraction of the 30% of the MCD spectrum of the oxidized [3Fe-xS] cluster from the low-pH spectrum, under identical conditions, produces relatively minor changes in the low-pH MCD spectrum and does not alter the conclusion that the reduced [3Fe-xS] cluster in *A. vinelandii* FdI can exist in two distinct forms dependent on the pH of the buffer. Magnetization data for the low-pH form were collected at 385 nm, 439 nm and 483 nm (data not shown). The data show much more rapid magnetization than would be expected for an $S = 1/2$ ground state and show pronounced nesting that is wavelength-dependent. While it is not possible to analyse the data in detail due to the contributions from the $S = 1/2$ oxidized [3Fe-xS] cluster, the data are indicative of a ground state with $S = 1$ or 2.

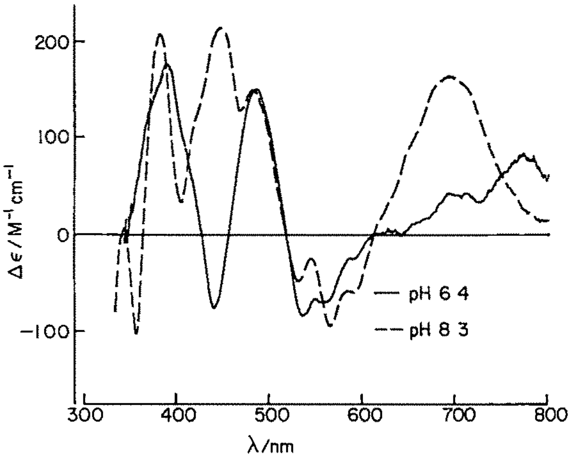

Fig 10. pH dependence of the low-temperature MCD spectrum of partially reduced *A. vinelandii* FdI. Broken line, 0.101 mM Fd in 100 mM Taps with 50% v/v ethylene glycol, pH 8 3, pathlength 0.170 cm. Solid line, 0.080 mM Fd in 100 mM Pipes with 50% v/v ethylene glycol, pH 6.4, pathlength 0.165 cm. Both spectra recorded at 4.22 K with a magnetic field of 4 5 T.

An identical pH effect has been observed for the reduced [3Fe-xS] cluster in *A. chroococcum* Fd [32], except that the low-pH sample was reported to be devoid of any significant EPR signals in this instance. The similarity in the properties of these two ferredoxins is not surprising in light of the fact that the EPR, MCD and CD characteristics of *A. chroococcum* Fd are indistinguishable from those of *A. vinelandii* FdI [32]. The ferredoxins from *A. vinelandii* and *A. chroococcum* are, however, reported to differ in the cluster conversion properties of the reduced [3Fe-xS] cluster [16,32].

EPR and MCD studies of fully reduced T. thermophilus Fd

Reduction of both clusters in *T. thermophilus* Fd was effected by anaerobic addition of excess solid dithionite and subsequent addition of 50% v/v ethylene glycol. The EPR spectrum, shown in Fig. 11, exhibits a complex signal centered at $g = 1.94$, in addition to the broad low-field resonance attributed to the reduced [3Fe-xS] cluster.

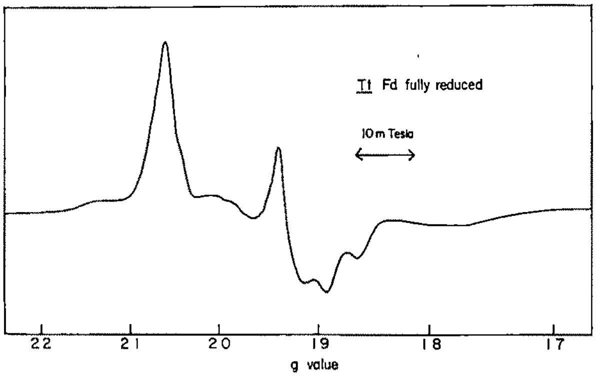

Fig 11 X-band EPR spectrum of fully reduced *T. thermophilus* Fd Sample was identical to the fully reduced sample used in Fig. 1. Temperature 10 K, microwave power 1 mW, modulation amplitude 0.63 mT, microwave frequency 9.02 GHz.

The EPR signal in the $g = 2$ region is identical to that previously reported [3,8,18], and is assigned to an $S = 1/2$ $[4Fe\text{-}4S]^{1+}$ cluster interacting via weak spin-spin interaction with the $S = 2$ reduced [3Fe-xS] cluster [18]. The $g = 1.94$ EPR signal observed in this work accounted for between 0.6 and 0.7 spins/molecule.

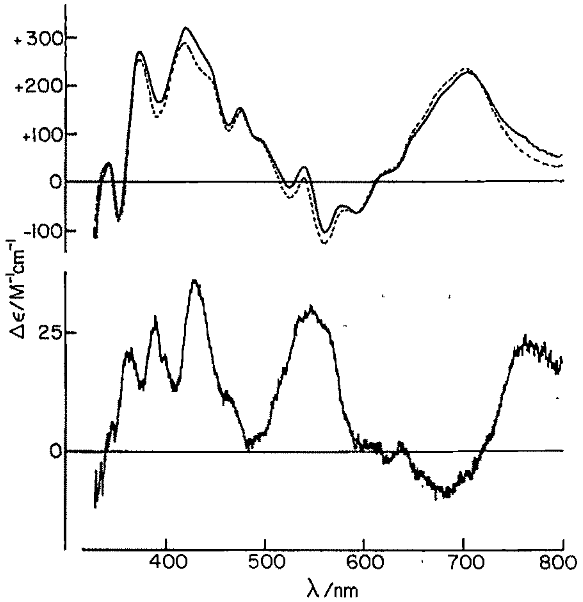

Fig. 12. Comparison of the low-temperature MCD spectra of fully and partially reduced *T thermophilus* Fd. Upper panel: comparison of MCD spectra of fully reduced (solid line) and partially reduced (broken line) *T. thermophilus* Fd at 1 57 K and 4.5 T. Samples were identical to those used in Fig 1 Lower panel: difference spectrum, fully reduced minus partially reduced at 1 57 K and 4 5 T

Fig. 12 shows the low-temperature MCD spectra for fully and partially reduced samples of *T. thermophilus* Fd at 1.57 K and 4.5 T. Comparison of the two spectra shows that the reduced [3Fe-xS] cluster dominates the MCD spectra in both redox states and that the intensity of the low-temperature MCD from the paramagnetic $S = 1/2$ $[4Fe\text{-}4S]^{1+}$ is an order of magnitude weaker than that of the reduced [3Fe-xS] cluster. The form of the low-temperature MCD spectrum for the $[4Fe\text{-}4S]^{1+}$ cluster was obtained by taking the difference between the fully and partially reduced spectra; see Fig. 12. The resultant spectrum has the characteristic features associated with that of a $[4Fe\text{-}4S]^{1+}$, i.e. positive bands centered at 750 nm and 550 nm, multiple positive bands between 460 and 330 nm, and negative band(s) between 600 and 700 nm [35,36]. The intensity of the MCD spectrum is consistent with the EPR spin quantitation.

Attempts to produce the fully reduced form of *A. vinelandii* FdI proved unsuccessful. No EPR signals attributable to a $[4Fe\text{-}4S]^{1+}$ cluster were observed in samples reduced with dithionite over the pH range 6.3 to 8.5, in the presence or absence of ethylene glycol. Stephens et al. have recently reported [16] formation of the fully reduced form and conversion of the reduced [3Fe-xS] cluster to a $[4Fe\text{-}4S]^{1+}$ cluster, albeit in very low yields, on reduction by dithionite at pH 9. However, these conditions also result in destruction of a large fraction of the iron-sulfur clusters.

Discussion

The results presented here permit a critical comparison of the electronic and magnetic properties of the iron-sulfur clusters in 7Fe ferredoxins from *A. vinelandii* and *T. thermophilus*. The low-temperature MCD studies confirm the presence of approximately one [3Fe-xS] cluster in both ferredoxins and show no indication of cluster conversion to yield a [4Fe-4S] cluster under reducing conditions (cf. aconitase [37]). Reduction and identification of the additional cluster as a $[4Fe\text{-}4S]^{2+,1+}$ center was only possible in the case of *T. thermophilus* Fd. However, the presence of a $[4Fe\text{-}4S]^{2+}$ cluster in *A. vinelandii* FdI has been demonstrated by both Mössbauer spectroscopy [7] and X-ray crystallography [5,6]. Our results are consistent with a midpoint reduction potential below -600 mV for the [4Fe-4S], which is in accord with previous investigations [16,17]. As well as differing in terms of midpoint potential, the [3Fe-xS] clusters in these two ferredoxins also differ with respect to their oxidative lability. The $[4Fe\text{-}4S]^{2+}$ cluster in *A. vinelandii* FdI is readily degraded by oxidizing agents such as ferricyanide [17,19], whereas the equivalent center in *T. thermophilus* Fd is extremely resistant to such oxidative breakdown.

The low-temperature MCD and EPR results reported here attest to a close similarity in electronic and magnetic properties of the oxidized [3Fe-xS] clusters in these ferredoxins. Taken together with the existing Mössbauer [7] and resonance Raman [9] data, it seems probable that the almost 200 mV difference in reduction potential of these clusters is a consequence of protein environment rather than major differences in the structures of the clusters. Perhaps the most significant difference in the spectroscopic properties of the oxidized [3Fe-xS] clusters in *A. vinelandii* FdI and *T. thermophilus* Fd is found in the anisotropy and spin relaxation of their EPR signals. However, the factors affecting these properties are presently not well understood. It is of interest to note that, of the presently characterized [3Fe-xS] clusters, the one in *D. gigas* hydrogenase exhibits the smallest anisotropy and slowest spin relaxation [27], whereas the one in *Escherichia coli* nitrate reductase has the largest anisotropy and fastest spin relaxation [28]. The data reported here also indicate a correlation between spin relaxation rates and g-value anisotropy. This correlation is best rationalized in terms of differences in the energy of a low-lying excited state, with a significant orbital moment, that can mix with the ground state and enhance spin-lattice relaxation.

The spectra reported here give no indication of any heterogeneity in the oxidized [3Fe-xS] clusters in *A. vinelandii* FdI as a function of pH over the range 6.3 to 8.5. Moreover, the currently available spectroscopic data, including that presented in this work, point to a similar structure for all the oxidized [3Fe-xS] clusters identified to date. Therefore the only way to reconcile the different structures reported for the oxidized [3Fe-xS] cluster in *A. vinelandii* FdI [5,6,9,12] is to invoke a structure in the crystalline state different from that in solution. However, resonance Raman studies do not support such a hypothesis [9]. Since the available spectroscopic and analytical data for a wide range of [3Fe-xS] clusters are consistent with a [3Fe-4S] core structure with Fe–Fe distances of 2.7 Å, the possibility of an error in the analysis of the X-ray crystallographic data for *A. vinelandii* FdI should be considered.

Low-temperature MCD studies, including detailed investigations of the temperature and magnetic field dependence of the spectra, are particularly informative concerning the electronic and magnetic properties of the reduced [3Fe-xS] clusters in these ferredoxins. MCD magnetization data for the partially reduced ferredoxins are consistent with an $S=2$ ground state with zero-field splitting such that the $M_s = \pm 2$ levels are lowest in energy, i.e. $D < 0$. The observed differences in magnetization data are interpretable in terms of the nature of the ground-state zero-field splitting, with the reduced [3Fe-xS] cluster in *A. vinelandii* FdI having a significant rhombic component compared to the predominantly axial zero-field splitting for the equivalent center in *T. thermophilus* Fd. The nature and magnitude of the structural perturbations that are responsible for the difference in the ground-state zero-field splitting are presently unknown. The magnitudes of the axial zero-field splitting parameters were found to be comparable for the two reduced [3Fe-xS] clusters; $D = -2.2 \pm 1.0$ cm^{-1} for *T. thermophilus* Fd, and $D = -2.5 \pm 1.5$ cm^{-1} for *A. vinelandii* FdI.

The interpretation of the MCD magnetization data for the reduced [3Fe-xS] clusters in these two ferredoxins does permit rationalization of the absence of a $\Delta M = 4$, X-band EPR transition for partially reduced *A. vinelandii* FdI in terms of the zero-field splitting of the $S = 2$ ground state. Resonance will not be possible for a ground state with significant rhombic zero-field splitting such that the splitting of the $M_s = \pm 2$ doublet, Δ ($\Delta = 3E^2/D$), is greater than the microwave energy (approx. 0.3 cm^{-1} at X-band); see Fig. 8. We conclude that although observation of low-field EPR signal for a reduced iron-sulfur protein is indicative of a reduced [3Fe-xS] cluster, the absence of such a signal does not preclude the presence of this type of center.

While no heterogeneity was observed as a function of pH for the oxidized [3Fe-*x*S] clusters in *A. vinelandii* Fd, MCD studies do reveal distinct low- and high-pH forms of the reduced [3Fe-*x*S] cluster. This behavior is analogous to that reported for the [3Fe-*x*S] cluster in *A. chroococcum* Fd [32], but is not observed for the [3Fe-*x*S] clusters in *T. thermophilus* Fd or *D. gigas* FdII [32]. The structural changes accompanying the interconversion of the two forms are presently unclear; however, the ease and rapidity of the interconversion make it unlikely that a major structural reorganization is involved. More likely, the change reflects a protonation-deprotonation equilibrium involving either a cysteinyl sulfur or a cluster sulfide ion. Since this cluster heterogeneity is only observed for the reduced [3Fe-*x*S] cluster, it seems unlikely that it is responsible for the inconsistency in the structural data that has been reported for the oxidized cluster.

Finally we turn our attention to the question of whether the [3Fe-*x*S] clusters in *A. vinelandii* Fd and *T. thermophilus* Fd are present in vivo or are isolation artifacts originating from degradation of a [4Fe-4S] cluster. The latter is certainly the case for the [3Fe-*x*S] clusters in aconitase [37] and *C. pasteurianum* Fd [30], whereas our recent investigations of fumarate reductase from *E. coli* suggest that some [3Fe-*x*S] clusters are intrinsic components of functional enzymes [29] and are present in vivo [38]. No definitive conclusions can be made at this time concerning the clusters in *A. vinelandii* Fd I and *T. thermophilus* Fd. However, the present study does provide two pieces of information that argue against the isolation artifact hypothesis. First, a full complement of oxidized [3Fe-*x*S] clusters were present in anaerobically isolated *A. vinelandii* FdI, and, second, no significant conversion to [4Fe-4S] clusters accompanied dithionite reduction of either Fd over the pH range 6.3 to 8.5. Perhaps the best argument in favor of these [3Fe-*x*S] clusters being isolation artifacts comes from the reported reconstitution of *A. vinelandii* Fd as an 8Fe Fd, comprised of two [4Fe-4S] clusters [15]. However, in our opinion, the spectroscopic data reported in Ref. 15 do not support the claim that reconstituted *A. vinelandii* FdI contains two [4Fe-4S] clusters. Rather the form and spin quantitation of the EPR spectrum of the reduced sample, as well as the UV-visible absorption data (see Ref. 15), provide evidence for no more than one [4Fe-4S]$^{2+,1+}$ cluster. Whether or not the site that is responsible for binding the [3Fe-*x*S] cluster in as-isolated *A. vinelandii* FdI can also accommodate a [4Fe-4S] cluster, therefore, remains to be determined.

Acknowledgements

We thank Carol J. Nettleton for purification of *T. thermophilus* Fd. This work was supported by grants from the National Institutes of Health (GM-33806 to M.K.J. and GM-30974 to J.A.F.), the National Science Foundation (DMB 86-03546 to M.K.J.), Research Corporation, and the American Chemical Society Petroleum Research Fund (to M.K.J.).

References

1 Shethna, Y.I. (1970) Biochim. Biophys. Acta 205, 58–62
2 Yoch, D.C and Arnon, D I. (1972) J. Biol. Chem. 247, 4514–4520
3 Ohnishi, T., Blum, H., Sato, S., Nakazawa, K , Hon-nami, K. and Oshima, T. (1980) J. Biol. Chem. 255, 345–348
4 Sato, S., Nakazawa, K., Hon-nami, K. and Oshima, T. (1981) Biochim. Biophys. Acta 668, 277–289
5 Ghosh, D., Furey, W., O'Donnell, S. and Stout, C.D (1981) J. Biol Chem 256, 4185–4192
6 Ghosh, D., O'Donnell, S , Furey, W., Robbins, A H. and Stout, C D (1982) J. Mol Biol 158, 73–109
7 Emptage, M.H., Kent, T.A., Huynh, B H , Rawlings, J , Orme-Johnson, W.H and Münck, E (1980) J. Biol. Chem 255, 1793–1796
8 Hille, R , Yoshida, T., Tarr, G.E., Williams, C.H., Ludwig, M.L , Fee, J A , Kent, T A., Huynh, B.H. and Münck, E (1983) J Biol. Chem 258, 13008–13013
9 Johnson, M.K., Czernuszewicz, R S , Spiro, T G., Fee, J A and Sweeney, W V. (1983) J. Am Chem. Soc 105, 6671–6678
10 Antonio, M.R., Averill, B A , Moura, I , Moura, J J.G , Orme-Johnson, W.H., Teo, B.K and Xavier, A V (1982) J Biol Chem 257, 6646–6649
11 Beinert, H , Emptage, M H , Dreyer, J L , Scott, R A , Hahn, J.E , Hodgson, K O. and Thomson, A.J. (1983) Proc. Natl. Acad. Sci USA 80, 393–396
12 Stephens, P J , Morgan, T.V., Devlin, F , Penner-Hahn, J E , Hodgson, K.O., Scott, R.A., Stout, C.D. and Burgess, B.K. (1985) Proc. Natl Acad. Sci. USA 82, 5661–5665
13 Johnson, M K., Czernuszewicz, R S., Spiro, T G., Ramsay, R.R and Singer, T.P (1983) J. Biol Chem. 258, 12771–12774

14 Sweeney, W.V, Rabinowitz, J.C and Yoch, D C. (1975) J. Biol. Chem. 250, 7842–7847

15 Morgan, T V., Stephens, P.J., Burgess, B.K. and Stout, C.D. (1984) FEBS Lett. 167, 137–140

16 Stephens, P.J., Morgan, T V., Stout, C.D. and Burgess, B.K. (1986) in Frontiers of Bioinorganic Chemistry (Xavier, A.V., ed.), pp 637–646, VCH Publishers, Weinheim

17 Morgan, T.V, Stephens, P J., Devlin, F, Stout, C.D., Melis, K A. and Burgess, B.K (1984) Proc. Natl Acad Sci USA 81, 1931–1935

18 Hagen, W.R., Dunham, W.R., Johnson, M.K. and Fee, J A. (1985) Biochim. Biophys. Acta 828, 369–374

19 Morgan, T.V., Stephens, P J., Devlin, F, Burgess, B.K and Stout, C.D. (1985) FEBS Lett. 183, 206–210

20 Nagayama, K., Imai, T., Ohmori, D and Oshima, T (1984) FEBS Lett. 169, 79–84

21 Sweeney, W.V (1981) J. Biol. Chem. 256, 12222–12227

22 Johnson, M.K., Morningstar, J.E., Bennett, D E., Ackrell, B.A.C and Kearney, E B. (1985) J. Biol Chem 260, 7368–7378

23 Aasa, R. and Vänngård, T (1976) J Magn Resonance 19, 308–315

24 Beinert, H. and Thomson, A.J. (1983) Arch Biochem Biophys. 222, 333–361

25 Johnson, M.K., Thomson, A.J, Richards, A.J.M., Peterson, J, Robinson, A.E., Ramsay, R.R. and Singer, T P. (1984) J. Biol Chem 259, 2274–2282

26 Thomson, A.J., Robinson, A.E, Johnson, M.K., Moura, J J.G., Moura, I, Xavier, A.V and LeGall, J (1981) Biochim Biophys. Acta 670, 93–100

27 Johnson, M.K., Zambrano, I.C., Czechowski, M.H, Peck, H.D. Jr., DerVartanian, D V. and LeGall, J. (1986) in Frontiers of Bioinorganic Chemistry (Xavier, A V., ed), pp 36–44, VCH Publishers, Weinheim

28 Johnson, M.K., Bennett, D.E., Morningstar, J.E., Adams, M W.W. and Mortenson, L E (1985) J. Biol. Chem 260, 5456–5463

29 Morningstar, J.E, Johnson, M.K., Cecchini, G., Ackrell, B A.C and Kearney, E B (1985) J Biol. Chem. 260, 13631–13638

30 Thomson, A.J, Robinson, A.E., Johnson, M.K., Cammack, R, Rao, K.K. and Hall, D.O. (1981) Biochim Biophys Acta 637, 423–432

31 Thomson, A.J and Johnson, M.K (1980) Biochem J. 191, 411–420

32 George, S.J, Richards, A.J.M., Thomson, A J. and Yates, M.G. (1984) Biochem J. 224, 247–251

33 Abragam, A. and Bleaney, B. (1970) Electron Paramagnetic Resonance of Transition Ions, pp. 209–216, Clarendon Press, Oxford

34 Browett, W.R., Fucaloro, A.F., Morgan, T V. and Stephens, P.J. (1983) J. Am Chem. Soc 105, 1868–1872

35 Johnson, M K., Thomson, A J., Robinson, A.E., Rao, K.K. and Hall, D O. (1981) Biochim. Biophys. Acta 667, 433–451

36 Hatchikian, E.C, Cammack, R., Patil, D.S., Robinson, A.E., Richard, A J.M, George, S. and Thomson, A.J. (1984) Biochim. Biophys. Acta 784, 40–47

37 Kent, T.A., Dreyer, J-L., Kennedy, M.C, Huynh, B H., Emptage, M.H., Beinert, H. and Münck, E (1982) Proc. Natl. Acad. Sci. USA 79, 1096–1100

38 Johnson, M.K., Morningstar, J.E, Cecchini, G. and Ackrell, B.A C. (1985) Biochem. Biophys Res Commun. 131, 653–658

39 Bennett, D.E. and Johnson, M K. (1987) Biochim. Biophys. Acta 911, 71–80

Biochimica et Biophysica Acta 911 (1987) 95–101
Elsevier

BBA 32694

Purification and some properties of peroxidases of rat bone marrow

Kimio Kariya [a], Eibai Lee [a], Masaaki Hirouchi [a], Mikio Hosokawa [b] and Hiroteru Sayo [b]

Departments of [a] Pharmacology and [b] Analytical Chemistry, Faculty of Pharmaceutical Sciences, Kobe-Gakuin University, Ikawadani-cho, Nishi-ku, Kobe 673 (Japan)

(Received 7 July 1986)

Key words Myeloperoxidase, Eosinophil peroxidase; ESR, Heme iron; (Rat bone marrow)

Myeloperoxidase and eosinophil peroxidase were separated and purified from rat bone marrow cells using cetyltrimethylammonium bromide as the solubilizer and then with column chromatographies on CM-Sephadex C-50 and Con A-Sepharose. Both purified enzymes were observed to be apparently homogeneous by SDS-polyacrylamide gel electrophoresis. Myeloperoxidase consisted of two subunits of M_r 57000 and 15000, and eosinophil peroxidase two of 53000 and 14000. On structural analysis of the enzymes, their visual and ESR spectra revealed that the structure surrounding the heme in myeloperoxidase was different from that in eosinophil peroxidase. Moreover, substrate specificity and sensitivity to inhibitors such as azide and cyanide differed between the two enzymes. Rat bone marrow possesses two distinct peroxidases, myeloperoxidase and eosinophil peroxidase, which have different subunits and different heme microenvironments. Therefore, the difference in enzymatic function between the two peroxidases may be due to their structures.

Introduction

Myeloperoxidase (donor:hydrogen peroxide oxidoreductase, EC 1.11.1.7) is present in mammalian leukocytes [1–3] and plays a role in the bacteriocidal function [4,5]. Eosinophils also contain peroxidase activity, called eosinophil peroxidase, the function of which is thought to be antiparasitic [6–8]. On the other hand, the peroxidase activity is observed in bone marrow granulocytes grown from stem cells. Peroxidase in the bone marrow is also a marker enzyme in the neutrophilic granulocytes [9], and its activity changes in their differentiation stages [10]. The above evidence shows that the peroxidase activity in the bone marrow may be involved in the growth of the granulocytes.

On the other hand, although myeloperoxidase and eosinophil peroxidase were also isolated from the bone marrow cells of guinea-pigs [11], their enzymatic properties and physiological and biological functions in bone marrow have been unclear. Previously, we found that leukopenia in rats treated with propylthiouracil was accompanied by the inhibition of peroxidase activity in the bone marrow [12]. Thus, we have attempted to isolate and purify the peroxidases from rat bone marrow, and to analyse their enzymatic characteristics and subunit compositions. Visual and ESR spectra and catalytic activities have been determined.

Materials and Methods

Materials

Guaiacol was purchased from Sigma Chemical

Correspondence: Professor K. Kariya, Department of Pharmacology, Faculty of Pharmaceutical Sciences, Kobe-Gakuin University, Ikawadani-cho, Nishi-ku, Kobe 673, Japan.

0167-4838/87/$03.50 © 1987 Elsevier Science Publishers B V. (Biomedical Division)

Co. Pyrogallol and N,N'-dimethyl-p-phenylenediamine were from Wako Pure Chemicals and Kanto Chemical Co., respectively. CM-Sephadex C-50 and Con A-Sepharose were obtained from Pharmacia. All other chemical of the highest grade were obtained from commercial sources.

Purification of enzymes

Erythrocyte-free bone marrow cells were prepared as described previously [12]. The 105 000 × *g* pellet of bone marrow homogenate was suspended in 10 mM potassium phosphate buffer (pH 7.0) containing 0.5% cetyltrimethylammonium bromide. The suspension was stirred overnight at 4°C and then centrifuged at 20 000 × *g* for 20 min. The supernatant fraction (referred to as cetyltrimethylammonium bromide extract) was dialyzed against 100 vol. of 25 mM acetate buffer (pH 4.7) containing 0.2 M NaCl. Then the dialyzed solution was applied to a CM-Sephadex C-50 column (0.9 × 20 cm) equilibrated with the same buffer. After washing with the same buffer, chromatography was carried out with 300 ml of a 0.2–2.0 M linear gradient of NaCl in the buffer. As shown in Fig. 1, two peroxidase activities were separated and are referred to as myeloperoxidase and eosinophil peroxidase, respectively. Both active fractions were dialyzed twice against 100 mM acetate buffer (pH 5.6) containing 5 mM $CaCl_2$, 5 mM $MgCl_2$, 5 mM $MnCl_2$ and 0.05% cetyltrimethylammonium bromide, and samples were applied to Con A-Sepharose columns (0.9 × 10 cm) equilibrated with the above acetate buffer. The column was washed with the same buffer, and purified peroxidase was eluted with the buffer containing 0.2 M methyl α-D-glucoside. Then the highly purified myeloperoxidase and eosinophil peroxidase were dialyzed again against 50 mM phosphate buffer (pH 7.0) containing 0.1 M NaCl, 0.02% cetyltrimethylammonium bromide and 2% glycerol.

Determination of enzyme activity

Peroxidase activity was assayed according to the previous report [12] with minor modifications. The standard reaction mixture (1.0 ml) consisted of 100 mM potassium phosphate buffer (pH 7.0), 0.33 mM H_2O_2 and guaiacol (33 mM), KI (5 mM), N,N'-dimethyl-p-phenylenediamine (10 mM) or pyrogallol (5 mM). The enzymatic oxidation of guaiacol, KI, N,N'-dimethyl-p-phenylenediamine and pyrogallol was monitored spectrophotometrically at 470, 350, 515 and 430 nm, respectively. When guaiacol and KI were used as the substrate, one unit of activity was defined as the amount of enzyme oxidizing 1 μmol substrate per min, using 5.57 $mM^{-1} \cdot cm^{-1}$ and 26.0 $mM^{-1} \cdot cm^{-1}$ as the extinction coefficients, respectively [13]. One unit of activity in the case of N,N'-dimethyl-p-phenylenediamine or pyrogallol was defined as the amount of enzyme catalyzing a change in absorbance of 1.0 unit/min.

Protein was assayed by the method of Lowry et al. [14].

Physicochemical analysis

SDS-PAGE was performed as described by Laemmli [15] using 12.5% acrylamide. For the estimation of the molecular weight of the enzymes, bovine serum albumin (68 000), ovalbumin (43 000), soybean trypsin inhibitor (21 500) and cytochrome *c* (12 300) were used as the standard compounds.

ESR spectra of myeloperoxidase and eosinophil peroxidase were measured at 4.3 K with an X-band spectrometer (type JES-FE-3X). Instrumental settings were as follows: microwave power, 4 mW; field modulation frequency, 100 kHz; modulation width, 6.3 G; scan rate, 2500 G/min.

Results and Discussion

Purifications of myeloperoxidase and eosinophil peroxidase

Since peroxidase catalyzes the oxidation of various compounds in the presence of hydrogen peroxide, the enzyme activity was determined using guaiacol and KI as substrate. The peroxidase activities of the rat bone marrow were separated into two forms by CM-Sephadex C-50 column chromatography as shown in Fig. 1. This result is compatible with data on the guinea-pig reported by Desser et al. [11]. The activities eluted with 0.5 and 1.2 M NaCl were referred to as myeloperoxidase and eosinophil peroxidase, respectively. Myeloperoxidase was specific for the oxidation of guaiacol rather than that of KI, whereas eosinophil peroxidase predominantly oxidized KI (Fig. 1). Therefore, the catalytic activity of myeloperoxi-

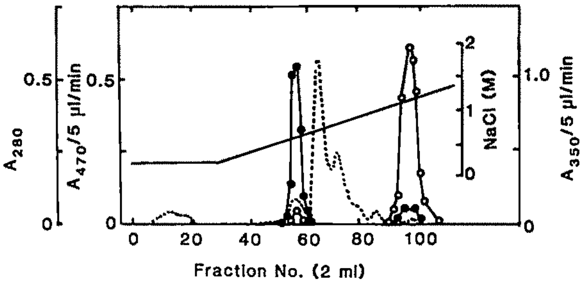

Fig. 1. CM-Sephadex C-50 column chromatography of peroxidases from rat bone marrow After extraction with cetyltrimethylammonium bromide, the peroxidase was loaded on a CM-Sephadex C-50 column (0.9×20 cm). The peroxidase activity was determined using guaiacol (●) or KI (○) as substrate ------, A_{280}.

dase is exactly opposite to that of eosinophil peroxidase. As the peroxidases have been recognized to be glycoproteins [16], the enzymes were further purified by the use of Con A-Sepharose. The enzymes were adsorbed on a Con A-Sepharose column and eluted with methyl α-D-glycoside (data not shown).

Table I represents the summary of purification of the peroxidases from the rat bone marrow. Using guaiacol as the substrate, this purification procedure caused about a 45-fold increase of the activity in myeloperoxidase, with an overall yield of 17.5%. In the case of eosinophil peroxidase, the specific activity was increased by 134-fold with a yield of 13.1% using KI as the substrate. Further, extraction with cetyltrimethylammonium bromide resulted in a larger increase in total activity. The ratios of the absorbance at the Soret maximum to the absorbance at 280 nm (RZ value) were 0.80 and 0.76 for purified myeloperoxidase and eosinophil peroxidase, respectively.

Molecular forms and sizes of myeloperoxidase and eosinophil peroxidase

An analysis by SDS-PAGE revealed that myeloperoxidase was comprised of two major polypeptides (M_r = 57000 and 15000) with minor bands (M_r 74000 and 43000) (Fig. 2). The minor band of M_r 43000 is similar to that reported in human neutrophils [17]. This polypeptide may be derived from the large subunit by proteolytic digestion. Although the origin of the band of M_r 74000 has not been reported yet, it may be a precursor of the large and small subunits. On the other hand, eosinophil peroxidase consisted of two bands (M_r 53000 and 14000) with minor contaminations (Fig. 2).

Generally, myeloperoxidase in human neutrophilic granulocytes is comprised of the large (α) and small (β) subunits [16,18–20]. It has been reported that the enzyme molecules have a molecular weight of about 140000 and $\alpha_2\beta_2$ structure [16,18–20]. Myeloperoxidase in the bone marrow seems to consist of the large (57000) and small (15000) subunits. Similarly, eosinophil peroxidase is comprised of large (53000) and small (14000) subunits as is myeloperoxidase, and its molecular weight is lower than that of myeloperoxidase. The two enzymes also differ in molecular size.

TABLE I

PURIFICATION OF RAT BONE MARROW MYELOPEROXIDASE AND EOSINOPHIL PEROXIDASE

The purification was carried out as described in Materials and Methods. The activity of peroxidase was determined using guaiacol or KI as the electron donor. MPO, myeloperoxidase; EPO, eosinophil peroxidase; CETAB, cetyltrimethylammonium bromide.

	Total protein (mg)	Specific activity (units/mg)		Total activity (units)		Purification factor		Yield (%)	
		guaiacol	KI	guaiacol	KI	guaiacol	KI	guaiacol	KI
105000× g pellet	194.9	4.4	5.0	853.7	966.7	1.0	1.0	100.0	100.0
CETAB extract	120.4	14.6	30.0	1757.8	3612.0	3.3	6.0	205.9	373.6
CM-Sephadex C-50									
MPO	6.0	59.1	3.0	354.0	20.9	13.5	0.7	41.5	2.2
EPO	0.9	179.0	556.7	161.9	506.9	40.7	111.3	19.0	52.4
Con A-Sepharose									
MPO	0.8	198.1	4.1	149.6	3.1	45.3	0.8	17.5	0.5
EPO	0.2	262.1	668.8	49.3	127.1	59.6	133.8	5.8	13.1

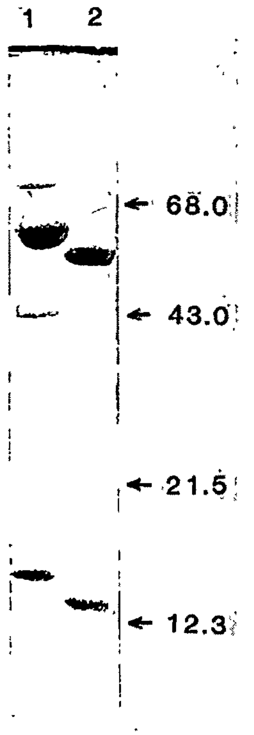

Fig 2 SDS-PAGE of peroxidases purified from the rat bone marrow Lane 1, purified myeloperoxidase; Lane 2, purified eosinophil peroxidase. The arrows show the standard proteins: bovine serum albumin (68000) ovalbumin (43000), soybean trypsin inhibitor (21500) and cytochrome *c* (12300)

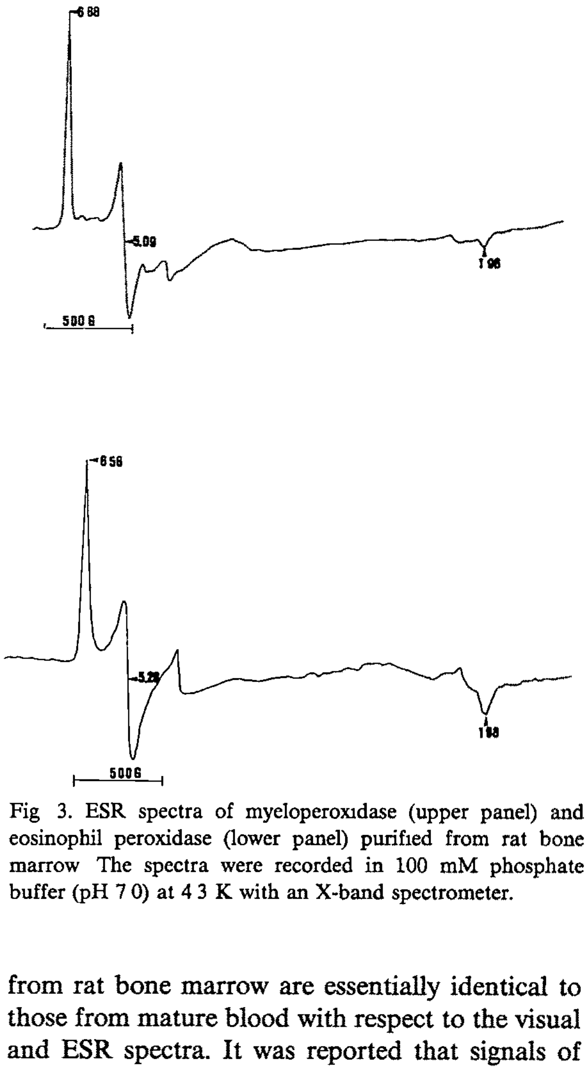

Fig 3. ESR spectra of myeloperoxidase (upper panel) and eosinophil peroxidase (lower panel) purified from rat bone marrow The spectra were recorded in 100 mM phosphate buffer (pH 7 0) at 4 3 K with an X-band spectrometer.

Spectral properties

Myeloperoxidase, in the oxidized state, showed a high peak at 430 nm and additional peaks at 575 and 620 nm. These spectra are in good agreement with the report on human neutrophils [16,19–23]. Eosinophil peroxidase had a maximum adsorption at 415 nm, with minor peaks at 500 and 610 nm. These observations are compatible with the results obtained in guinea-pig [12] and human blood [16,24,25].

Fig. 3 shows the ESR spectra of the two enzymes. The spectra show well-resolved signals near $g = 6$, characteristic of high-spin ferric heme iron in an environment of rhombic symmetry (myeloperoxidase, $g_x = 6.88$, $g_y = 5.09$ and $g_z = 1.96$; eosinophil peroxidase, $g_x = 6.58$, $g_y = 5.28$ and $g_z = 1.98$). These g values are in general agreement with previous reports [23,26,30]. Therefore, myeloperoxidase and eosinophil peroxidase from rat bone marrow are essentially identical to those from mature blood with respect to the visual and ESR spectra. It was reported that signals of both high spin-heme and non-heme iron were found in myeloperoxidase from mature leukocytes [23,26–30]. The purification procedure carried out in the present study remarkably decreased the intensity of the $g = 4.3$ ESR signal of myeloperoxidase, which is attributed to non-heme iron, and greatly increased the specific activity of myeloperoxidase in the catalysis of the H_2O_2-supported oxidation of guaiacol. Therefore, non-heme iron is considered to be independent of the catalytic activity of myeloperoxidase. It should be noted that the ESR spectra of the myeloperoxidase was different from that of eosinophil peroxidase. This suggests that the microenvironment surrounding the heme iron is different in the two enzymes.

Catalytic properties of myeloperoxidase and eosinophil peroxidase

Table II indicates the catalytic activities of the enzymes using various substrates. The activity of myeloperoxidase was highest toward guaiacol among the substrates tested. Trace activity could be shown in the other compounds. However, eosinophil peroxidase oxidized all substrates with hydrogen peroxide. The lowest activity of eosinophil peroxidase was observed with guaiacol as substrate. In addition, eosinophil peroxidase showed specific activities toward all substrates higher than those of myeloperoxidase. Therefore, this is the first distinct characterization of differences between myeloperoxidase and eosinophil peroxidase. These differences in catalytic activity between the two enzymes may be due to the structure surrounding the heme, namely the active centers.

The results of the kinetic analysis of the enzymes are shown in Table III. Although the K_m value for hydrogen peroxide of eosinophil peroxidase toward guaiacol was higher than that toward KI, the value of myeloperoxidase toward guaiacol is the same as that toward KI. The K_m values for guaiacol and KI of eosinophil peroxidase were lower than those of myeloperoxidase. These discrepancies in the kinetic constants may depend on the structures surrounding the heme.

It is well known that peroxidases are inhibited in their activities by the presence of azide and cyanide. Thus the effects of azide and cyanide on the activities of the two enzymes were examined. Azide markedly inhibited the activities of both using guaiacol or KI as the substrate (Fig. 4). However, the sensitivity of myeloperoxidase to azide was higher than that of eosinophil peroxidase using guaiacol, and lower than that of eosinophil peroxidase using KI as the substrate. In the case of cyanide, when guaiacol was used as the substrate, this compound inhibited both activities in a concentration-dependent manner (Fig. 5). Thus the two enzymes differed not only in their catalytic activities, but also in their sensitivities to heme inhibitors. These results suggest that the difference in the degree of inhibition by azide and cyanide is relevant to the mechanism of enzymatic reactions. In relation to this evidence, thyroid peroxidase forms the complex $[EOI]^-$ when KI is used as substrate [31] (Scheme I). However, such a

TABLE II

CATALYTIC ACTIVITY OF MYELOPEROXIDASE (MPO) AND EOSINOPHIL PEROXIDASE (EPO) PURIFIED FROM RAT BONE MARROW

The enzyme activities are expressed as units/mg protein. The values are the means of three experiments. DMPD, *N,N'*-dimethyl-*p*-phenylenediamine.

	Substrates			
	guaiacol	KI	DMPD	pyrogallol
MPO	198.4	4.1	41.4	7.2
EPO	262.1	668.8	2528.2	755.0

TABLE III

KINETIC CONSTANTS OF MYELOPEROXIDASE AND EOSINOPHIL PEROXIDASE PURIFIED FROM RAT BONE MARROW

The kinetic constants were calculated from Lineweaver-Burk plots. The values of K_m and V_{max} were determined in the presence of 33 mM guaiacol or 10 mM KI as the electron donor (a) and of 0.33 mM H_2O_2 (b).

		K_m (mM)	V_{max} (units/mg)
(1) Myeloperoxidase			
H_2O_2 [a]	Guaiacol	0.052	239.8
	KI	0.004	4.8
Guaiacol [b]		44.3	204.5
KI [b]		181.7	549.3
(2) Eosinophil peroxidase			
H_2O_2 [a]	Guaiacol	0.071	334.3
	KI	0.076	611.6
Guaiacol [b]		14.6	363.1
KI [b]		7.5	1280.0

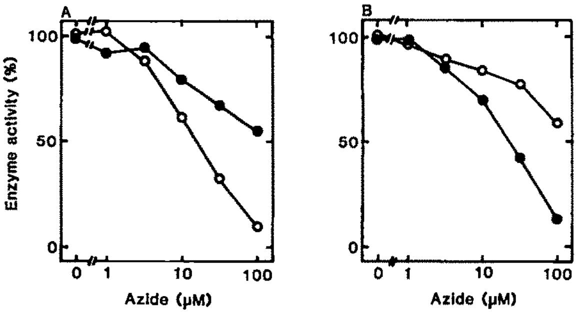

Fig 4. Effect of azide on the activities of myeloperoxidase (A) and eosinophil peroxidase (B) The activities of the peroxidases were determined using guaiacol (○) or KI (●) as substrate

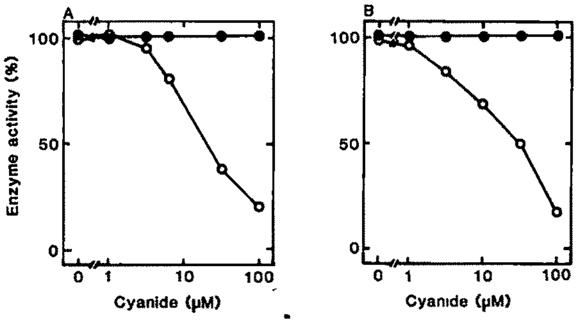

Fig. 5. Effect of cyanide on the activities of myeloperoxidase (A) and eosinophil peroxidase (B) The activities of the peroxidases were determined using guaiacol (O) or KI (●) as substrate.

complex is not formed using guaiacol as the substrate.

As shown in Scheme I, the reaction mechanisms of peroxidase differ according to the substrates used. Therefore, different inhibitor specificities will apply to the mechanism depending on the substrate. When KI was used as substrate, no effect on peroxidases was seen in the case of cyanide addition (Fig. 5). As it has been reported that Cl^- inhibits the binding of cyanide to chloroperoxidase [32], a halogen ion such as I^- might antagonize the binding of cyanide to the peroxidase. However, since Bakkenist et al. [33] reported that the dissociation constant of the myeloperoxidase-iodide complex was about 50 mM at pH 7.0, the possibility is uncertain at present. The action of cyanide on the oxidation of iodide catalyzed by myeloperoxidase and eosinophil peroxidase still remains to be elucidated in detail.

$$E+H_2O_2 \rightarrow EO \xrightarrow{I^-} [EOI]^- \xrightarrow[H_2O]{I^-} I_2 + 2OH^- + E \qquad (1)$$

$$E+H_2O_2 \rightarrow EO \xrightarrow{\text{guaiacol}} \text{tetraguaiacol} + E \qquad (2)$$

Scheme I

In this report it has been demonstrated that two peroxidases, myeloperoxidase and eosinophil peroxidase, are present in rat bone marrow. In addition, these enzymes were isolated from the same preparation. Both peroxidases had distinct enzymatic properties and showed differences in many aspects, including subunit composition, visual and ESR spectra and catalytic activities. From these results, we propose that the microenvironments surrounding the heme iron in myeloperoxidase and eosinophil peroxidase influence their catalytic activity. Such differences are related to their differing physiological significance in the bone marrow. Those findings are also thought to be a clue to the elucidation of the physiological roles of the two enzymes in the bone marrow.

Acknowledgement

This research was supported in part by a Grant-in-Aid (No. 58771687) from the Ministry of Education, Science and Culture of Japan.

References

1 Agner, K. (1941) Acta Physiol. Scand. 2, 1–62
2 Schultz, J., R , Oddi, F., Kaminker, J. and Jones, W. (1965) Arch Biochem Biophys 111, 73–79
3 Bos, A., Wever, R. and Roos, D. (1978) Biochim. Biophys. Acta 525, 37–44
4 Klebanoff, S J. (1975) Semin Hematol. 12, 117–142
5 Rosen, H. and Klebanoff, S J. (1977) J. Biol. Chem 252, 4803–4810
6 McLaren, D.J., Mackenzie, C.D. and Ramalho-Pinto, F.J (1977) Clin. Exp. Immunol 30, 105–118
7 Buys, J , Wever, R , von Stigt, R. and Ruitenberg, E.J. (1981) Eur. J. Immunol 11, 843–845
8 Nogueira, N N., Klebanoff, S.J. and Cohn, Z A (1982) J Immunol 128, 1705–1708
9 Bainton, D.F., Ullyot, J.L and Farquhar, M.G (1971) J. Exp. Med. 134, 907–934
10 Rovera, G., Santoli, D. and Damsky, C (1979) Proc Natl. Acad Sci USA 76, 2779–2783
11 Desser, R K., Himmelhoch, S R., Evans, W.H., Januska, M., Mage, M. and Shelton, E. (1972) Arch Biochem Biophys 148, 452–465
12 Kariya, K., Lee, E. and Hirouchi, M (1984) Japan. J. Pharmacol 36, 217–222
13 Hosoya, T and Morrison, M. (1967) J Biol. Chem 242, 2828–2836
14 Lowry, O.H., Rosebrough, N.J , Farr, A.L. and Randall, R.J. (1951) J. Biol. Chem. 193, 265–275
15 Laemmli, U.K. (1970) Nature 227, 680–685
16 Olsen, R.L. and Little, C. (1983) Biochem. J. 209, 781–787
17 Olsen, R.L. and Little, C. (1984) Biochem. J. 222, 701–709
18 Harrison, J.E., Pabalan, S and Schultz, J. (1977) Biochim Biophys. Acta 493, 493, 247–259
19 Andrews, P C. and Krinsky, N.I. (1981) J Biol. Chem 256, 4211–4218
20 Andersen, M.R., Atkin, C.L. and Eyre, H J. (1982) Arch Biochem. Biophys 214, 273–283

21 Pember, S.O., Shapira, R. and Kinkade, J.M., Jr. (1983) Arch. Biochem. Biophys. 221, 391–403

22 Schultz, J. and Shmukler, H.W. (1964) Biochemistry 3, 1234–1238

23 Bakkenist, A.R.J., Wever, R., Vulsma, T., Plat, H. and Van Gelder, B.F. (1978) Biochim. Biophys. Acta 524, 45–54

24 Bolscher, B.G.J.M., Plat, H. and Wever, R. (1984) Biochim. Biophys. Acta 784, 177–186

25 Carlson, M.G.C., Peterson, C.G.B. and Venge, P. (1985) J. Immunol. 134, 1875–1879

26 Ehrenberg, A. (1962) Arki. Kemi 19, 119–128

27 Wever, R., Roos, D., Weening, R.S., Vulsma, T. and Van Gelder, B.F. (1976) Biochim. Biophys. Acta 421, 328–333

28 Wever, R. and Bakkenist, A.R.J. (1980) Biochim. Biophys. Acta 612, 178–184

29 Odajima, T. (1980) J. Biochem. 87, 379–391

30 Wever, R., Hamers, M.N., Weening, R.S. and Roos, D. (1980) Eur. J. Biochem. 108, 491–495

31 Magnusson, R.P., Taurog, A. and Dorris, M.L. (1984) J. Biol. Chem. 259, 197–205

32 Lambeir, A.M. and Dunford, H.B. (1983) J. Biol. Chem. 258, 13558–13563

33 Bakkenist, A.R.J., De Boer, J.E.G. and Wever, R. (1980) Biochim. Biophys. Acta 613, 337–348

Biochimica et Biophysica Acta 911 (1987) 102–108
Elsevier

BBA 32599

Chemical modification of bovine liver rhodanese with tetrathionate: differential effects on the sulfur-free and sulfur-containing catalytic intermediates

A.R.S. Prasad and Paul M. Horowitz

Department of Biochemistry, University of Texas Health Science Center, San Antonio, TX 78284 (U.S.A.)

(Received 14 August 1986)

Key words. Rhodanese; Chemical modification; Enzyme inactivation; Sulfhydryl group; Tetrathionate

Sulfhydryl groups of bovine liver rhodanese (thiosulfate:cyanide sulfurtransferase, EC 2.8.1.1) were modified by treatment with tetrathionate. There was a linear relationship between loss of enzyme activity and the amount of tetrathionate used. At a ratio of one tetrathionate per mole of rhodanese, 100% of enzyme activity was lost in the sulfur-free E-form as compared with a 70% loss for the sulfur-containing ES-form of the enzyme. Addition of up to a 100-fold molar excess of tetrathionate to ES gave no further inactivation. Addition of cyanide to the maximally inactivated ES-tetrathionate complex gave complete loss of activity. Kinetic studies of maximally inactivated ES and partially inactivated E gave K_m (K_s) values that were essentially the same as native enzyme, indicating that the active enzyme, in all cases, bound thiosulfate similarly. Reactivation was faster with the ES-form than with the E-form. The substrate, thiosulfate, could reactivate the enzyme up to 70% in 1 h with ES as compared to 24 h with E. Tetrathionate modification of rhodanese could be correlated with the changes in intrinsic fluorescence and with the binding of the active site reporter 2-anilinonaphthalene-8-sulfonic acid (2,8-ANS). Circular dichroism spectra of the protein suggested increased ordered secondary structure in the protein after reaction with tetrathionate. Cadmium chloride and phenylarsine oxide totally inactivated the enzyme at levels usually associated with their effect on enzymes containing vicinal sulfhydryl groups. Further, cadmium inhibition could be reversed by EDTA. Tetrathionate modification of rhodanese may proceed through the formation of sulfenylthiosulfate intermediates at sulfhydryl groups, close to but not identical with the active-site sulfhydryl group, which then can react further with the active-site sulfhydryl group to form disulfide bridges.

Introduction

Rhodanese (thiosulfate:cyanide sulfurtransferase, EC 2.8.1.1) catalyzes the transfer of the outer sulfur atom of thiosulfate to the nucleophilic acceptor substrate cyanide [1–3]. The enzyme is a single polypeptide chain containing 293 amino acid residues [4] and contains 4 cysteine residues at positions 63, 247, 254 and 263. There are no disulfide bridges in the protein. Cysteine 247 is at the active site and holds the transferred sulfur as a persulfide. The polypeptide chain is folded into two domains connected by a loop of 16 amino acid residues [5] and the active site is at the interface of these two domains. Several sulfhydryl reagents have been shown to inactivate this enzyme [6–11]. Disulfide-bond formation between the active-site cysteine residue and a nearby sulf-

---

Abbreviations: 2,8-ANS, 2-anilinonaphthalene-8-sulfonic acid, E, the sulfur-free form of rhodanese, ES, the sulfur-substituted form of rhodanese

Correspondence: Dr. Paul M. Horowitz, Department of Biochemistry, University of Texas Health Science Center at San Antonio, 7703 Floyd Curl Drive, San Antonio, TX 78284, U.S.A.

4167-4838/87/$03.50 © 1987 Elsevier Science Publishers B.V. (Biomedical Division)

hydryl group has been implicated in the mechanism of inactivation by a wide variety of reagents [9]. The crystal structure, on the other hand, indicates that such disulfide-bond formation is not likely. The importance of sulfhydryl groups to the activity of rhodanese and the structural similarity between tetrathionate and thiosulfate, together with the known reactivity of this reagent with the sulfhydryl groups, prompted us to look into the effect of this reagent on rhodanese. The results presented here indicate that tetrathionate reacts with rhodanese in a complex pattern to form an inactive enzyme in the E-form, and a partially active derivative with the ES-form. The results can be rationalized by a model that incorporates the results of previous work showing that the individual sulfhydryl groups have differing reactivities and that disulfides can form within soluble conformers of the enzyme.

Materials and Methods

Materials

2-Anilinonaphthalene-8-sulfonic acid (2,8-ANS) was from Molecular Probes (Junction City, OR). All other reagents used were of the analytical grade.

Methods

Preparation and assay of rhodanese. Rhodanese purified from bovine liver was stored as a frozen ammonium sulfate pellet at −40°C and was assayed for activity as described by Horowitz [12]. Protein concentration was determined using an extinction of $E_{280}^{0.1\%} = 1.75$ [13]. The molecular weight of the protein was taken to be 33 000 [4,14]. All experiments were done in 20 mM sodium phosphate buffer containing 1 mM EDTA at pH 7.5 at 23°C unless otherwise stated. Sulfur-free rhodanese (E form) was obtained by adding a 10-fold molar excess of cyanide to a rhodanese solution containing no thiosulfate as described previously [15,16]. Kinetic studies to assess the effect of tetrathionate on the catalysis by rhodanese were performed using the rhodanese assay previously described [6] and were carried out in 50 mM KCN, 50 mM KH_2PO_4 and $K_2S_2O_3$ between 0 and 50 mM. Potassium sulfate (0–50 mM) was added to maintain the asay pH at 7.6. Initial velocities were calculated from the best straight-line fits to the initial portions of the progress curve.

Purified rhodanese was separated into A and B forms by chromatography on DE-52 according to the method of Blumenthal and Heinrikson [17].

Fluorescence measurements. Fluorescence measurements were carried out with an SLM Aminco model SPF-500C spectrophotofluorometer operated in the ratio mode. Temperature was maintained at 23°C by circulating water through the cell holder. Time-dependent fluorescence changes were measured using a strip chart recorder that monitored the instrument response.

Circular dichroism. CD measurements were made on a Jasco J 500C spectropolarimeter equipped with a model DP 500 data processor. Spectra were run at 23°C in a cell with 0.1 cm path lenth. Spectra were scanned from 260 to 195 nm and were corrected using a blank containing all components except the rhodanese. CD spectra were run on both the E and the ES forms of the enzyme in the presence (1-fold molar excess) and absence of tetrathionate. Mean residue ellipticities, $[\theta]$ MRW, were calculated using a mean residue weight of 115.

Difference absorption spectroscopy. Spectral measurements were made on a Cary 219 spectrophotometer in the region specific for persulfide groups. To get the base-line, a sample cuvette containing 1 ml of buffer with E or ES at 0.23 mg/ml was scanned against a reference cuvette containing an identical enzyme solution. To titrate the E or ES sample with tetrathionate, microliter quantities of a tetrathionate solution made in buffer were added to the sample cuvette. The same volume of buffer without tetrathionate was added to the reference cuvette to compensate for dilution of the sample.

Results and Discussion

Sulfur-free rhodanese (E) was completely inactivated at a 1:1 molar ratio of tetrathionate to enzyme as shown in Fig. 1. The inactivation was instantaneous and a linear function of the tetrathionate concentration. The sulfur-containing form of rhodanese (ES) was also inactivated by tetrathionate. 70% of the enzyme activity was lost at a

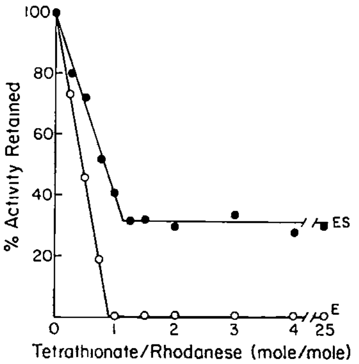

Fig. 1. Tetrathionate inactivation of rhodanese in E and ES forms. Rhodanese (7 μM) in 100 μl of 20 mM sodium phosphate, 1 mM EDTA, pH 7.6, was incubated with various concentrations of sodium tetrathionate at 0 °C for 1 h 5-μl aliquots of the enzyme were assayed for 15 s in triplicate ○, E form; ●, ES form

1:1 molar ratio of the reagent to rhodanese. Increasing the concentration of tetrathionate further, up to 100-fold molar excess over the enzyme, gave no additional inactivation of ES. Addition of cyanide at any point in an experiment similar to that shown in Fig. 1 resulted in total inactivation of ES (data not shown), suggesting the importance of the free active-site sulfhydryl group (Cys-247) in the tetrathionate modification of rhodanese. The fact that ES could only be 70% inactivated might be due to the following reasons: (a) rhodanese as normally prepared contains two electrophoretic variants (A and B) and they may differ in their reactivity towards tetrathionate; or (b) there may be differential reactivity of the sulfhydryl groups in rhodanese. In order to decide between these possibilities, we separated the A and B forms of rhodanese by anion-exchange chromatography on DE-52 as described previously [17]. Purified B rhodanese, the form with the least cross-contamination, was inactivated in both its E and its ES forms in exactly the same manner by tetrathionate as the original enzyme, suggesting differential reactivity of sulfhydryl groups as responsible for the effects observed. The result with ES is intriguing, as its suggests two mutually exclusive modes of tetrathionate binding to rhodanese, only one of which leads to inactivation. In the model shown in Fig. 6 (path A) the inactive species would involve modification of cystein 254.

Sodium thiosulfate is known to reactivate rhodanese that has been inactivated with various sulfhydryl reagents [6,8,9]. Hence, we tried to reactivate the rhodanese that had been inactivated with tetrathionate using sodium thiosulfate. The results are shown in Fig. 2. Nearly 70% of the activity could be recovered from both the E and the ES forms of the enzyme. However, reactivation of the ES form of the enzyme (1 h to reach 70% reactivation) was much more rapid than for the E form of rhodanese (24 h to reach 70% reactivation). We were able to reactivate the tetrathionate-inactivated enzyme at relatively low concentrations of thiosulfate (100-fold molar excess) in 24 h. Wang and Volini [6] were able to reactivate the mercaptoethanol-inactivated enzyme with 1-fold molar excess of a thiosulfate in 5 days. Weng et al. [10] used similar conditions to reactivate rhodanese inactivated by phenylglyoxal. Reactivation of rhodanese inactivated with tetrathionate at concentrations greater than 1-fold molar excess of tetrathionate was much easier than at low concentrations of the reagent. This suggests that the mode of inactivation of rhodanese by tetrathionate is concentration-dependent. Low concentrations of tetrathionate seem to introduce disulfide bonds in the protein which are much harder to reactivate.

Tetrathionate is structurally similar to thiosulfate and, in fact, can be visualized as a dimer of thiosulfate. Hence, it is natural to think that it will

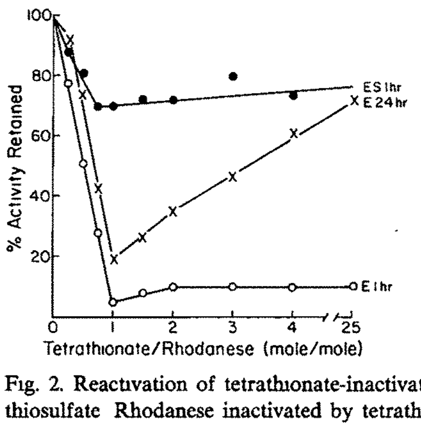

Fig. 2. Reactivation of tetrathionate-inactivated rhodanese by thiosulfate Rhodanese inactivated by tetrathionate in both E and ES forms as in Fig. 1 was made 100 mM with respect to thiosulfate and incubated at 23 °C. Activity was measured in an aliquot as indicated in the figure. The E samples were assayed either 1 h (○) or 24 h (×) after adding thiosulfate.

bind at the same site as thiosulfate and it is of interest to know the effect of tetrathionate on the binding of thiosulfate to rhodanese. As already noted, tetrathionate inactivation of the ES form of rhodanese led to 70% inactivated enzyme. In order to characterize this form of the enzyme in more detail, kinetic studies were performed using this enzyme and compared with results generated with partially inactivated E having the same total activity. The modified enzyme obtained with both E and ES forms of rhodanese showed very similar kinetics with respect to the substrate thiosulfate. Lineweaver-Burk plots of the kinetic data (not shown) gave K_m values of 8.06 mM and 7.57 mM vor thiosulfate for maximally inactivated ES and the partially active, E, respectively. Since K_m for thiosulfate has been shown to be equivalent to K_s [6], these results imply that the tetrathionate modification apparently had no effect on the affinity of the active enzyme for the thiosulfate. It is possible, therefore, that 30% active ES achieved at 1 : 1 tetrathionate to rhodanese contained fully active enzyme, with tetrathionate bound in such a way that thiosulfate binding was unaffected, but the reaction with tetrathionate leading to inactivation was prevented.

In order to assess the sulfhydryl titer of the various tetrathionate-inactivated rhodanese forms, DTNB titrations were performed and the data are presented in Table I. In keeping with previous results, E gave 1 sulfhydryl group under native conditions and 4 sulfhydryl groups when denatured with 6 M guanidinium chloride. When the enzyme was inactivated at 1 : 1 tetrathionate to rhodanese, two sulfhydryl groups were measured whether the protein was denatured or not. When the tetrathionate was present at a 50-fold molar excess over enzyme, fewer than one sulfhydryl group was detected independent of the presence of denaturant. In fact, in the absence of denaturant, enzyme so modified still had 30% of its initial activity. These results are consistent with a conformational change in the protein that accompanies the inactivation, and seem to indicate, further, that tetrathionate can modify additional sulfhydryl groups beyond those required for the activity.

TABLE I

SULFHYDRYL TITER OF NATIVE AND TETRATHIONATE-MODIFIED RHODANESE

Rhodanese (ES) (0.5 mg) was reacted with tetrathionate at indicated concentrations as described under Methods and converted into E form by the addition of 10-fold molar excess of CN. The modified enzyme was passed through a PD-10 column to remove excess cyanide and tetrathionate. 0.2 mg of this was used for DTNB titration according to Ellman's procedure as described by Glazer et al. [27]. For denatured rhodanese, protein was run into a solution containing 6 M guanidine hydrochloride and DTNB values reported are individual determinations in duplicate analyses.

Tetrathionate/ rhodanese	Sulfhydryl groups titrated (mole/mole)	
	buffer	6 M guanidine-HCl
0	0.72	3.84
	0.97	3.66
1	1.54	2.42
	2.06	1.96
50	0.40	0.38
	0.66	0.60

Binding of several effectors near the active site of rhodanese has been shown to perturb the chromophores in the hydrophobic cluster in the interdomain cleft so as to alter the optical properties of the enzyme [18,19]. Hence, we looked at the effect of tetrathionate on the intrinsic fluorescence, absorption spectra, circular dichroism spectra and 2,8-ANS binding in E and ES forms of rhodanese. It has been shown earlier that the E and ES rhodanese differ in their intrinsic fluorescence [16]. Addition of cyanide, which removes the sulfur from the active-site cysteine residue, leads to a stoichiometric increase in fluorescence. Since reaction at the active-site sulfhydryl group affects the intrinsic fluorescence, it was of interest to see the effect of tetrathionate modification on the fluorescence of E and ES. As shown in Fig. 3, addition of tetrathionate had no effect on ES at any concentration tested, but there was a stoichiometric quenching of the intrinsic fluorescence of E. In fact, the equivalence point in the fluorescence titration of E was consistent with the 1 : 1 stoichiometry observed in the activity-based titration. Cannella et al. [18] have shown that the sulfur in the ES form of the enzyme is in a persulfide linkage with a characteristic absorption at 335 nm. Removal of this sulfur to produce the E form of the enzyme leads to the loss of this

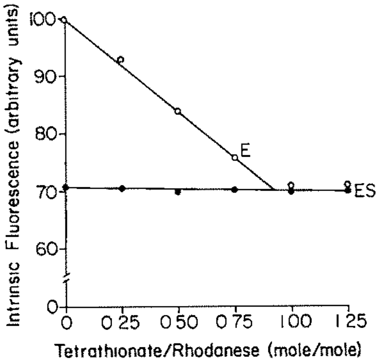

Fig. 3. Effect of tetrathionate modification on rhodanese intrinsic fluorescence Rhodanese intrinsic fluorescence was measured as a function of tetrathionate/rhodanese ratio. Excitation was at 280 nm and emission was at 335 nm. Rhodanese was at 0.2 mg/ml ●, fluorescence of the ES form of rhodanese; ○, fluorescence of the E form of rhodanese.

absorption. Addition of tetrathionate to the E form of the enzyme did not result in any absorption increase at 335 nm. There was no change in the absorption spectrum over the wavelength range 280 to 400 nm of either the E or the ES forms of the enzyme treated with 1.5-fold molar excess of tetrathionate. This suggests that the mechanism of quenching of the intrinsic fluorescence of rhodanese by tetrathionate is not due to resonance energy transfer between the tryptophan residues and the bound tetrathionate as has been suggested for the quenching due to the introduction of sulfur in forming ES [20;21].

Addition of cyanide to a sample of rhodanese treated with tetrathionate at high protein concentrations (greater than 0.5 mg/ml) led to the precipitation of the protein at room temperature. Such a precipitation was not observed when the sample was cooled to 0°C before cyanide was added, suggesting exposure of hydrophobic areas on the protein as a result of tetrathionate modification and leading to the aggregation of the protein. This is in agreement with increased binding of 2,8-ANS to the tetrathionate-modified enzyme (see below).

Circular dichroism spectral studies of rhodanese have revealed differences in the secondary structure of the E and ES forms of the protein. We looked at the CD spectra of rhodanese treated with tetrathionate in E and ES forms of the enzyme. As shown in Table II, the effect of added tetrathionate was to increase ordered secondary structure of the protein. This result is in keeping with a reorganization of the protein backbone following reaction with tetrathionate.

TABLE II

ELLIPTICITY VALUES FOR RHODANESE IN E, ES AND E-TETRATHIONATE FORMS

Circular dichroism spectra of rhodanese (6 μM) in 10 mM Tris-sulfate, pH 8.6, were measured at 23°C as described under Methods in E, ES and E-tetrathionate forms. The E-tetrathionate form was obtained by reacting the E-form of the enzyme with 10-fold excess of tetrathionate. Ellipticity values were calculated as described under Methods

Enzyme form	Molar ellipticity (10^3 deg·cm^2·dmol^{-1})		
	208 nm	215 nm	220 nm
ES	8.32	7.01	6.13
E	7.89	6.79	5.91
E-tetrathionate	10.08	8.54	7.45

The hydrophobic fluorescent probe, 2,8-ANS, binds to rhodanese at the active site [22]. Hence, any changes in the binding of this probe reveal changes around the active site. As shown in Fig. 4, the effect of added tetrathionate to E was to increase the 2,8-ANS fluorescence in a stoichiometric manner. There was a gradual increase in the fluorescence up to 1-fold molar excess of tetrathionate over the enzyme, after which there

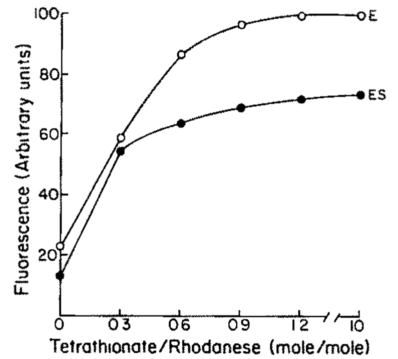

Fig. 4. Effect of tetrathionate on 2,8-ANS binding to E and ES forms of rhodanese. Rhodanese (0.2 mg/ml) in the E and ES forms was incubated with 50 μM 2,8-ANS in 20 mM Tris-sulfate buffer, pH 8.5. Excitation was at 350 nm. Emission was measured at 450 nm at the indicated concentrations of tetrathionate at 23°C.

was no further increase. Addition of tetrathionate to ES also gave an increase in the 2,8-ANS fluorescence, but even at very high ratios of tetrathionate over rhodanese the fluorescence was less than with the E form.

The results presented above are consistent with tetrathionate modification of rhodanese at more than one cysteine residue, although the stoichiometry of the effects implies that each enzyme molecule need incorporate only one tetrathionate molecule to become inactivated. A variety of solution results have indicated that at least 3 of the 4 sulfhydryl groups in rhodanese are close to each other at the active site [4]. The presence of sulfhydryl groups close together can result in the formation of disulfide bridges by displacement of thiosulfate from the sulfenylthiosulfonate formed as a result of modification with tetrathionate [23]. Hence we looked at the possible presence of vicinal dithiols at the active site of rhodanese using the criteria provided by Gaber and Fluharty [24]. The results of such a study are shown in Fig. 5. Cadmium chloride at 20 mM was able to totally inactivate rhodanese in both the E and the ES forms, in a first-order process. However, the rates of inactivation were different. E was inactivated with a half-time of 5 min, as compared to 20 min for ES. Cadmium-inactivated rhodanese could be reactivated to 70% by 100 mM EDTA but not by reducing agents such as dithiothreitol, mercaptoethanol or thiosulfate (data not shown). This is understandable, since reducing agents themselves cause inactivation of rhodanese [6,7[. Phenylarsine oxide, another reagent used to detect the presence of vicinal dithiols [25,26], also caused inactivation of E at a 10-fold molar excess, with no effect on the ES form of rhodanese. Phenylarsine oxide inactivation of rhodanese could not be reversed by EDTA or dithiothreitol (data not shown).

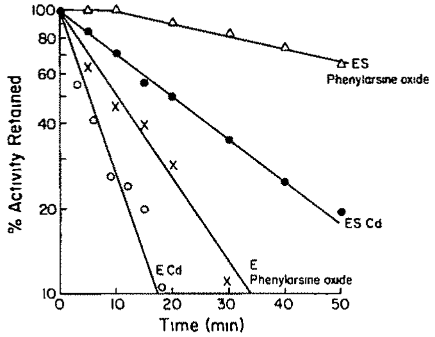

Fig. 5 Time course for cadmium chloride and phenylarsine oxide inhibition of E and ES forms of rhodanese. Rhodanese (0.2 mg/ml) in the E and ES forms was incubated with a 20-fold molar excess of cadmium chloride in 50 mM Tris-sulfate, pH 8.6. Activity was measured with an aliquot of the enzyme at various time intervels In a similar fashion rhodanese was incubated with a 50-fold molar excess of phenylarsine oxide The figure shows a semilog plot ●, ES form, ○, E form with cadmium,; △, ES form, ×, E form with phenylarsine oxide.

Studies of the sulfhydryl groups of rhodanese have been critical for understanding all aspects of its structure and function. The results of the present study are consistent with the many solution studies that show that sulfhydryl groups in soluble rhodanese can be brought into close enough proximity so that the active-site sulfhydryl group (Cys-247) can interact with other sulfhydryl groups in the enzyme. This is particularly evident in the oxidative inactivation of E by phenylglyoxal in which it was shown that a disulfide forms with cysteine 247 whose partner is cysteine 254 70% of the time and cysteine 263 30% of the time. These results are of particular interest, since the *X*-ray structure has been reported not to favor disulfide formation. This discrepancy has been the focus of studies that have sought to compare the solution and crystal structure.

The scheme presented in Fig. 6 fits the observations made in this paper and is in keeping with the many other studies of this aspect of the rhodanese structure previously reported. In both the E and the ES forms of the enzyme, tetrathionate does not react with the cysteine residue at position 247, instead it reacts 70% of the time with cysteine 254 and 30% of the time with cysteine 263 (paths A and B). These modifications are proposed to be mutually exclusive and are in keeping with the reactivities reported by Weng et al. [10]. Formation of sulfenylthiosulfate at cystein 254 prevents thiosulfate binding at the active site sterically and electrostatically, leading to the observed inactivation. Modification at cysteine 263 is far enough from the active site that the resulting enzyme has an apparently unmodified K_m. This is quite in keeping with the explanation proposed for the cyanolytic reactivation of the rhodanese-

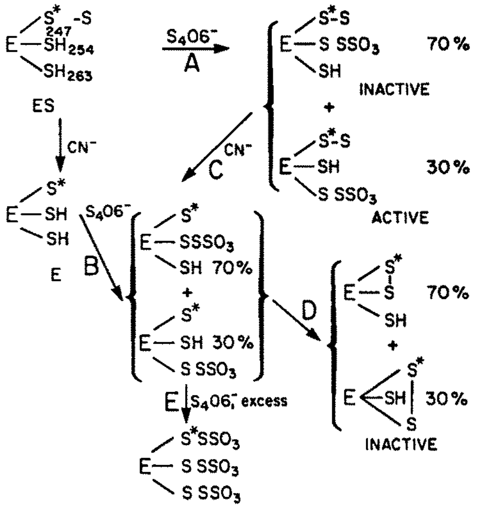

Fig. 6. Proposed scheme for the inactivation of rhodanese in the E and ES forms by tetrathionate.

thionitrobenzoate complex with the concomitant incorporation of cyanide [8]. Addition of cyanide to 70% inactivated ES leads to total inactivation of the enzyme (see above). This would occur because cyanide addition makes the sulfhydryl group at the active site free (path C) and could result in the formation of disulfide bridges and totally inactive enzyme (path D). This form of the enzyme seems to be more resistant to reactivation by thiosulfate (Fig. 2), as is shown by the reactivation patterns of Pensa et al. [8]. In the presence of excess tetrathionate cysteine 247 also forms a sulfenylthiosulfate derivative and prevents the formation of disulfide bridges (path E). This form of the enzyme is reactivated much faster (Fig. 2). Inactivation of rhodanese by cadmium chloride and phenylarsine oxide suggests the presence of vicinal thiol groups in rhodanese, and further supports a model that invokes interactions among sulfhydryl groups that are close together in the soluble form of rhodanese. Hence, interaction of tetrathionate with rhodanese seems to involve these vicinal thiol groups and can lead to the formation of disulfide bridges.

Acknowledgements

This work was supported by research grants GM25177 from NIH and Welch grant AQ-723 to P.M.H.

References

1 Westley, J. (1973) Adv. Enzymol. 39, 327–368
2 Westley, J. (1977) in Bioinorganic Chemistry (van Tamelen, ed.), Vol 1, pp. 371–390, Academic Press, New York
3 Sorbo, B. (1975) in Metabolic Pathways (Greenberg, D.M., ed.), pp. 433–456, Academic Press, New York
4 Ploegman, J.H., Drent, G., Kalk, K.H., Hol, W.G.J., Heinrikson, R.L., Keim, P, Weng, W. and Russel, J. (1978) Nature (London) 273, 124–129
5 Hol, W G.J., Lijk, L.J. and Kalk, K H (1983) Fund. Appl. Technol 3, 370–376
6 Wang, S F and Volini, M (1968) J. Biol. Chem 243, 5465–5470
7 Pecci, L., Pensa, B., Costa, M., Cignini, P.L. and Cannella, C. (1976) Biochim Biophys Acta 445, 104–111
8 Pensa, B , Costa, M., Pecci, L., Cannella, C. and Cavallini, D. (1977) Biochim. Biophys. Acta 484, 368–374
9 Costa, M., Pecci, L., Pensa, B. and Cannella, C (1977) Biochem. Biophys. Res. Commun. 78, 596–603
10 Weng, L., Heinrikson, R.L. and Westley, J. (1978) J. Biol Chem. 253, 8109–8119
11 Horowitz, P. and Criscimagna, N.L. (1982) Biochim. Biophys Acta 702, 173–177
12 Horowitz, P. (1978) Anal. Biochem 86, 751–753
13 Sorbo, B H. (1953) Acta Chem Scand. 7, 1123–1130
14 Trumpower, B.L., Katki, A. and Horowitz, P. (1974) Biochem. Biophys. Res. Commun. 57, 532–538
15 Wasylewski, Z. and Horowitz, P.M. (1982) Biochim. Biophys. Acta 701, 12–18
16 Horowitz, P. and Criscimagna, N (1983) J. Biol Chem. 258, 7894–7896.
17 Blumenthal, K.L. and Heinrikson, R L. (1971) J. Biol. Chem 246, 2430–2437
18 Cannella, C., Pecci, L , Ascoli, F., Costa, M., Pensa, B. and Cavallini, D. (1980) in Natural Sulfur Compounds (Cavallini, D., Gaull, G E and Zappiav, eds.), pp. 471–481, Plenum Press, New York
19 Chow, S.F. and Horowitz, P.M (1985) J. Biol. Chem 260, 15516–15521
20 Finazzi Agro, A., Federici, G , Giovagnoli, C., Cannella, C and Cavallini, D. (1972) Eur. J Biochem. 28, 83–89
21 Guido, K and Horowitz, P (1975) Biochem. Biophys. Res. Commun. 67, 670–676.
22 Horowitz, P.M. and Criscimagna, N. (1985) Biochemistry 24 2587–2593
23 Means, G.E. and Feeny, R.E (1971) Chemical Modification of Proteins, p 159, Holden-Day Inc., San Francisco
24 Gaber, P.B. and Fluharty, A L (1968) Q Rep. Sulfur Chem. 3, 318–337
25 Webb, J.L. (1966) Enzyme and Metabolic·Inhibitors, Vol. 3, p. 595, Academic Press, New York
26 Voordouw, G., Vandervie, S.M , Veeger, C. and Stevenson, K J. (1981) Eur. J Biochem. 118, 541–546
27 Glazer, A.N., Delange, R.J. and Sigman, D.S. (1975) Chemical Modification of Proteins, pp 113, Elsevier, New York

Biochimica et Biophysica Acta 911 (1987) 109–113
Elsevier

BBA 32662

The structure and formation of the glucose 6-phosphate adduct of hemoglobin A: a ^{31}P-NMR study

Irene K. Ropiak and Mary E. Fabry

Division of Experimental Hematology, Department of Medicine, Albert Einstein College of Medicine, Bronx, NY 10461 (U.S.A.)

(Received 18 June 1986)

Key words: Glucose 6-phosphate adduct; Hemoglobin A; ^{31}P-NMR

The glucose 6-phosphate adduct of hemoglobin formed on deoxy incubation of the sugar with hemoglobin is primarily present in solution as the unstable aldimine compound; in contrast, the percent ketoamine is higher if the adduct is formed in the presence of carbon monoxide. The adduct has a ^{31}P nuclear magnetic resonance peak with a chemical shift which is 0.7 ppm up-field from the shift of unreacted glucose 6-phosphate at pH 7.0 and is constant between pH 6 and 8, while the unreacted sugar phosphate shows the characteristic change of chemical shift due to ionization of one of the phosphate protons. This suggests that, in the adduct, phosphate is involved in a salt bridge, probably at the 2,3-diphosphoglyceric acid binding site.

Introduction

Human hemolysates contain both HbA_0 and chromatographically fast hemoglobins. The most abundant of these is HbA_{1c}, which is formed by the non-enzymatic condensation of the β-N-terminal valine of hemoglobin with glucose [1–3]. Glycosylated hemoglobins are formed slowly and continuously during the 120-day life-span of the red cell [4]. Interest in the study of glycosylated hemoglobin has recently increased due to the widely accepted use of the measurement of the fast hemoglobin fraction as a quantitative index in the control of diabetes. Glycosylated proteins may exist in the aldimine form, which is in rapid equilibrium with the free sugar and reactive amino group, or in the ketoamine form, which is formed from the aldimine in a nearly irreversible reaction in which a carbonyl group is formed on the C-2 carbon. The contribution of the labile (aldimine) form to HbA_{1c} measurements has been a topic of recent concern [5,6].

Other sugars, sugar phosphates and metabolites can form adducts with hemoglobin which migrate as fast hemoglobins and may interfere with the quantitation of HbA_{1c} and may also be involved in the pathophysiology of diabetes. One of these is glucose 6-phosphate, which is present at high concentration in the red cell [7] and is a reasonable model for this class of compounds. The glucose 6-phosphate adduct of hemoglobin has been found to correlate with levels of blood glucose and migrates with the clinically determined fast hemoglobin. It forms more readily than does the glucose-Hb adduct because a higher proportion of glucose 6-phosphate molecules in solution are in the open-chain structure which has a reactive aldehyde [8], and because glucose 6-phosphate affinity for the 2,3-diphosphoglyceric acid binding site brings the glucose 6-phosphate into close proxim-

---

Abbreviations: HbA_0, unmodified hemoglobin; HbA_{1c}, hemoglobin with glucose at the N-terminal; G-6-P-Hb, glucose-6-phosphate-hemoglobin adduct; NMR, nuclear magnetic resonance.

Correspondence: Mary E. Fabry, Department of Medicine, Ullmann Room 925, Albert Einstein College of Medicine, 1300 Morris Park Avenue, Bronx, NY 10461, U.S.A.

0167-4838/87/$03 50 © 1987 Elsevier Science Publishers B.V (Biomedical Division)

ity for reaction with the β-N-terminal valine of hemoglobin. It has been demonstrated that the N-terminal of the β-chain is one of the sites involved in the binding of 2,3-diphosphoglyceric acid [9,10].

The experimental questions which will be addressed are: what is the predominant solution form of the G-6-P-Hb adduct (aldimine or ketoamine); and, what is the state of the phosphate on the adduct?

Methods

Hemoglobin without 2,3-diphosphoglyceric acid was prepared by chromatography in 0.05 Tris-HCl at pH 8.1 on DE-52 (Whatman, Clifton, NJ) and elution with the same buffer with 0.5 M NaCl added. ^{31}P-NMR was used to verify that the 2,3-diphosphoglyceric acid content was reduced to less than 0.2 mM per 5 mM of tetramer. Hemoglobin-A_{1c} was removed by Bio-Rex 70 chromatography as described by McDonald et al. [11]. The glucose 6-phosphate adduct was prepared by incubating 2–3 mM hemoglobin A tetramer with 50 mM glucose 6-phosphate in a 0.08 mM Tris-HCl buffer at pH 7.2 under CO or deoxy conditions in the presence of Garamycin (Schering Corp. Kenilworth, NJ) for 72 h at room temperature (20–25 ° C). The preparation to this point is called the glucose 6-phosphate reaction mixture. Shorter incubations carried out in the absence of Garamycin yielded the same adduct at the same rate. For NMR experiments unreacted glucose 6-phosphate was removed by Sephadex G-25 chromatography in 0.08 M Tris-HCl buffer followed by concentration by vacuum dialysis against the same buffer. The amount of the adduct present was estimated by use of Isolab Fast-Hemoglobin columns (Isolab Inc, Akron, OH). When the species present is in the aldimine form, mini-columns such as the Isolab indicate a higher percent fast hemoglobin present than other methods [12]. An aliquot of the deoxy reaction mixture was transferred to a separate flask and incubated under CO conditions for 48 h and the percent aldimine and ketoamine present was determined as described below. Another aliquot of the reaction mixture was reduced with borohydride by adding sodium borohydride at a 3 : 1 wt/wt (borohydride/hemoglobin) ratio in an ice bath for 15 min. The reaction was stopped by applying the mixture to a G-25 Sephadex column and rapidly eluting the hemoglobin with 0.08 M Tris-HCl at pH 7.2. The column is destroyed by this process but the hemoglobin can be successfully recovered with good yield. The ratio of the aldimine to ketoamine forms was determined by incubation of one part reaction mixture with five parts of Isolab's Aldimine Eliminator (Isolab Inc, Akron, OH) at room temperature for 1 h. The procedure is based on the instability of aldimines at low pH [13,14]. Bio-Rex 70 chromatography was carried out as described by McDonald et al. [11]. A Jeol 100 PFT NMR spectrometer operating at 40.5 MHz for phosphorus was used at room temperature with proton decoupling. Chemical shifts were determined as the distance from a reference line of 2 mM $^2H_3PO_4$ contained in a concentric tube which had ^2H_2O and $^2H_2SO_4$. Peak areas were determined by the integration software provided by Jeol after measurement at two repetition rates (4 and 10 s) demonstrated that a 4 s rate introduced no systematic errors. The pH titration was carried out by dialyzing one aliquot of the adduct to pH 6.2 and a second aliquot to pH 8 and mixing the two solutions for intermediate pH values. This procedure avoids dilution and degradation effects associated with adding strong acid or base to hemoglobin solutions. All samples were well oxygenated by exposure to 100% O_2, EDTA was added to a 1 mM concentration, and the hemoglobin concentration in the NMR tube was between 2 and 4 mM in Hb tetramer.

Results and Discussion

Stability of the G-6-P-Hb adduct

After deoxy incubation of glucose 6-phosphate and hemoglobin, Sephadex G-25 chromatography of the reaction mixture to remove unreacted glucose 6-phosphate yields a solution with a new ^{31}P-NMR peak which is characteristic of the G-6-P-Hb adduct. Chromatography on Bio-Rex (Fig. 1) resolves the more rapidly migrating G-6-P-Hb adduct, which co-chromatographs with HbA_{1a+b}, but is well separated from HbA_{1c} and HbA_0. When this fast peak is isolated and subjected to rechromatography on Bio-Rex, loss of the adduct

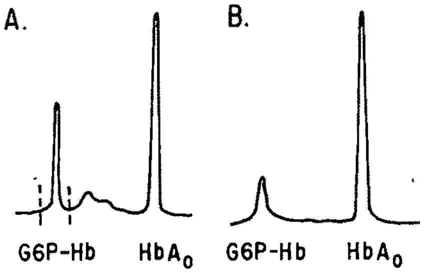

Fig. 1. Two cycles of Bio-Rex chromatography of the glucose 6-phosphate adduct of hemoglobin. The first is chromatography of the deoxy reaction mixture after glucose 6-phosphate has been removed by Sephadex G-25 chromatography. Panel B is re-chromatography of the first peak eluted (shown between dashed lines on panel A) with regeneration of HbA_0.

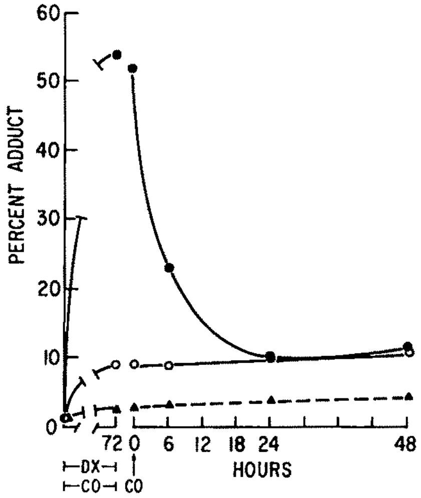

Fig 2. Percent G-6-P-Hb adduct formed under CO (○) and deoxy (●) conditions and the percent ketoamine formed in both cases (△) HbA from which 2,3-diphosphoglyceric acid and HbA_{1c} had been removed was incubated for 72 h under CO or deoxy conditions with 25 g/dl Hb, pH 7.2, 50 mM glucose 6-phosphate, Garamycin and 0.08 M Tris-HCl. The deoxy mixture was then transferred to a CO atmosphere and the incubation was continued for 48 h. Aldimine and ketoamine concentrations were determined as indicated in the text

is detected and HbA_0 is regenerated (Fig. 1), which implies that the adduct is not stable to chromatography on Bio-Rex and that determinations by this method (which includes the Isolab columns) may underestimate the amount of adduct present. If the first peak eluted is examined by ^{31}P-NMR after the first chromatography, no adduct is detected. Reaction of the adduct with borohydride allowed Bio-Rex chromatography without decomposition and NMR detection of the adduct. Therefore it is the sugar–protein bond which is labile rather than the sugar–phosphate bond. Chromatography on Isolab fast hemoglobin columns before exposure to glucose 6-phosphate revealed that there was 0.59 ± 0.26% fast Hb. Incubation under deoxy conditions for 72 h at 25 °C gave 52.9 ± 1.8% adduct before incubation at low pH to remove the aldimine form and 3.0 ± 0.1% after, while low-pH incubation of the borohydride-reduced adduct gave 52.35% before and 51.97% adduct after incubation. We can conclude that the adduct is unstable to chromatography because about 90% is present in the aldimine form. In contrast, low-pH incubation of the reaction product formed under CO conditions reveals 9.1 ± 0.1% before and 2.9 ± 0.1% after (or 30% in the ketoamine form), which suggests that although less adduct is formed under CO conditions, a greater percent of the adduct formed is in the ketoamine form. Incubation of the deoxy reaction product in the presence of excess glucose 6-phosphate for 48 h with CO resulted in rapid decomposition, with a half-life of about 6 h (Fig. 2), and no excess ketoamine formation. This observation suggests that decomposition of the aldimine due to the CO conformation is faster than conversion to the ketoamine form. These results suggest that the discrepancies in the reports of different workers on the amount of glycosylated hemoglobin formed on in vitro incubation may be due to different percents of the ketoamine form due to differences in the incubation conditions, as well as different sensitivities of various assays to the aldimine form.

The solution structure of the adduct

The investigation of the glucose 6-phosphate adduct of hemoglobin is complicated by the tendency of sugars and sugar phosphates to decompose and rearrange. Such complications make quantitation and structural determination difficult. ^{31}P-NMR is sensitive to the quantity and solution structure of any adduct formed and can be used to elucidate the state of the phosphate group in the G-6-P-Hb adduct. Fig. 3 illustrates the ^{31}P-NMR behavior of inorganic phosphate, glucose 6-phosphate and the G-6-P-Hb adduct in solution as a function of pH. The area of the peak identified as the adduct is proportional to the

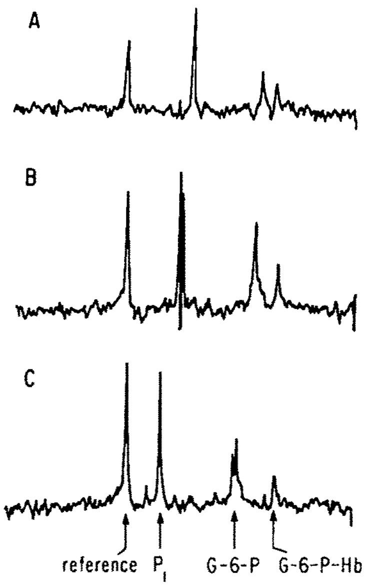

Fig 3. ^{31}P-NMR spectra of P_i, glucose 6-phosphate (G-6-P) and G-6-P-Hb formed by deoxy incubation at three different pH values: A, 7.55; B, 7.1; C, 6.6. Spectra were collected at 25°C and 40.5 MHz. They are reversed from left to right because of the quadrature detection on the JEOL-100

amount of the adduct detected by Bio-Rex chromatography.

Fig. 4 illustrates that, although a change in chemical shift is observed with a change in pH for the phosphate group of glucose 6-phosphate and inorganic phosphate, a change is not observed for the glucose 6-phosphate adduct of hemoglobin or its borohydride-reduced form. The chemical shift, which is similar to that of the fully titrated glucose 6-phosphate, and the fact that the proton on the phosphate group of the G-6-P-Hb adduct is no longer titratable, suggest that the phosphate is involved in a salt bridge with an amino acid on the hemoglobin. However, the chemical shift may be the sum of several compensating factors and the present data cannot rule out the possibility of a internal hydrogen bond. Since the primary site of glycosylation is the β-N-terminal, the phosphate is probably interacting with a group at the 2,3-diphosphoglyceric acid binding site. This observation is consistent with the observations of Chiou et al. [15] that the oxygen affinity of the glucose 6-phosphate adduct is reduced; that the oxygen affinity of the adduct is insensitive to the potent 2,3-diphosphoglyceric acid competitor inositol hexaphosphate [13]; and the observation of Haney and Bunn [16] that 2,3-diphosphoglyceric acid interferes with formation of the adduct of glucose 6-phosphate and deoxy hemoglobin. The observation that the borohydride-reduced adduct has a chemical shift and pH-dependence similar to that of the unreduced glucose 6-phosphate adduct suggests that the predominant conformation of the sugar is the open-chain form. The aldimine and ketoamine forms can form six- or five-membered rings, respectively, but the borohydride-reduced adduct has no carbonyl to form a ring.

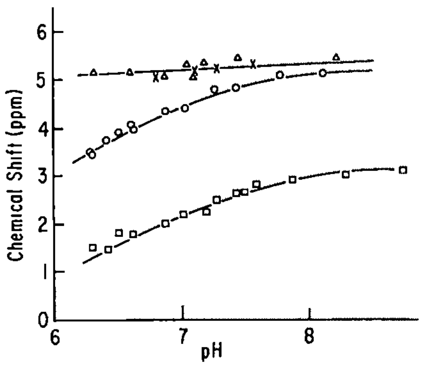

Fig. 4. Plot of ^{31}P-NMR chemical shift of the G-6-P-Hb adduct formed under deoxy conditions (△), G-6-P-Hb adduct after borohydride reduction (×), unreacted glucose 6-phosphate (○), and inorganic phosphate (□) as a function of pH. Spectra were collected at 25°C and 40.5 MHz with proton decoupling.

The glucose 6-phosphate adduct of hemoglobin, prepared by deoxy incubation, is unstable because it is mainly in the aldimine form. In contrast, the product of the CO incubation contains significant amounts of the stable ketoamine form. The ^{31}P-NMR peak associated with the adduct shows no change in chemical shift between pH 6 and 8, which suggests that it is involved in a salt bridge, probably at the 2,3-diphosphoglyceric acid binding site of hemoglobin. The predominant form of the sugar phosphate on the hemoglobin is probably the open-chain form.

Acknowledgements

We wish to thank Dr. Ronald Nagel for the valuable discussions and support which made this work possible. The expert technical assistance of

Sandra Suzuka is gratefully acknowledged. This work was supported by Grants HL 21016-06 and AM 20541-03 from the National Institutes of Health.

References

1 Bunn, H.F., Haney, D.N., Gabbay, K.H. and Gallop, P.M (1975) Biochem. Biophys. Res Commun. 67, 103–109

2 Fluckinger, R. and Winterhalter, K.H. (1976) FEBS Lett. 71, 356–360

3 Stevens, V J., Vlassara, H , Abati, A. and Cerami, A (1977) J Biol. Chem 252, 2998–3002

4 Bunn, H.F., Haney, D.N., Kamin, S., Gabbay, K.H. and Gallop, P.M. (1976) J Clin. Invest 57, 1652–1659

5 Nathan, D.M (1981) Clin. Chem 27, 1261–1263

6 Huisman, W., Kuijken, J.P.A A., Tan-Tjiong, H.L., Durkoop, E.P. and Leijnse, B. (1982) Clin. Chim Acta 118, 303–309

7 Tegos, C. and Beutler, E. (1980) J. Lab. Clin. Med. 96, 85–89

8 Gray, G.R (1976) Acc. Chem. Res. 9, 418–424

9 Bunn, H F. and Breihl, R W (1970) J Clin. Invest. 49, 1088–1091

10 Arnone, A (1972) Nature 237, 146–149

11 McDonald, M J., Shapiro, R., Bleichman, M., Solway, J. and Bunn, H.F. (1978) J Biol. Chem. 253, 2327–2332

12 Ploybutr, S., Burria, J.M. and Alberti, K G.M.M. (1982) Clin. Chem. 28, 1233–1234

13 Bisse, E., Berger, W and Fluckiger, R. (1982) Diabetes 31, 630–633

14 Bannon, P. (1982) Clin Chem. 28, 2183

15 Chiou, S.-H., Garrick, L.M. and McDonald, M.J. (1982) Biochemistry 21, 13–20

16 Haney, D.N and Bunn, H.F. (1976) Proc Natl. Acad. Sci. USA 73, 3534–3538

Biochimica et Biophysica Acta 911 (1987) 114–116
Elsevier

BBA 30158

BBA Report

Is thermally denatured protein unfolded? The example of α-lactalbumin

Wolfgang Pfeil

Central Institute of Molecular Biology, Academy of Sciences of the GDR, 1115 Berlin (G.D.R.)

(Received 16 July 1986)

Key words: Thermal denaturation, α-Lactalbumin; Protein unfolding

The degree of unfolding of various forms of human and bovine α-lactalbumin was characterized by the chromatographically determined distribution coefficient. Molecular size increases as follows: native protein ≈ apo form < acid form ≪ thermally unfolded form ≈ guanidine hydrochloride-unfolded protein.

During the past decade differential scanning calorimetry has gained importance in the study of thermal transitions of proteins [1,2]. However, the value of calorimetrically determined thermodynamic quantities remains questionable, since thermal unfolding might be incomplete as judged by circular dichroism and viscosity measurements [3]. Recently studies of α-lactalbumin by viscosity [4], light and X-ray scattering [5–11] became available showing that both the thermally denatured protein (T-state) and a well-characterized intermediate (A-state at pH 2 [12]) are only slightly expanded compared with the native protein (N-state) [4,5,9,11]. Accordingly, the T-state was proposed to be substantially different from the guanidine hydrochloride (GuHCl) unfolded protein (U-state), which has far-reaching consequences for the value of thermal unfolding studies. In these experiments, however, a protein concentration up to 100 mg/ml was required, and difficulties due to aggregation and extrapolation to zero protein concentration were reported. To avoid these problems, in the present paper we characterize various states of α-lactalbumin by analytical column chromatography using a protein concentration of the same order of magnitude as in optical and calorimetric investigations.

Analytical chromatography was performed according to Refs. 13 and 14 using thermostatted columns (0.9 × 100 cm and 0.9 × 50 cm) packed with Sephadex G-100. 0.5 mg protein in 0.5 ml buffer with Blue Dextran and DNP-glycine as internal standards was supplied, except for the experiments in inset B in Fig. 1. The flow rate was 5 ml per h. Buffer conditions are given in Table I. The distribution coefficient given below is defined by $K_d = (v_e - V_0)/(v_i - V_0)$, where v_e is the elution volume of the protein, V_0 is the void volume and v_i is the elution volume of the low molecular weight internal standard. α-Lactalbumin was prepared as described in Ref. 15.

Chromatographically determined distribution coefficients of various states of α-lactalbumin at 4°C are given in Table I. In agreement with X-ray and light scattering studies [5–11] the acid form, a native-like intermediate, is characterized by only a slight reduction in K_d (corresponding to about a 10% increase of Stokes radius according to Ref. 5) when compared with the native and GuHCl-unfolded protein (corresponding to about a 40% increase in Stokes radius [5]). The K_d of the apo-form is indistinguishable from that of the native protein. As an exception, however, the apo-form of bovine α-lactalbumin was found to

---

Correspondence: Dr. W Pfeil, Central Institute of Molecular Biology, Academy of Sciences of the GDR, 1115, Berlin, G.D.R.

0167-4838/87/$03.50 © 1987 Elsevier Science Publishers B.V (Biomedical Division)

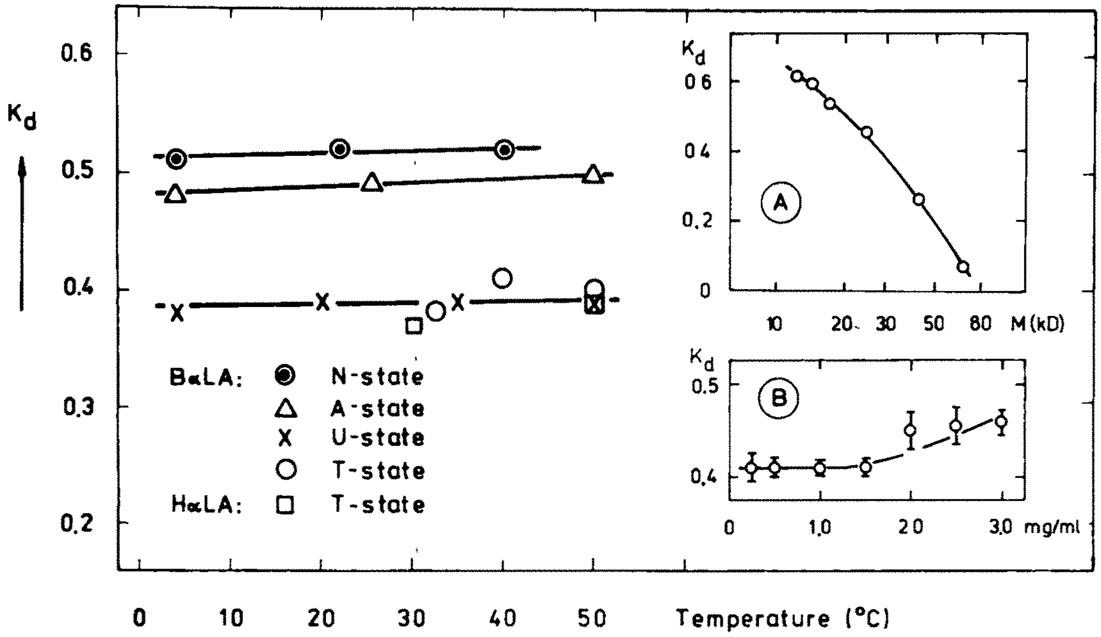

Fig. 1. Temperature dependence of the distribution coefficient K_d for native (N), acid (A), GuHCl-unfolded (U), and thermally unfolded (T) bovine (BαLA) and human (HαLA) α-lactalbumin. Inset (A): K_d as determined at 4°C using protein standards: cytochrome *c*, lysozyme, myoglobin, chymotrypsinogen, egg albumin and bovine serum albumin. Inset (B): K_d of thermally unfolded bovine apo-α-lactalbumin at 40°C versus amount of protein supplied to the column. Buffer: 10 mM borate, 1 mM EDTA, pH 8.0

be expanded in the absence of sodium chloride. It is known from calorimetric studies that the thermodynamic properties (transition temperature and enthalpy) of bovine apo-α-lactalbumin are dependent on ionic strength, in contrast to the human protein [15].

The chromatographically determined distribution coefficient of various α-lactalbumin forms (N, A and U) remains almost constant over a temperature range from 4 to 50°C (Fig. 1). The thermally unfolded protein which was obtained from the apo-form because of its lower transition temperature [15,16] shows a K_d value close to that of the GuHCl-unfolded protein. Thus, the size of the thermally unfolded protein is close to that of the GuHCl-unfolded protein and is significantly different from that of the less-expanded intermediate, the A-state.

TABLE I

DISTRIBUTION COEFFICIENT K_d OF VARIOUS α-LACTALBUMIN STATES DETERMINED BY CHROMATOGRAPHY AT 4°C

State	α-Lactalbumin	K_d	Buffer
Native (N)	bovine	0.51 ± 0.01	20 mM Tris, 0.1 mM $CaCl_2$, pH 7.5
Native (N)	human	0.50 ± 0.01	20 mM Tris, 0.1 mm $CaCl_2$, pH 7.5
Acid (A)	bovine	0.48 ± 0.01	50 mM KCl/HCl, pH 2.0
Acid (A)	human	0.48 ± 0.01	50 mM KCl/HCl, pH 2.0
Unfolded (U)	bovine	0.38 ± 0.01	6.5 M GuHCl, pH 7.5
Unfolded (U)	human	0.37 ± 0.01	6.5 M GuHCl, pH 7.5
Apo	bovine	0.46 ± 0.01	10 mM borate, 1 mM EDTA, pH 8.0
Apo	human	0.51 ± 0.01	10 mM borate, 1 mM EDTA, pH 8.0
Apo + NaCl	bovine	0.53 ± 0.02	10 mM borate, 1 mM EDTA, 0.25 M NaCl, pH 8.0
Apo + NaCl	human	0.51 ± 0.01	10 mM borate, 1 mM EDTA, 0.25 M NaCl, pH 8.0

The transition of the native protein into the intermediate (A-form) is accompanied by an enthalpy change which is nearly the same as in GuHCl-induced unfolding [17], although the secondary structure is completely retained, and the molecule size is only slightly increased. In contrast to the transition of the native protein into the A-form, the thermal transition is accompanied by reduction of the CD amplitude in the far ultraviolet region [18], a considerable increase in size (this work) and the same enthalpy change as in GuHCl-induced unfolding [19]. Thus, the degree of unfolding as determined by nonthermodynamic quantities (circular dichroism, size) does not seem to be relevant to calorimetrically determined thermodynamic quantities. Therefore, the often observed 'residual structure' in thermal unfolding must not be overestimated in thermodynamic considerations.

References

1 Privalov, P.L. (1979) Adv Protein Chem. 33, 167–241
2 Privalov, P.L. (1982) Adv Protein Chem 35, 1–104
3 Tanford, C. (1968) Adv Protein Chem. 23, 121–282
4 Dolgikh, D A., Gilmanshin, R.I., Brazhnikov, E.V, Bychkova, V.E, Semisotnov, G.V., Venyaminov, S Yu. and Ptitsyn, O B. (1981) FEBS Lett 136, 311–315
5 Gast, K., Zirwer, D., Welfle, H., Bychokova, V.E. and Ptitsyn, O B. (1986) Int J. Biol Macromol. 8, 231–236
6 Krigbaum, W.R and Kügler, F R (1970) Biochemistry 9, 1216–1223
7 Pessen, H., Kumosinski, T.F. and Timasheff, S.N. (1971) J Agr. Food Chem. 19, 698–702
8 Izumi, Y., Miyake, Y., Kuwajima, K., Sugai, S., Inoue, K, Izumi, M. and Katano, S. (1983) Physica 120B, 444–448
9 Dolgikh, D.A., Abaturov, L V., Bolotina, I.A., Brazhnikov, E.V., Bushuev, V.N., Bychkova, V.E, Gilmanshin, R.I., Lebedev, Yu.O, Semisotov, G.V., Tiktopulo, E.I. and Ptitsyn, O.B. (1985) Eur. J. Biophys. 13, 109–121
10 Timchenko, A.A., Dolgikh, D.A., Damaschun, H. and Damaschun, G. (1986) Studia Biophys 112, 201–206
11 Ptitsyn, O.B., Damaschun, G, Gernat, C., Damaschun, H. and Bychkova, V.E. (1986) Studia Biophys. 112, 207–211
12 Kuwajima, K, Nitta, K, Yoneyama, M. and Sugai, S. (1976) J. Mol. Biol. 106, 359–373
13 Ackers, G.K. (1970) Adv. Protein Chem. 24, 343–446
14 Mann, K.G and Fish, W.W. (1972) Methods Enzymol 26, 28–42
15 Pfeil, W. and Sadowski, M.L. (1985) Studia Biophys 109, 163–170
16 Hiraoka, Y and Sugai, S. (1984) Int. J Peptide Protein Res 23, 535–542
17 Okuda, T. and Sugai, S. (1977) J. Biochem. 81, 1051–1056
18 Kuwajima, K., Hiraoka, Y., Ikeguchi, M. and Sugai, S. (1985) Biochemistry 24, 874–881
19 Pfeil, W. (1981) Biophys Chem. 13, 181–186

Biochimica et Biophysica Acta 911 (1987) 117–120
Elsevier

BBA 30159

BBA Report

Lipase-catalyzed reactions in organic media: competition and applications

H. Deleuze [a], G. Langrand [a], H. Millet [a], J. Baratti [b], G. Buono [a]
and C. Triantaphylides [a]

[a] *Ecole Supérieure de Chimie de Marseille, Centre de Saint-Jérôme, rue Henri Poincaré, 13397 Marseille Cédex 13 (France) and* [b] *Laboratoire de Chimie Bactérienne du C.N R S., B.P. 71, 13277 Marseille Cédex 9 (France)*

(Received 1 July 1986)

Key words: Lipase; Transesterification; Organic solvent; Enzyme kinetics; Reaction selectivity

Lipases (triacylglycerol acylhydrolase, EC 3.1.1.3) have been used in organic media for the catalysis of reactions such as hydrolysis, esterification and transesterification. In these conditions it was confirmed that all reactions proceed through an acyl enzyme intermediate in two successive steps: acyl enzyme formation and solvolysis. The competition between two acyl acceptors (acyl donors) for reaction with a donor (acceptor) is described for the first time. A kinetic model is proposed using a competitive factor which is in good accordance with experimental results. The model was used successfully for the prediction of alcohol (acid) separations and resolutions by lipases.

Ester hydrolysis of emulsified substrates by lipases (EC 3.1.1.3) obeys complex kinetics [1–4]. In organic media ester synthesis and transesterification have been described [5–16] with an insoluble enzymatic preparation. As reported by others [17], and observed by us in this study, the reaction rate v_A, in organic solvent, increased with the substrate concentration [A] according to a Michaelis-Menten equation:

$$v_A = \frac{V_A[A]}{K_A + [A]} \quad (1)$$

Furthermore a ping-pong mechanism has been proposed including the formation of an acyl enzyme intermediate [17]. When two substrates (A and B) are present at the same time in the reaction mixture, a competitive factor α is then defined by the ratio of the catalytic powers according to Eq. 2 [20]:

$$\alpha = \frac{V_A/K_A}{V_B/K_B} \quad (2)$$

This formalism was also used by Chen et al. [18] for two enantiomers of the same substrate. The competitive factor can be calculated from one of the following equations [20]:

$$\frac{v_A}{v_B} = \alpha\frac{[A]}{[B]} \quad (3)$$

$$\log([A]/[A]_0) = \alpha \log([B]/[B]_0) \quad (4)$$

In this paper we describe the use of the preceding model for reactions in organic media using different acyl donors and acceptors. For instance, when two different esters (AcX and AcY) of the same acid are used as acyl donor a competitive donor factor α_D can be calculated (Fig. 1, full arrows). When two acceptors (X and Y) are used a competitive acceptor factor α_A can be calculated (Fig. 1, dotted arrows). The competitive factors

---

Correspondence: Dr C. Triantaphylides, Ecole Supérieure de Chimie de Marseilles, Centre de Saint-Jérôme, rue Henri Poincaré, 13397 Marseille Cédex 13, France.

0167-4838/87/$03.50 © 1987 Elsevier Science Publishers B V. (Biomedical Division)

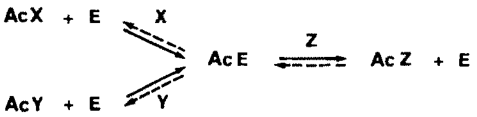

Fig. 1 Lipase competition reactions. AcX, AcY and AcZ = acyl donors (esters or acids). E = lipase, X, Y and Z, acyl acceptors (alcohols or water); AcE = acyl enzyme; full arrows, competition between two acyl donors (AcX and AcY); dotted arrows, competition between two acyl acceptors (X and Y).

were estimated from the variations of substrate concentrations (A and B) with time plotted according to Eq. 4. Fig. 2 shows a typical result for the competition between butanol (A) and water (B) with isopentyl butyrate as acyl donor. In the same figure the competition between the *R* and *S* enantiomers of 2-butylbutyrate is also shown.

Table I shows the results for the competitive donor factors α_D for four different couples of acyl donor, three different acceptors and two lipases. It is seen that the competitive donor factor α_D was independent of the alcohol used as acceptor when a given mixture of acyl donor was used. For instance α_D was 3.6 for the competition between cyclohexyl butyrate and isopentyl butyrate independently of the acceptor (geraniol, lauryl alcohol or (−)-menthol). This conclusion was true for every couple of acyl donor tested (AcX and AcY) even when butyric acid or tributyrin were used. The lipases from *Candida Cylindracea* (recently renamed *Candida rugosa*) and *Mucor miehi* showed the same property and identical results were observed using different substrate concentrations. Thus it can be concluded that this is a general property of the lipase-catalyzed reactions in organic solvents.

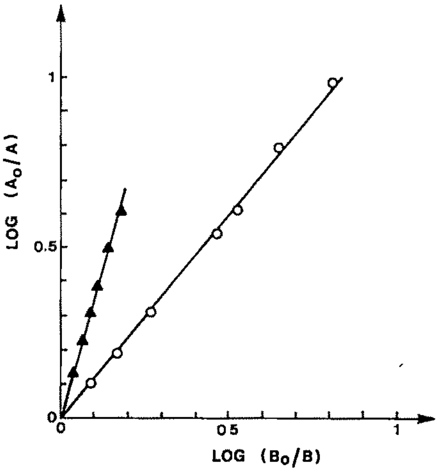

Fig 2. Estimation of competitive factor. ▲, competition between butanol ($[A]_0 = 0.25$ M) and water ($[B]_0 = 0.235$ M) with isopentyl butyrate as acyl donor (2 M) in tetrahydrofuran. ○, competition between *R* and *S* 2-butyl butyrate ($[A]_0 = [B]_0 = 0.25$ M) with lauryl alcohol (0.5 M) as acceptor in hexane Temperature was 40 °C and *C. cylindracea* was used

The competitive acceptor factors α_A were also measured using the same method. The results are shown in Table II for three different donors, three couples of acceptors and two lipases. The competitive acceptor factor α_A was independent of the ester (AcZ) used as donor and of the lipase tested.

For instance, α_A was 2.2 for the competition between geraniol and nerol independently of the donor (tributyrin, isopentyl butyrate and butyric acid). The same conclusion can be drawn for the

TABLE I

ACYL DONOR COMPETITIVE FACTORS α_D IN LIPASE-CATALYZED REACTIONS IN ORGANIC MEDIA

The reaction conditions were: 40 °C, acyl donors and acceptors 0.5 M in hexane Crude commercial lipase preparations were used at a concentration of 1 to 6% (w/v). The activity of the lipases on tributyrin was 14000 I.U./g for *C. cylindracea* (lipase My, Meito Sangyo) and 120000 I.U./g for *M. miehi* (Novo); for definition of units see Ref. 22. Esters and alcohols were assayed by GLC using silica fused capillary columns SE52 or DB5, 25 m. Acids were assayed by titration and water by the Karl Fischer method.

Acyl donor (AcX, AcY)	*C. cylindracea* lipase			*M. Mielhi* lipase	
Acceptor (Z):	geraniol	lauryl alcohol	(-)-menthol	geraniol	lauryl alcohol
Cyclohexyl butyrate/isopentyl butyrate	3.64 ± 0.06	3.66 ± 0.11	3.67 ± 0 07	–	–
Butyric acid/butyl butyrate	3.19 ± 0.08	3.14 ± 0.04	3.14 ± 0.01	3.02 ± 0.02	2.88 ± 0.10
Butyl butyrate/isopentyl butyrate	2.66 ± 0.06	2.58 ± 0 10	2.57 ± 0.06	1.32 ± 0.01	1.41 ± 0.01
Tributyrin/butyl butyrate	20.09 ± 2 7	20 09 ± 3.9	–	6.1 ± 1.6	6.1 ± 0.4

TABLE II

ACYL ACCEPTOR COMPETITIVE FACTOR α_A IN LIPASE-CATALYZED REACTIONS IN ORGANIC MEDIA

Experimental conditions were the same as in Table I Geraniol and nerol were 0.25 M in pure tributyrin or isopentyl butyrate and in 1 M butyric acid in heptane. Butanol was 0.25 M, water 0.235 M and esters 2 M in tetrahydrofuran The lipase concentrations were 0.25% (w/v).

Donor (AcZ)		*C. cylindracea* lipase		*M. miehei* lipase	
	Acceptor (X, Y).	geraniol/nerol	butanol/water	geraniol/nerol	butanol/water
Tributyrin		2.25 ± 0.04	3.86 ± 0.03	1.93 ± 0.02	1.08 ± 0.01
Isopentyl butyrate		2.20 ± 0.04	3.58 ± 0.02	1.57 ± 0.02	1.08 ± 0.01
Butyric acid		2.20 ± 0.08	–	1.99 ± 0.03	–

competition between butanol and water and for both lipases tested.

From the results in Tables I and II it can be concluded that esters (or acids) and alcohols (or water) bind to different enzyme species which are, most probably, the free and acyl enzymes (E and AcE in Fig. 1). In organic solvent, the formation and the solvolysis of the acyl enzyme occur in two independent steps. This result for *C. cylindracea* and *M. miehi* is in agreement with a previous report for pancreatic lipase [17] in organic solvent. The use of competitive factors α_D is a simple and easy way of describing the kinetics of the lipase-catalyzed reaction with two substrates. This is not the case in a biphasic system, where the kinetics are usually much more complex [3].

The domain of application of the model was further extended to comparison with equilibrium constants. Application of the Haldane [19–21] equation to the following equilibrium:

$$AcX + Y \rightleftharpoons AcY + X \quad (5)$$

allows the derivatization of Eqn. 6 which correlates the equilibrium constant with the competitive factors:

$$K_{eq} = \alpha_D/\alpha_A = \frac{V_{AcX}/K_{AcX}}{V_{AcY}/K_{AcY}} \cdot \frac{V_Y/K_Y}{V_X/K_X}$$

The competitive factors α_D and α_A were measured for different donors (AcX and AcY) with lauryl alcohol as acceptor (Z) and for different acceptors (X and Y) with tributyrin as donor. The results are shown in Table III. The equilibrium constant (K_{eq}) was estimated by measuring the substrate and product concentrations (AcX, Y, AcY and X) at equilibrium and compared to the ratio α_D/α_A. The two values were identical within

TABLE III

RELATIONSHIP BETWEEN COMPETITIVE FACTORS (α_D AND A_A) AND THE EQUILIBRIUM CONSTANT OF THE REACTION $AcX + Y \rightleftharpoons AcY + X$ FOR *C. CYLINDRACEA* LIPASE

For experimental conditions see Table I. The enantiomeric excess was determined by GLC on the alcohols according to the method of Konig [23]. For 3,3-dimethyl-2-butanol derivatization was done with (*R*)-(+)-phenylethylisocyanate

(X, Y):	Acyl donor	Acyl acceptor		
	butyryl esters (AcX, AcY), lauryl alcohol (Z): α_D	tributyrin (AcZ), alcohols (X, Y): α_A	α_D/α_A	K_{eq}
Butyl/isopentyl	2.58 ± 0.10	3.91 ± 0.07	0.66	0.56
Cyclohexyl/isopentyl	3.66 ± 0.11	1.13 ± 0.07	3.2	3.1
Cyclohexyl/butyl	1.39 ± 0.01	0.30 ± 0.29	4.6	4.9
(*R*/*S*)-2-Butyl	1.18 ± 0.01	1.13 ± 0.01	1.04	–
(*R*/*S*)-3,3-Dimethyl-2-butyl	26.0 ± 3.5	26.9 ± 1.4	0.97	–

experimental errors, for the three different equilibria tested. This is a strong confirmation of the validity of the kinetic model in organic media.

An important application of the model is the classification of acyl donors (or acceptors) according to their competitive factors. For instance, from the results in Tables I and II with the *C. cylindracea* lipase, taking butyl butyrate as reference, the following scale of acyl donor can be deduced: tributyrin (20.9) > butyric acid (3.19) > cyclohexylbutyrate (1.39) > isopentyl butyrate (1/2.66). Then one can easily compare the reactivity of different acyl donors in transesterification reactions. If all the acyl donors are present at the same time in the reaction mixture the model allows the prediction of reaction rates for each of them. This will be very useful when natural mixtures of esters are used in transesterification reactions. For acyl acceptors, the same approach gives the following scale in the case of butyryl transfer with *c. cylindracea* lipase: butanol (3.7) > cyclohexanol (1.1) > water (1.0) > isopentanol (0.95).

Some examples of kinetic separations are now given using *C. cylindracea* lipase.

In the case of alcohol resolution, the two enantiomers are considered as competitors towards the enzyme active site [18]. According to the microreversibility principle one should expect that $\alpha_D = \alpha_A$. The results are given in Table III for two alcohols. 2-Butanol could not be easily resolved ($\alpha = 1.15$) under our conditions. A different result with this alcohol has been reported by others [10,11]. In contrast the other alcohol, (R/S)-3,3-dimethyl-2-butanol could be easily resolved ($\alpha = 26.5$). The *R* enantiomer was prepared in large amounts (50 g) in two steps. In the first step the butyryl ester was synthesized and then ester solvolysis was done in the experimental conditions given in Table III. The conversion yield was 40% for both reactions and the enantiomeric excesses were respectively 88 and more than 98%.

Acid separations were demonstrated using butyric-lauric competition. When geraniol was used as acceptor the selectivity was higher for triacylglycerides ($\alpha_D = 32 \pm 3$) than for free acids ($\alpha_D = 8.9 \pm 0.9$). Thus the separation of butyric and lauric acid can be easily done using tributyrin and trilaurin. In these competitive reactions, two different acyl enzymes are concerned, in contrast with alcohol separations, where the same acyl enzyme is involved. Both the leaving and the acceptor groups played a role in the reaction selectivity. This approach can be easily extended to acid resolutions for which a systematic search for better acceptor and leaving groups has to be carried out.

References

1 Densnuelle, P (1972) in The Enzymes 3rd Edn (Boyer, P D , ed.), Vol 7, pp. 575–616, Academic Press, New York
2 Brockerhoff, H and Jensen R.G. (1974) Lipolytic Enzymes, pp 34–90, Academic Press, New York
3 Verger, R and De Haas, G H. (1976) Annu. Rev. Biophys Bioeng 5, 77–117
4 Verger, R (1980) Methods Enzymol 64, 340–392
5 Bell, G., Blain, J.A., Patterson, J.D.E. and Todd, R. (1976) J Appl. Chem Biol. 26, 582–583
6 Bell, G., Blain, J.A., Patterson, J D.E , Shaw, C.E L. and Todd, R. (1978) FEMS Microbiol. Lett. 3, 223–225
7 Patterson, J.D.E., Blain, J A , Shaw, C.E.L , Todd, R. and Bell, G (1979) Biotechnol. Lett. 1, 211–216
8 Seo, C.W., Yamada, Y. and Okada, H. (1982) Agric. Biol. Chem 46, 405–409
9 Zaks,A. and Klibanov, A.M (1984) Science 224, 1249–1251
10 Cambou, B. and Klibanov, A.M. (1984) J. Am. Chem Soc 106, 2687–2692
11 Cambou, B and Klibanov, A.M. (1984) Biotechnol. Bioeng. 26, 1449–1454
12 Kirchner, G., Scollar, M P. and Klibanov, A.M (1985) J Am Chem. Soc 107, 7072–7076.
13 Koshiro, S , Sonomoto, K., Tanaka, A. and Fukui, S J. (1985) Biotechnology 2, 47–57
14 Langrand, G., Secchi, M., Buono, G., Baratti, J. and Triantaphylides, C. (1985) Tetrahedron Lett. 26, 1857–1860
15 Marlot, C., Langrand, G., Triantaphylides, C. and Baratti, J (1985) Biotechnol. Lett. 7, 647–650
16 Langrand, G., Baratti, J., Buono, G. and Triantaphylides, C (1986) Tetrahedron Lett. 27, 29–32
17 Zaks, A. and Klibanov, A.M. (1985) Proc Natl. Acad. Sci. USA 82, 3192–3196
18 Chen, C.S , Fujimoto, Y., Girkaudas, G and Sih, C.J. (1982) J Am. Chem. Soc. 104, 7294–7299
19 Haldane, J.B.S. (1965) in Enzymes, p. 80, MIT Press Paperback
20 Laidler, K.J. and Bunding, P S. (1973) in The Chemical Kinetics of Enzyme Action, 2nd Edn., pp. 173–175, Clarendon Press, Oxford
21 Segel, S.H. (1975) in Enzyme Kinetics, pp 34-37, Wiley Interscience, New York
22 Lavayre, J. and Baratti, J. (1982) Biotechnol Bioeng. 24, 1007–1013
23 Konig, W.A., Francke, W. and Benecke, I. (1982) J. Chromatogr. 239, 227–231

Biochimica et Biophysica Acta 911 (1987) 121–126
Elsevier

BBA 30161

BBA Report

Enzyme kinetic evidence of active-site involvement in the interaction between aldolase and muscle myofibrils

Simon J. Harris and Donald J. Winzor

Department of Biochemistry, University of Queensland, St Lucia, Queensland 4067 (Australia)

(Received 19 August 1986)

Key words: Aldolase–myofibril interaction; Enzyme kinetics; Fructose 1,6-bisphosphate

The interaction of aldolase with the myofibrillar matrix of rabbit skeletal muscle has been investigated by means of its effect on kinetic parameters for the enzyme-catalyzed cleavage of fructose 1,6-bisphosphate. Involvement of the active site in the enzymic interaction with the thin filament of muscle is indicated, the association constant for competitive inhibition of catalysis (420 000 M^{-1}) being in excellent agreement with the value of 410 000 M^{-1} obtained under the same conditions (pH 6.8, *I* 0.16) from partition equilibrium studies of the aldolase–myofibril interaction (Kuter, M.R., Masters, C.J. and Winzor, D.J. (1983) Arch. Biochem. Biophys. 225, 384–389). A second kinetic study, designed to take into greater account the inhibitory effects of substrate and other phosphate-containing metabolites on the interaction of enzyme with myofibrils, has substantiated further the concept of aldolase existing as an equilibrium mixture of cytoplasmic and filament-bound forms in muscle tissue.

Equilibrium partition studies of the interaction between aldolase and the thin filaments of rabbit skeletal muscle have provided quantitative evidence of the physiological significance of the phenomenon [1–4]. Furthermore, the similarity of the equilibrium constants for the aldolase–phosphate interactions responsible for the competitive inhibition of enzyme catalysis and enzyme adsorption to muscle myofibrils was taken to signify identity of these interactions [4]. Such evidence for the involvement of the active-site region in the reversible binding of aldolase to the myofibrillar matrix is, however, seemingly in conflict with an earlier enzyme-kinetic investigation [5], which reported an enhanced maximal velocity for aldolase bound to synthetic thin filaments. In view of this discrepancy, a further study has been undertaken to ascertain the effect of enzyme adsorption on kinetic parameters for the aldolase-catalyzed cleavage of fructose 1,6-bisphosphate.

Rabbit muscle aldolase was obtained as an ammonium sulphate suspension from Sigma Chemical Co., who also supplied fructose 1,6-bisphosphate, glucose 1-phosphate, creatine phosphate and ATP. Other chemicals were of reagent grade. Before use the aldolase was freed of ammonium sulphate by extensive dialysis against 0.01 M imidazole-HCl buffer, pH 6.8, containing 0.15 M KCl, 0.001 M $MgCl_2$ and 0.001 M dithiothreitol. Concentrations of the dialyzed enzyme solutions were determined spectrophotometrically on the basis of an absorption coefficient ($A_{1cm}^{1\%}$) of 9.1 at 280 nm [6] and a molecular weight of 160 000 [7].

Myofibrils, prepared from rabbit skeletal muscle by the method of Etlinger and coworkers [8], were equilibrated with the above imidazole-chloride buffer (pH 6.8, *I* 0.16) by repeated cycles of centrifugation and resuspension of the pellet in

---

Correspondence: Dr D.J. Winzor, Department of Biochemistry, University of Queensland, St. Lucia, Qld 4067, Australia.

0167-4838/87/$03.50 © 1987 Elsevier Science Publishers B V (Biomedical Division)

buffer [4]. The protein concentrations of the myofibrillar suspensions were based on colorimetric assays [9,10] with bovine serum albumin as standard, the detailed protocol for these determinations having been described elsewhere [4].

Reaction mixtures (1 ml) containing aldolase (20 nM), fructose 1,6-bisphosphate (20–250 μM), hydrazine sulphate (1 mM), and, in alternate mixtures, myofibrillar suspension (27.4 mg/ml protein) in the imidazole-chloride buffer (pH 6.8, I 0.16) were incubated at 25°C for 5 min, after which ammonium sulphate (0.5 ml, 3.5 M) was added to prevent further product formation. Myofibrils were then removed by centrifugation for 5 min at $12\,000 \times g$, and hydrazone formation was monitored at 240 nm [11]. Complete enzymic cleavage of fructose 1,6-bisphosphate (0.1 mM) was used to calibrate absorbance changes in terms of substrate cleavage; and experiments were performed to test the validity of considering hydrazone production in reaction mixtures during the 5-min incubation period to reflect initial velocities, v. Best-fit values of the two Michaelis parameters (V_m, K_m^{app}) describing the observed dependence of $\bar{v}$ upon fructose 1,6-bisphosphate concentration, $[\bar{S}]$, were obtained by nonlinear regression analysis of the results in terms of a rectangular hyperbolic relationship [12].

A second series of experiments was designed to obtain kinetic parameters reflecting more closely the inhibitory effects of prevailing concentrations of phosphate-containing metabolites in muscle [13]. Creatine phosphate (15 mM) and inorganic phosphate (5 mM) were incorporated into the imidazole-chloride buffer (pH 6.8), as were glucose 1-phosphate (6 mM) and ATP (6 mM) to approximate metabolic concentrations of hexose phosphates and nucleoside phosphates, respectively. The inclusion of phosphate-containing metabolites in the buffer was compensated for by a decrease in the KCl concentration to 0.04 M in order to maintain the ionic strength in the vicinity of 0.16. Furthermore, since the relatively large ultraviolet absorbance of the revised buffer system precluded measurement of hydrazone formation at 240 nm, the hydrazone produced during the 5-min assay period was converted to the 2,4-dinitrophenylhydrazone [14] in order to allow a change in the monitoring wavelength to 540 nm. The inhibition of enzymic catalysis by the phosphate-containing metabolites was countered by amending the substrate concentration range examined (100–500 μM).

Because of possible complications arising from adsorption, to myofibrils, of the additional enzymes employed in coupled assays of aldolase activity [15,16], these assays have necessarily been bypassed in favour of a less sensitive method based on hydrazone formation [11]. Furthermore, the presence of myofibrillar suspension in some reaction mixtures had precluded the estimation of initial velocities by continuous spectrophotometric assay. Some comment is therefore required on the method used to determine initial velocities.

Fig. 1a presents progress curves obtained for the aldolase-catalyzed cleavage of fructose 1,6-bisphosphate present at various concentrations in myofibril-free reaction mixtures. Solid lines represent the relationships obtained by continuous monitoring of the absorbance change at 240 nm, whereas the symbols denote the corresponding absorbance changes inferred from subsequent analysis of reaction mixtures in which catalysis was stopped after incubation for the indicated periods: these absorbances have been multiplied by 1.5 to take into account the dilution incurred in stopping the enzymic reaction with ammonium sulphate. Measurement of absorbance changes in mixtures incubated for different periods seems to exhibit effectively linear time-dependence, but the continuously recorded progress curves are clearly curvilinear. Consequently, the absorbance change measured after catalysis for 5 min cannot be interpreted directly in terms of an initial velocity. That quantity has been obtained empirically from a calibration plot (Fig. 1b) relating the measured absorbance changes to corresponding initial velocities obtained by more sensitive, coupled assays of aldolase catalysis [16]. The adoption of such a procedure for determining initial velocities is clear testimony to the extreme difficulties and limitations imposed by the presence of a concentrated (approx. 30 mg/ml) protein suspension in quantitative assessment of catalysis by aldolase in the presence of myofibrils.

The effect of the interaction between aldolase and myofibrillar sites on the enzymic cleavage of fructose 1,6-bisphosphate is presented schemati-

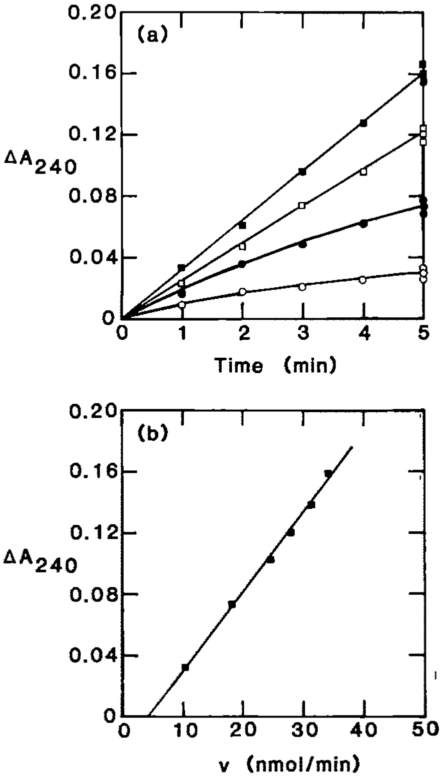

Fig. 1. Measurement of initial velocities for the aldolase-catalyzed cleavage of fructose 1,6-bisphosphate (pH 6.8, *I* 0.16, 25 °C). (a) Time-dependence of substrate depletion as measured by hydrazone formation [11] in mixtures containing aldolase (20 nM), hydrazine sulphate (1 mM) and 234 μM (■), 104 μM (□), 33 μM (●) and 13 μM (○) fructose 1,6-bisphosphate. (b) Relationship between the absorbance change resulting from catalysis for 5 min and the initial velocity as measured by a more sensitive coupled assay of aldolase activity [16].

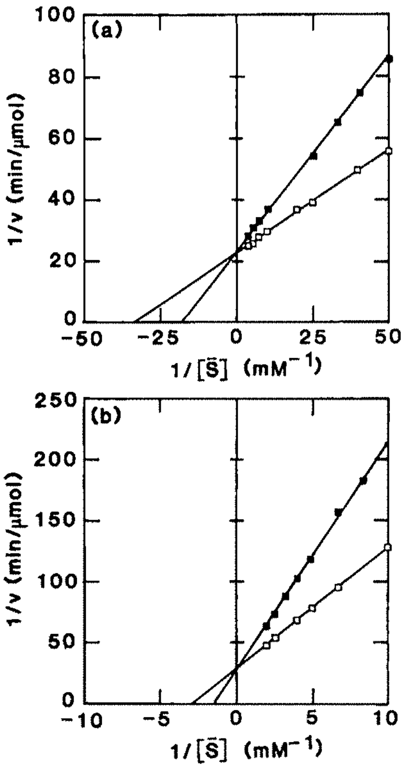

Fig. 2. Inhibitory effects of muscle myofibrils on the catalytic cleavage of fructose 1,6-bisphosphate by aldolase. (a) Results obtained in imidazole-chloride buffer (pH 6.8, *I* 0.16) (b) Effect of phosphate-containing metabolites (32 mM) on the inhibition of catalysis under comparable conditions (pH 6.8, *I* 0.16). Open symbols refer to results obtained in the absence of myofibrils, and closed symbols to results obtained in their presence (27.4 mg/ml myofibrillar protein).

cally (Lineweaver-Burk format) in Fig. 2a, the quantitative analysis of which is summarized in Table I. Several points are noted. (i) Results obtained in the absence of myofibrils (□) signify a Michaelis constant of 28–29 μM (lines 1 and 2 of Table I), a value in reasonable accord with that of 31–35 μM obtained previously [19] under similar conditions (pH 7.4, *I* 0.15). (ii) The results obtained in the presence of myofibrils (■) are also described adequately by a rectangular hyperbolic dependence of v upon substrate concentration, the impairment of the Michaelis constant and virtual lack of effect on maximal velocity being symptomatic (but not definitive) of competitive inhibition by the myofibrils. Since the interaction of aldolase with myofibrillar matrix sites under the present conditions has already been characterized by partition equilibrium studies [4], comparison of that equilibrium constant with the inhibition constant deduced from the kinetic studies should provide further comment on the competitive nature of enzyme catalysis and enzyme adsorption. (iii) On the basis of the previously reported [4] binding capacity of rabbit muscle myofibrils for aldolase under the present conditions [69.4 nmol/g myofibrillar protein), the total concentration of matrix sites, $[\bar{X}]$, in a 27.4 mg/ml myofibrillar suspension is 1.90 μM. Consideration of the kinetic results in terms of classical competitive inhibition, i.e., $K_m^{app} = K_m(1 + k_{EX}[\bar{X}])$ where

TABLE I

KINETIC PARAMETERS FOR ALDOLASE CATALYSIS OF FRUCTOSE 1,6-BISPHOSPHATE

Experiments were performed at 25°C in imidazole-chloride buffer, pH 6.8, I 0.16.

Reaction mixture [a]	K_m (μM) [b]	V_m (nmol/min) [b]
Fructose 1,6-bisphosphate (FBP)	29 ± 1 [c]	43 ± 1 [c]
FBP	28 ± 1 [d]	41 ± 1 [d]
FBP/myofibrils	52 ± 2 [c]	42 ± 1 [c]
FBP/physiological phosphates	350 ± 12 [d]	40 ± 1 [d]
FBP/physiological phosphates/ myofibrils	670 ± 30 [d]	39 ± 2 [d]

[a] Components in addition to enzyme (20 nM).

[b] Parameters obtained by nonlinear regression analysis of results [12]

[c] Results obtained from measurements of hydrazone formation [11].

[d] Results obtained from measurements of dinitrophenylhydrazone formation [14]

k_{EX} is the intrinsic association constant for the enzyme–matrix interaction, yields a value of $420\,000\pm70\,000$ M^{-1} for k_{EX}. The fact that this value is in excellent agreement with that of $410\,000\pm20\,000$ M^{-1} inferred from partition equilibrium studies of aldolase-binding under the same conditions [4] clearly adds weight to interpretation of Fig. 2a in terms of competitive inhibition by myofibrillar sites. These enzyme kinetic studies are therefore considered to provide direct support for the concept [4] that the active site of aldolase is involved in the interaction of the enzyme with the thin filament of skeletal muscle.

By substantiating the concept of active-site involvement in the aldolase-myofibril interaction, the present enzyme kinetic results refute their earlier counterparts [5], which signified activation (enhanced V_m) to be an outcome of enzyme adsorption to the thin filament matrix. However, in agreement with present findings, those results [5] also indicated that the presence of thin filaments caused impairment of K_m for the aldolase-catalyzed cleavage of fructose 1,6-bisphosphate. Indeed, the degree of impairment (20-fold to 150-fold increase in K_m^{app}) resulting from inclusion of a relatively low concentration (0.5 mg/ml) of synthetic thin filament seems to be much greater than that attributable to aldolase adsorption alone. It is suggested that adsorption, to the thin filaments, of the α-glycerophosphate dehydrogenase and/or triose-phosphate isomerase used in the coupled assay system may have been a contributing factor to the earlier findings [5].

A corollary of the above demonstration that the myofibrillar matrix acts as a competitive inhibitor of the aldolase-catalyzed cleavage of fructose 1,6-bisphosphate is, of course, that the substrate for aldolase is a competitive inhibitor of enzyme adsorption to myofibrils. Since phosphate and, presumably, other phosphate-containing metabolites also act in similar vein [4], the likely extent of the aldolase–myofibril interaction in the physiological environment clearly requires further examination. This problem has been addressed to some extent by repeating the enzyme kinetic studies in buffer supplemented with a selection of such metabolites, the concentrations of which were based on an NMR analysis of muscle tissue [13]. Some ADP is presumably formed from the ATP (6 mM) by the ATPase activity of the myofibril preparation [17], but should then be reconverted to ATP by the myofibril-bound creatine kinase [18]. Calculations based on those findings [18] predict the consequent conversion of 1 mM creatine phosphate to creatine and phosphate during the 5-min incubation period used for assays of aldolase activity. Any such variations in metabolite concentrations do not affect present consideration of the supplemented buffer as an approximate 'physiological phosphate' mixture.

Results of this second enzyme kinetic investigation are summarized in Fig. 2b and the final two lines of Table I. The metabolite-containing buffer clearly exerts a marked inhibitory effect on enzymic catalysis by aldolase, there being a 12-fold increase in the apparent Michaelis constant. Consideration of this K_m^{app} in terms of competitive inhibition by the 32 mM 'physiological phosphate' solution, i.e., $K_m^{app} = K_M(1 + k_{EP}[\bar{P}])$, leads to a calculated magnitude of 350 M^{-1} for k_{EP}, the weighted association equilibrium constant describing the competitive inhibition of aldolase by a concentration $[\bar{P}]$ of 'physiological phosphate' mixture. Inclusion of myofibrillar suspension (with $[\bar{X}] = 1.90$ μM as before) in reaction mixtures again leads to competitive inhibition, since, as required, the k_{EX} of $480\,000\pm100\,000$ M^{-1} so obtained compares favourably with the values deduced from Fig. 2a and from the earlier partition equilibrium study of the aldolase–myofibril interaction [4].

The combined competitively inhibitory effects of physiological concentrations of substrate and other phosphate-containing metabolites on the distribution of aldolase between adsorbed and soluble states may be described quantitatively by the expression [4,19]

$$\bar{k}_{\mathrm{EX}} = \frac{\{1-([\mathrm{E}]/[\bar{\mathrm{E}}])^{1/4}\}}{([\mathrm{E}]/[\bar{\mathrm{E}}])^{1/4}[[\bar{\mathrm{X}}]-4[\bar{\mathrm{E}}]\{1-([\mathrm{E}]/[\bar{\mathrm{E}}])^{1/4}\}]} \qquad (1a)$$

$$\bar{k}_{\mathrm{EX}} = k_{\mathrm{EX}}/(1+k_{\mathrm{ES}}[\bar{\mathrm{S}}]+k_{\mathrm{EP}}[\bar{\mathrm{P}}]) \qquad (1b)$$

in which $[\bar{\mathrm{E}}]$ refers to the total enzyme concentration (soluble and adsorbed forms), and [E] to the total concentration of enzyme in the liquid phase: $\bar{k}_{\mathrm{EX}}$ is a composite equilibrium constant that takes into account the inhibitory effects of competing ligands (substrate and phosphates) on the partition of enzyme. For the application of Eqn. 1 to the distribution of aldolase in the physiological environment, $[\bar{\mathrm{S}}]$, the muscle tissue concentration of fructose 1,6-bisphosphate, may be taken as approximately 0.1 mM [20]; and, provided that enzymic catalysis is considered to be the rate-limiting step, k_{ES} ($\equiv 1/K_{\mathrm{m}}$) as 34000 M^{-1} (Table I). Their combination in Eqn. 1b with a value of 410000 M^{-1} for k_{EX} [4] and the values of k_{EP} and $[\bar{\mathrm{P}}]$ discussed above leads to an estimate of 26000 M^{-1} for $\bar{k}_{\mathrm{EX}}$, the effective association constant describing the partition of aldolase under such conditions. Combination of this $\bar{k}_{\mathrm{EX}}$ with the values of 14 μM and 40 μM for the respective concentrations of myofibrillar sites and aldolase in muscle [4] yields an estimate of 0.75 for the ratio $[\mathrm{E}]/[\bar{\mathrm{E}}]$ in Eqn. 1a. The earlier prediction [4] that 26% of the aldolase should be adsorbed to resting muscle filaments is thus essentially unaltered by this more rigorous consideration of the effects of competitive inhibition by phosphate-containing metabolites (including substrate) on the aldolase–myofibril interaction. This value could be enhanced slightly by thermodynamic nonideality arising from the space-filling effects of other proteins present in the physiological environment [21]. For example, on the basis that the apparent thermodynamic binding constant is likely to be an order of magnitude greater than $\bar{k}_{\mathrm{EX}}$ [22], the calculated proportion of bound aldolase would increase to 30%.

By taking into greater account the inhibitory effects of substrate and other phosphate-containing metabolites on the interaction of aldolase with muscle myofibrils, the present investigation substantiates further the concept that under physiological conditions aldolase should not be regarded as a purely cytoplasmic enzyme, but rather as an equilibrium mixture of free and myofibril-bound forms, the relative proportions of which are a function of the metabolic state of the cell [4].

The partial support of this investigation by the Australian Research Grants Scheme is gratefully acknowledged, as is the receipt (by S.J.H.) of a Commonwealth Postgraduate Research Award.

References

1 Walsh, T.P., Winzor, D.J., Clarke, F.M., Masters, C.J. and Morton, D.J. (1980) Biochem. J. 186, 89–98

2 Masters, C.J., Winzor, D.J and Nichol, L.W. (1981) Biochem J. 195, 297–299

3 Kuter, M.R., Masters, C.J., Walsh, T.P and Winzor, D.J (1981) Arch Biochem. Biophys 212, 306–310

4 Kuter, M.R., Masters, C.J and Winzor, D.J. (1983) Arch Biochem. Biophys. 225, 384–389

5 Walsh, T.P., Clarke, F.M and Masters, C.J (1977) Biochem J 165, 165–167

6 Baranowski, T and Niederland, T.R (1949) J. Biol Chem. 180, 543–555

7 Kawahara, K and Tanford, C. (1966) Biochemistry 5, 1578–1584

8 Etlinger, J.D, Zak, R. and Fischman, D.A. (1976) J Cell Biol. 68, 123–141

9 Lowry, O.H., Rosebrough, N.J., Farr, A.L and Randall, R.J. (1951) J. Biol. Chem 193, 265–275

10 Peterson, G.L. (1977) Anal Biochem 83, 346–356

11 Jagannathan, V., Singh, K. and Damodaran, M. (1956) Biochem. J 63, 95–105

12 Duggleby, R.G. (1981) Anal. Biochem. 110, 9–18

13 Hoult, D.I., Busby, S.J.W., Gadian, D.G., Radda, G.K., Richards, R.E. and Seeley, P.J (1974) Nature (London) 252, 285–287

14 Sibley, J.A and Lehninger, A.L (1949) J. Biol. Chem 177, 859–872

15 Wu, R. and Racker, E. (1959) J. Biol. Chem 234, 1029–1035

16 Scopes, R.K (1977) Biochem J. 161, 253–263

17 Goodno, C.C., Wall, C.M. and Perry, S.V (1978) Biochem J 175, 813–821

18 Wallimann, T., Schlösser, T and Eppenberger, H.M (1984) J. Biol. Chem 259, 5238–5246

19 Nichol, L.W., Ward, L.D. and Winzor, D.J. (1981) Biochemistry 20, 4856–4860
20 Newsholme, E A and Leach, A.R (1983) Biochemistry for the Medical Sciences, p. 314, Wiley, New York
21 Minton, A P (1981) Biopolymers 20, 2093–2120
22 Harris, S.J. and Winzor, D.J (1985) Arch. Biochem Biophys 243, 598–604

Biochimica et Biophysica Acta **Vol. 911, No. 1**
Protein Structure and Molecular Enzymology P39(1) January 5, 1987

Contents

Biochimica et Biophysica Acta 40 years on v

Regular Papers

A covalent complex between horse heart cytochrome *c* and yeast cytochrome *c* peroxidase: kinetic properties (BBA 32594)
by J E Erman, K.L Kim, L B. Vitello, S.J. Moench and J D Satterlee (U.S.A) 1

Spectroscopic studies on the structural organization of the lectin discoidin I homologies with fibronectin (BBA 32651)
by A. Valencia, A Cano, R. Caballero and A. Pestaña (Spain) 11

Conformational and activity changes during guanidine denaturation of D-glyceraldehyde-3-phosphate dehydrogenase (BBA 32689)
by G.-F. Xie and C.-L Tsou (China) 19

Conformation similarities of the globular and tailed forms of acetylcholinesterase from *Torpedo californica* (BBA 32595)
by C.-S.C. Wu, L Gan and J.T. Yang (U.S.A.) 25

Spectroscopic properties of spinach catalase (BBA 32596)
by M Hirasawa, K.A. Gray, R.W. Shaw and D.B. Knaff (U S.A) 37

Functional differentiation of amphiphilic helices of the apolipoproteins by hydrophobic moment analysis (BBA 32690)
by H De Loof, M. Rosseneu, R Brasseur and J -M. Ruysschaert (Belgium) 45

The association reaction of yeast alcohol dehydrogenase with coenzyme is partly diffusion-controlled in solvents of increased viscosity (BBA 32677)
by B B Hasinoff, R. Dreher and J.P. Davey (Canada) 53

Oxidation reaction of human oxyhemoglobin with nitrite: a reexamination (BBA 32688)
by C Spagnuolo, P. Rinelli, M Coletta, E Chiancone and F. Ascoli (Italy) 59

Comparison of the kinetic behavior of human and bovine proteins in the heparin-catalyzed antithrombin III/thrombin reaction (BBA 32687)
by M T. Cunningham and G.L Nelsestuen (U.S.A.) 66

The electronic and magnetic properties of rubredoxin: a low-temperature magnetic circular dichroism study (BBA 32597)
by D E. Bennett and M.K. Johnson (U S.A.) 71

Spectroscopic studies of the seven-iron-containing ferredoxins from *Azotobacter vinelandii* and *Thermus thermophilus* (BBA 32598)
by M.K. Johnson, D.E. Bennett, J.A. Fee and W V Sweeney (U.S.A.) 81

Purification and some properties of peroxidases of rat bone marrow (BBA 32694)
by K Kariya, E. Lee, M Hirouchi, M Hosokawa and H Sayo (Japan) 95

Chemical modification of bovine liver rhodanese with tetrathionate: differential effects on the sulfur-free and sulfur-containing catalytic intermediates (BBA 32599)
by A.R.S Prasad and P M Horowitz (U.S A.) 102

continued

Cited in. Current Contents Life Sciences - Biological Abstracts - Chemical Abstracts - Index Chemicus - Index Medicus - Excerpta Medica (EMBASE)

INFORMATION FOR CONTRIBUTORS TO BIOCHIMICA ET BIOPHYSICA ACTA

The 1982 edition of this booklet, offering detailed guidance to authors, is available free of charge from the BBA Editorial Secretariat, P.O. Box 1345, 1000 BH Amsterdam, The Netherlands. It is also published as Biochim. Biophys. Acta 715 (1982) 1–23.

The structure and formation of the glucose 6-phosphate adduct of hemoglobin A: a ^{31}P-NMR study (BBA 32662)
by I K Ropiak and M E Fabry (U S.A) 109

Reports

Is thermally denatured protein unfolded? The example of α-lactalbumin (BBA 30158)
by W Pfeil (G.D.R.) 114

Lipase-catalyzed reactions in organic media. competition and applications (BBA 30159)
by H. Deleuze, G. Langrand, H. Millet, J. Baratti, G Buono and C Triantaphylides (France) 117

Enzyme kinetic evidence of active-site involvement in the interaction between aldolase and muscle myofibrils (BBA 30161)
by S.J Harris and D.J Winzor (Australia) 121

BIOCHIMICA ET BIOPHYSICA ACTA
International Journal of Biochemistry and Biophysics
Founded in 1947 by H G K. Westenbrink, Managing Editor 1947–1964

© 1987, Elsevier Science Publishers B V (Biomedical Division)
Printed in The Netherlands

All rights reserved No part of this publication may be reproduced, stored in a retrieval system, or transmitted, in any form or by any means, electronic, mechanical, photocopying, recording or otherwise, without the prior written permission of the publisher, Elsevier Science Publishers B V (Biomedical Division), P O Box 1527, 1000 BM Amsterdam, The Netherlands Submission of a paper to this journal entails the author's irrevocable and exclusive authorization of the publisher to collect any sums or considerations for copying or reproduction payable by third parties (as mentioned in article 17 paragraph 2 of the Dutch Copyright Act of 1912 and in the Royal Decree of June 20, 1974 (S 351) pursuant to article 16b of the Dutch Copyright Act of 1912) and/or to act in or out of Court in connection therewith

Special regulations for readers in the U.S.A. This journal has been registered with the Copyright Clearance Center, Inc. Consent is given for copying of articles for personal or internal use, or for the personal use of specific clients. This consent is given on the condition that the copier pays through the Center the per-copy fee stated in the code on the first page of each article for copying beyond that permitted by Sections 107 or 108 of the U S. Copyright Law The appropriate fee should be forwarded with a copy of the first page of the article to the Copyright Clearance Center, Inc., 27 Congress Street, Salem, MA 01970, U S.A. If no code appears in an article, the author has not given broad consent to copy and permission to copy must be obtained directly from the author. All articles published prior to 1980 may be copied for a per-copy fee of US$ 2 25, also payable through the Center. This consent does not extend to other kinds of copying, such as for general distribution, resale, advertising and promotion purposes, or for creating new collective works. Special written permission must be obtained from the publisher for such copying.

Special regulations for authors. Upon acceptance of an article by the journal, the author(s) will be asked to transfer copyright of the article to the publisher This transfer will ensure the widest possible dissemination of information.

biomembranes

SAMPLE COPY

for additional information contact:

ALLIED/ELSEVIER JOURNALS
MARKETING GROUP
30, WEST COTT ROAD, Ph: 82468
MADRAS - 600 014./
750, MOUNT ROAD,
MADRAS - 600 002.

BBA

Biochimica et Biophysica Acta (M)

Managing Editors: P. Borst, P Cohen,
. van Dam, L.L.M. van Deenen (Chairman),
P. Kennedy and G.K. Radda

Honorary Managing Editor: E.C. Slater

Vol. 896, No. 1, pp. 1-128
nuary 9, 1987
sevier

SN 0006-3002
0005-2736
BACAQ 896 (1) 1-128 (1987)
3MBS 896 (1) 1-128 (1987)

40 YEARS OF BBA!

PUBLICATION SCHEDULE FOR 1987

BBA is published according to a volume-numbering scheme that embraces all sections of the journal In addition, each regular section has its own sequential volume-numbering system, running parallel to the overall BBA scheme, as set out below
Full subscription 42 volumes plus Cumulative Index 1986

	BIO-ENERGETICS	BIO-MEMBRANES	GENE STRUCTURE AND EXPRESSION	PROTEIN STRUCTURE AND MOLECULAR ENZYMOLOGY	LIPIDS AND LIPID METABOLISM	GENERAL SUBJECTS	MOLECULAR CELL RESEARCH	BBA REVIEW SECTIONS
	6 volumes [a]	11 volumes [b]	3 volumes	6 volumes	6 volumes	4 volumes	5 volumes	3 volumes
Jan	890-1 = B80-1	896-1 = M145-1 896-2 = M145-2	908-1 = N17-1	911-1 = P39-1 911-2 = P39-2	917-1 = L82-1 917-2 = L82-2	923-1 = G126-1	927-1 = C17-1	BBA REVIEWS ON BIOENERGETICS
Feb	890-2 = B80-2 890-3 = B80-3	897-1 = M146-1 897-2 = M146-2		911-3 = P39-3	917-3 = L82-3	923-2 = G126-2	927-2 = C17-2 927-3 = C17-3	895-1 = BR15-1
March	891-1 = B81-1	897-3 = M146-3 898-1 = M147-1	908-2 = N17-2	912-1 = P40-1 912-2 = P40-2	918-1 = L83-1 918-2 = L83-2	923-3 = G126-3	928-1 = C18-1	895-2 = BR15-2 895-3 = BR15-3
April	891-2 = B81-2	898-2 = M147-2 898-3 = M147-3	908-3 = N17-3	912-3 = P40-3	918-3 = L83-3	924-1 = G127-1	928-2 = C18-2	
May	891-3 = B81-3	899-1 = M148-1 899-2 = M148-2		913-1 = P41-1 913-2 = P41-2	919-1 = L84-1 919-2 = L84-2	924-2 = G127-2	928-3 = C18-3	BBA REVIEWS ON BIOMEMBRANES
June	892-1 = B82-1 892-2 = B82-2	900-1 = M149-1 900-2 = M149-2	909-1 = N18-1	913-3 = P41-3	919-3 = L84-3	924-3 = G127-3	929-1 = C19-1 929-2 = C19-2	906-1 = MR16-1 906-2 = MR16-2
July	892-3 = B82-3	901-1 = M150-1 901-2 = M150-2	909-2 = N18-2	914-1 = P42-1 914-2 = P42-2	920-1 = L85-1 920-2 = L85-2	925-1 = G128-1	929-3 = C19-3	906-3 = MR16-3
Aug	893-1 = B83-1	902-1 = M151-1 902-2 = M151-2	909-3 = N18-3	914-3 = P42-3	920-3 = L85-3	925-2 = G128-2	930-1 = C20-1	BBA REVIEWS ON CANCER
Sept	893-2 = B83-2	902-3 = M151-3 903-1 = M152-1	910-1 = N19-1	915-1 = P43-1 915-2 = P43-2	921-1 = L86-1 921-2 = L86-2	925-3 = G128-3	930-2 = C20-2	907-1 = CR14-1 907-2 = CR14-2
Oct	893-3 = B83-3	903-2 = M152-2 903-3 = M152-3	910-2 = N19-2	915-3 = P43-3	921-3 = L86-3	926-1 = G129-1	930-3 = C20-3	907-3 = CR14-3
Nov	894-1 = B84-1 894-2 = B84-2	904-1 = M153-1 904-2 = M153-2		916-1 = P44-1 916-2 = P44-2	922-1 = L87-1 922-2 = L87-2	926-2 = G129-2	931-1 = C21-1 931-2 = C21-2	
Dec	894-3 = B84-3	905-1 = M154-1 905-2 = M154-2	910-3 = N19-3	916-3 = P44-3	922-3 = L87-3	926-3 = G129-3	931-3 = C21-3	

[a] This includes BBA Reviews on Bioenergetics, Vol 895 [b] This includes BBA Reviews on Biomembranes, Vol 906

Authors should submit their manuscripts (four copies) for publication in BIOCHIMICA ET BIOPHYSICA ACTA by sending them to one of the Managing Editors
Dr P Borst, c/o BBA Editorial Secretariat, P O Box 1345, 1000 BH Amsterdam, The Netherlands
Dr P Cohen, Department of Biochemistry, Medical Sciences Institute, University of Dundee, Dundee, DD1 4HN, U K
Dr K. van Dam, c/o BBA Editorial Secretariat, P O. Box 1345, 1000 BH Amsterdam, The Netherlands
Dr L.L M van Deenen, c/o BBA Editorial Secretariat, P O Box 1345, 1000 BH Amsterdam, The Netherlands
Dr E P Kennedy, c/o BBA Editorial Secretariat (Boston), Box C 9123, Brookline, MA 02146, U S A
Dr G K Radda, Department of Biochemistry, University of Oxford, South Parks Road, Oxford, OX1 3QU, U K

Detailed information for contributors may be found in Biochim. Biophys Acta 715 (1982) 1–23, also published as the 1982 edition of
INFORMATION FOR CONTRIBUTORS TO BIOCHIMICA ET BIOPHYSICA ACTA
a booklet which is available free of charge from the BBA Editorial Secretariat.

Subscription information

1987 BBA Biomembranes, Volumes 896–906 (including Reviews) (11 volumes in 27 issues), Dfl 2695 (US$ 1086 75) + Dfl 275 (US$ 111.00) postage, packaging and handling Total price Dfl 2970 (US$ 1197 25)
1987 BBA full subscription, Volumes 890–931 (42 volumes in 120 issues), Dfl 7812 (US$ 3150 00) + Dfl 1050 (US$ 423 50) postage, packaging and handling Total price Dfl 8862 (US$ 3573.50).
The Dutch guilder price is definitive. The U S dollar price is subject to exchange-rate fluctuations and is given only as a guide. Journals are sent by surface delivery to all countries, except the following countries where SAL air delivery (Surface Airlifted Mail) is ensured U S.A , Canada, Japan, Australia, New Zealand, P R China, India, Israel, South Africa, Malaysia, Singapore, South Korea, Taiwan, Pakistan, Hong Kong, Brazil, Argentina, Mexico and Thailand Airmail rates for other countries are available on request
Subscription orders can be entered only by calendar year (Jan -Dec) and should be sent to Elsevier Science Publishers, Journals Department, P O. Box 211, 1000 AE Amsterdam, The Netherlands, Telex 18582 ESPA NL, or to your usual subscription agent Claims for missing issues should be made within 3 months of publication, otherwise they cannot be honoured free of charge The Publisher reserves the right to issue additional volumes during the course of the year Such volumes will be invoiced before publication and delivered after receipt of payment.
In the U S A and Canada. for further information contact Elsevier Science Publishers, Journal Information Center, 52 Vanderbilt Avenue, New York, NY 10017, U S A , Tel. (212) 370-5520.

Biochimica et Biophysica Acta

BIOCHIMICA ET BIOPHYSICA ACTA

MANAGING EDITORS

L.L.M. van Deenen (Utrecht)
(Chairman)
P. Borst (Amsterdam)
P. Cohen (Dundee)
E.P. Kennedy (Boston, MA)
G.K. Radda (Oxford)
K. van Dam (Amsterdam)

HONORARY MANAGING EDITOR

E.C. Slater (Southampton)

EDITORS

H.R.V. Arnstein (London)
J. Barber (London)
I. Björkhem (Huddinge)
B. Borgström (Lund)
J. Brachet (Brussels)
J. Bremer (Oslo)
R. Burgess (Madison, WI)
E. Carafoli (Zürich)
J.E. Cleaver (San Francisco, CA)
C. Crane-Robinson (Portsmouth)
J.W. Daly (Bethesda, MD)
E.A. Dawidowicz (Boston, MA)
B. de Kruijff (Utrecht)
J.G. Demaille (Montpellier)
J.J.H.H.M. de Pont (Nijmegen)
B. Deuticke (Aachen)
K.T. Douglas (Colchester)
S. Ebashi (Tokyo)
L. Ernster (Stockholm)
S. Ferguson (Birmingham)
I. Fridovich (Durham)
F. Gibson (Canberra)
W.B. Gratzer (London)
M. Hamberg (Stockholm)
T.E. Hardingham (London)
J.L. Harwood (Cardiff)
E. Heinz (Dortmund)
E.J.M. Helmreich (Würzburg)
F. Hofmann (Homburg)
M.D. Houslay (Glasgow)
R.C. Hughes (London)
J.B. Jackson (Birmingham)
P. Jollès (Paris)
P.L. Jørgensen (Aarhus)
Y. Kagawa (Tochigi)
K.-A. Karlsson (Gothenburg)
M. Kates (Ottawa)
J. Kay (Cardiff)
Y. Kaziro (Tokyo)
R. Kinne (Dortmund)
C. Klee (Bethesda, MD)
A. Kleinzeller (Philadelphia, PA)
L. Läuger (Constance)
A.G. Lee (Southampton)
D.M. Lee (Oklahoma City, OK)
F. Maley (Albany, NY)
D. Marsh (Göttingen)
V. Massey (Ann Arbor, MI)
D.J. Morré (West Lafayette, IN)
J.F. Morrison (Canberra)
L.E. Mortenson (Athens, GA)
G. Nelsestuen (St. Paul, MN)
D.G. Nicholls (Dundee)
Y. Nishizuka (Kobe)
R.C. Nordlie (Grand Forks, ND)
S. Numa (Kyoto)
C. Pace-Asciak (Toronto)
P.G.W. Plagemann (Minneapolis, MN)
I. Ragan (Harlow)
P. Randle (Oxford)
A. Razin (Jerusalem)
A.M. Scanu (Chicago, IL)
H.J. Schatzmann (Bern)
G.L. Scherphof (Groningen)
J. Seelig (Basel)
N. Sharon (Rehovot)
G.G. Shipley (Boston, MA)
D. Shugar (Warsaw)
W.D. Stein (Jerusalem)
J.M. Tager (Amsterdam)
T. Taniguchi (Tokyo)
J.P. Thornber (Los Angeles, CA)
I. Tinoco (Berkeley, CA)
K.F. Tipton (Dublin)
I.P. Trayer (Birmingham)
I. Trowbridge (San Diego, CA)
C.L. Tsou (Beijing)
D.E. Vance (Edmonton)
H.J. van Gorkom (Leiden)
T. Vänngård (Gothenburg)
A. Watts (Oxford)
C. Weissmann (Zürich)
R.J.P. Williams (Oxford)
R.G. Williamson (London)
C. Wraight (Urbana, IL)
K. Wüthrich (Zürich)
R.F.A. Zwaal (Maastricht)

ELSEVIER SCIENCE PUBLISHERS B.V.
AMSTERDAM

BIOCHIMICA
ET BIOPHYSICA ACTA

INTERNATIONAL JOURNAL OF BIOCHEMISTRY AND BIOPHYSICS

biomembranes

896 (1987)
(M145)

ELSEVIER SCIENCE PUBLISHERS B.V.
AMSTERDAM

PUBLICATION SCHEDULE FOR 1987

BBA is published according to a volume-numbering scheme that embraces all sections of the journal In addition, each regular section has its own sequential volume-numbering system, running parallel to the overall BBA scheme, as set out below

Full subscription 42 volumes plus Cumulative Index 1986

	BIO-ENERGETICS	BIO-MEMBRANES	GENE STRUCTURE AND EXPRESSION	PROTEIN STRUCTURE AND MOLECULAR ENZYMOLOGY	LIPIDS AND LIPID METABOLISM	GENERAL SUBJECTS	MOLECULAR CELL RESEARCH	BBA REVIEW SECTIONS
	6 volumes [a]	11 volumes [b]	3 volumes	6 volumes	6 volumes	4 volumes	5 volumes	3 volumes
Jan	890-1 = B80-1	896-1 = M145-1 896-2 = M145-2		911-1 = P39-1 911-2 = P39-2	917-1 = L82-1 917-2 = L82-2	923-1 = G126-1	927-1 = C17-1	BBA REVIEWS ON BIOENERGETICS
Feb	890-2 = B80-2 890-3 = B80-3	897-1 = M146-1 897-2 = M146-2	908-1 = N17-1	911-3 = P39-3	917-3 = L82-3	923-2 = G126-2	927-2 = C17-2	895-1 = BR15-1
March	891-1 = B81-1	897-3 = M146-3 898-1 = M147-1	908-2 = N17-2	912-1 = P40-1 912-2 = P40-2	918-1 = L83-1 918-2 = L83-2	923-3 = G126-3	927-3 = C17-3 928-1 = C18-1	895-2 = BR15-2 895-3 = BR15-3
April	891-2 = B81-2	898-2 = M147-2 898-3 = M147-3	908-3 = N17-3	912-3 = P40-3	918-3 = L83-3	924-1 = G127-1	928-2 = C18-2	
May	891-3 = B81-3	899-1 = M148-1 899-2 = M148-2		913-1 = P41-1 913-2 = P41-2	919-1 = L84-1 919-2 = L84-2	924-2 = G127-2	928-3 = C18-3	BBA REVIEWS ON BIOMEMBRANES
June	892-1 = B82-1 892-2 = B82-2	900-1 = M149-1 900-2 = M149-2	909-1 = N18-1	913-3 = P41-3	919-3 = L84-3	924-3 = G127-3	929-1 = C19-1	906-1 = MR16-1 906-2 = MR16-2
July	892-3 = B82-3	901-1 = M150-1 901-2 = M150-2	909-2 = N18-2	914-1 = P42-1 914-2 = P42-2	920-1 = L85-1 920-2 = L85-2	925-1 = G128-1	929-2 = C19-2 929-3 = C19-3	906-3 = MR16-3
Aug	893-1 = B83-1	902-1 = M151-1 902-2 = M151-2	909-3 = N18-3	914-3 = P42-3	920-3 = L85-3	925-2 = G128-2	930-1 = C20-1	BBA REVIEWS ON CANCER
Sept	893-2 = B83-2	902-3 = M151-3 903-1 = M152-1	910-1 = N19-1	915-1 = P43-1 915-2 = P43-2	921-1 = L86-1 921-2 = L86-2	925-3 = G128-3	930-2 = C20-2	907-1 = CR14-1 907-2 = CR14-2
Oct	893-3 = B83-3 894-1 = B84-1	903-2 = M152-2 903-3 = M152-3	910-2 = N19-2	915-3 = P43-3	921-3 = L86-3	926-1 = G129-1	930-3 = C20-3	907-3 = CR14-3
Nov	894-2 = B84-2	904-1 = M153-1 904-2 = M153-2		916-1 = P44-1 916-2 = P44-2	922-1 = L87-1 922-2 = L87-2	926-2 = G129-2	931-1 = C21-1 931-2 = C21-2	
Dec	894-3 = B84-3	905-1 = M154-1 905-2 = M154-2	910-3 = N19-3	916-3 = P44-3	922-3 = L87-3	926-3 = G129-3	931-3 = C21-3	

[a] This includes BBA Reviews on Bioenergetics, Vol 895 [b] This includes BBA Reviews on Biomembranes, Vol 906

© 1987, Elsevier Science Publishers B.V (Biomedical Division)

All rights reserved. No part of this publication may be reproduced, stored in a retrieval system, or transmitted, in any form or by any means, electronic, mechanical, photocopying, recording or otherwise without the prior written permission of the publisher, Elsevier Science Publishers B V (Biomedical Division), P O Box 1527, 1000 BM Amsterdam, The Netherlands. Submission of a paper to this journal entails the author's irrevocable and exclusive authorization of the publisher to collect any sums or considerations for copying or reproduction payable by third parties (as mentioned in article 17 paragraph 2 of the Dutch Copyright Act of 1912 and in the Royal Decree of June 20, 1974 (S. 351) pursuant to article 16b of the Dutch Copyright Act of 1912) and/or to act in or out of Court in connection therewith.

Special regulations for readers in the U.S.A. This journal has been registered with the Copyright Clearance Center, Inc Consent is given for copying of articles for personal or internal use, or for the personal use of specific clients This consent is given on the condition that the copier pays through the Center the per-copy fee stated in the code on the first page of each article for copying beyond that permitted by Sections 107 or 108 of the U S Copyright Law. The appropriate fee should be forwarded with a copy of the first page of the article to the Copyright Clearance Center, Inc , 27 Congress Street, Salem, MA 01970, U.S.A If no code appears in an article, the author has not given broad consent to copy and permission to copy must be obtained directly from the author. All articles published prior to 1980 may be copied for a per-copy fee of US$ 2.25, also payable through the Center. This consent does not extend to other kinds of copying, such as for general distribution, resale, advertising and promotion purposes, or for creating new collective works. Special written permission must be obtained from the publisher for such copying

Special regulations for authors Upon acceptance of an article by the journal, the author(s) will be asked to transfer copyright of the article to the publisher This transfer will ensure the widest possible dissemination of information.

Printed in The Netherlands

Biochimica et Biophysica Acta: 40 years on

Professor H.G.K. Westenbrink

Professor E.C. Slater

Biochimica et Biophysica Acta, the first truly international journal in the field of biochemistry and biophysics, and now undoubtedly one of the largest, is celebrating its 40th anniversary with this issue.

The journal was founded in 1947 by Professor H.G.K. Westenbrink, who remained Managing Editor of the journal until 1964. He was succeeded by Professor E.C. Slater, who was able to fulfil this function until his recent retirement as Chairman of the Board of Managing Editors. Professor Slater was encouraged to write a history of BBA, recalling its remarkably rapid growth and some of the intricacies involved in the journal's birth and early development [1].

On the auspicious occasion of the journal's 40th birthday, the Publisher would like to take the opportunity of thanking all those who have played an active role in the journal's development, and looks forward to further stimulating developments over subsequent decades.

The photograph of E.C. Slater is reproduced by permission of Godfrey Argent, U.K., photographers.

[1] *Biochimica et Biophysica Acta: The Story of a Biochemical Journal* by E.C. Slater (1986) Elsevier Science Publishers, ISBN 0-444-80769-1; Price Dfl.75.00.

Biochimica et Biophysica Acta 896 (1987) 1–10
Elsevier

BBA 73181

Fourier transform infrared and differential scanning calorimetric studies of a surface-active material from rabbit lung

Alan J. Mautone [a],*, Kim E. Reilly [b] and Richard Mendelsohn [b],*

[a] *Pulmonary Division Research Center, Schneider Children's Hospital, Long Island Jewish Medical Center,*
270-05 76th Avenue, New Hyde Park, New York, NY 11042, and
[b] *Department of Chemistry, Newark College of Arts and Sciences,*
Rutgers University, 73 Warren Street, Newark, NJ 07102 (U.S.A.)

(Received 1 July 1986)

Key words: Pulmonary surfactant, Fourier transform, Infrared spectroscopy; Phase transition;
Surface-active material; Differential scanning calorimetry; (Rabbit lung)

A surface-active material with a chemical composition consistent with lung surfactant and with the ability to lower surface tension on a Wilhelmy balance to about 6 mN/m, has been isolated from rabbit pulmonary lavage. The thermotropic properties have been characterized with the techniques of Fourier transform infrared spectroscopy (FT-IR) and Differential Scanning Calorimetry (DSC). FT-IR melting curves were constructed from the temperature-dependence of the lipid CH_2 symmetric stretching vibrational frequencies near 2850 cm^{-1}. A broad gel-liquid crystal phase transition with an onset temperature of about 22°C, and a completion temperature of about 38°C was observed, with slight sample-to-sample variations in temperatures. A similar completion temperature was noted in DSC endotherms. Ca^{2+} (5–10 mM) increased the onset temperature of the lipid-melting event, and induced an ordering of surfactant and of its lipid extract at all temperatures studied. The effect on the lipids was suggestive of a Ca^{2+}-induced phase separation caused by ion binding to phosphatidylglycerol and other acidic components. Evidence for a direct interaction between Ca^{2+} and the phosphate groups was suggested through small Ca^{2+}-induced shifts in the 1090 cm^{-1} symmetric PO_2 stretching frequency. Removal of most of the protein component from a 10:1 (lipid/protein, w/w) sample caused an ordering of the resultant lipid fractions. In contrast, removal of most of the protein component from a 20:1 sample resulted in no change in lipid order or thermotropic behavior. These observations are discussed in light of the roles played both by Ca^{2+} and protein in the spreading of surfactant. The power of FT-IR to acquire useful structural information from complex biological tissues is demonstrated.

Introduction

Pulmonary surfactant functions by reducing the surface tension at the air-liquid interface in the alveoli of mammalian lung. The physiological requirements for an effective surfactant have been discussed [1,2]. These include the ability of a compressed monolayer to produce a surface tension of less than 9 dyn/cm, to sustain a low surface tension for sufficient time to avoid al-

---

* To whom reprint requests should be addressed.

Abbreviations: FT-IR, Fourier-transform infrared spectroscopy; DSC, differential scanning calorimetry; DPPC, 1,2-dipalmitoylphosphatidylcholine; POPG, 1-palmitoyl,2-oleoylphosphatidylglycerol; DMPC, 1,2-dimyristoylphosphatidylcholine; PC, phosphatidylcholine; PG, phosphatidylglycerol

Correspondence: Dr. R. Mendelsohn, Department of Chemistry, Newark College of Arts and Sciences, Rutgers University, 73 Warren Street, Newark, NJ 07102, U.S.A.

0005-2736/87/$03.50 © 1987 Elsevier Science Publishers B.V. (Biomedical Division)

veolar collapse and to spread rapidly from the subphase. Chemical analysis of surfactant reveals the presence of lipids, primarily phospholipids, and protein. The predominant lipid of mammalian lung surfactant is dipalmitoylphosphatidylcholine (DPPC). In bilayer systems, DPPC undergoes its gel-liquid crystal transition at 41°C. Therefore, under high compression at 37°C, the rigidity of the molecule enables it to sustain high surface pressures. However, the very rigidity of the acyl chains (necessary for the first two requirements above), constitutes a detriment to the third requirement, namely, the ability of surfactant to spread rapidly. It has been suggested [3] that a delicate balance of fluid lipids (such as unsaturated phospholipids) and rigid lipids is to be expected, and indeed, appears to occur [4]. In addition, it has recently been shown [5] that specific Ca^{2+}-protein–lipid interactions are important for determining surfactant structure and function. Notter, et al. [6], showed that whole lung surfactant will form a surface film when Ca^{2+} (but not Mg^{2+}) is present in the subphase, while Hawgood, et al. [5] suggest that the threshold concentration for Ca^{2+}-induced aggregation of unilamellar liposomes was reduced from 13 to 0.5 mM by a protein fraction isolated from surfactant. It has been previously suggested [7,8] that both Ca^{2+} and specific proteins modify the state of dispersion of surfactant lipids. As a Ca^{2+} concentration of 1.6 mM has been recently measured for adult rabbit lungs [9], the protein-induced reduction of the Ca^{2+} threshold could have functional consequences. Physical studies of the interaction between the components in this complex system are therefore indicated.

The physical techniques used to date for the study of lung surfactant have centered around surface balance determination of monolayer film properties (for a review see Notter [10]) and the use of (most frequently) turbidimetric [5,11] or DSC determination [12] of surfactant phase properties. Yet these methods do not provide information about the molecular configuration or conformation of surfactant components. A recent exception to this [13] involved electron paramagnetic spectroscopic studies of lipid fluidity in surfactant. While this method has provided much useful data on lipid structure in general [14], the requirement of the technique for a probe molecule such as 5-doxylmethylstearate in the aforementioned study, leads to the possibility of probe-induced alterations in lipid order [15], and partitioning of the probe into particular regions of the lipidic system. Thus, the application of additional physical methods to the problem of interacting components in lung surfactant is in order.

The techniques of FT-IR spectroscopy offer several advantages for the study of surfactant, as follows:

(1) Both lipid configuration and protein secondary structure are monitored in a single experiment.
(2) No probe molecules are required.
(3) Small amounts of material (1–500 μg) may be studied in a variety of physical states, including monolayers both on IR substrates such as germanium (via the techniques of attenuated total reflectance) and on an aqueous surface [16,17].

The current study reports the first FT-IR investigations of rabbit lung surfactant. The study focuses on the thermotropic properties of surfactant and their modification by Ca^{2+} and surfactant protein. Complementary DSC investigations are also presented.

Materials and Methods

Isolation and purification of surfactant

New Zealand white rabbits were anesthetized with sodium pentobarbital (30 mg/kg of body weight, intravenously) and exsanguinated by severing the abdominal aorta. The chest was opened and the lungs lavaged through a tracheal cannula with a volume of cold saline equal to the functional residual capacity, i.e., 30 ml/kg of body weight. The saline was gently infused and withdrawn five times. This procedure was repeated five times, the total volume of saline in the lungs never exceeding the functional residual capacity.

Surfactant was isolated by the method of Suzuki, et al. [18]. Briefly, lavage fluid was centrifuged at 100 × g for 10 min to remove cells and debris. The supernatant was centrifuged at 16 000 × g for 1 h at 0°C. The precipitate was resuspended in 0.145 M NaCl containing 0.01 M Tris-HCl and 1 mM EDTA (buffered NaCl), layered over a discontinuous gradient of 0.25 M and 0.68

M sucrose and centrifuged at 78 000 × g for 1 h at 0 °C. The material at the interface was collected by aspiration and washed three times with buffered NaCl. The pellet was resuspended in buffered NaCl and stored at −20 °C.

Chemical characterization

Total phosphorus was determined by the method of Chen et al. [19]. Protein was determined by the method of Lowry [20]. Lipid and protein components were separated using Bligh-Dyer or Folch [21] extraction protocols. The lipid classes were determined by analytical thin-layer chromatography using a $CHCl_3/MeOH/NH_4OH$ (65 : 25 : 5) solvent system. The phospholipid spots were scraped, and total phosphorus for each spot was determined as per Chen et al. [19]. Acyl chain lengths of the lipid component were assayed by gas chromatography on a Hewlett Packard 5890A gas liquid chromatograph following formation of the methyl esters. Protein molecular weights were evaluated by 10% SDS-polyacrylamide gel electrophoresis.

Dynamic surface tension

A 1 ml aliquot of surfactant with a lipid/protein ratio of 10 : 1 (w/w) and containing 1.8 mg total lipid/ml was gently spread on the surface of buffered Ringer's solution (pH 7.4) in a vertical film surface balance [22] at 37 °C, 100% humidity, and the subphase was gently stirred. The minimum surface area was 30.2 cm^2 and maximal surface area was 161.4 cm^2. The rate of cycling between the minimum and maximum surface areas was 5.25 min/cycle. Surface tension was measured via a Cahn electrobalance (Cahn Instrument Co., Paramont, CA, U.S.A.). Cycling was continued until the maximum and minimum surface areas were stable.

FT-IR spectroscopy

Samples were prepared for FT-IR examination as follows:

(1) Surfactant without calcium-surfactant in NaCl buffer was centrifuged at 100 000 × g for 1 h at 0 °C.

(2) Surfactant with calcium-surfactant was centrifuged at 10 000 × g for 1 h at 0 °C. The pellet was resuspended in 0.145 M NaCl containing 0.01 M Tris-HCl and 5 mM or 10 mM $CaCl_2$ (calcium buffer) and recentrifuged at 100 000 × g for 1 h at 0 °C.

(3) Lipid extract without calcium-lipid component was extracted as above and the organic solvent evaporated. The lipids were resuspended in buffered NaCl and centrifuged as for surfactant

(4) Lipid extract with calcium-prepared in the same manner as the sample without calcium except that the lipids were resuspended in calcium buffer and then centrifuged.

The samples were examined in a Harrick cell (pathlength 25 μM) equipped with CaF_2 windows. Spectra were recorded on a Mattson Instruments Sirius 100 spectrometer equipped with a mercury-cadmium-telluride detector. Routinely, 200 interferograms were collected, co-added, apodized with a triangular function and Fourier transformed to give a resolution of 4 cm^{-1} with data encoded every 2 cm^{-1}. Temperature was controlled with a Haake circulating bath and monitored with a Bailey BAT-12 digital thermometer, with a thermocouple sensor placed close to the IR windows in the cell. Frequencies were measured by fitting a parabola to the top three data points followed by finding the maximum in the parabola. The spectrum of water (matched for temperature and path length) was subtracted from all data sets. Residual sloping baselines were removed with a linear baseline leveling routine supplied with the instrument software.

Differential scanning calorimetry

Calorimetry experiments were performed in a Micro-cal MC1 unit. Sample volumes were 0.70 ml. Samples were heated at about 24° C/h following 1–2 h of equilibration in the instrument.

Results

Biochemical characterization of surfactant

The phospholipid composition (only components present in > 1% quantities are listed) of surfactant as determined by quantitative TLC is summarized in Table I. The results are in general accord with those of Hook et al. [13], whose value for phosphatidylglycerol (9.4%) was somewhat lower. The fatty acid composition of the phospholipids is also given in Table I. Palmitic acid

TABLE I
PHOSPHOLIPID COMPOSITION OF SURFACTANT

Phospholipid Class	% of P recovered
PC	78.5
PG	15.1
PE	3.7
LysoPC	2.7

FATTY ACID COMPOSITION OF TOTAL LIPID EXTRACT

Chain length: C = C bonds	(%)
14:0	3.0
16:0	64.9
16:1	4.6
18:0	3.8
18:1	15.5
18:2	6.2
Unidentified	2.0

TABLE II

ASSIGNMENTS OF FT-IR FREQUENCIES IN THE 1000–1800 cm^{-1} REGION OF SURFACTANT

Symbols: s, m, w, sh, v stand for strong, medium, weak, shoulder and very, respectively.

Frequency in cm^{-1}	Assignment
1018 sh	
1065 s	ester C-O sym. stretch
1088	phosphate sym. stretch
1114 sh	
1148 sh	
1175 w	ester C-O asym stretch
1200 1225 1242 1263 1287	CH_2 wagging progression superimposed on the phosphate antisymmetric stretch at 1225 cm^{-1}
1342 w	CH_2 wagging
1379 w	CH_2 symmetric bend
1403 vs	choline CH_3 sym bend
1420 w	alpha CH_2 scissoring
1437 sh	
1458 sh	CH_3 asym bend
1468 s	CH_2 scissoring
1487 sh	choline asym bend
1543 1550 1557	protein amide II
1638 sh	protein amide I + H_2O
1651 s	
1738 s	C = O stretch

was the major fatty acid, accounting for 64.9% of the total fatty acid present. Substantial amounts of oleic and linoleic acid were also noted. These results are in excellent accord with those of Magoon et al. [23], who observed that palmitic and oleic acids constituted the main fatty acid constituents in both the PC and PG fractions of rabbit lamellar bodies.

Five major protein fractions were observed with SDS-polyacrylamide gel electrophoresis. The molecular weights (kDa) were 15, 24, 32, 45 and 66. Wright, et al. [24] observed and characterized two fractions of protein with apparent molecular mass 30–36 kDa and 10–15 kDa. In addition, they observed prominent bands (possibly serum derived) with approximate molecular masses of 25, 50, 65–67 and 75 kD, in excellent accord with the current preparation.

Some sample-to-sample variation in the lipid/protein ratio has been noted. Values ranged from 10:1 to 5:1 with occasional samples falling outside these levels. Our variation was similar to that noted by Keough et al. [12], who noted variation in the lipid/protein ratio from 10.8:1 to 6.6:1 depending on the number of centrifugation steps used in the isolation protocol.

Dynamic surface tension studies

Slow cycling of surface area resulted in a stable maximum surface tension of 50 mN/m and minimum surface tension of 6 mN/m. This fits the criterion for surface tension lowering ability of surfactant as discussed in the Introduction.

FT-IR and DSC studies

Typical FT-IR spectra from the 1000–1800 and 2700–3100 cm^{-1} spectral regions are shown in Fig. 1. The observed intense spectral features arise from the phospholipid components of surfactant with two exceptions – the contour near 1650 cm^{-1} is due to overlapped solvent bending and protein Amide I (peptide C = O stretch) modes, and the features between 1540 and 1560 cm^{-1} arise from protein Amide II (mixed N-H in-plane bend and C-N stretch) modes. Spectral assignments are given in Table II.

Lipid thermotropic behavior is conveniently monitored [26] through temperature-induced alterations in the frequency of the CH_2 symmetric

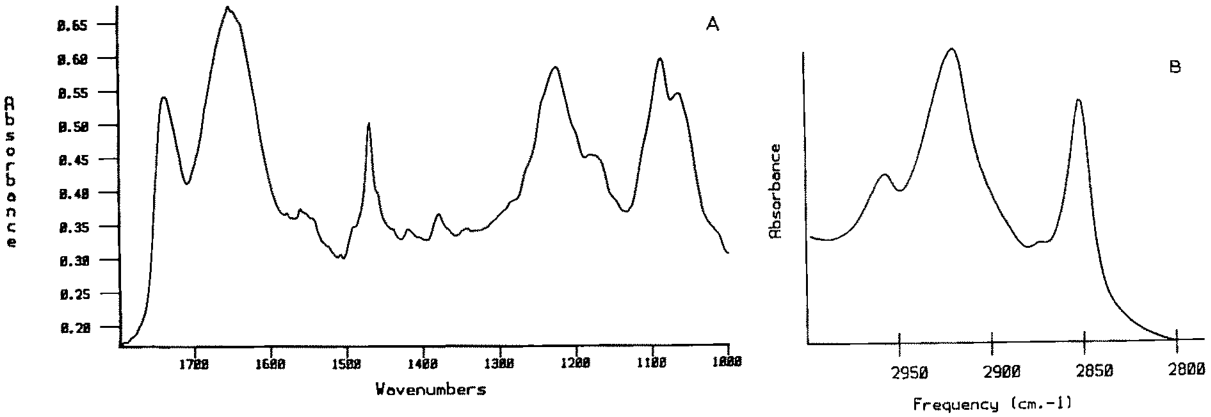

Fig. 1 Typical FT-IR spectra for surfactant (A) The 1000–1800 cm^{-1} spectral region of a sample of surfactant with 5 mM Ca^{2+} The experiment was performed at 5.7°C. The majority of the spectral features arise from the lipids; exceptions to this are the weak protein features between 1500–1580 cm^{-1}, and some of the intensity underlying the 1650 cm^{-1} band. (B) The 2800–3000 cm^{-1} spectral region of a sample of surfactant with 5 mM Ca^{2+} The experiment was performed at 5.7°C. The spectral features arise primarily from the lipidic components. The band near 2850 cm^{-1} had little underlying contribution from protein and, therefore, was the band of choice for monitoring the thermotrophic behavior of phospholipids.

stretching bands of the lipid acyl chains near 2850 cm^{-1}. This spectral feature is one of the strongest in the spectrum and suffers no interference from overlapping protein bands. Although frequency increases are small (1–3 cm^{-1}) during gel-liquid crystal phase transitions, they may be monitored with a precision of 0.01–0.05 cm^{-1} through use of the center of gravity algorithm for band positions developed by Cameron et al. [27]. The origin of the frequency increase on melting has been traced by Snyder et al. [28] to changes in the interaction constants between C-H stretching coordinates on adjacent methylene groups when the lipid physical state is altered through, for example, the formation of *gauche* rotamers in the acyl chains. Although the procedures of Snyder et al. [28] permit no rigorous correlation between the frequency and the number of *gauche* rotamers in the chain, procedures have been developed [29] for conversion of FT-IR melting curves into quantitative indicators of fractions of lipid melted.

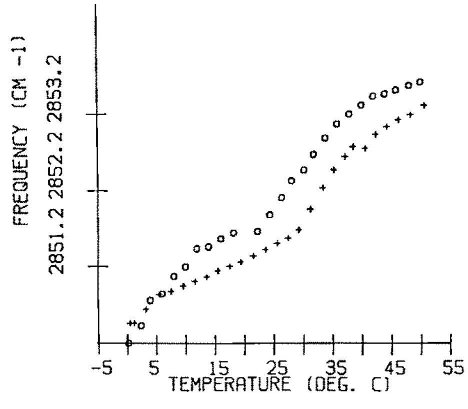

Fig. 2 Thermotropic behavior for surfactant (O) and surfactant+10 mM Ca^{2+} (+) with lipid/protein ratios (w/w) of 7:1 The parameter monitored is the frequency of the CH_2 symmetric stretching modes of the lipid acyl chains near 2850 cm^{-1}

The temperature dependence of the 2850 cm^{-1} band for a surfactant preparation (lipid/protein ratio 7:1) is shown in Fig. 2. Although some scatter in the data points is evident at low temperatures, a broad phase transition with an onset temperature of 22–23°C and a completion temperature of about 36–39°C is clearly discernable. As the monitored IR frequency arises from the lipid component of the preparation, the observed transition evidently arises from a gel-liquid crystal transition of the surfactant phospholipids, which are probably in multibilayer form in the current preparation. Thus, at physiological temperatures, the lipids are almost entirely in the liquid crystalline state. The magnitude of the change in the spectral parameter used is similar to, although slightly smaller than, that usually observed in single component phospholipid systems (e.g. Ref. 30). Slight variations in the onset and completion temperatures were noted from sample to sample. Further evidence for the temperature-induced disordering of the acyl chains comes from examination of the 1200–1300 cm^{-1} spectral region (Table II). At low temperatures, the observed series of bands at 1200, 1225, 1242, 1262 and 1284 cm^{-1} arises from a progression in the CH_2 wagging mode. The series arises essentially from coupling between similar vibrations along a sequence of unit cells and only occurs if the acyl chain configuration is all-*trans*. Thus at 5°C (data of Table II), a substantial all-*trans* character exists in the chains. As the temperature is raised (data not shown) the shoulders of the series progressively diminish in intensity so that at 48°C, only a single broad peak at 1225 cm^{-1} due to the antisymmetric PO_2 double bond stretching mode remains. The elimination of the band progression arises due to disruption of the coupling between adjacent unit cells upon *gauche* rotamer formation.

The effect of Ca^{2+} on the 7:1 surfactant sample is also shown in Fig. 2. Addition of 10 mM Ca^{2+} produces a 5–7 Cdeg increase in the onset temperature with no large alteration of the completion temperature. The midpoint of the transition is also shifted to higher temperatures. In addition, the CH_2 frequency is lowered from the Ca^{2+}-free surfactant at all temperatures, indicating a Ca^{2+}-induced ordering of the acyl chains.

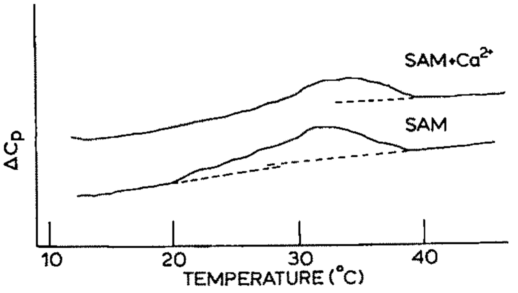

Fig. 3 Differential scanning calorimetry endotherms for surfactant (SAM) and surfactant +10 mM Ca^{2+} The lipid/protein (w/w) ratio was 6:1 The dashed lines are estimated baselines. Note that for the calcium-containing sample the onset temperature was difficult to estimate due to the continuous curvature of the trace.

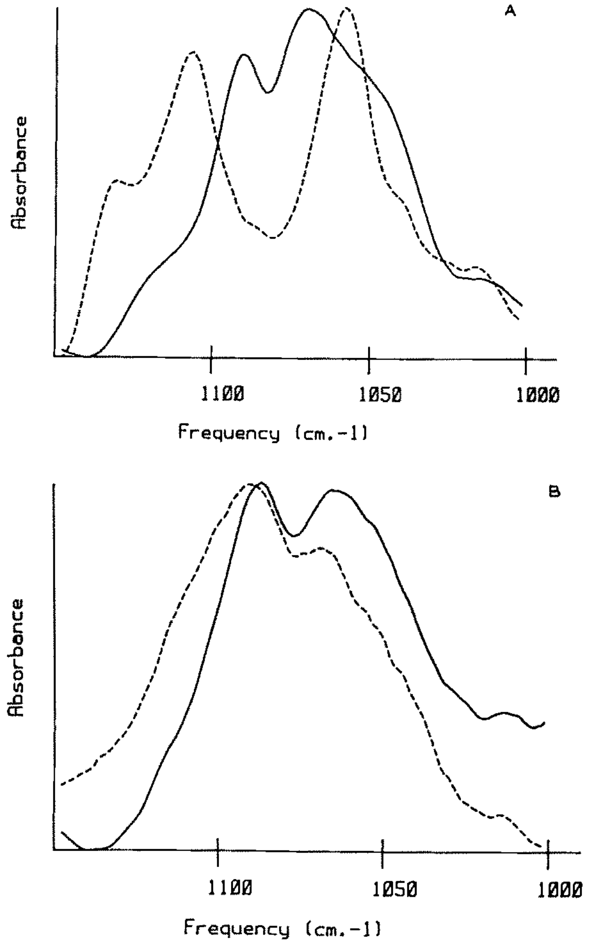

Fig. 4 FT-IR evidence for the interaction of calcium with the phosphate group. (A) The spectral region of 1000–1200 cm^{-1} for POPG (———) and for POPG+ 10 mM Ca^{2+} (------). (B) The spectral region of 1000–1200 cm^{-1} for surfactant (———) and for surfactant+10 mM Ca^{2+} (------).

The results from DSC experiments are shown in Fig. 3. Surfactant (lipid/protein ratio 6:1) shows a broad endotherm with an onset temperature of about 20°C, a completion temperature of 38.5°C and a maximum at about 31°C. The onset and completion temperatures are in reasonable accord with those determined from FT-IR data. We note that our DSC results differ slightly from those recently reported by Keough et al. [12], who observed higher completion temperatures although the temperature of the maximum was about the same. Part of the discrepancy may arise from difficulties in establishing accurate baselines for samples which have broad, weak endotherms. Ca^{2+}-induced effects, similar to those seen in the FT-IR melting profiles, were observed in the DSC experiments (Fig. 3). A comparison of the endotherms generated in the absence and presence of

Ca^{2+} (10 mM) shows a 1–2 Cdeg increase in the position of maximum excess enthalpy as well as a 1 Cdeg increase in the completion temperature induced by the ion. The occurrence of changes in the onset temperatures were difficult to determine (Fig. 3) due to continually changing baselines in the low temperature (single phase?) regions of surfactant in the presence of Ca^{2+}.

Direct FT-IR evidence for the interaction of Ca^{2+} with lipid head-groups was sought from an experiment whose results are depicted in Fig. 4. The vibrational mode known to respond most strongly to Ca^{2+}/phosphate interaction [31] is the symmetric PO_2^- double bond stretching mode near 1090 cm^{-1}. The control system (Fig. 4a) shows the effect of addition of 10 mM Ca^{2+} to POPG. Substantial alterations in the pattern of frequencies and intensities in the 1000–1150 cm^{-1} region are noted. Much smaller changes are observed when Ca^{2+} is added to surfactant (Fig. 4b). A frequency increase of about 4 cm^{-1} is seen in the 1090 cm^{-1} band and a frequency increase of 2 cm^{-1} is seen in the 1067 cm^{-1} band along with an intensity increase in the shoulder near 1115 cm^{-1}. Direct interaction of the ion with (at least) some of the phospholipid head-groups is therefore suggested.

The effect of calcium on the lipidic components alone is shown in Fig. 5. Lipids were extracted either with a Folch wash or with Bligh-Dyer extraction protocols. Rehydration of the dried lipids was accomplished either in an EDTA-containing buffer or in a buffer containing Ca^{2+}. FT-IR melting curves (Fig. 5) reveal a slight Ca^{2+}-induced ordering as measured from the CH_2 symmetric stretching frequency and upward shifts of the onset and completion temperatures of the lipid phase transition. An attempt was made to

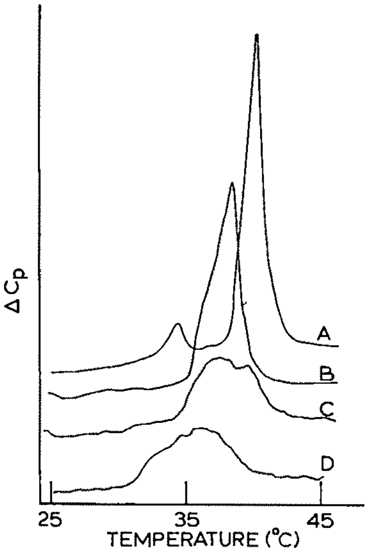

Fig. 6 Differential scanning calorimetry traces for·

(A) a 9:1 DPPC/POPG mixture in the presence of 10 mM Ca^{2+}

(B) a 9:1 DPPC/POPG mixture in the absence of Ca^{2+}

(C) a 4:1 DPPC/POPG mixture in the presence of 10 mM Ca^{2+}

(D) a 4:1 DPPC/POPG mixture in the absence of Ca^{2+}

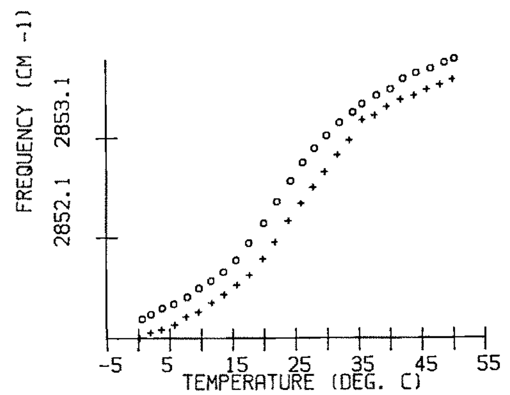

Fig. 5 The thermotropic behavior of a lipid extract from the surface-active material in the absence (O) and presence (+) of 10 mM Ca^{2+}. The parameter monitored is the same as that in Fig. 1.

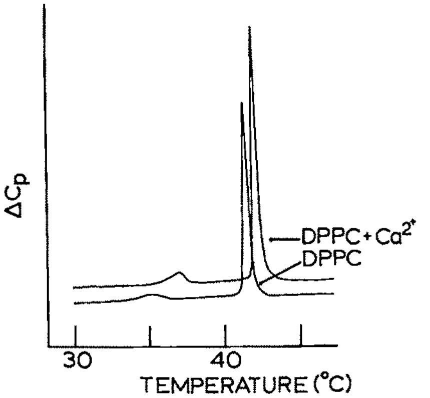

Fig 7. Differential scanning calorimetry traces for DPPC in the presence and absence of 10 mM Ca^{2+}. The slight Ca^{2+}-induced increases in melting temperatures of both the pre-transition and main transition are evident

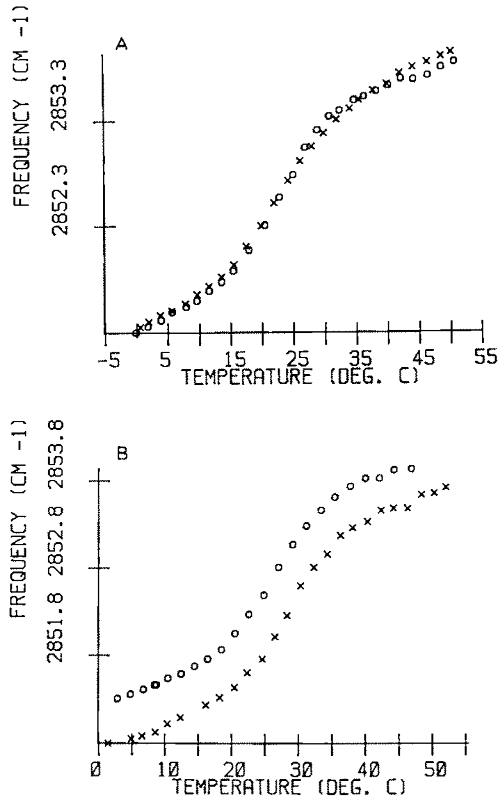

Fig. 8. The effect of protein on the thermotropic behavior of surfactant (A) A sample with a lipid/protein ratio of 20:1. The curves for the surfactant (O) and for the lipid extract (x) are virtually superimposed (B) A sample with a lipid/protein ratio of 10:1. The curve for the lipid extract (x) shows increased order, onset temperature and midpoint temperature from that of surfactant (O). The parameter monitored is the same as that in Fig. 1.

model this effect using DSC with phospholipid samples containing DPPC and POPG at molar ratios of 9:1 and 4:1, respectively. The results are shown in Figs. 6 and 7. In the absence of Ca^{2+}, the DSC traces for the 9:1 and 4:1 samples show (Fig. 6b and d) a broadening and shift to lower temperatures compared with pure DPPC (Fig. 7). Addition of Ca^{2+} to pure DPPC results in minor changes in the endotherms. As shown in Fig. 7, the main transition and pre-transition are shifted up in temperature by 0.6 Cdeg and about 1.6 Cdeg, respectively. In contrast, addition of 10 mM Ca^{2+} to the 9:1 sample results in major changes and leads to a trace (Fig. 6a) in which the pretransition is restored and the main endotherm is markedly reduced in width and increased in temperature. An upward shift is onset and completion temperatures are also noted for the 4:1 sample upon the addition of Ca^{2+} (Fig. 6c).

The final experiments involve the effect of protein on lipid melting. Extraction of the lipid component was followed by rehydration and FT-IR examination of samples found to have two different lipid/protein ratios, 20:1 and 10:1 (w/w), respectively. The FT-IR thermotropic data for the 20:1 sample and for its lipid extract are shown in Fig. 8a. The melting curve for the lipid fraction is virtually superimposed on that for intact surfactant. However, for the sample containing higher levels of protein (10:1 w/w), the removal of protein reveals (Fig. 8b) a general ordering of the lipid component. This is revealed by an increase in the CH_2 symmetric stretching frequency at all temperatures as well as a 3–5 Cdeg increase in the onset and mid-point temperatures of the phase transition. The completion temperature is less altered.

Discussion

The qualitative nature of the interactions between Ca^{2+}, surfactant lipids and the 35 kDa protein fraction of surfactant has been addressed by King and coworkers [8,11,32]. The efficiency of formation of complexes reconstituted from purified apoprotein and phospholipid mixtures was enhanced both by PG and Ca^{2+} [11]. Reconstitution studies of the protein with DMPC using DSC suggest that 9 mol of DMPC are immobilized upon complexation [32]. Whether similar effects occur in native surfactant is unclear. This and several additional issues would appear to require further reconstitution experiments and molecular spectroscopic techniques for their resolution. These include the effects of Ca^{2+} on the secondary structure of the various protein fractions and lipid-induced alterations therein, and the structure of tubular myelin.

The ability of FT-IR spectroscopy to determine the molecular nature of the interaction between surfactant components and hence resolve some of the issues alluded to above is evident from the current preliminary studies. The sites of Ca^{2+} action and its effect on surfactant lipid thermotropic properties are revealed in Figs. 2, 3 and 4. The interaction between the ion and the lipid head-group is revealed by alterations in the PO_2 symmetric stretching region. While the spectral perturbations (Fig. 4) are weaker than those produced by Ca^{2+} on phosphatidylserine [31] or on POPG, (Fig. 4) they nevertheless are indicative of the site of action. A possible explanation for the relatively small magnitude of the ion-induced shifts is that mainly the PG is directly affected by Ca^{2+}. The IR spectrum, however is dominated by the (less-affected) PC component, hence, is not strongly perturbed. The effect of Ca^{2+} on acidic lipid phase behavior is to rigidify the lipids and either to increase the midpoint temperature of the thermotropic transition [33] or, as noted in our recent FT-IR studies of Ca^{2+}-phosphatidylserine interaction [31], to abolish the cooperative melting event completely. Our current FT-IR and DSC observations of an increased ordering and melting temperatures suggest a calcium-induced sequestering (phase separation) of the acidic components. If this is indeed the case, the remainder of the surfactant would be enriched in DPPC compared with the Ca^{2+}-free preparation and would melt at higher temperatures. Data for the model systems formed from DPPC/POPG are consistent with this interpretation. The restoration of a pre-transition upon Ca^{2+} addition to the 9:1 DPPC/POPG mixture provides (Fig. 6) particularly good evidence for phase separation as the pre-transition is abolished by small amounts of a second component in an otherwise pure phase. In addition, this description would help explain the speculation [34] that during compression of a surface film of surfactant, non-DPPC components are selectively eliminated from the monolayer. Our data suggest that Ca^{2+} plays a key role in this process.

The two proteins expected to interact hydrophobically with phospholipids are the 32 and 14 kDa species [24], while the other species observed by SDS-polyacrylamide gel electrophoresis in the current work have been tentatively suggested (in studies of other species) as arising from serum [24]. The effect of protein on the thermotropic behavior of the lipid fraction is minimal at a lipid/protein ratio of 20:1 (Fig. 7). At higher protein levels, the observed protein-induced disordering of the lipid fraction is very similar to that observed by FT-IR in studies of Ca-ATPase reconstituted with a variety of lipid classes [30]. We note that the current FT-IR spectral parameter, which measures *gauche* rotamer formation in the acyl chains, reflects in part the bending of the hydrocarbon chains to accommodate the protein surface, in addition to the rates of acyl chain motion. Thus, the effect of protein on lipid order/mobility as revealed by FT-IR differs substantially compared with other techniques that monitor events that occur on slower time scales.

What can be concluded from the current work about the roles of Ca^{2+} and protein in surfactant function? The observation that PG liposomes rapidly aggregate and fuse in the presence of 10 mM Ca^{2+} [35], coupled with the indication from the current experiments of direct interaction of Ca^{2+} with PG head-group phosphates, is suggestive of a mechanism for calcium-induced aggregation of surfactant liposomes [5]. In addition, the observation of protein-induced disordering of surfactant lipids at relatively high protein levels suggests a means for control of lipid order. Not all of the molecular details of the interactions are accessible from the current experiments. It is possible that one or more of the several proteins present interacts strongly with a small subclass of lipid molecules or, alternatively, that more non-specific events occur. These possibilities can only be distinguished with reconstitution experiments. Further, it is reasonable to assume that ternary interactions between the lipids, Ca^{2+} and protein take place. In any event, there appear to be a number of possibilities by which the order of the lipids (hence their ease of spreading and rigidity) may be controlled. Further details may become available when interactions between purified proteins and lipid components are analyzed. FT-IR spectroscopy promises to be useful in studies of Ca^{2+} or lipid-induced alterations in protein secondary structure.

Acknowledgements

This work was supported by a grant (GM 29864) to R.M. from the National Institutes of Health. We thank Mr. A. Hassankhani for acquiring some of the DSC data. Additional support was provided from the Busch Memorial Fund of Rutgers University.

References

1 Clements, J.A. (1977) Am. Rev. Respir. Dis. 115, 67–71

2 King, R.J. (1984) in Pulmonary Surfactant (Robertson, B., Van Golde, L.M.G. and Batenburg, J.J. eds.), Chap 1, Elsevier, Amsterdam

3 Hawco, M W., Davis, P.J. and Keough, K.M.W. (1981) J Appl. Physiol. Respir. Environ Exercise Physiol. 57, 509–515

4 Trauble, H., Eibl. H. and Sawada, H. (1974) Naturwissenschaften 61, 334–354

5 Hawgood, S. Benson, B.J and Hamilton, R.L., Jr. (1985) Biochemistry 24, 184–190

6 Notter, R.H., Finkelstein, J.H. and Taubold, R D. (1983) Chem Phys. Lipids 33, 67–80

7 Gil, J. and Reiss, O.K. (1973) J. Cell. Biol. 58, 152–171

8 King, R.J., Carmichael, M.C. and Horowitz, P.M. (1983) J. Biol Chem. 258, 10672–10680

9 Neilson, D.W. (1984) Pediatr. Res. 18, 400–401

10 Notter, R.H. (1984) in Pulmonary Surfactant (Robertson, B., Van Golde, L.M.G. and Batenburg, J J., eds.), Chap 2, pp. 17–65

11 King, R.J. and MacBeth, M.C. (1979) Biochim. Biophys. Acta 557, 86–101

12 Keough, K.M.W., Farrell, E., Cox, M., Harrell, G. and Teusch, H.W , Jr. (1985) Can. J. Physiol. Pharmacol. 63, 1043–1051

13 Hook, G.E.R., Spalding, J.W., Ortner, M.J., Tombropoulos, E G., and Chignell, C.F. (1984) Biochem J. 223, 533–542

14 Marsh, D. (1981) in Membrane Spectroscopy (Grell, E., Ed.), Springer, Berlin

15 Taylor, M.O. and Smith, I.C.P. (1980) Biochim. Biophys. Acta 599, 140–149

16 Dluhy, R. and Cornell, D.G. (1985) J. Phys. Chem 89, 3195–3197

17 Briggs, M.S., Cornell, D.G., Dluhy, R.A. and Gierasch, L.M. (1986) Science, in the press

18 Suzuki, Y., Nakai, E. and Ohkawa, K. (1982) J. Lipid Res. 23, 563–61

19 Chen, P.S., Toribara, T.Y. and Warner, H. (1956) Anal. Chem. 28, 1756–1758

20 Lowry, O.H., Rosebrough, N J , Farr, A.L. and Randall, R J. (1951) J Biol. Chem 193, 265–275

21 Kates, M. (1972) in Laboratory Techniques in Biochemistry and Molecular Biology (Work, T.S. and Work, E., eds), North-Holland Publishing Company, Amsterdam

22 Boyle, J. and Mautone, A.J. (1982) Colloids Surf. 4, 77–85

23 Magoon, M.W , Wright, J.R., Baritussio, A , Williams, M C. Goerke, J., Benson, B.J , Hamilton, R L. and Clements, J.A. (1983) Biochim. Biophys. Acta 750, 18–31

24 Wright, J.R., Benson, B.J., Williams, M.C., Goerke, J. and Clements, J.A. (1984) Biochim. Biophys. Acta, 791, 320–332

25 Mendelsohn, R. and Mantsch, H.H. (1986) in Progress in Protein-Lipid Interactions 2 (Watts, A W. and De Pont, J.J.H.H.M., eds.), p 103–146, Elsevier, Amsterdam

26 Cameron, D.G., Kauppinen, J.K., Moffatt, D.J. and Mantsch, H.H. (1981) Biochemistry 20, 4496–4500

27 Cameron, D.G., Kauppinen, J.K., Moffatt, D.J. and Mantsch, H.H. (1982) Appl Spectrosc. 3613, 245–249

28 Snyder, R G., Strauss, H.L. and Elliger, C.A. (1982) J. Phys. Chem. 86, 5145–5150

29 Dluhy, R.A., Moffatt, D., Cameron, D G., Mendelsohn, R and Mantsch, H.H. (1985) Can. J. Chem 63, 1925–1932

30 Anderle, G. and Mendelsohn, R. (1986) Biochemistry 25, 2174–2179

31 Dluhy, R., Cameron, D.G., Mantsch, H.H and Mendelsohn, R. (1983) Biochemistry 22, 6318–6325

32 King, R.J. (1984) Experimental Lung Research 6, 237–253

33 Jacobson, K. and Papahadjopoulos, D. (1975) Biochemistry 14, 152–161

34 Goerke, J. and Clements, J.A. (1986) In The Handbook of Physiology (Fishman, A.P., ed.), Vol. 3, p.247, American Physiological Society, Bethesda, MD

35 Rosenberg, J , Duzgunes, N. and Kayalar, C. (1983) Biochim. Biophys. Acta 735, 173–180

Biochimica et Biophysica Acta 896 (1987) 11–18
Elsevier

BBA 73173

Effect of chlorophyll *a* on the phase behavior of hydrated monogalactosyldiacylglycerols

Phoebe Dea [a],*, Laurence T. Pearson [a], Martin Caffrey [b]
and Sunney I. Chan [a],**

[a] *Arthur Amos Noyes Laboratory of Chemical Physics ***, California Institute of Technology, Pasadena, CA 91125*
and [b] *Section of Biochemistry, Molecular and Cell Biology, Cornell University, Ithaca, NY 14853 (U.S.A.)*

(Received 4 July 1986)
(Revised manuscript received 24 September 1986)

Key words: Chlorophyll *a*; Freeze-fracture; Monogalactosyldiacylglycerol, Phase transition; X-ray diffraction

We have studied the effect of chlorophyll *a* (chl *a*) on the X-ray diffraction patterns and the appearance of freeze-fracture electron micrographs of aqueous dispersions of monogalactosyldiacylglycerols (MGDG), the most abundant lipid in the thylakoid membrane. In MGDG systems containing 0–18 mol% of chl *a*, the diffraction patterns indicate the presence of a well-ordered reverse hexagonal phase. When 30 mol% of chl *a* was incorporated into the MGDG, the low-angle X-ray diffraction lines of the hexagonal lattice were slightly broadened and were accompanied by additional weak lines. With higher mol percents of chl *a*, the low-angle lines could no longer be indexed on a hexagonal or lamellar lattice. The freeze-fracture electron micrographs of similar samples showed that the patterns characteristic of the reverse hexagonal phase of an aqueous dispersion of pure MGDG were replaced by large liposomes, the fracture pattern of which is circular. We conclude that chl *a* in excess of 20 mol% destabilized the orderly reverse hexagonal phase of aqueous MGDG dispersions and disturbed the long-range order of the lipid array. These results are summarized in a temperature-composition isobaric phase diagram over a temperature range of −60°C to 60°C.

Introduction

Photosynthesis occurs at specialized chloroplast membranes which consist of approximately 50% protein, 40% lipid and 10% chlorophyll by weight [1]. The monogalactosyldiacylglycerols (MGDG) and digalactosyldiacylglycerols (DGDG) represent the main constituents of the lipid matrix in the thylakoid membranes, being nearly 40% and 20% of the lipid mass, respectively [2]. It is both tempting and logical to correlate this unique chemical composition with its unique biochemical functions.

X-ray diffraction and freeze-fracture electron microscopy studies by Shipley et al. [3] have shown that MGDG from *Pelargonium* leaves do not form bilayers in an aqueous dispersion but exist in a reverse hexagonal lipid-water phase (H-II) with the polar groups facing inwards towards the aqueous phase. Esterification with a second galactose unit to form DGDG completely alters the phase

---

* Permanent address: Department of Chemistry and Biochemistry, California State University at Los Angeles, Los Angeles, CA 90032, U.S.A.

** To whom reprint requests should be addressed.

*** Contribution No. 7064 of the Department of Chemistry, California Institute of Technology.

Abbreviations: chl *a*, chlorophyll *a*; H-II, reverse hexagonal phase; MGDG, monogalactosyldiacylglycerols; DGDG, digalactosyldiacylglycerols

Correspondence address: Department of Chemistry and Biochemistry, California State University at Los Angeles, Los Angeles, CA 90032, U.S.A

0005-2736/87/$03.50 © 1987 Elsevier Science Publishers B.V. (Biomedical Division)

morphology, and a lamellar bilayer phase is formed. In the presence of excess water, DGDG forms dispersions of liposomes [4]. More recently, Williams and co-workers [5–8] have carried out rather extensive freeze-fracture studies on MGDG and DGDG/water systems from broad bean plants (*Vicia faba* L., var. Express). Their results indicate that when hydrated, MGDG forms an H-II phase, DGDG forms liposomes, while a mixture of these lipids in the molar ratio of 2:1 (MGDG/DGDG) forms bilayers in which there are either interbilayer lipid particles corresponding to an inverted micellar phase or arrays of particles between apposed bilayers.

Many studies of unsaturated phosphatidylethanolamines have shown that their phase states are modified by the presence of other components. For example, when phosphatidylcholine is mixed with phosphatidylethanolamine, the bilayer-forming phosphatidylcholine tends to stabilize the bilayer or lamellar phase over the reverse hexagonal phase [9]. Two components of different molecular shape can often form a new phase when mixed. In a dispersion of lysophosphatidylcholine/cholesterol (1:1), the lipids are found to be organized in extended bilayers [10]. Furthermore, monoolein and dioleoyl-phosphatidylcholine when mixed in equimolar amounts at 5% water form an inverted hexagonal phase. In isolation under the same conditions, they form the lamellar phase [11]. It is possible that a mixture of chl *a* and MGDG may form a phase other than that formed by the pure lipids. In particular, if the chlorophyll and galactolipids form stable complexes, the molecular shape of such complexes may be such as to permit stabilization of a bilayer phase.

In this paper, we report the effect of chl *a* on the phase behavior of aqueous dispersions of MGDG as revealed by freeze-fracture electron microscopy and X-ray diffraction.

Materials and Methods

Chlorophyll *a* was isolated from spinach extracts following the dioxane precipitation procedures of Iriyama et al. [12] and powdered sugar chromatographic purification [13,14]. Final purification was carried out in milligram quantities with high pressure liquid chromatography, using an Alltech 5 μm C-18 reverse phase column on a Waters High Pressure Liquid Chromatography apparatus with a UV detector at 254 nm. Complete resolution of chlorophyll *a* was achieved using a mobile phase consisting of 6% water in methanol at a column flow rate of 4 ml/min. Care was taken to minimize exposure of the chlorophyll *a* samples to room light and to keep the samples under nitrogen.

Monogalactosyldiacylglycerols (average M_r 773) from wheat flour were purchased from Sigma Chemical Co. The predominant fatty acid of monogalactosyldiacylglycerols is linoleic acid [15].

Galactolipids in benzene and chlorophyll *a* in chloroform were thoroughly mixed in a sample vial and the solvent evaporated under a stream of nitrogen. The residual solvent was removed by drying the sample under vacuum overnight. The dried film was then hydrated by adding excess nitrogen-saturated water and vortexing at room temperature. For X-ray diffraction measurements, samples were prepared similarly and transferred to thin-walled 1 mm diameter quartz capillaries (Blake Industries, Inc.) and flame sealed under vacuum.

Wide-angle and low-angle X-ray diffraction patterns were recorded on X-ray-sensitive film as a function of temperature over the range −60°C–60°C. Diffraction measurements were carried out using monochromatic (1.5 Å) wiggler-enhanced synchrotron radiation at the Cornell High Energy Synchrotron Source as described previously [16,17]. Radiation damage was minimized by implementing the precautions outlined in an earlier publicaiton [18]. Some of the measurements were made using the newly developed time-resolved X-ray diffraction method [19,20]. The samples contained in 1 mm capillaries were placed in a brass holder and clamped in a brass block through which water from a thermostated water bath was circulated. Sample temperatures were stable to ±0.5°C from 7°C to 55°C. Lower temperatures were achieved by passing over the sample capillary a stream of dry nitrogen gas that had been cooled in a methanol/solid CO_2 bath or an FTS crystal cooling device. Sample temperature was recorded by a copper-constantan thermocouple positioned in or next to the sample capillary to within 2 mm of the X-ray beam. The sample assembly was mounted on a concentric goniometer head (Supper) attached to a Buerger precession camera (Supper) which acted as an optical bench in the alignment of collimator, sample, beam stop and film. Exposure times varied from 1 to 15 min depending on the electron current and sample concentration.

Freeze fracturing was carried out on a Balzer 360 M instrument using a 'Clamshell' type sample holder. Approximately 1.5 μl of sample was loaded into a sandwich consisting of 25 μm thick copper discs which had been cleaned by dipping in 50% nitric acid. The sample was quenched rapidly from 20°C by plunging the sandwich into liquid Freon 22. In some experiments, a 58% solution of ethylene glycol in water was used as cryoprotectant. The frozen sandwich was then mounted, fractured at −130°C and etched for 30 s using the surface of a knife at −190°C. The etched surface was shadowed with platinum from 30° to the horizontal, then coated with carbon. Replicas were freed from the copper discs by dissolving the discs in 50% nitric acid. The replicas were then washed in dimethylformamide, followed by water, then floated onto formvar coated grids for observation in a Philips 201C electron microscope at 80 kV.

TABLE I

LONG-SPACINGS FOR FULLY HYDRATED MGDG/CHL *a* AGGREGATES

Lipid	Temp. (°C)	Long-spacing (nm)
MGDG	20	(5.31 vs [a], 3.03 s, 2.66 s) [b]
	−40	3.78 vs
18 mol% chl *a* in MGDG	18	(4.97 vs, 2.90 s, 2.51 s)
	−63	4.0 vs
30 mol% chl *a* in MGDG	20	(5.19 s, 3.03 m, 2.64 w), 2.23 vw, 0.75 vw
	−40	4.16 s, 2.36 vw, 2.03 vw, 0.75 vw
46 mol% chl *a* in MGDG	20	5.13 s, 3.00 m, 2.79 vw, 2.28 m, 2.01 vw, 0.75 vw
	−40	[1.00 vs, 1.85 w, 2.07 vw, 5.61 vw] [c]
chl *a*	20	2.8 vw

[a] Relative intensities are denoted vs, very strong; s, strong; m, medium; w, weak; vw, very weak.

[b] Bracketed reflections index according to a hexagonal lattice.

[c] Because of uncertainties in sample-to-film distance absolute long-spacing determinations could not be made. The values reported correspond to radial position relative to that of the lowest angle reflection (see Fig. 3).

Results

We have carried out both static and time-resolved X-ray diffraction mesurements over the temperature range −60°C–60°C on a series of fully hydrated samples ranging from pure MGDG to pure chl*a*. The long-spacing data on representative samples are presented in Table I. In every condition examined but one (vide infra), the pure lipid and lipid/chl *a* mixtures were in the fluid or liquid-crystalline phase as evidenced by diffuse scatter in the vicinity of $(0.46\ \mathrm{nm})^{-1}$.

The diffraction patterns of fully hydrated MGDG at 20°C and −40°C are shown in Fig. 1. The low-angle region consists of a series of extremely sharp reflections indexing on a hexagonal

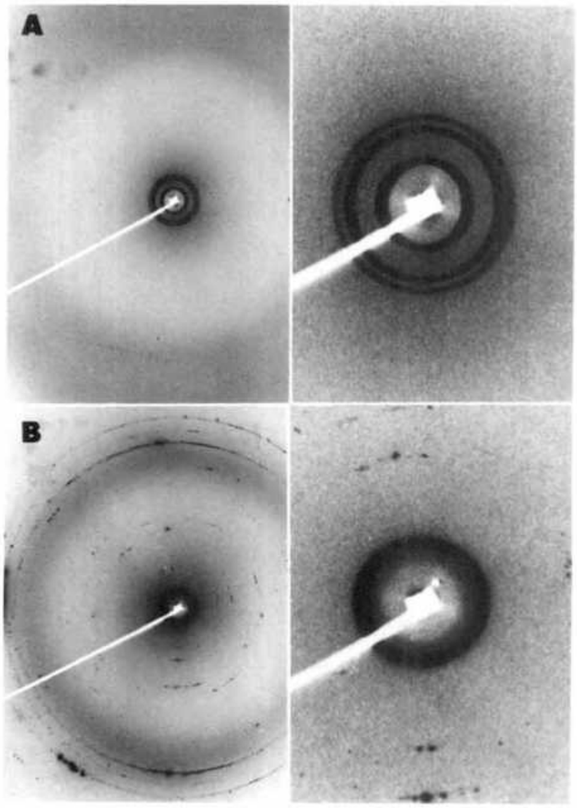

Fig. 1. X-ray diffraction patterns obtained for an aqueous dispersion of MGDG at 20°C (A), and at −40°C (B).

lattice with line spacings in the ratio $1/1 : 1/\sqrt{3} : 1/\sqrt{4}$. The hexagonal pattern persists upon cooling down to approximately −15°C in the presence of supercooled water. However, once ice crystal formation occurs the low-angle diffraction pattern changes dramatically and exhibits a single strong reflection at $(3.78\ \mathrm{nm})^{-1}$ down to −60°C. A single reflection such as this precludes lattice type and symmetry determination and thus phase identification. As the sample is heated from −60°C to −3°C, the diffraction pattern changes little, if at all. However, between −3°C and 0°C, diffraction lines corresponding to a hexagonal phase emerge and the dimensions of the hexagonal lattice increase, perhaps due to water uptake, with increasing temperature up to 0°C. Thereafter, and as is observed with other systems [20], lattice size decreases with tempeature. At 20°C, the MGDG d_{11} reflection at $(3.03\ \mathrm{nm})^{-1}$ (Table I) corresponds to a distance between cylinder axis in the hexagonal phase of 6.06 nm. This may be compared with the results of Shipley et al. [3] who observed a value of 6.05 nm at 20°C for fully hydrated MGDG prepared from *Pelargonium* leaves.

The addition of chl *a* up to 18 mol% has no observable effect on the phase properties of MGDG. The hexagonal pattern was still present and it underwent similar changes upon ice formation as was observed with MGDG alone. The lattice parameters did undergo slight changes as shown in Table I. At 30 mol% chl *a*, the diffraction pattern continues to show reflections indexing on a hexagonal lattice (Table I, Fig. 2) and, as noted with pure MGDG, the lattice dimensions have a negative temperature coefficient above 0°C. Additional reflections which do not index on a hexagonal lattice are seen in this sample (Table I)

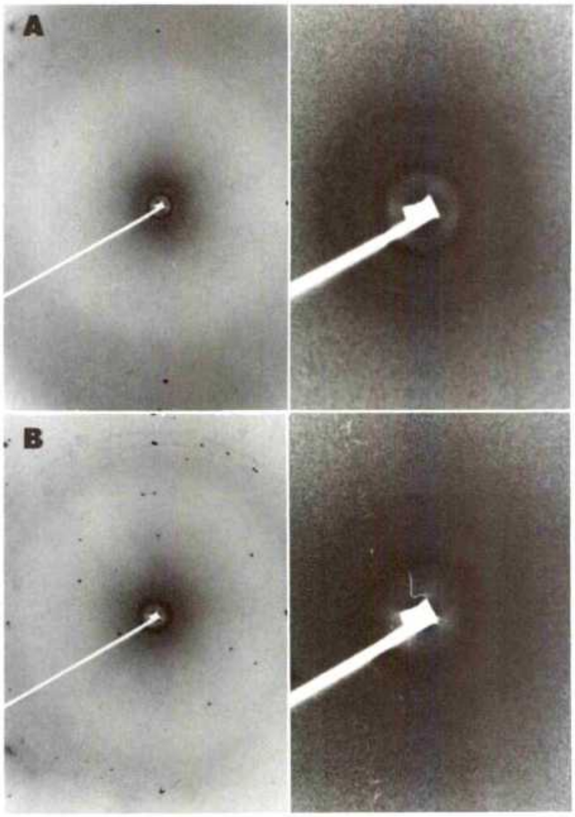

Fig. 2. X-ray diffraction patterns of a fully hydrated MGDG sample containing 30 mol% of chl *a* at 20°C (A), and at −40°C (B).

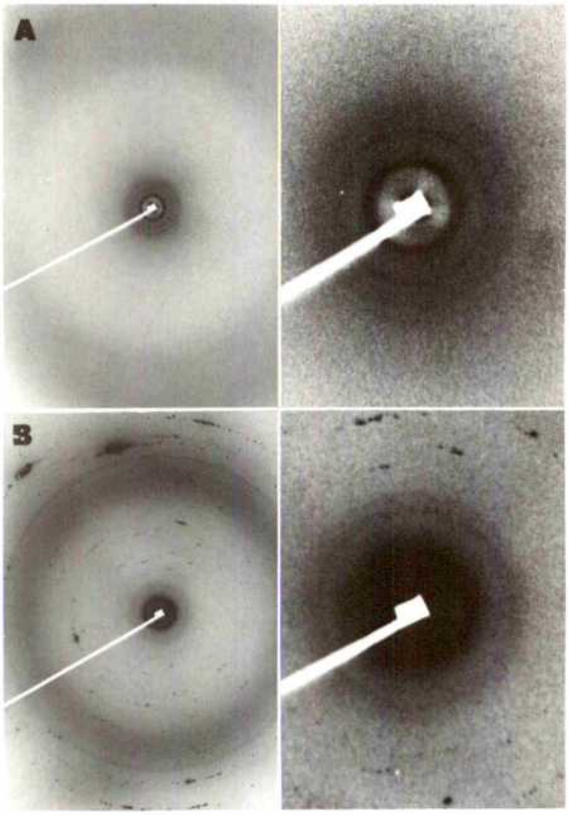

Fig. 3. X-ray diffraction patterns of a fully hydrated sample containing 46 mol% of chl *a* in MGDG at 20°C (A), and at −40°C (B).

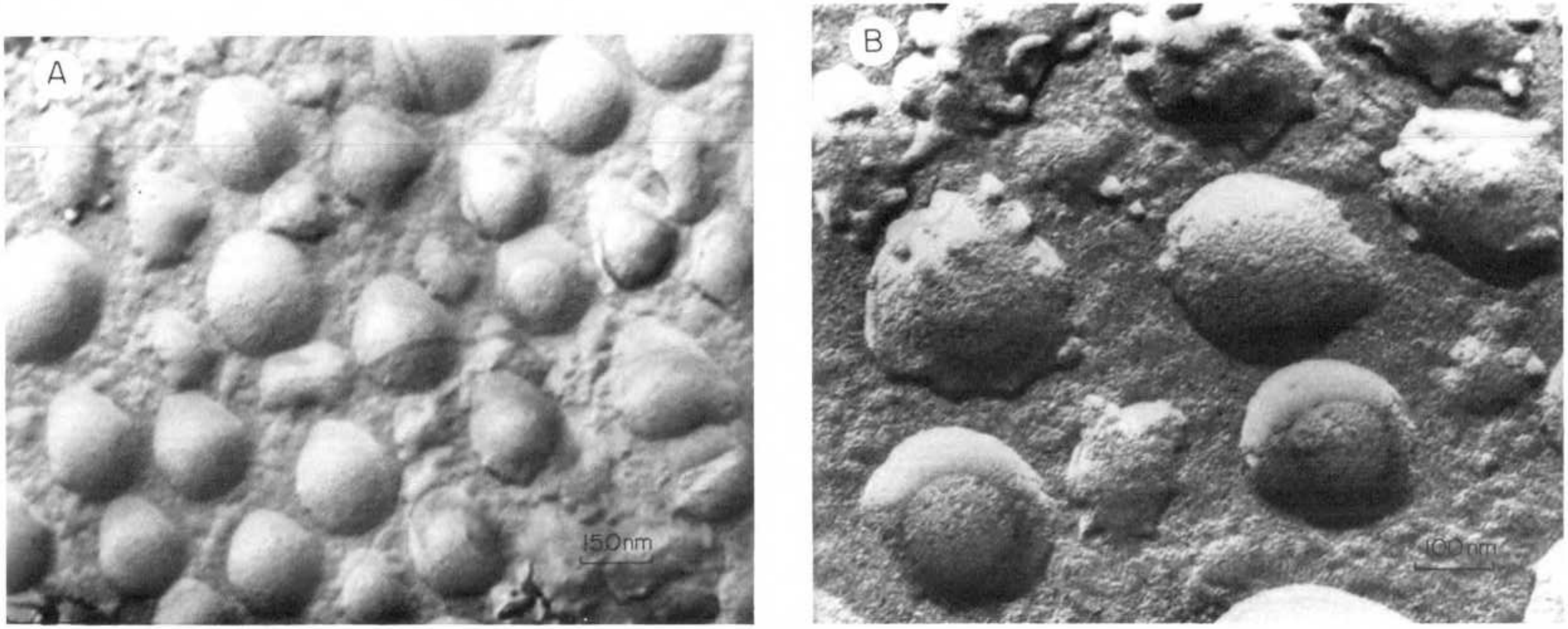

Fig. 4. Freeze-fracture electron micrograph of a fully hydrated sample containing 46 mol% of chl *a* in MGDG, with 58% ethylene glycol added as cryoprotectant. A, a representative micrograph; B, a magnified region showing the presence of blisters.

and we note also that the hexagonal lines are considerably broader than observed at the lower chl concentrations. This suggests that at 30 mol% chl *a*, the sample is probably in a mixed phase region and that the orderly hexagonal arrangement of lipid aggregates is being disrupted.

At an even higher chl *a* level of 46 mol%, indexing of the low-angle diffraction lines was not possible at any of the temperatures examined (Table I, Fig. 3). It appears that at this level, chl *a* and MGDG do not accommodate each other in either the hexagonal packing arrangement or indeed any other unique geometry recognizable by X-ray diffraction. This is the only sample in which additional sharp lines to the wide-angle side of the $(0.46\ \mathrm{nm})^{-1}$ peak were observed at −40°C. However, the phase state of the acyl chains cannot be established unequivocally under these conditions because of interference in this region by ice reflections (Fig. 3).

Diffraction patterns were also recorded on pure chl samples dispersed in water. Measurements were made at five temperatures in the range −39°C–50°C. At low angles, the diffraction patterns are featureless except for a single diffuse, ill-defined line centered at approximately $(2.81\ \mathrm{nm})^{-1}$ possibly indicating the presence of micellar aggregates. The wide-angle region shows a diffuse peak centered at $(0.43\ \mathrm{nm})^{-1}$ in the presence of ice. Above 0°C, the broad wide-angle peak due to water overlaps with that of chlorophyll and a well-defined pigment peak is no longer visible.

In the mixed MGDG/chl *a* systems containing in excess of 18 mol% chl *a*, a relatively sharp reflection at $(0.75\ \mathrm{nm})^{-1}$ was consistently observed in the diffraction patterns at all temperatures examined. The origin of this reflection is not known, and given the observations with pure chl *a*, it is unlikely to represent phase-separated chl *a*. However, it was absent in the 18 mol% chl *a* sample, the lowest concentration of chl *a* in MGDG examined in this study.

In conjunction with X-ray diffraction, freeze-fracture electron microscopy was carried out. Fig. 4A shows a characteristic region of a replica prepared from 46 mol% of chl *a* in MGDG. The dominant structure has the appearance of large (250 nm diameter) bilayer liposomes. The fracture pattern of the structures is circular, with the 'halo' that is characteristic of single bilayer vesicles which have been fractured and from which ice has then been removed from the outside surface by sublimation during etching. In addition, there appear to be blisters on or around the liposomes (Fig. 4B). The blisters may be due to areas of concentration of chl *a*. In none of the micrographs examined was there any evidence of the H-II phase normally associated with MGDG.

Discussion

Pure MGDG in the fully hydrated state adopts the H-II phase over the entire temperature range examined when water is part of the system. Ice formation drives the MGDG into an as yet unidentified phase with fluid acyl chains. Indeed, over the entire phase diagram, liquid-crystalline hydrocarbon packing prevails with only one possible exception at −40°C for the 46 mol% chl *a* where evidence for the coexistence of gel and liquid-crystalline phase was obtained.

The addition of 18 mol% chl *a* to MGDG perturbs the lipid system very little. The MGDG H-II phase accommodates this level of chl *a* with slight changes in the dimensions of the hexagonal lattice. Beyond 18 mol%, the H-II phase begins to disorder and additional phase(s), as yet unidentified, begin to emerge. 30 mol% appears to be a transition region. It is here that a well-defined, albeit somewhat disordered, reverse hexagonal phase is seen in the presence of small amounts of these other phases.

Worthy of note in this context is the result concerning the interaction of chl *a* with certain phosphatidylcholines. Several groups [21–23] have demonstrated that chlorophyll can be integrally incorporated into the bilayer, with the porphyrin headgroup in the polar region of the membrane and the nonpolar phytol chain inserted into the hydrophobic core of membrane along the fatty acyl chains. Eigenberg et al. [24,25] have obtained evidence for compound formation between chl *a* and distearoylphosphatidylcholine involving interaction of the lipid phosphate with the magnesium ion in chlorophyll. More recently, Dea and Chan [26] have mapped the phase diagram of chl *a* in a bilayer membrane of dimyristoylphosphatidylcholine and showed that chlorophyll-rich domains are formed in this lipid system. The monolayer solubility limit of chl *a* in both gel and liquid-crystalline dimyristoylphosphatidylcholine have also been reported by Heithier and Möhwald [27] to be in excess of 20 mol%. While the lipid phase and dispersion type differ considerably between these systems, a similar conclusion is drawn, namely that the two lipid systems accommodate chl *a* to the extent of at least 20 mol%.

The hydrocarbon chains of galactolipids are characterized by a high degree of unsaturation resulting in extremely low liquid-crystalline-to-gel phase transition temperatures. This may enable the phytol chain to insert easily into the hydrophobic region along the acyl chains. While some long-range order is maintained in the MGDG/chl *a* mixtures, the X-ray diffraction results showed that the order is different from that of pure MGDG when the chlorophyll mol% is 30% or greater. This is confirmed by the large liposomes observed with freeze-fracture electron microscopy and the absence of any H-II fracture patterns. Thus, when chl *a* is incorporated into MGDG, it destabilizes the orderly H-II phase structure and disturbs the long-range order of the lipid array.

The phases adopted by MGDG and chl *a* are consistent with the idea that the phase behavior of amphiphiles is strongly dependent on the relative cross-sectional area of headgroup and hydrocarbon regions of each molecule [28,29]. In this sense, chl *a* and MGDG represent opposite extremes, the former having a large headgroup (the porphyrin ring) relative to a single hydrocarbon chain, and the latter a small headgroup (a galactose residue) and two unsaturated hydrocarbon chains giving it a wedge shape. Consistent with these dimensions, chl *a* forms normal micelles [30] when hydrated whereas MGDG forms a reverse hexagonal phase.

A schematic representation of the H-II phase is shown in Fig. 5A. Upon incorporation of the chl *a* molecules, the disruption which arises from large differences in molecular shape between chl *a* and MGDG may allow the H-II cylinders to open up to form pseudobilayers, as schematically exemplified in Fig. 5B. The same may also be responsible for interrupting the long-range order of the lipid as reflected in the X-ray diffraction patterns. These models are consistent with those that have been proposed as possible intermediates in the lamellar-to-H-II phase transition [20,31] and in the process of membrane fusion such as alamethicin-mediated fusion of lecithin vesicles [32].

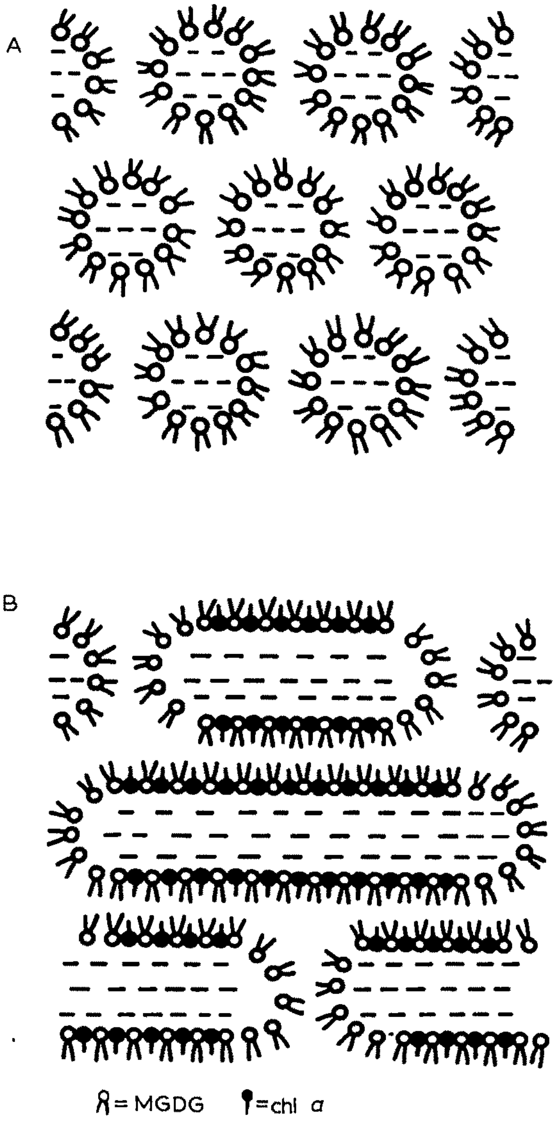

Fig. 5 Diagrammatic representation of (A) the H-II structure of pure MGDG, and (B) the structures formed upon incorporation of chl *a* into MGDG.

Acknowledgments

This research was supported in part by Grants GM-22432 (S.I.C.), GM-08117 and RR-08101 (P.D.), and IR23AM-36849 (M.C.) from the National Institute of General Medical Sciences, U.S. Public Health Service. This work was also supported in part by a Grant-in-Aid of research, Sigma Xi to M.C. Acknowledgment is made to the Donors of The Petroleum Research Fund, administered by the American Chemical Society, for partial support of this research (P.D.). We wish to thank Dr. G.W. Feigenson (Cornell University) for valuable discussion of this work and Dr. J.P. Revel and his research group (CalTech) for expert advice with the freeze-fracture electron microscopy.

References

1 Stryer, L. (1981) Biochemistry, pp. 434–435, Freeman, New York

2 Hashimoto, H. and Murakami, S (1975) Plant Cell Physiol. 16, 895–902

3 Shipley, G.G., Green, J.P. and Nichols, B.W (1973) Biochim. Biophys. Acta 311, 531–544

4 Larsson, J. and Puang-Ngern, S. (1979) in Advances in the Biochemistry and Physiology of Plant Lipids (Appelqvist, L A and Liljenberg, C., eds.), pp 27–33, Elsevier, New York

5 Sen, A., Williams, W P , Brain, A.P R., Dickens, M J and Quinn, P.J. (1981) Nature 293, 488–490

6 Sen, A , Williams, W P , Brain, A P.R. and Quinn, A J. (1982) Biochim. Biophys. Acta 685, 297–306

7 Sen, A., Brain, A.P.R., Quinn, A.J and Williams, W.P (1982) Biochim. Biophys. Acata 686, 215–224

8 Gounaris, K., Sen, A., Brain, A.P.R., Quinn, P.J and Williams, W.P. (1983) Biochim Biophys. Acta 728, 129–139

9 Boni, L.T and Hui, S.W. (1983) Biochim. Biophys. Acta 731, 177–185

10 Van Echteld, C.J.A , De Kruijff, B , Mandersloot, J.G. and DeGier, J. (1981) Biochim Biophys. Acta 649, 211–220

11 Rilfors, L., Lindblom, G , Wieslander, A. and Christianson, A. (1984) Biomembranes 12, 205–245

12 Iriyama, K., Ogura, N. and Takamiya, A. (1974) J. Biochem. 76, 901–904

13 Strain, H.H., Thomas, M.R., Crespi, H.L , Blake, M.I. and Katz, J.J (1960) Ann N.Y. Acad. Sci 84, 617–666

14 Strain, H.H., Thomas, M.R. and Katz, J.J. (1963) Biochim Biophys Acta 75, 306–311

15 Carter, H.E., Ohno, K., Nojima, S., Tipton, C.L. and Stanacev, N.Z. (1961) J Lipid Res. 2, 215–222

16 Caffrey, M. and Bilderback, D.H (1984) Biophys. J. 45, 627–631

17 Caffrey, M. and Feigenson, G.W (1984) Biochemistry 23, 323–331

18 Caffrey, M. (1984) Nucl Instrum. Methods Phys. Res 222, 329–338

19 Caffrey, M. and Bilderback, D.H. (1983) Nucl. Instrum Methods Phys. Res. 208, 495–510

20 Caffrey, M (1985) Biochemistry 24, 4826–4844

21 Lee, A G (1975) Biochemistry 14, 4397–4402

22 Oettmeier, W., Norris, J.R. and Katz, J.J. (1976) Biochem Biophys Res. Commun. 71, 445–451

23 Podo, F , Cain, J.E. and Blasie, J.K. (1976) Biochim. Biophys. Acta 419, 19–41

24 Eigenberg, K.E., Croasmun, W.R. and Chan, S.I. (1982) Biochim. Biophys Acta 679, 353–360

25 Eigenberg, K.E., Croasmun, W.R. and Chan, S I. (1982) Biochim Biophys Act 679, 361–368

26 Dea, P and Chan, S.I (1986) Biochim. Biophys Acta 854, 1–8

27 Heithier, H. and Möhwald, H (1983) Z. Naturforsch. 38c, 1003–1010

28 Israelachvilli, J.N , Mitchell, D.J and Ninham, B W. (1977) Biochim. Biophys Acta 470, 185–201

29 Mitchell, D.J. and Ninham, B.W. (1981) J. Chem. Soc. Faraday Trans. II 77, 601–629

30 Flaumenhaft, E. and Katz, J.J. (1973) J. Inorg Nucl Chem. 35, 1719–1725

31 Siegel, D.P. (1984) Biophys J. 45, 399–420

32 Lau, A.L.Y. and Chan, S I (1975) Proc. Natl. Acad. Sci. USA 72, 2170–2174

Biochimica et Biophysica Acta 896 (1987) 19–25
Elsevier

BBA 73182

Changes in myoblast membrane order during differentiation as measured by EPR

Maria T. Santini [a,b], Pietro L. Indovina [a] and Robert E. Hausman [b]

[a] *Laboratorio di Fisica, Istituto Superiore di Sanità, Viale Regina Elena 299, 00161 Rome (Italy)*
and [b] *Biological Science Center, Boston University, 2 Cummington St., Boston, MA 02215 (U.S.A.)*

(Received 11 June 1986)
(Revised manuscript received 9 September 1986)

Key words: ESR; Membrane order, Myogenesis, Cell-cell recognition; Membrane fusion; Differentiation; (Chicken myoblast)

The events which make possible the characteristic fusion of the cell membranes of embryonic myoblasts are known to involve modification of the cell membrane (Hausman, R.E., Dobi, E.T., Woodford, E.J., Petrides, S., Ernst, M. and Nichols E.B. (1986) Dev. Biol. 113, 40–48). Myoblasts from chick embryos were allowed to differentiate in gyrotory aggregate culture and the order of their membranes was measured by EPR. Two spin-labels which insert at different depths into the lipid bilayer were used. Measurement with the 5-nitroxystearate label showed an increase in myoblast membrane order ($2T_{\parallel}'$) from 0–15 h of culture and again from 26–38 h of culture. Measurement with the 12-nitroxystearate label showed the 0–15 h increase in order but the second increase was greatly reduced and shifted in time. While the specific sources of these changes in membrane order cannot yet be identified, the changes observed correlated well with known events of myogenic differentiation in vitro. The initial increase in membrane order occurred while the myoblasts were recovering from the effects of trypsin dissociation and undergoing gyrotory aggregation. The second increase in membrane order occurred during the known period of prostaglandin receptor activity and increased cell-cell adhesion.

Introduction

The differentiation of embryonic myoblasts in vitro has been a useful system for the study of development. Two processes, the elaboration of specific cytoskeletal proteins which form the contractile apparatus of mature muscle [1–4] and fusion of myoblast membranes [5–10], while not fully understood, have been extensively investigated.

Myoblast fusion in vitro creates the myotube necessary for full elaboration of the characteristic proteins [11]. However, it is clear that many of the molecules specific for myogenic differentiation appear before membrane fusion [12–14]. This has led to increased interest in those aspects of myogenic differentiation which precede fusion of the myoblast cell membranes [12,15–20].

Several of these early differentiation events during myogenesis in vitro are localized at the cell surface and may play a role in the cell-cell communication necessary to coordinate both fusion and the synchronous development of contractile proteins [21]. Electron paramagnetic resonance (EPR) study of membrane bilayers with spin-labels provides a very sensitive means of detecting events at the cell membrane [22]. It has been used to detect changes in membrane fluidity during pas-

---

Correspondence: Dr. R E. Hausman, Biological Science Center, Boston University, 2 Cummington St, Boston, MA 02215, U.S.A.

0005-2736/87/$03.50 © 1987 Elsevier Science Publishers B.V. (Biomedical Division)

sage of Chinese hamster ovary cells through the cell cycle [23], and to establish correlations between membrane fluidity and thermosensitivity of mammalian cells [24].

While changes in the membrane fluidity or order of some differentiating cells have been reported [25,26], EPR has not (to our knowledge) been used to investigate changes in membrane order during embryonic myogenesis. We demonstrate here dynamic changes in the membrane order of embryonic chick myoblasts. We discuss the correlation of these changes with the processes of gyrotory aggregation of the cells, binding of secreted prostaglandin by cell membrane receptors and a consequent change in myoblast adhesion. Finally, we confirm with one EPR spin-label the known increase in membrane fluidity which precedes membrane fusion.

Materials and Methods

Materials

Trypsin was obtained from Difco, soybean trypsin inhibitor and DNAase from Sigma, Dulbecco's modified Eagle's medium and penicillin/streptomycin from Gibco Europe, fetal bovine serum from Flow and potassium ferricyanide [$K_3Fe(CN)_6$] from Merck. The spin-labels, 5-nitroxystearate (2-(3-carboxypropyl)-4,4-dimethyl-2-tridecyl-3-oxazolidinyloxyl) and 12-nitroxystearate (2-(10-carboxydecyl)-2-hexyl-4,4-dimethyl-3-oxazolidinyloxyl) were purchased from Aldrich. All other chemicals were obtained from Farmitalia Carlo Erba.

Myoblast cell cultures

Primary cultures were prepared from pectoral muscles of 11-day embryonic chicks by a modification of standard procedures [21]. After washing in calcium and magnesium-free Tyrode's solution, minced tissue was incubated in 0.25% trypsin in the same salt solution for 20 min at 37°C. The cells were washed twice by centrifugation with 50 mg/ml of soybean trypsin inhibitor and twice with 2 mg/ml DNAase, both in calcium and magnesium-free Tyrode's solution. Cells were resuspended in Dubecco's modified Eagle's medium supplemented with 5% fetal bovine serum, 5000 units/ml penicillin and 5 mg/ml streptomycin to a total volume of 10 ml. Loose aggregates of cells were broken up by fire-polished Pasteur pipet, the cells counted by hemocytometer and diluted in the same medium to a final concentration of $5 \cdot 10^6$ cell/ml. This suspension of single cells was then pipeted into sterile 50 ml Erlenmeyer flasks (6 ml per flask), gassed with a mixture of 5% CO_2/95% air and the flasks were plugged. Flasks were gyrotory rotated (100 rpm, 37°C). Under these conditions only the myoblasts aggregate, the fibroblasts adhere to the flask [21]. The suspended myoblast aggregates were collected for measurement.

Microscopy

Suspensions of myoblast cells or aggregates were pipeted onto glass slides, examined and photographed with a Zeiss Ultrophot microscope. Magnifications are specified in the figure legends.

EPR measurements

Myoblasts ($40 \cdot 10^6$) were collected, centrifuged, washed three times and resuspended in phosphate-buffered saline (0.5 ml). Thorough washing was necessary to eliminate the paramagnetic signal from fetal bovine serum. The supernatant from the third phosphate-buffered saline wash was tested and gave no signal. For both 5-nitroxystearate and 12-nitroxystearate, a $3.25 \cdot 10^{-2}$ M stock solution was made in 100% ethanol and stored at -20°C until needed. 1 μl of either stock solution was added to the cell suspension, and the suspension was vortexed and rotation-incubated for 15 min at 37°C. 20 μl of a 1 M $K_3Fe(CN_6)$ solution (0.04 M) in phosphate-buffered saline was added, and the suspension was vortexed and added to capillary tubes. EPR measurement was on a temperature-controlled Varian E-4 X-band Spectrophotometer. It was operated at a microwave frequency of 9.12 GHz, at a power of 10 mW with a field modulation of 100 kHz. Temperature was monitored by digital thermometer with its thermocouple inserted into the capillary tube holder where silicon oil was added to maintain even temperature distribution. Temperature was maintained to within ±0.5 Cdeg. The data obtained were analyzed as detailed below.

Results

Spin-labels

Both spin-labels are thought to orient themselves inside the cell membrane noncovalantly (intercalate) with their longitudinal molecular axis perpendicular to the membrane surface. For 5-nitroxystearate, the location of the oxazolidine ring at position 5 of the hydrocarbon chain of the stearic acid allows the polar position of the hydrophobic tail of the lipid bilayer to be sampled. The ring motion is, therefore, related to the rotation of the adjacent segment of the molecule [27]. The structure of the spectrum obtained from myoblasts labeled with 5-nitroxystearate did not change significantly over the 48 h of experimentation; a typical spectrum is shown in Fig. 1. 12-Nitroxystearate is thought to insert deeper into the lipid bilayer [22,28,29]. Its spectra consist of at least two components [30]; a typical spectrum is shown in Fig. 2. As with 5-nitroxystearate, the structure of the 12-nitroxystearate spectra did not change significantly over the period studied. For both spin-labels, the distance between the outer hyperfine splitting ($2T_{\parallel}'$) was measured directly from the spectra and used as an indicator of membrane order. For a complete theoretical treatment of the use of spin-labels in membranes see Ref 28. We measured the $2T_{\parallel}'$ with the smallest hyperfine splitting because this distance could be more precisely measured at all time points. The signal due to the second component ($2T_{\parallel}'$ with the larger hyperfine splitting) was very small and could not be easily measured as it was sometimes masked by noise.

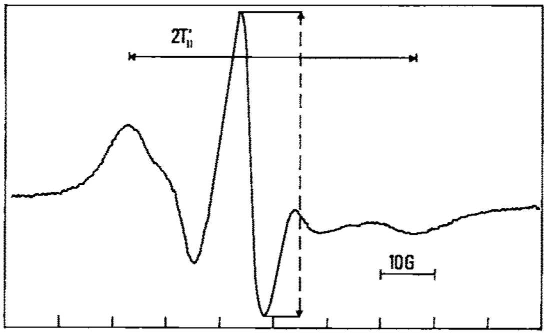

Fig. 1. Representative EPR spectrum obtained from embryonic chick myoblasts in rotation culture after labeling with 5-nitroxystearate The external ($2T_{\parallel}'$) hyperfine resonance extrema of the *T*-tensor is indicated. The dotted line shows the mid-field line height The marked scale indicates 10 G intervals

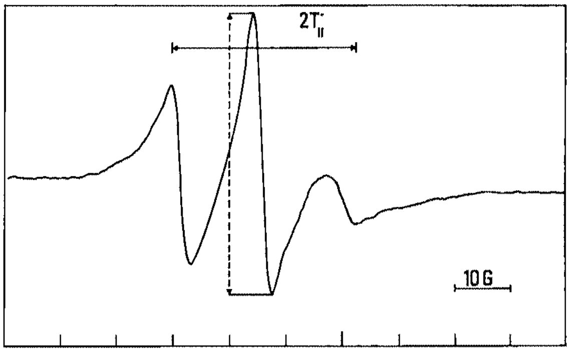

Fig. 2. Representative EPR spectrum obtained from embryonic chick myoblasts in rotation culture after labelling with 12-nitroxystearate Parameters are marked as in Fig 1

The 5-nitroxystearate resonance signal obtained at each time point from the myoblasts in the presence of potassium ferricyanide remained quite stable. Measurements of the mid-field line height (Fig. 1) at intervals after introduction of the spin-label showed no decay of the signal. This observation justified the addition of potassium ferricyanide to the samples. Not only did this substance quench any free spin-labile, but (since it does not enter cells) it continuously oxidized the fatty acid spin-label which was being reduced at the cell surface [27]. The increase in signal stability thus obtained demonstrated that the spin-label was not being internalized by the cells, otherwise the ferricyanide would not be active. Thus, it is reasonably certain the the 5-nitroxystearate spin-label was probing the outer surface of the myoblast plasma membrane. In contrast, the measurements of mid-field line height from 12-nitroxystearate spectra (Fig. 2) showed a 30% decay in 1 h which was not inhibited by ferricyanide. While this decay was slow enough to allow use of the spin-label, the lack of ferricyanide protection suggested that the membrane was being probed at a deeper level.

The parameters which contribute to EPR spectra of cell membranes are not fully understood but include fluidity of phospholipids in the bilayer, local changes in charge across the membrane and molecular ordering [22]. While we have referred to changes in $2T'_{\parallel}$ as changes in membrane order, $2T'_{\parallel}$ should be understood as an empirical measure of molecular motion in the immediate vicinity of the spin-label probe.

Kinetics of gyrotory aggregation

Single myoblasts (Fig. 3) rapidly formed large (> 100 cell) aggregates during the first 15 h of gyrotory rotation (Fig. 4). In aggregates from later stages (> 44 h), areas of smooth outer edge could be observed. These indicate the close membrane apposition and subsequent fusion characteristic of myoblasts [21].

Changes in membrane order

Investigation of membrane order over the first 48 h of differentiation in vitro with 5-nitroxystearate spin-label yielded the results shown in Fig. 5. The membrane order increased almost 8% for the first 15 h, while the single cells were undergoing gyrotory aggregation. The membrane order then decreased until 26–28 h of culture. At this time, important in myoblast membrane interactions [21], the order again began to increase with a point of maximum order reached at 38 h. The order then decreased until the end of the 48-h study.

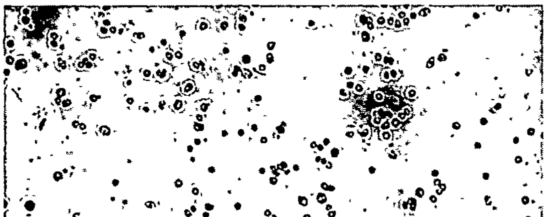

Fig. 3 Light micrograph of a suspension of 11-day embryonic chick muscle cells after 10 min of gyrotory rotation culture. Bar = 100 μm

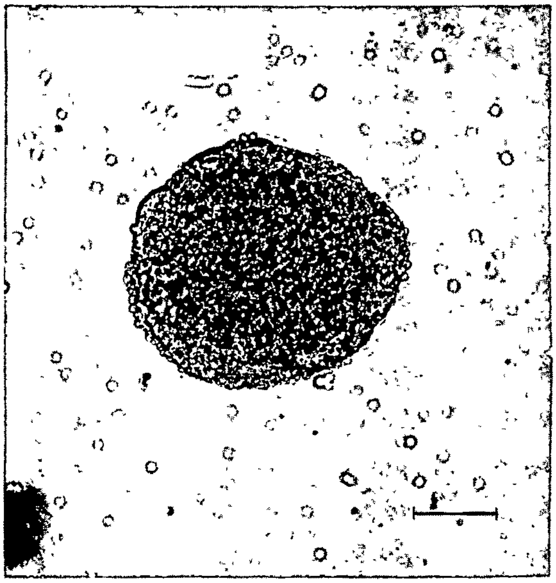

Fig. 4. Light micrograph of an aggregate of 11-day embryonic chick myoblasts and remaining single cells after 24 h of gyrotory rotation culture The cells remaining single are virtually depleted of myoblasts. Bar = 100 μm.

Probing deeper into the membrane bilayer with 12-nitroxystearate spin-label yielded a different picture (Fig. 6). The increase in membrane order associated with the period of gyrotory cell aggregation remained but that associated with subse-

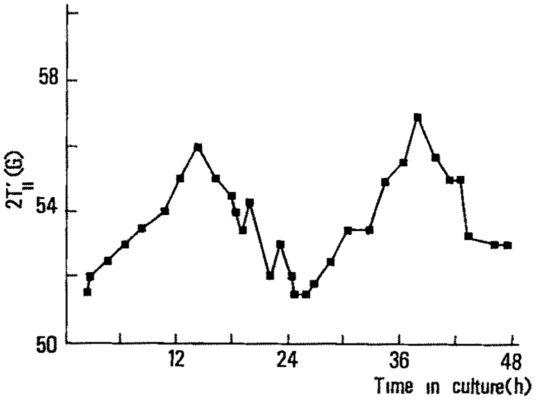

Fig. 5. Myoblast membrane order as represented by $2T'_{\parallel}$ using the 5-nitroxystearate spin-label plotted as a function of time in culture. The plot represents measurements from five separate experiments with overlapping time points At each data point, the average value is shown. For each experiment, five measurements of $2T'_{\parallel}$ were taken per time-point The curve was obtained by connecting the experimental points.

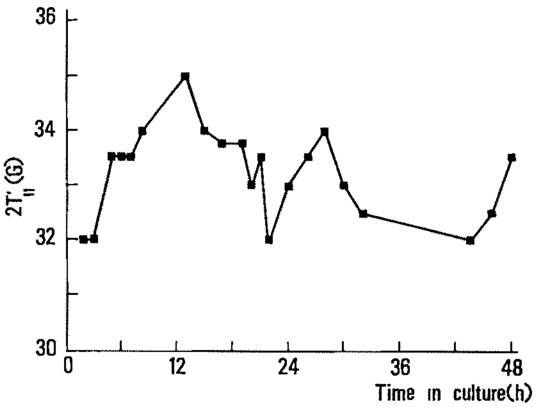

Fig 6. Myoblast membrane order as represented by $2T'_{\parallel}$ using the 12-nitroxystearate spin-label plotted as a function of time in culture. The plot was obtained as described in Fig 5.

quent myoblast membrane interactions was greatly reduced and shifted in time.

Discussion

The magnitude of the changes in $2T'_{\parallel}$ seen in this study are greater than those observed in most other complex cellular systems [23,24,26]. This is particularly significant since the changes in EPR spectra observed here are the result of gyrotory-mediated cell aggregation and myogenic differentiation in vitro, not the result of any direct experimental modification of the cell membrane. As noted earlier, the spectra of 12-nitroxystearate appears to consist of at least two spectral components. These may be due to lipid–protein interactions [30] or arise from a characteristic distribution of the spin-label between plasma and intracellular membranes. The similar changes in membrane order seen over the first 15 h of culture with the 5-nitroxystearate and 12-nitroxystearate spin-labels and their known degrees of insertion into the lipid bilayer [22,28,29] give us confidence that the value of $2T'_{\parallel}$ with the smallest hyperfine splitting of the deeper-inerting spin-label is not due to insertion of the label primarily into intracellular membranes. Thus, we are observing molecular order changes in the myoblast plasma membrane. This conclusion is further supported by the ability (reported here) of ferricyanide to enhance the 5-nitroxystearate signal and by work currently in progress.

Most investigations of the structure of embryonic myoblast cell membranes have focused on membrane fusion. This occurs between the membranes of closely apposed myoblasts beginning at 40 h in our culture system and continuing through 60 h [21]. Thus, the period of culture from 38–48 h is that immediately preceding membrane fusion for most myoblasts in the aggregates. Prives and Shinitzky [6] and Herman and Fernandez [7], using fluorescence spectroscopy, have both reported an increase in membrane fluidity during the period immediately preceding myoblast fusion. Our results with the 5-nitroxystearate spin-label, showing a decrease of four Gauss in $2T'_{\parallel}$ from 38–48 h of culture confirm their findings. However, our results with the deeper-inserting spin-label show no decrease in membrane order over this period of differentiation.

Our primary interest is in the earlier events of myogenic differentiation, specifically those which occur at the myoblast cell surface. There are three discrete events which occur over the period of differentiation investigated here. They are gyrotory aggregation, binding of prostaglandin to a cell membrane receptor, and the change in cell-cell adhesion called recognition [21]. The latter two events are necessary for subsequent fusion and differentiation [31]. Throughout this period of culture, the myoblast aggregates also synthesize and secrete prostaglandins [21] which are known to affect membrane fluidity [22].

The initial increase in membrane order from 0 to 15 h of culture seen with both spin-labels correlates with two events unique to aggregate culture: recovery of the cell membranes from the effects of trypsin [32] and gyrotory aggregation of the myoblasts [21]. Because fibroblasts are gradually being selected out of the cell suspension [21], the composition of the EPR sample is also changing. The similar observation with both labels suggests that this change in membrane order occurs at both the outer surface and in the interior of the lipid bilayer, and perhaps is associated with the events of gyrotory aggregation and replacement of cell surface proteins.

The subsequent increase in membranes order (from 28 to 38 h of culture) appears to be associated with the surface of the lipid bilayer. It is seen only with the 5-nitroxystearate spin-label. This change in order occurs at the time when prostaglandin begins to bind to a specific membrane receptor on the myoblast membrane [21]. This causes a dramatic change in cell-cell adhesion [31] resulting in the close apposition of myoblast membranes which is so difficult to distinguish from actual membrane fusion [10,21].

Membrane order (as measured by $2T_{\parallel}'$) can be influenced by several processes simultaneously. These may contribute to the final spectra to differing extents. Furthermore, spin-label spectra obtained from fatty acid probes are sensitive to pH. Thus, the spectral changes observed may reflect contributions from local changes in membrane charge. These charge differences would themselves be significant in that they might directly affect cell-cell interactions. We have suggested some processes which are likely to contribute to the 0–15-h and 28–38-h increases in membrane order seen in this study. We cannot yet attribute these changes in order to specific processes such as gyrotory aggregation, especially since the myoblast membrane is unlikely to be homogeneous and different regions may contribute different signals [30]. However, the differences observed in membrane order between the two spin-labels from 28 to 38 h suggest that the factors affecting membrane order during this period of myoblast differentiation are different from those which contribute to the 0–15-h increase in order.

The finding by EPR of a change in myoblast membrane order which is associated with prostaglandin receptor activation and myoblast recognition and adhesion raises the possibility of understanding the biophysics of these myoblast membrane differentiation events. Toward this end, we are currently investigating the changes in membrane order after manipulation by probes for prostaglandin receptors and by inhibitors of prostaglandin metabolism.

Acknowledgments

We thank Mr. Giacomo Monteleone for expert photography and Dr. Barbara Caccia for mathematical assistance. This work was partially supported by Basic Research Grant 1-859 from the March of Dimes Birth Defects Foundation.

References

1 Buckingham, M E. (1977) Int. Rev. Biochem. 15, 269–332
2 Merlie, J.D., Buckingham, M.E and Whalen, R.G. (1977) Curr. Top. Dev. Biol. 11, 61–114
3 Nadal-Ginard, B (1978) Cell 15, 855–864
4 Pun, E.C., Caravatti, M , Periard, J.-C , Turner, D.C and Eppenberger, H M. (1980) Proc Natl. Acad. Sci. USA 77, 5297–5301
5 Curtis, D.H and Zalin, R.J. (1981) Dev. Biol 113, 40–48
6 Prives, J. and Shinitzky, M (1977) Nature 268, 761–763
7 Herman, B.A. and Fernandez, S.M (1978) J. Cell Physiol. 94, 253–264
8 Weidekamm, E., Schudt, G. and Brdiczka, D. (1976) Biochim Biophys. Acta 443, 169–180
9 Lipton, H.B. and Konigsberg, L R. (1972) J. Cell Biol. 53, 348–364
10 Shimada, Y. (1971) J. Cell Biol. 48, 128–142
11 Yaffe, D. (1971) Exp. Cell Res. 66, 33–48
12 Trotter, J.A and Nameroff, M. (1976) Dev. Biol. 49, 548–555
13 Vertel, B.M. and Fischman, D A. (1976) Dev. Biol. 48, 438–446
14 Konieczny, S.F., McKay, J. and Coleman, J.R. (1982) Dev. Biol. 91, 11–26
15 Furcht, L.T., Wendeschafer-Crabb, G. and Woodbridge, P.A. (1977) J. Supramol Struct. 7, 307–332
16 Friedlander, M. and Fischman, D.A (1979) J Cell Biol. 81, 193–214
17 David, J D , See, W.M. and Higginbotham, C.-A (1981) Dev. Biol. 82, 297–307
18 David, J.D. and Higginbotham, C.-A. (1981) Dev. Biol. 82, 308–316
19 Grove, B.K., Schwartz, G. and Stockdale, F E. (1981) J. Cell Biochem. 17, 147–152
20 Cates, G.A., Brickenden, A.M. and Sanwal, B.D (1984) J. Biol. Chem. 259, 2646–2650
21 Hausman, R.E., Dobi, E.T., Woodford, E J., Petrides, S., Ernst, M. and Nichols, E.B. (1986) Dev. Biol. 113, 40–48
22 Dodd, N.J.F. (1984) in Magnetic Resonance in Medicine and Biology (Foster, M.A., ed.), pp. 66–91, Pergamon, Oxford
23 Lai, C S., Hopwood, L.E. and Swartz, H.M (1980) Biochim. Biophys Acta 602, 117–126
24 Konings, A W.T. and Ruifrok, A.C.C. (1985) Rad. Res. 102, 86–98
25 Kawai, S. and Tanaka, K.L (1978) Cell Struct. Funct. 3, 31–37
26 Weeks, G. and Hernng, F.G. (1980) J. Lipid Res 21, 681–686
27 Kaplan, J., Canonico, P.G. and Caspary, W J. (1973) Proc Natl. Acad. Sci. USA 70, 66–70
28 McConnell, H M. and McFarland, B G. (1970) Q. Rev. Biophys 3, 91–136
29 Butterfield, D.A., Roses, A.D., Cooper, M.L., Appel, S.H. and Chestnut, D.B. (1974) Biochemistry 13, 5078–5082

30 Marsh, D. (1985) in Progress in Protein-Lipid Interactions (Watts, A. and De Pont, J.J H.H.M , eds), pp. 143–172, Elsevier, Amsterdam
31 Hausman, R.E. and Berggrun, D.A. (1986) Exp. Cell Res., in the press
32 Hausman, R E and Moscona, A.A. (1979) Exp. Cell Res. 119, 191–204

Biochimica et Biophysica Acta 896 (1987) 26–34
Elsevier

BBA 73200

Membrane lipid changes in erythrocytes, liver and kidney in acute and chronic experimental liver disease in rats

Sumio Kawata *, Aram Chitranukroh, James S. Owen and Neil McIntyre

Academic Department of Medicine, Royal Free Hospital School of Medicine (University of London), London (U.K.)

(Received 11 September 1986)

Key words: Membrane lipid, Liver disease; Cholesterol; Arachidonate; Brush-border membrane; (Rat)

Lipid molecules in lipoprotein surfaces exchange with their counterparts in cell plasma membranes. In human or experimental liver disease, plasma lipoprotein surfaces are enriched in cholesterol and deficient in arachidonate; corresponding alterations occur in membrane lipids of erythrocytes. To determine whether similar changes take place in membranes of nucleated cells, the lipid content of plasma and of erythrocyte, liver and kidney membranes was measured in rats with acute (3-day) galactosamine-induced hepatitis or chronic (3-week) biliary obstruction. In both models of liver injury the cholesterol:phospholipid ratio in plasma and in erythrocytes was significantly increased ($P < 0.001$). Although this ratio was also elevated in liver and kidney microsomes, only in liver microsomes of obstructed rats was the increase significant ($P < 0.001$). However, the cholesterol:phospholipid ratio of kidney brush-border membranes, was significantly higher in bile-duct-ligated rats; presumably, compensating mechanisms limit cholesterol accumulation in intracellular membranes. Kidney brush-border membranes from obstructed rats were deficient in arachidonate as were plasma and erythrocytes. However, arachidonate levels were unchanged in kidney microsomes; renal Δ^6-desaturase, the rate-limiting enzyme in the conversion of linoleic acid to arachidonic acid, was increased by 50% ($P < 0.001$) and may have counteracted a reduced supply of exogenous lipoprotein arachidonate. We conclude that in experimental liver disease lipoprotein-induced lipid abnormalities can occur in renal membranes, although compensatory mechanisms may operate; the alterations seen, cholesterol accumulation and arachidonate depletion, would be expected to interfere with sodium transport and prostaglandin production, respectively. Our findings support the hypothesis that lipid abnormalities in kidney membranes contribute to the renal dysfunction which is a frequent complication of human liver disease.

Introduction

In both human and experimental liver disease, characteristic changes occur in the lipid composition of the surface coat of plasma lipoproteins. These include a reduction of arachidonyl fatty acyl chains in the phospholipids and, as a consequence of diminished hepatic synthesis and/or secretion of lecithin–cholesterol acyltransferase (EC 2.3.1.43), an accumulation of cholesterol and phosphatidylcholine molecules [1]. Cholesterol and phospholipid molecules in lipoprotein surfaces tend to exchange and equilibrate with their counterparts in cell plasma membranes [2,3] and it is not surprising, therefore, that in liver disease,

---

* Permanent address: The Second Department of Internal Medicine, Osaka University Medical School, Fukushima-ku, Osaka, Japan 553.

Correspondence: Dr. J.S. Owen, Academic Department of Medicine, Royal Free Hospital School of Medicine, Rowland Hill Street, London, NW3 2PF, U.K.

0005-2736/87/$03.50 © 1987 Elsevier Science Publishers B.V (Biomedical Division)

platelets [4,5] and erythrocyte membranes [6–9] show lipid abnormalities similar to those of the plasma lipoproteins.

The erythrocyte and platelet lipid abnormalities seen in jaundiced patients appear to correlate with changes in cellular and cell membrane functions. Cholesterol enrichment of the erythrocyte membrane decreases its fluidity [9] and there is an associated impairment of Na^+ transport [8,10] and inhibition of anion exchange via the band 3 transmembrane protein [11]. Platelets from patients with liver disease aggregate less readily [4], apparently because there is insufficient arachidonic acid in platelet membrane phospholipids to convert to prostaglandins and thromboxane A_2 [4,12]. It seems likely, though experimentally unproven, that such membrane lipid abnormalities occur in tissues and organs and that membrane dysfunction will be widespread in liver disease.

Patients with severe liver disease develop several renal functional abnormalities, and may retain Na^+ and water [13–17]. No obvious histological changes are seen in the kidneys and the cause of the renal dysfunction is uncertain, since many of the proposed mechanisms may be secondary rather than primary events in their genesis [13–15]. One possibility is that renal membrane lipid abnormalities play an important role; accumulation of cholesterol may directly interfere with Na^+ transport, whilst reduced arachidonic acid levels may limit production of renal prostaglandins, including the vasodilator prostaglandin E_2 which helps to regulate renal vascular resistance, affects renal Na^+ and water excretion, and interacts with the renin-angiotensin system [16,17]. As a preliminary step in testing the hypothesis that membrane lipid changes contribute to renal dysfunction in liver disease, we have measured the cholesterol content and phospholipid fatty acid composition in kidney microsomes and brush-border membranes in rats with either acute galactosamine-induced hepatitis or chronic biliary obstruction.

Materials and Methods

Experimental animals

Male Sprague-Dawley rats initially weighing 180–200 g were used; they were fed on commercial rat chow. Two models of liver injury were employed.

(i) Galactosamine hepatitis. Rats were given intraperitoneal D-galactosamine hydrochloride (1 g/kg body weight) dissolved in saline on the 1st and 3rd days. Control rats were given saline alone and all were killed on the 4th day.

(ii) Bile duct ligation. Double ligation of the common bile duct, with section between the two ligatures, was performed under diethyl ether anaesthesia. Other rats were subjected to sham-operations and both groups were studied 3 weeks after the operations.

Preparation of microsomes from liver and kidney and of brush-border membranes from kidney cortex

Rats were killed by diethyl ether inhalation and their liver and kidneys were perfused in situ with 100 ml of ice-cold 10 mM Tris-HCl buffer (pH 7.5)/0.25 M sucrose. Microsomes were obtained from a cell-free homogenate by centrifugation at 105 000 × *g* for 1 h at 4°C as described previously [18]. The microsomal pellet obtained was suspended in buffer and washed once by re-centrifugation. One portion was used immediated for lipid analysis, while another was stored at −75°C for assay of Δ^6-desaturase activity.

For preparation of the brush-border membrane the kidneys were placed on ice and the medulla removed by dissection. The remaining cortex was homogenized in 50 mM mannitol and, following addition of 0.4 ml of 1 M $CaCl_2$, the final volume was adjusted to 40 ml. The suspension was gently mixed for 20 min and centrifuged at 3000 × *g* for 10 min at 4°C. The supernatant was removed and recentrifuged at 18 000 × *g* for 10 min to pellet the brush-border membrane [19]. Protein concentrations were determined with the Folin-Ciocalteau reagent [20] using bovine serum albumin as standard.

Lipid analyses

Lipids were extracted from plasma by the procedure of Folch et al. [21], from washed erythrocytes with isopropanol and chloroform [22] and from microsomes and brush-border membranes by the method of Bligh and Dyer [23]. Plasma free and total cholesterol concentrations were measured by gas-liquid chromatography as described previously [24] and membrane cholesterol and plasma triacylglycerols using commercial enzymatic kits (Boehringer Corporation Ltd., Lewes, East Sussex, U.K.). Lipid phosphorus was measured as inorganic phosphorus following digestion with H_2SO_4 at 180 ° C [25]. The phospholipid fatty acid composition of microsomes and brush-border membranes was determined by gas-liquid chromatography following separation of total phospholipids from neutral lipids on silica-gel G (Merck) thin-layer chromatograms with hexane/diethyl ether/acetic acid, 90 : 20 : 1 (v/v) as solvent. The phospholipid fraction was transmethylated by heating at 90 ° C for 1 h under N_2 in 14% (w/v) BF_3 in MeOH. The fatty acid methyl esters were extracted into hexane and separated at 185 ° C on a 150 cm column of 10% EGSS-X on Gas-Chrom P, 100/120 mesh; detection was by flame ionization.

Enzyme assays

Plasma lecithin–cholesterol acyltransferase activity was assayed using endogenous lipoproteins pre-labelled with [^{14}C]cholesterol as substrate [26]. The incubation time (30 min) was within the linear period and, following separation of cholesterol and cholesteryl ester by thin-layer chromatography as described previously [27], the percentage of cholesterol esterified per h was determined.

In man, arachidonic acid (20:4($n-6$) is derived almost entirely from dietary linoleic acid (18:2($n-6$) by desaturation and chain elongation [28]. The rate-limiting step is the initial conversion of linoleic acid to γ-linolenic acid (18:3($n-6$) by a Δ^6-desaturase. This enzyme was assayed in liver and kidney microsomes by incubating microsomal protein (0.2–1.0 mg) with 50 nmol NADH, 50 μmol potassium phosphate buffer (pH 7.4) and 50 nmol [^{14}C]linoleoyl-CoA (0.1 μCi) in a final volume of 0.6 ml for either 10 min (liver) or 60 min (kidney) at 37 ° C. Reactions were stopped by addition of $CHCl_3$/MeOH (1 : 2, v/v) [22]. The lipid extracts were dried and the fatty acids transmethylated for 1 h at 90 ° C with 14% (w/v) BF_3 in MeOH. The methyl esters were extracted into hexane and separated on silica-gel H thin-layer chromatograms containing 10% (w/w) $AgNO_3$ [29]. The esters of linoleic acid and linolenic acid were removed and the percentage conversion was calculated from the distribution of ^{14}C between substrate and product fatty acids.

Statistics

All results are expressed as means ± S.E.; statistical differences were determined by the unpaired Student's *t*-test.

Results

Plasma lipids and lecithin–cholesterol acyltransferase activity

The plasma concentrations of triacylglycerol were significantly reduced ($P < 0.001$) in both models of liver injury, but total phospholipid levels were unchanged (Table I). Total cholesterol (i.e., free cholesterol and cholesteryl esters) was 25% higher ($P < 0.05$) in bile-duct-ligated rats than in sham-operated animals, but was unchanged in galactosamine-treated rats when compared to their controls. Plasma lecithin–cholesterol acyltransferase activity was significantly reduced in both galactosamine-treated and bile-duct-ligated rats, whether expressed as an absolute or fractional amount of cholesterol converted into cholesteryl esters. As expected, in both galactosamine-treated and bile-duct-ligated rats, these reduced lecithin–cholesterol acyltransferase activities resulted in significant increases ($P < 0.001$) in the proportion of plasma total cholesterol present as free cholesterol and in the cholesterol:phospholipid molar ratio, *C/PL*. The proportions of linoleate, dihomo-γ-linoleate (20:3($n-6$) and arachidonate in the plasma total fatty acyl chains of bile-duct-ligated rats were significantly decreased ($P < 0.05$) compared to those in the sham-operated rats (20.6 ± 0.8, 0.7 ± 0.1 and 9.6 ± 0.5% compared to 27.2 ± 0.5, 1.3 ± 0.1 and 11.0 ± 0.3%, respectively). In the galactosamine-treated rats these proportions were unchanged compared to the control rats.

Lipid content of erythrocytes and microsomal membranes of liver and kidney

The cholesterol content per mg protein was significantly higher ($P < 0.001$) in liver microsomal membranes in both galactosamine-treated and bile-duct-ligated rats (Table II). However, in kidney microsomes the increase in mean

TABLE I

PLASMA LIPID COMPOSITION AND LECITHIN–CHOLESTEROL ACYLTRANSFERASE (LCAT) ACTIVITY IN RATS WITH ACUTE GALACTOSAMINE-INDUCED HEPATITIS OR CHRONIC BILIARY OBSTRUCTION

Groups of rats were injected with D-galactosamine hydrochloride (GalN) or saline and killed 3 days later or were subjected to bile-duct ligation (BDL) or sham-operation for 3 weeks as described in Materials and Methods. Results are means ± S.E. and significance of differences from control values are indicated in the footnotes

Animals (No.)	Triacylglycerol (mmol/l)	Total phospholipid (mmol/l)	Total cholesterol (mmol/l)	Percentage of free cholesterol (%)	LCAT activity		Cholesterol/ phospholipid ratio (mol/mol)
					%/h	nmol/ml per h	
GalN (13)	0.64 ± 0.08 ***	1.55 ± 0.09	1.50 ± 0.09	61.4 ± 3.4 ***	4.9 ± 0.7 ***	41.6 ± 5.7 *	0.61 ± 0.05 **
Saline-injected (6)	1.91 ± 0.21	1.63 ± 0.06	1.47 ± 0.12	31.0 ± 0.7	14.1 ± 1.5	62.9 ± 6.2	0.28 ± 0.02
BDL (7)	0.72 ± 0.04 ***	1.41 ± 0.11	1.71 ± 0.13 *	43.2 ± 1.7 ***	4.9 ± 0.1 ***	36.0 ± 2.7 ***	0.52 ± 0.01 ***
Sham-operated (8)	1.93 ± 0.33	1.64 ± 0.03	1.37 ± 0.05	29.0 ± 0.3	17.2 ± 0.8	67.2 ± 2.2	0.24 ± 0.01

* $P < 0.05$. ** $P < 0.01$. *** $P < 0.001$.

cholesterol content was less than 10% and reached significance ($P < 0.05$) only in the bile-duct-ligated rats. Phospholipid content per mg of liver or kidney microsomal protein was unchanged, except in liver microsomes of galactosamine-treated rats which showed a small increase ($P < 0.05$).

Membrane lipid analyses are better expressed as ratios or proportions, rather than absolute amounts per cell or per mg of membrane protein, since the former are good indicators of lipid–lipid interactions within biomembranes. For example, in erythrocytes from patients with liver disease reduced membrane fluidity correlates closely with the C/PL molar ratio but not with the cholesterol content per mg of membrane protein [9]. In both bile-duct-ligated and galactosamine-treated rats the C/PL ratios of erythrocyte membranes were significantly elevated ($P < 0.001$) (Table II). The mean C/PL ratios of kidney and liver microsomal membranes were higher in bile-duct-ligated and galactosamine-treated rats than in the corresponding controls, suggesting that their fluidity may have been reduced. However, the rises in the C/PL ratio were small and not significant ($0.05 < P < 0.01$), except for liver microsomes of bile-duct-ligated rates, which showed a marked increase ($P < 0.001$).

Phospholipid fatty acyl chains in erythrocytes and in microsomal fractions of liver and kidney

The proportion of arachidonate in erythrocyte phospholipid fatty acyl chains was significantly lower in the galactosamine-treated or bile-duct-ligated rats, albeit less than 10%, than in the corresponding controls (Table III). However, this reduction was not reflected in the phospholipids of liver or kidney microsomes, since no decrease in arachidonate was seen in either experimental

TABLE II

LIPID COMPOSITION OF LIVER AND KIDNEY MICROSOMES AND OF ERYTHROCYTE MEMBRANES FROM RATS WITH ACUTE GALACTOSAMINE-INDUCED HEPATITIS OR CHRONIC BILIARY OBSTRUCTION

Groups of rats and presentation of results are as described in Table I. Values in nmol/mg protein C/PL, cholesterol:phospholipid molar ratio.

Animals (No.)	Liver microsomes			Kidney microsomes			Erythrocyte membranes (C/PL)
	cholesterol	phospholipid	C/PL	cholesterol	phospholipid	C/PL	
GalN (13)	128 ± 5	822 ± 40	0.15 ± 0.01	210 ± 2	586 ± 6	0.36 ± 0.00	0.84 ± 0.01 ***
Saline-injected (6)	97 ± 2	702 ± 26	0.14 ± 0.00	194 ± 14	562 ± 32	0.34 ± 0.01	0.73 ± 0.00
BDL (7)	169 ± 8 ***	668 ± 19	0.25 ± 0.01 ***	222 ± 2 *	570 ± 20	0.39 ± 0.02	0.82 ± 0.01 ***
Sham-operated (8)	96 ± 4	720 ± 15	0.13 ± 0.01	207 ± 5	549 ± 13	0.38 ± 0.00	0.74 ± 0.01

* $P < 0.05$ *** $P < 0.001$.

TABLE III

COMPOSITION OF PHOSPHOLIPID FATTY ACYL CHAINS IN ERYTHROCYTE MEMBRANES AND KIDNEY AND LIVER MICROSOMES FROM RATS WITH ACUTE GALACTOSAMINE-INDUCED HEPATITIS OR CHRONIC BILIARY OBSTRUCTION

Groups of rats are as described in Table I. Results (weight %) of major fatty acids with retention times up to and including arachidonic acid (20:4(*n* – 6) are means ± S E and significance of differences from control values are indicated in the footnotes

Animals	(No.)	Erythrocyte membranes					
		16:0	18:0	18:1	18.2	20:3	20:4
GalN	(13)	33.9 ±0 2	11.6 *** ±0.1	12.8 ±0 2	13.4 ** ±0.2	1.9 * ±0.1	26.3 * ±0.2
Saline-injected	(6)	32.7 ±0.9	12 6 ±0 2	12.9 ±0.5	11.1 ±0 5	2.4 ±0.1	28.5 ±0.7
BDL	(7)	31.6 ±0 1	10.5 *** ±0.5	17 2 *** ±0.5	8.9 ** ±0.4	1 7 ±0 5	26.2 * ±0.4
Sham-operated	(8)	32 7 ±0.4	13.7 ±0.3	13.0 ±0.3	10.9 ±0 4	2.0 ±0 5	27.7 ±0.4

* $P < 0.05$. ** $P < 0\ 01$. ***$P < 0.001$.

Animals	(No.)	Liver microsomes						Kidney microsomes					
		16:0	18:0	18:1	18:2	20:3	20:4	16:0	18:0	18:1	18:2	20:3	20:4
GalN	(13)	22.7 *** ±0.4	25 3 ±0.6	9.6 ±0.2	18.1 ±0.3	1.9 ** ±0.2	22.7 ±0.5	21.7 ** ±0.9	19.0 ±0.2	11 7 ±0.1	15.6 ±0.4	2.6 ±0.4	29.6 * ±0.9
Saline-injected	(6)	24.9 ±0.2	24.1 ±0.5	9.1 ±0.2	16.7 ±0.6	3.0 ±0 2	22.3 ±0.4	24.5 ±0.2	18.2 ±0.4	11 1 ±0.3	16.1 ±0.4	2 8 ±0 4	27.5 ±0.5
BDL	(7)	25 8 * ±0.8	19.9 *** ±0.2	18.7 *** ±0.4	11.7 ** ±0.5	1.5 *** ±0.2	21.6 ±1.1	24.4 ±0.6	19.8 ±0.9	14.3 *** ±0.6	11.6 *** ±0.6	2.4 ±0.3	27.5 ±1.2
Sham-operated	(8)	22.6 ±0 6	25.5 ±0.5	9.7 ±0 3	16.8 ±0.5	2 9 ±0.2	22.0 ±0 4	24.6 ±0.6	19.0 ±0.2	11.0 ±0.1	15 5 ±0.3	1.9 ±0.1	28.0 ±0.8

model. Linoleate, the main dietary precursor of arachidonate, was significantly reduced in the phospholipids of both liver and kidney microsomes in bile-duct-ligated rats but it was unchanged in galactosamine-treated animals.

Microsomal Δ^6-desaturase activity in liver and kidney

The Δ^6-desaturase activities in microsomal fractions from normal rat liver (107–270 pmol linoleic acid converted per min per mg protein) were similar to those reported by other workers [30,31] and at least 4-fold greater than in fractions from kidney (Table IV). The mean activity in liver microsomes was significantly lower in both galactosamine-treated rats ($P < 0.001$) and bile-duct-ligated rats ($P < 0.05$) when compared to their control groups. Unexpectedly, the mean value in

TABLE IV

MICROSOMAL Δ^6-DESATURASE ACTIVITY IN LIVER AND KIDNEY FROM RATS WITH ACUTE GALACTOSAMINE-INDUCED HEPATITIS OR CHRONIC BILIARY OBSTRUCTION

Groups of rats and presentation of results are as described in Table I.

Animals (No.)	Microsomal Δ^6-desaturase activity (pmol/min per mg protein)	
	liver	kidney
GalN (13)	131 ± 12 ***	19 1 ± 1.6
Saline-injected (6)	270 ± 35	22.0 ± 1.8
BDL (7)	106 ± 4 *	23.3 ± 1.8 **
Sham-operated (8)	132 ± 7	15.2 ± 1.0

* $P < 0.05$. ** $P < 0.01$. *** $P < 0.001$.

TABLE V

LIPID COMPOSITION IN KIDNEY BRUSH-BORDER MEMBRANE FROM RATS WITH CHRONIC BILIARY OBSTRUCTION

Groups of rats were subjected to either bile-duct ligation (BDL) or sham-operation and killed 3 weeks later. Results are means ± S.E. for the numbers in parentheses and significance of differences between the groups are indicated in the footnotes. *C/PL*, cholesterol:phospholipid molar ratio.

Animals	(No.)	Cholesterol (nmol/mg protein)	Phospholipid (nmol/mg protein)	*C/PL*	Phospholipid fatty-acid composition (wt%)					
					16.0	18:0	18:1	18:2	20:3	20:4
BDL	(7)	429 ± 9 ***	643 ± 15 **	0.668 ± 0.009 *	24.7 ± 0.8	23.9 ± 0.8 **	10.2 ± 0.6	8.5 ± 0.5	2.5 ± 0.7	28.9 ± 0.6 ***
Sham-operated	(6)	343 ± 9	545 ± 21	0.631 ± 0.013	25.9 ± 0.4	22.7 ± 0.6	7.4 ± 0.4	8.6 ± 0.5	2.0 ± 0.5	33.4 ± 0.4

* $P < 0.05$. ** $P < 0.01$. *** $P < 0.001$.

the sham-operated rats was half that in the group injected with saline as control for the galactosamine-treated rats, even though all samples were assayed in the same run. The reason for this difference was not investigated. One possibility is that experiments with sham-operated (and bile-duct-ligated) rats lasted 18 days longer than those with saline-injected (and galactosamine-treated) rats and were begun 2 months later in the year; Δ^6-desaturase activity is known to vary with the age of the animal and with the season of the year [30], whilst the 2-month extra storage time of microsomes from saline-injected rats may also have affected enzymatic activity. In kidney microsomes the Δ^6-desaturase activity was significantly increased in bile-duct-ligated rats ($P < 0.001$) but was unchanged in the galactosamine-treated animals (Table IV).

Lipid composition of brush-border membranes in the kidney cortex of biliary-obstructed rats

To assess whether lipid changes might be more pronounced in kidney plasma membranes, we isolated the brush-border membranes from seven bile-duct-ligated rats. The cholesterol content and C/PL ratio were both significantly raised in these membranes (Table V), although we had been unable to detect a change in the C/PL ratio of the microsomal fraction (Table II). In addition, the amount of arachidonate in brush-border membrane phospholipids was 15% lower in bile-duct-ligated rats compared to sham-operated controls ($P < 0.001$), but there was no difference in the microsomal fractions.

Discussion

Results from the present study establish for the first time that lipid abnormalities occur in renal membranes in experimental liver disease; they appear to be induced by changes in plasma lipoprotein lipid composition. Rat kidney brush-border membranes were found to have accumulated cholesterol and to have lost arachidonate in phospholipid fatty acyl chains 3 weeks after bile-duct ligation, alterations expected to interfere with Na^+ transport and to diminish prostaglandin synthesis, respectively. These findings provide support for the hypothesis that lipid abnormalities in kidney membranes contribute to the renal dysfunction which is commonly seen in patients with severe liver disease.

As expected from previous studies [32–34], liver injury in rats induced by either bile-duct ligation or galactosamine treatment resulted in a fall in plasma lecithin–cholesterol acyltransferase activity, an accumulation of cholesterol in lipoprotein surfaces and a rise (of up to 15%) in the cholesterol : phospholipid ratio of red cell membranes. Liver microsomes from bile-duct-ligated rats were also enriched in cholesterol, but no change was found in those from galactosamine-treated rats. This difference was unexpected; cholesterol exchange between lipoproteins and membranes is rapid [2] and the red cell membranes of both groups were enriched to a similar extent. Nucleated cells have two ways to handle a net influx of exogenous cholesterol which are unavailable to red cells; they can reduce endogenous cholesterol synthesis and they can divert cholesterol from their membrnes into an intracellular cholesteryl ester storage pool. It is conceivable that these mechanisms were still able to function during the 3-day period of galactosamine treatment but were impaired by prolonged biliary obstruction.

Kidney microsomes in bile-duct-ligated rats, however, accumulated no more cholesterol than those in galactosamine-treated animals; in both cases the mean rise in the C/PL ratio was small (less than 4%) and statistically insignificant. Kidney cells differ from those in liver by being exposed only to the lipoproteins of the extravascular fluid; fenestrations in the thin layer of sinusoidal endothelium enables all of the plasma lipoproteins, except chylomicrons and large very-low density lipoproteins, to interact with the hepatocyte surface [35]. The relationship between lipoproteins in plasma and in interstitial fluid is poorly defined; current evidence suggests that as well as differences in concentration there may be dissimilarities in composition and morphology of particles of the same lipoprotein class [36,37]. Cholesterol uptake by red-cell membranes from cholesterol-rich plasma in vitro depends on the incubation time, the C/PL ratio of the plasma and the relative amounts of membrane cholesterol and plasma cholesterol [38]. Whether the inability of kidney microsomes in bile-duct-ligated rats to amass cholesterol compared with liver microsomes can be attributed to diminished concentrations and/or lower *C/PL* ratios of renal interstitial fluid lipoproteins compared to plasma lipoproteins remains to be established. The plasma membrane forms only a small percentage of a microsomal fraction and, although cholesterol equilibrates relatively freely between surface membranes and membranes of intracellular organelles [2], it is possible that our analysis of whole kidney microsomes may have masked a greater cholesterol enrichment of the plasma membrane. Analysis of brush-border membranes from the kidney cortex of bile-duct-ligated rats supported this possibility; their *C/PL* ratio was significantly raised, indicating that brush-border membranes cannot maintain a normal cholesterol content when kidney cells are exposed to abnormal, cholesterol-rich lipoproteins.

Most arachidonic acid in mammalian cells is present as an ester in the 2-position of glycerophospholipids. It is derived predominantly from dietary linoleic acid by desaturation and chain elongation; the initial introduction of a double bond by Δ^6-desaturase, to form γ-linolenic acid, is the rate-limiting step [28,39,40]. In rat, and probably man, liver has the highest desaturase activity [40]. It has been suggested that the liver could be the major source of arachidonic acid for other tissues in the rat [40]; this function probably involves lipoproteins as transport vehicles, since circulating complexes of albumin and free-fatty acids contain relatively little arachidonic acid [41].

Red cells cannot synthesize fatty acids or elongate or desaturate fatty acyl chains, turnover of these lipids occurs by utilization of exogenous free-fatty acids in the phospholipid deacylation-reacylation cycle and by equilibrium exchange of intact phospholipid molecules between membrane and plasma. It is not surprising, therefore, that there is a significant reduction of arachidonate in the phospholipids of red cell membranes in bile-duct-ligated rats and that this reflects the decreased proportion of arachidonate in plasma. The reasons for plasma arachidonate deficiency are less clear [42]. Abnormal lipoprotein metabolism may be one factor, inasmuch as patients with familial lecithin–cholesterol acyltransferase deficiency have good liver function but reduced arachidonate levels in plasma, red cells and platelets [43]. Impaired absorption of dietary linoleic acid may also contribute, but decreased hepatic conversion of linoleate to arachidonate probably plays the predominant role. The reduced Δ^6-desaturase activity in liver of bile-duct-ligated rats suggests reduced production of arachidonic acid and decreased availability for export in the phospholipids of lipoprotein surfaces. Despite this diminished Δ^6-desaturase activity, normal arachidonate levels were found in the phospholipids of hepatic microsomes; the liver may be able to conserve this eicosanoid precursor [44]. The proportion of arachidonate in phospholipids of kidney microsomes was also unchanged in bile-duct-ligated rats. However, when renal brush-border membranes were analysed a significant reduction in arachidonate was found; conceivably, the 50% increase in Δ^6-desaturase activity in kidney microsomes of bile-duct-ligated rats could represent a mechanism to compensate for a diminished exogenous supply of lipoprotein arachidonate.

In conclusion, our analyses of renal brush-border membranes establish that both the cholesterol and fatty-acid contents of these membranes can be influenced by the lipid composition of interstitial fluid lipoproteins. Similar alterations in the lipids of intracellular renal membranes were not detected, suggesting that compensatory mechanisms, such as changes in lipid synthetic rates, may have been operating. Whether these putative mechanisms can adequately compensate if cellular exposure to the altered lipoproteins is more prolonged is uncertain; gross cholesterol accumulation occurs in the renal cortex of patients with familial lecithin–cholesterol acyltransferase deficiency [43], but in mice given fat-free diets the renal cortex tenaciously retains arachidonate in all phospholipid classes except phosphatidylinositol [44]. By analogy with studies in red cells [8,10] and platelets [4,12] from jaundiced patients, cholesterol enrichment and arachidonate depletion of renal membranes are likely to perturb Na^+ transport and prostaglandin production, respectively; whether kidney membrane lipid abnormalities play a significant role in the impaired renal handling of sodium and water reported in biliary-obstructed rats [45] or can contribute to a better understanding of the aetiology of renal dysfunction in human liver disease must await additional investigations.

Acknowledgement

This work was supported by a grant from the Medical Research Council.

References

1 Harry, D.S., Owen, J.S. and McIntyre, N (1985) in Liver and Biliary Disease (Wright, R , Millward-Sadler, G H., Alberti, K.G M.M. and Karran, S., eds.), pp. 65–85, Baillière Tindall, London

2 Bruckdorfer, K R. and Graham, J.M. (1976) in Biological Membranes, Vol III (Chapman, D. and Wallach, D.F H., eds), pp. 103–151, Academic Press, New York

3 Owen, J.S , McIntyre, N and Gillett, M.P.T (1984) Trends Biochem. Sci. 9, 238–242

4 Owen, J.S , Hutton, R A , Day, R.C., Bruckdorfer, K R and McIntyre, N (1981) J Lipid Res 22, 423–430

5 Langley, P.G , Cove, C.D. and Williams, R (1984) in Advances in Hepatic Encephalopathy and Urea Cycle Diseases (Kleinberger, G., Ferenci, P., Riederer, P. and Thaler, H., eds.), pp. 706–710, Karger, Basel.

6 Neerhout, R.C. (1968) J. Lab. Clin. Med 71, 438–447

7 Cooper, R.A , Diloy-Puray, M., Lando, P. and Greenberg, M.S (1970) J. Clin Invest. 51, 3182–3190

8 Owen, J.S. and McIntyre, N. (1978) Biochim Biophys Acta 510, 168–176

9 Owen, J S., Bruckdorfer, K.R., Day, R.C. and McIntyre, N (1982) J Lipid Res. 23, 124–132

10 Jackson, P A. and Morgan, D B (1982) Clin Sci 62, 101–107

11 Jackson, P A and Morgan, D.B. (1982) Biochim Biophys. Acta 693, 99–104

12 Laffi, GT , La Villa, G., Pinzani, M., Ciabattoni, G , Patrignani, P , Mannelli, M., Cominelli, F and Gentilini, P. (1986) Gastroenterology 90, 274–282

13 Epstein, M. (1979) Gastroenterology 76, 622–635

14 Papper, S (1983) in The Kidney in Liver Disease (Epstein, M., ed), pp 3–10, Elsevier, Amsterdam

15 Epstein, M. (1983) in The Kidney in Liver Disease (Epstein, M., ed) pp 25–49, Elsevier, Amsterdam

16 Dunn, M.J. (1984) Gastroenterology 87, 1392–1395

17 Arroyo, V., Planas, R , Gaya, J., Deulofeu, R., Rimola, A , Perez-Ayuso, R., Rivera, F and Rodes, J (1983) Eur. J. Clin. Invest. 13, 271–278

18 Kawata, S., Trzaskos, J M and Gaylor, J.L (1985) J Biol Chem 260, 6609–6617

19 Evers, C., Haase, W., Murer, H and Kinne, R. (1978) J Membrane Biochem. 1, 203–219

20 Lowry, O H., Rosebrough, N J., Farr, A.L. and Randall, R.J. (1951) J. Biol. Chem. 193, 265–275

21 Folch, J , Lees, M and Sloane-Stanley, G.H. (1957) J. Biol Chem. 226, 497–503

22 Rose, H.G. and Oklander, M. (1965) J Lipid Res 6, 428–431

23 Bligh, E.G. and Dyer, W.J. (1959) Can. J. Biochem. Physiol. 37, 911–917

24 Owen, J.S , Goodall, H., Mistry, P., Harry, D S , Day, R.C. and McIntyre, N. (1984) J. Lipid Res. 25, 919–931

25 Bartlett, G R. (1959) J. Biol. Chem 234, 466–468

26 Stokke, K.T and Norum, K.R. (1971) Scand. J. Clin. Lab Invest. 27, 21–27

27 Owen, J.S., Ramalho, V., Costa, J.C.M and Gillett, M P.T. (1979) Comp Biochem Physiol. 63B, 261–265

28 Sinclair, H M. (1984) Hum. Nutri. Clin. Nutr. 38C, 245–260

29 Safford, R , Jeffcoat, R. and James, A.T (1975) Biochim Biophys. Acta 409, 86–96

30 Peluffo, R.O. and Brenner, R R. (1974) J Nutr. 104, 894–900

31 Okayasu, T , Nagao, M and Imai, Y. (1979) FEBS Lett. 104, 241–243

32 Sabesin, S.M., Kuiken, L.B. and Ragland, J.B (1975) Science 190, 1302–1304

33 Calandra, S., Martin, M J., O'Shea, M J. and McIntyre, N. (1972) Biochim. Biophys Acta 260, 424–432

34 Taniguchi, M., Tanake, F., Ishikawa, H. and Sakagami, T. (1983) Biochim. Biophys. Acta 753, 22–31

35 Fraser, R., Bosanquet, A G. and Day, W.A (1978) Atherosclerosis 29, 113–123

36 Raymond, T.L. and Reynolds, S.A (1983) J. Lipid Res. 24, 113–119

37 Dory, L , Boquet, L M., Hamilton, R.L., Sloop, C H. and Roheim, P.S (1985) J Lipid Res. 26, 519–527

38 Cooper, R.A , Arner, E.C., Wiley, J.S. and Shattil, S.J. (1975) J. Clin. Invest 55, 115–126

39 Willis, A.L. (1981) Nutr Rev. 39, 281–301

40 Leat, W.M.F. (1981) Trends Biochem. Sci 6, IX–X

41 Skipski, V.P (1972) in Blood Lipids and Lipoproteins: Quantitation, Composition, and Metabolism (Nelson, G.J., ed.), pp. 471–583, Wiley-Interscience, New York

42 Johnson, S.B., Gordon, E , McClain, C., Low, G. and Holman, R.T. (1985) Proc. Natl Acad. Sci. USA 82, 1815–1818

43 Stokke, K.T , Bjerve, K.S., Blomhoff, J P.. Öystesse, B , Flatmark, A , Norum, K.R. and Gjone, E (1974) Scand J Clin Invest. 33 (Suppl. 137), 93–100

44 Lefkowith, J.B , Flippo, V., Sprecher, H. and Needleman, P (1985) J. Biol. Chem. 260, 15736–15744

45 Yarger, W.E. (1972) J Clin. Invest. 57, 408–418

Biochimica et Biophysica Acta 896 (1987) 35–46
Elsevier

BBA 73183

Further characterization of a fodrin-containing transmembrane complex from mouse T-lymphoma cells

Suzanne J. Suchard and Lilly Y.W. Bourguignon

Department of Anatomy and Cell Biology, University of Miami, School of Medicine, Miami, FL 33101 (U.S.A.)

(Received 23 May 1986)

Key words: Fodrin; Transmembrane complex; Cytoskeleton; Membrane glycoprotein; (Lymphoma)

A transmembrane complex containing fodrin (an actin-binding protein) and a major surface glycoprotein (GP 180) was previously isolated from mouse T-lymphoma cells by the complementary techniques of non-ionic detergent extraction and sucrose gradient centrifugation (Bourguignon et al. (1985) J. Cell Biol. 101, 477–487). The analysis of this complex has been extended to verify the structural association and further define the interaction between fodrin and GP 180. The association between fodrin and GP 180 has been confirmed by the following evidence: (1) co-sedimentation of fodrin and GP 180 in a single peak on a sucrose gradient with a sedimentation coefficient of 20 S; (2) a constant ratio of fodrin and GP 180 across the 20 S peak; (3) the specific co-precipitation of GP 180 with fodrin from the 20 S peak using anti-fodrin antibody; and (4) the colocalization of fodrin and GP 180 from the 20 S peak on actin filaments using an immuno-electron microscopic technique. Furthermore, this fodrin-GP 180 complex can be readily dissociated and reassembled in the presence and absence of 0.6 M NaCl, respectively. The fact that this fodrin-GP 180 complex displays actin-binding ability indicates that this transmembrane complex may play an important role in the linking event between receptors and the cytoskeleton during lymphocyte patching and capping.

Introduction

A direct connection between transmembrane cell surface proteins and the underlying cytoskeleton may be essential for processes such as cell motility, cell-cell recognition, phagocytosis, endocytosis etc. (for a general review see Ref. 2) that require the lateral movement of cell surface receptors. Plasma membrane-cytoskeleton interactions have been demonstrated in a number of differing cell types. Such interactions may be relatively static as in erythrocytes [3,4], the microvilli of intestinal brush-border cells [5,6] or ascites tumor cells [7]. On the other hand, plasma membrane-cytoskeleton interactions may be the result of an inducible event such as receptor redistribution in lymphocytes and fibroblasts [8–11].

Currently, the most comprehensive view of the protein composition and structural arrangement of plasma membrane–cytoskeleton interactions is from the more structured systems of erythrocytes and intestinal brush-border cells. In erythrocytes, binding of cytoskeletal spectrin to the transmembrane anion-channel protein, band 3, is mediated by the membrane attachment protein, ankyrin [3,12]. The binding of spectrin to actin, in turn, appears to be mediated by band 4.1 [4]. Band 4.1 may also serve as a membrane attachment protein, since it can also bind to the erythrocyte membrane through its direct interaction with the glycophorins and band 3 [13,14]. In brush-border cells,

---

Correspondence: Dr. L.Y.W Bourguignon, Department of Anatomy and Cell Biology, University of Miami, School of Medicine, Miami, FL 33101, U.S.A.

0005-2736/87/$03.50 © 1987 Elsevier Science Publishers B.V (Biomedical Division)

recent evidence indicates that the 110 kDa actin-binding protein may be an integral membrane protein [6]. The direct attachment of this protein to cytoskeletal actin would represent a simpler system of membrane–actin interaction and an alternative model to that represented by the erythrocyte system.

In lymphocytes, the initial implication of an interaction between membrane and cytoskeletal components was provided by immunofluorescent experiments. It was demonstrated that during ligand-induced cell-surface receptor redistribution there was a parallel accumulation of actin, myosin, and α-actinin directly beneath receptor patches and caps [8,15,16]. More direct evidence of an association between specific surface receptors and the underlying cytoskeleton was suggested by non-ionic detergent extraction of isolated plasma membranes to obtain a detergent insoluble, membrane-associated cytoskeletal residue [17]. For example, when surface immunoglobulin molecules are induced to patch and/or cap, they become tightly linked to the detergent insoluble cytoskeleton [10,11].

Because so little is known about the detailed molecular organization of transmembrane-cytoskeletal protein associations in lymphocytes, we have sought to draw analogies to the well-defined erythrocyte system. The existence of cytoskeletal proteins common to both lymphocytes and erythrocytes has provided insight into how such cytoskeletal elements may regulate lymphocyte receptor mobility. For example, the co-localization of actin and myosin with receptor patches and caps influenced Bourguignon and Singer [8] to propose that surface receptors were clustered into caps via a sliding filament mechanism analogous to that occurring during muscle contraction. Subsequent experiments demonstrated that (i) myosin light chain phosphorylation occurs during lymphocyte capping [18], (ii) a myosin light-chain kinase is associated with the lymphocyte cytoskeleton [19], and (iii) a Ca^{2+}-activated myosin light-chain kinase is responsible for the regulation of receptor capping [20].

Even as we begin to understand the regulation of the movement of cell surface molecules following their linkage to the cytoskeleton, we still know very little about the protein or proteins that mediate the interactions between transmembrane proteins and the cytoskeleton. Recently, several laboratories have investigated a group of nonerythroid spectrins (fodrin, TW 260/240) that have the ability to cross-link actin and bind to spectrin-depleted erythrocyte membranes [21–25]. The widespread distribution of fodrin has led Glenney and Glenney [26] to suggest that fodrin could provide the general linkage system between microfilaments and the membrane in nonerythroid and nonmuscle cells. Fodrin has been identified in both plasma membrane and membrane-associated cytoskeleton fractions obtained from lymphocytes [1,27]. Indirect evidence from immunofluorescent studies demonstrated that fodrin localizes beneath concanavalin A caps in fibroblasts and concanavalin A, immunoglobulin, and H2 caps in lymphocytes [27–29], suggesting a possible role in receptor reorganization. Moreover, the amount of fodrin associated with the Nonidet P-40-insoluble cytoskeleton increases significantly during lymphocyte patching and capping [1,27]. In addition to fodrin, a major cell-surface transmembrane glycoprotein with a molecular weight of 180000 is also recruited to the lymphocyte cytoskeletal fraction during patching and capping [1,27]. Interestingly, when this 180 kDa glycoprotein (GP 180) is immunoprecipitated by anti-GP 180 antibody from Nonidet P-40-solubilized plasma membrane, fodrin is also selectively co-precipitated [1]. Bourguignon et al. [1] have also demonstrated that GP 180 can be preferentially separated from other cell-surface proteins following Triton X-114 extraction and partitioning. This GP 180-enriched fraction also contained fodrin, and preliminary analysis of this material, coupled with the co-recruitment and immunoprecipitation data, led these authors to suggest that GP 180 and fodrin are closely associated in vivo.

In the present paper, we have conducted a variety of experiments including stoichiometric measurements, dissociation and reassembly assays, immunoprecipitation, immunoelectron microscopic localization, and actin-binding analyses to demonstrate further the close interaction between fodrin and GP 180 as a transmembrane complex. We believe that this fodrin-GP 180 complex may be very important for the transmembrane interactions occurring between membrane proteins and the cytoskeleton.

Materials and Methods

Cell culture and plasma membrane isolation. Mouse T lymphoma cells (BW5147), provided by R. Hyman (The Salk Institute), were grown and plasma membranes isolated as previously described [1].

Radioactive labeling of cellular proteins. Surface proteins were labeled with ^{125}I using the iodogen method of Fraker and Speck [30]. To label proteins metabolically with [^{35}S]methionine or [^{3}H]glucosamine, approx. $1 \cdot 10^5$ cells/ml were incubated with either [^{35}S]methionine (1000 Ci/mmol) or [^{3}H]glucosamine (100 Ci/mmol) (ICN, Irvine, CA) in Dulbecco's modified Eagle's medium under standard culture conditions for 16 h.

Concanavalin A blotting. Isolated plasma membrane was electrophoresed as described below. The polypeptides were then transferred to nitrocellulose sheets [31], incubated with 30 μg of ^{125}I-labeled concanavalin A ([30]; Calbiochem, La Jolla, CA), dried and analyzed by autoradiography.

Con A-Sepharose affinity chromatography. A Con A-Sepharose (Pharmacia, Piscataway, NJ) column (6.0×0.5 cm) was washed with 0.15 M NaCl/10 mM Tris-HCl (pH 7.3) containing 0.5% Triton X-114. Plasma membrane isolated from ^{125}I-labeled cells was extracted in 1% Triton X-114 as described below. The material was passed over the column at least ten times to allow for sufficient binding. The column was then washed until no further radioactivity was removed. Wash buffer containing 1 M methyl α-D-mannoside was then used to elute the column. Fractions containing unbound and specifically eluted radioactive proteins were separately pooled and analyzed by SDS-gel electrophoresis.

Non-ionic detergent extraction. ^{125}I- or [^{35}S]methionine-labeled lymphocyte plasma membrane was isolated from intact cells, washed in 0.15 M NaCl/10 mM Tris-HCl (pH 7.3) and then resuspended in 200 μl of 1.0% (v/v) Triton X-114 in the same buffer. The protein concentration in all samples was kept at about 2.5 mg/ml. Extraction and partitioning was carried out as previously described [1]. Since GP 180 can be separated from other cell surface proteins by its preferential partitioning into the upper, aqueous phase, we used the Triton X-114 aqueous phase as the starting material for all subsequent experiments.

Isolation of a native 20 S transmembrane complex. ^{125}I- or [^{35}S]methionine-labeled plasma membrane was isolated from intact cells, extracted with Triton X-114 and partitioned as described above. The aqueous phase was then loaded onto a linear sucrose gradient (7–28%) with a 0.5 ml cushion of 65% sucrose and centrifuged at 70 000 $\times g_{av}$ for 22 h. Fractions were counted on a LKB MiniGamma gamma counter (LKB Instruments, Rockville, MD) to determine the distribution of surface-iodinated protein within the gradient. Total protein concentration in each fraction was determined by absorbance at 280 nm. Fractions that corresponded with either the 280 nm protein peak or ^{125}I-labeled peak were pooled, precipitated with 10% trichloroacetic acid, and subsequently analyzed by SDS-polyacrylamide gel electrophoresis and autoradiography. The [^{35}S]-methionine-labeled fractions that corresponded to the ^{125}I-labeled peak were precipitated with trichloroacetic acid and the individual fractions were analyzed by SDS-polyacrylamide gel electrophoresis autoradiography, and scanning densitometry. The ^{125}I-labeled peak fractions corresponded to a sedimentation value of 20 S as calculated using protein standards of tetrameric fodrin, tetrameric spectrin (11 S), and G-actin (3.7 S) as described previously [1]. In order to iodinate the proteins in the 20 S peak fractions (i.e., fodrin and GP 180), the Triton X-114 aqueous fraction was iodinated prior to centrifugation on sucrose gradients.

SDS-polyacrylamide gel electrophoretic and autoradiographic analysis. Electrophoresis was conducted using an exponential polyacrylamide gradient (6.0–17.0%) slab gel and the discontinuous buffer system described by Laemmli [32]. Gels containing samples labeled with either ^{125}I or [^{35}S]methionine were stained, fluorographed [33], vacuum dried, and exposed to Kodak X-ray (X-Omat, AR-5) film at −70°C. In order to quantitate the relative amounts of GP 180 and fodrin in gel lanes, silver-stained gels and autoradiograms of [^{35}S]methionine-labeled or ^{125}I-labeled proteins were scanned on a Quick Scan R & D (Helena Laboratories, Beaumont, TX) scanning densitometer.

Isolation of 9 S, GP 180 by high salt extraction and sucrose gradient centrifugation. The ^{125}I-labeled 20 S material was isolated as described above, diluted with 0.15 M NaCl/10 mM Tris-HCl (pH 7.3) containing 0.01% Triton X-114, and concentrated using a 3 ml Amicon stirred filtration cell. This material was then divided into an experimental sample exposed to high salt and a control. The experimental sample was adjusted to 0.6 M NaCl/10 mM Tris-HCl (pH 8.0)/0.5% Triton X-114; the control sample to 0.15 M NaCl/10 mM Tris-HCl (pH 7.2)/0.5% Triton X-114. The extraction buffer was modeled after ones used to extract cytoskeletal proteins [21,22,34]. 9 S, GP 180 was obtained by an overnight incubation of 20 S material with high salt (0.6 M NaCl) at 4°C followed by centrifugation on a linear sucrose gradient (7–28%) for 22 h at $70000 \times g_{av}$. 20 S control material, incubated overnight in physiological strength salt (0.15 M), was run on a parallel 7–28% sucrose gradient. The high-salt sample was centrifuged on a sucrose gradient containing 0.6 M NaCl, whereas the control sample was run on a gradient containing 0.15 M NaCl. Parallel high-salt and control gradients containing ^{125}I-labeled human transferrin and spectrin were included as internal controls to demonstrate that high salt had no inherent effect on S values.

In vitro reassembly of a transmembrane complex from 9 S, GP 180 and fodrin. (1) Preparation of a 9 S, GP 180-Con A-Sepharose column. Isolated 9 S, GP 180 material was first dialyzed overnight against physiological strength salt (0.15 M NaCl/10 mM Tris-HCl (pH 7.3)/0.1% Triton X-114) to reduce the salt concentration and remove sucrose, and then passed over a Con A-Sepharose column. This 9 S, GP 180 bound column was used for the following in vitro reassembly assay. (2) In vitro reassembly assay. After washing the 9 S, GP 180-Con A-Sepharose column with physiological strength salt (0.15 M NaCl buffer), 3–5 μg of ^{125}I-labeled [30] pig brain fodrin was passed over the unlabeled 9 S, GP 180-Con A-Sepharose column at least ten times to insure maximum fodrin binding, and the column was then washed until no more radioactivity was removed. A parallel Con A-Sepharose column with no bound GP 180 was run as a control for nonspecific binding and/or elution of ^{125}I-labeled fodrin. Following washing, columns were eluted with 1 M methyl α-D-mannoside and 0.5 ml fractions collected. To demonstrate specific sugar elution profiles, 9 S, GP 180-bound and 20 S-bound Con A-Sepharose columns were also prepared as positive controls. Fractions from all four columns were then counted and plotted vs. fraction number to establish an elution profile for each column. (3) Characterization of in vitro assembled 9 S, GP 180-fodrin transmembrane complex. The newly formed 9 S, GP 180-fodrin transmembrane complex was preferentially eluted by methyl α-D-mannoside from a Con A-Sepharose column and analyzed by sucrose gradient (7–28%) centrifugation for 22 h at $70000 \times g_{av}$. 9 S, GP 180 alone, sugar-eluted from a Con A-Sepharose column, was run on a parallel gradient as a control.

Immunoprecipitation procedure. The 20 S, GP 180-containing peak fraction (isolated by sucrose density centrifugation as described above) was incubated with a polyclonal rabbit anti-fodrin antibody (kindly provided by Dr. Shin Lin, Johns Hopkins University) or pre-immune serum at 4°C for 30 min. This step was followed by an overnight incubation with goat anti-rabbit immunoglobulin [35]. The resulting immunoprecipitates were pelleted by centrifugation at $700 \times g_{av}$ for 5 min, washed three times with 0.1% Triton X-114 in 0.15 M NaCl/10 mM Tris-HCl (pH 7.3) solubilized in sample buffer and analyzed by SDS-polyacrylamide gel electrophoresis autoradiography.

Actin-binding analysis. The ^{125}I-labeled 20 S, GP 180-containing peak was isolated and concentrated as described above. F-actin was prepared according to the procedure of Pardee and Spudich [36]. For these analyses, the peak material was incubated with actin under two different sets of conditions. Peak material was incubated with 40 μg of F-actin, an estimated 50 molar excess, in a solution comprising 0.1 M NaCl/2 mM $MgCl_2$/1 mM EGTA/10 mM imidazole-Cl (pH 7.0) [37]. In the second type of experiment, the peak material was incubated with equimolar concentrations of F-and G-actin (20 μg of each) in 0.1 M NaCl/2 mM Tris-HCl (pH 8.0)/1.2 mM $MgCl_2$/1.2 mM $CaCl_2$/ and 0.5 mM 2-mercaptoethanol, a buffer favoring actin polymerization [36]. In parallel controls, peak material was incubated in the absence of actin. After an incubation period of 4–12 h at 4° C, the material was loaded onto a standard linear sucrose gradient (7–28%) and centrifugated at $70\,000 \times g_{av}$ for 22 h. The gradients were then fractionated and the ^{125}I-labeled peak was determined by gamma counting.

Immunoelectron microscopy. The isolated ^{125}I-labeled 20 S, GP 180-containing peak material was dialyzed overnight against G-actin buffer comprising 5 mM Tris-HCl (pH 8.0)/0.2 mM ATP/0.2 mM $CaCl_2$/0.5 mM 2-mercaptoethanol. This dialyzed material was then added to G-actin and polymerization was initiated by the addition of 50 mM KCl/1 mM ATP/1 mM $MgCl_2$ [36]. Polymerization was carried out for 1 h at room temperature or overnight at 4° C. Following polymerization, anti-GP 180 or anti-fodrin was added and the material incubated at 4° C for 30 min. This step was followed by the addition of protein A-gold [38]. Control samples, which were either incubated with antisera preabsorbed with GP 180 or fodrin or in which the primary antibody addition step was omitted, were run in parallel with the experimental samples. Following 30 min incubation with protein A-gold, aliquots of material were removed, applied to formvar-coated grids, washed extensively with buffer, and negative stained [39]. Grids were then examined in a Philips 300 electron microscope operating at 60 kV and photographed.

Results

GP 180 as a concanavalin-A-binding glycoprotein

The Coomassie blue staining pattern after SDS-polyacrylamide gel electrophoresis of isolated plasma membrane from ^{125}I-labeled mouse T-lymphoma cells revealed many membrane-associated polypeptides with molecular weights ranging from about 300 000 to 17 000 (Fig. 1A). We have previously identified the high-molecular-weight doublet above myosin in lane 1A as the actin-binding protein, fodrin [1]. The corresponding autoradiogram shows several ^{125}I-labeled cell surface proteins with molecular weights ranging from 25 000 to 250 000 (Fig. 1B). An M_r 180 000 protein appears to be one of the major iodinated proteins (Fig. 1B). The results of blotting and binding of plasma membrane with ^{125}I-labeled concanavalin (Fig. 1C) and Con A-Sepharose columns (Fig. 1D) indicate that the 180 000 protein is a major concanavalin A-binding glycoprotein previously identified as GP 180 (also known as T200) [1,40]. The binding specificity of GP 180 for concanavalin A was confirmed by its specific binding and elution from Con A-Sepharose columns [Fig. 1D). In addition to GP 180, at least three other cell-surface proteins, with molecular weights ranging from 130 000 to 70 000, were specifically bound and eluted from Con A-Sepharose.

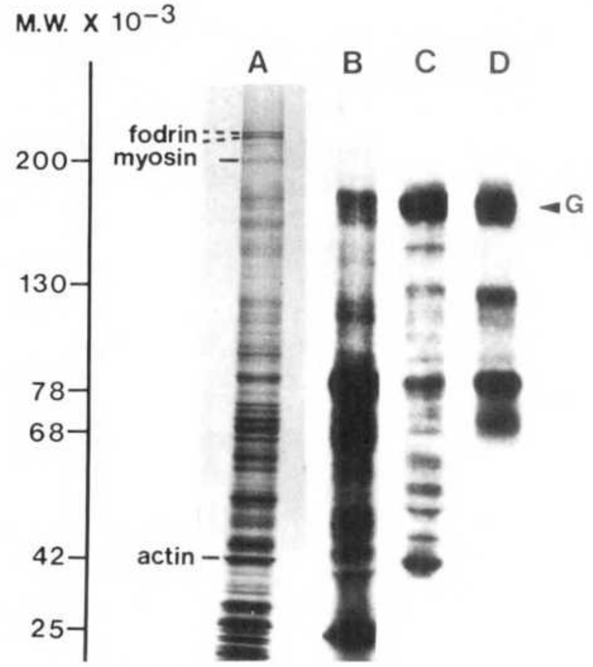

Fig. 1. Characterization of mouse T-lymphoma plasma membrane proteins. (A) Coomassie blue staining of total plasma membrane. (B) Autoradiogram of ^{125}I-surface-labeled plasma membrane. (C) Autoradiogram of total plasma membranes that are processed by SDS-polyacrylamide gel electrophoresis, electrophoretically transferred to nitrocellulose sheets, and then incubated with ^{125}I-labeled concanavalin A. G indicates the M_r 180000 (GP 180) band. (D) Autoradiogram of detergent solubilized, ^{125}I-labeled plasma membrane proteins that were bound to a Con A-Sepharose column and specifically eluted with methyl α-D-mannoside. (Molecular weight markers: myosin, 200000; β-galactosidase, 130000; lactoperoxidase, 78000; bovine serum albumin, 68000; actin, 42000; concanavalin A, 25000).

Characterization of the fodrin-GP-180-containing peak material

A fodrin-GP 180 complex can be routinely isolated by a selective Triton X-114 extraction procedure [1,41] followed by sucrose gradient centrifugation as described previously (Ref. 1; Fig. 2a, 2a-A; 2a-B). To characterize the fodrin-GP-180-containing peak material, we determined the sedimentation coefficient (S value) of the peak and the [^{35}S]methionine ratio of GP 180 to fodrin across the peak. Using 3.7 S G-actin [42] and 11 S tetrameric spectrin or fodrin [24] as protein standards, we were able to confirm that the sedimentation coefficient of the fodrin-GP 180 peak is 20 S (Fig. 2a). The relative ratio of fodrin to GP 180 in the individual gradient fractions corresponding to the 20 S peak was examined using plasma membrane isolated from cells metabolically labeled with [^{35}S]methionine. (Previously [1], we had pooled the 20 S peak fractions to estimate a 1 : 1 ratio of fodrin to GP 180.) The analysis was done on [^{35}S]methionine autoradiograms instead of Coomassie-blue-stained gel lanes because GP 180, like many other glycoproteins, does not stain well with Coomassie. The ratio of fodrin to GP 180 was determined by integration of the area under the respective peaks generated by scanning densitometry of SDS-electrophoresis autoradiograms. For our ratio calculations we compared relative arbitrary units of fodrin and GP 180. The relative ratio of fodrin to GP 180 is constant across the 20 S peak (compare Figs. 2a and 2b), suggestive of a specific association between fodrin and GP 180. Similar results were also obtained following the analysis of total ^{125}I-labeled and silver-stained 20 S material (data not shown).

Next, we wanted to examine the effect of high salt on the components of the 20 S peak, since similar treatments have been shown to dissociate fodrin from membranes [21,22] and spectrin from the band 3-ankyrin complex of erythrocytes [34]. Following incubation in 0.6 M NaCl, the ^{125}I-labeled GP 180 exhibits a lower sedimentation coefficient (Fig. 3b) than the control (Fig. 3a). When compared to ^{125}I-labeled transferrin with an average S value of 5 [43], the high-salt-treated peak has an apparent S value of 9. The control peak retains an S value of 20, identical to the value calculated during the original isolation procedure (Fig. 2). Parallel high-salt and control gradients containing ^{125}I-labeled transferrin were run to demonstrate that the high salt gradient has no apparent effect on S value. Note that the ^{125}I-labeled 9 S peak obtained under high-salt conditions displayed a significant shoulder, with an S value of more than 10. When all the 9 S peak material is collected (including the shoulder), and dialyzed against physiological strength buffer (0.15 M NaCl), the 20 S peak is partially reformed (data not shown). Previous controls demonstrated that tetrameric fodrin, with an S value of 11, would be included in the shoulder of the 9 S peak.

Further analysis indicates that both native fodrin-GP 180 (20 S) complex (Fig. 2a and 3a) and GP 180 (9 S) (Fig. 3b), but not fodrin (Fig. 4b) bind specifically to Con A-Sepharose and can be eluted by the sugar, methyl α-D-mannoside (Fig. 4a). In order to demonstrate the direct binding between fodrin and GP 180, in the absence of high salt, an in vitro reassembly assay that involves the addition of ^{125}I-labeled fodrin to 9 S, GP 180 material bound to a Con A-Sepharose column was performed. Our data reveals that ^{125}I-labeled fodrin can associate with GP 180 as shown by the following two pieces of evidence: (1) the ^{125}I-labeled fodrin-GP 180-Con A-Sepharose bound material was eluted by the specific sugar, methyl α-D-mannoside, suggesting the co-elution of ^{125}I-labeled fodrin and GP 180; and (2) the sugar eluted material containing the newly formed ^{125}I-labeled fodrin-GP 180 complex displayed a sedimentation coefficient of 20 S (Fig. 5), similar to that of the native fodrin-GP 180 complex (Figs. 2a and 3a). (A parallel gradient of 9 S, GP 180 alone was run as a control (Fig. 5).) Our data demonstrate that fodrin and GP 180 can be dissociated and reassembled in the presence and absence of high salt, respectively, implying that the binding between these two molecules is rather specific.

To provide further evidence of a close association between fodrin and GP 180 in the 20 S peak, we immunoprecipitated fodrin from the ^{125}I-labeled GP 180-containing 20 S peak material using an anti-fodrin antibody. Analysis of the precipitated proteins by SDS-electrophoresis and silver staining [44], demonstrated that fodrin was the major visible protein precipitated from the 20

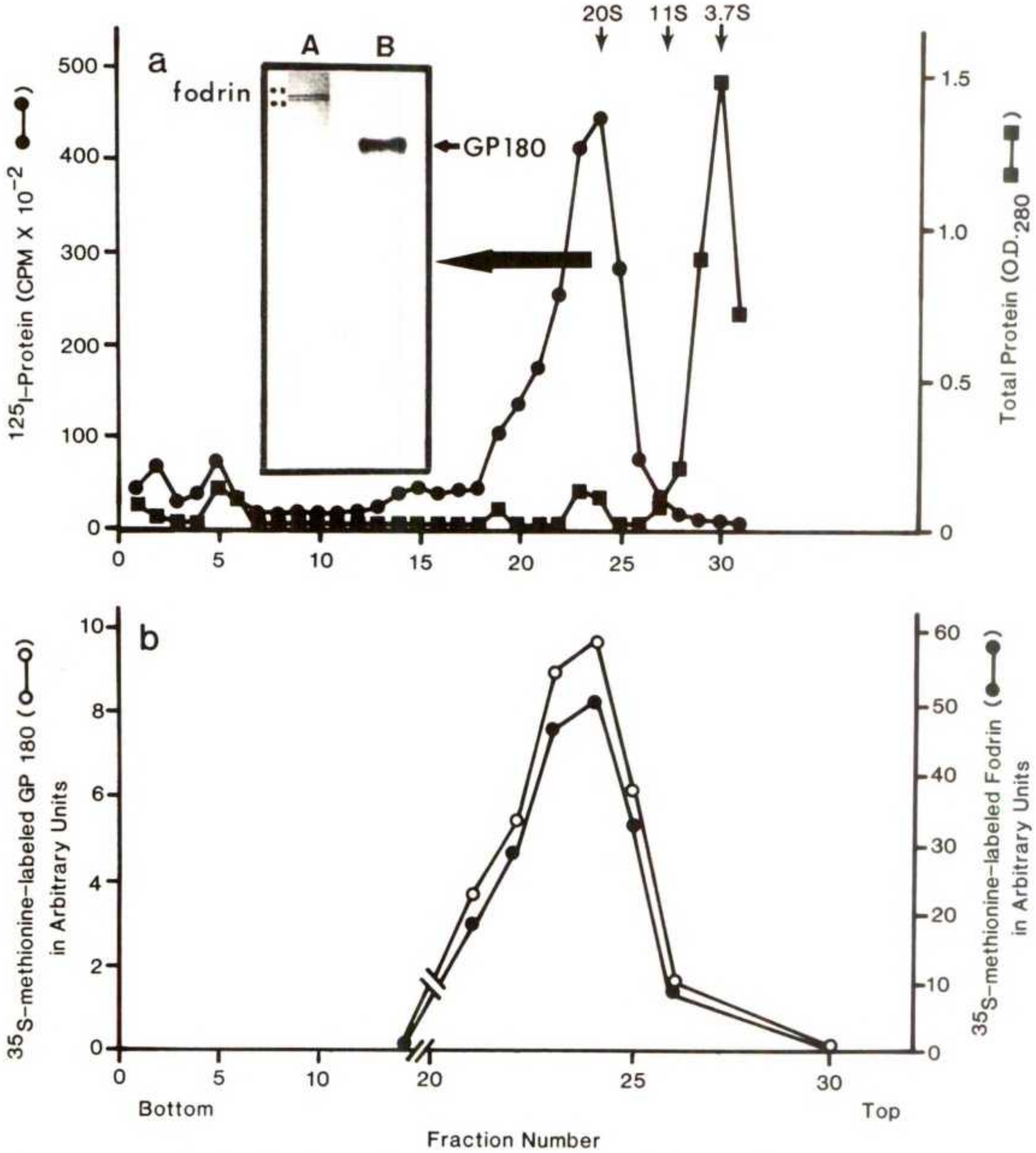

Fig. 2. Analysis of ^{125}I-labeled Triton X-114 aqueous phase by sucrose gradient centrifugation. (a) The total protein profile as determined by absorbance at 280 nm (■) vs. the ^{125}I-labeled proteins (●). Protein standards of G-actin and tetrameric spectrin or fodrin with respective S values of 3.7 and 11 were used to determine the S value of the ^{125}I-labeled peak. (A and B): SDS-polyacrylamide gel electrophores analysis of the pooled ^{125}I-labeled 20 S peak fractions with Coomassie blue staining pattern (A) showing the actin-binding protein, fodrin (240/235) and corresponding autoradiogram (B) demonstrating the presence of ^{125}I-labeled GP 180. (b) Profiles of [^{35}S]methionine-labeled GP 180 and fodrin across the 20 S peak fractions indicated in (a). The relative ratios of fodrin (●) and GP 180 (○) were calculated from densitometry tracings of autoradiograms obtained from individual fractions within the peak. Similar results were also obtained with both ^{125}I-labeled and silver-stained material.

S peak material (Fig. 6A). A band in the range of M_r 180000 suggested that GP 180 was co-precipitated along with fodrin. Autoradiographic analysis of this same gel lane confirmed the presence of GP 180 in the immunoprecipitated material (Fig. 6B). Analysis of this immunoprecipitated material

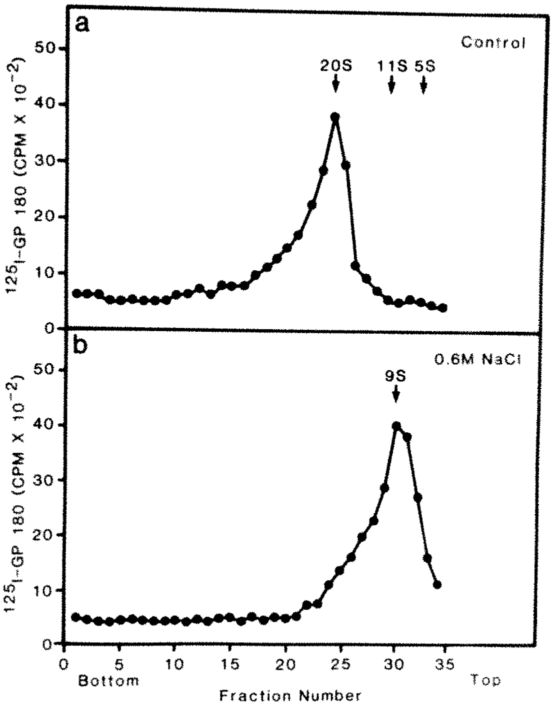

Fig. 3. High-salt treatment of the 20 S, ^{125}I-labeled GP 180-containing material. (a) Sucrose gradient centrifugation of the control 20 S material. (b) Sucrose gradient centrifugation of the 20 S material after exposure to 0.6 M NaCl. Following high-salt treatment the 20 S, GP 180-containing material is reduced to a value of 9 S.

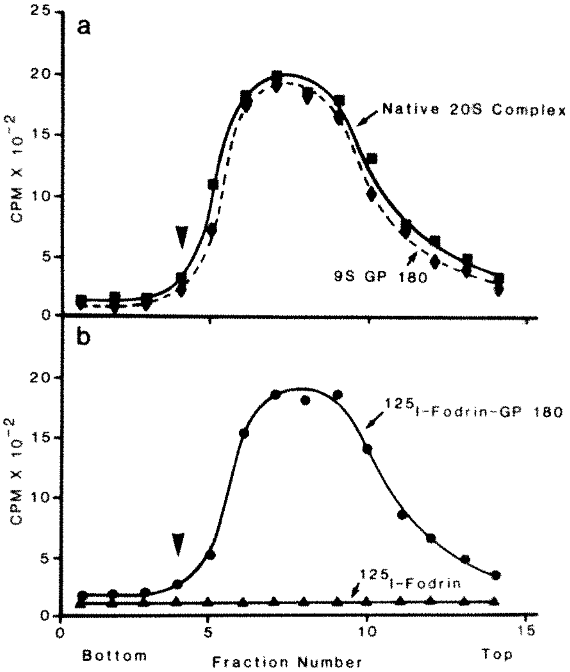

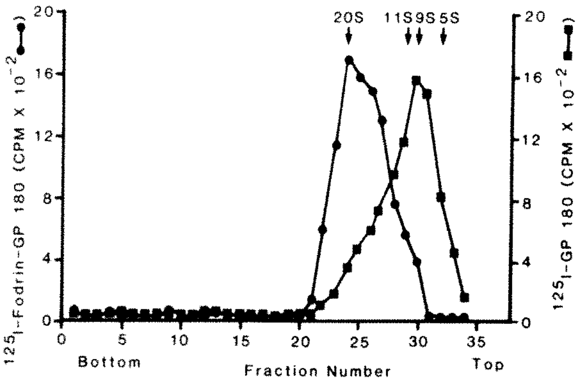

Fig. 5. Sucrose gradient centrifugation of newly formed ^{125}I-labeled fodrin-GP 180 material (prepared according to the procedure outlined in Materials and Methods and shown in Fig. 4b (●)) eluted from Con A-Sepharose by the addition of methyl α-D-mannoside. The ^{125}I-labeled fodrin containing material (●) sediments with a sedimentation coefficient of approx. 20 S, indicating that the fodrin-GP 180 complex can be assembled by the addition of exogenous fodrin. A parallel gradient of 9 S, ^{125}I-labeled GP 180-containing material alone, sugar eluted from a Con A-Sepharose column, was run as a control (■). Protein standards of G-actin (3.7 S), transferrin (5 S), and tetrameric fodrin or spectrin (11 S) were used to determine S value.

indicates that fodrin and GP 180 appear in a ratio similar to that observed in the 20 S peak fractions (Fig. 2) and in our previously published immunoprecipitation experiments [1]. The control precipitate showed neither fodrin (Fig. 6C) nor GP 180 (Fig. 6D). These data provide more evidence that GP 180 and fodrin are specifically associated in the 20 S peak.

Fig. 4. In vitro reassembly of exogenous pig brain fodrin with lymphocyte GP 180. (a) Con A-Sepharose binding properties of native 20 S complex and 9 S, GP 180. Native 20 S, fodrin-^{125}I-labeled GP 180 complex (■) is first bound to a Con A-Sepharose column and then specifically eluted by addition of the sugar, methyl α-D-mannoside (arrowhead). This parallels the pattern of binding and elution of 9 S, GP 180 (◆). b. Binding of ^{125}I-labeled fodrin to a GP 180-Con A-Sepharose column and specific elution with the sugar, methyl α-D-mannoside. ^{125}I-labeled fodrin is bound to GP 180 (9 S)-Con A-Sepharose (●) and then specifically eluted following the addition of the sugar, methyl α-D-mannoside (arrowhead). ^{125}I-labeled fodrin that is nonspecifically bound to Con A-Sepharose in the absence of GP 180 (▲) is not eluted by the addition of sugar. The elution of ^{125}I-fodrin from the GP 180-Con A-Sepharose column parallels that of both 9 S, GP 180 alone and the native 20 S, fodrin-GP 180 complex.

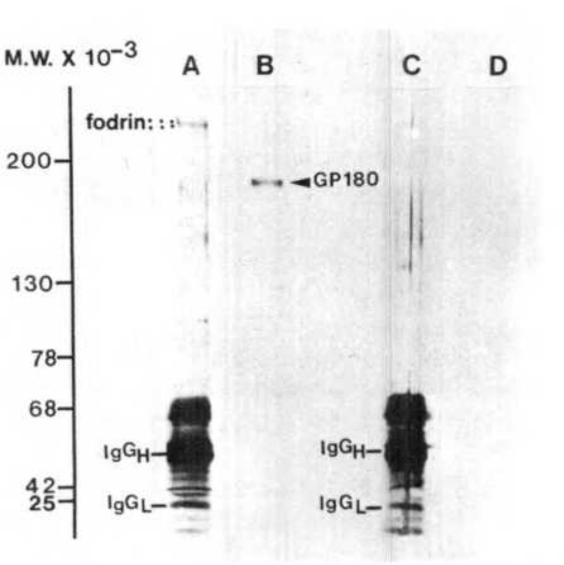

Fig. 6. Immunoprecipitation of the 20 S peak material with rabbit anti-fodrin antibody followed by goat anti-rabbit immunoglobulin (IgG). (A) Silver staining pattern of the immunoprecipitate showing fodrin as the major specific precipitated protein. (B) Corresponding autoradiogram indicating the co-precipitation of GP 180. (C) Control lane showing the nonspecifically precipitated bands and (D) the corresponding control autoradiogram indicating the absence of GP 180 (IgG_H = heavy chain of IgG; IgG_L = light chain of IgG).

Additional evidence that fodrin is associated with GP 180 in the 20 S peak came from examining the localization of these proteins along actin filaments formed in the presence of the 20 S complex material. The localization of fodrin using anti-fodrin antibody followed by protein A-gold showed labeling of small clusters along actin filaments (Fig. 7a and 7b). A very similar labeling pattern was observed when the distribution of GP 180 along actin filaments, using anti-GP 180 antibody followed by protein A-gold, was examined (Fig. 7c and 7d). No labeling was observed on control grids that were either treated with fodrin or GP 180 pre-adsorbed serum or in which the primary antibody step was omitted.

Since the 20 S, fodrin-GP 180-containing peak material was shown to be associated with F-actin filaments by cytochemical procedures, we decided to examine biochemically its ability to bind actin. When isolated ^{125}I-labeled 20 S peak material is incubated in the presence of actin, it moves farther into the sucrose gradient than control material (Fig. 8). Protein standards demonstrated that the actin-incubated material had sedimentation coefficient of 34 S. The increased S value indicated that

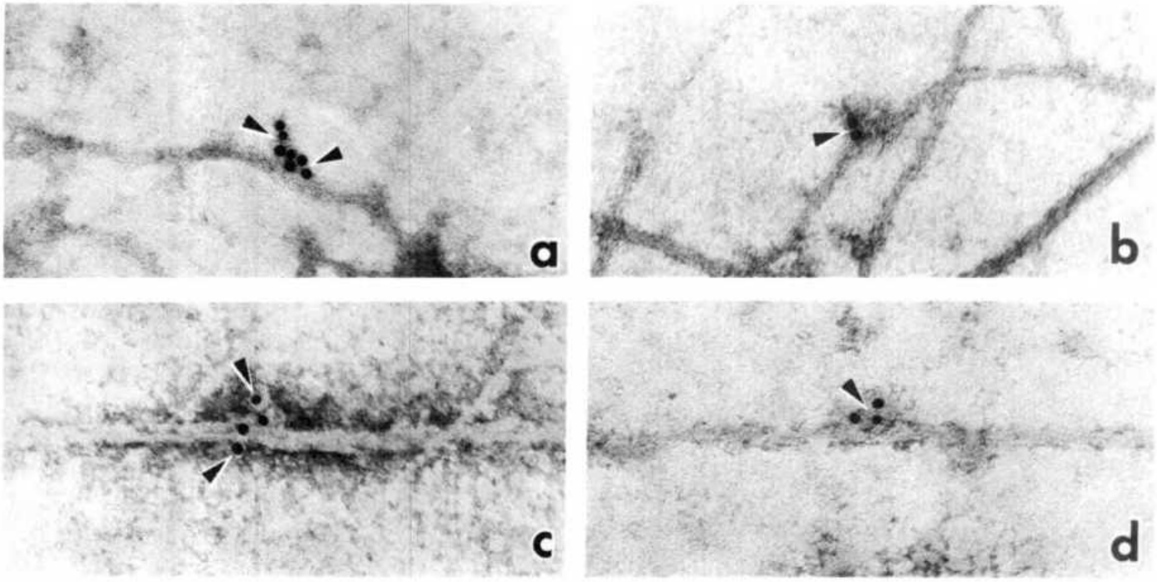

Fig. 7. Immuno-gold localization of both GP 180 and fodrin on actin filaments that were formed in the presence of the 20 S, GP 180-fodrin containing material. (a and b) Negative-stain image of actin filaments showing the association of fodrin (arrowheads; 108000). (c and d) Negative-stain image of actin filaments showing the association of GP 180 (arrowheads; 108000).

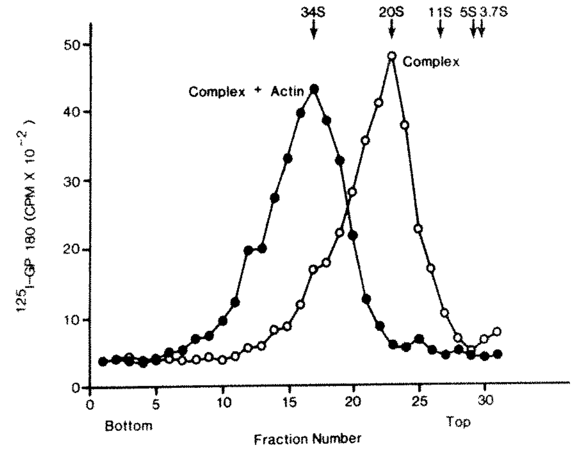

Fig. 8. The ^{125}I-labeled 20 S peak material was incubated with G-actin under polymerizing conditions and then analyzed by sucrose gradient centrifugation. Following incubation with actin, the S value of the complex shifted from 20 S to 34 S, indicating that the complex has the ability to bind to actin. Fodrin (11 S), transferrin (5 S) and G-actin (3.7 S) were used as protein standards of known S values.

the isolated 20 S peak could bind actin. Actin binding with the fodrin and GP 180 complex was verified by SDS-electrophoretic analysis (data not shown). The immuno-gold localization of fodrin and GP 180 along the actin filaments in the 34 S peak fractions was very similar to that observed in Fig. 7 (data not shown). The results from these aforementioned experiments, examined as a whole, suggest that lymphoma fodrin and GP 180 are closely associated as a stable transmembrane complex with the ability to bind actin. This transmembrane complex might thereby mediate or participate in the interaction of cell-surface receptors with the cytoskeleton during patching/capping in mouse T-lymphocytes.

Discussion

Previously, we have identified a transmembrane complex from T-lymphoma plasma membrane that may play a role in linking one or more surface receptors to the cytoskeleton during ligand-induced cell-surface capping or other cytoskeleton-mediated surface events [1]. In this study, we have carried out further structural analysis of this transmembrane complex in order to understand the linkage properties between membrane protein (s) and the cytoskeleton. One of the proteins in this complex, GP 180, is a transmembrane glycoprotein that has been shown to be very similar if not equivalent to T-200 (a major T-lymphocyte-specific glycoprotein) [1]. Like T200 [40], GP 180 binds concanavalin A and can be specifically eluted from columns of Con A-Sepharose.

During Triton X-114 extraction of mouse T-lymphoma membranes, GP 180 partitions into the Triton X-114 aqueous phase along with such cytoskeletal proteins as actin and the actin-binding protein, fodrin [1]. For this reason, we hypothesized that GP 180 might be closely associated with certain hydrophilic cytoskeletal components in unstimulated lymphoma cells. Glenney and Glenney [6] used this same type of extraction procedure to isolate the M_r 110000 brush-border protein from other cytoskeletal proteins and characterize it as an integral membrane protein.

Further analysis of the aqueous phase of Triton X-114-extracted ^{125}I-labeled lymphoma membranes enabled us to identify a distinct peak on sucrose density gradients in which ^{125}I-labeled GP 180 and the actin-binding protein, fodrin, are major components (Fig. 2; Ref. 1). The co-sedimentation of fodrin and GP 180 suggests that these two proteins may be closely associated. Carraway et al. [7] have used similar separation procedures to isolate a transmembrane protein-actin complex from detergent-extracted microvillar membranes. Our ability to co-isolate fodrin and GP 180 from this 20 S peak material with anti-fodrin antibody (data not shown) further strengthens the evidence that GP 180 and fodrin are specifically associated.

By running protein standards with known S values during the isolation of the GP 180 containing material on sucrose gradients, we were able to calculate a sedimentation coefficient of 20 S for the associated fodrin-GP 180 material. To determine the fodrin : GP 180 ratio throughout the 20 S, GP 180-containing peak, we isolated this material from cells metabolicity labeled with [^{35}S]methionine. SDS-electrophoresis autoradiography followed by scanning densitometry of the autoradiogram established a constant ratio of fodrin to GP 180 across the 20 S peak. In addition, these two proteins appear to be labeled to a similar extent by silver staining, ^{125}I-labeling, and [^{35}S]methionine labeling. Therefore, it is possible for us to speculate on the stoichiometry of these proteins based on the following assumptions. The assumptions are: (1) fodrin is present in a tetrameric form (combined M_r 950 000); (2) GP 180 is present in a monomeric form (M_r 180 000); and (3) both proteins are labeled equivalently. According to the aforementioned assumptions, we can calculate a 1 : 1 molar ratio of fodrin to GP 180 in the pooled fractions of the 20 S peak as described previously [1]. In this study, the results of similar calculations also reveal a 1 : 1 molar ratio of fodrin to GP 180 in the individual fractions across the 20 S peak. Therefore, we believe that a close association exists between these two molecules. The same 1 : 1 molar ratio has been demonstrated for the ankyrin-band 3 transmembrane complex from erythrocytes [34], and the actin-CAG transmembrane complex from the microvillar membranes of ascites tumor cells [7].

Following exposure to the same high salt conditions previously used to remove fodrin from membranes [21,22], the ^{125}I-labeled GP 180 containing material sediments at an S value of 9, less than that estimated for isolated tetrameric fodrin (11 S). This reduced S values suggested that fodrin was separated from GP 180 under high-salt conditions. Similar high-salt conditions have been shown to cause the dissociation of the ankyrin-band 3 complex from spectrin [34]. The shift in S value of the GP 180, 9 S peak material to its original 20 S value can occur following the binding of ^{125}I-labeled fodrin to 9 S, GP 180 in the absence of high salt (Fig. 4). These data suggest that these two proteins are able to reassemble as a transmembrane complex. Most importantly, our reassociated fodrin-GP 180 complex also displays lectin-binding properties similar to those of the native 20 S complex, implying that the in vitro assembly of these two proteins may be similar to that of the native complex. Our ability to high-salt-dissociate the 20 S, fodrin-GP 180-containing material and then reform it by the addition of fodrin to the 9 S, GP 180-containing material in the absence of high salt further corroborates our evidence that there is an interaction between fodrin and GP 180.

Both cytochemical (Fig. 7) and biochemical (Fig. 8) data indicate that the 20 S, fodrin-GP 180 complex is capable of binding F-actin. In addition, the amount of both fodrin and GP 180 in the actin-containing cytoskeleton increases significantly during lymphocyte patching and capping [1,27]. Since fodrin is an actin-binding protein, it is reasonable to assume that, functionally, the interaction of the fodrin-GP 180 complex with actin is through fodrin.

From this study, we have further demonstrated that fodrin is closely associated with a specific transmembrane protein, GP 180, in T-lymphoma plasma membranes. Additionally, this transmembrane complex has the ability to interact with actin, and such an interaction may be responsible for the linkage of the GP 180 receptor to the cytoskeleton. Apparently missing from our fodrin-GP 180 complex is an ankyrin-like or 4.1-like protein, spectrin-binding proteins that appear to mediate the binding of spectrin to erythrocyte membranes [23,45]. Although both an ankyrin-like protein and a 4.1-like protein have been localized in the subcap region of capped lymphocytes [27,46,47], and polypeptides of both proteins have been isolated from lymphocytes [46,47], these proteins have not been successfully identified in our 20 S material. It is possible that these proteins (present in small quantities in the complex) are responsible for linking GP 180 and fodrin. Alternatively, GP 180 may itself have certain ankyrin-like or 4.1-like fodrin-binding properties in its cytoplasmic domain that allows it to bind directly to fodrin in mouse T-lymphoma cells. This possibility is under active investigation in our laboratory.

Acknowledgements

We thank Dr. J.E. Magnusen for help in the preparation of this manuscript and Dr. K.L. Carraway for suggestions and reading this article. This work was supported by U.S. Public Health Grants AI 19188 and GM 36353; NIH grant DRR, S07 RR 05 363 awarded under the Biomedical Research Support Grant Program, American Cancer Society, Florida Division Grant No. F86UM-3, and American Heart Association grants. L.Y.W.B. is an Established Investigator from the American Heart Association.

References

1 Bourguignon, L.Y.W., Suchard, S.J., Nagpal, M.L. and Glenney, J R., Jr. (1985) J. Cell Biol. 101, 477–487

2 Geiger, B. (1983) Biochim. Biophys. Acta 737, 305–341

3 Bennett, V. and Stenbuck, P J. (1979) Nature (Lond) 280, 468–473

4 Branton, D., Cohen, C.M. and Tyler, J. (1981) Cell 24, 24–32

5 Matsudaira, P.T. and Burgess, D.R. (1979) J Cell Biol. 83, 667–673

6 Glenney, J.R and Glenney, P. (1984) Cell 37, 743–751

7 Carraway, C.A C., Jung, G. and Carraway, K L. (1983) Proc Natl. Acad. Sci. USA 80, 430–434

8 Bourguignon, L.Y.W. and Singer, S.J. (1977) Proc Natl Acad. Sci USA 74, 5031–5035

9 Bourguignon, L Y.W , Hyman, R., Trowbridge, I. and Singer, S.J. (1978) Proc. Natl. Acad Sci. USA 75, 2406–2410

10 Flanagan, J. and Koch, G.L.E (1978) Nature (Lond) 273, 278–281

11 Braun, J., Hochman, P S. and Unanue, E.R. (1982) J Immunol. 128, 1198–1204

12 Bennett, V and Stenbuck, P J (1979) J Biol Chem. 254, 2533–2541

13 Anderson, R.A. and Lovrien, R E. (1984) Nature 307, 655–658

14 Pasternak, G R., Anderson, R A , Leto, T L. and Marchesi, V.T. (1985) J. Biol. Chem 260, 3676–3683

15 Geiger, B. and Singer, S.J. (1979) Cell 16, 213–222

16 Hoessli, D., Rungger-Brandle, E , Jockusch, B.M. and Gabbiani, G. (1980) J Cell Biol 84, 305–314

17 Osborn, M and Weber, K. (1977) Exp Cell Res 106, 339–349

18 Bourguignon, L.Y.W., Nagpal, M. and Hsing, Y.C. (1981) J. Cell Biol. 91, 889–894

19 Bourguignon, L.Y.W., Nagpal, M.L., Balazovich, K., Guerriero, V and Means, A.R. (1982) J. Cell Biol. 95, 793–797

20 Kerrick, W G.L and Bourguignon, L.Y.W. (1984) Proc Natl Acad Sci USA 81, 165–169

21 Levine, J. and Willard, M. (1981) J. Cell Biol 90, 631–643

22 Bennett, V., Davis, J. and Fowler, W.E (1982) Nature (Lond.) 299, 126–131

23 Burridge, K., Kelly, T and Mangeat, P. (1982) J Cell Biol. 95, 478–486

24 Glenney, J.R., Jr., Glenney, P., Osborn, M. and Weber, K. (1982) Cell 28, 843–854

25 Glenney, J.R., Jr., Glenney, P. and Weber, K. (1982) J. Biol. Chem. 257, 9781–9787

26 Glenney, J R., Jr., and Glenney, P. (1983) Cell 34, 503–512

27 Bourguignon, L Y.W and Bourguignon, G.J. (1984) Int. Rev. Cytol. 87, 195–224

28 Levine, J. and Willard, M. (1983) Proc. Natl. Acad. Sci. USA 80, 191–195

29 Nelson, W J., Colaco, C.A.L. and Lazarides, E (1983) Proc. Natl. Acad Sci. USA 80, 1626–1630

30 Fraker, P.J. and Speck, J C., Jr. (1978) Biochem. Biophys. Res. Commun. 80, 849–857

31 Burnette, W.N. (1981) Anal Biochem. 112, 195–203

32 Laemmli, U.K. (1970) Nature (Lond.) 227, 680–685

33 Bonner, W.M. and Laskey, R.A. (1974) Eur. J. Biochem 46, 83–88

34 Bennett, V. (1982) Biochim. Biophys Acta 689, 475–484

35 Trowbridge, I.S and Mazauskas, C. (1979) Eur. J Immunol. 6, 557–562

36 Pardee, J.D. and Spudich, J A (1982) in Methods in Cell Biology (Wilson, L , ed), Vol 24, pp. 271–289, Academic Press, New York

37 Pearl, M., Fishkind, D., Mooseker, M., Keene, D. and Keller, T , III (1984) J. Cell Biol 98, 66–78

38 Slot, J.W. and Geuze, H.J. (1981) J Cell Biol. 90, 533–536

39 Hinkley, R.E. (1976) J. Ultrastruct. Res. 57, 237–250

40 Trowbridge, I.S., Nilsen-Hamilton, M., Hamilton, R.T., and Bevan, M.J (1977) Biochem J. 163, 211–217

41 Bordier, C. (1981) J Biol. Chem. 256, 1604–1607

42 Sheeler, P. (1981) Centrifugation in Biology and Medical Science, p. 26, John Wiley & Sons, New York

43 Smith, M.H (1968) in CRC Handbook of Biochemistry. Selected Data for Molecular Biology (Sober, H.A., ed.), pp. C3-C193, Chemical Rubber Co., Cleveland, OH

44 Merril, C.R., Goldman, D., Sedman, S.A. and Ebert, M.H. (1981) Science 211, 1437–1438

45 Bennett, V. (1985) Annu. Rev. Biochem 54, 273–304

46 Bourguignon, L.Y.W., Walker, G., Suchard, S J. and Balazovich, K.J. (1986) J Cell Biol. 102, 2115–2124

47 Bourguignon, L.Y.W., Suchard, S.J., and Kalomiris, E.L. (1986) J. Cell Biol. 103, 5229–2540.

Biochimica et Biophysica Acta 896 (1987) 47–51
Elsevier

BBA 73179

Divalent cation effects on the binding of human anti-phospholipid antibodies

F.A. Green and P.B. Costello

Departments of Medicine and Microbiology, State University of New York at Buffalo and the Veterans Administration Medical Center, Buffalo, NY (U.S.A.)

(Received 15 August 1986)

Key words: Anti-phospholipid antibody; Cardiolipin; Magnesium ion; Calcium ion; Phospholipid structure

(1) Anti-phospholipid antibodies from sera of subjects with documented syphilis were measured as a result of their individual interactions with cardiolipin, phosphatidylserine and phosphatidic acid, each impregnated in nitrocellulose paper from chloroform solution, followed by reaction with a labelled second antibody. Binding curves generated by increasing the cardiolipin concentration over a standard area of nitrocellulose paper showed saturation. (2) The presence of Ca^{2+} or Mg^{2+} during the antibody binding step resulted in a complex pattern of binding as a function of the cation concentration. When the extent of binding was normalized to percent of maximum bound, virtually superimposible patterns were seen with different sera. These patterns were distinctive for both the phospholipid and the cation. (3) The speculation is presented, albeit without any direct evidence, that the extent of antibody binding is sensitive to a variety of intermediate phospholipid phase structures which may be initiated by the presence of the specific divalent cation at a particular concentration.

Introduction

The influences of individual phospholipids on membrane structure/function, and membrane-bound enzyme activity are fundamental biological characteristics about which much has yet to be learned [1]. Cardiolipin, 1,3-diphosphatidylglycerol [2], is curious in that it is present in substantial concentration in mammals only in the inner leaf of the mitochondrial membrane [3] where it has an important role in cytochrome *c* oxidase [4] and cytochrome P-450_{scc} activities [5]. Antibodies to cardiolipin have been well described in patients with syphilis [6] and more recently in patients with systemic lupus erythematosus [7] where there could be important clinical correlations [8]. The biological significance of these antibodies is not clear [9] and the phospholipid-antibody interactions have not been well characterized in molecular terms.

The traditional method of measuring anti-cardiolipin antibodies by flocculation tests appears to require other phospholipids and cholesterol [10] which may not be central to the antigen-antibody interaction. The requirement of the test for secondary interactions may be one of the reasons for conflicting results of measurements based on flocculation to answer questions regarding the antibody interactions with caridolipin, phosphatidylcholine, and cholesterol [9]. There is no doubt, however, that the active phospholipid is diphosphatidylglycerol and that the synthesized phospholipid reacts well in flocculation tests [11].

We have previously demonstrated that syphilitic sera contain antibodies to cardiolipin, phosphatidic acid, and phosphatidyl serine [12]. In the

---

Correspondence: Dr. F.A Green, Department of Medicine, State University of New York at Buffalo, 3495 Bailey Avenue, Buffalo, NY 14215, U.S A

0005-2736/87/$03.50 © 1987 Elsevier Science Publishers B.V. (Biomedical Division)

present studies we measured specific and reproducible effects of Ca^{2+} and Mg^{2+} on antibody binding to phospholipids impregnated in nitrocellulose paper. The observed binding patterns in the presence of the cations showed striking similarity using different sources of donor serum and were specific to the phospholipid.

Materials and Methods

Normal human sera were obtained from the Red Cross (Buffalo, NY), and sera from syphilitic patients were obtained through the courtesy of the Public Health Division of the Erie County Laboratories. The latter were defined as sera exhibiting positive flocculation tests in routine screening procedures for syphilis, and positivity in two specific tests for spirochetal antigens. Affinity purified goat anti-human IgG was obtained from Bio-Rad Laboratories (Rockville Center, NY) and rabbit anti-human IgG from Jackson ImmunoResearch Laboratories (Avondale, PA). [1-^{14}C]Acetic anhydride (30–40 mCi/mmol) was obtained from New England Nuclear (Boston, MA). The purified antibody was labelled with [^{14}C]acetic anhydride as previously described [13]. The labelled second antibodies from goat and rabbit sources could be used interchangeably. Measurement of the specific activity of the labelled antibody protein permitted the conversion from disintegrations per minute to moles of second antibody. The phospholipids were obtained from Sigma Chemical Company (St. Louis, MO) and from Avanti Polar Lipids (Birmingham, AL). These were studied for purity in two-dimensional thin-layer chromatography as previously described [14]. Lipid phosphorus was measured with the Barlett technique [15].

Cardiolipin (bovine heart), phosphatidylserine (bovine brain), and phosphatidic acid (egg yolk) were dried separately under ultrapure nitrogen and dissolved in chloroform in the specified concentrations. 5-μl aliquots were spotted on circles of nitrocellulose paper (Bio-Rad) which had been cut into 1-cm diameter membranes. After drying, these membranes were then blocked for 1 h in a buffer containing 0.05 M Tris (pH 7.4), 0.15 M NaCl, 0.05% Tween 20, 0.02% NaN_3 and 3% gelatin and added cation were indicated. The papers were then incubated overnight at room temperature with the sera in dilutions of 1 : 50 to 1 : 1000 in blocking buffer to a final volume of 4.0 ml. The papers were then washed three times in the same buffer.

The circles were reacted for 1 h with ^{14}C-labelled anti-human IgG, diluted 1 : 200 in 20 mM phosphate (pH 7.4) containing 150 mM NaCl in a final volume of 10 ml. After washing, the circles were placed in suitable scintillation media and the radioactivity was measured in a Packard 460CD scintillation counter.

The cations were tested in the form of $MgCl_2$ and $CaCl_2$, EDTA or EGTA at the concentrations specified, and were added to the blocking buffer during the serum incubation. Membranes with no added phospholipid were used for the assessment of the non-specific binding of IgG from the patients' serum to nitrocellulose paper. Such binding was usually very low, was almost linear in form, and was subtracted for most calculations. There was negligible binding of the diluted labelled second antibody to the nitrocellulose paper itself and to the paper with phospholipid but without human serum.

Results

Fig. 1 shows binding curves of two individual sera from patients with syphilis and two normals. The binding of ^{14}C-anti-IgG was measured as a function of the amount of cardiolipin added. It can be seen that the binding curves for syphilitics rose fairly steeply to plateau levels at approximately 50 nmol of cardiolipin. The measurement at zero cardiolipin concentration gave an indication of the non-specific binding to nitrocellulose paper. Further inspection of these binding curves revealed that at the plateau binding level one antibody molecule was bound per 8000 molecules of antigen.

In Fig. 2 the binding of labelled anti-IgG was measured as a function of the concentration of Mg^{2+} added at plateau levels of other reactants. Data are shown for cardiolipin and for phosphatidylserine. It is apparent in the case of cardiolipin that the binding first decreased slightly, exhibited an apparent peak at 1 mM, then a later rise. The pattern with phosphatidylserine was quite different, showing a broader peak at lower con-

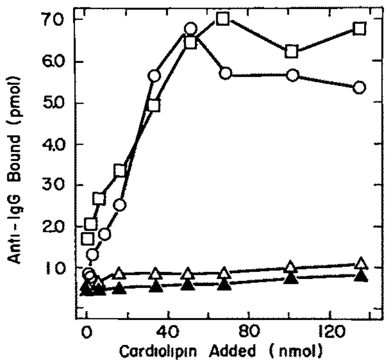

Fig 1. Binding curves of two sera from syphilitic subjects (open squares, open circles) and two normals (open triangles, closed triangles). Cardiolipin in chloroform in the indicated amounts was spotted on 1 cm diameter nitrocellulose papers, dried, blocked and 50 μl sera added for overnight incubation. After washing, ^{14}C-labelled goat anti-human IgG was added as indicated in Methods.

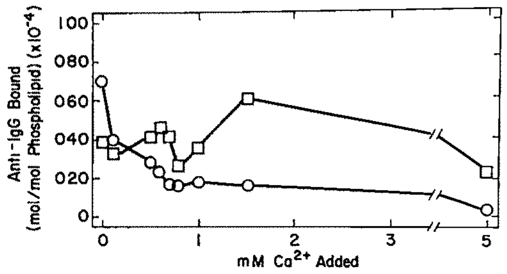

Fig. 3 Effect of Ca^{2+} on anti-phospholipid antibody binding Cardiolipin (open squares), phosphatidylserine (open circles)

centrations of Mg^{2+} and clearly no peak at 1 mM. The effects of Mg^{2+} on antibody binding to these phospholipids was reproducible. For cardiolipin, antibody binding peaked at exactly 1.0 mM Mg^{2+} in 11 of 15 experiments. For phosphatidylserine, binding peaked at 0.75–0.80 mM Mg^{2+} in 4 of 4 experiments. Binding patterns were otherwise similar for each phospholipid.

In Fig. 3 the data for Ca^{2+} and the same two phospholipids are illustrated. There was no increased binding over the amount measured with no added cation and no peak at 1 mM, but a small one at 1.5 mM. A total of six experiments with cardiolipin and Ca^{2+} was done. In each case a decrease in binding was evident in the 0.8–0.9 mM Ca^{2+} range. The small peak at 1.5 mM Ca^{2+} was less consistently seen (2 of 6 experiments). For phosphatidylserine the curve was less dramatic showing an irregular decrease in the amount of binding with increased Ca^{2+}. The same pattern of antibody binding was seen in three additional experiments with Ca^{2+} and phosphatidylserine.

In Fig. 4, data have been normalized by referring the extent of binding to the percent of maximum achieved. In these experiments, anti-cardiolipin antibody binding was measured in three additional individual sera from syphilis patients as a function of the concentration of Mg^{2+} added. Antibody binding was decreased in the

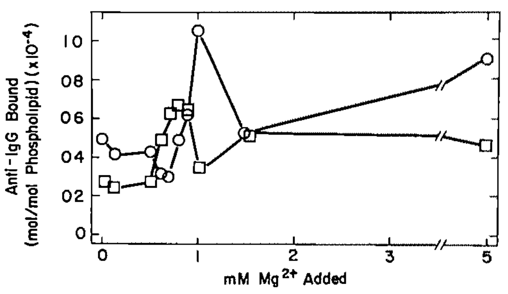

Fig. 2. Effect of Mg^{2+} on anti-phospholipid antibody binding Extent of anti-human IgG bound using constant serum concentrations (50 μl) from a patient with syphilis, and constant phospholipid (100 μmol). Cardiolipin (open circles), phosphatidylserine (open squares), and increasing concentrations of added Mg^{2+} during the blocking and human serum incubation stages. Otherwise as in Fig. 1.

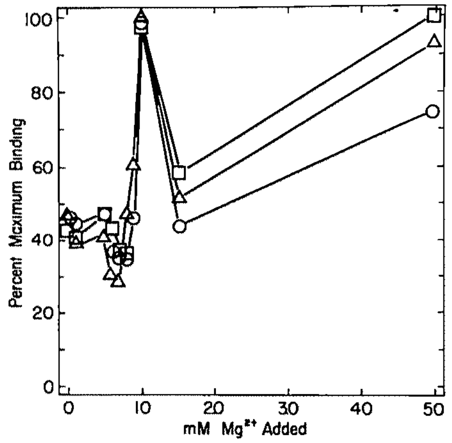

Fig. 4. Effect of Mg^{2+} on human antibody binding to cardiolipin Binding data for sera from three additional syphilitic subjects are presented, normalized to percent maximum bound.

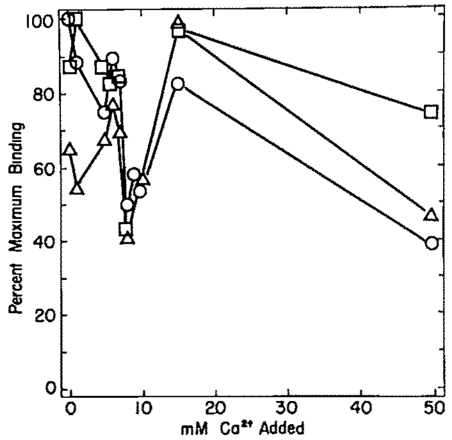

Fig 5 Effect of Ca^{2+} on human antibody binding to cardiolipin, normalized to maximum percent bound Otherwise as in Fig 4.

concentration range of 0.5 to 1.0 mM but a peak at 1mM was noted which was approximately twice the control value. Although the absolute extent of binding in these three sera was substantially different (data not shown) when the data were normalized the results were remarkably consistent with these sera as well as for others not shown. In general, there was a 2–4-fold increase in binding at 1 mM Mg^{2+} compared to control. Normalized data are also shown for Ca^{2+} in Fig. 5. In these sera there was slightly more variability but it is apparent that there was a reduction at just under 1 mM, no peak at 1 mM but a peak at 1.5 mM or higher. There is also either a peak or a shoulder at 0.6 mM. At higher concentrations of both Ca^{2+} and Mg^{2+} (20 mM) there was uniform depression of binding to near baseline levels (data not shown).

Discussion

In the system used for the present studies all syphilitic sera which were examined (more than 50) showed antibodies to cardiolipin, and most also to phosphatidylserine and to phosphatidic acid [12]. The latter were found at a lower level of binding activity and usually did not reach saturation under the conditions employed. With increasing amounts of Ca^{2+} and Mg^{2+}, a polyphasic pattern of binding was found, one which was specific to both the phospholipid and the cation.

When normalized to percent of maximum binding, the patterns were highly reproducible from serum to serum. The mechanism of the effect of phospholipid structural polymorphism on antibody binding is not clear. There would seem to be too much reproducibility among different serum samples for the explanation to simply be limitation of antibody access to closed structures. Furthermore, in preliminary experiments the hyperbolic (sometimes sigmoid) binding curves generated as a function of increasing serum concentration and with added Mg^{2+} (1.0 mM) became flattened in the presence of EGTA (1.0 mM). This would indicate that the cation had a significant effect on binding affinity. This in turn might suggest specific effects of phospholipid structural changes on antibody binding rather than simply being a function of limiting antibody excess.

Although the stoichiometry between the second antibody and the antibody to cardiolipin is not known the results are quite similar to what was found with ^{14}C-labelled protein A [12] where a 2:1 stoichiometry is known to exist [16]. In any case, one antibody molecule is apparently reacting with 5000 to 25 000 molecules of antigen. This observation itself could suggest a structural requirement, yet marked phospholipid specificity is retained. No reactivity was found, for example, with phosphatidylcholine or phosphatidylethanolamine. Interaction of hydrated cardiolipin might occur with the nitrocellulose paper itself, analogous to the charge mediated binding of phospholipids to glass [17]. Such interaction could have some effect on the apparently large molar ratio of cardiolipin molecules to antibody.

Extensive investigations have been made of the influence of divalent cations on the phase structures of phospholipids, including cardiolipin. X-ray diffraction [18] and ^{31}P-NMR techniques [19] have been employed to demonstrate that Ca^{2+} and Mg^{2+} could induce hexagonal (H_{II}) structures from bilayer phase cardiolipin in model systems. In the freeze-fracture system an intermediate phase which consisted of 'inverted' structures was evident [19]. These phase changes were evident in the 1–3 mM concentration range for Ca^{2+} in the case of bacterial cardiolipin [20]. The structure of the hydrated lipid in the nitrocellulose paper and on its surface is not known. Although the present studies do not directly address this question, one could hypothesize that cation induced intermediate phase phospholipid structures modulated the antibody binding patterns seen in syphilitic sera. In data not shown, high levels of divalent cation (20 mm) resulted in greatly reduced binding, both in the case of Ca^{2+} and Mg^{2+}. Although without supporting data, this might suggest that the polyphasic binding observed in the region of 1 mM could be due to the formation and possibly disappearence of (different) intermediate structures preceding hexagonal phase formation, and that this polymorphism greatly effects antibody binding.

Perhaps the most fascinating aspect of these studies is repeatibility of the pattern of binding with different concentrations of each cation in different syphilitic sera. That biological molecules in the form of human antibodies to phospholipid antigens are so strikingly sensitive to alterations in the cation environment opens up interesting possibilities to probe the structural/functional role of cardiolipin.

Acknowledgements

Supported by the Veterans Administration, the National Institute of Health HL 24009, and the Arthritis Foundation of Western New York.

References

1 Freedman, R.B. (1981) in New Comprehensive Biochemistry, Vol. 1 (Neuberger, A. and Van Deenen, L L M , Gen. eds., Finean, J.B. and Michell, R H., eds.), pp. 161–214, Elsevier/North-Holland, Amsterdam
2 De Haas, G.H., Bonsen, P.P.M and Van Deenen, L.L.M. (1986) Biochim. Biophys Acta 116, 114–124
3 Fleischer, S., Rouser, G., Fleischer, B., Casu, A. and Kritchevsky, G (1967) J Lipid Res. 8, 170–180
4 Robinson, N C. (1982) Biochemistry 21, 184–188
5 Lambeth, J.D. (1981) J. Biol. Chem 256, 4757–4762
6 Pangborn, M.C (1942) J. Biol. Chem. 143, 247–256
7 Hughes, G.R.V. (1984) Br. Med. J. 289, 339–342
8 Harris, E.N., Boey, M.L., Mackworth-Young, C.G., Hughes, G.R.V , Gharavi, A.E , Patel, B.M. and Loizou, S. (1983) Lancet ii, 1211–1214
9 Ioannou, P.B. and Golding, B.T. (1979) in Progress in Lipid Research (Holman, R.T., ed.), Vol. 17, pp. 279–318, Pergamon Press, Oxford
10 Inoue, K. and Nojima, S. (1967) Chem. Phys. Lipids 1, 360–367
11 De Haas, G.H. and Van Deenen, L.L.M. (1965) Nature 935
12 Costello, P.B. and Green, F.A. (1986) Infect Immun 51, 771–775
13 Owens, N.A., Hui, H.L. and Green, F.A. (1982) J. Immunol. 129, 1471–1473
14 Green, F A , Hui, H L , Green, L.A D., Heubusch, P and Pudlak, W. (1984) Mol. Immunol. 21, 433–438
15 Bartlett, G.R. (1959) J Biol Chem. 234, 466–471
16 Langone, J.J. (1982) in Advances in Immunology (Dixon, F.J. and Kunkel, H.G., eds.), Vol. 32, pp. 157–241, Academic Press, New York
17 Green, F.A. (1969) J. Lipid Res. 10, 710–711
18 Rand, R.P. and Sengupta, S. (1972) Biochim. Biophys Acta 255, 484–492
19 Cullis, P R., Verkleij, A J. and Ververgaert, P.H.J.T. (1978) Biochim. Biophys. Acta 513, 11–20
20 Vasilenko, I., De Kruijff, B and Verkleij, A.J. (1982) Biochim. Biophys Acta 684, 282–286

Biochimica et Biophysica Acta 896 (1987) 52–56
Elsevier

BBA 73180

Cholesterol effects on the interaction of cardiolipin with anti-cardiolipin antibody

P.B. Costello and F.A. Green

Departments of Medicine and Microbiology, State University of New York at Buffalo and the Veterans Administration Medical Center, Buffalo NY (U.S.A.)

(Received 15 August 1986)

Key words Cholesterol–cardiolipin interaction; Cholesterol; Cardiolipin; Anti-phospholipid antibody

(1) Human antibodies to cardiolipin, phosphatidic acid and phosphatidylserine were assessed by binding to nitrocellulose paper and subsequent reaction with an enzyme-linked or radioactively labelled second antibody to human IgG. (2) The addition of cholesterol to constant amounts of cardiolipin impregnated in the nitrocellulose paper resulted in a profound fall in antibody binding beginning at a 0.5 to 1 molar ratio of cholesterol to cardiolipin and stabilizing at about 15% of the original level. (3) Antibody binding to phosphatidic acid and phosphatidylserine also showed extensive cholesterol-induced inhibition beginning at a slightly lower molar ratio of cholesterol to phospholipid. (4) The structural array of neither the cardiolipin alone impregnated in nitrocellulose nor the phospholipid together with cholesterol is known. It is possible that the specific cardiolipin phase structure required for human antibody recognition was disrupted by cholesterol.

Introduction

The structural role of cholesterol in the phospholipid bilayers of cell membranes is complex and affects membrane characteristics in diametrically opposed ways in different model systems [1–4]. A functional role for cholesterol in membrane adhesion has been recently proposed [5]. The physical effects of the interaction of cholesterol and cardiolipin in model membranes could not be assessed in one spin-label study in which such attempts were made [6]. In the case of cytochrome P-450$_{scc}$ cardiolipin appeared to exert its specific effect by enhancement of cholesterol binding to the enzyme rather than any direct interaction with cholesterol [7]. It has been suggested that the effect of cholesterol in enhancing the flocculation test for anti-cardiolipin antibodies in syphilis is related to a spacing role of the sterol for the phospholipid [8]. Modulation of the interaction of human antibodies with cardiolipin and other acidic phospholipids by cholesterol provides an interesting model to examine possible structural aspects of cardiolipin–antibody interaction.

Materials and Methods

Sera were obtained from individuals with documented cases of syphilis through the courtesy of the Erie County Health Department, Division of Public Health. The fluorescent treponemal antibody absorption test for syphilis was positive in each patient and all sera were reactive in the venereal disease research laboratory (VDRL) flocculation test. Nitrocellulose paper was purchased from Bio-Rad Laboratories (Rockville Center,

---

Correspondence: Dr. F.A Green, Department of Medicine, State University of New York at Buffalo, 3495 Bailey Avenue, Buffalo, NY 14215, U.S.A.

0005-2736/87/$03 50 © 1987 Elsevier Science Publishers B.V. (Biomedical Division)

NY). Affinity purified goat and rabbit anti-human IgG were purchased from Jackson ImmunoResearch Laboratories (Avondale, PA). These antibodies could be used interchangeably. [1-^{14}C]Acetic anhydride (30–40 mCi/mmol) was obtained from New England Nuclear (Boston, MA). Anti-human IgG peroxidase conjugates and diaminobenzidine were purchased from Sigma Chemcial Company (St. Louis, MO). Cardiolipin (bovine heart), phosphatidic acid (egg yolk), and phosphatidylserine (bovine brain) were obtained from Sigma Chemical Company and Avanti Polar Lipids (Birmingham, AL) and were checked for purity in two-dimensional thin-layer chromatography as previously described [9]. Hydrofluor was supplied by National Diagnostics (Somerville, NJ).

Qualitative anti-phospholipid antibody assessment

Cardiolipin and cholesterol were dried under N_2, dissolved inchloroform, and then mixed in varying cholesterol: cardiolipin molar ratios. 10 μl of each mixture (containing a constant 27 nmol cardiolipin) were spotted on nitrocellulose papers (3.5 × 8 cm) and dried. The papers were agitated in 3% gelatin blocking buffer (50 mM Tris (pH 7.4), 150 mM NaCl, 1 mM Mg^{2+}, 0.02% NaN_3, 0.1% Tween 20) for 90 min at 25 °C. The papers were then incubated for 16 h in blocking buffer and patient serum (400 μl in a total volume of 20 ml). The strips were then washed three times in blocking buffer for 10 min and were incubated with goat anti-human IgG-peroxidase conjugate according to the manufacturers instructions, 1 : 1000 in 20 mM sodium phosphate buffer (pH 7.4), containing 150 mM sodium chloride (phosphate-buffered saline) at room temperature for 90 min. The papers were rewashed three times with phosphate-buffered saline and color development was visualized after addition to diaminobenzidine solution (50 mg/100 ml phosphate-buffered saline and 0.04% H_2O_2).

Quantitative anti-phospholipid antibody measurement

Nitrocellulose papers were cut in 1 cm diameter circles and spotted with 10 μl of cholesterol/phospholipid mixtures in the same molar ratios as for the qualitative experiments with the cardiolipin concentration held constant at 68.0 nmol. The circles and controls without phospholipid were placed in 50 ml conical centrifuge tubes containing 4 ml of 3% gelatin blocking buffer and were incubated for 1 h in a 33° angled centrifuge rack. Syphilitic serum (80 μl) was then added up to a final volume of 4.0 ml. The tubes were agitated for 16 h at 25 °C, and the papers were then removed and washed three times for 15 min in 50 ml of blocking buffer. The circles were subsequently reacted for 1 h with affinity purified goat or rabbit ^{14}C-labelled anti-human IgG, which had been prepared by reaction with [^{14}C]acetic anhydride as previously described [10]. The papers were then washed three times, and were counted in a Packard Tricarb 460CD scintillation counter after addition of 10 ml hydrofluor. The extent of antibody binding was plotted as a function of cholesterol: cardiolipin molar ratios after subtraction of the level of background counts (no phospholipid) for each experimental point. This non-specific binding was low level. Non-specific binding of the labelled second antibody to the paper with and without phospholipid but without the human serum step was negligible.

Results

In the more than 50 syphilitic sera tested, all had detectable antibodies to cardiolipin, phosphatidic acid, and phosphatidylserine [11]. In the qualitative tests there was no reactivity with phosphatidylcholine (egg or dicaproylphosphatidylcholine), or phosphatidylethanolamine (data not shown). Fig. 1 shows the results of two qualitative binding experiments in which a syphilitic serum was reacted with cardiolipin and phosphatidylserine respectively with increasing concentrations of cholesterol impregnated in nitrocellulose papers. Inspection of the staining intensity reveals that anti-cardiolipin antibody binding began to decrease at molar ratios of cholesterol : phospholipid in the 2.5–5.0 range and was undetectable in the 10.0–20.0 range. Anti-phosphatidylserine binding was suppressed at a lower molar ratio.

Figs. 2–4 show the effects of increasing cholesterol : phospholipid molar ratios on quantitative antibody binding to different phospholipids in sera from eight different syphilitic patients. In

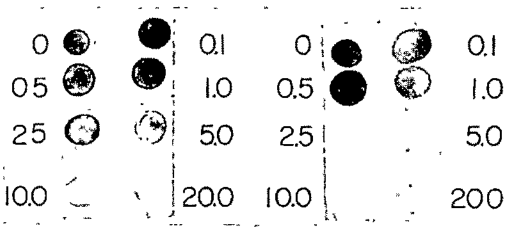

Fig. 1. Cholesterol-induced suppression of anti-phospholipid binding. Nitrocellulose organic blots contained, respectively, 27 nmol cardiolipin (left panel) and phosphatidylserine (right panel) in 10 μl chloroform, as well as cholesterol at the indicated molar ratios. Incubation in serum (1 : 50 in blocking buffer) was followed by washing and incubation in peroxidase-linked anti-human IgG. Visualization was accomplished with diaminobenzidine and hydrogen peroxide.

each case binding is plotted as the amount of anti-IgG bound as a function of increasing molar ratio of cholesterol to the particular phospholipid with the concentration of the latter held constant. The results of three separate experiments, in which anti-cardiolipin binding was measured in different syphilitic sera, are shown in Fig. 2. In each case as the ratio increased, binding to cardiolipin began to decline at the 0.5–1.0 molar ratio point. Binding consistently reached a minimum at a ratio of 2.5 and remained relatively constant thereafter at approx. 15% of the original level. The results of four additional experiments with different sera showed the same pattern.

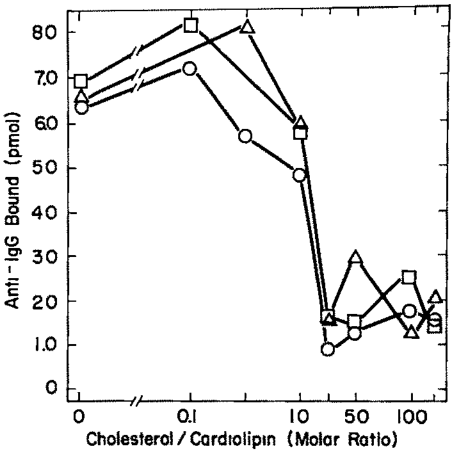

Fig. 2. Suppression of anti-cardiolipin antibody binding by cholesterol Cardiolipin (68 nmol) and increasing cholesterol at the indicated molar ratios were spotted on 1 cm nitrocellulose circles in 10 μl chloroform followed by incubation with three separate sera (80 μl, separate symbols) from syphilitic patients in 4.0 ml of blocking buffer. After washing the circles were incubated with excess ^{14}C-labelled anti-human IgG.

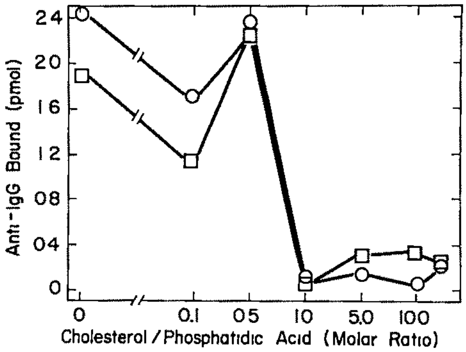

Fig. 3 Suppression of anti-phosphatidic acid binding by cholesterol Details as in Fig. 2

The effect of cholesterol on binding to phosphatidic acid and phosphatidylserine resulted in similar binding inhibition. In the two sera which were incubated with cholesterol and phosphatidic acid (Fig. 3) the inhibition was in close parallel and maximum depression (approx. 90%) were seen at molar ratios of 0.5–1.0. A further experiment showed a nearly superimposable binding curve although the absolute values were lower. Reproducibility was also seen in the case of binding to phosphatidylserine (Fig. 4). In the three syphilitic sera tested with this phospholipid, the levels of

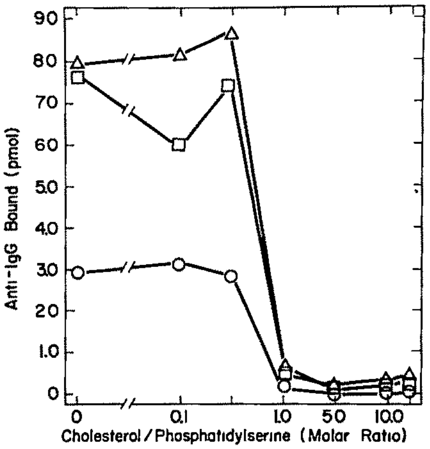

Fig. 4. Suppression of anti-phosphatidylserine antibody binding by cholesterol Details as in Fig. 2.

anti-IgG binding varied at the control points and lower cholesterol concentrations but in each case began to diminish above a ratio of 0.5 and reached almost 90% inhibition at a ratio of 1.0 where it remained.

Discussion

Cholesterol is an important component of many biological membranes, but its specific role in membrane structure/function has yet to be fully elucidated [12]. Apparently very little work has been done on cardiolipin-cholesterol interactions in model systems, perhaps because they tend not to be found in substantial concentration together in the same membranes [8].

The results of the present experiments demonstrated that there was consistent inhibition by cholesterol of human antibody binding to different phospholipids in sera from different syphilitic subjects. Surprisingly, there was impressive uniformity in these sera, both with regard to the magnitude of suppression and with regard to the molar ratio at which it occurred with each phospholipid. Overall, anti-cardiolipin binding tended to be higher but uniformly began to decline at the 0.5–1.0 molar ratio range and showed maximum depression at 2.5. A similar pattern was evident for phosphatidic acid and phosphatidylserine at even lower cholesterol : phospholipid ratios. Cholesterol has been used along with phosphatidylcholine to amplify the flocculation reactions of anti-cardiolipin antibodies with cardiolipin in syphilis [8], but the molecular basis of the cholesterol effect is not clear. The mechanism may be unrelated to the interaction of cardiolipin and antibody described here.

Why the quantitative antibody measurement with labelled anti-IgG appeared to show inhibition of anti-cardiolipin and anti-phosphatidylserine at a lower molar ratio than the assessment by peroxidase-linked anti-IgG is not clear. In any case there was consistency in that cholesterol-induced suppression of anti-phosphatidylserine antibody binding was observed at a lower cholesterol : phospholipid ratio than that for anti-cardiolipin by both methods.

Concentration-dependent disruption of membrane phospholipid and bilayer stability by cholesterol may occur through different mechanisms [13]. At relatively low cholesterol levels site-specific hydrogen bond formation between cholesterol and the cardiolipin fatty acid residue occurred. At higher cholesterol concentrations cardiolipin disruption was thought to take place as a result of head group disengagement. In other studies mixtures of unsaturated cardiolipin in membranes were disrupted by cholesterol as a result of assumption of dynamic wedge or cone-shaped structures [14,15]. This indirect evidence would point to the provisional hypothesis that cholesterol-induced changes in the physical array of the cardiolipin molecules render the binding of anti-cardiolipin antibody molecules unfavorable. These effects of cholesterol an anti-phospholipid antibody binding are complementary to the observations outlined in the companion paper (divalent cation effects on antibody binding) [16]. The disruptive role of cholesterol in a system of biological interest may provide another reason for the dissimilar membrane distribution of cardiolipin and cholesterol. Cholesterol and related sterols could be useful as molecular probes for the interaction of cardiolipin with anti-cardiolipin antibodies.

Acknowledgements

Supported by the Veterans Administration, the National Institutes of Health HL 24009, and the Arthritis Foundation of Western New York.

References

1 Jain, M.K. (1975) Curr Top. Membrane Transp. 6, 1–57

2 Estep, T.N , Mountcastel, D.B., Ciltonen, R.L. and Thompson, T.E (1978) Biochemistry 17, 1984–1989

3 Mabrey, S., Mateo, P.L. and Sturtevant, J.M. (1978) Biochemistry 17, 2464–2468

4 Houslay, M.D. and Stanely, K.K. (1982) Dynamics of Biological Membranes: Influence on Synthesis Structure and Function, pp. 330, Wiley, New York

5 Ohki, S. and Leonards, K.S. (1984) Biochemistry 23, 5578–5581

6 Boggs, J.M. and Hsia, J C (1973) Can. J Biochem. 51, 1451–1459

7 Lambeth, J.D., Kamin, H. and Seybert, D.W. (1980) J. Biol. Chem. 255, 8282–8288

8 Ioannou, P.B and Golding, B.T. (1979) in Progress in Lipid Research (Holman, R.T., ed.), Vol. 17, pp. 279–318, Pergamon Press, Oxford

9 Green, F.A, Hui, H L., Green, L A.D, Heubusch, P and Pudlak, W. (1984) Mol. Immunol. 21, 433–438

10 Owens, N.A, Hui, H.L. and Green, F A. (1982) J. Immunol. 129, 1471–1473

11 Costello, P.B. and Green, F A (1986) Infect. Immun 51, 771–775

12 Yeagle, P.L (1985) Biochim. Biophys Acta 815, 33–36

13 Yeagle, P.L., Hutton, W.C., Huang, C H. and Martin, R B (1975) Proc. natl. Acad Sci. USA 72, 3477–3481

14 Cullis, P.R., Van Kijck, P W.M., De Kruijff, B. and De Gier, J. (1978) Biochim. Biophys. Acta 513, 21–30

15 Cullis, P.R. and De Kruijff, B. (1978) Biochim. Biophys. Acta 507, 207–218

16 Green, F.A. and Costello, P.B. (1987) Biochim. Biophys Acta 896, 47–51

Biochimica et Biophysica Acta 896 (1987) 57–63
Elsevier

BBA 73175

The mobility of concanavalin A receptors and surface immunoglobulins on rat hepatocyte plasma membranes

György Lustyik *, Kenichi Kitani ** and Minoru Ohta

Tokyo Metropolitan Institute of Gerontology, First Laboratory of Clinical Physiology, 35-2 Sakaecho,
Itabashi-ku, Tokyo 173 (Japan)

(Received 3 September 1986)

Key words: Cell surface; Concanavalin A receptor; Protein mobility;
Photobleaching recovery; FRAP; Aging; (Rat liver)

Lateral mobilities of lectin receptors and surface immunoglobulins were measured in plasma membranes of hepatocytes prepared by smearing small pieces of rat liver tissue and then using the fluorescence recovery after photobleaching (FRAP) technique. Smears were treated with various doses of fluorescein isothiocyanate (FITC) conjugated concanavalin A (ConA), succinylated ConA (SConA), wheat germ agglutinin (WGA), and soybean agglutinin (SBA), as well as with rabbit anti-rat IgG (RARa/IgG) and goat anti-rat IgM(Fc) (GARa/IgM(Fc)) antisera. 10 μg/ml ConA and SConA concentrations and a 55 × dilution of the GARa/IgM(Fc) antiserum were found to be suitable for measuring the lateral mobilities dependent on age. Diffusion constant and mobile fractions of receptor complexes were measured in different age groups of female Fisher rats (from 1 to 26 month-old). The FRAP measurements revealed that at least two major receptor sites can be distinguished in cell membranes of compact tissue (similar to the cultured and isolated cells), forming a mobile and an immobile fraction. The mobile fractions of both the lectin receptors and the surface immunoglobulins tended to decrease with age, while the age differences of the diffusion constants were not statistically significant. The observed alterations could be due to the covalent crosslinking of the mobile receptors to immobile patches and/or to the retardation of free diffusion by the cytoskeleton, dependent on age.

Introduction

Since the redistribution of macromolecules in the intramembrane plane was first demonstrated by fusing together mouse and human cultured cell lines and the spreading of the surface antigens observed on the fused heterocaryons [1], the lateral mobility of many membrane proteins has been clearly established in wide variety of cells. A very effective optical technique, fluorescence recovery after photobleaching (FRAP), is the most widely used method for measuring lateral mobilities in both living cells and model systems [2–8]. Attention has been focused predominantly on three areas: (1) quantitation of the observed mobilities in terms of diffusion constant (D) and fractional recovery (R) [9–14]; (2) revealing the importance of the protein movement in determining the functional properties of the cell membranes [15–19] and (3) gaining insight into factors which control

---

* Dr. G. Lustyik was the awardee of the visiting scientist scholarship from the Tokyo Metropolitan Institute of Gerontology

** To whom reprint requests should be addressed.

Correspondence: Dr. G. Lustyik, Fritz Verzar International Laboratory for Experimental Gerontology (VILEG), Hungarian Section, University Medical School, H-4012 Debrecen, Hungary

0005-2736/87/$03.50 © 1987 Elsevier Science Publishers B.V. (Biomedical Division)

the mobility of membrane components [20–26].

Experimental data accumulated for mammalian cells showed several common characteristics of the lateral diffusion of membrane proteins. The two most important observations in plasma membrane have been that: (1) the diffusion constant of diffusible membrane proteins is considerably lower than expected theoretically from the hydrodynamic model of Saffman and Delbruck [27] and also lower than that measured with proteins reconstituted into lipid bilayers; (2) the diffusible fraction (R) of proteins is generally less than 100%, and certain proteins are virtually nondiffusible (an exception being rhodopsin in the amphibian rod outer segment disk [28]).

Most of our knowledge of the mobility characteristics of membrane proteins is derived from observations on cultured or isolated cells. However, it is important to assess the extent to which these results can be extrapolated to parenchymal cells of compact tissues, like liver, muscle, nervous system, etc. One of the problems that needs to be solved in this context is that diffusion measurements on living cells of compact tissue require special preparation methods. By virtue of the findings reported in the papers of Zs.-Nagy et al. [29,30] we tried to circumvent the preparation problem in rat hepatocytes by using exogenous markers in smeared liver specimens.

The present study is concerned with the age dependence of the translational movement of membrane proteins of rat liver cells. Hepatocytes were labeled with concanavalin A (ConA) and succinylated concanavalin A (SConA) lectins and goat anti-rat IgM(Fc) antiserum conjugated with fluorescein isothiocyanate (FITC). We chose lectin receptors and surface immunoglobulins for our first investigation on smeared samples with exogenous ligands because their properties are well characterized in isolated and cultured cells. It was expected that membrane damage, predominantly the accumulation of covalent crosslinks between membrane components during aging, would retard the diffusion in the cell membrane. The results demonstrate that under certain conditions the smearing technique can be useful for studies of protein mobilities in plasma membrane of cells of solid tissues, like the liver.

Materials and Methods

General. Female Fisher 344 rats (Japan, Charles River Astugi) were maintained in the institute's SPF aging farm on a standard diet (CRF, Oriental, Tokyo) with free access to acidified water (pH 2.5–3.0, residual chlorine 10 ppm). Their survival and other conditions are described elsewhere [31]. The animals were killed by decapitation and hepatocytes were prepared from the freshly removed livers (usually within one minute subsequent to the removal) by smearing small tissue pieces between two slides. In order to minimize the cell damage during smearing and to standardize the method we used a preparation procedure similar to that described in detail recently [29,30], with the exceptions that non-frosted slides were used in order to improve the cell recognition, and 50 μm thick plastic tape was used on the smearing slide only, to avoid any influence of the tape components on the smears. The smears were then incubated with the FITC-labeled lectins and immunoconjugates as detailed below.

Two series of experiments were performed. First, four labeled lectins, concanavalin A (ConA-FITC), succinyl concanavalin A (SConA-FITC), wheat germ agglutinin (WGA-FITC) and soybean agglutinin (SBA-FITC) as well two immunoconjugates, FITC-labeled rabbit anti-rat IgG (RARa/IgG-FITC) and goat anti-rat IgM(Fc) (GARa/IgM(Fc)-FITC) antisera, were applied at various concentrations to the incubating solution. The purpose of these 'preliminary' experiments was to establish the optimal label concentrations for the measurement of protein mobility dependent on age.

In the second series of experiments different age groups of female rats (from one to 26 month-old) were used as test animals. Lateral mobility of membrane proteins of liver cells was measured after labeling the cells with ConA-FITC, SConA-FITC and GARa/IgM(Fc)-FITC (see below).

Materials. ConA-FITC and SConA-FITC were obtained from Sigma (U.S.A.). WGA-FITC, SBA-FITC and RARa/IgG-FITC was from Miles Laboratories (Israel). GARa/IgM(Fc)-FITC was purchased from Nordic (The Netherlands).

Incubation and slide preparation. The incubating solutions were prepared with Krebs-Ringer bicarbonate buffer (pH 7.4) [32]. The prepared smears were covered immediately with a 200 μl solution containing the FITC conjugated label and incubated for 10 min at 37°C. They were then washed intensively with the buffer saline, and wet mounted and sealed with paraffin in order to avoid drying during the fluorescence recovery experiments.

In preliminary experiments the following concentrations were tested:

ConA-FITC: 5, 10, 20 and 50 μg/ml.
WGA-FITC: 1, 2, 5 and 10 μg/ml.
SBA-FITC: 1, 5, 10, 50, 100 and 200 μg/ml.
RARa/IgG-FITC: 11x, 22x, 55x and 110x dilution of the antiserum.
GARa/IgM(Fc)-FITC: 11x, 22x, 55x and 110x dilution of the antiserum.

In the experiments in which the lateral mobility of membrane proteins were measured in relation to rat age, 10 μg/ml ConA-FITC and SConA-FITC and 55x dilution of the GARa/IgM(Fc)-FITC were used, these concentrations having been found to be optimal for labeling liver cells.

Fluorescence recovery after photobleaching. Diffusion coefficients and recoveries (immobile fractions) were determined by the FRAP technique using the instrument described in detail by Zs.-Nagy et al. [29]. Attenuated laser beam ($\lambda = 476.5$ nm) from a NEC GLG 3200 argon ion laser was focused on the cell membrane through the objective (FLPL 40,˙- NA = 0.75) of a phase contrast/epifluorescence microscope. The approximately gaussian beam was focused to 1.5 μm of its $1/e^2$ radius. A beam splitting system consisting of two 10 mm thick optical flats (Melles Griot 02 FQD 007 type) which produced an approximately 10^4-fold attenuation of the full laser beam (100–150 mW). The unattenuated beam could be turned on and off by means of a shutter which allowed bleaching pulses greater than 10 ms to be used.

Approximately 50–60% of the FITC in the illuminated area was irreversibly bleached by a short (100–200 ms) pulse of the unattenuated beam created by opening the shutter. The fluorescence of the bleached spot, as well as the prebleaching fluorescence were followed with a Hamamatsu R649 type photomultiplier operated in the photon counting mode at −20°C. Typical recovery curves are shown in Fig. 1. Fluorescence was measured in a duty circle of 1 s every 4 s. Intensity signals were applied to a Hamamatsu C 1230 type photon counter providing digital data of the intensities for the on line NEC PC-9801E computer. The data were converted into diffusion coefficients and percent recoveries by using the calculation procedure described by Yguerabide et al. [33].

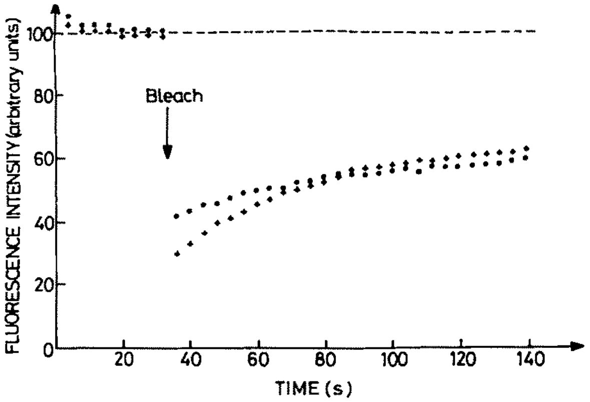

Fig. 1. Two typical photobleaching recovery curves. ConA-FITC bound to hepatocyte membrane of an old rat (●) and GARa/IgM(Fc)-FITC bound to the liver cell membrane of a young animal (+) The diffusion constants were $1\,3 \cdot 10^{-10}$ cm^2/s and $1.5 \cdot 10^{-10}$ cm^2/s, respectively. Mobile fractions were 43% and 69%

Prepared specimens were examined using the microscope's phase contrast mode. The overall fluorescence of the cell membranes could be observed under epi-illumination using the completely defocused laser beam. Monolayered cells showing intact morphology and homogeneous fluorescent labeling were chosen for measurements. Only a single bleach was applied to each of the measured cells. The FRAP measurements started immediately after the specimen preparation and continued for approximately 90–110 min. All the measurements were performed at 25–26°C.

Results

Concentration dependence of the labeling

The phase contrast microscopic picture of the liver smear showed that mononuclear hepatocytes were the predominant form among the morphologically intact cells. The cells displayed a relatively weak labeling with ConA-FITC and SConA-FITC. Sufficiently high FITC fluorescence intensity for FRAP measurements could be obtained only with concentrations higher than 5 μg/ml of the incubating medium. The ConA receptors were generally uniformly distributed without any cap-like asymmetrical arrangement.

Both the diffusion constant and the mobile fraction varied depending on the concentration of the probe (Fig. 2). The recovery decreased to about 20% with ConA concentrations above 20 μg/ml. Since at concentrations of 5 μg/ml or below the intensity was too low to allow an appropriate measurement, 10 μg/ml ConA-FITC and SConA-FITC concentrations of the incubating media were chosen for the measurement of the lateral mobility of ConA receptor complexes dependent on age.

A homogenous, sufficiently intensive labeling was obtained with WGA-FITC lectin. Unlike smear preparations labeled with the other two

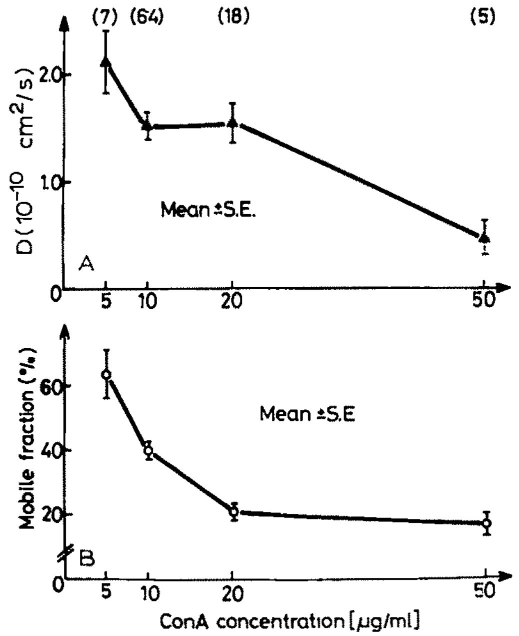

Fig 2 Diffusion coefficients (▲) of ConA receptors and mobile fractions (O) as measured on rat liver cells incubated with various doses of ConA-FITC in smear. Concentrations below 5 μg/ml did not provide appropriate fluorescent labeling. The data were obtained from measurements on the number of cells indicated in parentheses

TABLE I

LATERAL MOBILITY OF ConA RECEPTORS IN THE PLASMA MEMBRANE OF HEPATOCYTES

Labeling with 10 μg/ml ConA-FITC. *D* and *R* values are presented as means ± S.E. Abbreviations: ANOVA, one-way analysis of variance; M.Sqr, mean squares; df, degree of freedom (numerator, denominator); n.s, not significant.

Age of rats [a]	Diffusion constant (*D*) $(10^{-10}\ \mathrm{cm^2/s})$	Mobile fraction (*R*) (%)
1 month (40)	1.95±0.13	50.5±1.8
2.5 months (39)	1.74±0.10	49.8±2.0
6 months (61)	1.97±0.12	50.4±1.7
12 months (48)	1.86±0.12	50.3±1.7
17.5 months (52)	1.68±0.14	45.3±1.6
23.5 months (65)	1.66±0.07	43.7±1.4
ANOVA:		
M Sqr. between groups:	102.46	440.15
within groups:	62.79	125.48
F:	1.632	3.508
df (num, denom):	5, 299	5, 299
Significance:	n.s. ($P > 0.1$)	$P < 0.005$

[a] In parentheses: number of measured cells.

TABLE II

LATERAL MOBILITY OF SUCCINYL-CONCANAVALIN A BOUND TO HEPATOCYTES IN LIVER SMEAR

Labeling with 10 μg/ml SConA-FITC. *D* and *R* values are presented as means ± S.E. Abbreviations: ANOVA, one-way analysis of variance; M. Sqr, mean squares; df, degree of freedom (numerator, denominator).

Age of rats [a]	Diffusion constant (*D*) $(10^{-10}\ \mathrm{cm^2/s})$	Mobile fraction (*R*) (%)
1 month (40)	2.43±0.17	60.4±2.1
2.5 months (49)	2.82±0.14	61.8±2.0
4.5 months (18)	2.03±0.21	58.7±3.8
6 months (45)	1.91±0.11	49.4±2.0
7.5 months (51)	2.04±0.13	56.4±2.2
12 months (51)	1.85±0.14	59.2±2.2
17.5 months (48)	1.80±0.10	51.1±1.7
23.5 months (29)	2.09±0.13	46.0±2.5
ANOVA:		
M. Sqr. between groups:	561.13	1304.83
within groups:	78.09	202.18
F:	7.185	6.545
df (num, denom):	7, 323	7, 323
Significance:	$P < 0.005$	$P < 0.005$

[a] In parentheses: number of measured cells.

TABLE III

LATERAL MOBILITY OF GARa/IgM(Fc)-FITC IMMUNOGLOBULINS BOUND TO HEPATOCYTES IN LIVER SMEAR

D and R values are presented as means ± S.E. Abbreviations: ANOVA, one-way analysis of variance; M.Sqr., mean squares; df, degree of freedom (numerator, denominator); n.s., not significant.

Age of rats [a]	Diffusion constant (D) (10^{-10} cm^2/s)	Mobile fraction (R) (%)
1 month (20)	1.69±0.20	67.2±2.5
2.5 months (15)	1.79±0.23	62.8±2.3
17 months (14)	1.91±0.20	54.8±3.0
26 months (23)	1.44±0.16	59.0±3.6
ANOVA:		
M.Sqr. between groups:	107.01	480.33
within groups:	67.18	173.32
F:	1.593	2.771
df (num, denom):	3, 68	3, 68
Significance.	n.s. ($P > 0.1$)	$P < 0.025$

[a] In parentheses: number of measured cells.

lectins both the plasma membrane and the cell nuclei in 30–40% of the liver cells showed fluorescence after incubation. The percentage of cells showing nucleus fluorescence increased with incubation time. The fluorescence intensity of nuclei exceeded the intensity of plasma membrane. The diffusion coefficients and mobile fractions measured in the nucleus membrane of these cells were found to be significantly lower than those recently reported for isolated nuclei by Schindler et al. [34].

Since labeling of nuclei membrane can be the result of a certain type of plasma membrane damage resulting in an increased permeability for macromolecules, we did not extensively study WGA-FITC. The lateral mobility of WGA receptors of cell membrane, however, showed a concentration dependence similar to the ConA receptors.

When SBA-FITC was used as a cell label no measurable fluorescence was obtained even at higher incubating concentrations (up to 250 μg/ml) and longer incubation times (2 h). The RARa/IgG-FITC produced a mottled fluorescence pattern on hepatocytes membranes at all concentrations (dilutions) of the antiserum which were used. No FRAP measurement was performed with either the SBA-FITC or RARa/IgG-FITC probes.

The incubation of liver smears with GARa/IgM(Fc)-FITC resulted in a homogeneous labeling of the cell surface. The lateral mobility of the fluorescent complexes as well as the mobile fraction showed a clear concentration dependence.

Lateral mobility dependent on age

The diffusion constant as well as the percent recovery of ConA receptor complexes labeled with ConA-FITC and SConA-FITC and surface immunoglobulins are shown in Table I, II and III, respectively. The results indicate, that the diffusion constants of the ConA and the GARa/IgM(Fc) did not change significantly with age, although the D of the ConA receptors tended to decrease over time. The diffusion constant of the SConA was significantly higher in the young (1 and 2.5 month-old) animals than in the older. A greater difference can be seen among the age-groups in the mobile fraction of the receptors. The mobile fractions of both lectins and GARa/IgM(Fc) were considerably lower in the 23.5–26 month-old rats than in the young ones. The diffusion constants and the mobile fractions of the individual cells were scattered over a wide range.

Discussion

Since increasing ConA doses and longer incubation times were reported to reduce the diffusion constant and the mobile fraction [35], we used the lowest possible lectin concentrations for cell labeling. The lectins showed a relatively weak binding to the surface receptors of rat liver cells in smears. In our experiments the 10 μg/ml ConA (and SConA) concentration was found to be the lowest concentration at which a relatively stable and measurable green FITC fluorescence could be observed. Others have stained hepatocytes with both fluorescein and peroxydase labeled lectins using lectin concentrations similar to or higher than that applied in the present experiments [36–38].

Photobleaching measurements reported in the present study demonstrated that in young (1 and

2.5 month-old) animals both the diffusion constant and the mobile fraction of the lectin receptors were lower in the plasma membrane of liver cells treated with ConA than in the SConA-treated cells. This agrees with previous reports demonstrating a greater decrease for the tetravalent ConA than for its succinylated derivative [35,39].

The (1.5–2.8) $\cdot 10^{-10}$ cm^2/s values of the diffusion coefficients of lectin receptors on liver cells found in our study are larger than generally measured on other cell membranes [2,21,35,40]. On the other hand, the present results are comparable with the receptor mobilities in normal and virus transformed mouse fibroblasts [41] and even higher diffusion coefficients were calculated from electrophoretic measurements on embryonic muscle cells [42]. Diffusion constants of receptors labeled with SConA fell into the same range as that of the unfertilized and fertilized mouse eggs [15]. It is noteworthy that we obtained relatively low fractional recoveries: in ConA treated hepatocytes 40–50%, and in SConA-treated ones 45–60% of the receptors was mobile. This may be due to: (1) the receptors exist in at least two states on hepatocytes, forming a mobile and an immobile fraction or (2) lectin labeling itself caused two apparently different receptor states.

Basically, the same conclusion can be drawn for the lateral mobility of surface antigens. The diffusion coefficient and the mobile fraction of both the lectin receptors and surface immunoglobulins strongly depended upon the dose of the probe, most probably due to the aggregation of the receptor complexes. Since ConA is rather tetravalent in the circumstances of our labeling procedure [43] crosslinking can produce impermeable (but fluorescently invisible) patches forming an 'archipelago' on the cell membrane, and consequently reduce the diffusion coefficient [44]. On the other hand, links between originally mobile and immobile complexes may reduce the mobile fraction. Thus, our results suggest that none of ligands used in the present study is ideal for the purpose of FRAP measurement, although we could obtain some information on the hepatocyte plasma membrane that was not accessible up to now.

In our previous work using autofluorescence [30] we observed a significantly linear decrease of the diffusion constant of membrane proteins in relation to age, and much higher recoveries (> 80% even in old rats). The results obtained from the present measurement tends to be similar to our previous work but the age differences are less clear. Discovery of the real causes for the differences between the two studies using exogenous and endogenous fluorescent markers awaits future work.

Although the results presented in this paper do not offer a final answer to the behavior of the surface receptors of liver cells, the acceptable agreement with previous experimental results suggests that the most important properties of the receptors are preserved during the smearing and the preparation. Moreover, the results indicate the utility of the FRAP technique for research on rat liver cells.

Acknowledgements

This study was supported in part by Grants in Aid from the Ministry of Science and Technology of Japan and from the Tokyo Metropolitan Institute of Gerontology 'The pharmacodynamics in the elderly' and from the Life Science Foundation. G. Lustyik was the awardee of a visiting scientist scholarship from the Tokyo Metropolitan Institute of Gerontology.

References

1 Frye, L.D. and Edidin, M. (1970) J. Cell. Sci. 7, 319–336
2 Cherry, R.J. (1979) Biochim. Biophys. Acta 559, 289–327
3 Axelrod, D. (1983) J. Membrane Biol. 75, 1–10
4 Lauffenburger, D. and DeLisi, C. (1983) Int. Rev. Cytol. 84, 269–302
5 Shinitzky, M. and Henkart, P. (1969) Int. Rev. Cytol. 60, 121–147
6 Nicolson, G.L., Poste, G. and Ji, T.H. (1977) in Dynamic Aspects of Cell Surface Organization pp. 1–73, North-Holland, Amsterdam
7 Vaz, W.L.C., Criado, M., Madeira, V.M.C., Schoellmann, G. and Jovin, T.M (1982) Biochemistry 21, 5608–5612
8 Criado, M., Vaz, W.L.C., Barrantes, F.J. and Jovin, T.M. (1982) Biochemistry 21, 5750–5755
9 Axelrod, D., Koppel, D.E., Schlessinger, J., Elson, E.L. and Webb, W.W. (1976) Biophys. J. 16, 1055–1069
10 Koppel, D.E., Axelrod, D., Schlessinger, J., Elson, E.L. and Webb, W.W. (1976) Biophys. J. 16, 1315–1329
11 Koppel, D.E. (1979) Biophys. J. 28, 281–292
12 Koppel, D.E and Sheetz, P.M. (1983) Biophys. J. 43, 175–181

13 Jacobson, K., Derzko, Z., Wu, E.-S., Hou, Y. and Poste, G. (1976) J. Supramol. Struct. 5, 565–576

14 Davoust, J., Devaux, P.F. and Leger, L. (1982) Eur. Mol. Biol. Organ. J. 1, 1233–1238

15 Wolf, D.E. and Ziomek, C.A. (1983) J. Cell Biol. 96, 1786–1790

16 Aizenbud, B.M. and Gershon, N.D. (1982) Biophys. J. 38, 287–293

17 Peters, R. (1981) Cell. Biol. Int. Rep. 5, 733–760

18 Golan, D.E. Alecid, M.R., Veatch, W.R. and Rando, R.R (1984) Biochemistry 23, 332–339

19 Damjanovich, S., Trón, L., Szöllősi, J., Zidovetzki, R., Vaz, W.L C., Regateiro, F., Arndt-Jovin, D. and Jovin, T.M. (1983) Proc. Natl. Acad. Sci. USA 80, 5985–5989

20 Wu, E.-S., Tank, D.W. and Webb, W.W. (1982) Proc. Natl Acad. Sci. USA 79, 4962–4966

21 Schlessinger, J., Elson, E.L., Webb, W.W., Yhara, I., Rutishauser, U. and Edelman, G.M. (1977) Proc. Natl. Acad. Sci. USA 74, 1110–1114

22 Henis, Y.I. and Elson, E.L. (1981) Proc. Natl. Acad. Sci. USA 78, 1072–1076

23 Tank, D.W., Wu, E.-S and Webb, W.W. (1982) J. Cell Biol. 92, 207–212

24 McCloskey, M and Poo, M.-M. (1984) Int. Rev. Cytol. 87, 19–81

25 Jacobson, B.S. (1983) Tissue Cell 15, 829–852

26 Pink, D.A. (1985) Biochim. Biophys. Acta 818, 200–204

27 Saffman, P.G. and Delbruck, M. (1975) Proc. Natl. Acad. Sci. USA 72, 3111–3113

28 Poo, M.-M. and Cone, R.A (1974) Nature (Lond.) 247, 438–441

29 Zs.-Nagy, I., Ohta, M., Kitani, K and Imahori, K. (1984) Mikroskopie (Wien) 41, 12–25

30 Zs.-Nagy, I., Kitani, K., Ohta, M., Zs-Nagy, V., and Imahori, K. (1986) Arch. Gerontol. Geriatr. 5, 131–146

31 Nokubo, M. (1985) J. Gerontol 40, 409–414

32 Umbreit, W.W., Burris, R.H. and Stauffer, J.F. (eds.) (1964) Manometric Techniques, pp. 1932, Burges, Minneapolis

33 Yguerabide, J., Schmidt, J A. and Yguerabide, E.E. (1982) Biophys. J. 40, 69–75

34 Schindler, M., Holland, J.F. and Hogan, M. (1985) J. Cell Biol. 100, 1408–1414

35 Schlessinger, J., Koppel, D.E., Axelrod, D , Jacobson, K , Webb, W W. and Elson, E.L. (1976) Proc Natl Acad. Sci USA 73, 2409–2413

36 Roth, J., Neupert, G. and Block, F. (1975) Exp. Pathol. 10, 143–155

37 Roth, J. and Thoss, K. (1975) Exp. Pathol. 10, 258–267

38 Roth, J., Neupert, G. and Thoss, K. (1975) Exp. Pathol. 10, 309–317

39 Edelman, G.M. (1976) Science 192, 218–226

40 Metcalf, T N., Wang, J.L., Schubert, K.R. and Schindler, M. (1983) Biochemistry 22, 3969–3975

41 Eldridge, C.A., Elson, E.L. and Webb, W W. (1980) Biochemistry 19, 2075–2079

42 Poo, M.-M., Poo, W.-J H. and Lam, J.W. (1978) J. Cell Biol. 76, 483–501

43 Senear, D.F. and Teller, D.C. (1981) Biochemistry 20, 3076–3083

44 Saxton, M.J. (1982) Biophys. J. 39, 165–173

Biochimica et Biophysica Acta 896 (1987) 64–76
Elsevier

BBA 73199

Depth-dependent fluorescent quenching of a tryptophan residue located at defined positions on a rigid 21-peptide helix in liposomes

Klaus-Peter Voges [a], Günther Jung [a] and William H. Sawyer [b]

[a] Institut für Organische Chemie, Universität Tübingen, Tübingen (F.R.G.)
and [b] Russell Grimwade School of Biochemistry, University of Melbourne, Parkville (Australia)

(Received 1 August 1986)

Key words: Membrane–protein interaction; Alamethicin analog, Tryptophan fluorescence, Fluorescence quenching; Circular dichroism; Doxyl stearic acid

Five lipophilic 21-peptide analogs of the potential-dependent pore-former, alamethicin, were synthesized bearing tryptophan residues at the position 1, 6, 11, 16 and 21 on a long, conformationally rigid, α-helix. The α-helical conformation was induced and stabilized using the sequential oligomers (Ala-Aib-Ala-Aib-Ala)$_n$ as analyzed by CD and NMR. The partitioning of the *N*-*t*-butoxycarbonyl 21-peptide methyl esters and the *N*-terminally deprotected α-helices was followed by fluorescence enhancement in phospholipid bilayer vesicles. Quenching experiments were performed by titrating with *n*-doxyl stearic acids bearing the nitroxide label at positions 5, 7, 10, 12 and 16. This well-defined system revealed that the N- and C-terminal tryptophan residues become situated in the hydrophilic region. Tryptophan at position 11 was found in the lipophilic core, whereas the tryptophan at positions 6 and 16 were localized at intermediate depths of the lipid membrane. Therefore, the helices span the lipid bilayer with their long axis normal to the membrane surface.

Introduction

A variety of α helical polypeptides are known to form voltage-dependent pores in lipid bilayer membranes: alamethicin [1], suzukacillin [2], trichotoxin A40 [3], and several natural and chemically modified analogs, a synthetic nonadecapeptide, melittin, and modified analogs [4]. Simple analogs of natural helical peptides such as Boc-(LAla-Aib-Ala-Aib-Ala)$_n$-OMe ($n = 1$–4) also induce voltage-dependent, ion-conducting pores, although at higher concentrations than alamethicin [5,6]. It has been concluded that a lipophilic, rigid and α-helical rod is a sufficient prerequisite for the formation of voltage-gated pores. The opening and closing of ion-conducting pores has been explained by a flip-flop within aggregates of antiparallel and parallel arranged helix dipoles in the bilayer [7]. Rigid α-helices may be used also as carriers for drugs such as hormones or for the presentation of antigens on cell surfaces [8].

These applications and the interpretation of results in bilayer experiments require a detailed knowledge of the behavior and position of the helices within the membrane. Recently the quenching processes of *n*-anthroyloxy stearic acids and *n*-doxyl stearic acids in egg-yolk phosphatidylcholine vesicles were investigated [9,10]. On this basis we were able to check the transverse disposition of helical peptides carrying a

---

Abbreviations: Aib (or α), α-aminoisobutyric acid; Boc, *t*-butoxycarbonyl; *n*-NS, *n*-doxyl stearic acids (n = 5, 7, 10, 12, 16). See also Scheme I.

Correspondence: Dr G. Jung, Institut für Organische Chemie, Universität Tübingen, Auf der Morgenstelle 18, D-7400 Tübingen 1, F.R.G.

0005-2736/87/$03.50 © 1987 Elsevier Science Publishers B.V (Biomedical Division)

tryptophan fluorophore, using the set of *n*-doxyl stearic acids as a gauge within the membrane. In order to obtain suitable helices we modified the icosapeptide Boc-(L-Ala-Aib-Ala-Aib-Ala)$_4$-OMe, the pore-forming properties of which had been investigated [5,6], by incorporating a tryptophan residue at different positions. Thus a set of five henicosapeptides resulted with tryptophan at the sequence positions 1,6,11,16 and 21.

Materials and Methods

Phospholipid vesicles

Unilamellar vesicles of egg-yolk phosphatidylcholine (Lipid Products, U.K.) were prepared as described previously [11,12]. Sonication of the liposome suspension was performed with a probe-type sonicator (MSE Soniprep 150) for 4 × 30 s burst, with cooling periods between each burst. The final suspension contained 0.1 mM phospholipid in 0.1 M Tris-HCl buffer (pH 7.0).

n-Doxyl stearates

Quenching of tryptophan fluorescence was carried out using *n*-doxyl stearates (*n*-NS, $n=$ 5,7,10,12) purchased from Molecular Probes (U.S.A.).

Peptide syntheses

The peptides were synthesized by fragment condensation as outlined in Fig. 1. Boc-LAla-Aib-Ala-Aib-Ala-OH [13], Boc-LAla-Aib-Ala-Aib-Ala)$_2$-OH and H-(LAla-Aib-Ala-Aib-Ala)$_n$-OMe HCl ($n = 1$–4) [14] were the key products for the synthesis of the tryptophan helices. The syntheses [14], spectroscopic studies [14,15] and dipole moments [16] of the helices Boc-(Ala-Aib-Ala-Aib-Ala)$_n$-OMe ($n = 1$–4) were published elsewhere. The identity and purity of the tryptophan-containing helices was checked by TLC (detection with ninhydrin and chlorine/4,4′-methylenebis(N,N'-dimethylaniline) TDM reagent), amino-acid analysis (addition of thioglycolic acid to 6 M HCl,

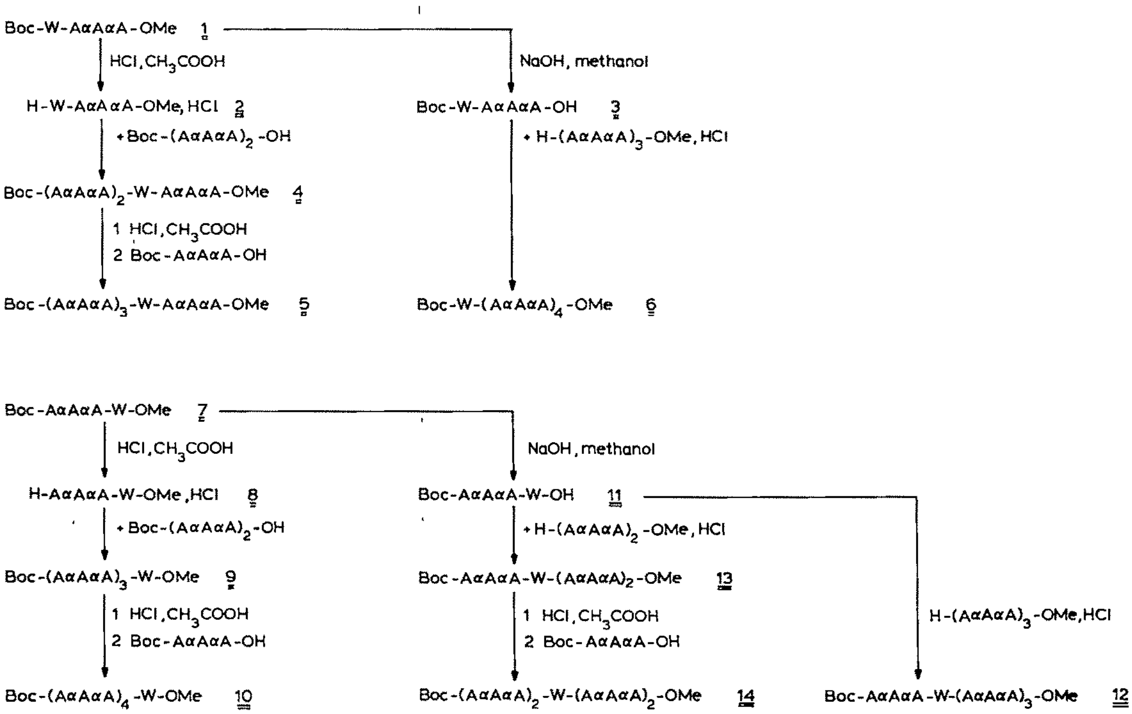

Fig. 1. Scheme of fragment condensations used for the synthesis of five tryptophan-containing α-helical 21-peptides (A, alanine: α = α-aminoisobutyric acid; Boc = *tert*-butoxycarbonyl; W, tryptophan)

110°C, 18 h), and ^{1}H-NMR. R_F values were determined on silica-gel plates (Merck, No. 5729) with chloroform/methanol/acetic acid/ (65 : 25 : 3 : 4, v/v).

Boc-Trp-Ala-Aib-Ala-Aib-Ala-OMe (1)

At −10°C, a 1 M solution of *N,N'*-dicyclohexylcarbodiimide in dichloromethane (1.43 ml, 1.43 mmol) is added to Boc-Trp-OH (402 mg, 1.32 mmol) and 1-hydroxybenzotriazole (180 mg, 1.32 mmol) in dimethylformamide (1 ml). After 10 min at −10°C, *N,N'*-dicyclohexylurea precipitates and H-Ala-Aib-Ala-Aib-Ala-OMe · HCl [13] (500 mg, 1.1 mmol) and *N*-methylmorpholine (0.121 ml, 1.1 mmol) in dimethylformamide (3 ml) are added. After 1 h at −10°C, 4 h at 0°C, and 18 h at room temperature acetic acid (50 μl) is added and the urea is removed by centrifugation. The supernatant is concentrated in vacuo, and the dry residue is dissolved in ethyl acetate/1-butanol (1 : 1, v/v) and washed thrice with 5% sodium hydrogen carbonate, thrice with 5% potassium hydrogen sulfate and five time with water. After drying over sodium sulfate Boc-Trp-Ala-Aib-Ala-Aib-Ala-OMe (**1**) is precipitated by addition of light petroleum (b.p. 30–50°C), and chromatographed on Sephadex LH-20 (column 60 × 2.7 cm). Yield: 680 mg (88%); $R_F = 0.81$.

H-Trp-Ala-Aib-Ala-Aib-Ala-Aib-Ala-OMe –HCl (2)

Hexapeptide **1** (200 mg, 0.285 mmol) is deprotected with 1.2 M HCl/acetic acid (1.54 ml, 1.85 mmol) at 5°C. After 10 min the solution is concentrated in vacuo, the dry residue is dissolved in methanol and evaporated again. After freeze-drying from *t*-butanol/water (3 : 1) the ester is stored over potassium hydroxide in vacuo. Yield: 173 mg (95%); $R_F = 0.86$.

N-Boc-Trp-Ala-Aib-Ala-Aib-Ala-OH (3)

Hexapeptide **1** (200 mg, 0.285 mmol) is saponified in methanol (7.5 ml) and 0.5 M NaOH (1.73 ml, 0.86 mmol). After 2 h at room temperature the solution is neutralized at 0°C, and methanol is removed on a rotary evaporator. After acidification to pH 2 and extraction with ethyl acetate (five times) the combined extracts are washed twice with water, dried over sodium sulfate and evaporated in vacuo. The hexapeptide acid **3** is chromatographed on Sephadex LH-20 and freeze-dried from *t*-butanol/water (3 : 1). Yield: 154 mg (80%); $R_F = 0.42$.

Boc-(Ala-Aib-Ala-Aib-Ala)$_2$-Trp-Ala-Aib-Ala-Aib-Ala-OMe (4)

Boc-(Ala-Aib-Ala-Aib-Ala)$_2$-OH [14] (150 mg, 0.17 mmol) is activated at 0°C with 1-hydroxybenzotriazole (23 mg, 0.17 mmol) in dimethylformamide (1.5 ml) by addition of *N,N'*-dicyclohexylcarbodiimide (38.5 mg, 0.19 mmol). After precipitation of urea the mixture is warmed up to room temperature, and after 15 min the hexapeptide ester hydrochloride (**2**) (130 mg, 0.2 mmol) and *N*-methylmorpholine (22 μl, 0.2 mmol) in dimethylformamide (1 ml) are added. After 18 h, acetic acid (50 μl) is added, the urea is removed by centrifugation, and the supernatant is concentrated in vacuo. The residue is dissolved in dichloromethane and purified as described for **1**. Yield: 240 mg (95%); $R_F = 0.85$.

Boc-(Ala-Aib-Ala-Aib-Ala)$_3$-Trp-Ala-Aib-Ala-Aib-Ala-OMe (5)

Hexapeptide **4** (240 mg, 0.165 mmol) is dissolved in 1.2 M HCl/acetic acid (2 ml) and concentrated in vacuo after 10 min. After drying in a desiccator over potassium hydroxide, the peptide ester is dissolved in dimethylformamide (2 ml) and neutralized with *N*-methylmorpholine (18 μl, 0.165 mmol). Boc-Ala-Aib-Ala-Aib-Ala-OH [13,14] (166 mg, 0.33 mmol) is activated at 0°C with 1-hydroxybenzotriazole (45 mg, 0.33 mmol) in dimethylformamide (1.5 ml) and *N,N'*-dicyclohexylcarbodiimide (39 mg, 0.19 mmol). After precipitation of urea the activated pentapeptide acid is added to the solution of the hexadecapeptide ester. After 18 h, acetic acid (50 μl) is added and the solvent is evaporated in vacuo. The heneicosapeptide, **5**, is purified on Sephadex LH-20 in dichloromethane/methanol (11 : 1, v/v). Further purification is achieved on a silica-gel column followed again by Sephadex LH-20 chromatography. Yield: 89 mg (30%); $R_F = 0.70$; m.p. 205°C (dec.).

Boc-Trp-(Ala-Aib-Ala-Aib-Ala)$_4$-OMe (6)

This 21-peptide can be prepared via two different routes. Boc-Trp-OH (28.5 mg, 95 μmol) is activated at 0°C with 1-hydroxybenzotriazole (13 mg, 94 mmol) in dimethylformamide (0.5 ml) and N,N'-dicyclohexylcarbodiimide (21 mg, 19 μmol). After precipitation of urea, the mixture is pipetted into a solution of H-(Ala-Aib-Ala-Aib-Ala)$_4$-OMe · HCl (30 mg, 19 μmol) and N-methylmorpholine (19 μl, 19 μmol) in dimethylformamide/dichloromethane (1 : 1, v/v; 200 μl). After 4 h the icosapeptide ester has disappeared (TLC), and the isolation of **6** is performed as described for **5**. Yield: 10 mg (29%); $R_F = 0.70$.

Boc-Trp-Ala-Aib-Ala-Aib-Ala-OH (101 mg, 148 μmol) is activated at 0°C with 1-hydroxybenzotriazole in dimethylformamide (1.5 ml) and N,N'-dicyclohexylcarbodiimide (37 mg, 1.80 μmol). A solution of H-(Ala-Aib-Ala-Aib-Ala)$_3$-OMe (150 mg, 123 μmol) and N-methylmorpholine (14 μl, 123 μmol) in dimethylformamide (1.5 ml) is added. After 10 h at room temperature the polypeptide **6** is isolated as described for **5**. Yield: 70 mg (31%); $R_F = 0.70$.

Boc-Ala-Aib-Ala-Aib-Ala-Trp-OMe (7)

To Boc-Ala-Aib-Ala-Aib-Ala-OH (575 mg, 1.15 mmol) and 1-hydroxybenzotriazole (156 mg, 1.15 mmol) in dimethylformamide (5 ml) is added a 1 M solution of N,N'-dicyclohexylcarbodiimide in dichloromethane (1.26 ml, 1.26 mmol) at 0°C. After 30 min (precipitation of urea) H-Trp-OMe · HCl (350 mg, 1.38 mmol) and N-methylmorpholine (152 μl, 1.38 mmol) in dimethylformamide is added. After 24 h at room temperature the isolation follows the procedure for **1**. The hexapeptide **7** is purified by gel chromatography on Sephadex LH-20. Yield: 565 mg (70%); $R_F = 0.90$.

H-Ala-Aib-Ala-Aib-Ala-Trp-OMe · HCl (8)

Hexapeptide 7 (400 mg, 570 μmol) is deprotected in 1.2 M HCl/acetic acid (3 ml, 3.7 mmol) at 0°C. After 10 min the solution is concentrated in vacuo. The dry residue is dissolved in methanol and evaporated again several times, and lyophilized from t-butanol/water (3 : 1, v/v). Yield: 291 mg (80%); $R_F = 0.45$.

Boc-(Ala-Aib-Ala-Aib-Ala)$_3$-Trp-OMe (9)

Boc-(Ala-Aib-Ala-Aib-Ala)$_2$-OH (176 mg, 197 μmol) is activated at 0°C with hydroxybenzotriazole (27 mg, 197 μmol) in dimethylformamide (1.5 ml) and a 1 M solution of N,N'-dicyclohexylcarbodiimide in dichloromethane (215 μl, 215 μmol). After precipitation of urea (15 min) a solution of hexapeptide ester **8** (105 mg, 164 μmol) and N-methylmorpholine (17 μl, 164 μmol) in dimethylformamide (1 ml) is added. After 15 h the hexadecapeptide is isolated according to the procedure described for **5**. Chromatography on Sephadex LH-20, silica gel and again Sephadex LH-20 in methanol yield peptide **9**. Yield: 200 mg (83%); $R_F = 0.85$.

Boc-(Ala-Aib-Ala-Aib-Ala)$_4$-Trp-OMe (10)

Hexapeptide ester **9** (300 mg, 204 μmol) is deprotected with 1.2 M HCl/acetic acid at 5°C. After 10 min the solution is evaporated and the residue is dried over KOH in vacuo for 12 h. The ester and N-methylmorpholine (23 μl, 399 μmol) are dissolved in dimethylformamide (2 ml) and a solution of Boc-Ala-Aib-Ala-Aib-Ala-OH (200 mg, 399 μmol), preactivated with 1-hydroxybenzotriazole (54 mg, 399 μmol) and 1 M N,N'-dicyclohexylcarbodiimide/dichloromethane (440 μl, 440 μmol) in dimethylformamide/dichloromethane (1 : 1, 2 ml) is added. Acetic acid (50 μl) is added after 18 h and the henicosapeptide **10** is isolated as described for **5**. Yield: 100 mg (27%); $R_F = 0.85$; m.p. 170°C (dec.).]

Boc-Ala-Aib-Ala-Aib-Ala-Trp-OH (11)

Hexapeptide ester **7** (200 mg, 0.28 mmol) was saponified in methanol (7.5 ml) with 0.5 M NaOH (1.73 ml, 0.86 mmol). After 2 h the hexapeptide acid **11** was isolated as described for **3** and chromatographed on silica-gel and Sephadex LH-20 in methanol. Yield 170 mg (88%); $R_F = 0.42$; m.p. 195°C (dec.).

Boc-Ala-Aib-Ala-Aib-Ala-Trp-(Ala-Aib-Ala-Aib-Ala)-OMe (12)

Hexapeptide acid **11** (113 mg, 164 μmol) in dichloromethane (1.5 ml) is activated with 1-hydroxybenzotriazole (22 mg, 164 μmol) and N,N'-dicyclohexylcarbodiimide (37.3 mg, 180.5 μmol) at 0°C. After the activation becomes evident (precipitation of urea) H-(Ala-Aib-Ala-Aib-Ala)$_3$-OMe [14] (100 mg, 82 μmol) and N-methylmorpholine (9 μl, 82 μmol) in dimethylformamide (1 ml) are added. After 4 h acetic acid (40 μl) is added, the solvent is removed and the residue is dissolved in dichloromethane. After filtering off the insoluble urea, the peptide **12** is chromatographed on Sephadex LH-20, silical-gel and again on Sephadex LH-20 in methanol/dichloromethane (1 : 1, v/v). Yield 150 mg (49%); $R_F = 0.78$; m.p. 172°C (dec.).

Boc-Ala-Aib-Ala-Aib-Ala-Trp-(Ala-Aib-Ala-Aib-Ala)$_2$-OMe (13)

Hexapeptide acid **11** (200 mg, 0.29 mmol) is activated with 1-hydroxybenzotriazole (39 mg, 0.29 mmol) and *N,N'*-dicyclohexylcarbodiimide (70 mg, 0.34 mmol) in dimethylformamide (2 ml) at 0°C. After 10 min H-(Ala-Aib-Ala-Aib-Ala)$_2$-OMe · HCl (202 mg, 0.24 mmol) in dimethylformamide (1.5 ml) are added. After 18 h and addition of acetic acid (50 μl) the filtrate of the reaction mixture is evaporated and the residue is taken up in chloroform and washed with 5% potassium hydrogen sulfate and water. Final purification of **13** is achieved by gel chromatography on Sephadex LH-20. Yield: 300 mg (84%); $R_F = 0.72$; m.p. 170°C.

Boc-(Ala-Aib-Ala-Aib-Ala)$_2$-Trp-(Ala-Aib-Ala-Aib-Ala)$_2$-OMe (14)

Hexapeptide **13** (300 mg, 204 μmol) is deprotected in 1.2 M HCl/acetic acid (2 ml, 204 μmol) at 0°C. After 10 min the solvent is removed and the resulting peptide ester hydrochloride is chromatographed on Sephadex LH-20 in methanol in order to remove decomposition products. The main fraction (200 mg, 143 μmol, yield 70%) and *N*-methylmorpholine (16 μl, 143 μmol) are dissolved in dimethylformamide (1.5 ml). Boc-Ala-Aib-Ala-Aib-Ala-OH [13] (143 mg, 285 μmol) is activated with 1-hydroxybenzotriazole (39 mg, 285 μmol) and *N,N'*-dicyclohexylcarbodiimide (65 mg, 314 μmol) in dichloromethane and, after 10 min, is added to the hexadecapeptide ester. After 5 h acetic acid (50 μl) is added, the solution is evaporated and the residue chromatographed on Sephadex LH-20, silica-gel, and again on Sephadex LH-20 in dichloromethane/methanol (1 : 1, v/v). Yield: 103 mg (49%); $R_F = 0.70$; m.p. 173°C (dec.).

21-Peptide methyl esters with free N-terminus

After treatment of henicosapeptides **5, 6, 10, 12** and **14** with HCl/acetic acid for 10 min at 4°C, a second set of henicosapeptides is obtained possessing free, positively charged N-terminus. After lyophilisation from *t*-butanol these peptides are checked by TLC, CD, ultraviolet and fluorescence spectroscopy.

Analyses of tryptophanyl peptides

The *N*-Boc-protected hexapeptides **1, 3, 7** and **8** were characterized by ^{1}H- and ^{13}C-NMR spectra. After acidolytic removal of the *t*-butoxycarbonyl group the hexapeptide ester hydrochlorides **2** and **8** were analyzed by ^{1}H-NMR and found to contain the intact indolyl ring. On the amino-acid analyzer, peak separation of Ala/Aib could not be achieved quantitatively (ratio of color factors Ala/Aib = 7 : 1) for the five henicosapeptides. Threfore the Ala/Aib and the Trp peaks (addition of thioglycolic acid for hydrolysis) were taken for the determination of recovery factors. Only Boc-Trp-(Ala-Aib-Ala-Aib-Ala)$_4$-OMe (**6**) contained larger amounts of silica gel (recovery factor 0.26), whereas the other four 21-peptides showed excellent recovery factors: 1.00(**12**), 0.98 (**14**), 0.95(**5**) and 0.95(**10**). Gas chromatography of the *N*-pentafluoropropionylamino acid *n*-propyl esters of the hydrolysate (prepared in the presence of 2-propanethiol) on a Chirasil-Val capillary column gave satisifying results.

The analyses of all peptides which do not contain tryptophan are reported elsewhere [13–15].

Spectroscopy

Ultraviolet spectra of the polypeptides were measured in ethanol at concentrations from $c = 1 \cdot 10^{-7}$ to $c = 1 \cdot 10^{-8}$ mol/l on a Cary ultraviolet spectrometer (path-length $d =$ 1 cm; slit-width 1 nm; temperature 22°C). Circular dichroism spectra were measured on a CD 195 spectrometer (Roussel-Jouan) in methanol ($c = 1 \cdot 10^{-3}$ mol/l; temperature 20°C). The intensity of the Cotton effects is given in mean residue ellipticities $[\theta]_m$. Epiandosterone in dioxan with $[\theta] = 10.925$ deg · cm^2 · dmol^{-1} at 304 nm was used for calibration of the spectrometer. Fluorescence spectra of tryptophan-containing peptides were recorded with a

Hitachi-Perkin Elmer MPF3 spectrofluorimeter using an excitation wavelength of 290 nm. Peptide solutions ($c = 4 \cdot 10^{-6}$ mol/l) were prepared in the following solvents: (a) 0.1 M Tris-HCl (pH 7.0); (b) ethanol; (c) 0.1 mM egg phosphatidylcholine vesicles in 0.1 M Tris-HCl buffer (pH 7.0).

Quenching experiments

Stock solutions (1 mM) of the *n*-doxyl stearic acids (*n*-NS) were prepared in methanol and their relative concentrations measured by ESR. Aliquots (6 × 5 μl) were added to 2.5 ml of vesicle suspension (0.1 mM phospholipid containing 4 μM peptide) in a cuvette, and the fluorescence intensity was determined at 340 nm. The use of *n*-NS probes to determine the transverse position of fluorophore bilayers requires a knowledge of the partition coefficients of the quenchers. These were determined according to methods published elsewhere [9,10].

Analysis of peptide partitioning

The partitioning [17] of the polypeptides into the bilayer phase was determined by analysis of the enhancement of tryptophan fluorescence that occurs during uptake. At a given concentration of peptide and membrane, the observed fluorescence is determined by the fluorescence of the peptide in the membrane (M) and aqueous (A) phases.

$$F_{\mathrm{obs}} = F_{\mathrm{M}} + F_{\mathrm{A}} \tag{1}$$

$$= F_{\mathrm{M}} \cdot f + F_{\mathrm{A}}(1-f) \tag{2}$$

where f is the fraction of total peptide which is in the lipid phase.

$$f = \frac{F_{\mathrm{obs}} - F_{\mathrm{A}}}{F_{\mathrm{M}} - F_{\mathrm{A}}} \tag{3}$$

The concentration of the peptide in the membrane ($[\mathrm{P}]_{\mathrm{M}}$) is given by:

$$[\mathrm{P}]_{\mathrm{M}} = [\mathrm{P}]_{\mathrm{T}} \cdot f = \langle P \rangle \cdot [\mathrm{ves}] \tag{4}$$

where $[\mathrm{P}]_{\mathrm{T}}$ is the total concentration of peptide, $\langle P \rangle$ is the number of peptide molecules per vesicle, and [ves] is the concentration of vesicles. The total concentration of peptide is the sum of the concentration in each phase:

$$[\mathrm{P}]_{\mathrm{T}} = [\mathrm{P}]_{\mathrm{M}} + [\mathrm{P}]_{\mathrm{A}} \tag{5}$$

$$= \langle P \rangle\ [\mathrm{ves}] + [\mathrm{P}]_{\mathrm{A}} \tag{6}$$

Thus, uptake experiments at a range of vesicle concentrations provide data for a plot of Eqn. 6, values of $\langle P \rangle$ and $[\mathrm{P}]_{\mathrm{A}}$ being determined from the slope and intercept, respectively. The concentration of peptide in the lipid phase, expressed with respect to the volume of the lipid phase becomes:

$$[\mathrm{P}]_{\mathrm{L}} = \langle P \rangle = K_{\mathrm{p}} \cdot [\mathrm{P}]_{\mathrm{A}} \tag{7}$$

where K_{p} is the partition coefficient and V_{L} is the volume of 1 mol of vesicles. K_{p} can therefore be determined from a plot of $\langle P \rangle$ versus $[\mathrm{P}]_{\mathrm{A}}$. Where the uptake is determined by binding to predetermined sites on or in the membrane, as well as by partition, the ordinate intercept of this plot can provide a measure of the number of binding sites [9].

Results and Discussion

By conventional peptide fragment condensations five α-helices were synthesized (compare Fig. 1) each containing one tryptophan residue. According to the sequence position of the tryptophan residue the *t*-butoxycarbonyl-protected henicosapeptides (21-peptides) and the corresponding *N*-deprotected peptides used in this investigation were abbreviated as shown in Scheme I.

Boc-W-(AαAαA)$_4$-OMe **6** +H$_2$-W-(AαAαA)$_4$-OMe	B-21$_1$-OMe H-21$_1$-OMe
Boc-AαAαA-W-(AαAαA)$_3$-OMe **12** +H$_2$-AαAαA-W-(AαAαA)$_3$-OMe	B-21$_6$-OMe H-21$_6$-OMe
Boc-(AαAαA)$_2$-W-(AαAαA)$_2$-OMe **14** +H$_2$-(AαAαA)$_2$-W-(AαAαA)$_2$-OMe	B-21$_{11}$-OMe H-21$_{11}$-OMe
Boc-(AαAαA)$_3$-W-AαAαA-OMe **5** +H$_2$-(AαAαA)$_3$-W-AαAαA-OMe	B-21$_{16}$-OMe H-21$_{16}$-OMe
Boc-(AαAαA)$_4$-W-OMe **10** +H$_2$-(AαAαA)$_4$-W-OMe	B-21$_{21}$-OMe H-21$_{21}$-OMe

Scheme I. Peptide abbreviations.

The conformationally stable α-helical henicosapeptides with tryptophan in defined positions were embedded in liposomes and examined as follows:

(a) Upon excitation at 290 nm the Stokes' shift of the emission band was recorded for the henicosapeptides in solvents of different polarity.

(b) The partition coefficients in the polypeptides were determined from the enhancement of tryptophan fluorescence according to Eqns. 6 and 7.

(c) The liposomes were titrated with n-doxyl stearic acids ($n = 5, 7, 10, 12, 16$) to determine the transverse position of tryptophan residues in the bilayer.

Using this experimental approach we tried to prove that each helix buries its fluorophore at a defined depth – the depth which is predicted by perpendicular insertion of the helices into the membrane. If the fluorescent oligopeptides span the bilayer in a helical form, they could be classified into three arbitrary groups:

1. B/H-21_1-OMe and B/H-21_{21}-OMe would have terminal fluorophores near the membrane surface.
2. B/H-21_{11}-OMe and B/H-21_{16}-OMe would have fluorophores located within the lipophilic center of the membrane.
3. B/H-21_6-OMe cannot be classified in an a priori way.

The above classification does not exclude the possibility that the polypeptide structures are tilted at some angle to the membrane normal.

Absorption spectra

The indolyl chromophore of the tryptophan residue showed the same wavelengths of absorption bands at 274, 282 and 290 nm for all α-helical 21-peptides (Fig. 2). The intensity ratios of these bands were about the same within the series of B-21_x-OMe, and it was assumed that the molar extinctions were independent of the position of the tryptophan residue along the α-helix. Therefore ultraviolet absorption was taken as a measure for the relative concentration within the series of B-21_x-OMe and H-21_x-OMe peptides. Not only were almost coincident ultraviolet spectra found within these two series, but the maxima of the spectra were also very similar to those of N-stearoyl-L-tryptophan-n-hexyl ester and 3-methylindole.

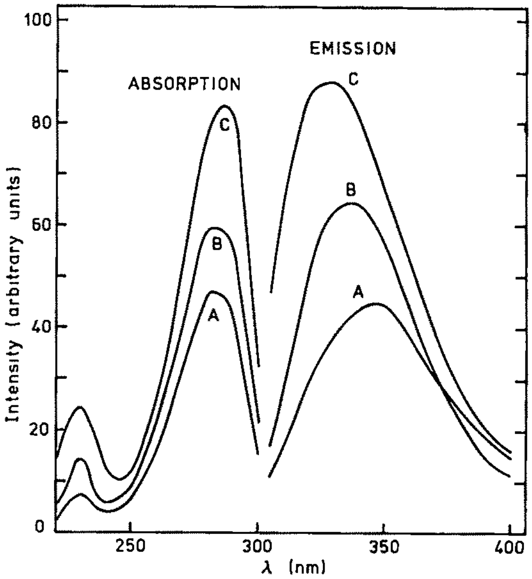

Fig. 2. Solvent dependence of the absorption and emission spectra of 21-peptide Boc-(AαAαA)$_3$-W-AαAαA-OMe (B-21_{16}-OMe, 5) in 0.1 M Tris-HCl (pH 7.0) (A), ethanol (B) and 0.1 mM phosphatidylcholine (C).

Circular dichroism

Obviously the α-helix content is sensitive to the position of tryptophan in the polypeptide chain, which is documented by the different CD spectra of the 21-peptides (Fig. 3). Although aminoisobutyrate peptides may not be appropriate examples in this context, it should be emphasized that N-terminal tryptophan on helices has a higher α-propensity ($H_\alpha = 1.45$) than in other α-helical positions ($H_\alpha = 1.15$) [18].

Henicosapeptides of B-21_{11}-OMe and B-21_{16}-OMe have identical ultraviolet absorption, yet have different circular dichroic spectra. In methanol, higher ellipticities were observed for B-21_1-OMe, B-21_6-OMe and B-21_{21}-OMe; these peptides have ellipticities as found for alamethicin [1] and Boc-(Ala-Aib-Ala-Aib-Ala)$_3$-OMe. We found earlier that the prolongation of the latter pentadecapeptide to the icosapeptide Boc(Ala-Aib-Ala-Aib-Ala)$_4$-OMe reduces the α-helix content from 80% to 40% [14]. In the present case of the henicosapeptides B-21_1-OMe and B-21_6-OMe, the strong helix-former tryptophan restores the α-helix to 80%. It is not clear, however, why tryptophan in the C-terminal position in B-21_{21}-OMe also leads

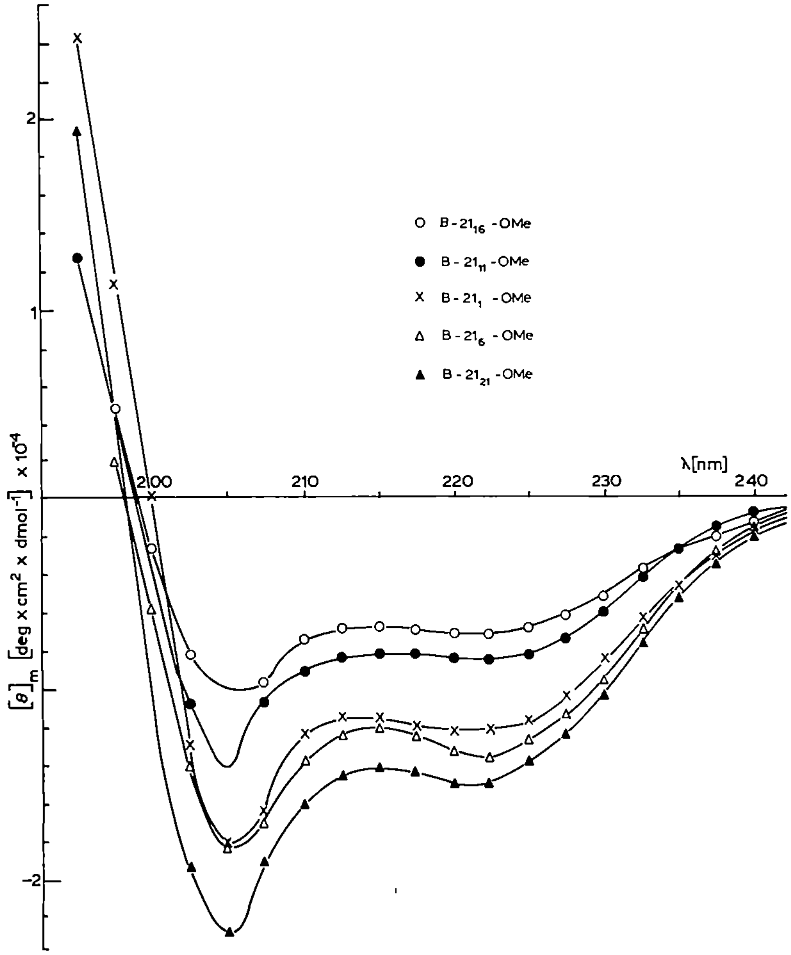

Fig. 3. Circular dichroism spectra of the five tryptophan containing α-helical 21-peptides (1 mM; ethanol, 20 °C).

to high ellipticities. According to the CD measurements, the tryptophan residue in the middle of the molecule destabilizes the still-dominating α-conformation in B-21$_{11}$-OMe and B-21$_{16}$-OMe.

The CD spectra of the series are homogeneous with respect to the wavelengths of the Cotton effects and their intensity ratios (Table I). The maxima of π,π^* transitions are shifted by 2 nm to 205 nm with respect to the non-tryptophan-containing icosapeptide, Boc-(Ala-Aib-Ala-Aib-Ala)$_4$-OMe.

TABLE I

CIRCULAR DICHROISM DATA OF THE TRYPTOPHAN-HELICES B-21$_x$-OMe (METHANOL, 1 mM, 20 °C)

x	1	6	11	16	21
$[\theta]_m^{205}$	−18100	−18320	−14070	−10250	−22670
$[\theta]_m^{222}$	−12200	−13590	−8500	−7190	−15000
$R = [\theta]_m^{222}/[\theta]_m^{205}$	0.67	0.74	0.60	0.70	0.66
% α-Helix	80	81	62	45	100
Residues in α-Helix	17	17	13	9-10	21

TABLE II

SOLVENT DEPENDENCE OF THE TRYPTOPHAN FLUORESCENCE MAXIMUM (nm) OF THE 21-PEPTIDE HELICES

In parentheses are given shifts ($\Delta\lambda$) of the fluorescence maximum referred to buffer solution ($\Delta\lambda = 0$).

	Tris-HCl	Ethanol	Phosphatidylcholine bilayers
Boc-21_1-OMe	346	338 (−8)	337 (−9)
H-21_1-OMe	352	342 (−10)	348 (−4)
Boc-21_6-OMe	320	330 (+10)	320 (0)
H-21_6-OMe	349	335 (−14)	322 (−27)
Boc-21_{11}-OMe	346	339 (−7)	324 (−22)
H-21_{11}-OMe	352	339 (−13)	338 (−14)
Boc-21_{16}-OMe	345	340 (−5)	330 (−15)
H-21_{16}-OMe	350	339 (−11)	332 (−18)
Boc-21_{21}-OMe	–	–	–
H-21_{21}-OMe	350	350 (0)	345 (−5)

Fluorescence spectra

The fluorescence spectra of the helical polypeptide esters **5**, **6**, **10**, **12**, **14** (Fig. 1) and their N-deprotected esters were recorded in three solvent systems:

(A) aqueous buffer (0.1 M Tris-HCl (pH 7.0));
(B) ethanol;
(C) bilayer vesicles.

Generally, a blue shift of fluorescence band is observed on changing the solvents from A to C (Fig. 2), whereas the ultraviolet band does not shift.

Due to the positively charged N-terminus, the series H-21_x-OMe is expected to form a larger solvent cage than the uncharged series B-21_x-OMe. Thus, according to the Lippert equation, the compounds H-21_x-OMe exhibit a Stokes' shift which is about 5 nm larger than for the compounds B-21_x-OMe (Table II). Both compounds, B-21_1-OMe and H-21_1-OMe, locate the fluorophore near the hydrophilic surface of the membrane, where the polarity of the environment is similar to the buffer solution, resulting in a minimal Stokes' shift (Fig. 4).

Similarly, a blue shift of only 5 nm is observed for H-21_{21}-OMe on changing the medium from buffer to ethanol to bilayer vesicles. We would expect the charged N-terminus to be about 30 Å from the fluorophore in this helical compound.

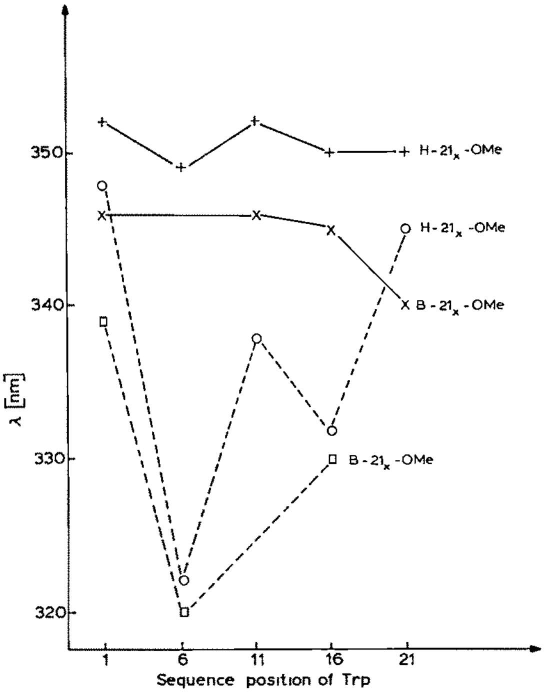

Fig. 4. Dependence of the fluorescence emission maximum on the position of the tryptophan residue in N-Boc and protonated 21-peptide helices in 0.1 M Tris-HCl (———) and in liposomes (- - - -)

Therefore, the induced small blue shift at the C-terminal tryptophan must be attributed to charge effects of N-termini of neighboring helices in antiparallel position. The fact that both N- and C-terminal fluorophores are in a polar environment leads to the conclusion that the H-21_{21}-OMe helices are inserted perpendicular to the membrane surface and span the membrane.

The behavior of B-21_6-OMe cannot be explained satisfactorily. This compound seems to agregate strongly in aqueous solution thus producing a lipophilic environment for the fluorophore. Except for B-21_{16}-OMe and H-21_{16}-OMe, the charged and uncharged species behave similarly. Obviously the positive charge at the N-terminus of the 21-peptide helices does not influence the orientation of the helix or depth of the fluorophore. This is consistent with the results of bilayer experiments, in which the N-terminally charged helices induce voltage-dependent, ion-conducting pores, but with different pore-state characteristics [5,6].

TABLE III

PARTITION COEFFICIENTS (K_p) OF THE TRYPTOPHAN α-HELICES IN EGG PHOSPHATIDYLCHOLINE BILAYERS

Peptide	K_p[cm$^{-3}\cdot$mol^{-1}] (×10^4)	r [a]
B-21$_1$-OMe	1 390 ±0.42	0.89
B-21$_6$-OMe	0.632 ±0 09	0.97
B-21$_{11}$-OMe	0 461 ±0.15	0.87
B-21$_{16}$-OMe	4.570 ±0.11	0.99
Indole	3.340 ±1.0	0.95
Trp-Sta	5.700 ±0.6	–
H-21$_1$-OMe	1 560 ±0 47	0.86
H-21$_6$-OMe	1.540 ±0.23	0.99
H-21$_{11}$-OMe	3 690 ±0 50	0.97
H-21$_{16}$-OMe	3 490 ±0.52	0.97
H-21$_{21}$-OMe	80 30 ±27.6	0.83

[a] Correlation coefficient for plot of Eqn 7 ($[P]_L$ vs. $[P]_A$)

Two conclusions may be drawn from the fluorescence spectra:

(1) B-21$_1$-OMe and H-21$_{21}$-OMe locate their terminal tryptophan fluorophores near the hydrophilic membrane surface.

(2) Helices with tryptophan in positions 6, 11 and 16 locate their fluorophores in the lipophilic, inner part of the membrane.

Fluorescence enhancement

The mechanism of association of the helical polypeptide with the lipid bilayer can be inferred from data plotted according to Eqn. 6. When partition is the only type of association process, such plots are linear and pass through the origin. When the association involves both partition and binding processes the plots are nonlinear [9]. In the present study, these plots were linear and intercepted the ordinate axis close to the origin, indicating that partition was the dominant mode of association. The K_p values for the polypeptides are summarized in Table III and confirm their high lipophilicity. These values are comparable to those determined for doxyl stearates in bilayer systems [12]. Since the overall lipophilicity of the butoxycarbonyl-protected polypeptides is the same, the observed difference in K_p must be attributed to the influence of sequence and conformation. The same is true of differences within the deprotected series of polypeptides.

Quenching of fluorescence

Table IV summarizes the expected transverse positions of the doxyl groups and tryptophan residues in the lipid bilayer for the n-NS and H-21$_x$-OMe molecules, respectively. After incorporation of the polypeptide into the bilayer, the highest quenching efficiency should be observed for the n-doxyl stearate which places its doxyl moiety closest to the tryptophan fluorophore. Quenching data are normally presented as a Stern-Volmer plot of the quenching efficiency, QE ($= I_0/I - 1$) versus total quencher concentration, $[Q]_T$; I and I_0 being the fluorescence intensities in the presence and absence of quencher, respectively. In the two-phase system dealt with here the appropriate value of [Q] is that pertaining to the lipid phase rather than to the total volume. Indeed, the use of $[Q]_T$ can lead to serious errors [9,10]. Thus, the abscissa in Figs. 5 and 6 are scaled in terms of the average number of quencher molecules per vesicle rather than $[Q]_T$.

TABLE IV

DEPTHS OF THE DOXYL LABELS AND TRYPTOPHAN RESIDUES IN A LIPID BILAYER MEMBRANE

	$x =$	1	6	11	16	21
H-21$_x$-OMe	$d_{\text{theor}} =$	1 5	9	16 5	24	31.5
	$d_{\text{obs}} =$	1–5	6–9	15	25	38–33
n-NS [a]	$n =$	5	7	10	12	16
	$d =$	6.25	8.75	12.5	15	20
	$d' =$	30.75	28.25	25.5	22	17

[a] For n-NS, two values for the depth of a quencher (d and d') are given, because the carboxy groups are anchored on both polar sides of the bilayer membrane (thickness: 37 Å) The theoretical depths of a fluorophore was calculated assuming an ideal α-helix spanning the membrane, using the relation $d_{\text{theor}} = 1.5 \times n$ Å (n, sequence position of tryptophan residues). d_{obs} are the values taken from the modified Stern-Volmer plots for the observed maximal quenching efficiency

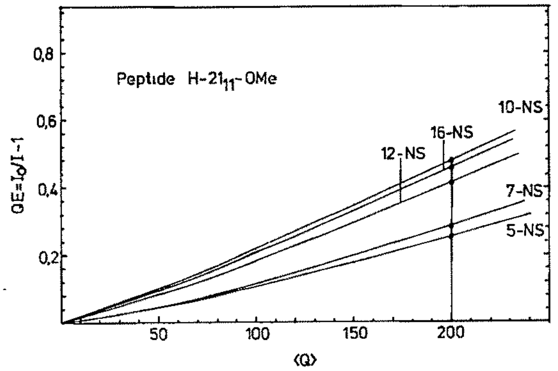

Fig. 5. Stern-Volmer plot for the quenching of the tryptophan fluorophore in H-21_{11}-OMe by the doxyl stearic acids *n*-NS ($n = 5, 7, 10, 12, 16$). The quenching efficiency (QE) at $\langle Q \rangle = 200$ normalized with respect to QE(5-NS) gives data for the secondary plots shown in Fig. 7.

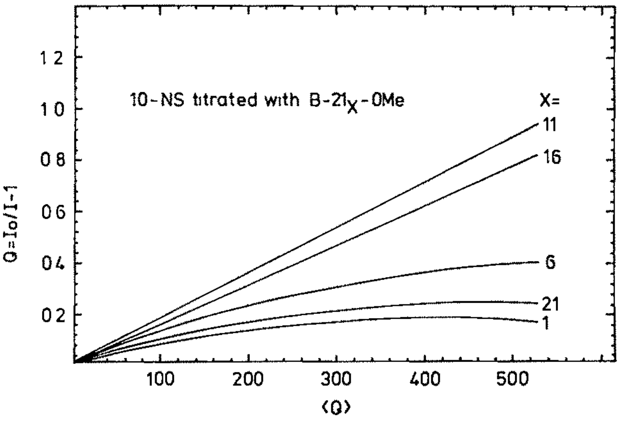

Fig. 6. Stern-Volmer plots of titration of *n*-doxyl stearic acids with the five butoxycarbonyl-protected helices B-21_x-OMe ($x = 1, 6, 11, 16, 21$).

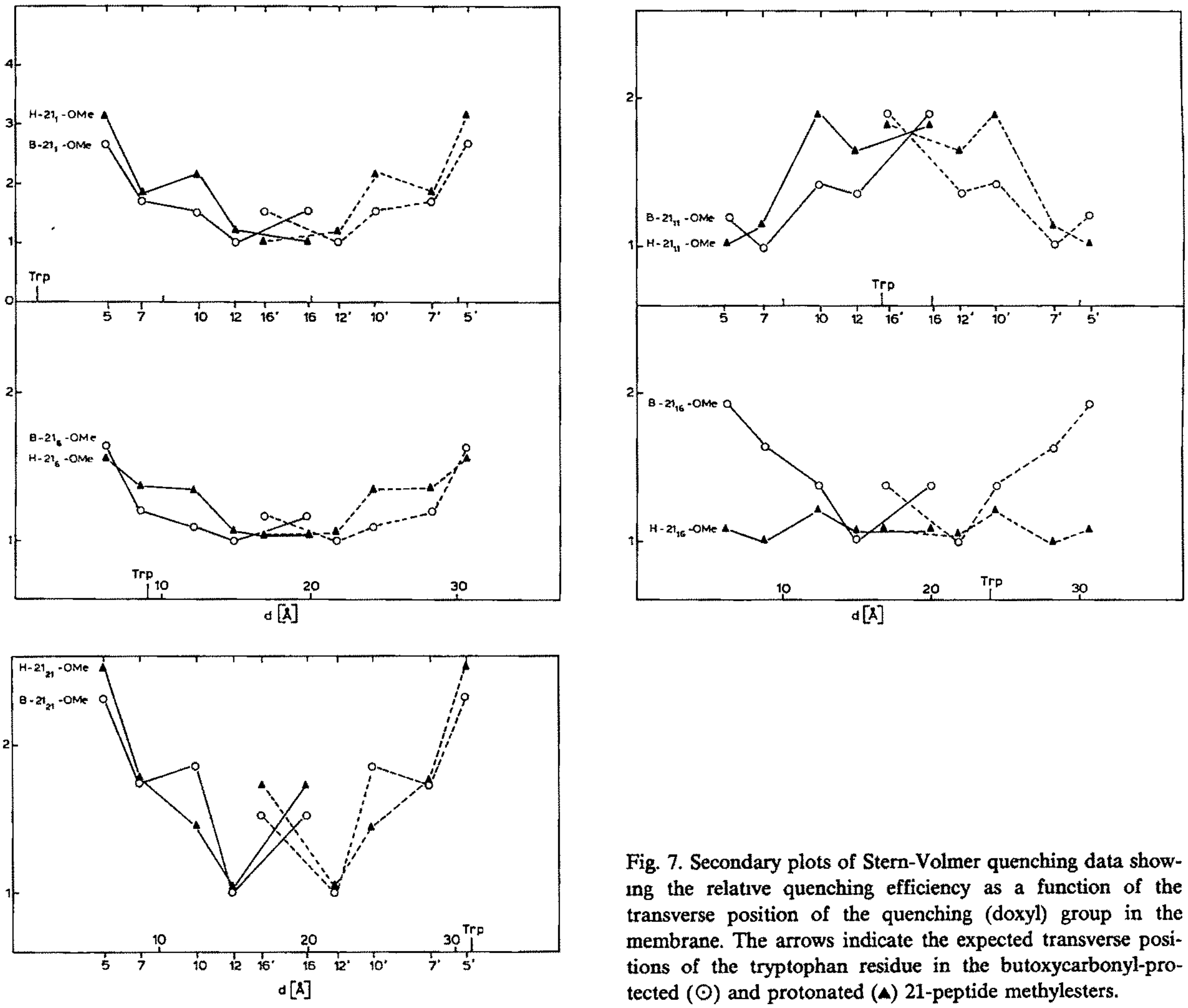

Fig. 7. Secondary plots of Stern-Volmer quenching data showing the relative quenching efficiency as a function of the transverse position of the quenching (doxyl) group in the membrane. The arrows indicate the expected transverse positions of the tryptophan residue in the butoxycarbonyl-protected (○) and protonated (▲) 21-peptide methylesters.

A comparison of the relative quenching efficiency of the five *n*-NS quenchers can be obtained by comparing the quenching efficiencies at a single value of $\langle Q \rangle$; e.g. $\langle Q \rangle = 200$. The resulting quintuplet of data points ($QE_1 \ldots QE_5$) can be normalized to the lowest value (QE_5) thus:

$$\overline{QE_i} = QE_i/QE_5 \ (i = 1-5).$$

These normalized values can now be plotted against the depth of the quenching moiety (i.e., the doxyl group) in the membrane as depicted in Fig. 7. Such a plot reflects the transverse or depth proximity of the fluorophore to the quenching group and therefore indicates the transverse position of the tryptophan residue in the membrane. For the individual peptides the following results were obtained.

B/H-21$_1$-OMe (theoretical depth 1.5 Å). Protected and protonated peptide esters exhibit similar behavior. Optimum quenching is achieved by 5-NS, which places its paramagnetic doxyl group at a depth of approx. 6.25 Å from the hydrophilic surface of the membrane. The influence of the quenchers decreases as they are placed deeper in the membrane.

B/H-21$_6$-OMe (theoretical depth 9 Å). The tryptophan fluorophore is placed within the steep gradient of the membrane potential. The quenchers 5-, 7-, 10-NS whose doxyl groups are centered at 6.2, 8.7, 12.5 Å, respectively, from the surface show a stronger effect than 12- and 16-NS, which bury the doxyl moiety in the interior of the membrane. Obviously, the fluorophore is shifted somewhat from the theoretical depth towards the surface.

B/H-21$_{11}$-OMe (theoretical depth 16.5 Å). A highly pronounced change in the Stern-Volmer-plot can be observed, and charged and uncharged helices show similar behavior. Optimum quenching is now achieved by deeper quenchers (10-, 12-, 16-NS). Remarkably, 12-NS quenches with high efficiency, although it is a poor quencher in other cases. Thus, the tryptophan fluorophore is assumed to be placed approx. 15 Å from the bilayer surface.

B/H-21$_{16}$-OMe (theoretical depth 24 Å). N-protected and deprotected species behave differently in this case, although the N-terminus of H-21$_{16}$-OMe is bound to the membrane surface by its positive charge, the peptide shows similar accessibility for all quenchers. Optimum quenching efficiency is achieved for 10-NS, corresponding to a depth of 24.5 Å.

In contrast, the fluorophore of B-21$_{16}$-OMe is mostly accessible to the outer quenchers 5- and 7-NS, thus resembling B-21$_6$-OMe. As evaluated from its CD-spectrum, B-21$_{16}$-OMe has an α-helical content of about 50%. Obviously tryptophan at position 16 causes high conformational flexibility, and thus this molecule is unlikely to form a rigid dipole which spans the membrane.

B/H-21$_{21}$-OMe (theoretical depth 31.5 Å). We would expect the tryptophan fluorophore of this peptide to be placed in the hydrophilic section of the membrane, with 5-NS being an optimum quencher. The observed Stern-Volmer plot confirms the expected orientation (Fig. 7).

Other studies on the fluorescence of ionophores in lipid bilayers have been reported. The association of a synthetic N-terminally dansylated nonapeptide of emericin with phosphatidylcholine liposomes has been studied by Nagaraj and Balaram [19], and the behavior of N-dansylated 13- and 17-residue fragments of alamethicin has been examined in liposomes and rat liver mitochondria [20,21]. The self-association of melittin and its binding to lipid vesicles has been investigated by using the fluorescence of the intrinsic tryptophan residue [22,23]. These studies are noteworthy because of some similarities of melittin to alamethicin [4] with respect to α-helical conformation [24,25], lytic properties [26], stimulation of membrane-bound enzymes [27], and high dipole moment [28]. The recent finding of a naturally occurring analog of alamethicin named trichorzianine AIIIc [29] carrying a C-terminal tryptophanol residue is most interesting in the light of our studies on the 21-peptide helices carrying N- and C-terminal tryptophan residues. C-terminally dansylated alamethicin [30] and trichotoxin [4] have been used already in voltage-dependent bilayer experiments, but not in fluorescence spectroscopic studies.

Conclusion

Tryptophan residues at the N- or C-terminal positions in the peptide are situated in a hydrophilic environment near the bilayer surface. For H-21_1-OMe this is not surprising, as the positive charge is situated on the amino group of tryptophan itself. The experimental behavior of the other synthetic polypeptides proves the original assumption of long helical structures capable of spanning the membrane.

On the other hand, the peptides B/H-21_{11}-OMe would be expected to locate their tryptophan residues in the lipophilic interior of the membrane. This expectation is borne out by experiment.

The compounds B/H-21_6-OMe and H-21_{16}-OMe locate their fluorophores within the steep gradient of the membrne potential. Here small deviations from the theoretical depth of the fluorophores may obscure the differences in quenching efficiency for the *n*-doxyl stearic acids, as shown in the Stern-Volmer-plots for these compounds.

Acknowledgements

This study has been supported by the Deutsche Forschungsgemeinschaft (SFB 76, project B2; G.J.) and by the Australian Research Grants Committee (W.H.S.). K.-P.V. was a stipendiate of the Studienstiftung des Deutschen Volkes.

References

1 Schmitt, H. and Jung, G. (1985) Liebigs Ann. Chem. 321–344
2 Katz, E., Aydin, M., Lucht, N., König, W.A., Ooka, T. and Jung, G. (1985) Liebigs Ann. Chem. 1041–1062
3 Brückner, H., König, W A., Aydin, M. and Jung, G. (1985) Biochim. Biophys Acta 827, 51–62
4 Hanke, W., Methfessel, C., Wilmsen, H.-U., Katz, E , Jung, G. and Boheim, G. (1983) Biochim. Biophys. Acta 727, 108–114
5 Jung, G., Katz, E., Schmitt, H., Voges, K.-P. and Boheim, G. (1983) in Physical Chemistry of Transmembrane Ion Motions (Spach, G., ed.), Elsevier, Amsterdam; (1963) Stud Phys. Theor. Chem. 24, 349–357
6 Menestrina, G , Voges, K.-P., Jung, G. and Boheim, G (1986) Biophys. J , in the press
7 Boheim, G., Hanke, W. and Jung, G. (1983) Biophys. Struct. Mech. 9, 181–191
8 Jung, G. (1984) in Synthetic Antigens, Proc. Int. Conf. Annali Sclavo 1984, 191–208
9 Blatt, E and Sawyer, W H (1985) Biochim. Biophys Acta 822, 43–62
10 Blatt, E., Chatelier, R C. and Sawyer, W.H. (1984) Photochem Photobiol 39, 477–483
11 Chatelier, R.C., Blatt, E. and Sawyer, W H. (1984) Chem Phys Lipids 36, 131–136
12 Blatt, E., Chatelier, R.C. and Sawyer, W.H. (1984) Chem. Phys. Lett. 108, 397–400
13 Schmitt, H., Winter, W , Bosch, R. and Jung, G. (1982) Liebigs Ann. Chem., 1304–1321
14 Voges, K.-P. (1985) Dissertation, University Tübingen
15 Jung, G , Voges, K -P., Schmitt, H., Becker, G., Kolshorn, H. and Albert, K (1984) in Forum Peptides (Castro, B. and Martinez, J , eds.), pp. 217–220, Centre de Pharmacologie-Endocrinologie, Montpellier
16 Rizzo, V , Schwarz, G., Voges, K.-P and Jung, G. (1985) Eur Biophys. J 12, 67–73
17 Blatt, E , Chatelier, R C and Sawyer, W.H (1986) Biophys J. 50, 349–356
18 Chou, P.Y. and Fasman, G.D. (1977) Adv Enzymol. 47, 45–148
19 Nagaraj, R. and Balaram, P. (1979) Biochem. Biophys. Res Commun. 89, 1041–1049
20 Mathew, M.K., Nagaraj, R. and Balaram, P. (1979) Biochim. Biophys. Acta 649, 339–342
21 Mathew, M.K Nagarai, R and Balaram, P. (1981) J. Biol Chem. 257, 2170–2176
22 Dufourcq, J. and Faucon, J.-F. (1977) Biochim. Biophys Acta 467, 1–11
23 Faucon, J -F., Bufourcq, J. ad Loussan, C. (1979) FEBS Lett. 102, 187–190
24 Fox, R.O. and Richards, F.M. (1981) Nature 300, 325–330
25 Terwilliger, T.C., Weissman, L. and Eisenberg, D. (1982) Biophys. J. 37, 353–361
26 Irmscher, G and Jung, G (1976) Eur. J. Biochem 80, 165–174
27 Klumpp, S., Jung, G and Schultz, J.E. (1984) Biochim. Biophys Acta 800, 145–151
28 Sano, T. and Schwarz, G. (1983) Biochim. Biophys. Acta 745, 189–193
29 Bodo, B., Rebufrats, S , ElHajji, M. and Davoust, D. (1985) J. Am. Chem. Soc. 107, 6011–6017
30 Eisenberg, M., Kleinberg, M.E. and Shaper, J.H. (1977) Ann. N.Y. Acad. Sci. 303, 291–291

Biochimica et Biophysica Acta 896 (1987) 77–88
Elsevier

BBA 73195

Conformation and packing properties of membrane lipids: The crystal structure of sodium dimyristoylphosphatidylglycerol

I. Pascher [a]*, S. Sundell [a], K. Harlos [b] and H. Eibl [c]

[a] *Department of Structural Chemistry, Göteborg University, Box 33031, S-400 33 Göteborg (Sweden),*
[b] *Laboratory of Molecular Biophysics, University of Oxford, Oxford OX1 3QU (U.K.)*
and [c] *Max-Planck-Institut für Biophysikalische Chemie, D-3400 Göttingen, Nikolausberg (F.R.G.)*

(Received 20 June 1986)

Key words: Phosphatidylglycerol; Crystal structure, Phospholipid conformation; Molecular packing; Headgroup interaction

The conformation and molecular packing of sodium 1,2-dimyristoyl-*sn*-glycero-phospho-*rac*-glycerol (DMPG) have been determined by single crystal analysis ($R = 0.098$). The lipid crystallizes in the monoclinic spacegroup $P2_1$ with the unit cell dimensions $a = 10.4$, $b = 8.5$, $c = 45.5$ Å and $\beta = 95.2°$. There are two independent molecules (A and B) in the asymmetric unit which with respect to configuration and conformation of their glycerol headgroup are mirror images. The molecules pack tail to tail in a bilayer structure. The phosphoglycerol headgroups have a layer-parallel orientation giving the molecules an L-shape. At the bilayer surface the (−) phosphoglycerol groups are arranged in rows which are separated by rows of (+) sodium ions. Laterally the polar groups interact by an extensive network of hydrogen, ionic and coordination bonds. The packing cross-section per molecule is 44.0 Å^2. The hydrocarbon chains are tilted (29°) and have opposite inclination in the two bilayer halves. In the chain matrix the chain planes are arranged according to a so far unknown hybride packing mode which combines the features of $T_{\parallel}$ and $O_{\perp}$ subcells. The two fatty acid substituted glycerol oxygens have mutually a − synclinal rather than the more common + synclinal conformation. The conformation of the diacylglycerol part of molecule A and B is distinguished by an axial displacement of the two hydrocarbon chains by four methylene units. This results in a reorientation of the glycerol back bone and a change in the conformation and stacking of the hydrocarbon chains. In molecule A the β-chain is straight and the γ-chain is bent while in molecule B the chain conformation is reversed.

Introduction

Phosphatidylglycerol (PG) is an abundant lipid in the plasmamembrane of microorganisms [1,2] and in the chloroplast membrane of plants [3]. In mammalian systems PG occurs in minor amounts only, notably in lung surfactants [4,5] and in mitochondrial membranes [6], where it can function as a precursor of cardiolipin [7].

Like other negatively-charged phospholipids, PG exhibits a very complex phase behaviour in aqueous media. The phase transitions and structural organization of PG are affected both by temperature, surface pH and concentration of monovalent and divalent cations [8–15]. Depending on the environmental conditions (proton, ion,

---

Abbreviations. DMPG, dimyristoylphosphatidylglycerol; DPPG, dipalmitoylphosphatidylglycerol; PG, phosphatidylglycerol; PC, phosphatidylcholine; sc, synclinal (= *gauche*); ac, anticlinal (= anti-*gauche*); ap, antiperiplanar (*trans*-planar)

Correspondence: Dr. I. Pascher, Department of Structural Chemistry, Göteborg University, Box 33031, S-400 33 Göteborg, Sweden.

0005-2736/87/$03.50 © 1987 Elsevier Science Publishers B.V. (Biomedical Division)

TABLE I

COORDINATES AND EQUIVALENT ISOTROPIC TEMPERATURE FACTORS

Atomic fractional coordinates and equivalent isotropic temperature factors ($\times 10^2$) for the non-hydrogen atoms of DMPG. $U_{eq} = 1/3(U_{11} + U_{22} + U_{33} + 2^{*}U_{13}^{*}\cos\beta)$.

Molecule A

Atom	X	Y	Z	U_{eq}
Na (1)	0.1593 (9)	0.4944 (14)	0.0075 (3)	4.7 (0.7)
P (1)	0.0790 (7)	0.1754 (10)	0.0391 (2)	4.1 (0.5)
O (11)	0.1192 (20)	0.1510 (25)	0.0731 (4)	5.3 (1.3)
O (12)	−0.0131 (19)	0.3275 (23)	0.0381 (5)	5.0 (1.3)
O (13)	0.0049 (17)	0.0226 (23)	0.0298 (5)	6.0 (1.4)
O (14)	0.1883 (16)	0.2313 (25)	0.0226 (5)	5.6 (1.3)
C (11)	−0.1521 (26)	0.3090 (39)	0.0417 (8)	5.7 (2.2)
C (12)	−0.1908 (24)	0.4541 (41)	0.0598 (7)	4.9 (1.9)
C (13)	−0.3406 (33)	0.4364 (40)	0.0639 (9)	6.8 (2.3)
O (15)	−0.1717 (20)	0.6001 (25)	0.0441 (5)	5.6 (1.4)
O (16)	−0.4172 (18)	0.4488 (28)	0.0379 (5)	5.6 (1.3)
C (1)	0.2181 (37)	0.2613 (46)	0.0866 (12)	10.6 (3.3)
C (2)	0.3033 (51)	0.1729 (64)	0.1109 (10)	12.2 (3.8)
C (3)	0.4403 (30)	0.2402 (44)	0.1151 (10)	8.1 (2.5)
O (21)	0.2324 (22)	0.1610 (35)	0.1382 (6)	8.0 (1.8)
O (22)	0.3546 (25)	−0.0469 (40)	0.1537 (7)	10.5 (2.3)
C (21)	0.2740 (45)	0.0474 (59)	0.1573 (10)	8.3 (3.2)
C (22)	0.1975 (35)	0.0559 (44)	0.1828 (8)	7.0 (2.4)
C (23)	0.2234 (34)	−0.0644 (57)	0.2067 (9)	9.0 (2.8)
C (24)	0.1434 (37)	−0.0569 (65)	0.2330 (9)	10.0 (3.2)
C (25)	0.1866 (41)	−0.1868 (63)	0.2554 (9)	10.1 (3.3)
C (26)	0.1092 (45)	−0.1843 (69)	0.2809 (12)	12.0 (3.9)
C (27)	0.1384 (39)	−0.3100 (65)	0.3035 (8)	9.8 (3.2)
C (28)	0.0656 (36)	−0.3090 (63)	0.3311 (10)	10.0 (3.2)
C (29)	0.0958 (47)	−0.4339 (62)	0.3530 (9)	11.3 (3.6)
C (210)	0.0239 (48)	−0.4350 (69)	0.3791 (10)	12.2 (3.9)
C (211)	0.0636 (49)	−0.5389 (89)	0.4032 (10)	14.1 (4.5)
C (212)	−0.0031 (68)	−0.5506 (105)	0.4301 (15)	18.7 (6.4)
C (213)	0.0224 (67)	−0.6426 (131)	0.4583 (18)	22.0 (8.1)
C (214)	−0.0490 (79)	−0.6283 (118)	0.4843 (15)	22.0 (8.4)
O (31)	0.4140 (25)	0.4033 (32)	0.1258 (6)	9.4 (1.9)
O (32)	0.6302 (27)	0.4079 (48)	0.1391 (10)	13.7 (2.9)
C (31)	0.5301 (64)	0.4729 (66)	0.1389 (10)	11.9 (4.2)
C (32)	0.4805 (48)	0.6121 (52)	0.1520 (12)	10.6 (3.6)
C (33)	0.4899 (55)	0.6050 (55)	0.1852 (13)	12.4 (4.2)
C (34)	0.4372 (38)	0.4922 (54)	0.2000 (9)	7.7 (2.7)
C (35)	0.4441 (48)	0.4752 (65)	0.2308 (13)	12.2 (4.1)
C (36)	0.3899 (47)	0.3542 (61)	0.2480 (10)	11.1 (3.6)
C (37)	0.4051 (45)	0.3496 (69)	0.2802 (11)	11.4 (3.9)
C (38)	0.3510 (43)	0.2285 (75)	0.2969 (13)	11.4 (4.0)
C (39)	0.3643 (58)	0.2136 (70)	0.3279 (16)	14.5 (5.0)
C (310)	0.3080 (44)	0.1049 (60)	0.3442 (13)	10.3 (3.6)
C (311)	0.3289 (59)	0.0881 (95)	0.3768 (15)	16.2 (5.9)
C (312)	0.2683 (66)	−0.0047 (95)	0.3954 (14)	16.1 (5.8)
C (313)	0.2900 (63)	−0.0258 (89)	0.4308 (21)	18.2 (6.7)
C (314)	0.2200 (90)	−0.1420 (122)	0.4437 (22)	24.2 (9.3)

Molecule B

Atom	X	Y	Z	U_{eq}
Na (2)	0.6580 (9)	−0.3216 (14)	0.0081 (2)	4.2 (0.6)
P (1)	0.5778 (7)	0.0000 (–)	0.0390 (2)	4.2 (0.4)
O (11)	0.6116 (18)	0.0175 (24)	0.0730 (4)	5.1 (1.2)
O (12)	0.4794 (17)	−0.1549 (24)	0.0370 (5)	5.7 (1.4)
O (13)	0.5097 (16)	0.1492 (24)	0.0296 (4)	4.7 (1.2)
O (14)	0.6904 (15)	−0.0608 (24)	0.0239 (4)	5.2 (1.2)
C (11)	0.3476 (27)	−0.1235 (37)	0.0437 (9)	6.1 (2.2)
C (12)	0.3104 (27)	−0.2795 (47)	0.0584 (9)	7.1 (2.4)
C (13)	0.1621 (36)	−0.2783 (38)	0.0641 (9)	7.0 (2.4)
O (15)	0.3314 (19)	−0.4190 (25)	0.0427 (6)	5.7 (1.4)
O (16)	0.0839 (19)	−0.2785 (24)	0.0377 (5)	4.9 (1.2)
C (1)	0.6724 (61)	−0.1066 (55)	0.0918 (9)	12.1 (3.8)
C (2)	0.8015 (51)	−0.0500 (82)	0.1041 (11)	11.1 (4.1)
C (3)	0.8018 (44)	0.0617 (56)	0.1241 (11)	9.3 (3.3)
O (21)	0.8366 (38)	−0.2067 (42)	0.1228 (9)	11.6 (2.8)
O (22)	1.0382 (43)	−0.1420 (63)	0.1235 (9)	15.3 (3.9)
C (21)	0.9583 (89)	−0.2258 (71)	0.1289 (17)	12.9 (5.9)
C (22)	1.0015 (51)	−0.3761 (99)	0.1472 (13)	17.1 (5.8)
C (23)	0.9187 (52)	−0.3694 (59)	0.1722 (11)	13.1 (4.2)
C (24)	0.9712 (41)	−0.5164 (61)	0.1939 (10)	10.1 (3.3)
C (25)	0.9033 (40)	−0.5219 (59)	0.2205 (13)	11.4 (3.7)
C (26)	0.9360 (46)	−0.6473 (61)	0.2440 (11)	10.7 (3.6)
C (27)	0.8649 (46)	−0.6516 (69)	0.2704 (14)	13.7 (4.6)
C (28)	0.9038 (43)	−0.7640 (59)	0.2939 (10)	10.3 (3.3)
C (29)	0.8264 (40)	−0.7625 (59)	0.3179 (11)	10.5 (3.3)
C (210)	0.8629 (50)	−0.8717 (67)	0.3439 (11)	11.6 (4.0)
C (211)	0.7817 (48)	−0.8884 (74)	0.3667 (13)	13.4 (4.5)
C (212)	0.8191 (47)	−0.9873 (69)	0.3940 (11)	12.3 (3.9)
C (213)	0.7429 (63)	−1.0022 (90)	0.4194 (14)	17.0 (5.8)
C (214)	0.7834 (60)	−1.1137 (92)	0.4421 (13)	17.7 (5.9)
O (31)	0.7167 (22)	0.0450 (31)	0.1466 (5)	7.8 (1.7)
O (32)	0.8714 (33)	0.0595 (58)	0.1824 (7)	15.4 (3.3)
C (31)	0.7516 (42)	0.0430 (48)	0.1733 (10)	8.9 (3.0)
C (32)	0.6726 (36)	0.0292 (56)	0.1979 (8)	7.9 (2.7)
C (33)	0.7179 (31)	−0.0619 (51)	0.2239 (8)	6.9 (2.3)
C (34)	0.6240 (40)	−0.0865 (74)	0.2476 (9)	11.1 (3.7)
C (35)	0.6719 (38)	−0.1818 (61)	0.2740 (12)	10.4 (3.5)
C (36)	0.5914 (41)	−0.2008 (69)	0.2977 (10)	10.3 (3.5)
C (37)	0.6307 (40)	−0.2914 (69)	0.3227 (11)	10.8 (3.6)
C (38)	0.5444 (45)	−0.3108 (85)	0.3465 (11)	13.3 (4.3)
C (39)	0.5922 (37)	−0.4229 (68)	0.3723 (12)	11.2 (3.7)
C (310)	0.5117 (56)	−0.4450 (69)	0.3965 (11)	12.7 (4.3)
C (311)	0.5535 (45)	−0.5510 (78)	0.4210 (13)	12.6 (4.3)
C (312)	0.4786 (59)	−0.5684 (91)	0.4448 (12)	15.3 (5.0)
C (313)	0.5093 (66)	−0.6586 (120)	0.4742 (17)	20.0 (7.1)
C (314)	0.4268 (73)	−0.6595 (173)	0.4942 (14)	25.9 (9.6)

and non-electrolyte concentrations) PG was shown to form lamellar structures with great variations in bilayer thickness [10,12]. This indicates a great flexibility in the lateral interactions and packing requirements of the phosphoglycerol headgroup at the bilayer surface. The hydrocarbon chains accommodate to these different molecular cross-sections by forming either layer-perpendicular, tilted or even interdigitating chain matrices [10, 12–15].

In order to obtain insight in interactions and packing properties of PG we have performed a X-ray single crystal analysis of sodium 1,2-dimyristoyl-*sn*-glycerol-3-phospho-*rac*-glycerol.

Experimental

Monosodium 1,2-dimyristoyl-*sn*-glycerol-3-phospho-*rac*-glycerol,(2,3-dimyristoyl-D-glycerol-1-phospho-DL-glycerol) DMPG (for numbering conventions and configurational notations in structural studies of lipids see Ref. 21) was obtained from Calbiochem (Ca, U.S.A.).

It is of interest to note that attempts to grow crystals of DMPG with natural L (*sn*-1-*P*) configuration at the phosphoglycerol headgroup were so far unsuccessful, while for the corresponding diasteromeric pair with DL (*rac*) phosphoglycerol headgroups suitable crystals for X-ray analysis could be obtained.

For crystallization the lipid was dissolved (1 mg/ml) in a solvent mixture of carbon tetrachloride/ethanol/water (100 : 10 : 0.3, by vol.). The crystallization was induced by diffusion of diethyl ether vapours into the lipid solution. Thin plate-like crystals appeared after several days.

A crystal with the dimensions 0.35 × 0.35 × 0.02 mm was used for data collection with an Enraf-Nonius CAD4F-11 diffractometer. The angular settings of 25 reflections ($8° < \theta < 23°$) were measured to calculate the lattice parameters. Intensity data were collected by the $\theta/2\theta$ scan method using monochromatized CuK_α radiation. Three intensity control reflections were measured every 2 h. At the end of the data collection the intensities of these reflections had dropped to about 90% of their original values. All reflections were rescaled to account for this decay. A total of 5408 independent reflections ($1° < \theta < 55°$) were recorded and of these 1247 reflections with $I > 3\sigma(I)$ were considered observed. All intensities were corrected for Lorentz and polarization effects but not for absorption or extinction.

Crystal data

Molecular formula $C_{34}H_{66}O_{10}NaP$, space group $P2_1$, unit cell $a = 10.370(8)$, $b = 8.482(7)$, $c = 45.52(2)$ Å, $\beta = 95.22(4)°$, $V = 3987$ Å^3, $Z = 4$, $M_r = 688.16$, $D_c = 1.146$ g · m^{-3}, $\mu(\text{Cu}K_\alpha) = 11.2$ cm^{-1}.

The structure was solved by direct methods using the programs DIRDIF [16] and MITHRIL [17] which provided the non-hydrogen atom positions. Refinement was carried out by the full-matrix least-squares method and anisotropic temperature factors were applied for the non-hydrogen atoms. Hydrogen atoms connected to carbon atoms (except those connected to methyl end groups) were included at expected positions and were assigned a common isotropic temperature factor (5 Å^2). The hydrogen atom parameters were not refined. The refinement was terminated with residuals $R = 0.098$ and $R_w = 0.115$. The weighting scheme used in the later part of the refinement was $w = 1/(1 + ((|F_{obs}| - 32)/35)^2)$ [18]. The form factors used were those given by Cromer and Mann [19]. All calculations have been performed on a DEC-system-10 computer using mainly the X-ray 72 program system [20].

Description of the structure

The coordinates of the non-hydrogen atoms are given in Table I. Observed and calculated structure factors, anisotropic temperature parameters and coordinates of the hydrogen atoms can be obtained from the Department of Structural Chemistry, Göteborg University. The numbering of the atoms and notation of torsion angles is shown in Fig. 1. For configurational and conformational notation used in structural studies of glycerophospholipids see Ref. 21.

Molecular packing

The DMPG molecules are arranged in a typical bilayer structure. The packing pattern and the extension of the unit cell is shown in Fig. 2 in views along the two short unit cell axes *a* and *b*.

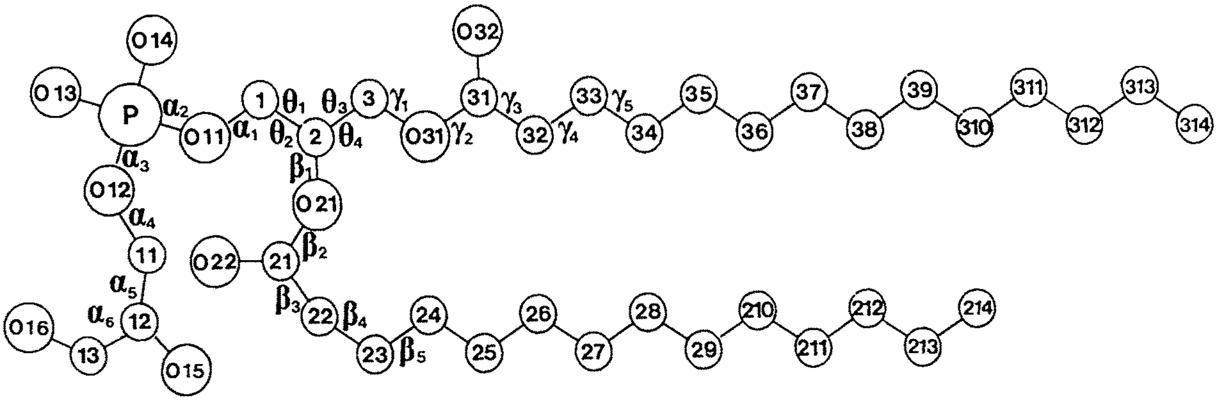

Fig. 1. Schematic drawing of a DMPG molecule showing atom numbering and notation of torsion angles according to the conventions used in conformational studies [21].

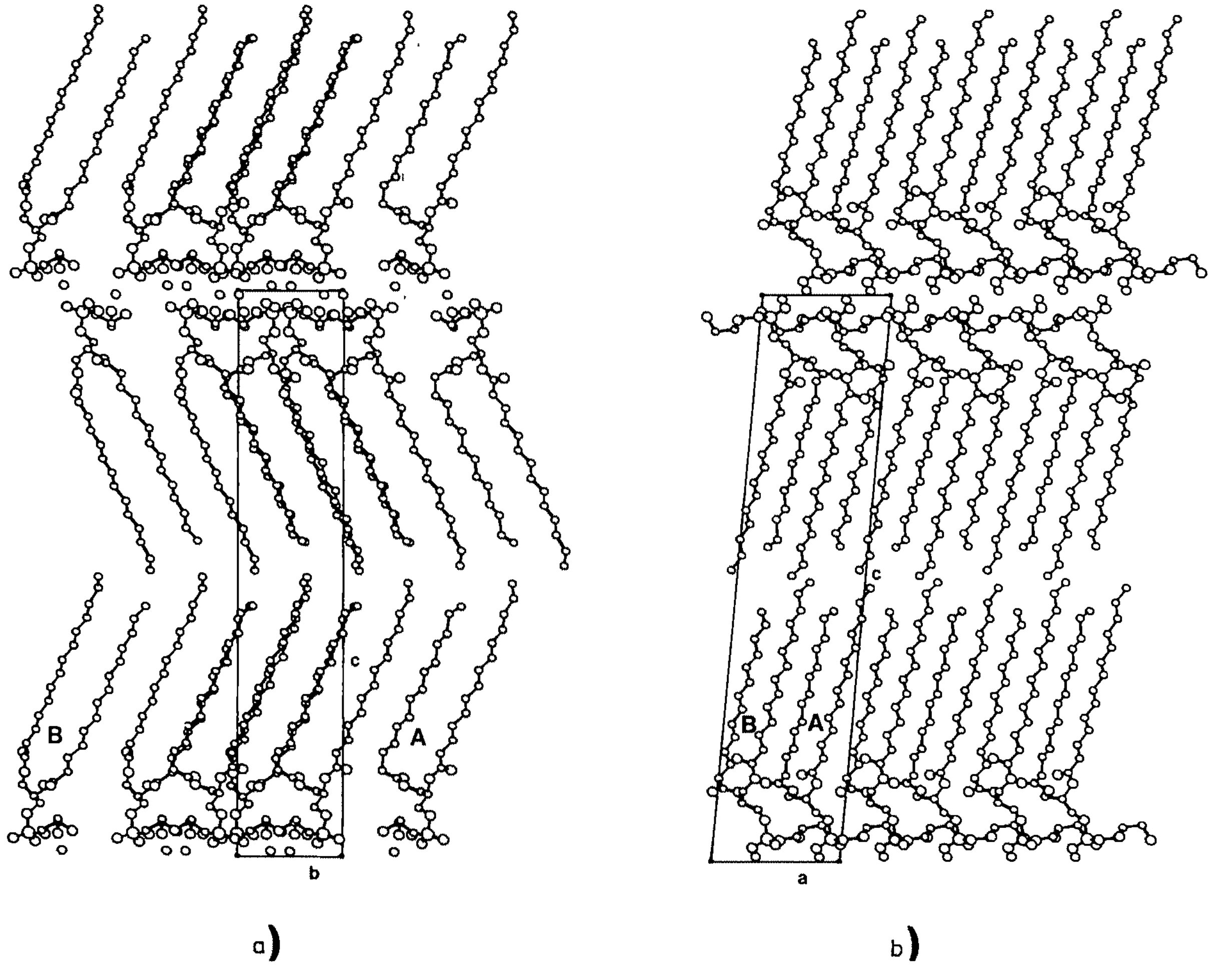

Fig. 2. Molecular packing of DMPG in views (a) along the unit cell a-axis and (b) along the b-axis. In the projection (a) DMPG molecules A and B overlap (center). For clarity, on the right side of the bilayer only A molecules and on the left side only B molecules are reproduced.

The unit cell contains four molecules, two of which (A and B) constitute the asymmetric unit and are related to the opposite pair by a 2-fold screw axis. The two molecules A and B in each pair are diastereomers, differing with respect to the configuration of their glycerol headgroups. The diacylglycerol moiety has natural D-configuration (*sn*-3-*P*) in both molecules while the glycerol headgroup has natural L-configuration (*sn*-1-*P*) in molecule A, but D-configuration (*sn*-3-*P*) in molecule B. The headgroups of molecule A and B are mirror images also with respect to their conformation (see molecular conformation below).

The phosphoglycerol headgroups are oriented parallel to the bilayer plane forming a rather smooth surface. The headgroup layers of two adjacent bilayers sandwich a layer of sodium ions at the bilayer interface.

The packing requirement of the layer-parallel phosphoglycerol headgroup determines the molecular packing cross-section in the layer plane ($S = 44.0$ Å^2). The hydrocarbon chains accommodate to this headgroup area by adopting a tilt of 29°. The chains thereby are inclined both in direction of the *a*- and *b*-axes. Furthermore, as obvious from Fig. 2a the hydrocarbon chains of the two bilayer halves have opposite tilt direction. In the projection along the *b*-axis (Fig. 2b) the chains appear parallel.

Chain packing mode

Laterally the chains pack according to a hitherto unknown hybride packing mode. The chain packing pattern in a view along the chain axes (c_s-axis) is shown in Fig. 3. The subcell combines features of both triclinic parallel $T_{\parallel}$ and orthorhombic

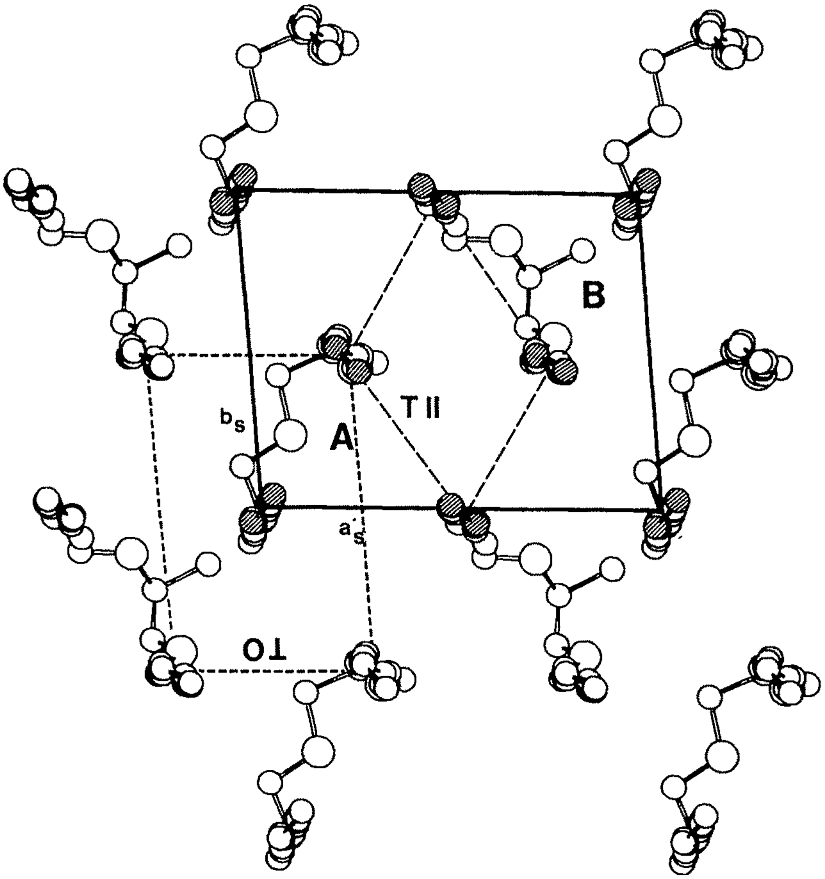

Fig. 3. Lateral packing of the hydrocarbon chains of DMPG in a view along the chain axes (c_s-axis). The hybrid subcell (solid lines) combines features of both $T_{\parallel}$ and $O_{\perp}$ chain packing modes (broken lines)

perpendicular $O_\perp$ chain packing modes [22]. The packing pattern can be regarded as a variation of the hybrid subcells (HS1 and HS2) [22] which earlier have been observed in phosphatidylethanolamine [23] and cerebroside [24]. The hybrid subcell of DMPG has the dimensions:

$a_s = 10.1(1)$ Å, $b_s = 7.8(1)$ Å, $c_s = 2.54(3)$ Å and $\alpha_s = 101(2)°$, $\beta_s = 90(1)°$, $\gamma_s = 97(1)°$,

which corresponds to a packing cross-section per chain of $\Sigma = 19.2$ Å^2. The parameters of the $T_\parallel$ 'sub'-subcell are: $a_s = 4.4(1)$ Å, $b_s = 5.4(1)$ Å, $c_s = 2.54(3)$ Å, $\alpha_s = 67(1)°$, $\beta_s = 105(1)°$, $\gamma_s = 118(2)°$ and of the distorted $O_\perp$ 'sub'-subcell: $a_s = 5.0(1)$ Å, $b_s = 7.8(1)$ Å, $c_s = 2.54(3)$ Å, $\alpha_s = 83(2)°$, $\beta_s = 84(1)°$, $\gamma_s = 92(1)°$.

As obvious from Figs. 3 and 4 the zigzag planes of the two hydrocarbon chains of molecule A are oriented at a right angle to each other, while they are parallel in molecule B. The hybrid subcell thus is constituted of four chains, three with mutually parallel chain planes and one perpendicular to the others.

Molecular conformation

The conformation of the two DMPG molecules A and B is shown in Fig. 4 in projections along the unit cell axes *a* and *b*. Torsion angles in comparison to those of other membrane lipids are given in Table II.

Diacylglycerol part. The diacylglycerol moiety displays conformational features that recently have been reported for phosphatidyl-*N*,*N*-dimethylethanolamine [25]. Typical for this conformation is that the two fatty acid substituted glycerol oxygens O(21) and O(31) have mutually a −sc (θ_4) rather than the well known +sc position [21,26] (compare θ_4 Table II).

The two DMPG molecules, however, differ with respect to orientation of their glycerol back bone and their chain stacking. In molecule A the C(2)-O(21) glycerol bond points approximately in the direction of the layer normal and the C(3)-O(31) bond has an almost layer-parallel orientation. The adherent β-chain is straightly extended while the γ-chain is bent perpendicularly at carbon atom

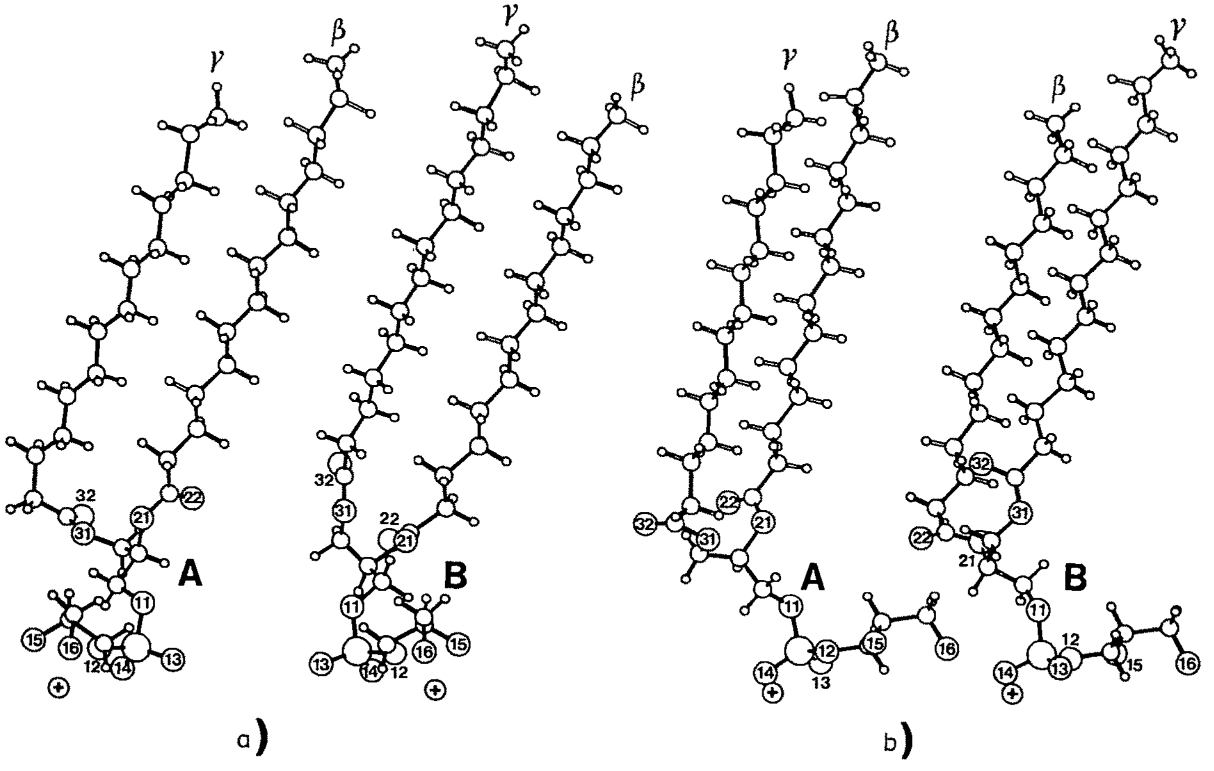

Fig. 4 Molecular conformation of DMPG molecules A and B in views (a) along the unit cell *a*-axis and (b) along the *b*-axis Note the difference in the orientation of the diacylglycerol part of molecule A and B and the lateral and axial shift of the β and γ chains (projection b).

TABLE II

TORSION ANGLES

For torsion angle notations see Fig. 1. DLPEM$_2$, dilauroylphosphatidyl-*N*,*N*-dimethylethanolamine [25], DMPC, dimyristoylphosphatidylcholine [27]; DMPA, dimyristoylphosphatidate [28].

	α_1	α_2	α_3	α_4	α_5	α_6	θ_1	θ_2	θ_3	θ_4	β_1	β_2	β_3	β_4	γ_1	γ_2	γ_3	γ_4
DMPG A	−146	−76	−86	143	180	−66	151	−78	64	−63	159	178	178	−179	164	−170	110	−57
DMPG B	116	58	78	−147	−173	67	71	179	45	−58	157	180	−50	−175	122	179	142	174
DLPEM$_2$	179	65	54	144	−96		176	−66	56	−60	148	173	−57	176	129	−167	166	175
DMPC	177	−74	−47	−150	54		168	−80	166	51	120	179	−134	67	102	176	180	180
DMPA	153						−54	62	−179	62	87	172	164	179	−142	180	−119	73

C(31). This bend is produced by a +ac ($\gamma_3 = 110°$) and −sc ($\gamma_4 = -57°$) twist about the C(31)-C(32) and C(32)-C(33) bond, respectively.

Compared to molecule A the glycerol backbone of molecule B is turned by approximately 60° (see Fig. 5). This changes the orientation of the glycerol bonds C(2)-O(21) and C(3)-O(31) form 'vertical' to 'horizontal' and vice versa. Thereby the two hydrocarbon chains get axially displaced by four methylene units. The β-chain becomes bent and

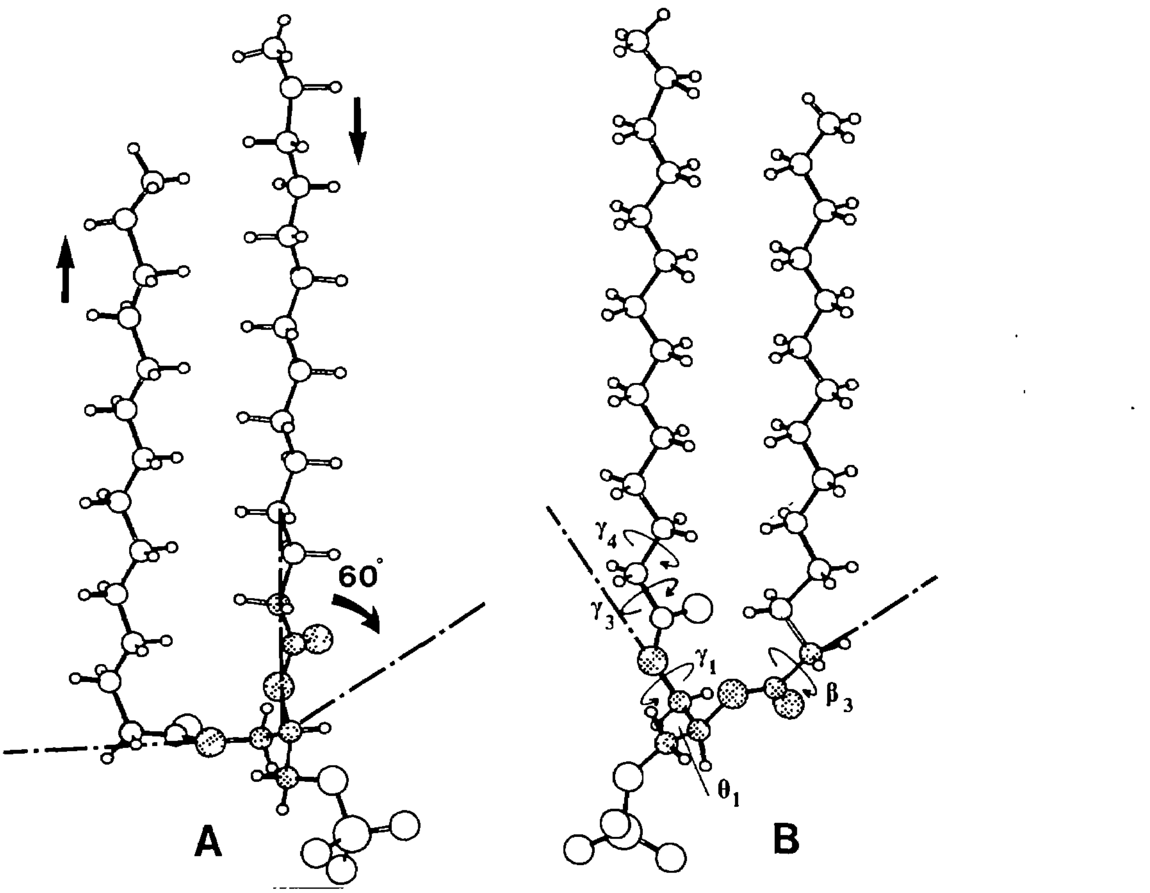

Fig. 5. Conformational differences between DMPG molecules A and B can be attributed to an axial displacement of the fatty acid chains (arrows) and a reorientation of the central diacylglycerol part (dotted atoms). The fatty acids thereby change their conformation from straight to bent and vice versa The bonds involved in this conformational change are indicated (rotation arrows). The glycerol headgroup has been omitted for clarity

the γ-chain straightens and projects beyond the β-chain. As indicated in Fig. 5 and obvious from the torsion angles in Table II, the conformation of the central part of the diacylglycerol group (dotted atoms) is largely unaffected. Changes are confined to torsion angles γ_1, γ_3, γ_4 and β_3 (see Table II). Compared to molecule A this leads to a lateral shift of the chains (compare Fig. 4b).

Headgroup conformation. As shown in Figs. 2b and 4b the phosphoglycerol headgroup is turned away from the diacylglycerol part and extends parallel to the bilayer surface. This gives the molecule an L-shape. As mentioned above the headgroups of molecule A and B are mirror images both with respect to configuration and conformation. The α-torsion angles (Table II) of the headgroups of molecule A and B thus are practically identical but of opposite direction. Note, however, that molecules A and B are not related by any crystallographic symmetry and thus this mirror image conformation is not perfect.

At the glycerol bond C(1)-C(2) the pseudo mirror symmetry is discontinued. The torsion angles about this bond (θ_1/θ_2) are ap/$-$sc and $+$sc/ap in molecule A and B, respectively.

The three oxygens of the glycerol headgroup O(12), O(15) and O(16) have mutually (α_5/α_6) $+$sc/$+$sc (molecule A) or $-$sc/$-$sc conformation (molecule B). The two unsubstituted glycerol oxygens are oriented towards the layer interface and are involved in hydrogen bonds and coordination bonds (see below).

Polar group packing and interactions

Fig. 6 shows the arrangement and interactions of the phosphoglycerol headgroups in views parallel and perpendicular to the bilayer interface. The sodium ions form a layer that is sandwiched by phosphoglycerol groups of adjacent bilayers. The sodium ions are placed ±0.3 Å and the phosphate groups ±1.8 Å from the bilayer interface. As it can be seen in the projection onto the layer plane (Fig. 6b) the (+) and (−) charges are not distributed uniformly at the bilayer surface. The (+) sodium ions as well as the (−) phosphate groups are aligned in zigzag rows extending in *a*-direction. In *b*-direction rows of phosphate groups alternate with rows of sodium ions.

The glycerol groups project alternatingly to the left and to the right from the phosphate rows. Laterally, the headgroups interact by an extensive network of hydrogen bonds, ionic bonds and coordination bonds.

A sequence of two hydrogen bonds (2.8 and 2.7

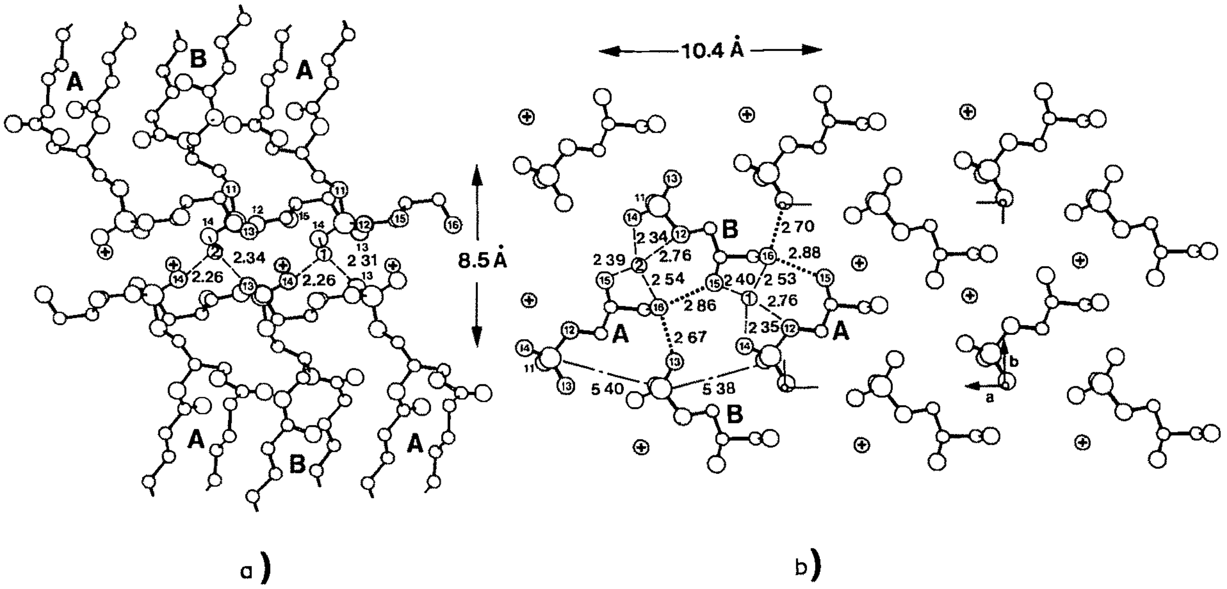

Fig 6. Packing and interactions of the phosphoglycerol headgroups of DMPG viewed (a) parallel and (b) perpendicular to the bilayer interface Hydrogen bonds (dotted lines) and ionic and coordination bonds (borken lines) are indicated. The contact distances are given in Å

Å) starts at the glycerol hydroxyl oxygen O(15) of molecule A. The bonds are directed via hydroxyl oxygen O(16) of molecule B and terminated at a phosphate oxygen O(14) of another A molecule. A corresponding sequence of bonds, but with opposite orientation in the bilayer plane, runs between molecules B–A–B.

The sodium ions form bond contacts both laterally and across the bilayer interface. Each sodium ion is coordinated by six oxygen atoms. Three of these contacts are formed with unsubstituted (−) charged phosphate oxygens and have the character of short ionic bonds (< 2.40 Å). The other three contacts are established with formally neutral oxygens (one esterfied phosphate oxygen O(12) and two unsubstituted glycerol oxygens O(15), O(16)) and may be considered as co-ordination bonds. The $Na^+ \cdots O$ contact distance of these three latter bonds is somewhat longer (2.40–2.76 Å) than those of the ionic bonds. Differences in bond lengths appear to reflect the degree of negative polarisation of the oxygen atoms. The rather short coordination bond between $Na^+ \cdots O(15)$ thus might be due to the fact, that this hydroxyl oxygen serves as a proton donator only and becomes more polarized than O(16) which acts both as a donor and acceptor.

Discussion and Conclusions

The present crystal analysis provides important information on the structural organization of DMPG and of membrane lipids in general. In particular with respect to conformation of the hydrophobic diacylglycerol moiety, the chain packing mode and the headgroup packing the DMPG structure reveals a variety of new interesting features. Moreover the structural parameters of DMPG closely resemble the parameters recorded for the gel phase of DPPG indicating that the structure observed in crystals is largely preserved on hydration.

Preferred conformations

Regarding the conformation of the diacylglycerol part, the DMPG structure now confirms earlier observations, that the fatty acid carrying glycerol oxygens O(21) and O(31) can mutually adopt both a +sc and a −sc conformation about the C(2)-C(3) glycerol bond (torsion angle θ_4) [21,25,26]. The $\theta_4 = +\mathrm{sc}$ conformation is the most predominant one and has been found in a great number of crystal structures of both double chain [23,26–28] and single chain (lyso)glycerophospholipids [29–31].

The $\theta_4 = -\mathrm{sc}$ conformation has so far only been observed in three glycerolipids, in dilauroylphosphatidyldimethylethanolamine [25], in diacylglycero-*p*-toluenesulphonate (a model lipid) [32] and now in DMPG.

Moreover, for lipids with the $\theta_4 = +\mathrm{sc}$ confirmation it could be shown that the glycerol back bone can change its orientation towards the bilayer plane from layer perpendicular to layer-parallel and vice versa by an axial displacement of the hydrocarbon chains [25,31]. The present DMPG structure shows that a similar axial displacement of the hydrocarbon chains and a reorientation of the glycerol back bone also occurs for the lipids with the $\theta_4 = -\mathrm{sc}$ conformation. Thus we can now distinguish four minimum energy conformations for the diacylglycerol group which arise from two simple motions of the hydrocarbon chains:

(1) an axial ±120° rotation of the hydrocarbon chain about the C(2)-C(3) glycerol bond giving rise to the +sc and −sc conformation of the two fatty acid carrying glycerol oxygens [25] and

(2) an axial displacement of the chains producing a reorientation of the glycerol back bone and a shift of the chain bend from the β-fatty acid to the γ-fatty acid and vice versa (compare Fig. 5 and Ref. 28).

According to NMR-studies these kind of rotational and translational motions of the chains are actually the fundamental motions that occur in the diacylglycerol part in the liquid-crystalline state [33] and the described minimum energy conformations co-exist in the bilayer in a dynamic equilibrium (Ref. 34, and Hauser, Pascher and Sundell, unpublished data).

Hybride subcells

With regard to the lateral chain packing, the subcell of DMPG (Fig. 3) and other complex membrane lipids [23,24] show that simple packing modes, such as $O_\perp$, $M_\parallel$ and $T_\parallel$ [22] can combine to a variety of hybride packing modes. These hybride packing modes have to be considered as intermediate states between the well-ordered, simple chain packing modes and the less ordered hexagonal chain matrix [35].

The great variability of the chain packing modes apparently can give rise to statistical disorder in the chain matrices of multilamellar lipid crystals and thus lead to complications in the solution of single crystal structures. Furthermore, these hybride packings obstruct the interpretation of the chain arrangement from high-angle reflexions (short spacings) of X-ray powder diffractions and from infrared and Raman spectra. Little or no information is at present available on the interpretation of hybrid packing modes by the above mentioned techniques.

Lateral packing of the headgroup

The packing pattern of the phosphoglycerol headgroup (Fig. 6) displays far reaching similarities with that of the phosphocholine headgroup [21]. In both headgroup arrangements the (−) phosphate groups and the (+) sodium ions or choline groups, respectively are aligned in separate rows. Similarly to the glycerol groups the choline groups extend to the left and right from these phosphate rows.

There is however a significant dissimilarity. The phosphate groups of PC are linked to rows by water molecules of hydration. In PG there is no such direct interactions. A contact between the phosphate groups is mediated by the distal glycerol-hydroxyl group O(16).′ Nevertheless the phosphate-phosphate distances and packing geometry is almost identical. In the PC pattern the distance between the phosphate rows (*b*-axis) is 1 Å longer than in the PG structure. This difference is due to the longer ionic bond contacts between the phosphate group and the bulky quarternary ammonium groups (3.7 Å) compared to the phosphate-sodium contacts (2.4 Å).

TABLE III

STRUCTURAL PARAMETERS

Comparison of structural parameters of DPPG in the gel phase at pH 8 [10] and in the anhydrous crystal phase (calculated from the DMPG structure).

	d_1(Å)	S(Å)	ϕ(°)	$\bar{V}_1$(ml·g^{-1})
DPPG gel phase	51.1	48.0	32	1.01
DPPG crystal phase	50.0	44.0	29	0.889

Ressemblance of the PG crystal structure and the gel phase

From X-ray diffraction studies of aqueous dispersions of DPPG, Watts et al. [10] have calculated the bilayer-thickness d_1, molecular area S, chain tilt ϕ and partial specific volume $\bar{V}_1$ of the gel phase at pH 8 (see Table III). Based on the crystal structure of DMPG and with consideration of the increased chain length of the dipalmitoyl homologue the corresponding structural parameters for the anhydrous crystal phase of DPPG can be calculated. As shown in Table III the main difference between gel and crystal phase concerns the partial specific volume. The value $\bar{V}_1 = 1.01$ ml · g^{-1} recorded for the gel state no doubt, appears to be very large compared to that of the crystal phase $\bar{V}_1 = 0.889$ ml · g^{-1}.

The determination of $\bar{V}_1$ in aqueous dispersions, however, is a rather troublesome task. Any error in $\bar{V}_1$ also affects the value of the molecular area and of the chain tilt. Assuming that $\bar{V}_1$ is 0.91 instead of 1.01 ml · g^{-1}, the molecular area of the gel phase is reduced from 48 to 44 Å^2, the packing cross-section of the crystal phase. The minor difference in bilayer thickness then can be attributed to the less effective chain packing and thus to a diminished chain tilt (25° instead of 29°).

Regardless of possible experimental errors the structural parameters of the gel phase and the crystal phase are similar to an extent indicating that the structural features observed in the anhydrous crystal are largely preserved also in the hydrated gel state.

Acknowledgement

We wish to thank M. Lundmark for skilful technical assistance. K.H. wishes to thank Dr. A. Watts, Department of Biochemistry, Oxford for his help and support. The work was supported by the Swedish Medical Research Council (grant 006), the Knut and Alice Wallenberg Foundation and the Deutsche Forschungsgemeinschaft (grant HA 1291/1-2).

References

1 Galliard, T. (1973) in Form and Function of Phospholipids (Ansell, G.B., Hawthorne, J N. and Dawson, R.M.C., eds), pp. 253–288, Elsevier, New York

2 Knitt, M.D. and Harwood, J.L. (1985) Biochem J 228, 707–711

3 McMurray, W.C. (1973) in Form and Function of Phospholipids (Ansell, G.B., Hawthorne, J.N. and Dawson, R M C., eds.), pp 205–251, Elseiver, New York

4 Rooney, S.A., Canavan, P.M. and Motiyama, E.K. (1974) Biochim Biophys Acta 360, 56–67

5 Hallman, M., Enhorning, G and Possmayer, F. (1985) Pediatr. Res. 19, 286–292

6 Daum, G. (1985) Biochim Biophys. Acta 822, 1–42

7 Hostetler, K.Y (1982) in Phospholipids (Hawthorne,, J N and Ansell, G B., eds), pp. 215–261, Elsevier Biomedical Press, Amsterdam

8 Cevc, G., Watts, A. and Marsh, D. (1980) FEBS Lett 120, 267–270

9 Harlos, K. and Eibl, H. (1980) Biochemistry 19, 895–899

10 Watts, A., Harlos, K. and Marsh, D (1981) Biochim Biophys. Acta 654, 91–96

11 Boggs, J.M. and Rangaraj, G. (1983) Biochemistry 22, 5425–5435

12 Rank, J.L., Keira, T. and Luzzati, V. (1977) Biochim. Biophys Acta 488, 431–441

13 Boggs; J.M. and Rangaraj, G. (1985) Biochim. Biophys. Acta 816, 221–233

14 Rank, J.L. and Tocanne, J.F. (1982) FEBS Lett. 143, 171–174

15 Sacre, M.M , Hoffman, W., Turner, M., Toscanne, J.-F. and Chapman, D. (1979) Chem. Phys. Lipids 25, 69–83

16 Beurskens, P.T., Bosman, W.P.J.H., Doesburg, H.M., Gould, R.O., Van den Hark, T.E.M., Prick, P.A J , Noordik, J.H , Beurskens, G. and Parthasarathi, V. (1981) Technical Report 1981/2, Crystallography Laboratory, Toernooiveld, 6525 ED Nijmegen, The Netherlands

17 Gilmore, C J. (1984) MITHRIL A Computer Program for the Automatic Solution of Crystal Structures from X-ray Data, University of Glasgow, Glasgow, U.K.

18 Mills, O.S. and Rollet, J.S. (eds) (1961) in Computing Methods and the Phase Problem in X-ray Crystal Analysis, pp 107–124, Pergamon, London

19 Cromer, D.T. and Mann, J.B (1968) Acta Crystallogr. A24, 321–324

20 Stewart, J.M., Kruger, G.J., Ammon, H.L., Dickinson, C and Hall, S.R. (1972) The X-ray System - version of June 1972 Technical Report TR-192, Computer Science Center, University of Maryland, College Park

21 Hauser, H , Pascher, I., Pearson, R.H., Sundell, S. (1981) Biochim. Biophys. Acta 650, 21–51

22 Abrahamsson, S., Dahlen, B., Löfgren, H. and Pascher, I. (1978) Progr. Chem. Fats Lipids 16, 125–143

23 Elder, M., Hitchcock, P.B., Mason, R and Shipley, G.G. (1977) Proc. R. Soc. London, Ser. A 354, 157–170

24 Pascher, I. and Sundell, S (1977) Chem. Phys. Lipids 20, 175–191

25 Pascher, I. and Sundell, S. (1986) Biochim Biophys. Acta 855, 68–78

26 Pascher, I., Sundell, S. and Hauser, H. (1981) J Mol Biol. 153, 791–806

27 Pearson, R.H. and Pascher, I. (1978) Nature 281, 499–501

28 Harlos, K., Eibl, H., Pascher, I. and Sundell, S. (1984) Chem Phys. Lipids 34, 115–126

29 Pascher, I., Sundell, S. and Hauser, H. (1981) J. Mol. Biol. 153, 807–824

30 Pascher, I. and Sundell, S (1985) Chem. Phys. Lipids 37, 241–250

31 Pascher, I., Sundell, S., Eibl, H and Harlos, K. (1986) Chem Phys Lipids 39, 53–64

32 Watts, P.H., Pangborn, W.A. and Hybl, A (1972) Science 175, 60–61

33 Seelig, J. and Seelig, A. (1980) Biophys. 13, 19–61

34 Hauser, H., Guyer, W., Pascher, I , Skrabal, P and Sundell, S. (1980) Biochemistry 19, 366–373

35 Small, D.M. (1986) in Physical Chemistry of Lipids, Handbook of Lipid Research (Hanahan, D J , ed.), Vol. 4, pp. 21–41, Plenum Press, New York

Biochimica et Biophysica Acta 896 (1987) 89–95
Elsevier

BBA 73196

Relation between Ca^{2+} uptake and fluidity of brush-border membranes isolated from rabbit small intestine and incubated with fatty acids and methyl oleate

A.R. Merrill [a], H. Aubry [a] and P. Proulx [a] and A.G. Szabo [b]

[a] *Department of Biochemistry, School of Medicine, University of Ottawa, 451 Smyth Road, Ottawa K1H 8M5 (Canada)* and [b] *Division of Biological Sciences, National Research Council of Canada, Ottawa K1A OR6 (Canada)*

(Received 29 April 1986)
(Revised manuscript received 22 July 1986)

Key words: Calcium uptake; Membrane fluidity; Oleic acid; Fatty acid, Brush-border membrane

The rate of incorporation of oleic acid into isolated brush-border membranes was found to be considerably faster than methyl oleate incorporation under similar experimental conditions. The effects of fatty acids and methyl oleate incorporation on Ca^{2+} uptake and fluidity were monitored. Whereas treatment with 0.01–0.05 mM oleic acid corresponding to incorporations smaller than 90 nmol/mg protein enhanced Ca^{2+} transport, exposures to higher concentrations of this fatty acid corresponding to incorporations larger than 150 nmol/mg protein, decreased uptake of this cation. On the other hand, treatment with 0.01–0.2 mM methyl oleate corresponding to incorporations of up to 220 nmol/mg protein had only a stimulatory effect on the Ca^{2+} uptake. Oleic acid, linoleic acid and methyl oleate decreased the fluorescence anisotropy of membranes labelled with diphenylhexatriene in a dose-dependent manner. In contrast, palmitic acid had little or no effect on the diphenylhexatriene-reportable order of the membrane within the range of concentrations used. Monitored as a function of temperature, the anisotropy values showed a gradual melting for both the control and lipid-treated membranes. The results support the concept that saturated and *cis*-unsaturated fatty acids dissolve in different lipid domains and this in itself appears to be an important factor defining whether the biological function of the membrane is affected by the uptake. Incorporation of *cis*-unsaturated fatty acids in domains harboring the Ca^{2+} uptake process increases Ca^{2+} uptake in concert with increased diphenylhexatriene-monitored fluidity. However, when concentrations of such fatty acids in these domains become sufficiently great, the presence of a largely increased number of free carboxyl groups at the membrane surface causes inhibition of Ca^{2+} uptake.

Introduction

Previous reports have indicated that brush-border membranes isolated from rabbit small intestine can incorporate a variety of lipids in vitro including phospholipids, fatty acids and cholesterol [1–4]. Compositional changes brought about by such incorporations would be expected to change some of the biological properties of the membranes. Accordingly it was shown that the rate of Ca^{2+} uptake was stimulated by treatment of the membranes with low concentrations of *cis*-unsaturated fatty acids (0.05 mM) as well as with various concentrations of caprylic acid (0.10–3.00 mM) and inhibited by treatment with higher concentrations of *cis*-unsaturated fatty acids (0.10–0.60 mM). Saturated fatty acids had no marked effects on Ca^{2+} uptake and glucose and fructose

---

Correspondence. Dr P. Proulx, Department of Biochemistry, School of Medicine, University of Ottawa, 451 Smyth Road, Ottawa, Canada K1H 8M5.

0005-2736/87/$03.50 © 1987 Elsevier Science Publishers B.V. (Biomedical Division)

transports were unaffected by any of these incorporations [5].

The dual effects of unsaturated fatty acids on Ca^{2+} uptake could not be easily explained although it was suggested that the extent of fluidization of the membrane may be an important factor in determining whether stimulation or inhibition ensues. In the present report we compare the effects of fatty acids and methyl oleate on the fluidity of the membrane as determined by changes in anisotropy using membrane preparations labelled with diphenylhexatriene (DPH). We also compare the effects of oleic acid and methyl oleate on the rate of Ca^{2+} uptake.

Materials and Methods

[1-^{14}C]Oleic acid and tri[1-^{14}C]oleoyl glycerol were purchased from New England Nuclear Corp. (Boston) and diluted to required specific activity. Methyl [1-^{14}C]oleate was formed by alkaline methanolysis of tri[^{14}C]oleoylglycerol [6] and purified by thin-layer chromatography on silica gel G plates prepared with 0.4 M boric acid using petroleum ether (b.p. 60–80 °C)/ethyl ether/acetic acid (90 : 10 : 1, v/v) as solvent [7].

Uptake of fatty acids and methyl oleate. Unlabelled or (1-^{14}C)-labelled fatty acids as well as methyl [1-^{14}C]oleate were dissolved together with sodium taurocholate in chloroform/ethanol (1 : 1, v/v). The solvent was removed by evaporation in vacuo and the residue was suspended in 10 mM Hepes-Tris buffer (pH 7.5), containing 100 mM mannitol. After shaking at room temperature for 15 min, the suspension was sonicated twice for 2 min with the small probe of an Ultrasonics sonicator at a setting of 5. In the case of palmitic acid, the large probe was used instead at a setting of 11. Suspensions that were not completely clear were clarified by centrifugation at 10^7 $g \cdot$ min.

The term, uptake, used in the present report is meant to signify an intercalation of fatty acids within the core of the membrane as opposed to adsorption or loose association at the surface of the membrane. The evidence supporting this was presented in previous reports [4,5] although the possibility of some adsorption cannot be completely precluded. Lipid extraction of the membranes followed by thin-layer chromatographic analyses of the extract indicated that no significant conversion to more complex lipids occurred and essentially all of the incorporated lipid was recovered as free fatty acid.

Brush-border membranes were prepared [8] and checked for purity by electron microscopy and by assay of marker enzymes [9]. For lipid uptake studies, mixtures consisting of membranes (300 μg protein/ml) and various concentrations of micellized fatty acid or methyloleate, as specified in the text, were incubated at 25 °C for 10 min in the case of fatty acids and up to 4 h in the case of methyl oleate. The final taurocholate concentration was 7.2 mM in all cases except for palmitate which required 10 mM bile salt. After the incubation, the membranes were centrifugated at 40 000 $\times g$ for 30 min and the pellet was washed with 1 incubation volume of Hepes-Tris, mannitol buffer. The washed pellet was either counted to estimate the amount of lipid incorporated [5] or resuspended in buffer for further experimentation involving measurements of Ca^{2+} uptake or of fluorescence anisotropy. Protein concentrations were determined by the method of Lowry et al. [10].

Ca^{2+} uptake. The procedure followed was that of Miller and Bronner [11]. Briefly, the uptake was initiated by addition of 10 μl of brush-border membrane vesicles (30 μg protein) to 25 μl of $^{45}CaCl_2$, 0.36 mM final concentration. Incubations were at 25 °C and terminated after 5 min by addition of 40 vol. of ice-cold stop solution containing 10 mM Hepes/Tris buffer (pH 7.5), 5 mM EDTA, 20 μM $LaCl_3$ and 100 mM mannitol. The suspension was then filtered through a 0.45 μm nitrocellulose filter which was then washed twice with 2.5 ml of ice-cold stop solution, air-dried and transferred to counting vials containing PCS (Amersham International)/toluene (1 : 1, v/v) and counted. The rate of uptake under these conditions was linear for at least 5 min [5] and reflected a transport process similar to one described earlier [11].

Spectroscopic measurements. To 2.5 ml of brush-border membranes, (0.16 mg protein/ml) 10 μl of $1 \cdot 10^{-4}$ M diphenylhexatriene in tetrahydrofuran (spectroscopic grade) were added to give a probe: phosphoacylglycerol ratio of 1 : 100. After thorough mixing with a Vortex shaker and incubation at room temperature for 30 min, at which time little or no odor of tetrahydrofuran could be detected, the suspension was transferred to a 1 cm quartz cell in which mixing was continued by means of a small teflon stir bar. Steady-state anisotropy measurements were made with a Perkin-Elmer spectrofluorimeter, model MPF-44A equipped with a DCSU-2 corrected spectra unit and interfaced with an analog-to-digital converter and a Commodore PET computer. The sample temperature was increased from 0°C at a rate of approx. 1 K/min. Excitation and emission wavelengths were 350 nm and 430 nm and excitation and emission bandpasses were 5 nm and 10 nm, respectively. Corrections for background fluorescence and light scattering were made with blanks containing brush-border membranes and no probe.

Absorbance measurements were conducted with a Varian, Model Cary-219 double beam spectrophotometer equipped with temperature control.

Anisotropy (r) was calculated from the fluorescence intensities measured parallel and perpendicular to the plane of the light of excitation according to the following equation:

$$r=\frac{I_{\parallel}-I_{\perp}(G)}{I_{\parallel}+2I_{\perp}(G)}$$

where $g=\mathrm{HV}/\mathrm{HH}$, a correction factor for the anisotropy of the instrument [12].

Total lipids were extracted from microvillus membranes by the method of Bligh and Dyer [13]. For preparation of the sonicated dispersions of lipids (liposomes), the dried, extracted lipid was suspended in 100 mM mannitol 10 mM Hepes-Tris buffer (pH 7.5) to a final concentration corresponding to the studies of the intact vesicles. The mixture was sonicated twice with the small probe of an Ultrasonics sonicator at a setting of 5 for 2 min under N_2 at 25°C. The resulting solutions were clear and were used as such for anisotropy studies.

Results

Results illustrated in Fig. 1 indicate that the incorporation of oleic acid into brush-border vesicles is very rapid, equilibrium being attained immediately. As reported earlier, attempts to reduce this rate by modifying the incubation conditions and sample processing conditions within practical limits were unsuccessful [4]. On the other hand, the incorporation of methyl oleate proceeded at a much slower rate equilibrium being attained after 2 h. It can be noticed that even with methyl oleate, incorporation continues to some extent during processing which extends over a 30 min period corresponding to the time required to pellet the membranes by centrifugation. Some incorporation is consequently seen at zero time.

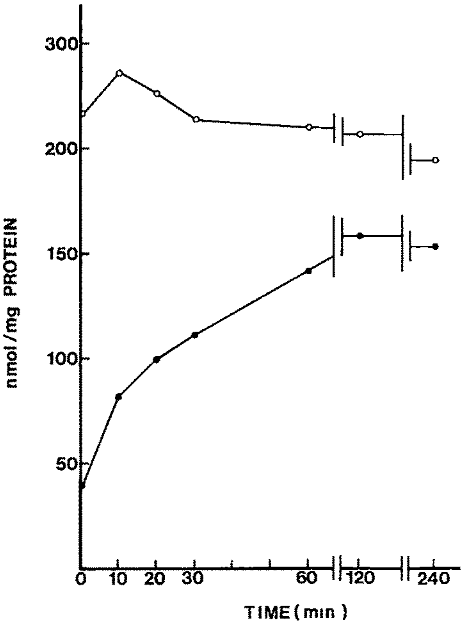

Fig 1. Time-course of oleic acid (○) and methyl oleate (●) incorporation into brush-border membranes. The incubation mixture contained in 1 ml, 0.3 mg membrane protein, 7.2 mM taurocholate, 0.10–0.11 mM lipid, 100 mM mannitol and 10 mM Hepes-Tris buffer (pH 7.5). Incubations were maintained at 25°C for the times indicated. The values are averages of 3–6 determinations giving variations < 3% and are representative of several other experiments performed under similar conditions with different animals

Results shown in Table I compare the effects of increasing concentrations of oleic acid and methyl oleate on the rate of uptake of Ca^{2+}. Whereas oleic acid stimulated at lower and inhibited at higher concentrations, the methyl ester analogue was stimulatory over the entire range of concentrations tried. Linoleic acid was shown previously to have the same dual effects as oleic acid whereas palmitic acid had no marked effect [5].

It has been reported that the anisotropy of

TABLE I

EFFECT OF OLEIC ACID AND METHYL OLEATE ON Ca^{2+} UPTAKE

The results represent the mean ± S.E. from 6 to 20 determinations with membranes from 3 to 5 rabbits.

Lipid	Lipid uptake (nmol/mg protein)	Rate of Ca^{2+} uptake (percent of control) [a]
Oleic acid [b]		
0.010 mM	18 ± 1	113 ± 10
0.025 mM	48 ± 0	117 ± 7
0.050 mM	89 ± 4	137 ± 11
0.100 mM	148 ± 3	65 ± 8
0.200 mM	342 ± 17	48 ± 8
Methyloleate [c]		
0.010 mM	14 ± 1	118 ± 7
0.050 mM	68 ± 4	124 ± 8
0.090 mM	101 ± 4	133 ± 9
0.120 mM	119 ± 8	143 ± 7
0.180 mM	182 ± 10	156 ± 10
0.180 mM [d]	220 ± 21	207 ± 29

[a] The control uptake was 7.5 ± 1.5 nmol/mg protein per 5 min.

[b] Values for oleic acid-treated membranes were reported previously [5].

[c] All methyloleate values represent incubations of 1 h with membranes except for (d) in which case incubations were for 4 h.

diphenylhexatriene in membrane preparations was dependent on the membrane concentration [14,15]. This was due to a depolarization of the light caused by scattering in such suspensions. In order to avoid such an artifact we monitored the anisotropy of both the control and treated vesicles at different concentrations of vesicles, as suggested by Teale [14] and Lentz and co-workers [15] and observed this scattering effect. We found that a vesicle concentration corresponding to 0.16 mg protein/ml gave an anisotropy reading which was close to the anisotropy value at infinite dilution (results not shown) and this concentration was used in the experiments that follow.

Results illustrated in Fig. 2 show that treatment of membranes with low and higher concentrations of oleic acid decreased the fluorescence anisotropy in a dose-related manner and these differences became more apparent above 15 °C. The results for linoleic acid (Fig. 3 show that for low incorporation of this lipid there is a slight decrease in the anisotropy while for high levels of incorporation (1074 nmol/mg protein) the anisotropy was markedly reduced. Since these fatty acids at low and high concentrations caused stimulation and inhibition of the Ca^{2+} transport, respectively, no

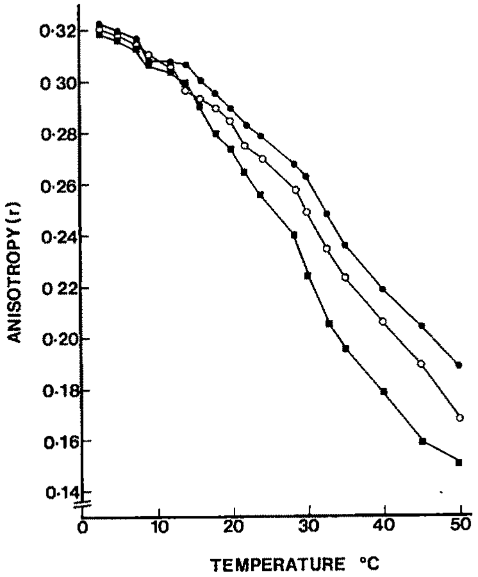

Fig. 2. The effect of oleic acid on anisotropy (●) control, no oleic acid incorporated; (○) 89 nmol (■) 341 nmol oleic acid incorporated/mg protein. The samples contained 0.16 mg of brush-border membrane protein.

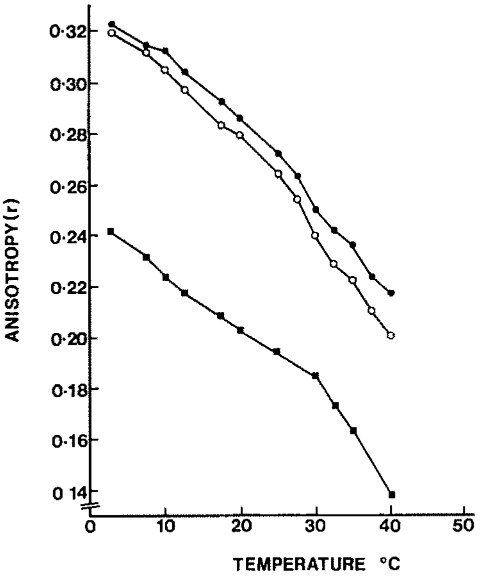

Fig 3. The effect of linoleic acid on anisotropy (●) control, no linoleic acid incorporated (○) 50 nmol, (■) 1074 nmol linoleic acid incorporated/mg protein The samples contained 0.16 mg of brush-border membrane protein.

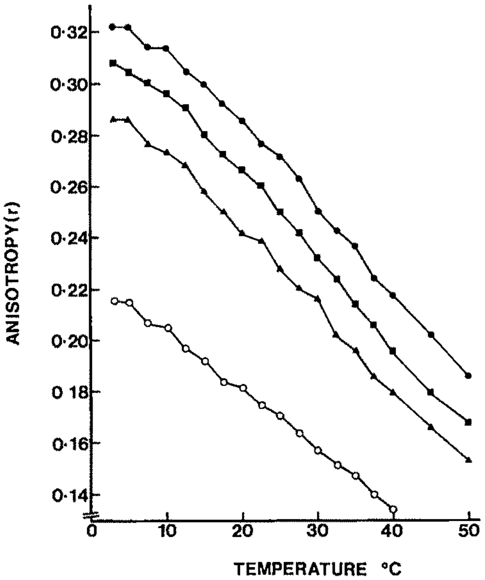

Fig 4. The effect of methyl oleate on anisotropy (●) control, no methyl oleaete incorporated; (■) 68 nmol, (▲) 101 nmol, (O) 220 nmol methyl oleate incorporated/mg protein The samples contained 0.16 mg of brush-border membrane protein.

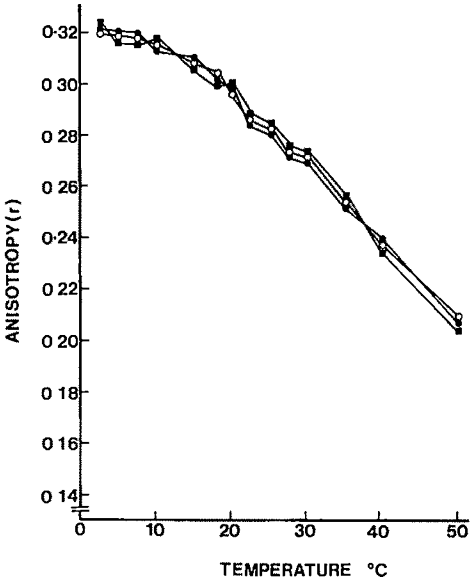

Fig. 5. Effect of palmitic acid on anisotropy (●) control, no palmitic acid incorporated (O) 153 nmol, (■) 275 nmol palmitic acid incorporated/mg protein. The samples contained 0 16 mg of brush-border membrane protein

simple relationship between fluidization and transport activation could be found. It was suggested previously that the inhibition seen at high levels of *cis*-unsaturated fatty acid might result from an excess of fluidity which might lead to disorganization of the transport process. However, results in Fig. 4 do not support such a conclusion. Incorporations of 79–220 nmol/mg protein of methyl oleate decreased the anisotropy in a dose-dependent manner yet with this lipid, only a stimulatory effect on Ca^{2+} uptake was seen. By comparison, incorporations of 340 nmol/mg protein of oleic acid inhibited Ca^{2+} uptake (Table I) while the anisotropy of diphenylhexatriene was greater than that found when 220 nmol/mg protein of methyl oleate was incorporated.

It must be noted that the effect on the fluorescence anisotropy of diphenylhexatriene in brush-border membrane vesicles treated with methyl oleate is markedly different from those treated with oleic acid in the same concentration range. As successive amounts of methyl oleate were incorporated into the vesicles the entire anisotropy-temperature plot was shifted to lower values. For example, when 220 nmol/mg protein of methyl oleate was incorporated the anisotropy at 25 °C was 0.17 compared with the value of the control sample which was 0.27. When 341 nmol/mg protein of oleic acid was taken up, the anisotropy

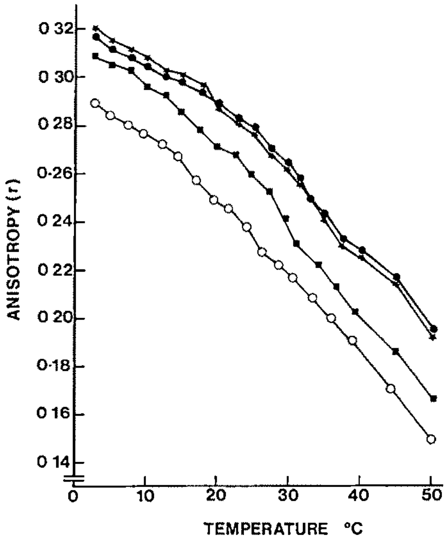

Fig. 6 The lipid extracts of fatty acid-treated brush-border membrane vesicles (●) control; (*) 153 nmol palmitic acid; (■) 89 nmol oleic acid; (O) 341 nmol oleic acid. The lipid concentrations of the extracts are identical to those used for intact brush-border membrane vesicles.

value was 0.255 at 25 °C. The effect on the fluorescence anisotropy was greater for methyloleate even though less was incorporated than for the oleic acid-treated samples.

Treatment of brush-border membranes with palmitic acid had no significant effect on the anisotropy (Fig. 5). In all cases, the decrease in anisotropy as a function of temperature indicated gradual melting and no sharp transition temperatures.

The results shown in Fig. 6 show a different behavior for the lipids from oleic acid-treated vesicles than was observed for the corresponding intact vesicles. The curve is shifted to lower values over the entire temperature range in the lipid extracts. This contrasts with the intact brush-border membrane vesicles where differences in the anisotropy of the oleic acid-treated vesicles were readily observed only at temperatures greater than 15 °C. The extracts from palmitic acid-treated vesicles gave results similar to those from control samples. Generally, the anisotropy values were lower for the lipid extracts compared to the intact membrane vesicles at temperatures below 30 °C.

Discussion

The reason for the difference in rates of uptake of oleic acid and its methyl ester is not certain. This difference could be related to the negative charge intensity and/or to the size of the lipid-bile salt micelles both of which could affect possible interactions of these aggregates with the membrane. The observation could also be due to differences in concentration of these two lipids in the monomer phase. This point requires further investigation.

It is difficult at this point to provide a fully satisfactory rationalization of the differences in the anisotropy results observed for oleic acid and methyl oleate-treated membranes. The presence of the carboxyl group in the *cis*-unsaturated fatty acids could favor interactions with endogenous membrane constituents such as protein for example which would not occur with the methyl ester derivatives of these fatty acids. Such interactions could restrict the extent of mixing with endogenous lipids and limit the effect of acyl chain unsaturation. The effect of unsaturation would become apparent, however, when relatively high levels of incorporation are attained or when the temperature of the membrane becomes sufficiently elevated.

The results obtained with lipid extracts of the brush-border membranes suggests that the proteins influence the membrane fluidity as has been demonstrated by others [16,17]. This is especially evident with oleic acid-treated membranes the extracts of which display decreased anisotropy even throughout the lower temperature range. These effects of protein become apparent, however, only at temperatures well below physiological.

The present study indicates that while *cis*-unsaturated fatty acids affect the fluidity of the membranes as reported by diphenylhexatriene fluorescence, saturated fatty acids apparently had no effect when similar amounts had been incorporated into the membrane. Our findings are similar to those of Klausner et al. [18], who making use of diphenylhexatriene and 8-anilino-1-naphthalene sulfonic acid as fluorescent probes showed that the membranes of mouse lymphocytes and baby hamster kidney cells contained lipid domains of different fluidities. Saturated and *trans*-unsaturated fatty acids were taken up by the less fluid domains without apparent change in order of the interior apolar regions and consequently diphenylhexatriene fluorescence polarization was unaffected. *Cis*-unsaturated fatty acids on the other hand were taken up by more fluid domains where they caused further disruption of acyl chain packing and a lowering of the diphenylhexatriene fluorescence polarization.

The Ca^{2+} transport channels must in some way interact with such fluid domains since Ca^{2+} transport responds to uptake of *cis*-unsaturated fatty acids as well as to their CoA and methyl ester derivatives [19,20]. Excess fluidization, in response to large incorporations of *cis*-unsaturated fatty acid, cannot be in itself the cause of inhibition of Ca^{2+} transport since higher levels of methyl oleate uptake would have exerted a similar inhibitory effect. One must suppose therefore that the accumulation of a large number of free carboxyl groups in the vicinity of the Ca^{2+} channels is in some manner responsible for the inhibitory effects of oleic and linoleic acids at higher levels of incorporation. The binding of Ca^{2+} to these carboxyl groups at the exterior of the membrane would compete with Ca^{2+} transport through the channels. Such superficially bound divalent cation would be removed by the wash procedures used in our method for studying Ca^{2+} transport [11] and consequently decreased Ca^{2+} uptake values would be seen. The complete lack of, or relatively weak, inhibitory effect of saturated fatty acids which have been reported to be much more effective in binding Ca^{2+} than *cis*-unsaturated fatty acids, either alone in solution or following uptake by sarcoplasmic reticulum [21–23], could be explained on the basis of their being incorporated in less fluid areas away from the Ca^{2+} channel sites. The presence of free carboxyl groups could also effect conformational changes in the channel proteins or modify charged group relationships across the channel which would in turn alter transport ability. The stimulatory effect of lower levels of *cis*-unsaturated fatty acids could be explained on the basis of increased fluidity at the temperature prevailing during the Ca^{2+} uptake studies since methyl oleate causes the same enhancement of uptake. It could be argued, however, that the stimulation observed at low levels of unsaturated fatty acid is due to some extent to an increase in free calcium at the transport site resulting from the calcium buffer action of carboxyl groups. These points require further clarification and in this respect it would be of interest to test the effect of other unsaturated lipids such as dioleoylphosphatidylcholine, dioleolylphosphatidic acid, alkenylamines and alkenols on Ca^{2+} transport.

The luminal membrane of intestinal cells is constantly exposed to exogenous lipids derived from the diet. The uptake of these lipids modifies the composition of the membrane and this in turn would affect its structure relationships. Some of the possible changes in structure and function are described in the present study which reveals that oleic acid and methyl oleate increases the fluidity of the membrane in a dose-dependent manner while affecting transport of Ca^{2+}. The effects on Ca^{2+} transport are complex however and do not relate only to general physical effects on the membrane but also to specific differences in the molecular structure of the incorporated lipids. Purification of the transporter proteins and their reconstitution into liposomes could shed additional light on the overall effects of lipids on Ca^{2+} transport as it occurs in brush-border membranes.

Acknowledgements

This study was supported by the Medical Research Council and the National Science and Engineering Research Council of Canada.

References

1 Proulx, P, McNeil, J., Brglez, I. and Williamson, D G (1982) Can. J. Biochem 60, 904–909
2 Proulx, P., Aubry, H, Brglez, I. and Williamson, D G (1984) Biochim. Biophys Acta 775, 341–346
3 Proulx, P., Aubry, H., Brglez, I. and Williamson, D G (1984) Biochim. Biophys Acta 778, 586–593
4 Proulx, P., Aubry, H., Brglez, I. and Williamson, D G (1985) Can. J. Biochem. Cell Biol 63, 249–256
5 Merrill, A.R., Proulx, P. and Szabo, A. (1986) Biochim Biophys. Acta 855, 337–344
6 Marshall, M.O. and Kates, M. (1972) Biochim. Biophys Acta 260, 558–570
7 Mangold, H.K. and Malins, D.C (1960) J. Am. Oil Chem Soc. 37, 383–385
8 Bligh, E.G. and Dyer, W J. (1959) Can. J. Biochem. Physiol. 37, 911–917
9 Selhub, J. and Rosenberg, I.H. (1981) J. Biol Chem. 256, 4489–4493
10 Aubry, H., Merrill, A R and Proulx, P. (1986) Biochem. Biophys. Acta 856, 610–614
11 Lowry, O H., Rosebrough, N.J., Farr, A L and Randall, R J. (1951) J Biol. Chem. 193, 265–275
12 Miller, A and Bronner, F. (1981) Biochem J. 196, 391–401
13 Parker, C A. (1978) in Photoluminescence of Solutions, p 51, Elsevier Publishing Co., Amsterdam
14 Teale, F.W J. (1969) Photochem. Photobiol 10, 363–374
15 Lentz, B.R, Moore, B.M. and Barrow, D.A (1979) Biophys J. 25, 489–494
16 Brasitus, T A., Davidson, N.O. and Schachter, D. (1985) Biochim. Biophys Acta 812, 460–4144
17 Brasitus, T.A., Schachter, D and Mamouneas, T G. (1979) Biochem. 18, 4136–4144
18 Klausner, R.D., Kleinfeld, A.M., Hoover, R.L. and Karnovsky, M.J (1980) J. Biol. Chem. 255, 1286–1295
19 Fontaine, O., Matsumoto, J, Goodman, D B P. and Rasmussen, H. (1981) Proc. Natl. Acad Sci. USA 78, 1751–1754
20 Kreutter, O., Lafreniere, D.C. and Rasmussen, H (1984) Biochim Biophys. Acta 777, 261–266
21 Watras, J., Messineo, F.C. and Herbette, L.G (1984) J. Biol. Chem. 259, 1319–1324
22 Herbette, L.G., Favreau, C, Segalman, K, Napoletano, C.A. and Watras, J. (1984) J. Biol Chem. 259, 1325–335
23 Messineo, C., Rathier, M., Favreau, C., Watras, J. and Takanaka, H. (1984) J. Biol. Chem. 259, 1336–1343

Biochimica et Biophysica Acta 896 (1987) 96–102
Elsevier

BBA 73194

Enhanced uptake of carnitine by perfused rat liver following starvation

Gyula Kispal, Bela Melegh, Istvan Alkonyi and Attila Sandor

Institute of Biochemistry, University Medical School of Pecs, Pecs (Hungary)

(Received 4 June 1986)
(Revised manuscript received 25 September 1986)

Key words: Carnitine transport; Liver perfusion; Starvation; (Rat liver)

Previously, the release of carnitine from the perfused rat liver was found to be protein-mediated, dependent on the nutritional state but not on metabolic energy. Further, it was shown to exceed the physiological demand by about 10-fold (Sandor et al. (1985) Biochim. Biophys. Acta 835, 83–91). In the present study the uptake of carnitine by perfused rat liver has been investigated. (1) The liver tissue and the perfusate were in equilibrium when the carnitine concentration in the perfusate was close to 45 μM, physiological in the rat plasma. Under this condition, when no net carnitine transport occurred, an unidirectional uptake of L-[^{3}H]carnitine was observed. Quantitatively, the uptake rate was 355 ± 60 (S.D.) nmol/h per 100 g body weight at 45–50 μM perfusate concentration. This uptake capacity balances the previously reported excessive release (Sandor et al., op. cit.). On this basis we propose that a futile release/uptake cycle operates in carnitine transport across the liver cell membrane. (2) Liverse of 24-h starved rats took up L-[^{3}H]carnitine at 56% higher rate from the perfusate (75 μM) than livers of fed rats. Kinetic analysis revealed that fasting caused a decrease in K_m value from 4.22 mM to 2.59 mM, whereas V_{max} remained practically unchanged, average 0.95 μmol/min per 100 g body weight. D-[^{3}H]Carnitine was transported at the same rate as L-carnitine and underwent the effect of fasting as well. (3) The uptake was partially inhibited by 1 mM 2,4-dinitrophenol and 5 mM KCN, showing its dependency on metabolic energy. If Li^+ replaced Na^+ a strong inhibitory effect (to 20% of control) was observed, which suggests a co-transport of carnitine with Na^+. Mersalyl, an SH reagent, had no effect on the uptake, whereas it practically abolished the release of carnitine from the perfused livers. This observation suggests that the inward and outward transport of carnitine are mediated by two different proteins.

Introduction

It has been well documented the rat liver in the fasting state accumulates carnitine (i.e., L-(−)-carnitine: 3-hydroxy-4-*N*-trimethylammoniobutanoate) [1–3], an essential substance for fatty acid oxidation and ketogenesis. The increase of carnitine content on a g liver basis is undoubted, but the mechanism(s) whereby rat liver concentrates carnitine during fasting is not completely understood. Whereas some workers found an absolute rise in liver carnitine content [2,3], others found that the increased concentration could be accounted for by loss of liver mass [1]. We pointed out earlier [3] that shrinkage of the liver during starvation cannot be the cause by itself. An elevated concentration in liver should equilibrate with the serum at the earlier fed level, unless the kinetic parameters of cellular transport are changed. In a previous work [3] we demonstrated

---

Correspondence: Dr. A. Sandor, Institute of Biochemistry, University Medical School of Pecs, 7624 Pecs, Szigeti ut 12, Hungary.

0005-2736/87/$03.50 © 1987 Elsevier Science Publishers B.V. (Biomedical Division)

a decreased rate of carnitine release from the liver during starvation, which is due to a decrease of rate constant (to 5.0 min^{-1} from 8.4 min^{-1}). In the present paper, the uptake side of carnitine transport has been investigated. As will be demonstrated, the enhanced uptake also contributes to developing the increased liver carnitine concentration seen in starvation.

The uptake process, characterized hereafter, deserves attention in two points when compared to the efflux. In rat, the liver synthesizes carnitine and supplies the whole organism with that. However, the efflux of carnitine from the liver [3] exceeds several times the estimated physiological demand and rate of biosynthesis [1,4,5]. Thus, most of the released carnitine has to reenter the liver. A question to be answered is whether or not the influx rate matches the excessive release? In a qualitative sense, the uptake process will be characterized through its sensitivity to inhibitors. Comparing these properties of influx to those of the efflux process we can obtain further information about the transport mechanism: do the uptake and release share a common protein?

Materials and Methods

Male Wistar rats (200–250 g) were used in all experiments and fed commercial laboratory chow ad libitum. Fasted rats were deprived of food at 8:00 a.m. the day before the experiment.

Materials

L-Carnitine, internal salt, was a kind gift from Sigma-Tau, Rome. D,L-[*methyl*-^{3}H]Carnitine and [1-^{14}C]acetyl-CoA were purchased from Amersham. Inulin [^{14}C]carboxylic acid from Amersham was rechromatographed on a Sephadex G-25 column before use. Acetyl-CoA was prepared as described [6]. L-[^{3}H]Carnitine was prepared from the commercially available racemic mixtures by paper chromatography after the enzymatic acylation of the L-isomer with pripionyl-CoA [3,7]. The separation of propionyl-L-carnitine from D-carnitine and the subsequent alkaline hydrolysis resulted in D-[^{3}H]carnitine and L-[^{3}H]carnitine. The overall yield was 90% with 99% purity as determined by TLC. Carnitine acetyltransferase and 3-hydroxybutyrate dehydrogenase were obtained from Boehringer-Mannheim. All other chemicals were market-available analytical grade compounds.

Experimental procedures

Livers were perfused with 30 ml perfusion fluid as described by Mortimore [8] with some modifications [3]. Samples of perfusion fluid were taken at time intervals shown in the figures, and of livers at the end of perfusion. Perfusate and liver samples were assayed for total carnitine after alkaline hydrolysis by modified enzymatic analysis [3] originally described by Cederblad [9]. To determine the unidirectional uptake rate we introduced L-[^{3}H]carnitine (usually 1000 cpm/nmol) into the perfusate and measured radioactivity in the perfusion fluid. To express the changes in nmol the initial specific activity was used. For calculations of uptake rates we used the initial straight part of the curves between 5 and 15 min. (The diluting effect of released carnitine on the specific activity was neglected because it could affect the calculation less than 10%.) Ketone bodies were determined in the deproteinized extracts by described methods [10,11] (the term ketone bodies refers to the sum of acetoacetate and 3-hydroxybutyrate).

Extracellular space of perfused livers was determined with [*carboxy*-^{14}C]inulin in separate experiments, tissue total water was determined by drying as described [3] and the intracellular water was calculated by subtraction. Application and standardization of Mersalyl was also described earlier [3]. Radioactive determinations in 10 ml toluene/Triton X-100 (2:1, v/v) scintillant were performed using Beckman LS 230 counter. ^{3}H activities were measured in separate aliquots in absence of ^{14}C. ^{14}C activities were measured by using narrow window if tritium activity was present.

Terminology

'Uptake' or 'unidirectional uptake' means the influx. 'Release' means the efflux. 'Net uptake' means the resultant inward transport of the concomitant influx and efflux. For example, when the influx and efflux are equal not net uptake occurs.

Results

Fed and fasted state

The carnitine concentration in the perfusate and tissue were compared during perfusion of livers from fed and 24-h fasted rats. In respect to ketone body production the perfused liver preserved the in vivo fed-fasted relationship. The 'fed' livers produced 18 μmol, 'fasted' livers produced 80 μmol total ketone bodies per h per 100 g body weight (data not shown), consistent with the value reported in the literature [12].

Carnitine concentrations in the perfusate during the perfusion are shown in Fig. 1. When the initial carnitine concentration in the perfusate was 45 μM (considered physiological), this level remained constant during the 2 h of perfusion (Fig. 1, set I). This steady-state concentration is the result of the concommitant uptake and release. The steady state was achieved at a lower perfusate concentration by livers from fasted animals (Fig. 1). Hepatic carnitine content at the end of perfusion was 170 nmol/g and 356 nmol/g in fed and starved rats, respectively. These levels correspond to 307 μM and 622 μM intracellular concentrations, when calculated on intracellular water basis. (The intracellular water content increased slightly from 552 to 572 μl/g wet weight during starvation, in accordance with other reports [8]). The liver-to-perfusate concentration ratios of carnitine at equilibrium were 6.9 vs. 18.2 when livers derived from fed and fasted animals, respectively. In vivo the liver/serum ratio undergoes the same shift (because the liver develops its higher concentration at practically unchanged serum level). Thus, the recirculating perfusion system maintains the liver-serum relationship with respect to the carnitine concentration, as well. When perfusate carnitine concentration was higher, 78–80 μM, livers took up carnitine, approaching the steady-state condition (Fig. 1, set II). The rate of net uptake in fasted state was increased by 62.5% when compared with the rate seen in livers from fed rats. This apparent increase in the net uptake raised two questions. First, because the decreased release in the fasted state [3] contributes to this effect, what was the effect of starvation on the unidirectional uptake process? Second, might this effect be due to metabolism, i.e., enhanced esterification of carnitine?

To answer the first question, we introduced L-[^{3}H]carnitine into the perfusate to determine the unidirectional uptake. Fig. 2 shows the unidirectional and net uptake simultaneously in both nutritional states. The divergence between the net and unidirectional curve is due to the concomitant release. The unidirectional uptake rates were 36 and 56 nmol/min per liver by livers from fed (Fig.

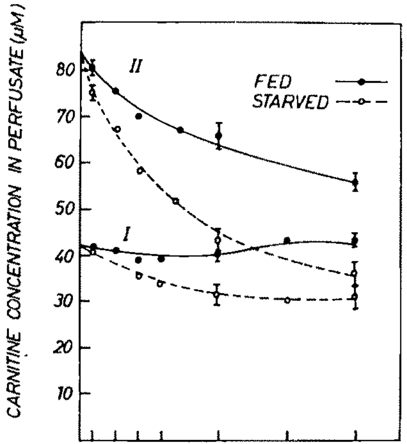

Fig. 1. Total carnitine concentration in perfusate during recirculating perfusion of fed and fasted rats Livers were 12.5±0.6 g and 9.4±0.5 g at the end of perfusion in the fed and fasted state, respectively. (In this and all other experiments the pre-fasting body weights were the same in the two groups.) Values presented in the figure are means of four experiments. For clarity, S.E. is shown by bars only at 60 and 120 min

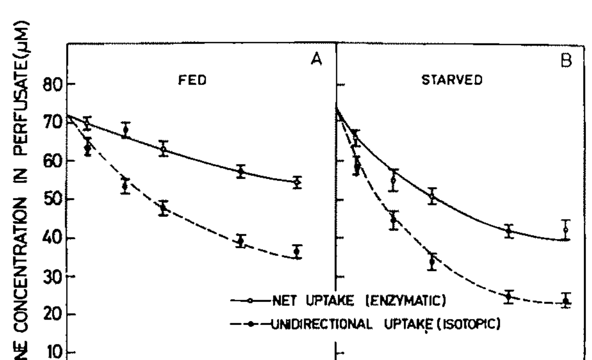

Fig. 2 (A, B) Unidirectional and net uptake of carnitine in fed and fasted states. Rat livers were perfused with 30 ml medium as described in Materials and Methods. Livers were 10.5 and 7.8 g in the fed and starved states, respectively. Unidirectional uptake was measured by the isotopic, net uptake by the enzymatic method, as detailed in Materials and Methods Values are means±S.E. for four experiments.

2A) and fasted (Fig. 2B) rats, respectively. Thus, 24-h fasting resulted in a 56% increase in the influx of total carnitine. (The comparison on whole liver basis seems to be very resasonable, because the prefasting liver weights were the same in the two groups. Comparison on 100 g body weight basis would have exaggerated the difference by about 10%.)

To answer the second question the uptake of D-[^{3}H]carnitine was also examined. As seen (Fig. 3A), there was no significant difference between the unidirectional uptake of L- and D-carnitine. This finding is consistent with observation made on isolated rat hepatocytes [13]. Further, D-carnitine uptake was also enhanced by starvation (Fig. 3B); the tissue/perfusate ratio increased from 2.09 to 6.20. This observation rules out the possibility that increased esterification of carnitine was responsible for the enhanced uptake seen in the fasted state.

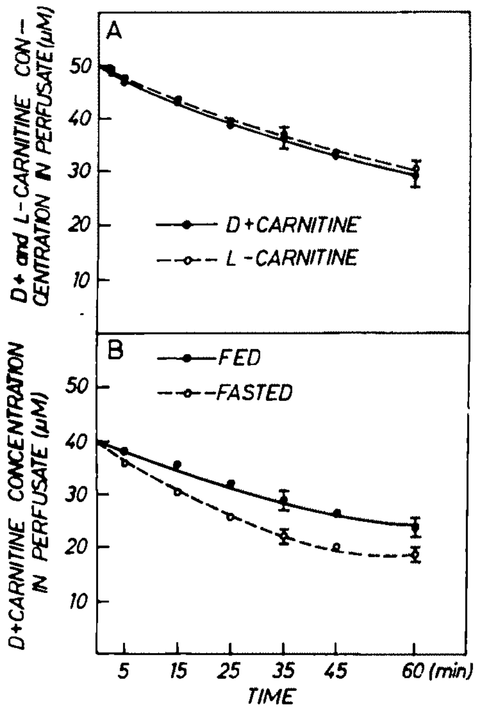

Fig. 3. (A) Uptake of D-[^{3}H]carnitine and L-[^{3}H]carnitine by perfused livers from fed rats. 8.5 ± 0.5 g livers were perfused at concentrations showed on the scale. Values are means of four experiments; S.E. is shown by bars at two points. (B) Uptake of D-[^{3}H]carnitine by perfused livers of fed and starved rats 9.5 ± 0.5 g fed and 6.5 ± 0.6 g starved livers were perfused as described above. Concentrations of D-carnitine in the liver and the end of perfusion were 68.2 and 133.2 nmol/g in the fed and fasted cases, respectively.

The perfusion model also enabled us to characterize the kinetics of hepatocellular carnitine transport. For this purpose a separate experimental series was performed at the perfusate concentrations shown in Fig. 4. The initial rate of unidirectional uptake was saturable (not shown). Double-reciprocal plots of these data (Fig. 4) showed a decrease in the K_m value from 4.22 mM to 2.59 mM, whereas the V_{max} remained unchanged (average 0.95 μmol $\cdot$ min^{-1} per 100 g prefasting body weight).

Effect of different inhibitors

All experiments with inhibitors were performed using livers of fed animals. The sensitivity of the transport to sulfhydryl reagent was examined by using mersalyl. As shown in Fig. 6C, mersalyl had no effect on unidirectional carnitine uptake. We demonstrated previously that mersalyl strongly inhibits the release of carnitine from the perfused rat liver [3]. Simultaneous measurement of the mersalyl effect on the unidirectional and net uptake enabled us to compare the effect on the uptake and release in the same liver under the same conditions. In Fig. 5A, the unidirectional and net uptake in 'fed' livers are shown. (The divergence between the two curves is due to the

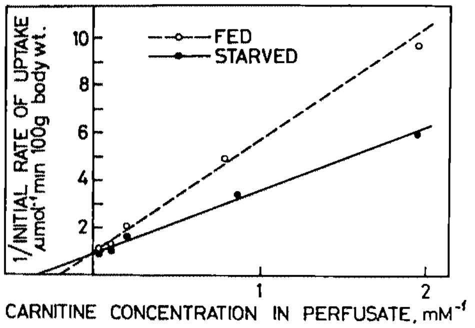

Fig. 4. Double-reciprocal plot of carnitine uptake rate by perfused livers from fed and fasted rats against perfusate carnitine concentration. The unidirectional uptake was measured isotopically; initial rates were assumed as reasoned under Materials and Methods. All points are means for four perfusions. Lines were fitted with least-squares regression. The K_m values: 4.22 mM for fed rats, 2.59 mM for fasted ones. The V_{max} values are 0.92 and 0.98 μmol/min per 100 g body weight.

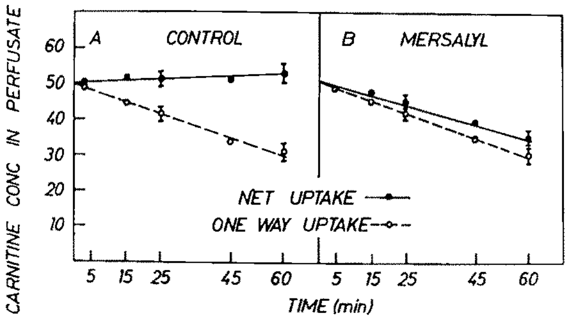

Fig 5 (A, B) Unidirectional and net uptake of carnitine in the presence (B) and absence (A) of mersalyl. 8.4±0.3 g livers from fed rats were perfused. The effective mersalyl concentration was 380 μM Values are means for four perfusions, S E is shown by bars at important points.

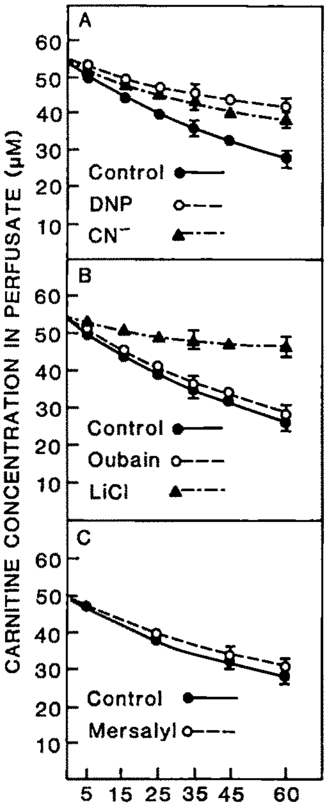

Fig. 6. (A, B, C) Effects of different inhibitors on unidirectional uptake of carnitine 8 5±0.5 g livers were perfused as described in Materials and Methods. Perfusion medium contained 5 mM KCN, 1 mM 2.4-dinitrophenol, 1 mM ouabain and 380 μM effective mersalyl in different sets of experiments, respectively. In the experiment where the effect of LiCl was examined, the NaCl content of the medium was replaced totally with LiCl Values are means of four experiments, S E is shown by bars at two points

release of carnitine.) Mersalyl abolished the divergence, that is, abolished the release, while the unidirectional uptake rate was uneffected (Fig. 5B).

Previous studies of carnitine transport by different tissues [13–21] revealed that the uptake process was energy-dependent. Our results, obtained in recirculating perfusion system yielded the same results. Measuring the initial rate of unidirectional uptake of L-[^{3}H]carnitine, significant inhibition by 1 mM 2,4-dinitrophenol and 5 mM KCN was found (Fig. 6A). The 50% and 30% inhibitory effects of 2,4-dinitrophenol and KCN are consistent with results obtained by others on extrahepatic tissues [14–16,18]. Replacement of Na^+ with Li^+ inhibited the inward transport by 80% (Fig. 6B), suggesting a close connection between the Na^+ transmembrane gradient and carnitine transport. Oubain, an inhibitor of (Na^+-K^+)-ATPase, did not affect the uptake (Fig. 6B) and neither did changes in perfusate pH from 6.5 to 8.0 (not shown).

Discussion

At carnitine concentration in the perfusate close to the physiological plasma concentrations (45–50 μM), the perfused liver maintained the perfusate concentration constant. Under this condition, when no net carnitine transport occurred, we observed unidirectional uptake using isotopic techniques (Figs. 1, 2, 5A, 6 control curves). This finding proves that concomitant uptake and release processes are operating in the hepatocellular carnitine transport and that they are balanced under steady-state conditions. In rat, the liver is devoted to supplying the organism with carnitine, and the established daily release from the liver, 9.93 μmol per 100 g body weight [3], exceeds by 4–10-fold the estimated demand. In this work, the uptake of carnitine by rat liver, that is, the re-entry of the released carnitine, has been characterized. Quantitatively, the unidirectional uptake rate average 354 ± 60 (S.D.) nmol/h per 100 g body weight at 45–50 μM perfusate concentration. (Compiled data from Figs. 3, 5, 6. Specific liver weights were 4.79 g/100 g body weight.) (The uptake rate calculated from the kinetic parameters would be somewhat higher (582 nmol/h per 100 g body wt.). This is fairly consistent, if we consider that the kinetic measurements were performed at another (higher) range of substrate concentrations.) On a daily basis, 8.5 μmol of carnitine were taken up per 100 g body weight, which matches fairly well the previously established release rate. Since this uptake is energy-dependent, this release and uptake cycle can be considered an energy-consuming futile cycle. The significance of this cycle is shown by the fact that the amount of carnitine turning over each day is 10-times higher than the carnitine content of liver. Numerous futile cycles have already been described [22], stressing the ability of these cycles to amplify metabolic signals, if the two opposite processes are simultaneously controlled. We looked at how the hepatocellular carnitine transport is controlled in the fasting state.

Starvation results in a marked increase in liver carnitine on a g wet tissue basis [1–3]. Calculated on an intracellular water basis, the concentrations found in this work were 307 μM and 622 μM in the perfused liver of fed and fasted rats, respectively. Due to the reduced weight of livers from fasted animals, the increase in total liver carnitine (nmol/g per g organ) is smaller (Refs. 2, 3 and this work) or there is no increase [1] compared to the fed state. We stress that the liver shrinkage cannot cause and maintain an increased concentration, that is, the increased liver/plasma ratio. Searching for changes in transport properties, we found that the uptake of carnitine is increased by 56% on the effect of fasting (when starting from 75–80 μM perfusate concentration; Fig. 2). It has also been shown that this increase in transport rate is due to a decrease in K_m value while the V_{max} is slightly changed (Fig. 4). The observation that D-(+)carnitine transport also undergoes the effect of fasting proves that the change is not due to further metabolic conversion (esterification). Earlier [3], we demonstrated a decreased release of carnitine from the perfused livers of fasted animals. Returning to the futile cycle outlined above, the liver takes advantage of release/uptake futile cycle: both directions are controlled in the fasting state in favor of developing and maintaining the higher liver:plasma carnitine ratio (Fig. 1). Presumably, the endocrine background, more exactly, the decreased insulin:glucagon ratio during fasting [2], is responsible for changing the hepatocellular carnitine transport.

Being concentrative, the uptake of carnitine into liver cells is sensitive to metabolic inhibitors is consistence with Bremer's results [13] and other data obtained in extrahepatic tissues [14,16]. The relatively low sensitivity to metabolic inhibitors anticipates that the process is not related directly to ATP utilization but to some other energy-dependent process. In fact, our finding (Fig. 6B) suggests a dependency on an Na^+ gradient. A co-transport mechanism with Na^+ for carnitine is also described in perfused rat heart [16]. (Neither those workers nor ourselves have observed any effect of oubain, probably because carnitine uses the already built up Na^+ gradient for transport.) Mersalyl (SH reagent) did not inhibit the uptake of carnitine (Fig. 6C), but markedly inhibited the release of carnitine (Fig. 5), as, confirming our previous finding [3]. These observations strongly suggest that the inward and outward transport of carnitine through the liver cell membrane are mediated by two different proteins. Alternatively, one carrier protein with two oriented sides may be operating: one is mersalyl-sensitive and the other is not.

Acknowledgments

We wish to thank Dr. Charles L. Hoppel and Dr. Athur Zinn for helpful discussions and Cherice Edmonds for typing. We also thank Maria Miklosvari and Zsuzsa Hillebrand for their skilled technical assistance.

References

1 Brass, E.P. and Hoppel, C.L. (1978) J Biol. Chem. 253, 2688–2693
2 McGarry, J.D., Robles-Valdes, C and Foster, D.W. (1975) Proc. Nat. Acad. Sci. USA 72, 4385–4388
3 Sandor, A., Kispal, G., Melegh, B. and Alkonyi, I. (1985) Biochim. Biophys. Acta 835, 83–91
4 Cederblad, G. and Lindstedt, S (1976) Arch. Biochem. Biophys. 175, 173–180
5 Brooks, D E and Intosh, E (1975) Biochem J 148, 439–455
6 Stadtman, E R. (1957) Methods Enzymol. 3, 931–941
7 Tsai, A C., Romsos, D.R. and Leveille, C.A. (1975) J. Nutr 105, 301–307
8 Mortimore, G.E (1963) Am. J. Physiol. 200, 1315–1319
9 Cederblad, G., Lindstedt, S and Lundholm, K. (1974) Clin. Chim. Acta 53, 311–321

10 Williamson, D.H. and Mellanby, J (1974) in Methods of Enzymatic Analysis (Bergmayer, H.U., ed.), pp. 1836–1839, Verlag Chemie, Weinheim

11 Mellamby, J. and Williamson, D.H. (1974) in Methods of Enzymatic Analysis (Bergmayer, H.U., ed), pp. 1840–1843, Verlag Chemie, Weinheim

12 McGarry, J.D. and Foster, D.W. (1971) J. Biol. Chem. 246, 6247–6253

13 Christiansen, R.Z. and Bremer, J. (1976) Biochim Biophys Acta 448, 562–577

14 Rebouch, C.J. (1977) Biochim. Biophys. Acta 471, 145–155

15 Vary, T.C. and Neely, J.R. (1982) Am. J Physiol 242, H585–H595

16 Vary, T.C. and Neely, J.R. (1983) Am. J. Physiol. 244, H247–H254

17 T. Bohmer, K.E. and Jonsen, J (1977) Biochim. Biophys. Acta 465, 627–633

18 Huth, P.J. and Shug, A.L. (1980) Biochim. Biophys. Acta 602, 621–634

19 James, M.J., Brooks, D.E. and Snoswell, A M (1981) FEBS Lett. 126, 53–56

20 Zoccarato, F., Siliprandi, N. and Mugolo, M. (1983) Biochim. Biophys. Acta 734, 381–383

21 Parvin, R. and Pande, S.V. (1979) J Biol. Chem. 254, 5423–5429

22 Hue, L. (1982) in Metabolic Compartmentation (Sies, H , ed.) pp 71–94, Academic Press, London

Biochimica et Biophysica Acta 896 (1987) 103–108
Elsevier

BBA 73349

Nitrite uptake and its regulation in the cyanobacterium *Anacystis nidulans*

Enrique Flores, Antonia Herrero and Miguel G. Guerrero

Departamento de Bioquímica, Facultad de Biología y C.S.I.C., Apartado 1095, E-41080 Sevilla (Spain)

(Received 28 July 1986)

Key words: Nitrite transport; Nitrogen control; (*A. nidulans*)

Two different components seem to participate in the uptake of nitrite by the cyanobacterium *Anacystis nidulans*, namely a transport system sensitive to *N*,*N′*-dicyclohexylcarbodiimide and a passive influx. The relative contribution of each component depended on the pH of the medium, that of the active system being prevalent at high pH values. The active transport of nitrite appears to be mediated by a high-affinity system, whereas the affinity for nitrite of the passive system is lower, similar to that of nitrite reductase. The utilization of nitrite was inhibited by products of the assimilation of ammonium via glutamine synthetase, apparently acting at the level of the active component involved in nitrite uptake.

Introduction

Most cyanobacteria are able to use nitrate, nitrite or ammonium as the sole nitrogen source for growth [1]. Whereas several studies concerning the uptake of nitrate [2–7] and ammonium [6,8–10] by different strains of cyanobacteria have appeared, the published information about nitrite uptake is scarce [4,11].

The proposal has been raised that two components, namely, active transport and passive diffusion, contribute to nitrite uptake in *Anacystis nidulans* [4]. In this report evidence is presented in support of the operation of both systems in nitrite acquisition by *A. nidulans* cells. Some features of the energy-requiring system have been characterized. The active component of nitrite uptake is regulated by ammonium and carbon dioxide availability, to which it responds in a similar way to that previously described for the nitrate uptake system [3,5].

Materials and Methods

Anacystis nidulans (strain L 1402-1 from the Göttingen University Algal Culture Collection; also known as *Synechococcus leopoliensis* or *Synechococcus elongatus* [12]) was grown photoautotrophically at 39°C with nitrate as the nitrogen source on a medium previously described [13]. Cellular chlorophyll was determined in methanolic extracts [14].

The cells were harvested and washed by filtration through Milipore filters (type HA-0.45 μm). When a treatment with DCCD or MSX was carried out before the uptake experiments, the cells were suspended in 30 mM Tricine-NaOH buffer (pH 8.1) (unless otherwise indicated) and incubated in air-opened conical flasks at 40°C in the light (100 W · m^{-2}, white light). Nitrite uptake

---

Abbreviations: DCCD, *N*,*N′*-dicyclohexylcarbodiimide; Mops, 4-morpholinepropanesulfonic acid; MSX, L-methionine-D,L-sulfoximine; MTA, mixed alkyltrimethylammonium bromide; Tricine, *N*-[2-hydroxy-1,1-bis(hydroxymethyl)-ethyl]glycine.

Correspondence: Dr E. Flores, Departamento de Bioquímica, Facultad de Biología y C.S.I.C., Apartado 1095, E-41080 Sevilla, Spain.

0005-2736/87/$03.50 © 1987 Elsevier Science Publishers B.V (Biomedical Division)

was studied with washed cells at 40°C in the light (as above) under the particular conditions described for each experiment. Nitrite uptake was followed as nitrite disappearance from the medium; the cells were removed by filtration and nitrite in the medium determined by the method of Snell and Snell [15]. Alternatively, aliquots of the cell suspension were directly added to the nitrite determination assay, removing the cell debris by low-speed centrifugation. Similar results were obtained with any of the two methods. Ammonium was determined in the filtrates with glutamate dehydrogenase [16].

The K_m (NO_2^-) of nitrite reductase was determined in cells made permeable to small molecules by the detergent mixed alkyltrimethylammonium bromide (MTA). *A. nidulans* cells (2 μg chlorophyll) were added to a reaction mixture containing in a final volume of 1 ml: MTA, 750 μg; Mops-NaOH buffer (pH 7.2), 25 μmol; methyl viologen, 5 μmol; 20 μmol of $Na_2S_2O_4$ in 0.1 ml of 0.3 M $NaHCO_3$; and KNO_2 at the indicated concentration. After incubation at 30°C for 5 min, nitrite was determined [15]. Activity units correspond to μmol of nitrite disappeared per min. (Mixed alkyltrimethylammonium bromide did not interfere with the assay for nitrite determination.)

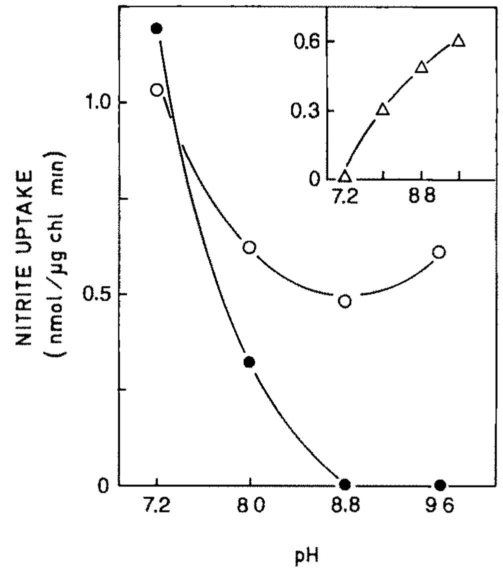

Fig. 1. Effect of extracellular pH on nitrite utilization by DCCD-treated *Anacystis nidulans* cells. The cells (8 μg chlorophyll/ml) were preincubated for 15 min in the light, at 40°C, suspended in 30 mM Tricine-NaOH buffer (pH 8.1) supplemented (●) or not (○) with 10 μM DCCD. After washing by filtration, the cells were suspended (8 μg chlorophyll/ml) in 10 mM Mops/10 mM Tricine/10 mM glycine-NaOH buffer of the indicated pH value and, after addition of nitrite (0.5 mM KNO_2, final concentration), nitrite utilization was assayed for 30 min. The insert shows the pH dependence of the DCCD-sensitive nitrite uptake (nitrite utilization by untreated cells minus nitrite utilization by DCCD-treated cells).

Results and Discussion

Two different components in nitrite uptake

Nitrate-grown cells of the cyanobacterium *Anacystis nidulans* exhibit high activities of nitrite utilization in the light, in the range of 1–3 nmol · μg^{-1} (chlorophyll) · min^{-1}. Nitrite uptake in *Anacystis* is sensitive to DCCD [4], an inhibitor of bacterial ATPases [17], suggesting the involvement in nitrite uptake of an active transport system and the participation of ATP in the link between energy metabolism and the uptake process [4]. The extent to which nitrite utilization was inhibited by DCCD-treatment of the cells depended on the pH of the medium. Treatment of the cells with DCCD did not affect nitrite utilization at neutral pH, whereas a negative effect was manifest at higher pH values, the degree of inhibition increasing as the pH raised (Fig. 1). Increasing the pH would reduce the concentration of available nitrous acid (pK_a NO_2^-/HNO_2, 3.4), which suggests that diffusion of uncharged nitrous acid might account for the passive nitrite influx. On the other hand, a DCCD-sensitive activity of nitrite uptake is manifest at the higher pH values tested. Consequently, DCCD can be used to evaluate the relative contribution of diffusion and active transport to the net nitrite uptake by *A. nidulans* cells. Interestingly enough, the pH dependence of the DCCD-sensitive uptake (Fig. 1, insert) is very similar to the pH dependence of nitrate uptake in *A. nidulans* [18], which takes place in an active way [4].

Under conditions in which active nitrite uptake is operative, *Anacystis* cells exhibit a high affinity for nitrite, the K_m (NO_2^-) being below 10 μM [4]. However, when contribution of the active component was low (pH 7.2), a biphasic pattern was apparent in the response of nitrite utilization by whole *A. nidulans* cells to changes in nitrite concentration (Fig. 2). For the low concentration range, a K_m (NO_2^-) of about 6 μM (V_{max} about 0.6 nmol $NO_2^- \cdot \mu g^{-1}$ (chlorophyll) $\cdot$ min^{-1}) could be calculated, whereas for the higher nitrite concentration range, the calculated K_m (NO_2^-) was higher (about 450 μM), the V_{max} being about 3.5 nmol $NO_2^- \cdot \mu g^{-1}$ (chlorophyll) $\cdot$ min^{-1}. This can be interpreted in terms of the contribution of two systems with different affinities for the substrate to nitrite utilization by *Anacystis*. The high-affinity component might correspond to the active (DCCD-sensitive) system, scarcely active at pH 7.2, whereas the low-affinity component probably reflects passive influx of nitrous acid. As a matter of fact, the K_m (NO_2^-) of nitrite uptake by DCCD-treated cells was estimated to be 400 μM (Fig. 3).

Active uptake of nitrite by whole cells of *A. nidulans* may well be mediated by a permease with a high affinity for the substrate. On the other hand, under conditions in which nitrite uptake takes place mainly as a passive process, the affinity for nitrite exhibited by the cells might be determined by nitrite reductase, the first enzyme involved in the assimilation of nitrite. To test this possibility, the K_m (NO_2^-) of nitrite reductase has been estimated under in situ conditions, in *Anacystis* cells made permeable to small molecules by the detergent alkyltrimethylammonium bromide, and a value of about 120 μM was found (Fig. 4). This compares well to the K_m (NO_2^-) of intact untreated cells under conditions favoring passive uptake of nitrite (about 450 μM; Fig. 2) or to that of DCCD-treated cells (400 μM; Fig. 3).

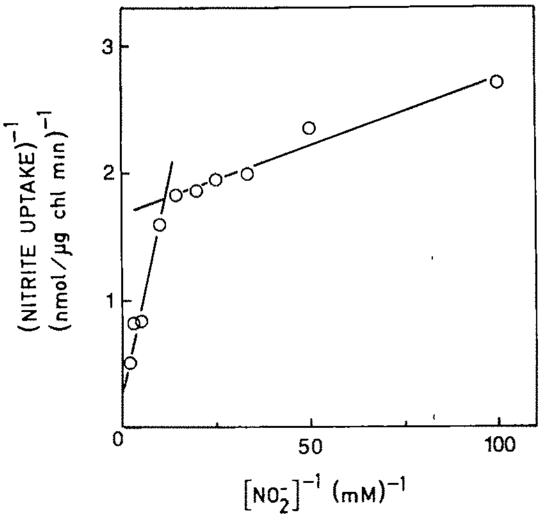

Fig 2 Lineweaver-Burk plot of the effect of the concentration of nitrite on the rate of nitrite utilization by *A. nidulans* at pH 7.2. The assays were started by the addition of washed cells (3 μg chlorophyll/ml, final concentration) to solutions containing different concentrations of KNO_2 in 25 mM Mops-NaOH buffer (pH 7 2).

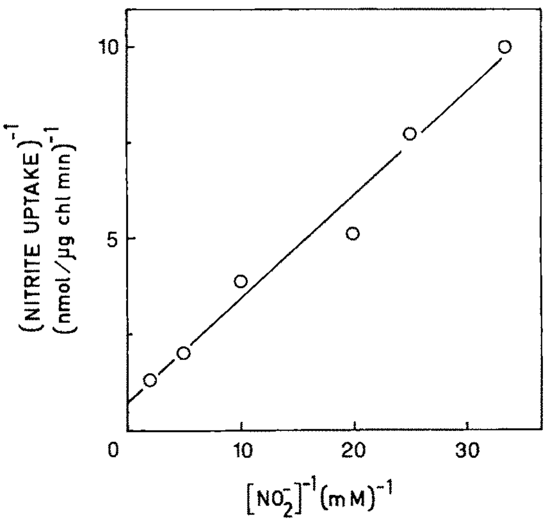

Fig 3. Lineweaver-Burk plot of the effect of the concentration of nitrite on the rate of nitrite utilization at pH 7.2 by DCCD-treated *A. nidulans*. A cell suspension (10 μg chlorophyll/ml) in 30 mM Tricine-NaOH buffer (pH 8 1) was treated with 30 μM DCCD for 15 min After washing, the cells were added (4 μg chlorophyll/ml, final concentration) to solutions containing different concentrations of KNO_2 in 25 mM Mops-NaOH buffer (pH 7 2), and the nitrite uptake rates determined.

Because cyanobacteria generally have been found in alkaline natural waters and exhibit optimal rates of growth and photosynthesis at an alkaline pH [19–22], the active transport of nitrite probably contributes significantly to nitrite-dependent growth, especially at the low concentrations of nitrite usually found in Nature [23] which are below the value of the K_m (NO_2^-) of the active system.

Regulation of nitrite uptake

Both ammonium and CO_2 have a prominent role in the regulation of nitrate utilization in *A. nidulans* [3,5,7]. The effect of these two com-

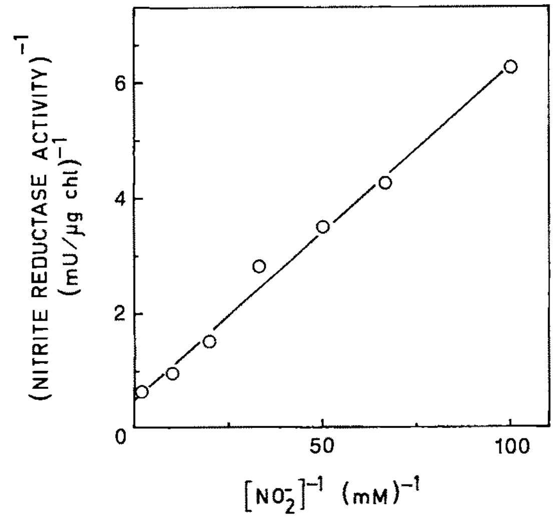

Fig 4 Lineweaver-Burk plot of the effect of the concentration of nitrite on nitrite reductase activity of *A. nidulans* estimated in situ. See Materials and Methods for the experimental procedure.

pounds on nitrite uptake has been tested. Nitrite uptake was inhibited by ammonium and stimulated by CO_2, the magnitude of the effect of either compound being pH-dependent (Table I). Both the inhibition by ammonium and the positive effect of carbon dioxide on nitrite utilization were in fact more pronounced at the higher pH values tested (Table I), conditions under which the contribution to nitrite uptake of the active component is prevalent. The active component of nitrite uptake, rather than its passive counterpart or any intracellular component involved in nitrite assimilation, seems thus to be the target of the effects of ammonium and CO_2 on nitrite utilization.

The nitrite taken up in the absence of CO_2 was quantitatively recovered as ammonium in the outer medium (Table II). This can be expected from the requirement of CO_2-fixation products as substrates for ammonium assimilation, which is also evident for the uptake of exogenously supplied ammonium (Table II; see also Ref. 8).

The glutamine synthetase/glutamate synthase pathway is the main route for ammonium assimilation by the strain of *A. nidulans* used throughout this work [6], the incorporation of ammonium into carbon skeletons being drastically hampered [4,6] by L-methionine-D,L-sulfoximine (MSX), a gluta-

TABLE I

EFFECT OF AMMONIUM AND CARBON DIOXIDE ON NITRITE UTILIZATION BY *A. NIDULANS* AT DIFFERENT VALUES OF EXTRACELLULAR pH

Suspensions containing 7 μg chlorophyll per ml of 15 mM Tricine/15 mM glycine-NaOH buffer of the indicated pH were used. Experiment 1 was carried out in air-opened conical flasks and, where indicated, the suspensions were supplemented with 0.5 mM NH_4Cl. Experiment 2 was carried out in closed Warburg vessels, in which the cell suspension was placed in the main compartment, containing either CO_2-free or CO_2-enriched air as the gas phase; this was achieved by placing in the center well 20% KOH or 0.5 M $NaHCO_3/Na_2CO_3$ buffer (pH 9.6), respectively The assays were started by the addition of 0.5 mM KNO_2 (final concentration).

Expt.	pH	Nitrite taken up (nmol/μg chlorophyll per 30 min)		Ratio
1		$-NH_4^+$	$+NH_4^+$	$+NH_4^+/-NH_4^+$
	7.5	29.7	27.7	0.93
	8.5	12.1	9.9	0.81
	9.5	19.1	5.0	0.26
2		$+CO_2$	$-CO_2$	$+CO_2/-CO_2$
	7.5	34.7	20.6	1.69
	8.5	27.6	11.3	2.44
	9.5	26.3	8.3	3.17

TABLE II

EFFECT OF CARBON DIOXIDE ON NITRITE OR AMMONIUM UPTAKE AND ON NITRITE-DEPENDENT AMMONIUM RELEASE BY *A. NIDULANS*

The experiment was carried out in closed Warburg vessels containing in the main compartment cell suspensions (7 μg chlorophyll/ml) in 25 mM Tricine-NaOH buffer (pH 8.3). CO_2-free or CO_2-enriched air as the gas phase was achieved as described in Table I. The assays were started by the addition of 0.4 mM KNO_2 or NH_4Cl (final concentration). n.d., not determined.

Substrate added	Conditions	Substrate taken up (nmol/μg chlorophyll per 30 min)	Ammonium released (nmol/μg chlorophyll per 30 min)
Nitrite	$+CO_2$	27.6	0.0
	$-CO_2$	6.6	6.4
Ammonium	$+CO_2$	25.9	n.d
	$-CO_2$	0.0	n.d.

mate analog that inactivates glutamine synthetase [24]. The inhibition by ammonium of nitrite utilization was prevented by treatment of the cells with L-methionine-D,L-sulfoximine (Table III). Thus, in analogy to what happens with nitrate uptake [3], ammonium must be assimilated via glutamine synthetase in order to inhibit nitrite uptake. Results in Table III also show that treatment of *Anacystis* cells with L-methionine-D,L-sulfoximine allowed increased rates of nitrite utilization. This may result from the prevention by MSX of the assimilation of the ammonium resulting from nitrite reduction. Thus, the regulatory system modulating nitrite uptake via the active transport system seems to involve products of the assimilation of ammonium via glutamine synthetase.

If the inhibitory metabolites resulting from ammonium assimilation specifically modulate the active component of nitrite uptake, L-methionine-D,L-sulfoximine should affect the active uptake of nitrite but not its passive utilization. As shown in Table IV, this was actually the case, since nitrite utilization by DCCD-treated cells was not affected at all by MSX, whereas MSX promoted an increase in nitrite uptake by untreated cells.

The results presented in this paper show that uptake of nitrite in *A. nidulans* is subject to regulation by a system similar to that modulating nitrate uptake [4,5,6], involving products of ammonium assimilation via glutamine synthetase as negative effectors. No direct evidence is available about the nature of the target of the regulation system in nitrate assimilation, although the nitrate transport system appears to be a good candidate [6]. The above results indicate that the control of nitrite utilization is exerted at the level of the active transport of nitrite. Analogously, the nitrate transport system might well be the target of the regulatory system modulating nitrate utilization in *Anacystis*.

TABLE III

RELEASE BY MSX OF THE AMMONIUM-PROMOTED INHIBITION OF NITRITE UTILIZATION IN *A. NIDULANS*

The cells (7 μg chlorophyll/ml) were preincubated for 15 min in the light, at 40°C, in 30 mM Tricine-NaOH buffer (pH 8.1) supplemented or not with 1 mM L-methionine-D,L-sulfoximine (MSX). After washing by filtration, the cells were resuspended (7 μg chlorophyll/ml) in 30 mM glycine-NaOH buffer (pH 9.6) and the assays were started by the addition of 0.5 mM KNO_2 and, where indicated, 0.5 mM NH_4Cl.

Treatment	Additions	Nitrite taken up (nmol/μg chlorophyll per 30 min)
None	NO_2^-	27.9
None	NO_2^-, NH_4^+	7.1
MSX	NO_2^-	45.7
MSX	NO_2^-, NH_4^+	42.9

TABLE IV

EFFECT OF DCCD AND MSX ON NITRITE UPTAKE BY *A. NIDULANS* AT pH 7.2

The assays were started by the addition of KNO_2 to cell suspensions (8 μg chlorophyll/ml 25 mM Mops-NaOH, pH 7.2) that had been preincubated for 15 min (at 40°C in the light) without any addition or in the presence of 20 μM DCCD, 1 mM L-methionine-D,L-sulfoximine (MSX) or 20 μM DCCD and 1 mM MSX. Neither MSX or DCCD interfered with the assay for nitrite determination

Inhibitor added	Nitrite taken up (nmol/μg chlorophyll per 10 min)
None	10.1
MSX	17.5
DCCD	7.5
DCCD, MSX	7.5

Acknowledgments

This work was supported by Comisión Asesora de Investigación Científica y Técnica (Spain). We thank Professor M. Losada for encouragement and help.

References

1 Fogg, G.E., Stewart, W.D.P., Fay, P and Walsby, A E (1973) The Blue-green Algae, Academic Press, London, New York
2 Ohmori, M., Ohmori, K. and Strotmann, H. (1977) Arch Microbiol 114, 225–229
3 Flores, E, Guerrero, M.G and Losada, M (1980) Arch. Microbiol. 128, 137–144
4 Flores, E., Guerrero, M.G. and Losada, M (1983) Biochim. Biophys. Acta 722, 408–416
5 Flores, E, Romero, J.M., Guerrero, M.G and Losada, M (1983) Biochim. Biophys Acta 725, 529–432

6 Flores, E, Ramos, J.L., Herrero, A and Guerrero, M G (1983) in Photosynthetic Prokaryotes: Cell Differentiation and Function (Papageorgiou, G. and Packer, L., eds.), pp 363–387, Elsevier/North-Holland, New York

7 Romero, J.M., Lara, C. and Guerrero, M.G. (1985) Arch Biochem Biophys 237, 396–401

8 Boussiba, S., Resch, C M and Gibson, J (1984) Arch. Microbiol. 138, 287–292

9 Boussiba, S., Dilling, W and Gibson, J. (1984) J Bacteriol 150, 204–210

10 Rai, A N, Rowell, P. and Stewart, W.D.P. (1984) Arch. Microbiol. 137, 241–246

11 Hattori, A. (1962) Plant Cell Physiol. 3, 355–369

12 Rippka, R. and Cohen-Bazire, G (1983) Ann. Microbiol (Inst Pasteur) 134 B, 21–36

13 Herrero, A, Flores, E. and Guerrero, M G (1981) J Bacteriol. 145, 175–180

14 MacKinney, G. (1941) J. Biol. Chem. 140, 315–322

15 Snell, F.D. and Snell, C.T (1949) Colorimetric Methods of Analysis, Vol 3, pp 804–405, Van Nostrand, New York

16 Bergmeyer, H.U. (1974) Methoden der enzymatischen Analyse, 2nd Edn., Verlag Chemie, Weinheim

17 Harold, F N., Baarda, J R, Baron, C. and Abrams, A (1969) J. Biol. Chem. 244, 2261–2268

18 Flores, E. (1982) Ph.D. Thesis, Universidad de Sevilla

19 Kratz, W.A. and Myers, J (1955) Am J. Bot. 42, 282–287

20 Wolk, C.P (1973) Bacteriol. Rev 37, 32–101

21 Coleman, J.R. and Colman, B. (1981) Plant Physiol. 67, 917–921

22 Miller, A.G, Turpin, D H. and Canvin, D.T (1984) J. Bacteriol 159, 100–106

23 Svensson, B.H. and Söderlund, R (1976) Ecol. Bull (Stockholm) 22, 23–73

24 Prusiner, S. and Stadtman, E.R (1973) The Enzymes of Glutamine Metabolism, Academic Press, New York

Biochimica et Biophysica Acta 896 (1987) 109–112
Elsevier

BBA 70368

BBA Report

Competition between nitrate and nitrite uptake in the cyanobacterium *Anacystis nidulans*

Francisco Madueño, Enrique Flores and Miguel G. Guerrero

Departamento de Bioquímica, Facultad de Biología y C.S.I.C., Apartado 1095, E-41080 Sevilla (Spain)

(Received 4 August 1986)

Key words: Nitrate transport; Nitrite transport; Nitrate reductase; Nitrite reductase, (*A. nidulans*)

Nitrate and nitrite reciprocally inhibited the utilization of each other in the unicellular cyanobacterium *Anacystis nidulans*. Nitrate hampered active nitrite uptake both in wild-type cells lacking active nitrate reductase and in a nitrate reductase-defective mutant. Nitrate uptake in a nitrite reductase-defective mutant was inhibited by nitrite. The competitive interaction between nitrate and nitrite utilization in *A. nidulans* seems to take place at the level of substrate transport into the cell.

Cyanobacteria can use nitrate or nitrite as the source of nitrogen for growth [1]. The assimilation of both nitrogenous compounds in this group of organisms has been studied mainly in the unicellular species *Anacystis nidulans* (= *Synechococcus elongatus*, see Ref. 2). The systems involved in nitrate and nitrite uptake are both operative in nitrate-grown cells. Nitrate uptake appears to be mediated by an active transport system with a high affinity for nitrate [3–5]. Nitrite entrance into the cell seemingly takes place both by diffusion (probably in the form of nitrous acid) and via active transport of the nitrite anion [4,6]; the relative contribution of each component depends on the pH of the medium, that of the active system being prevalent at high pH values [6]. Nitrate uptake and the active component of nitrite uptake share common properties in *A. nidulans*, as they exhibit analogous pH-dependence profiles and are subject to regulation by ammonium and carbon dioxide in a similar fashion [6]. In view of the above similarities it seems plausible that a common transport system participates in both nitrate and nitrite uptake. The results presented in this report actually show that there is a marked competitive interaction between nitrate and nitrite uptake in *A. nidulans*.

Anacystis nidulans (strain L 1402-1 from Göttingen University's Algal Culture Collection, also known as *Synechococcus leopoliensis*) cells incubated in the presence of both nitrate and nitrite took up both substrates simultaneously, but at rates lower than those observed in control cell suspensions supplemented with only one nitrogenous compound (Table I). This was also the case for cells treated with L-methionine-D,L-sulfoximine (Table I), a glutamate analog that inactivates glutamine synthetase [7], the L-methionine-D,L-sulfoximine-treated cells quantitatively releasing to the outer medium the ammonium resulting from reduction of the nitrate or nitrite taken up [4]. Thus, the competition between nitrate and nitrite utilization takes place at the early stages of the processes, prior to the assimilation, via glutamine synthetase, of the ammonium resulting from

---

Abbreviations: Mops, 4-morpholinepropanesulfonic acid; Tricine, *N*-[2-hydroxy-1,1-bis(hydroxymethyl)ethyl]glycine.

Correspondence: Dr. E. Flores, Departamento de Bioquímica, Facultad de Biología y C.S.I.C., Apartado 1095, E-41080-Sevilla, Spain.

0005-2736/87/$0.3.50 © 1987 Elsevier Science Publishers B V (Biomedical Division)

TABLE I

COMPETITION BETWEEN NITRATE AND NITRITE UPTAKE IN *ANACYSTIS NIDULANS*

Nitrate-grown cells [10] were harvested and resuspended (20 μg chlorophyll/ml) in 25 mM Tricine-NaOH buffer (pH 8.3) with or without 1 mM L-methionine-D,L-sulfoximine (MSX). After 15 min of incubation at 40°C in the light (100 W/m^2), the assays were started by the addition of KNO_3 or/and KNO_2 at a concentration of 0.32 mM each (Expt 1) or 0.4 mM KNO_3 or/and 0.6 mM KNO_2 (Expt. 2) Samples were withdrawn at different times, filtered (Millipore HA 0.45 μm), and the remaining substrates determined in the filtrates [13,14]

Expt	Addition	Substrate taken up (nmol/μg chlorophyll per 25 min)	
		NO_3^-	NO_2^-
1	KNO_3	12.1	-
	KNO_2	-	10.7
	KNO_3, KNO_2	3.7	6.4
2	MSX, KNO_3	16.0	-
	MSX, KNO_2	-	21.0
	MSX, KNO_3, KNO_2	12.5	15.6

reduction of the substrates.

Because in *A. nidulans* both nitrate reductase and nitrite reductase use reduced ferredoxin as the physiological electron donor [8], a competition between the enzymes for reductant could account for the observed competitive interaction above described. Alternatively, competition might take place at the level of substrate transport into the cell. To decide between these two possibilities, cells devoid of nitrate reductase or nitrite reductase have been used in studies of the effect of nitrate on nitrite uptake and vice versa.

Cells of *Anacystis nidulans* L 1402-1 essentially devoid of active nitrate reductase but with full activity of other components of the nitrate assimilating system were obtained by treatment with tungstate as described in Ref. 9. Nitrate reductase activity [10] in these cells was only 0.02 mU/μg chlorophyll (chlorophyll measured as in Ref. 11), which represents about 0.5% of the activity level of normal untreated cells. The tungstate-treated cells exhibited high rates of nitrite uptake and reduction, whereas they did not show any detectable nitrate utilization activity. Nitrite uptake by these cells was effectively inhibited by nitrate, however (Table II), suggesting an effect at the level of nitrite transport, since nitrate could not be reduced, which excludes a competition at the reduction stage. The extent of the inhibition of nitrite uptake caused by nitrate depended on the pH of the outer medium, increasing with the alkalinization of the medium (Table II). This pattern of inhibition resembles the activity profile with respect to pH of the active nitrite transport system [6], supporting the contention of the active transport of nitrite as the likely target of the nitrate effect on nitrite uptake. Increasing the nitrate concentration in the medium resulted in enhanced inhibition of nitrite uptake. Under conditions in which nitrite uptake takes place almost exclusively via the active transport system (L-methionine-D,L-sulfoximine-treated cells, pH 9.6; see Ref. 6), nitrate at 20 mM concentration caused 95% inhibition of the utilization of 0.2 mM nitrite (data not shown).

The effect of nitrate on nitrite uptake has also been studied in a nitrate reductase-defective mutant of *A. nidulans*. This mutant (strain FM10), which will be described in detail elsewhere, is a derivative of *Anacystis nidulans* R2 (a strain closely related to *A. nidulans* L 1402-1; Ref. 2) obtained by transposon mutagenesis by the method described by Kuhlemeier et al. [12]. Nitrate reductase level in nitrite-grown cells of strain FM10

TABLE II

NITRATE INHIBITION OF NITRITE UPTAKE IN TUNGSTATE-TREATED *A. NIDULANS* CELLS

Ammonium-grown cells were treated with 1 mM sodium tungstate and the nitrate utilization system induced in the presence of nitrate and tungstate as described in Ref. 9 The cells were harvested and resuspended (11 μg chlorophyll/ml) in 25 mM Mops-NaOH buffer (pH 7.2), 25 mM Tricine-NaOH buffer (pH 8.1), or 25 mM glycine-NaOH buffer (pH 9.6). The assays were started by the addition of 0.2 mM KNO_2 and carried out at 40°C in the light (100 W/m^2), in the absence or in the presence of 2 mM KNO_3. Samples were withdrawn at different times (0–15 min) and the remaining nitrite determined [13]

pH	Nitrite uptake (nmol/μg chlorophyll per min)		Inhibition by nitrate (%)
	$-NO_3^-$	$+NO_3^-$	
7.2	1.66	1.17	30
8.1	1.28	0.56	56
9.6	1.29	0.31	76

was negligible, below 0.02 mU/μg chlorophyll. Nitrate also inhibited nitrite utilization by cells of this strain, but no negative effect of nitrate up to 50 mM on nitrite reductase activity could be observed (nitrite reductase activity was about 0.8 mU/μg chlorophyll as estimated in situ in cells made permeable with mixed alkyltrimethylammonium bromide [9]). These results again suggest that competition between nitrate and nitrite uptake does not take place at the reduction stage but rather at the level of transport of the anions into the cell.

Results from kinetic studies of the effect of nitrate on nitrite uptake by L-methionine-D,L-sulfoximine-treated FM10 cells at different nitrite concentrations showed that nitrate actually behaves as a competitive inhibitor of nitrite uptake (Fig. 1). L-Methionine-D,L-sulfoximine-treated cells were used in this experiment in order to avoid regulatory interferences resulting from the assimilation via glutamine synthetase of the ammonium resulting from nitrite reduction (see Refs. 3 and 6). The calculated K_i value for nitrate was 24 μM, quite close to the K_m value for nitrite of nitrite uptake, which was 22 μM (Fig. 1).

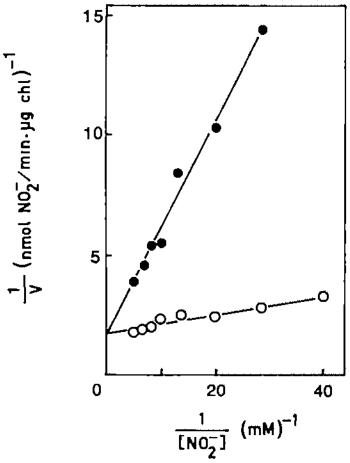

Fig. 1. Lineweaver-Burk plot of the effect of nitrite concentration on the rate of nitrite uptake by *A. nidulans* strain FM10 (defective in nitrate reductase) in the absence (○) or in the presence (●) of 0.25 mM KNO_3. Nitrite-grown cells (9 μg chlorophyll per ml of 50 mM Tricine-NaOH buffer, pH 8.1) were treated with 1 mM L-methionine-D,L-sulfoximine for 15 min in the light at 40°C. After harvesting, the cells were resuspended in 25 mM glycine-NaOH buffer (pH 9.6), and the nitrite uptake assays were carried out as described in Table II.

The effect of nitrite on nitrate uptake has also been investigated. For this study, another transposon-induced mutant of *A. nidulans* R2 (strain FM2) has been used. Strain FM2 is a nitrite reductase-defective mutant exhibiting undetectable nitrite reductase level. (Nitrite reductase activity of strain R2 estimated as described in Ref. 9 was about 1 mU/μg chlorophyll.) The effect of nitrite on nitrate uptake was tested in cell suspensions of strain FM2 at pH 9.6, conditions under which nitrite uptake takes place almost exclusively via the active transport system. Nitrite effectively inhibited nitrate uptake in FM2 cells, 1 mM nitrite inhibiting the utilization of 0.1 mM nitrate by 75% (Table III). Because nitrite at moderately high concentrations is toxic for cyanobacteria, the effect of nitrite on [^{14}C]CO_2 fixation by FM2 cells has been tested. No inhibition was detected, the CO_2-fixation rate being 5.8 nmol/μg chlorophyll per min in the absence or in the presence of KNO_2 at concentrations up to 1 mM. These experiments show that nitrite inhibition of nitrate utilization in *Anacystis* does not result from a competition for reducing equivalents or from non-specific inhibition of photosynthetic electron flow which is required for nitrate utilization [3,4].

The data presented in this paper indicate a reciprocal competition between the active trans-

TABLE III

NITRITE INHIBITION OF NITRATE UPTAKE BY NITRITE REDUCTASE-DEFECTIVE *A. NIDULANS* STRAIN FM2

Ammonium-grown cells were incubated for 3 h in culture medium lacking any added nitrogen source, in order to induce the nitrate-assimilating system. The assays were carried out as described in Table II and were started by addition of 0.1 mM KNO_3 to cells suspended in 25 mM glycine-NaOH buffer (pH 9.6), with or without KNO_2. At different time intervals samples were withdrawn and filtered (Millipore HA-0.45 μm filters), the remaining nitrate being measured in the filtrates [14].

Nitrite added (mM)	Nitrate uptake (nmol/μg chlorophyll per min)
0	0.34
0.2	0.25
0.5	0.13
1.0	0.09

port of nitrate and that of nitrite in the cyanobacterium *Anacystis nidulans*. These results support the contention that in *A. nidulans* nitrate and nitrite might share a common permease for their transport into the cell. Our results with *Anacystis* are in contrast to those reported for *Neurospora*, where nitrite behaves as a non-competitive inhibitor of nitrate uptake [15] and nitrate does not inhibit nitrite uptake [16]. However, for the diatom *Phaeodactylum*, the similarities between nitrate and nitrite uptake have led to the suggestion that both anions may be taken up by the same mechanism [17].

This work was supported by Comisión Asesora de Investigación Científica y Técnica (Spain). We thank Professor M. Losada for encouragement and help, and Dr. A. Herrero for helpful discussion.

References

1 Fogg, G E, Stewart, W D.P., Fay, P and Walsby, A.E (1973) The Blue-green Algae, Academic Press, London, New York
2 Rippka, R and Cohen-Bazire, G. (1983) Ann Microbiol. (Inst Pasteur) 134 B, 21–36
3 Flores, E., Ramos, J L., Herrero, A and Guerrero, M.G (1983) in Photosynthetic Prokaryotes· Cell Differentiation and Function (Papageorgiou, G and Packer, L., eds), pp 363–387, Elsevier/North-Holland, New York
4 Flores, E., Guerrero, M.G. and Losada, M. (1983) Biochim. Biophys. Acta 722, 408–416
5 Tischner, R. and Schmidt, A. (1984) Arch. Microbiol. 137, 151–154
6 Flores, E., Herrero, A. and Guerrero, M G (1987) Biochim. Biophys. Acta 896, 103–108
7 Prusiner, S. and Stadtman, E.R. (1973) The Enzymes of Glutamine Metabolism, Academic Press, London, New York
8 Manzano, C., Candau, P., Gómez-Moreno, C., Relimpio, A.M. and Losada, M (1976) Mol. Cell. Biochem. 10, 161–169
9 Herrero, A. and Guerrero, M G (1986) J. Gen. Microbiol 132, 2463–2468
10 Herrero, A, Flores, E and Guerrero, M.G. (1981) J. Bacteriol 145, 175–180
11 MacKinney, G. (1941) J. Biol. Chem. 140, 315–322
12 Kuhlemeier, C.J., Logtenberg, T, Stoorvogel, W., Van Heugten, H.A.A., Borrias, W.E. and Van Arkel, G A (1984) J. Bacteriol. 159, 36–41
13 Snell, F.D. and Snell, C.T. (1949) Colorimetric Methods of Analysis, Vol. 3, pp. 804–805, Van Nostrand, New York
14 Cawse, P A. (1967) Analyst 92, 311–315
15 Schloemer, R.H. and Garrett, R.H (1974) J Bacteriol 118, 259–269
16 Schloemer, R.H. and Garrett, R.H (1974) J. Bacteriol 118, 270–274
17 Cresswell, R C. and Syrett, P.J (1982) J Exp Bot. 33, 1111–1121

Biochimica et Biophysica Acta 896 (1987) 113–116
Elsevier

BBA 70267

BBA Report

Inositol trisphosphate and calcium mobilisation in permeabilised enterocytes

A. Ilundain *, J.A. O'Brien, K.A. Burton and F.V. Sepúlveda

AFRC Institute of Animal Physiology, Babraham, Cambridge (U.K.)

(Received 30 June 1986)

Key words: Intestinal transport; Ca^{2+} transport; Inositol trisphosphate; (Chicken intestine)

Saponin-permeabilised epithelial cells isolated by hyalurodinase incubation from chicken small intestine were used to study ^{45}Ca uptake into intracellular stores. At low ($6.7 \cdot 10^{-7}$ M) free Ca^{2+} concentration most of the Ca^{2+} appears to be taken up into non-mitochondrial stores, whilst the mitochondria seem to play a major role at high ($2 \cdot 10^{-5}$ M) Ca^{2+} concentration. Addition of inositol trisphosphate (IP_3) causes a rapid and reversible release of ^{45}Ca from non-mitochondrial stores, with a half-maximal effect of approximately 1 μM.

The importance of cytoplasmic Ca^{2+} in the regulation of intestinal transport has been well established. Studies with both small and large intestine have demonstrated that manoeuvres supposedly affecting cytoplasmic Ca^{2+} concentration alter transepithelial Na^+ and Cl^- transport [1,2]. Work with isolated intestinal cells or perfused intestine has also demonstrated a dependence of K^+ fluxes upon intracellular Ca^{2+} [3–5]. The free Ca^{2+} concentration of the cytoplasm is thought to be determined by the interplay between the rate of Ca^{2+} entry from the extracellular space, the pumping of the Ca^{2+} out of the cell through the plasma membrane and the action of intracellular buffering systems. The role of the plasma membrane systems has been studied using isolated plasma membrane vesicles [6]. The ability of intracellular organelles of intestinal cells to act as stores or buffer systems for Ca^{2+} has been explored using cells whose plasma membrane had been previously rendered highly permeable [7,8] or in subcellular membrane fractions [9,10]. No information is available, however, on the possible ways by which external stimuli could modify intracellular Ca^{2+} in transporting enterocytes. It has recently become apparent that inositol 1,4,5-trisphosphate (IP_3) is produced as a response to external stimuli in various cell types and that its liberation into the cytoplasm is followed by Ca^{2+} mobilization from intracellular stores [11,12] but no information on this is available for intestinal epithelial cells. In the present report we demonstrate that inositol 1,4,5-trisphosphate is capable of releasing Ca^2, probably accumulated in a non-mitochondrial store, in transporting intestinal epithelial cells with highly permeable plasma membrane.

White Leghorn chickens 5–10-weeks old were used throughout. Intestinal cells were isolated as described in Ref. 13 with minor modifications. After isolation cells were washed twice in a modified Hank's buffer and then immediately suspended in a high K^+ medium of the following composition (mM): 120 KCl, 10 $MgCl_2$, 1.2 KH_2PO_4, 1 EGTA, 0.5 mg/ml bovine serum albumin (BSA) and 25 Tris-Hepes (pH 7.2), that

---

* Permanent address Departamento de Fisiologia Animal, Facultad de Farmacia, Seville, Spain.

Correspondence: Dr F.V. Sepúlveda, AFRC Institute of Animal Physiology, Babraham, Cambridge CB2 4AT, U.K.

0005-2736/87/$03.50 © 1987 Elsevier Science Publishers B.V. (Biomedical Division)

contained 50 μg/ml saponin and incubated for 5 min at 37°C. This incubation was terminated by washing in saponin-free, high potassium medium. The cells obtained in this way are defined as permeabilised cells.

Ca^{2+} transport experiments were performed in cells previously exposed to saponin, a detergent that is thought to render the plasma membrane permeable by complexing with cholesterol [14]. The membranes which contain low amounts of cholesterol, such as those of the mitochondria and endoplasmic reticulum, do not seem to be affected by this treatment. The cell suspension was diluted, generally 1 ml of cells plus 4 ml of buffer of the following composition (mM): 120 KCl, 10 $MgCl_2$, 1.2 KH_2PO_4, 5 Tris ATP, 5 sodium phosphocreatine, 9.5 units/ml creatine phosphokinase, 0.5 mg/ml bovine serum albumin and 25 Tris-Hepes (pH 7.2) which contained in addition ^{45}Ca (5 μCi/ml). Samples of the cell suspension (200 μl) were taken at timed intervals to measure ^{45}Ca content of the cells. These were added to ice-cold microcentrifuge tubes containing an upper layer of radioactivity-free high potassium solution and a lower layer of dense immiscible oil [3] and immediately centrifuged (20 s, $12000 \times g$). ^{45}Ca in the cells was measured by liquid scintillation counting. In some experiments Ca^{2+} uptake was measured at fixed external free Ca^{2+} concentrations of $2 \cdot 10^{-5}$ M and $6.7 \cdot 10^{-7}$ M obtained with the chelators *N*-hydroxyethylethylenediamine triacetic acid (HEDTA) and ethyleneglycol bis(β-aminoethyl-*N*,*N*′-tetraacetic acid (EGTA), respectively. The necessary amounts of $CaCl_2$ and ligand were calculated by iteration using a microcomputer programme [15].

As demonstrated previously for rabbit enterocytes [7], leaky chicken intestinal epithelial cells take up ^{45}Ca from a medium mimicking the intracellular composition (Fig. 1). The upper panel shows that rapid uptake occurred at $2 \cdot 10^{-5}$ M Ca^{2+}, and that this was sensitive to a mixture of the mitochondrial blockers oligomycin and rotenone. The reduction in uptake was of the order of 65%. Addition of the ATPase inhibitor vanadate, caused only a very small further decrease in Ca^{2+} uptake. When the free Ca^{2+} concentration was reduced to $6.7 \cdot 10^{-7}$ M the inhibition by mitochondrial inhibitors was only about 30%. Addition of vanadate, however, caused a further inhibition that lowered uptake to 10% of that under control conditions. These results suggest that, as reported before for rabbit enterocytes [8], permeable chicken enterocytes transport Ca^{2+} into mitochondrial and non-mitochondrial intracellular stores. No uptake was observed when ATP in the solution was decreased by addition of hexokinase and glucose (not shown). Uptake into mitochondrial stores was predominant at high ($2 \cdot 10^{-5}$ M) free Ca^{2+} concentration, while the non-mitochondrial stores became dominant at lower ($6.7 \cdot 10^{-7}$ M) free Ca^{2+}.

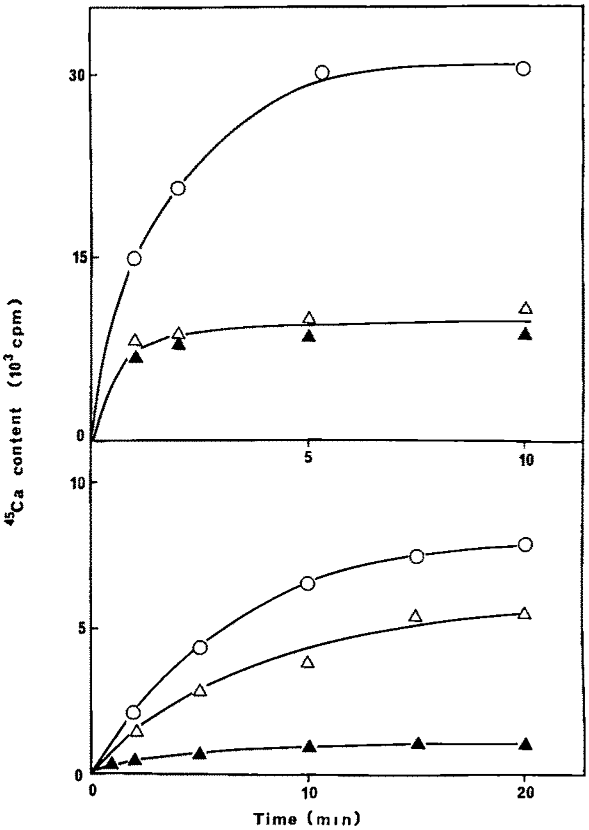

Fig. 1. ^{45}Ca uptake by leaky chicken-enterocytes. Cells previously permeabilised with saponin were incubated at 37°C and pH 7.2 in a buffer mimicking the intracellular composition and containing 5 mM ATP and an ATP-regenerating system. Initial free Ca^{2+} concentration was either $2 \cdot 10^{-5}$ M (upper panel) or $6.7 \cdot 10^{-7}$ M (lower panel) obtained by HEDTA and EGTA buffering, respectively Incubation solutions contained either 3 μg/ml oligomycin and 0.5 μg/ml rotenone (△); 3 μg/ml oligomycin, 0.5 μg/ml rotenone and 5 mM vanadate (▲). Control solution (○).

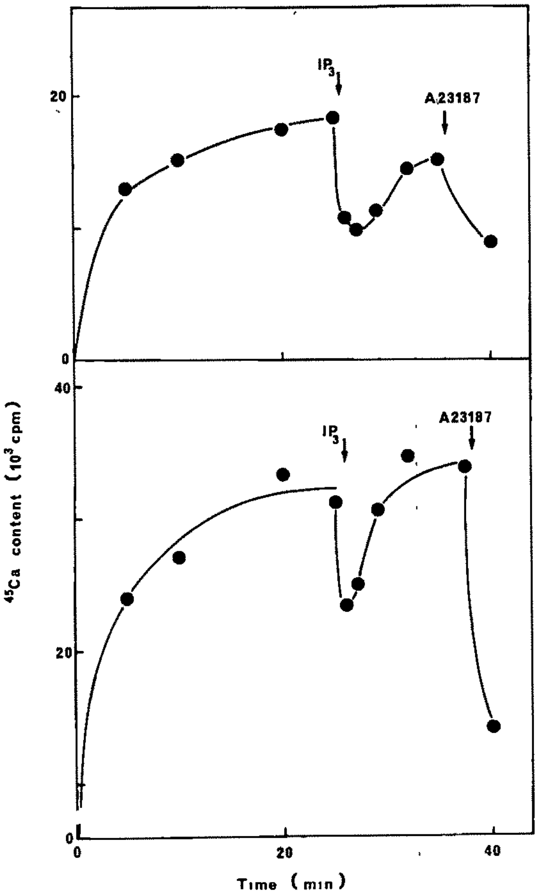

Fig. 2. Effect of IP_3 on the ^{45}Ca content of leaky chicken-enterocytes Cells were incubated in the same buffer as that used in Fig. 1, but with no added Ca^{2+} or chelators. The initial Ca^{2+} concentration was 500 nM as measured with a Ca^{2+}-selective electrode Incubations were performed in the absence (lower panel) or presence (upper panel) of oligomycin (3 μg/ml) and rotenone (0.5 μg/ml). Additions: 5 μM IP_3; 10^{-5} M Ca^{2+}-ionophore A23187.

To test the effect of the intracellular messenger IP_3, leaky chicken enterocytes were allowed to take up ^{45}Ca from a solution similar to that in the experiments described above but containing no added Ca^{2+} or chelators. Fig. 2 shows the time course of ^{45}Ca uptake, either in the absence of inhibitors (lower panel) or when the mitochondrial inhibitors rotenone and oligomycin were present in the medium (upper panel). Under both conditions addition of IP_3 induced a rapid and transient release of accumulated ^{45}Ca. The decrease in ^{45}Ca associated with the cells was from 19.5 ± 1.5 to 10 ± 1.4 10^3 cpm ($P < 0.01$ by paired t-test) and from 310 ± 30 to 232 ± 28 10^3 cpm ($P < 0.05$ by paired t-test) in the presence and absence of inhibitors, respectively (means ± S.E., $n = 4$). Most of this Ca^{2+} was lost within the first minute of stimulation with IP_3. The magnitude of the release was similar in both situations but the re-uptake process was slower in the inhibited cells. Release of accumulated ^{45}Ca could also be induced by addition of the calcium-ionophore A23187, suggesting that ^{45}Ca sequestration was in a membrane-enclosed compartment. Substances with no effect included Inositol 1,4-bisphosphate (IP_2, 10 μM) and *myo*-inositol (20 μM). Similar results were obtained with rabbit enterocytes with highly permeable plasma membranes (not shown). The concentration-dependence of IP_3-induced ^{45}Ca release from leaky chicken enterocytes in the presence of mitochondrial inhibitors is shown in Fig. 3. A maximal release of 51 ± 7 percent of the accumulated ^{45}Ca was extrapolated assuming that the relationship between release and IP_3 concentration was a rectangular hyperbola. The concentration of IP_3 giving half maximal release was 1.0 ± 0.4 μM (mean ± S.D. of four separate experiments). This value is similar to the half-maximal concentrations previously described for other cell types [12].

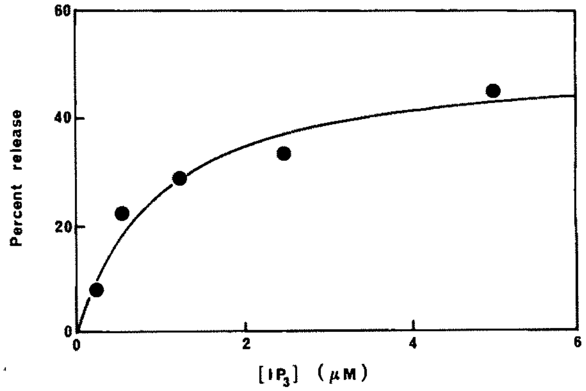

Fig. 3. Concentration-dependence of IP_3-induced ^{45}Ca release from leaky epithelial cells isolated from chicken intestine. Saponin-treated cells were incubated in the presence of ^{45}Ca for 20 min as described for the upper panel of Fig. 2. Percent release indicates the percent of total accumulated ^{45}Ca lost by the cells upon addition of the appropriate concentration of IP_3 and is based on the maximal loss of ^{45}Ca occurring after addition; this was usually one minute after IP_3 addition. Results are means of four separate experiments.

Release of Ca^{2+} under the effect of IP_3 could also be shown by monitoring ambient free Ca^{2+} concentration in the presence of leaky cells, with a Ca^{2+}-selective electrode [8]. In these experiments release is assessed by comparison between elevation in Ca^{2+} concentration induced by IP_3 with that observed upon direct addition of known amounts of $CaCl_2$. These measurements (not shown) revealed that 5 μM IP_3 evoked the release of about 2.4 nmol Ca per mg of cell protein.

Intracellular Ca^{2+} has been proposed to play a crucial role in regulating intestinal transport, and there are numerous recent reports showing that in many cells IP_3 is an important link between receptor-agonists binding and Ca^{2+} mobilisation from intracellular stores [11,12]. The fact that IP_3 produces Ca^{2+} mobilisation in leaky enterocytes suggests that this compound might act in these cells as an intracellular signal mediating the response of the intestine to external stimuli, such as secretagogues, which are known to be Ca^{2+}-dependent [1,2]. In addition this effector might be the signal involved in intestinal transport regulation events which appear to be accompanied by Ca^{2+} mobilisation [16].

Part of this work was presented at the April 1986 meeting of the Physiological Society [17].

We thank Dr. Robin Irvine for the supply of IP_2 and IP_3 and to Dr. C.J.M. Nicol for making his computer programme available to us. A.I. acknowledges the support of the Junta de Andalucia and the British Council Acciones Integradas travel grant.

References

1 Fondacaro, J.D. (1986) Am J. Physiol. 250, G1–G8

2 Donowitz, M. and Welsh, M.J (1986) Annu Rev. Physiol. 48, 135–150

3 Brown, P.D. and Sepúlveda, F V. (1985) J Physiol. 365, 271–285

4 Sepúlveda, F.V. and Mason, W.T (1985) FEBS Lett. 191, 87–91

5 Boyd, C.A.R. and Walley, G.J. (1985) J. Physiol. 358, 77P

6 Van Corven, E.J.J.M., Roche, C. and Van Os, C.H. (1985) Biochim. Biophys. Acta. 820, 274–282

7 Sepúlveda, F.V. (1985) J. Physiol. 367, 58P

8 Sepúlveda, F.V. and Smith, S.M. (1986) Pflügers Arch. in the press

9 Rubinoff, M.J. and Nellans, H.N. (1985) J. Biol. Chem. 260, 7824–7828

10 Bikle, D.D., Askew, E.W., Zolock, D.T., Morrissey, R.L. and Herman, R.H. (1980) Biochim. Biophys Acta 598, 561–574

11 Berridge, M.J. and Irvine, R.F. (1984) Nature, 312, 315–321

12 Sekar, M.C. and Hokin, L.E. (1986) J. Membrane Biol. 89, 193–210

13 Kimmich, G.A. (1970) Biochemistry 9, 3659–3668

14 Burgess, G.H., McKinney, J.S., Fabiato, A., Leslie, B.A. and Putney, J.W. (1983) J. Biol. Chem. 258, 15336–15345

15 Nicol, C.J.M. (1985) J. Physiol 367, 10P

16 Sepúlveda, F.V., Burton, K.A. and Brown, P.D. (1986) Biochim. Biophys. Acta. 856, 185–187

17 Burton, K.A., Ilundain, A, O'Brien, J.A and Sepúlveda, F.V. (1986) J. Physiol. 378, 77P

Biochimica et Biophysica Acta 896 (1987) 117–122
Elsevier

BBA 70369

BBA Report

A simple method for the preparation of small unilamellar vesicles

Danilo D. Lasič, Jurkica Kidrič and Silva Zagorc

Boris Kidrič Institute of Chemistry, Ljubljana (Yugoslavia)

(Received 2 September 1986)

Key words: Small unilamellar vesicle; Vesicle preparation; Size distribution; Vesicle formation, spontaneous

A simple and quick method for the preparation of small unilamellar vesicles (SUV) was developed. SUV are spontaneously formed by swelling of the specially prepared phospholipid film in water/buffer. Normally, large multilamellar vesicles (MLV) are formed when a phospholipid film is dissolved in water. To prevent the formation of multilamellar structures we used the slightly charged phospholipids which exhibit infinite swelling while the formation of large structures was prevented by the deposition of the phospholipid film on the support with small surfaces. These two requirements were met by mixing a small amount of ionic detergent into phospholipid which was deposited on microcrystals. The size and size distribution of the produced vesicles depend on the size and homogeneity of the microcrystals. When 1.5 wt% of cetyltetramethylammonium bromide (CTAB) in egg yolk phosphatidylcholine was deposited on zeolite X microcrystals with crystallite sizes of approx. 0.4 μm a homogeneous population of vesicles with average diameter 21.5 nm was obtained.

Phospholipid vesicles can be prepared by many different techniques [1,2]. The most frequently used are sonication [3] or French press extrusion [4] of MLV, removal of detergent from phospholipid-detergent mixed micelles by dilution [5], chromatography [6], dialysis [7], or absorption [8], injection of phospholipid dissolved in the organic solvent into aqueous solution under controlled conditions [9], cyclic titration of dispersions of phospholipid mixed with charged lipids [10], or depleting the organic phase from water in oil emulsion of phospholipid and water in an organic phase [11].

All these techniques require rather demanding laboratory equipment and operations. Therefore our aim was the spontaneous formation of SUV, resembling the spontaneous formation of MLV, only by swelling of the phospholipid film in water.

It was suggested that vesicles are formed by bending and vesiculation of small bilayered phospholipid flakes [12] which are formed by different preparation techniques in a different way [13].

When isoelectric phospholipid film is swelling in water/buffer the bunches of lamellae peel off and close upon themselves to protect the exposed hydrocarbon chains at their edges from water and large MLV are formed [14]. However, if LUV are desired repulsion between the lamellae has to be induced. This can be done by charging the surfaces of the lamellae because charged bilayers exhibit infinite swelling [15–18]. To reduce the size of lamellae (bilayered phospholipid flakes which peel off when the system is swelling) one must reduce the dimensions of the support on which the film is deposited. This can be done by replacing the round bottomed glass flask with a support offer-

---

Abbreviations: SUV, small unilamellar vesicles; MLV, multilamellar vesicles; LUV, large unilamellar vesicles; PC, phosphatidylcholine; CTAB, cetyltetramethylammonium bromide.

Correspondence: Dr. D.D. Lasič, Boris Kidrič Institute of Chemistry, P.O. Box 30, 61115 Ljubljana, Yugoslavia.

0005-2736/87/$03.50 © 1987 Elsevier Science Publishers B.V. (Biomedical Division)

ing much smaller surfaces. This was achieved in the following way.

We deposited egg yolk phosphatidylcholine (egg yolk PC) mixed with 1.5 wt% of cetyltetramethylammonium bromide (CTAB) in $CHCl_3/CH_3OH$ on various supports. Besides blank samples (egg

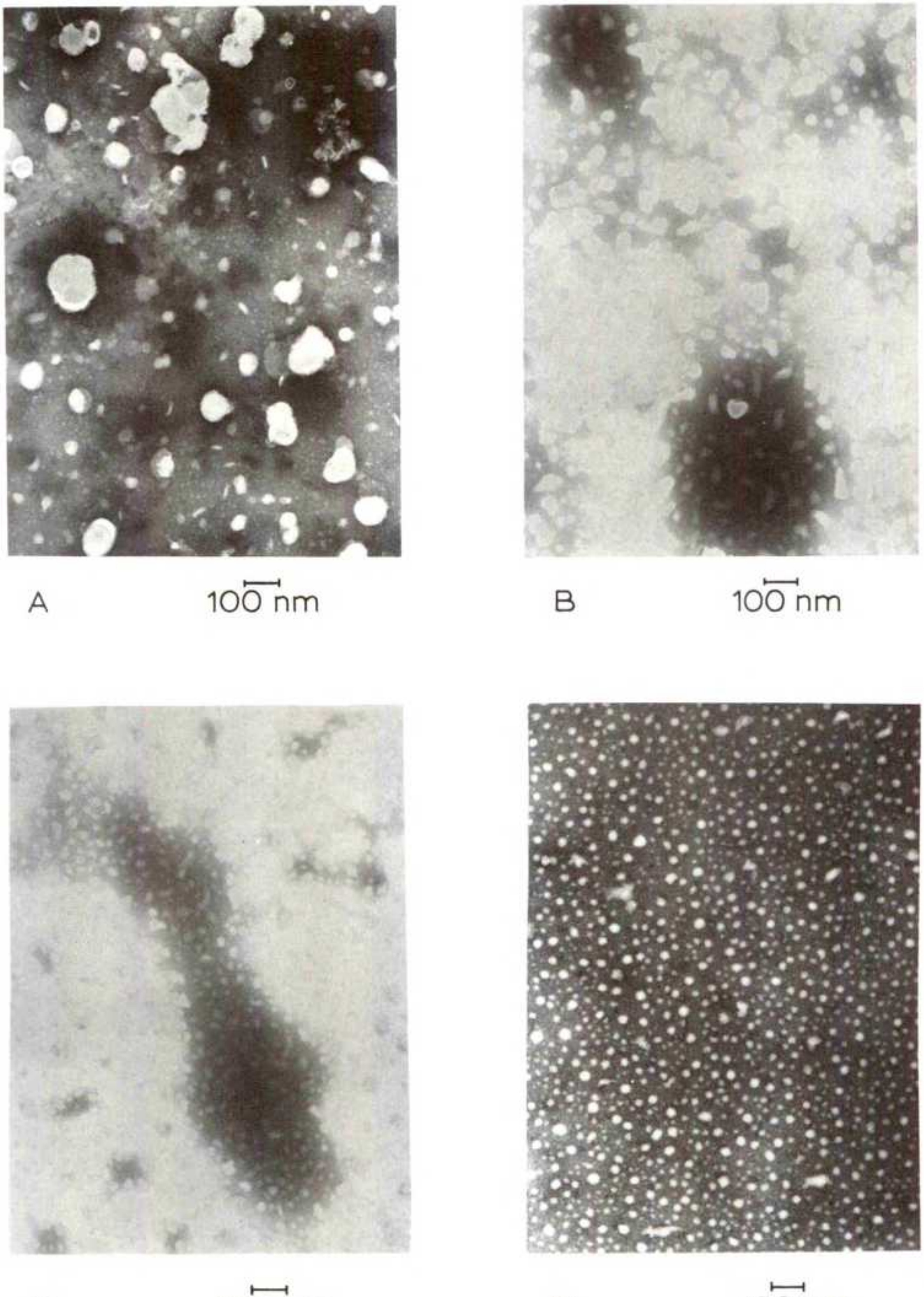

Fig. 1. Negative staining EM micrographs of vesicles formed by resuspending the egg yolk PC film with 1.5 wt% CTAB deposited on A: glass wool (Sample III), B: silica gel (Sample IV), C: zeolite ZSM 5 (Sample V) and D: zeolite X (Sample VI) in water. The samples were stained with 2% potassium phosphotungstate.

yolk PC alone on the round bottomed flask, Sample I and egg yolk PC/CTAB on the round bottomed flask, Sample II) we deposited this mixture on glass wool (Sample III), silica gel powder (Sample IV) and the microcrystals of zeolite ZSM5 (Sample V, size of crystallites 3 μm) and zeolite X (Sample VI, size approx. 0.4 μm). For additional reference, pure egg yolk PC was deposited on zeolite X (Sample VII). Normally 2–5 mg of the phospholipid mixture (1.5 wt% of CTAB) was deposited on 0.5–1 g of the support. After removal of the organic phase (overnight at 10^{-2} torr) the system was resuspended by shaking or stirring in distilled water or 5 mM NaCl to the concentration of 1–2 mg/ml. The vesicle solution was decanted (to increase the yield and save time a desk top centrifuge can be used). The losses due to adsorption of water on silica gel and zeolites are negligible (powders were handled at normal humidity) but wetting of the powder results in losses less than 5 wt% of the weight of the added powder. Losses due to the adsorption of phospholipid on the supports are 10–20% in the case of glass wool, zeolite ZSM 5, approx. 70% in the case of silica gel, and above 95% in the case of zeolite X.

After the support was removed the solutions of vesicles were investigated. All were turbid with the turbidity (naked eye and laser beam) decreasing in the order $\mathrm{I} \gg \mathrm{VII} > \mathrm{III} \approx \mathrm{II} \gg \mathrm{IV} > \mathrm{V} \gg \mathrm{VI}$. The values of the absorbance (A) at 330 nm are shown in Table I. The concentration of phosphorus in these solutions was also determined to monitor the losses due to the absorption of egg yolk PC on the support and to normalize the measured A (see Table I).

The produced vesicles were also investigated by negative staining electron microscopy (EM) and gel permeation chromatography (GC). To increase the resolution of GC we used Sephacryl S1000 gel medium [19]. The EM micrograph of the egg yolk PC dispersion (Sample I) shows typical multilamellar structures [14] which are very large and heterogeneous in size. Sample II shows big multilamellar structures and also some SUV [17]. The micrographs of samples III–VI are shown in Figs. 1A–D, respectively. The histograms of the corresponding samples, which were counted on different grids of different sample preparations, are shown in Figs. 2A–D. The histograms of egg yolk PC/CTAB film on glass wall (Sample II) and egg yolk PC on zeolite X (Sample VII) also are shown in Fig. 2. E and F, respectively, while the histogram of I is not shown because the extremely heterogeneous sample has particles with diameters with diameters from approx. 0.1 to approx. 10 μm [14]. Figs. 1 and 2 show that with the decreasing size of the support the size of the produced vesicles also decreases while the homogeneity of the produced vesicles increases. These results were confirmed by gel chromatography. The elution profiles are shown in Fig. 3 and the radii of the vesicles calculated from the calibration curve, are listed in Table I. The shapes of the curves give also some qualitative estimates of the size distribution of vesicles although the linewidth cannot be a quantitative measure for the size distribution of particles [20]. However, the elution profiles of

TABLE I

SOME PHYSICAL AND CHEMICAL PROPERTIES OF THE PRODUCED VESICLES

EYC, egg yolk PC; EM, electron microscopy; GC, gel permeation chromatography.

Property support	Sample I EYL glass wall	Sample II EYL/CTAB glass wall	Sample III EYL/CTAB glass wool	Sample IV EYL/CTAB silica gel	Sample V EYL/CTAB zeolite ZSM	Sample VI EYL/CTAB zeolite X	Sample VII EYL zeolite X
$2r$ (nm) (EM)	100–10000	80–500	30–200	50	25.0	21.5	25–100
$2r$ (nm) (GC)	> 300	–	–	90–20	29	22	–
Homogeneity	no	no	no	bad	intermediate	good	no
$A_{330\mathrm{nm}}$	2.53	1.116	1.038	0.099	0.329	0.014	1.99
C_{EYL}(mg/ml)	2.1	1.64	1.53	0.31	1.50	0.07	–
A/C_{EYl}	1.2	0.68	0.68	0.32	0.22	0.20	–

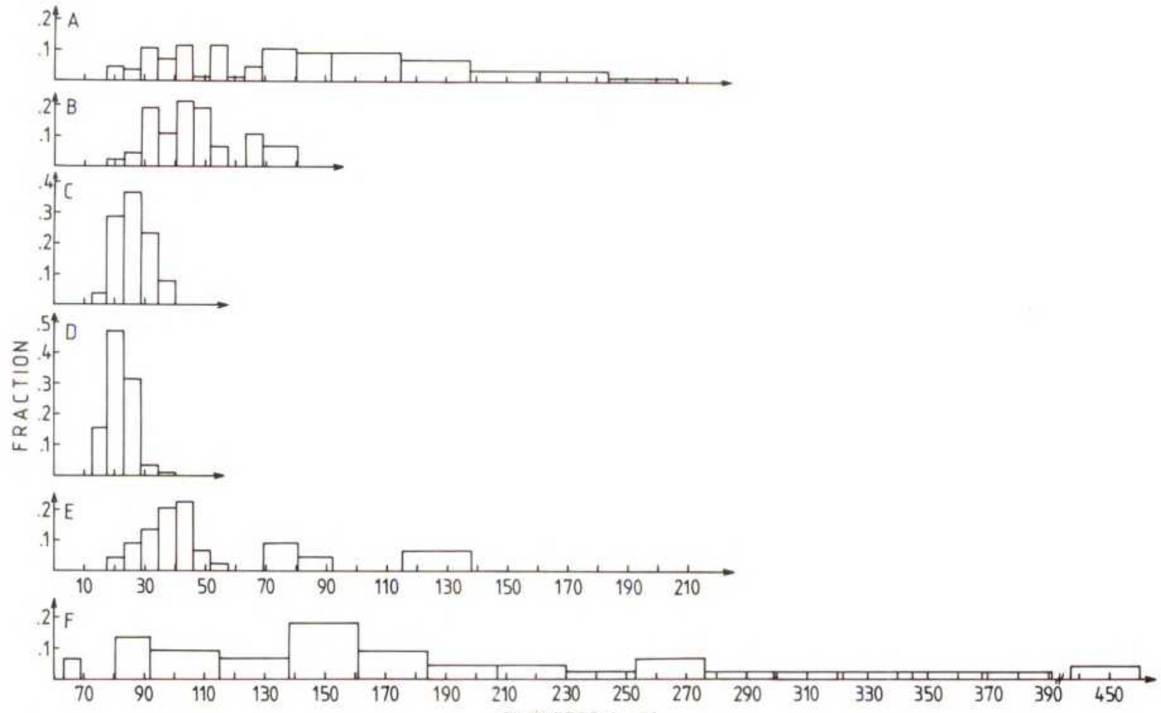

Fig. 2. The histograms of size distribution of the samples III (A), IV (B), V (C) and VI (D); E: sample VII (egg yolk PC deposited on zeolite X) and F: sample II (phospholipid film on glass wall).

samples I, IV, V and VI show that the vesicles of samples V and VI are rather small and homogeneous, sample IV is a mixture of large and small vesicles while sample I has practically only large structures (most of the phospholipid material actually stayed on the top of the column and even clogged it). SUV (samples V and VI) are stable at least for several days at 20°C as confirmed by constant *A* readings and reproducible EM micrographs.

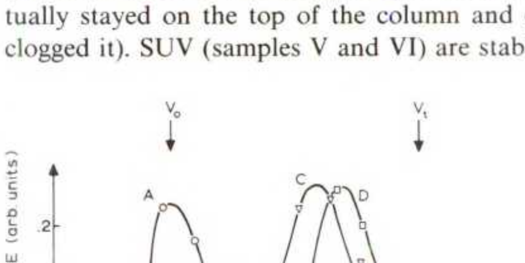

Fig. 3. Elution patterns on the Sephacryl S1000 column (39 × 0.7 cm, flow rate 6 ml/h, presatured with egg yolk PC) for four preparations: A, sample I (egg yolk PC on glass wall); B, sample IV (phospholipid film on silica gel); C, sample V (zeolite ZSM 5); and D, sample VI (zeolite X).

It is probable that many characteristics of the produced vesicles could be varied by changing of the support for the deposited phospholipid film. In addition to the size (and homogeneity) of the support the hydrophobicity of the support could also be varied. In our case the hydrophobicity of all supports is rather similar except of the zeolite X where a large ratio Al_2O_3/SiO_2 makes it even more hydrophilic than other materials which are composed predominantly from SiO_2.

The main characteristics of the support must be chemical inertness towards all substances used in the preparation process, small size of the microcrystals and low adsorption capacity. The last requirement is not satisfactory in using zeolite X which has a very large adsorption capacity (size of cages approx. 1.3 nm, channels approx. 0.74 nm) [21]. Below the saturation limit of adsorption (approx. 1 mg egg yolk PC/1.8 mg zeolite X) the yield is very low ($\leqslant 5\%$) while above this limit it begins to increase. However, the fraction of LUV and MLV, which also are at lower ratios negligible, begin to increase indicating that the lipid film has coated several microcrystals. Zeolite ZSM5 has smaller channels (0.5–0.55 nm and no cages) [21] and this results in larger yield (about 70–80%). The use of zeolite A (channels 0.42 nm, cages 1.14 nm) and sodalite (channels 0.22 nm, cages 0.6 nm) [21] also results in larger yields (about 40 and 55%, respectively). Preliminary results show that vesicle populations are heterogeneous in size probably due to the undefined size of the support or slightly higher values of pH in these suspensions. On the other hand, amorphous silica powders cannot be used due to their thixotropic behaviour while we have not yet been able to obtain small and uniform crystals of quartz.

Changes may also be expected by changing the swelling behaviour of the phospholipid film, which can be varied from finite to infinite, depending on the surface charge [15–18].

To investigate the permeability properties we also have used γ-Al_2O_3 for support (size of crystallites approx. 1 μm) where larger yield (approx. 80%) enables trapped volume and NMR measurements. These samples show wide size distribution; besides SUV there are also LUV and some MLV, as determined by EM and phase contrast optical microscopy. ^1H high-resolution NMR spectrum of these vesicles is shown in Fig. 4. The addition of paramagnetic shift reagents (3 mM $EuCl_3$, 3 mM $PrCl_3$) does not split the $N(CH_3)_3$ signal. This indicates that vesicles are permeable to cations what can be expected from the presence of detergent. Trapped volume measurements by ESR (water soluble spin label and bleaching agent $[Cr(C_2O_4)_3]^{-3}$), show, on the other hand, that vesicles are impermeable to this anion. The measured value of the trapped volume 0.67 litre per mol of phospholipid, which corresponds to the average diameter of approx. 35 nm of the hypothetic monodisperse sample, cannot be used to calculate the vesicle size because the vesicles are rather heterogeneous and a few bigger structures were also observed by optical microscopy. The permeability of vesicles induced by CTAB within the bilayers can be eliminated by mixing charged phospholipids instead of ionic detergents, into the bilayer. Permeability studies of mixed egg yolk PC/phosphatidic acid vesicles [22,23] show that their permeability is similar to egg yolk PC vesicles prepared by sonication.

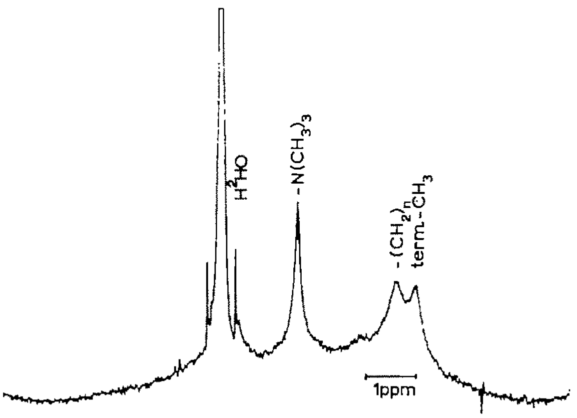

Fig. 4. 90 MHz ^1H-NMR of vesicles (6 mM egg yolk PC with 1.5 wt% CTAB) which were obtained by swelling of the lipid film deposited on Al_2O_3 (10 mg of lipid was deposited on 0.5 g Al_2O_3) and resuspended with 1.3 ml ^2H_2O).

In addition to the novelty, simplicity and rapidness of this method for the preparation of vesicles, the results obtained also shed some light on the mechanism of the vesicle formation.These results are in agreement with the proposed model where a bilayered phospholipid flake is an intermediate structure in the vesicle formation process [12,13]. Because the surface area of the support was several times larger than the area of the phospholipid film we can assume that the phospholipid film was deposited more or less as a monolayer. The swelling and peeling of the film produced bilayered phospholipid flakes which bend and close upon themselves due to their instability at the edges. The results of this work, considering the size and homogeneity of the produced vesicles, are in qualitative agreement with the proposed model. On the basis of these findings and with proper variation of the experimental parameters LUV could also be probably produced.

Besides their permeability to cations the produced vesicles are similar to SUV prepared by sonication or by detergent (sodium cholate) removal. The advantage of these two techniques are higher concentrations of the produced vesicles. The yield of egg yolk PC (mass of resuspended egg yolk PC as SUV/mass of deposited egg yolk PC) is in the case of zeolite X very low but with another support it can increase. The advantage of this method is its simplicity and therefore avoidance of sonication, organic solvents, detergents (by the use of charged phospholipid), or pH changes what makes it very suitable for the drug or genetic material encapsulation. The subjects of our present studies are to increase the yield, increase the concentration of vesicles and additional physicochemical characterizations of the spontaneously formed SUV.

The authors are thankful to Professor D. Hadži for the critical reading of the manuscript, Dr. M. Pšeničnik for the EM micrographs and Mss. M.T. Lešnjak, M.Sc., for synthesis of the inorganic materials. One of us (D.D.L.) is indebted to Professor H. Hauser for helpful discussions.

References

1 Szoka, F.C. and Papahadjopoulos, D. (1980) Annu. Rev. Biophys. Bioeng. 9, 467–508
2 Hauser, H. (1982) Trends Pharm. Sci. 3, 274–277
3 Huang, C. (1969) Biochemistry 8, 344–352
4 Lichtenberger, D., Freire, E., Schmidt, C.F., Barenholz, Y., Felgner, P. and Thompson, T.E. (1981) Biochemistry 20, 3462–3467
5 Razin, S. (1972) Biochim. Biophys. Acta 265, 241–296
6 Brunner, J., Skrabal, P. and Hauser, H. (1976) Biochim. Biophys. Acta 455, 322–331
7 Baron, C. and Thompson, T.E. (1975) Biochim. Biophys. Acta 382, 276–285
8 Gerritsen, W.J., Verkleij, A.J., Zwaal, R.F. and Van Deenen, L.L. (1978) Eur. J. Biochem. 85, 255–261
9 Batzri, S. and Korn, E.D. (1973) Biochim. Biophys. Acta 298, 1015–1019
10 Hauser, H. and Gains, N. (1982) Proc. Natl. Acad. Sci. USA 79, 1683–1687
11 Szoka, F.and Papahadjopoulos, D. (1978) Proc. Natl. Acad. Sci. USA 75, 4194–4198
12 Lasič, D.D. (1982) Biochim. Biophys. Acta 692, 501–502
13 Lasič, D.D. (1986) J. Theor. Biol., in the press
14 Bangham, A.D. and Horne, R.W. (1964) J. Mol. Biol. 8, 660–668
15 Krzewycki, T.G., Tardieu, A. and Luzzati, V. (1969) Mol. Cryst. Liq. Cryst. 8, 285–291
16 Hauser, H. (1984) Biochim. Biophys. Acta 712, 37–50
17 Hauser, H., Gains, N. and Lasič, D.D. (1983) in Physics of Amphiphiles (Corti, M. and Di Giorgio, V., eds.), pp. 648–662, North Holland, Amsterdam
18 Hauser, H. and Lasič, D.D. (1985) in Lecithin and Health (Paltauf, F. and Lekim, D., eds.), pp. 221–231, Semmelweis Verlag, Hoya
19 Nozaki, Y., Lasič, D.D., Tanford, C. and Reynolds, J.A. (1982) Science 217, 366–367
20 Lasič, D.D. (1986) J. Colloid Interface Sci., 110, 282–286
21 Breck, D.W. (1974) Zeolite Molecular Sieves, pp. 1–771, J. Wiley and Sons, New York
22 Gains, N. and Hauser, H. (1983) Biochim. Biophys. Acta 731, 31–39
23 Hauser, H., Gains, N. and Müller, M. (1983) Biochemistry 22, 4775–4781

Biochimica et Biophysica Acta 896 (1987) 123–127
Elsevier

BBA 70314

BBA Report

The combined and separate effects of low temperature and freezing on membrane lipid mesomorphic phase behavior: relevance to cryobiology

Martin Caffrey

Section of Biochemistry, Molecular and Cell Biology, Clark Hall, Cornell University, Ithaca, NY 14853 (U.S.A.)

(Received 11 August 1986)

Key words: Cryobiology; Dehydration; Lipid membrane; Phosphatidylserine; Time-resolved X-ray diffraction; X-ray diffraction; Water freezing; Phase transition

Time-resolved X-ray diffraction is used to demonstrate that for certain lipids low temperature alone may not be sufficient to bring about changes in mesomorphic phase state. However, when combined with slow freezing of the aqueous substrate, the fluid bilayer phase is destabilized as a result of dehydration, and thus more prone to undergoing deleterious thermotropic phase transformations. The cryobiological relevance of these results is discussed.

The systematic study of the physiochemical properties of lipids promises an understanding of lipid phase relations in cellular membranes and in other biological and reconstituted lipid aggregates. The lipid fraction of natural membranes consists of a vast array of different lipid species each with their own unique thermotropic, lyotropic and miscibility properties. The behavior of the native membrane reflects to some extent the behavior of its individual components. To understand how the biomembrane responds to environmental stresses such as extremes of temperature and hydration we must first of all establish the behavior of the individual lipid components in isolation and subsequently in more complex mixtures under similar conditions [1].

In the present study the combined and separate effects of temperature and hydration on the mesomorphic phase properties of membrane lipids is addressed. It is shown that slow freezing causes dehydration and that for phospholipids with suitably poised transition temperatures (T_t), this can effect a direct lyotropic (solvent-induced) lamellar liquid crystal-to-gel phase transformation. Such an effect occurring in a native biological membrane could trigger undesirable, possibly irreversible, lateral phase separations in the plane of the membrane or simply destabilize the bilayer structure leading to loss of trans-membrane electrical potential and eventually to cell death.

In this study time-resolved X-ray diffraction (TRXRD) [2–4] is used and is shown to be an effective and revealing method for monitoring the combined and separate effects of temperature and freezing on the mesomorphic phase properties of hydrated dioleoylphosphatidylserine (DOPS). The method reports directly and continuously on the phase state and degree of hydration of the lipid, and the phase state of the suspending aqueous medium. Thermal events occurring during the heating and cooling scans are monitored simultaneously by recording sample temperature.

Time-resolved X-ray diffraction was used to decipher the structural rearrangements undergone when fully hydrated DOPS is cycled in temperature between 20°C and −25°C. Static measure-

---

Correspondence: M. Caffrey, Section of Biochemistry, Molecular and Cell Biology, Clark Hall, Cornell University, Ithaca, NY 14853, U.S.A.

0005-2736/87/$03.50 © 1987 Elsevier Science Publishers B.V. (Biomedical Division)

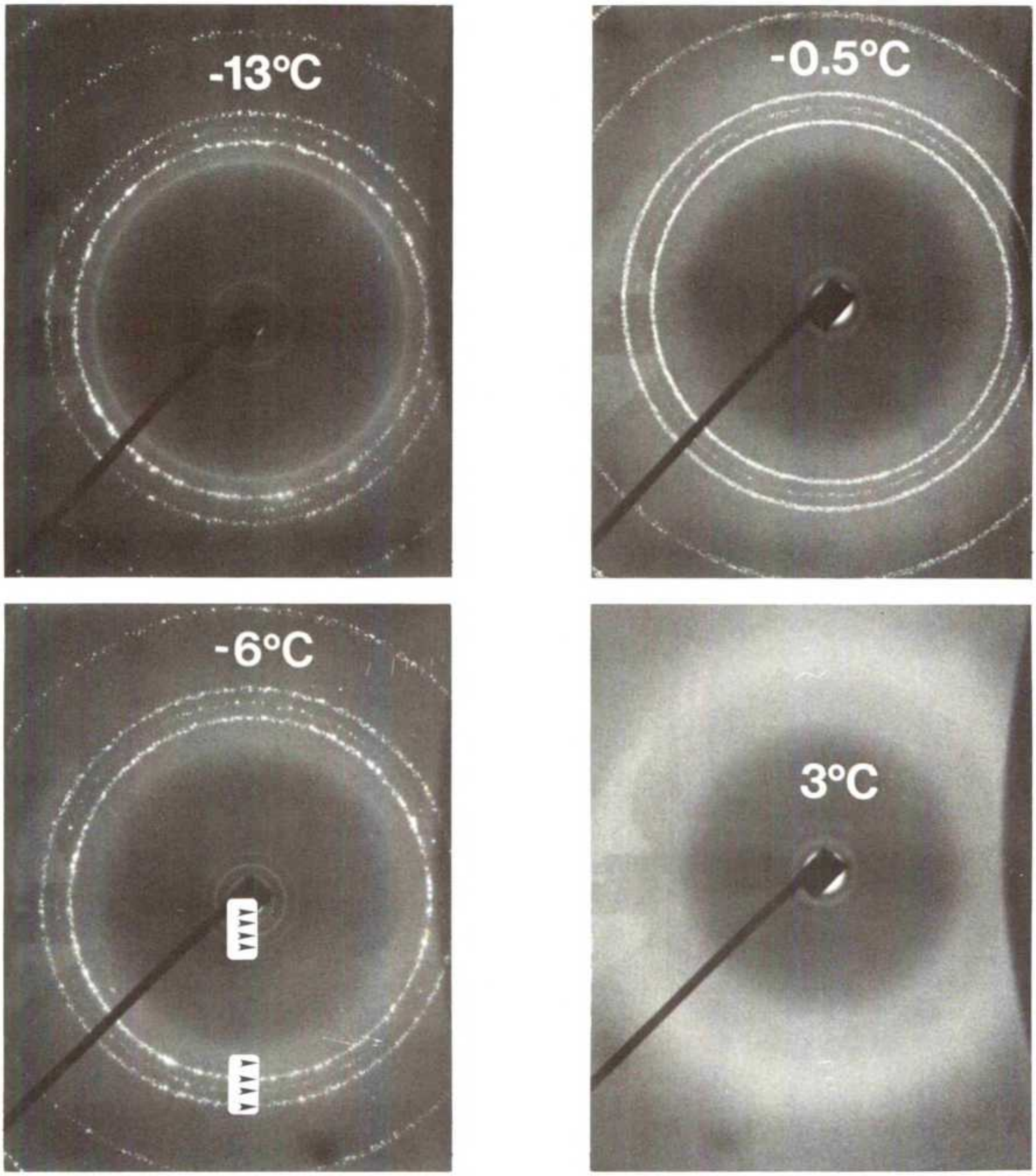

Fig. 1. X-Ray diffraction patterns from fully hydrated dioleoylphosphatidylserine above and below the freezing ($-18°$C) and melting ($\sim 0°$C) temperature of the aqueous phase. Samples were slowly (≤ 6 K/min) cooled to $\leq -25°$C and subsequently warmed to the temperature indicated. At $-6°$C, the arrowed reflections correspond to lipid peaks at $(5.5\text{ nm})^{-1}$, $(2.75\text{ nm})^{-1}$, $(1.83\text{ nm})^{-1}$, and about $(0.46\text{ nm})^{-1}$ and to ice peaks at $(0.39\text{ nm})^{-1}$, $(0.366\text{ nm})^{-1}$ and $(0.346\text{ nm})^{-1}$. The lipid, obtained from Avanti Polar Lipids, Inc., gave a single spot by thin-layer chromatography [2] and was used without further purification. It was dispersed at approx. 20 mM lipid in excess buffer (0.1 M KCl/0.01 M Hepes (pH 7)) by vortexing at room temperature in an argon atmosphere and concentrated by centrifugation [2,5]. The hydrated lipid pellet was transferred to a thin-walled (10 μm) capillary (1 mm internal diameter, Supper), flame-sealed under argon and hermetically sealed with 5-min epoxy. X-Ray diffraction measurements were carried out on the A-1 line at the Cornell High Energy Synchrotron Source as previously described [2–5]. Sample temperature was controlled by using a gas crystal heating/cooling system. A thermocouple positioned outside but touching the capillary next to the X-ray beam was used to record sample temperature [2]. Placing the thermocouple inside the capillary essentially eliminated undercooling and resulted in ice formation upon cooling at close to 0°C. Static diffraction patterns were recorded on X-ray sensitive polaroid film (Polaroid, Type 57) with an exposure time of 2 min, a sample-to-film distance of 46 mm, and a 0.3 mm collimator (Supper).

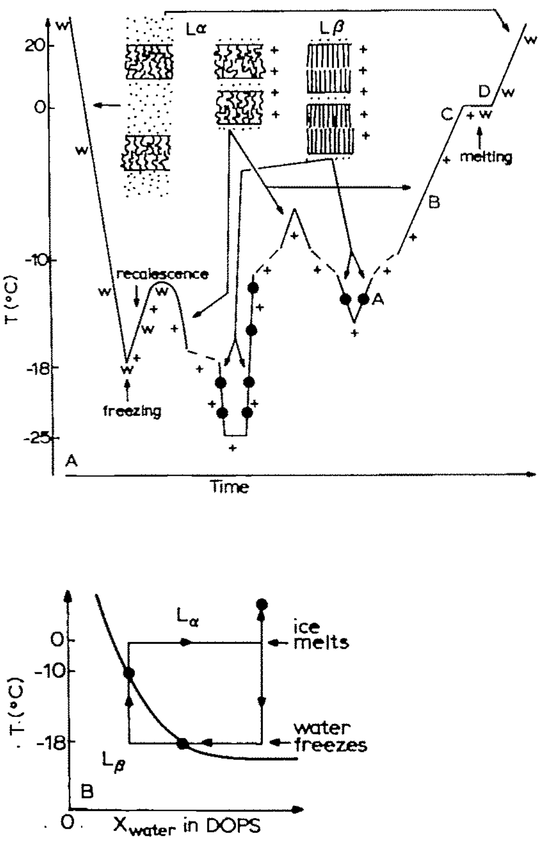

Fig. 2. (A) Heating and cooling curve for hydrated dioleoylphosphatidylserine. A schematic view of phase changes undergone by the lipid and aqueous components of the system is also included. Linearity along the time and temperature axis is not implied. The figure incorporates time-resolved and static X-ray diffraction data along with measurements of elapsed time and sample temperature. The following notation is used: ———, and ●———● denote the lamellar liquid crystal and gel phases, respectively; — — —, gel/liquid crystal phase coexistence; +, ice; w, water. The points labelled A–D correspond to the temperatures at which the diffraction patterns in Fig. 1 were recorded. (B) An interpretation of the effects of freezing and low temperature on the phase properties of dioleoylphosphatidylserine in terms of a typical temperature/composition isobaric phase diagram (see for example, Ref. 7). The sample begins at high temperature in the fully hydrated L_α phase. Cooling procedes down to −18°C at which point water freezes. In so doing it dehydrates the lipid effecting a disorder-to-order transition in the vicinity of −18°C. Warming the sample facilitates an order-to-disorder transition in the presence of ice at −10°C. At 0°C, ice melts and the lipid imbibes water to restore the original fully hydrated L_α phase. The important point to note is that a higher transition temperature is observed in the heating compared to the cooling direction which reflects the lower hydration level of the lipid in the presence of ice.

ments were made using X-ray sensitive polaroid film at intervals during the thermal cycles [5]. The lipid was dispersed in an excess of aqueous buffer (pH 7) as described in the legend to Fig. 1.

A summary of the experimental observations along with an interpretation of the results are presented in Fig. 2. At 20°C and in the presence of excess aqueous substrate electrostatic repulsion causes the liquid crystalline DOPS bilayers to separate and the interbilayer region to imbibe large quantities of fluid. This corresponds to the swollen or fully hydrated lamellar liquid crystal (L_α) phase [7]. The corresponding diffraction pattern from this phase is shown in Fig. 1. It consists of a series of diffuse continuous low-angle peaks accompanied by a broad peak centered at (0.46 nm)$^{-1}$ arising from the disordered acyl chains and a broad water peak at approx. (0.33 nm)$^{-1}$ [8–12]. Upon slowly cooling the sample, the above condition is maintained in that no phase change occurs down to −18°C in the presence of an undercooled aqueous substrate. At −18°C, ice crystals spontaneously form, the system experiences a reduction in available water and the lipid undergoes dehydration. During freezing, the latent heat of crystallization released (recalescence) raises sample temperature and upon continued cooling sample temperature slowly decreases. At about −16°C, the phase state of the lipid undergoes a dramatic change from liquid crystalline-to-gel corresponding to the direct lyotrope-induced transformation. The diffraction pattern below −16°C (cf. Fig. 1) shows a series of sharp reflections in the low-angle region and a sharp line at (0.42 nm)$^{-1}$ characteristic of ordered or gel-like acyl chain packing. Also present in the diffraction pattern are the tell-tale spotty reflections from hexagonal ice at ≥ (0.3 nm)$^{-1}$ [13]. Further cooling to −25°C does not noticeably change the system from that of a dehydrated or partially dehydrated (referred to as low moisture) gel phase lipid in the presence of ice.

If the sample is now warmed, very little occurs (see Fig. 1) until the system reaches −10.5°C. At this temperature the lipid undergoes a reversible thermotropic chain 'melting' transition from the low moisture gel to the low moisture L_α phase in the presence of ice. Note that this transition occurs some 5–6 K above the T_t recorded upon sample cooling, a result which is in agreement with the expected behavior of desiccation raising the chain 'melting' T_t [7–10]. That this difference is due to undercooling of the lipid transition seems unlikely in view of the current evidence. In the vicinity of the T_t, changes are seen to occur in both the low- and wide-angle regions of the diffraction pattern (cf. Fig. 1).

At −6°C in the L_α phase the diffraction pattern reveals a lamellar repeat spacing of 5.50 nm (Fig. 1). The corresponding wide-angle region contains a diffuse liquid crystalline peak centered at approx. $(0.46\ \mathrm{nm})^{-1}$ along with characteristic ice crystal reflections. This suggests that the lipid is only partially hydrated given a bilayer thickness increment of 0.105 nm/methylene group in the L_α phase, a water layer thickness increment of 0.16 nm/water molecule and a glycerophosphorylserine headgroup thickness of about 0.7 nm [7,14].

As sample temperature rises it was observed in the time-resolved diffraction patterns that the ice crystals become noticeably mobile beginning at T_t as evidenced by fluctuations in intensity of the individual ice reflections. These fluctuations become progressively more rapid and dramatic with temperature up to 0°C at which point ice melting is complete. As the ice melts and water becomes available the low moisture L_α phase imbibes water and swells to restore the original condition of the fully hydrated L_α phase.

The temperature of ice crystal formation was repeatedly found to occur in this and similar lipid systems in the vicinity of −18°C (unpublished data). Interestingly, if ice formation is nucleated at −11.1°C, the fluid lipid phase persists for many (up to 15) minutes in the presence of ice. Following this protocol, cooling effects the disorder-to-order transition at approx. −15°C.

These results demonstrate that freezing reduces water activity which in turn can bring about lipid dehydration. It is noted in this regard that ice at −20°C in a one-component system has a vapor pressure equal to that of a 10.8 osmolal solution and is capable of exerting an equivalent osmotic pressure of 244 bars (241 atm, 2.44 dyn/cm^2, ~ 24 MPa) [15]. In the case of certain lipids a freeze-induced dehydration occurring at the appropriate temperature, of and by itself, can induce a liquid crystal-to-gel phase transformation. Worthy of note in this connection is (1) the reversibility of the chain melting transition at −10.5°C in the presence of ice, and (2) the observation that ice crystal formation precedes the appearance of the gel phase lipid upon cooling. This precludes gel phase formation acting to trigger ice crystallization. The latter possibility is not unreasonable given that an organized 'rigid' lattice such as exists at the gel phase lipid/water interface is more likely to act as a heterogeneous ice nucleation site than is the fluid surface that obtains at the lipid/water interface of the L_α phase. This ties in with the fact that heterogeneous nucleation of ice can be prevented by emulsifying water as small droplets in an inert carrier fluid [16].

Throughout these measurements samples were slowly cooled and frozen in contrast to an ultrarapid freezing protocol which would fix the system in the fully hydrated, swollen state. This slow cooling approach facilitates extramembranal ice formation and the local condensation of stacked membranes [17,18].

These results have far reaching implications when considered from a cryobiological perspective. Organisms, subcellular organelles, isolated membranes and other lipid-rich systems that are exposed to low temperatures may be in a position to resist or to tolerate such a stress by virtue of their lipid composition. If, however, in addition to low temperature, a freezing stress is imposed, the lipid components may no longer be able to withstand the low temperatures because of the freeze-induced dehydration which destabilizes the lamellar liquid crystal in favor of the gel phase. A lyotropic bilayer-to-nonbilayer transition is also possible since in a variety of lipid systems low moisture stabilizes the nonbilayer phases [2,8,9,19]. In either case, the lipid mesomorphic phase change is likely to profoundly influence membrane structure and thus function.

The knowledge that water freezing can be effected in the hydrated DOPS system by nucleating at −11°C without an accompanying mesomorphic phase transformation has been put to use in experiments where a freeze-thaw method is employed to equilibrate metal ions in aqueous dispersions of DOPS [20]. Multiple freeze-thaw cycling between 22°C and −11.1°C effectively equilibrates Ca^{2+} ions without inducing a thermotropic or lyotropic phase transition which could conceivably alter the properties of the PS-Ca^{2+} complex.

The following funding agencies are acknowledged: Sigma Xi, The Scientific Research Society and NIH Grant No. DK36849 (M.C.), NSF Grant No. DMR81-12822 (B.W. Batterman), NIH Grant No. HL-18255 (G.W. Feigenson), and NIH Grant Nos. RR-01646, and GM29044 (J.K. Moffat).

References

1 Caffrey, M. (1986) in Membranes, Metabolism and Dry Organisms (Leopold, A.C., ed.), pp. 242–258, Cornell University Press, New York

2 Caffrey, M. (1985) Biochemistry 24, 4826–4844

3 Caffrey, M. and Bilderback, D.B. (1983) Nucl. Instrum. Methods 208, 495–510

4 Caffrey, M. and Bilderback, D.B. (1984) Biophys. J. 45, 627–631

5 Caffrey, M. and Feigenson, G.W. (1984) Biochemistry 23, 323–331

6 Tsui, F.C., Ojcius, D.M. and Hubbell, W.L. (1986) Biophys. J. 49, 459–468

7 Hauser, H., Paltauf, F. and Shipley, G.G. (1982) Biochemistry 21, 1061–1067

8 Luzzati, V. (1968) in Biological Membranes, Physical Fact and Function (Chapman, D., Ed.), Vol. 1, pp. 71–123, Academic Press, New York

9 Shipley, G.G. (1973) in Biological Membranes (Chapman, D. and Wallach, D.F.H., eds.), Vol. 2, pp. 1–89, Academic Press, New York

10 Levine, Y.K. (1973) Prog. Surf. Sci. 3, 279–352

11 Blaurock, H.E. (1982) Biochim. Biophys. Acta 650, 167–207

12 Engelman, D.M. (1970) J. Mol. Biol. 47, 115–117

13 Dowell, L.G., Moline, S.W. and Rinfret, A.P. (1962) Biochim. Biophys. Acta 59, 158–167

14 Cevc, G., Seddon, J.M. and Marsh, D. (1985) Biochim. Biophys. Acta 814, 141–150

15 Nobel, P.S. (1983) Biophysical Plant Physiology and Ecology, W.H. Freeman and Co., San Francisco

16 Franks, F., Mathias, S.F., Galfe, P., Webster, S.D. and Brown, D. (1983) Cryobiology 20, 298–309

17 Franks, F. (1985) Biophysics and Biochemistry at Low Temperatures, Cambridge University Press, New York

18 Finean, J.B., Bunn, T.K., Hutchinson, A. and Mills, D. (1984) Biochim. Biophys. Acta 777, 140–146

19 Seddon, J.M., Cevc, G., Kaye, R.D. and Marsh, D. (1984) Biochemistry 23, 2634–2644

20 Feigenson, G.W. (1986) Biochemistry 25, 5819–5825

Biochimica et Biophysica Acta
Biomembranes M145(1)

Vol. 896, No. 1
January 9, 1987

Contents

Biochimica et Biophysica Acta: 40 years on v

Regular Papers

Fourier transform infrared and differential scanning calorimetric studies of a surface-active material from rabbit lung (BBA 73181)
by A.J. Mautone, K.E. Reilly and R. Mendelsohn (U.S.A.) 1

Effect of chlorophyll *a* on the phase behavior of hydrated monogalactosyldiacylglycerols (BBA 73173)
by P. Dea, L.T. Pearson, M. Caffrey and S.I. Chan (U.S.A.) 11

Changes in myoblast membrane order during differentiation as measured by EPR (BBA 73182)
by M.T. Santini, P.L. Indovina and R.E. Hausman (Italy, U.S.A.) 19

Membrane lipid changes in erythrocytes, liver and kidney in acute and chronic experimental liver disease in rats (BBA 73200)
by S. Kawata, A. Chitranukroh, J.S. Owen and N. McIntyre (U.K.) 26

Further characterization of a fodrin-containing transmembrane complex from mouse T-lymphoma cells (BBA 73183)
by S.J. Suchard and L.Y.W. Bourguignon (U.S.A.) 35

Divalent cation effects on the binding of human anti-phospholipid antibodies (BBA 73179)
by F.A. Green and P.B. Costello (U.S.A.) 47

Cholesterol effects on the interaction of cardiolipin with anti-cardiolipin antibody (BBA 73180)
by P.B. Costello and F.A. Green (U.S.A.) 52

The mobility of concanavalin A receptors and surface immunoglobulins on rat hepatocyte plasma membranes (BBA 73175)
by G. Lustyik, K. Kitani and M. Ohta (Japan) 57

Depth-dependent fluorescent quenching of a tryptophan residue located at defined positions on a rigid 21-peptide helix in liposomes (BBA 73199)
by K.-P. Voges, G. Jung and W.H. Sawyer (F.R.G., Australia) 64

Conformation and packing properties of membrane lipids: The crystal structure of sodium dimyristoylphosphatidylglycerol (BBA 73195)
by I. Pascher, S. Sundell, K. Harlos and H. Eibl (Sweden, U.K., F.R.G.) 77

Relation between Ca^{2+} uptake and fluidity of brush-border membranes isolated from rabbit small intestine and incubated with fatty acids and methyl oleate (BBA 73196)
by A.R. Merrill, H. Aubry, P. Proulx and A.G. Szabo (Canada) 89

Enhanced uptake of carnitine by perfused rat liver following starvation (BBA 73194)
by G. Kispal, B. Melegh, I. Alkonyi and A. Sandor (Hungary) 96

Nitrite uptake and its regulation in the cyanobacterium *Anacystis nidulans* (BBA 73349)
by E. Flores, A. Herrero and M.G. Guerrero (Spain) 103

continued

Cited in: Current Contents Life Sciences - Biological Abstracts - Chemical Abstracts - Index Chemicus - Index Medicus - Excerpta Medica (EMBASE)

INFORMATION FOR CONTRIBUTORS TO BIOCHIMICA ET BIOPHYSICA ACTA

The 1982 edition of this booklet, offering detailed guidance to authors, is available free of charge from the BBA Editorial Secretariat, P.O. Box 1345, 1000 BH Amsterdam, The Netherlands. It is also published as Biochim. Biophys. Acta 715 (1982) 1–23.

Reports

Competition between nitrate and nitrite uptake in the cyanobacterium *Anacystis nidulans* (BBA 70368)
by F. Madueño, E. Flores and M.G. Guerrero (Spain) 109

Inositol trisphosphate and calcium mobilisation in permeabilised enterocytes (BBA 70267)
by A. Ilundain, J.A. O'Brien, K.A. Burton and F.V. Sepúlveda (U.K.) 113

A simple method for the preparation of small unilamellar vesicles (BBA 70369)
by D.D. Lasič, J. Kidrič and S. Zagorc (Yugoslavia) 117

The combined and separate effects of low temperature and freezing on membrane lipid mesomorphic phase behavior: relevance to cryobiology (BBA 70314)
by M. Caffrey (U.S.A.) 123

BIOCHIMICA ET BIOPHYSICA ACTA
International Journal of Biochemistry and Biophysics
Founded in 1947 by H.G.K. Westenbrink, Managing Editor 1947–1964

© 1987, Elsevier Science Publishers B.V. (Biomedical Division)
Printed in The Netherlands

All rights reserved. No part of this publication may be reproduced, stored in a retrieval system, or transmitted, in any form or by any means, electronic, mechanical, photocopying, recording or otherwise without the prior written permission of the publisher, Elsevier Science Publishers B.V. (Biomedical Division), P.O. Box 1527, 1000 BM Amsterdam, The Netherlands. Submission of a paper to this journal entails the author's irrevocable and exclusive authorization of the publisher to collect any sums or considerations for copying or reproduction payable by third parties (as mentioned in article 17 paragraph 2 of the Dutch Copyright Act of 1912 and in the Royal Decree of June 20, 1974 (S. 351) pursuant to article 16b of the Dutch Copyright Act of 1912) and/or to act in or out of Court in connection therewith.

Special regulations for readers in the U.S.A. This journal has been registered with the Copyright Clearance Center, Inc. Consent is given for copying of articles for personal or internal use, or for the personal use of specific clients. This consent is given on the condition that the copier pays through the Center the per-copy fee stated in the code on the first page of each article for copying beyond that permitted by Sections 107 or 108 of the U.S. Copyright Law. The appropriate fee should be forwarded with a copy of the first page of the article to the Copyright Clearance Center, Inc., 27 Congress Street, Salem, MA 01970, U.S.A. If no code appears in an article, the author has not given broad consent to copy and permission to copy must be obtained directly from the author. All articles published prior to 1980 may be copied for a per-copy fee of US$ 2.25, also payable through the Center. This consent does not extend to other kinds of copying, such as for general distribution, resale, advertising and promotion purposes, or for creating new collective works. Special written permission must be obtained from the publisher for such copying.

Special regulations for authors. Upon acceptance of an article by the journal, the author(s) will be asked to transfer copyright of the article to the publisher. This transfer will ensure the widest possible dissemination of information.

lipids and lipid metabolism

SAMPLE COPY

for additional information contact :

ALLIED/ELSEVIER JOURNALS
MARKETING GROUP
30, WEST COTT ROAD, Ph : 82468
MADRAS – 600 014./
750, MOUNT ROAD,
MADRAS – 600 002.

BBA

Biochimica
et Biophysica Acta (L)

Managing Editors: P. Borst, P. Cohen,
C. van Dam, L.L.M. van Deenen (Chairman),
.P. Kennedy and G.K. Radda
Honorary Managing Editor: E.C. Slater

Vol. 917, No. 1, pp. 1–210
anuary 13, 1987
Elsevier

SSN 0006-3002
0005-2760
BBACAQ 917 (1) 1–210 (1987)
BBLLA6 917 (1) 1–210 (1987)

40 [illegible]ARS OF BBA!

PUBLICATION SCHEDULE FOR 1987

BBA is published according to a volume-numbering scheme that embraces all sections of the journal. In addition, each regular section has its own sequential volume-numbering system, running parallel to the overall BBA scheme, as set out below.
Full subscription: 42 volumes plus Cumulative Index 1986.

	BIO-ENERGETICS	BIO-MEMBRANES	GENE STRUCTURE AND EXPRESSION	PROTEIN STRUCTURE AND MOLECULAR ENZYMOLOGY	LIPIDS AND LIPID METABOLISM	GENERAL SUBJECTS	MOLECULAR CELL RESEARCH	BBA REVIEW SECTIONS
	6 volumes [a]	11 volumes [b]	3 volumes	6 volumes	6 volumes	4 volumes	5 volumes	3 volumes
Jan	890-1 = B80-1	896-1 = M145-1 896-2 = M145-2		911-1 = P39-1 911-2 = P39-2	917-1 = L82-1 917-2 = L82-2	923-1 = G126-1	927-1 = C17-1	BBA REVIEWS ON BIOENERGETICS
Feb	890-2 = B80-2 890-3 = B80-3	897-1 = M146-1 897-2 = M146-2	908-1 = N17-1	911-3 = P39-3	917-3 = L82-3	923-2 = G126-2	927-2 = C17-2	895-1 = BR15-1
March	891-1 = B81-1	897-3 = M146-3 898-1 = M147-1	908-2 = N17-2	912-1 = P40-1 912-2 = P40-2	918-1 = L83-1 918-2 = L83-2	923-3 = G126-3	927-3 = C17-3 928-1 = C18-1	895-2 = BR15-2 895-3 = BR15-3
April	891-2 = B81-2	898-2 = M147-2 898-3 = M147-3	908-3 = N17-3	912-3 = P40-3	918-3 = L83-3	924-1 = G127-1	928-2 = C18-2	
May	891-3 = B81-3	899-1 = M148-1 899-2 = M148-2		913-1 = P41-1 913-2 = P41-2	919-1 = L84-1 919-2 = L84-2	924-2 = G127-2	928-3 = C18-3	BBA REVIEWS ON BIOMEMBRANES
June	892-1 = B82-1 892-2 = B82-2	900-1 = M149-1 900-2 = M149-2	909-1 = N18-1	913-3 = P41-3	919-3 = L84-3	924-3 = G127-3	929-1 = C19-1	906-1 = MR16-1 906-2 = MR16-2
July	892-3 = B82-3	901-1 = M150-1 901-2 = M150-2	909-2 = N18-2	914-1 = P42-1 914-2 = P42-2	920-1 = L85-1 920-2 = L85-2	925-1 = G128-1	929-2 = C19-2 929-3 = C19-3	906-3 = MR16-3
Aug	893-1 = B83-1	902-1 = M151-1 902-2 = M151-2	909-3 = N18-3	914-3 = P42-3	920-3 = L85-3	925-2 = G128-2	930-1 = C20-1	BBA REVIEWS ON CANCER
Sept	893-2 = B83-2	902-3 = M151-3 903-1 = M152-1	910-1 = N19-1	915-1 = P43-1 915-2 = P43-2	921-1 = L86-1 921-2 = L86-2	925-3 = G128-3	930-2 = C20-2	907-1 = CR14-1 907-2 = CR14-2
Oct	893-3 = B83-3	903-2 = M152-2 903-3 = M152-3	910-2 = N19-2	915-3 = P43-3	921-3 = L86-3	926-1 = G129-1	930-3 = C20-3	907-3 = CR14-3
Nov	894-1 = B84-1 894-2 = B84-2	904-1 = M153-1 904-2 = M153-2		916-1 = P44-1	922-1 = L87-1 922-2 = L87-2	926-2 = G129-2	931-1 = C21-1 931-2 = C21-2	
Dec	894-3 = B84-3	905-1 = M154-1 905-2 = M154-2	910-3 = N19-3	916-2 = P44-2 916-3 = P44-3	922-3 = L87-3	926-3 = G129-3	931-3 = C21-3	

[a] This includes BBA Reviews on Bioenergetics, Vol. 895. [b] This includes BBA Reviews on Biomembranes, Vol. 906

Authors should submit their manuscripts (four copies) for publication in BIOCHIMICA ET BIOPHYSICA ACTA by sending them to one of the Managing Editors:
Dr. P. Borst, c/o BBA Editorial Secretariat, P.O. Box 1345, 1000 BH Amsterdam, The Netherlands
Dr. P. Cohen, Department of Biochemistry, Medical Sciences Institute, University of Dundee, Dundee, DD1 4HN, U.K.
Dr. K. van Dam, c/o BBA Editorial Secretariat, P.O. Box 1345, 1000 BH Amsterdam, The Netherlands
Dr. L.L.M. van Deenen, c/o BBA Editorial Secretariat, P.O. Box 1345, 1000 BH Amsterdam, The Netherlands
Dr. E.P. Kennedy, c/o BBA Editorial Secretariat (Boston), Box C 9123, Brookline, MA 02146, U.S.A.
Dr. G.K. Radda, Department of Biochemistry, University of Oxford, South Parks Road, Oxford, OX1 3QU, U.K.

Detailed information for contributors may be found in Biochim. Biophys. Acta 715 (1982) 1–23, also published as the 1982 edition of
INFORMATION FOR CONTRIBUTORS TO BIOCHIMICA ET BIOPHYSICA ACTA
a booklet which is available free of charge from the BBA Editorial Secretariat.

Subscription information

1987 BBA Lipids and Lipid Metabolism, Volumes 917–922 (6 volumes in 18 issues), Dfl. 1470 (US$ 592.75) + Dfl. 150 (US$ 60.50) postage, packaging and handling. Total price: Dfl. 1620 (US$ 653.25).
1987 BBA full subscription, Volumes 890–931 (42 volumes in 120 issues), Dfl. 7812 (US$ 3150.00) + Dfl. 1050 (US$ 423.50) postage, packaging and handling. Total price: Dfl. 8862 (US$ 3573.50).
The Dutch guilder price is definitive. The U.S. dollar price is subject to exchange-rate fluctuations and is given only as a guide.
Journals are sent by surface delivery to all countries, except the following countries where SAL air delivery (Surface Airlifted Mail) is ensured: U.S.A., Canada, Japan, Australia, New Zealand, P.R.China, India, Israel, South Africa, Malaysia, Singapore, South Korea, Taiwan, Pakistan, Hong Kong, Brazil, Argentina, Mexico and Thailand. Airmail rates for other countries are available on request.
Subscription orders can be entered only by calendar year (Jan.–Dec.) and should be sent to Elsevier Science Publishers, Journals Department, P.O. Box 211, 1000 AE Amsterdam, The Netherlands, Telex 18582 ESPA NL, or to your usual subscription agent.
Claims for missing issues should be made within 3 months of publication, otherwise they cannot be honoured free of charge. The Publisher reserves the right to issue additional volumes during the course of the year. Such volumes will be invoiced before publication and delivered after receipt of payment.
In the U.S.A. and Canada: for further information contact Elsevier Science Publishers, Journal Information Center, 52 Vanderbilt Avenue, New York, NY 10017, U.S.A., Tel. (212) 370-5520.

Biochimica et Biophysica Acta

BIOCHIMICA
ET BIOPHYSICA ACTA

MANAGING EDITORS

L.L.M. van Deenen (Utrecht)
(Chairman)
P. Borst (Amsterdam)
P. Cohen (Dundee)
E.P. Kennedy (Boston, MA)
G.K. Radda (Oxford)
K. van Dam (Amsterdam)

HONORARY MANAGING EDITOR

E.C. Slater (Southampton)

EDITORS

H.R.V. Arnstein (London)
J. Barber (London)
I. Björkhem (Huddinge)
B. Borgström (Lund)
J. Brachet (Brussels)
J. Bremer (Oslo)
R. Burgess (Madison, WI)
E. Carafoli (Zürich)
J.E. Cleaver (San Francisco, CA)
C. Crane-Robinson (Portsmouth)
J.W. Daly (Bethesda, MD)
E.A. Dawidowicz (Boston, MA)
B. de Kruijff (Utrecht)
J.G. Demaille (Montpellier)
J.J.H.H.M. de Pont (Nijmegen)
B. Deuticke (Aachen)
K.T. Douglas (Colchester)
S. Ebashi (Tokyo)
L. Ernster (Stockholm)
S. Ferguson (Birmingham)
I. Fridovich (Durham)
F. Gibson (Canberra)
W.B. Gratzer (London)
M. Hamberg (Stockholm)
T.E. Hardingham (London)
J.L. Harwood (Cardiff)
E. Heinz (Dortmund)
E.J.M. Helmreich (Würzburg)
F. Hofmann (Homburg)
M.D. Houslay (Glasgow)
R.C. Hughes (London)
J.B. Jackson (Birmingham)
P. Jollès (Paris)
P.L. Jørgensen (Århus)
Y. Kagawa (Tochigi)
K.-A. Karlsson (Gothenburg)
M. Kates (Ottawa)
J. Kay (Cardiff)
Y. Kaziro (Tokyo)
R. Kinne (Dortmund)
C. Klee (Bethesda, MD)
A. Kleinzeller (Philadelphia, PA)
P. Läuger (Constance)
A.G. Lee (Southampton)
D.M. Lee (Oklahoma City, OK)
F. Maley (Albany, NY)
D. Marsh (Göttingen)
V. Massey (Ann Arbor, MI)
D.J. Morré (West Lafayette, IN)
J.F. Morrison (Canberra)
L.E. Mortenson (Athens, GA)
G. Nelsestuen (St. Paul, MN)
D.G. Nicholls (Dundee)
Y. Nishizuka (Kobe)
R.C. Nordlie (Grand Forks, ND)
S. Numa (Kyoto)
C. Pace-Asciak (Toronto)
P.G.W. Plagemann (Minneapolis, MN)
I. Ragan (Harlow)
P. Randle (Oxford)
A. Razin (Jerusalem)
A.M. Scanu (Chicago, IL)
H.J. Schatzmann (Bern)
G.L. Scherphof (Groningen)
J. Seelig (Basel)
N. Sharon (Rehovot)
G.G. Shipley (Boston, MA)
D. Shugar (Warsaw)
W.D. Stein (Jerusalem)
J.M. Tager (Amsterdam)
T. Taniguchi (Tokyo)
J.P. Thornber (Los Angeles, CA)
I. Tinoco (Berkeley, CA)
K.F. Tipton (Dublin)
I.P. Trayer (Birmingham)
I. Trowbridge (San Diego, CA)
C.L. Tsou (Beijing)
D.E. Vance (Edmonton)
H.J. van Gorkom (Leiden)
T. Vänngård (Gothenburg)
B.R. Velthuys (Gif-sur-Yvette)
A. Watts (Oxford)
C. Weissmann (Zürich)
R.J.P. Williams (Oxford)
R.G. Williamson (London)
C. Wraight (Urbana, IL)
K. Wüthrich (Zürich)
R.F.A. Zwaal (Maastricht)

ELSEVIER SCIENCE PUBLISHERS B.V.
AMSTERDAM

BIOCHIMICA
ET BIOPHYSICA ACTA

INTERNATIONAL JOURNAL OF BIOCHEMISTRY AND BIOPHYSICS

lipids and lipid metabolism

917 (1987)
(L82)

ELSEVIER SCIENCE PUBLISHERS B.V.
AMSTERDAM

PUBLICATION SCHEDULE FOR 1987

BBA is published according to a volume-numbering scheme that embraces all sections of the journal. In addition, each regular section has its own sequential volume-numbering system, running parallel to the overall BBA scheme, as set out below.
Full subscription: 42 volumes plus Cumulative Index 1986.

	BIO-ENERGETICS	BIO-MEMBRANES	GENE STRUCTURE AND EXPRESSION	PROTEIN STRUCTURE AND MOLECULAR ENZYMOLOGY	LIPIDS AND LIPID METABOLISM	GENERAL SUBJECTS	MOLECULAR CELL RESEARCH	BBA REVIEW SECTIONS
	6 volumes [a]	11 volumes [b]	3 volumes	6 volumes	6 volumes	4 volumes	5 volumes	3 volumes
Jan	890-1 = B80-1	896-1 = M145-1 896-2 = M145-2	908-1 = N17-1	911-1 = P39-1 911-2 = P39-2	917-1 = L82-1 917-2 = L82-2	923-1 = G126-1	927-1 = C17-1	BBA REVIEWS ON BIOENERGETICS
Feb	890-2 = B80-2 890-3 = B80-3	897-1 = M146-1 897-2 = M146-2		911-3 = P39-3	917-3 = L82-3	923-2 = G126-2	927-2 = C17-2 927-3 = C17-3	895-1 = BR15-1
March	891-1 = B81-1	897-3 = M146-3 898-1 = M147-1	908-2 = N17-2	912-1 = P40-1 912-2 = P40-2	918-1 = L83-1 918-2 = L83-2	923-3 = G126-3	928-1 = C18-1	895-2 = BR15-2 895-3 = BR15-3
April	891-2 = B81-2	898-2 = M147-2 898-3 = M147-3	908-3 = N17-3	912-3 = P40-3	918-3 = L83-3	924-1 = G127-1	928-2 = C18-2	
May	891-3 = B81-3	899-1 = M148-1 899-2 = M148-2		913-1 = P41-1 913-2 = P41-2	919-1 = L84-1 919-2 = L84-2	924-2 = G127-2	928-3 = C18-3	BBA REVIEWS ON BIOMEMBRANES
June	892-1 = B82-1 892-2 = B82-2	900-1 = M149-1 900-2 = M149-2	909-1 = N18-1	913-3 = P41-3	919-3 = L84-3	924-3 = G127-3	929-1 = C19-1 929-2 = C19-2	906-1 = MR16-1 906-2 = MR16-2
July	892-3 = B82-3	901-1 = M150-1 901-2 = M150-2	909-2 = N18-2	914-1 = P42-1 914-2 = P42-2	920-1 = L85-1 920-2 = L85-2	925-1 = G128-1	929-3 = C19-3	906-3 = MR16-3
Aug	893-1 = B83-1	902-1 = M151-1 902-2 = M151-2	909-3 = N18-3	914-3 = P42-3	920-3 = L85-3	925-2 = G128-2	930-1 = C20-1	BBA REVIEWS ON CANCER
Sept	893-2 = B83-2	902-3 = M151-3 903-1 = M152-1	910-1 = N19-1	915-1 = P43-1 915-2 = P43-2	921-1 = L86-1 921-2 = L86-2	925-3 = G128-3	930-2 = C20-2	907-1 = CR14-1 907-2 = CR14-2
Oct	893-3 = B83-3 894-1 = B84-1	903-2 = M152-2 903-3 = M152-3	910-2 = N19-2	915-3 = P43-3	921-3 = L86-3	926-1 = G129-1	930-3 = C20-3 931-1 = C21-1	907-3 = CR14-3
Nov	894-2 = B84-2	904-1 = M153-1 904-2 = M153-2		916-1 = P44-1 916-2 = P44-2	922-1 = L87-1 922-2 = L87-2	926-2 = G129-2	931-2 = C21-2	
Dec	894-3 = B84-3	905-1 = M154-1 905-2 = M154-2	910-3 = N19-3	916-3 = P44-3	922-3 = L87-3	926-3 = G129-3	931-3 = C21-3	

[a] This includes BBA Reviews on Bioenergetics, Vol 895 [b] This includes BBA Reviews on Biomembranes, Vol 906

© 1987, Elsevier Science Publishers B.V. (Biomedical Division)

All rights reserved. No part of this publication may be reproduced, stored in a retrieval system, or transmitted, in any form or by any means, electronic, mechanical, photocopying, recording or otherwise without the permission of the publisher, Elsevier Science Publishers B.V. (Biomedical Division), P.O. Box 1527, 1000 BM Amsterdam, The Netherlands. Submission of a paper to this journal entails the author's irrevocable and exclusive authorization of the publisher to collect any sums or considerations for copying or reproduction payable by third parties (as mentioned in article 17 paragraph 2 of the Dutch Copyright Act of 1912 and in the Royal Decree of June 20, 1974 (S. 351) pursuant to article 16b of the Dutch Copyright Act of 1912) and/or to act in or out of Court in connection therewith.

Special regulations for readers in the U.S.A. This journal has been registered with the Copyright Clearance Center, Inc. Consent is given for copying of articles for personal or internal use, or for the personal use of specific clients. This consent is given on the condition that the copier pays through the Center the per-copy fee stated in the code on the first page of each article for copying beyond that permitted by Sections 107 or 108 of the U.S. Copyright Law. The appropriate fee should be forwarded with a copy of the first page of the article to the Copyright Clearance Center, Inc., 27 Congress Street, Salem, MA 01970, U.S.A. If no code appears in an article, the author has not given broad consent to copy and permission to copy must be obtained directly from the author. All articles published prior to 1980 may be copied for a per-copy fee of US$ 2.25, also payable through the Center. This consent does not extend to other kinds of copying, such as for general distribution, resale, advertising and promotion purposes, or for creating new collective works. Special written permission must be obtained from the publisher for such copying.

Special regulations for authors. Upon acceptance of an article by the journal, the author(s) will be asked to transfer copyright of the article to the publisher. This transfer will ensure the widest possible dissemination of information.

Printed in The Netherlands

Biochimica et Biophysica Acta: 40 years on

Professor H.G.K. Westenbrink

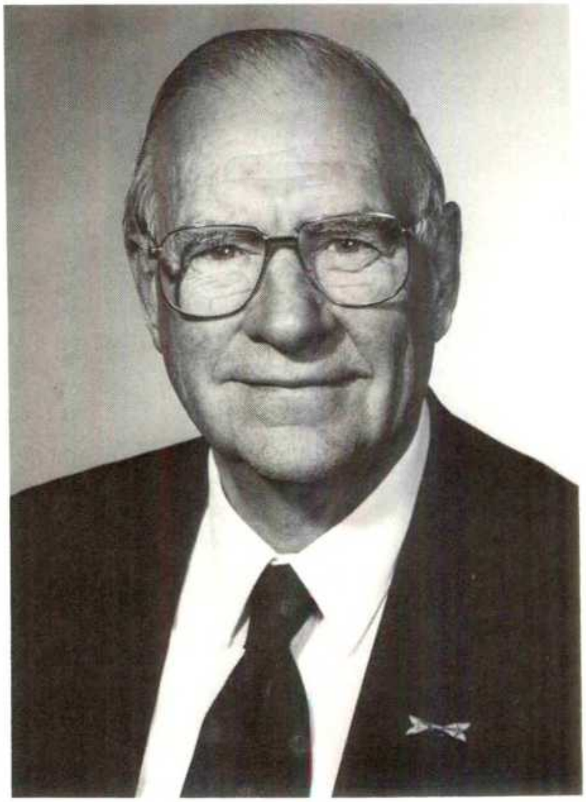

Professor E.C. Slater

Biochimica et Biophysica Acta, the first truly international journal in the field of biochemistry and biophysics, and now undoubtedly one of the largest, is celebrating its 40th anniversary with this issue.

The journal was founded in 1947 by Professor H.G.K. Westenbrink, who remained Managing Editor of the journal until 1964. He was succeeded by Professor E.C. Slater, who was able to fulfil this function until his recent retirement as Chairman of the Board of Managing Editors. Professor Slater was encouraged to write a history of BBA, recalling its remarkably rapid growth and some of the intricacies involved in the journal's birth and early development [1].

On the auspicious occasion of the journal's 40th birthday, the Publisher would like to take the opportunity of thanking all those who have played an active role in the journal's development, and looks forward to further stimulating developments over subsequent decades.

The photograph of E.C. Slater is reproduced by permission of Godfrey Argent, U.K., photographers.

[1] *Biochimica et Biophysica Acta: The Story of a Biochemical Journal* by E.C. Slater (1986) Elsevier Science Publishers, ISBN 0-444-80769-1; Price Dfl.75.00.

Biochimica et Biophysica Acta 917 (1987) 1–8
Elsevier

BBA 52299

Effect of chloroquine on the activity of some lysosomal enzymes involved in ganglioside degradation

Pam Fredman, George W. Klinghardt and Lars Svennerholm

Department of Psychiatry and Neurochemistry, Gothenburg University, St. Jörgen's Hospital,
S-422 03 Hisings Backa (Sweden)

(Received 17 March 1986)
(Revised manuscript received 15 September 1986)

Key words Chloroquine, Lysosomal enzyme, Ganglioside degradation

Chronic chloroquine treatment of miniature pigs resulted in increased activity of several lysosomal enzymes of the liver and brain. The most affected enzyme was α-fucosidase which showed a 3-fold increase in liver ($P < 0.001$) and a 2-fold increase in the brain ($P < 0.01$). The increased activity of the other lysosomal enzymes was generally slightly more pronounced in the liver, in which β-hexosaminidase, α-mannosidase and acid phosphatase were also significantly ($P < 0.01$) increased. In contrast, chloroquine added in vitro reduced the activity of the lysosomal enzymes. Three of these, α-fucosidase, β-hexosaminidase and acid phosphatase, were further investigated, and at a drug concentration of 15 mM and optimum pH for each respective enzyme, the activity was reduced to 20–30% of the initial value. Kinetic analyses revealed that this inhibition was non-competitive with regard to β-hexosaminidase but competitive with regard to α-fucosidase. These results indicate that there is a multifactorial effect of chloroquine on the lysosomal enzymes, and that the inhibitory effect of α-fucosidase and β-hexosaminidase might well explain the ganglioside storage found in liver and brain.

Introduction

Chloroquine is a lysosomotropic drug that accumulates selectively in lysosomes [1], used in the therapy of rheumatoid diseases and in the prophylaxis of malaria. Prolonged treatment with chloroquine can have serious side effects of which the most severe are retinopathy and myopathy [2–4]. Several studies on the effect of chloroquine in man and animals have shown that the affected tissues contain lamellated cytoplasmic bodies (lysosomal residual bodies) similar to those found in inherited lipid storage disorders, like Tay-Sachs disease [5]. These findings have led to the expression 'drug-induced lipidoses' and were thought to be an experimental model for the inherited disorders.

In three reports [6–8] we have examined lipid storage by electron-microscopic, histochemical and biochemical methods in various tissues of miniature pigs, subjected to chronic chloroquine intoxication. Nervous tissues, skeletal muscles and visceral organs all showed both qualitative and quantitative differences of the stored lipids. This storage involved gangliosides, neutral glycosphin-

---

Abbreviations: ganglioside abbreviations follow the nomenclature system of Svennerholm, IUPAC-IUP Commission on Biochemical Nomenclature CBN, The Nomenclature of Lipids [20]. GM2, $II^3(NEuAc)_2$-$GgOse_4Cer$, Fuc-GM1, IV^2Fuc, II^3NeuAc-$GgOse_4Cer$ and Fuc-GD1b, IV^2Fuc, $II^3(NeuAc)_2$-$GgOse_4Cer$

Correspondence: P. Fredman, Department of Psychiatry and Neurochemistry, St Jörgen's Hospital, 422 03 Hisings Backa, Sweden.

0005-2760/87/$03.50 © 1987 Elsevier Science Publishers B V (Biomedical Division)

golipids and, in the visceral organs, also phospholipids and cholesterol. Among the gangliosides, three components, GM2 and the fucose-containing gangliosides, Fuc-GM1 and Fuc-GD1b, increased more than the others. This finding led to the assumption that the lysosomal enzymes, β-hexosaminidase, degrading GM2 to GM3, and α-fucosidase, degrading Fuc-GM1 and Fuc-GD1b to GM1 and GD1b, respectively, were particularly sensitive to chloroquine.

In this study we have measured the in vitro effect of chloroquine on the β-hexosaminidase and the α-fucosidase activities in relation to some other lysosomal enzymes in liver and brain of chloroquine-treated and control pigs.

Materials and Methods

Tissue material. The tissue material was liver and forebrain from miniature pigs, of the Göttingen type [9]. Chloroquine was given to the pigs by addition of chloroquine diphosphate (Resorchin®) in doses of 2.0 or 3.0 g/kg fodder. The control pigs were given the same standard fodder without chloroquine. All data concerning the age, weight at death and duration and dose of chloroquine treatment of the individual animals are summarized in Table I. A brief description of the manifestations of the chronic chloroquine intoxication in the pigs has been described by Klinghardt et al. [6]. The pigs were killed by a shot in the medulla oblongata and the tissue was dissected immediately after death, placed in air-tight polyethylene bags, quick frozen and stored at −20°C until analysed.

Chemicals. 4-methylumbelliferyl derivatives of β-D-galactopyranoside, α-D-galactopyranoside, 2-acetamido-2-deoxy-β-D-glucopyranoside, α-L-fucopyranoside, α-D-mannopyranoside, β-D-glucoronide, α-L-iduronide, and D-glucuronate 1,4-lactone, phosphate and 4-methylumbelliferone were purchased from Koch-Light (Colnbrook, U.K.). [^{14}C]Glucosylceramide was prepared as described by Svennerholm et al. [10]. Sodium taurocholate, A grade, was obtained from Calbiochem (San Diego, CA) and Cutscum from Fischer Scientific Co. (Fair Lawn, NJ). Instagel was obtained from Packard Instrument Co., Inc. (Downers Grove, NJ). All other chemicals and organic solvents were of analytical reagent quality and used without purification.

Preparation of enzyme extracts. All procedures were performed at 1–4°C. The tissue was thawed and freed from connective tissue and vessels be-

TABLE I

SURVEY OF THE ANIMALS USED IN THE STUDY

Animal No	Age at death (days)	Duration of treatment (days)	Dose of chloroquine (g/kg diet)	Weight at death (kg)	Tissue
Control					
1	150	–	–	30	liver
2	223	–	–	53	liver
3	306	–	–	57	liver, brain
4	352	–	–	58	liver, brain
5	359	–	–	49	liver, brain
6	429	–	–	47	liver, brain
Chloroquine-treated					
7	325	212	2.0	31	liver
8	352	223	2.0	55	liver
9	360	230	2.0	48	liver
10	372	219	2.0	32	brain
11	435	188	2.0	55	liver
12	486	184	3.0	48	liver, brain
13	635	349	2.0	74	liver, brain
14	640	310	3.0	41	liver, brain

fore homogenization. Approximately 0.5 g of liver and 0.1 g of brain were homogenized in 4.5 ml and 4.9 ml, respectively, of distilled water in a scissor homogenizer for 1 min and then with six strokes in a Potter-Elvehjem homogenizer. The homogenate was then centrifuged at 900 × g for 10 min. The supernatant was frozen, thawed and ultrasonicated in a water bath ultrasonicator for 1 min. The procedure was repeated three times and this preparation was used in the studies.

Protein determination. protein was determined by the method of Hartree [11] with bovine serum albumin as standard.

Enzyme assays. A detailed description of the conditions for the enzyme assays is given in Table II. All the enzymes were determined at 37°C in a shaking water bath. The enzymic reactions with methylumbelliferyl substrates were stopped by addition of 3.0 ml 0.25 M glycine buffer (pH 10.3) and the liberated 4-methylumbelliferone was measured in a Perkin Elmer MPF 2A spectrofluorimeter with the exitation wavelength at 360 nm and the emission wavelength at 448 nm. α-Iduronidase was measured in micro-scale and the reaction was stopped with 0.6 ml 0.10 M glycine buffer (pH 10.7). The β-glucosidase activity was determined with [^{14}C]glucosylceramide as substrate and the reaction was stopped by addition of 2.5 ml of chloroform/methanol (2:1, v/v). Thereafter 0.4 ml 0.1% (w/v) glucose in water was added and the two phases were separated by centrifugation. The lower phase was removed, and the upper phase was washed with 1 ml of theoretical lower phase of chloroform/methanol/water (86:14:1, by vol.) solution. Finally 0.5 ml of the upper phase was added to 10 ml Instagel and the radioactivity was measured by liquid scintillation spectrometry.

For the studies of the in vitro drug effect, chloroquine diphosphate was added in different concentrations to homogenates of liver and brain. The pH in the assays was adjusted to 5.0 after addition of the chloroquine. The other conditions in the assays are described in Table II. The kinetic analysis was performed in the same manner but only one control and one chloroquine-treated pig was studied.

Chloroquine assay. Chloroquine and its metabolites, desethylchloroquine and bidesetheyl-

TABLE II

ASSAY CONDITIONS FOR DETERMINATION OF ENZYMIC ACTIVITY

MU-, methylumbelliferyl-

Enzyme	Enzyme protein μg)	Buffer	Detergent (g/l)	Substrate (nmol/l)	Incubation time (min)	Total volume (μl)
MU-α-galactosidase	15–50	Acetate 0.1 M (pH 5.0)	–	5.0	30	100
MU-β-galactosidase	2–20	Lactate 0.05 M (pH 3.8)	–	1.0	10	100
Glucosylceramide-β-glucosidase	10–50	Citrate-phosphate 0.05 mol/l (pH 5.8)	Sodium taurocholate, 2 mM Oleic acid, 1 mM	0.075	60	100
MU-*N*-acetylglucosaminidase (β-hexosaminidase)	1–10	Citrate 0.05 M (pH 4.4)	–	5.0	10	100
MU-α-fucosidase	5–50	Acetate 0.05 M (pH 5.0)	–	1.0	30	100
MU-α-mannosidase	5–50	Acetate 0.2 M (pH 4.0)	–	5.0	15	200
Acid phosphatase	2–30	Acetate 0.2 M (pH 5.0)	–	4.0	15	100
MU-α-L-iduronidase	10–25	Formiate 0.2 M (pH 3.3)	–	0.2	60	20
MU-β-glucuronidase	10–30	Acetate 0.2 M (pH 4.0)	–	1.0	30	100

chloroquine were extracted from the tissue with chloroform and determined by high-performance liquid chromatography as previously described [12].

Results

The enzymic activity of lysosomal hydrolases in liver and forebrain from chloroquine-treated pigs and controls

The specific activity was measured as described under 'Materials and Methods' at optimum pH (Table II) and the results are summarized in Table III.

The specific activity of four of the seven investigated lysosomal enzymes in liver was significantly increased in the chloroquine-treated pigs. Most affected was α-fucosidase, which showed a 3-fold increase ($P < 0.001$) followed by β-hexosaminidase, acidic phosphatase and α-mannosidase with an approximately 2-fold increase. The influence of chloroquine treatment on the activity of these enzymes in brain was less pronounced and only α-fucosidase showed a significant, 2-fold increase ($P < 0.01$). Another difference between liver and brain was the effect of chloroquine on α-galactosidase. This enzyme was unaffected in the liver but significantly increased ($P < 0.05$) in brain.

TABLE IV

CONCENTRATION OF CHLOROQUINE AND ITS METABOLITES IN LIVER AND CEREBRUM OF CHLOROQUINE-TREATED MINIATURE PIGS AND CONTROLS

Surveys of the animals are given in Table I. The values are mean values of duplicate determinations on the same homogenate. CQ, chloroquine; CQM, Desethylchloroquine; CQMM, Bidesethylchloroquine; n.d., not detectable.

Animal No.	Tissue	μmol/g wet tissue		
		CQ	CQM	CQMM
Control				
4	liver	0.03	0.02	n.d
5	liver	0.03	0.02	n.d
5	brain	n.d	n.d	n.d
Chloroquine-treated				
8	liver	0.87	1.04	0.44
9	liver	1.82	1.73	0.62
12	liver	3.87	2.72	0.54
13	liver	3.96	3.85	1.22
14	liver	8.53	3.11	1.19
14	brain	0.16	0.09	0.02

In addition to the lysosomal enzymes listed in Table III, α-iduronidase and β-glucuronidase were investigated in the liver of two controls and two chloroquine-treated animals. The activity was higher in the treated pigs than in the controls,

TABLE III

SPECIFIC ACTIVITY OF LYSOSOMAL ENZYMES IN LIVER AND BRAIN OF CHLOROQUINE-TREATED MINIATURE PIGS AND CONTROLS

The activity (μkat/kg protein) was measured in the tissue homogenate. The incubation was performed under optimum conditions as described in Table II. The values are means ± S.D. The statistical significance was calculated with the Student's *t*-test: *** 0.001 level; ** 0.01 level; * 0.05 level. MU-, methylumbelliferyl-

Enzyme	Liver		Brain	
	controls ($n = 6$)	chloroquine-treated ($n = 7$)	controls ($n = 4$)	chloroquine-treated ($n = 4$)
MU-α-galactosidase	53.7 ± 7.3	55.3 ± 7.5	8.1 ± 1.2	11.5 ± 1.8 *
MU-β-galactosidase	120 ± 39	152 ± 42	19.9 ± 4.9	23.8 ± 5.8
Glucosylceramide-β-glucosidase	13.6 ± 3.2	15.0 ± 3.2	29.1 ± 6.9	26.4 ± 2.2
MU-*N*-acetyl-β-glucosaminidase (β-hexosaminidase)	385 ± 68	835 ± 239 ***	421 ± 71	547 ± 246
MU-α-fucosidase	29.3 ± 7.0	88.2 ± 26.1 ***	24.6 ± 6.4	56.0 ± 5.1 **
MU-α-mannosidase	16.2 ± 3.0	27.0 ± 5.6 **	37 [a]	30 [a]
Acid phosphatase	547 ± 55	1066 ± 395 **	344 ± 67	382 ± 90

α-iduronidase increasing from 0.81 to 1.28 μkat/kg protein and β-glucuronidase from 41 to 56 μkat/kg protein.

There was no correlation between the increase in specific activity and age, weight at death, duration of treatment or drug concentration found in the tissue (Table IV). However, those pigs which had been given the higher dose, 3.0 g/kg diet, also had the highest specific activity of the most affected enzymes, α-fucosidase, *N*-acetyl-β-hexo-

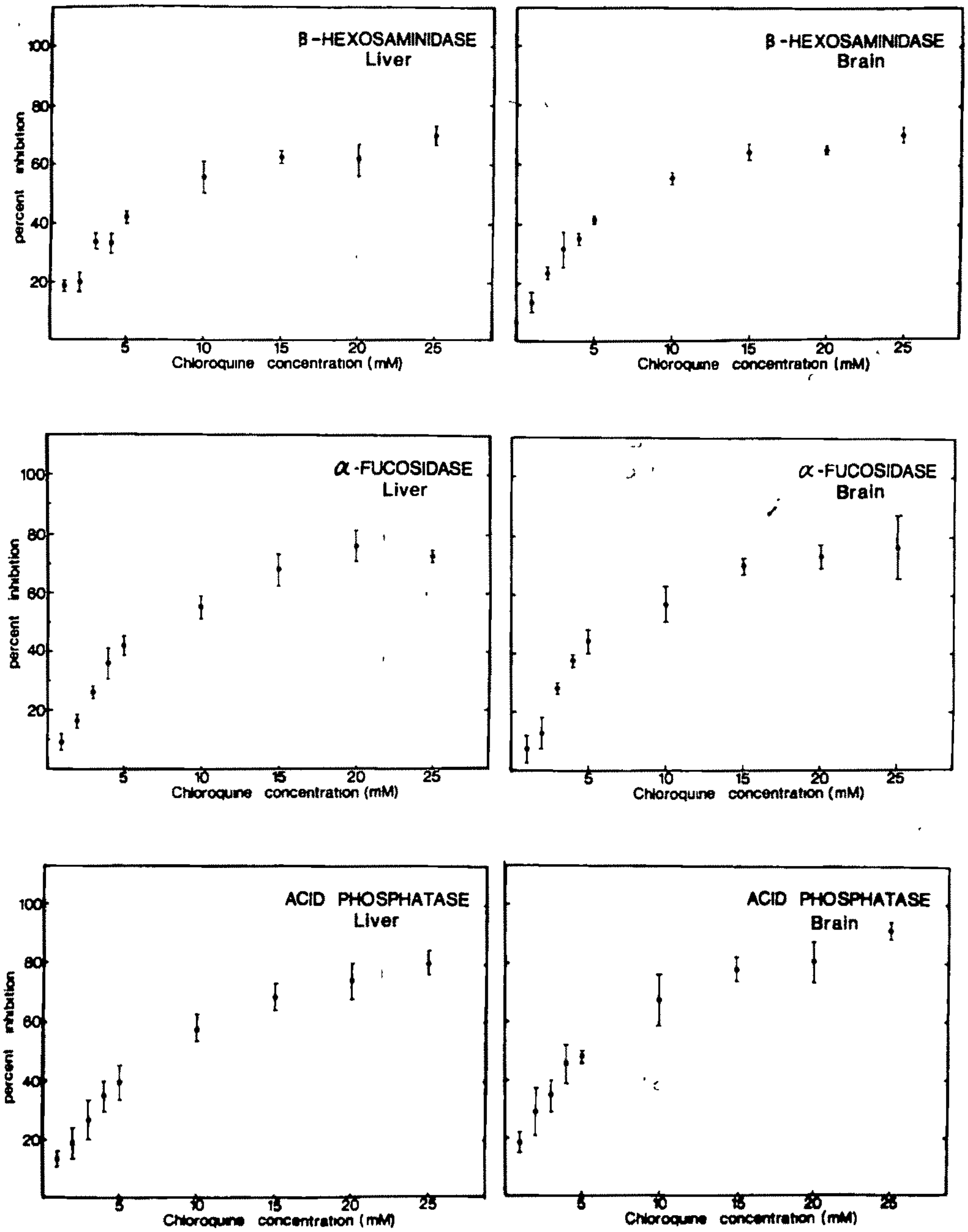

Fig 1 The effect of in vitro addition of chloroquine on the activities of β-hexosaminidase, α-fucosidase and acid phosphatase in homogenates of liver and brain from control miniature pigs The enzymic activities were measured in five liver and four brain homogenates and the values are mean values ± S D.

saminidase and acid phosphatase, both in liver and brain.

The effect of in vitro addition of chloroquine on lysosomal enzymes in liver and brain

The pH of the incubation mixture was held constant (the optimum pH for the respective enzyme as described in Table I) by adjustment after the addition of chloroquine. In liver and brain homogenates from control pigs the activity of three lysosomal enzymes were investigated – α-fucosidase, β-hexosaminidase, acid phosphatase – and the results are presented in Fig. 1 as percentage inhibition of their activity versus chloroquine concentration.

The activity of all three enzymes was reduced by the chhloroquine addition and the inhibition curves were most steep in the 0–5 mM interval. Further increase of the drug concentration caused only a slight reduction of the activities and the curves reached a plateau around a chloroquine concentration of 15 mM. A complete inhibition of the enzyme activities was never reached.

The in vitro effect of chloroquine on the activity of α-fucosidase and β-hexosaminidase in liver and brain homogenates from drug-intoxicated pigs was also investigated. The initial values of the enzyme activities in those pigs were, as expected from the values in Table III, higher than those of the controls but the effect of chloroquine addition was the same in both groups and the inhibition curves showed the same profiles as those presented in Fig. 1.

Kinetic analyses of the chloroquine inhibition in vitro on the β-hexosaminidase and α-fucosidase activities in liver and brain from control pigs

Enzyme sources were liver and brain homogenates from control pigs and the pH (the optimum pH for the respective enzyme) was adjusted after the addition of chloroquine.

The effect of chloroquine on β-hexosaminidase was a non-competitive inhibition (see Fig. 2) regardless of the enzyme source. The K_m values in brain and liver homogenates remained constant, 2.5 mM and 2.9 mM, respectively, after chloroquine addition. In liver homogenate the V_{max} value was reduced from 418 to 288 μkat/mg protein and in brain homogenate the corresponding decrease was from 697 to 477 μkat/kg protein – a reduction of around 30% in both cases.

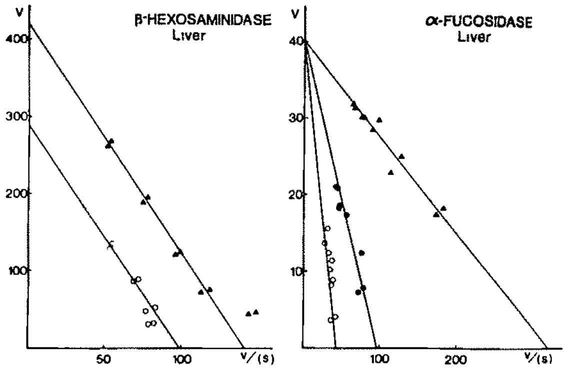

Fig 2. Kinetic analyses of the inhibition of chloroquine on β-hexosaminidase and α-fucosidase activities in liver homogenates from control miniature pigs The assays were performed in liver homogenate from animal No 3 (Table I). The symbols indicate the amount of drug in the assays: ○, 5 mM; ●, 2 mM; and ▲, no chloroquine $V = \mu$kat/kg protein and $S =$ mmol

In contrast to the findings with β-hexosaminidase, the effect of chloroquine on α-fucosidase was a competitive inhibition (see Fig. 2) and this effect was the same on the enzyme from liver and brain. The effect of the drug was measured at two concentrations, 2 and 5 mM. V_{max} remained unchanged and the value in liver homogenate was 40 μkat/mg protein and in brain homogenate 24.4 μkat/kg protein. The initial K_m value in liver homogenate, 0.12 mM, was raised to 0.41 and 0.89 mM at chloroquine concentrations of 2 and 5 mM, respectively. The corresponding values for brain homogenate were increases from 0.08 mM initially to 0.26 and 056 mM, respectively.

Discussion

The underlying mechanism for the lysosomal storage of several different lipids caused by lysosomotropic drugs is not clearly understood but several hypotheses have been put forward.

1. The drug forms a complex with the lipids, which leads to a delayed hydrolysis of the lipids by lysosomal enzymes. Such complex formation has been demonstrated by NMR both for lecithin and preferentially acidic lipids [13].

2. The drug interacts with the lysosomal enzymes, which leads to diminished enzymic activities.
3. The uptake of the cationic drug in the lysosomes leads to an increase of the intralysosomal pH; increases of more than one pH unit have been demonstrated [14]. Since most of the enzymes have optimum activity at the normal lysosomal pH, pH 4.0, or slightly above, an increase of the intralysosomal pH by one unit leads to a marked decrease of the activities of several lysosomal enzymes.

Since the chloroquine effect on the pH of the lysosomes has been well documented [1,15], we decided to run all the determinations of the enzyme activities at their respective optimum pH values to be able to evaluate whether chloroquine had any effect on the enzyme activities, in addition to increasing the lysosomal pH. We found that the activity of all the lysosomal enzymes examined was reduced to 20–30% of the control activity with chloroquine concentrations which occurred in the lysosomes of chloroquine-treated pigs (fig. 1). However, the actual enzymic activity of the chloroquine-intoxicated mini-pigs within the lysosomes is probably even lower since, in addition to the direct effect of the drug measured above, chloroquine also increased the lysosomal pH by more than one unit, which might have reduced the residual activities of many lysosomal enzymes to less than 10%. This reduction is of the same magnitude found for other lysosomal enzymes by other research groups. Wibo and Poole [16] found that 50 mM chloroquine inhibited cell-free preparation of cathepsin B by 90%. Matsuzava and Hostetler [17] showed that phosholipases A and C were partially inhibited by 200 mM chloroquine. Tager and collaborators [18] reduced the activity of α-galactosidase to 10% by incubating cell homogenates with 100 mM chloroquine.

We expected that chloroquine would cause a non-competitive inhibition of the lysosomal enzymes, as a result of the interaction between the drug and the enzyme. Such interaction leads to a diminution of the V_{max}, which was clearly manifested when the hexosaminidase activity was assayed (Fig. 2). It was more noteworthy that chloroquine caused a pure competitive inhibition when the α-fucosidase activity was assayed with artificial substrate (Fig. 2). These results suggest interaction between substrate and chloroquine. It is, however, difficult to conceive that chloroquine would interact with methylumbelliferyl-α-fucoside and not with the methylumbelliferyl-N-acetyl-β-glucosaminide substrate. Another theoretical possibility is an activation of endogenous substrate in the enzyme preparation by chloroquine. This substrate should then have a very low K_m value. Neither of these explanations seems plausible, and a reasonable interpretation of the phenomenon remains to be found.

The chronic chloroquine treatment led to a significant increase in the α-fucosidase activity in brain and in the activities of β-hexosaminidase, α-fucosidase and acid phosphatase in liver (Table III). In a study by Sly and co-workers [19], chloroquine treatment of normal human fibroblasts was shown to enhance the secretion of newly synthesized lysosomal enzymes, to deplete enzyme binding sites from the cell surface and to inhibit the pinocytosis of the exogenous enzyme. These findings explain how chloroquine, by raising the intralysosomal pH, can disrupt both the intracellular pathway for newly synthesized lysosomal enzymes and the uptake of exogenous enzyme by cell surface receptors. We have now demonstrted that chloroquine, in the concentrations that can be expected in the lysosomes in chloroquine treatment, strongly inhibits two key enzymes in the biodegradation of GM2 and fucogangliosides. All these effects of chloroquine explain the ganglioside storage that we have demonstrated in the nervous system [6] and parenchymatous organs [8] in chloroquine treatment.

Acknowledgements

We are grateful to Dr. Yngve Bergqvist (Department of Clinical Chemistry, Falun Central Hospital, Falun, Sweden) who performed the analyses of chloroquine and its metabolites in the tissues. We also thank Mrs. Inger Härnström and Mrs. Irene Andreasson for skillfull technical assistance and Mrs. Barbro Lundmark for typing the manuscript. The costs of this study have been partially defrayed by the Swedish Medical Research Council (No. 3X-627) and the Medical Faculty, University of Gothenburg.

References

1 De Duve, C., De Barsy, T, Poole, B , Trovet, A , Tulkens, P. and Van Hoof, F. (1974) Biochem. Pharmacol. 23, 2495–2531

2 Goldman, L and Preston, R H. (1957) Am. J Trop Med. 6, 654–657

3 Hobbs, H.E , Sorsby, A. and Freedman, A (1959) Lancet ii, 478–480

4 Whisnant, J.P., Espinosa, R.E., Kierland, R.R. and Lambert, E H (1963) Proc Staff Meet. Mayo Clin. 38, 501–513

5 Gleiser, C A., Bay, W W , Dukes, T.W., Brown, R S , Read, W.K. and Pierce, K.R (1968) Am. J Pathol. 53, 27–45

6 Klinghardt, G W , Fredman, P. and Svennerholm, L (1981) J. Neurochem. 37, 897–908

7 Nilsson, O., Fredman, P , Klinghardt, G W , Dreyfus, H. and Svennerholm, L (1981) Eur. J. Biochem 116, 565–571

8 Fredman, P., Klinghardt, G.W., Nilsson, O. and Svennerholm, L. (1982) Biochem J 201, 581–588

9 Haring, R , Gruhn, R , Smidt, D. and Scheven, B. (1967) Zentralbl Bakteriol. 189, 521–537

10 Svennerholm, L., Håkansson, G., Månsson, J.-E and Vanier, M -T. (1979) Clin. Chim. Acta 92, 53–64

11 Hartree, E F. (1972) Anal. Biochem. 48, 422–427

12 Bergqvist, Y and Domeij-Nyberg, B (1983) J Chromatogr. 272, 137–148

13 Seydel, J.K and Wasserman, O. (1976) Biochem Pharmacol. 25, 2357–2364

14 Reijngoud, D -J and Tager, J.M. (1976) FEBS Lett. 64, 231–235

15 Reijngoud, D -J. and Tager, J.M. (1977) Biochim Biophys. Acta 472, 419–449

16 Wibo, M. and Poole, B. (1974) J. Cell Biol. 63, 430–440

17 Matsuzawa, Y and Hostetler, K Y (1980) J Biol Chem. 255, 5190–5194

18 De Groot, P.G., Elferink, R O., Hollemans, M., Strijland, A., Westerveld, A , Khan, P M. and Tager, J M. (1981) Exp Cell Res. 136, 327–333

19 Gonzales, A., Grubb, J.H., Talkad, V. and Sly, W S (1980) J. Cell Biol. 85, 839–852

20 Svennerholm, L. (1977) Eur J. Biochem 79, 11–21

Biochimica et Biophysica Acta 917 (1987) 9–17
Elsevier

BBA 52315

The uptake of the apoprotein and cholesteryl ester of high-density lipoproteins by the perfused rat liver

Cynthia M. Arbeeny, Vincent A. Rifici and Howard A. Eder

Department of Medicine, Albert Einstein College of Medicine, Bronx, NY 10461 (U S.A)

(Received 14 July 1986)

Key words: HDL; Hepatic receptor; Apolipoprotein A-I, Cholesterol ester; Lipoprotein uptake; (Rat liver)

The uptake of the ^{125}I-labeled apolipoprotein and ^{3}H-labeled cholesteryl ester components of rat apolipoprotein E-deficient HDL by the perfused liver was studied. The uptake of the cholesteryl ester moiety was 4-fold higher than that of apolipoprotein. The concentration-dependent uptake of labeled protein was saturable and competed for by an excess of unlabeled HDL. The uptake of cholesteryl ester was not saturable over the concentration range studied. In the presence of a 50-fold excess of unlabeled HDL, the uptake of both radiolabeled components was decreased by over 75%, indicating that three-quarters of the hepatic uptake of HDL is by a receptor-mediated process. After 15 min of perfusion, 37% of the apolipoprotein radioactivity that was initially bound at 5 min was released into the perfusate as a more dense particle. After 5, 15, 30 and 60 min of perfusion the subcellular distribution of the apolipoprotein and cholesteryl ester components was analyzed by Percoll density gradient centrifugation. Over the 60 min period, there appeared to be transfer of radioactivity from the plasma membrane fraction to the lysosomal fraction. However, the internalization and degradation of cholesteryl ester was more rapid than that of the apolipoprotein. Our findings indicate that there is preferential uptake of HDL cholesteryl ester relative to protein by the liver and that the internalization of these components may occur independently.

Introduction

The liver is the major organ for the uptake of the cholesterol component of high-density lipoproteins [1]. The hepatic removal of cholesterol from HDL may be an important means of clearance of cholesterol from the plasma [2]. It has been shown that HDL cholesterol is preferentially incorporated into biliary sterols [3], and that HDL apolipoproteins are secreted into the bile [4]. A high-affinity binding site for HDL has been identified on the liver cell surface which is distinct from the hepatic LDL and chylomicron remnant receptors [5–7].

Recent studies by Glass et al. [8] indicate that there is a dissociation between the tissue uptake of HDL cholesteryl ester and protein. They found that the uptake of the cholesteryl ether component of reconstituted HDL by cultured hepatocytes was over 4-fold greater than that of apolipoprotein A-I [9]. This finding is in contrast to what has been described for the internalization of LDL and remnant lipoproteins by the liver which involves endocytosis of intact particles and subsequent degradation in the lysosomes [10,11]. However, the

---

Abbreviations: VLDL, very-low-density lipoproteins; LDL, low-density lipoproteins, HDL, high-density lipoproteins, EDTA, ethylenediaminetetraacetic acid; SDS, sodium dodecyl sulfate; LPDS, lipoprotein-deficient serum

Correspondence: Dr Cynthia M. Arbeeny, Albert Einstein College of Medicine, 1300 Morris Park Avenue, Ullmann Building, Room 511, Bronx, NY 10461, U S A

0005-2760/87/$03.50 © 1987 Elsevier Science Publishers B V (Biomedical Division)

processes mediating the internalization and degradation of HDL components by the liver have not been described and are the focus of this study.

Several mechanisms for the selective uptake of cholesteryl ester have been suggested [12–16]. It is possible that HDL binds to the cell surface and cholesteryl esters are preferentially transferred into the cell. Another possibility is that the entire HDL particle is internalized with the apoprotein component being released from the cell. Reaven et al. [15] have shown by morphological methods that in ovarian cells labeled HDL protein remains associated with the plasma membrane and that cholesteryl ester is transferred into the cell from the bound HDL particles. Schmitz et al. [16] have demonstrated that colloidal gold-labeled HDL was internalized by macrophages, but was not transported to lysosomes and was transported back to the cell surface. There is evidence that at least part of the HDL apoprotein is degraded by the liver. Havel et al. [17] have shown that a small fraction of the administered ^{125}I-labeled HDL is degraded by the perfused liver. We have shown that the ionophore monensin, which prevents the movement of ligand from the cell surface to lysosomes, partially inhibits the degradation of HDL apoprotein by hepatocytes [7].

In the present study we have investigated the receptor-mediated uptake of the protein and cholesteryl ester components of apolipoprotein E-deficient HDL by the perfused liver. This system has the advantage of using an intact organ, where the cellular architecture is maintained. We have also studied the internalization of HDL components by subcellular fractionation of the liver in order to elucidate the mechanisms involved in the metabolism of HDL.

Experimental procedures

Animals. Male Sprague-Dawley rats (Marland, Hewitt, NJ) that weighed 300–350 g were used in these studies. All animals were maintained on standard Purina rat chow. Animals were anesthetized with diethyl ether prior to exsanguination and all surgical procedures.

Preparation of radiolabeled HDL. Apolipoprotein E-deficient HDL was isolated from rat serum by a modification [18] of the polyanion precipitation method [19]. The serum lipoproteins that contain apolipoprotein B and apolipoprotein E were removed by precipitation of the rat serum with sodium phosphotungstate (NaPhT) and magnesium chloride. To 20 ml serum, 2.0 ml 4% NaPhT and 0.5 ml 2 M $MgCl_2$ was added and this solution was mixed vigorously. After incubation for 1 h at 20°C the mixture was centrifuged at 1500 × *g* and 20°C for 1 h. The supernatant was removed and dialyzed against 0.85% NaCl and 0.01% EDTA. The density of the supernatnat was adjusted to 1.21 g/ml with KBr and then centrifuged at 100 000 × *g* for 48 h. This HDL subfraction was then radiolabeled in the cholesteryl ester component by the procedure of Roberts et al. [20], in which radiolabeled ester is incorporated into the core of HDL by incubation with the lipid transfer protein present in the lipoprotein-free fraction. Specifically, 500 μCi of 1,2,6,7-^{3}H cholesteryl oleate (2.2 TBq/mmol, NEN Research Products, Boston, MA) was incubated for 45 min at 23°C with 12 ml of human LPDS. This mixture was then incubated for 30 min at 4°C with 3 mg of apolipoprotein E-deficient HDL cholesteryl (1 mg/ml). The density was then adjusted to 1.21 g/ml and the ^{3}H-labeled HDL was re-isolated by centrifugation. The HDL was dialyzed against 0.85% NaCl and 0.01% EDTA and radioiodinated [21] yielding apolipoprotein E-deficient HDL that contained ^{3}H-cholesteryl ester and ^{125}I-labeled apolipoprotein. The distribution of ^{3}H-radiolabel between cholesterol and cholesteryl ester was analyzed by thin layer chromatography [22] and indicated that 98% of the radiolabel was associated with the cholesteryl esters.

The protein content of HDL was determined by a modification [23] of the method of Lowry et al. [24]. Aliquots (50 μg of protein) were dried under vacuum and delipidated for analysis by SDS polyacrylamide electrophoresis utilizing gels with a gradient of 3–27% acrylamide [25]. The SDS-gradient gel analysis is shown in Fig. 1. In lane 1 is the apolipoprotein E-deficient HDL that was labeled with ^{3}H and ^{125}I. This fraction contained apolipoprotein A-IV, apolipoprotein A-I and the C-apolipoproteins. In lane 2 is the total HDL fraction (isolated by centrifugation at a density of 1.063–1.21 g/ml) which contained apolipoprotein E.

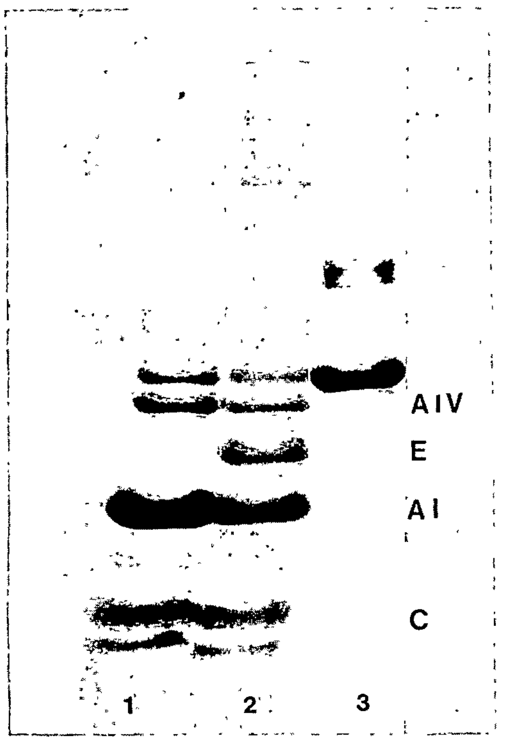

Fig. 1 SDS-gradient gel electrophoresis of rat HDL. An aliquot containing 50 μg of delipidated lipoprotein was applied to each position, except lane 3 which contained 20 μg of bovine serum albumin. Lane 1 is double-labeled apo E-deficient HDL, lane 2 is total rat HDL

The lipid composition of the HDL which was incubated with LPDS or saline alone was determined. Free and esterified cholesterol were assayed by enzymatic methods (Finnsugar Biochemicals, Elks Grove Village, IL). Triglycerides [26] and phospholipids [27] were measured by chemical methods. The results of these determinations are shown in Table I. Both the electrophoretic analysis and chemical composition data indicate that the incubation with LPDS had no effect on the lipid or protein components of the HDL used in these studies.

Liver perfusion. Non-recirculating liver perfusions were performed in situ as previously reported [28]. After a 15 min stabilization period, a bolus of labeled lipoprotein (10–500 μg of protein in 400 μl) was injected into the portal vein cannula in order to measure the concentration-dependent uptake of ^{3}H- and ^{125}I-labeled HDL. In competition studies, a bolus containing radiolabeled HDL (250 μg of protein in 200 μl) and a separate bolus of unlabeled competitor (0.5–12.5 mg in 200 μl) were simultaneously injected. The livers were perfused for an additional 5 min with lipoprotein-free perfusate and then flushed with saline. The livers were homogenized in ice-cold 0.15 M NaCl/0.01 M Tris-HCl (pH 7.6) by six strokes in a Dounce homogenizer using the loose-fitting pestle. The radioactivity from ^{125}I-labeled apolipoprotein that was associated with the liver homogenates was then determined using a gamma counter. The ^{3}H-labeled cholesteryl ester radioactivity was extracted from triplicate aliquots (0.5 ml) of the liver homogenates in 10 ml of chloroform methanol (3 : 1, v/v) and measured by liquid scintillation counting. The ^{3}H radioactivity that was extracted by chloroform-methanol was analyzed by thin layer chromatography [22] to determine the distribution of radiolabel in cholesteryl ester and unesterified cholesterol associated with the liver.

The catabolism of HDL protein and cholesteryl ester was studied over a 1 h interval. A bolus of radiolabeled HDL was injected into the portal vein cannula followed by a 10 min single-pass perfusion of lipoprotein-free perfusate to wash out

TABLE I

CHEMICAL COMPOSITION OF APOLIPOPROTEIN E-DEFICIENT HDL FOLLOWING INCUBATION WITH HUMAN LPDS OR SALINE

Values are percentages by weight.

	Unesterified cholesterol	Cholesteryl ester	Triglyceride	Phospholipid	Protein
HDL + LPDS	2.5	31.3	8.0	17.8	40.4
HDL + saline	3.1	32.0	6.6	17.9	40.3

any unbound lipoprotein. Then 80 ml of fresh perfusate was recirculated through the liver for 1 h. At 15 min intervals after the bolus injection, 250 μl aliquots of perfusate were removed from the reservoir, the erythrocytes were removed by centrifugation and the ^{125}I radioactivity that was soluble and insoluble in 10% trichloroacetic acid was determined. Bile samples were also collected during the entire period and assayed for trichloroacetic acid soluble and insoluble radioactivity from ^{125}I-labeled protein and radioactivity from ^{3}H-labeled cholesteryl ester.

Perfusate was collected after 15 min of perfusion and was concentrated by membrane dialysis in Aquacide (Calbiochem, La Jolla, CA). The density of the solution was then adjusted to 1.21 g/ml using KBr and centrifuged at $100\,000 \times g$ for 48 h. The radioactivities associated with both the $d <$ 1.21 and $d >$ 1.21 fractions were then measured to determine whether the radioactivity associated with the lipoproteins that were present in the perfusate was of the same density as the HDL that was originally injected into the liver. A control experiment was performed in which radiolabeled HDL was reisolated after circulation through the perfusion apparatus in the absence of the liver. The fraction that floated at $d < 1.21$ was then cleared of albumin by recentrifugation and the apolipoprotein constituents were analyzed by SDS gel electrophoresis.

The intracellular distribution of radiolabeled apoprotein and cholesteryl ester in the liver following perfusion with HDL was studied by Percoll (Pharmacia, Piscataway, NJ) density gradient centrifugation by the method of Harford et al. [29]. At 5, 15, 30 and 60 min of perfusion after injection of ^{3}H and ^{125}I-HDL, the livers were rinsed with 50 ml of 0.15 M NaCl/0.01 M Tris-HCl (pH 7.6) and then excised, weighed and placed on ice. All subsequent procedures were performed at 4°C. The livers were homogenized in 3 vol (w/v) of ice-cold 0.28 M sucrose/0.002 M $CaCl_2$/0.01 M Tris-HCl (pH 7.6) using a Dounce homogenizer (12 strokes of the loose fitting pestle and three strokes of the tight fitting pestle). The homogenates were then centrifuged at $300 \times g$ for 15 min and the supernatants were made to be 20% in Percoll. The samples were then centrifuged at $10\,000 \times g$ in a Beckman SW 41 rotor for 45 min. The gradients were fractionated into 0.6 ml fractions by displacement from the bottom with 50% sucrose. The ^{125}I and ^{3}H radioactivity in each of the gradient fractions was determined. The distribution of label between cholesteryl ester and unesterified cholesterol in each gradient fraction was detrmined by thin-layer chromatography. The location in the gradients of the plasma membrane marker enzyme 5′-nucleotidase [30] and the lysosome marker enzyme, β-hexosaminidase [31] were determined.

Results

The concentration-dependent uptake of apolipoprotein E-deficient HDL by the liver was measured to determine saturability of uptake of the radiolabeled components of HDL (Fig. 2). Perfusion of the livers with increasing amounts of radiolabeled HDL resulted in the saturable uptake of the ^{125}I-labeled apolipoprotein indicating that the uptake of HDL is mediated though a limited number of binding sites. The uptake of ^{3}H-cholesteryl ester increased linearly and did not saturate over the concentration range studied. The ^{3}H-labeled cholesteryl ester found in the liver was 4-fold higher than ^{125}I-labeled protein suggesting a dissociation of apolipoprotein and cholesteryl

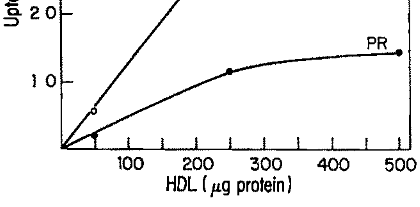

Fig 2. Concentration dependent uptake of HDL protein and cholesteryl ester components. The uptake of the ^{125}I-labeled protein (●– –●) and ^{3}H-labeled cholesteryl ester (O– –O) of apolipoprotein E-deficient HDL by the perfused liver was determined Each point is the mean of three perfusions

ester uptake by the liver. In order to determine receptor-mediated binding, a competition study was performed. Livers were perfused with a constant amount of radiolabeled HDL protein and an increasing amount of unlabeled HDL (Fig. 3). At a 50-fold excess of unlabeled HDL the uptake of apolipoprotein was decreased by 75% and cholesteryl ester was decreased by 77%, indicating that three-quarters of the hepatic uptake of HDL is receptor mediated.

In another study, a recirculating perfusion was used to mesure the degradation of HDL. After 15 min of perfusion 37% of the radioactivity that was initially bound at 5 min was present in the perfusate (Fig. 4). After 30 min this value represented 56% of that which was initially bound. At subsequent times there was no additional release of radioactivity into the perfusate. Of all the radioactivity present in the perfusate at 15 min, 93% was insoluble in 10% trichloroacetic acid, suggesting that this radioactivity represented undegraded HDL that was released from the liver. When the perfusate was centrifuged at a density of 1.21 g/ml, 32% of the protein radioactivity floated at this density. In a control experiment where HDL was recirculated through the perfusion apparatus in the absence of the liver and then reisolated by ultracentrifugation, 92% of the radioactivity floated at a density of 1.21 g/ml. SDS gel electrophoresis showed that the HDL that was released by the liver and present in the perfusate had a similar apolipoprotein distribution as the reisolated control HDL, indicating that there is no selective removal of any individual apoprotein.

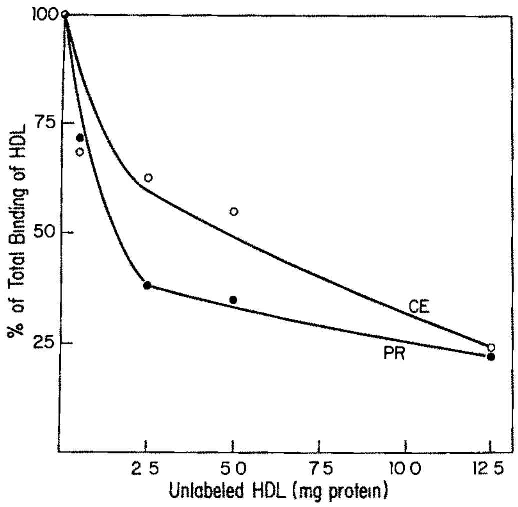

Fig. 3 Competition for the uptake of HDL protein and cholesteryl ester Livers were perfused with 250 μg of HDL protein and the uptake of ^{125}I-labeled protein (●--●) and ^{3}H-cholesteryl ester (O--O) was determined in the absence and presence of increasing amounts of unlabeled HDL. Each point is the mean of three perfusions

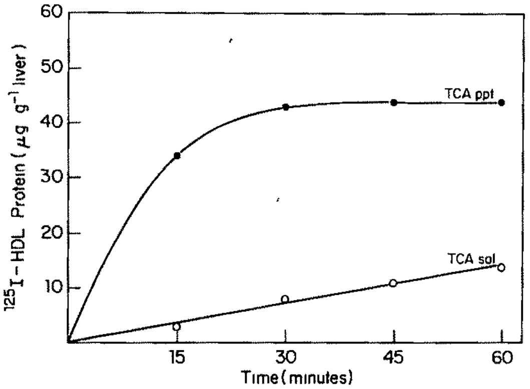

Fig. 4. Release of ^{125}I radioactivity into the perfusate. Livers were perfused with 250 μg of double labeled HDL and the accumulation of ^{125}I radioactivity that was trichloroacetic acid-insoluble (●--●) and soluble (O--O) was determined over a 60 min period.

During a 60 min recirculating perfusion, there was a linear increase of radioactivity in the perfusate that was soluble in 10% trichloroacetic acid. This finding suggests that some of the HDL protein is internalized and degraded within the lysosomes. After 15 min of perfusion less than 5% of the radiolabeled cholesteryl ester was present in the perfusate and remained constant over the next 45 min of perfusion. Thus it appears that more cholesteryl ester than protein is internalized and that the released HDL that was found in the perfusate is depleted in cholesteryl ester. After 60 min of perfusion the apoprotein and cholesteryl ester radioactivity that was present in the bile was minimal and represented 6.5% and 1.0% of the total uptake at 5 min of perfusion (data not shown).

The association of the protein and cholesteryl ester components of HDL after internalization by the liver with the plasma membrane and lysosomes was determined after centrifugation on Percoll density gradients (Fig. 5 and 6). The activity

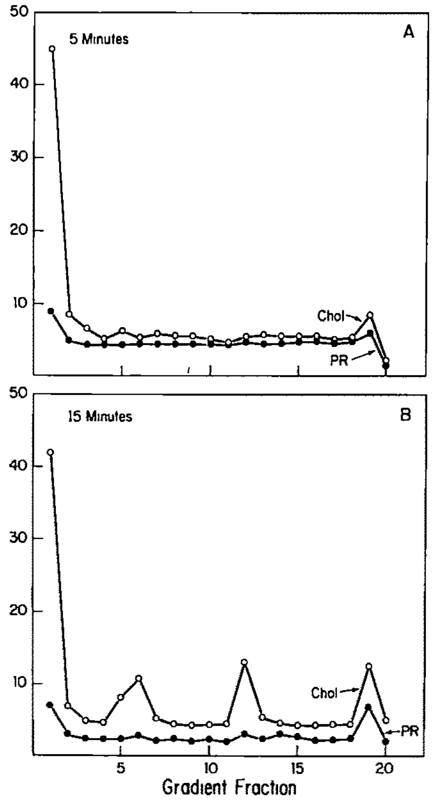

Fig. 5 Percoll density gradient analysis of internalized components of HDL after 5 (A) and 15 (B) min of perfusion. The ^{125}I-labeled protein (●- -●) and ^{3}H-labeled cholesterol (○- -○) radioactivity was determined for each gradient fraction Each time point is representative of three perfusions

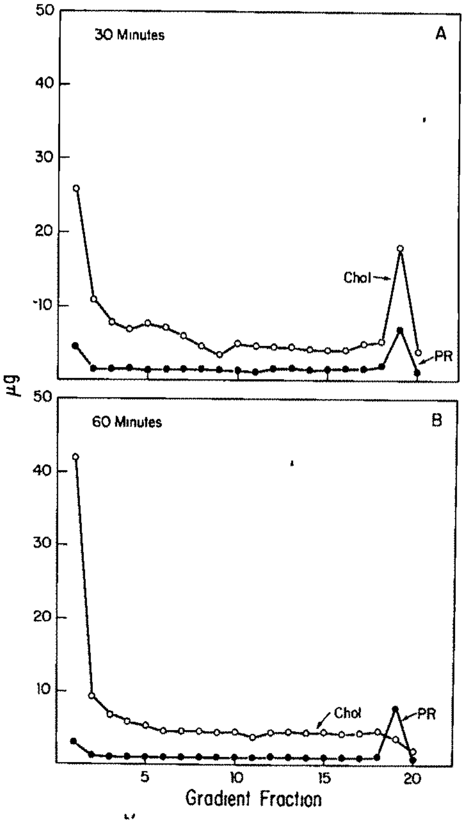

Fig 6 Percoll density gradient analysis of internalized components of HDL after 30 (A) and 60 (B) min of perfusion The ^{125}I-labeled protein (●- -●) and ^{3}H-labeled cholesterol (○- -○) radioactivity was determined Each time point is representative of three perfusions

for the plasma membrane marker, 5′-nucleotidase, was found in fraction 1, and the activity of the lysosome marker β-hexosaminidase, was found in fraction 19. Throughout the 60 min period, greater than 98% of the ^{125}I radioactivity in the gradient fractions was insoluble in 10% trichloroacetic acid, indicating that the radioactivity was still protein bound. At all times there was more cholesteryl ester than protein present in the liver. During the 60 min of perfusion, there appeared to be transfer of radioactivity from the plasma membrane to the lysosome fraction. However, cholesteryl ester transferred from the plasma membrane to the lysosome fraction more rapidly.

At 5 min after the injection of radiolabeled HDL, both labels were largely associated with the plasma membrane fraction (Fig. 5A). At this time there was 4-times more cholesteryl ester radioactivity than protein associated with the plasma membrane fraction. Lipid analysis by thin layer chromatography indicated that 97% of the ^{3}H-label in all gradient fractions was present as cholesteryl ester. After 15 min of perfusion (Fig. 5B), ^{3}H radioactivity was associated with the plasma membrane fraction, an intermediate density fractions as well as with the lysosomal fraction. At this time 96% of the ^{3}H-label was found as cholesteryl ester. ^{125}I-labeled protein radioactivity was decreased in the plasma membrane fraction and increased in the lysosomal fraction.

Both the ^{125}I and ^{3}H radioactivity in the plasma membrane fraction was diminished at 30 min (Fig. 6A), and at this time the ^{3}H radioactivity in the lysosomes was 2-fold higher compared to ^{125}I-labeled apoprotein. Of the ^3H radioactivity, 76% and 81% of the radioactivity associated with the plasma membrane fraction and lysosomal fraction was as cholesteryl ester. After 60 min of perfusion (Fig. 6B), there still appeared a small amount of ^{125}I-labeled apolipoprotein that was associated with the lysosomes, while all of the ^3H was associated with the plasma membrane fractions. Half of the ^3H-label was as cholesteryl ester and half was found as unesterified cholesterol. These results indicate a preferential uptake of cholesteryl ester from HDL by the liver and a more rapid movement of cholesteryl ester to the lysosomes compared to HDL apoprotein. In addition, there appears to be hydrolysis of the cholesteryl ester and appearance of unesterified cholesterol in the plasma membrane.

Discussion

Our results indicate that there is selective hepatic uptake of HDL cholesteryl ester relative to apoprotein and that the internalization and degradation of these components may occur independently. The uptake of the radiolabeled apolipoprotein was saturable and competed for by an excess of unlabeled HDL. The data indicate that 77% of the uptake is by a receptor mediated process. The uptake of radiolabeled cholesteryl ester was 4-fold higher than the uptake of apoprotein. These results are consistent with other studies which indicate that there is selective uptake of HDL cholesteryl ester by hepatocytes [8,9] and steroidogenic cells [8,12]. In contrast to what was found for apolipoprotein uptake, the uptake of cholesteryl ester by the liver did not saturate over the concentration range studied.

The results of the competition study show that in the presence of a 1-fold excess of unlabeled HDL, competition for the uptake of protein and cholesteryl ester were similar and may be due to the contribution of the nonspecific binding to the total binding. At a 1–25-fold excess of unlabeled HDL, the uptake of protein was competed for to a greater extent than was the cholesteryl ester, indicating that the uptake of protein saturates at a lower concentration than cholesteryl ester. At a 50-fold excess of unlabeled HDL, the competition for the uptake of both components was equal. This result suggests that the saturation of the capacity for uptake of cholesteryl ester occurs at a higher concentration than protein. Glass et al. [9] have also shown using rat hepatocytes that although the absolute uptake of cholesteryl ester was higher than protein, the degree of competition was similar at higher concentrations of unlabeled HDL. It is still unclear whether the binding of HDL apolipoprotein to the receptor is required for the uptake of cholesteryl ester.

In this study we observed that a fraction of the HDL that was initially bound was released from the surface of the hepatocyte into the perfusate. This particle was more dense than the initial starting material and may have been depleted of cholesteryl ester. This is consistent with the finding of Bachorik et al. [13] who showed that in cultured pig hepatocytes a portion of the ^{125}I-labeled HDL that was initially bound was internalized and a portion was modified at the cell surface and then released as a more dense lipoprotein. Bamberger et al. [32] has suggested that hepatic lipase, by its phospholipase activity, shifts the equilibrium of cholesterol between HDL and the plasma membrane resulting in the net delivery of cholesterol to the cell by a surface-transfer process. Reaven et al. [15] have shown using radioautography that in the luteunized ovary perfused in situ, HDL is not internalized as an intact particle. They showed that the protein moiety remained associated with the plasma membrane and speculate that the cholesterol is transferred to a specialized region of the plasma membrane. Others have suggested [16] that the HDL is internalized by the cell and the cholesterol is removed before the particle is returned to the exterior. This process of retroendocytosis has been visualized for the uptake of HDL colloidal gold conjugates by macrophages. Whether HDL is internalized by the liver as an intact particle is still not known. However, our results suggest that the dissociation of the HDL components may occur at the hepatocyte surface.

In the present study we have used apolipoprotein E-deficient HDL in order to exclude binding of HDL by the apolipoprotein E receptor. However, Quarfordt et al. [33] have shown that there was substantially greater uptake of apolipoprotein E-rich HDL than apolipoprotein E-deficient HDL by the perfused liver and suggest that apo E-rich HDL plays an important role in the return of cholesterol to the liver for subsequent metabolism. In a previous study [7] we have found that apo A-I was more effective than apo E in competing for the binding of HDL which contained apolipoprotein E, indicating that both apolipoprotein A-I and apolipoprotein E are ligands for the binding of HDL. It is possible that apolipoprotein E-rich HDL may be metabolized, in part, by a similar pathway mediating the intracellular processing of apolipoprotein E-deficient HDL.

The results of the Percoll density gradient analyses show that there was transfer of radioactivity from the plasma membrane to the lysosome fraction and that the movement of HDL cholesteryl ester to lysosomes was more rapid than protein. This finding suggests that the internalization and degradation of HDL constitutents may occur independently. We have previously shown [7] that the presence of monensin, an ionophore that inhibits receptor recycling, inhibited the degradation of ^{125}I-labeled HDL protein by isolated hepatocytes. Pittman et al. [14] using adrenal cells, found that chloroquine and monensin reduced apolipoprotein A-I uptake by 62% but reduced cholesteryl ester uptake by less than 25%. This suggests that the selective uptake of cholesteryl ester is by a mechanism different from that for protein.

Our results indicate that both HDL protein and cholesteryl ester are degraded within lysosomes, although the degradation of protein occurs more slowly. In contrast to our previous liver perfusion studies with ^{125}I-labeled VLDL remnants (Arbeeny, C.M., Rifici, V.A., Handley D.A. and Eder, H.A. unpublished observations), the rate of degradation of rat ^{125}I-labeled HDL was 4-fold slower than that of remnants. Using Percoll density gradient analyses to study the intracellular movement of ^{125}I-labeled VLDL remnants, we found that the movement of remnants to lysosomes occurred more rapidly than that of ^{125}I-labeled HDL. In a recent publication Bachorik et al. [13] reported that the ^{125}I-labeled HDL protein that was internalized by cultured pig hepatocytes was degraded by lysosomes at a rate that was half that of LDL. The reason for the slower delivery of HDL to lysosomes remains to be evaluated, but may explain the low rate of degradation of ^{125}I-labeled HDL by the perfused liver previously reported by Sigurdsson et al. [17].

Our findings suggest that internalized cholesteryl ester is processed in part by lysosomal hydrolases. However, since we found free cholesterol in the membrane fractions of the gradient, some cholesteryl ester may be metabolized at the plasma membrane and degraded by a cytosolic neutral sterol ester hydrolase [34]. Nestler et al. [35] found that treatment of ovarian cells with cholorquine and NH_4Cl which inhibit lysosomal hydrolysis, had little effect on the metabolism of HDL sterol esters. It is possible that there may be an intracellular partitioning of the HDL cholesterol within the hepatocyte. Previous studies have suggested that HDL cholesterol in preference to LDL cholesterol is the source for biliary cholesterol [3]. Robins et al. [26] have suggested that lipoprotein cholesterol may be transported directly from the plasma membrane of the hepatocyte to the bile canaliculus without equilibrating with newly synthesized intracellular cholesterol. The concept that intracelluar lipid transfer may be a highly specific process has been put forth by several investigators [37–39] and a sterol carrier protein present in the rat liver cytosol has been implicated in the intracellular transfer of cholesterol among organelles [40].

The results of these studies indicate that the binding, internalization and degradation of the apoprotein and cholesteryl ester components of HDL by the liver is a more complex process than that described for LDL and remnants of triglyceride-rich lipoproteins which are transported to the lysosomes as intact particles. Further study is necessary to elucidate the pathways that mediate the hepatic uptake of HDL.

Acknowledgements

The authors gratefully acknowledge the excellent technical assistance of Diane Edelstein and Craig Bliss. This study was supported by Research Grant HL 26817 from the National Institutes of Health and an Established Fellowship Award from the American Heart Association-New York City Affiliate (CMA).

References

1 Glass, C, Pittman, R.C, Keller, G A and Steinberg, D (1968) J. Biol. Chem 258, 7161–7167

2 Glomset, J A (1968) J Lipid Res. 9, 155–167

3 Schwartz, C.C, Halloran, L.G., Vlahcevic, Z.R, Gregory, D.H and Swell, L (1978) Science 200, 62–64

4 Sewell, R B., Mao, S.J.T, Kawamoto, T. and LaRusso, N.F (1983) J. Lipid Res. 24, 391–401

5 Bachorik, P.S., Franklin, F A., Virgil, D G and Kwiterovich, P.O. (1982) Biochemistry 21, 5675–5684

6 Soltys, P A, Portman, O W. and O'Malley, J.P. (1982) Biochim Biophys Acta 713, 300–314

7 Rifici, V.A and Eder, H A. (1984) J Biol. Chem. 259, 13814–13818

8 Glass, C, Pittman, R C, Weinstein, D B and Steinberg, D. (1983) Proc. Natl Acad. Sci. USA 80, 5435–5439

9 Glass, C., Pittman, R C, Civen, M and Steinberg, D (1985) J Biol Chem. 260, 744–750

10 Handley, D.A, Arbeeny, C M., Eder, H.A. and Chien, S. (1981) J. Cell. Biol. 90, 778–787

11 Jones, A.L., Hradek, G.T, Hornick, C., Renaud, G, Windler, E.E T and Havel, R.J (1984) J Lipid Res. 25, 1151–1158

12 Gwynne, J.T. and Hess, B. (1980) J Biol Chem 255, 10875–10883

13 Bachorik, P.S, Franklin, F.A., Virgil, D G. and Kwiterovich, P.O. (1985) Arteriosclerosis 5, 142–152

14 Pittman, R.C., Knecht, T P and Taylor, C A. (1985) Circulation 72, 377

15 Reaven, E., Chen, Y-D.I., Spicher, M. and Azhar, S (1984) J Clin. Invest. 74, 1384–1397

16 Schmitz, G, Robenek, H., Lohmann, U. and Assmann, G. (1985) EMBO J 4, 613–622

17 Sigurdsson, G, Noel, S P. and Havel, R.J (1979) J. Lipid Res. 20, 316–324

18 Arbeeny, C M. and Eder, H.A. (1983) J. Lipid Res 24, 1457–1467

19 Burstein, M., Scholnik, H.R and Morfin, R (1980) J Lipid Res. 11, 583–595

20 Roberts, D.C.K, Miller, N.E., Crook, D, Price, S.L., Cortese, C., LaVille, A., Masan, L. and Lewis, B (1985) Biochem J. 226, 319–322

21 Bilheimer, D.W, Eisenberg, S and Levy, R.J (1972) Biochim. Biophys Acta 260, 212–221

22 Chen, C H and Albers, J J (1983) Biochim Biophys Acta 753, 40–46

23 Sata, T, Havel, R J. and Jones, A.L. (1972) J Lipid Res 13, 757–768

24 Lowry, O.H, Rosebrough, N J., Farr, A.L. and Randall, R.J (1951) J. Biol. Chem 193, 265–275

25 Swaney, J B and Kuehl, K S (1976) Biochim Biophys Acta 446, 561–565

26 Fletcher, M.J. (1968) Clin. Chim Acta 22, 393–397

27 Norton, W.T and Autilio, L A (1966) J. Neurochem. 13, 213–222

28 Arbeeny, C.M and Rifici, V.A. (1984) J Biol. Chem. 259, 9662–9666

29 Harford, J., Wolkoff, A W., Ashwell, G. and Klausner, R D (1983) J. Cell Biol. 96, 1824–1828

30 Widnell, C C. and Unkeless, J.C (1968) Proc. Natl. Acad. Sci. USA 61, 1050–1057

31 Hall, C W., Liebars, I, DiNatale, P and Neufeld, E.F (1978) Methods Enzymol. 50, 439–456

32 Bamberger, M., Lund-Katz, S., Phillips, M.C. and Rothblat, G H. (1985) Biochemistry 24, 3693–3701

33 Quarfordt, S, Hanks, J., Jones, R S. and Shelburne, F (1980) J. Biol. Chem 255, 2934–2937

34 Khoo, J.C, Drevon, C A and Steinberg, D (1979) J Biol Chem. 254, 1785–1787

35 Nestler, J.E, Bamberger, M., Rothblat, G H and Strauss, III, J.F (1985) Endocrinology 117, 502–510

36 Robins, S.J, Fasulo, J.M Collins, M.A. and Patton, G.M (1985) J Biol. Chem 260, 6511–6513

37 Dempsey, M.E., McCoy, K.E., Baker, H N, Dimitriadou-Vafiadou, A, Lorsback, T and Howard, J.B, (1981) J. Biol. Chem. 256, 1867–1873

38 Gavey, K.L, Noland, B.J and Scallen, T J (1981) J Biol. Chem. 256, 2993–2999

39 Wetterau, J R and Zilversmit, D B. (1984) J Biol Chem 259, 10863–10866

40 Chanderbhan, R, Noland, B.J., Scallen, T J and Vahouny, G (1982) J. Biol Chem 257, 8928–8934

Biochimica et Biophysica Acta 917 (1987) 18–23
Elsevier

BBA 52316

Purinoceptor agonists stimulate phosphatidylcholine secretion in primary cultures of adult rat type II pneumocytes

Alasdair M. Gilfillan and Seamus A. Rooney

Division of Perinatal Medicine, Department of Pediatrics, Yale University School of Medicine,
P.O Box 3333, New Haven, CT 06510 (U S.A.)

(Received 22 April 1986)

Key words Lung surfactant; Adenosine, ATP, Purinergic system; Phosphatidylcholine secretion; (Rat type II cell)

We examined the effect of purinoceptor agonists on phosphatidylcholine secretion in primary cultures of type II pneumocytes from adult rats. Surfactant is a major product of the type II cell and phosphatidylcholine is its principal component. Adenosine, AMP, ADP and ATP stimulated phosphatidylcholine secretion in a concentration-dependent manner. At the optimum concentration (1 mM), adenosine and AMP stimulated phosphatidylcholine secretion more than 2-fold, while ATP stimulated 5-fold and ADP almost 7-fold. Because of the magnitude of the response it is tempting to speculate that secretion of surfactant may be under purinoceptor regulation. None of these agents influenced cellular phosphatidylcholine synthesis or lactate dehydrogenase release into the medium, so the effects were primarily on secretion and were not secondary to effects on synthesis or cell damage. Non-metabolizable analogs of adenosine, 5′-*N*-ethylcarboxyamidoadenosine (NECA) and L-N^6-phenylisopropyladenosine (L-PIA), stimulated secretion to the same extent as adenosine and the effect of NECA was antagonized by 8-phenyltheophylline, suggesting a P_1 purinoceptor-mediated mechanism. The stimulatory effect of ATP was diminished by α,β-methylene ATP but only slightly by 8-phenyltheophylline, suggesting that, although part of the ATP effect could be explained by catabolism to adenosine, the P_2 purinoceptor may also be involved in regulation of surfactant secretion.

Introduction

Lung surfactant, material which is believed to play a vital role in maintaining alveolar stability, is synthesized and secreted by the type II pneumocyte, one of the two cells lining the alveolus [1]. There is evidence that cholinergic and β-adrenergic agonists and prostaglandins have regulatory roles in surfactant secretion in vivo [1,2]. Phosphatidylcholine is the major component of surfactant and secretion of phosphatidylcholine in cultured type II cells has been reported to be stimulated by leukotrienes [3], by agents such as β-adrenergic agonists [4–6], cholera toxin [7] and forskolin [8], which elevate cAMP levels and are believed to act via cAMP-dependent protein kinase, and by agents such as 12-*O*-tetradecanoylphorbol-13-acetate [9] and 1-oleoyl-2-acetyl-*sn*-glycerol [10] which act via protein kinase C. Recently, evidence has accumulated for purinergic regulation of a variety of physiologic systems [11–13]. There are data which suggest the presence of purinoceptors in the lung [14] but it is not known if they play a role in surfactant production. To begin to address this question we examined the effects of adenosine and adenosine 5′-phosphates on phosphatidylcholine secretion in

---

Correspondence address: Dr A Rooney, Yale Department of Pediatrics, P.O. Box 3333, New Haven, CT 06510, U S A

0005-2760/87/$03.50 © 1987 Elsevier Science Publishers B V (Biomedical Division)

cultured type II pneumocytes from adult rat lung. An abstract of this work has been published [15].

Experimental procedures

Type II pneumocytes were isolated from the lungs of adult male Sprague-Dawley rats (approx. 175 g) by a modification of the procedure of Brown and Longmore [5] as described previously [16]. This method involves purification of the cells by passage through a discontinuous albumin density gradient and preferential attachment on plastic culture dishes.

For secretion studies, the freshly isolated cells were plated at a density of $3.5 \cdot 10^6$ cells per dish and cultured for 18–20 h in 1.5 ml Dulbecco's modified Eagle's medium containing [*methyl*-^{3}H]choline chloride (2 μCi/ml), 10% fetal bovine serum, streptomycin (100 μg/ml) and penicillin (100 U/ml). The cells were rinsed with fresh serum- and antibiotic-free medium to remove [^{3}H]choline and unattached cells. At this stage approx. $1 \cdot 10^6$ cells remained attached of which at least 95% were type II cells. After a 30 min preincubation in the fresh medium the test agents were added and the incubation continued. After 90 min, or various periods in the case of the time course experiments, the medium was aspirated, the cells lysed with ice-cold water and lipids extracted from both cells and medium with chloroform and methanol [16]. Phosphatidylcholine was separated from the other phospholipids by thin layer chromatography [3] and its radioactivity measured by liquid scintillation counting [17]. Secretion was expressed as the amount of [^{3}H] phosphatidylcholine in the medium as a percentage of that in the cells plus medium.

The rate of [*methyl*-^{3}H]choline incorporation into phosphatidylcholine was measured to assess effects on phosphatidylcholine synthesis. After the 18–20 h culture period the cells were incubated with [*methyl*-^{3}H]choline in the presence and absence of the test compounds and cellular [^{3}H] phosphatidylcholine was measured as described previously [3,18]. To assess cellular integrity, the activity of lactate dehydrogenase (EC 1.1.1.27) in the cells and medium was measured [17] after exposure to the test compounds.

Rats were purchased from Charles River (Kingston, NY), tissue culture medium from Grand Island Biological Co. (Grand Island, NY), fetal bovine serum from Hyclone (Logan, UT), [*methyl*-^{3}H]choline from New England Nuclear (Boston, MA), terbutaline sulfate (Brethine) from Geigy (West Caldwell, NJ), 8-phenyltheophylline, 5′-*N*-ethylcarboxyamidoadenosine (NECA), L-*N*^{6}-phenylisopropyladenosine (L-PIA), adenine, ADP (di{monocyclohexylammonium} salt), α,β-methylene ATP (lithium salt), other nucleosides and nucleotides (free bases or sodium salts) and other biochemicals from Sigma (St. Louis, MO).

Results

Addition of adenosine, AMP, ADP and ATP to the culture medium stimulated phosphatidylcholine secretion in primary cultures of type II pneumocytes. The stimulatory effect was dependent on concentration in the range 10 nM–1 mM (Fig. 1). At 1 mM, the concentration which produced the maximum effect, adenosine and AMP stimulated phosphatidylcholine secretion approx. 2-fold, while ATP stimulated 5-fold and ADP almost 7-fold

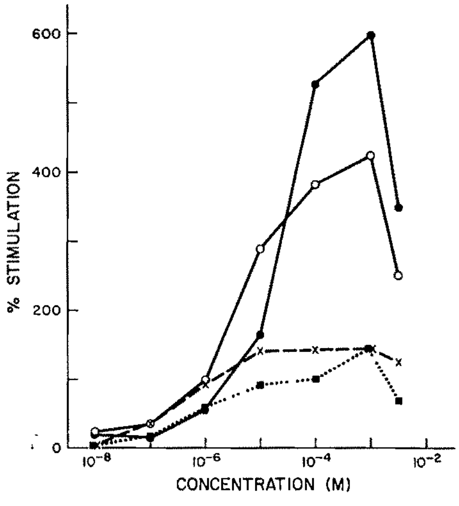

Fig. 1. The effect of different concentrations of adenosine, AMP, ADP and ATP on phosphatidylcholine secretion in type II pneumocytes The cells were cultured in the presence or absence of the indicated concentration of agonist for 90 min, after which [^{3}H]phosphatidylcholine in the cells and medium was measured. Stimulation is expressed as a percentage increase over the rate in the absence of agonist. The data are means from 3–6 experiments. ■ · · · ■, adenosine; × — — — ×, AMP; ● —— ●, ADP; ○ —— ○, ATP

TABLE I

EFFECTS OF ADENOSINE, AMP, ADP, ATP AND TERBUTALINE ON PHOSPHATIDYLCHOLINE SECRETION IN CULTURED TYPE II PNEUMOCYTES

Cells were incubated with and without the indicated test compound for 90 min, after which [^{3}H]phosphatidylcholine in the cells and medium was measured. Secretion is expressed as the amount of [^{3}H]phosphatidylcholine in the medium as percentage of the total (cells plus medium). The concentration of terbutaline (0.036 mM) was supramaximal [19]. All other concentrations were 1 mM. The data are means ±S.E. from the number of experiments indicated (n). The data were analysed statistically with Student's two-tailed t test for paired samples.

	n	Percent [^{3}H]phosphatidylcholine secreted		Treated/ control	P
		control	treated		
Adenosine	6	0.91±0.06	2.19±0.26	2.41	< 0.005
AMP	4	0.87±0.07	2.09±0.09	2.40	< 0.002
ADP	4	0.84±0.05	5.65±0.34	6.73	< 0.002
ATP	5	0.84±0.04	4.32±0.35	5.14	< 0.001
Terbutaline	11	0.90±0.04	1.77±0.07	1.97	< 0.001

(Table I). The EC$_{50}$ values (concentration which produced 50% of the maximum effect) for adenosine, AMP, ADP and ATP calculated from the data in Fig. 1 were 5.3, 0.6, 23.0 and 4.1 μM, respectively. In comparison, terbutaline stimulated phospatidylcholine secretion approx. 2-fold (Table I). This is similar to the stimulatory effect on phosphatidylcholine secretion previously reported for this and other β-adrenergic agonists in type II cells [4,5].

As shown in Table II none of the agents stimulated cellular phosphatidylcholine synthesis as

TABLE II

EFFECTS OF ADENOSINE, AMP, ADP, AND ATP ON THE RATE OF [^{3}H]CHOLINE INCORPORATION INTO PHOSPHATIDYLCHOLINE AND ON LACTATE DEHYDROGENASE RELEASE IN CULTURED TYPE PNEUMOCYTES

Cells were incubated with [*methyl*-^{3}H]choline in the presence and absence of the test compound (1 mM) for 2 h, after which [^{3}H]phosphatidylcholine in the cells and lactate dehydrogenase in the medium were measured. Choline incorporation is expressed as cpm/10^6 cells per h and lactate dehydrogenase as percent of the total (cells plus medium) released into the medium per h. The data are means ±S.E from the number of experiments indicated (n)

Agonist	Choline incorporation (n = 3)	Lactate dehydrogenase release (n = 4)
Control	3510±630	1.61±0.19
Adenosine	3550±456	1.53±0.21
AMP	3800±490	1.54±0.21
ADP	3260±360	1.55±0.21
ATP	3880±498	1.33±0.33

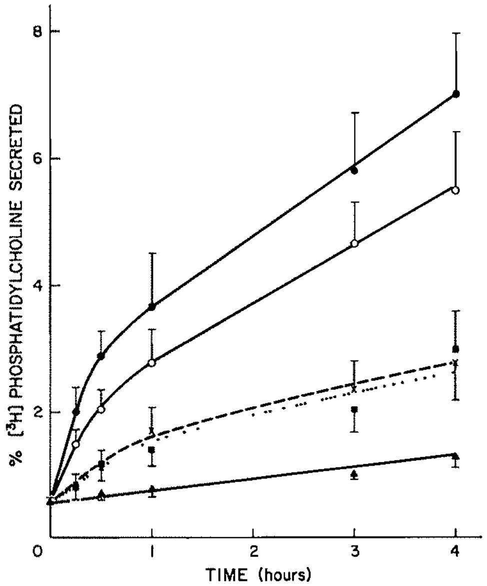

Fig. 2. The effect of adenosine, AMP, ADP and ATP on [^{3}H]phosphatidylcholine secretion in type II pneumocytes. The cells were cultured in the presence or absence of 1 mM agonist for the times indicated, after which [^{3}H]phosphatidylcholine in the cells and medium was measured. Secretion is expressed as the percentage of total phosphatidylcholine in the medium. The data are means ±S.E (bar) from 4 experiments ▲——▲, control; ■·····■, adenosine, ×———×, AMP; ●——●, ADP; ○——○, ATP.

TABLE III

EFFECTS OF ADDITIONAL PURINE AND PYRIMIDINE DERIVATIVES ON PHOSPHATIDYLCHOLINE SECRETION IN CULTURED TYPE II PNEUMOCYTES

Cells were incubated with and without the indicated test compound and [^{3}H]phosphatidylcholine secretion was measured as described in Table I. The concentration of terbutaline was 0.036 mM. All other concentrations were 1 mM. Each value was the mean derived from 2–4 culture dishes. In each experiment cells from 11 rats were distributed among the control and all treatment groups. The data are means ± S.E. from 5 experiments and were analysed statistically with Student's *t* test for paired samples. Significant differences from the control were determined from Sidak's multiple *t* test tables [20]. n.s., not statistically significant ($P > 0.05$)

	Percent [^{3}H]phosphatidylcholine secreted	Treated/ control	*P*
Control	0.96±0.06		
Terbutaline	1.79±0.15	1.86	< 0.05
ADP [a]	4.75±0.18	4.95	< 0.05
Adenine	0.85±0.04	0.89	n.s.
Guanosine	1.01±0.05	1.05	n.s.
Inosine	1.29±0.08	1.34	< 0.05
Cytidine	1.15±0.11	1.20	n.s
2′-AMP	1.94±0.12	2.02	< 0.01
3′-AMP	1.96±0.09	2.04	< 0.01
GDP	1.02±0.04	1.06	n.s
CDP	1.01±0.05	1.05	n.s.
UPD	1.91±0.18	1.99	< 0.05
TDP	1.07±0.07	1.11	n.s.

[a] Three experiments

measured by the rate of choline incorporation or increased release of lactate dehydrogenase into the medium. The stimulatory effects were, therefore, primarily on secretion and were not secondary to effects on synthesis or cellular injury.

Effects on secretion as a function of time are shown in Fig. 2. As reported previously by us [3,17] and others [4,5], basal secretion was linear with time for at least 4 h. Adenosine and adenosine phosphates caused an initial rapid stimulation of secretion in the first 30 min followed by a slower rate of stimulation over the next 3.5 h. The stimulatory effects, however, were apparent at all times examined. Similar time courses were reported for the stimulatory effects of terbutaline [4], 1-oleoyl-2-acetyl-*sn*-glycerol [10] and leukotriene E_4 [3] on phosphatidylcholine secretion in type II cells.

To determine whether the stimulation was a specific effect of adenosine and adenine nucleotides we examined the effects of other purine and pyrimidine nucleosides and nucleoside 5′-diphosphates. We also examined the effects of inosine, the deamination product of adenosine metabolism, as well as of adenine, 2′-AMP and 3′-AMP. For comparison, we included terbutaline and ADP in this experiment. The results (Table III) show that with the exception of a small effect of inosine the other nucleosides tested had no effect on phosphatidylcholine secretion. UDP did stimulate secretion but its effect was considerably less than that of ADP. The other nucleoside diphosphates tested did not stimulate. Adenine had no effect but 2′-AMP and 3′-AMP were as effective was 5′-AMP.

As shown in Table IV the non-metabolizable adenosine analogs, L-PIA and NECA, also stimulated phosphatidylcholine secretion. In preliminary experiments (data not shown) the effects of these agonists were dependent on concentration. At 0.01 mM, NECA and L-PIA were at least

TABLE IV

EFFECTS OF ADENOSINE, AMP, AND THE NON-METABOLIZABLE ANALOGS OF ADENOSINE, L-PIA AND NECA, ON PHOSPHATIDYLCHOLINE SECRETION IN CULTURED TYPE II PNEUMOCYTES

Cells were incubated with and without the indicated test compound (0.01 mM) for 90 min, after which [^{3}H]phosphatidylcholine secretion was measured. Other details as in Table I.

	n	Percent [^{3}H]phosphatidylcholine secreted		Treated/ control	*P*
		control	treated		
Adenosine	6	0.91±0.06	1.73±0.19	1.90	< 0.01
AMP	4	0.87±0.07	2.03±0.11	2.33	< 0.005
L-PIA	6	0.95±0.21	2.10±0.41	2.21	< 0.005
NECA	12	0.93±0.07	2.20±0.18	2.37	< 0.001

TABLE V

EFFECT OF 8-PHENYLTHEOPHYLLINE AND α,β-METHYLENE ATP ON THE STIMULATORY EFFECTS OF NECA AND ATP ON PHOSPHATIDYLCHOLINE SECRETION IN TYPE II CELLS

Cells were incubated with the agonists and secretion of [^{3}H]phosphatidylcholine was measured as described in Table I. 8-Phenyltheophylline and α,β-methylene ATP were added 5 and 30 min, respectively, prior to the agonist. The concentrations were: NECA, 0.001 mM; 8-phenyltheophylline, 0.01 mM; ATP and α,β-methylene ATP, 0.1 mM. Stimulation is expressed as percentage increase over the rate in the absence of agonist. 8-Phenyltheophylline alone had no effect on phosphatidylcholine secretion but α,β-methylene ATP stimulated 29% from 1.10 ± 0.09 (percent of total phosphatidylcholine in the medium) to 1.43 ± 0.12. Secretion in control dishes containing α,β-methylene ATP was therefore used to determine the percent stimulation in the presence of ATP plus α,β-methylene ATP. Statistical details as in Table I.

Antagonist	Agonist	n	Percent stimulation		+ Antagonist/ − antagonist	P
			− antagonist	+ antagonist		
8-Phenyltheophylline	NECA	4	105 ± 12	61 ± 8	0.58	< 0.025
	ATP	8	227 ± 26	182 ± 26	0.80	< 0.025
α,β-Methylene ATP	ATP	7	202 ± 6	96 ± 12	0.47	< 0.001

as stimulatory as adenosine and AMP (Table IV). These data, as well as the fact that adenine and inosine had little or no stimulatory effects (Table III), suggest that the effect of adenosine is not mediated by an adenosine metabolite. Since methylxanthines are competitive antagonists of P_1 receptors [11], we examined the effect of 8-phenyltheophylline on the stimulatory effects of NECA and ATP. As shown in Table V, 8-phenyltheophylline reduced the stimulatory effect of NECA by over 40%. It also reduced the stimulatory effect of ATP to a small, although significant, extent. This suggests that at least part of the stimulatory effect of ATP is mediated via a P_1 receptor. Since α,β-methylene ATP has been reported to selectively desensitize P_2 receptors in some systems [11], we examined the effect of this agent on the stimulatory effect of ATP on phosphatidylcholine secretion in type II cells. As shown in Table V, α,β-methylene ATP reduced the stimulatory effect of ATP by over 50%. Thus the effect of ATP is likely to be mediated at least in part by P_2 receptors.

Discussion

This is the first report that the purinoceptor agonists adenosine, AMP, ADP and ATP stimulate phosphatidylcholine secretion in type II pneumocytes. Gilfillan et al. [21] briefly reported that 1 mM ATP stimulated phosphatidylcholine secretion in a perifused lung slice model but did not examine other adenosine derivatives and did not speculate on whether this might be a purinoceptor-mediated effect. Ekelund and Enhorning [22] reported that the phosphodiesterase inhibitor enprofylline, but not theophylline, stimulated surfactant secretion in fetal rabbits and postulated that the difference in the effects of these two xanthine derivatives is due to the fact that theophylline is also an adenosine antagonist while enprofylline is not.

Purinoceptors have been divided into two subgroups: P_1 receptors are more responsive to adenosine and AMP than to ADP and ATP, while the reverse applies to the P_2 receptor [11,12,23]. Both the P_1 and P_2 receptors have been further subdivided based on differential effects of agonists in a variety of tissues [23]. Based on their effects on phosphatidylcholine secretion where ADP > ATP > AMP = adenosine, our data suggest mediation by the P_2 receptor. However, this is not supported by the EC_{50} values, since the order of potency was AMP > ATP $\geqslant$ adenosine > ADP. Since the non-metabolizable adenosine analogs L-PIA and NECA were at least as stimulatory as adenosine and AMP, and the stimulatory effect of NECA was diminished by the P_1 antagonist 8-phenyltheophylline, it is likely that at least some of the effects are mediated by P_1 receptors. It could be argued that the effects of AMP, ADP and ATP are due to metabolism to adenosine which then acts at a receptor site. However, since AMP was more potent than adenosine while ADP and ATP produced a much greater response, this possibility is unlikely. The fact that the stimulatory effect of ATP was diminished by α,β-methylene ATP suggests that the effect of this agonist is mediated at least in part by a P_2 receptor. This is also supported by the finding that the effect of ATP was diminished to a much smaller extent than that of NECA by 8-phenyltheophylline.

β-Adrenergic agonists and other agents which act via cAMP-dependent protein kinase were reported to stimulate phosphatidylcholine secretion 2–3-fold in type II cells isolated from rat [4–8,19] and human [24] lung. In the same systems, agents which are believed to act via protein kinase C were reported to stimulate phosphatidylcholine secretion 3.5–8.4-fold [4,7,9,10,24]. The response produced by ADP and ATP in the present study was therefore of the same order as that produced by agents acting via protein kinase C, while the effects of adenosine and AMP were more similar to those of agents acting via cAMP-dependent protein kinase.

Further studies are required to determine precisely which purinoceptor type or subtype mediates the observed effects. It is possible that more than one receptor may be involved. In a number of systems the A_2 subtype of the P_1 receptor has been linked to activation of adenylate cyclase and increased intracellular cAMP levels [11,14]. Whether the purinoceptor-mediated effect on secretion also involves cAMP-dependent protein kinase, protein kinase C or another mechanism needs to be established.

A variety of agents influence lung surfactant secretion in a number of different models and there is evidence that at least some of them are involved in the physiologic regulation of surfactant production [1,2]. In view of the magnitude of the response in comparison with other physiologic mediators of surfactant secretion it is tempting to speculate on such a role for purinoceptor agonists. Whether they do play such a role, however, must be established in a more physiologically appropriate model than isolated cells in culture.

Acknowledgement

This work was supported by a grant (HL-31175) from the National Heart, Lung and Blood Institute, United States Public Health Service.

References

1 Hollingsworth, M and Gilfillan, A.M (1984) Pharmacol Rev 36, 69–90
2 Rooney, S A (1985) Am Rev. Respir. Dis. 131, 439–460
3 Gilfillan, A M and Rooney, S.A (1986) Biochim. Biophys Acta 876, 22–27
4 Dobbs, L.G. and Mason, R.J (1979) J Clin Invest 63, 378–387
5 Brown, L A.S. and Longmore, W J (1981) J. Biol. Chem 256, 66–72
6 Mettler, N.R., Gray, M.E., Schuffman, S and LeQuire, V S (1981) Lab. Invest. 45, 575–586
7 Mescher, E J., Dobbs, L.G and Mason, R.J (1983) Exp Lung Res 5, 173–182
8 Rice, W.R., Hull, W.M, Dion, C A, Hollinger, B A. and Whitsett, J A. (1985) Exp Lung Res. 9, 135–149
9 Dobbs, L.G. and Mason, R.J. (1978) Am Rev Respir. Dis. 118, 705–713
10 Sano, K, Voelker, D R and Mason, R.J (1985) J. Biol Chem. 260, 12725–12729
11 Burnstock, G. and Buckley, N J. (1985) Methods Pharmacol 6, 193–212
12 Satchell, D (1984) Trends Pharmacol Sci. 5, 340–343
13 Daly, J.W. (1982) J Med Chem 25, 197–207
14 Ukena, D, Schirren, C G., Klotz, K N and Schwabe, U (1985) Naunyn-Schmiedeberg's Arch Pharmacol 331, 89–95
15 Rooney, S A and Gilfillan, A.M. (1986) Fed. Proc 45, 1665
16 Gilfillan, A.M., Chu, A J, Smart, D.A. and Rooney, S.A (1983) J. Lipid Res. 24, 1651–1656
17 Gilfillan, A.M. and Rooney, S A (1985) Biochim. Biophys. Acta 833, 336–341
18 Gilfillan, A.M., Chu, A J and Rooney, S.A. (1984) Biochim. Biophys Acta 794, 269–273
19 Gilfillan, A M., Lewis, A J. and Rooney, S A (1986) Fed. Proc 45, 1665
20 Rohlf, F.J and Sokal, R R. (1981) Statistical Tables, 2nd Edn., pp. 84–96, Freeman, New York
21 Gilfillan, A M., Hollingsworth, M. and Jones, A.W (1983) Br J Pharmacol 79, 363–371
22 Ekelund, L. and Enhorning, G. (1985) Pediatr. Res 19, 1000–1003
23 Gordon, J.L. (1986) Biochem. J 233, 309–319
24 Robinson, P.C, Voelker, D.R. and Mason, R.J (1984) Am Rev. Respir Dis 130, 1156–1160

Biochimica et Biophysica Acta 917 (1987) 24–32
Elsevier

BBA 52430

Some properties and subcellular distribution of acyl-coenzyme A: retinol acyltransferase activity in rat testes *

Lala R. Chaudhary ** and Eldon C. Nelson

Department of Biochemistry, Okalahoma Agricultural Experimental Station, Oklahoma State University, Stillwater, OK 74078 (U.S.A.)

(Received 5 August 1986)

Key words: Acyl-CoA : retinol acyltransferase; Acyltransferase, (Rat testis)

The present study was conducted to examine esterification of retinol by testicular microsomes. The microsomes were isolated from rat testes and were incubated under varying assay conditions with [^{3}H]retinol. [^{3}H]Retinylpalmitate was identified by reversed-phase high-performance liquid chromatography as an esterified product. The rate of esterification was increased by the addition of a fatty acyl-CoA. Coenzyme A esters of oleic, palmitic and stearic acids were equally effective substrates for retinol esterification. A 17-fold increase was observed in the presence of palmitoyl-CoA when microsomes had been pretreated with hydroxylamine, a reagent that reacts with coenzyme A thioesters to form hydroxamic acids. The esterifying activity was stimulated by the addition of dithiothreitol (4 mM) and fatty acid-free bovine serum albumin (1 mg/ml). The optimal concentrations for retinol and palmitoyl-CoA were 40 μM and 30–40 μM, respectively. The enzyme activity was inhibited by *p*-hydroxymercuribenzoate, sodium taurocholate and 5,5′-dithiobis-(2-nitrobenzoic acid), but not by EDTA. The enzyme activity was highest in microsomes (36%). However, some activity was present in mitochondria (29%). These results clearly show the presence of a fatty acyl-CoA : retinol acyltransferase that catalyzes the esterification of retinol in rat testes.

Introduction

Vitamin A is stored in the liver primarily as retinyl palmitate. Vitamin A esters are hydrolyzed before retinol is transported from the liver to peripheral target tissues as the retinol–retinol-binding protein-transthyretin complex which is a highly regulated process [1]. Although vitamin A is known to be essential for the maintenance of normal testicular development and function, and a specific requirement for retinol for the maintenance of normal spermatogenesis has been well established [2], its molecular mechanism of action is not yet known. In recent years much progress has been made in the area of enzymology of vitamin A, particularly the retinyl ester hydrolase [3–5] and retinol esterifying enzymes [6–9] in various animal tissues. However, no information is available about the nature of these enzymes in rat testes, a target tissue for vitamin A. In continuation of our work on the metabolism of vitamin A and related retnoids, we have recently shown the in vivo formation of various retinyl esters from [^{3}H]retinyl acetate injected directly into testes suggesting the presence of retinol esterifying enzyme

---

* Article number J-4851 of the Oklahoma Agricultural Experiment Station.

** Present address: Department of Biochemistry, Texas Tech University Health Sciences Center, Lubbock, TX 79430, U.S.A.

Correspondence: Dr. E.C Nelson, Department of Biochemistry, Okalhoma Agricultural Experiment Station, Oklahoma State University, Stillwater, OK 74078, U.S.A

0005-2760/87/$03.50 © 1987 Elsevier Science Publishers B.V. (Biomedical Division)

in rat testes [10]. Our preliminary studies showed that the addition of coenzyme A thioester of fatty acids enhanced the rate of retinol esterification by microsomes from rat testes and some of the results have been communicated in abstract form [11]. These observations prompted us to investigate further whether testicular microsomes can catalyze retinol esterification.

In this manuscript we describe the optimal assay conditions, some of the characteristics and subcellular distribution of a fatty acyl-CoA : retinol acyltransferase in rat testes.

Materials and Methods

[15-^{3}H(N)]Retinol (specific activity, 13.6 Ci/mmol) was purchased from New England Nuclear (Boston, MA, U.S.A.). Before use, radioactive retinol was purified by HPLC on reversed-phase Partisil PXS 10/25 ODS-2 column with methanol : water (90 : 10) at a flow rate of 1.0 ml/min (retention time, 17 min). Both labeled and unlabeled retinol were stored in ethanol at −80°C. Retinol (type X), bovine serum albumin (essentially fatty acid-free), dithiothreitol, butylated hydroxytoluene, hydroxylamine hydrochloride, disodium ethylenediaminetetraacetate (EDTA), 5,5′-dithiobis-(2-nitrobenzoic acid), succinic acid disodium hexahydrate, *p*-hydroxymercuribenzoate sodium salt, *p*-chloromercuriphenylsulfonic acid monosodium salt (*p*-CMPS), potassium cyanide, rotenone, sodium taurocholate, palmitoyl-CoA, oleoyl-CoA, stearoyl-CoA, *p*-nitrophenyl acetate, cytochrome *c* type III, β-nicotinamide adenine dinucleotide phosphate, reduced form (NADPH), *p*-iodonitrotetrazolium violet Grade I, were obtained from Sigma Chemical Company. Glass distilled residue-free solvents of HPLC grade were used for extractions and HPLC.

Male Sprague-Dawley Holtzman rats weighing 240–270 g (Charles River Breeding Labs, Inc., Wilmington, MA, U.S.A.) were used. Rats were sacrificed by cervical dislocation under light diethylether anaesthesia.

Isolation of subcellular fractions. After removing the tunica albuginea, the testes were immediately homogenized in 3 vols. of 0.25 M sucrose buffered with 0.01 M potassium phosphate buffer (pH 7.4) containing 1 mM EDTA in a glass vessel with a motor-driven Teflon pestle. Microsomes and subcellular fractions were isolated by differential ultracentrifugation according to the method described previously [12]. The homogenates were filtered through four layers of cheesecloth. The nuclear fraction was pelleted by centrifuging the homogenate at 800 × *g* for 10 min in a Sorvall RC 2-B centrifuge. The nuclear pellet was rehomogenized and recentrifuged as above. Both post-nuclear supernatant fractions were combined and centrifuged for 10 min at 11 000 × *g* to pellet mitochondrial fractions. The resulting supernatant fraction was further centrifuged at 110 000 × *g* for 90 min in a Beckman Model L5-65 ultracentrifuge with Ti75 rotor to obtain the microsomal fraction. The microsomal pellet was suspended in 0.15 M potassium phosphate buffer (pH 7.4) and stored at −80°C.

Assay of acyl-CoA : retinol acyltransferase activity. The enzyme activity was assayed according to the method described previously [8] with slight modifications. The incubation mixture consisted of 20 nmol [^{3}H] retinol (250 000–300 000 dpm) dispersed in 10 μl ethanol, 500 μg bovine serum albumin (essentially fatty-acid-free), 20 nmol palmitoyl-CoA, 2 μmol dithiothreitol and 100–150 μg microsomal protein in a final volume of 0.5 ml in 0.15 M potassium phosphate buffer (pH 7.4). The addition of microsomes started the reaction after 5 min of preincubation at 37°C in a shaking water bath. After 10 min incubation, the reactions were terminated by the addition of 1 ml ethanol containing 100 μg butylated hydroxytoluene/ml. To each tube 4 ml hexane was added and, after shaking, 0.8 ml water was added to obtain a clear hexane upper phase and lower aqueous ethanol phase. The hexane layer was removed and the extraction was repeated twice with 4 ml hexane each time to obtain maximum recovery (85–95%). The hexane extracts were combined, dried under a stream of nitrogen and redissolved in a known amount of acetonitrile : methanol (50 : 50, v/v). A known amount of the sample was used for separation of retinol and retinyl palmitate by HPLC. The activity was expressed as pmol retinol esterified after subtraction of values for incubations with boiled microsomes. All procedures with vitamin A compounds were carried out under gold light or in the dark.

Pretreatment of microsomes with hydroxylamine. Because CoA thioesters are known to react with hydroxylamine at neutral pH to form hydroxamic acids, the microsomes were pretreated with hydroxylamine to determine whether this treatment might reduce the ability of microsomes to esterify retinol in the absence of exogenous fatty acyl-CoA. Hydroxylamine hydrochloride in water was adjusted to pH 7.4 with NH_4OH and diluted to 2.5 M as described by Ross [6]. Frozen microsomes were thawed and diluted to 2.5 mg protein/ml in 0.15 M phosphate buffer. 1 ml of this microsomal suspension and 0.25 ml hydroxylamine solution were mixed and incubated at 37°C for 20 min, then diluted with 7 ml cold 0.15 M phosphate buffer (pH 7.4) and centrifuged at 4°C for 30 min at 40000 r.p.m. in a Beckman L5-65 ultracentrifuge in a Ti 75 rotor. The supernatant solution was discarded and pellets were rinsed with 4 ml phosphate buffer which was also discarded. The pellet was then homogenized in 5 ml of cold phosphate buffer and recentrifuged as above. The final washed pellets were homogenized in a small volume of phosphate buffer and stored at $-80°C$ until used for enzyme assay. In another experiment, the hydroxylamine was replaced by the buffer and used with the same treatment protocol as described above.

Enzyme assay. The following marker enzymes were assayed: Succinic dehydrogenase (E.C. 1.3.99.1) for mitochondrial fraction [13], rotenone-insensitive NADPH-cytochrome *c* reductase (EC 1.6.2.3) was measured in the presence of 0.15 μM rotenone by following the reduction of cytochrome *c* at 550 nm at $23 \pm 1°C$ [14] and carboxyl esterase (EC 3.1.1.1) was measured with *p*-nitrophenyl acetate as substrate by following the increased extinction at 400 nm at $23 \pm 1°C$ [15] for the microsomal fraction.

Protein was determined by the method of Lowry et al. [16] with bovine serum albumin (Fraction V powder, Sigma) as the standard.

All HPLC separations were performed on a system previously described [17] with a 6-port sample injector (Valco Instruments Co., Houston, TX, USA). The reversed-phase octadecylsilane (ODS) columns used were Partisil PXS ODS-2 and ODS-3, 10/25, 4.6 mm i.d. × 25 cm (Whatman Inc., Clifton, NJ, U.S.A.). All columns were protected by precolumns 2 mm i.d. × 2 cm length (Upchurch Scientific, Inc., Oak Harbor, WA, U.S.A.) packed with Co : Pell ODS. Internal standards were detected by their absorbance at 340 nm. Solvent composition for the separation of samples is described in the figure legends.

Fractions (1 ml) were collected from the column in 7-ml vials, and 5 ml scintillation fluid (Insta-Gel, Packard Instrument Company, Inc., Downers Grove, IL, U.S.A.) was added to each vial. The radioactivity was measured and corrected for quenching with a Model PO-1 PRIAS liquid scintillation spectrometer (Packard Instrument Company, Inc., Downers Grove, IL, U.S.A.).

Results

In the present study, the reaction product, retinyl palmitate and the substrate ([^{3}H]retinol) remaining after enzymatic reaction were separated and identified by HPLC as shown in Fig. 1. In one of the experiments the authenticity of the product was further confirmed by collecting the retinyl palmitate peak, subjecting it to alkaline ethanol

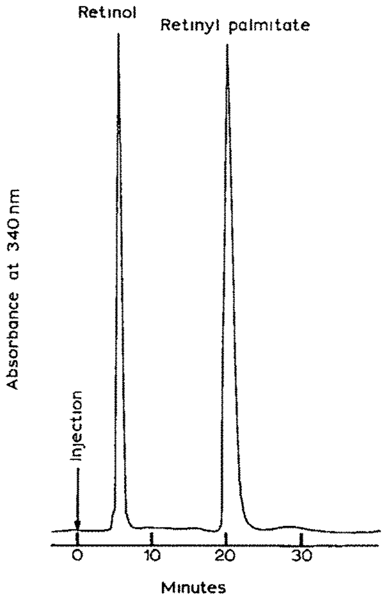

Fig. 1 The HPLC profile of a mixture of retinol and retinyl palmitate separated on a Partisil PXS 10/25 ODS-3 (4 6 mm i.d × 25 cm) column with acetonitrile/methanol (55:45) at a flow rate of 1 ml/min

hydrolysis, extracting and separating by HPLC. As shown in Fig. 2, all radioactivity comigrated with retinol. A negligible amount of radioactivity comigrated with retinyl palmitate when [^{3}H]retinol was incubated with heat-inactivated microsomes and served as control (Fig. 2A). These data not only provided evidence that the retinol esterification occurred during incubations with microsomes and not after their heat-inactivation, but also that the product comigrated with authentic retinyl palmitate and its formation was dependent on the presence of both retinol and palmitoyl-CoA.

Initial experiments were performed to determine what exogenous substrates and/or supplements are needed for the retinol esterification by testicular microsomes. The addition of fatty acyl-CoA, dithiothreitol, and bovine serum albumin to incubation mixture enhanced retinyl ester synthesis (Table I).

TABLE I

EFFECT OF DELETING ESSENTIAL COMPONENTS ON RETINOL ESTERIFICATION BY MICROSOMES FROM RAT TESTES

The complete system consists of 20 nmol of [^{3}H]retinol (250000–300000 dpm), 500 μg of bovine serum albumin-fatty acid free, 20 nmol of palmitoyl-CoA, 2 μmol of dithiothreitol and 135 μg of microsomal protein in a final volume of 0 5 ml in 0.15 M phosphate buffer (pH 7.4) The individual essential components as indicated, were omitted from the incubation mixture The values given are means ± S.D ($n = 4$).

	Percent enzyme activity
Complete system	100 [a]
(A) Palmitoyl-CoA	40.0 ± 13 0
(B) Dithiothreitol	53.0 ± 10 4
(C) Bovine serum albumin	51 0 ± 5.1
(D) (A, B and C)	25 7 ± 0 3

[a] Retinyl ester formed (236 pmol/mg protein per min)

Studies were conducted to define further the optimal conditions for the enzyme assay. As shown in Fig. 3, the rate of retinyl ester formation was linear with time for 10 min, but progressed with time for 30 min. A linear relationship was found between retinol esterification and microsomal protein and the optimal concentration was in the range of 100–130 μg/0.5 ml incubation mixture. The enzyme activity was stimulated by the addition of bovine serum albumin and dithiothreitol and optimal concentrations were 1 mg/ml and 4 mM, respectively. When microsomes were heated in a water bath at 70°C for 20 min, the enzyme

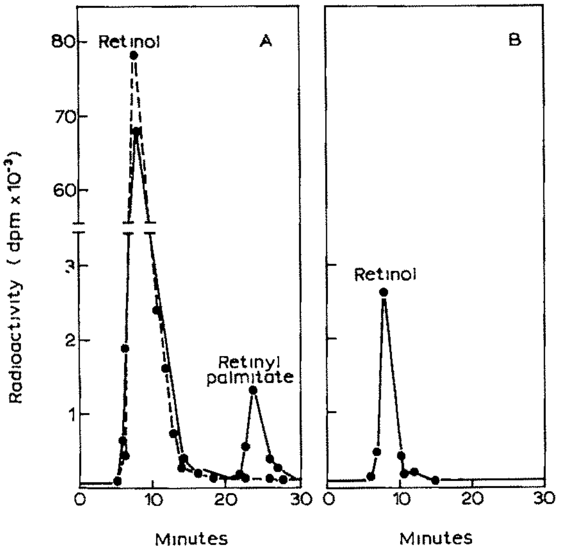

Fig 2 Enzymatic formation of [^{3}H]retinylester from [^{3}H]retinol and palmitoyl-CoA by rat testicular microsomes (A) The incubation mixture contained normal (———) and heat-inactivated (- - - - -) microsomes. Incubation time was 30 min The lipid extracts of the incubation mixtures were separated by HPLC as described in the legends of Fig. 1. (B) The [^{3}H]retinyl palmitate peak was collected (Fig 2A) and was subjected to alcoholic KOH hydrolysis The lipid extracts were separated by HPLC as described above

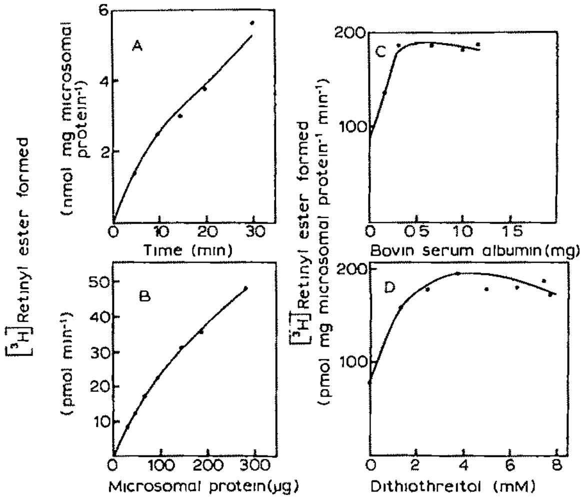

Fig. 3 The effect of time (A), concentration of microsomal protein (B), bovine serum albumin (C), and dithiothreitol (D) on retinol esterification by testicular microsomes

activity was completely abolished. This strongly indicates that testicular tissue contains the acyl-CoA : retinol acyltransferase activity. Maximal rate of esterification was obtained when retinol concentration was 30–40 μM and further increase was inhibitory (Fig. 4A). The acyl-CoA : retinol acyltransferase activity increased by the addition of palmitoyl-CoA and 40 μM was found to be optimal concentration (Fig. 4B).

To answer the question why there was a consistent formation of some retinyl esters by microsomes without the addition of exogenous fatty acyl-CoA, we treated microsomes with hydroxylamine hydrochloride, a reagent known to react with CoA thioesters to form hydroxamates at neutral pH [18,19]. Microsomes from testes pretreated with hydroxylamine were incubated with [^{3}H]retinol under optimal assay conditions in the absence or presence of palmitoyl-CoA. As shown in Table II, hydroxylamine-treated and buffer-treated microsomes could esterify 14 pmol/mg protein per min and 83 pmol/mg protein per min, respectively, a 6-fold decrease in the enzyme activity by the pretreatment of microsomes with hydroxylamine. When exogenous palmitoyl-CoA was added to the incubation mixture, a 17-fold increase in the esterification of retinol was observed in the hydroxylamine-treated microsomes, but with buffer-treated microsomes, only a 4-fold enhancement was seen. These results strongly suggested the presence of an endogenous pool of fatty acyl-CoA in rat testes and provide sufficient evidence that the retinol esterification observed in the absence of exogenous palmitoyl-CoA was due to the presence of the endogenous pool of fatty acyl-CoA.

Experiments were conducted to determine the fatty acid specificity of the retinol esterifying enzyme reaction. Coenzyme A esters of oleic, palmitic and stearic acids were incubated with testicular microsomes pretreated with hydroxylamine. No difference in retinol esterification was observed and each fatty acyl-CoA was an equally effective substrate for the enzyme activity (oleoyl-CoA, 191 ± 1.4 pmol/mg protein per min; palmitoyl-CoA, 194 ± 14.9; stearoyl-CoA, 180 ± 10.6; $n = 2$).

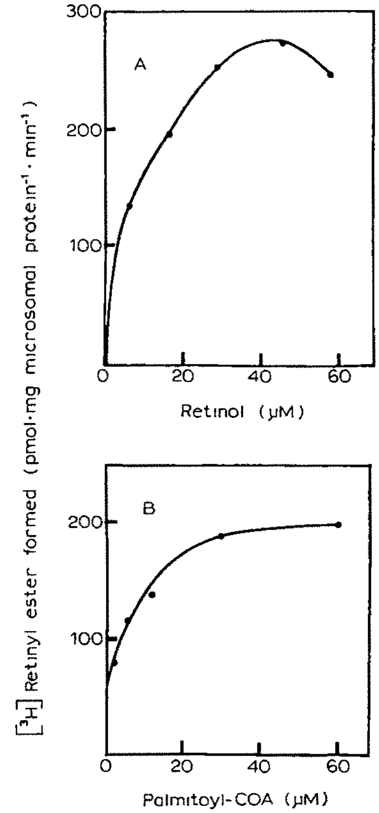

Fig 4 The effect of concentration of retinol (A) and palmitoyl-CoA (B) on retinol esterification by testicular microsomes.

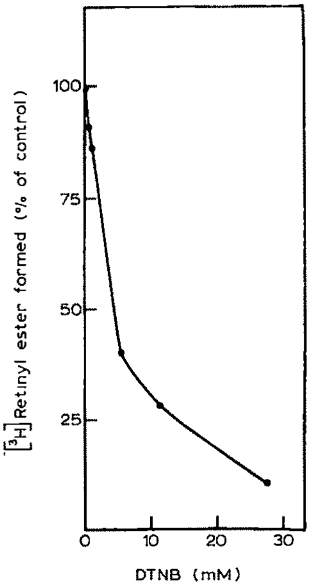

Fig 5 The effect of 5,5′-dithiobis-(2-nitrobenzoic acid) on the acyl-coenzyme A : retinol acyltransferase activity. The inhibitor was added in buffer before start of preincubation

TABLE II

EFFECT OF PRETREATMENT OF MICROSOMES ON THE ESTERIFICATION OF RETINOL

Rat testicular microsomes were treated with hydroxylamine or buffer. Values given are means ± S.D. of duplicate determinations.

Pretreatment of microsomes	Additions or omissions	Retinylester formed (pmol/mg protein per min)	Increase in the presence of acyl-CoA
Buffer	without palmitoyl-CoA	83 ± 8.7	
	with palmitoyl-CoA	303 ± 0.5	3.7-fold
Hydroxylamine	without palmitoyl-CoA	14 ± 0.3	
	with palmitoyl-CoA	232 ± 0.1	16.6-fold

TABLE III

SUBCELLULAR DISTRIBUTION OF ACYL-CoA RETINOL ACYLTRANSFERASE AND SOME MARKER ENZYMES IN SUBCELLULAR FRACTIONS ISOLATED FROM RAT TESTES

The data are from subcellular fractions isolated from four pooled testes. N, nuclear; M, mitochondrial; P, microsomal fractions; S, cytosol. The values given are means ± S.D. ($n = 4$).

Enzyme	Relative distribution of enzyme activity in percent of total activity (N + M + P + S)			
	N	M	P	S
Acyl-coenzyme A : retinol acyltransferase	20.6 ± 2.1	28.8 ± 1.6	36.3 ± 0.8	14.3 ± 2.7
Succinic dehydrogenase	33.7 ± 4.6	49.9 ± 0.3	6.9 ± 0.4	9.6 ± 0.4
NADPH-cytochrome *c* reductase	22.6 ± 3.42	29.9 ± 1.4	44.8 ± 1.5	4.1 ± 2.5
Carboxylesterase	7.4 ± 0.7	24.2 ± 4.3	63.0 ± 3.1	5.5 ± 1.8
Protein	23.3 ± 2.9	15.6 ± 0.5	15.4 ± 0.9	45.7 ± 2.6

TABLE IV

EFFECTS OF SOME ENZYME INHIBITORS ON THE ACYL-COENZYME A:RETINOL ACYLTRANSFERASE ACTIVITY

The enzyme inhibitors were added in buffer before preincubation. Values given are means ± S.D. of duplicate determinations.

Additions	Concentration (mM)	Retinylester formed (pmol/mg protein per min)	Enzyme activity (% of control)
None (control)	–	266 ± 10.5	100
p-Hydroxymercuribenzoate	2.0	168 ± 27.4	63
	6.0	66 ± 1.1	25
p-Chloromercuriphenylsulfonic acid	2	201 ± 5.0	76
	6	25 ± 2.8	9
	10	16 ± 5.0	6
Ethylenediaminetetraacetic acid	2	251 ± 2.8	94

The results in Table III show the distribution of acyl-CoA : retinol acyltransferase activity in subcellular fractions isolated from homogenates of total testicular tissue and known marker enzymes for mitochondrial and microsomal fractions. The acyl-CoA : retinol acyltransferase activity was 36% of the total activity in the microsomal fraction, whereas mitochondria contained 29% of the total activity.

The effect of various enzyme inhibitors, sulfhydryl blocking reagents, a chelator of divalent cations and a detergent, on the esterification of retinol was studied. *p*-Hydroxymercuribenzoate sodium salt, *p*-chloromercuriphenylsulfonic acid monosodium salt and 5,5′-dithiobis-(2-nitrobenzoic acid) inhibited the enzyme activity, suggesting that the reduced sulfhydryl groups are required either for the enzyme or its thioester substrate, fatty acyl-CoA (Table IV and Fig. 5). Addition of sodium taurocholate to incubation mixture markedly inhibited the retinyl ester formation by testicular microsomes and the inhibition was essentially complete at 8 mM concentration (Fig. 6).

Discussion

The main objective of this study was to demonstrate the presence of retinol-esterifying enzyme in rat testes and to investigate whether the esterification of retinol by testicular microsomes is catalyzed by a fatty acyl-CoA : retinol acyltransferase, like the esterification of cholesterol (acyl-CoA : cholesterol acyltransferase, EC 2.3.1.26) and other lipids or perhaps by a different type of reaction such as transesterification [12,20–23]. Our results have demonstrated for the first time the presence of acyl-CoA : retinol acyltransferase in rat testes, the enzyme catalyzing the esterification of retinol through the transfer of fatty acyl moiety from fatty acyl-CoA to retinol. Direct evidence came when [^{3}H]retinol was incubated with hydroxylamine-treated microsomes and enzyme activity increased 17-fold by the addition of palmitoyl-CoA. Thus, the basal enzyme activity observed in the absence of untreated microsomes was due to the presence of a fatty acyl-CoA pool in rat testes. Retinol esterification increased by addition of bovine serum albumin and dithiothreitol but the extent and kinetics were slightly different than observed in other tissues where either the increase was greater or the requirement was absolute [6–9]. The exact mechanism by which bovine serum albumin stimulated the retinol esterification is not clear; however, there are few possibilities: (i) the enzyme inhibition by long-chain fatty acyl-CoA at a concentration above their critical micellar concentration may be reversed by albumin due to its binding capacity and thus the molar ratio of acyl-CoA to albumin may be critical for the enzyme activity; or (ii) vitamin A is unstable in aqueous solutions and there is some evidence that bovine serum albumin may bind retinol and thereby increase its stability, but with hydroxyl group still free for enzymatic reaction or further metabolic transformation.

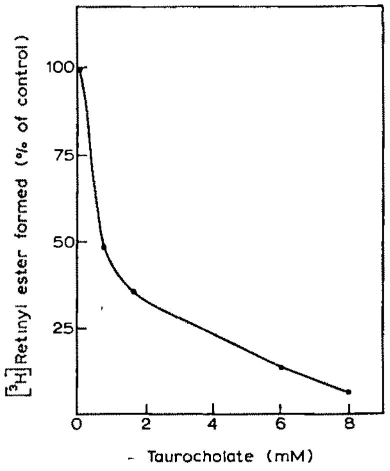

Fig. 6 The effect of taurocholate on the acyl-coenzyme A : retinol acyltransferase activity. The inhibitor was added in buffer before start of preincubation

Observations from several laboratories have established that the esterification of triacylglycerols, phospholipids, cholesterol [12,20–23] and retinol [6–9] takes place in microsomes of various tissue and organs. The esterification is generally catalyzed by acyl-CoA transferases using coenzyme A thioesters of fatty acids. The acyl-CoA : retinol acyltransferase activity in testes was mainly localized in testicular microsomes but significant activity was present in the mitochondrial fraction. The subcellular distribution of acyl-CoA : retinol acyltransferase has not been reported in other tissues. Our data on subcellular distribution of marker enzymes were in good agreement with the results reported by others [24]. It is still less certain whether acylation may occur at additional subcellular sites such as plasma membranes or mitochondria. However, acyltransferase activity has been reported in outer membrane of rat liver mitochondria which was not due to microsomal contamination [25–27] and in plasma membrane [28]. Therefore, whether the retinol esterification by subcellular fractions other than microsomal from rat testes is due to contamination of these fractions with microsomes or the activity is associated with mitochondria, at the moment, could not be established. The enzyme activity did not change when different fatty acyl-CoAs (oleoyl-, palmitoyl- and stearoyl-CoA) were used. It appears that retinol esterifying enzyme from testes displays a rather broad specificity towards activated fatty acids. However, acyl-CoA : retinol acyltransferase activity was higher with palmitoyl-CoA than with oleoyl-CoA in rat and human intestine [8,9], whereas higher activity has been reported in rat mammary gland with oleoyl-CoA [7].

The biological significance of the presence of acyl-CoA : retinol acyltransferase in testis can, at the present, only be conjectured. There is evidence that testicular tissue do contain various retinyl esters and retinyl palmitate is the major esterified form of vitamin A. Our earlier results have further suggested that vitamin A may also, in addition to liver, be stored in testis as retinyl esters [10]. If that is the case, acyl-CoA : retinol acyltransferase could play an important role in the regulation of retinol/retinyl ester ratio in testes, and thereby the metabolism of vitamin A. Free retinol is less stable, much more sensitive to oxidation and toxic to cell and cell membranes than the retinol complexed with protein(s). Thus, the holo-retinol-binding protein prevents membranolytic effects of free retinol during the transport of retinol from the liver to peripheral tissues [1] and another protein called cellular retinol-binding protein may act as a vehicle in the intracellular transport of retinol. Cellular retinol-binding protein has been implicated in the biological expression of retinol activity in the cell [29]. A retinol ester cycle may be operating in testes which could play an important role in the regulation of the flux of free retinol. The role of acyl-CoA : retinol acyltransferase may be to sense the level of free retinol in the cell and, by esterifying the excess, as well as to provide a store of retinyl esters, probably in Sertoli cells [30].

Since the properties of rat testicular acyl-coenzyme A : retinol acyltransferase correspond closely with those of acyl-CoA : cholesterol acyltransferase, activity of both enzymes is membrane bound, sensitive to detergents and inhibited by polar steroid progesterone and sulfhydryl blocking agents [6–9,21,23], one can raise the question whether the esterification of retinol and cholesterol in rat testes is catalyzed by the same enzyme. There is evidence that cholesterol and retinol acyltransferase might be different enzymes. This concept is further supported by the experiments showing that the acyl-coenzyme A : cholesterol acyltransferase activity is completely inhibited by a selective inhibitor 58-035 (3-[decyldimethyl]-*N*-[2-(4-methylphenyl)-1-phenylethyl]propanamide) without affecting the acyl-coenzyme A : retinol acyl transferase activity in both rat hepatoma and arterial smooth muscle cells in culture [31]. Rasmussen et al. [32] have recently reported that the activity of acyl-CoA : retinol acyltransferase in rat liver and small intestine increased significantly by feeding large doses of vitamin A. Using rat liver cells in culture, Drevon et al. [33] have further suggested that the esterification of retinol and cholesterol may be catalyzed by two different enzymes. At the moment, it is difficult to answer this question and much work is needed to say whether both enzyme activities are due to the same enzyme or different enzymes in rat testes.

Acknowledgements

The work was supported in part by Public Health Science Research Grant AM-09191 from NIADDK and the Competitive Research Grants. Office, Science and Education Administration, U.S. Department of Agriculture, agreement number number 85-CRCR-1-1711.

References

1 Goodman, D S (1984) in The Retinoids (Sporn, M B , Roberts, A.B. and Goodman, D.S , eds), Vol. 2, pp 41–88, Academic Press, New York
2 Ganguly, J , Rao, M R S , Murthy, S K and Sarada, K. (1980) Vitam Horm 38, 1–54
3 Mathur, S.N., Murthy, S.K , Ganguly, J (1972) Internat J Vit Nutr Res 42, 115–126
4 Harrison, E.H , Smith, J E. and Goodman, D S (1979) J Lipid Res 20, 760–771
5 Prystowsky, J.H , Smith, J.E and Goodman, D S. (1981) J Biol Chem 256, 4498–4503
6 Ross, A C (1982) J Biol Chem 257, 2453–2459
7 Ross, A C (1982) J Lipid Res 23, 133–144
8 Helgerud, P , Petersen, L B. and Norum, K R (1982) J Lipid Res 23, 609–618
9 Helgerud, P , Petersen, L B and Norum, K R (1983) J Clin Invest. 71, 747–753
10 Chaudhary, L R. and Nelson, E C. (1986) Ann Nutr Metab 30, 1–8
11 Chaudhary, L R. and Nelson, E C. (1985) Fed Proc 44, 545 (Abstract)
12 Chaudhary, L.R (1982) Biochimie 64, 211–217
13 Pennington, R J (1961) Biochem J. 80, 649–654

14 Sottocasa, G.L , Kuylensterna, B., Ernster, L and Bergstrand, A. (1967) J Cell Biol. 32, 415–438

15 Rommerts, F F G , Van Doorn, L G , Galjaard, H., Cooke, B A and Van der Molen, H.J (1973) J Histochem Cytochem 21, 572–579

16 Lowry, O H., Rosebrough, N.J , Farr, A L and Randall, R J (1951) J Biol. Chem 193, 265–275

17 Chaudhary, L.R and Nelson, E C. (1984) J Chromatogr 294, 466–470

18 Kornberg, A and Pricer, W.E., Jr. (1953) J Biol. Chem 204, 329–343

19 Torchinsky, Yu.M (1981) in Sulfur in Proteins, pp 10–13, Pergamon Press, New York

20 Holub, B J. and Kuksis, A. (1978) Adv Lipid Res 16, 1–125

21 Spector, A.A., Mathur, S.N and Kaduce, T L (1979) Prog Lipid Res 18, 31–53

22 Marcel, Y L (1982) Adv. Lipid Res. 19, 85–136

23 Suckling, K.E and Stange, E F. (1985) J Lipid Res 26, 647–671

24 Van der Vusse, G J., Kalkman, M L and Van der Molen, H J (1974) Biochim Biophys Acta 348, 404–414

25 Stoffel, W and Schiefer, H G (1968) Z Physiol. Chem. 349, 1017–1026

26 Sarzala, M G , Van Folde, L.M G., De Kruyff, B and Van Deenen, L L M (1970) Biochim Biophys Acta 202, 106–119

27 Waite, M , Sisson, P and Blackwell, E. (1970) Biochemistry 9, 746–753

28 Stein, Y., Widnell, C and Stein, O (1968) J. Cell Biol. 39, 185–192

29 Chytil, F and Ong, D E (1984) in The Retinoids (Sporn, M.B , Roberts, A B and Goodman, D S , eds), Vol 2, pp 89–123, Academic Press, New York

30 Ahulwalia, B S., Gambhir, K and Sekhon, H (1975) J Ntur. 105, 467–474

31 Ross, A.C., Go, K J , Heider, J.G and Rothblat, G H (1984) J Biol Chem 259, 815–819

32 Rasmussen, M , Petersen, L.B and Norum, K.R. (1984) Brit J Nutr. 51, 245–253

33 Drevon, C A , Blomhoff, R , Rasmussen, M., Kindberg, G.M , Berg, T. and Norum, K R (1985) Biochem. J 230, 617–623

Biochimica et Biophysica Acta 917 (1987) 33–41
Elsevier

BBA 52432

Metabolism of platelet-activating factor (alkylacetylphosphocholine) by type-II epithelial cells and fibroblasts from rat lungs

Raj Kumar [a], Richard J. King [b], Helen M. Martin [b] and Donald J. Hanahan [a]

Departments of [a] Biochemistry and [b] Physiology, The University of Texas Health Science Center at San Antonio,
San Antonio, TX 78284 (U S A)

(Received 3 July 1986)

Key words: Platelet-activating factor; Type II cell; (Rat lung)

The uptake and metabolism of ^{3}H-labeled platelet-activating factor by interstitial and epithelial cells from rat lungs was investigated. The uptake of 1-*O*-[^{3}H]octadecyl-2-acetyl-*sn*-glycero-3-phosphocholine (^{3}H-AGEPC) by alveolar type-II cells was linear with time from 5 to 60 min, with an average rate of 660 and 450 fmol / 10^6 cells for cells in primary culture for 48 to 72 h, respectively. AGEPC was rapidly metabolized and by 10 min 60% of AGEPC was converted into long-chain acylphosphatidylcholine (PC) (50%) and 1-*O*-alkyl-2-lyso-*sn*-glycero-3-phosphocholine (lyso-GEPC) (10%). By 60 min radioactivity in AGEPC was less than 10% of the total intracellular activity. Lyso-GEPC remained at about 10% throughout the incubation period. The uptake of ^{3}H-AGEPC by fibroblasts was very similar to type II cells, but the rate of metabolism was slower. AGEPC in fibroblasts constituted 85% of the cellular counts after 10 min of incubation, and 50% by 60 min. After 60 min only 30% of the AGEPC was converted to alkylacyl-PC. Characterization of the fatty acids in the alkylacyl-PC of both the type-II cells and lung fibroblasts indicated that arachidonic acid was preferentially (more than 90%) inserted at the 2-position.

Introduction

Platelet-activating factor, a phospholipid with the structure of an alkylacetyl glycerophosphocholine, has been shown to have a spectrum of diverse biological activities, and may be involved in several pathophysiological events [1–4]. In animal studies intravenous injection of less than 1 nmol/ kg induces severe cardiovascular and pulmonary alterations, including systemic hypotension, increased pulmonary resistance and decreased dynamic lung compliance [5,6], and the induction of pulmonary vasoconstriction and edema [7]. PAF is produced by a variety of activated cells, including platelets [8], neutrophils [9], monocytes [10], basophils [11], endothelial cells [12] and alveolar macrophages [13], and several of these cells are present in the parenchyma of the lungs. In an earlier study we reported that glycerylethers were present in the phosphatidylcholine fraction of lung surfactant, and that PAF-like activity could be found in the lavage fluids of mongrel dogs and rabbits [14]. Recently, Billah and Johnston [15] have observed PAF-like activity in the amniotic fluid of some women prior to onset of labor. Stenmark and coworkers [16] have reported the presence of PAF-like activity in the lavage fluids of nine out of nine infants with

---

Abbreviations ^{3}H-AGEPC, 1-*O*-[^{3}H]octadecyl-2-acetyl-*sn*-glycero-3-phosphocholine, lyso-GEPC, 1-*O*-alkyl-2-lyso-*sn*-glycero-3-phosphocholine; PC, phosphatidylcholine; TNS, 6-*p*-toluidine-2-naphthalenesulfonic acid; PAF, platelet-activating factor.

Correspondence: Dr Raj Kumar, Department of Biochemistry, The University of Texas Health Science Center at San Antonio, 7703 Floyd Curl Drive, San Antonio, TX 78284, U S.A.

0005-2760/87/$03 50 © 1987 Elsevier Science Publishers B V. (Biomedical Division)

bronchopulmonary dysplasia. We have found PAF-like activity in the lavage fluids obtained from premature baboons (140 days gestational age) who had been ventilated for 6 days with 100% O_2, but not in non-ventilated animals (unpublished observations). It is evident, therefore, that PAF is released into alveolar fluids of animals and humans, even under conditions not associated with severe lung injury. Since PAF has potent pathological effects which could exacerbate a pre-existing condition of lung damage, we considered it important to determine how its biological activity may be regulated.

The metabolic fate of this compound has been investigated in plasma [17], intact cells [18–21] as well as in vivo [22], and is generally associated with the removal of the acetyl group to form the inactive lyso derivative. In intact cells there is a transient formation of a lyso derivative, with the subsequent esterification of a long-chain fatty acid at the 2-position to form 1-*O*-alkyl-2-acyl-*sn*-glycero-3-phosphocholine (alkylacyl-PC), of which arachidonic acid appears to be the predominant molecular species. The existence of these pathways in certain lung cells has been investigated. Since PAF released into the alveolar fluid might interact with alveolar epithelial cells, and that released into the interstitial space might encounter fibroblasts, we have determined the capability of these cells to metabolize PAF. Further, we have determined the time course of the generation of its metabolites, and have characterized the composition of the formed alkylacyl-PC. The results show that type II cells in primary culture rapidly hydrolyze PAF, and form alkylacyl-PC containing arachidonic acid at the *sn* 2-position. Similar findings were obtained using lung fibroblasts, although the kinetics of the reactions were significantly different.

Experimental procedures

Materials

Labeled PAF 1-*O*-[^{3}H-10,11-octadecyl]-2-acetyl-*sn*-glycero-3-phosphocholine (^{3}H-18 : 0-AGEPC, 67 Ci/mmol) was prepared by tritation (New England Nuclear) of 1-*O*-[10,11-*cis*)-*sn*-glycero-3-phosphocholine. ^{3}H-18 : 0-lyso-GEPC was prepared by mild alkaline hydrolysis of ^{3}H-AGEPC, followed by purification to more than 99% radiopurity on thin layer chromatography and HPLC. Lipid standards for TLC were purchased from Sigma Chemical Co., St. Louis, MO and Serdary Research Laboratories. Vitride was obtained from Alfa Products. Fatty acid anhydrides (palmitoyl, oleoyl, linoleoyl, linolenoyl, and arachidonoyl) were products of Nu Chek Prep (Elysian, MN). 1-*O*-octadeyl-2-lyso-*sn*-glycero-3-phospholcholine was obtained from Nova Biochem, Switzerland. TNS spray for the identification of lipid spots on TLC under UV light was prepared in our laboratory as previously described [23]. TLC plates coated with 250 μm silica gel G were products of Analtech (Neward, NJ). 10% SP 2330 on 100/120 mesh Chromosorb was obtained from Supelco, Bellefonte, PA. Phospholipase C *Bacillus cereus*, (specific activity, 145 units per mg protein) was purchased from Calbiochem-Behring Corp. All fatty acid methyl ester standards were obtained from Applied Science Laboratories (State College, PA). The following materials were also used in this study; bovine serum albumin (Miles Laboratories Inc., Naperville, IL), fetal calf serum (GIBCO Laboratories, New York), trypsin (Sigma, type II), ACS scintillation cocktail (Liquiscint, Somerville, NJ), 2-7-dichlorofluorescein (Sigma Chemical Co.). All solvents used were of reagent grade.

Methods

Unless otherwise stated, all solvent mixtures for extraction and thin layer chromatography were prepared on a volume to volume basis. TLC plates were prewashed with the appropriate developing solvent and then activated by heating for 30 min at 140°C immediately before use. 1-*O*-octadecyl-2-acyl-*sn*-glycero-3-phosphocholine containing 16 : 0, 18 : 1, 18 : 2, 18 : 3, and 20 : 4 fatty acyl groups at the *sn-2* position were prepared by the method of Gupta et al. [24]. Lyso-GEPC was acylated with specific fatty acid anhydrides in anhydrous chloroform in the presence of 4,4-dimethylaminopyridine at room temperature for 36 h. The reaction mixture was extracted by the method of Bligh and Dyer [25]. The organic phase containing the acylated product was purified on TLC using chloroform/methanol/water system (65 : 35 : 6). The identity of each of the homologs was confirmed by analysing the methyl esters of the fatty acids, obtained after base-catalyzed methanolic hydrolysis of the compounds, using gas-liquid chromatography. Standards of 1-*O*-octadecyl-2-long chain acyl-3-acetyl-glycerol were prepared essentially by the method of Kumar et al. [26]. 1-*O*-alkyl-2-acyl-PC containing various fatty acyl groups at the 2-position (16 : 0, 18 : 1, 18 : 2, 18 : 3, 20 : 4) were subjected to phospholipase C treatment, and the resulting 1-*O*-alkyl-2-acyl-3-glycerol was purified by TLC and acetylated with acetic anhydride and perchloric acid. The product, 1-*O*-octadecyl-2-acyl-2-acetyl glycerol, was purified by preparative TLC using silica gel G plates developed in petroleum ether/diethylether/acetic acid (90 : 10 : 1).

Preparation of alveolar type II cells

Alveolar type II cells were prepared by a slight modification of the method of Dobbs and Mason [27]. Animals were anaesthetized by intraperitoneal injection of sodium pentabarbital (20 mg/kg). A tracheal cannula was inserted and the animals were ventilated with air. The lungs were perfused with RPMI 1640 (culture medium) at a pressure of about 20 cm H_2O until the lungs were visibly cleared of blood, and then quickly excised. Alveolar macrophages were partially removed by endobronchial lavage with Hanks buffer in the absence of calcium and magnesium. The lungs were then filled with 1 mg/ml trypsin dissolved in RPMI 1640, minced finely with small sharp scissors, and incubated for 20 min at 37°C on a rotary platform. The tissue was filtered through 100 μm nylon mesh, and the cells passing through the filter were collected. 10% (by volume) fetal calf serum was added, and the cells were pelleted by low-speed centrifugation. These cells were gently suspended in 90% RPMI 1640/10% fetal calf serum, and plated on a plastic dish for 60 min. The cells not adherent after 1 h were transferred to a plastic T flask and maintained for 48–72 hours in 90% RPMI 1640/10% fetal calf serum. Adherent cells consisted of nearly 90% type II cells, as indicated by the intracellular organelles associated with lamellar inclusions, visible by inverted-phase microscopy, and their staining with a modified Papanicolaou procedure [28]. Greater than 95% excluded trypan blue. In previous experiments [29] it had been determined that these cells synthesized dipalmitoyl phosphatidylcholine and the 35 kDa protein associated with pulmonary surfactant. Cells isolated from 2–4 rats were used for each experiment.

Preparation of lung fibroblasts

Lung fibroblasts were obtained from adult rat lung by enzymatic dissociation of cells using 1 mg/ml trypsin. Cells adhering to the plastic cell culture plates after 1 h were passed 4 times in 90% minimum essential media containing 10% fetal calf serum. Cell cultures appeared homogeneous by inverted phase contrast microscopy.

Incubation conditions and lipid analysis

Alveolar type-II cells were rinsed five times with serum free medium. 20 μl of 1-*O*-[^{3}H]-octadecyl-2-acetyl-*sn*-glycero-3-phosphocholine (AGEPC; specific activity, 65.7 Ci/mmol) bound to bovine serum albumin (2.5 mg%) were presented to cells in 2 ml serum free medium containing 0.05% bovine serum albumin which had been prewarmed to 37°C, to provide a final concentration of $1 \cdot 10^{-9}$ M. At the end of the incubation period, which varied from 2 to 60 min, the cells were washed three times with cold medium, scraped with a rubber policeman into chloroform/methanol (1 : 2, v/v) and the lipids were extracted by the method of Bligh and Dyer [25]. The medium was also extracted. The entire procedure took less than 2 min. These extracted materials were then spotted on silica gel G plates, together with carriers of nonlabeled AGEPC, lyso-GEPC, and egg PC. Lipids were separated in a solvent system of chloroform/methanol/water (65 : 25 : 6, v/v). The individual lipids were located under ultraviolet light after spraying with TNS. The fractions were scraped directly into vials and radioactivity was determined in a Beckman LS 6800 liquid scintillation spectrometer.

Chemical procedures

To determine if the ^{3}H-label was present in the alkyl moiety of the acylated GEPC, the PC fraction was isolated from TLC, extracted, and subjected to base-catalyzed methanolysis for 1 h at room temperature [26]. After neutralization of the mixture, the organic phase was separated and chromatographed on a silica gel G plate using chloroform : methanol : H_2O (65 : 35 : 6, v/v). The

TLC plate was sprayed with TNS and the area corresponding to various lipid standards was visualized under ultraviolet light, and scraped into the scintillation vial for radioactive determination.

Two methods were used to analyze the molecular species of the 1-*O*-[^{3}H]alkyl-2-long chain acyl-GEPC. First the phosphatidylcholines, separated on TLC, were subjected to an acetolysis procedure [30], using acetic anhydride and glacial acetic acid in the ratio of 2 : 3 at 150°C for 5 h; or alternatively by treatment with phospholipase C followed by acetylation with acetic anhydride and perchloric acid. The 1-*O*-[^{3}H]alkylacyl acetate derivatives were purified on TLC, using silica gel G plates developed in a solvent system of chloroform-acetone (94/6), and extracted from the plate with the solvent of Bligh and Dyer [25]. The purified acetate derivatives were mixed with the non-radiolabeled standards containing specific fatty acyl groups at the 2-position, and separated into various species by argentation chromatography using silica gel G plates coated with 10% silver nitrate. Plates were first developed in chloroform-methanol (95 : 5, v/v), followed by chloroform only [31], or with a solvent system of benzene/chloroform (99 : 1, v/v) [32]. The individual species were located under ultraviolet light after spraying the plates with 0.2% dichlorofluorescein. The distribution of the label in the various molecular species was determined by scintillation counting.

In the second method the composition of alkyl acyl PC was determined by reverse phase HPLC, using a modification of the procedure of Patton et al. [33]. The reverse phase HPLC was performed by employing a C-18 radial pack cartridge (Waters, Milford, MA) using a solvent system of methanol-acetonitrile-water (83 : 10 : 7, v/v) containing 200 mM choline chloride, with an elution rate of 1 ml/min. The radioactive molecular species were monitored by counting aliquots of the eluants, collected at the rate of 1 ml/min, or by using a radioactive flow detector (Flo One/Beta, Radiomatic Instruments and Chemical Co., Tampa, FL) fitted with a 0.25 mm plastic cell. The radioactive peaks were identified by coinjecting phospholipid standards mixed with the radioactive cell lysate, which was monitored by ultraviolet absorbance at 206 nm.

Results

Recovery of ^{3}H-AGEPC

The adsorption of ^{3}H-AGEPC of high specific activity to glass and plastic ware has been observed by many investigators [34]. It was therefore necessary to establish a protocol which would give good recovery of AGEPC and its metabolites. Culture medium in plastic dishes was incubated with $1 \cdot 10^{-9}$ M ^{3}H-AGEPC at 37°C for various time intervals. The medium was then extracted by a Bligh and Dyer [25] solvent partition and the chloroform soluble fraction was analyzed for radioactivity level. Greater than 90% of the label was recovered when the cultured medium contained 0.05% albumin. In contrast, when the medium did not contain any added albumin, only 36% of the label was recovered after 1 h. In another set of experiments, recoveries of radioactivity of up to 95% were obtained when ^{3}H-AGEPC was added to cells in culture medium containing 0.05% albumin (Fig. 1). All subsequent

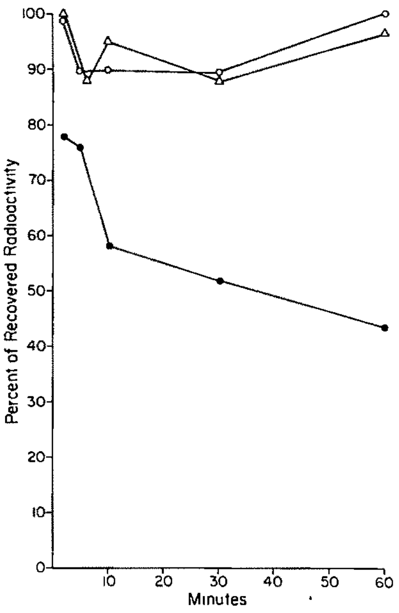

Fig 1 Recovery of ^{3}H-AGEPC after incubation with type-II cells at various time intervals. Cells (approx $1 \cdot 10^6$) in primary culture containing varying amounts of albumin were incubated with 2 μl (1 10^{-9} M) ^{3}H-AGEPC (specific activity, 65 7 Ci/mmol, 1 $2 \cdot 10^5$ c p.m.). Medium and cells were extracted together and analyzed for isotope recovery. ●——●, 0% albumin; ○——○, 0.05% albumin; △——△, 0.1% albumin ($n = 2$).

experiments therefore, were conducted in the presence of 0.05% albumin.

Cellular uptake and metabolism of ^{3}H-AGEPC

Alveolar type II cells and fibroblasts were incubated with ^{3}H-AGEPC at varying time intervals as described in the methods. The lipids from the cells and media were extracted and analyzed by TLC using a chloroform/methanol/water system. Three major areas of radio-labeled lipids were identified and isolated: lyso-GEPC, AGEPC, and PC. In Fig. 2 is shown the uptake of AGEPC by type-II cells in primary culture for 48 and 72 h. The uptake is approximately linear with time from 5 through 60 min (the longest time interval studied) with an average rate of 660 fmol AGEPC/h per million cells found for 48-h cultures and 450 fmol/h per million cells for 72-h cells. The slopes of the linear regression lines, however, were not statistically different. The intracellular metabolism of the AGEPC is shown in Figs. 3 and 4 expressed as either the percentage distribution of the radioactivity in the metabolites (Fig. 3) or the amount of radioactive metabolites found in the cells (fmol/10^6 cells) (Fig. 4). From Fig. 4 it can be seen that a constant intracellular level of AGEPC is reached in 10 min. Radioactivity in the alkyl acyl PC found in the media increased with time, suggesting that some of the cellular alkyl acyl PC was released into media (data not shown). When the intracellular counts are expressed as a percentage of the total radioactivity recovered at each time point, as in Fig. 3, the pattern of AGEPC metabolism could be determined. By 1 h AGEPC was less than 10% of the intracellular radioactivity. Lyso-GEPC remained at about 10% throughout the entire incubation period. Approx. 8–10% of the radioactivity was consistently found in the neutral lipid fractions on the TLC (data not shown), and the majority of these counts migrated in TLC as monoglycerides. Two types of control experiment were run concomitantly. In the first cell cultures which were maintained at 5°C and had essentially no metabolic activity towards AGEPC were presented with ^{3}H-AGEPC, and the

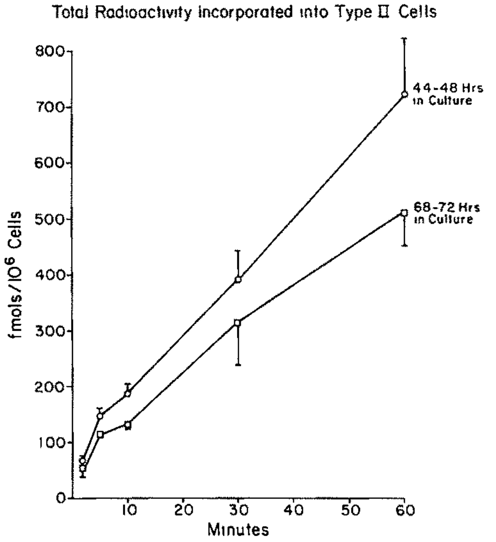

Fig 2 The uptake of ^{3}H-AGEPC by alveolar type-II cells in primary culture for 44–72 h. 2 pmol ^{3}H-AGEPC (specific activity 65.7 Ci/mmol) were presented to approx. 750000 cells as described in Methods At various time intervals the medium was removed, and the cells were washed three times with ice-cold medium These cells were then scraped from the plate into 1 ml of cold medium, repeating the procedure three times Shown are the means and standard errors for four experiments

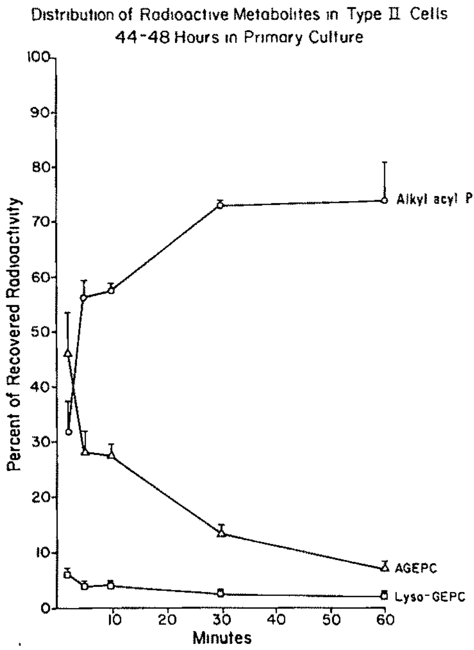

Fig. 3. Distribution of metabolites of ^{3}H-AGEPC in type-II cells. AGEPC and its metabolites were separated on TLC and the lipids were scraped into scintillation vials. The percentage of the radioactivity in individual samples was calculated based on total radioactivity applied to the TLC plate Shown are mean and standard errors of four experiments

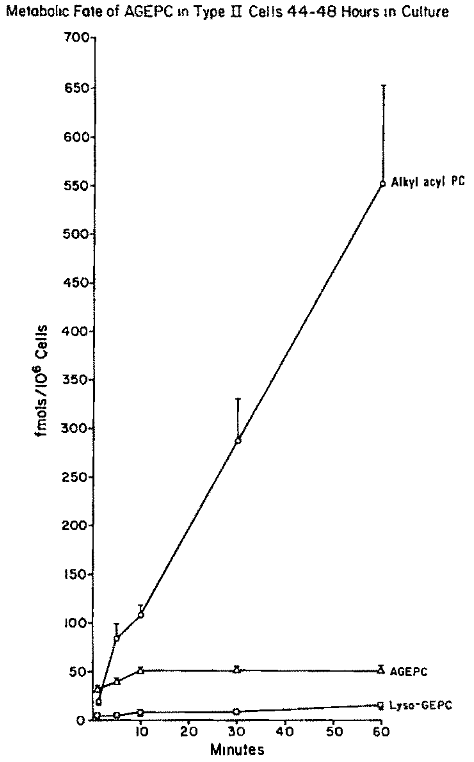

Fig 4. Distribution of metabolites of ^{3}H-AGEPC in type-II cells expressed as fmol of phospholipids per million cells

second in which labeled AGEPC was added to media only and maintained at 37°C for 1 h. In both control experiments AGEPC was recovered without any appreciable (less than 2%) breakdown.

In order to establish if alveolar type-II cells in primary culture for 70 h were capable of hydrolyzing all of its intracellular pool of AGEPC, when the AGEPC in the culture medium was removed, cells were incubated with ^{3}H-AGEPC (2 pmol) for 10 mi at 37°C. After the incubation period, the medium was replaced with fresh medium without AGEPC and the cells were incubated further for up to 60 min. Medium and cells were separately analysed for AGEPC and its metabolites. Lyso-GEPC constituted about 5% of the cellular counts, and remained constant throughout the incubation period. The intracellular level of ^{3}H-AGEPC at 10 min (i.e., 10 min after the 10 min preincubation with ^{3}H-AGEPC in the medium and subsequent wash) was 30% of cellular counts. Within 30 min its activity decreased to 10% (50 fmol) and remained approximately at this level up to 60 min. Similarly, a corresponding increase in the alkylacyl-PC was observed from 10 to 30 min. In the medium, the level of radioactivity of AGEPC dropped to 70% at 60 min, whereas in the lyso-GEPC fraction it increased to 18%. Alkylacyl-PC in the medium also increased from 1% to 5%, thereby indicating some release of this metabolite.

Metabolic activities of lung fibroblasts

The uptake and the intracellular distribution of metabolites of ^{3}H-AGEPC by fibroblasts are shown in Fig. 5. AGEPC is taken up by fibroblasts with kinetics which are approximately linear with time through 60 min, at a rate comparable to that seen by the type-II cells after 70 h of culture. The rate at which AGEPC was metabolized by fibroblasts, however, is about one-half of that of the type-II cells. AGEPC did not reach a constant intracellular level at times up to 60 min, and the formation of alkylacyl-PC was much slower than that of the type-II cells. At 10 min 85% of the

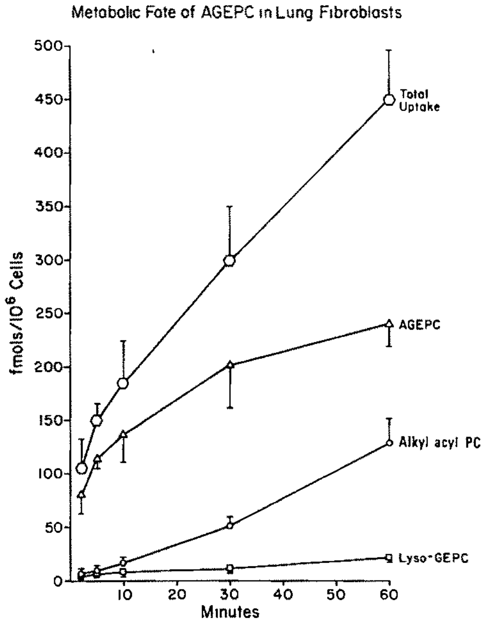

Fig. 5. Uptake and metabolism of ^{3}H-AGEPC by lung fibroblasts. Fibroblasts were obtained from adult rat lung as described in the Methods The other details of the experiments are similar to those described in Fig 2 Shown are the mean and standard errors of four experiments using four different cultures.

cellular counts in fibroblasts were in AGEPC. By contrast, in 10 min, type-II cells had metabolized 55% of the AGEPC to alkylacyl-PC, 8% to lyso-GEPC, and only about 32% of the recovered counts were in AGEPC. By 60 min about 50% of the recovered counts in fibroblasts were in AGEPC, while AGEPC in type-II cells was less than 10%. In control experiments using fibroblasts, as described for type-II cells, AGEPC remained unchanged.

Characterization of 1-O-[^{3}H]alkyl-2-acyl-PC

In order to confirm that radioactive counts were located exclusively in the 1-*O*-alkyl acyl PC molecule(s), the following experiments were conducted. First, the PC fraction was rechromatographed on silica gel G plates using the following solvent systems: chloroform/methanol/acetic acid/water (60 : 35 : 1 : 8), and chloroform/methanol/methylamine 20% (60 : 36 : 10). In each solvent more than 95% of the counts was found in the PC area. Secondly, when this PC was subjected to base catalyzed methanolysis, as described in Methods, and analyzed by TLC, 80–85% of the total counts were present at an R_f value similar to a lyso-GEPC standard. Approx. 4% of the counts were present at the origin and 10% of the total counts migrated at the solvent front. Similarly 90% of the radioactive counts of the acetate derivatives of the PC fraction obtained either by direct acetolysis or by phospholipase C treatment followed by acetylation, migrated on TLC as the 1-*O*-alkyl-2-acyl-3-acyl glycerol, while approx. 10% of the total counts were present in the 1,2-diacyl-3-acetyl-glycerol.

Further characterization of the fatty acyl composition of the ^{3}H-alkyl acyl PC synthesized by alveolar type-II cells and fibroblasts was achieved by using series of chemically synthesized 1-*O*-octadecyl-2-acyl-GEPC standards containing specific acyl chains at the *sn*-2 position of the molecule. ^{3}H-alkylacyl-PC (from the cells) and the non-radioactive standards were derivatized into alkylacyl-acetyl glycerols and separated by argentation chromatography using benzene/chloroform (99 : 1) [32] and chloroform/methanol (95 : 5). Nearly all of the label was found in the 18 : 0–20 : 4 species (95%), with minor amounts in the 18 : 0–18 : 2 (4%), and 18 : 0–18 : 1 (1%). The specificity of incorporation of the acyl chain in the alkylacyl-PC was further confirmed by reverse phase HPLC (Fig. 6). The distribution of alkylacyl-phosphatidylcholine was very similar to that found by argentation chromatography, in that nearly all of the diethyl ether-linked species contained arachidonic acid at the *sn*-2 position. Approx. 10% of the total counts were eluted with the same retention time as that of a diacyl-PC species, and approx. 5–10% of the total radioactivity was present near the solvent front, suggesting that some breakdown had occurred during separation by TLC or by HPLC. The other glyceryl ether phosphatidylcholines were 18 : 0–18 : 3 (1%), 18 : 0–18 : 2 (4%), and 18 : 0–18 : 1 (1%). Comparable results were also obtained with fibroblasts. The composition of alkylacyl-PC in these cells were as follows: 18 : 0–18 : 2 (4%), 18 : 0–18 : 1 (2%), 18 : 0–20 : 4 (84%). There was approx. 6% of the total counts eluting with the solvent front, and 4% counts had the same retention time as that of diacyl derivatives.

Acylation of 1-O-[^{3}H]alkyl-2-(lyso)-sn-glycero-3-phosphocholine

In order to directly determine if lyso-GEPC, a proposed precursor of AGEPC, could be acylated, Type II cells were incubated with ^{3}H-lyso-GEPC ($1 \cdot 10^{-9}$ M) for 4 h. Cellular lipids were extracted and analyzed by TLC. Up to 60% of the label in the medium was taken up by the cells after 4 h, and 90% of this radioactivity was converted into alkylacyl-PC. When the composition of this fraction was determined by HPLC, a pattern of acylation similar to that found using ^{3}H-AGEPC as a precursor was obtained (data not shown).

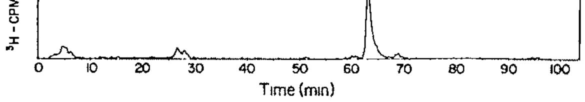

Fig 6. HPLC separation of 1-*O*-[^{3}H]-2-acyl-PC obtained from alveolar epithelial type-II cells Glycerylether standards containing fatty acids at the 2-position were added in the samples, and their elution is shown in the upper tracing

Discussion

The results of this study demonstrate that type-II cells and lung fibroblasts rapidly hydrolyze ^{3}H-AGEPC to lyso-GEPC, and reacylate it to alkylacyl-PC containing arachidonic acid at the *sn*-2 position. When type-II cells were incubated with AGEPC, 50% of the total intracellular activity was present in the AGEPC fraction and the remainder was metabolized into alkylacyl-PC (30%) and lyso-GEPC (10%) within 2 min. The level of intracellular lyso-GEPC remained approximately constant throughout the incubation period. There was no evidence of any lag period, and the alkylacyl-PC accumulated linearly for up to 30 min and then remained constant up to 60 min. When the medium was examined a small increase in the lyso-GEPC was observed. Approx. 0.5% of the counts were in lyso-GEPC at 2 min, while 6% was observed at 1 h. Experiments were not performed in the presence of unlabelled exogenous lyso-GEPC, and it is difficult to assess whether this small accumulation of lyso-GEPC was due to the release of cellularly deacylated AGEPC, or whether it was formed by extracellular degradation. However, these results are somewhat different from those reported by Robinson et al. [35], who observed a large accumulation of lyso-GEPC in alveolar macrophages after 2–4 h of incubation with AGEPC. Approx. 2.4% of the total counts in the extracellular medium of type-II cells were in the PC fraction, indicating a release of alkylacyl-PC by these cells, which is consistent with their capacity to secrete surfactant PC [36]. In contrast no such release was observed using lung fibroblasts.

In all experiments where ^{3}H-AGEPC was incubated with cells, a small but significant percentage (10–15%) of the total radioactivity was observed in the neutral lipid fractions. Further fractionation of these counts by TLC indicated that the majority of the counts were in the monoglyceride fraction. Because of the limited material available no attempt was made to rigorously characterize this material.

In certain experiments the medium containing the radioactive AGEPC was removed, fresh medium added, and the metabolic fate of the label was followed with time. 15% of the total intracellular counts, equivalent to 50 fmol, was still present as ^{3}H-AGEPC after 60 min incubation, suggesting that an intracellular pool of AGEPC may be maintained by type-II cells, with lyso-GEPC functioning as an intermediate between steady-state pools of AGEPC and alkylacyl-PC. The results of preliminary experiments investigating the capacity of type-II cells to synthesize PAF indicate that type-II cells acetylate ^{3}H-lyso-GEPC to AGEPC, and this activity is stimulated by ionophore A23187 [37]. Further experiments, however, are required to confirm these initial observations, and to explore them in detail.

An important aspect of these studies was the identification of the composition of fatty acids inserted at the *sn*-2 position of the alkylacyl-PC. Analysis of the molecular species of alkylacyl-PC by HPLC or argentation chromatography revealed that the predominant species was 1-*O*-octadecyl-2-arachidonyl-PC, consistent with the reported data on processing of AGEPC in platelets [38], and neutrophils [39]. We find this result very interesting, since there is very little arachidonic acid in any other phospholipids in type-II cells, and may suggest the presence of a specialized pool. Recently, it has been reported by Gilfillan and Rooney that arachidonic acid and leukotrienes may affect the metabolism of pulmonary surfactant [40]. Whether the arachidonic acid esterified to alkylacyl-PC might be released and serve in a regulatory capacity is unknown, but it is a intriguing question to be pursued in subsequent studies.

Acknowledgements

This investigation was supported by NIH grants HL-23578 and HL-22555. The authors are indebted to Anna Pittard for her technical assistance.

References

1 Benveniste, J. and Vargaftig (1983) Ether Lipids (Mangold, H K. and Paltauf, F , eds.), pp 365–376, Academic Press, New York
2 Snyder, F (1985) Med Res. Rev 5, 107–140
3 Snyder, F. (ed.) Platelet-Activating Factor, Plenum Publishing Co , New York, in the press
4 Pinckard, R.N , McManus, L.M , Halonen, M and Hanahan, D J (1982) in Immuno-pharmacology of the Lung (Lenfant, C. and Newball, H , eds.), pp. 73–107, Marcel Dekker, New York

5 Halonen, M, Palmer, J D., Lohman, I.C, McManus, L M. and Pinckard, R N (1980) Am Rev. Resp. Dis. 122, 915–924

6 Pinckard, R.N, McManus, L M, O'Rourke, R.A, Crawford, M H. and Hanahan, D.J (1980) Clin Res 28, 258 (Abstract)

7 Worthen, G S., Goins, A., Mitchell, B, Larsen, G, Reeves, J and Henson, P. (1982) Am. Rev. Resp Dis. 125, 274 (Abstract)

8 Chap, H., Mauco, G, Simon, M.F., Benveniste, J and Douste-Blazy, L. (1981) Nature 289, 312–314

9 Clark, P.O, Hanahan, D J. and Pinckard, R.N (1980) Biochim. Biophys Acta 625, 69–75

10 Benveniste, J., Henson, P.M and Cochrane, C.G (1972) J. Exp. Med. 136, 1356–1376

11 Camussi, G, Mencía-Huerta, J.M and Benveniste, J (1977) Immunology 33, 523–534

12 Zimmerman, G.A, McIntyre, T.M. and Prescott, S M (1985) Circulation 72, 718–727

13 Benveniste, J (1979) Monoger. Allergy 14, 138–141

14 Kumar, R., King, R J and Hanahan, D J. (1985) Biochim Biophys Acta 836, 19–26

15 Billah, M.M. and Johnston, J.M. (1983) Biochem. Biophys Res Commun 113, 51–58

16 Stenmark, K.R., Eyzaguirre, M., Remigo, L, Secome, J and Benson, P.M (1985) Am Rev. Res Dis 131, 236a

17 Farr, R S., Cox, C P, Wardlow, M L. and Jorgensen, R. (1980) Clin Immunol Immunopathol 115, 318–330

18 Tougui, L, Jacquemin, C. and Vargaftig, B B. (1983) Biochem. Biophys Res Commun 110, 890–893

19 Pieroni, G. and Hanahan, D.J. (1983) Arch. Biochem Biophys. 224, 485–493

20 Cabot, M C., Blank, M L., Welsh, C.J., Horan, M J, Cress, E.A and Snyder, F (1982) Life Sci 31, 2891–2898

21 Robinson, M, Blank, M.L. and Snyder, F (1985) J Biol Chem 260, 7889–7895

22 Blank, M.L., Cress, E.A., Whittle, T. and Snyder, F. (1981) Life Sci. 29, 769–775

23 Jon, M, Keenan, R W. and Horowitz, P (1982) J Chromatogr. 237, 522–524

24 Gupta, C M., Radhakrishnan, R. and Khorana, H.G. (1977) Proc. Natl Acad. Sci USA 74, 4315–4319

25 Bligh, E G and Dyer, W (1959) Can J. Biochem 37, 911–918

26 Kumar, R., Weintraub, S.T., McManus, L M., Pinckard, R N. and Hanahan, D J (1984) J Lipid Res 25, 198–208

27 Dobbs, L G. and Mason, R.J. (1978) J Clin Invest. 63, 378–387

28 Kikkawa, Y. and Yoneda, K (1974) Lab. Invest. 30, 76–84

29 King, R.J and Martin, H.M. (1981) Biochim. Biophys. Acta 663, 289–301

30 Kumar, R., Weintraub, S T and Hanahan, D J (1983) J Lipid Res. 24, 930–937

31 Okano, G, Kawamoto, T. and Akino, T (1978) Biochim Biophys Acta 528, 385–393

32 Renkonen, O. (1971) Progress in Thin-Layer Chromatography and Related Methods, Vol. II (Neiderwieser, A and Pataki, G, eds.

33 Patton, G M., Fasulo, J M. and Robins, J (1982) J Lipid Res 23, 190–196

34 Renooij, W and Snyder, F (1981) Biochim Biophys Acta 663, 545–556

35 Robinson, M. and Snyder, F (1985) Biochim. Biophys. Acta 837, 52–56

36 Goerke, J. (1974) Biochim Biophys Acta 344, 241–261

37 Kumar, R., King, R J. and Hanahan, D.J. (1986) in: New Horizons in Platelet-Activating Factor Research (Lee, M.L. and Winslow, C M., eds), John Wiley & Sons, New York, in the press

38 Malone, B., Lee, T-C and Snyder, F. (1985) J. Biol Chem 260, 1531–1534

39 Muller, H W., O'Flaherty, J T. and Wykle, R.L. (1984) J Biol Chem 259, 14554–14559

40 Gilfillan, A.M and Rooney, S.A (1985) Biochim. Biophys Acta 833, 336–341

Biochimica et Biophysica Acta 917 (1987) 42–47
Elsevier

BBA 52434

Metabolic activities in human skin fibroblasts preloaded with labeled G_{M2}-ganglioside

Srinivasa Raghavan, Timothy A. Lyerla *, Allan Krusell
and Edwin H. Kolodny

*Department of Biochemistry, Eunice Kennedy Shriver Center for Mental Retardation, Inc., Waltham, MA,
and the Neurology Department, Massachusetts General Hospital and Harvard Medical School, Boston, MA (U.S.A.)*

(Received 7 May 1986)

Key words Ganglioside G_{M2} metabolism; Gangliosidosis; (Human skin fibroblast)

Confluent cultures of human skin fibroblasts were maintained for 10 days with sphingosine labeled $[^3H]G_{M2}$. Labeled medium was then replaced with normal medium and the cells maintained for 42 days with weekly medium changes. Cells were harvested at regular intervals and cells, medium, and trypsin digest supernatant analyzed for $[^3H]G_{M2}$ and its metabolic products. The ganglioside can be membrane associated and removed by trypsin, or membrane incorporated and trypsin insensitive. The membrane incorporated material is apparently transported to the lysosomes slowly by membrane flow, where 80% of the cellular G_{M2} can be metabolized by day 42. $[^3H]G_{M2}$ as well as its metabolic products in control cells is continuously released into the medium, during which it can also become associated with the cell surface membrane. There is no detectable metabolism of the $[^3H]G_{M2}$ in G_{M2} gangliosidosis cell lines over the extended post-labeling period, indicating that there is no residual enzyme activity in these cells. Undegraded G_{M2} is continuously released into the medium and remains associated with the cell surface membrane as well.

Introduction

The neurological disorders Tay-Sachs and Sandhoff disease arise from an inability to hydrolyze G_{M2}-ganglioside [1] due to a deficiency in the activity of hexosaminidase A (EC 3.2.1.52). The hydrolysis, in vivo, of G_{M2} also requires an activator protein [2] whose deficiency leads to the AB variant neurological disorder [3]. Hydrolysis of radio-labeled G_{M2} in vitro by hexosaminidase A requires the presence of detergent [4,5] or the activator protein [6] for mediating substrate-enzyme interaction. Detergent alters the substrate specificity for the isozyme [7–10], while the activator is difficult to prepare and available in only a few laboratories [6].

We reported that the difficulties in using in vitro assays to diagnose G_{M2} gangliosidoses can be circumvented by an in vivo method using cultured skin fibroblasts challenged with ^{3}H-labeled G_{M2} [11]. These studies showed that in normal fibroblasts maintained for 10 days in medium containing 20 μM $[^3H]G_{M2}$, about half the labeled substrate taken up by the cells is metabolized. Cells deficient in hexosaminidase A activity or in activator factor, however, show little hydrolysis of

---

* Present address: Department of Biology, Clark University, Worcester, MA 01610, U.S.A

Nomenclature. The ganglioside nomenclature used here is that of Svennerholm (J. Neurochem (1963) 10, 613–623) G_{M3}, II^{3}NeuAc-LacCer; G_{M2}, II^{3}NeuAc-GgOse$_3$Cer, G_{M1}, II^{3}NeuAc-GgOse$_4$Cer.

Correspondence: Dr Srinivasa Raghavan, Department of Biochemistry, Eunice Kennedy Shriver Center, 200 Trapelo Road, Waltham, MA 02254, U S A.

0005-2760/87/$03.50 © 1987 Elsevier Science Publishers B.V (Biomedical Division)

the substrate over the same period. We find that the method is especially helpful in the evaluation of atypical cases of hexosaminidase deficiency for the definitive diagnosis of G_{M2}-gangliosidosis [12].

In order to follow the long-term kinetics of complete metabolism of G_{M2}, normal cells were preloaded with $[^3H]G_{M2}$ ganglioside and the cellular radioactivity was followed in the absence of $[^3H]G_{M2}$ in the medium for varying periods of time up to 42 days in culture. Radioactivity was examined in the cells, the media and trypsin removable cell surface material. Similar studies were performed in cells from patients with G_{M2}-gangliosidosis to determine whether residual G_{M2} metabolism occurs in these mutant cells.

Materials and Methods

Labeling cells with $[^3H]G_{M2}$

Fibroblasts from controls and patients with various types of G_{M2} gangliosidoses were first labeled with $[^3H]G_{M2}$ ganglioside as previously described [11]. Briefly, 6 cm dishes were seeded with $0.5 \cdot 10^6$ cells and 3 days later culture medium containing about 20 μM $[^3H]G_{M2}$ (specific activity, 48000 cpm/nmole) were added to each dish. The medium is Dulbecco's modified Eagle's medium containing 4.5 g glucose/l and supplemented with 10% fetal calf serum, 5 μg/ml gentamycin antibiotic, 1 mM pyruvate, 2 mM glutamine, 35 mM $NaHCO_3$ and 1 × minimal essential medium non-essential amino acids. ^3H-labeled ganglioside medium is prepared by drying an appropriate volume of a labeled ganglioside solution in chloroform/methanol (2 : 1, v/v) with a sterile stream of nitrogen, resuspending in the culture medium and sonicating for 30 min in a bath-type sonicator. After 10 days of labeling the cells were washed free of radioactivity by four successive rinses with phosphate-buffered saline and placed in fresh non-radioactive culture medium without G_{M2} (considered as day 0). Cultures were maintained in most cases for another 42 days with weekly medium changes. All sterile work is done in a vertical laminar flow hood and cells are maintained at 37°C in 95% air/5% CO_2 under 100% relative humidity. Cells are harvested by trypsinization in 2 ml enzyme medium, the reaction stopped with 0.2 ml fetal calf serum, pellets collected by centrifugation and rinsed two times in phopshate-buffered saline. They are analyzed immediately or kept frozen at −20°C until ^3H-labeled lipid analyses are made.

$[^3H]$glycine incorporation into proteins

Protein synthesis of cell cultures in 6 cm dishes between day 0 and day 42 was determined as $[^3H]$glycine uptake into hot trichloroacetic acid precipitable material. Duplicate cultures on days 0, 21 and 42 were rinsed twice in phopshate-buffered saline and fresh culture medium was added containing 5 μM $[^3H]$glycine per dish (New England Nuclear, specific activity 15 Ci/nmol). Cells were labeled for 4 h at 37°C in 95% air/5% CO_2. $[^3H]$glycine medium was removed, the cultures rinsed twice with phosphate-buffered saline and cells collected in 3 ml of cold 10% trichloroacetic acid with a rubber policeman. They were allowed to stand for 15 min on ice, then rinsed twice in cold 10% trichloroacetic acid by centrifugation at 1500 × *g*. The final pellet was resuspended in 1.5 ml cold 10% trichloroacetic acid, heated at 100°C for 15 min and subsequently chilled on ice for 15 min. The hot acid precipitable material was collected by centrifugation after one rinse in 95% ethanol and another in diethyl ether. The ether was dried under nitrogen and material solubilized in 0.5 ml 0.5 M NaOH overnight at 37°C. Samples were counted in a Packard Tricarb scintillation spectrometer. Total protein was determined from a 10 μl sample of solubilized pellet according to the method of Lowry et al. [13].

Extraction and analysis of sphingolipids

Media (10 ml) pooled from duplicate dishes during weekly changes and trypsin digests (4.4 ml) combined from two dishes at the time of harvesting cells were extracted overnight with 20 vols. of chloroform/methanol (2 : 1, v/v). The extract was filtered through a sintered glass funnel and residue washed with another 5 vols. of chloroform/methanol. The clear filtrate was taken to dryness in a rotary evaporator with the addition of toluene to remove water present in the lipid extracts. The sample was taken up in 10 ml of chloroform/methanol and partitioned as follows to remove the labeled ganglioside (approx. 95%) into an aqueous upper phase and to retain the lipid metabolites in the lower organic phase. The extract was mixed with 2 ml of water, vortexed and centrifuged briefly to separate the phases. The aqueous phase was withdrawn and saved. The lower phase was washed with 4 ml of theoretical upper phase consisting of chloroform/methanol/water (3 : 48 : 47, v/v/v) and the resultant upper phase combined with the first upper phase. The lower phase was taken to dryness, residue redissolved in 10 ml of chloroform/methanol (2 : 1) and the above partitioning procedure was repeated. We found it necessary to perform the partitioning procedure twice to remove more than 95% of labeled G_{M2} from chloroform/methanol extracts of culture medium containing the ganglioside. Due to the high salt concentration of the medium, G_{M2} is not completely removed into the aqueous phase with only cycle of the partitioning procedure. From the pooled upper phases (17.3 ml) containing labeled ganglioside and the final lower phase (7.2 ml) containing labeled lipid metabolites, 400 μl aliquots were taken in small counting vials for determining radioactivity as previously described [11]. The ganglioside present in the aqueous phase was purified on a small BondElut C18 cartridge as previously described [11] and radioactive component identified as G_{M2} by thin layer chromatography [11]. The total lipids from the lower phase were subjected to alkaline hydrolysis and fractionated on a small silicic acid column by successive elution with chloroform, acetone/methanol (9 : 1, v/v) and then methanol, and radioactivity in each fraction determined as described previously [11].

The fibroblast cell pellets were sonicated in 200 μl water. After removing a sample for protein determination [13], the homogenate was extracted with chloroform/methanol (2 : 1) and analyzed for radioactivity as previously described [11].

Results

In order to ensure the cells maintained metabolic activity over the long experimental time in culture, $[^3H]$glycine incorporation into protein was measured between day 0 and day 42. $[^3H]$glycine uptake into hot trichloroacetic acid precipitable material ranged from 28 000 to 53 000 cpm/mg protein over the 4 hour labeling period, with lowest values found on day 0, some 13 days after the cells were originally plated onto 6 cm dishes. Maximal incorporation was found on day 21, but day 42 had higher cpm/mg protein than day 0 (38 000 vs. 28 000), indicating that overall metabolic activity, as reflected in short-term protein synthesis, was not hampered as cell remained on the dishes for this extended period. No cell disruption was observed during routine examination with a microscope over the course of the experiment. Total cellular protein increased throughout this period from 0.33 mg on day 0 to 0.42 mg on day 21 and 0.58 mg per dish on day 42.

TABLE I

RELEASE OF RADIOACTIVITY INTO THE MEDIUM FROM CONTROL CELLS PRELOADED WITH LABELED G_{M2} DURING THE CHASE PERIOD

The medium collected during weekly changes was counted for radioactivity. Chloroform/methanol (2 1) extracts of media were partitioned to remove unhydrolyzed G_{M2} into the aqueous phase, while retaining the metabolic products in the organic phase.

Time	Counts per min per dish	Total percentage	Percentage in aqueous phase
Day 0– 7	65 760	36	39
Day 7–14	35 165	19	39
Day 14–21	28 306	15	42
Day 21–28	20 601	11	28
Day 28–35	19 140	10	39
Day 35–42	14 500	8	19
Total 0–42	183 472		

The continuing metabolic activities of the cells in handling $[^3H]G_{M2}$ was observed throughout the culture period after removing the labeled ganglioside from the medium. Radioactivity was released from control cells into the medium during this entire time (Table I). More than half of the total released radioactivity were recovered during the first and second weeks of the post-labeling period (36 and 19% of the total, respectively), which declined to only 8% of the total released during the last week. The lipid extracts of the medium were partitioned with water to remove the unhydrolyzed $[^3H]G_{M2}$ ganglioside into the aqueous upper phase. The radioactivity in the aqueous phase was present only in gangliosides and none as small water-soluble molecules as determined by

TABLE II

RADIOACTIVITY RELEASED IN THE TRYPSIN DIGEST WHEN CELLS WERE HARVESTED BY TRYPSINIZATION

For each time point, two dishes were harvested by trypsinization and the combined trypsin digests were counted for radioactivity. Chloroform/methanol (2:1) extracts of the trypsin digests were partitioned to remove unhydrolyzed G_{M2} into the aqueous phase, while retaining the metabolic products in the organic phase

Time	Counts per min per dish	Percentage in aqueous phase
Day 0	37070	70
Day 21	10813	60
Day 42	6486	31

chromatography on Bond Elut C_{18} cartridge [11]. The unhydrolyzed $[^3H]G_{M2}$ in the medium dropped from 39% in the first week to 19% by the last week in the unlabeled medium (Table I), indicating that metabolic products of labeled G_{M2} were continuously released from the cells into the medium.

Radioactivity in the trypsin-removable cell-surface material also declined steadily throughout this time, but unhydrolyzed $[^3H]G_{M2}$ predominated in this fraction for the first half of the post-label period (Table II). At the end of 6 weeks in non-labeled medium, almost a third of the radioactivity recovered in this component were still unhydrolyzed $[^3H]G_{M2}$ (Table II).

TABLE III

RADIOACTIVITY IN THE METABOLIC PRODUCTS OF LABELED G_{M2} PRESENT IN THE MEDIA AND TRYPSIN DIGESTS

Radioactive lipids from the lower organic phase of a washed lipid extract were fractionated on a silicic acid column.

	Chloroform fraction	Acetone · methanol fraction	methanol fraction
Media			
Day 21	39%	24%	37%
Day 42	43%	25%	32%
Trypsin digest			
Day 0	35%	40%	25%
Day 21	36%	33%	30%
Day 42	24%	35%	40%

Fractionation of the lipids in the lower organic phase by silicic acid column chromatography showed that both media and trypsin digest supernatants contained a variety of G_{M2} ganglioside metablic products (Table III). Thin-layer chromatography analysis of the chloroform fraction indicated that the radioactivity was in fatty acids originating from ester linkage in glycerolipids. All of the radioactivity of the methanol fraction was present as sphingomyelin. Cells from variant forms of G_{M2} gangliosidoses were also examined similarly in these same experiments. Like control cells, these cells also continuously released cellular radioactivity into the medium. However, unlike controls, this radioactivity consisted essentially of $[^3H]G_{M2}$ ganglioside with very little of its hydrolytic products (data not shown).

Because of this continuous release of radioactivity into the medium by both control and disease cell lines, the cell-associated radioactivity continued to decline during the course of the post-labeling period. Nevertheless, at any time point, the percent distribution of remaining intracellular radioactivity between the aqueous and organic phases of washed lipid extract reflected the extent

TABLE IV

G_{M2} HYDROLYSIS IN SITU IN FIBROBLASTS PRELOADED WITH THIS LABELED GANGLIOSIDE

Confluent cultures of normal human skin fibroblasts were maintained in the medium containing sphingosine labeled $[^3H]G_{M2}$ ganglioside (20 μM, 48000 cpm/nmol) for 10 days After this time, labeled media were replaced with a regular medium without any ganglioside, and the cultures were maintained for an additional 21 and 42 days with periodic changes of medium The cells were extracted with chloroform/methanol (2:1) and analyzed for unhydrolyzed ganglioside. Values for duplicate dishes are given separately for each time point Day 0 refers to the day on which the cells were changed into non-radioactive medium

Days after G_{M2} removal	Protein (mg) per dish	Counts per min per dish	Percentage aqueous phase
0	0.245	132170	55
	0.209	102654	51
21	0.362	69595	33
	0.398	68418	33
42	0.495	40411	20
	0.495	47352	21

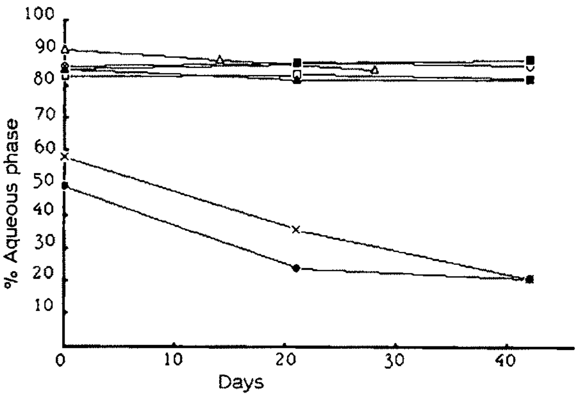

Fig 1 [^{3}H]G_{M2} metabolism in control and G_{M2} gangliosidosis skin fibroblasts Cells were labeled for 10 days in [^{3}H]G_{M2} when the medium was removed and replaced with unlabeled medium (day 0) Cells were harvested at day 0, and days 21 and 42 (or 14 and 28) during the post-labeling period Chloroform/methanol (2·1) extracts of the cells were partitioned with water to remove unhydrolyzed G_{M2} into the aqueous upper phase, while retaining the metabolic products in the organic lower phase The values on the ordinate represent unhydrolyzed G_{M2} in the aqueous phase All points are averages of duplicate or triplicate analyses of the same cell line Two different control lines were used, and one line for each G_{M2} gangliosidosis ◇——◇, Tay-Sachs, ■——■, Sandhoff, □——□, Juvenile Tay-Sachs, ▲——▲, Juvenile Sandhoff; △——△, AB Variant, ×——×, Control (No 2493), ◆——◆, Control (No. 4)

of the metabolic breakdown of the ingested [^{3}H]G_{M2} ganglioside in the cell (Table IV). Normal cells effectively metabolize the labeled ganglioside during the post-label period with only about 20% present as G_{M2} at the end of the experiment. In fibroblasts from various forms of G_{M2} gangliosidosis, intracellular radioactivity remained essentially as unhydrolyzed G_{M2} (approx. 90%) at all time points in the post-label period (Fig. 1). The small amount of radioactivity seen in the organic phase from day 0 to day 42 in extracts from these disease cell lines is not due to metabolism, but due to the partioning of a small amount of G_{M2} into the organic phase as determined by thin-layer chromatography (data not shown).

Discussion

In the earlier studies on uptake and metabolism of [^{3}H]G_{M2} ganglioside by human skin fibroblasts, a 10-day labeling period provided a method to distinguish between those individuals capable of metabolizing G_{M2} and those incapable of hydrolyzing this substrate [11]. Sonderfield et al. [14] noticed that incorporation of labeled G_{M2} by fibroblasts depended strongly on the concentration of fetal calf serum in the culture medium. Optimizing at 0.3% serum concentration with 50 μM G_{M2} in the medium, they have shown that 40% of G_{M2} ingested during 72–92 h was metabolized by control cells, whereas in fibroblasts from patients with G_{M2} gangliosidosis, 96% of cellular radioactivity remained as unhydrolyzed G_{M2}.

In the present study, metabolism of ingested [^{3}H]G_{M2} was followed over an extended period of time after removal of labeled ganglioside from the medium. Both control and disease cell lines continuously release radioactive material into the medium for this entire period: quickly at first, then more slowly towards the end. The released material from control cells mostly contained metabolic products with smaller amounts of unhydrolyzed ganglioside. The metabolic products consisted of esterified fatty acids, sphingomyelin and other neutral sphingolipids. The media collected from disease cell lines contained essentially unhydrolyzed ganglioside.

In contrast to the results found for medium of control cells, radioactivity in the trypsin removable pericellular surface component of these cells was present mostly as G_{M2} for the first half of the post-labeling period. These results suggest that exogenous [^{3}H]G_{M2} is strongly attached to the trypsin-removable surface material. It is apparently not incorporated readily into the plasma membrane for internalization and metabolism by lysosomes in control cells. After incorporation, radioactivity in the cell associated ganglioside declined with time, and there was an increase of its metabolic products. However, cell-associated G_{M2} was not completely hydrolyzed, suggesting that exogenous G_{M2} incorporated into plasma membrane is not directly transported to the lysosomes for complete hydrolysis. Instead, the ganglioside may move slowly within intracellular membranes by membrane flow until its eventual transfer to lysosomes where it can be catabolized. Also, these results suggest that as the [^{3}H]sphingosine-labeled G_{M2} was metabolized in control cells, the labeled products (consisting of ester-linked fatty acids in glycerolipids and sphingolipids, including sphingomyelin) were exocytosed into the medium, when they could be partly bound to the pericellular surface membrane and found as trypsin removable components. It can be calculated that on day 0, before trypsinization, there are 154482 cpm per dish and at the end of the experiment, day 42, there are 50368 cpm per dish showing that about 70% of ingested radioactivity is released from the cells during this time. This is recovered in the medium as cpm/dish collected from day 0 to day 42 (Table I).

In the disease cells, very little metabolism of the ingested labeled G_{M2} was seen in the entire period after removing labeled ganglioside from the medium. This suggests that hexosaminidase B in Tay-Sachs disease, hexosaminidase S in Sandhoff disease and normal hexosaminidase A without the activator protein in AB variant do not have any residual slow rate of hydrolytic activity on the intracellular G_{M2}. It appears that both normal hexosaminidase A and the activator protein are essential to detect even a small amount of metbaolism of G_{M2} in vivo using these methods.

Studies on sulfatide metabolism in fibroblasts from variant forms of metachromatic leukodystrophy have shown that there is no residual metabolism in cells from infantile metachromatic leukodystrophy, but cells from juvenile and adult metachromatic leukodystrophy could be distinguished by their residual slow metabolism of the ingested sulfatide [14–17]. Conzelmann et al. [18] have reported that when G_{M2} hydrolysis was assayed in vitro in the presence of activator protein, fibroblasts from adult type G_{M2} gangliosidosis had measurable residual activity compared to the total deficiency observed in cells from infantile G_{M2} gangliosidosis. We have also reported that cells from adult-type G_{M2} gangliosidosis exhibited a small amount of metabolism when preloaded with labeled G_{M2} and maintained for 42 days in the absence of $[^3H]G_{M2}$ [19]. This observation must be confirmed, however, using cells from several patients with adult type G_{M2} gangliosidosis. The kinetics of G_{M2} metabolism as described above, should be evaluated carefully in these adult variants to determine if this milder clinical course is explicable using these techniques and, thus, distinguishable in vivo from severe infantile G_{M2} gangliosidosis.

Acknowledgements

This study was supported by grants HD-05515 and HD-04147 and from the National Institutes of Health grant GM-28207. We thank Denise C. McDonough for her excellent assistance in preparing this manuscript.

References

1 O'Brien, J S (1983) in Metabolic Basis of Inherited Diseases (Stanbury, J B , Wyngaarden, J.B., Fredrickson, D S , Goldstein, J.L and Brown, M S , eds), pp 945–969, McGraw-Hill, New York

2 Conzelmann, E and Sandhoff, K (1979) Hoppe-Seylers Z. Physiol Chem 360, 1837–1849

3 Conzelmann, E and Sandhoff, K (1978) Proc Natl Acad Sci. USA 75, 3979–3983

4 O'Brien, J S , Norden, A G W., Miller, A L., Frost, R G and Kelly, T E (1977) Clin. Genet 11, 171–183

5 Poulos, A., Holding, J and Carey, W F (1982) Clin Chim. Acta 108, 361–368

6 Erzberger, A., Conzelmann, E and Sandhoff, K. (1980) Clin Chim Acta 108, 361–368

7 Tallmann, J.F , Brady, R O., Quirk, J.M , Villaba, M and Gal, A E (1974) J Biol. Chem 249, 3489–3499

8 Sandhoff, K , Conzelmann, E and Nekhorn, H (1977) Hoppe-Seylers Z. Physiol Chem 358, 779–787

9 Li, S.-C., Hirabayashi, Y and Li, Y -T. (1981) J Biol Chem 256, 6234–6240

10 Harzer, K (1983) Clin Chim Acta 135, 89–93

11 Raghavan, S , Krusell, A , Lyerla, T A , Bremer, E G and Kolodny, E.H (1985) Biochim Biophys Acta 834, 238–248

12 Raghavan, S , Krusell, A , Krusell, J , Lyerla, T.A and Kolodny, E H (1985) Am J Hum Genet 37, 1071–1082

13 Lowry, O H , Rosebrough, N J , Farr, A L and Randall, R J. (1951) J Biol Chem 193, 265–275

14 Sonderfeld, S , Conzelmann, E., Schwarzmann, B.J., Hinrichs, U and Sandhoff, K (1985) Eur J Biochem 149, 247–255

15 Porter, M.T , Fluharty, A.L., Harris, S E. and Kihara, H (1970) Arch Biochem Biophys 138, 646–652

16 Kihara, H , Tsay, K K and Fluharty, A.L (1983) Biochem. Med. 29, 278–284

17 Kudoh, T and Wenger, D.A (1982) J Clin. Invest 70, 89–97

18 Conzelmann, E , Kytzia, H -J , Navon, R and Sandhoff, K (1983) Am J. Hum Genet 35, 900–913

19 Kolodny, E.H and Raghavan, S (1983) Trends Neurosci 6, 16–20

Biochimica et Biophysica Acta 917 (1987) 48–56
Elsevier

BBA 52436

Incorporation of arachidonic acid into 1-acyl-2-lyso-*sn*-glycero-3-phosphocholine of the human neutrophil

Floyd H. Chilton, Jean S. Hadley and Robert C. Murphy

Department of Pharmacology, University of Colorado School of Medicine, Denver, CO 80262 (U.S.A.)

(Received 8 August 1986)

Key words: Arachidonoyl-CoA : lysophosphatidylcholine acyltransferase; Neutrophil; Arachidonic acid; 1-Acyl-2-lyso-GPC; 1,2-Diacyl-GPC; 1-*O*-Alkyl-2-acyl-GPC; Molecular species

In this study, the initial incorporation of arachidonic acid into human neutrophils has been examined. Neutrophils pulse labeled for 5 min with [^{3}H]arachidonic acid rapidly incorporated this fatty acid into 1,2-diacylglycerophosphocholine. However, when neutrophils were pulse labeled with [^{3}H]arachidonic acid for 5 min, washed, and allowed to incubate for an additional 120 min, the relative amount of [^{3}H]arachidonic acid increased in alkylacylglycerophosphocholine molecular species. Similar, when neutrophils were pulse labeled, washed, and allowed to incubate in the presence of 30 μM unlabeled arachidonic acid for 120 min, [^{3}H]arachidonic acid was also remodeled into alkylacylglycerophospocholine. These results implied that the initial incorporation of [^{3}H]arachidonic acid proceeded via a free fatty acid intermediate into 1,2-diacyl-GPC, while the subsequent remodeling of arachidonate-containing glycerophospholipids did not. This initial incorporation was further investigated in a number of cell-free systems. Disrupted neutrophils incubated with [^{14}C]arachidonoyl-CoA incorporated [^{14}C]arachidonic acid into 1,2-diacyl-GPC containing 16:0, 18:0, and 18:1 at their *sn*-1 position in a pattern similar to that seen when whole neutrophils were incubated with arachidonic acid for 5 min. A small percentage of [^{14}C]arachidonate from [^{14}C]arachidonoyl-CoA was incorporated into 1-alkyl-2-acyl-GPC. The enzymatic activity responsible was found predominately in the membrane fraction of the broken cell preparation. This selectivity of the CoA-dependent acyltransferase for 1-acyl-linked glycerophosphocholine was further examined by adding [^{14}C]arachidonoyl-CoA and various 1-radyl-2-lyso-GPC to neutrophil membrane preparations. These studies provide evidence that the initial incorporation of arachidonic acid into *sn*-glycero-3-phosphocholine takes place by an arachidonoyl-CoA : lysophosphatidylcholine acyltransferase(s) which is selective for the 1-acyl-2-lyso-GPC.

Introduction

It has been recognized for some time that arachidonic acid serves as a precursor for various mediators of cell fucntion. The endogenous stores of arachidonate which give rise to these bioactive mediators are located primarily at the *sn*-2 position of glycerophospholipids in the resting mam-

---

Abbreviations: AA, arachidonic acid, GPI, glycerophosphoinositol; GPE, glycerophosphoethanolamine; GPC, *sn*-glycero-3-phosphocholine; HPLC, high-pressure liquid chromatography; TLC, thin-layer chromatography; HBSS, Hanks' balanced salt solution.

Correspondence: Dr. R C Murphy, Department of Pharmacology, University of Colorado School of Medicine, Denver, CO 80262, U S A

0005-2760/87/$03 50 © 1987 Elsevier Science Publishers B V (Biomedical Division)

malian cell. Thus, a number of phospholipase-dependent mechanisms (i.e., phospholipase A_2 and/or C) which lead to the liberation of these endogenous stores from a variety of glycerophospholipids (phosphatidylethanolamine, phosphatidylcholine and phosphatidylinositol) have been proposed in the activated cell [1–3]. However, in resting cells, levels of free arachidonic acid are very low [4]; therefore liberation of arachidonic acid must be coupled to very efficient esterification mechanisms in order to maintain these low levels. Several enzyme systems may be responsible for maintaining low levels of free arachidonic acid within a cell. For example, it has been recognized for some time that free arachidonic acid enters into lysophospholipids such as lysophosphatidylcholine through CoA-dependent acyltransferase(s) [5,6]. However, arachidonic acid must first be converted to arachidonoyl CoA at the expense of ATP by an acyl-CoA synthetase. In fact, a specific arachidonoyl-CoA synthetase has been reported in a number of cells [7–9]. Recently, it has become clear that this CoA-dependent mechanism is not the only way in which arachidonate is shuttled through complex lipids of cells. A number of investigators have described other CoA-dependent and -independent enzyme systems which may be responsible for the acylation of individual molecular species of a glycerophospholipid class [10–12]. Of particular interest is a CoA-independent transacylase which shuttles arachidonate from 1,2-diacyl to 1-*O*-alkyl-2-acylglycerophosphocholine [13–16]. It has been suggested that this enzyme is responsible for the rapid acylation of lyso platelet-activating factor and the high amount of arachidonate found in alkylacylcholinephospholipids in a number of cells [17–23].

We recently reported that arachidonic acid complexed to albumin was rapidly taken up into 1,2-diacyl-linked glycerol-phospholipids (GPI, GPC, and PGE) in human neutrophils. However, this arachidonate at a latter time rapidly appeared in 1-alkyl and/or 1-alk-1-enyl molecular species of choline- and ethanolamine-linked glycerophospholipids [24]. With these findings, we proposed that the initial incorporation of exogenous arachidonic acid into 1,2-diacyl-GPC was mediated by arachidonoyl-CoA : 1-acyl-2-lyso-GPC-acyl transferase(s). Subsequently, this arachidonate was remodeled into alkylacylglycerophospholine by other enzyme systems. In order to support further this hypothesis within the human neutrophil, we have examined the initial incorporation of free arachidonic acid and arachidonoyl-CoA arachidonic acid from arachidonoyl-CoA into various 1-radyl-2-lyso-GPC's. These findings provide further evidence for different mechanisms which may be responsible for the initial incorporation and subsequent remodeling of arachidonate-containing phosphatidylcholine within the human neutrophil.

Experimental procedures

Materials. [5,6,8,9,1,12,14,15-^{3}H(N)]Arachidonic acid and [arachidonoyl-1-^{14}C]arachidonoyl coenzyme A were purchased from New England Nuclear (Boston, MA). All solvents were HPLC grade from Fisher Scientified Co. (St. Louis, MO). L-alpha-monopalmitoyllecithin and lipid standards used in TLC and HPLC were purchased from Avanti Polar Lipids (Birmingham, AL). 1-*O*-Hexadecyl-2-lyso-*sn*-glycero-3-phosphocholine was purchased from Bachem (Bubendorf, Switzerland). Essentially fatty-acid-free human serum albumin and arachidonoyl CoA was purchased from Sigma (St. Louis, MO). Hanks' balanced salt solution was purchased from Gibco Laboratories (Grand Island, NY). Molecular species of arachidonic acid containing glycerophospholipids were synthesized following published procedures [25].

Preparation of human neutrophil. Human neutrophils were obtained from normal volunteers and isolated by the procedure described by Haslett et al., [26] using the Percoll-plasma technique. The neutrophils were then suspended in Hanks' balanced salt solution and distupred by pulse sonication (3 times at 50% duty cycle) for 30 s. At this point, whole neutrophils were removed from the sonicate by centrifugation 225 × *g* for 10 min. In some experiments, [^{14}C]arachidonoyl CoA (1.0 μM) was added to the neutrophil sonicate from $500 \cdot 10^6$ neutrophils and then allowed to incubate at 37 °C for 5 min. This incubation was terminated by adding $CHCl_3$/MeOH (1 : 2, v/v) to the incubation mixture. In other experiments, the sonicate was then further fractionated into soluble and membrane components by centrifugation (100 000 × g for 45 min). The membrane pellet was washed with HBSS followed by a second centrifugation (100 000 × g for 45 min). Finally, the membrane pellet was suspended in HBSS and the protein concentrations in both the soluble and the membrane fraction were determined by the method of Bradford et al. [27]. All fractions were stored at −70 °C until they were used. The acyl transferase activity remained constant for at least 8 days after storage at −70 °C.

Incorporation of [^{3}H]arachidonate into whole neutrophils. An aqueous solution (50 μl) containing labeled arachidonate (2 μCi) complexed to human serum albumin (5.0 mg/ml) was added to 0.95 ml of the cell suspension ($5.0 \cdot 10^7$ neutrophils) bringing the final concentration of arachidonate to 0.07 μM. The reaction was terminated by the addition of ice-cold HBSS (5.0 ml) containing fatty-acid-free human serum albumin (0.25 mg/ml) to the cell pellet. The cells were washed twice with HBSS containing fatty-acid-free human serum albumin (0.25 mg/ml) to rid cells of any exogenous arachidonic acid and suspended in 1.0 ml HBSS containing fatty-acid-free human serum albumin (0.25 mg/ml). The reaction mixture was then incubated at 37 °C for an aditional 120 min. For some experiments, neutrophils were pulse labeled for 5 min (without unlabeled arachidonate) and washed as described and then allowed to incubate at 37 °C with 30 μM of unlabeled arachidonic acid for 120 min. In all experiments, cells were removed from the supernate by centrifugation (225 × g). The incubations were terminated by adding methanol to the pellet.

Acyl-transferase assay. Details of individual assays are presented in the figure legends. Under standard condition, different 1-radyl-2-lyso-glycerophosphocholines complexed to fatty-acid-free human serum albumin were prepared in HBSS. To this mixture, 75 000 dpm (2 μl) of [^{14}C]arachidonoyl CoA along with varying concentrations of unlabeled arachidonoyl-CoA in ethanol/water (1 : 1) was then added. All assays were started by the addition of enzyme to the reaction mixture. The reaction mixture was then allowed to incubate at 37 °C for 5 min. Incubations were terminated by the addition of $CHCl_3$/MeOH; (1 : 2) to the reaction mixture.

Extraction and chromatography of the neutrophil lipids Lipids were extracted by the method of Bligh and Dyer [28]. Solvents from the organic phase were removed by a stream of nitrogen and the lipids suspended in $CHCl_3$/MeOH (1 : 1, v/v) for TLC analysis. Glycerophospholipids were separated by TLC on layers of silica gel G developed in chloroform/methanol/acetic acid/water (50 : 25 : 8 : 4, v/v). Neutral lipids were separated by TLC on layers of silica gel G developed in hexane/ether/formic acid (90 : 60 : 6, v/v). Glycerophosphocholine was isolated from other phospholipid classes by normal phase HPLC using an Ultrasphere-Si column (4.6 × 2.50 mm; Rainin, Woburn, MA) eluted with isopropanol/25 mM phosphate buffer/hexane/ethanol (490 : 62 : 367 : 100 : 0.6, v/v) at 1.5 ml/min [29]. The various molecular species of glycerophosphocholine were separated by reverse phase HPLC using an Ultrasphere ODS reverse-phase column (4.6 mm × 250 mm; Rainin, Woburn, MA) eluted with methanol/water/acetonitrile (905 : 70 : 25, v/v) and 20 mM choline chloride at 2 ml/min at 40 °C [29]. Radioactive products eluting from the HPLC were monitored either directly by an on-line scintillation counting system (Ramona-D; IN/US, Fairfield, NJ) or by monitoring the distribution of radioactive label in the eluent fraction by liquid scintillation spectroscopy. The predominant arachidonate-containing molecular species which contained label were identified by elutions with synthetic standards and their elution order determined by fast atom bomdardment mass spectroscopy [30,31].

Results

Influence of arachidonic acid supplementation on the incorporation of arachidonic acid into glycerophosphocholine

The possibility that the acylation of [^{3}H]arachidonic acid into different 1-radyl-2-arachidonoyl-GPC could be influenced by high levels of arachidonic acid in the incubation mixture was explored. Neutrophils were labeled with low concentrations (0.07 μM) of arachidonic acid for 5 min. By 5 min, arachidonic acid was incorporated into a number of glycerolipids [24]. In these experiments reported here, 10.0% of the [^{3}H]arach-

TABLE I

DISTRIBUTION OF [^{3}H]ARACHIDONIC ACID IN MOLECULAR SPECIES OF PHOSPHATIDYLCHOLINES

Neutrophils were pulse-labeled for 5 min and analyzed (5 min) or incubated for an additional 120 min without (120 min) or with 30 μM cold arachidonic acid (120 min, 30 μM) Incubations were terminated by extracting lipids from the cell pellet GPC was separated from other glycerophospholipid classes by normal phase HPLC Molecular species of 1-radyl-2-[^{3}H]arachidonoyl-GPC were isolated by reverse phase HPLC The amount of label in 1-acyl and 1-*O*-alkyl was determined by liquid scintillation counting Unknown molecular species constituted less than 5% of the label These data are representative of three separate experiments

Time (min)	% of total [^{3}H]arachidonate in glycerophosphocholine		
	sn-1 linkage		alk-1-enyl + unknown molecular species
	acyl	alkyl	
5	66	18	16
120	42	39	19
120 (30 μM AA)	43	42	15

idonic acid was incorporated into glycerophosphocholine. The amount of [^{3}H]arachidonic acid found in GPI, GPE, phosphatidic acid and neutral lipids was found to be 26.1%, 3.9%, 0.9% and 56.9%, respectively. This incorporation pattern was typical for normal human neutrophils observed in over 50 experiments. However, it must be stressed that a significant variation has been observed in the absolute labelling level of exgenously added arachidonic acid by neutrophils from patient to patient with GPC occasionally exceeding absolute GPI labeling. Further examination of the newly synthesized 1-radyl-2-[^{3}H]arachidonoyl-GPC revealed that [^{3}H]arachidonate was incorporated predominantly (66%) into 1,2-diacyl molecular species 18% into 1-*O*-alkyl-GPC and 16% into plasmalogen species and unknown GPC species (Table I). In similar experiments, neutrophils were pulse labeled for 5 min with [^{3}H]arachidonic acid (0.07 μM) then incubated in the presence and absence of arachidonic acid (30 μM) for an additional 120 min. In this experiment, the distribution of [^{3}H]arachidonic acid in glycerophosphocholine remained relatively constant at approx. 11.0% of the cells total [^{3}H]arachidonate in the absence and presence of unlabeled arachidonic acid for 120 min. Neutrophils incubated for an additional 120 min (without exogenous arachidonic acid) redistributed their [^{3}H]arachidonate into 1-alkyl-2-[^{3}H]arachidonoyl-GPC 39% and 42%, respectively (Table I). HPLC analysis of the labeled 1,2-diacyl-glycerophosphocholine molecular species revealed 16 : 0, 18 : 0, and 18 : 1 at their *sn*-1 position (data not shown). In addition, neutrophils incubated with arachidonate (30 μM) remodeled [^{3}H]arachidonate in a pattern of the molecular species similar to neutrophils incubated without 30 μM arachidonic acid (Table I). These findings sugegst that the transfer of [^{3}H]arachidonate into alkyl-acyl-GPC may not involve a free acid intermediate, since high levels of unlabeled arachidonic acid did not inhibit the transfer process. However, it was possible that the arachidonic acid pool from which [^{3}H]arachidonic acid was transferred to 1-alkyl-2-lyso-GPC was not diluted in this experiment due to equilibration factors. It was not possible to test these hypotheses without major assumptions using an intact cell system. Therefore, the incorporation of arachidonic acid into 1-acyl-2-arachidonoyl-GPC was further examined in a cell-free system.

Incorporation of [^{14}C]arachidonoyl-CoA into neutrophil glycerophosphocholine

In these experiments, the arachidonoyl CoA synthetase step was bypassed by adding [^{14}C] arachidonoyl-CoA to disrupted neutrophil ($500 \cdot 10^6$) suspension for 5 min. Because the specific activity of the [^{14}C]arachidonoyl-CoA added in these experiments was approximately 10-fold lower than that of [^{3}H]arachidonic acid, this would mean that a total of 1 μM arachidonoyl-CoA would be added to the broken cell suspension. Therefore, the number of neutrophils ($500 \cdot 10^6$) used in this experiment was increased 10-fold to mimic the experiments in which $50 \cdot 10^6$ neutrophils were incubated with [^{3}H]arachidonic acid (0.07 μM). The distribution of [^{14}C]arachidonate in the various glycerophospholipids was determined by TLC and the [^{14}C]arachidonate associated with individual molecular species of GPC was analyzed by reverse phase HPLC. By 5 min, 90% of the added [^{14}C]arachidonoyl-CoA had been incorporated to a number of glycerophospholipids (Table II), GPC

TABLE II

DISTRIBUTION OF [^{14}C]ARACHIDONIC ACID INTO GLYCEROPHOSPHOLIPID CLASSES FROM [^{14}C]ARACHIDONOYL-CoA

Sonicated neutrophils were incubated with [^{14}C]arachidonoyl-CoA for 5 min as described in Experimental procedures The incubation was terminated by extracting the lipids from the cell pellet and supernatant followed by TLC separation of the combined extracts The distribution of [^{14}C]arachidonate is expressed as the percent of total labeled glycerolipids and is the average of three experiments (error bars ± S E M)

Class	% Total radioactivity
PC	28.6 ± 8.7
PI	4.6 ± 1.1
PE	26.0 ± 8.9
Neutral lipid	27.5 ± 3.3

had retained (28.6 ± 8.7%) of the total label incorporated into glycerophospholipids during this incubation. This [^{14}C]arachidonate was found by HPLC (Fig. 1) to be distributed into different 1-radyl-linked GPC's. Following this 5 min incubation, the majority (72%) of [^{14}C]arachidonate was associated with 1-acyl-2-[^{14}C]arachidonoyl-GPC (Fig. 1A). The newly synthesized 1-acyl-2-[^{14}C]arachidonoyl-GPC contained primarily 16 : 0, 18 : 0, and 18 : 1 at their *sn*-1 position. Only 17% of the [^{14}C]arachidonate was distributed in 1-alkyl-2-arachidonoyl-GPC (Fig. 1B). The remaining 11% of the label was associated with other minor components such as 1-alk-1-enyl-2-arachidonoyl-GPC (data not shown).

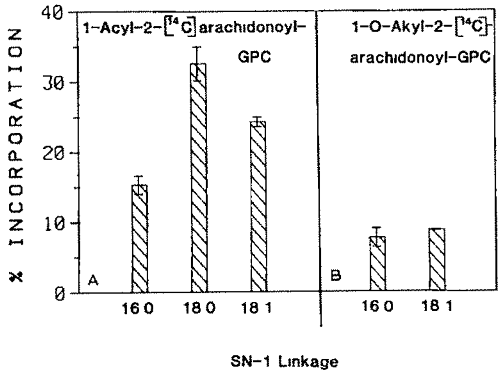

Fig. 1. Molecular species of PGC labeled with [^{14}C]arachidonoyl-CoA by the cell-free system Sonicated neutrophils (500 10^6) were incubated with [^{14}C]arachidonoyl-CoA for 5 min as described in the Methods The incubation was terminated by extracting the lipids from the cell pellet and supernatant GPC was isolated from other glycerol phospholipids by normal phase HPLC The distribution of [^{14}C]arachidonate in individual molecular species of GPC expressed here as the % incorporation was analyzed by reverse phase HPLC and is the average of three experiments (error bars ± S E M.) (A) 1,2-Diacyl-GPC molecular species; (B) 1-alkyl-2-acylGPC molecular species The radyl group at *sn*-1 is indicated either as 1-acyl or 1-*O*-alkyl with the total carbon chain: number of double bonds indicated.

Arachidonoyl transferase(s) activity within soluble and membrane components

The neutrophil sonicate was further fractionated into soluble and membrane components as described in the methods. An aqueous solution containing [^{14}C]arachidonoyl CoA (1.0 μM) along with 1-hexadecanoyl-2-lyso-GPC (40 μM) and 1-hexadecyl-2-lyso-GPC (40 μM) complexed to albumin was added to each of the neutrophil preparations and allowed to incubate for 5 min at 37°C. The incorporation of [^{14}C]arachidonoyl-CoA into GPC as a function of soluble or membrane protein concentration in the incubation mixture is shown in Fig. 2. These studies revealed that the membrane components contained most of the arachidonoyl transferase(s) activity found within the human neutrophils. In addition, the

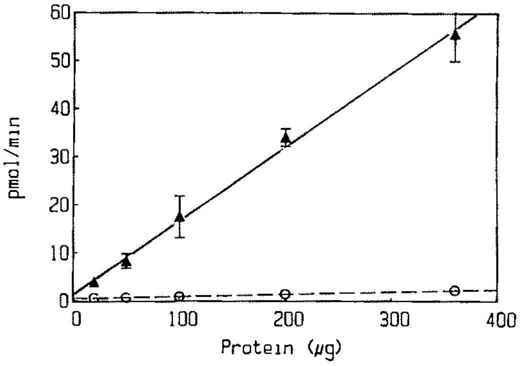

Fig 2. Incorporation of arachidonoyl-CoA into phosphatidylcholine as a function of protein concentration Neutrophil membranes (▲——▲) and soluble preparations (○——○) were incubated with 1-hexadecanoyl-2-lyso-GPC (40 μM) and 1-*O*-hexadecyl-2-lyso-GPC (40 μM) and [^{14}C]arachidonoyl CoA (1 μM) for 5 min. The incubation was terminated by extracting the lipids from the incubation mixture GPC was separated from other glycerophospholipids by TLC as described and is the average of three experiments (error bars ± S E M)

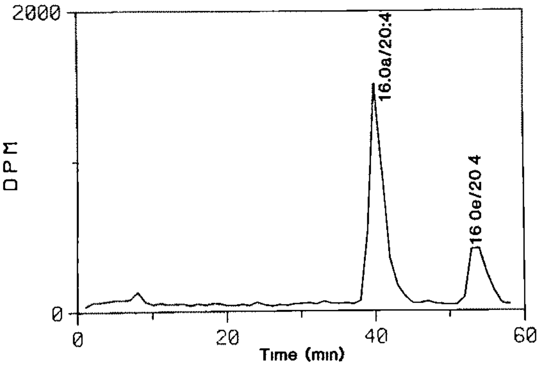

Fig 3. Reverse-phase HPLC separation of the lipid extract from the neutrophil membrane preparation (200 μg) incubated with 1-hexadecanoyl-2-lyso-GPC (40 μM), 1-*O*-hexadecyl-2-lyso-GPC (40 μM), and [^{14}C]arachidonoyl-CoA (1 μM for 5 min). The incubation was terminated by extracting the lipids from the incubation mixture. Phosphatidylcholine was isolated from other glycerophospholipids by normal phase HPLC prior to this separation These data are representive of two separate experiments

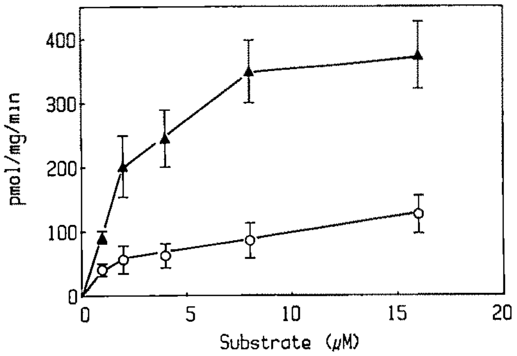

Fig 4 Incorporation of arachidonoyl-CoA into phosphatidylcholine as a function of lyso-GPC molecular species Neutrophil membrane preparation (200 μg) was incubated with [^{14}C]arachidonoyl-CoA (1 μM) and increasing concentrations of either 1-hexadecanoyl-2-lyso-GPC (▲——▲) or 1-O-hexadecyl-2-lyso-GPC (○——○) for 5 min The incubation was terminated by extracting the lipids from the incubation mixture Phosphatidylcholine was separated from other glycerophosphocholines by TLC and is the average of three experiments (error bars ± S.E.M.)

arachidonoyl transferase activity of the membrane fraction increased linearly over the protein range which was tested. Examination of the newly synthesized 1-radyl-2-[^{14}C]arachidonoyl-GPC from the membane preparation containing 200 μg of protein revealed that [^{14}C]arachidonate was primarily incorporated into 1-hexadecanoyl-2-[^{14}C]arachidonoyl-GPC (74%) and to a much lesser extent 1-hexadecyl-2-[^{14}C]arachidonoyl-GPC during the 5 min incubation (Fig. 3). However, it was not know if the endogenous levels of 1-hexadecanoyl-2-lyso-GPC and 1-hexadecyl-2-lyso-GPC in the membrane preparation were playing a role in the specificity observed here. In order to role out this possibility and further explore apparent specificity of the membrane arachidonoyl transferase(s) for 1-acyl-2-lyso-GPC, arachidonoyl transferase(s) activity of the neutrophil membrane fraction was measured as a function of increasing 1-radyl-2-lyso-GPC concentrations found within the incubation mixture (Fig. 4). A large percentage of [^{14}C]arachidonate from [^{14}C]arachidonoyl CoA was incorporated into 1-hexadecanoyl-2-lyso-GPC at all lyso concentrations when this substrate alone was added to the membrane preparation. In contrast to the 1-hexadecanoyl-2-lyso-GPC, 1-hexadecyl-2-lyso-GPC was a poorer substrate for the membrane enzymes at all concentrations tested. Maximal enzyme activity using 1-hexadecanoyl-2-lyso-GPC as a substrate was observed at (16 μM) and this activity declined at concentrations higher than 25 μM (data not shown). To ascertain further that 1-hexadecanoyl-2-[^{14}C]arachidonoyl-GPC was being produced during the incubation, we further examined the distribution of [^{14}C]arachidonate by reverse-phase HPLC in the labeled phosphatidylcholine obtained from our assay mixture (16 μM, 1-hexadecanoyl-2-lyso-GPC). As expected, [^{14}C]arachidonate was found only in the molecular species 1-hexadecanoyl-2-[^{14}C]arachidonoyl-GPC (data not shown).

Experiments designed to evaluate enzymatic parameters of the crude arachidonoyl-CoA transferase did not demonstrate saturation kinetics when arachidonoyl-CoA was varied from 1 to 200 μM. These experiments were carried out with an equal molar mixture of 1-acyl-lyso-GPC and 1-*O*-alkyl-lyso-GPC at 200 and 400 μM in order to limit substrate availability for the higher concentrations of [^{14}C]arachidonoyl CoA. Unfortunately, inhibition of the transferase by the lyso substrates as mentioned above reduced the apparent enzymatic activity. However, in these experiments the amount of glycerophosphocholine product detected as [^{14}C] extracted by the Bligh-

Dyer technique, linearly increased from 135 to 310 pmol/min per mg protein as arachidonoyl-CiA increase from 1 μM to 200 μM (200 μM lyso-GPC). When 400 μM lyso-GPC was employed, a parallel but reduced amount of product resulted. HPLC analysis of the product revealed 1,2-diacyl-GPC as the major product as seen above. In control experiments, with no lyso GPC substrate added, 10% of the radioactivity from [^{14}C]arachidonoyl CoA (1 μM) was extractable using Bligh-Dyer conditions and less than 5% at 200 μM. In both cases, the radioactive product was predominately free arachidonic acid.

Finally, it was important to determine the stability of the [^{14}C]arachidonoyl-CoA in our assay system. For example, it was possible that the free [^{14}C]arachidonic acid which was found to be formed by arachidonoyl-CoA hydrolase activity during the incubation (data not shown) could account for the acylation of 1-radyl-2-lyso-GPC. However, when [^{3}H]arachidonic acid was added to the assay mixture (200 μg of membrane protein) at an identical concentration as [^{14}C]arachidonoyl-CoA, no [^{3}H]arachidonic acid was incorporated into glycerophospholipids. This experiment revealed that the [^{14}C]arachidonate which was incorporated in GPC arose from [^{14}C]arachidonoyl-CoA and not free [^{14}C]arachidonic acid.

Discussion

Previous experiments revealed that arachidonic acid complexed to albumin was selectively incorporated into the 1,2-diacyl-linked glycerophospholipids GPC, GPE, and GPI. However, this label over time appeared in 1-alk-1-enyl and 1-*O*-alkyl linked molecular species in choline and ethanolamine-linked glycerophospholipids [24]. The initial incorporation of arachidonic acid into 1,2-diacyl glycerophospholipids could arise in several ways. Firstly, 1-acyl-linked products could be located within a cell domain more accessible to exogenous arachidonic acid and indeed, studied by Record et al. [32] revealed that 1-acyl-linked phosphatidylcholine is located in the outer leaflet of the plasma membrane of ascites cells. However, other studies in neutrophils (data not shown) and fibroblasts [33], which localized by autoradiography labeled arachidonate in experimental protocols similar to that described above, indicated that the nuclear envelope contained the highest specific activity of arachidonate within the first 5 min of labeling. It cannot be determined from these studies where the initial acylation of arachidonic acid into 1,2-diacyl glycerophospholipids had taken place, but the final location of the 1,2-diacyl glycerophospholipids at these early time points could be observed. An alternative hypothesis to the proximity argument is that there are enzyme systems responsible for the selectivity seen in the initial incorporation of arachidonic acid into 1,2-diacylglycerophospholipids. Other enzymes might be responsible for the appearance of arachidonate in 1-*O*-alkyl-2-acyl-GPC. In the present investigation, we have focused on the incorporation of arachidonic acid into glycerophosphocholine and obtained evidence in support of the hypothesis for selectivity in initial esterification.

Experiments suggested that the incorporation of arachidonic acid into 1,2-diacyl-GPC and the subsequent appearance of arachidonate in 1-*O*-alkyl-2-acyl-GPC may be mediated by different enzyme systems. In these experiments, the majority of the trace amounts of labeled arachidonic acid was initially incorporated into 1,2-diacyl PC. However, more of the [^{3}H]arachidonic acid appeared in the 1-*O*-alkyl-2-acyl-GPC fraction following a 120 min incubation. This subsequent remodeling of arachidonic acid was not influenced by high levels of unlabeled arachidonic acid (30 μM) suggesting that free arachidonic acid is not a requisite intermediate in this process. However, this result must be interpreted with caution because the labeled and free arachidonic acid pools may differ in location in these two situations.

Using a cell-free system, the arachidonoyl CoA synthetase was bypassed by adding arachidonoyl-CoA directly and the initial acylation of arachidonic acid from arachidonoyl-CoA into various GPC's was examined. In these experiments disrupted neutrophils selectively incorporated [^{14}C] arachidonic acid from [^{14}C]arachidonoyl-CoA into 1,2-diacyl-GPC in a pattern similar to that seen when intact neutrophils were incubated with trace levels of free arachidonic acid complexed to albumin. It is important to stress that the selectivity seen here cannot be accounted for by the availability of alkyl or acyl substrate, since composition studies of human neutrophil indicate that 44% of 1-radyl-1-acyl-GPC is 1-*O*-alkyl linked and 47% is 1-acyl linked [19]. An alternative explanation is that a larger 1-acyl-2-lyso-GPC pool could arise from a specific phospholipase A_2 which would favor diacyl-GPC over alkylacyl-GPC. This could not be ruled out from the whole cell or broken cell preparation. However, when various concentrations of each lyso substrates were added to the membrane preparation, diacyl-GPC synthesis predominated over alkyl acyl-GPC synthesis.

This apparent specificity of the acyl transferase for 1-acyl-2-lyso-GPC was further tested in isolated membrane and cytosolic preparations from the human neutrophils. In these studies, the majority of the acyl transferase activity was located in the membrane preparation when both hexadecanoyl-2-lyso-GPC were added as substrates. Examination of the newly synthesized phosphatidylcholine from this membrane preparation revealed that [^{14}C]arachidonate from [^{14}C]arachidonoyl-CoA was distributed primarily in 1-hexadecanoyl-2-lyso-GPC. In addition, the same specificity of the membrane acyl transferase(s) for 1-acyl-2-lyso-GPC was observed at all concentrations of arachidonoyl CoA tested. Furthermore, as mentioned above, this apparent selectivity was further confirmed in experiments in which each substrate (1-alkyl-2-lyso-GPC and 1-acyl-2-lyso-GPC) was added individually to membrane preparations at identical concentrations (Fig. 4). Here, both rate and maximal activity of the acyl transferase were higher for the acyl substrates than the corresponding alkyl counterpart; but the specificity for the acyl substrate was not absolute. The possibility that small amounts 1-alkyl-2-arachidonoyl-GPC formed in the assay may originate from a small amount of transfer of arachidonate from 1,2-diacyl-GPC or other glycerophospholipids to 1-*O*-alkyl-2-acyl-GPC (i.e., transacylase) during the 5 min incubation period cannot be ruled out, since this enzyme is also found in the membrane preparation. However, the selectivity observed here could not be accounted for by a specific phospholipase A_2, since high levels of both substrates were added.

Earlier studies have provided evidence for a specific arachidonoyl CoA synthetase in the human platelet [7]. In addition, this enzyme has also been reported in a number of other cell types including granulocytes [8,9]. In this study, evidence is provided to suggest that an initial incorporation of arachidonic acid into phosphatidylcholine probably involves an arachidonoyl-CoA : lysophosphatidylcholine acyltransferase that is selective for 1-acyl-linked glycerophosphocholine (Fig. 5). It should be noted that approx. 65% of the arachidonate in the 1-radyl-2-acyl-GPC is in 1-*O*-alkyl-GPC fraction; and yet, free arachidonic acid or arachidonic acid from arachidonoyl CoA is incorporated into 1,2-diacyl-linked phosphocholines initially in every system tested. This would suggest that another enzyme maybe responsible for the acylation of 1-*O*-alkyl-2-lyso-GPC. While the subsequent appearance of arachidonate in 1-*O*-alkyl-2-acyl-GPC was not addressed directly in this study, we and others have proposed that this step takes place through a CoA-independent transacylase [13–16,24]. In addition, this enzyme appears to be responsible for the selective acylation of lyso platelet-activating factor by arachidonate during platelet-activating factor inactivation. From these studies, we have proposed a three-step mechanism which may account for the initial uptake and the subsequent remodeling of arachidonate-containing phosphatidylcholine in the neutrophil (Fig. 5). These pathways may account for the high amount of arachidonate in 1-*O*-alkyl-2-acylglycerophosphocholine and further emphasize the potential role of 1-*O*-alkyl-2-arachidonoylglycerophosphocholine as

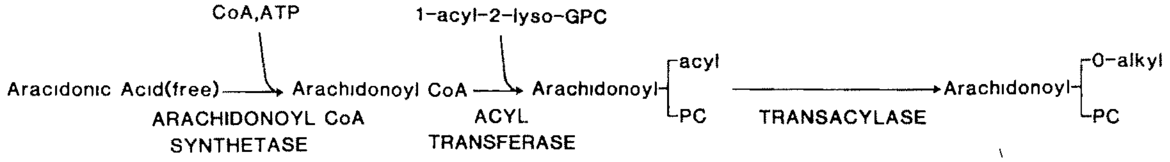

Fig 5 Proposed pathway for the initial incorporation and subsequent remodeling of arachidonate containing phosphatidylcholine.

a precursor for platelet-activating factor and eicosanoids [34,35].

Acknowledgements

The authors wish to acknowledge Dr. Peter M. Henson for the isolated human neutrophils as well as helpful discussions throughout the course of these investigations. This work was supported in part by a grant from the National Institutes of Health (AI 20774 and HL34303).

References

1 Van den Bosch, H. (1982) Phospholipase in Phospholipids (Hawthorn, J N. and Ansell, G B , ed), pp 313–357, Elsevier Biomedical Press, Amsterdam

2 Rittenhouse-Simmons, S (1979) J. Clin Invest 63, 580–587

3 Bell, R L , Kennerly, D A., Stanford, N and Majerus, P.W (1979) Proc Natl. Acad Sci USA 76, 3238–3241

4 Bills, T K., Smith, J B and Silver, M J. (1977) J. Clin. Invest 60, 1–6

5 Hill, E E., Husbands, D.R. and Lands, W E M (1968) J Biol Chem 243, 440–4451

6 Lands, W E M and Crawford, C G. (1976) in: The Enzymes of Biological Membranes (Martonosi, A , ed) Vol. 2, pp 3–20, Plenum Press, New York

7 Wilson, D B , Prescott, S M. and Majerus, P.W (1982) J Biol Chem. 257, 3510–3515

8 Neufeld, E J , Bross, T E and Majerus, P W. (1984) J Biol Chem 259, 1986–1992

9 Laposata, M , Reich, E L and Majerus, P W (1985) J. Biol Chem 260, 11016–11020

10 Kameyama, Y., Yoshioka, S , Imai, A and Nozawa, Y. (1983) Biochim. Biophys Acta 752, 244–250

11 Trotter, J , Flesch, I , Schmidt, B and Ferbes, E (1982) J Biol Chem 257, 1816–1823

12 Kramer, R M , Pritzker, C R. and Deykin, D (1984) J Biol Chem 259, 2403–2406

13 Kramer, R.M., Patton, G M , Pritzker, C R and Deykin, D (1984) J Biol. Chem 259, 13316–13320

14 Kramer, R M. and Deykin, D (1983) J Biol. Chem 258, 13806–13811

15 Sugiura, T. and Waku, K. (1985) Biochem. Biophys Res Commun 127, 384–390

16 Robinson, M , Blank, M L. and Snyder, F (1985) J. Biol Chem 260, 7889–7895

17 Chilton, F.H., O'Flaherty, J T , Ellis, J.M., Swendsen, C L and Wykle, R.L. (1983) J. Biol Chem. 258, 6357–6361

18 Chilton, F H , O'Flaherty, J.T , Ellis, J.M , Swendsen, C.L and Wykle, R.L (1983) J. Biol. Chem 258, 7268–7271

19 Mueller, H.W , O'Flaherty, J.T , Green, D G., Samuel, M P and Wykle, R L. (1984) J Lipid Res 25, 383–388

20 Mueller, H W , O'Flaherty, J.T and Wykle, R L (1982) Lipids 17, 72–77

21 Sugiura, T , Nakajima, M., Sekguchi, M , Nakahawa, Y and Waku, K (1983) Lipids 18, 125–129

22 Sugiura, T , Masuzawa, Y. and Waku, K (1980) Lipids 15, 475–478

23 Yoshioka, S , Nakashima, S., Okano, Y , Hasegawa, H , Ichiyama, A and Nozawa, Y (1985) J Lipid Res 26, 1134–1141

24 Chilton, F H. and Murphy, R.C (1986) J. Biol. Chem 261, 7771–7777

25 Gupta, C M., Radhakrishnan, R and Khorana, H G. (1977) Proc Natl. Acad. Sci. USA 74, 4315–43194

26 Haslett, C., Guthrie, L.A , Kopaniac, M.M , Johnston, R.B and Henson, P M (1985) Am J. Pathol. 119, 101–110

27 Bradford, M. (1976) Anal Biochem. 72, 248–254

28 Bligh, E G. and Dyer, W J. (1959) Can J. Biochem Physiol. Res 23, 190–196

29 Patton, G M., Fasulo, J M and Robins, S.J. (1982) J Lipid Res. 23, 190–196

30 Chilton, F.H. and Murphy, R C. (1986) Biomed Mass Spectrom. 13, 71–76

31 Chilton, F H and Murphy, R C. (1986) Prostagl Leukotr. and Med. 23, 141–148

32 Record, M., Tamer, A E , Chap, H and Douste-Blazy, L (1984) Biochim. Biophys Acta 556, 434–446

33 Neufield, E.J , Majerus, P W., Krueger, C M. and Saffitz, J E (1985) J. Cell Biol. 101, 573–581

34 Chilton, F.H , Ellis, J M , Olson, S C and Wykle, R L (1984) J Biol Chem 259, 12014–12019

35 Swendson, C L., Ellis, J.M. and Chilton, F.H , O'Flaherty, J T and Wykle, R.L. (1983) Biochem Biophys. Res Commun. 13, 72–79

Biochimica et Biophysica Acta 917 (1987) 57–61
Elsevier

BBA 52322

Increased response to peroxisomal proliferators in starved rats

Rachel Hertz and Jacob Bar-Tana

Department of Biochemistry, Hebrew University – Hadassah Medical School, P O Box 1172, Jerusalem 91010 (Israel)

(Received 7 August 1986)

Key words. Peroxisomal proliferation; Bezafibrate; Beta-oxidation; (Rat)

The induction of liver peroxisomal β-oxidation activities by bezafibrate or Wy 14,643 was 2–4-fold higher in starved rats than in fed animals. The increased response to peroxisomal proliferators in starved rats was independent of the mode of administration of the proliferator, given either orally or by intraperitoneal injection. Inhibitors of carnitine acyltransferase I could prevent the induction of peroxisomal activities in starved rats but not in fed animals. In contrast to fasted rats, the induction of liver peroxisomal activities in streptozotocin-diabetic rats was not susceptible to bezafibrate. The higher sensitivity to peroxisomal proliferators under conditions of starvation may allow for the detection of xenobiotic peroxisomal proliferators of low proliferative potency.

Introduction

Peroxisomal β-oxidation has been reported to increase in livers of starved or alloxan-diabetic rats [1,2]. The induction of peroxisomal activities in the fasting or diabetic states is significantly less than that observed in rats treated by xenobiotic peroxisomal proliferators [3]. However, it is of special interest since it may help in identifying natural peroxisomal proliferators as well as metabolic steps involved in the induction of peroxisomal activities.

The induction of peroxisomal activities in cultured rat hepatocytes by long chain fatty acids added to the culture medium [4] or by fat-rich diets in vivo [5,6], taken together with the extensive accumulation of long chain fatty acyl-CoA during starvation or diabetes [15] seems to point to long chain fatty acids as the putative natural peroxisomal proliferators in the fasted or diabetic rat. The relatively low induction of peroxisomal activities in fasted, diabetic or fat-fed rats as compared to that exerted by xenobiotic proliferators may be accounted for by the fast metabolic elimination of the natural long chain fatty acids, as compared to the sustained prevalence of xenobiotic peroxisomal proliferators.

The present study aims at evaluating the role played by starvation or diabetes in the induction of peroxisomal activities by xenobiotic peroxisomal proliferators. The present report seems to indicate that the rat is highly susceptible to peroxisomal proliferators under conditions of starvation but not during diabetes.

Materials and Methods

Male rats of the Hebrew University strain weighing 150–200 g were maintained on purina chow diet ad libitum. Starved rats were fasted for 4 consecutive days prior to death. Streptozotocin-diabetic rats were prepared by injecting the rats

---

Correspondence: Dr J. Bar-Tana, Department of Biochemistry, Hebrew University Hadassah Medical School, P.O Box 1172, Jerusalem 91010, Israel.

0005-2760/87/$03.50 © 1987 Elsevier Science Publishers B V (Biomedical Division)

once with 10 mg/100 g body weight of streptozotocin and they were selected by following their urine glucose and ketobodies. Insulin-treated diabetic rats were prepared by injecting streptozotocin-diabetic rats subcutaneously with 2 units of protamine zinc insulin every 12 h. The specified drugs were administered daily by gastric tube in 2 ml of 1% methylcellulose 400 and were given for 3 days prior to death. Alternatively, bezafibrate was dissolved in 1 ml of saline and was injected intraperitoneally daily for 3 consecutive days prior to death. The animals were killed under ether anaesthesia 18 h after the last dosage. Liver homogenate was prepared in 4 vols. of 0.25 M sucrose – 0.1% ethanol, centrifuged at 700 × *g* for 10 min and the respective activities were measured in the 700 × *g* supernatant. Enoyl-CoA hydratase was assayed spectrophotometrically as described by Steinman and Hill [12]. The reaction mixture contained 0.3 M Tris-HCl buffer (pH 7.4), 5 mM EDTA, 0.005% of egg albumin and 0.2 mM of crotonyl-CoA in a final vol. of 1 ml. The peroxisomal activity was defined as the fractional activity which was heat-inactivated at 57°C for 5 min [7]. Cyanide-insensitive palmitoyl-CoA oxidation was determined according to the method described in ref. 8. The reaction mixture contained 0.4 ml of modified Krebs-Henseleit bicarbonate buffer (pH 7.4), 20 μM of [1-^{14}C]palmitoyl-CoA (spec. act. 7 μCi/μmol), 4 mM ATP, 0.5 mM CoA, 2 mM NAD$^+$, 2 mM KCN, and 2 mM dithiothreitol in a final vol. of 0.5 ml. Incubation was carried out at 37°C for 5 min and was terminated by adding $HClO_4$ to a final concentration of 6%. Acid-soluble oxidation products were determined according to Mannaerts et al. [8]. Catalase was determined in the sonicated (10 s) 700 × *g* supernatant as previously described [4]. Protein was determined according to Lowry et al. [9]. Significance was analyzed by the Mann-Whitney U-test.

[1-^{14}C]Palmitoyl-CoA was synthesized enzymatically according to Kornberg and Price [10] and was purified on an octyl sepharose column as described in Ref. 11. Crotonyl-CoA was synthesized from crotonic anhydride according to Steinman and Hill. Bezafibrate was kindly donated by Boehringer (Mannheim, F.R.G.). WY 14,643 and 2-[5-4(-chlorophenyl)-pentyl]-oxirane-2-carboxylate (POCA) were kindly donated by Merrell Dow Pharmaceuticals (Cincinnati, Ohio, U.S.A.) and Byk Gulden (Konstanz, F.R.G.), respectively.

Results and Discussion

The basal specific activities of liver peroxisomal enoyl-CoA hydratase and cyanide-insensitive palmitoyl-CoA oxidase in starved rats were 1.5–2.0-fold higher than in fed animals (Fig. 1), while catalase remained practically unaffected during starvation (137 ± 11 and 169 ± 8 nmol H_2O_2 decomposed/min per mg protein in starved and fed rats, respectively). These findings corroborate previous results of Ishii et al. [1] in Wistar rats as opposed to those reported in Ref. 13 in Sprague-Dawley rats. The induction of liver peroxisomal activities by bezafibrate was much more pronounced in starved than fed rats (Fig. 1). This observed increase in bezafibrate-dependent induction of peroxisomal activities was again characteristic of the β-oxidative activities while catalase remained unaffected in starved or fed animals treated with bezafibrate up to 8.5 mg/100 g body weight (not shown). The affinity for bezafibrate at its target site was essentially not affected by starvation as the ED_{50} for bezafibrate amounted to 1.25 and 1.4 mg/100 g body weight in starved and fed animals, respectively. .Hence, the observed sensitivity to bezafibrate in the fasting state presumably resulted from the respective increase in the number of target sites for bezafibrate binding.

The increased response to bezafibrate could not be accounted for by the intestinal absorption of the drug, since it was also observed upon injecting the drug intraperitoneally (Table I). Moreover, the higher sensitivity of the fasted animal involved a step which was presumably perturbed by all peroxisomal proliferators, natural or xenobiotic. Thus, the increase in the respective specific activities of the fasted compared to the fed rat was observed in the absence or presence of bezafibrate (Fig. 1, Table I), as well as other xenobiotic peroxisomal proliferators not related in structure to fibrate drugs (Table II).

The increased response to peroxisomal proliferators in the starved rat is presumably related to the carnitine acyltransferase reaction. Thus, oxirane inhibitors of the transferase (e.g., POCA)

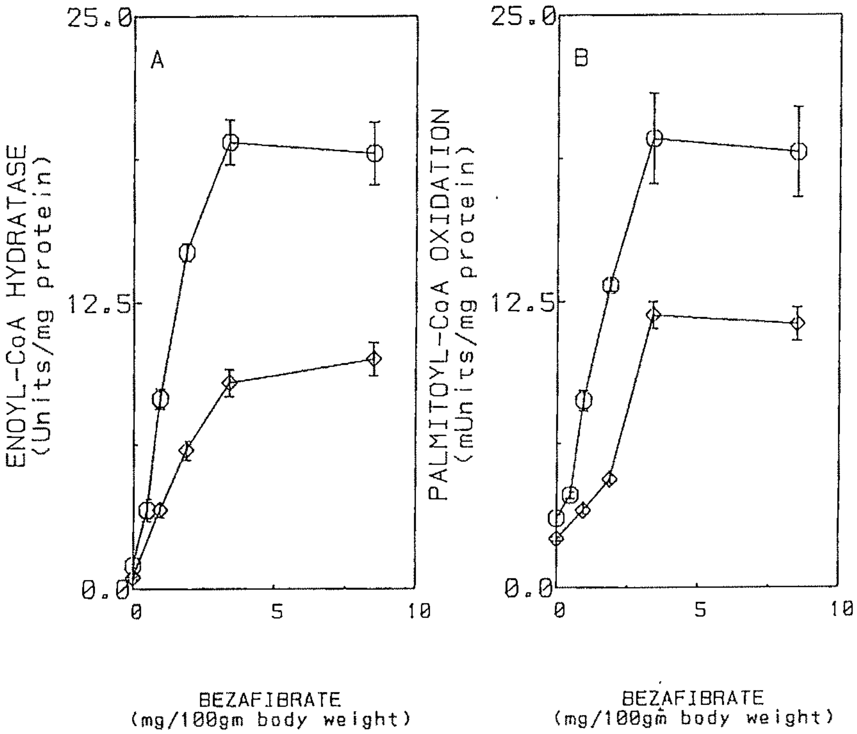

Fig. 1 Induction of peroxisomal β-oxidation activities by bezafibrate introduced per orum in fed and starved rats. Bezafibrate was administered daily by a gastric tube to fasted (○) or fed (◇) rats for 3 consecutive days. A Peroxisomal enoyl-CoA hydratase. B Peroxisomal palmitoyl-CoA oxidation. Mean ± S.D. ($n = 4$)

could prevent the induction of peroxisomal activities in the fasted but not the fed rat (Table III). The prevention of bezafibrate-dependent induction of peroxisomal activities by POCA in the fasted animal in vivo resembles that observed in cultured rat hepatocytes in the presence of POCA,

TABLE I

INDUCTION OF PEROXISOMAL β-OXIDATION ACTIVITIES BY BEZAFIBRATE INTRODUCED INTRAPERITONEALLY IN FED AND STARVED RATS

Bezafibrate (1.4 mg/100 g body weight) was injected intraperitoneally daily to fasted or fed rats for 3 consecutive days. Mean ± S.D. ($n = 4$)

	Peroxisomal enoyl-CoA hydratase (U/mg protein)	Peroxisomal palmitoyl-CoA oxidation (mU/mg protein)
Nontreated, fed	0.5±0.1	2.0±0.2
Nontreated, fasted	0.8±0.1 [a]	3.0±0.4 [a]
Bezafibrate, fed	1.6±0.4	4.4±0.8
Bezafibrate, fasted	6.0±0.3	16.0±2.0

[a] Significantly different from the nontreated-fed value; $P < 0.03$

TABLE II

INDUCTION OF PEROXISOMAL β-OXIDATION ACTIVITIES BY WY 14,643 INTRODUCED PER ORUM IN FED AND STARVED RATS

Wy 14,643 (0.25 mg/100 g body weight) was administered daily by gastric tube to fasted or fed rats for 3 consecutive days. Mean ± S.D. ($n = 4$)

	Peroxisomal enoyl-CoA hydratase (U/mg protein)	Peroxisomal palmitoyl-CoA oxidation (mU/mg protein)
Nontreated, fed	0.5±0.1	2.0±0.2
Nontreated, fasted	1.0±0.1 [a]	3.0±0.3 [a]
Wy 14,643, fed	6.8±1.0	8.6±1.5
Wy 14,643, fasted	16.0±2.0	13.0±2.0

[a] Significantly different from the nontreated fed value, $P < 0.03$.

TABLE III

THE EFFECT OF POCA ON THE INDUCTION OF PEROXISOMAL β-OXIDATION ACTIVITIES IN FED AND STARVED RATS

Bezafibrate (1.88 mg/100 g body weight) was administered daily by gastric tube to fasted or fed rats for 3 consecutive days. POCA was administered daily by means of a gastric tube where indicated, at 0.2 mg/100 g body weight and 0.9 mg/100 g body weight to starved and fed rats, respectively. Mean ± S.D. ($n = 4$)

	Peroxisomal enoyl-CoA hydratase (U/mg protein)	
	fed rats	starved rats
Nontreated	0.5±0.05	0.8±0.1
POCA-treated	0.5±0.1	2.0±0.2
Bezafibrate-treated	6.6±0.8	12.0±0.8
POCA- and bezafibrate-treated	6.0±0.8	4.4±1.4

tetradecylglycidic acid or 2-bromopalmitate added to the culture medium. Hence, the putative susceptible step may consist of the carnitine acyltransferase reaction which could be obligatory for the induction of peroxisomal activities in the fasted but not in the fed, animal where an alternative translocation route could be effective. The role played by carnitine transferases in the induction of peroxisomal proliferation in the fasted rat still remains to be investigated.

TABLE IV

INDUCTION OF PEROXISOMAL β-OXIDATION ACTIVITIES IN STREPTOZOTOCIN-DIABETIC AND INSULIN-TREATED DIABETIC RATS

Bezafibrate (2.0 mg/100 g body weight) was administered daily by gastric tube to streptozotocin-diabetic or insulin-treated diabetic rats for 3 consecutive days. Mean ± S.D. ($n = 4$)

	Peroxisomal enoyl-CoA hydratase (U/mg protein)	Peroxisomal palmitoyl-CoA oxidation (mU/mg protein)
Diabetic	1.4±0.5	7.5±0.6
Diabetic, bezafibrate	2.0±0.4 [a]	9.6±1.1 [a]
Insulin-treated	1.2±0.2	4.9±0.4
Insulin-treated, bezafibrate	2.6±0.3 [b]	8.8±1.9 [b]

[a] Significantly different from the diabetic value; $P < 0.03$

[b] Significantly different from the insulin-treated value; $p < 0.03$

In contrast to the fasted rat, the induction of liver peroxisomal activities by bezafibrate in streptozotocin-diabetic rats was similar to that observed in insulin-treated diabetic rats (Table IV). These results confirm earlier findings reported in Ref. 14 and may point to the requirement for insulin for the expression of the concerned susceptible step in the fasted rat.

The induction of peroxisomal activities in the starved rat appears, therefore, to result from both the accumulation of long chain fatty acids acting as natural proliferators as well as the involvement of a step presumably related to carnitine acyltransferase. The induction of peroxisomal activities by xenobiotic proliferators in the fasted rat appears to involve a sequel similar to that engaged by long chain fatty acids acting as natural proliferators. The increased response of the fasted animal to peroxisomal proliferators may thus be exploited for the detection of xenobiotic peroxisomal proliferators of low proliferating potency.

Acknowledgement

This research was supported by the Herta Schnap Foundation for Cancer Research.

References

1 Ishii, H., Horie, S. and Suga, T. (1980) J. Biochem. 87, 1855–1858

2 Horie, S., Ishii, H. and Suga, T. (1981) J. Biochem. 90, 1691–1696

3 Hess, R., Staubli, W. and Reiss, W. (1965) Nature (Lond.) 208, 856–858

4 Hertz, R., Arnon, J. and Bar-Tana, J. (1985) Biochim. Biophys. Acta, 836, 192–200

5 Ishii, H., Fukumori, T., Horie, S. and Suga, T. (1980) Biochim. Biophys. Acta 617, 1–11

6 Neat, C.E., Thomassen, M.S. and Osmundsen, H. (1981) Biochem. J. 196, 149–159

7 Lalwani, N.D., Reddy, N.K., Mangkornkanole-Mark, M. and Reddy, J.K. (1981) Biochem. J. 198, 177–186

8 Mannaerts, G.P., Debeer, L.J., Thomas, J. and Deschepper, P.J. (1979) J. Biol. Chem. 154, 4585–4595

9 Lowry, O.H., Rosebrough, N.J., Parr, A.L. and Randall, R.J. (1951) J. Biol. Chem. 193, 265–275

10 Kornberg, A. and Pricer, W.E. (1953) J. Biol. Chem. 204, 329–343

11 Merrill, A.H., Gidwitz, S and Bell, R M. (1982) J Lipid Res. 23, 1368–1373
12 Steinman, H.M. and Hill, R L (1975) in Methods Enzymol 35, 136–151
13 Slauter, R W and Yamazaki, R K. (1984) Arch. Biochem Biophys. 233, 197–202
14 Kawashima, Y., Katoh, H and Kozuka, H. (1983) Biochim Biophys Acta 750, 365–372
15 Tubbs, P K , Garland, P B. (1964) Biochem J 93, 550–557

Biochimica et Biophysica Acta 917 (1987) 62–73
Elsevier

BBA 52441

Composition and properties of very low density lipoproteins secreted by the perfused rat liver and subfractionated by affinity chromatography

Friedhelm Schroeder [a], Ann B. Kier [b], Darrell A. Kinden [b], Henry G. Wilcox [c] and Thomas P. Mawhinney [d]

Departments of [a] Pharmacology and [d] Biochemistry, University of Missouri-Columbia School of Medicine, Columbia, MO 65212, [b] Department of Veterinary Pathology, University of Missouri-Columbia College of Veterinary Medicine, Columbia, MO 65211 and [c] Department of Pharmacology, The University of Tennessee Center for the Health Sciences, 874 Union Avenue, Memphis, TN 38163 (U.S.A.)

(Received 3 April 1986)
(Revised manuscript received 1 October 1986)

Key words. VLDL; Lipoprotein secretion; (Rat liver)

Very low density lipoproteins (VLDL) were isolated from the perfusate of rat livers infused with a complex of oleic acid bound to bovine serum albumin. Very low density lipoprotein (VLDL) secretion, bile flow, histopathology, and transmission electron microscopy indicated that secretory functions but not morphologic integrity of the livers were maintained during the procedure. Plasma VLDL and liver perfusate VLDL did not have similar size distribution. VLDL isolated from recycling perfusate and single pass perfusate were also subfractionated with concanavalin A-Sepharose 4B affinity chromatography. Three subfractions were eluted sequentially from the perfusate VLDL: a non-adherent fraction A and two adherent fractions B and C. The size of these VLDL, determined after negative staining and examination by transmission electron microscopy, was significantly decreased by affinity chromatography. VLDL in fractions A, B and C were spherical and had diameters of 935 ± 17, 881 ± 34 and 415 ± 30 Å respectively. Fraction A, which did not adhere to the column, contained 65% of the lipid applied to the column. The carbohydrate composition of fraction A VLDL was 11.2 ± 0.6% fucose, 14.7 ± 1.2% galactose, 43.7 ± 2.3% *N*-acetylglucosamine, and 30.5 ± 1.9% sialic acid. Sugars such as glucose and mannose, which bind to concanavalin A, were not detected. In contrast, VLDL fractions B and C, which adhered to the column, contained both glucose (17.7 and 2.5%) and mannose (5.8 and 8.3%) as well as the other sugars present in VLDL fraction A. Sodium dodecyl sulfate gradient gel electrophoresis revealed that the affinity column procedure clearly altered the apolipoprotein patterns of the applied VLDL, thereby producing abnormal fractions B and C. Fractions B and C also differed from unfractionated VLDL and fraction A VLDL in lipid composition, in surface/interior core lipid ratio, and in fatty acid composition of the interior core lipids, primarily triacylglycerols. The steady-state anisotropy, the limiting anisotropy and the lipid order parameter of fluorescence probe molecules 1,6-diphenyl-1,3,5-hexatriene and *trans*-parinaric acid incorporated into the VLDL were of the following order: fraction B > fraction A > fraction C. These results are consistent with the interpretation that concanavalin A-Sepharose 4B affinity chromatography may artificially produce a series of VLDL subfractions whose composition and structural properties do not resemble those of native VLDL.

Correspondence address: Department of Pharmacology, University of Missouri-Columbia School of Medicine, Columbia, MO 65212, U S A.

0005-2760/87/$03 50 © 1987 Elsevier Science Publishers B V (Biomedical Division)

Introduction

The VLDL obtained from plasma are a heterogeneous group of particles with respect to density [1–3], carbohydrate content [4,5], size [6] and metabolism [7,8]. However, it is not known whether the origin of this heterogeneity is solely due to intravascular metabolism and/or exchange or whether the liver also secretes a heterogeneous class of nascent VLDL. Concanavalin A-Sepharose 4B affinity chromatography has been used to isolate from human plasma a large number of VLDL subfractions differing in apolipoprotein content [4,5]. In addition, selective binding of concanavalin A to human lipoproteins containing apolipoprotein B was reported. In the present work the VLDL secreted by the isolated perfused rat liver were subfractionated by affinity chromatography on concanavalin A-Sepharose 4B in order to determine whether the concanavalin A-Sepharose 4B affinity column procedure can itself alter VLDL or whether the liver secretes a homogeneous or heterogeneous class of VLDL particles with regard to carbohydrates, lipids and structure. The isolated rat liver perfused with a chemically defined, blood-free medium provides a model system that minimizes the intravascular variables and may thereby allow heterogeneity analysis of secreted VLDL. A considerable body of information on the sensitivity of the lipid composition, size, density and physiochemical properties of the VLDL, secreted by the perfused rat liver, to nutritional variables [9–12] and to endocrine status [13,14] are already available. Presented herein are the results of electron microscopy, carbohydrate, apolipoprotein, lipid composition, and structural analyses of VLDL subfractions isolated by concanavalin A-Sepharose 4B chromatography.

Materials and Methods

Bovine serum albumin (fraction V) was obtained from Miles Research Laboratories (Elkhart, IN). The bovine serum albumin was delipidized as described earlier [15]. *trans*-parinaric acid was from Molecular Probes, Inc. (Junction City, OR), while 1,6-diphenyl-1,3,5-hexatriene was from Aldrich Chemical Co., Milwaukee, WI. Oleic acid was from the Hormel Institute (Elysian, MN). Concanavalin A-sepharose 4B was obtained from Pharmacia (Uppsala, Sweden). All solvents were glass distilled and all lipid analysis glassware washed before use. [^{3}H]oleic acid was from New England Nuclear (Boston, MA).

Liver perfusion. Sprague-Dawley male rats (200–250 g body weight) were obtained from Charles River Breeding Laboratories (Wilmington, MA). The animals were maintained on water and Purina Laboratory Chow ad libitum. After at 16 h overnight fast, livers were isolated from the animals and perfused with a blood-free medium containing 70 ml Krebs-Ringer bicarbonate buffer, (pH 7.4), 100 mg/dl glucose and 3 g/dl purified bovine serum albumin was described previously [16]. Oleic acid-albumin complex, prepared as described elsewhere [17], was infused into the perfusion medium at the rate of 166 μmol/h for 4 h. Alternatively, the 6% albumin-oleate complex in Ca^{2+}- and Mg^{2+}-free Krebs-Henseleit buffer (pH 7.8) contained 50 μCi [^{3}H]oleic acid. The rate of triacylglycerol output in the perfusate calculated from the radioisotope precursor specific activity was 6 μmol/g liver per 4 h, a value similar to that obtained by other investigators [18]. Livers were perfused either by recycling the perfusate [11] for 4 h, or by single pass perfusion for 1 h. In the latter procedure the infusate was not recycled through the liver. In either case, immediately after the perfusate was collected EDTA and NaN_3 were added at a final concentration of 0.01% and 0.02%, respectively, and the temperature was lowered to 4°C. The presence of EDTA and NaN_3 inhibited bacterial growth and reduced potential proteinase activity. Antibiotics were not included in the infusate during liver perfusion in order to avoid potential alterations in liver function. The omission of antibiotics from the infusate is standard procedure in the field. It should be noted that especially in the recycling perfusion system containing red blood cells, hepatic lipase is active and uptake of VLDL from the perfusate occurs [19]. However, in the present work recirculating and non-recirculating perfusions were performed without red blood cells. Despite this difference, effects of lipolysis on VLDL should be considered. The VLDL were isolated from the perfusate as described below. Liver function was assessed by several criteria before and after perfusion [20,21].

Liver histopathology and electron microscopy. Liver specimens were taken from the median lobes before and after a 4 h perfusion, fixed with neutral buffered formalin, paraffin processed, cut, and stained with hematoxylin and eosin. For electron microscopy, tissues were fixed with 2.5% glutaraldehyde in 0.1 M cacodylate buffer containing 1% sucrose, washed, post-fixed with 1% OsO_4 in the same buffer, and dehydrated in a graded ethanol series. The specimens were then infiltrated and embedded in poly/bed 812, cut, and post-stained with uranyl acetate and lead citrate [22]. Micrographs were obtained with an RCA EMU-3G electron microscope operating at an accelerating voltage of 100 kV.

Isolation and subfractionation of the VLDL. The VLDL from the rat liver perfusate were isolated as described previously [23]. Briefly, the perfusate was centrifuged at 4°C for 18 h in a 50.2 Ti Rotor (Beckman Instr., Fullerton, CA) at 39000 rpm ($1.6 \cdot 10^8$ g min). The VLDL were then resuspended in 10 vol. 0.9% NaCl/0.02% NaN_3/0.01% EDTA (pH 7.4) and again centrifuged. The solvent density employed for VLDL flotation was less than 1.006 g/ml. The VLDL isolated from the perfusate as above were fractionated at 24°C according to concanavalin A-Sepharose 4B column chromatography essentially following the procedure of Shore and Shore [4]: concanavalin A-Sepharose 4B (Pharmacia) was the column matrix (0.7 × 11 cm column). Unless otherwise specified, the bed volume was 5.5 ml and the flow rate was 2 ml/min. The concanavalin A-Sepharose 4B was washed ten times with 5 ml buffer A (0.2 M NaCl/0.1 M sodium acetate/0.01% EDTA/0.02% NaN_3 (pH 6.8)) and then poured into the column. The VLDL sample (20 mg lipid) was applied to the column in 2 ml buffer A. The column was then washed with 12 ml buffer A. All subsequent elution buffers (B through G) contained buffer A in order to maintain pH and inhibit microbial growth: 12 ml buffer B (0.05 M glucose), 12 ml C (0.1 M glucose), 12 ml D (0.05 M mannose), 12 ml E (0.1 M mannose), 12 ml F (0.1 M methyl-α-D-glucopyranoside), 18 ml G (1 M methyl-α-D-glucopyranoside) and 10 ml H (0.2 M NaCl/0.1 Tris (pH 9.5)). Unless otherwise specified, 2 ml fractions were collected and immediately cooled to 4°C. The amount of protein ($A_{280\,\mathrm{nm}}$) was determined in the eluant. Recoveries of lipid from the column were 90 ± 5%. The three major subfractions identified by absorbance at 280 nm were concentrated at 4°C by Amicon filtration using XM50 ultrafiltration membranes with Model 52, Model 12, or Model 3 stirred ultrafiltration cells (Amicon Corp., Lexington, MA). All VLDL samples were routinely stored at 4°C until use.

Very low density lipoprotein transmission electron microscopy. VLDL were dispersed in a 0.9% NaCl/1 mM EDTA/0.02% NaN_3 (pH 7.2) buffer solution. Sample preparation for negative staining was performed basically as described by Clark et al. [24]. Negatively stained samples were examined immediately with an RCA EMU-3G electron microscope as described above. VLDL diameters were measured directly from known magnification factors and prints made of electron micrographs. In cases where the VLDL were not spherical in shape, an average diameter was obtained from the long and short axes. Aggregated VLDL were not measured.

Carbohydrate analysis. Neutral and amino sugar were quantitated as described earlier by Mawhinney et al. [25]. Sialic acid content was determined by a colorimetric assay [26] and by gas liquid chromatography as described by Mawhinney et al. [27].

Electrophoresis. Delipidization and apolipoprotein electrophoresis of VLDL, isolated as described earlier [28], were performed as described elsewhere [29,30]. Sodium dodecyl sulfate gel electrophoresis was carried out in 0.1% sodium dodecyl sulfate on a 3.5–20% polyacrylamide gel gradient (top to bottom).

Lipid analysis. Lipids were extracted from VLDL fractions by the method of Bligh and Dyer [31]. Nonlipid contaminants in the extract were removed by Sephadex chromatography [32] and silicic acid chromatography (Unisil, 100–200 mesh, Clarkson Chemical Co., Williamsport, PA). Triacylglycerol, cholesteryl esters and phospholipids were separated by thin layer chromatography using Silical Gel G plates (250 μm thick, Analtech Inc., Newark, DE), visualized with 0.01% rhodamine 6G [33], scraped and eluted with chloroform, and quantitated by colorimetric procedures [15]. Fatty acid methyl esters were prepared by heating under

N_2 with BF_3-methanol (Supelco, Inc., Bellefonte, PA) at 100°C for 90 min [30]. The fatty acid methyl esters were identified by comparison of their retention times with standards on a 0.25 inch, 6-foot, 10% SP-2340 (on Chromosorb WAW, 100 mesh, Supelco, Inc., Bellefonto, PA) column at 185°C using a Sigma 2 Gas Chromatograph (Perkin Elmer Corp., Norwalk, CT) and 3390A Recorder-Integrator (Hewlett Packard, Inc., Avondale, PA).

Fluorescence probe incorporation and instrumentation. *trans*-Parinaric acid and 1,6-diphenyl-1,3,5-hexatriene were incorporated into the VLDL (50 μg/ml phosphate-buffered saline (pH 7.4)) at 1:100 probe-to-lipid molar ratios as described earlier [9–12]. Absorption, absorption-corrected fluorescence, relative fluorescence efficiency, and corrected fluorescence emission were determined with the computer-centered spectrofluorimeter of Holland et al. [34] as described by Schroeder et al. [9–12]. *trans*-Parinaric acid and 1,6-diphenyl-1,3,5-hexatriene were excited at 313 and 362 nm, respectively, while emission was determined at 415 and 424 nm, respectively. Arrhenius plots, fluorescence lifetime, τ, steady-state fluorescence polarization, P, limiting anisotropy, rotational relaxation time, order parameter and mole fractions were determined using a T format spectrofluorimeter obtained from SLM (SLM 4800 Subnanosecond Spectrofluorimeter, SLM Instruments, Inc., Champaign-Urbana, IL) basically as described earlier [12,35].

Results

Function and structure of perfused rat livers

The following experiments were performed to determine whether the VLDL secreted by isolated rat livers perfused with a chemically defined, blood-free medium were released by functionally and morphologically normal livers. The liver average wet weight was 9.1 ± 0.4 and 8.8 ± 0.6 g/rat, bile production was unaltered at 0.13 ± 0.02 ml/4 h/g per liver, perfusate flow rate was 6.3 ± 0.8 and 7.0 ± 0.3 ml/min per g liver, and VLDL triacylglycerol output was linear for 4 h in livers perfused with and without oleate-bovine serum albumin. These findings confirm results of others [18]. Infusion of 166 μmol oleate/h for 4 h stimulated VLDL triacylglycerol from 3.2 ± 0.3 to 6.1 ± 0.4 mol/g liver per 4 h. Light microscopy of hepatocytes in non-perfused livers, fixed at 37°C [36], exhibited normal morphology at the light and ultrastructural level. After perfusion, there was apparent intracellular swelling and some of the hepatocytes lost their normal polygonal shape. Electron microscopic examination of the rat liver before perfusion indicated the following prominent cytological features of the hepatocytes: a conspicious nucleus, dense cytoplasm containing abundant mitochondria and rough and smooth endoplasmic reticula, few lipid droplets, and absence of glycogen. After liver perfusion, the hepatocytes had more and larger lipid droplets, indicative of increased triacylglycerol formation reported by others [37]. The normal parallel arrays of smooth endoplasmic reticulum appear more disordered after perfusion. Smooth endoplasmic reticulum and peroxisomes also appeared more abundant, indicating increased metabolic activity.

Affinity chromatography of VLDL secreted by perfused rat livers

VLDL were isolated from livers perfused with oleate-bovine serum albumin and fractionated on concanavalin A-Sepharose columns as described in Materials and Methods. Three VLDL subfractions were obtained by sequential elution of the VLDL with buffers containing displacing sugars of increasing affinity for concanavalin A. Both absorbance at 280 nm (Fig. 1) and [^{3}H]oleate incorporation (data not shown) demonstrated the sequential elution of three VLDL subfractions: a non-adherent fraction A, an adherent fraction B that was displaced by glucose and mannose, and a tightly adherent fraction C that was displaced by 1-*O*-methyl-α-D-glucopyranoside. Regeneration of the column and elution of VLDL obtained from a single pass perfusate also showed that same elution profile (Fig. 1). However, the distribution of material in the three peaks varied, depending on the type of perfusion carried out. This result may indicate that some degradation of VLDL (e.g., peak B) occurred during the recycling perfusion. Regeneration of the column had no effect on separation of a second VLDL application. A non-adherent fraction A eluted first followed by two adherent fractions B and C.

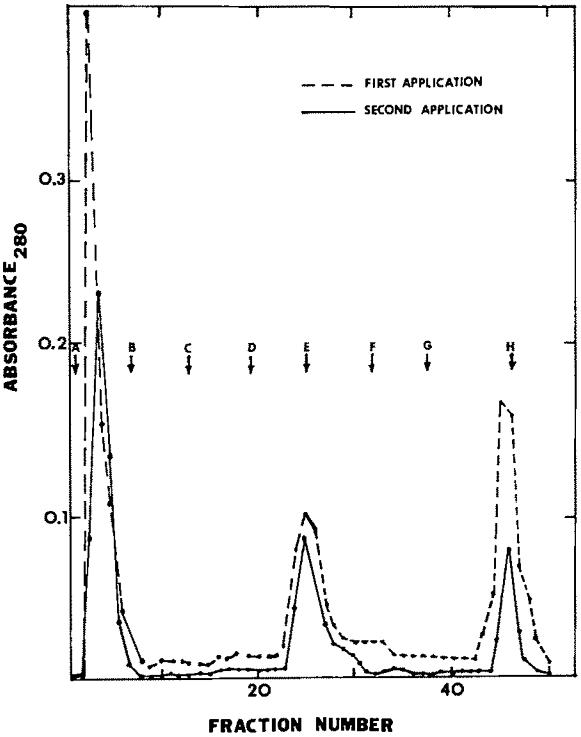

Fig 1 Elution profile of VLDL from affinity columns. VLDL were isolated from the perfusate of the perfused rat liver and affinity chromatography was carried out with concanavalin A-Sepharose 4B. The VLDL were resolved at 24°C At lower temperatures the VLDL adhered very poorly to the column The eluted fractions were designated from left to right as fraction A, fraction B and fraction C First application refers to VLDL from recycling perfusate applied to fresh column Second application refers to VLDL from single pass perfusate Recoveries from the columns were 90–95%

TABLE I

SIZE OF VLDL ISOLATED FROM PLASMA OR FROM THE PERFUSED RAT LIVER AND SUBFRACTIONATED BY AFFINITY CHROMATOGRAPHY

VLDL were isolated from rat plasma and from a recycling (4 h) infusate through the perfused rat liver. VLDL were negatively stained at room temperature, examined by transmission electron microscopy, and were photographed at a magnification of ×20000 to ×60000. Most of the particles were spherical The n refers to the number of particles measured. Values represent the means ±S E An asterisk (*) refers to $P < 0.05$ for fractions A, B or C compared to unfractionated VLDL in the single pass perfused liver while a dagger (†) refers to $P < 0.05$ as compared to VLDL from plasma (Student's 't' test).

Sample	Diameter (Å)	n
Blood		
plasma VLDL	708±40	55
Perfused liver (recycling)		
unfractionated	$866 \pm 33^{\dagger}$	60
fraction A	$935 \pm 17^{\dagger}$	83
fraction B	$881 \pm 34^{\dagger}$	55
fraction C	$415 \pm 30^{*,\dagger}$	67

Transmission electron microscopy of plasma VLDL and VLDL secreted by perfused rat livers

Differences in morphology of VLDL isolated from rat plasma versus the isolated perfused rat liver indicated that the rat liver perfused for 4 h with recycling perfusate secreted a heterogeneous group of particles that were mostly spherical in shape, but aggregates also appeared. The diameters of non-aggregated VLDL from recycling liver perfusate and from plasma were 866 ± 33 vs. 708 ± 40 Å (Table I; $P < 0.05$). This difference could result from more extensive intravascular metabolism and corresponding size reduction in plasma as compared to isolated liver perfusate. The VLDL isolated from the recycling perfusate and eluted from a concanavalin A-Sepharose 4B affinity chromatography column had a similar morphology to those of plasma VLDL and unfractionated VLDL. Each of the three fractions, A, B and C, eluted primarily as a single size peak, although fraction A contained some larger diameter particles. The mean diameters of the non-adherent fraction A and the adherent fraction B (935 ± 17 Å vs. 881 ± 34 Å) were not significantly different from each other. In contrast, fraction C was comprised of much smaller VLDL particles with a mean diameter of 415 ± 30 Å, which were significantly smaller ($P < 0.05$) than those from either fractions A and B or plasma (Table I). Thus, passage of VLDL from the recycling perfusate (mean diameter 866 ± 33 Å) over the affinity column resulted in elution of some particles with diameters much smaller, indicating disruption of VLDL on the column.

Carbohydrate analysis of VLDL subfractionated by affinity chromatography

The unfractionated VLDL obtained from the isolated perfused rat liver contained 1.77 ± 0.15 mg carbohydrate/100 mg protein (Table II). The

TABLE II

CARBOHYDRATE COMPOSITION OF VLDL OBTAINED FROM THE ISOLATED PERFUSED RAT LIVER AND SUBFRACTIONATED BY AFFINITY CHROMATOGRAPHY

Very low density lipoproteins (VLDL) were isolated from the perfused rat liver, subfractionated by affinity chromatography on concanavalin A-Sepharose 4B, and protein and carbohydrate analyses were determined Values represent the means ±S E ($n = 7$ or 8) An asterisk (*) refers to $P < 0.001$ as compared to unfractionated VLDL while a dagger (†) refers to $P < 0.001$ for fractions B or C compared to fraction A (Student's 't' test)

Sugars, measured as:	Sample			
	unfractionated	fraction A	fraction B	fraction C
mg carbohydrate/100 mg protein)				
total	1.767±0.150	0.348±0.031*	0.654±0.063*,†	2.832±0.194*,†
Percent composition by weight				
fucose	6.6 ±0.3	11.2 ±0.6*	13.0 ±0.6*	5.9 ±0.2†
mannose	16.1 ±2.1	0.0*	5.8 ±0.6*,†	17.7 ±2.4†
glucose	2.9 ±0.2	0.0*	8.3 ±0.7*,†	2.5 ±0.2†
galactose	25.1 ±2.0	14.7 ±1.2*	26.0 ±2.1†	25.3 ±2.2†
N-acetyl-glucosamine	30.3 ±2.4	43.7±2.3*	27.7 ±3.2†	30.2 ±1.6†
sialic acid	18.9 ±1.2	30.5 ±1.9*	19.3 ±2.3†	18.4 ±0.9†
total	100	100	100	100

non-adherent VLDL fraction A had the lowest carbohydrate content (0.35 ± 0.03 mg/100 mg protein), while the VLDL fraction C with the highest affinity for concanavalin A had the highest carbohydrate content (2.83 ± 0.19 mg/100 protein). More importantly, carbohydrates that have a high affinity for concanavalin (glucose and mannose) were absent in VLDL fraction A, but were present at 0.038 and 0.054 mg/100 mg protein in fraction B and at 0.502 and 0.068 mg/100 mg protein in fraction C. Mannose is 5-fold and 10-fold more potent in binding to concanavalin A than are glucose and *N*-acetylglucosamine, respectively, while galactose, fucose and sialic acid are poorly bound, if at all [38]. The content of sialic acid increased 5-fold in the order fraction A < fraction B < fraction C. Thus, the relative content of concanavalin A binding residues normalized for binding affinity of the various sugars was: fraction A, 1.0; fraction B, 2.3; and fraction C, 4.9. These differences were also reflected in the percent carbohydrate composition by weight and can account for the relative binding of VLDL fractions A, B, and C to concanavalin A-sepharose 4B beads.

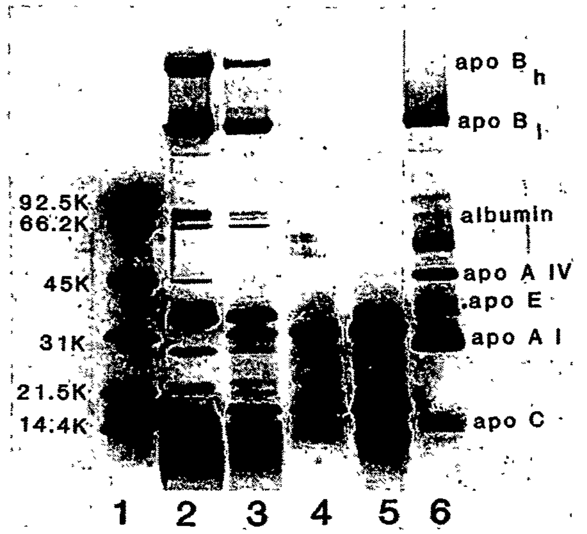

Fig. 2. SDS gradient gel electrophoresis of VLDL and VLDL subfractions isolated by affinity chromatography Track 1, molecular weight standards; track 2, unfractionated VLDL; track 3, fraction A VLDL; track 4, fraction B VLDL, track 5, fraction C VLDL, track 6, rat lymph. Apo, apolipoprotein.

Distribution of lipid in VLDL subfractions

The composition of the unfractionated VLDL was 7.1, 6.8, 4.2, and 32.5 mg/dl of protein, phospholipid, cholesterol, and triacylglycerol, respectively. Greater than 90% of the VLDL lipid

TABLE III

RELATIVE PERCENT COMPOSITION OF VLDL APOLIPOPROTEINS

The percent composition of the VLDL apolipoproteins (Apo) was obtained from gel scans of the gels in Fig. 1 by use of an LKB Laser Gel Scanner

	Unfractionated	Fraction A	Fraction B	Fraction C
Apo B_h	15.1	5.1	0	0
Apo B_l	25.2	21.6	0	0
Albumin	6.4	6.6	7.6	0
Apo AIV	1.4	0	0	0
Apo E	24.0	18.4	0	0
X_1	0	12.6	20.6	32.6
Apo AI	3.5	2.4	0	0
X_2	0	0	2.9	7.2
Apo II	2.2	3.2	1.6	3.6
X_3	0	9.2	43.7	33.7
Apo C	22.1	20.9	23.6	23.5

applied to the column was recovered and approximately 65 ± 7% of the lipid recovered from the column appeared in the non-adherent peak designated fraction A. Two smaller peaks (B and C) contained 22 ± 6% and 12 ± 3% of the lipid recovered from the column, respectively. Thus, the VLDL secreted by the perfused liver appeared to be comprised of a major fraction and two significant smaller fractions when fractionated by concanavalin A affinity chromatography.

Electrophoretic analysis of apolipoproteins from VLDL subfractions

To characterize further the glycoapolipoprotein composition of VLDL secreted by the perfused rat liver, sodium dodecyl sulfate gradient gel electrophoresis was performed on unfractionated VLDL, fractions A, B, and C and rat lymph VLDL (Fig. 2 and Table III). As expected, apolipoproteins B, E and C were the major components of the unfractionated VLDL, comprising 40.3, 24.0 and 22.1% of the total. Small amounts of apolipoproteins AI, AII and AIV were also present. VLDL fraction A contained all of the aforementioned apolipoproteins plus certain other proteins with molecular weights of 31000 ($X_1 = 12.6\%$) and 15000–20000 ($X_2 + X_3 = 9.2\%$). Although beyond the scope of the present work, immunoblotting techniques could help in identifying the source of the 'X' proteins. VLDL fractions B and C were deficient in apolipoproteins B, E, AI and AIV while being enriched 67% and 73%, respectively, in unidentified apolipoproteins not present in the starting material. The C apolipoproteins appeared to be present in all the VLDL fractions. The presence of low molecular weight new proteins as well as the absence of high molecular weight proteins, e.g. apolipoprotein B, in fractions B and C, strongly suggests proteolysis during the column procedures. Thus, the identification of fractions B and C as normal VLDL species devoid of apolipoproteins B and E is not warranted at this stage of the investigation. It would appear that apolipoprotein modification on the column may also give rise to the considerable loss or proteolytic modification of apolipoprotein B_h in fraction A as well (Table III). The ratio of apolipoprotein B_h to apolipoprotein B_l in the unfractionated VLDL and in fraction A was 0.59 vs. 0.24, respectively. These data were also consistent with the possible loss of some fraction A apolipoproteins either on the column or during the column eluant concentration and washing procedure. Lastly, rat plasma VLDL were also electrophoresed by the above procedure and demonstrated the presence of apolipoproteins AI and AII, as well as apolipoproteins C, E and D (data not shown). The gel patterns and relative apolipoprotein compositions of plasma VLDL were not similar to any of the VLDL subfractions presented here.

Lipid composition of VLDL secreted by the perfused rat liver

The lipid composition of VLDL is a primary determinant of VLDL structure, density, and flotation behavior. Considerable lipid compositional differences between the VLDL subfractions were observed (Table IV). The ratio of surface lipids (phospholipid plus cholesterol) to interior core lipids (triacylglycerol plus cholesteryl ester) and the cholesterol-to-phospholipid ratio were markedly different between the three fractions. The former ratio (surface/interior core lipid) was smallest in VLDL from fraction C (0.14) as compared to VLDL in fraction A (0.30).

The fatty acid composition of the phospholipid from fractions A, B and C showed no statistical differences except for the decreased content of

TABLE IV

LIPID COMPOSITION OF HEPATIC VERY LOW DENSITY LIPOPROTEIN SUBFRACTIONATED BY CONCANAVALIN A-SEPHAROSE 4B AFFINITY CHROMATOGRAPHY

Triacylglycerol, phospholipid, cholesterol, and cholesterol esters were quantitated and expressed on a molar basis Molar values were then assigned relative values with triacylglycerols arbitrarily assigned a value of 100 This calculation was described earlier [10] Values represent the means ±S.E. ($n = 6$) An asterisk (*) signifies $P < 0.01$ as compared to fraction A.

Lipid	VLDL subfraction		
	A	B	C
Triacylglycerol (TG)	100	100	100
Phospholipid (PL)	22.8 ±2.0	36.6 ±3.8*	8.5 ±1.4*
Cholesterol (C)	22.3 ±5.7	23.4 ±5.0	8.6 ±2.9*
Cholesteryl ester (CE)	4.0 ±1.0	15.2 ±4.2*	3.4 ±0.9
(PL + C)/(TG + CE)	0.30±0.04	0.34±0.05	0.14±0.02*
(C/PL)	0.97±0.03	0.64±0.07*	1.01±0.2

TABLE V

FATTY ACID COMPOSITION OF PHOSPHOLIPIDS AND TRIACYLGLYCEROLS OF THE VERY LOW DENSITY LIPOPROTEINS SECRETED BY THE PERFUSED RAT LIVER AND FRACTIONATED BY CONCANAVALIN A-SEPHAROSE 4B AFFINITY CHROMATOGRAPHY

Values represent the means ±S.E ($n = 6$) An asterisk refers to $P < 0.05$ as compared to A L, S and U refer to long-chain (more than 18 carbons), short-chain (less than 18 carbons) and unsaturated fatty acids, respectively

Fatty acid composition (% by weight)	VLDL subfraction		
	A	B	C
Phospholipid			
14:0	1.7±0.6	3.3±1.2	1.9±0.8
15:0	0.3±0.1	0.5±0.3	–
16:0	21.3±2.1	21.4±4.3	17.4±1.2
16:1	1.3±0.3	1.2±0.8	1.4±0.2
18:0	20.0±2.8	24.1±2.7	21.2±4.4
18:1	36.6±2.7	30.5±4.1	38.7±4.8
18:2	7.2±3.1	1.2±0.4*	8.9±1.2
20:4	3.5±1.7	7.7±0.3*	6.7±1.8*
other	8.1±2.0	10.1±1.1	3.8±1.2*
L/S	3.0	2.8	3.0
U/S	1.3	1.0	1.5
Triacylglycerol			
14:0	2.5±0.9	16.3±6.4*	3.8±1.0
15:0	0.4±0.2	0.7±0.3	0.3±0.1
16:0	15.4±1.0	15.8±1.4	12.8±0.6
16:1	4.3±2.8	1.4±0.4	1.8±0.6
18:0	2.5±1.3	5.0±2.6	1.0±0.1
18:1	60.1±2.3	39.6±5.8*	73.2±1.0*
18:2	3.4±2.3	0.9±0.8	2.9±0.7
20:4	0.3±0.1	2.8±1.3*	0.6±0.4
other	11.1±2.0	17.5±2.8	3.6±0.8*
L/S	3.4	1.9*	4.4*
U/S	3.8	1.7*	4.6*

18:2 in fraction B and elevated content of 20:4 in B and C (Table V). In contrast, the triacylglycerols varied as much as 2-fold between fractions (Table V). The triacylglycerol unsaturated/saturated fatty acid ratio was 3.8, 1.7 and 4.6 for VLDL subfractions A, B and C, respectively. The triacylglycerols in fraction B have a unique fatty acid composition, low in oleate, the fatty acid infused. This could perhaps represent preformed VLDL released by the liver. Fatty acid composition of the cholesteryl esters was not shown since the cholesteryl esters usually comprised only a small fraction of the total VLDL lipids. In summary (Table V), the above data indicate that the VLDL subfractions resolved by concanavalin A-Sepharose 4B affinity chromatography were compositionally heterogeneous. This heterogeneity may be responsible for the structural heterogeneity detailed below.

Static and dynamic properties of fluorescence probe molecules in VLDL subfractions

The possible structural heterogeneity of VLDL isolated from perfused rat livers and subfractionated on concanavalin A-Sepharose 4B was determined. A quantitative summary of fluorescence probe spectral parameters in VLDL subfractions is given in Table VI. The corrected fluorescence and relative fluorescence efficiency (directly proportional to quantum yield) differed as much as 2-fold in the three VLDL subfractions. The corrected fluorescence and relative fluo-

TABLE VI

FLUORESCENCE OF 1,6-DIPHENYL-1,3,5-HEXATRIENE AND *TRANS*-PARINARIC ACID IN VLDL SUBFRACTIONATED BY CONCANAVALIN A-SEPHAROSE AFFINITY CHROMATOGRAPHY

Values represent the means ± S.E. ($n = 6$). An asterisk (*) signifies $P < 0.01$ as compared to A

Fluorescence probe spectral parameters	VLDL fraction		
	A	B	C
1,6-Diphenyl-1,3,5-hexatriene			
absorbance corrected fluorescence	87.0 ± 0.1	105.3 ± 3.1*	109.9 ± 0.1*
relative fluorescence efficiency	167 ± 15	251 ± 12*	307 ± 13*
polarization, P	0.222 ± 0.004	0.245 ± 0.005*	0.203 ± 0.003*
lifetime, τ (ns)	8.4 ± 0.3	8.9 ± 0.2	8.7 ± 0.4
steady-state anisotropy, r	0.159 ± 0.002	0.178 ± 0.003*	0.145 ± 0.002*
limiting anisotropy, r_∞	0.159 ± 0.002	0.125 ± 0.002*	0.085 ± 0.002*
rotational rate (ns)	2.09 ± 0.007	2.20 ± 0.06	2.11 ± 0.09
order parameter, S	0.50 ± 0.01	0.56 ± 0.02*	0.46 ± 0.01*
trans-Parinaric acid			
absorbance corrected fluorescence	86.0 ± 3.2	154.1 ± 2.9*	217.0 ± 2.1*
relative fluorescence efficiency	176 ± 8	302 ± 21*	490 ± 30*
polarization, P	0.303 ± 0.004	0.334 ± 0.004*	0.277 ± 0.003*
lifetime, τ_1 (ns)	2.9 ± 0.3	3.3 ± 0.2	2.1 ± 0.3
lifetime, τ_2 (ns)	9.8 ± 0.8	10.6 ± 0.5	9.3 ± 0.4
fractional fluorescence, F_1	0.40 ± 0.05	0.38 ± 0.06	0.34 ± 0.06
fractional fluorescence, F_2	0.60 ± 0.05	0.62 ± 0.06	0.66 ± 0.06
steady-state anisotropy, r	0.224 ± 0.003	0.251 ± 0.003*	0.203 ± 0.002*
limiting anisotropy, r_∞ [a]	0.188 ± 0.003	0.224 ± 0.003*	0.161 ± 0.002*
rotational rate (ns) [a]	1.53 ± 0.002	1.52 ± 0.03	1.53 ± 0.02

[a] Values were calculated according to Weber's Law for additivity of polarization anisotropy [46] and represent average values based on fractional fluorescence

rescence efficiency of 1,6-Diphenyl-1,3,5-hexatriene and *trans*-parinaric acid were highest in fraction C, while the steady-state polarization of 1,6-diphenyl-1,3,5-hexatriene was highest in fraction B (0.245 in B vs. 0.222 in A and 0.203 in C). The motional properties of lipids were also determined with fluorescence probe molecules (Table VI). The limiting anisotropy (sensitive to the degree of restriction to probe rotational motion) and the lipid order parameter of 1,6-diphenyl-1,3,5-hexatriene were significantly higher in fraction B VLDL and lower in fraction C VLDL, respectively, as compared to fraction A VLDL. The rotational relaxation time, in contrast, was near 2.1 ns and was unchanged. The fluorescence probe molecule *trans*-parinaric acid partitions into two membrane lipid environments, fluid and solid, and displays a 4-fold preference for solid lipid [39]. Similarly, in the VLDL subfractions *trans*-parinaric acid displayed two fluorescence lifetime components near 3 and 10 ns. Approximately 0.69, 0.66 and 0.69 mole fraction of the *trans*-parinaric acid was associated with the lipid environment with the short lifetime component in VLDL subfractions A, B and C, respectively. The remaining mole fraction was with the longer lifetime component. Because of its 4-fold higher affinity for solid lipid approximately only 7.7%, 8.5% and 7.8% of the lipid environment detected by *trans-parinaric acid in VLDL subfractions A, B and C, respectively, was solid at 24°C. Arrhenius plots of trans*-parinarate corrected fluorescence or polarization in fractions A, B and C had breakpoints near 17 and 24°C (fraction A), 39°C (fraction B) and no breakpoints (fraction C). 1,6-Diphenyl-1,3,5-hexatriene showed breakpoints only in fractions B and C near 26°C and 35°C, respectively. These data indicate a very different structure and phase behavior in the three VLDL subfractions.

Discussion

Recent results from several laboratories indicate that a structural and metabolic heterogeneity may exist not only for the plasma high and low density lipoproteins but also for the VLDL released by the liver [1–8]. Other investigators [4,5] have used concanavalin A-Sepharose 4B chromatography to resolve plasma VLDL subfractions. The effect of concanavalin A-Sepharose 4B chromatography itself on VLDL properties has not heretofore been reported. VLDL secreted by the isolated perfused liver were used instead of plasma VLDL wherein exchange of components and extensive metabolism may already modify the VLDL. The secretory but not all morphological criteria showed that the perfused liver was functionally normal. Standard criteria, such as loss of endothelial cells, reduced microvilli, fragmentation and/or dissociation of hepatocytes, which are characteristic of necrosis, were not observed in either non-perfused or perfused livers. Although the hepatocytes were slightly swollen, mitochondrial swelling inclusions within mitochondria, indicative of early cell injury [40,41], were not present either before or after perfusion. The hepatocyte swelling after perfusion may be due to the flow rate of perfusate through the liver (7 ml/min per g) which is higher than in vivo rates indicated from previous studies in other species [42]. The increased appearances of lipid droplets was consistent with uptake of oleate from the perfusate, and increased triacylglycerol synthesis.

The data presented herein demonstrated that the three subfractions separated by concanavalin A-Sepharose 4B chromatography differed 8-fold (fractions A vs. C) in carbohydrate content and even more dramatically in carbohydrate composition. The elution profile of the subfractions could be explained by their quantity and relative content of mannose, glucose and *N*-acetylglucosamine – all sugar residues that bind to concanavalin A. These sugars were primarily found in the column adherent fractions B and C. However, sialic acid, fucose and galactose were found in all three subfractions. All of the above sugars are normal constituents of plasma lipoproteins [43]. In addition, sialic acid, which is the carbohydrate whose relative distribution in the C apolipoproteins regulates VLDL catabolism, was compositionally greatest in the VLDL fraction C and least in the non-adherent VLDL fraction A (5-fold difference).

A number points consistent with the conclusion that the concanavalin A affinity chromatography altered VLDL properties were obtained. First, the size of the VLDL was altered by the column fractionation procedure. Second, the apolipoprotein pattern of the three VLDL subfractions differed markedly. Although the apolipoproteins B, E, AI, AII, AIV and C were present in relative expected amounts in the unfractionated VLDL and fraction A VLDL [29,44], the apolipoproteins B_h and B_l were essentially absent from adherent fractions B and C. Third, preferential loss of apolipoprotein B_h and AIV apparently occurred in all three fractions as compared to the unfractionated VLDL. Fourth, several smaller molecular weight and as yet unidentified apolipoproteins appearing in the vicinity of the C apolipoproteins were enriched in VLDL fractions B and C. Several types of lipoprotein degradation must be considered, e.g., intravascular metabolism by hepatic lipase. The isolated perfused liver may secrete this and other enzymes including proteinases. Sources of proteinase activity in the perfusate and buffers could include bacteria as well as proteinase released from the liver. Bacterial growth was inhibited with NaN_3 and low temperature in the present study. VLDL themselves can contain attached proteinases [45]. Possibly, such proteinases could be activated during the affinity chromatography procedure. It is obvious that the activity of proteinases could be further reduced by including a proteinase inhibitor such as phenylmethylsulfonyl fluoride in the perfusate and/or the buffers used to isolate the VLDL. However, since these substances could be toxic to the liver, were not utilized by many investigators in the field using perfused liver techniques [9–18,20,21,28,29], and because they were not added by others using concanavalin A-Sepharose 4B chromatography

[4,5], proteinase inhibitors were also not used herein. This allowed for better comparisons with the data of earlier workers. The above enzymes could break down large VLDL into smaller VLDL and cause concomitant loss of some apolipoproteins such that a heterogenous population of particles may be obtained. However, such breakdown would be less likely in perfusate from the 1 h single pass perfusate which remained at 37°C only while passing through the liver in minutes and was then immediately cooled at 4°C. In contrast the recycling perfusate was kept at 37°C for 4 h. However, VLDL from both single pass and recycling perfusate displayed similar elution patterns on concanavalin A-Sepharose 4B columns.

The physiological importance of VLDL heterogeneity is not understood at this time. The results presented here clearly show that concanavalin A-Sepharose 4B affinity chromatography resolves several VLDL subfractions differing dramatically in lipid, protein and carbohydrate composition as well as structure. However, these subfractions appear to be produced by or artifactually modified by the affinity column procedure. The electron microscopic and electrophoretic data clearly established that the affinity column procedure produced artifacts, especially in fractions B and C. Therefore, these subfractions probably do not represent newly secreted VLDL, but instead VLDL modified during the affinity chromatography procedures. Whether VLDL apolipoprotein modification on the column also results in altered lipid composition and structure is not known, but is suspected. Use of the concanavalin A-Sepharose 4B affinity isolation procedure is therefore not recommended for investigating normal VLDL heterogeneity.

Acknowledgements

The authors wish to thank Ms. Nancy Malin, Mr. Eugene Hubert, Mr. Michael Brady and Mr. Jim Case for their excellent technical assistance and Mrs. Lindy Corkins for preparation of the manuscript. This investigation was supported primarily by a grant from the American Heart Association – Missouri Affiliate and, in part, by a grant from the NIH (Special Emphasis Career Development Award to A.B.K.) RR00013.

References

1 Patsch, W., Patsch, J.R., Kostner, G.M., Sailer, S and Braunsteiner, H. (1978) J Biol Chem. 253, 4911–4915

2 Kashyap, M.L., Srivastava, L S, Hynd, B A, Perisutti, G and Robinson, K (1979) Circulation 60, 73a

3 Streja, D A (1979) Atherosclerosis 32, 57–67

4 Shore, V G. and Shore, B. (1973) Biochemistry 12, 502–507

5 McConathy, W J. and Alaupovic, P (1974) FEBS Lett. 41, 174–178

6 Eisenberg, S., Bilheimer, D., Lindgren, F and Levy, R.I (1972) Biochim Biophys. Acta 269, 329–333

7 Smith, L C., Pownall, H J and Gotto, A M. (1978) Annu Rev Biochem 47, 751–777

8 Higgin, J.M and Fielding, C J (1975) Biochemistry 14, 2288–2294

9 Schroeder, F., Goh, E H and Heimberg, M (1979) FEBS Lett 97, 233–236

10 Schroeder, F, Goh, E.H and Heimberg, M. (1979) J. Biol. Chem 254, 2456–2463

11 Schroeder, F and Goh, E H (1979) J. Biol. Chem. 254, 2464–2470

12 Hale, J and Schroeder, F (1981) J. Lipid Res 22, 838–851

13 Schroeder, F., Wilcox, H.G, Keyes, W.G and Heimberg, M (1982) Endocrinology 110, 551–562

14 Schroeder, F, Keyes, W.G, Wilcox, H G. and Heimberg, M. (1983) Drug-Nutrient Interactions 1, 249–263

15 Wilcox, H.G, Dunn, G.D. and Heimberg, M. (1975) Biochim. Biophys Acta 389, 39–54

16 Goh, E H and Heimberg, M (1979) Biochem. J 184, 1–6

17 Soler-Argilaga, C, Danon, A., Wilcox, H.G and Heimberg, M (1976) Lipids 11, 517–525

18 Olubadewo, J., Morgan, D W. and Heimberg, M (1983) J Biol Chem 258, 938–945

19 Berry, E.M, Aldini, R, Bar-On, H and Eisenberg, S (1981) Eur. J. C I 11, 151–159

20 Azain, M.J., Fukuda, N, Chao, F-F., Yamamoto, M and Ontko, J.A. (1985) J Biol Chem 260, 174–181

21 Goh, E H (1974) Ph.D thesis, Vanderbilt University, Nashville, TN

22 Steinman, R M., Brodie, S.E and Cohn, Z A (1976) J. Cell Biol 68, 665–687

23 Wilcox, H.G and Heimberg, M. (1970) J Lipid. Res (1970) 11, 7–22

24 Clark, S.B, Atkinson, D, Hamilton, J.A., Forte, T., Russell, B, Feldman, E B and Small, D M (1982) J Lipid Res 23, 28–41

25 Mawhinney, T P, Feather, M S., Barbero, G.J. and Martinez, J R (1980) Anal Biochem 101, 112–117

26 Warren, L (1959) J Biol. Chem. 234, 1971–1978

27 Mawhinney, T P, Madson, M.A., Rice, R H, Feather, M.S and Barbero, G J (1982) Carbohydr. Res 104, 169–181

28 Keyes, W G. and Heimberg, M. (1979) J Clin Invest. 64, 182–190

29 Wilcox, H G., Keyes, W.G, Hale, T A, Frank, R., Morgan, D.W and Heimberg, M. (1982) J. Lipid Res 23, 1159–1166

30 Laemmli, U.K (1970) Nature 227, 680–685

31 Bligh, E G. and Dyer, W N (1959) Can J Biochem. Physiol 37, 911–917

32 Rouser, G., Kritchevsky, G and Yamamoto, A (1967) in Lipid Chromatographic Analysis (Marinetti, G , ed), Vol 1, pp 99–161, Marcel Dekker, Inc , New York

33 Morrisett, W R. and Smith, L M. (1964) J Lipid Res. 5, 600–615

34 Holland, J.F., Teets, R E and Timnick, A (1973) Anal Chem 45, 145–153

35 Schroeder, F , Goetz, I.E and Roberts, E. (1984) J. Neurochem 43, 526–539

36 Bowers, W., Hubbard, R , Wagner, D , Chisolm, M A P , Murphy, M., Leav, B S I , Hamlet, M. and Maher, J. (1981) Lab. Invest. 44, 99–104

37 Kohout, M , Kohouteva, B and Heimberg, M. (1971) J. Biol Chem 246, 5067–5074

38 Goldstein, I J. (1976) in Concanavalin A as a Tool (Bittinger, H , and Schnebli, H.P , eds.), pp 55–78, John Wiley and Sons, New York, NY

39 Schroeder, F. (1983) Eur. J. Biochem 132, 509–516

40 Hagler, H K , Sherwin, L and Buja, L M (1979) Lab. Invest 40, 529–544

41 Laiho, K.U and Trump, B F. (1975) Lab Invest. 32, 163–182

42 Greenway, C V and Stark, R D. (1971) Physiol Rev 51, 23–65

43 Parggaonkar, P.S., Radhakrishnamurthy, B , Srinivason, S.R. and Berenson, G S (1977) Comp. Biochem. Physiol. 56B, 293–299

44 Vega, G L , Goszek, E , Wolf, R. and Grundy, S.M (1982) J Lipid Res 23, 811–822

45 Bradley, W A , Gilliam, E B., Gotto, A M. and Gianturco, S H. (1982) Biochem Biophys. Res Commun. 109, 1360–1367

46 Weber, G. (1953) Adv Protein Chem 8, 415–460

Biochimica et Biophysica Acta 917 (1987) 74–80
Elsevier

BBA 52300

Cell-density-dependent uptake of chylomicron remnants in rat hepatocyte monolayers. Effects of compactin and mevalonic acid

Elmo Jensen, Claes-Henrik Florén and Åke Nilsson

Department of Medicine, University of Lund, Lund (Sweden)

(Received 10 July 1986)

Key words: Chylomicron uptake; Cell density; Compactin; Mevalonate; LDL receptor, (Hepatocyte)

In rat hepatocytes cultured in lipoprotein-deficient serum, the uptake and degradation of chylomicron remnant cholesteryl ester per mg cell protein varies inversely with cell density. Compactin, a competitive inhibitor of 3-hydroxy-3-methylglutaryl-coenzyme-A reductase, stimulates the uptake at all cell densities. Mevalonic acid, on the other hand, can suppress a significant part of the remnant uptake. Chylomicron remnant uptake in hepatocyte cultures can thus be influenced by factors known to regulate the apolipoprotein-BE receptor activity.

Introduction

Dietary and endogenous cholesterol is transported from the intestine mainly as chylomicrons. During the rapid lipolysis of chylomicron triacylglycerols, chylomicron remnants are formed which carry the major part of the cholesteryl ester [1]. These particles are rapidly taken up by the liver [2], by an endocytic process located mainly at the hepatocytes [3–5]. This uptake may be mediated both by the receptor that exclusively binds apolipoprotein E (the remnant or E-receptor) and the low-density lipoprotein (LDL) receptor (the B, E-receptor) [6].

Metabolic regulation of the hepatic apolipoprotein-E-mediated remnant uptake cannot be easily demonstrated in vivo, i.e., in cholesterol-fed hypothyreotic rats that accumulate apolipoprotein-E-rich lipoproteins in plasma the remnant clearance is normal [7]. In dog liver membranes an increased binding of remnants is observed after bile acid drainage or cholestyramine treatment, but this can be ascribed to an induction of the apolipoprotein-BE receptor [8]. In vivo an increased catabolism of low-density lipoprotein (LDL) by the liver after biliary drainage and cholestyramine treatment has been demonstrated in several species, including man [9–11]. Administration of mevinolin or compactin, which are efficient competitive inhibitors of 3-hydroxy-3-methylglutaryl-CoA-reductase, not only inhibits cholesterol synthesis but also induces the hepatic LDL-receptor in vivo [11,12].

In cultured rat hepatocytes, chylomicron remnants are taken up more efficiently than native chylomicrons [13], although the absolute rates of uptake are lower than in the intact perfused liver [14,15]. Rat hepatocyte monolayers also take up LDL [16], and this uptake is cell-density-dependent and inducible with compactin [17]. In other cell types apolipoprotein-E-rich chylomicron remnants bind avidly to the apolipoprotein-BE receptor [18,19]. Both the apolipoprotein-BE and the apolipoprotein-E receptor could thus contrib-

---

Abbreviations. LDL, low-density lipoprotein, Hepes, 4-(2-hydroxyethyl)-1-piperazineethanesulphonic acid

Correspondence Dr. E. Jensen, Department of Medicine, University of Lund, 22185 Lund, Sweden

0005-2760/87/$03.50 © 1987 Elsevier Science Publishers B V (Biomedical Division)

ute to the chylomicron remnant uptake in hepatocyte monolayers. In the present study the cell-density dependence of the chylomicron remnant uptake in hepatocyte monolayers was examined. In addition, the effects of compactin and of mevalonic acid were examined in order to see whether the remnant uptake in this model system is subject to a metabolic regulation similar to that of the apolipoprotein-BE receptor.

Material and Methods

[1,2-^{3}H]Cholesterol and [1-^{14}C]linoleic acid were obtained from Amersham International, U.K. Male white Sprague-Dawley rats weighing 250–300 g were obtained from ALAB AB, Stockholm, Sweden. Thoracic duct cannulations were performed according to Bollman et al. [20], and the rats were treated postoperatively as described earlier [13]. The rats were fed 1.0 ml corn oil containing 20 mg unlabeled cholesterol plus 500 μCi [1,2-^{3}H]cholesterol and 50 μCi [1-^{14}C]linoleic acid. The fat was given divided in three doses over 2 h. Lymph was collected and stored at 4°C with 2 mM Na_2-EDTA present [21]. Chylomicron remnants were prepared by injecting chyle into eviscerated rats [15]. After 30 min, blood was drawn from the abdominal aorta using Na_2-EDTA as an anticoagulant. The density of the plasma was adjusted to 1.063 kg/l by adding a stock solution ($d = 1.35$ kg/l) of KBr and NaCl. It was then layered under saline ($d = 1.006$ kg/l) and centrifuged in a Beckman L 5-65 ultracentrifuge with an SW Ti 40 rotor at 32000 rpm ($120000 \times g$) for 12 h. The top layer containing the chylomicron remnants was collected under sterile conditions and used within 24 h. Lipoprotein deficient serum was prepared from fetal calf serum (Flow Laboratories, Irvine, U.K.) by ultracentrifugation at d = 1.25 kg/l [22]. After centrifugation the $d > 1.25$ kg/l fraction was extensively dialyzed against 0.15 M NaCl/1 mM Na_2-EDTA (pH 7.4). The cholesterol content in lipoproten-deficient serum ranged between 0.10 and 0.18 mmol/l.

Leibovitz L-15 medium, fetal calf serum and Hepes were obtained from Flow Laboratories, U.K. Acid-soluble calf-skin collagen and mevalonolactone were obtained from Sigma Chemical Co., St. Louis, MO, U.S.A. The mevalonolactone was subjected to alkaline hydrolysis before use [23]. Triacylglycerol and cholesterol concentrations were determined by the commercial enzymatic kit methods of Boehringer-Mannheim, Mannheim, F.R.G. Compactin was a kind gift from Dr. Endo, Tokyo, Japan.

Hepatocytes were prepared by a collagenase procedure [24], using the conditions of Seglen [25]. The initial cell viability of cells in suspenion was better than 85% as determined by the Trypan blue exclusion test. Sterilized equipment and aseptic technique were used during operation. Hepatocytes were cultured in primary monolayers according to Lin and Snodgrass [26]. The culture medium was Leibovitz L-15 containing 28 mM Hepes (pH 7.4), 1 mM sodium succinate, 100 μg penicillin and 50 μg gentamicin per ml. Collagen coated 60 mm Petri dishes (Falcon No 1007) were used. Varying numbers of hepatocytes were plated in each dish ($0.1 \cdot 10^6 - 4 \cdot 10^6$ hepatocytes) in a volume of 2.5 ml medium containing 5% lipoprotein-deficient fetal calf serum. The dishes were placed in humidified air at 37°C. Medium was changed 4 h after plating and then every 24 h except as described otherwise in the text. Before the incubation with chylomicron remnants, new medium containing 5% lipoprotein-deficient fetal calf serum was added. The incubation with remnants lasted for 4 h. After incubation with remnants the cells were washed according to a standard procedure [27], ans solubilized with 2.6 ml 0.5 M NaOH. Aliquots were taken for protein determination [28]. After neutralization with HCl, lipids were extracted from cells and media with chloroform/methanol (1:2). Lipids were separated by thin-layer chromatography on silica-gel G plates developed in light petroleum/diethyl ether/acetic acid (80:20:1, v/v). Spots were identified by staining with iodine vapour, and scraped into vials. 1 ml methanol/water (1:1) and 9 ml Instagel/toluene (1:1) were added and radioactivity was determined in a Packard TC 460 CD Liquid Scintillation system, using the computerized automatic Scintillation system, using the computerized automatic external standard for quench correction.

Net hydrolysis of remnant cholesteryl ester was calculated as described earlier [13]. Cell association of chylomicron remnant cholesterol is the amount of unesterified labelled cholesterol plus cholesteryl ester found in the washed cells. When the remnant uptake at different cell densities was investigated we found that cell association and hydrolysis per mg cell protein varied inversely with cell density. In a double-log plot the points centered round a line. Normalization has been described earlier [17,29]. In short, through each point representing an observation a line is drawn parallel with the main line, the intercept with the line $x = 3$ (1000 µg/dish) gives the normalized value for each dish. As long as the points are arranged symmetrically round a common axis the normalized values will also be comparable and thus they will have the same k_{m}. Evaluation of the normalized values was done with Student's t-test and Wilcoxon's rank sum test.

Results

The remnant particles prepared by injecting chyle into eviscerated rats had lost 85–95% of their original triglyceride content. 60–80% of the [^{3}H]cholesterol radioactivity of the chylomicrons was in cholesteryl ester. Due to loss of unesterified [^{3}H]cholesterol during preparation of remnants, the proportion of ^{3}H that was in cholesteryl ester in incubated remnants was 81.3–88.4%.

Uptake of chylomicron remnants was cell-density-dependent. After a 4 h incubation at low cell density (500 µg protein/dish), cell association of radioactively labelled cholesterol and cholesteryl ester was on average 35 ng/mg cell protein. At a high cell density (1.5 mg cell protein/dish) the average value was 10 ng/mg cell protein (Fig. 1).

The net hydrolysis of chylomicron remnant cholesteryl ester was also cell-density-dependent. At a low cell density (0.5 mg protein/dish) 20 ng cholesteryl ester were hydrolysed per mg cell protein and at a high cell concentration (1.5 mg cell protein/dish) 8 ng were hydrolysed per mg cell protein.

In order to normalize cell association and hydrolysis to 1 mg cell protein a double-log plot was drawn (Fig. 1B). This normalization was carried out to make it possible to compare the effects of compactin at different cell densities.

Incubation with compactin for 48 h had a stimulatory effect on cell association and hydrolysis of chylomicron remnant cholesteryl-ester (Table I, Fig. 2). The effect was most pronounced at subconfluent densities (Fig. 2).

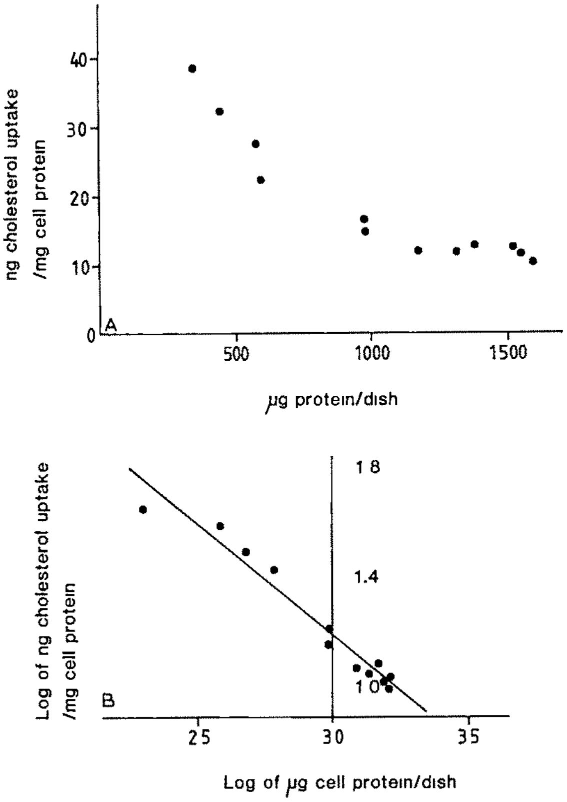

Fig. 1. Effect of cell density on the uptake of chylomicron remnant cholesterol. Double-log transformation of the uptake of chylomicron remnant cholesterol per mg cell protein vs µg cell protein. After culture for 48 h in the presence of 5% lipoprotein-deficient serum, new medium containing chylomicron remnants was added per dish These remnants contained 300 ng cholesterol, of which 81% (5170 dpm ^{3}H) was cholesteryl ester and 19% cholesterol (1213 dpm ^{3}H). The added chylomicron remnants contained 2 19 µg triacylglycerol (5287 dpm ^{14}C). The incubation was continued for 4 h (A) Cholesterol uptake as a function of µg protein per dish. The mean value for chylomicron remnant uptake is 17.4±7,4 (S.D.) ng cholesterol/mg cell protein, $N = 12$. The coefficient of variation is 0.43. In B the uptake is normalized. The mean value is here 15 9±1.2 ng cholesterol per mg cell protein. The coefficient of variation is 0.08. Each point represents one dish All the values are from one experiment.

Using normalization (i.e., to 1 mg cell protein per dish), ten different experiments were carried out with compactin added at a concentration of 20 µmol/l. In all experiments both cell association of

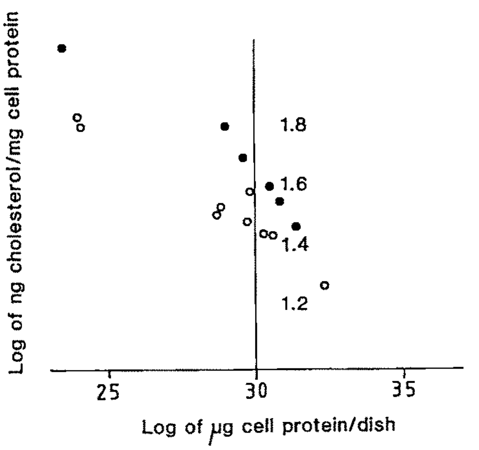

Fig 2 Effect of compactin on chylomicron remnant cell association. The basal conditions were the same as described in Fig. 1. Also the same amount – 300 ng – of labeled remnant cholesterol was added per dish for the final 4 h of the experiment. Open circles (○) symbolize dishes without compactin and black circles (●) dishes with 20 µmol/l compactin present. Incubations included compactin during the whole experiment Compactin elevated cell association from 28 8±3 3 (S.D.) (n = 9) ng/mg (normalized) to 43.5±6 0 (n = 6) ng/mg (i.e +51%, $P < 0.001$). The corresponding values for hydrolysis of cholesteryl-ester were 13 0±2.6 ng/mg (n = 9) to 16 3±2.2 (n = 6) ng/mg (i.e., +20%, $P < 0.05$). Each point represents one dish.

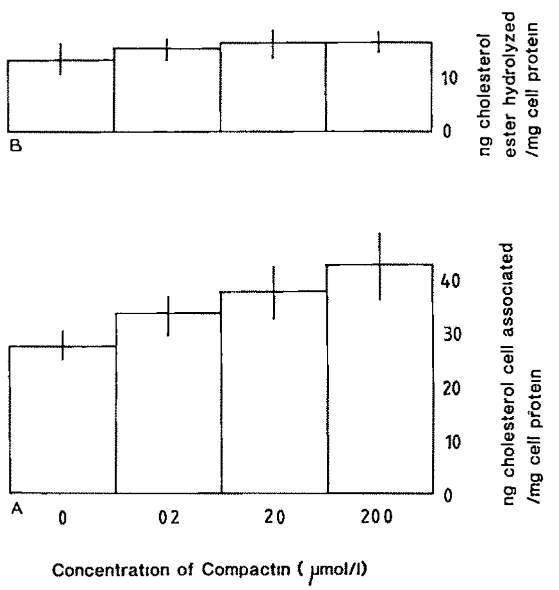

Fig 3. Effect of different concentrations of compactin on (A) cell association of remnant cholesteryl ester plus cholesterol and (B) hydrolysis of remnant cholesteryl ester in cultured rat hepatocytes. The basal conditions are those described in Fig 2. Cells were incubated 48 h with 0, 0.2, 2.0 and 20.0 µmol/l compactin. The range of µg cell protein per dish was 163–1763. Each bar represents the mean value±S.D from 6–10 normalized values, i.e., corresponding to 1 mg cell protein per dish.

TABLE I

EFFECT OF COMPACTIN ON REMNANT UPTAKE AND HYDROLYSIS

The table shows the effect of 20 µmol compactin/l on cell association of chylomicron remnant cholesteryl ester plus cholesterol and hydrolysis of cholesteryl ester in cultured rat hepatocytes. The amount of remnant cholesterol added per dish was 100–300 ng. Values represent the effect of compactin on the normalized values, i.e., per 1 mg cell protein per dish from ten consecutive experiments. For all the experiments taken together the P values are less than 0.005 for both the effect on uptake and hydrolysis.

Experiment number	Numbers of dishes	Range of µg cell protein per dish	Effect of compactin on cell association (%)	P less than	Effect of compactin on hydrolysis (%)	P less than
1	16	270–1110	+36	0 01	+31	0.01
2	18	132–1109	+82	0 001	+51	0.02
3	20	300–1830	+7	n.s.	+26	0.01
4	12	120–2000	+16	n.s.	+1	n.s.
5	20	225–1413	+51	0.001	+20	0 05
6	16	104–1404	+18	0.05	+14	n.s.
7	18	94–1872	+32	0.05	+23	n s.
8	16	187–1544	+15	0.001	+13	0.02
9	10	130–1240	+2	n s.	+14	n.s.
10	16	192–1048	+36	n.s.	+10	n.s.
Mean ± SD:			30±24		21±14	

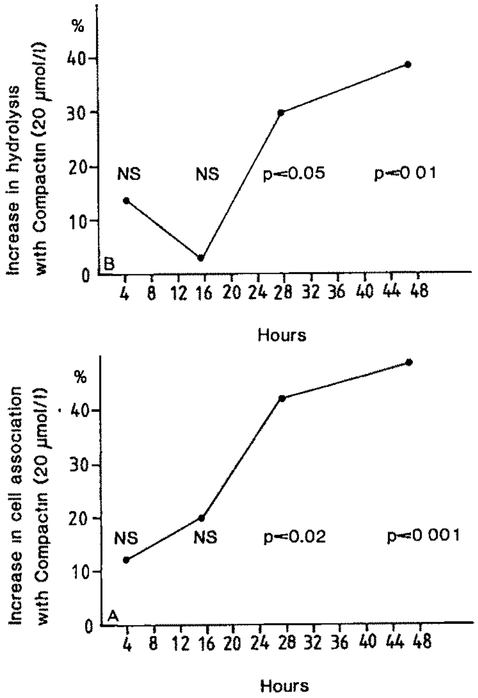

Fig. 4. Time-course for the effect of compactin on cell association (A) and hydrolysis (B) of chylomicron remnant cholesterol and cholesteryl ester by hepatocyte monolayers. Cells were plated at different densities. All the dishes were cultured for 48 h before interruption. At different times before this – 4, 15, 27 and 46 h – cells were incubated with 20 µM compactin. The added chylomicron remnants that contained 200 ng of labelled chylomicron remnant cholesteryl ester were incubated with cells for the last 4 h. Each point represents the difference between the means of four dishes preincubated with 20 µmol/l compactin and four dishes without compactin For each dish uptake and hydrolysis has been normalized to 1 mg cell protein per dish. The range of µg cell protein per dish in the experiment was 208–1326.

chylomicron remnant cholesterol and cholesteryl ester and hydrolysis of chylomicron remnant cholesteryl ester increased (Table I), although the increase caused by compactin varied between individual experiments. Cell association increased 2–82% with a mean of 30% ± 24% (± S.D.). The increase was statistically significant ($P < 0.005$). Hydrolysis of chylomicron cholesteryl-ester increased 1–56% with a mean of 21% ± 14% (S.D.). The increase in hydrolysis was also statistically significant ($P < 0.005$). The effect of compactin was also dose-dependent when compactin concentrations varying between 0.2 and 20 µmol/l were compared (Fig. 3). Fig. 4 shows the effect of preincubation time with compactin on chylomicron remnant cell association and hydrolysis. Cell association of chylomicron remnant cholesterol and cholesteryl ester and hydrolysis of chylomicron remnant cholesteryl ester increased with preincubation time.

Incubations with 10 mmol/l of mevalonic acid gave a suppression of chylomicron remnant cell association and hydrolysis (Fig. 5 and Table II). In order to see if cell-density-dependent uptake of chylomicron remnants also occurred in the presence of mevalonic acid, cells were planted at varying densities (65–1240 µg protein/dish) – without and with 10 mmol/l mevalonic acid. Normalization was carried out in regard to cell mass as described in Fig. 1. The two resulting lines were essentially parallel, indicating the same cell-density-dependence without and with mevalonic acid.

TABLE II

THE EFFECT OF MEVALONIC ACID ON CHYLOMICRON REMNANT UPTAKE AND HYDROLYSIS

Expt. 1 is described in the legend to Fig. 5. Expts. 2 and 3 were done essentially the same way. All the values are in % of controls (without mevalonic acid) ± S.D. Each observation is based on normalized values (i e., to 1 mg cell protein per dish) from 2–4 dishes. The range of µg cell protein per dish was for experiments 1, 2 and 3: 577–887, 356–757 and 406–868, respectively.

Mevalonic acid (mmol per l)	Expt No.	Uptake (% control)			Hydrolysis (% control)		
		1	2	3	1	2	3
0.0 (control)		100±5	100±6	100±14	100± 8	100±10	100± 3
0.3		–	–	120±27	–	–	96±17
1.0		57± 4	–	–	38±11	–	–
3.0		44± 5	–	86±16	15± 2	–	48±15
10.0		50±13	54±4	79±17	21±10	44±10	54±12
30.0		49± 2	–	–	15± 3	–	–

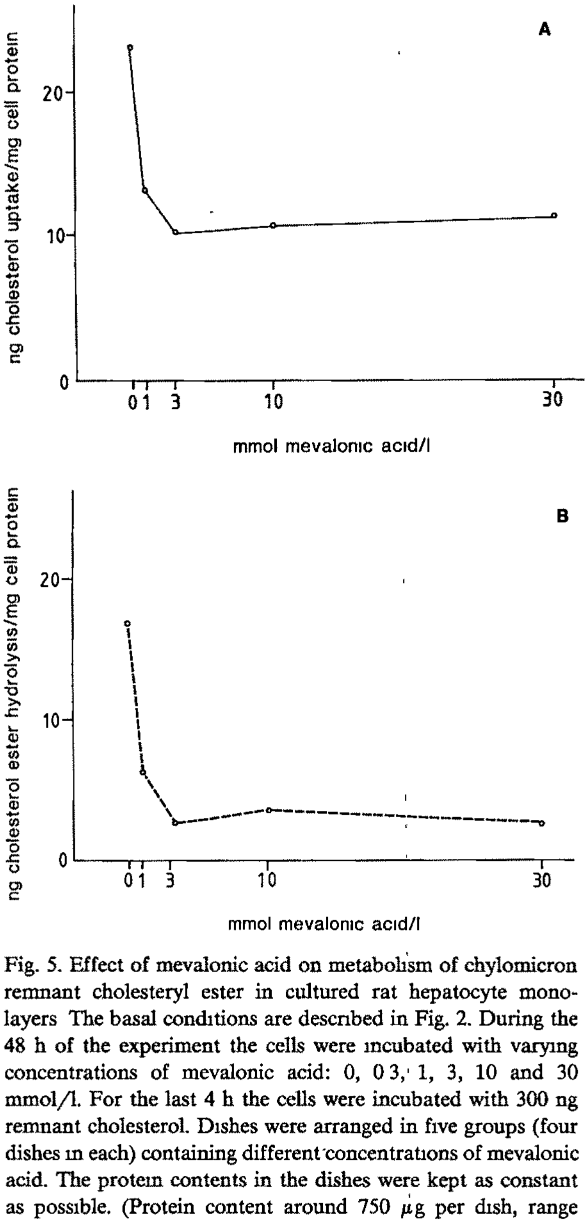

Fig. 5. Effect of mevalonic acid on metabolism of chylomicron remnant cholesteryl ester in cultured rat hepatocyte monolayers The basal conditions are described in Fig. 2. During the 48 h of the experiment the cells were incubated with varying concentrations of mevalonic acid: 0, 0 3, 1, 3, 10 and 30 mmol/l. For the last 4 h the cells were incubated with 300 ng remnant cholesterol. Dishes were arranged in five groups (four dishes in each) containing different concentrations of mevalonic acid. The protein contents in the dishes were kept as constant as possible. (Protein content around 750 μg per dish, range 577–887 μg.) (A) Effect of mevalonic acid on chylomicron remnant cell association; (B) effect on chylomicron remnant hydrolysis

Discussion

The present study demonstrates that the chylomicron remnant uptake in hepatocyte monolayer cultures is influenced by cell density in a similar way as the uptake of LDL, i.e., the uptake per mg cell protein varies inversely with cell density [17]. In addition, the uptake can be induced with the 3-hydroxy-3-methylglutaryl-CoA-reductase inhibitor compactin to about the same extent as the uptake of LDL, and suppressed by adding mevalonic acid (Fig. 5), which forces the cholesterol synthesis in the cells by supplying an intermediary of the cholesterol synthesis beyond the rate-limiting step [23]. In hepatocytes cultured in lipoprotein-deficient serum the regulation of the chylomicron remnant uptake is thus influenced by factors known to regulate the apolipoprotein-BE receptor, i.e., cell density and the cholesterol content of the cell. Since in other cell types apolipoprotein-E-containing lipoprotein particles bind avidly to the apolipoprotein-BE receptor [18,19], one possible interpretation of the data would be that a significant part of the remnant uptake in hepatocyte monolayer cultures may occur by the apolipoprotein-BE receptor under the conditions used. If this is so, hepatocyte monolayers cultured at low cell densities in the presence of lipoprotein-deficient serum may provide a convenient model system for further studies of the interaction between remnant particles and the hepatic B,E-receptor. Further studies are, however, necessary to test the possibility that the apolipoprotein E recpetor may also be influenced by cell density and factors that regulate the cellular cholesterol content of the hepatocytes, although evidence for this is so far lacking in vivo.

The mechanism behind the effect of cell density on the uptake of LDL and chylomicron remnants is not clear. A similar cell density dependence of the LDL uptake has been demonstrated in cultures of fibroblasts and endothelial cells [30–32].

In a variety of mammalian cell lines cell density has been shown to have other effects on lipid metabolism. For example 3-hydroxy-3-methylglutaryl-CoA reductase increases at low cell densities [33–35] and the rate of cholesterol esterification changes [35–36]. Since dividing cells have more LDL-receptors than quiescent cells [37], this effect has been ascribed to an effect on cell proliferation. Rat hepatocyte monolayers are, however, non-proliferating primary cultures in which other causes may thus operate.

In summary, the study thus demonstrates a cell-density dependence of chylomicron remnant uptake in non-proliferating hepatocyte monolayers that may be influenced by factors effecting the cholesterol supply to the cells. This model system can be used for further studies of the hormonal and metabolic control of the remnant uptake via different receptor types.

Acknowledgements

Ms Birgit Persson and Ms Gertrud Ohlsson provided skilful technical assistance. The work was supported by grants from the Swedish Medical Research Council (No 03X-3969 and 03X-6802), the Swedish Diabetes Association, Lundgrens Stiftelse, Nordisk Insulinfond and the Medical Faculty, University of Lund.

References

1 Noel, S.-P, Dolphin, P.J. and Rubinstein, D. (1975) Biochem Biophys Res. Commun 63, 764–772
2 Goodman, D.W.S (1962) J Clin. Invest 41, 1886–1896
3 Stein, O, Stein, Y., Goodman, D.W.S. and Fidge, N.H (1969) J. Cell. Biol. 43, 410–430
4 Nilsson, A. and Zilversmit, D.B. (1971) Biochim Biophys Acta 248, 137–142
5 Jones, A.L., Hrakek, G.T, Hornick, C, Renaud, G., Windler, E.E T. and Havel, R J. (1984) J Lipid. Res 25, 1151–1158
6 Mahley, R W., Hui, D Y, Innerarity, T.L and Weisgraber, K.H. (1981) J. Clin. Invest. 68, 1197–1206
7 Florén, C.H. and Nilsson, Å. (1981) Eur J. Clin Invest 11, 11–18
8 Hui, D.Y, Innerarity, T.L. and Mahley, R W (1981) J. Biol Chem 256, 5646–5655
9 Slater, H R., Packard, C.J, Bicker, S. and Shepherd, J. (1980) J. Biol. Chem 255, 10210–10213
10 Shepherd, J., Packard, C.J, Bicker, S., Lawrie, T D.V. and Morgan, H.G. (1980) N. Engl. J. Med. 302, 1219–1222
11 Kovanen, P.T., Bilheimer, D W., Goldstein, J.L., Jaramillo, J J. and Brown, M S. (1981) Proc Natl. Acad. Sci. 78, 1194–1198
12 Mabuchi, H., Sakai, T, Sakai, Y, Yosimura, A, Watanabe, A., Wakasugi, T., Koisumi, J. and Takeda, R. (1983) N. Engl. J. Med. 308, 609–613
13 Florén, C.H and Nilsson, Å. (1977) Biochem. J. 168, 483–494
14 Cooper, A.D and Yu, P.Y.S. (1978) J Lipid. Res. 19, 635–643
15 Sherril, B.C. and Dietschy, J.M. (1978) J Biol Chem 253, 1859–1867
16 Pangburn, S.H, Newton, R.S., Chang, C.M., Weinstein, D.B. and Steinberg, D (1981) J. Biol. Chem. 256, 3340–3347
17 Jensen, E., Florén, C.H. and Nilsson, Å. (1985) Biochim. Biophys Acta 834, 279–283
18 Florén, C.H., Albers, J J., Kudchodkar, B.J and Bierman, E.L. (1981) J. Biol. Chem. 256, 425–433
19 Florén, C.H. and Chait, A. (1981) Biochim. Biophys. Acta 665, 608–611
20 Bollman, J.L., Cain, J.C. and Grindlay, J H. (1948) J. Lab Clin. Med 33, 1349–1354
21 Onkto, J.A. (1970) J. Lip Res. 11, 367–375
22 Chait, A., Bierman, E.L. and Albers, J.J (1978) Biochim. Biophys Acta 529, 292–299
23 Nilsson, Å (1975) Eur. J Biochem. 51, 337–342
24 Berry, M.N. and Friend, D.S. (1969) J. Cell Biol 43, 506–520
25 Seglen, P.O. (1973) Exp. Cell. Res. 82, 391–398
26 Lin, R.C. and Snodgrass, P.J. (1975) Biochem. Biophys. Res. Commun 64, 725–734
27 Goldstein, J.L, Basu, S K., Brunschede, G.Y. and Brown, M.S. (1976) Cell 7, 85–95
28 Lowry, O H, Rosebrough, N.J., Farr, A.L. and Randall, R J (1951) J. Biol Chem 193, 265–275
29 Chait, A, Bierman, E L. and Albers, J.J. (1979) Diabetes 28, 914–918
30 Kruth, H.S, Avigan, J., Gamble, W. and Vaughan, M. (1979) J. Cell. Biol. 83, 588–594
31 Leren, T P. and Berg, K (1985) Scand J. Lab Invest 45, 379–385
32 Kenagy, R., Bierman, E.L., Schwartz, S and Albers, J.J. (1984) Arteriosclerosis 4, 365–371
33 Chen, H.W. (1983) J. Cell Physiol 117, 123–127
34 Chen, H.W. (1981) J. Cell. Physiol 108, 91–97
35 Gal, D, MacDonald, P.C., Porter, J C, Smith, J.W. and Simpson, E R (1981) Cancer Res 41, 473–477
36 Kenagy, R.D. and Bierman, E.L. (1983) Biochim. Biophys Acta 754, 174–180
37 Chait, A., Ross, R., Albers, J.J and Bierman, E.L. (1980) Proc. Natl. Acad Sci USA 77, 4084–4088

Biochimica et Biophysica Acta 917 (1987) 81–85
Elsevier

BBA 52313

1,25-Dihydroxycholecalciferol stimulates renal phosphate transport by directly altering membrane phosphatidylcholine composition

Brenda R.C. Kurnik, Margaret Huskey and Keith A. Hruska

Renal Division, Department of Medicine, Washington University and Jewish Hospital, St. Louis, MO 63110 (USA)

(Received 21 April 1986)
(Revised manuscript received 2 September 1986)

Key words: Phosphatidylcholine content, 1,25-Dihydroxycholecalciferol; Vitamin D; Phosphate transport, Renal transport; (Brush-border membrane vesicle)

Controversy exists regarding the mechanisms by which 1,25-dihydroxycholecalciferol ($1,25(OH_2)D_3$) alters membrane lipid composition and ion transport. Recent studies have demonstrated stimulation of the transfer of 1-acyl-2-(*N*-4-nitrobenz-2-oxa-1,3-diazole)aminocaproylphosphatidylcholine (NBD-PC) by $1,25(OH)_2D_3$. In the present studies, brush border membrane vesicle phosphatidylcholine content was increased after incubation with liposomes composed of dioleoylphosphatidylcholine or β-linoleyl, γ-palmitoyl phosphatidylcholine and $1,25(OH)_2D_3$ (10^{-7} M). Vesicular phosphatidylcholine content was increased from control levels of 49.5 μg/mg protein to 56.9 and 58.5, respectively, after treatment with the liposomes containing $1,25(OH)_2D_3$, $P < 0.05$. When the vesicles were incubated with liposomes composed of β-linoleyl, γ-palmitoyl phosphatidylcholine, phosphate transport was stimulated from 231 ± 20 to 431 ± 41 pmol/mg protein per 15 s in the presence of $1,25(OH)_2D_3$ if the vesicles were derived from vitamin D deficient rats and from 443 ± 33 to 601 ± 42 pmol/mg protein per 15 s if the vesicles were prepared from normal rats. Despite phosphatidylcholine transfer, incubation with liposomes composed of dioleoylphosphatidylcholine and $1,25(OH)_2D_3$ did not stimulate phosphate transport. Furthermore, incubation of vesicles with liposomes and $1,25(OH)_2D_3$ did not alter glucose transport.

Introduction

Current evidence suggests that the mechanism of action of several hormones may be mediated through alterations in membrane lipid composition [1–4]. Both membrane phosphatidylcholine (PC) content and its degree of fatty acid unsaturation are decreased in renal proximal tubular and duodenal brush border membranes by vitamin D deficiency. This is reversed by physiologic repletion of 1,25-dihydroxycholecalciferol ($1,25(OH)_2D_3$) [5,6]. In both the intestine [6,7] and the kidney [8], indirect evidence suggests that these lipid changes may be important in stimulating calcium and phosphate transport. Recent studies using fluorescent phospholipid derivatives demonstrate that $1,25(OH)_2D_3$ rapidly and directly stimulates the transfer of PC from lipposomes to renal brush border membrane vesicles [9,10]. The following studies were performed to investigate the effects of $1,25(OH)_2D_3$ stimulated phospholipid transfer on phosphate transport.

Abbreviations: $1,25(OH)_2D_3$, 1,25-dihydroxycholecalciferol; NBD-PC, 1-acyl-2-(*N*-4-nitrobenz-2-oxa-1,3-diazole)aminocaproylphosphatidylcholine, BBMV, brush-border membrane vesicles; Mes, 4-morpholineethanesulfonic acid; DOPC, dioleoylphosphatidylcholine, P_i, inorganic phosphate; PC, phosphatidylcholine.

Correspondence: Dr. Keith A Hruska, Renal Division, Jewish Hospital of St. Louis, 216 South Kingshighway, St. Louis, MO 63110, U.S.A.

0005-2760/87/$03.50 © 1987 Elsevier Science Publishers B.V. (Biomedical Division)

Methods

Preparation of brush-border membrane vesicles (BBMV). Renal RBMV were prepared from either normal or vitamin D deficient rats by a technique of divalent cation precipitation and differential centrifugation. Detailed discussions of the model of vitamin D deficiency, and the preparation and characterization of the BBMV have been published [5,11]. The final vesicle preparation was suspended in 150 mM KCl, 2 mM 4-morpholine-ethanesulfonic acid-2 amino-2-hydroxymethyl propane-1,3-diol (Mes-Tris) (pH 7.5) and incubated with various liposome preparations as detailed below.

Preparation of liposomes. Small unilamellar liposomes, 25–75 nm in diameter, were prepared by a method of bath sonication and ultracentrifugation [10]. The liposomes were composed of dioleoylphosphatidylcholine (DOPC) or β-linoleyl, γ-palmitoyl phosphatidylcholine (β-linoleic-PC) with or without $1,25(OH)_2D_3$ at specified concentrations. Scanning electron micrographs and chromatogrpahic elution patterns of the liposomes were the same and independent of hormone or phospholipid composition.

Modification of BBMV lipid composition. Following their preparation, liposomes (50 μg lipid/ml) and BBMV (1 mg vesicle protein/ml), were incubated together and subsequently used for either analysis and quantitation of vesicle lipids or for transport studies.

Quantitation of vesicle lipids. Vesicle phospholipid content was analyzed following their incubation with liposomes composed of either DOPC or β-linoleic-OC and various concentrations of $1,25(OH)_2D_3$. Following a 1 h incubation at 0°C the vesicles were pelleted by centrifugation (35000 $\times g$), the supernatant (free liposomes) discarded, and the pellet washed two more times. The pellets containing vesicle lipid were extracted by the method of Bligh and Dyer [12], beginning with chloroform/methanol/0.1 M HCl (1 : 2 : 0.8). Lipid extracts were analyzed by chromatography on Silica Gel 60 thin-layer plates (E. Merck, Darmstadt, F.R.G.) using a chloroform/methanol/28% ammonium hydroxide (65 : 35 : 5) solvent system along with appropriate standards [10]. The phosphatidylcholine spot was scraped and re-extracted with chloroform/methanol/water (1:2:0.8). Extracted phosphatidylcholine was dried, reconstituted, and quantitated using a phosphate assay [13].

Transport studies. Following incubation with various liposome preparations for 30 min at 0°C, the vesicles were seprated by centrifugation (35000 $\times g$ for 10 min) and resuspended in 150 mM KCl/2 mM Mes-Tris (pH 7.5) to achieve a final protein concentration of 10–20 μg/μl. The preparation was aliquoted into individual test tubes and used for transport studies as previously described [11]. BBMV were preincubated for one minute at 30°C following which a solution composed of 150 mM sodium chloride, 5 mM Mes-Tris (pH 7.5) and 31 μM phosphate ($^{32}P_i$, $25 \cdot 10^6$ cpm/ml) was added to initiate phosphate transport. Transport was studied at 15 s, 1 min and 90 min (steady state) of incubation and stopped using an ice-cold solution composed of 150 mM sodium chloride/5 mM Mes-Tris (pH 6.5)/5 mM arsenate. Values for nonspecific retention of radioactivity on the filters were subtracted from the values obtained with vesicle samples. All points were carried out in triplicate and uptakes expressed in pmol/mg protein.

Glucose transport was performed using a solution of 150 mM sodium chloride/5 mM Mes-Tris (pH 6.5)/50 μM glucose, (D-[2-^{3}H(N)]glucose). Glucose transport was also measured at 15 s, 1 min and 90 min of incubation and stopped with a solution of ice-cold 150 mM sodium chloride/5 mM Mes-Tris (pH 6.5).

Materials. Vitamin D metabolites were a gift from Hoffman-LaRoche (Nutley, New Jersey). Other chemicals were of the highest purity available for commercial sources. All solutions were filtered through a 0.45 μm Millipore filter on the day of the experiment.

Analytical methods. The Student's *t*-test for non-paired data was used for comparisons between groups when the BBMV were derived from different animals. For comparison of results using BBMV preparations from the same animals, a paired *t*-test was used.

Results

Quantitation of BBMV PC content

The results of incubating BBMV derived from

TABLE I

PHOSPHATIDYLCHOLINE CONTENT OF BBMV PREPARED FROM VITAMIN-D-DEFICIENT RATS FOLLOWING INCUBATION WITH LIPOSOMES

Liposomes composed of either DOPC or β-linoleic-PC with or without $1,25(OH)_2D_3$ at the specified concentrations were incubated with BBMV prepared from vitamin-D-deficient rats for 1 h at 0°C. The vesicle phospholipids were extracted and quantitated as described in the Methods

	Vesicle PC content (μg/mg prpotein)
Control ($N=10$)	49.5 ± 2.3
DOPC+10^{-7} M $1,25(OH)_2D_3$ ($N=7$)	56.9 ± 2.3 [a]
DOPC+10^{-1} M ($N=3$)	49.5 ± 5.2
β-linoleic-PC+10^{-7} M ($N=3$)	58.5 ± 3.2 [a]
β-linoleic-PC+10^{-11} M ($N=5$)	48.8 ± 3.4
β-linoleic-PC+10^{14} M ($N=3$)	45.5 ± 11

[a] $D^+ > D^-$; $P < 0.05$.

vitamin-D-deficient rats with various liposome preparations and quantitating their phosphatidylcholine content are shown in Table I. Control BBMV were vesicles not incubated with liposomes. Following incubation of BBMV with liposomes composed of 10^{-7} M $1,25(OH)_2D_3$ and DOPC, the vesicle PC content increased from 49.5 ± 2.3 μg/ml protein to 56.9 ± 2.3 μg/mg protein. When the liposomes were composed of β-linoleic-PC and $1,25(OH)_2D_3$ (10^{-7} M), the vesicle PC content was increased similarly to 58.5 ± 3.2 μg/mg protein. Concentrations of $1,25(OH)_2D_3$ of 10^{-11} M and below did not affect the vesicle PC content regardless of the liposome lipid composition. In a separate set of experiments, an intermediate level of $1,25(OH)_2D_3$ (10^{-9} M) incorporated into the DOPC liposomes increased PC content of BBMV after incubation to 51.4 ± 3.0 μg/mg protein, and to 54.6 with β-linoleic-PC liposomes, $N = 3$ and $N = 2$, respectively.

Phosphate transport

Na^+-dependent phosphate (P_i) transport in BBMV prepared from both vitamin D deficient and normal rats was studied following incubation with liposomes of specified compositions. Table II demonstrates that Na^+-dependent phosphate transport at 15 s of incubation was stimulated in BBMV prepared from vitamin-D-deficient rat kidneys following incubation with liposomes consisting of β-linoleic-PC and $1,25(OH)_2D_3$. P_i uptake in BBMV was increased from 231 ± 20 to 431 ± 41 pmol/mg protein per 15 s. when the β-linoleic-PC liposomes included 10^{-7} M $1,25(OH)_2D_3$. Phosphate transport was not stimulated if the liposomes were composed of DOPC in the presence or absence of $1,25(OH)_2D_3$ or β-linoleic-PC without $1,25(OH)_2D_3$. Uptakes of P_i at 90 min, repre-

TABLE II

EFFECT OF $1,25(OH)_2D_3$ STIMULATED PC TRANSFER FROM LIPOSOMES TO VITAMIN-D-DEFICIENT RAT RENAL BRUSH-BORDER MEMBRANE VESICLES

Liposomes composed of either DOPC or β-linoleic-PC with or without 10^{-7} M $1,25(OH)_2D_3$ were prepared and incubated with BBMV from vitamin-D-deficient rats for 30 min at 0°C. Phosphate transport was measured as described in the Methods. Data are expressed as mean ± SE, $N = 6$ in each group

	15 s	90 min
Control	287 ± 31	183 ± 25
DOPC	289 ± 33	271 ± 29
DOPC+$1,25(OH)_2D_3$	290 ± 39	225 ± 26
β-Linoleic-PC	231 ± 20	180 ± 19
β-linoleic-PC+$1,25(OH)_2D_3$	431 ± 41 [a]	217 ± 50

[a] Greater than control, $P < 0.05$.

TABLE III

P_i TRANSPORT EFFECTS OF $1,25(OH)_2D_3$ STIMULATED PC TRANSFER FROM LIPOSOMES TO NORMAL RAT RENAL BRUSH-BORDER MEMBRANE VESICLES

Liposomes composed of β-linoleic-PC with or without $1,25(OH)_2D_3$ at the specified concentrations were incubated with BBMV derived from normal rats for 30 min at 0°C. Phosphate transport was measured as described in the Methods. Data are expressed as mean ± SE, $N = 6$ in each group

	15 s	90 min
Control	443 ± 33	249 ± 45
β-linoleic-PC	431 ± 41	234 ± 63
β-linoleic-PC+10^{-7} M	601 ± 42 [a]	317 ± 86
β-linoleic-PC+10^{-11} M	406 ± 42	178 ± 22
β-linoleic-PC+10^{-14} M	463 ± 45	193 ± 37

[a] Greater than other groups, $P < 0.02$.

senting the steady state, were not different between groups.

Phosphate transport was also stimulated following incubation with liposomes of β-linoleic-PC and 1,25(OH)$_2$D$_3$ (10^{-7} M) when the BBMV were prepared from normal rats. P_i uptake was increased from 443 ± 33 to 601 ± 42 pmol/mg protein per 15 s (Table III). Incubation with liposomes without 1,25(OH)$_2$D$_3$, or those containing 10^{-11} M or 10^{-14} M 1,25(OH)$_2$D$_3$ did not exhibit stimulation of phosphate transport. Steady-state phosphate uptakes were again unchanged between groups. In separate experiments, inclusion of an intermediate level of 1,25(OH)$_2$D$_3$ in the β-linoleic-PC liposomes increased P_i transport to 575 ± 80 pmol/mg protein from a control value of 410 pmol/mg protein.

Na$^+$-dependent P_i uptake was significantly less in BBMV from kidneys of vitamin-D-deficient rats compared to normal rats (compare control studies in Tables II and III). The degree of stimulation by 1,25(OH)$_2$D$_3$ incorporated into β-linoleic-PC liposomes was greater in BBMV from vitamin D deficient rat kidneys (150% vs. 135%) and developed in association with increased BBMV β-linoleic-PC only (Table I). The relatively greater stimulation of P_i transport in BBMV from vitamin D deficient animals by 1,25(OH)$_2$D$_3$ compared to the stimulation seen in BBMV from normal rats agrees with our previous reports [10,11]. The dependency on unsaturated fatty acid of P_i transport stimulation requires further analysis of the specificity for individual fatty acids.

TABLE IV

Na-DEPENDENT GLUCOSE UPTAKE INTO BBMV-PREPARED FROM VITAMIN-D-DEFICIENT RATS

Liposomes composed of β-linoleic-PC ± 1,25(OH)$_2$D$_3$ (10^{-7} M) were incubated with BBMV prepared from vitamin-D-deficient rats for 30 min at 0 °C. The vesicles were isolated and used for glucose transport as described in the Methods

	pmol/mg protein			*N*
	15 s	1 min	90 min	
Control vesicles	121 ± 19	296 ± 50	76 ± 16	3
Liposome incubations				
β-linoleic-PC	114 ± 23	236 ± 37	74 ± 8	3
β-linoleic-PC + 1,25(OH)$_2$D$_3$ (10^{-7} M)	115 ± 13	272 ± 42	56 ± 11	3

Glucose transport

Sodium-dependent glucose transport was studied into BBMV from both normal and vitamin D deficient rats (Table IV). Uptake at 15 s of incubation was 114 ± 23 pmol/mg protein using BBMV derived from vitamin-D-deficient animals, and 115 ± 13 pmol/mg protein when the vesicles were pre-incubated with liposomes composed of β-linoleic-PC and 1,25(OH)$_2$D$_3$ (10^{-7} M). Uptakes at 90 min of incubation (steady state) were also unchanged between groups. Glucose uptakes were similar when the BBMV were derived from normal animals and were not affected by incubaitons with liposomes.

Discussion

Previous studies from this laboratory demonstrated an increase in PC of the renal brush border membranes, following 1,25(OH)$_2$D$_3$ treatment in vivo [5]. Partial mediation of this increase through facilitation of direct PC transfer to the BBM was suggested by recent studies [10]. The previous studies were performed using both fluorescent phospholipid derivatives, and endogenous forms of PC. The structure of the fluorescent derivatives and their inherent property of spontaneous transfer are not physiologic. Thus, the current experiments were performed using liposomes composed of DOPC or β-linoleic-PC with or without 1,25(OH)$_2$D$_3$. The results confirm that 1,25-(OH)$_2$D$_3$ stimulated phospholipid transfer. In addition, a quantitatively similar increase in total vesicle phosphatidylcholine content occurred whether the liposomes were composed of DOPC or β-linoleic-PC and 1,25(OH)$_2$D$_3$. Thus, these data suggest that the 1,25(OH)$_2$D$_3$-induced stimulation of lipid transfer, which may be mediated by a phospholipid-exchange protein, does not involve a structural specificity for chain length [14] or fatty acid desaturation.

In order to relate the membrane phospholipid alterations to solute transport functions of the BBMV, Na$^+$-dependent phosphate and glucose transport were studied. The results show that phosphate transport is stimulated into BBMV from either normal or vitamin-D-deficient rats following incubation with liposomes composed of β-linoleic-PC and 1,25(OH)$_2$D$_3$ (10^{-7} M). Transport was not stimulated if the liposomes were composed of a more saturated PC, despite a quantitatively similar transfer of this species.

The relationship of the above observations to the effects of 1,25(OH)$_2$D$_3$ on membrane phospholipid metabolism and P_i transport remain unclear. Further studies are required to understand the role of the sterol in phospholipid transfer, the dose dependency of the 1,25(OH)$_2$D$_3$ effect, and the specificity of β-linoleic-PC. Previous studies in both the intestine [6] and kidney [5] have demonstrated an increase in membrane phosphatidylcholine content and its degree of fatty acid unsaturation after in vivo 1,25(OH)$_2$D$_3$ administration. β-linoleic-PC was specifically chosen for these studies because it is increased following 1,25(OH)$_2$D$_3$ treatment [5]. The stimulation of phosphate transport following an increase in membrane β-linoleic-PC content induced in vitro provides a functional mechanism by which 1,25(OH)$_2$D$_3$ may act to alter ion transport.

Physiologic concentrations of 1,25(OH)$_2$D$_3$ (10^{-11} M) had no effect on either vesicle PC content or phosphate transport. However, the function of this process under different conditions may disclose enhanced sensitivity clarifying the potential biologic relevance of the observations reported here. In addition, intracellular compartmentalized concentrations of 1,25(OH)$_2$D$_3$ have not been measured. It is possible that they may be higher than serum levels in view of the fact that 1,25(OH)$_2$D$_3$ is produced in renal proximal tubular cells.

Specificity for the effect of the 1,25(OH)$_2$D$_3$-induced membrane lipid alterations on phosphate transport was shown by the data demonstrating that glucose transport is not altered by 1,25-(OH)$_2$D$_3$-stimulated phospholipid exchange.

In conclusion, these studies suggest that 1,25(OH)$_2$D$_3$ may directly modify the cell membrane phosphatidylcholine composition and that a specific increase in membrane β-linoleic-PC content results in a stimulation of sodium-dependent phosphate transport.

References

1 Farese, R.V., Barnes, D E., Davis, J.S., Standaert, M.L. and Pollett, R.J. (1984) J. Biol. Chem. 259, 7094–7100

2 Marver, D. and Kokko, J.P. (1983) Miner. Electrolyte Metab. 9, 1–18

3 Litosch, I., Lin, S.H and Fain, J.N. (1983) J. Biol. Chem. 258, 13727–13732

4 Meltzer, V., Weinreb, S., Bellorin-Font, E and Hruska, K.A. (1982) Biochim Biophys. Acta 712, 258–267

5 Tsutsumi, M., Alvarez, U., Avioli, L.V. and Hruska, K.A. (1985) Am. J. Physiol. 249, F117–F123

6 Matsumoto, T, Fontaine, O. and Rasmussen, H. (1981) J Biol Chem. 256, 3354–3360

7 Matsumoto, T., Fontaine, O. and Rasmussen, H (1980) Biochim. Biophys. Acta 599, 13–23

8 Kurnik, B R.C. and Hruska, K.A (1985) Biochim Biophys. Acta 817, 42–51

9 Kurnik, B.R.C. and Hruska, K.A. (1985) Kidney Int. 27, 119

10 Kurnik, B R.C., Huskey, M., Hagerty, D and Hruska, K A (1986) Biochim Biophys. Acta

11 Kurnik, B R.C. and Hruska, K.A. (1984) Am J Physiol. 247, F177–F182

12 Bligh, E.G. and Dyer, W.J (1959) Can J. Biochem Physiol 37, 911–917

13 Ames, B.N. and Dubin, D.T. (1960) J Biol. Chem 235, 769–775

14 Welti, R and Helmkamp, G.M, Jr. (1984) J Biol. Chem 259, 6937–6941

Biochimica et Biophysica Acta 917 (1987) 86–91
Elsevier

BBA 52321

Use of the fluorescence activated cell sorter for studying uptake of fluorescent fatty acids into cultured cells

Nabeel Nahas [a], Eitan Fibach [b], Haim Giloh [c] and Shimon Gatt [a]

[a] *Department of Membrane Biochemistry and Neurochemistry,* [b] *Department of Hematology and* [c] *The Interdepartmental Equipment Unit, The Hebrew University–Hadassah Medical School, Jerusalem 91010 (Israel)*

(Received 10 June 1986)
(Revised manuscript received 6 October 1986)

Key words: Fluorescence; Flow cytometry; Fatty acid; (Cell culture)

A procedure is described for the continuous monitoring and recording of fatty acid transport into cultured cells. Uptake of the fluorescent fatty acid derivative, 12-(1-pyrene)dodecanoic acid [P12] by a suspension of human promyelocytic leukemia (HL-60) cells was analyzed and recorded by the Fluorescence Activated Cell Sorter (FACS). A major advantage of the FACS is its ability for measuring the fluorescence of the cells only, without interference by that of the fatty acids dissolved or dispersed in the medium or complexed with serum albumin. The time-dependent fluorescence increase due to uptake of the acid by the cells could thus be monitored and recorded directly without a need for sedimenting, washing and extracting the cellular lipids. This procedure provided an accurate measurement of the kinetics of uptake of the fatty acid into the cells and permitted study of the effect of various parameters such as temperature, glucose, albumin or serum. The results indicated a biphasic uptake of P12 into the cells. The first, a rapid, energy-independent phase, lasted 3–4 min. This was followed by a slower uptake which was directly related to the metabolic utilization of the acid in the cells. This second phase represents the overall process of translocation across the cell membrane, activation to acyl coenzyme A and incorporation into the cellular neutral lipids and phosphoglycerides. When compared to HL-60, murine erythroleukemia (MEL) cells took up considerably lesser quantities of P12. This was utilized for setting up a model system, in which mixtures of these two respective cell types could be identified and separated from each other on the basis of their relative rates of uptake of the fluorescent fatty acid.

Introduction

The fluorescence activated cell sorter (FACS) is employed for the analysis and sorting of cells according to two properties: forward light scattering, which defines cell size, and fluorescence intensity [1]. Cells can be rendered fluorescent by conjugation with a fluorescent antibody or by administration of fluorescent molecules into the membrane or cell interior. In previous reports from this laboratory, cultured cells were treated with several fluorescent derivatives of fatty acids. Following insertion into the plasma membrane, these compounds were translocated and incorporated into cellular lipids [2], thereby imparting a considerable fluorescence to the cells. Of several fluorescent fatty acids examined, 12-(1-pyrene)

Abbreviations: P12, 12-(1-pyrene)dodecanoic acid; FACS, fluorescence activated cell sorter; MEL, murine erythroleukemia cells; PBS, phosphate buffered saline

Correspondence: Dr. E. Fibach. Department of Hematology, The Hebrew University–Hadassah Medical School, Jerusalem 91010, Israel.

0005-2760/87/$03.50 © 1987 Elsevier Science Publishers B V (Biomedical Division)

dodecanoic acid (P12) was taken up and incorporated into cellular lipids at rates similar to those observed using radioactively labelled palmitic acid [2]. Following incubation with fluorescent [2] or radioactive fatty acids [3], the cells were collected, washed extensively to remove excess fatty acid, the cellular lipids were extracted and their fluorescence intensity measured in a spectrofluorometer. The extract was then chromatographed on columns of aluminum oxide for separation of the neutral lipids and phospholipids.

We herewith report the use of the FACS for studying the uptake of fluorescent derivatives of fatty acids into suspensions of cultured cells. This method permitted continuous measurements of the association and uptake of the fatty acid by intact, living cells and obviated the necessity for separating and washing the cells and, most important, the background fluorescence of dispersions of the free acid or its complexes with serum albumin did not interfere with the measurements of fluorescence of the cells.

Using the FACS also permitted the identification, separation and reculture of mixed populations of cells which differed in their relative uptake of the fluorescent fatty acid. Some of these results have been presented as a symposium report [4].

Materials and Methods

Cells. The HL-60 cell line was originally established from the peripheral blood of a patient with acute promyelocytic leukemia [5] and the murine erythroleukemia (MEL, Friend) cell line was established from a Friend virus-infected leukemic mouse [6]. Either line was subcultured every 3–4 days, in alpha minimal essential medium supplemented with 10% fetal calf serum, and incubated at 37 °C in a humidified atmosphere of 5% CO_2 in air.

Preparation of P12-albumin complex. A solution of 12-(1-pyrene)dodecanoic acid (P12; Molecular Probes, Junction City, OR) in chloroform/methanol (2 : 1 v/v) was evaporated under a stream of nitrogen. Six to eight equivalents of KOH in 100–200 μl were added, and the tubes were heated for 10 min at 60 °C with occasional stirring. Bovine serum albumin (fatty acid free, Sigma Chemical Company, St. Louis, MO) in phosphate-buffered saline devoid of Ca^{2+} was added and the solution was incubated at 37 °C for 30 min. The P12-albumin complex thus formed was stored at -20 °C and thawed immediately before use.

Measurement of P12 uptake. 5–20 μM P12, dissolved in 1 μl dimethylsulfoxide or alternatively complexed with serum albumin, was added to $(1\text{–}2) \cdot 10^6$ washed cells. The tube containing the cell suspension was immediately attached to the sample line of the FACS and maintained at constant temperature by a water-jacketed device. P12 uptake was analyzed using the FACS-440 (Becton Dickinson FACS Systems, Sunnyvale, CA). P12 fluorescence was excited by the combined UV lines (351 nm, 364 nm) at 30 mW power. An LP-420 dielectric filter was used to exclude scattered laser light from the fluorescence detector. PMT voltage was set at 420 V. Cells were passed at a rate of approximately 1000 cells per s through an 80 nm nozzle, using phosphate-buffered saline as the sheath fluid. Light scatter and fluorescence of about 5000 cells were analyzed at various time intervals and the resulting histograms of cell distribution as a function of fluorescence intensity were stored in the computer memory. The mean relative fluorescence intensity of the population at each time point, expressed as the channel number of the fluorescence at the peak of the histogram, was obtained by a curve-fitting algorithm of the FACS computer. Each experiment was repeated at least three times and in each individual case the variability did not exceed 10%.

Results

Uptake of P12 by HL-60 cells

Fig. 1 shows results of five consecutive FACS measurements of the association of P12 with HL-60 cells over a period of 12 min. From 5000 single-cell data accumulated at each time point, the FACS computer constructed a pair of histograms, showing the distribution of cells according to their forward light scatter and fluorescence intensities, respectively. The five light scatter histograms coincided (Fig. 1A), indicating that cell size was maintained during the entire incubation period. The symmetric, Gaussian-type shape of the histograms suggested that the HL-60 indeed

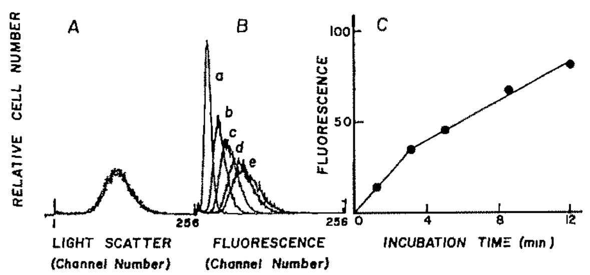

Fig. 1. FACS analysis of the time-dependent uptake of P12 by HL-60 cells 20 nmol P12, complexed with 10 nmol bovine serum albumin, were added to 1 ml phosphate-buffered saline containing 10^6 HL-60 cells, and the distribution of cells according to the forward light scatter (A) and fluorescence (B) were recorded. Incubation times. 1.2 min (a), 3.0 min (b), 5.0 min (c), 8.5 min (d) and 12.0 min (e). Fig. C presents the data of Fig. B as a kinetic curve representing the mean fluorescence of the population as a function of incubation time. Light scatter did not change with time.

consisted of a single cell species. The width of the histograms reflected the natural diversity of cell size among the unsynchronized HL-60 population.

Fig. 1B shows that the fluorescence histograms shifted with time from low (left edge of the figure) towards gradually increasing fluorescence intensities, representing an increasing time-dependent association of the fatty acid with the cells. Since the fluorescence histograms were also approximately symmetrical, the distance from the origin ('channel number') of the histogram peak at each time point was considered as representing the mean relative fluorescence intensity of the entire cell population at the respective incubation time. These respective values were recorded as a function of time and provided the kinetics of fatty acid uptake by the HL-60 cells (Fig. 1C). This curve, which relates the relative fluorescence of the population to the time of incubation, was biphasic. The first rapid phase lasted about 4 min and was followed by a second slower phase. This pattern (see also Figs. 2 and 3) is similar to that observed in previous experiments in which P12 uptake was analyzed by spectrofluorometry following extraction of cell lipids [2].

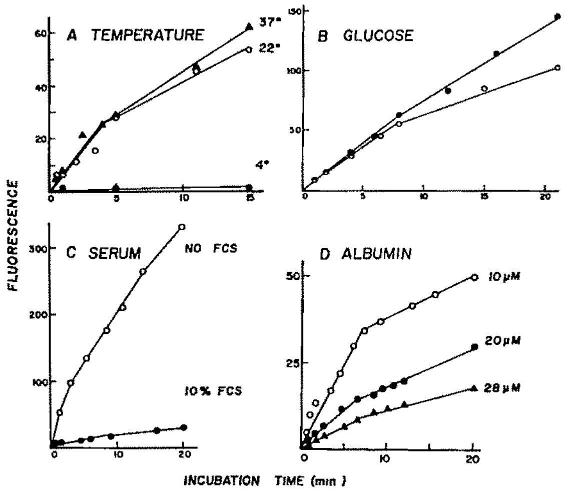

Fig. 2. FACS analysis of parameters controlling P12 uptake by HL-60 cells. Conditions were as follows. (A) 20 nmol P12 in 2 μl dimethyl sulfoxide were added to 10^6 HL-60 cells in 1 ml of medium containing 10% fetal calf serum (FCS), and the temperature was maintained as shown in the figure. (B) 20 nmol P12 were complexed with 20 nmol bovine serum albumin and added to HL-60 cells in 1 ml phosphate-buffered saline, without (○) or with (●) 5 mM glucose. (C) 20 nmol P12 in dimethyl sulfoxide were added to HL-60 cells suspended in 1 ml phosphate-buffered saline without or with 10% fetal calf serum (D) 20 nmol P12 were complexed with bovine serum albumin at the indicated concentrations and added to cells in 1 ml each of phosphate-buffered saline.

Parameters affecting the time-dependent uptake of P12

The FACS was used to delineate several parameters affecting the uptake of P12 by HL-60 cells (Fig. 2). Fig. 2A shows the effect of temperature. At 4°C there was little association of P12 with the cells; at 22 or 37°C, higher rates of uptake were observed. Fig. 2B shows that addition of 5 mM glucose had little effect on the first phase but increased the rate of uptake of P12 in the second phase. Increasing the glucose concentration to 10 mM did not cause any further increase in P12 uptake (data not shown). Fig. 2C and D shows the effects of fetal calf serum and bovine serum albumin, respectively, on the rates of uptake of P12. Similar to previous findings [3], the rates of association of the acid with the cells were considerably reduced when compared to those observed in the absence of serum or albumin. This is most probably due to competition by albumin with the cell surface for molecules of free fatty acid. Fig. 3 shows the time-dependent uptake of increasing concentrations of P12, complexed to serum albumin in 1:1 (M/M) ratio. The biphasic shapes of the respective curves were retained, but the

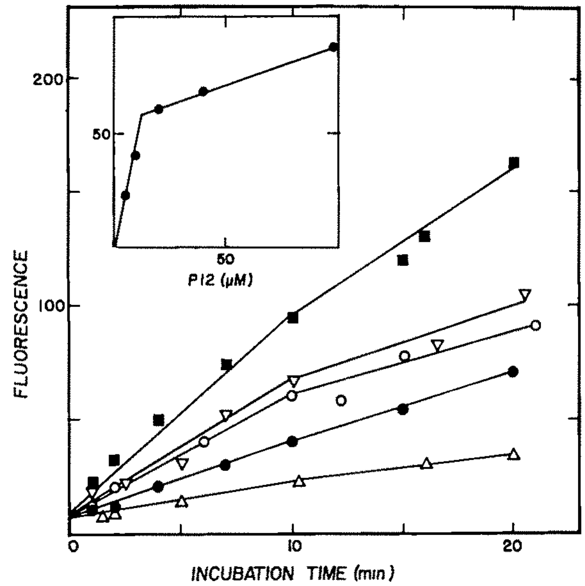

Fig. 3. The effect of increasing concentrations of P12 complexed to albumin on uptake by the HL-60 cells. A P12-albumin complex at a ratio of 1.1 (M/M) was prepared and added to washed cells suspended in 1 ml phosphate-buffered saline to final concentrations of 5 μM (△), 10 μM (●), 20 μM (○), 40 μM (▽) and 100 μM (■), respectively. The values of the channel number at maximum fluorescence were plotted as a function of the incubation time In the inset, the values of fluorescence obtained at various concentrations of the P12-albumin complex, at 10 min incubation, were plotted against the concentration of P12

relative rates of uptake of the acid increased with increasing concentration of the P12-albumin complex (see inset to Fig. 3).

Analysis and sorting of a mixed population of Friend and HL-60 cells

Friend cells take up considerably lesser quantities of P12 relative to HL-60 cells [4]. This was utilized for separating a mixture of Friend and HL-60 cells into their individual components; this system was employed as a model for possible similar experiments using natural cell mixtures.

Fig. 4 shows the distribution of size and fluorescence in a mixed population of Friend and HL-60 cells and demonstrates (A, C) the considerable differences in uptake of P12 as reflected by the fluorescence intensities of these respective two cell lines. Fig. 4B and D shows that the FACS could be used for separating and collecting each of these respective species (i.e., HL-60 or Friend cells in Fig. 4B and D, respectively).

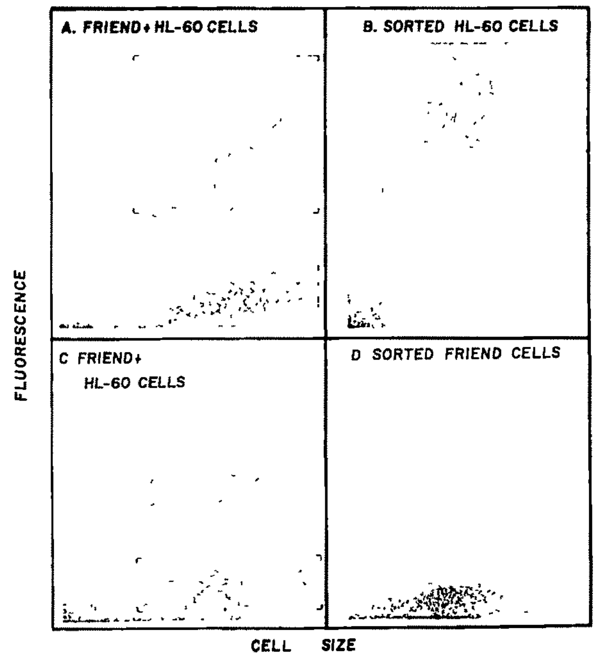

Fig. 4. FACS analysis and sorting of a mixture of HL-60 and MEL (Friend) cells A mixture of HL-60 and mEL cells was incubated for 5 h with 20 M P12 complexed with bovine serum albumin (1:1 molar ratio) in phosphate-buffered saline. The distribution of cells according to fluorescence and cell size was recorded as a two-parameter correlated dot plot. In panels A and C, two distinct subpopulations are evident Sorting according to the gatings presented in A or C produced populations which are presented in panels B and D, respectively. Morphological examination of cells in panel B showed mostly HL-60 cells, while the population presented in panel D consisted mostly of MEL cells. Dots in the lower left corners of the panels represent damaged cells and cell debris

Discussion

The uptake of fatty acids and their incorporation into cellular lipids has been extensively studied [2,3,7–12]. Most of these studies employed radioactively labelled fatty acids [3,7–12]. Reports from this laboratory have shown that fluorescent derivatives of fatty acids could be used to study the uptake and metabolism of fatty acids by cultured cells [2,3].

In this paper we describe a novel procedure for measuring the time-dependent uptake of fluorescent derivatives of fatty acids, utilizing the ability of the FACS to measure the fluorescence intensities of individual cells. The fluorescence background of fatty acid molecules, micelles or complexes with serum albumin did not interfere and only fluorescence associated with the cells was actually measured and recorded by the FACS. The high sensitivity of the FACS for cell fluorescence permits utilization of the instrument for recording rates of fatty acid uptake starting 30 s after exposing the cells to the fluorescent acid. This was the time required for mixing the suspension, transferring the tube to the FACS and for the cells to travel through the sample line to the point of excitation and detection of fluorescence. This time lag could be shortened by introducing the fatty acid directly into a cell suspension already attached to the instrument, and by maximally shortening the FACS line to the nozzle.

Since the FACS recorded only the cell-bound fluorescence, it obviated the need for washing and extracting the cells before analysis. One further advantage was the continuous monitoring of cell-associated fluorescence, coupled to computer-assisted analysis of the uptake kinetics. Changes of cell size, granularity or integrity could be recorded in the course of the experiment, since they would affect the 90° light scattering properties of the cells [1,13]. Also, since the FACS measures fluorescence of individual cells, accurate data could be obtained using a relatively small number of cells. In this study each point of analysis represents the fluorescence of 5000 cells. This should be compared to 100–1000-fold greater cell numbers used in other analytical procedures. Furthermore, each of the experimental data represents a histogram of the distribution of the cell population with respect to uptake of P12, compared with the mean value of numerous cells provided by other techniques. Also, each histogram provides information about the distribution of the cell population with regard to fatty acid uptake, permitting its separation into subpopulations differing in their ability to accumulate fatty acids.

In the present study we used P12 as a representative fluorescent fatty acid, since it is taken up and incorporated into cellular lipids at a rate similar to that of the natural, palmitic acid [2]. However, this procedure could no doubt be extended for studying interaction of other fluorescent compounds with cells. Thus, we have followed the uptake of several fatty acids labelled with anthracene, e.g., 10-(9-anthracene)decanoic acid and *N*-acetyl-*N*-(9-methyleneanthracene)-12-aminododecanoic acid. The results (not shown) indicate that the uptake of the former acid provide a similar pattern to that of P12 with a somewhat lesser intensity, while the latter was taken up rapidly during the first phase, which lasted for 2 min, but the second phase did not follow. These results concur with a previous report from this laboratory showing that the latter compound associated with the plasma membrane, but was not translocated or incorporated into cellular lipids [2].

It therefore seems reasonable to assume that for P12 the first phase represents association with and/or insertion into the plasma membrane of the cells, while the second phase represents the overall process of translocation, activation to acyl CoA and incorporation into cellular lipids. Glucose had practically no effect on the first phase of the uptake of fatty acid, but increased the rate of uptake during the second phase. This suggested a dependence of the latter on glucose as a source of energy or for supplying glycerol 3-phosphate for synthesis of phospholipids and triacylglycerols. The inhibition of the fatty acid uptake by serum or albumin is probably the consequence of competition for the fatty acid, by this protein and the cell membrane. This suggests that the free molecular form of the fatty acid is the species interacting with the cell surface, as previously suggested by several authors [7–10], rather than the fatty acid-albumin complex [12]. A parallel study of uptake of [^{14}C]palmitic acid by HL-60 cells using conventional techniques of radioactive analysis provided data very similar to those reported in this paper (unpublished data). This suggests that fluorescent derivatives of fatty acids could indeed be used as a reliable model for fatty acid transport and utilization. The direct measurements and accurate analysis provided by the FACS make this instrument a very useful tool for analyzing uptake of biological precursors suitably labeled with fluorescent probes.

The experiments of Fig. 4 were set up as a model for using fluorescent derivatives of fatty acids for separating mixed populations of cells.

For this purpose equal numbers of HL-60 and MEL cells were mixed and pulsed with P12. The differences in the uptake of P12 by these two respective cells permitted identification of the respective individual species, and their subsequent separation and recloning. We have recently utilized this procedure for identifying, quantifying and separating mixtures of normal and leukemic peripheral blood cells (unpublished data).

Acknowledgement

This work was supported in part by a grant from the Muscular Dystrophy Association of the U.S.A. to S.G.

References

1 Melamed, M.R, Mullaney, P.F and Mendelson, M.L. (1979) in Flow Cytometry and Cell Sorting, John Wiley and Sons, New York

2 Morand, O., Fibach, E., Dagan, A. and Gatt, S (1982) Biochim. Biophys. Acta 711, 539–550

3 Morand, O, Fibach, E and Gatt, S. (1982) Biochim. Biophys Acta 693, 143–150

4 Nahas, N., Fibach, E., Giloh, H. and Gatt, S (1987) in Enzymes of Lipid Metabolism (Freysz, C., Dreyfuss, H., Massarelli, R and Gatt, S., eds.), Plenum Press, in the press

5 Collins, S.J., Gallo, R.C. and Gallagher, R.E (1977) Nature 20, 347–349

6 Friend, L., Scher, W, Holland, J G and Sato, T. (1971) Proc Natl Acad. Sci USA 68, 378–382

7 DeGrella, R.F. and Light, R.J. (1980) J Biol. Chem. 225, 9739–9745

8 Spector, A.A, Steinberg, D and Tanaka, A. (1965) J Biol Chem 240, 1032–1041

9 Mishkin, S, Yalousky, M and Kessler, J I. (1972) J. Lipid Res. 13, 155–167

10 Goodman, D.S (1958) J Clin Invest. 37, 1729–1735

11 Spector, A.A. (1975) J. Lipid Res 16, 165–179

12 Weisiger, R., Gollan, J. and Ockner, R (1981) Science 211, 1048–1051

13 Crissman, H.A., Mulaney, P.F. and Steinkamp, T.A. (1975) Methods Cell Biol. 9, 1979–1988

Biochimica et Biophysica Acta 917 (1987) 92–100
Elsevier

BBA 52433

Increase in hepatic low-density lipoprotein receptor activity during pregnancy in Watanabe heritable hyperlipidemic rabbits; an animal model for familial hypercholesterolemia

Masashi Shiomi, Takashi Ito and Yoshio Watanabe

Institute for Experimental Animals, Kobe University School of Medicine, Kobe (Japan)

(Received 1 July 1986)

Key words: Pregnancy; LDL receptor; Cholesterol level; (Rabbit serum)

In homozygous Watanabe heritable hyperlipidemic (WHHL) rabbits, the serum cholesterol level and serum low-density lipoprotein (LDL) level decreased from 562 ± 76 (mean ± S.E.) to 144 ± 34 mg/dl and 410 ± 56 to 90 ± 25 mg/dl, respectively, during pregnancy, although the LDL receptor in this rabbit is genetically deficient. When Tyroxapol, which inhibits the degradation of very-low-density lipoprotein (VLDL), as well as Triton WR-1339, was injected into WHHL rabbits, the rate of the increase in serum cholesterol level in pregnant rabbits was not statistically different from that in non-pregnant rabbits. This result implied that the secretion rate of VLDL-cholesterol, the precursor of LDL-cholesterol, did not decrease during pregnancy. The amount of ^{125}I-labeled LDL bound to LDL receptor was increased 1.8-fold in normal rabbits (from 29.3 ± 4.3 to 52.3 ± 4.6 ng/mg protein) and 12-fold in WHHL rabbits (from 0.5 ± 0.2 to 6.0 ± 0.7 ng/mg protein) during pregnancy. These results suggest that the decrease in serum cholesterol level in WHHL rabbits during pregnancy was associated with an increase in hepatic LDL receptor activity, which plays an important role in the regulation of serum cholesterol level.

Introduction

In the homozygous Watanabe heritable hyperlipidemic (WHHL) rabbit, the amount of low-density lipoprotein (LDL) bound to LDL receptor is under 5% of that in normal rabbits [1–3]. Since a deficiency of LDL receptors leads to an enhanced conversion of very-low-density lipoprotein (VLDL) to LDL [4], in the WHHL rabbit LDL accumulates in the plasma and the serum cholesterol level is 400 to 1000 mg/dl from birth [5,6]. As a result of this hypercholesterolemia, severe atherosclerosis spontaneously occurs in the aorta and coronary arteries from an early age [5,7,8] and consequently myocardial infarction occurs [9]. Since these findings are similar to those of familial hypercholesterolemia in humans, WHHL rabbits have been used for the study of lipid metabolism, atherosclerosis and so forth as the only animal model for human familial hypercholesterolemia.

It is difficult to reduce the serum cholesterol level to normal when the LDL receptor is deficient. For the reduction of serum cholesterol level in WHHL rabbits, various hypolipidemic drugs [10,11], partial ileal bypass [12] and plasmapheresis [13] have been used with a consequent reduction of the serum cholesterol level by 20–50%.

Abbreviations: VLDL, very-low-density lipoprotein(s); IDL, intermediate-density lipoprotein(s); LDL, low-density lipoprotein(s); HDL, high-density lipoprotein(s)

Correspondence. Dr. M. Shiomi, Institute for Experimental Animals, Kobe University School of Medicine, 7-Kusunoki-cho, Chuo-ku, Kobe 650, Japan.

0005-2760/87/$03.50 © 1987 Elsevier Science Publishers B.V (Biomedical Division)

However, the serum cholesterol level in WHHL rabbits has been shown to decrease by about 75% during pregnancy without any of these treatments. A similar phenomenon has been observed in normal rabbits and cholesterol-fed rabbits [14–17]. Although the secretion rate of VLDL [15] and the level of excretion of cholesterol into feces and urine [16] have been determined in both pregnant and non-pregnant rabbits in order to study the cause of this decrease in serum cholesterol level, no differences in these points have been noted between the two types of rabbit. In addition, the amount of cholesterol transfer from maternal plasma to fetuses has been shown to be less than that of cholesterol excretion into feces [16]. It has been reported that estrogen reduces the plasma cholesterol level in rats [18,19] and rabbits [20,21], and that the degradation of LDL in rats treated with estradiol is increased [22,23]. Since the serum estrogen level increases during pregnancy in many species, the decrease in serum cholesterol level in pregnant rabbits may be due to the action of estrogens.

It is an interesting problem as to why the serum cholesterol level decreases during pregnancy in LDL-receptor-deficient WHHL rabbits. In the present study, we investigated the decrease in serum cholesterol level during pregnancy in WHHL rabbits, and observed an increase in the amount of LDL bound to hepatic LDL receptors in pregnant WHHL rabbits.

Materials and Methods

Materials. Sodium [^{125}I]iodide (carrier-free in 0.1 M NaOH) was purchased from the Radiochemical Center (Amersham, U.K.). Tyroxapol and 17α-ethinylestradiol were purchased from Sigma Chemical Co. (St. Louis, MO, U.S.A.). Dowex 1-X8 was purchased from Dow Chemical Co. (Midland, MI, U.S.A.). Evans blue was purchased from Nakarai Chemical Co. (Tokyo, Japan).

Animals. Female WHHL and normal rabbits (Japanese white rabbits) at the age of 8–14 months were used. WHHL rabbits were bred and raised at Kobe University and normal rabbits were purchased from Fukusaki Rabbit Center (Fukusaki-cho, Hyogo Prefecture, Japan). The day of mating was designated as day zero of pregnancy. The gestation period of WHHL rabbits is about 31 days. Rabbits were individually housed in metal cages, fed a standard rabbit chow (Type GC-4: Oriental Yeast Co., Tokyo, Japan) at 120 g/day, and were given water ad libitum. Room temperature was set at $22 \pm 2°$C and relative humidity was set at $55 \pm 5\%$. The room was illuminated with fluorescent lamps and the photo period was set at 12 h.

Fractionation of lipoproteins. Blood samples of WHHL rabbits were obtained from a marginal ear vein after 12 h overnight fasting at days 0, 7, 14, 21 and 28 of pregnancy. Since each lipoprotein fraction prepared by Airfuge was contaminated by NaBr or KBr used for adjustment of serum density, we used sucrose for this purpose. VLDL (containing intermediate-density lipoprotein (IDL)) ($d < 1.019$), LDL (d 1.019–1.063) and high-density lipoprotein (HDL) ($d > 1.063$) were fractionated by ultracentrifugation using Airfuge (Beckman) with an 18° angle rotor ($100\,000 \times g$ for 3 h). Each lipoprotein fraction from WHHL rabbits ($n = 12$) prepared by Airfuge was compared with that by normal ultracentrifuge using Hitachi 65P Ultracentrifuge with RPS-56T rotor (Hitachi Co., Tokyo, Japan) according to the method of Hatch and Lees [33] (Fig. 1). The coefficient of correlation was 0.978 in the VLDL fraction, 0.980 in the LDL fraction, and 0.921 in the HDL fraction. The ratio of the lipoprotein cholesterol level by Airfuge to that by normal ultracentrifuge was 1.00 ± 0.29 ($n = 12$) (mean $\pm$ S.E.) in the VLDL fraction, 1.01 ± 0.03 in the LDL fraction, and 0.90 ± 0.05 in the HDL fraction. These results suggest that our Airfuge method was available for fractionation of lipoproteins.

Determination of plasma volume. Both non-pregnant and pregnant (21 day) WHHL rabbits were used after 12 h overnight fasting. According to the method of Gregersen [25], 1 ml of a 0.1% aqueous solution of Evans blue was injected into a marginal ear vein. Blood samples were obtained before injection of dye solution and at 10 min after injection. The optical absorbance of serum was measured at 524 nm.

Intravenous injection of tyroxapol. Both non-pregnant and pregnant (21-day) WHHL rabbits were used after 12 h overnight fasting. According

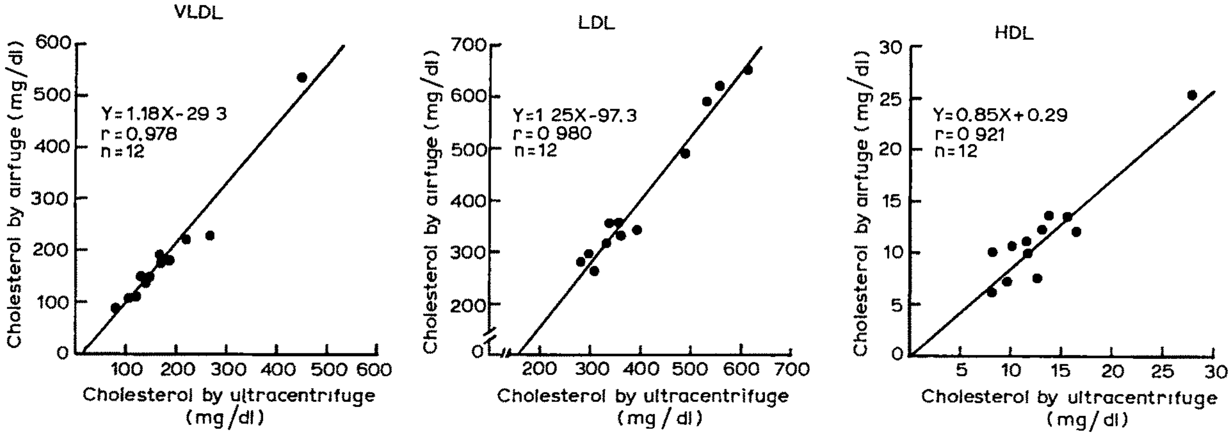

Fig 1 Correlation between lipoprotein cholesterol level prepared by Airfuge and that by normal ultracentrifuge Serum density was prepared with sucrose in the Airfuge method and with NaBr in normal ultracentrifuge according to the method of Hatch and Lees [24] A VLDL fraction containing IDL was prepared by the ultracentrifugation with density < 1 019, an LDL fraction was prepared by the ultracentrifugation with density 1.019–1 063, and an HDL fraction was prepared by the ultracentrifugation with density > 1 063.

to the method of Hornick et al. [26], Tyroxapol, which is the same poly(ethylene glycol) as Triton WR-1339, at 200 mg/ml of 0.15 M NaCl was injected into a marginal ear vein at a dose of 400 mg/kg of body weight. Blood samples were periodically obtained from a marginal ear vein.

Radioiodination of LDL. Blood was obtained from a WHHL rabbit and plasma was prepared with the antagonist EDTA. LDL (*d* 1.03–1.05) was isolated by preparative ultracentrifugation with Hitachi RP-55P Ultracentrifuge with RP-40 rotor (Hitachi Co., Tokyo, Japan) using NaBr for adjustment of plasma density [27]. This LDL fraction was recentrifuged with density 1.05 to clear the LDL of contaminating proteins such as albumin and HDL. LDL was radioiodinated with sodium [^{125}I]iodide by the iodine monochloride method [28] and purified by ion-exchange with Dowex 1-X8.

Binding of ^{125}I-labeled LDL to liver membrane. Non-pregnant and pregnant (21-day) normal rabbits, and non-pregnant and pregnant (21-day) WHHL rabbits were used. According to the method of Kovanen et al. [22], hepatic membrane fractions were prepared by centrifugation (500 × *g* for 10 min, 8000 × *g* for 15 min and 100000 × *g* for 60 min). Then, according to the method of Kita et al. [2], assay of the binding of ^{125}I-labeled LDL to the membrane fractions was conducted in buffer (20 mM NaCl/0.63 mM CaCl$_2$/50 mM Tris-HCl (pH 8.0) plus 20 mg bovine serum albumin per ml) containing about 150 μg of membrane protein and 3.0 μg/ml of ^{125}I-labeled LDL with 578 cpm/ng of specific activity in the absence or presence of 5 mM EDTA and in the absence or presence of 280 μg/ml of unlabeled LDL. The reaction mixture was incubated for 60 min in an ice/water bath at 0°C. After incubation, the reaction mixture was ultracentrifuged at 100000 × *g* for 20 min using an Airfuge with an 18° angle rotor, and the radioactivity of the pellet was counted with Crystal Multi Detector Gamma System (Packard Instruments Co., Downersgrove, IL, U.S.A.).

Administration of 17α-ethinylestradiol. 17α-Ethinylestradiol was dissolved in propylene glycol (5 mg/ml) at 37°C and administered daily to WHHL rabbits subcutaneously at a dose of 5 mg/kg of body weight.

Chemical assays. Serum cholesterol level was measured by the cholesterol-oxidase method (Iatrolipo TC kit: Iatron Laboratories, Inc., Tokyo, Japan), serum triacylglycerol level by the glycerol-oxidase methdo (Determiner TG kit: Kyowa Medex Co., Tokyo, Japan), serum phospholipid level by the choline-oxidase method (Phospholipids B-test kit: Wako Pure Chemical Ind., Osaka, Japan) and protein concentration by the method of Lowry et al. [30].

Statistical analysis. Data were analyzed by paired t-test for the mean of serum lipoprotein lipid levels during pregnancy, by Student's t-tst for the means of others, and by analysis of covariance for the difference of the regression line.

Results

Lipoprotein lipid levels in WHHL rabbits during pregancy

Fig. 2 shows each of the lipoprotein lipid levels in WHHL rabbits during pregnancy ($n = 7$). Serum cholesterol level was 562 ± 76 mg/dl before mating and decreased to 145 ± 19 mg/dl by day 28 of pregnancy ($P < 0.001$). The decrease in serum cholesterol level up to day 21 of pregnancy was due to that in the LDL-cholesterol level (from 410 ± 56 to 106 ± 33 mg/dl ($P < 0.001$)) and that between day 21 of pregnancy and day 28 was due to that in the VLDL-cholesterol level (from 122 ± 27 to 45 ± 9 mg/dl ($P < 0.01$)). The HDL-cholesterol level was 11.0 ± 0.9 mg/dl before mating and there were almost no changes during pregnancy. At 14 day after delivery, the serum cholesterol level reverted to about 84% in that

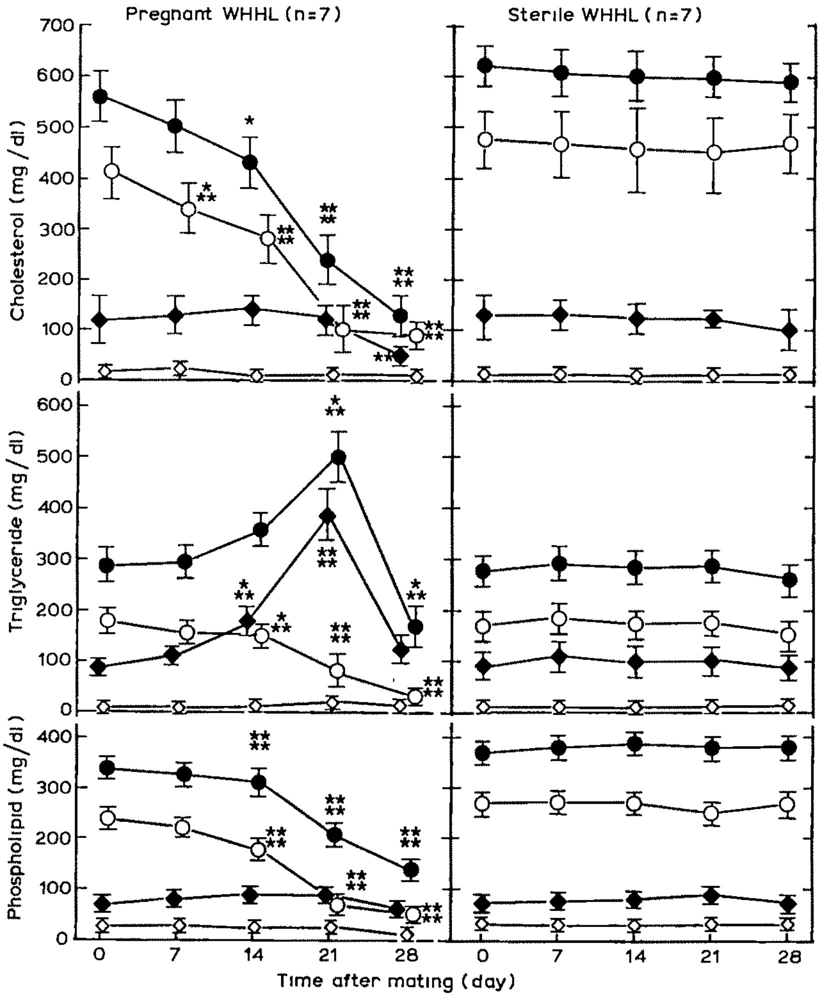

Fig. 2 Lipid levels in each lipoprotein (●, total; ◆, VLDL containing IDL; ○, LDL; ◇, HDL) in WHHL rabbits during pregnancy Significantly different from values in before mating by paired t-test: $P < 0.05$ *, $P < 0.01$ **, $P < 0.005$ *** and $P < 0.001$ **** Error bars mean ± S.E

TABLE I

PLASMA VOLUME OF NON-PREGNANT AND PREGNANT WHHL RABBITS

The plasma volume was determined by dye dilution method using Evans blue solution. Each value is presented as mean ± S.E.

		Body weight (B) (kg)	Plasma volume (P) (ml)	P/B (ml/kg)
Non-pregnant	($n = 5$)	3.6 ± 0.2	123 ± 12	34.4 ± 1.5
Pregnant 21 days	($n = 5$)	3.8 ± 0.2	184 ± 16 *	47.5 ± 2.7 **

Significant difference between non-pregnant and pregnant by Student's t-test: * $P < 0.05$ and ** $P < 0.01$.

before mating. The serum triacylglycerol level was 284 ± 37 mg/dl before mating, increased to 510 ± 61 mg/dl ($P < 0.005$) by day 21 of pregnancy, and decreased to 159 ± 24 mg/dl ($P < 0.005$) by day 28 of pregnancy. This change in serum triacylglycerol level was due to that in the VLDL-triacylglycerol level. The change in phospholipid level was similar to that in cholesterol. There were hardly any changes in lipid levels of each lipoprotein in sterile WHHL rabbits.

Comparison of plasma volume in the pregnant state with that in the non-pregnant state

As the plasma volume increased 1.4-fold during pregnancy in normal rabbits [15], plasma volume was determined in both non-pregnant and pregnant WHHL rabbits (Table I). Plasma volume for body weight was 47.5 ± 2.7 ml/kg in pregnant WHHL rabbits ($n = 5$), which was increased 1.4-fold in that in non-pregnant rabbits ($n = 5$) (34.4 ± 1.5 ml/kg) ($P < 0.001$).

Comparison of VLDL secretion rate in the pregnant state with that of the non-pregnant state

Since Tyroxapol, which is the same poly(ethylene glycol) as Triton WR-1339, inhibits the degradation of VLDL [30], Tyroxapol was used in order to determine the secretion rate of VLDL-

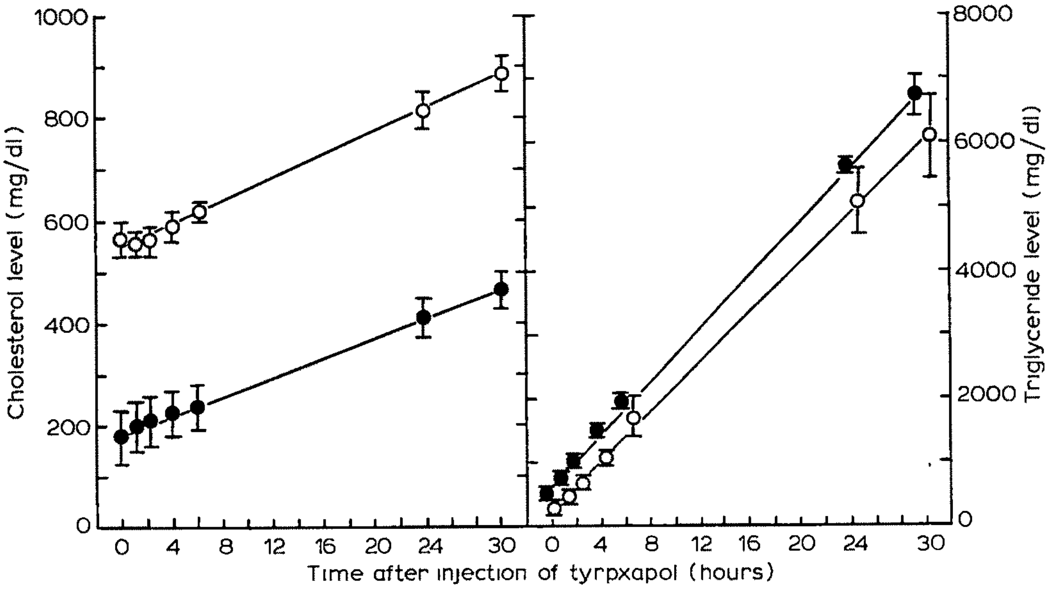

Fig 3. Serum lipid levels of WHHL rabbits treated with Tyroxapol both in non-pregnant (○: $n = 4$) and pregnant (day-21) states (●: $n = 5$). Tyroxapol was injected into a marginal ear vein at a dose of 400 mg/kg body weight. The average of the rate of increase in serum cholesterol and triacylglycerol was 11.1 ± 0.5 (mean ± S.E.) and 194 ± 20 mg/dl per h, respectively, in the non-pregnant state, and 9.5 ± 0.6 and 207 ± 8 mg/dl per h, respectively, in the pregnant state.

cholesterol and triacylglycerol in both non-pregnant and pregnant WHHL rabbits (Fig. 3). As the lipoprotein secreted from liver is only VLDL in WHHL rabbits [26], the secretion rates of VLDL-cholesterol and triacylglycerol were represented as the rates of increase in serum cholesterol and triacylglycerol level. The secretion rates of VLDL-cholesterol and triacylglycerol from the liver were 11.1 ± 0.5 and 194 ± 20 mg/dl per h, respectively, in non-pregnant WHHL rabbits (n = 4), and 9.5 ± 0.6 and 207 ± 8 mg/dl per h, respectively, in pregnant WHHL rabbits (n = 5). When these secretion rates were corrected by plasma volume for body weight, the secretion rates of VLDL-cholesterol and triacylglycerol were 3.8 ± 0.2 and 67 ± 13 mg/kg per h, respectively, in non-pregnant WHHL rabbits, and 4.6 ± 0.3 and 100 ± 4 mg/kg per h, respectively, in pregnant WHHL rabbits. The secretion rate was increased 1.2-fold for VLDL-cholesterol and 1.5-fold for VLDL-triacylglycerol ($P < 0.005$) during pregnancy.

Binding assay of ^{125}I-labeled LDL to liver membrane

^{125}I-labeled LDL (^{125}I-LDL) from a WHHL rabbit showed a saturable binding to hepatic membrane fractions from a normal rabbit over 3.0 μg/ml of ^{125}I-LDL, which was similar to the binding of ^{125}I-LDL from normal rabbits [2]. The assay of the binding of ^{125}I-LDL from a WHHL rabbit to liver membranes from non-pregnant and pregnant normal rabbits, and non-pregnant and pregnant WHHL rabbits was carried out (Table II). LDL-receptor-dependent binding is represented as EDTA-sensitive binding, which was calculated by subtracting the amount of ^{125}I-LDL bound in the presence of EDTA from that bound in the absence of EDTA, and LDL-receptor-independent binding is represented as EDTA-resistant binding, which was calculated by subtracting the amount of ^{125}I-LDL bound in the presence of excess unlabeled LDL from that bound in the absence of unlabeled LDL and the presence of EDTA [2]. The amount of ^{125}I-LDL bound to the receptor was 0.5 ± 0.2 ng/mg protein in non-pregnant WHHL rabbits (n = 4), 6.0 ± 0.7 ng/mg protein in pregnant WHHL rabbits (n = 4), 29.3 ± 4.3 ng/mg protein in non-pregnant normal rabbits (n = 3), and 52.3 ± 3.3 ng/mg protein in pregnant normal rabbits (n = 2). The receptor-dependent binding of ^{125}I-LDL was increased 12-fold in WHHL rabbits and the ratio of this binding in WHHL rabbits to that in normal rabbits was

TABLE II

BINDING OF ^{125}I-LDL FROM A WHHL RABBIT TO LIVER MEMBRANES FROM EACH RABBIT

Each tube containe 150 μg of membrane protein, 0.63 mM $CaCl_2$, ^{125}I-LDL at 3.0 μg/ml and the indicated addition. LDL-receptor-dependent binding was presented as EDTA-sensitive site, which was calculated by subtracting the amount of ^{125}I-LDL bound in the presence of EDTA from that bound in its absence, and LDL-receptor-independent binding was calculated by subtracting the amount of ^{125}I-LDL bound in the presence of unlabeled LDL from that bound in the absence of unlabeled LDL and the presence of EDTA. Each value is presented as mean ± S.E.

	^{125}I-LDL bound to membrane (ng/mg protein)			
	WHHL rabbit		normal rabbit	
	non-pregnant (n = 4)	pregnant [a] (n = 4)	non-pregnant (n = 3)	pregnant [a] (n = 2)
Addition to assay				
None	20.8 ± 1.6	26.8 ± 1.7	49.4 ± 4.0	73.6 ± 6.5
5 mM EDTA	20.3 ± 1.5	20.7 ± 1.1	20.1 ± 1.2	21.8 ± 3.3
LDL at 280 μg/ml	8.5 ± 0.7	8.7 ± 0.5	8.5 ± 0.4	8.2 ± 0.9
Binding site				
Receptor-dependent	0.5 ± 0.2	6.0 ± 0.7	29.3 ± 4.3	52.3 ± 4.6
Receptor-independent	11.8 ± 1.0	12.1 ± 0.8	11.6 ± 0.8	13.1 ± 3.4
Total	12.3 ± 1.1	18.1 ± 1.5	40.9 ± 4.5	65.4 ± 8.0

[a] Day 21 of pregnancy.

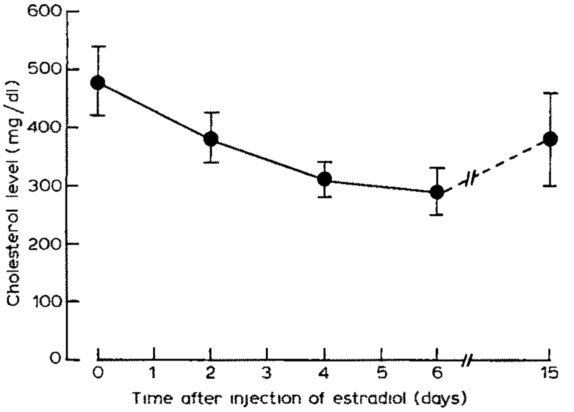

Fig 4 Hypocholesterolemic effect of 17α-ethinylestradiol in WHHL rabbits. 17α-Ethinylestradiol was dissolved in propylene glycol at 37°C and administered daily to WHHL rabbits ($n = 3$) subcutaneously at a dose of 5 mg/kg of body weight ———, treatment; — — —, no drug, Error bars: mean ± S E

incresed from 2% to 21% during pregnancy. Receptor-dependent binding of ^{125}I-LDL in normal rabbits was incresed 1.8-fold during pregnancy. The amount of receptor-independent binding of ^{125}I-LDL was 11.6–13.1 ng/mg protein in each type of rabbit.

Hypocholesterolemic effect of 17α-ethinylestradiol

Fig. 4 shows the hypocholesterolemic effect of 17α-ethinylestradiol in WHHL rabbits ($n = 3$). Serum cholesterol level was 479 ± 59 mg/dl before treatment and was reduced to 290 ± 39 mg/dl by day 6 of treatment, which was about 60% that before treatment. At 9 days after cessation of treatment, serum cholesterol level was 377 ± 78 mg/dl, which was about 80% in that before treatment.

Discussion

In WHHL rabbits, serum cholesterol level and LDL-cholesterol level were decreased by about 75% and by about 80%, respectively, during pregnancy (Fig. 2) in spite of the genetic deficiency of LDL receptors. The level of cholesterol decrease in maternal plasma was not associated with litter size (unpublished data). Ross and Zilversmit [16] reported similar results in normal rabbits and showed that the amount of cholesterol transfer from maternal plasma to fetuses was less than that of cholesterol excretion into feces. The decrease in serum cholesterol level during pregnancy was not due to decreased secretion of VLDL-cholesterol, the precursor of LDL-cholesterol, but was associated with both a 1.4-fold increase in plasma volume (Table I) and a 12-fold increase in hepatic LDL receptor activity (Table II). About two-thirds of the circulating LDL pool is cleared by receptor-dependent means and about one-third of the LDL in the plasma pool is cleared by receptor-independent menas; the clearance of LDL in hepatic LDL receptor is about 70% of the receptor-dependent clearance in whole animals [23,31]. In normal rabbits the LDL receptor mediated the rapid removal of VLDL and IDL from plasma and in WHHL rabbits a deficiency of LDL receptors led to an enhanced conversion of VLDL to LDL [4]. Therefore, the hepatic LDL receptor has been considered to regulate the serum cholesterol level. The increase in the binding activity of this receptor is important for decreasing the serum cholesterol level.

During pregnancy, the increse in the secretion rate of cholesterol (1.2-fold) was less than that of triacylglycerol (1.5-fold) when Tyroxapol was injected into both non-pregnant and pregnant WHHL rabbits (Fig. 3). This difference may be due to an increase in LDL degradation as a result of the increase in hepatic LDL receptor, and/or to an increase in the triacylglycerol content in VLDL during pregnancy (Fig. 2). It has been reported that the VLDL-triacylglycerol level is increased in various animals treated with estradiol [32–35].

The change in serum cholesterol level during pregnancy varies between species. Serum cholesterol level during pregnancy increases in humans [36], does not change in dogs [15], and decreases in baboons [37], rhesus monkeys [38] and rabbits [14–17]. In healthy women, an increase in serum cholesterol level during pregnancy has been shown to be due to that in VLDL and IDL cholesterol levels, and the LDL cholesterol level tends to be decreased [36]. In healthy women and patients with heterozygous familial hypercholesterolemia, the serum cholesterol level and cholesterol level in LDL containing IDL were increased during pregnancy, but were reduced by 25% and 33%, respectively, when a cholesterol-free diet was induced [39,40]. These reports imply that the increase in serum cholesterol level in humans during pregnancy is associated with an increase both in the VLDL and IDL-cholesterol levels and in the absorption of exogenous cholesterol.

Plasma LDL level has been shown to be reduced in estradiol-treated rats [18,19] and cholesterol-fed rabbits [20,21]. Kovanen et al. [22] and Spady et al. [23] showed that membranes prepared from the livers of rats treated with estradiol exhibited a 3- to 10-fold increase in saturable binding site for LDL. When estrogen was injected into humans, plasma and LDL-cholesterol levels were reduced [41,42]. Recently, Ma et al. [43] showed that the level of the mRNA for LDL receptor increased 6- to 8-fold in the liver of rabbits treated with estradiol and that the increase in the receptor number was correlated with that in the mRNA level. Mabuchi et al. [44] observed, in one patient with heterozygous familial hypercholesterolemia, that the serum cholesterol level and LDL cholesterol level were decreased by 63% and 83%, respectively, during pregnancy, and by 25% and 40%, respectively, in the non-pregnant state following treatment with estradiol. They considered that the reduction in serum cholesterol level during pregnancy was probably brought about by the action of estrogens. When non-pregnant WHHL rabbits were subcutaneously injected with 17α-ethinylestradiol at a dose of 5 mg/kg per day, the serum cholestrol level decreased by about 40% within 6 days (Fig. 4). These results and reports suggest that, in WHHL rabbits, the increase in hepatic LDL receptor activity during pregnancy may be due to the action of estrogens.

Schneider et al. [45] showed that, in homogzygous WHHL fibroblasts, LDL receptor was processed from a precursor with an apparent molecular mass on SDS polyacrylamide gels from 120 kDa, to a 160 kDa mature form at a rate that was markedly slower than normal, and that only about 25% of the receptors were converted to the mature form. However, in the present study the binding of ^{125}I-LDL to hepatic LDL receptor in non-pregnant WHHL rabbits was only about 2% of that in normal rabbits (Table II). Similar results have been reported in WHHL fibroblasts [1] and WHHL liver and adrenal cells [2,3]. These results and reports suggest that the LDL receptor in WHHL rabbits is mutated both in its ability to be processed at a normal rate and in its ability to bind LDL. In heterozygous WHHL fibroblasts, about 65% of the receptor were converted to the mature form [45]. Although, as well as fibroblasts from homozygous WHHL rabbits, it is uncertain that all of 65% of the receptor shows the binding ability, serum cholesterol level in heterozygotes is 59 ± 6 mg/dl [46], which is 1- to 1.5-fold increse in normal level. In pregnant homozygous WHHL rabbits, the binding activity of hepatic LDL receptor was about 21% of normal and serum cholesterol level was 144 ± 34 mg/dl. The secretion rate of VLDL in WHHL rabbits was almost equal to that in normal rabbits [26]. These reports and results suggest that in homozygous WHHL rabbits, the decrease in serum cholesterol level during pregnancy is closely associated with an increase in hepatic LDL receptor activity.

Acknowledgments

We are grateful to Drs. T. Kita, M. Arai, Y. Tsujita, and M. Kuroda for their valuable discussions and criticisms. We are grateful to Dr. H. Enomoto and Mr. Y. Yoshikuni for their kind support.

References

1 Tanzawa, K., Shimada, Y , Kuroda, M., Tsujita, Y., Arai, M and Watanabe, Y (1980) FEBS Lett. 118, 81–84

2 Kita, T., Brown, M.S., Watanabe, Y. and Goldstein, J.L (1981) Proc. Natl. Acad Sci. USA 78, 2268–2282

3 Huettinger, M , Schneider, W.J , Ho, Y K., Goldstein, J.L and Brown, M S (1984) J Clin. Invest. 74, 1017–1026

4 Kita, T., Brown, M.S , Bilheimer, D.W. and Goldstein, J.L. (1982) Proc. Natl. Acad. Sci USA 79, 5693–5697

5 Watanabe, Y (1980) Atherosclerosis 36, 261–268

6 Havel, R J , Kita, T , Kotite, L , Kane, J.P., Hamilton, R.L., Goldstein, J.L. and Brown, M.S. (1982) Arteriosclerosis 2, 467–474

7 Buja, M.L., Kita, T., Goldstein, J.L., Watanabe, Y. and Brown, M.S. (1983) Arteriosclerosis 3, 87–101

8 Watanabe, Y., Ito, T and Shiomi, M. (1985) Atherosclerosis 56, 71–79

9 Hatanaka, K., Ito, T , Shiomi, M., Yamamoto, A. and Watanabe, Y. (1986) Am. Heart J., in the press

10 Watanabe, Y., Ito, T. Saeki, M., Kuroda, M., Tanzawa, K , Mochizuki, M., Tsujita, Y. and Arai, M. (1981) Atherosclerosis 38, 27–31

11 Naruszewics, M., Carew, T.E , Pittman, R.C., Witztum, J L. and Steinberg, D (1984) J. Lipid. Res 25, 1206–1213

12 Niekerk, J.L.M., Demacker, P.N.M., Hendrics, T.H and Boer, H H M. (1983) Atherosclerosis 48, 243–252

13 Yokoyama, S , Hayashi, R , Kikkawa, T , Tani, N., Takada, S., Hatanaka, K and Yamamoto, A (1984) Arteriosclerosis 4, 276–282

14 Popjak, G. (1946) J. Physiol 105, 236–254

15 Zilversmit, D.B , Hughes, B L and Remington, M. (1972) J Lipid Res. 13, 750–756

16 Ross, C.A and Zilversmit, D.B (1976) Am J Physiol 230, 754–761

17 Kovanen, P T , Goldstein, J L. and Brown, M.S (1978) J Biol Chem. 253, 5126–5132

18 Hay, R V , Pottenger, L A , Reingold, A L., Getz, G.S and Wissler, R.W. (1971) Biochem Biophys Res. Commun 44, 1471–1477

19 Chao, Y , Windler, E.E , Chen, G. and Havel, R.J (1979) J Biol Chem 254, 11360–11366

20 Kushwaha, R.S. and Hazzard, W B (1981) Am. J. Physiol 241, E372–E377

21 Floren, C.H , Kushwaha, R.S., Hazzard, W R. and Albers, J.J (1981) Metabolism 30, 367–375

22 Kovanen, P T , Brown, M.S. and Goldstein, J L (1979) J Biol Chem 254, 11367–11373

23 Spady, D K , Turley, S D and Dietschy, J M (1985) J Clin. Invest 76, 1113–1122

24 Hatch, F T. and Lees, R S. (1968) Adv Lipid Res. 6, 1–68

25 Gregersen, M.I. (1944) J. Lab. Clin Med. 29, 1266–1286

26 Hornick, C.A., Kita, T., Hamilton, R L , Kane, J.P. and Havel, R.J (1983) Proc. Natl. Acad Sci USA 80, 6096–6100

27 Havel, R J., Eder, H.A. and Bragdon, J.H. (1955) J Clin Invest. 34, 1345–1353

28 Bilheimer, D W., Goldstein, J.L , Grundy, S M. and Brown, M.S. (1975) J Clin Invest. 56, 1420–1430

29 Lowry, O.H., Rosebrough, N J , Farr, A.L. and Randall, R.J. (1951) J. Biol. Chem. 193, 265–275

30 Bilheimer, D.W , Eisenberg, S. and Levy, R I (1972) Biochim. Biophys Acta 260, 212–221

31 Pittman, R.C , Carew, T.E., Attie, A.D , Witztum, J.L., Watanabe, Y. and Steinberg, D (1982) J. Biol. Chem. 257, 7994–8000

32 Hamosh, M. and Hamosh, P (1975) J Clin. Invest 55, 1132–1135

33 Kim, H.-J and Kalkhoff, R.K. (1975) J. Clin Invest 56, 888–896

34 Applebaum, D.M., Goldberg, A.P., Pykalisto, O.J., Brunzell, J D. and Hazzard, W.R. (1977) J Clin Invest 59, 601–608

35 Chan, L., Bradley, W A , Jackson, R L and Means, A R (1980) Endocrinology 106, 275–283

36 Worth, M.R., Arky, R.A. and Knopp, R H (1975) J. Clin. Endocrinol. Metabol 41, 649–655

37 Zyl, V (1957) J. Endocrinol 14, 317–324

38 Martine, D.E., Wolf, R.C. and Meyer, R.K (1971) Proc Exp. Biol Med 138, 638–641

39 Glueck, C.J., Christopher, C., Tsang, R C and Mellies, M.J (1980) Metabolism 29, 949–955

40 McMurry, M.P., Connor, W.E. and Goplerad, C.P. (1981) Metabolism 30, 869–879

41 Wallace, R.B., Hoover, J., Barrett-Connor, E., Rifkind, B M , Hunninghake, D.B., Mackenthun, A. and Heiss, G. (1979) Lancet ii, 111–114

42 Appleboum-Boden, D., Hazzard, W., Mclean, P., Steinmetz, A., Mathis, C., Fontana, D., Warnick, R and Albers, J (1982) Arteriosclerosis 2, 415a

43 Ma, P T S., Yamamoto, T., Goldstein, J.L and Brown, M.S. (1986) Proc. Natl. Acad. Sci USA 83, 792–796

44 Mabuchi, H., Sakai, Y., Watanabe, A , Haba, T., Koizumi, J and Takeda, R. (1985) Metabolism 34, 309–315

45 Schneider, W.J , Brown, M.S and Goldstein, J L. (1983) Mol Biol Med 1, 353–367

46 Shiomi, M , Ito, T and Watanabe, Y (1986) Lab Anim Sci., in the press

Biochimica et Biophysica Acta 917 (1987) 101–107
Elsevier

BBA 52435

Partial purification and characterization of 7α-hydroxysteroid dehydrogenase from rat liver microsomes

Yoshiki Amuro, Wataru Yamade, Tetsuo Yamamoto, Akio Maebo,
Toshikazu Hada and Kazuya Higashino

Third Department of Internal Medicine, Hyogo College of Medicine, Nishinomiya (Japan)

(Received 1 July 1986)

Key words: Bile acid; Keto bile acid; Hydroxysteroid dehydrogenase, (Rat liver)

An NADPH-dependent 7α-hydroxysteroid dehydrogenase acting on 3α-hydroxy-7-keto-5β-cholanoic acid was partially purified 160-fold with a yield of 13% from rat liver microsomes using DEAE-cellulose, hydroxyapatite and Affi-Gel® Blue column chromatography. The specific activity of the purified enzyme was 91.3 nmol chenodeoxycholic acid formed/min per mg of protein. The reaction was reversible, and the optimum pH of the enzyme for the oxidation was about 8.5, whereas that for the reduction was about 5.0. A molecular weight of the enzyme was estimated to be about 130000 by Superose 6™ gel filtration chromatography. The apparent K_m value for 3α-hydroxy-7-keto-5β-cholanoic acid was 35.7 μM and that for NADPH was 90.9 μM. The preferred substrate for the enzyme was 3α-hydroxy-7-keto-5β-cholanoic acid rather than 3α,12α-dihydroxy-7-keto-5β-cholanoic acid, a 7-keto-bile acid analogue. The enzyme also preferred the unconjugated form to the conjugated forms. The enzyme activity was inhibited by *p*-chloromercuribenzoate; however, the inhibition was prevented by addition of reduced form of glutathione to the reaction mixture, indicating that the enzyme requires a sulfhydryl group for activity.

Introduction

Chenodeoxycholic acid is a main bile acid [1] and is extensively used for solubilizing cholesterol gallstones by decreasing the cholesterol saturation in the bile [2]. This bile acid is probably oxidized further to 3α-hydroxy-7-keto-5β-cholanoic acid by bacterial 7α-dehydrogenation in the intestine [3], resulting in the occurrence of 3α-hydroxy-7-keto-5β-cholanoic acid in the feces. However, 3α-hydroxy-7-keto-5β-cholanoic acid is not found in an appreciable amount in the bile of rats and humans, suggesting that 3α-hydroxy-7-keto-5β-cholanoic acid absorbed from the intestine is again reduced to chenodeoxycholic acid during passage through the liver. Thus several in vivo studies on bile acid metabolism demonstrated that 3α-hydroxy-7-keto-5β-cholanoic acid could be reduced to chenodeoxycholic acid in the liver of rats [4], dogs [5] and humans [6]. These results indicate the presence of 7α-hydroxysteroid dehydrogenase acting on 3α-hydroxy-7-keto-5β-cholanoic acid in mammalian liver, and suggest that some chenodeoxycholic acid in the bile is formed from 3α-hydroxy-7-keto-5β-cholanoic acid in the liver.

The detailed nature of hepatic 7α-hydroxysteroid dehydrogenase remains to be clarified, although bacterial 7α-hydroxysteroid dehydrogenases have been purified and characterized [3,7,8]. Recently, we found that rat liver preparations could reduce 3α-hydroxy-7-keto-5β-cholanoic acid to chenodeoxycholic acid, and that

---

Correspondence. Dr Y. Amuro, The Third Department of Internal Medicine, Hyogo College of Medicine, Mukogawa-cho, Nishinomiya, Hyogo 663, Japan

0005-2760/87/$03.50 © 1987 Elsevier Science Publishers B V (Biomedical Division)

the reductase required NADPH but not NADH as coenzyme and was mainly localized in the microsomes [9]. In this paper, we describe the solubilization, purification and characterization of 7α-hydroxysteroid dehydrogenase acting on 3α-hydroxy-7-keto-5β-cholanoic acid from rat liver microsomes.

Materials and Methods

Chemicals

The sources of the chemicals used in this study were as follows: pyridine nucleotides, cholylglycine hydrolase, sodium taurodeoxycholate, chenodeoxycholic acid, cholic acid and 3-keto-5β-cholanoic acid from Sigma Chemical Co. (St. Louis, MO); 3α-hydroxy-7-keto-5β-cholanoic, 3α,12α-dihydroxy-7-keto-5β-cholanoic and 3α,7α-dihydroxy-12-keto-5β-cholanoic acids from Steraloids (Wilton, NH); 7α,12α-dihydroxy-5β-cholanoic acid from Calbiochem-Behring Corp. (La Jolla, CA); DEAE-cellulose (DE-52) from Whatman (U.K.); Affi-Gel® Blue from Bio-Rad (Richmond, CA); Superose 6™ from Pharmacia Fine Chemicals (Sweden); calibration proteins from Boehringer-Mannheim (F.R.G.) and Sigma; hydroxyapatite, Tween 80 and other chemicals from Wako Pure Chemicals (Osaka, Japan). Taurine- and glycine-conjugated 3α-hydroxy-7-keto-5β-cholanoic acids were synthesized from its free form by the method of Tserng et al. [10].

Purification of 7α-hydroxysteroid dehydrogenase

Male Wistar strain rats weighing 200–250 g were anesthetized with diethyl ether and killed by decapitation 5 min later. The liver (45 g) was homogenized with 3 vol. 0.25 M sucrose in a Teflon homogenizer. Liver microsomes were prepared by the method of Wilgram et al. [11] and washed with 20 mM phosphate buffer (pH 7.4) containing 20% (w/v) glycerol and 1.0 mM reduced form of glutathione (GSH). The protein concentration was adjusted to 30 mg/ml, and then Tween 80 and sodium taurodeoxycholate were added to final concentrations of 0.1 and 0.5% (w/v), respectively. The suspension was stirred for 60 min and centrifuged at 105 000 × g for 1 h. The supernatant was dialyzed against 20 mM phosphate buffer (pH 7.4) containing 20% glycerol, 1 mM GSH, 0.1% Tween 80 and 0.05% sodium taurodeoxycholate (buffer A) and was applied to DEAE-cellulose column (4 × 13 cm), previously equilibrated with buffer A. The column was washed with the same buffer, and the protein was eluted with a linear gradient of concentration from 0 to 0.3 M NaCl in buffer A. The active fractions were dialyzed against buffer A and applied to second DEAE column (2 × 20 cm) equilibrated with buffer A. The column was washed with the same buffer and the protein was eluted with a linear gradient of concentration from 0 to 0.15 M NaCl in buffer A (Fig. 1). The fractions containing enzyme activity were concentrated using Amicon Diaflo membrane and dialyzed against 20 mM phosphate buffer (pH 7.4) containing 20% glycerol, 1 mM GSH, 0.2% Tween 80 and 0.1% sodium taurodeoxycholate (buffer B). The fractions were applied to hydroxyapatite column (4 × 5 cm) equilibrated with buffer B. The column was washed with the same buffer and the protein was eluted with 70 mM phosphate buffer (pH 7.4) containing 20% glycerol, 1 mM GSH, 0.2% Tween 80 and 0.1% sodium taurodeoxycholate. The two peaks containing 7α-hydroxysteroid dehydrogenase activity were found on hydroxyapatite chromatography (Fig. 2). The nonbound enzyme fractions (peak 1), which contained 65% of the total activity obtained from the hydroxyapatite column, were applied to Affi-Gel® Blue column (1 × 7 cm) equilibrated with buffer B. The column was washed with the same buffer and the protein was eluted with a linear gradient of concentration from 0 to 4 M NaCl in buffer B. The fractions containing enzyme were combined and used as the purified 7α-hydroxysteroid dehydrogenase.

Gel filtration

Gel filtration of the enzyme was performed on an HR 10/30 column prepacked with Superose 6™ using Pharmacia Fast Protein Liquid Chromatography system.

Sodium dodecyl sulfate polyacrylamide gel electrophoresis

Sodium dodecyl sulfate polyacrylamide gel electrophoresis was carried out according to Laemmli [12] using a 9% acrylamide gel.

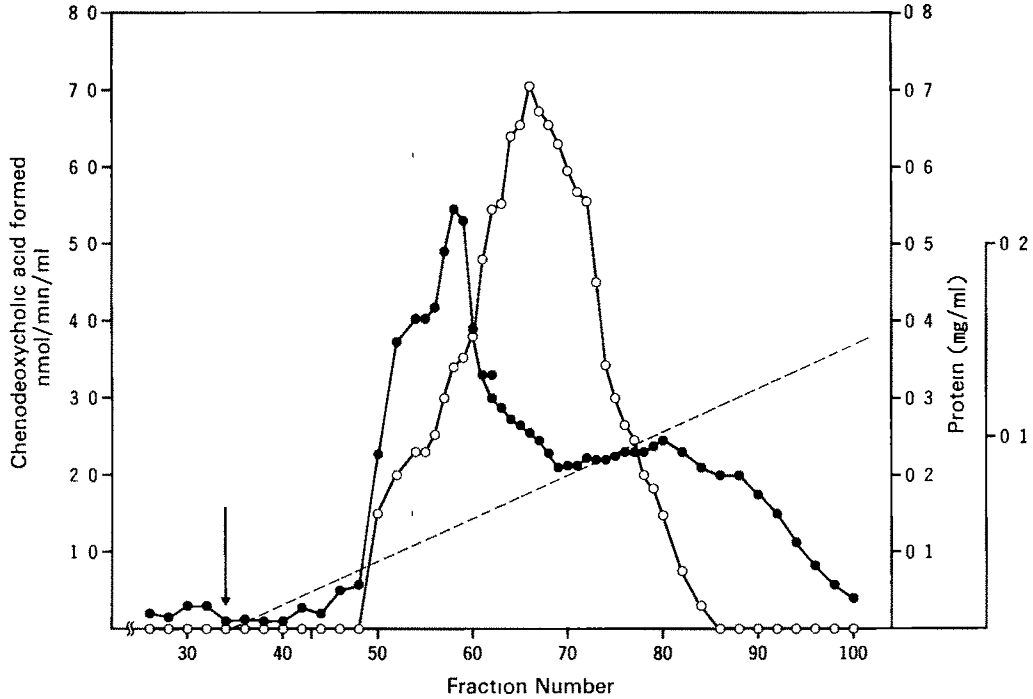

Fig 1. DEAE-cellulose chromatography (DEAE-2) of 7α-hydroxysteroid dehydrogenase The eluate from first DEAE-cellulose column was applied. Fractions of 6.5 ml were collected and analyzed for enzyme activity (○) and for protein concentration (●) The standard incubation conditions were used as in text. The arrow indicates the start of a linear NaCl gradient.

Determination of protein concentration

Protein concentration was determined by the method of Lowry et al. [13] or from the absorbance at 280 nm with bovine serum albumin as standard.

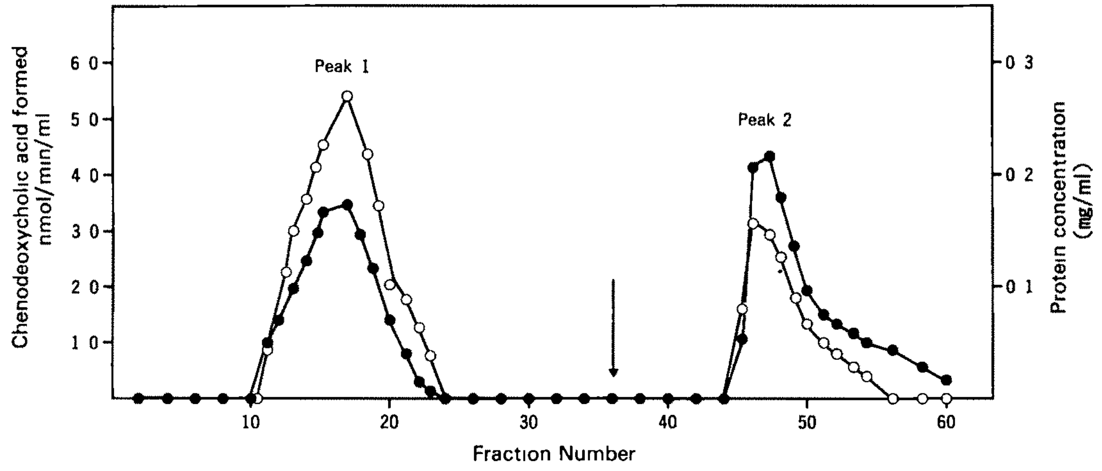

Fig 2. Hydroxyapatite chromatography of 7α-hydroxysteroid dehydrogenase The fractions containing enzyme activity from second DEAE column were applied to hydroxyapatite column chromatography. The fractions of 7.0 ml were collected and the enzyme activity (○) and protein concentration (●) were analyzed as in text The arrow indicates the start of the elution by 70 mM phosphate buffer (pH 7.4) containing 20% glycerol, 1 mM GSH, 0.2% Tween 80 and 0.1% sodium taurodeoxycholate.

Incubation procedure and analysis of the product formed

Activity of 7α-hydroxysteroid dehydrogenase acting on 3α-hydroxy-7-keto-5β-cholanoic acid was assayed by the method as described previously with slight modifications [9]. The standard incubation mixture in a total volume of 3.0 ml contained 170 μM 3α-hydroxy-7-keto-5β-cholanoic acid in 100 μl of ethanol, an appropriate amount of microsomes or purified enzyme, 0.1 M sodium-citrate-phosphate buffer (pH 5.0), and 0.8 mM NADPH or NADH. The mixture was incubated at 37°C for 15 min, and the reaction was stopped by adding 0.2 ml of 4 M hydrochloric acid. Then 100 μg of 7α,12α-dihydroxy-5β-cholanoic acid was added as an internal standard. The bile acids extracted with diethyl ether from the incubation mixture were converted to the hexafluoroisopropyl-trifluoroacetyl derivatives [14] and were subjected to gas chromatography (Shimadzu GC9A) on a glass column (3.0 mm × 1.6 m) of 3% DC QF-1 at 230°C. The amount of chenodeoxycholic acid formed was determined by measuring the peak areas of chenodeoxycholic acid and the internal standard.

Results and Discussion

The purification of 7α-hydroxysteroid dehydrogenase acting on 3α-hydroxy-7-keto-5β-cholanoic acid from microsomes of rat liver was summarized in Table I. The solubilization from the microsomes with a mixture of Tween 80 and sodium taurodeoxycholate resulted in a complete recovery of activity of 7α-hydroxysteroid dehydrogenase in the 105000 × g supernatant. On hydroxyapatite chromatography of the active fractions obtained from two DEAE-cellulose chromatographies, two peaks containing 7α-hydroxysteroid dehydrogenase were found in the nonbound and eluate fractions, respectively (Fig. 2). The nonbound fraction containing more abundant enzyme activity was purified further about 160-fold as compared to the original microsomes in a yield about 13% by Affi-Gel Blue chromatography. The specific activity of the partially purified 7α-hydroxysteroid dehydrogenase acting on 3α-hydroxy-7-keto-5β-cholanoic acid was 91.3 nmol chenodeoxycholic acid formed/min per mg protein. However, the purified enzyme could reduce 3α-hydroxy-7-keto-5β-cholanoic acid to ursodeoxycholic acid in a trace amount. Thus, the purified enzyme preparation still contained small amount of 7β-hydroxysteroid dehydrogenase, which was unable to be removed by the present purification procedures.

The stability of the enzyme was examined with the solubilized microsomes which were stored in buffer A at 4°C or −80°C. When the enzyme was stored in the presence of 20% glycerol at 4°C, the activity remained unchanged for at least 1 week, whereas it decreased to less than one-half over a week in the absence of glycerol. On the other hand, when the enzyme was stored at −80°C, its activity remained unchanged for 3 weeks, regardless of the presence or absence of glycerol.

The reduction of 3α-hydroxy-7-keto-5β-cholanoic acid to chenodeoxycholic acid was linear with time for at least 20 min. Furthermore, the reduction rate was proportional to the concentration of enzyme protein. The reduction required the addition of NADPH but not NADH as coen-

TABLE I

PURIFICATION OF 7α-HYDROXYSTEROID DEHYDROGENASE FROM RAT LIVER MICROSOMES

CDCA, chenodeoxycholic acid.

	Protein (mg)	Enzyme activity (nmol of CDCA formed/min)	Purification (-fold)	Yield (%)
Microsomes	1819.0	1040.7	1.0	100.0
Solubilization	869.3	992.6	2.0	95.4
DEAE-1	168.0	646.1	6.7	62.1
DEAE-2	42.0	446.6	18.6	42.9
Hydroxyapatite (peak 1)	8.6	257.0	52.5	24.7
Affi-Gel Blue	1.5	137.0	160.2	13.2

zyme. These results were consistent with those observed previously with crude liver homogenate [9].

As shown in Fig. 3, the reaction was found to be reversible. The optimum pH for the oxidation was about 8.5 in the phosphate buffer, whereas the pH for the reduction was found to be about 5.0 in the citrate-phosphate buffer, which was similar to that observed previously with crude liver homogenate [9].

When the purified 7α-hydroxysteroid dehydrogenase (peak 1) was applied to gel-filtration chromatography on a column of Superose 6, a single peak of the enzyme appeared in the region of molecular weight of about 130 000 (Fig. 4). However, the electrophoretogram of sodium dodecyl sulfate-polyacrylamide gel electrophoresis of the purified enzyme (Fig. 5) showed two bands in the molecular weight range of 66 000–70 000. The band corresponding to the molecular weight of 130 000 was not found. These results indicate that this enzyme may exist as a dimer.

The apparent K_m for 3α-hydroxy-7-keto-5β-cholanoic acid calculated from a Lineweaver-Burk plot was 35.7 μM, which was similar to that observed with crude liver homogenate [9] and that for NADPH was 90.9 μM.

The substrate specificity for the purified 7α-hydroxysteroid dehydrogenase is shown in Table II. The purified enzyme could reduce only 7-keto bile acids but not 3- or 12-keto bile acid, indicating that the 7α-hydroxysteroid dehydrogenase is different from 3- and 12-hydroxysteroid dehydrogenases and is an enzyme specific for 7-keto bile acids. The preferable substrate for the enzyme was the unconjugated form rather than the conjugated forms. Moreover, when 3α,12α-dihydroxy-7-keto-5β-cholanoic acid, a 7-keto-bile acid analogue, was used as substrate, the rate of reduction to cholic acid was slower than that of 3α-hydroxy-7-keto-5β-cholanoic acid to chenodeoxycholic acid. The result suggests that the 7α-hydroxysteroid dehydrogenase has more affinity for 3α-hydroxy-7-keto-5β-cholanoic acid than 3α,12α-dihydroxy-7-keto-5β-cholanoic acid, and is consistent with the in vivo study that 3α-hydroxy-7-keto-5β-cholanoic acid was reduced to a greater extent than that of 3α,12α-dihydroxy-7-keto-5β-cholanoic acid in dog liver [5].

Table III shows the effect of a sulfhydryl com-

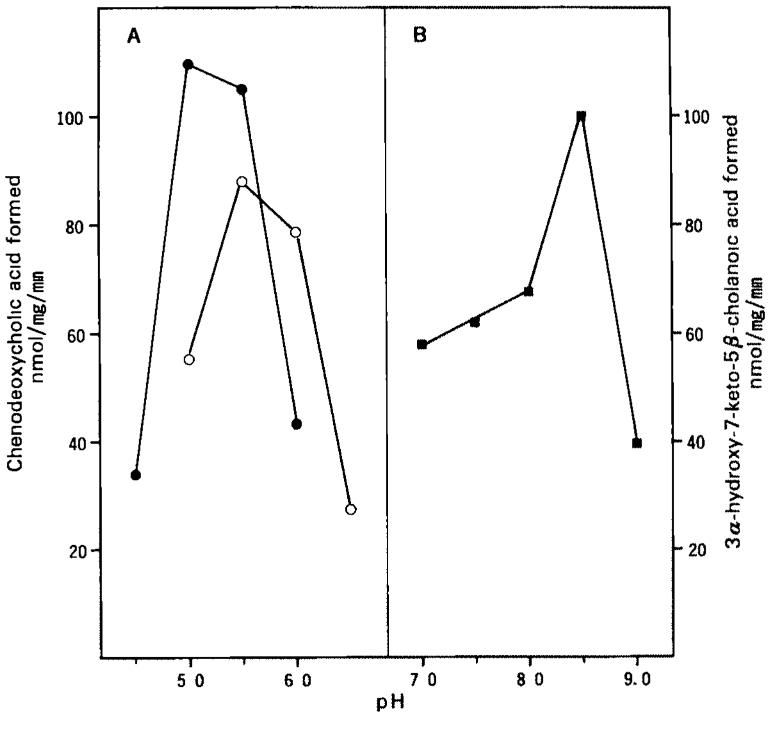

Fig. 3. Effect of pH on reduction of 3α-hydroxy-7-keto-5β-cholanoic acid (A) and on oxidation of chenodeoxycholic acid (B) by the purified 7α-hydroxysteroid dehydrogenase. The purified enzyme was incubated at various pH levels with 170 μM 3α-hydroxy-7-keto-5β-cholanoic acid in 0.1 M potassium phosphate buffer (○) or 0.1 M sodium-citrate-phosphate buffer (●) containing 0.8 mM NADPH. The enzyme was also incubated at various pH levles with 170 μM chenodeoxycholic acid in 0.1 M potassium phosphate buffer containing 0.8 mM NADP. The amount of 3α-hydroxy-7-keto-5β-cholanoic acid formed (■) was determined by gas-chromatographic analysis (1.5% SE-30 column)

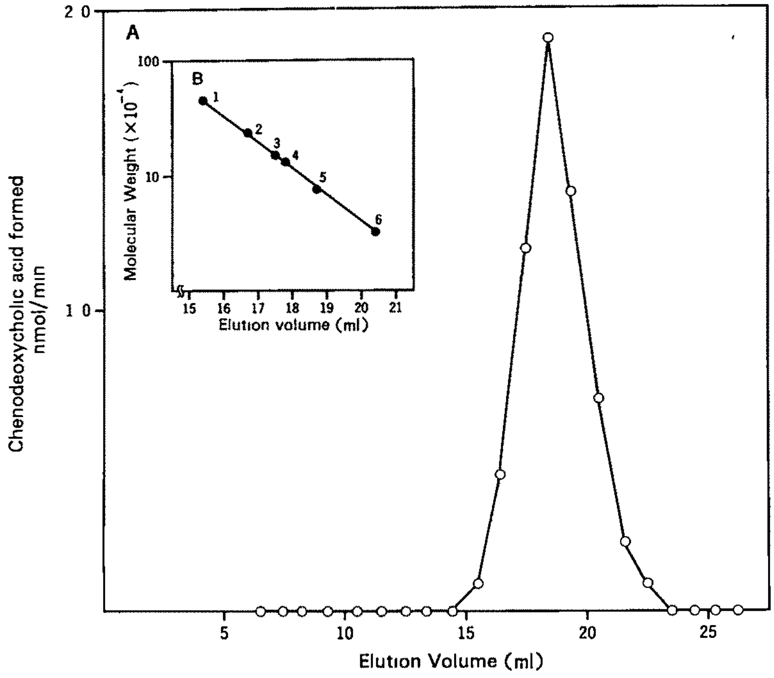

Fig. 4. (A) Gel-filtration chromatography of the purified 7α-hydroxysteroid dehydrogenase on a column of Superose 6. The purified 7α-hydroxysteroid dehydrogenase, 60 μg of protein, was applied to a column of Superose 6 in buffer B. Fractions of 0.5 ml were collected and analyzed for the enzyme activity (○) as described in text. (B) Molecular weight determination of 7α-hydroxysteroid dehydrogenase: 1, ferritin (M_r 450000); 2, catalase (240000); 3, aldolase (158000); 4, 7α-hydroxysteroid dehydrogenase (peak 1); 5, albumin (66 000); 6, chymotrypsinogen (25000).

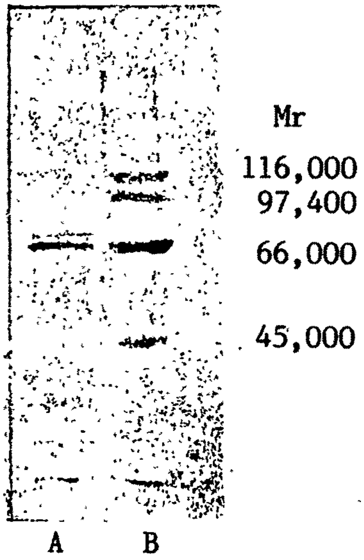

Fig. 5 Sodium dodecyl sulfate polyacrylamide gel electrophoresis of the purified 7α-hydroxysteroid dehydrogenase. Migration was from top to bottom. (A) The purified 7α-hydroxysteroid dehydrogenase (2 μg of protein); (B) a mixture of β-galactosidase (M_r 116000), phosphorylase *b* (97400), bovine serum albumin (66000), ovalbumin (45000) (3 μg of each).

TABLE II

SUBSTRATE SPECIFICITY

The substrate, 170 μM, was incubated with purified 7α-hydroxysteroid dehydrogenase (peak 1) in the presence of 0 8 mM NADPH under the standard assay conditions as described in text. In the experiments which the conjugated substrates were used, the acidified reaction mixture was neutralized with 0.5 ml of 1.25 M sodium hydroxide and was filtered. The filtrate was hydrolyzed with cholylglycine hydroalse as described previously [15]. Thereafter, the bile acids were extracted with ethyl ether from the acidified hydrolyzate and were analyzed by gas chromatography.

Substrates	The corresponding hydroxy bile acids formed (nmol/mg per min)
3α-Hydroxy-7-keto-5β-cholanoic acid	
unconjugated	102.0
glycine conjugate	56.0
taurine conjugate	44.0
3α,12α-Dihydroxy-7-keto-5β-cholanoic acid	21 0
3-Keto-5β-cholanoic acid	0.0
3α,7α-Dihydroxy-12-keto-5β-cholanoic acid	0.0

TABLE III

EFFECT OF PCMB ON REDUCTION OF 3α-HYDROXY-7-KETO-5β-CHOLANOIC ACID

The purified enzyme was used PCMB, *p*-chloromercuribenzoate; CDCA, chenodeoxycholic acid.

PCMB added	CDCA formed (nmol/mg per min)	Inhibition (%)
None	106.5	0.0
5 μM	25.5	76.1
10 μM	9.5	91.1
10 μM + 3 mM GSH	103.0	3.3

pound, *p*-chloromercuribenzoate, on the reduction of 3α-hydroxy-7-keto-5β-cholanoic acid. The enzyme activity was highly inhibited by addition of 10 μM *p*-chloromercuribenzoate. However, the inhibition was prevented by addition of 3 mM GSH. The enzyme is therefore considered as an enzyme containing a sulfhydryl group reversibly reactive to the sulfhydryl compound.

On the other hand, another enzyme (peak 2) was also purified about 67-fold by Affi-Gel Blue chromatography. Although the characterization of the partially purified enzyme (peak 2) was performed as described above (data not shown), its enzymological properties were not different from those of the peak 1 except for a physicochemical property, binding to the hydroxyapatite column in buffer B.

Until recently, the NADP(H)-dependent 7α-hydroxysteroid dehydrogenases have been purified and characterized from several strains of bacteria [3,7,8]. The properties of the enzyme were found to be dependent partly on the species of bacterium. In comparison with the bacterial enzymes, the 7α-hydroxysteroid dehydrogenase from rat liver microsomes presented in this study had some different properties. For example, the hepatic enzyme had a molecular weight of about 130000, which differed from the enzyme isolated from *Clostridium welchii* [3]. The optimum pH for the hepatic enzyme was lower than that for the enzymes from *Clostridium welchii* [3], *Bacteroides fragilis* [7] and *Clostridium absonum* [8]. Moreover, the substrate specificity for the hepatic enzyme was different from that for the enzymes isolated from *Clostridium welchii* and *Bacteroides fragilis,* which had more affinity for trisubstituted than disubstituted bile acid.

References

1 Danielsson, H and Sjövall, J (1975) Annu. Rev. Biochem 44, 233–253

2 Thistle, J L and Hofmann, A F (1973) N. Engl J Med 289, 655–659

3 Aries, V.C. and Hill, M J (1970) Biochim. Biophys. Acta 202, 535–543

4 Mahowald, T.A., Yin, M.W , Matschiner, J T., Hsia, S L., Doisy, E A., Elliott, W H. and Doisy, E.A (1958) J Biol Chem. 230, 581–588

5 Nakagaki, M , Danzinger, R G., Hofmann, A.F. and Roda, A (1983) Am J. Physiol 245, G411–G417

6 Fromm, H., Carlson, G.L , Hofmann, A F., Farivar, S. and Amin, P. (1980) Am J. Physiol. 239, G161–G166

7 Hylemon, P B. and Sherrod, J.A. (1975) J. Bacteriol 122, 418–424

8 Macdonald, I.A. and Roach, P D. (1981) Biochim. Biophys Acta 665, 262–269

9 Amuro, Y , Yamade, W., Nakano, T , Hayashi, E., Hada, T and Higashino, K (1985) Biochim. Biophys. Acta 841, 229–231

10 Tserng, K.-Y., Hachey, D.L. and Klein, P.D. (1977) J Lipid Res. 18, 404–407

11 Wilgram, G.F. and Kennedy, E.P. (1963) J. Biol Chem 238, 2615–2619

12 Laemmli, U.K (1970) Nature 227, 680–685

13 Lowry, O.H., Rosebrough, N J , Farr, A.L. and Randall, R J. (1951) J. Biol. Chem. 193, 265–275

14 Imai, K , Tamura, Z., Mashige, F. and Osuga, T .(1976) J Chromatogr. 120, 181–186

15 Van Berge Henegouwen, G.P., Ruben, A and Brandt, K.-H (1974) Clin. Chim. Acta 54, 249–261

Biochimica et Biophysica Acta 917 (1987) 108–111
Elsevier

BBA 52318

Covalently bound ω-hydroxyacylsphingosine in the stratum corneum

Philip W. Wertz and Donald T. Downing

The Marshall Dermatology Research Laboratories, Department of Dermatology, University of Iowa College of Medicine, Iowa City, IA (U.S.A.)

(Received 4 August 1986)

Key words: Ceramide; Water barrier; Stratum corneum, ω-Hydroxyacid; (Pig skin)

Pig epidermis was heat separated, and the stratum corneum was isolated after trypsinization. Exhaustive extraction of the stratum corneum fraction with chloroform/methanol mixtures yielded 14.7% lipid on a dry weight basis. After mild saponification of the extracted residue, additional lipid could be extracted which accounted for 2.1% of the stratum corneum weight. This bound lipid proved to consist mainly (91.9%) of *N*-(ω-hydroxyacyl)sphingosines in which the amide-linked ω-hydroxyacids were 28 to 34 carbon atoms in length. The release of this lipid by mild alkaline hydrolysis indicates that it is bound through an ester linkage. Half of the hydroxyceramide molecules reacted in situ with acidic acetone, suggesting that half of these molecules are attached to the stratum corneum through the ω-hydroxyl function, while the other half may be linked through one of the hydroxyl groups of the sphingosine.

Introduction

Full thickness mammalian epidermis has been shown to contain a complex array of lipids including phospholipids, ceramides, glucosylceramides, free fatty acids, cholesterol and cholesteryl sulfate [1–4]. After removal of these lipids by extraction with chloroform/methanol, a further quantity of lipid can be recovered from the residue following mild alkaline hydrolysis [5]. It was proposed that this additional lipid, consisting of fatty acids, ω-hydroxy acids, and ω-hydroxyacylsphingosines, is present in ester linkage with an insoluble macromolecular constituent of the epidermis, presumably protein [5]. In the present study, isolated stratum corneum was investigated, and *N*-(ω-hydroxyacyl)sphingosines were found to be the principal covalently bound lipids. The composition of this material has been determined and the mode of its attachment has been elucidated.

Methods

Isolation of stratum corneum. Sections of fresh pig skin were placed in water at 60°C for 1 min and the epidermis was scraped off in sheets. The epidermal sheets were placed in 1% trypsin (type III, Sigma Chemical Co., St. Louis, MO, U.S.A.) in phosphate-buffered saline for 2 h at 37°C, after which the liberated unkeratinized cells were scraped off with a spatula. The sheets were thoroughly rinsed with phosphate-buffered saline to remove additional loosened cells, and the entire process of trypsinization, scraping and rinsing was repeated. Histologic examination showed that the sheets of remaining tissue consisted almost entirely of stratum corneum cells. The stratum corneum sheets were dried under vacuum without a desiccant, weighed and stored at −20°C before use.

Extraction of unbound lipids. The sheets of stratum corneum were suspended successively in three separate mixtures of chloroform/methanol (2:1, 1:1 and 1:2, v/v) for 2 h each and were recovered each time by filtration. This sequence of

---

Correspondence: Dr P.W. Wertz, 270 Medical Laboratories, University of Iowa College of Medicine, Iowa City, IA 52242, U.S.A.

0005-2760/87/$03.50 © 1987 Elsevier Science Publishers B.V. (Biomedical Division)

extractions was repeated with solvent changes at 1 h intervals to thoroughly remove nonpolar lipids and ceramides, and the stratum corneum was finally extracted with methanol overnight to remove traces of polar lipids. The extracts were combined, concentrated to dryness, weighed and redissolved in chloroform/methanol prior to analysis by thin-layer chromatography (TLC).

Extraction of chemically bound lipids. Sheets of stratum corneum recovered after the extraction described above were heated at 60°C for 1 h with 1 M NaOH in 90% methanol [5]. The mixture was then acidified to pH 4 with 2 M HCl and shaken with chloroform. After filtration through a coarse sintered glass filter, the chloroform layer was separated and the aqueous phase was reextracted with chloroform. The chloroform extracts were washed with water and recombined before evaporation to recover the lipids released by the alkaline hydrolysis. The recovered lipids were dissolved in a small volume of chloroform/methanol, 2:1, and filtered through a 0.5 μm teflon millipore filter (Millex-SR; Millipore Corp., Bedford, MA, U.S.A.) to remove fine particulate material prior to weighing and analysis by TLC.

Derivatization of chemically bound lipids in situ. Sheets of stratum corneum from which unbound lipids had been extracted were suspended in dry acetone containing a trace of HCl, in order to form the acetonides of any ceramides in which both the 1- and 3-hydroxyl groups of the sphingosine moiety were a free. In one experiment, HPLC grade acetone was used without additional drying. The reaction was allowed to proceed for 2 h at room temperature. In two other experiments, the acetone was stored over molecular sieve 4A for 1 week prior to use, and reaction times of 4 h and 16 h were employed. Acetonide formation was terminated by the addition of 2% aqueous excess K_2CO_3 prior to filtration. The derivatized stratum corneum was immediately subjected to alkaline hydrolysis with recovery of the liberated lipid.

Lipid analysis. Each of the lipid extracts obtained was first analyzed by quantitative TLC [6], using individual lipids from pig epidermis, previously isolated and characterized [2–4], as reference compounds.

The material recovered after mild alkaline hydrolysis of extracted stratum corneum sheets was subjected to vigorous acid hydrolysis with 1 M HCl in methanol containing 20 M water at 65°C for 18 h [2,7]. The products were recovered by extraction of the reaction mixture before and after neutralization with NaOH. ω-Hydroxyacids and sphingosine bases were separated by preparative TLC.

The hydroxyacids were converted to methyl esters by treatment with 10% BCl_3 in methanol at 60°C for 1 h, and subsequently the ω-hydroxyl group was acetylated by treatment with acetic anhydride in pyridine [2]. Each step in this conversion was monitored by TLC using previously prepared standards [2]. The ω-*O*-acetyl methyl esters were separated according to degree of unsaturation by argentation TLC [3]. Each fraction was then subjected to quantitative TLC [6] and to gas-liquid chromatography (GLC) using a 25 m quartz capillary column with a BP-1 bonded silicone stationary phase (Scientific Glass Engineering, Austin, TX, U.S.A.) to determine the chain-length distribution. This column was operated isothermally at 300°C.

The sphingosines were converted to aldehydes by periodate oxidation [8], which were analyzed by GLC, on the column described above, at 220°C.

Results

The unbound lipids extracted from sheets of isolated stratum corneum amounted to 14.7 ± 1.4% ($n = 4$) by dry weight and consisted predominantly of six series of ceramides, cholesterol and free fatty acids as reported previously [1,9]. Minor components included cholesteryl sulfate and cholesteryl esters.

The material subsequently recovered from extracted tissue following mild alkaline hydrolysis amounted to 2.1 ± 0.2% of the dry tissue weight and consisted almost entirely of a material with the TLC mobility of ω-hydroxyacylsphingosine. This one component represented 91.9 ± 6.5% of the total bound lipid. Small amounts of free fatty acids (1.9 ± 3.2%) and ω-hydroxyacids (6.2 ± 6.3%) were also present; however, the high degree of variability associated with these minor components suggests that they may arise from the small pockets of unkeratinized epidermal material con-

TABLE I

COMPOSITION OF THE AMIDE-LINKED ω-HYDROXY ACIDS FROM COVALENTLY ATTACHED CERAMIDES OF THE STRATUM CORNEUM

The relative amounts of saturated, monoenoic and dienoic hydroxyacids (given in parentheses) were determined by quantitative TLC after separation by argentation TLC Fatty acid compositions, determined by gas-liquid chromatography, are presented as weights percent for each class of unsaturation. The values are the mean ± S.D. for four separate samples.

Carbon No	Saturates (50.5 ± 4.5)	Monoenes (44.5 ± 4.2)	Dienes (5.0 ± 1.6)
28	5.9 ± 1.6	1.4 ± 0.6	4.7 ± 1.0
29	3.5 ± 1.8	1.1 ± 0.5	3.2 ± 2.7
30	63.3 ± 3.3	8.5 ± 0.4	13.6 ± 5.8
31	7.0 ± 0.3	2.3 ± 1.4	2.8 ± 2.1
32	18.8 ± 1.8	66.9 ± 4.6	40.4 ± 7.6
33	0.5 ± 0.2	1.5 ± 0.4	3.7 ± 1.8
34	1.0 ± 0.2	18.3 ± 2.1	31.6 ± 3.4

taminating the stratum corneum preparations.

TABLE II

COMPOSITION OF THE SPHINGOSINE BASES FROM COVALENTLY ATTACHED CERAMIDES OF THE STRATUM CORNEUM

The chain length distribution of the sphingosine bases was determined by gas-liquid chromatography as described in Methods and the results are presented as weight percent Each value represents the mean ± S D. from four samples

Long-chain base	Weight percent
16:0	0.4 ± 0.1
16:1	2.1 ± 0.4
17:0	2.6 ± 0.1
17:1	11.8 ± 0.9
18:0	4.5 ± 1.1
18:1	21.9 ± 4.2
19:0	0.8 ± 0.2
19:1	2.2 ± 0.3
20:0	8.7 ± 0.4
20:1	34.0 ± 2.3
21:0	0.8 ± 0.2
21:1	3.7 ± 0.5
22:0	1.4 ± 0.2
22:1	5.3 ± 0.4

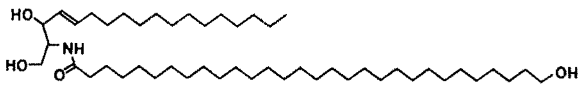

Fig. 1. Representative structure of *N*-(ω-hydroxyacyl)sphingosine

The observation that ω-hydroxyacylsphingosine was the only ceramide recovered from the saponified residue supports the interpretation that this lipid is covalently bound to the keratinocyte. If this ceramide were present in the stratum corneum residue simply as a result of incomplete extraction of free lipids, then other epidermal ceramides [2] should have been present also. Since other ceramides were not recovered from the extracted residue after saponification, it can be concluded that ω-hydroxyacylsphingosine is specifically and probably covalently bound within the stratum corneum.

Acid hydrolysis confirmed the identity of ω-hydroxyacylsphingosine. The only products of this reaction, as judged by both TLC and GLC, were ω-hydroxyacids and sphingosines. The composition of the ω-hydroxyacids is given in Table I and the composition of the sphingosines is presented in Table II. Each of these is similar to the compositions previously reported for corresponding materials contained in the mixture of lipids extractable from epidermis without hydrolysis [2]. A representative structure of *N*-(ω-hydroxyacyl) sphingosine is shown in Fig. 1.

The experiments in which the ceramide hydroxyl functions were derivatized with acetone prior to alkaline hydrolysis resulted in half of the recovered material appearing as acetonides (50.3 ± 5.3). This indicates that half of the ceramides were attached to the stratum corneum by esterification to the ω-hydroxyl function and half by esterification to one of the sphingosine hydroxyls. Although poor penetration of the reagent or local neutralization of the acid cannot be entirely ruled out as an explanation for this observation, increasingly more rigorous conditions did not change this result. Furthermore, free ω-hydroxyacylceramide was completely converted to an acetonide under all of the reaction conditions used.

Discussion

The present results show that, compared with full thickness epidermis, isolated stratum corneum contains a much higher content of lipid that is extractable only after alkaline hydrolysis. Moreover, the covalently bound lipid thus liberated from stratum corneum consists almost entirely of a single class of compound, namely *N*-(ω-hydroxyacyl)sphingosines, whereas full thickness epidermis yielded, in addition, significant levels of free fatty acids and ω-hydroxyacids [5].

Although the present results strongly indicate ester linkages as the most likely means of attachment of ω-hydroxyacylsphingosine to the stratum corneum, little evidence has been obtained regarding the site of the attachment. It seems highly probable that the substrate to which the hydroxyceramides are bound consists of protein, so that bonding would involve the carboxylic side chains with which certain epidermal proteins abound [10,11]. We have suggested [5] that the presence of the hydroxyacid derivatives on the outer surface of the horny cell envelope would facilitate the attraction between this otherwise hydrophilic surface and the extracellular lipid bilayers that constitute the epidermal water barrier. Such an interaction could be of major importance for both the epidermal water barrier function and the cohesiveness of the stratum corneum. Continuing studies using ultrastructural techniques are providing evidence to support these speculations.

Acknowledgement

This study was supported in part by a grant from the United States Public Health Service (AM 32374) and by Richardson-Vicks Inc. Wilton, CT.

References

1 Yardley, H.J. (1983) Epidermal Lipids, in Biochemistry and Physiology of the Skin (Goldsmith, L.A , ed), Oxford University Press

2 Wertz P.W. and Downing, D.T. (1983) J. Lipid Res 24, 759–765

3 Wertz, P W. and Downing, D.T. (1983) J. Lipid Res 24, 1135–1139

4 Abraham, W , Wertz, P.W and Downing, D T. (1985) J. Lipid Res. 26, 761–766

5 Wertz, P.W and Downing, D T. (1986) Biochem. Biophys Res. Commun. 137, 992–997

6 Downing, D.T. (1968) J. Chromatog. 38, 91–99

7 Gaver, R.C. and Sweeley, C C. (1965) J Am Oil Chem. Soc 42, 294–298

8 Sweeley, C.C and Moscatelli, E.A. (1959) J Lipid Res. 1, 40–47

9 Long, S A., Wertz, P.W., Strauss, J.S and Downing, D T (1985) Arch. Dermatol Res 77, 284–287

10 Peterson, L.L., Zettergren, J G. and Wuepper, K D (1983) J. Invest. Dermatol. 81, 95–100

11 Simon, M and Green, H. (1985) Cell 40, 677–683

Biochimica et Biophysica Acta 917 (1987) 112–120
Elsevier

BBA 52437

Age-dependent changes in the distribution and concentration of human lens cholesterol and phospholipids

Lu-Ku Li, Lydia So and Abraham Spector

Biochemistry and Molecular Biology Laboratory, Department of Ophthalmology, College of Physicians and Surgeons, Columbia University, New York, NY 10032 (U S A)

(Received 18 August 1986)

Key words Age; Cholesterol distribution; Phospholipid distribution; (Human lens)

Analyses of total lipid in individual lenses 1.8–63 years of age indicate that both the cholesterol and the phospholipid concentrations have reached a high level of 10 and 14 $\mu g/mg$ lens dry weight, respectively, after the first ten years of growth. Thereafter, the rate of phospholipid accumulation was greatly reduced to a value of 0.05 $\mu g/mg$ per year while that of cholesterol reduced to 0.19. Analyses of the distribution of lipid in successive lens fiber layers indicate that both the cholesterol and phopsholipid levels increase in the entire lens between the age of 1.8 and 9 years. Older lenses showed a continuous increase in the accumulation of cholesterol in the deep cortical fibers, while little or no increase in phospholipid concentration was observed. These results indicate that the accumulation of lipids is greater than that of lens dry mass (protein) during the first decade of lens growth. Since more than 90% of lenticular lipids are associated with fiber cell membranes, these data suggest a gradual change in the differentiation of the newly formed secondary fibers from the epithelium during this period. Analyses of the phospholipid composition of the successive fiber fractions indicate that the major phospholipids of phosphatidyl ethanolamine (PE), phosphatidylserine (PS) and sphingomyelin maintained a uniform distribution in the 1.8- and 5-year-old lenses. While no change was observed with the cortical fibers, older lenses showed a gradual loss of PE and PS in the nuclear fiber up to 63 years of age. By the late teen years, nuclear PS can no longer be detected, while high levels of PE are maintained in lens nucleus. The disappearance of nuclear PE begins in the teen years and is completed by the age of 40. The decrease in PE and PS resulted in a continuous increase in the cholesterol/phopsholipid ratio, a measure of membrane rigidity in the nuclear fiber in lenses 20 years of age and older. This decrease is also responsible for the exceedingly high rigidity of the nuclear fibers of lenses 60 years of age and older. Possible lamellar cholesterol organization in the lens fiber membrane is discussed.

Introduction

The avascular lens is an ideal organ for the study of aging. The bulk is made of concentric layers of fiber cells differentiated continuously from a single layer of epithelium underneath the anterior lens capsule. Since there is no fiber loss or turnover, lens weight and lipid content increase throughout life. Membrane lipid synthesis and accumulation in the outer cortex and differences in lipid in lens regions have been reported (Refs. 1–3; see Refs. 4 and 5 for a review). Analysis of lipids isolated from consecutive layers of individual human lenses 54 years of age and older indicates a unique lipid distribution along the optical axis. Fibers at various stages of elongation and aging are characterized by a distinct lipid content and composition [6].

Due to lens geometry and the fact that the dry

Correspondence address: Department of Ophthalmology. Research, Columbia University, College of Physicians and Surgeons, 630 West 168th Street, New York, NY 10032, U S A

0005-2760/87/$03 50 © 1987 Elsevier Science Publishers B V (Biomedical Division)

weight is proportional to the volume occupied by the fiber layers, the inner nuclear 10% of lens mass containing the embryonic primary fibers has been estimated to account for more than 50% of the optical pathlength [6]. This region, identified as the fetal lens that hardens during the onset of presbyopia, is responsible for the nuclear opacification during senile cataractogenesis [7]. The cortical region of the lens contains all the metabolically active newly formed fibers and elongated fibers. It increases in proportion as the lens grows. Lipid changes in this region are the results of age-dependent changes in fiber differentiation and aging of mature fibers [6]. Although lipid alterations in lens aging have been studied with operationally defined lens parts [1–3], little information is available on the lipid changes characteristic of fiber cells at various stages of development and aging.

In the present study, lipid analyses were carried out with concentric layers obtained from individual human lenses 1.8–63 years of age. A large increase in lipid during the first decade of lens growth was observed. The disappearance of major phospholipids in lens nucleus reported previously [1,6] was found to begin in the teen years. The accumulated loss of these phospholipids results in the highest cholesterol/phospholipid ratio in the nuclear region of old lenses that has ever been observed with cell membrane lipid. An abstract of this paper has been presented at the annual meeting of the Association for Research in Vision and Ophthalmology in Sarasota, FL, May, 1985.

Materials and Methods

Preparation of successive fiber layers and protein fractions

Normal human lenses were obtained in pairs from the Eye Bank for Sight Restoration, Inc. (New York, NY) within 24 h of death and stored at −70°C before use. Successive concentric fractions from individual lenses were isolated by rolling the decapsulated lens on a cooled metal block covered with parafilm [6]. Lenses younger than 50 years of age were frozen in liquid nitrogen and the procedure was performed while the lenses were thawing under a stream of argon. The location of the fractions on the lens axis is expressed as the percent dry weight occupied by each fiber fraction. In Figs. 2–4 and 7, the 0% represents the surface, while the 100% represents the center of the lens. A total of 23 lenses, in the age range 1.8–63 years, were fractionated and analyzed.

To maintain a constant protein (dry mass) concentration, lens fractions were suspended in a final volume of 0.3–0.5 ml water and homogenized in a 12 ml polypropylene tube with a Ross microemulsifier (Hauppauge, NY) at a setting of 3.5 for 20 s under argon. After the removal of aliquots for dry weight and protein determinations, the remainder was extracted for lipid with chloroform/methanol (2 : 1, v/v) in the same tube [8]. The lipid extracts were dried in a Savant Vac concentrator (Hicksville, NY) and kept at −20°C until use. Solvent blanks and extractions containing known amounts of cholesterol, protein, phospholipid and fatty acid were run. Recoveries of approximately 90% were obtained in all cases.

Dry weight and protein determination

The dry weight was determined by heating 10–20 μl lens homogenates in the microbalance aluminum pan (Cahn Instr., Cerritos, CA) at 110°C for 4–6 h. Values obtained from duplicate samples are within 1.5%. Some of the samples were hydrolyzed in 6 M HCl and analyzed in a Beckman amino acid analyzer.

Cholesterol and phospholipid determination

Cholesterol was measured by the cholesterol oxidase (EC 1.1.3.6; *Brevibacterium* sp.) assay (Cholesterol kit, Boehringer, Indianapolis, IN) in Triton X-100 (Baker) [9]. Total phospholipid was determined as phosphorus after digestion of lipid samples with perchloric acid [10]. Individual phospholipids were identified by thin layer chromatography (TLC) with standards from Supelco (Bellefonte, PA), on silica gel 60 TLC plates (EM Darmstadt, Cincinnati, OH). The plates were washed in the first solvent, heated to 110°C for 30 min and then developed with two solvents in one dimension [11]. The first solvent contains chloroform, methanol, acetic acid and water (35 : 15 : 6 : 1, v/v), while the second is made of hexane, isopropyl ether and acetic acid (65 : 35 : 2, v/v). After charring the plates with 10% cupric sulfate in 8% phosphoric acid [12], the individual lipids were quantitated by densitometry using an LKB-soft laser densitometer (LKB Instrument, Paramus, NJ). The detector response was calibrated with known amounts of standards. For the same quantity of phosphatidylethanolamine (PE), phosphatidylserine (PS), phosphatidylcholine (PC) and sphingomyelin, the areas detected were within ±7%. No color yield correction was made for the small amounts of lysoPE and lysoPS because of difficulty in resolving the lyso-phospholipids from PC in the TLC system employed.

Fatty acid composition

Lipid extracts were hydrolyzed in 5% sulfuric acid in acetonitrile/water, 9:1 [13]. Tricosanoic acid (Supelco) was added as internal standard for quantitation. Fatty acid methyl esters were prepared by heating the hexane extracts of the lipid hydrolysate with 3 M methanolic HCl (Supelco) at 80°C for 20 min and analyzed by gas-lipid chromatography (GLC) with an HP 5080 gas chromatogram (Hewlett-Packard) as described [3]. The identity of the fatty acid methyl esters was established by a comparison with standards.

Results

Age dependence of total lens cholesterol and phospholipid concentration

The overall cholesterol and phopsholipid contents of human lenses were obtained from the sum of lipids in the concentric fiber fractions divided by the total lens dry weight. The lowest cholesterol value of 3.8 μg/mg was observed with the youngest (1.8-year-old) lens examined (Fig. 1). This value was more than doubled in the 9-year-old lens to 9.6 μg/mg. Thereafter, the cholesterol content increase at a slower rate of 0.188 μg/mg per year. The phospholipid content also increases with age; in a manner similar to cholesterol, the major increases occurred during the first decade of growth. Increase after the first ten years is minimal, approximately 0.053 μg/mg per year. Phospholipid values obtained from lenses between 40 and 63 years of age are within the range of experimental variation; 16.1 ± 1.6 μg/mg.

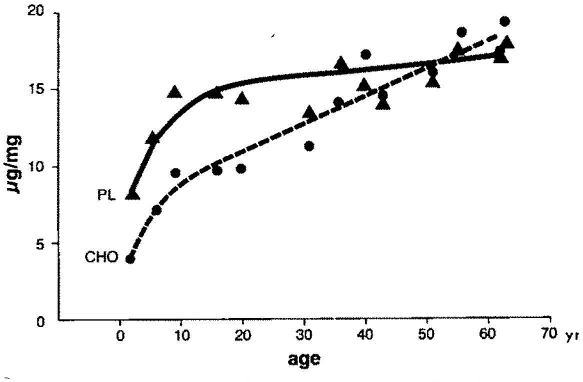

Fig. 1. Increase in total cholesterol (●) and phospholipid (▲) concentration (μg lipid/mg dry weight) as lens ages. Rates of increase in cholesterol and phospholipid concentration are 1.17 and 1.03 μg/mg per year, respectively, for the first ten years of lens growth. For lenses from 10 to 63 years of age, the rates are reduced to 0.19 for cholesterol and 0.05 for phospholipid. Values are the averages from paired lenses, except those of 1.8, 36 and 40 years of age.

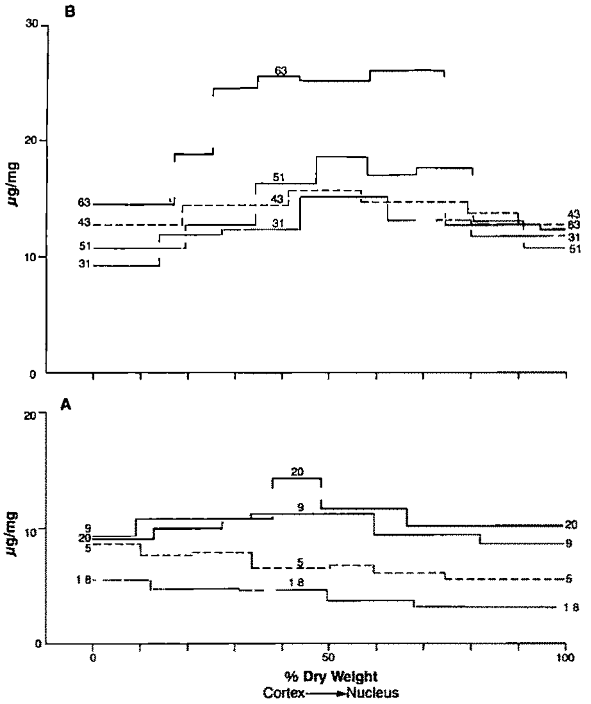

Fig. 2. Age-dependent changes in the concentration distribution of cholesterol. The location of the concentric fractions are represented as percent dry weight on the lens cortex-to-nucleus axis; The 0% and 100% depict the surface and center of the lens, respectively. Panel A: 1.8-year, ······; 5-year, ------; 9-year, ——; 20-year ——. Panel B: 31-year, ······; 43-year, ------; 51-year, ——; 63-year, ——. Except for the single 1.8-year-old, data from one of the paired lenses having the greater number of successive fiber fractions are presented. Variation in cholesterol content between the paired lenses is ±7% or less for fiber fractions occupying comparable locations on the lens axis. Duplicate lipid determinations performed for a given lipid extract were within ±4%.

Age-dependent changes in the distribution of cholesterol

Fig. 2 shows the distribution of the cholesterol level in individual human lenses from 1.8 to 63 years of age. During the first five years of postnatal life, the cholesterol concentration increases in all lens regions, while the highest level is found in the cortical 10–15% of the total lens dry weight. In the 9-year-old lens examined, a cholesterol content of about 9.6 µg/mg was found with the cortical 10% lens dry weight. This cortical level is maintained constant until after the 4th decade of life where it averages to approximately 12 µg/mg (Fig. 2B). The cholesterol level in the nuclear 10% lens dry weight attained a high value Of 8.6 µg/mg in the 9-year-old lens; further increases in the nuclear cholesterol levels are small and become insignificant after the third decade of lens growth. The major accumulation of cholesterol is in the deep cortex (30–70% of lens cortex-to-nucleus dry weight axis). Thus, in lenses of 9 years of age and older, this region has the highest cholesterol content. This maximal cholesterol level in the inner cortex increases continuously with age, up to the oldest lens examined, 63 years of age. The increase in cholesterol concentration in the deep cortex suggests the presence of another source of cholesterol in addition to the de novo synthesis that occurs in the metabolically active superficial cortex. This source of cholesterol is responsible for the observed overall increase in lens cholesterol content for individuals of 5 years and older.

Age-dependent changes in the distribution of phopsholipid content

The distribution of phospholipid concentration in the lens is characterized by a cortex-to-nucleus decrease in all ages studied (Fig. 3). The maximal phospholipid level associated with the superficial cortex (about 10% of total lens dry weight) increases from a value of 9.2 µg/ml in the 1.8-year-old lens to 19.3 µg/mg in the 5-year-old lens. Thereafter, no further significant increase was found. Following a similar pattern, the phospholipid concentration in the deep cortex and nucleus increases continuously during the first decade of lens growth. After 9 years of age, there is little change in the distribution or concentration of phospholipid with the exception of the 63-year-old, that showed a somewhat higher value. In the nucleus (approximately 10% of total lens dry weight), the phospholipid values for lenses of 31–63 years of age varies in a range of 6–9 µg/mg (Fig. 3B). The higher values of 10 and 11.6 µg/mg observed with the 9- and 20-year-old lenses (Fig. 3A) are probably due to the use of a larger weight fraction to represent the nuclear region of these relatively 'soft', young lenses.

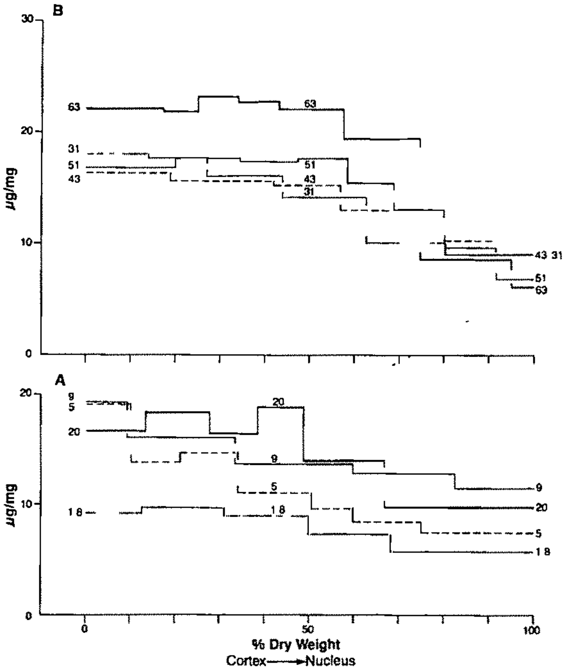

Fig 3. Age-dependent changes in the concentration distribution of phospholipid The same samples as in Fig. 2 were used. See legend of Fig. 2 for details.

Age dependence in the distribution of the cholesterol /phospholipid ratio in the lens

The molar cholesterol/phospholipid ratio of the lenses examined is shown in Fig. 4 to indicate changes in fiber membrane physical properties. All lenses except the youngest, 1.8 years, showed a cortex-to-nucleus increase in cholesterol/phospholipid; the magnitude of this increase becomes greater as the lenses age. The average value for the cortical 15% lens dry mass is 0.94 for lenses 20 years of age or younger (Fig. 4A). For lenses older than 30 years, the average cholesterol/phospholipid ratio in this region is about 1.20 (Fig. 4B).

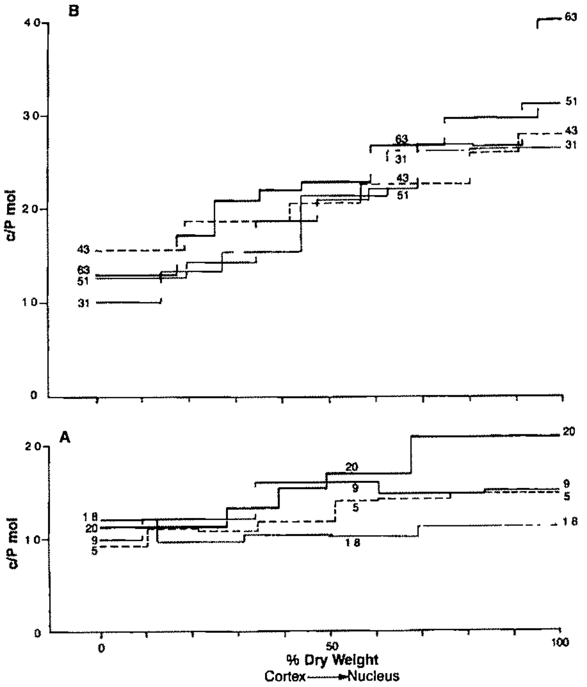

Fig 4 Changes in the distribution of the cholesterol/phospholipid ratio as human lenses age The same samples as in Fig. 2 were used. See Fig 2 for details.

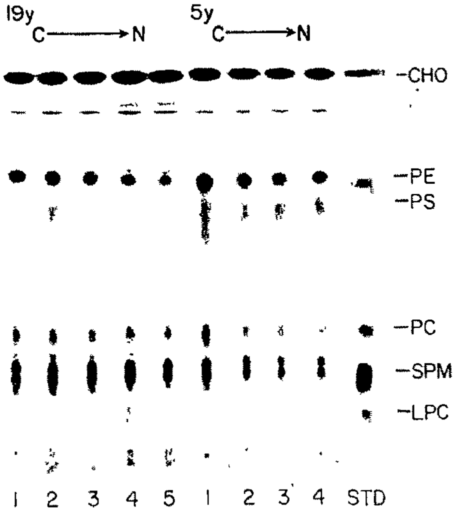

Fig. 5 Thin layer chromatography of lipids isolated from the fiber fractions of a 5-year-old (5y) and a 19-year-old (19y) lens. The numbers represent successive fractions from the cortex to the nucleus of the lens Standard lipids are; CHO, cholesterol; PE, phosphatidylethanolamine; PS, phosphatidylserine (Fig 6); PC, phosphatidylcholine; SPM, palmitoyl and nervonyl sphingomyelins; and LPC, lysoPC. LPE, lysoPE (Fig 6) and lysoPS (not shown) migrate closely with PC

In the deep cortex (30–70% of total lens dry weight), the cholesterol/phospholipid increases with age primarily as a result of the cholesterol accumulation in these deep fibers (see Fig. 2). For the nuclear 20% of the total lens dry mass, the cholesterol/phospholipid ratio increases continuously with age; from 1.15 for the 1.8-year-old to an average of about 3.2 for the 43–63-year-old. Beyond the age of 30 years, the increases in cholesterol/phospholipid ratio were observed primarily in the nuclear region, especially the innermost 10% of total lens dry weight. The highest cholesterol/phospholipid value of 4.1 was observed in the nuclear 6% of the 63-year-old lens. A small nuclear fraction was not obtained from younger lenses. A high cholesterol/phospholipid ratio of 3.2 has been reported previously for 1 72-year-old nucleus [4].

Age-dependent changes in phopsholipid composition in individual lenses

The phospholipid compositions of the lipid extracts isolated from concentric lens fractions were analyzed by TLC developed with two solvent systems in one dimension. One lens at each age in the range of 1.8–63 years, shown in Fig. 1, was analyzed. Selected examples are shown in Figs. 5 and 6. The major phospholipids are the PE, PS and sphingomyelins. The sum of these three phospholipids accounts for greater than 70% of the total. From the youngest, 1.8-, to the 5-year-old lenses, the phospholipid composition remained the same throughout the entire lens, as indicated by that of the 5-year-old lens in Fig. 5. The relative abundance of PE, PS and sphingomyelin is maintained at 36.5, 15.0 and 27.5%, respectively, based on densitometry of the charred TLC plate (Fig. 7). In the 19-year-old lens examined, a decrease in the nuclear PE levels and a low PS content in all the fractions became apparent. A cortex-to-nucleus decrease in PE was also observed with the 31-year-old lens (data not shown). In 40-year and older lenses, both PE and PS disappeared almost completely from the deep cortical and nuclear fractions (Fig. 6). The decrease in PE and PS was compensated for by a relative increase in SPM, as shown in Fig. 7. The increase in the intensity in

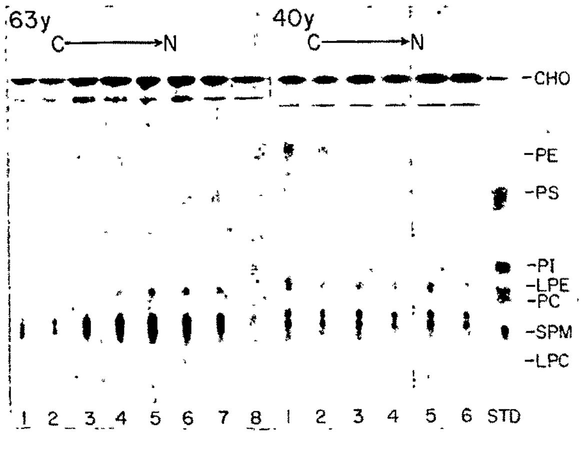

Fig 6. Thin layer chromatography of lipids isolated from consecutive fractions from a 40-year-old (40y) and a 63-year-old (63y) human lens Experimental conditions and abbreviations used are the same as in Fig. 5. Phosphatidylinositol (PI) was included in the standard lipids

the lysoPE, lysoPS regions in the nuclear fibers of lenses older than 40 years indicates the breakdown of the corresponding phospholipids as reported previously by Broekhuyse [1]. In the 63-year-old lens, the changes in phospholipid composition occurred in the cortical region corresponding to 18% of total lens mass. It is interesting to note that trace amounts of PE and PS remain in the nuclear fractions of the 63-year-old lens.

Changes in the distribution and composition of fatty acids in aging lenses

The fatty acid acyl chain of the phospholipid also determines the physical properties of the membrane lipid. Saturated fatty acids having a higher melting temperature increase the rigidity of the lipid. Fatty acid methyl esters obtained by transesterification of the lipid extracts from lens regions were analyzed by GLC and the relative composition for 5-, 20-, 42- and 62-year-old lenses are given in Table I. The data indicate that three major fatty acids, palmitic (16 : 0), oleic (18 : 1) and nervonic (24 : 1), accounted for more than 90% of the total. Several minor components were observed as reported [3,4] and only stearic acid (18 : 0) could be found with reasonable reproducibility. The decrease in the abundance of 18 : 1 in deeper fibers of lenses 20 years of age and older conforms with the disappearance of PE and PS shown by the TLC data in Figs. 5 and 6. The increase in 16 : 0 and 24 : 1 is due to the relative increase in sphingomyelin.

The level of fatty acid saturation in lens fiber lipid was maintained at about 40% for the entire lens. The cortex-to-nucleus decrease in 18 : 1 is compensated for by a corresponding increase in 24 : 1. The results suggest that the average acyl chain saturation remains almost unchanged throughout the lens as well as during aging and therefore does not contribute significantly to the

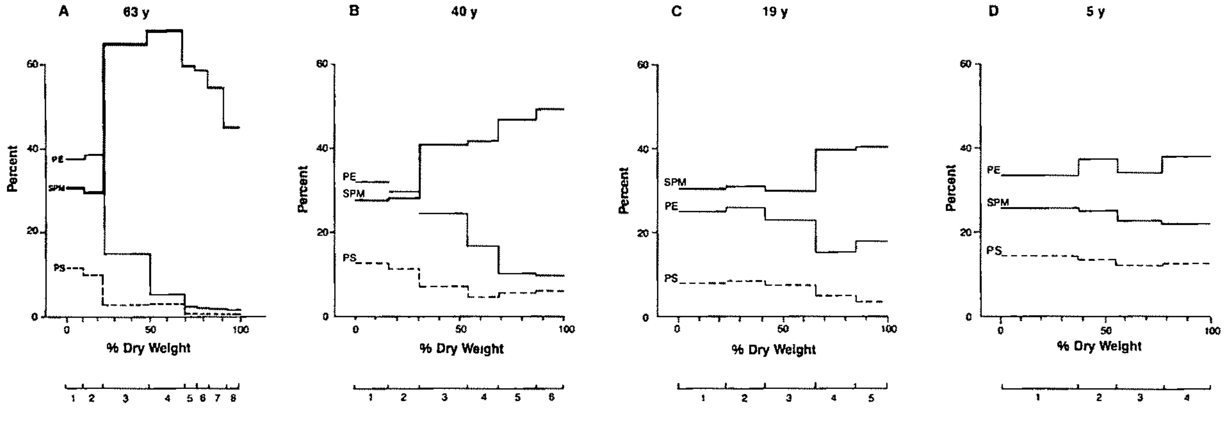

Fig 7 Relative phospholipid composition of human lens fiber fractions from densitometric scanning of the TLC plates shown in Figs. 5 and 6. The percentages of the major phospholipids, PS ------, PE ——— and sphingomyelin (SPM) ———, in the consecutive lens fractions (indicated by numbers) are given as a function of the location of the fractions on the lens dry weight axis Panel A, 63-year; B, 40-year; C, 19-year; and D, 5-year-old lens

TABLE I

PERCENT FATTY ACID COMPOSITION IN HUMAN LENS PARTS

Fatty acids were determined as the methyl esters by GLC after hydrolysis of the lipid extracts with 5% sulfuric acid in acetonitrile/water 9:1 and esterification with methanolic HCl Values are means of three to five determinations. S.D. is 9% except for 18:0 where it is 19% The outer cortex represents the outermost 18–28% of the total lens dry weight while the nucleus the innermost 15–20 and 30–35%, respectively, of the 42- and 62-, and 5- and 20-year-old lenses The inner cortex represents 25–35% of total lens mass intermediate between the cortex and nucleus.

	Fatty acid			
Lens age (years): section	16:0	18:0	18:1	24:1
5: outer cortex	28.9	11.1	48.3	11.7
inner cortex	31.5	14.8	44.4	9.3
nucleus	29.1	9.9	48.0	13.0
20: ounter cortex	26.1	8.1	45.2	20.6
inner cortex	31.0	7.7	32.8	28.5
nucleus	43.5	7.4	19.6	29.6
42: outer cortex	29.2	12.2	41.4	17.2
inner cortex	32.8	6.7	33.0	27.5
nucleus	43.3	6.2	17.2	33.3
62: outer cortex	32.6	8.8	35.7	22.8
inner cortex	41.2	5.2	25.6	28.0
nucleus	47.4	4.7	9.5	38.4

age-dependent increase in the rigidity of fiber membrane lipid.

Discussion

High cholesterol content in lens membrane lipid

The molar cholesterol/phospholipid ratio are exceedingly high in lens fibers and most of the lipids are in the plasma membrane (see Refs. 4 and 5 for a review). A high cholesterol/phospholipid value of 3.2 was reported previously for a 72-year-old nucleus [4]. In the nucleus of the 63-year-old a value of 4.0 was observed (Fig. 4). Other cell membranes have considerably lower cholesterol content [14]. The highest known value of 1.32 was observed with myelin [15]. The much lower aqueous solubility of cholesterol compared to phospholipid serves to insulate the nerve fiber for the transduction of electric pulses. The high cholesterol concentration in lens membrane suggests a cholesterol molecular organization other than the configuration with the 3′-OH spanning the acetyl region, with the rigid non-polar ring in the hydrocarbon interior of the phospholipid bilayer [16]. The tendency of cholesterol to aggregate into clusters at a cholesterol/phospholipid ratio of greater than 0.3 [17] suggests that lamellar packing of cholesterol into mono- or multi-layers is the preferred molecular orientation. The low lipid content of the lens [4,6] necessitates an efficient packing of the enveloping lipid material. The dimension observed for the fiber cell membrane is in the range of 5–7 nm, comparable to that observed with other cells [18,19]. These results suggest that mono- or bi-layer cholesterol may characterize the unique structure of fiber memrbane.

Embryonic (primary) versus postnatal (secondary) lens fiber cells

Since new fiber cells are added to lens periphery continuously throughout life while the mature and nuclear cells are metabolically rather inactive, the age-dependent increase in total lipid concentration reflects changes brought about by the newly formed secondary fibers, i.e., they are characterized by a higher lipid content than that of the embryonic primary fibers. The lipid data shown in Figs. 1, 2 and 3 as well as those on phospholipid from lens parts by Broekhuyse [1] support this contention. Furthermore, since mature fibers contain low concentrations of internal organelles and most lens cholesterol and phospholipid is associated with plasma membrane [4,20], the higher lipid content of the newly formed fibers indicates the availability of a greater amount of enveloping material for the cell mass. These results suggest that the volume (size) of the secondary fibers is smaller than that of the primary fibers or that their membrane structures are different. Microscope examination of adult rabbit lenses showed the large size of the primary nuclear fibers [19].

Changes in the differentiation of lens epithelium during the first ten years of lens growth

The large increase in total lipid concentration during the first decade of lens growth is due to the large increase in both cholesterol and phospholipid concentration in the newly formed cortical fibers (Figs. 2A and 3A). An early study suggests that the period of rapid phospholipid increase extends well beyond into the third decade of lens growth [1]. This discrepancy may be due to the use of lens wet weight in estimating lipid concentrations while the lens water content decreases much faster in the young than old lenses [21]. These lipid increases reflect changes in the formation of secondary fibers from the differentiating epithelium during the first ten years of postnatal life.

Morphologically, a reduction in the volume (size) of the new fibers during early postnatal life was reported [18]. The cholesterol/phospholipid ratio, a measure of membrane rigidity, remains almost unchanged during this period of rapid lens growth, ranging from 0.8 to 1.2 for the cortical region. The large variation may be due to the inclusion of a greater number of mature fibers having a higher cholesterol content in the older cortex. These results suggest that the transport and/or cell-to-cell communication requirement(s) of the newly formed fibers remain relatively constant despite the reduction in cell volume. The greater variation in the cortical cholesterol/phospholipid ratio observed with 30-year or older lenses (Fig. 4B) may reflect the decrease in the relative contribution of the superficial cortex, having the lowest cholesterol/phospholipid ratio, to the total lens mass.

Accumulation of membrane cholesterol in inner cortex

That the inner cortical fibers have the highest cholesterol level can be detected as early as in the 9-year-old lens (Fig. 2A). This high cholesterol level becomes even greater as lens ages. Similar high levels of cholesterol accumulation in brain tissue during early childhood have been reported [22] and suggest a possible regulatory function of this lipid during lens development in addition to its role as a fiber membrane structural component (see Ref. 14 for a review). Changes in protein polypeptides in the same inner cortex region have been described [23] to indicate that this is the region where metabolic activities associated with fiber development and elongation (maturation) have almost stopped.

Nuclear protein insolubilization occurred after age-dependent phospholipid changes

The age-dependent disappearance of PE and PS and the concurrent increase in the relative amount of sphingomyelin in human lens nucleus appears to be a complex process. The data in Fig. 5 indicate that while PS has almost completely disappeared from the nucleus of a 19-year-old lens, high levels of nuclear PE remained. The high nuclear PS levels found for 20- and 32-year-old lenses by Broekhuyse [1] may be due to the use of the inner 30% wet weight to represent the nuclear region. In the 40-year-old lens, the PE can no longer be detected in the nucleus. Since these are normal and transparent lenses, the destruction of PS and PE and the consequent membrane fluidity alterations [15] do not appear to result in lens opacification. On the other hand, analyses of the proteins from the concentric fiber fractions [23] did show a rather small increase in nuclear protein insolubilization in 40-year-old lenses. A large increase in water-insoluble protein was found in 50-year or older lenses without further change in PS and PE. These results indicate that the nuclear lipid changes precede those of the proteins and that membrane lipid changes may be a prerequisite for nuclear protein insolubilization responsible for the hardening of lens nucleus. This possibility is currently under investigation.

Acknowledgements

We thank Ms. Gloria Jenkins for performing the amino acid analyses. This work was supported by grants from the National Eye Institute, National Institutes of Health.

References

1 Broekhuyse, R.M. (1969) Biochim. Biophys Acta 187, 354–365
2 Cenedella, R.J (1982) J Lipid Res. 23, 619–626
3 Rosenfeld, L and Spector, A (1981) Exp Eye Res. 33, 641–650
4 Broekhuyse, R M (1981) in Mechanisms of Cataract Formation in the Human Lens (Duncan, G., ed.), pp. 151–192, Academic Press, New York
5 Zelenka, P S. (1984) Curr Eye Res 3, 1337–1359
6 Li, Lu-Ku, So, L and Spector, A. (1985) J Lipid Res 26, 600–609
7 Brown, N A.P. (1973) Ciba Foundation Symposium, Vol 19 (new series), pp 65–78, Elsevier, Amsterdam
8 Folch, J , Lees, M and Stanley, G.H. (1957) J. Biol. Chem. 226, 497–509

9 Ott, P, Binggeli, Y. and Brodbeck, U (1982) Biochim Biophys. Acta 685, 211–213

10 Hess, H H. and Derr, J.E (1975) Anal. Biochem 63, 607–613

11 Ando, S., Kon, K. and Tanaka, Y. (1980) in Membrane Fluidity (Kates, M. and Kuksis, A, ed), pp. 43–56, The Humana Press, Clifton, NJ

12 Touchstone, J C., Levin, S S, Dobbins, M.F and Beers, P C (1983) J Liq. Chromatogr. 6, 179–192

13 Aveldano., M I and Horrocks, L.A. (1983) J. Lipid Res 24, 1101–1105

14 Yeagle, P L (1985) Biochim Biophys. Acta 822, 267–287

15 Shinitzky, M and Barenholz, Y. (1978) Biochim. Biophys Acta 515, 367–394

16 Ashcroft, R.G., Coster, H G L and Smith, J.R. (1983) Biochim. Biophys Acta 730, 231–238

17 Engelman, D.M. and Rothman, J.E (1972) J. Biol Chem. 247, 3694–3697

18 Kuwabara, T (1975) Exp Eye Res 20, 427–443

19 Harding, C.V., Susan, S and Murphy, H. (1976) Ophthalmol. Res 8, 443–445

20 Lange, Y. and Ramos, V. (1983) J Biol Chem 258, 15130–15134

21 Hockwin, O., Rast, F, Rink, H., Minninghoff, J. and Twenhoven, H. (1978) Interdisciplinary Top. Gerontol 13, 102–108

22 Altman, P L. and Dittmer, D.S (ed) (1972) Biology Data Book, Vol. 2, pp. 1208–1210, Federation of American Societies for Experimental Biology, Bethesda, MD

23 Li, L.-K., Roy, D and Spector, A (1986) Curr Eye Res. 5, 127–135

Biochimica et Biophysica Acta 917 (1987) 121–130
Elsevier

BBA 52438

Glucocorticoid-induced elevation of serum high-density lipoprotein-cholesterol and its reversal by adrenocorticotropin in the rat

Takeshi Mitamura

Department of Laboratory Medicine, Hokkaido University School of Medicine, Sapporo (Japan)

(Received 13 June 1986)

Key words: Lipoprotein; Cholesterol; Glucocorticoid, ACTH; (Rat serum)

The effect of administration of a high dose of glucocorticoid (triamcinolone) on serum lipids and lipoproteins was studied in rats. Changes in serum lipids, especially cholesterol, were most marked when 5 mg/kg body weight of triamcinolone was injected daily for 5 days. Serum lipoproteins were separated by ultracentrifugation followed by gel-filtration chromatography. Cholesterol distribution between apolipoprotein B-containing lipoproteins (very-low-density and low-density lipoproteins), high-density lipoprotein$_1$ (HDL$_1$), and HDL$_2$ was determined after administration of triamcinolone with or without additional treatment with adrenocorticotropin (ACTH; Cortrosyn, 6 IU/rat). When triamcinolone was administered, cholesterol concentrations in HDL$_1$ and HDL$_2$ were elevated in a dose-dependent manner, but there was no significant change in apolipoprotein B-containing lipoprotein cholesterol levels. When ACTH was administered in combination with triamcinolone, the concentrations of all serum lipids except triacylglycerol were significantly lowered compared with rats treated with triamcinolone alone. HDL$_1$-cholesterol concentration in serum was significantly ($P < 0.001$) lowered from 69 ± 13 mg/dl (mean ± S.D.) in triamcinolone-treated rats to 36 ± 4 mg/dl by the administration of ACTH plus triamcinolone. The additional administration of ACTH in triamcinolone-treated rats caused a slight, but significant, decrease in cholesterol concentration in apolipoprotein B-containing lipoproteins; however, HDL$_2$-cholesterol level was not significantly affected, although there was a tendency for it to be lowered.

Introduction

Administration of glucocorticoids can cause hyperlipidemia both in man [1] and in other animal species, including rats [2–5]. The pattern and extent of hyperlipidemia varies depending on the dosage of glucocorticoids and on the animal species. It has been reported that rats maintained on a low dose of triamcinolone (0.5 mg/kg body weight) showed a 2-fold increase in serum triacylglycerol concentration, while a high dose of triamcinolone (over 5 mg/kg) produced an increase in serum cholesterol and high-density lipoprotein (HDL), without much change in serum triacylglycerol and very low density lipoprotein (VLDL) concentrations [5]. Cole et al. [6] reported that the concentration of plasma HDL lipid and protein tended to be elevated following dexamethasone treatment in the rat.

HDL is the major lipoprotein component transporting serum cholesterol in rats [7–9]. Lipoprotein cholesterol, rather than cholesterol newly synthesized in the glands, is the major substrate for the production of steroid hormones in the adrenal gland, ovary, and testis of the rat. These three endocrine glands preferentially take up and utilize HDL cholesterol for steroidogenesis in rats [10], although bovine adrenal cells predominantly utilize low-density lipoprotein (LDL) cholesterol [11].

Correspondence. Dr T. Mitamura, Department of Laboratory Medicine, Hokkaido University School of Medicine, Kita-15, Nishi-7, Sapporo 060, Japan.

0005-2760/87/$03 50 © 1987 Elsevier Science Publishers B V. (Biomedical Division)

Treatment with excessive glucocorticoids in experimental animals would suppress ACTH secretion and would lead to a reduction in the uptake of cholesterol from lipoproteins by adrenal cortex. Therefore, the present study was undertaken to obtain additional information concerning the changes in rat serum lipoproteins caused by treatment with a high dose of triamcinolone with or without additional administration of ACTH, primarily focusing on HDL subfractions. Lipoprotein classes were separated using agarose gel-filtration chromatography after preparing the total lipoproteins by means of a vertical ultracentrifugation.

Materials and Methods

Animals and treatments

Normally fed, male Wistar rats weighing 280–370 g were used. Triamcinolone diacetate was given for 1–5 days by a daily subcutaneous injection of 0.1 ml (0.25 or 2.5 mg triamcinolone/ml) per 100 g body weight. Where indicated, rats were treated with ACTH (tetracosactide acetate, Cortrosyn; 6 IU/rat) given subcutaneously daily for 5 days. Control animals were injected with the same volume of saline instead of the drugs. Blood was drawn from the aorta under light ether anesthesia. Animals were fed ad lib. before blood collection.

Isolation of lipoproteins

Blood was allowed to clot at 5°C for approx. 3 h, and serum was separated by centrifugation. Sera from several animals of the same treatment groups were pooled and subjected to the isolation procedures described as previously [12]. Briefly, the density of the sera was raised to 1.225 g/ml by additions of solid KBr, EDTA-Na_2, and 5,5′-dithiobis-2-nitrobenzoic acid [13]. Then the solution was centrifuged in a Hitachi 70P-73 ultracentrifuge with a vertical rotor (RPV-50T). The floated lipoproteins were collected by pipetting. Recovery of lipoproteins under these conditions was more than 95% in terms of cholesterol. The lipoprotein solutions were diluted to about 3-fold with 0.15 M NaCl/5 mM Tris-HCl/0.27 mM EDTA/3 mM NaN_3 (pH 7.4) and concentrated to 3–4 ml by ultrafiltration with an Amicon filter membrane (XM-50). The lipoprotein concentrate was then applied to an agarose gel chromatography column. The column (1.9 × 95 cm) consisted of Bio-Gel A50m, and was equilibrated and eluted with the same buffer described above at 10°C. The absorbance at 280 nm of the effluent was read for each fraction. Lipoproteins were separated into three major fractions (Fig. 1). Fraction I was composed of chylomicrons (if any) and large VLDL with preβ-mobility, and fraction II contained VLDL (pre-β-migrating) and LDL (β-migrating). The major component of the third peak, fraction III, was composed of lipoproteins with α-mobility. Lipoproteins with β-mobility were also found in this fraction, with small amount of contaminating albumin. Therefore, fractions corresponding to the third peak were pooled, concentrated to approx. 3.5 ml, and subjected further to Bio-Gel A5m column chromatography (Fig. 2). The column (1.5 × 95 cm) was eluted at 10°C with the same buffer as used for Bio-Gel A50m column chromatography. The absorbance at 280 nm of the effluent was continuously monitored.

Lipid and protein analyses

Total and free cholesterol in serum and in lipoprotein fractions were determined by an enzymatic method [14] using commercial kits purchased from Kyowa Medex Co. Ltd. (Tokyo, Japan). Cholesteryl ester was estimated as the difference between the total and the free cholesterol. Triacylglycerol [15] and phospholipid [16] was quantitated as described previously [12]. Protein was determined by the method of Lowry et al. [17] as modified by Markwell et al. [18].

Other procedures

Agarose gel electrophoresis was carried out by using Corning Universal Electrophoresis Film from Corning ACI (Palo Alto, CA, U.S.A.) in 0.05 M barbital buffer (pH 8.6), and lipoproteins were stained with Fat Red 7B. Sodium dodecyl sulfate (SDS) polyacrylamide gel electrophoresis was performed by the method of Weber and Osborn [19] after lipoproteins had been delipidated according to Scanu and Edelstein [20]. Protein standards of known molecular weight were run. The molecular weight standards employed were cytochrome *c* (12500), chymotrypsinogen A (25000), hen egg albumin (45 000) and bovine serum albumin (68 000) obtained from Boehringer-Mannheim (F.R.G.). The gels were stained with 0.25% Coomassie brilliant blue R in $CH_3OH/CH_3COOH/H_2O$ (46 : 9 : 45, v/v) and destained in 7.5% acetic acid in 5% methanol. Serum HDL-cholesterol were determined also by phosphotungstate-Mg^{2+}/dextran sulfate-Mg^{2+} precipitation method using a test kit 'Determiner HDL' obtained from Kyowa Medex Co. Ltd. (Tokyo, Japan).

Results

In preliminary experiments, rats were injected with triamcinolone in a dose of 5 mg/kg body weight for 1, 3 and 5 days, and serum lipids and HDL-cholesterol were determined. Serum total and free cholesterol continued to increase with the duration of triamcinolone treatment. Phospholipid and HDL-cholesterol were also elevated, though less marked than cholesterol, and these lipids reached maximal levels after 3–5 days of treatment. Serum triacylglycerol concentration was eventually unaffected, although it decreased temporarily after 1 day treatment. Thus, in later experiments animals were treated with triamcinolone for 5 days.

Table I shows the changes induced by increasing the amount of triamcinolone doses in serum lipids and HDL-cholesterol. Total and free cholesterol, phospholipid, and HDL-cholesterol levels were gradually elevated by the injection of increasing amount of triamcinolone doses, reaching almost a maximal level in a dose of 5 mg/kg body weight. Serum triacylglycerol concentration was unaffected again by the triamcinolone treatment.

Fig. 1 shows that the $d < 1.225$ g/ml fractions (total lipoproteins) were separated roughly into three fractions by gel-filtration chromatography on Bio-Gel A50m. As described under 'Materials and Methods', fractions I and II contained lipoproteins of non-HDL species or collectively named apolipoprotein B-containing lipoproteins. Fraction III was composed of mostly α-lipoproteins (or HDL species) and minor amount of β-lipoproteins.

When lipoproteins of fraction III were further subjected to Bio-Gel A5m column chromatography, lipoproteins were separated into two major subfractions, III-1 and III-2, although the separation was incomplete (Fig. 2). Subfractions III-1 and III-2 were collected and subjected to further analyses. Fig. 3 shows the electrophoretograms of the lipoproteins separated on agarose gel. In control animals, subfraction III-1 contained both α- and β-lipoproteins, while subfraction III-2 was composed of only α-lipoprotein. In triamcinolone-treated rats, β-lipoprotein in subfraction III-1 decreased as increasing amount of triamcinolone was administered, and was almost absent when it was injected in a dose of 5 mg/kg body weight. Subfraction III-2 from triamcinolone-treated rats was also composed of only α-lipoprotein.

TABLE I

CHANGES IN SERUM LIPIDS AND HDL-CHOLESTEROL AFTER 5 DAYS OF TREATMENT WITH INCREASING DOSES OF TRIAMCINOLONE

Values are mg/dl, means ± S.D., for eight rats in each group. HDL-cholesterol was determined by precipitation method. P values were obtained by Student's t-test. n.s., not significant.

Triamcinolone dose (mg/kg)	Total cholesterol	Free cholesterol	Phospholipid	Triacylglycerol	HDL-cholesterol
A 0	59 ± 6	14 ± 4	115 ± 14	147 ± 60	38 ± 3
B 0.5	96 ± 16	28 ± 6	162 ± 26	129 ± 24	57 ± 6
C 5.0	163 ± 35	56 ± 15	236 ± 56	129 ± 58	72 ± 8
D 10.0	175 ± 23	60 ± 12	240 ± 23	129 ± 82	78 ± 6
P values for					
A vs. B	< 0.001	< 0.001	< 0.001	n.s.	< 0.001
B vs. C	< 0.001	< 0.001	< 0.005	n.s	< 0.001
C vs. D	n.s	n.s	n.s	n.s	n.s

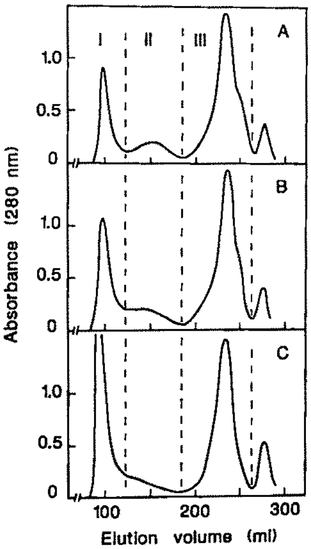

Fig. 1 The elution patterns of total lipoproteins ($d < 1.225$ g/ml) on a 1.9×95 cm column of Bio-Gel A50m 3–4 ml of concentrated lipoprotein solution corresponding to 18–22 ml of serum was applied to the column and approx. 3.5-ml fractions were collected. Lipoproteins were separated into three fractions, I (eluting at approx. 85–124 ml), II (eluting at approx. 124–182 ml), and III (eluting at approx. 182–265 ml) as indicated in the figure, which were quantitatively collected and cholesterol mass was determined for each lipoprotein fraction. The last (fourth) peak represents 5,5′-dithiobis-2-nitrobenzoic acid which was added to the sera during the lipoprotein isolation procedure. (A) Control rat, (B) triamcinolone (0.5 mg/kg) treated rat; (C) triamcinolone (5 mg/kg) treated rat.

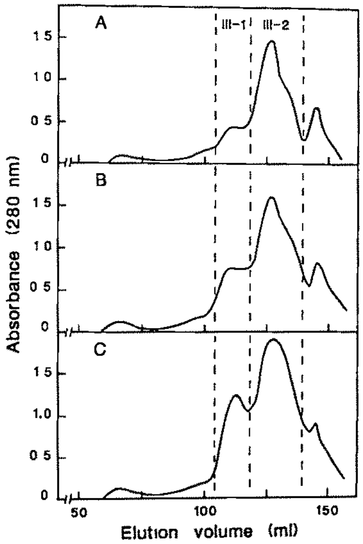

Fig. 2. The elution patterns of fraction III lipoproteins from Bio-Gel A50m column chromatography on a 1.5×95 cm column of Bio-Gel A5m 3–3.5 ml of concentrated fraction III lipoprotein solution was applied to the column and approx. 2.5-ml fractions were collected. Lipoproteins were separated into subfractions III-1 (eluting at approx. 105–120 ml) and III-2 (eluting at approx. 120–140 ml) as indicated in the figure, which were quantitatively collected and cholesterol mass was determined for each lipoprotein fraction. (A), control rat; (B), triamcinolone (0.5 ml/kg) treated rat, (C), triamcinolone (5 mg/kg) treated rat.

Table II depicts the chemical compositions of fraction III lipoprotein subfractions separated by gel-filtration chromatography on a Bio-Gel A5m column (Fig. 2). Although subfraction III-1 from saline-treated control rats was found to be composed of both α- and β-lipoproteins on agarose gel electrophoresis, the chemical composition was rather similar to subfraction III-2 lipoprotein which was composed of almost exclusively α-lipoproteins. When increasing amount of triamcinolone was administered to the animals, the relative contents of cholesteryl ester, free cholesterol and phospholipid increased and the relative content of protein decreased in subfraction III-1 lipoprotein. The chemical composition of subfraction III-1 lipoprotein from rats injected with triamcinolone in a dose of 5 mg/kg body weight is similar to that of rat HDL_1 isolated by density gradient centrifugation [21–23]. The chemical composition of subfraction III-2 lipoproteins from either control or triamcinolone-treated rats is also similar to HDL_2. It has been reported that the rat completely lacks HDL_3 [22].

Fig. 4 shows the apolipoprotein patterns of

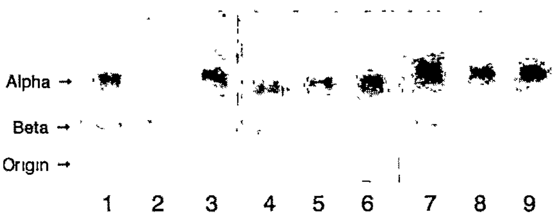

Fig. 3. Agarose gel electrophoresis of lipoproteins from control rats (lanes 1–3), triamcinolone (0.5 mg/kg) treated rats (lanes 4–6) and triamcinolone (5 mg/kg) treated rats (lanes 7–9). Lanes 1, 4 and 7 = fraction III lipoproteins from Bio-Gel A50m column chromatography, lanes 2, 5 and 8 = subfraction III-1 lipoproteins; lanes 3, 6 and 9 = subfraction III-2 lipoproteins.

TABLE II

CHEMICAL COMPOSITION OF FRACTION III LIPOPROTEIN (HDL) SUBFRACTIONS

Values are means ± S.D. for the number of experiments indicated in parentheses. Four to eight rats were used in each experiment

Treatment	Sub-fraction	Components (% by weight)				
		triacyl-glycerol	cholesteryl ester	free cholesterol	phospholipid	protein
Saline (5)	III-1	6.7±0.9	17.0±1.5	5.3±0.9	27.2±4.2	43.8±5.3
	III-2	1.6±0.7	14.8±0.6	3.2±0.3	31.9±1.5	48.7±1.1
Triamcinolone (5) (0.5 mg/kg)	III-1	4.0±1.1	18.0±1.5	6.2±1.5	35.3±1.8	36.6±2.8
	III-2	1.8±0.8	13.7±0.3	3.4±0.3	35.6±2.0	45.4±1.6
Triamcinolone (7) (5.0 mg/kg)	III-1	2.2±0.9	19.2±1.1	9.4±1.3	39.9±3.2	29.4±3.9
	III-2	1.3±0.5	14.8±0.6	4.5±0.3	37.5±1.3	41.9±0.9
Triamcinolone (4) (5.0 mg/kg)	III-1	1.9±0.3	18.2±0.7	9.2±1.1	40.0±0.8	30.7±2.7
+ACTH (6 IU)	III-2	0.3±0.1	14.8±1.4	4.2±0.6	38.0±1.9	42.7±3.8
ACTH (6 IU) (3)	III-1	2.5±0.8	19.5±2.3	6.6±1.0	39.8±2.7	31.5±1.5
	III-2	0.4±0.1	14.5±1.0	3.2±0.4	37.3±2.7	44.7±3.0

subfractions III-1 and III-2 lipoproteins from control and triamcinolone (5 mg/kg)-treated rats. In subfraction III-1 lipoproteins both from control and triamcinolone-treated rats, apolipoprotein E was preponderant over apolipoprotein A-I. Apolipoprotein A-I was the major component in subfraction III-2 lipoproteins from both control and triamcinolone-treated rats.

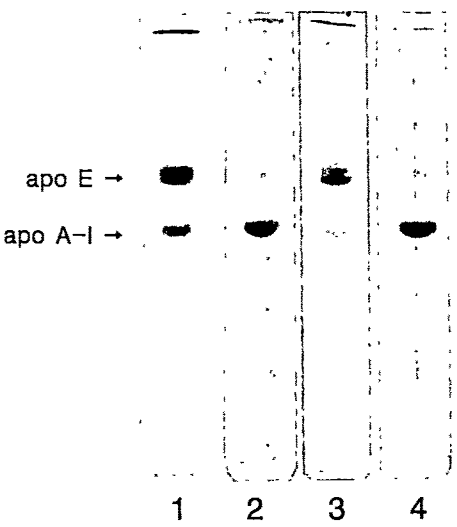

Fig. 4. Sodium dodecyl sulfate polyacrylamide gel electrophoresis of apolipoproteins of subfractions III-1 and III-2 lipoproteins from control (gels 1 and 2) and from triamcinolone (5 mg/kg)-treated rats (gels 3 and 4). Gels 1 and 3 = subfractions III-1; gels 2 and 4 = subfractions III-2. apo, apolipoprotein

On the basis of these observations presented above, subfractions III-1 and III-2 lipoproteins were here designated HDL_1 and HDL_2, respectively.

It was attempted to determine the cholesterol distribution among the lipoprotein subfractions. This was accomplished by estimating the cholesterol mass in the pooled fractions eluted from gel filtration chromatography columns. Fraction I plus II lipoproteins which correspond to chylomicrons (if any), VLDL and LDL were pooled collectively. Table III shows the results of these experiments. The triamcinolone treatment showed no significant changes in the cholesterol concentrations in fraction I plus II (VLDL plus LDL). HDL_1-cholesterol concentration was elevated by the administration of triamcinolone in a dose-dependent manner, and the increase was probably more than 5-fold compared with the control level when triamcinolone in a dose of 5 mg/kg body weight was administered, since LDL contributed considerably to the cholesterol concentration in subfraction III-1 from control animals. The administration of triamcinolone in a

TABLE III

CHOLESTEROL CONCENTRATIONS IN LIPOPROTEIN (SUB)FRACTIONS FROM CONTROL AND TRIAMCINOLONE-TREATED RATS

Values are means ± S.D. for the number of experiments given in parentheses. Five rats were used in each experiment. P values were obtained by Student's t-test. n.s., not significant

Treatment	Cholesterol in lipoprotein (sub)fractions (mg/dl)		
	Fraction I + II (VLDL + LDL)	Subfraction III-1 (HDL$_1$)	Subfraction III-2 (HDL$_2$)
A Saline (3)	16.5 ± 3.7	12.0 ± 6.3	34.2 ± 7.0
B Triamcinolone (0.5 mg/kg) (4)	21.3 ± 7.3	28.7 ± 7.1	43.5 ± 2.3
C Triamcinolone (5.0 mg/kg) (4)	18.9 ± 3.0	58.1 ± 8.4	73.3 ± 11.3
P values for			
A vs. B	n.s.	< 0.025	n.s.
A vs. C	n.s.	< 0.001	< 0.005
B vs. C	n.s.	< 0.005	< 0.005

dose of 0.5 mg/kg body weight did not make any significant change in the concentration of HDL$_2$-cholesterol compared with control rats. When a dose of 5 mg/kg was given, HDL$_2$-cholesterol concentration increased about 2-fold compared with the control level. Results shown in Table III indicate that the hypercholesterolemia induced by the administration of triamcinolone to rats was derived almost entirely from the elevation of cholesterol concentration in HDL fractions.

The effect of ACTH administration on the distribution of cholesterol among the lipoprotein fractions was investigated, since chronic administration of ACTH has been shown to increase the transfer of cholesterol from HDL into rat adrenal glands [24]. Control rats were injected with the same volume of vehicle solution (saline) as used for the hormone-treated animals.

Table IV shows the changes in serum lipids and HDL-cholesterol levels induced by administration of triamcinolone alone, triamcinolone plus ACTH, or ACTH alone. When both ACTH and tri-

TABLE IV

CHANGES IN SERUM LIPIDS AND HDL-CHOLESTEROL INDUCED BY ADMINISTRATION OF TRIAMCINOLONE, ACTH, AND THEIR COMBINATION

Rats were injected with triamcinolone (5 mg/kg b.wt.) or ACTH (Cortrosyn, 6 IU/rat) alone, or the two hormones in combination for 5 days. HDL-cholesterol was determined by precipitation method. Values (mg/dl) are means ± S.D. for the number of rats indicated in parentheses. P values were obtained by Student's t-test. n.s., not significant

Treatment	Total cholesterol	Free cholesterol	Phospholipid	Triacylglycerol	HDL-cholesterol
A Triamcinolone	157 ± 17 (8)	49 ± 7 (8)	283 ± 31 (7)	92 ± 40 (8)	73 ± 15 (7)
B Triamcinolone + ACTH	104 ± 12 (6)	31 ± 4 (6)	214 ± 12 (5)	58 ± 18 (6)	56 ± 5 (5)
C ACTH	67 ± 8 (4)	18 ± 3 (4)	154 ± 13 (3)	92 ± 27 (4)	40 ± 5 (3)
D Saline	61 ± 12 (5)	15 ± 3 (5)	132 ± 15 (4)	87 ± 17 (5)	37 ± 7 (4)
P values for					
A vs. B	< 0.001	< 0.001	< 0.001	n.s.	< 0.05
B vs. C	< 0.001	< 0.001	< 0.001	< 0.05	< 0.005
C vs. D	n.s.	n.s.	n.s.	n.s.	n.s.
A vs. D	< 0.001	< 0.001	< 0.001	n.s.	< 0.005

amcinolone were administered, the serum levels of total and free cholesterol, phospholipid and HDL-cholesterol were intermediate between those from control rats and from animals treated with triamcinolone alone. The administration of ACTH alone produced no change in serum lipids and HDL-cholesterol levels by itself, when compared with the saline-treated control rats. Serum triacylglycerol concentrations were unaffected again by any treatment except when both triamcinolone and ACTH were administered, where the triacylglycerol level tended to be lowered.

The elution patterns of the $d < 1.225$ g/ml fraction (total lipoproteins) from ACTH-treated rats and from rats injected with triamcinolone plus ACTH were essentially similar to those from saline-treated control rats and from triamcinolone (5 mg/kg)-treated rats, respectively. The electrophoretograms of lipoproteins on agarose gel were also similar to those shown in Fig. 3 (data not shown).

The administration of ACTH in triamcinolone-treated rats did not induce any significant alterations in chemical compositions of HDL_1 (subfraction III-1) and HDL_2 (subfraction III-2) (Table II). In rats treated with ACTH alone, the chemical compositions of HDL_1 and HDL_2 (subfractions III-1 and III-2 in Table II, respectively) were very similar to those from rats treated with triamcinolone (0.5 or 5 mg/kg).

Table V shows the cholesterol concentrations in lipoprotein fractions from these various groups of rats. When rats were injected with ACTH in addition to triamcinolone, the cholesterol concentration in HDL_1 was significantly ($P < 0.001$) reduced from 69 mg/dl in the triamcinolone-treated rats to 36 mg/dl in the animals treated with triamcinolone plus ACTH. In contrast, no significant difference in the cholesterol concentration in HDL_2 was found between the groups of rats injected with triamcinolone plus ACTH and rats treated with triamcinolone alone, although the former group tended to have a lower concentration of HDL_2-cholesterol than the latter. The cholesterol concentrations in HDL_1 and HDL_2 from rats injected with triamcinolone plus ACTH were both significantly higher than those from either ACTH-treated or control rats. ACTH-treated rats had significantly higher cholesterol concentration in HDL_1 than control rats, but in other lipoprotein fractions no significant difference in the cholesterol concentration was found between the two groups of animals.

The free cholesterol to phospholipid ratios in HDL_1 and HDL_2 are shown in Table VI. HDL_1 had a significantly higher free cholesterol-to-phospholipid ratio than HDL_2 within each group of rats. Also, HDL_1 from both triamcinolone- and

TABLE V

CHOLESTEROL CONCENTRATIONS IN LIPOPROTEIN (SUB)FRACTIONS FROM RATS TREATED WITH TRIAMCINOLONE, ACTH, AND THEIR COMBINATIONS

Rats were injected with triamcinolone (5 mg/kg b.wt.) or ACTH (Cortrosyn, 6 IU/rat) alone, or the two hormones in combination for 5 days. Values are means ± S.D. for the number of experiments indicated in parentheses Three to six rats were used in each experiment. P values were obtained by Student's t-test. n.s., not significant

Treatment		Cholesterol in lipoprotein (sub)fractions (mg/dl)		
		Fraction I + II (VLDL + LDL)	Subfraction III-1 (HDL_1)	Subfraction III-2 (HDL_2)
A Triamcinolone	(8)	17.6 ± 2 6	68 9 ± 13 2	70.2 ± 11 0
B Triamcinolone + ACTH	(5)	13.1 ± 2 9	35.9 ± 4.4	56.6 ± 13 5
C ACTH	(4)	11.7 ± 3 1	21.0 ± 2.3	34.6 ± 3.7
D Saline	(5)	14.3 ± 5.1	13.7 ± 5 4	33.1 ± 5.9
P values for				
A vs B		< 0.025	< 0.001	n.s
B vs C		n.s	< 0 001	< 0.025
C vs. D		n.s.	< 0.05	n.s
A vs. D		n s	< 0 001	< 0 001

TABLE VI

FREE CHOLESTEROL-TO-PHOSPHOLIPID RATIO IN HDL SUBFRACTIONS

Treatment of rats was the same as described in Table V. Values are means ± S.D. for the number of experiments indicated in parentheses. Three to six rats were used in each experiment. *P* values were obtained by Student's *t*-test. FC, free cholesterol; PL, phospholipid

Treatment	Sub-fraction	FC/PL ratio (w/w)	*P* values for HDL_1 vs. HDL_2
Triamcinolone (4)	HDL_1	0.238 ± 0.027	< 0.001
	HDL_2	0.120 ± 0.019	
Triamcinolone + ACTH (4)	HDL_1	0.231 ± 0.024	< 0.001
	HDL_2	0.109 ± 0.011	
ACTH (3)	HDL_1	0.166 ± 0.018	< 0.005
	HDL_2	0.086 ± 0.004	
Saline (3)	HDL_1	0.182 ± 0.023	< 0.01
	HDL_2	0.098 ± 0.015	

triamcinolone plus ACTH-treated rats showed significantly higher free cholesterol to phospholipid ratios than those from either of the other two groups of rats.

Discussion

In most of the studies in animals, the density limits defined for human serum lipoproteins have been used, tacitly assuming that they are also applicable to the serum lipoproteins of the various animal species. Studies on the metabolism of rat serum lipoproteins are usually also carried out with methods developed for similar experiments in humans. However, there is evidence that the density profile of rat serum lipoproteins is quite divergent from that in man [25]. In this study, lipoproteins were separated by gel-filtration chromatography which fractionates the lipoproteins on the basis of particle size, thus avoiding the inadequacy deriving from resorting to the ultracentrifugal procedure developed for human serum lipoproteins described above.

Although the separation of HDL_1 from HDL_2 was incomplete, the peak which corresponds to HDL_1 was consistently observed in the gel-filtration chromatography. There was a clear distinction between the two lipoprotein fractions in chemical compositions and in apoprotein patterns on SDS-polyacrylamide gel electrophoresis.

HDL_1, originally defined as a cholesteryl ester-rich lipoprotein in which apolipoprotein E is the predominant apolipoprotein, is reported to represent about 24% of the total HDL-cholesterol in male rats [23], while Quarfordt et al. [26] showed that the apolipoprotein E-rich HDL occupied about 10% of the total HDL. The concentration of this minor HDL subfraction is varied according to the dietary and hormonal status or under a certain pathological condition [12,27–29].

The administration of triamcinolone increased the serum concentration of HDL_1-cholesterol most significantly (more than 5-fold control level), followed by HDL_2-cholesterol (about 2-fold compared with the control level). The origin of this increased HDL_1(-cholesterol) is not clear. Eisenberg [30] suggested that HDL_1 is formed in plasma, probably from HDL_2 (or heavier HDL populations), and the origin of apolipoprotein E in HDL_1 is most probably lipolysis of triacylglycerol-rich lipoproteins.

The change in HDL-cholesterol concentration shown in Table I is a relatively small fraction of the change in total cholesterol, while in Table III is shown that VLDL plus LDL was not altered. This discrepancy is due to the different methods used. In Table I, HDL-cholesterol was determined by a precipitation method in which apolipoprotein E-containing lipoproteins, i.e. HDL_1, would be readily precipitable as suggested by Mahley and Innerarity [31], while in Table III the cholesterol concentrations in lipoprotein classes were determined following separation of the lipoproteins by a combination of ultracentrifugation and gel-filtration chromatography. Thus, the HDL-cholesterol concentrations obtained by the precipitation method would represent mostly HDL_2, which is apolipoprotein E-poor, rather than HDL_1 plus HDL_2.

It is suggested that hepatic triacylglycerol lipase plays a role in the uptake of HDL by the liver in rats [32,33]. It has also been shown that the lipase activity in the liver decreased when rats were rendered hypercortisolic by the administration of a corticotrophin analogue (Synacthen), and that liver lipase activities in the liver and the adrenal gland change in an opposing way during prolonged corticotrophin administration to rats [34]. Similar situations may have occurred in our triamcinolone-treated rats, though the lipase activity was not measured in this study. Thus, the administration of triamcinolone may reduce the uptake of HDL by the liver in rats. Jansen et al. [34] also suggested that the liver lipase-like activities in liver, adrenals and ovaries may be involved in the hydrolysis of HDL-phospholipids, thereby inducing a flow of free cholesterol to these tissues [35]. These situations seem to occur also in the hypercortisolic rats.

It is conceivable that if the ratio of free cholesterol to phospholipids in the surface of the lipoprotein particle is high, then the lipoprotein is suitable as a donor of free cholesterol to the lipase-containing tissues such as adrenal glands. In this regard, HDL_1, which was accumulated by triamcinolone treatment, might be preferentially utilized as a donor of free cholesterol, since the ratio of free cholesterol to phospholipid in HDL_1 is much higher than in HDL_2 as shown in Table VI.

The changes in HDL levels may be secondary to alterations in liver lipase activity under various conditions including hormonal status. ACTH treatment in rats lowers liver lipase activity [34,36] which seems to facilitate the uptake of HDL by the liver. Thus, ACTH treatment might be expected to raise the plasma HDL level by reducing the hepatic uptake of HDL. In this study, however, ACTH treatment reduced the HDL_1-cholesterol concentration in triamcinolone-treated rats without significantly affecting the HDL_2-cholesterol concentration (Table V). This may be explained partly by an increased adrenal uptake of HDL_1-cholesterol through a stimulation of adrenal cortex by the ACTH treatment. However, this mechanism may not be sufficient to explain the marked fall of HDL_1-cholesterol, and at present we have no alternative explanation. Further work is necessary to clarify this phenomenon.

Acknowledgement

The author is grateful to Dr. H. Matsumiya, Head of the Department of Laboratory Medicine, Hokkaido University School of Medicine, for his continuing interest and support in this study.

References

1 Stern, M.P., Kolterman, O G., Fries, J F., McDevitt, H.O. and Reaven, G M. (1973) Arch. Intern Med. 132, 97–101
2 Friedman, M, Van den Bosch, J, Byers, S.O and St George, S (1965) Am J. Physiol. 208, 94–105
3 Barrett, A.M. (1966) J Endocrinol. 36, 301–316
4 Reaven, E P., Kolterman, O.G and Reaven, G M. (1974) J Lipid Res. 15, 74–83
5 Krausz, Y, Bar-On, H and Shafrir, E. (1981) Biochim Biophys Acta 663, 69–82
6 Cole, T.G., Wilcox, H G and Heimberg, M. (1982) J. Lipid Res. 23, 81–91
7 Schonfeld, G, Felski, C and Howald, M A (1974) J. Lipid Res 15, 457–464
8 Mahley, R W. and Holcombe, K.S. (1977) J Lipid Res. 18, 314–324
9 Gwynne, J.T. and Hess, B. (1980) J Biol Chem 255, 10875–10883
10 Andersen, J.M and Dietschy, J.M. (1978) J Biol. Chem. 253, 9024–9032
11 Kovanen, P T, Faust, J R., Brown, M S. and Goldstein, J.L. (1979) Endocrinology 104, 599–609
12 Mitamura, T. (1984) J. Biochem. 95, 29–36
13 Rudel, L L., Lee, J A., Morris, M D. and Felts, J.M. (1974) Biochem. J. 139, 89–95
14 Allain, C C., Poon, L S., Chan, C S.G, Richmond, W. and Fu, P C (1974) Clin Chem. 20, 470–475
15 Fletcher, M.J (1968) Clin Chim. Acta 22, 393–397
16 Hoeflmayr, J and Fried, R. (1966) Medizin Ernährung 7, 9–10
17 Lowry, O.H., Rosebrough, N J., Farr, A L and Randall, R.J (1951) J Biol. Chem 193, 265–275
18 Markwell, M.A., Haas, S.M., Bieber, L L and Tolbert, N E (1978) Anal. Biochem 87, 206–210
19 Weber, K. and Osborn, M. (1975) in The Proteins (Neurath, H. and Hill, R L, eds), Vol I, pp. 179–223, Academic Press, New York
20 Scanu, A.M and Edelstein, C. (1971) Anal Biochem 44, 576–588
21 Lusk, L T., Walker, L F., DuBien, L H and Getz, G S. (1979) Biochem. J 183, 83–90
22 Oschry, Y and Eisenberg, S (1982) J Lipid Res 23, 1099–1106
23 Jansen, H., Schoonderwoerd, G.C. and Dallinga-Thie, G M. (1983) Biochim. Biophys Acta 754, 271–278
24 Gwynne, J.T., Mahaffee, D, Brewer, H B., Jr, and Ney, R L. (1976) Proc. Natl Acad. Sci. USA 73, 4329–4333
25 Terpstra, A H.M., Sanchez-Muniz, F J, West, C.E and Woodward, C J H (1982) Comp Biochem Physiol. 71B, 669–673
26 Quarfordt, S.H, Jain, R S., Jakoi, L, Robinson, S and Shelburne, F (1978) Biochem. Biophys. Res Commun. 83, 786–793
27 Weisgraber, K H., Mahley, R.W and Assmann, G (1977) Atherosclerosis 28, 121–140
28 Mitamura, T., Keimatsu, M and Imai, Y (1979) Biochim. Biophys Acta 575, 92–101

29 Patsch, W., Kim, K., Wiest, W. and Schonfeld, G (1980) Endocrinology 107, 1085–1094

30 Eisenberg, S. (1984) J. Lipid Res. 25, 1017–1058

31 Mahley, R.W. and Innerarity, T L. (1977) J Biol Chem. 252, 3980–3986

32 Kuusi, T , Kinnunen, P.K.J. and Nikkilä, E A. (1979) FEBS Lett 104, 384–388

33 Jansen, H., Van Tol, A. and Hülsmann, W.C. (1980) Biochem Biophys Res. Commun. 92, 53–59

34 Jansen, H., Schoonderwoerd, K., Baggen, M.G.A and De Greef, W.J (1983) Biochim. Biophys. Acta 753, 205–212

35 Jansen, H. and Hülsmann, W.C. (1980) Trends Biochem. Sci. 5, 265–268

36 Schoonderwoerd, K , Hülsmann, W C. and Jansen, H. (1983) Biochim. Biophys. Acta 754, 279–283

Biochimica et Biophysica Acta 917 (1987) 131–139
Elsevier

BBA 52439

Isolation of protein components from rat lung lamellar bodies

J.G. Nijssen [a], D. Hardeman [a], H.N.M. Lucas Luyckx [a], L.W. Promes [a], J.A. Post [b] and H. van den Bosch [a]

[a] *Laboratory of Biochemistry and*
[b] *Institute of Molecular Biology, State University of Utrecht, Utrecht (The Netherlands)*

(Received 30 May 1986)

Key words: Lamellar body; Protein component; (Rat lung)

Lamellar bodies isolated from 10% (w/v) rat lung homogenates by discontinuous sucrose gradient centrifugation were shown to contain variable amounts of adhering proteins. These contaminating proteins could be removed by either Sepharose 4B gel filtration or precipitation of the crude preparation at pH 11.5. Both purification methods yielded membrane preparations with a phospholipid-to-protein ratio of 10.0 μmol/mg. Nearly complete separation of lamellar body phospholipid and protein could be achieved upon application of the purified membranes to DEAE-cellulose in the presence of 0.2% (v/v) Triton X-100. Phospholipid analyses showed that 83% of total lipid phosphorus was recovered in phosphatidylcholine. In phosphatidylethanolamine, phosphatidylglycerol, phosphatidylserine and phosphatidylinositol recoveries amounted to 4, 8, 2 and 2%, respectively. Molecular mass determinations of the isolated protein component of lamellar bodies by means of SDS polyacrylamide gel electrophoresis and staining with Coomassie brilliant blue revealed the presence of three protein bands with molecular masses of 64, 33 and 31 kDa. Upon staining with silver a 16 kDa protein was also visible. Sephadex G-100 gel filtration showed only one protein peak corresponding to a molecular mass of 64 kDa when protein was assayed with Coomassie brilliant blue.

1. Introduction

Pulmonary surfactant is a complex of phospholipids and proteins, synthesized in type II pneumocytes. The most important function of surfactant is to maintain a low and variable surface tension at the alveolar air/liquid interface (See Refs. 1 and 2 for recent reviews). It is generally accepted that the lamellar bodies are the intracellular storage sites for surfactant. The lamellar bodies are secreted from the type II pneumocyte into the alveolar lumen by exocytosis. There, the lamellar body is converted into tubular myelin. Tubular myelin is considered to be another morphologic form of surfactant and is composed of membranes arranged into a square lattice [8,9]. This structure is thought to be the immediate precursor of the surfactant film that lines the alveolar surface. The morphogenesis of the lamellar body is still unclear, though it has been suggested that it is a modified lysosome [3]. This hypothesis was supported by the observations that lamellar bodies, as well as the precursors of lamellar bodies, i.e. the multivesicular bodies, contain lysosomal marker enzyme activities [4–7].

The discovery of phosphatidate phosphohydrolase activity in the lamellar body membrane [10–15] has led to a number of controversial reports on the possible role of this organelle in phospholipid biosynthesis. However, it has now

---

Correspondence: Dr. H van den Bosch, Laboratory of Biochemistry, State University of Utrecht, Padualaan 8, NL-3584 CH Utrecht, The Netherlands

0005-2760/87/$03.50 © 1987 Elsevier Science Publishers B V. (Biomedical Division)

been demonstrated that lamellar bodies lack both cholinephosphotransferase [16] and glycerophosphate acyltransferase [17]. The absence of cholinephosphotransferase excludes the possibility that lamellar bodies can synthesize phosphatidylcholine de novo. Furthermore, it was shown that lamellar bodies are incapable of de novo phosphatidylglycerol biosynthesis [18].

Lamellar bodies are characterized by a high content of phosphatidylcholine, 50–70% of which is the dipalmitoyl species [19–22]. The high phospholipid content of the lamellar bodies allows the separation from other organelles by density gradient centrifugation. The recoveries and the composition of the lamellar bodies isolated with density gradients, however, showed considerable differences [23–25].

In this paper we describe a simple and rapid isolation of rat lung lamellar bodies from 10% (w/v) lung homogenates yielding organelles with highly reproducible phospholipid-to-protein ratios. The isolation procedure includes a discontinuous sucrose gradient centrifugation and the subsequent removal of variable amounts of non-lipid associated protein by filtration over Sepharose 4B. Precipitation of the crude lamellar body preparation at alkaline pH yielded membranes with similar lipid/protein ratios. After delipidation, SDS-gel electrophoresis gave four protein bands, corresponding to molecular masses of 64, 33, 31 and 16 kDa, after staining with silver. Coomassie brilliant blue did not stain the 16 kDa protein. Sephadex G-100 gel filtration revealed only one protein peak, corresponding to a molecular mass of 64 kDa.

Materials and Methods

Materials

Sephadex G-100 and Sepharose 4B were purchased from Pharmacia, Sweden. [*phenyl*(n)-^{3}H]Triton X-100 (5 mCi/mg) was bought from New England Nuclear, U.S.A. Triton X-100 was a product of Rohm and Haas, U.S.A., and Bio-Beads SM-2 of Bio-Rad, U.S.A. Aquacide III was obtained from Calbiochem, France, and DEAE-cellulose DE 52 from Whatman, U.K. All other chemicals were products of either Merck, F.R.G., or Fluka, Switzerland, and were of standard laboratory grade.

Methods

The isolation of rat lung lamellar bodies and derived membranes. Lungs of adult male Wistar rats (200–250 g) were excised after decapitation and washed in 0.75 M sucrose/1 mM EDTA/10 mM Tris, adjusted to pH 7.4 with 6 M HCl (buffer A). A 10% (w/v) homogenate was prepared in the same buffer. The homogenate was centrifuged for 10 min at 600 × *g*. The pellet was discarded. 6-ml aliquots of the supernatant were overlaid with 9 ml each of 0.66 M and 0.30 M sucrose in buffer, consecutively. The gradients were centrifuged overnight at 20000 rpm at 4°C in a Beckman L2-65 ultracentrifuge with an SW-27 rotor. When the run was completed, the crude lamellar body material was collected from the interface between 0.66 M and 0.30 M sucrose. Subsequently, lamellar bodies were purified by gel-permeation chromatography on Sepharose 4B (conditions specified in the legend of Fig. 1). Lamellar body membranes were prepared from the crude preparation by a precipitation at alkaline pH as described by Fujiki et al. [26]. In the latter procedure the lamellar body material from the gradient was dialyzed overnight against 100 mM NH_4HCO_3 (pH 7.4) and concentrated by dialysis against Aquacide III to a final concentration of 0.2–0.5 mg protein per ml. Subsequently, the solution was adjusted to pH 11.5 with 6 M NaOH, incubated for 30 min at 0°C and finally centrifuged for 30 min at 35000 rpm at 4°C in an SW-41 rotor When the run was completed the supernatant was discarded and the pellet was rinsed once with ice-cold water.

Delipidation of purified lamellar bodies. The delipidation of the lamellar bodies was performed essentially as described by Sueishi and Benson for the delipidation of surfactant protein [27]. After precipitation at pH 11.5 as described, the pellet, containing the lamellar bodies, was dissolved in 0.1 M NaCl/0.2% (v/v) Triton X-100/5 mM Tris/3 mM EDTA (pH 8.0) (buffer B) to a final concentration of about 1 mg protein per ml. The solubilized lamellar bodies were applied onto DEAE-cellulose. The column was eluted with 60 ml buffer B before a linear NaCl gradient was started, ranging from 0.1 to 0.5 M. The lipid and protein peaks were collected separately and Triton X-100 was removed by extensive dialysis against 1

M KCl/10% (v/v) glycerol/1 mM EDTA/10 mM Tris (pH 7.4) (buffer C). Dialysis was facilitated by the addition of 6 mg/ml Bio-Beads SM-2 to the dialysis buffer, according to the method of Philippot et al. [28]. The protein peak was concentrated by dialysis against Aquacide III to a final concentration of about 200 μg/ml and stored at 4°C.

Electrophoresis. Sodium dodecyl sulfate (SDS) polyacrylamide gel electrophoresis was performed according to the method of Laemmli [29]. A 10% polyacrylamide gel was run with phosphorylase *b*, bovine serum albumin, ovalbumin, carbonic anhydrase, soybean trypsin inhibitor and α-lactalbumin as molecular weight standards. After delipidation and subsequent removal of Triton X-100, the protein sample was dialyzed against 100 mM NH_4HCO_3 (pH 7.4) and lyophilized. The lyophilized protein was mixed with 4% (w/v) SDS/10% (v/v) glycerol/65 mM Tris (pH 6.7) in presence or absence of 100 mM dithiothreitol with Bromophenol blue as a tracking dye. The gel was stained, according to the method of Righetti and Chillemi [30] and then with silver, according to Merril [31].

Phospholipid composition of rat lung lamellar bodies. Lamellar bodies were isolated from 10% (w/v) rat lung homogenates and purified by precipitation at pH 11.5 as described. Phospholipids were extracted according to the method of Bligh and Dyer [32] and separated by two-dimensional chromatography on silica-gel type 60 H thin-layer plates. The plates were developed in $CHCl_3$/CH_3OH/14 M NH_4OH/H_2O (90:54:5.5:5.5, v/v) and $CHCl_3$/CH_3OH/CH_3COOH/H_2O (90:40:12:2, v/v), respectively. Lipid phosphorus was determined from the silica gel as described by Rouser et al. [33].

Analytical Procedures. Protein was determined according to the method of Bradford [34], as modified by Vianen and van den Bosch [35]. When Triton X-100 was present, protein was quantitated as described by Lowry et al. [36], after centrifugation of the precipitate formed [37]. Phosphorus in lipid extracts was measured after ashing [38], according to Chen et al. [39]. Radioactivity was measured after addition of Packard emulsifier scintillation fluid in a Packard 3320-Tricarb liquid scintillation spectrometer.

Morphological studies. Lamellar bodies were isolated from 10% (w/v) lung homogenates and purified by either Sepharose 4B gel-filtration or precipitation at pH 11.5, as described. Membrane preparations were fixed by incubation for 1 h in 2.5% glutaraldehyde/2% tannic acid in 100 mM phosphate buffer (pH 7.2). Post-fixation was performed by incubation for 30 min in 1% OsO_4/1.5% $K_4Fe(CN)_6$ in the same buffer. The samples were stained en bloc with 1% uranyl acetate, dehydrated with the use of acetone and embedded in araldite resin. Thin sections were cut on a Rickert Om-U_2 ultramicrotome using a diamond knife. The sections were stained with 1% $KMnO_4$ and examined in a Philips 201 electron microscope.

Results and Discussion

In this paper we describe the isolation of rat lung lamellar body protein. For that purpose we developed a two-step isolation procedure for lamellar bodies, including a discontinuous sucrose gradient centrifugation and a subsequent purification of the lamellar body material recovered from the gradient. Fig. 1 shows the elution profiles on Sepharose 4B of two lamellar body preparations recovered from different sucrose gradient centrifugations. From this figure it becomes evident that lamellar bodies separated from other organelles by a single-step gradient centrifugation may contain a variable amount of adhering protein that is not associated with phospholipid. Since these adhering proteins are not an integral constituent of the lamellar body it is possible that they originate from other subcellular fractions and aspecifically interact with the lamellar body membrane. It was demonstrated by Fujiki et al. [26] that membranes can be freed from peripheral proteins by centrifugation at pH 11.5. At alkaline pH the proteins become negatively charged and are repelled by the membrane through electrostatic forces. After centrifugation, the membrane phospholipids together with the membrane-bound proteins are recovered in the pellet. This method appeared applicable to the purification of lamellar bodies. In Table I the results of both purification procedures are summarized. The total yield of purified rat lung lamellar bodies ranged between 300–500 μg protein/g wet weight. Both purification on

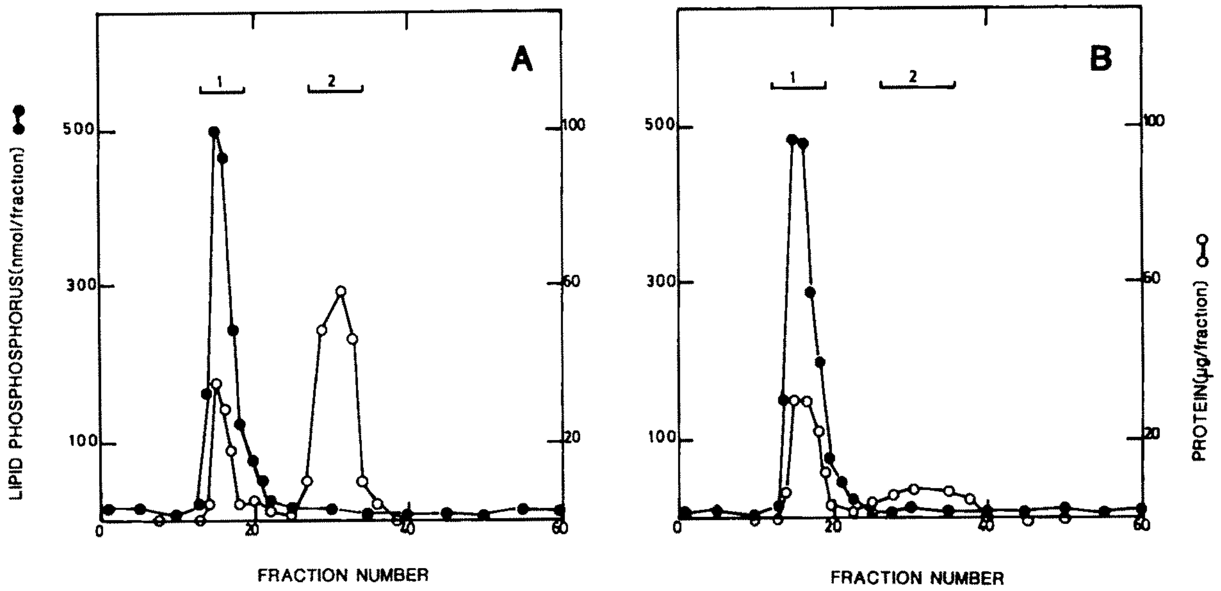

Fig. 1. Lamellar bodies from sucrose gradient centrifugations on Sepharose 4B. Lamellar bodies were isolated from 600 × *g* rat lung supernatants as described under Materials and Methods Sepharose 4B column (65 × 0.8 cm) was run with 0.3 M sucrose/1 mM EDTA/10 mM Tris (pH 7.4) at a flow rate of 20 ml/h and 10 min fractions were collected. Panels A and B show the elution patterns of lamellar body preparations, from repeated sucrose gradients, containing 555 and 168 μg protein, respectively In B, the pooled fractions under 1 and 2 contained 104 and 40 μg protein, respectively. In (A), 94 μg protein was recovered in pool 1 and 388 μg in pool 2. Total recovery of lipid phosphorus amounted to 91 and 92% for experiments A and B, respectively. The content per fraction of lipid phosphorus (●——●) and protein (○——○) is depicted

Sepharose 4B and precipitation at pH 11.5 at 0°C yielded membranes with phospholipid-to-protein ratios of 10.0 μmol/mg. In the purified preparations no microsomal marker enzyme activity could be detected. The same phospholipid-to-protein ratios were found when freshly isolated, perfused rat lungs were used (data not shown). For rat lung lamellar bodies phospholipid to protein ratios have been reported ranging from 4 to 16 μmol/mg [25,40–43]. It is quite likely that the isolation techniques used yielded lamellar body preparations together with contaminating adhering proteins as shown in Fig. 1 and Table I. In the following experiments for the isolation of the protein components we used the precipitation at alkaline pH as purification for the lamellar bodies membranes from the sucrose gradients. This procedure is less laborious than Sepharose 4B chromatography and the lamellar bodies are recovered as a pellet, allowing them to be dissolved in any solvent required.

However, upon precipitation at alkaline pH the ultrastructure of the lamellar body is destroyed. In

TABLE I

PHOSPHOLIPID-TO-PROTEIN RATIOS OF LAMELLAR BODIES PURIFIED BY SEPHAROSE 4B GEL CHROMATOGRAPHY OR PRECIPITATION AT pH 11.5 AT 0°C

Sepharose 4B was run as described in the legend of Fig 1. The precipitation at pH 11.5 at 0°C was performed as described under Materials and Methods. Ratios are expressed as μmol lipid phosphorus per mg protein. Letters A and B refer to the experiments shown in Fig 1. In both experiments the fractions under peak 1 were pooled, prior to phospholipid and protein analysis The results of the purification by precipitation at alkaline pH are given as means ± S.E from three experiments

Purification	Ratio before purification (μmol/mg)	Ratio after purification (μmol/mg)
Sepharose 4B		
Expt. A	2.5	10.0
B	7.4	10.0
Precipitation at 0°C, pH 11.5	6.9 ± 2.0	10.4 ± 0.2

agreement with the results of Fujiki et al. [26], we observed sheets of membranes rather than the typical multilamellar structures (micrographs not shown). In contrast, when Sepharose 4B gel filtration was used as a means for purification of the crude lamellar body preparation, the structural integrity of the organelle is maintained to the same degree as observed after sucrose gradient isolation alone (Fig. 2).

Afer purification, the lamellar bodies were solubilized in 0.2% Triton X-100. The lipid and protein components were separated on a DEAE-cellulose anion exchanger at pH 8.0. In Fig. 3 the elution profile of the solubilized lamellar bodies on DEAE-cellulose is depicted. This figure shows that nearly complete separation of phospholipid and protein could be achieved. All phospholipid, with minor amounts of protein, passed through by the column at pH 8.0, whereas the major protein peak could be eluted only in the presence of 0.35 M NaCl. In the protein peak no phospholipid was detectable. Application of rat-lung surfactant on DEAE-cellulose in 1% Triton X-100 at pH 8.0 showed, three different protein peaks, as reported by Sueishi and Benson [27]. Two peaks that eluted with 0.1 M and 0.15 M NaCl, respectively, were designated by the authors to be serum components. The third peak eluted with 0.35 M NaCl and was shown to be the surfactant-associated apolipoprotein with a molecular mass of 73 kDa. Table II shows the phospholipid composition of the purified lamellar bodies. Phosphatidylcholine is the most abundant phospholipid in the lamellar body membrane (83% of lipid phosphorus). Phosphatidylglycerol, phosphatidylethanolamine, phosphatidylinositol and phosphatidylserine are only minor constituents of the lamellar body. These results are in reasonable agreement with reported values for the phospholipid composition of surfactant [44] and lamellar bodies [25,39]. Since the lamellar body protein and the major surfactant apolipoprotein have comparable elution pro-

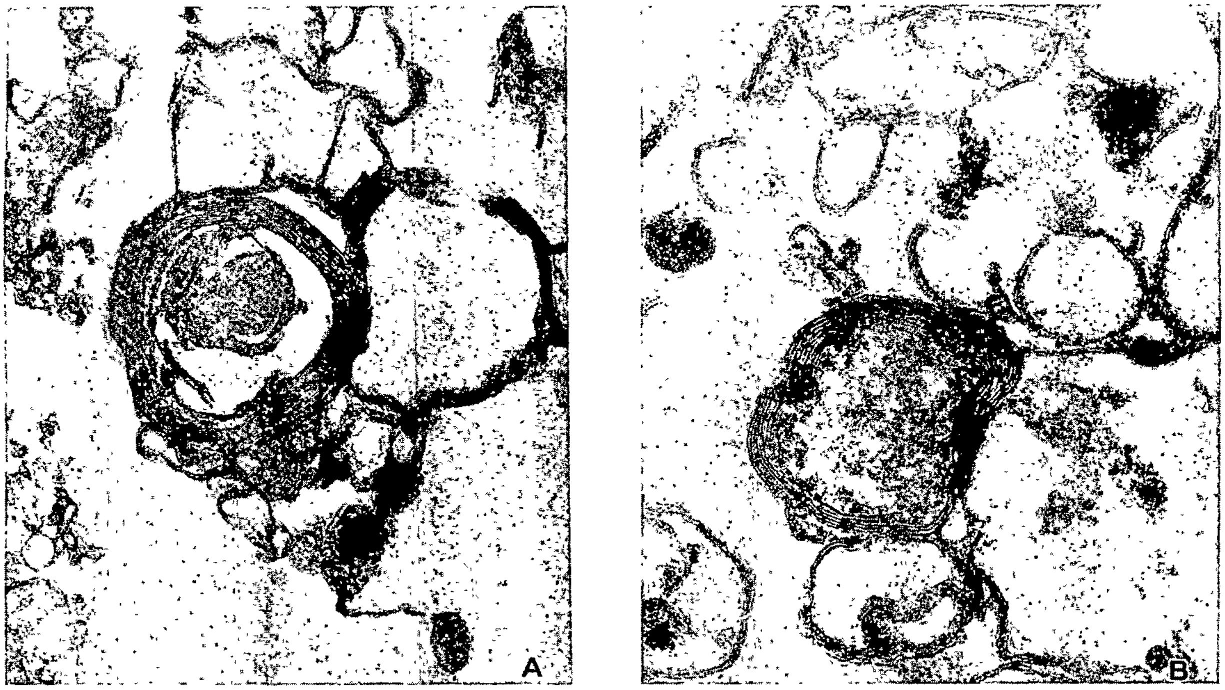

Fig. 2. Effect of Sepharose 4B gel filtration on the ultrastructure of lamellar bodies Lamellar bodies were isolated from 10% (w/v) lung homogenates by density gradient centrifugation and purified by Sepharose 4B gel filtration. Samples were taken and prepared for thin-section electron microscopy, as described in Materials and Methods. (A) Lamellar bodies isolated by sucrose gradient centrifugation alone (×43300 as shown), (B) Lamellar bodies purified by Sepharose 4B gel filtration (×43300 as shown)

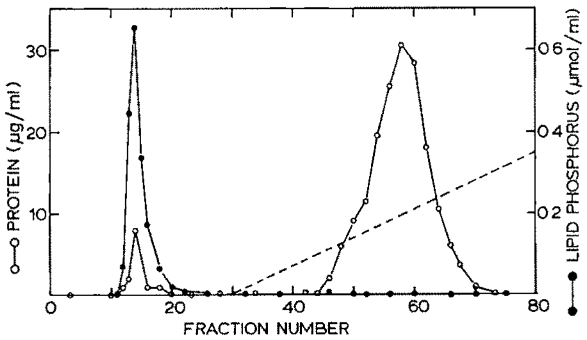

Fig. 3. Lamellar bodies chromatographed on DEAE-cellulose in 0.2% Triton X-100. Lamellar bodies from sucrose gradient centrifugations were purified by precipitation at pH 11.5 at 0 °C and subsequently solubilized in 0.2% (v/v) Triton X-100 as described in Materials and Methods. The DEAE-cellulose column (45×0.6 cm) was run at a flow rate of 12 ml/h and 12-min fractions were collected. Purified lamellar bodies, containing 950 µg protein were applied onto the column. The broken line (— — —) indicates the slope of the NaCl gradient, ranging from 0.1 to 0.5 M. The protein (O———O) and lipid phosphorus (●———●) concentration of the fractions are given. Recoveries of protein and lipid phosphorus amounted to 89 and 91%, respectively.

files on DEAE-cellulose, we decided to investigate further the similarity of these proteins. Interestingly, recent immunohistochemical studies have demonstrated that antibodies against the surfactant apoprotein react with lamellar bodies [45,56,57]. Vice versa, antibodies against proteins from lamellar body-enriched homogenates were shown to react with type II cells as well as the surfactant [46].

TABLE II

PHOSPHOLIPID COMPOSITION OF RAT LUNG LAMELLAR BODIES

Phospholipids from rat lung lamellar bodies were extracted and separated by two-dimensional thin-layer chromatography as described in Materials and Methods. Data are given as percentage of total lipid phosphorus and are expressed as means ± S.E. from three experiments.

Phospholipid	Relative abundance (%)
Phosphatidylcholine	83±2
Phosphatidylethanolamine	4±2
Phosphatidylglycerol	8±1
Phosphatidylserine	2±1
Phosphatidylinositol	2±1

We performed molecular mass determinations on the isolated lamellar body protein. Prior to the molecular mass determinations, Triton X-100 had to be removed from the protein. This was done by dialysis, as described in the Materials and Methods section. Despite the addition of 6 mg/ml Bio-Beads SM-2 to the buffer, a dialysis time of 72 h was required to remove 95% of added [^{3}H]Triton X-100. Addition of Bio-Heads SM directly to the protein solution resulted in a complete loss of protein from the supernatant, probably due to binding of the protein itself to the Bio-Beads (data not shown). After removal of Triton X-100, the protein was subjected to molecular weight determinations by Sephadex G-100 gel filtration and SDS polyacrylamide gel electrophoresis.

In Figs. 4 and 5 are depicted the results of the molecular mass determination on Sephadex G-100. The lamellar body protein eluted in one peak with a molecular mass of about 64 kDa. When the protein was kept at 4°C for several weeks and re-eluted over Sephadex G-100, a second peak appeared with an apparent molecular mass of about 35 kDa (data not shown). SDS-polyacrylamide gel electrophoresis (Fig. 6) of the lamellar body protein revealed the presence of three protein bands corresponding to molecular masses of 64, 33 and 31 kDa, respectively. The molecular masses are in good agreement with the value reported for the surfactant apolipoproteins [44,47,48]. In the presence of a sulfhydryl reducing agent, the surfactant apolipoprotein with a molecular weight of about 68 kDa is reduced to a molecular mass of 35–38 kDa [49,50]. The protein isolated from lamellar bodies was unaffected by the presence of dithiothreitol. The reason behind this different behavior of the surfactant apolipoprotein and the lamellar body protein towards sulfhydryl reducing agents is not known. We suppose that the 33 and 31 kDa proteins as seen in SDS gels associate to a 64 kDa component under the conditions of Sephadex G-100 filtration. Whether the 16 kDa protein seen in SDS gels with silver staining also associated under the conditions of the Sephadex filtration cannot be deduced from the experiments performed, since this protein may not have been detected in the fractions eluted from the Sephadex G-100 column because of its low response in Coomassie brilliant blue binding

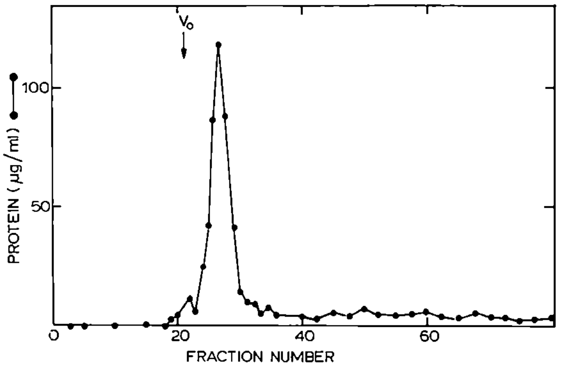

Fig. 4 Lamellar body protein subjected to Sephadex G-100 gel filtration. Lamellar body protein was isolated as described under Materials and Methods and dissolved in 1 M KCl/10% (v/v) glycerol/1 mM EDTA/10 mM Tris (pH 7.4) Lamellar body protein, 965 µg, was eluted in the same buffer. Sephadex G-100 column (45×1 cm) was run at 20 ml/h and 6 min fractions were collected. Void volume (V_0) was determined with Dextran blue. Protein recovery amounted to 86%

(compare Fig. 5). In this respect it is striking that also the 11–16 kDa protein isolated from lung surfactant was found to stain poorly with Coomassie brilliant blue [51]. Hence, it cannot be excluded that part of this protein is also present in the breakthrough peak of the DEAE-cellulose column (Fig. 3) together with the phospholipids. Only a few reports are available on the characterization of lamellar body proteins [45,47,52–54,58]. In these papers proteins are described with molecular masses ranging from 16–130 kDa. Most reports show the presence of a protein with a molecular mass of about 65–70 kDa together with other proteins with variable molecular masses. The wide range of molecular weights for lamellar body proteins can probably be explained in the same way as the wide range in phospholipid-to-protein ratios reported for lamellar bodies, i.e., by the occurrence of a variable amount of adhering, non-lamellar body proteins.

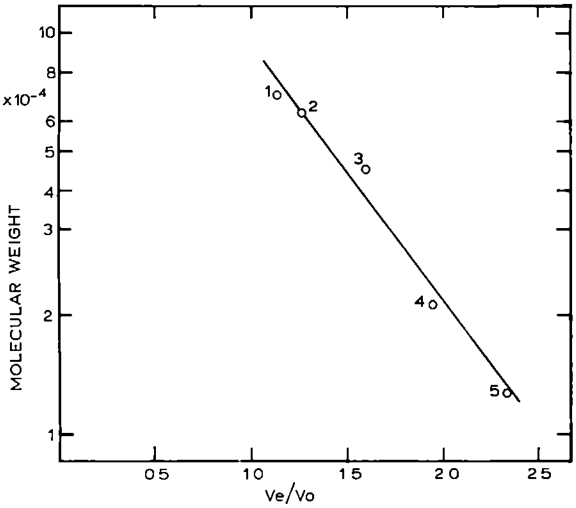

Fig. 5. Molecular mass estimation of lamellar body protein on Sephadex G-100. Sephadex G-100 was run under the same conditions as described in the legend of Fig. 4. Void volume was determined with Dextran blue. Standard proteins and lamellar body protein were eluted from the column and the ratio of the respective elution volume over void volume (V_e/V_o) was plotted against the molecular mass (1) Bovine serum albumin. (2) Rat lung lamellar body protein. (3) Ovalbumin (4) Soybean trypsin inhibitor (5) Cytochrome *c*

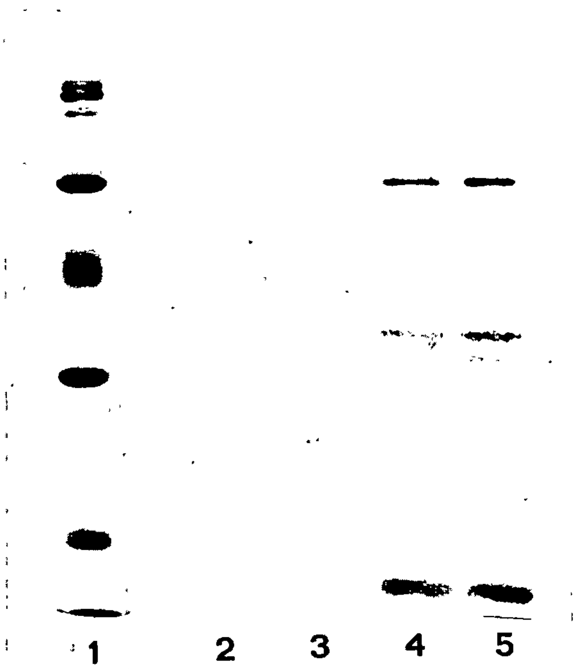

Fig. 6. SDS-polyacrylamide gel electrophoresis of lamellar body protein. Lamellar body protein was isolated from lung homogenates as described in Materials and Methods. Electrophoresis was performed with 30 µg lamellar body protein in the presence (lanes 2 and 4) or absence (lanes 3 and 5) of 100 mM dithiothreitol A 10% gel was run. Lane 1 shows the electrophoretic pattern of marker proteins with molecular masses of 94, 67, 43, 30, 20.1 and 14.4 kDa, respectively. The gel was stained with Coomassie brilliant blue (lanes 1–3) and subsequently with silver (4 and 5)

Collectively, the isolation of lamellar bodies described in this paper eliminates the problem of adhering proteins and could therefore be a useful means in studies on the role of this organelle in surfactant metabolism. Some aspects of the interaction of the protein from lamellar body with phospholipids are described in the accompanying paper [55].

Acknowledgements

These studies were carried out under the auspices of the Netherlands Organization for the Advancement of Pure Research (Z.W.O.) with financial aid from the Netherlands Foundation for Chemical Research (S.O.N.).

References

1 Possmayer, F., Yu, S-H., Weber, J.M. and Harding, P.G.R. (1984) Can. J. Biochem Cell Biol. 62, 1121–1133
2 Rooney, S.A. (1985) Am. Rev. Respir Dis. 131, 439–460
3 Hoffman, L. (1972) J. Cell. Physiol 79, 65–72
4 Balis, J. and Conen, P.E. (1964) Lab Invest. 13, 1214–1229
5 Kuhn, C. (1968) Am. J. Pathol. 53, 809–833
6 Heath, M.F., Gandy, G and Jacobson, W (1976) in Lysosomes in Biology and Pathology (Dingle, J T and Dean, R T, eds), Vol 5, pp. 33–58, Elsevier/North-Holland, Amsterdam
7 DiAugustine, R P (1974) J. Biol. Chem. 249, 584–593
8 Williams, M.C. (1982) Exp. Lung Res 4, 37–46
9 Williams, M.C. (1978) J Ultrastructure Res. 64, 352–361
10 Schultz, F.M, Jimenez, J.M., McDonald, P C.M. and Johnston, J.M. (1974) Gynecol. Invest 5, 222–229
11 Adamson, I Y.R. and Bowden, R H. (1973) Exp Mol Pathol. 18, 112–124
12 Meban, C.J (1972) J. Cell. Biol 53, 249–252
13 Spitzer, H.L. and Johnston, J.M (1978) Biochim. Biophys Acta 531, 275–285
14 Crecelius, C A and Longmore, W J. (1983) Biochim. Biophys. Acta 750, 447–456
15 Casola, P G., McDonald, P M, McMurray, W.C C and Possmayer, F (1982) Exp. Lung Res 3, 1–16
16 Baranska, J. and van Golde, L.M G (1977) Biochim Biophys. Acta 488, 285–293
17 Garcia, A, Sener, S F and Mavis, R.D. (1976) Lipids 11, 109–112
18 Hallman, M. and Gluck, L. (1980) Pediatr. Res 14, 1250–1259
19 Engle, M J, Sanders, R.L and Longmore, W.J (1976) Arch. Biochem Biophys 173, 586–595
20 Jobe, A., Kirkpatrick, E. and Gluck, L. (1978) J Biol. Chem. 253, 3810–3816
21 King, R.J. and Clements, J.A. (1972) Am. J Physiol. 223, 715–726
22 Rooney, S.A., Page-Roberts, B A and Motyama, E.K. (1975) J Lipid Res. 16, 418–425
23 Gil, J. and Reiss, O K (1973) J Cell. Biol 58, 152–171
24 Page-Roberts, B.A (1972) Biochim. Biophys. Acta 260, 334–338
25 Hallman, M and Gluck, L. (1975) Biochim. Biophys. Acta 409, 172–191.
26 Fujiki, Y, Hubbard, A L., Fowle, S. and Lazarow, P B (1982) J. Cell Biol. 93, 97–102
27 Sueishi, K. and Benson, B J (1981) Biochim. Biophys. Acta 665, 442–453
28 Philippot, J. Mutaftschiev, S. and Liautard, J P (1983) Biochim Biophys Acta 734, 137–143
29 Laemmli, U.K. (1970) Nature 227, 680–685
30 Righetti, P.G. and Chillemi, F (1978) J. Chromatogr 157, 243–251
31 Merril, C.C. (1981) Science 211, 1437–1438
32 Bligh, E.G. and Dyer, W J. (1959) Can J. Biochem 37, 911–917
33 Rouser, G. Siakotos, A N and Fleisher, S. (1966) Lipids 1, 85–86
34 Bradford, M.M. (1976) Anal. Biochem 72, 248–254
35 Vianen, G.M. and van den Bosch, H. (1978) Arch Biochem Biophys. 190, 373–384
36 Lowry O.H, Rosebrough, N J., Farr, A L. and Randall, R J (1951) J. Biol. Chem 193, 165–175
37 Shiu, R P.C and Friesen, H.G. (1974) J Biol Chem 249, 7902–7911
38 Ames, B.N. and Dubin, D.T. (1960) J Biol. Chem. 235, 769–775
39 Chen, P.S., Toribara, T.Y. and Warner, H (1956) Anal Chem. 28, 1756–1758
40 Chander, A, Dodia, C.R., Gil, J and Fisher, A.B (1982) Biochim Biophys. Acta 753, 119–129
41 Boudreau, J., Beaudoir, A.R. and Nadeau, D (1982) Can J Biochem Cell Biol. 61, 231–239
42 Duck-Chong, C.G. (1978) Life Sci 22, 2025–2030
43 Gilder, H, Haschemeyer, R.H, Flairclough, Jr., G.F. and Mynarick, D.C (1981) J. Lipid Res. 22, 1277–1285
44 Yu, S, Harding, P G R, Smith, N and Possmayer, F. (1983) Lipids 18, 522–529
45 Balis, J U., Paterson, J F, Paciga, J.E., Haller, E.M. and Shelly, S A. (1985) Lab. Invest 52, 657–669
46 Kumar, R.K, Lykke, A.W.J., Truskott, J.Y., Watkins, S.G. and Smith, G.J (1985) Lung 163, 243–253
47 Bhattacharyya, S N., Passero, M.A., DiAugustine, R P and Lynn, W.S (1975) J. Clin. Invest. 55, 914–920
48 Katyal, S L and Singh, G (1984) Biochim Biophys Acta 794, 411–418
49 King, R.J. (1974) Fed. Proc. 33, 2238–2247
50 King, R J and Martin, H. (1980) J. Appl Physiol Respirat. Environ. Exercise Physiol 48, 812–820
51 Claypool, W.D, Wang, D.L., Chander, V. and Fisher, A.B. (1984) Exp. Lung Res 6, 215–222
52 Tsao, F H C and Zachman, R D (1977) Pediatr Res 11, 849–857
53 Phizackerley, P.J R., Town, M h and Newman, G.E (1979) Biochem. J 183, 731–736

54 Cavalieri, R L and Woodling, S (1984) Am J. Obstet Gynecol 150, 409–414

55 Nijssen, J.G , Promes, L W , Hardeman, D. and van den Bosch, H (1987) Biochim Biophys. Acta 917, 140–149

56 Coalson, J J., Winter, V T., Martin, H.M. and King, R.J (1986) Am. Rev. Respir Dis 133, 230–237

57 Walker, S.R., Williams, M.C and Benson, B.J. (1984) Am. Rev. Respir. Dis. 129, A295

58 Bhattacharyya, S N., Rose, M.C , Lynn, M.G , MacLeod, C., Alberts, M. and Lynn, W S. (1976) Am Rev. Respir Dis. 114, 843–850

Biochimica et Biophysica Acta 917 (1987) 140–147
Elsevier

BBA 52440

Phospholipid-protein interactions in rat lung lamellar bodies

J.G. Nijssen, L.W. Promes, D. Hardeman and H. van den Bosch

Laboratory of Biochemistry, State University of Utrecht, Utrecht (The Netherlands)

(Received 30 May 1986)

Key words: Lamellar body; Microsome; Phospholipid–protein interaction; (Rat lung)

We investigated the specificity of the cytosol-mediated phosphatidylcholine transfer between isolated rat lung microsomes and rat lung lamellar bodies. For that purpose we labeled the microsomes with 1-acyl-2-[1-^{14}C]palmitoyl- and 1-acyl-2-[9,10-^{3}H]oleoylphosphatidylcholine through protein-catalyzed phosphatidylcholine exchange. Incubation in buffer resulted in 3–5% transfer of label from microsomes to lamellar bodies. Lung cytosol stimulated this transfer about 2-fold and the presence of 12 μg/ml phosphatidylcholine-transfer protein from bovine liver resulted in a 30 to 35% recovery of radioactivity in the lamellar bodies. When microsomal donor membranes with a ^{3}H/^{14}C ratio of 2.6 were used, the ^{3}H/^{14}C ratios of the lamellar bodies were 3.9, 3.7 and 3.7, after incubation in buffer, with cytosol and with bovine liver exchange protein, respectively. Doubling the amount of lamellar body acceptor membranes resulted in ^{3}H/^{14}C ratios in the lamellar bodies of 4.6 and 4.1, after incubation in buffer and with cytosol, respectively. Furthermore, we isolated the protein component from rat lung lamellar bodies and performed reconstitution experiments with phospholipids. Reconstituted and non-reconstituted phospholipid and protein were separated by either Sepharose 4B gel filtration or discontinuous sucrose gradient centrifugation. The presence of lamellar body protein in the reconstitution mixture resulted in the formation of larger structures with higher density than those formed in control experiments without protein. When 1-acyl-2-[1-^{14}C]palmitoyl- and 1-acyl-2-[9,10-^{3}H]oleoylphosphatidylcholine were included in the reconstitution mixture, the structures containing lamellar body protein had 2- to 4-fold lower ^{3}H/^{14}C ratios than initially present in the incubation. These results suggest that lamellar body proteins associate preferentially with disaturated phosphatidylcholine species.

Introduction

The alveoli of the lung are lined with surfactant, a complex of phospholipid and protein. The main function of the lung surfactant is to stabilize the alveolus during expiration by lowering the surface tension at the air/water interface (see Refs. 1 and 2 for recent reviews). The most important surface active component of lung surfactant is dipalmitoylphosphatidylcholine [3,4]. Together with other constituents of the surfactant, this phospholipid is thought to be synthesized in the alveolar type II cell [1,2,5,6]. Intracellularly, the surfactant material is stored in the lamellar bodies [7,8]. After secretion into the alveolar space, the lamellar body is converted into tubular myelin, the immediate precursor of the surfactant film.

The lamellar body is characterized by a high content of phospholipids, phosphatidylcholine being the most abundant [9,10]. It is generally accepted that phosphatidylcholine is synthesized at the endoplasmatic reticulum. Compared to the phospholipid composition of this organelle, the lamellar body is particularly enriched in dipalmi-

---

Correspondence: Dr. H. van den Bosch, Laboratory of Biochemistry, State University of Utrecht, Padualaan 8, NL-3584 CH, Utrecht, The Netherlands.

0005-2760/87/$03.50 © 1987 Elsevier Science Publishers B.V. (Biomedical Division)

toylphosphatidylcholine. Since the lamellar body lacks the capacity for phosphatidylcholine biosynthesis [11,12], a phospholipid-transfer system is probably involved in the transport of phosphatidylcholine species from the endoplasmatic reticulum to the lamellar body. Most likely, the overall specificity of this transport process has to account for the enrichment of disaturated phosphatidylcholine species in lamellar bodies. It has been demonstrated that lung cytosol contains phospholipid-transfer proteins [13–18]. In these reports, however, a preference for the transfer of saturated phosphatidylcholine could not be established unequivocally. When transfer from lung microsomes to mitochondria was measured. unsaturated phosphatidylcholines were transferred better than the saturated species of this phospholipid [14]. With phospholipid vesicles as donor membranes and rat liver mitochondria as acceptors a purified phospholipid-transfer protein from lung transported dipalmitoylphosphatidylcholine 1.5-fold better than unsaturated phosphatidylcholines [18]. Phospholipid transfer from donor vesicles to lamellar bodies has been demonstrated [13] and has been found to be influenced by the fatty acyl composition of the phosphatidylcholines composing the donor membranes, but the selectivity with respect to molecular species transferred to the lamellar bodies was not investigated. In this paper we report on the cytosol-mediated phosphatidylcholine transfer between rat lung microsomes and lamellar bodies. In addition, we isolated the protein component of rat lung lamellar bodies by methods described in the accompanying paper [19] and performed reconstitution experiments of the lipid-free lamellar body proteins with phospholipids. The results may be indicative for an as yet unknown role of the lamellar body proteins in the enrichment of disaturated phosphatidylcholine species in this organelle.

Materials and Methods

Materials

1-Palmitoyl-2-[1-^{14}C]palmitoylphosphatidylcholine (57 mCi/mmol) and [9,10-^{3}H]oleic acid (3.4 Ci/mmol) were purchased from Amersham, U.K. 1-Acyl-2-[9,10-^{3}H]oleoylphosphatidylcholine was synthesized from 1-acyl-2-lysophosphatidylcholine and oleoyl-CoA as originally described for the synthesis of 1-acyl-2-[1-^{14}C]linoleoylphosphatidylethanolamine by van den Bosch et al. [20]. [*phenyl*(n)-^{3}H]Triton X-100 (5 mCi/mg) was a product of New England Nuclear, U.S.A.. Unlabeled Triton X-100 was obtained from Rohm and Haas, U.S.A.. Egg-yolk phosphatidylcholine was purified on HPLC and kindly donated by Mr. W.S.M. Geurts van Kessel from this laboratory. Phosphatidylcholine-exchange protein as purified from bovine liver [21] was a generous gift from Dr. D. van Loon from this laboratory. Aquacide III was a product of Calbiochem, France. DEAE-cellulose (DE-52) was obtained from Whatman, U.K.. All other chemicals were products of either Merck, F.R.G. or Fluka, Switzerland, and were of standard laboratory grade.

Methods

Isolation of microsomes. Lungs from adult male Wistar rats were excised after decapitation and homogenised with a Potter-Elvehjem homogenizer in 0.30 M sucrose/1 mM EDTA/10 mM Tris (pH 7.4) (buffer A) to yield a 10% (w/v) homogenate. After centrifugation at 600 × *g* for 10 min and at 20000 × *g* for 20 min, microsomes were pelleted by centrifugation for 60 min at 105000 × *g*. The microsomal pellet was resuspended in buffer A to a concentration of 5 mg protein per ml.

Isolation of lamellar bodies. Lamellar bodies were isolated from 10% (w/v) lung homogenates and subsequently freed from aspecifically adsorbed proteins by gelfiltration on Sepharose 4B as described [19]. The purified lamellar bodies were concentrated by dialysis against Aquacide III to a concentration of 250 μg protein per ml.

Preparation of labeled phosphatidylcholine vesicles. Vesicles were prepared by sonication of 1-acyl-2-[1-^{14}C] palmitoylphosphatidylcholine (12000 dpm/nmol) together with 1-acyl-2-[9,10-^{3}H] oleoyl phosphatidylcholine (28 000 dpm/nmol) at a final phospholipid concentration of 35 μM in the presence of 2 mol% phosphatidic acid in 3 ml of buffer A with a Branson B12 sonifier for 45 min at 50 W under a stream of N_2 at 0°C. Subsequently, the sonicate was centrifuged at 105000 × *g* for 60 min. Vesicles from the supernatant were used for labeling of the microsomes.

Labeling of microsomes with radioactive phos-

phatidylcholine. Equal volumes of radiolabeled vesicles and microsomal suspension were incubated for 45 min at 37°C in the presence of 12 μg/ml phosphatidylcholine-exchange protein from bovine liver. After the incubated microsomes had been reisolated from the mixture by centrifugation at 105000 × *g* for 60 min, the resulting microsomal pellet was resuspended in buffer A to a concentration of 5 mg protein per ml.

Transfer of radioactive phosphatidylcholine from microsomes to lamellar bodies. Microsomes were labeled with 1-acyl-2-[1-^{14}C] palmitoylphosphatidylcholine and 1-acyl-2-[9,10-^{3}H] oleoylphosphatidylcholine as described. Incubations were performed with 100 μl microsomal suspension, containing 5 mg protein/ml, and either 100 or 200 μl lamellar body-suspension, containing 250 μg protein/ml, in the presence of either 700 μl rat lung cytosol or 12 μg/ml phosphatidylcholine-exchange protein purified from bovine liver in buffer A. After incubation for 30 min at 37°C, 2 ml of ice-cold 0.975 M sucrose/1 mM EDTA/10 mM Tris (pH 7.4) was added to the incubation mixture. The resulting solution was overlaid with two consecutive layers of 4.2 ml 0.66 M sucrose/1 mM EDTA/10 mM Tris (pH 7.4) and 0.3 M sucrose/1 mM EDTA/10 mM Tris (pH 7.4), respectively. Lamellar bodies and microsomes were separated by centrifugation for 3 h at 35000 rpm at 4°C in a Beckman L2-65 ultracentrifuge with an SW-41 rotor.

Isolation of rat lung lamellar body proteins. Lamellar bodies were isolated from 10% (w/v) lung homogenates and adhering proteins were removed by precipitation at pH 11.5. The purified lamellar bodies were delipidated by elution over a DEAE-cellulose anion exchanger in the presence of 0.2% (v/v) Triton X-100. All procedures were executed as described [19]. Triton X-100 was subsequently removed from the protein on a DEAE-cellulose anion exchanger at pH 8.0. The protein peak was concentrated by dialysis against Aquacide III to a concentration of 0.1–1.0 mg/ml.

Cholate reconstitution of isolated lamellar body-protein with lamellar body phospholipid and egg phosphatidylcholine. Lamellar body phospholipids were extracted according to the method of Bligh and Dyer [22] from the phospholipid peak after DEAE-cellulose chromatography of lamellar bodies in 0.2% (v/v) Triton X-100. Phospholipid and protein were dissolved in buffers that contained 7.5 mg/ml sodium cholate by sonication for three times 15 sec at 50 W under N_2 at 0°C. Subsequently, cholate was removed by dialysis against buffer A and reconstituted and non-reconstituted phospholipid and protein were separated by either Sepharose 4B gel filtration or sucrose gradient centrifugation. When Sepharose 4B gel filtration was used for this separation, the incubation mixture contained 200 μg lamellar body protein, 2 μmol lamellar body phospholipid and 2 μmol egg phosphatidylcholine in a final volume of 2 ml of buffer A. In the incubation were included 10 nmol 1-acyl-2-[9,10-^{3}H] oleoylphosphatidylcholine (52800 dpm/nmol) and 0.4 nmol 1-acyl-2[1-^{14}C] palmitoylphosphatidylcholine (150 000 dpm/nmol). Sepharose 4B gel filtration was performed with 0.4 ml of this mixture, as specified in the respective figure legend. When sucrose gradient centrifugation was used, 200 nmol lamellar body phospholipid, 200 nmol egg phosphatidylcholine and 20 μg lamellar body protein were incubated together with 3 nmol 1-acyl-2-[9,10-^{3}H] oleoylphosphatidylcholine (20000 dpm/nmol) and 0.1 nmol 1-acyl-2-[1-^{14}C] palmitoylphosphatidylcholine (200000 dpm/nmol). The sample, in a final volume of 0.8 ml, was applied onto a discontinuous sucrose gradient, consisting of 1 ml 0.75 M sucrose, 4 ml 0.66 M sucrose and 5.6 ml 0.3 M sucrose, each containing 10 mM Tris and 1 mM EDTA (pH 7.4). Gradients were centrifuged for 3 h at 37000 rpm in a Beckman SW 41 rotor. After ending of the run, gradients were fractionated in 0.5 ml portions and assayed for protein and for lipid phosphorus after extraction [22].

Analytical procedures. Protein was measured according to the method of Bradford [23] as modified by Vianen and van den Bosch [24]. When Triton X-100 was present protein was determined according to Lowry et al. [25]. Lipid phosphorus was measured according to Chen et al. [26], after ashing [27]. Radioactivity was quantitated in a Packard 3320-Tricarb liquid scintillation spectrometer after addition of Packard emulsifier scintillation fluid. Rotenone-insensitive NADPH:cytochrome *c* reductase activity was measured as described by Margiolash [28].

Results and Discussion

In this paper we describe some experiments on the interaction of the protein component of lamellar bodies with phospholipids. Compared to the endoplasmic reticulum, i.e. the main intracellular site of phospholipid biosynthesis, the lamellar body is particularly enriched in disaturated phosphatidylcholine [9,10]. Since it has been demonstrated that the lamellar body is incapable of phosphatidylcholine synthesis [11,12], it has been proposed that saturated phosphatidylcholine species are specifically transfered from the endoplasmatic reticulum to the lamellar body through action of soluble phospholipid-transfer proteins. Lung cytosol was shown to contain transfer proteins for phosphatidylcholine [13–15,17,18]. However, a specificity for the transfer of saturated phosphatidylcholine was not convincingly observed [14,18]. We reinvestigated the specificity of the cytosol-mediated phosphatidylcholine transfer from microsomes to lamellar bodies, i.e., from the putative donor to acceptor membranes. For that purpose we labeled microsomes with radioactive phosphatidylcholines via protein-mediated exchange. In a preliminary experiment we investigated whether lamellar bodies and microsomes could be adequately separated again by sucrose gradient centrifugation, after incubation of the isolated organelles for 30 min at 37°C. In fig.1 the result of the such an experiment is depicted. This figure shows two peaks of lipid phosphorus, one associated with microsomal marker enzyme activity and another at the interface between 0.66 and 0.30 M sucrose. This density corresponds to the place in the gradient where lamellar bodes are expected. Since there was no microsomal marker enzyme activity detectable in the lamellar body peak, we concluded that sucrose gradient centrifugation is a good means for the separation of lamellar bodies and microsomes. Using this method, we studied the transfer of 1-acyl-2-[9,10-^{3}H]oleoyl- and 1-acyl-2-[1-^{14}C]palmitoylphosphatidylcholine from microsomes to lamellar bodies. In buffer, from 3–5% of initial radioactivity was transferred to the lamellar bodies. Lung cytosol stimulated the phospholipid transfer about 2-fold and the presence of 12 μg/ml phosphatidylcholine-transfer protein purified from bovine liver resulted in a 30–35% recovery of radiolabel in the lamellar bodies. When microsomal donor membranes with a $^3H/^{14}C$ ratio of 2.6 were used, the $^3H/^{14}C$ ratio of the lamellar bodies was 3.9, 3.7 and 3.7 after incubation in buffer, with cytosol and with bovine liver exchange protein, respectively. When the amounts of acceptor lamellar bodies in the incubations were doubled the ratios in the lamellar bodies had even further increased, to 4.6 and 4.1 in buffer and with cytosol, respectively. These results indicate that the lamellar body can act as an acceptor for phospholipids of microsomal origin. The increased $^3H/^{14}C$ ratios in the lamellar bodies after incubation indicate that 1-acyl-2-[9,10-^{3}H]oleoylphosphatidylcholine is more effectively transferred from the microsomal membrane than 1-acyl-2-[1-^{14}C]palmitoylphosphatidylcholine. This conclusion is in good agreement with results of Engle et al. [14]. These authors reported a slight preference of the lung phosphatidylcholine-transfer protein for unsaturated species in the transport from lung microsomes to mitochondria. In contrast, Funkhouser and co-workers noticed a 1.5-fold preference for transport of dipalmitoyl-

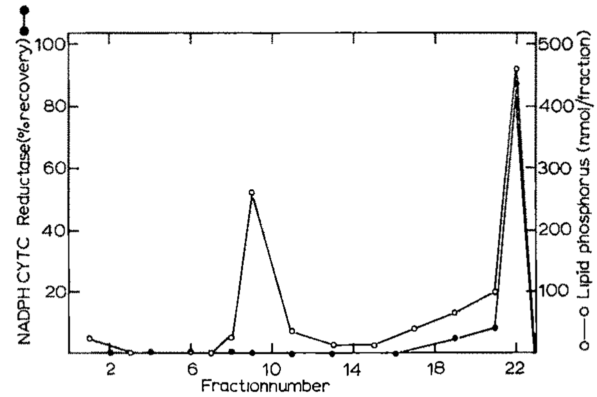

Fig 1. Separation of lamellar bodies and microsomes by sucrose gradient centrifugation. Lamellar bodies and microsomes were isolated from 10% (w/v) lung homogenates as described under Materials and Methods. Subsequently, both organelles were incubated at 37°C for 30 min and separated in a discontinuous sucrose gradient by centrifugation at 37000 rpm in a Beckman SW41 rotor at 4°C Gradients were fractionated in portions of 0.5 ml and assayed for microsomal marker enzyme activity and lipid phosphorus The figure shows a typical experiment from a series of three Fractions are numbered from top to bottom of the gradient Recoveries of phospholipid and enzyme activity amounted to 118% and 101%, respectively

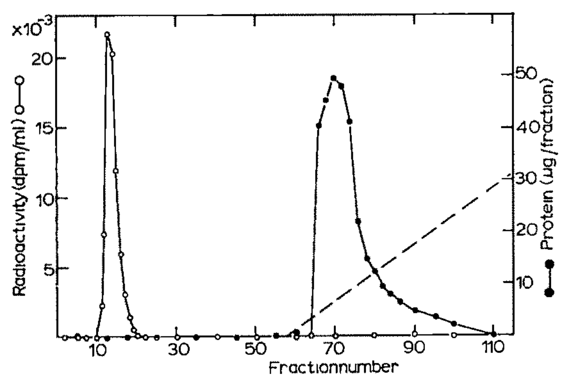

Fig. 2. Separation of lamellar body-protein and Triton X-100 on DEAE-cellulose. Lamellar bodies were isolated from 10% (w/v) lung homogenates and delipidated by elution on DEAE-cellulose in presence of 0 2% (v/v) Triton X-100 as described. For the removal of Triton X-100 from the protein a second DEAE-cellulose column was used. This column (75 × 1 cm) was run in buffer A (pH 8.0) at a flow rate of 9 ml/h and 20-min fractions were collected. The broken line indicates the slope of the salt gradient from 0 to 1 M NaCl. A 1 ml aliquot of lamellar body protein (960 μg/ml) in 0.2% (v/v) Triton X-100 containing 0.1 μCi [*phenyl*(n)-^{3}H] Triton X-100 was chromatographed. Fractions were assayed for protein and radioactivity Recoveries of protein and radioactivity amounted to 96% and 101%, respectively.

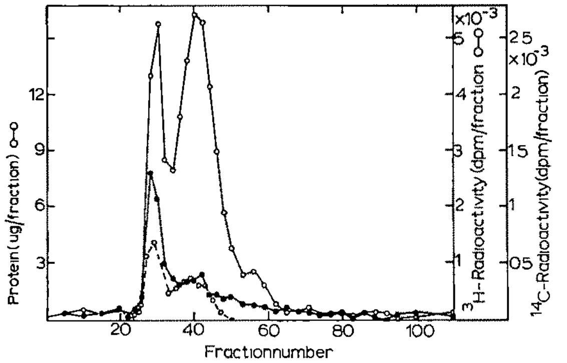

Fig 3 Reconstituted lamellar body protein and phospholipid on Sepharose 4B. Lamellar bodies were isolated and delipidated as indicated in the legend of Fig 2. Lamellar body protein was dissolved together with equimolar amounts of lamellar body phospholipids and egg phosphatidylcholine in 7 5 mg/ml cholate as described under Materials and Methods After dialysis of the cholate, a sample was filtered over a Sepharose 4B column (65 × 1.2 cm) in buffer A at a flow rate of 17 ml/h and 3-min fractions were collected The column was loaded with 0.4 ml of the incubation mixture, containing 40 μg protein, 400 nmol lamellar body phospholipid and 400 nmol egg phosphatidylcholine together with 2 nmol 1-acyl-2-[9,10-^{3}H]oleoylphosphatidylcholine (52800 dpm/nmol) and 0.08 nmol 1-acyl-2-[1-^{14}C]palmitoylphosphatidylcholine (150000 dpm/nmol) Protein was determined after lyophilization of 0.5 ml aliquots of the fractions. Radioactivity was measured as described Recoveries of protein, ^{3}H, and ^{14}C radioactivity amounted to 76, 110 and 90%, respectively

phosphatidylcholine from liposomal donor vesicles to rat liver mitochondria [18]. Transport to the relatively saturated lamellar body membranes was 2- to 3-fold lower than to the more unsaturated liver mitochondria [13], but the selectivity in the transfer of phosphatidylcholine species to lamellar bodies was not investigated. Collectively, these data suggest that soluble phosphatidylcholine-transfer proteins are not likely involved in the enrichment of lamellar bodies in saturated phosphatidylcholine species.

In the next series of experiments we investigated whether the protein component of the lamellar body could be important in the specific uptake of saturated phosphatidylcholine. To investigate this possibility we performed cholate reconstitution experiments with isolated lamellar body protein with equimolar amounts of lamellar body phospholipid and egg phosphatidylcholine. To isolate the lamellar body protein we applied purified lamellar bodies on DEAE-cellulose in the presence of 0.2% (v/v) Triton X-100. This procedure separates the protein and lipid components of lamellar bodies [19]. Subsequently, Triton X-100 was removed from the protein peak by a second elution on DEAE-cellulose. Fig. 2 shows a typical elution profile upon DEAE-cellulose chromatography. Triton X-100 is barely retarded by the column, whereas the protein can only be eluted in the NaCl gradient without any apparent overlap. This method is less time-consuming, and thus provides a more favorable method for the removal of Triton X-100 than the extensive dialysis used previously [19]. We determined that 83% of lamellar body phospholipids is phosphatidylcholine [19]. Under the assumption that 80% of this phospholipid is saturated and that egg phosphatidylcholine consists of 5% saturated species, the reconstitution mixture contained saturated and unsaturated phosphatidylcholine in a mole ratio of about 1 : 1.8. The phospholipid-to-protein ratio in the mixtures used for reconstitution amounted to 20 μmol/mg, i.e., twice the value of purified lamellar bodies [19]. Two independent methods were used to separate reconstituted and non-reconstituted phospholipid and protein: Sepharose 4B gel-filtration and sucrose gradient centrifugation. In Fig. 3 the elution profile on Sepharose 4B is depicted of phosphatidylcholine-associated radioactivity and protein after reconstitution. Both radioactivity and protein are recovered in two peaks. One eluted in the void volume of the column and a second peak was somewhat retarded. Interestingly, the peak with the apparent higher molecular mass is enriched in 1-acyl-2-[1-^{14}C]palmitoylphosphatidylcholine. In contrast, the lower-molecular-mass peak contains relatively more 1-acyl-2-[9,10-^{3}H]oleoylphosphatidylcholine. Starting from a ^{3}H/^{14}C ratio of 8.8 in the initial incubation mixture, in the pooled void volume peak a ratio of 4.9 was measured. At the same time the ratio in the lower-molecular-mass peak was increased to 15.5. When this experiment was performed without lamellar body protein being present, only the peak with the apparent lower molecular mass was observed, without any shift in the ^{3}H/^{14}C ratio (data not shown). These results indicate that, upon reconstitution, phospholipid-protein complexes are formed with a higher molecular weight than phospholipid vesicles made through cholate reconstitution alone. Furthermore, in the reconstituted complexes saturated phosphatidylcholine is more readily incorporated than unsaturated species of this phospholipid.

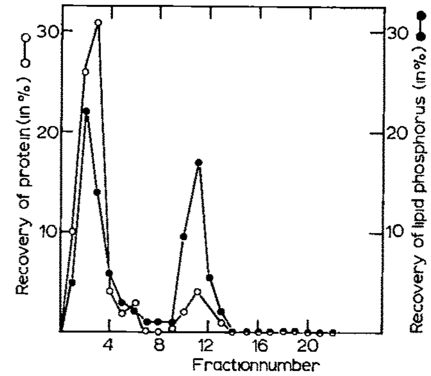

Fig. 4. Separation of reconstituted and non-reconstituted lamellar body protein and phospholipid by sucrose gradient centrifugation. Lamellar bodies were isolated and delipidated as described in the legend of Fig. 2. Reconstitution was performed with 90 μg lamellar body protein, 900 nmol lamellar body phospholipid and 900 nmol egg phosphatidylcholine as described in the Materials and Methods. The mixture (0.8 ml) was applied onto a discontinuous sucrose gradient as described. When the run was completed, gradients were collected in 0.5 ml fractions and assayed for protein and lipid phosphorus. Results are expressed as % recovery of protein and lipid phosphorus in each fraction. A typical example from a series of three experiments is shown. Fractions were numbered from top to bottom.

Lamellar bodies are characterized by a high phospholipid content, which enables isolation of this organelle by density gradients. We investigated whether reconstituted lamellar body-protein and phospholipid could be separated from non-reconstituted entities by sucrose gradient centrifugation. Fig. 4 shows the distribution of protein and phospholipid in the gradient after cholate reconstitution and centrifugation. Both protein and lipid phosphorus are recovered at two discrete places in the gradient, i.e. at the interfaces between 0.1 and 0.3 M (fractions 1–4) and 0.3 and 0.66 M sucrose (fractions 9–13). Lipid phosphorus is recovered for about 32% at the higher density and for 68% at the lower. Protein is found with 90% recovery at lower and for only 10% at higher density. Since lamellar bodies can be isolated at the interface between 0.3 and 0.66 M sucrose, we concluded that the phospholipid and protein recovered at that density upon cholate reconstitution is most likely to be the reconstituted phospholipid-protein complex. This was confirmed in the next series of experiments in which the specificity of the lamellar body protein for the incorporation of saturated phosphatidylcholine species was investigated by means of cholate reconstitution, using sucrose gradient centrifugation for the separation of reconstituted and non-reconstituted phospholipid and protein. Fig. 5 shows that, in presence of lamellar body protein, two peaks of phosphatidylcholine-associated radioactivity can be recovered at the same positions in the gradient as lipid phosphorus and protein in Fig. 4. However, 1-acyl-2-[1-^{14}C]palmitoyl- and 1-acyl-2-[9,10-^{3}H]oleoylphosphatidylcholine were distributed disproportionately over the two peaks, the former being more abundant at higher density and the latter at lower density, with ^{3}H/^{14}C ratios of 0.7 and 4.2, respectively. The ratio before reconstitution was 3.0. Without lamellar body protein present, only the lower-density peak was observed,

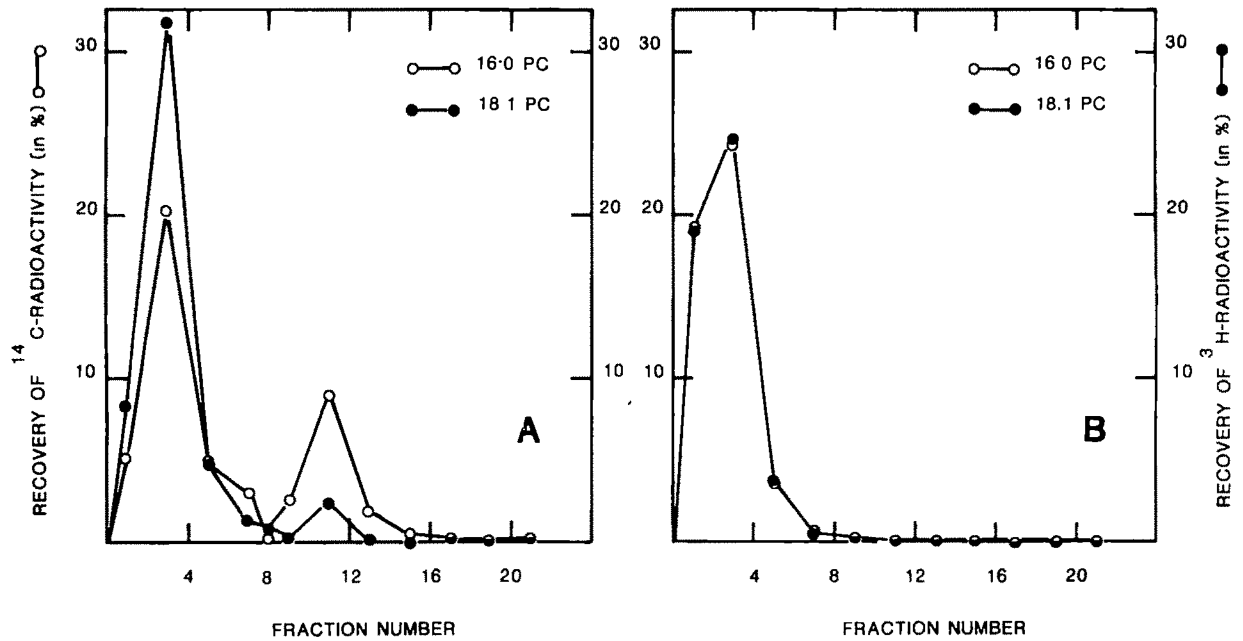

Fig 5. Distribution of reconstituted lamellar body protein and phospholipid in sucrose gradients Lamellar body protein and phospholipid were isolated as described under Materials and Methods The reconstitution mixture contained 200 nmol lamellar body phospholipid and 200 nmol egg phosphatidylcholine, together with 3 nmol 1-acyl-2-[9,10-^{3}H] oleoylphosphatidylcholine (20000 dpm/nmol) (18·1 PC) and 0.1 nmol 1-acyl-2-[1-^{14}C] palmitoylphosphatidylcholine (200000 dpm/nmol) 16.0 PC) Experiments were carried out in presence (panel A) or absence (panel B) of 20 μg lamellar body protein After removal of the cholate, the incubation mixtures (0.8 ml) were centrifuged in a discontinuous sucrose gradient, as described Results are expressed as % recovery of ^{3}H and ^{14}C radioactivity in each fraction. Fractions were numbered as in Fig 4.

indicating that the appearance of the higher-density peak is due to to the formation of phospholipid-protein complexes.

A comparison of the results in Figs. 3 and 5 strongly suggests that the reconstituted structures are not homogeneous. Whereas about 50% of the protein after reconstitution is recovered in large structures (Fig. 3), not all of this protein is present in structures with a density comparable to that of lamellar bodies, as evidenced by the fact that only about 10% of the protein is recovered in such fractions (Fig. 5). Both the size and density analyses, however, show a preference for the association of disaturated phosphatidylcholine with lamellar body protein. In this respect it is interesting to note that Tsao [28] demonstrated that, upon incubation of rabbit lung slices with multilamellar liposomes, 30–50% more dipalmitoylphosphatidylcholine was incorporated into the lamellar bodies than dioleoylphosphatidylcholine. Tsao suggested that phosphatidylcholine-transfer proteins specific for disaturated species were involved in this transfer. Possibly the lamellar body protein could be responsible for the observed preferential uptake of dipalmitoylphosphatidylcholine.

Until now, reassembly studies of isolated lamellar body proteins with phospholipid have not been reported. Some data are available, however, on the interaction of phospholipids with surfactant protein. It has been shown that isolated surfactant protein can readily reassemble with phospholipids [30–34]. Unfortunately, in the reports a possible specificity of the surfactant protein towards saturated phosphatidylcholine was not investigated. It could be of interest to compare the behavior of the proteins from surfactant and lamellar bodies in order to gain further evidence for both protein pools' being identical. Further investigations will also be necessary to elucidate the mechanism for the specific recognition of saturated phosphatidylcholine and to assess which of the lamellar body proteins is responsible for this phenomenon.

Acknowledgements

These studies were carried out under the auspices of the Netherlands Organization for the Advancement of Pure Research (Z.W.O.) with financial aid from the Netherlands Foundation for Chemical Research (S.O.N.).

References

1 Possmayer, F., Yu, S-H., Weber, J.M and Harding, P G.R (1984) Can. J. Biochem. Cell Biol 62, 1121–1133

2 Rooney, S.A (1985) Am. Rev Respir Dis. 131, 439–460

3 Klaus, M.H., Clements, J.A. and Havel, R. (1961) Proc. Natl. Acad. Sci. USA 47, 1858–1859

4 King, R J and Clements, J.A. (1972) Am. J. Physiol. 223, 715–726

5 Goerke, J (1974) Biochim. Biophys Acta 344, 241–261

6 Van Golde, L M.G. (1976) Am. Rev Resp. Dis 114, 977–1000

7 Williams, M.C. and Mason, R.J. (1977) Am. Rev. Resp. Dis. 115, 37–47

8 Engle, M.J , Sander, R.L and Longmore, W.J. (1976) Arch Biochem. Biophys. 173, 586–595

9 Hallman, M. and Gluck, L. (1975) Biochim Biophys. Acta 409, 172–191

10 DiAugustine, R P. (1974) J. Biol Chem 249, 584–593

11 Baranska, J. and van Golde, L.M G. (1977) Biochim. Biophys Acta 488, 285–293

12 Garcia, A., Sener, S F. and Mavis, R D. (1976) Lipids 11, 109–112

13 Funkhouser, J.D. and Hughes, E R. (1983) Arch. Biochem Biophys. 221, 499–506

14 Engle, M J , van Golde, L.M G and Wirtz, K W A (1978) FEBS Lett. 86, 277–281

15 Van Golde, L M G , Oldenborg, V., Post, M., Batenburg, J J., Poorthuis, B.J H M. and Wirtz, K.W A (1980) J Biol. Chem 255, 6011–6013

16 Whitlow, C.D., Pool, G.L., Brumley, G.W. and Lumb, R H (1980) FEBS Lett. 113, 221–224

17 Funkhouser, J.D and Read, R.J (1985) Chem. Phys. Lipids 38, 17–27

18 Read, R.J. and Funkhouser, J.D. (1984) Biochim. Biophys Acta 794, 9–17

19 Nijssen, J G., Hardeman, D., Lucas Luyckx, H., Promes, L.W., Post, J A and van den Bosch, H (1987) Biochim Biophys. Acta 917, 131–139

20 Van den Bosch, H., Aarsman, A J and van Deenen, L L.M (1974) Biochim Biophys Acta 348, 197–209

21 Westerman, J., Kamp, H H. and Wirtz, K.W A. (1983) Methods Enzymol. 98, 581–586

22 Bligh, E.G. and Dyer, W J (1959) Can J Biochem 37, 911–917

23 Bradford, M.M. (1976) Anal. Biochem 72, 248–254

24 Vianen, G.M. and van den Bosch, H (1978) Arch Biochem. Biophys. 190, 373–384

25 Lowry, O.H., Rosebrough, N.J , Farr, A.L. and Randall, R.J. (1951) J Biol Chem 193, 265–275

26 Chen, P S , Toribara, T.Y. and Warner, H. (1956) Anal Chem. 28, 1756–1758

27 Ames, B.N. and Dubin, D.T (1960) J. Biol Chem 235, 769–775

28 Margoliash, E. (1954) Biochem J. 56, 535–543

29 Tsao, F.H.C. (1980) Biochim Biophys. Acta 601, 415–426

30 King, R.J. and MacBeth, M.C (1979) Biochim Biophys Acta 557, 86–101

31 King, R.J. and MacBeth, M.C. (1981) Biochim. Biophys. Acta 647, 159–168

32 Benson, B.J. and Hawgood, S. (1985) Eur. J. Resp. Dis. 67 Suppl. 142, 29–36

33 Hawgood, S , Benson, B J and Hamilton, R L , Jr. (1985) Biochemistry 24, 184–190

34 King, R.J. (1984) Exp. Lung Res 6, 237–253

Biochimica et Biophysica Acta 917 (1987) 148–161
Elsevier

BBA 52317

Astrocytes synthesize apolipoprotein E and metabolize apolipoprotein E-containing lipoproteins

Robert E. Pitas, Janet K. Boyles, Susan H. Lee, Donna Foss
and Robert W. Mahley

Gladstone Foundation Laboratories for Cardiovascular Disease, Cardiovascular Research Institute, Departments of Pathology and Medicine, University of California, San Francisco, CA 94140-0608 (U.S.A.)

(Received 8 September 1986)

Key words: LDL receptor; Apolipoprotein E synthesis; Astrocyte; (Rat brain)

We have previously demonstrated that astrocytes synthesize and secrete apolipoprotein E in situ. In the present work, primary cultures of rat brain astrocytes were used to study apolipoprotein E synthesis, secretion, and metabolism in vitro. The astrocytes in culture contained immunoreactive apolipoprotein E in the area of the Golgi apparatus. Incubation of the astrocytes with [^{35}S]methionine resulted in the secretion of labeled immunoprecipitable apolipoprotein E, which constituted 1–3% of the total secreted proteins. The apolipoprotein E secreted in culture and the apolipoprotein E in rat brain extracts differed from serum apolipoprotein E in two respects: both had a slightly higher apparent molecular weight (approx. 36000) and more acidic isoforms than serum apolipoprotein E. Sialylation of the newly secreted apolipoprotein accounted for the difference in both the apparent molecular weight and isoelectric focusing pattern of newly secreted apolipoprotein E and plasma apolipoprotein E. The astrocytes possessed apolipoprotein B,E(LDL) receptors capable of binding and internalizing apolipoprotein E-containing lipoproteins. The uptake of lipoproteins by the cells led to a reduction in the number of cell surface receptors and to the intracellular accumulation of cholesteryl esters. Since apolipoprotein E is present within the brain, and since brain cells can express apolipoprotein B,E(LDL) receptors, apolipoprotein E-containing lipoproteins may function to redistribute lipid and regulate cholesterol homeostasis within the brain.

Introduction

Plasma lipoproteins, which contain apolipoprotein B and apolipoprotein E, play key roles in the transport of lipid and in cholesterol homeostasis [1–3]. Lipoproteins that contain apolipoprotein B bind to the low density lipoprotein (LDL) receptor in hepatic and extrahepatic tissues, whereas lipoproteins that contain apolipoprotein E bind to both the LDL receptor (often called the apolipoprotein B,E(LDL) receptor because of its dual apolipoprotein specificity) and an apolipoprotein E-specific receptor present in the liver [3,4]. Up-

---

Abbreviations: AcAc, acetoacetylated; apolipoprotein B,E(LDL) receptor, LDL receptor; apolipoprotein E HDL$_c$, a cholesterol-induced canine lipoprotein, which contains apolipoprotein E as its only protein constituent; β-VLDL, cholesterol-rich β-migrating very low density lipoproteins; DiI, 1,1′-dioctadecyl-3,3,3′,3′-tetramethylindocarbocyanine; GFAP, glial fibrillary acidic protein; HDL, high density lipoproteins; HDL$_1$, rat lipoproteins that contain apolipoprotein E and apolipoprotein A-I and that float at $d = 1.02$–1.063 g/ml upon centrifugation; IgG, immunoglobulin G, LDL, low density lipoproteins; SDS, sodium dodecyl sulfate

Correspondence: Dr R.E. Pitas, Gladstone Foundation Laboratories for Cardiovascular Disease, P O Box 40608, San Francisco, CA 94140-0608, U S.A.

0005-2760/87/$03.50 © 1987 Elsevier Science Publishers B.V (Biomedical Division)

take of cholesteryl ester-rich lipoproteins by cells expressing the apolipoprotein B,E(LDL) receptor leads to the liberation of free cholesterol within the cells and a reduction both in the number of receptors and in the endogenous synthesis of cholesterol.

Cerebrospinal fluid contains apolipoprotein E but not apolipoprotein B [5,6]. Roheim et al. [5] observed that the amount of apolipoprotein E in human cerebrospinal fluid was 2.7% of the level found in plasma, whereas albumin and apolipoprotein A-I (a lower-molecular-weight apolipoprotein) were present at 0.5 and 0.4%, respectively, of their plasma levels. These data suggested that apolipoprotein E was present in cerebrospinal fluid at a concentration higher than would be expected for a filtered plasma protein and that apolipoprotein E might be produced and secreted by tissues of the nervous system. More recently, Elshourbagy et al. [7] noted that brain tissue of humans, marmoset monkeys, and rats contains high concentrations of apolipoprotein E mRNA (approximately 30% the level in the liver) and therefore has the capacity for apolipoprotein E synthesis.

Recently, the specific cells in the brain that synthesize apolipoprotein E have been identified immunocytochemically [8]. Within the central nervous system, all astrocytes, including the specialized astrocytes (Bergmann glia, tanycytes, pituicytes, and Müller cells), contain appreciable concentrations of apolipoprotein E. Electron microscopic immunocytochemical studies demonstrated apolipoprotein E in the Golgi apparatus of these cells, indicating that the astrocytes secrete apolipoprotein E. In the peripheral nervous system, apolipoprotein E was found in satellite cells of the superior cervical sympathetic ganglion and dorsal root ganglion, enteric glia, and a subset of nonmyelinating Schwann cells (but not in myelinating Schwann cells).

Increasing evidence suggests that apolipoprotein E plays an important role in nervous tissue metabolism. A 37 000-Da protein that accumulates in nerve tissue after injury to the nerve has been identified as apolipoprotein E [9–11]. Skene and Shooter [12] and Müller et al. [13] have reported that synthesis of the 37 000-Da protein increases in response to crush injury of central and peripheral nerves, coincident with Wallerian degeneration and the need to mobilize lipid from degenerating myelin. More recent studies of the 37 000-Da protein in sciatic nerve of neonatal rats suggest that apolipoprotein E may also play a role in normal nerve growth and maturation [14].

Since apolipoprotein E-containing lipoproteins are present in cerebrospinal fluid and apolipoprotein E has been extracted from brain tissue, it is probable that apolipoprotein E-containing lipoproteins serve a lipid transport role within the brain, just as they do within the general circulation. This possibility is strengthened by the observation that certain brain cell lines metabolize lipoproteins: human malignant glioma cells (U-251MG) possess receptors for LDL [15], and LDL regulate the synthesis of cholesteryl ester and cholesterol in C-6 glioma cells [16]. No characterization of the apolipoprotein specificity of these receptors has been reported, however, nor have lipoprotein receptors been characterized in primary cultures of normal brain cells. The present studies were initiated to demonstrate directly the synthesis and secretion of apolipoprotein E by astrocytes and to characterize the lipoprotein receptors of astrocytes in primary culture.

Materials and Methods

Materials. Ascites fluid containing the mouse monoclonal antibody against glial fibrillary acidic protein (GFAP), biotinylated anti-mouse immunoglobulin G (IgG), and Texas Red-labeled strepaviden were purchased from Amersham/Searle (Arlington Heights, IL). Fluorescein-labeled goat anti-rabbit IgG was obtained from Zymed Laboratories (South San Francisco, CA). Rabbit anti-rat apolipoprotein E antiserum was raised against purified rat apolipoprotein E, and is known to be monospecific, as determined by immunoblotting of rat brain and liver extracts and rat plasma [8]. The fluorescent probe 1,1′-dioctadecyl-3,3,3′,3′-tetramethylindocarbocyanine (DiI) was purchased from Molecular Probes Inc. (Eugene OR).

Cell isolation. Primary cultures of rat brain cells were prepared from tissues of either fetal or newborn rats. Pregnant Sprague-Dawley rats (at 19–21 days gestation) were anesthetized with pentobarbital (65 mg/kg, I.P.), and their fetuses were removed and decapitated prior to removal of their brains. Newborn rats (1–3 days old) were etherized and decapitated. The meninges were carefully removed from the brains, and the tissue finely diced. The cells were dispersed by vortexing [17] for 3 min in Dulbecco's modified Eagle's medium containing 20% fetal calf serum before passage through nylon mesh (80 μm, then 10 μm) to remove debris. The cells were grown in monolayer culture on tissue culture dishes (cells from one brain were grown on 75–100 35-mm dishes) or tissue culture chamber slides at an equivalent density. Cells were routinely grown in Dulbecco's modified Eagle's medium containing streptomycin, penicillin, and 10% fetal calf serum. Three days after isolation, the cells were washed two times and the medium was changed. The medium was then changed every 3 days until the cells were used. In initial studies, the diced brain tissue was digested with trypsin prior to sieving. However, similar experimental results were obtained using the Vortex-disrupted brain cells, which produced cultures with a higher percentage of astrocytes. Therefore, cells obtained from Vortex-disrupted brains were used in all subsequent experiments.

Unstimulated mouse peritoneal macrophages were isolated and human fibroblast cultures established as described previously [18–20].

Immunocytochemistry. The immunocytochemical techniques used were similar to those performed by Boyles et al. [8]. Cells were washed three times with phosphate-buffered saline and then fixed for 3 h at 4°C in 0.15 M phosphate buffer (pH 7.4) containing 4% formaldehyde prepared from paraformaldehyde. The plates were washed three times with phosphate-buffered saline. Nonspecific binding sites were then blocked and the cells made permeable by incubation for 30 min to 3 h in buffer containing goat serum (1 : 50 dilution), 1% ovalbumin, 0.15% Triton X-100, and 150 mM ammonium acetate in half-strength phosphate-buffered saline (pH 7.4). The primary antiserum was then diluted (apolipoprotein E antiserum, 1 : 20000; anti-GFAP, 1 : 1500) in incubation buffer (phosphate-buffered saline containing 0.1% ovalbumin, 15 mM ammonium acetate, with 0.15% Triton X-100) and incubated with the cells for 16–24 h. The cells were washed as previously described and then reacted in one of two ways, either with immunoperoxidase reagents to localize apolipoprotein E and GFAP separately as previously described [8] or with immunofluorescence reagents, which permitted the detection of both apolipoprotein E and GFAP in the same cells.

The dual-label immunofluorescence visualization was performed as follows. The cells, which had been incubated with both primary antibodies simultaneously, were washed and incubated with biotinylated anti-mouse IgG (1 : 300 dilution) and fluorescein-labeled goat anti-rabbit IgG (1 : 500 dilution) for 3 h in incubation buffer without Triton X-100. They were then washed for 2 h, incubated for 30 min with a 1 : 1000 dilution of Texas Red-labeled strepaviden in the same buffer, and washed. The cells were mounted with 75% glycerol in phosphate-buffered saline.

Apolipoprotein E synthesis. Dissociated brain cells were grown for 1–2 weeks in Dulbecco's modified Eagle's medium containing 10% fetal calf serum. Before the experiment, the tissue culture plates were washed two times with Dulbecco's modified Eagle's medium and one time with methionine-free Dulbecco's modified Eagle's medium. Medium (Dulbecco's modified Eagle's medium with 25% of the normal L-methionine) containing [^{35}S]methionine (100–200 μCi/ml) was added to each tissue culture plate and incubated at 37°C for 16 h. The medium was removed and centrifuged at 3000 × g for 10 min to remove cellular debris, and the trichloroacetic acid-precipitable [^{35}S]methionine-labeled proteins were measured. Medium from the cells was incubated with monospecific rabbit anti-rat apolipoprotein E immune serum, and then the apolipoprotein E-IgG complex was precipitated with Protein A (IgGSORB, The Enzyme Center, Boston, MA). Nonspecific immunoprecipitable material had been previously removed with nonimmune rabbit serum. Whole medium and immunoprecipitates were analyzed by 10% sodium dodecyl sulfate (SDS)-polyacrylamide slab gel electrophoresis and visualized by autoradiography. The relative amount of apolipoprotein E synthesized was calculated as the percentage of the total [^{35}S]methionine-labeled protein (trichloroacetic acid-precipitable counts) immunoprecipitated with anti-rat apolipoprotein E immune serum and by densitometric scanning of autoradiograms of total proteins separated by electrophoresis on SDS-polyacrylamide gels.

Newly synthesized [^{35}S]methionine-labeled apolipoprotein E was also examined by isoelectric focusing before and after neuraminidase digestion. For this purpose, the apolipoprotein E was first separated from other labeled proteins. This was accomplished by raising the density of the cell culture medium to 1.21 g/ml with solid KBr and ultracentrifugation (59000 rpm) for 24 h at 4°C in a Beckman 60 Ti rotor. The material that floated was dialyzed prior to the performance of neuraminidase digestion and isoelectric focusing as previously described [21].

Lipoprotein preparation. Rat high density lipoproteins (HDL) ($d = 1.125$–1.21 g/ml) and rat LDL and HDL_1 ($d = 1.02$–1.063 g/ml) were isolated by ultracentrifugation [22]. The rat LDL, containing only apolipoprotein B, and HDL_1, containing apolipoprotein E and apolipoprotein A-I, were separated by preparative electrophoresis [23]. Canine apolipoprotein E HDL_c ($d = 1.006$–1.02 g/ml) and canine β-VLDL ($d < 1.006$ g/ml) were isolated from the plasma of cholesterol-fed dogs [24] by a combination of centrifugation and preparative electrophoresis as previously described [23,25]. The apolipoprotein E HDL_c contain only apolipoprotein E, while β-VLDL contain apolipoproteins B and E. Lipoprotein-deficient human serum ($d > 1.21$ g/ml) was prepared as described [26]. Lipoproteins were iodinated by the procedure of Bolton and Hunter [27]. Lipoproteins were labeled with the fluorescent probe DiI as previously described [28] and acetoacetylated by reaction with diketene [19,28]. The purity of the lipoprotein fractions, which was assessed by SDS-polyacrylamide gel electrophoresis [29], was similar to that previously obtained [18,30].

Cell binding studies. Primary cultures of brain cells were used for binding studies when the cells were essentially confluent, 1–2 weeks after isolation. In some experiments, the medium was changed to Dulbecco's modified Eagle's medium containing 10% lipoprotein-deficient human serum (the $d > 1.21$ g/ml ultracentrifugal fraction of human serum) 48 h before the experiment to deplete the cells of cholesterol and to up-regulate the expression of the apolipoprotein B,E(LDL) receptors.

For direct and competitive binding experiments at 4°C, the tissue culture plates containing the primary cultures of astrocytes were cooled to 4°C for 5 min prior to addition of the lipoproteins in ice-cold Dulbecco's modified Eagle's medium containing 10% lipoprotein-deficient human serum. Direct binding experiments were conducted for 3 h at 4°C [31]. Equilibrium dissociation constants for rat lipoproteins were calculated as previously described [30]. Competitive binding experiments were conducted for 2 h at 4°C. After the incubation, cells were washed three times with phosphate-buffered saline containing 10% bovine serum albumin and then left in the same solution for 10 min. The second 10-min wash was followed by a final washing with phosphate-buffered saline before cells were solubilized using three 0.5-ml aliquots of 0.1 M NaOH. Radioactivity was measured and the protein was assayed [32].

Direct binding experiments were also conducted at 37°C to demonstrate degradation of the lipoproteins by the cells. Cells were incubated for 5 h at 37°C with lipoproteins in Dulbecco's modified Eagle's medium containing 10% lipoprotein-deficient human serum as described previously [33]. After incubation, the cells were washed and cell-associated (bound and internalized) radioactivity was determined as described above. The degraded lipoproteins that accumulated in the medium were measured as described [33]. Nonspecific binding of the iodinated ligands has been subtracted from both the 4°C and 37°C direct binding data. Nonspecific binding was measured in the presence of a 60-fold excess of nonlabeled canine β-VLDL.

The effect of incubation of the cells with lipoprotein on cholesteryl ester synthesis was determined either by the incorporation of [^{14}C]oleate into cholesteryl ester or by the effect on the cholesteryl ester mass within the cells. Both of these procedures were conducted at 37°C as described previously [33,34].

Results

Identification of the cell producing apolipoprotein E in culture

Nearly pure cultures of astrocytes can be prepared by the vortexing procedure of Hertz et al. [17]. Astrocytes represented approx. 95% of the cells in the brain cell cultures produced by this procedure as determined by their morphological response to incubation with dibutyryl cyclic AMP and their content of glial fibrillary acidic protein (GFAP). When the cultured cells were incubated with fluorescently labeled acetoacetylated (AcAc) LDL, a lipoprotein that is internalized by macrophages through specific receptors [35–37], only approx. 2–3% of the cells were labeled. These cells were identified as either microglia or monocyte-derived macrophages.

To assess the ability of astrocytes in primary cultures to produce apolipoprotein E, dual-label immunofluorescence studies were performed. Astrocytes were identified by the presence of GFAP, and apolipoprotein E was identified with a monospecific antibody. As shown in Fig. 1, cells that reacted positively with the anti-GFAP antibody contained apolipoprotein E as well. The apolipoprotein E was localized to one side of the nucleus of the astrocytes, as would be expected for a secretory protein in the Golgi apparatus, whereas the intermediate filament protein GFAP occurred in fibers in the cell processes and in the cell body. The location of apolipoprotein E within the cells was more clearly visualized by an immunoperoxidase procedure. As shown in Fig. 2, the apolipoprotein E occurred in stacks near the nucleus of the astrocytes, indicating the presence of this protein in multiple Golgi apparatus, whereas the GFAP was visualized as a filamentous network within the cells. Another type of cell present in small numbers also contained apolipoprotein E, as has been reported previously [9]. These small round cells, which were not positive for GFAP, were identical to cells that bound and internalized DiI-labeled AcAc LDL and were therefore identified as macrophages.

Apolipoprotein E synthesis by primary cultures of brain cells

The primary cultures of rat brain cells (95% astrocytes) were incubated in medium containing [^{35}S]methionine to label the newly synthesized apolipoprotein E. The apolipoprotein E was then precipitated from the cell medium using rabbit

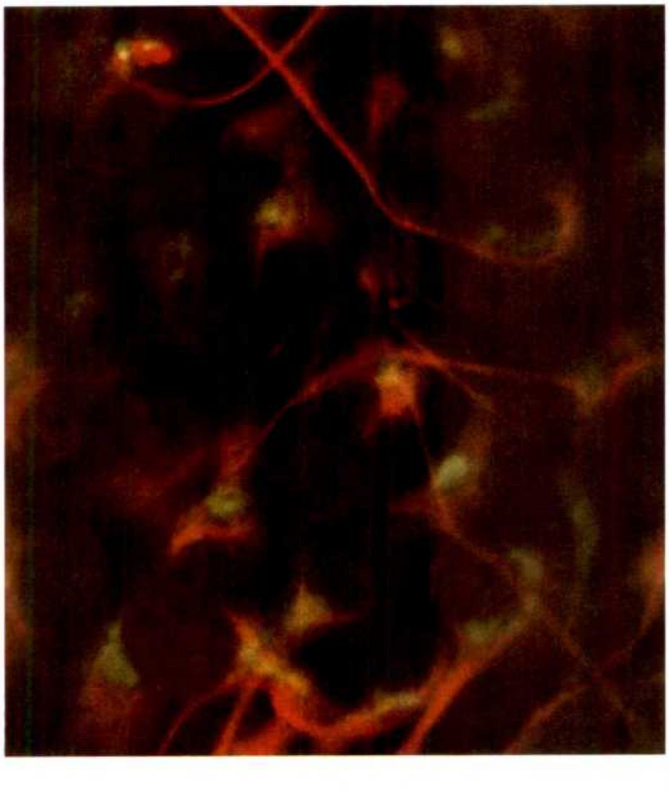

Fig. 1. Fluorescent photomicrograph showing the occurrence of apolipoprotein E (green) and glial fibrillary acidic protein (GFAP) (red) in the same astrocytes in vitro. Both apolipoprotein E and GFAP are visualized in the same cells by dual-label immunofluorescence (see Materials and Methods). ×750.

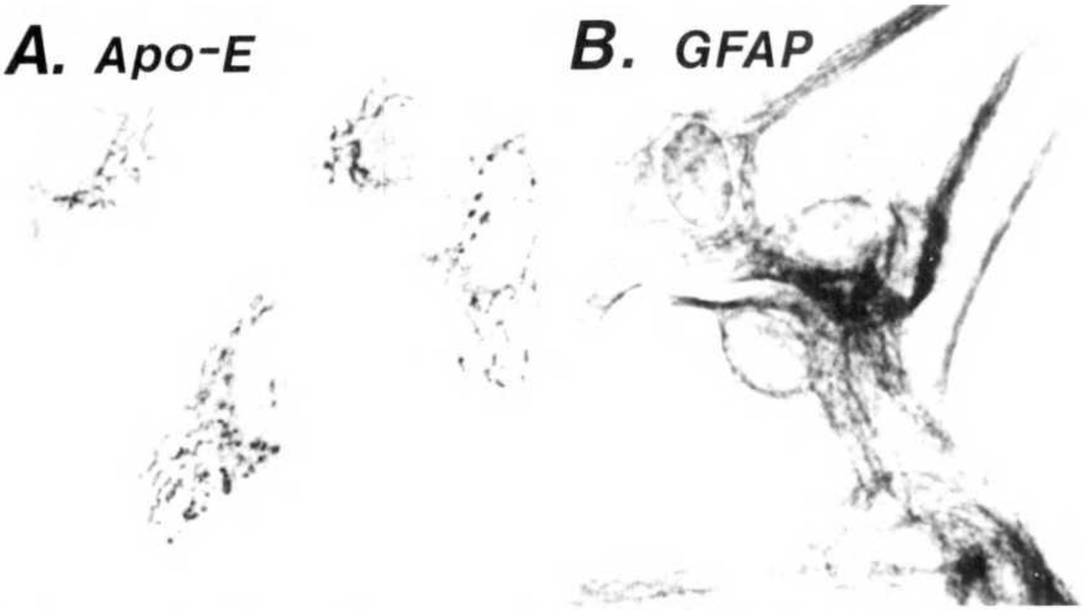

Fig. 2. Immunoperoxidase visualization of apolipoprotein E (panel A) and GFAP (panel B) within astrocytes in primary culture ×700.

anti-rat apolipoprotein E immune serum. As shown in the autoradiogram in Fig. 3, [^{35}S]methionine-labeled apolipoprotein E (apparent $M_r \approx 36000$) was immunoprecipitated from the [^{35}S]methionine-labeled proteins in the medium. (In addition to apolipoprotein E, the antibody also precipitated a variable small amount of other material, as can be seen in both Figs. 3 and 4. This material probably represents aggregates of apolipoprotein E or nonspecific precipitation.) In this particular experiment the immunoprecipitated apolipoprotein E represented 1.5% of the secreted protein. Measurements of apolipoprotein E secretion ranged between 1 and 3% of total secreted proteins in additional experiments. Quantitation based on immunoprecipitation of [^{35}S]methionine-labeled apolipoprotein E agreed with the results obtained from densitometric scanning of the autoradiograms of SDS-polyacrylamide gels of whole medium.

The apolipoprotein E in rat brain extracts has previously been shown by SDS-polyacrylamide gel electrophoresis to have a slightly higher apparent molecular weight than apolipoprotein E of rat serum or apolipoprotein E extracted from rat liver [8]. To determine whether the apparent molecular weight of the newly synthesized apolipoprotein E from brain cell cultures was similar to that of the apolipoprotein E present in the brain in vivo, the migration of ^{125}I-labeled serum apolipoprotein E and ^{125}I-labeled brain apolipoprotein E was compared with [^{35}S]methionine-labeled apolipoprotein E produced by astrocytes in culture. As shown in Fig. 4, the [^{35}S]methionine-labeled apolipoprotein E that was immunoprecipitated from brain cell culture medium had an apparent molecular weight similar to that of the ^{125}I-apolipoprotein E immunoprecipitated from rat brain extract and a higher apparent molecular weight than that of the major component of ^{125}I-apolipoprotein E immunoprecipitated from rat serum. The immunoprecipitated apolipoprotein E from the cultures often appeared as a diffuse band on SDS-polyacrylamide gels and sometimes separated into multiple bands (as seen in Fig. 4), suggesting the presence of multiple sialylated forms. Sialylated forms of apolipoprotein E are known to have a higher apparent molecular weight than nonsialylated forms [38].

To determine whether the newly secreted apoli-

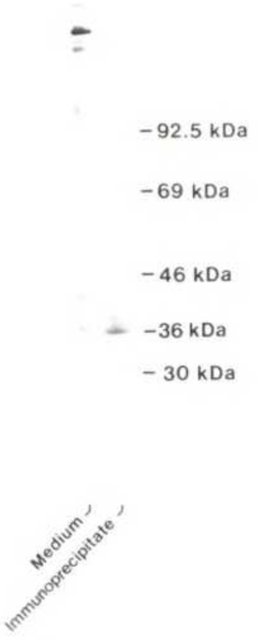

Fig. 3. Autoradiogram of [^{35}S]methionine-labeled protein secreted by astrocytes in vitro (left lane) and apolipoprotein E immunoprecipitated from the medium with an anti-apolipoprotein E antibody (right lane). Primary cultures of rat brain astrocytes were established and grown in culture for 6 days. The cells were then incubated for 16 h in serum-free medium containing 100 μCi of [^{35}S]methionine/ml. The proteins secreted into the medium were immunoprecipitated with an anti-apolipoprotein E, separated by SDS-polyacrylamide gel electrophoresis, and visualized by autoradiography.

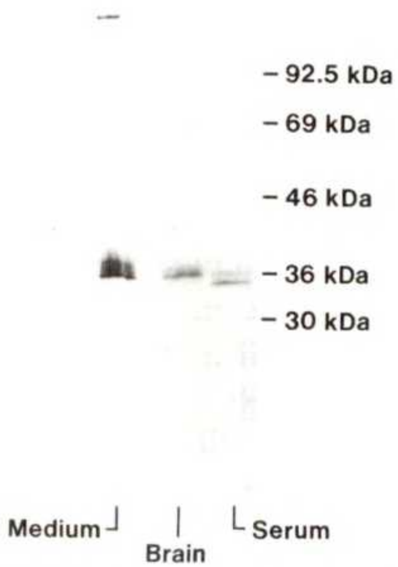

Fig. 4. Comparison of the apparent molecular weight of apolipoprotein E immunoprecipitated from astrocyte culture medium, rat brain extract, and rat serum. The [^{35}S]methionine-labeled apolipoprotein E from the medium of the cultured rat astrocytes was immunoprecipitated as described in Fig. 3. The apolipoprotein E in rat brain extract and rat serum was labeled with ^{125}I and then immunoprecipitated with anti-apolipoprotein E. The samples were separated by SDS-polyacrylamide gel electrophoresis and visualized by autoradiography.

poprotein E was sialylated, the pattern of isoforms was examined by isoelectric focusing before and after neuraminidase digestion. For this purpose, the newly synthesized [^{35}S]methionine-labeled apolipoprotein E was first separated from other labeled proteins by flotation at a density of 1.21 g/ml. A variable proportion of newly synthesized apolipoprotein E floated at this density and was separated easily from other labeled proteins. Both brain apolipoprotein E and the apolipoprotein E secreted by astrocytes in vitro (lanes a and c, respectively, in Fig. 5) consisted predominantly of more acidic isoforms than were found in rat serum apolipoprotein E (lane b in Fig. 5). As expected if the higher-molecular-weight forms are sialylated, neuraminidase digestion of the apolipoprotein E secreted by the astrocytes resulted in a shift in the isoelectric focusing pattern to more basic forms (lane d in Fig. 5). The existence of two forms after neuraminidase digestion may be due to incomplete hydrolysis; however, the possibility that additional forms are present cannot be excluded.

Characterization of lipoprotein receptors expressed by primary cultures of brain cells

The ability of the cultured brain cells to bind and internalize lipoproteins was determined by using lipoproteins labeled with the fluorescent probe DiI. The canine apolipoprotein E HDL$_c$, lipoproteins that contain only apolipoprotein E, were labeled with DiI and incubated with the cells. As shown in Fig. 6 (left panel), almost all of the cells showed punctate fluorescence as a result of the internalization of the labeled lipoproteins and their sequestration into lysosomes. Incubation of the cells with DiI-labeled human LDL, which contain apolipoprotein B as their only protein constituent, gave similar results, i.e., most of the cells were fluorescently labeled but with a lower labeling intensity. The binding of the DiI-labeled apolipoprotein E HDL_c and LDL to the brain cells was highly specific. No uptake of the fluorescent lipoproteins was observed when the cells were incubated with DiI-labeled apolipoprotein E HDL_c in the presence of a 100-fold excess of nonlabeled apolipoprotein E HDL_c. In addition, chemical modification of the lysine residues of the human LDL by acetoacetylation blocked binding to the receptor, as assessed by the lack of uptake of DiI-labeled AcAc LDL. (It has been shown

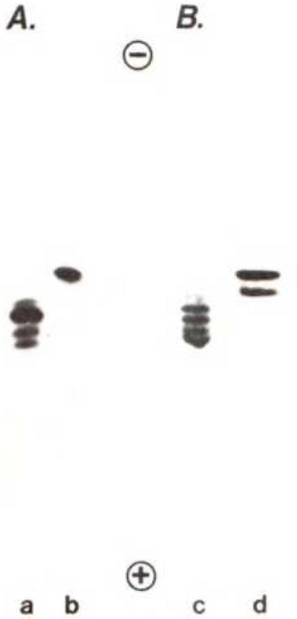

Fig. 5. Isoelectric focusing of rat brain apolipoprotein E, rat serum apolipoprotein E, and apolipoprotein E secreted by astrocytes in vitro. Panel A (an autoradiogram of an immunoblot) compares the isoform pattern of apolipoprotein E from rat brain extract (lane a) and rat serum (lane b). Panel B is an autoradiogram of $[^{35}S]$methionine-labeled apolipoprotein E secreted by astrocytes in culture before (lane c) and after (lane d) neuraminidase treatment. The apolipoprotein E secreted by the astrocytes was first separated from other labeled proteins by centrifugation (see Materials and Methods).

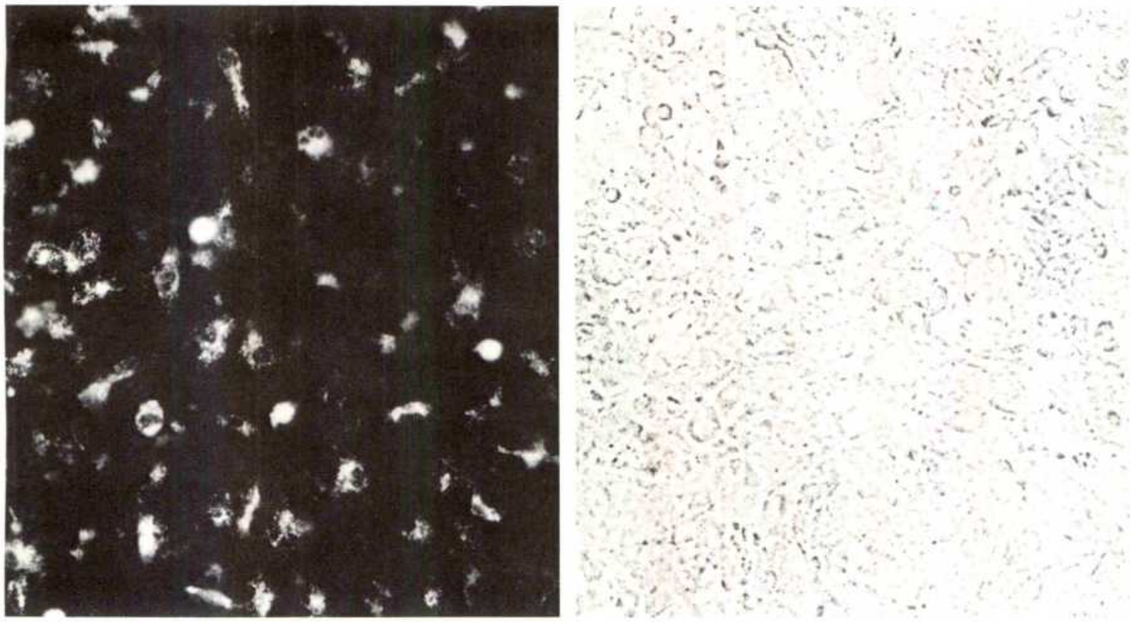

Fig. 6. The uptake of fluorescently labeled apolipoprotein E HDL_c by a primary culture of rat brain astrocytes. The same field has been photographed under fluorescence (left panel) and phase contrast (right panel) illumination. Primary cultures of astrocytes were established and maintained in culture in medium containing 10% fetal calf serum. The cells were then incubated for 24 h in medium containing 10% lipoprotein-deficient human serum to up-regulate apolipoprotein B,E(LDL) receptors. The cells were incubated for 5 h with apolipoprotein E HDL_c labeled with the fluorescent probe 1,1′-dioctadecyl-3,3,3′,3′-tetramethylindocarbocyanine (5 μg of protein/ml of medium). ×180.

that such modification blocks lipoprotein binding to apolipoprotein B,E(LDL) receptors on fibroblasts (for review, see Ref. 3).)

The receptors on the cultured astrocytes were further characterized by studying the direct binding of canine apolipoprotein E HDL$_c$, rat LDL, and rat HDL$_1$. The apolipoprotein E HDL$_c$ contain apolipoprotein E as their only protein constituent, rat LDL contain only apolipoprotein B, and rat HDL$_1$ contain apolipoprotein E and a variable small amount of apolipoprotein A-I. As shown in Fig. 7, direct binding experiments conducted at 4°C revealed that the binding of both rat LDL and apolipoprotein E HDL$_c$ was saturable, indicating that the lipoproteins bound to a limited number of receptors. When the data were analyzed as described by Scatchard [39], the K_d for the binding of apolipoprotein E HDL$_c$ and rat LDL was 0.10 (0.18 nM) and 3.2 μg/ml (3.5 nM), respectively. At receptor saturation, the cells bound approximately twice as much rat LDL as canine apolipoprotein E HDL$_c$. The rat lipoprotein HDL$_1$ also bound to receptors with high affinity (K_d, average of 2.9 μg/ml (3.4 nM)) (data not shown). At 37°C the cells bound, internalized, and degraded both rat LDL and rat HDL$_1$ (Fig. 8).

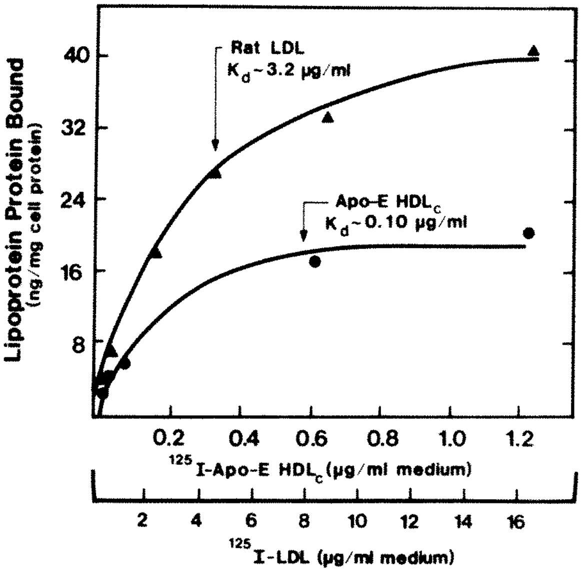

Fig. 7. The direct binding of rat LDL and canine apolipoprotein (apo) E HDL$_c$ to rat brain cells. Primary cultures of rat brain cells were derived from fetal rats and grown in culture for 5 days in Dulbecco's modified Eagle's medium containing 10% fetal calf serum. The medium was then changed to Dulbecco's modified Eagle's medium containing 10% lipoprotein-deficient human serum, and experiments were conducted 2 days later. The plates were cooled to 4°C, and the indicated concentrations of either ^{125}I-labeled rat LDL or ^{125}I-labeled apolipoprotein E HDL$_c$ were added in ice-cold Dulbecco's modified Eagle's medium containing 10% lipoprotein-deficient human serum. The plates were incubated in the cold room at 4°C for 3 h prior to washing the cells (see Materials and Methods). Nonspecific binding (i.e., binding that occurred in the presence of a 60-fold excess of nonlabeled β-VLDL) has been subtracted.

Competitive binding studies demonstrated that the rat LDL and HDL$_1$ were binding to the same receptors (Fig. 9). The rat LDL and HDL$_1$ were both capable of competing to the same extent for the binding (i.e., were able to compete for the same percentage of the total binding) of rat ^{125}I-labeled LDL or ^{125}I-labeled HDL$_1$. In contrast, normal rat HDL ($d = 1.125$–1.21 g/ml), which contain little apolipoprotein E, were not capable of competing for binding. Thus, the receptor responsible for binding the apolipoprotein B- and E-containing lipoproteins is the apolipoprotein B,E(LDL) receptor.

Rat LDL, rat HDL$_1$, and canine β-VLDL (a cholesteryl ester-rich lipoprotein that binds to the apolipoprotein B,E(LDL) receptor via the apolipoprotein E present on its surface [40]) were capable of stimulating the incorporation of [^{14}C]oleate into cholesteryl esters by the isolated brain cells (Fig. 10), whereas HDL without apolipoprotein E were not. The maximum level of stimulation observed with the rat LDL and HDL$_1$ was twice the level observed in the control brain cells, whereas incubation with β-VLDL resulted in a 4-fold increase in cholesteryl ester synthesis over the level seen in the control brain cells. The apparent cholesterol [^{14}C]oleate formation of control brain cells was 6-times greater than the amount observed for fibroblasts and macrophages. However, no significant differences were observed in the mass of cholesteryl ester in the control brain cells, fibroblasts, and macrophages. These data suggested that the cholesterol moiety of the cholesteryl esters within the control brain cells might have become radiolabeled. To test the ability of the cultured cells to metabolize [^{14}C]oleate, they were incubated with [^{14}C]oleate, and the cholesterol mass and the distribution of the radioactivity in the free and esterified cholesterol were analyzed.

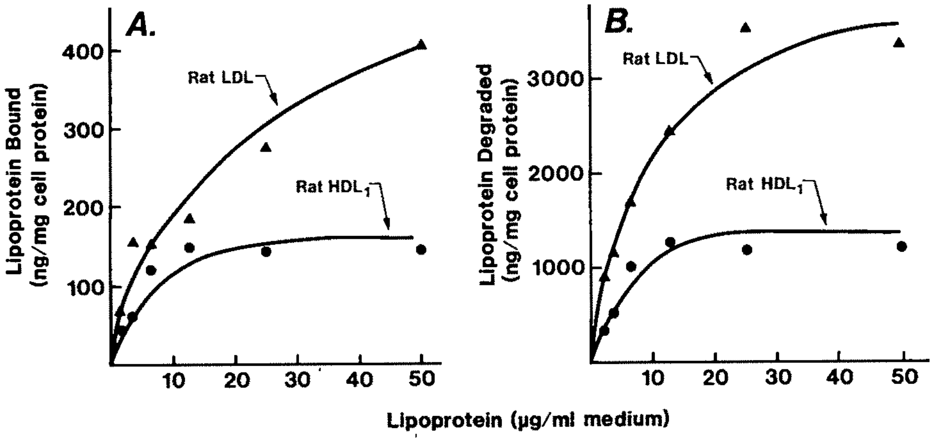

Fig. 8 Specific concentration-dependent binding and internalization (panel A) and degradation (panel B) of ^{125}I-labeled rat LDL (▲) and ^{125}I-labeled rat HDL$_1$ (●) by rat brain cells. Cells were obtained and maintained as described in Fig. 7. Following incubation with 10% lipoprotein-deficient human serum, the cells were incubated for 5 h at 37°C with the indicated concentration of either labeled rat LDL or rat HDL$_1$. Determination of cell-associated lipoproteins and degraded lipoproteins was performed as described in Materials and Methods. Nonspecific cell-associated binding and degradation, determined in the presence of a 60-fold excess of nonlabeled β-VLDL, has been subtracted.

The free cholesterol from the brain cells contained 4-times more radioactivity than was seen in the cholesterol from the fibroblasts and 8 times more than was observed in the macrophage cholesterol. Brain cells, therefore, oxidized [^{14}C]oleate and incorporated the acetate units into cholesterol more

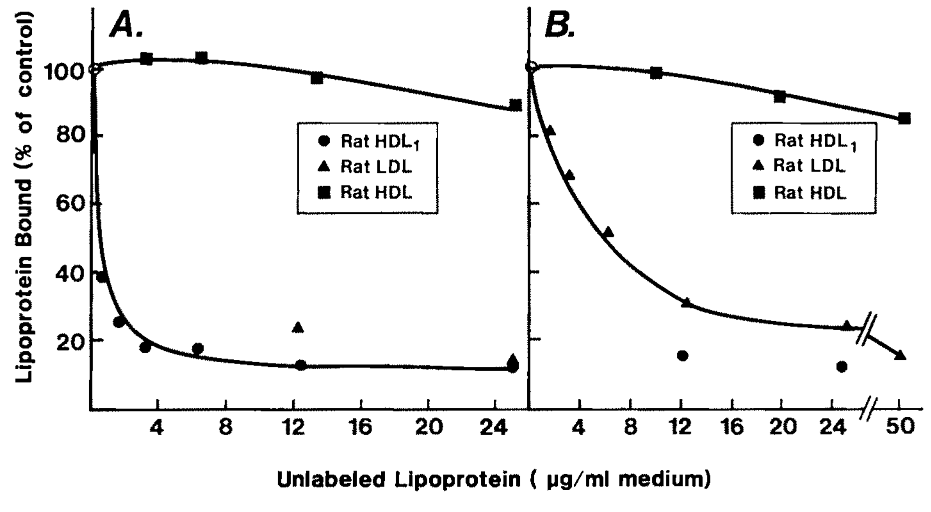

Fig. 9 Competition for the binding of ^{125}I-labeled rat LDL (panel A) and ^{125}I-labeled rat HDL$_1$ (panel B) by an excess of nonlabeled rat LDL, rat HDL$_1$, or rat HDL. Cells from fetal rat brains were grown in primary cultures for 5 days in Dulbecco's modified Eagle's medium containing 10% fetal calf serum. The medium was then changed to Dulbecco's modified Eagle's medium containing 10% lipoprotein-deficient human serum, and experiments were conducted on day 7 of growth in culture. The cells were cooled to 4°C and incubated for 2 h at 4°C with medium containing either 0.5 µg of ^{125}I-labeled rat LDL protein/ml or 0.5 µg of ^{125}I-labeled rat HDL$_1$ protein/ml along with the indicated concentrations of nonlabeled lipoprotein. The plates were then washed, the cells solubilized in 0.1 M NaOH, and the plates counted for radioactivity. The binding of ^{125}I-labeled rat LDL and ^{125}I-labeled rat HDL$_1$ in the absence of competing lipoproteins was 7.1 and 4.6 ng/mg of cell protein, respectively.

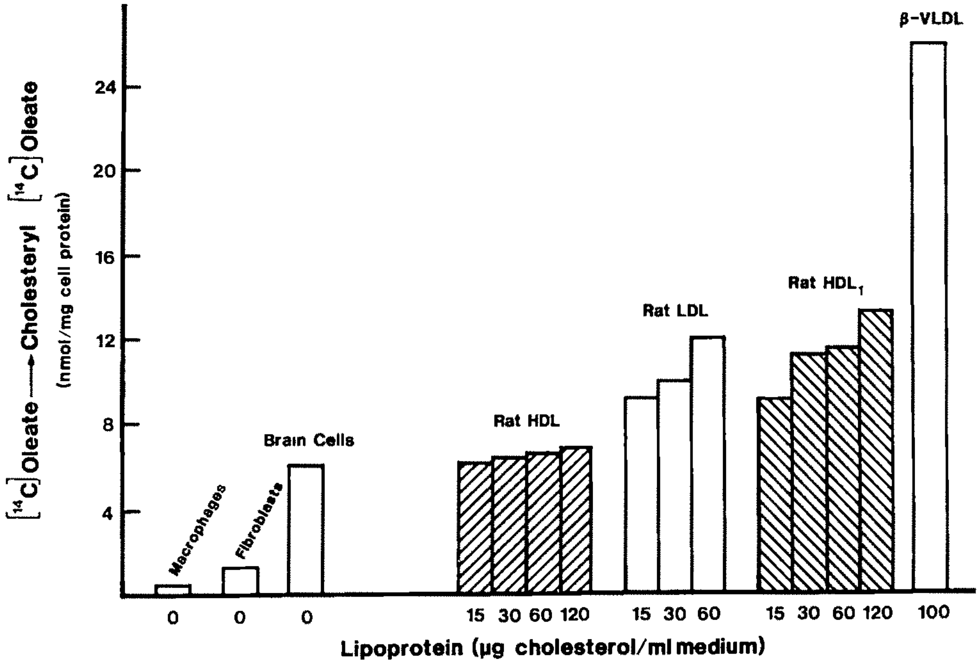

Fig 10 Stimulation of the incorporation of [^{14}C]oleate into cholesteryl [^{14}C]oleate by rat astrocytes as a function of the concentration of normal rat HDL, LDL, HDL$_1$. Primary cultures of rat brain astrocytes and human fibroblasts were grown for 6 days in Dulbecco's modified Eagle's medium containing 10% fetal calf serum Mouse peritoneal macrophages were assayed 2 days following isolation The cells were incubated for 16 h in serum-free Dulbecco's modified Eagle's medium containing 0 1 mM [^{14}C]oleate (24000 dpm/nmol) per dish, as well as the indicated concentration of either rat HDL, LDL, HDL$_1$, or β-VLDL The cells were harvested, and the concentration of cholesteryl [^{14}C]oleate in the cells was determined.

readily than did fibroblasts or macrophages.

Since the stimulation of the incorporation of [^{14}C]oleate into cholesteryl esters in response to incubation with lipoproteins did not provide a reliable measure of cholesteryl ester synthesis in astrocytes, the mass of cholesteryl ester was determined directly. Incubation of the cells at 37°C with β-VLDL (100 μg of lipoprotein cholesterol/ml of medium) for 16 h in serum-free medium resulted in a 21-fold increase in the amount of cholesteryl esters within the brain cells (1.15 μg of cholesteryl ester/mg of cell protein in control cells and 24.3 μg of cholesteryl ester/mg of cell protein after incubation with β-VLDL).

To determine whether the number of receptors was regulated by the content of cellular cholesterol, binding studies were performed following prior incubation of the cells with either fetal calf serum, lipoprotein-deficient human serum, or canine β-VLDL. Binding of rat LDL and canine apolipoprotein E HDL$_c$ was decreased by only 10% by preincubation with fetal calf serum compared with the binding to cells grown in the presence of lipoprotein-deficient human serum (data not shown). By contrast, when cells were preincubated with β-VLDL and the ability of the cells to bind ^{125}I-labeled apolipoprotein E HDL$_c$ was tested, a 75% reduction in binding was noted at the highest concentrations of β-VLDL (Fig. 11).

Discussion

A previous study showed that astrocytes of the brain synthesize and secrete apolipoprotein E in situ [8]. Our in vitro study now demonstrates that primary cultures of rat brain cells composed of approx. 95% astrocytes (and 3% macrophages and 2% other cell types) synthesize and secrete apolipoprotein E and metabolize apolipoprotein B- and E-containing lipoproteins in vitro. Dual-label immunocytochemical techniques revealed that cultured astrocytes, which were identified by their

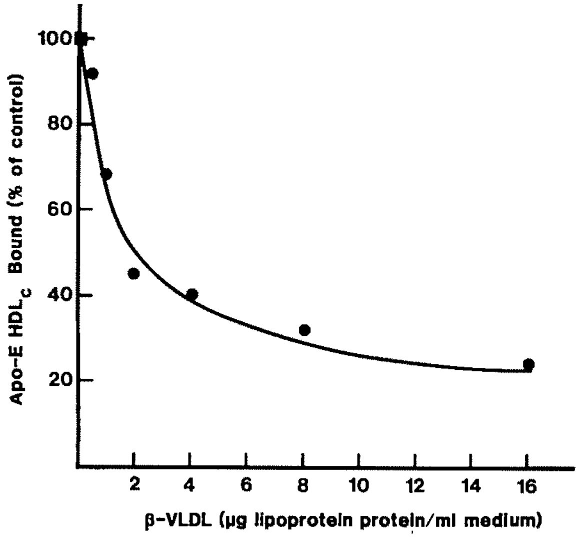

Fig. 11. Regulation of receptor expression by preincubation of brain cells with β-VLDL. Primary cultures of brain cells derived from fetal rats were grown for 5 days in Dulbecco's modified Eagle's medium containing 10% fetal calf serum. On day 5 the medium was changed: the control cells received Dulbecco's modified Eagle's medium containing 10% lipoprotein-deficient human serum, while the other cells received medium containing 10% lipoprotein-deficient human serum and increasing concentrations of canine β-VLDL. The plates were incubated for 40 h at 37°C and were washed three times with Dulbecco's modified Eagle's medium containing 10% fetal calf serum and once with Dulbecco's modified Eagle's medium containing 10% lipoprotein-deficient human serum. The cells were then incubated for 1 h at 37°C to internalize any bound lipoproteins. The plates were cooled to 4°C, and ^{125}I-labeled apolipoprotein (apo-) E HDL$_c$ was added (0.15 μg of HDL$_c$ protein/ml of Dulbecco's modified Eagle's medium containing 10% lipoprotein-deficient human serum) and incubated for 2 h at 4°C. The plates were then washed, the cells solubilized in 0.1 M NaOH, and the amount of radioiodine in the solubilized cells determined. The control value for the binding of the ^{125}I-labeled apolipoprotein E HDL$_c$ was 18 ng/mg of cell protein.

content of GFAP, contained apolipoprotein E within their secretory apparatus. Macrophages within brain cell cultures, which were identified by the presence of receptors for AcAc LDL, also contained apolipoprotein E in the region of the Golgi apparatus. Earlier work [41] established that mouse peritoneal macrophages synthesize and secrete apolipoprotein E at levels of less than 1% of their total secreted protein. As shown in the present study, primary cultures of rat brain cells secreted apolipoprotein E at a level of 1–3% of total secreted proteins. Since the astrocytes represented 95% of the cells in culture and clearly contained apolipoprotein E within their Golgi apparatus, it is reasonable to assume that they account for the majority of the apolipoprotein E produced by the cultures.

The apolipoprotein E secreted by the astrocyte cultures and the apolipoprotein E in rat brain extract both had a higher apparent molecular weight on SDS-polyacrylamide gels and a higher percentage of more acidic isoforms than did plasma apolipoprotein E. Neuraminidase digestion of the apolipoprotein E secreted by astrocytes demonstrated that the acidic isoforms resulted from multiple sialylation. (We have recently demonstrated that the apolipoprotein E present in both human and canine cerebrospinal fluid is more highly sialylated than plasma apolipoprotein E (unpublished data).) Sialylated forms of apolipoprotein E are known to be more acidic and to have a higher apparent molecular weight than nonsialylated forms [38]. Sialylated apolipoprotein E is secreted by other cell types in vitro [42,43].

Primary cultures of astrocytes were also shown to metabolize apolipoprotein E-containing lipoproteins by a specific, saturable high-affinity binding process. The receptor responsible for the uptake of lipoproteins by astrocytes is the apolipoprotein B,E(LDL) receptor, which has been previously characterized on rat fibroblasts [30] and other cells (for review, see Ref. 3). The apolipoprotein B,E(LDL) receptors on astrocytes bind both apolipoprotein B- and E-containing lipoproteins. Furthermore, the receptors are down-regulated by the internalization of lipoprotein cholesterol. These data are consistent with previous reports of the interaction of LDL with various glioma-derived cell lines [15,16].

One difference was noted between the processing of free fatty acids by the rat brain cells in primary culture and in macrophages and fibroblasts. The brain cells in culture were observed to oxidize free fatty acids and utilize these products for the de novo synthesis of cholesterol. Therefore, the incorporation of [^{14}C]oleate into cholesteryl esters cannot be used as a reliable measure of cholesteryl ester synthesis or acyl CoA : cholesterol acyltransferase activity in brain cells by methods used with other cell types [33].

These data are not unexpected; when [^{14}C]stearate is injected in vivo, a substantial proportion taken up by the brain is degraded and incorporated into cholesterol [44].

The role or roles of apolipoprotein E within the nervous system remain unknown; it may participate in the redistribution of lipids and in cholesterol homeostasis as it does in the plasma. Since apolipoprotein B is not present within the cerebrospinal fluid, apolipoprotein E is the major apolipoprotein in cerebrospinal fluid that is capable of lipid transport and regulation of lipid metabolism through known receptor-mediated processes. While the brain is capable of synthesizing cholesterol, it can also acquire cholesterol from the blood [45]. Boyles et al. [8] have noted that apolipoprotein E is present within the foot processes of astrocytes and suggest that it is secreted where these foot processes terminate at blood vessels. The apolipoprotein E secreted by astrocytes within the brain might transport this cholesterol to cells where it is needed and suppress the synthesis of cellular cholesterol. In addition, in the face of excess cholesterol, apolipoprotein E-containing lipoproteins passing into the cerebrospinal fluid could serve to transport lipid out of the brain into the plasma compartment. This transport could prevent the accumulation of cholesterol within the central nervous system.

Human cerebrospinal fluid contains 0.3–0.5 mg/dl cholesterol [46], or a total of 450–750 μg of cholesterol in 150 ml of cerebrospinal fluid [47]. Since the cerebrospinal fluid is replaced almost completely every 8 h [47], this clearance could account for the removal of 1.35–2.25 mg of cholesterol per day. This amount might be sufficient to maintain cholesterol homeostasis within the brain. A role for apolipoprotein E in reverse cholesterol transport (i.e., the removal of cholesterol from peripheral cells for clearance by the liver) has been postulated [48,49]. In addition, the ability of apolipoprotein E-rich lipoproteins to remove cholesterol from cholesterol-loaded cells has been clearly demonstrated [50,51]. While the precise function of apolipoprotein E within the nervous system has not been determined, mounting evidence suggests that it is involved in lipid movement. However, other important roles for apolipoprotein E within the nervous system cannot be ruled out.

Acknowledgments

The authors acknowledge the excellent technical assistance of Jim McGuire and Elizabeth Wilson, the preparation of figures by James X. Warger and Norma Jean Gargasz, the editorial assistance of Al Averbach and Sally Gullatt Seehafer, and the manuscript preparation by Kerry Humphrey. The anti-apolipoprotein E antibody was provided by Dr. Karl H. Weisgraber of Gladstone Foundation Laboratories.

References

1 Goldstein, J.L. and Brown, M.S. (1974) J. Biol Chem 249, 5153–5162
2 Goldstein, J L and Brown, M S (1977) Annu Rev. Biochem. 46, 897–930
3 Mahley, R.W and Innerarity, T L. (1983) Biochim. Biophys. Acta 737, 197–222
4 Brown, M S., Kovanen, P T. and Goldstein, J L (1981) Science 212, 628–635
5 Roheim, P S., Carey, M., Forte, T and Vega, G.L. (1979) Proc. Natl Acad. Sci. USA 76, 4646–4649
6 Pitas, R E., Weisgraber, K H., Boyles, J.K , Lee, S. and Mahley, R.W. (1986) Fed Proc 45, 587
7 Elshourbagy, N.A., Liao, W S , Mahley, R W. and Taylor, J.M. (1985) Proc Natl. Acad Sci. USA 82, 203–207
8 Boyles, J.K., Pitas, R.E , Wilson, E., Mahley, R.W. and Taylor, J.M (1985) J. Clin. Invest 76, 1501–1513
9 Ignatius, M.J , Gebicke-Härter, P.J , Skene, J.H P., Schilling, J.W , Weisgraber, K H., Mahley, R W. and Shooter, E.M (1986) Proc. Natl. Acad Sci. USA 83, 1125–1129
10 Boyles, J K., Weisgraber, K H , Mahley, R W., Ignatius, M J., Gebicke-Harter, P., Schilling, J. and Shooter, E.M. (1985) J. Cell Biol. 101, 125a
11 Snipes, G.J , McGuire, C B., Norden, J J. and Freeman, J.A. (1986) Proc Natl. Acad. Sci. USA 83, 1130–1134
12 Skene, J.H.P and Shooter, E M (1983) Proc. Natl. Acad Sci. USA 80, 4169–4173
13 Müller, H W , Gebicke-Härter, P.J., Hangen, D.H. and Shooter, E M (1985) Science 228, 499–501
14 Müller, HW., Ignatius, M.J., Hangen, D.H and Shooter, E M (1986) J. Cell Biol 102, 393–402
15 Rudling, M.J., Collins, V.P and Peterson, C.O. (1983) Cancer Res. 43, 4600–4605
16 Volpe, J J., Hennessy, S.W. and Wong, T. (1978) Biochim. Biophys Acta 528, 424–435
17 Hertz, L., Juurlink, B H J , Fosmark, H. and Schousboe, A (1982) in Neuroscience Approached through Cell Culture (Pfeiffer, S.E., ed.), pp. 175–186, CRC Press, Boca Raton, FL
18 Innerarity, T.L. and Mahley, R.W. (1978) Biochemistry 17, 1440–1447

19 Weisgraber, K.H., Innerarity, T.L. and Mahley, R.W (1978) J Biol. Chem. 253, 9053–9062

20 Goldstein, J L., Ho, Y.K., Brown, M.S., Innerarity, T L and Mahley, R.W (1980) J. Biol. Chem 255, 1839–1848

21 Weisgraber, K.H , Rall, S.C., Jr , Innerarity, T.L., Mahley, R.W , Kuusi, T. and Ehnholm, C (1984) J. Clin Invest. 73, 1024–1033

22 Weisgraber, K H. and Mahley, R W. (1983) in CRC Handbook of Electrophoresis, Vol. IV: Lipoproteins of Nonhuman Species (Lewis, L.A. and Naito, K H., eds), pp 103–132, CRC Press, Boca Raton, FL

23 Mahley, R.W and Weisgraber, K.H (1983) in CRC Handbook of Electrophoresis, Vol. IV: Lipoproteins of Nonhuman Species (Lewis, L.A. and Naito, H K., eds), pp. 151–173, CRC Press, Boca Raton, FL

24 Mahley, R.W , Innerarity, T.L., Weisgraber, K.H. and Fry, D.L. (1977) Am J. Pathol. 87, 205–226

25 Fainaru, M., Mahley, R.W , Hamilton, R.L. and Innerarity, T.L (1982) J. Lipid Res 23, 702–714

26 Pitas, R E., Innerarity, T.L. and Mahley, R W. (1980) J Biol. Chem 255, 5454–5460

27 Bolton, A.E and Hunter, W.M. (1973) Biochem. J. 133, 529–539

28 Pitas, R.E., Innerarity, T.L., Weinstein, J.N and Mahley, R.W (1981) Arteriosclerosis 1, 177–185

29 Laemmli, U.K. (1970) Nature 227, 680–685

30 Innerarity, T.L., Pitas, R.E. and Mahley, R W. (1980) J Biol Chem 255, 11163–11172

31 Pitas, R.E., Innerarity, T.L , Arnold, K.S. and Mahley, R.W (1979) Proc. Natl. Acad. Sci. USA 76, 2311–2315

32 Lowry, O H , Rosebrough, N.J , Farr, A.L and Randall, R.J (1951) J Biol Chem. 193, 265–275

33 Goldstein, J.L., Basu, S.K and Brown, M.S. (1983) Methods Enzymol. 98, 241–260

34 Innerarity, T.L., Pitas, R.E. and Mahley, R.W. (1986) Methods Enzymol. 129, 542–566

35 Brown, M S., Basu, S.K., Falck, J.R , Ho, Y.K. and Goldstein, J.L. (1980) J Supramol. Struct. 13, 67–81

36 Mahley, R W , Innerarity, T L , Weisgraber, K H. and Oh, S Y (1979) J Clin Invest. 64, 743–750

37 Pitas, R.E , Innerarity, T L. and Mahley, R W. (1983) Arteriosclerosis 3, 2–12

38 Zannis, V.I., Breslow, J.L , Utermann, G , Mahley, R W , Weisgraber, K H., Havel, R.J , Goldstein, J.L., Brown, M.S., Schonfeld, G., Hazzard, W R. and Blum, C (1982) J Lipid Res. 23, 911–914

39 Scatchard, G (1949) Ann. N.Y. Acad. Sci 51, 660–672

40 Innerarity, T.L., Arnold, K S., Weisgraber, K H. and Mahley, R.W (1986) Arteriosclerosis 6, 114–122

41 Basu, S.K., Brown, M.S., Ho, Y K., Havel, R J. and Goldstein, J L. (1981) Proc. Natl. Acad. Sci. USA 78, 7545–7549

42 Basu, S.K., Ho, Y.K., Brown, M.S., Bilheimer, D.W., Anderson, G W and Goldstein, J.L (1982) J. Biol Chem. 257, 9788–9795

43 Zannis, V.I., Breslow, J.L., SanGiacomo, T.R., Aden, D P. and Knowles, B.B. (1981) Biochemistry 20, 7089–7096

44 Gozlan-Devillierre, N , Baumann, N. and Bourre, J -M. (1978) Biochim. Biophys Acta 528, 490–496

45 Horrocks, L.A. and Harder, H.W. (1983) in Handbook of Neurochemistry (Lajtha, A , ed), Vol. 3, pp. 1–16, Plenum Press, New York

46 Illingworth, D R. and Glover, J (1971) J Neurochem. 18, 769–776

47 Pollay, M. (1977) in Proceedings of the Congress of Neurological Surgeons· Clinical Neurosurgery, pp. 254–269, Williams & Wilkins, Baltimore, MD

48 Mahley, R.W (1982) Med. Clin North Am. 66, 375–402

49 Mahley, R.W (1983) Arch. Pathol Lab Med. 107, 393–398

50 Gordon, V., Innerarity, T L. and Mahley, R.W. (1983) J Biol. Chem. 258, 6202–6212

51 Koo, C , Innerarity, T.L. and Mahley, R W (1985) J. Biol Chem. 260, 11934–11943

Biochimica et Biophysica Acta 917 (1987) 162–168
Elsevier

BBA 52323

Enzyme immunoassay of a plant phospholipid transfer protein

Michèle Grosbois, Françoise Guerbette, Dominique Douady
and Jean-Claude Kader

Laboratoire de Physiologie Cellulaire, Université Pierre et Marie Curie, Paris (France)

(Received 18 July 1986)

Key words. Phospholipid transfer protein; Enzyme immunoassay; Antibody; (Maize seed)

An antibody against the phospholipid transfer protein from maize seedlings has been raised in rabbits and purified by ion-exchange or affinity chromatography. When checked by double-immunodiffusion, the antibody gave a single precipitin line with the pure protein or a crude extract. An immunoinhibition of the transfer activity was observed when the antibody was incubated with phospholipid transfer protein. This specific antibody was used to develop an enzyme immunoassay. The enzyme immunoassay measured transfer protein levels in the range 1–20 ng. The enzyme immunoassay was used to detect the transfer protein after high-performance liquid chromatography of a partially purified extract and to determine the amount of the transfer protein in crude extracts. The values found (2% of the postmicrosomal proteins or 4.1% of the total proteins precipitated by ammonium sulfate) indicate that the maize cytosol is rich in phospholipid transfer protein. This work, which describes for the first time in plants the use of enzyme immunoassay to quantify phospholipid transfer proteins, opens new perspectives in the study of the regulation of their biosynthesis.

Introduction

Phospholipid transfer proteins are widely distributed among eucaryotic (animals, higher plants, yeast) or procaryotic (*Rhodopseudomonas sphaeroides*) cells (for reviews, see Refs. 1–4). These proteins, detected in various plants [4], have been purified to homogeneity from maize seedlings [5,6], spinach leaves [7] or castor bean seedlings [8]. Plant phospholipid transfer proteins have similar biochemical properties: high isoelectric point (around 9) and low molecular mass (9 kDa for spinach; 9.2 kDa for castor bean; 10 kDa (which forms a dimer of 20 kDa) for maize).

These proteins have been demonstrated to facilitate in vitro a nonspecific intermembrane transfer of phospholipids [4]. This led to the hypothesis suggesting that these proteins may carry phospholipids from sites of active synthesis (for example, endoplasmic reticulum) to membranes unable to synthesize these lipids [1,3,5].

In order to try to demonstrate this hypothesis, it could be of interest to determine the levels of the phospholipid transfer proteins in different tissues under a variety of physiological conditions. One of the best approaches for such studies is the use of immunochemical techniques. These methods have been employed to study the specific and nonspecific phospholipid transfer proteins from normal and cancerous hepatocytes [9,11].

In the present paper, we have used an enzyme immunoassay to carry out – for the first time in higher plants – a qualitative and quantitative study

---

Correspondence: Dr. J.-C. Kader, Laboratoire de Physiologie Cellulaire (Unité Associée C N.R.S. 1180), Université Pierre et Marie Curie, 4 place Jussieu, 75005 Paris, France

0005-2760/87/$03 50 © 1987 Elsevier Science Publishers B V (Biomedical Division)

of a phospholipid transfer protein from maize seedlings.

Materials and Methods

Plant materials. Maize (*Zea mays* L. cv INRA 508) seeds were grown in darkness at 30°C for 3 days. In some experiments maize seedlings were grown for 10 days under fluorescent light (14 h light periods).

Chemicals. Agarose (Indubiose) was obtained from IBF, CNBr-activated Sepharose 4B and CM-Sepharose were purchased from Pharmacia, Tris-barbiturate buffer (pH 8.6) from LKB, poly(ethylene glycol) 30 000, egg phosphatidylcholine and Brilliant blue R were obtained from Sigma, sodium dodecyl sulfate and CM Affi-Gel Blue from Bio-Rad, microtiter plates certified from NUNC, Denmark, and sheep anti-rabbit IgG antibodies conjugated with alcaline phosphatase from Biosys, France. All other chemicals were reagent grade.

Preparation of phospholipid transfer proteins. Phospholipid transfer protein was purified to homogeneity from maize seedlings, according to the previously published techniques [6]. After precipitation of the proteins from membrane-free supernatant by ammonium sulfate, the dialyzed proteins were submitted to a gel-filtration step (Sephadex G-75). The active low molecular-mass fractions were chromatographed on a carboxymethyl-Sepharose column. The fractions containing the pure proteins were collected. The purified protein was thoroughly washed with distilled water, with 0.02% sodium azide through ultrafiltration membrane (Amicon Y M2). The concentrated protein, (average concentration, 1 mg · ml^{-1}) determined according to Lowry et al. [12] was kept at +4°C or frozen with 50% glycerol at −20°C until use. In some experiments, crude protein extracts were prepared according to the previously described technique [6] from roots or stems of 3-day-old etiolated corn seedlings (cultivated at 30°C in darkness).

Immunization of rabbits against maize phospholipid transfer protein. Maize purified phospholipid transfer protein (1 mg · ml^{-1}) was inserted into liposomes prepared from egg yolk phosphatidylcholine (1 mg · ml^{-1}) by sonication (1 min in melting ice) under nitrogen [11]. The protein-containing liposomes were emulsified with complete Freund's adjuvant for the first two immunizations. The mixtures were subcutaneously injected in several points in the back and shoulders of rabbits (New Zealand); the booster injections (with incomplete Freund adjuvant) were performed every month. Sera were periodically collected (8–10 days after a booster injection) and tested for immunoreactivity by Ouchterlony double immunodiffusion [13]. Active sera were usually obtained 3–4 months after the first injection.

Purification of immunoglobulin fractions. IgGs were prepared from active sera or preimmune sera by ammonium sulfate precipitation follwed by DEAE-cellulose chromatography for double-diffusion tests. For enzyme immunoassay, total IgGs were purified from the serum by CM Affi-Gel Blue. This solution of IgGs was adjusted to the initial serum dilution and constituted the antibody stock solution. For the immunoinhibition experiments, a specific IgG fraction was obtained by affinity chromatography. Maize phospholipid transfer protein (10 mg) was coupled to CNBr-activated Sepharose 4B (1 g); the immunoadsorbent was then packed in a small column and washed with 0.015 M potassium phosphate buffer/0.15 M NaCl (pH 7.5). Then, 30 mg of IgG fraction purified by CM Affi-Gel Blue were deposited on the column. Bound IgGs, which represent 5% of the total IgGs, were eluted with 0.53 M formic acid (pH 2.0) according to Ref. 11.

Double immunodiffusion. Immunodiffusion was carried out according to the method of Ouchterlony and Nilsson [13] on 1% Agarose/Tris-barbiturate (pH 8.6) gels at 25°C for 24 h. For some immunodiffusion 4% poly(ethylene glycol) was incorporated in the gel to increase the sensitivity of the precipitin reaction as previously reported by Chua and Blomberg [14]. The immunoprecipitates were visualized by staining the plates in 0.5% Coomassie Brilliant blue R/45% ethanol/10% CH_3COOH for 15 min.

Inhibition studies. Purified maize phospholipid transfer protein was incubated for 30 min at 30°C with increasing concentration of specific anti-maize phospholipid transfer protein IgG (affinity purified) in 0.05 M Tris-HCl/0.25 M sucrose/0.001 M EDTA (pH 7.2). The mixture was cooled to 0°C and centrifuged after 3 h. The phosphatidylcholine transfer activity was determined in the supernatant. Transfer assays were performed by measuring the transfer of [^{3}H]phosphatidylcholine from liposomes to mitochondria as previously described [5].

High-performance liquid chromatography of proteins. A fast protein liquid chromatography equipment (Pharmacia, Sweden) was used. The pure protein or the active fractions from the Sephadex G-75 column were injected into a Mono S column equilibrated with 10 mM Tris/3 mM sodium azide/8 mM 2-mercaptoethanol (pH 7.5). The column was then eluted at a flow rate of 1 ml · min^{-1} with a gradient of NaCl in the same buffer.

Enzyme immunoassay. Qualitative and quantitative determinations of maize phospholipid transfer protein have been performed by an immunoassay in which the phospholipid transfer protein is immobilized on a plastic plate (96-well microtiter plates) and detected indirectly by a second antibody (i.e., anti-rabbit IgG antibody conjugated with alcaline phosphatase).

A typical experiment was performed as follows. Each well was coated with 100 μl solution of variable concentration of pure phospholipid transfer protein or unknown samples of phospholipid transfer protein in 10 mM Tris/0.15 M NaCl (pH 7.4). The plate was left overnight at 4°C. During each incubation period, the plate was covered with a plastic lid and put inside a plastic bag, in contact with a damp paper towel, to lower the surface charge effects.

The plate was then rinsed four times with 10 mM Tris/0.15 M NaCl/0.01% Triton X-100 (pH 7.4). 100 μl of this buffer containing 10 μg/ml of casein were added and the plate was incubated 1 h at 37°C. After incubation the plate was washed four times with the buffer and 100 μl of specific anti-phospholipid transfer protein antibody was added (before use, the stock solution was diluted 10000-times in the same buffer containing 50 μg/ml of casein).

Immune complex was allowed to form at 4°C for 2 h. The plate was then washed four times with the same Tris/NaCl/Triton buffer. The remaining immobilized antigen-antibody complex was revealed by sheep anti-rabbit IgG antibodies conjugated with alcaline phosphatase diluted to 1/5000 in the same buffer. An additional incubation period of 1 h at 37°C was followed by three washings with the buffer and one washing with 10 mM Tris/0.15 M NaCl (pH 8).

The quantity of enzyme remaining in individual wells was determined by adding 100 μl of the substrate solution (0.26 mg · ml^{-1} of *p*-nitrophenylphosphate in 1 M Tris buffer (pH 8)).

The plate was incubated again at 37°C for 1 h, then the enzyme was inhibited by addition of 50 μl of 0.2 M K_2HPO_4.

Absorbance measurements were then performed at 405 nm with a COOKE-AM 120 autoreader.

Results

Immunodiffusion studies

After Ouchterlony double immunodiffusion, anti-maize phospholipid transfer protein produced a single precipitin line with the pure protein (Fig. 1). It is to be noted that this reaction was only observed at least 3 months after the first injection. Crude protein extracts, prepared from stems or roots excised from 3-day-old etiolated maize seedlings or green leaves, gave a precipitin line fusing with that found with the pure protein (data not shown). These results suggest that the antibody is specific for maize phospholipid transfer protein,

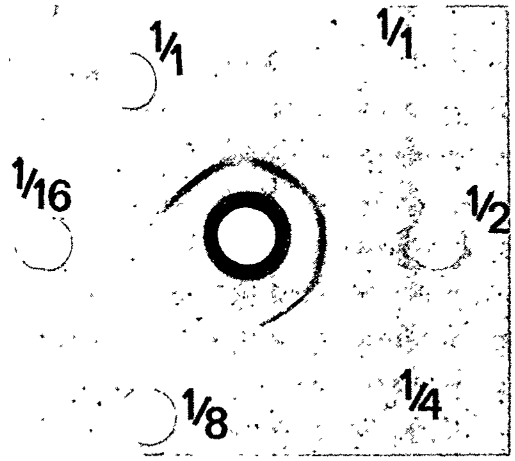

Fig. 1 Ouchterlony double immunodiffusion. The center well contained 20 μl of anti-maize phospholipid transfer protein IgG. Peripheric wells contained 20 μl of antigen (pure maize phospholipid transfer protein) at different concentrations from 1/1 to 1/16 (1/1 = 1 mg · ml^{-1})

since the crude extracts gave only one precipitin line fusing with that observed with the purified protein.

Immunoprecipitation of maize phospholipid transfer protein

After incubation of pure maize phospholipid transfer protein with increasing amounts of the affinity purified antibody and centrifugation of the mixture, the supernatants were checked for phospholipid transfer activity. A progressive inhibition of the activity was observed. A complete inhibition of the transfer activity was seen at an IgG/transfer protein ratio of 10:50 (w/w). Incubation with preimmune IgGs in the same conditions had no effect on the transfer activity. This result confirms that the anti-maize IgG is truly reactive with the phospholipid transfer protein (Fig. 2).

Specificity of the immunoassay

The specificity of the enzyme immunoassay was tested to make sure that no cross-reaction would interfere with the detection of phospholipid transfer protein or with the quantitative determinations.

For this purpose, the first two steps of the

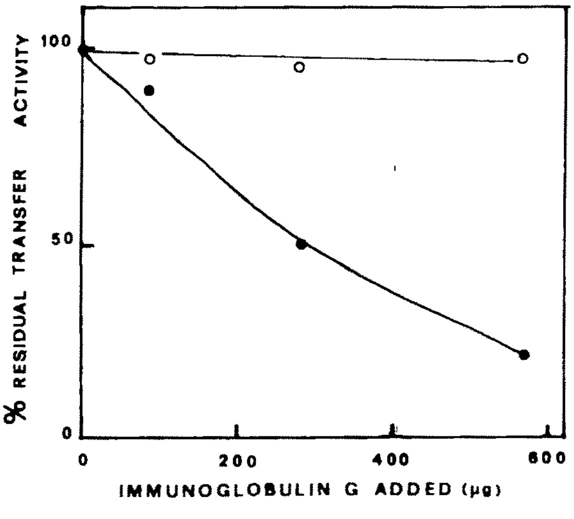

Fig 2. Effect of anti-maize phospholipid transfer protein monospecific IgG on phospholipid transfer activity 140 µg of phospholipid transfer protein were incubated with increasing amounts of IgG (affinity purified) and assayed for activity as described in Materials and Methods (●) The same test was carried out with preimmune IgG prepared by DEAE-chromatography (○) Results are expressed as % residual activity vs. IgG quantities.

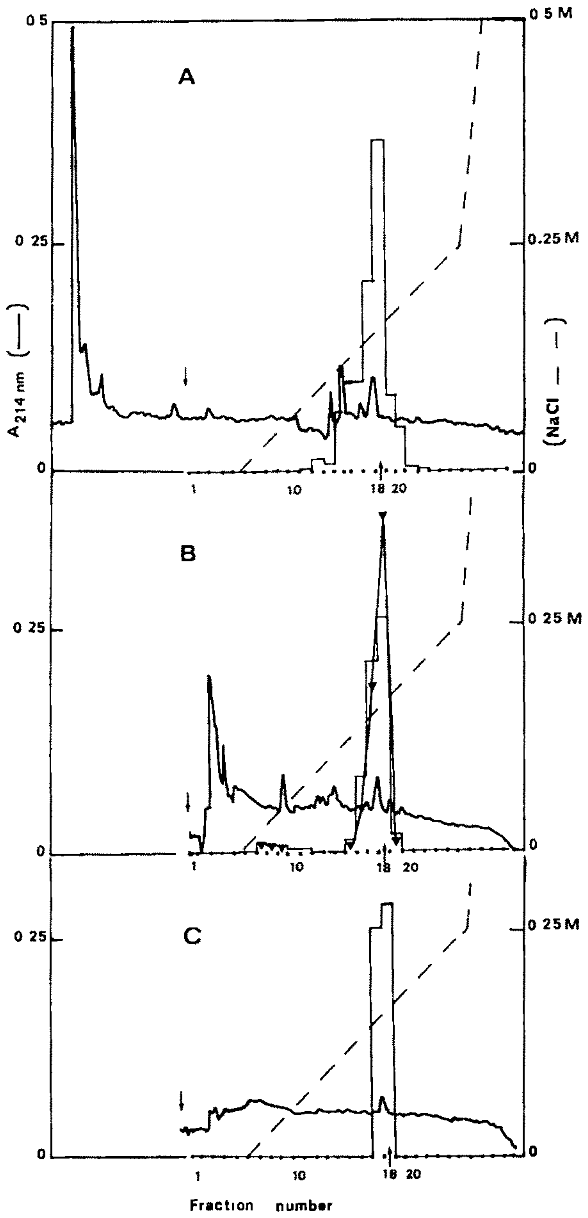

Fig 3. Immunohistograms corresponding to different steps of purification of phospholipid transfer protein after separation by fast protein liquid chromatography A, Protein extract; B, Sephadex G-75 fraction; C, pure phospholipid transfer protein. ———, absorbance at 214 nm; □, level of phospholipid transfer protein determined by enzyme immunoassay, absorbance at 405 nm. ▼, Transfer activity; - - - - - -, NaCl concentration (M).

transfer protein purification, according to the technique previously described [5] were tested. The corresponding fractions were: (1) the total protein extract obtained after ammonium sulfate precipitation and dialysis; (2) Sephadex G-75 fraction, corresponding to a low molecular-mass fraction – the only active – detected after separation of the whole protein extract on a molecular sieve.

Protein extract and Sephadex G-75 fractions were separated by fast-protein liquid chromatography. The fractions eluted by the NaCl gradient were subjected to enzyme immunoassay. The immunohistogramm obtained from the protein extract (Fig. 3A) showed a single peak of immunoreactivity with a maximum response at the same elution volume as the pure phospholipid transfer protein in the same conditions (Fig. 3C). Sephadex G-75 fractions were both assayed for phospholipid transfer activity and subjected to enzyme immunoassay. The immunohistogram obtained (Fig. 3B) exhibited a single peak of immunoreactivity strictly superimposed on the peak of transfer activity, and at the same elution volume as the pure protein. Of interest, this peak corresponded to a peak of absorbance at 214 nm in the Sephadex G-75 fraction as well as in the protein extract. A similar peak is obtained with pure phospholipid transfer protein. For each analysis, the non-retained proteins were collected in bulk. This fraction tested by enzyme immunoassay did not show any immunoreactivity.

These results showed there was no cross-reactive material in the protein extract or in the Sephadex G-75 fraction. This result assured the detection of phospholipid transfer protein in a complex mixture corresponding to any of its steps of purification and allowed us to quantitate the protein from both steps without further purification.

Quantitative tests

Fig. 4 shows that increasing concentrations of pure maize phospholipid transfer protein, in the range of 1–20 ng/100 μl, gave a linear response. This indicates that the adsorption of the pure protein to the plastic surface of the plate was linear up to 20 ng. Measurements concerning unknown amounts of phospholipid transfer protein present in complex mixtures have been made using different dilutions so as to ascertain that values to be compared to the dose-response line actually lie on the curve. Levels of phospholipid transfer proteins at different purification steps were obtained

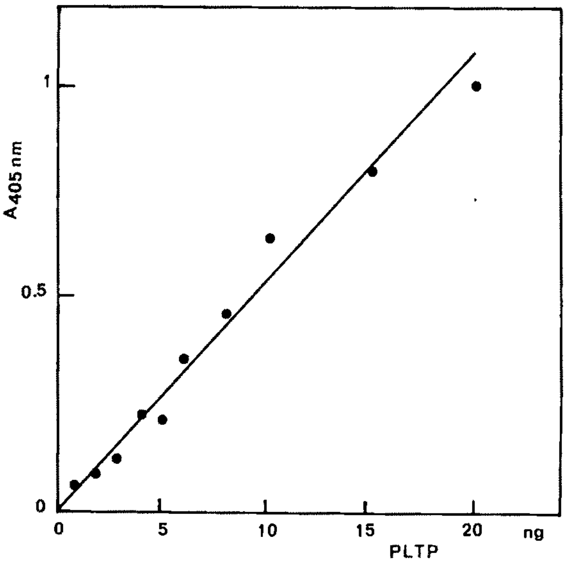

Fig 4. Enzyme immunoassay standard curve for maize phospholipid transfer protein (PLTP). Specific IgG concentration: 1/10000 of the original serum concentration.

TABLE I

QUANTITATION OF MAIZE PHOSPHOLIPID TRANSFER PROTEIN IN COMPLEX MIXTURES

Steps of purification	Dilution factor	Phospholipid transfer protein (% of total protein [c])
Protein extract [a]	1/10000	4.7 (2)
	1/12500	4.0 (2)
	1/15000	3.6 (2)
	1/17500	3.8 (2) $X = 4.1 \pm 0.7$
	1/20000	3.3 (2)
Sephadex G-75 [b]	1/5000	15.9 (2)
	1/6250	15.8 (3)
	1/7500	15.9 (3)
	1/10000	15.0 (2) $X = 15.6 \pm 0.8$

[a] Obtained after ammonium sulfate precipitation and dialysis (19.2 mg protein/ml).

[b] Pooled active fractions from Sephadex G-75 column (1.7 mg protein/ml).

[c] The amount of phospholipid transfer protein is expressed in percent of total protein present in the fraction Values represent mean of several independent enzyme immunoassay: numbers in parentheses are the number of samples tested for each dilution X represents mean±standard deviation of values obtained from several dilutions of a given extract.

(Table I): phospholipid transfer proteins accounted for 4.1% of the total proteins recovered after ammonium sulfate precipitation and 15.5% of Sephadex G-75 fraction. The transfer protein enrichment between those two steps of purification is a factor of 3.8. These results are consistent with those obtained previously [6] for the improvement of specific activity during the same steps of purification. Specific activity has been shown to be enhanced by a factor of 3.3 between protein extract and Sephadex G-75 steps. In some experiments, immunoassays were carried out on postmicrosomal supernatants (obtained after centrifugation at 100 000 × *g* for 1 h) without any precipitation by ammonium sulfate. Phospholipid transfer protein accounted for 2% of the postmicrosomal supernatant proteins.

Discussion

Although immunochemical techniques using antibodies directed against animal phospholipid transfer proteins have been developed [9–11], these methods have never been applied to similar proteins from higher plants. This work describes, for the first time, the use of an enzyme-immunoassay for the study of a plant phospholipid transfer protein. By using this approach, it was found that the phospholipid transfer protein is abundant in maize seedlings (about 4% of the total proteins recovered after ammonium sulfate precipitation).

The specific character of the antibody used in this work was shown by enzyme immunoassay coupled to high-performance liquid chromatography. No fraction other than that corresponding to the phospholipid transfer protein was reactive. In contrast, IgG directed against lipid transfer protein from rat tissues reacted with the low-molecular mass protein as well as with a high-molecular-mass fraction [11], probably a higher-molecular-mass precursor [15]. The specificity of the anti-maize IgG was demonstrated by the inhibition of the phospholipid transfer activity of maize protein. Immunoinhibition of the lipid transfer activity has been studied in the case of specific and nonspecific phospholipid transfer proteins from animals [9,10].

In this work, a one-step immunoassay method, based on the adsorption of the antigen on plastic plates, was used, giving a linear response up to 20 $\mathrm{ng} \cdot 100\ \mu\mathrm{l}^{-1}$; this is not true for larger amounts of proteins. Two-step competitive immunoassays have also been performed according to Engvall [16]; however, the results were not satisfactory for maize phospholipid transfer protein. As a comparison, rat liver lipid transfer protein was measured by enzyme immunoassay in the range 0.2 to 2 ng [11]. Using radioimmunoassay, with labelled specific phospholipid transfer protein from rat liver, a linear curve was found between 5 and 50 ng [17].

The acquisition of a highly specific enzyme immunoassay for maize protein allowed the determination of its amount in crude extracts prepared from maize seedlings. The results given by several experiments performed on different batches indicated that phospholipid transfer protein is abundant in the total protein extract from maize seedlings. This new finding is in agreement with the four different observations: (i) high amounts of pure phospholipid transfer proteins were obtained from seeds (as an example, 60 mg starting from 2 kg of dry seeds); (ii) only a 100-fold purification factor is needed for obtaining a homogeneous protein [6]; (iii) a peak of absorbance corresponding to phospholipid transfer protein is clearly seen after separation of low-molecular-mass proteins by fast protein liquid chromatography (Fig. 3B); (iv) when low-molecular-mass fractions obtained after gel filtration were separated by SDS-electrophoresis, the staining of the band corresponding to the phospholipid transfer protein (9 kDa) was about 15–20% of the total staining intensity determined by densitometry in all the detected bands. In contrast, nonspecific phospholipid transfer proteins from rat tissues are minor proteins; they represent 0.08% of the total 105 000 × *g* supernatant proteins from rat liver and 0.01% of lung. The value for liver agrees with the need of 1500-fold purification to obtain a homogeneous protein [1].

The abundance of phospholipid transfer protein in maize cytosol is similar to that found for fatty acid binding proteins in animal cells; in liver, values equal to 5% have been published [18]. Of interest, it has been also demonstrated that phospholipid transfer protein from spinach [19] and maize (unpublished data) are able to bind fatty acids.

In conclusion, the development of enzyme immunoassay for the determination of maize phospholipid transfer protein provides a sensitive method to quantitate this protein without the need to determine its transfer activity. This is important in plant extracts containing several interfering compounds and degradative enzymes which perturb the measurement of this activity [20]. The enzyme immunoassay approach will facilitate, in future studies, the determinations of the variations of the levels of maize phospholipid transfer protein during crucial physiological stages of the plant. This may give new information on the relations between the biosynthesis of the phospholipid transfer protein and the biogenesis or turnover of membrane lipids.

Acknowledgements

The authors are much indebted to Dr. Quintin-Colonna and Mrs. Mnich (Ecole Nationale Vétérinaire d'Alfort, Service de M. le Professeur Pilet) for rabbit immunizations.

References

1 Wirtz, K.W A (1982) in Lipid-Protein Interactions (Jost, P. and Griffiths, H., eds), pp 151–231, Wiley Interscience, New York

2 Zilversmit, D.B. and Hughes, M E (1976) Methods Membrane Biol 7, 211–259

3 Kader, J.C., Douady, D. and Mazliak, P. (1982) in Phospholipids (Hawthorne, J N and Ansell, G.B., eds.), pp 279–311, Elsevier/North-Holland, Amsterdam

4 Kader, J C. (1985) Chem Phys Lipids 38 51–62

5 Douady, D., Grosbois, M., Guerbette, F. and Kader, J C (1982) Biochim. Biophys. Acta 710, 143–153

6 Douady, D., Guerbette, F, Grosbois, M and Kader, J.C (1985) Physiol. Vég 23, 373–380

7 Kader, J.C., Julienne, M and Vergnolle, C (1984) Eur J Biochem. 139, 411–416

8 Watanabe, S. and Yamada, M (1986) Biochim Biophys Acta 876, 116–123

9 Poorthuis, B J.H.M., Van der Krift, T P, Teerlink, T, Akeroyd, R., Hostetler, K.Y. and Wirtz, K.W.A (1980) Biochim Biophys. Acta 600, 376–386

10 Teerlink, T, Van der Krift, T., Post, M and Wirtz, K.W A (1982) Biochim Biophys Acta 713, 61–67

11 Teerlink, T, Van der Krift, T P, Van Heusden, P.H. and Wirtz, K W.A (1984) Biochim. Biophys Acta 793, 251–259

12 Lowry, O.H., Rosebrough, N.J, Farr, A L and Randall, R.J (1951) J Biol Chem. 193, 265–275

13 Ouchterlony, O and Nilsson, L.A (1973) Handbook of Experimental Immunology (Weire, D M, ed), 1, 10 1–19 39, blackwell Scientific Publications, Oxford

14 Chua, N.H. and Blomberg, F. (1979) J. Biol Chem 254, 215–223

15 Van der Krift, P., Leunissen, J., Teerlink, T., Van Heusden, G.P H, Verkleij, J. and Wirtz, K W.A. (1985) Biochim Biophys Acta 812, 387–392

16 Engvall, E. (1980) Methods Enzymol. 70A, 419–439

17 Teerlink, T, Poorthuis, B.J H M., Van der Krift, T. and Wirtz, K.W.A (1981) Biochim. Biophys Acta 665, 74–81

18 Ockner, R.K., Manning, J.S and Kane, J P (1982) J Biol. Chem 257, 7872–7878

19 Rickers, J., Tober, I. and Spener, F (1984) Biochim Biophys Acta 794, 313–319

20 Kader, J.C. (1975) Biochim. Biophys Acta 380, 31–44

Biochimica et Biophysica Acta 917 (1987) 169–177
Elsevier

BBA 52325

Hydrolysis of membrane-associated phosphoglycerides by mitochondrial phospholipase A_2

J.M. de Winter, H.B.M. Lenting, F.W. Neys and H. van den Bosch

Laboratory of Biochemistry, State University of Utrecht, Utrecht (The Netherlands)

(Received 11 July 1986)

Key words: Phospholipase A_2, Phosphoglyceride hydrolysis; Active site inhibition; (Rat liver mitochondrion)

Conversion of membrane-bound substrates by membrane-associated enzymes can proceed in principle via intramembrane and intermembrane action. By using rat-liver mitochondria containing labeled phosphatidylethanolamine and inactivated phospholipase A_2 as substrate source, and mitochondria containing unlabeled substrate and active enzyme, it is shown that hydrolysis of phosphatidylethanolamine by mitochondrial phospholipase A_2 proceeds nearly entirely via intramembrane enzyme action. A study of the characteristics of this mode of enzyme action showed that all mitochondrial phosphoglycerides were hydrolyzed. Plots of approximate initial velocities of hydrolysis against the remaining amounts of each individual phospholipid, indicated that phosphatidylethanolamine was hydrolyzed fastest, with a rate about twice that for phosphatidylcholine and about 10-fold that for cardiolipin. The initial rates remained nearly constant in the initial phase of the hydrolysis, suggesting that the enzyme is surrounded by excess substrate.

Introduction

Rat liver mitochondria contain a membrane-associated phospholipase A_2 capable of hydrolyzing endogenous mitochondrial phospholipids [1–4]. Generally, it has to be realized that there are two possible modes of action when membrane-bound enzymes are assayed in vitro for their action towards membrane-bound substrates. Firstly, an intramembrane action in which the enzyme acts on substrate in its own membrane, and secondly, an intermembrane route in which enzyme of one membrane acts on substrate in a second membrane and vice versa (compare Fig. 1). Thus, in such systems the measured conversion of a radioactive membrane-bound substrate is the sum of intra- and intermembrane routes, and the contribution of each of these routes cannot be assessed.

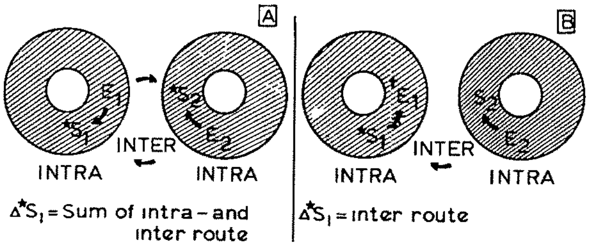

Fig 1. Comparison of intra- and intermembrane mode of action of membrane-bound enzyme. (A) Total conversion of radioactive substrate ($\Delta{}^*S_1$) in membranes 1 and 2 is the sum of intramembrane action of enzymes E_1 and E_2 on $^*S_1$ and $^*S_2$, respectively, and the intermembrane actions of enzymes E_1 on $^*S_2$ and E_2 on $^*S_1$. (B) Schematic representation of a procedure to determine the contribution of the intermembrane route, i.e., by using membranes containing radioactive substrate and inactivated enzyme (†E_1) in combination with membranes containing unlabeled substrate and active enzyme (E_2)

Correspondence: Dr. H. van den Bosch, Laboratory of Biochemistry, State University of Utrecht, Transitorium 3, Padualaan 8, NL-3584 CH Utrecht, The Netherlands

0005-2760/87/$03.50 © 1987 Elsevier Science Publishers B.V (Biomedical Division)

Although intuitively it is felt that the intramembrane route is most important, a number of papers have recently stressed the importance of intermembrane routes [5–8]. These contributions were deduced from experiments in which membranes containing radioactive substrate but inactivated enzyme, were incubated with membranes having non-labeled substrate and active enzyme (compare Fig. 1). Unfortunately, both in the case of a diglyceride lipase from rat brain [5] and rat liver [8] microsomes, as well as of a lysophospholipase in *Mycoplasma gallisepticum* membranes [7], membrane-bound substrate had to be generated by pretreatment of the membranes with the lipolytic enzymes phospholipase C and phospholipase A_2, respectively. In addition, inactivation of enzyme in membranes containing the substrate, was done by heat treatment of such membranes. Both procedures are likely to exert considerable effect on membrane structure. Nevertheless, even by using similar techniques – i.e., phosphatidic acid generation in microsomal membranes by phospholipase D treatment and inactivation of membrane-bound CTP : phosphatidate cytidylyltransferase and phosphatidate phosphohydrolase by heat treatment – no indications for conversion of phosphatidate by intermembrane mode of enzyme action were obtained [9]. Likewise, from studies on the synthesis of sphingomyelin by transfer of the phosphocholine moiety of phosphatidylcholine to ceramide in mouse fibroblasts, an exclusively intramembrane utilization of ceramide was inferred. In these studies, it was found that phosphatidylcholine might be used in an intermembrane mechanism as well, although to a lesser extent than intramembrane substrate utilization [10].

Hydrolysis of endogenous phosphatidyl [^{14}C]ethanolamine by rat liver mitochondrial phospholipase A_2 can be initiated by addition of Ca^{2+} [11]. By using mitochondrial membranes in which the phospholipase A_2 is inactivated by pretreatment with the active-site-directed inhibitor *p*-bromophenacyl bromide, rather than by heat treatment, we show in this paper that hydrolysis of phosphatidylethanolamine proceeds completely by intramitochondrial enzyme action. The characteristics of this intramembrane action of the enzyme towards the main mitochondrial phosphoglycerides are described.

Materials and Methods

Materials

[2-^{14}C]Ethan-1-ol-2-amine hydrochloride and [1-^{14}C]linoleate were obtained from Amersham International, U.K. *p*-Bromophenacyl bromide was a product of Fluka A.G., Buchs, Switzerland. ATP and Coenzyme A were obtained from Boehringer, Mannheim, F.R.G. Phosphatidylethanolamine and phosphatidylcholine containing [1-^{14}C]linoleate at the *sn*-2-position were prepared biosynthetically using rat-liver microsomes as previously described [11].

Methods

Preparation of mitochondria. Unlabeled and [2-^{14}C]ethanolamine-labeled mitochondria were isolated as described earlier [11].

Preparation of mitoplasts. Mitoplasts were prepared by a combination of the method of Parsons and Williams [12], and of Sottacasa et al. [13], with minor modifications. The mitochondria, isolated from one rat liver, were resuspended in 50 ml 20 mM potassium phosphate buffer (pH 7.2), containing 0.2% (w/v) bovine serum albumin. After the mitochondria had been allowed to swell for 30 min at 0°C, the suspension was centrifuged for 15 min at 2000 × *g* in a Sorval RC2B centrifuge (SS-34 rotor). The pelleted crude inner membrane fraction was resuspended in 50 ml of the same swelling medium, and again centrifuged for 15 min at 2000 × *g*. The pellet was resuspended in 11.25 ml 10 mM Tris/potassium phosphate buffer (pH 7.5). Then, 3.75 ml of 1.8 M sucrose/2 mM ATP/2 mM $MgSO_4$ was added to the suspension. After 5 min stirring at 0°C, during which there was a visible increase in turbidity, the suspension was sonicated in aliquots of 3.5 ml with a Branson Sonifier for 15 s at 16 W and 0°C. The total volume of the sonicated suspension (15 ml) was layered over 20 ml 1.18 M sucrose/0.5 mM EDTA/5 mM Tris-HCl (pH 7.5), and centrifuged in the SW 27 rotor at 80000 × *g* for 1.5 h in a Beckman L5-65 ultracentrifuge. After centrifugation, the supernatant was carefully pipetted off and the tightly packed brown pellet was washed three times with 2 ml 0.25 M sucrose/5 mM Tris-HCl (pH 8.0). The pellet was finally suspended in 0.25 M sucrose/0.1 M Tris-HCl (pH

8.5) with the aid of a Teflon pestle to yield the mitoplast preparation used in the experiments.

Assay of mitochondrial phospholipase A_2. When exogenous 1-acyl-2-[1-^{14}C]linoleoylphosphatidylethanolamine or 1-acyl-2-[1-^{14}C]linoleoylphosphatidylcholine was used as substrate, the incubations and the determinations of the amount of [1-^{14}C]linoleate release were carried out as previously described [11].

The assay of the enzyme using endogenous substrate was done by incubating the indicated amounts of [^{14}C]ethanolamine-labeled mitochondria for 30 min at 37 °C in 1 ml 0.25 M sucrose/0.1 M Tris-HCl (pH 8.0)/10 mM $CaCl_2$. The reaction was terminated by extraction of the lipids [14]. Phospholipids were separated on silica-gel G thin-layer plates with chloroform/ methanol/ acetic acid/water (65 : 50 : 1 : 4, v/v). Spots were detected by iodine staining and scraped into vials for radioactivity measurement after addition of Packard emulsifier scintillation fluid. The percentage hydrolysis was calculated from the decrease in phosphatidylethanolamine radioactivity.

For the determination of the hydrolysis of endogenous phospholipids, 5 mg mitochondrial protein was incubated at 37 °C in 1 ml 0.25 M sucrose/0.1 M Tris-HCl (pH 8.0)/10 mM $CaCl_2$. At the indicated times the reaction was terminated by addition of EDTA to a final concentration of 10 mM followed by an extraction of the lipids according to Bligh and Dyer [14]. The chloroform phase was evaporated to dryness, dissolved in a few drops of chloroform/methanol (1 : 2, v/v), and transferred to silica gel 60 HR plates containing 2% (w/v) florisil. The plates were developed in two dimensions; in the first dimension with chloroform/ methanol/ ammonia/ water (90 : 54 : 5.5 : 5.5, v/v), in the second dimension with chloroform/methanol/ammonia (100 : 50 : 12, v/v). Phospholipid spots were detected with iodine staining. After evaporation of the iodine, the spots were scraped into tubes and the amount of phosphorus was determined according to Rouser et al. [15]. Phospholipid hydrolysis in mitoplasts was determined in the same way, except that 3 mg mitoplast protein was incubated at a final Ca^{2+} concentration of 250 μM.

Inactivation of mitochondrial phospholipase A_2 with p-bromophenacyl bromide. A mitochondrial suspension (2 mg protein/ml) in 0.25 M sucrose/3 mM EDTA/50 mM Tris-HCl (pH 7.2) was incubated for 3 h at 30 °C with 2 mg *p*-bromophenacyl bromide per mg mitochondrial protein. The inhibitor was dissolved in acetone to give a final acetone concentration of 2.5% (v/v). This percentage acetone was shown to have no effect on phospholipase A_2 activity. After incubation, the excess of inhibitor was removed by sedimentation at 500 rpm for 5 min in a Christ centrifuge and subsequent incubation of the supernatant in buffer comprising 0.25 M sucrose/3 mM EDTA/1 M imidazole (pH 7.2), for 30 min at 37 °C. Afterwards, the mitochondria were sedimented at 12 000 × *g* for 20 min. The pellet was resuspended in 0.25 M sucrose/3 mM EDTA/50 mM Tris-HCl (pH 7.2).

Analytical procedures. Protein was determined according to Lowry et al. [16] with bovine serum albumin as standard. Total lipid phosphorus was determined according to the method of Chen et al. [17] after destruction of the sample as described by Ames and Dubin [18]. Monoamine oxidase activity was measured according to Weissbach et al. [19] and succinate dehydrogenase according to Green et al. [20].

Results

To determine the mode of action, i.e., intra- and/or intermembrane hydrolysis of mitochondrial phospholipid, increasing concentrations of [^{14}C]ethanolamine-labeled mitochondria were incubated in the presence of Ca^{2+}. Inasmuch as these mitochondria contain both labeled phosphatidyl[^{14}C]ethanolamine substrate and active enzyme, total hydrolysis of labeled substrate is the sum of, as yet, unknown contributions of intra- and intermembrane action of the mitochondrial phospholipase A_2. As can be seen in Fig. 2, the rate of phosphatidylethanolamine hydrolysis increases linearly with protein concentration. This indicates that the reaction is first-order with respect to mitochondria concentration, compatible with a predominate intramembrane enzyme action. A predominance of intermembrane action, which, according to the particle-collision theory, is proportional to the square of organelle concentration, would be expected to result in an upward

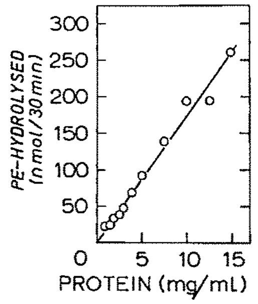

Fig. 2. Phosphatidylethanolamine hydrolysis as a function of protein concentration. The indicated amounts of [^{14}C]ethanolamine-labeled mitochondria were incubated for 30 min in the presence of 10 mM Ca^{2+}.

curvature of the line in Fig. 2.

To determine in a more quantitative manner the contribution of the intermembrane route to total substrate hydrolysis, experiments as indicated in Table I, using three types of mitochondrion, were done. Under the experimental conditions the original [^{14}C]ethanolamine-labeled mitochondria, M_0, degraded 20.1% of their endogenous phosphatidyl[^{14}C[ethanolamine, corresponding to a total of 40.2 nmol per 2.5 mg protein. When these mitochondria were treated with *p*-bromophenacyl bromide to yield mitochondria, M_1, containing radioactive substrate and inactivated enzyme, only 3.4 nmol of phosphatidylethanolamine was degraded upon incubation. This indicates that the phospholipase A_2 is inhibited for over 90% by treatment with the inhibitor. Control experiments using exogenous 1-acyl-2-[1-^{14}C]linoleoylphosphatidylethanolamine indicated a seemingly 100% inhibition of the phospholipase A_2. When mitochondria M_0 were incubated with equal amounts of *p*-bromophenacyl bromide-treated mitochondria M_1, the specific activity of the phospholipase A_2 was half of that measured in M_0 alone (data not shown). These control experiments established that the *p*-bromophenacyl bromide-treated mitochondria M_1 were sufficiently freed of excess inhibitor so as to cause no inhibition of the phospholipase A_2 activity of the original mitochondria, M_0. The low phospholipase A_2 activity remaining in mitochondria M_1, when measured with endogenous substrate, may be due to some residual activity of the enzyme in the inner membrane. When the mitochondria M_1 were incubated in the presence of mitochondria M_2, containing unlabeled substrate and active enzyme, the increase in [^{14}C]phosphatidylethanolamine hydrolysis in comparison to that observed in M_1 alone is a quantitative measure of the contribution of the intermembrane route. As can be seen in Table I, a contribution of intermembrane phospholipase A_2 action became only apparent at higher protein concentrations. In the extreme case where 10 mg of mitochondrial protein M_2 is added, the hydrolysis of radioactive phosphatidylethanolamine due to intermembrane action

TABLE I

ABSENCE OF INTERMITOCHONDRIAL ACTION OF MITOCHONDRIAL PHOSPHOLIPASE A_2

The indicated amounts of mitochondria protein were incubated for 30 min with 10 mM Ca^{2+} M_0, [^{14}C]ethanolamine-labeled mitochondria; M_1 [^{14}C]ethanolamine-labeled mitochondria containing *p*-bromophenacyl bromide- (BrPhBr-) inactivated phospholipase A_2; M_2, mitochondria containing unlabeled phosphatidylethanolamine (S_2, compare Fig. 1) and active phospholipase A_2 (E_2, compare Fig 1). Hydrolysis of phosphatidyl [^{14}C]ethanolamine (Δ^*S) was measured after thin-layer chromatography of lipid extracts The mitochondria contained 80 nmol phosphatidylethanolamine per mg protein. For further explanation, see text

Incubation (mg protein/ml)			Δ^*S (%)	Δ^*S (nmol)		Inter route (% of total expected)
M_0	M_1	M_2		total	inter	
2.5	–	–	20.1	40.2	?	–
–	2.5	–	1.7	3.4	?	–
–	2.5	0.6	0.7	1.4	0	0
–	2.5	2.5	1.6	3.2	0	0
–	2.5	5.0	3.1	6.2	2.8	3.3
–	2.5	10.0	4.3	8.6	5.2	3.2

amounted to 5.2 nmol. By contrast, when 10 mg of mitochondrial protein M_0 were incubated, total hydrolysis of phosphatidylethanolamine due to inter- and intramembrane enzyme action amounted to about 160 nmol (Fig. 2 and Table I, first line). It follows from these data that at least 97% of total substrate degradation takes place by intramitochondrial enzyme action. Both intermitochondrial enzyme action due to organelle collision and apparent intermitochondrial enzyme action as a result of substrate transport between organelles or fusion of organelles are negligible, certainly at organelle concentrations up to 5 mg protein/ml. This conclusion is valid only provided the phospholipase A_2 in mitochondria M_2 remained fully active during the 30 min incubation period and did not become inhibited by the free fatty acids and lysophospholipids formed in the membranes of M_2. Fig. 3 shows that phospholipase activity remains linear with time up to 60 min, thus indicating that this condition is met.

The conclusion that intermitochondrial enzyme action is nearly absent is fully corroborated by experiments in which a constant amount of mitochondria, M_2, containing active enzyme, was incubated with increasing amounts of mitochondria, M_1, having labeled substrate but inactivated enzyme (Table II). This experiment represents a substrate concentration curve for the intermembrane route of substrate hydrolysis. As can be seen in Table II, substrate hydrolysis by the intermembrane route in this experiment never amounted to more than 2% of the total hydrolysis expected, when the sum of intra- and intermembrane hydrolysis would have been measured under these conditions. Thus, although an accurate substrate concentration curve for the intermembrane route cannot be given because of the low amounts of substrate hydrolysis, the data clearly indicated the negligible contribution of the intermembrane enzyme action in total substrate hydrolysis upon incubation of mitochondria in the presence of Ca^{2+}.

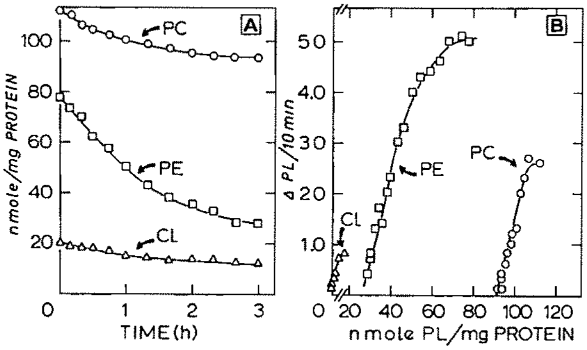

Fig 3. Hydrolysis of endogenous mitochondrial phospholipids (A) Incubation of mitochondria in the presence of 10 mM Ca^{2+} for the indicated time periods and determination of residual phospholipids was done as described in the Materials and Methods section. (B) Replot of the data in (A) giving the decrease in 10 min intervals of the indicated phospholipids ($\Delta PL/10$ min) as function of the remaining amounts of these phospholipids at the beginning of each 10 min interval. Abbreviations: PC, phosphatidylcholine; PE, phosphatidylethanolamine; CL, cardiolipin; PL, phospholipid Mean values of three independent experiments are given.

Having established that substrate hydrolysis upon incubation of mitochondria with Ca^{2+} proceeds by intramembrane action of the phospholipase A_2, we can now determine how the velocity of this mode of enzyme action changes with time as more phospholipid substrate is converted into free fatty acids and lysophospholipids. This is done by measuring phospholipid hydrolysis as a function of time (Fig. 3A). The curves obtained can then be converted into curves in which the phospholipid decrease during intervals of 10 min, as an approximation of initial velocity, is plotted against the remaining amount of that phospholipid in nmol phospholipid/mg protein still present at the beginning of the time interval (Fig. 3B). Several interesting phenomena become apparent upon inspection of these curves. Firstly, the curves for phosphatidylethanolamine and phosphatidylcholine tend to plateau and near-maximal hydrolysis rates for these phospholipids are found at the amounts at which they occur naturally in mitochondria. Secondly, phosphatidylethanolamine hydrolysis proceeds at a rate almost twice that for phosphatidylcholine at the initial ratio in which these phospholipids occur in mitochondria. Thirdly, the rates drop dramatically during the course of the experiment, and hydrolysis of the main mitochondrial phospholipids does not seem to proceed to completion. In fact, phospholipid degradation nearly has stopped while there is still about 90 nmol phosphatidylcholine, 25 nmol phosphatidylethanolamine, and 10 nmol cardiolipin remaining per mg protein. This is not due to

TABLE II

INFLUENCE OF ORGANELLE CONCENTRATION ON SUBSTRATE HYDROLYSIS BY INTERORGANELLE ENZYME ACTION

The indicated amounts of mitochondria M_0, M_1, and M_2 (compare legend of Table I for explanation) were incubated for 20 min at 37°C in the presence of 10 mM $CaCl_2$ to measure hydrolysis of phosphatidyl [^{14}C]ethanolamine (Δ^*S) The mitochondria contained 86 nmol phosphatidylethanolamine per mg protein.

Incubation (mg protein/ml)			Δ^*S (%)	Δ^*S (nmol)		Inter route (% of total expected)
M_0	M_1	M_2		total	inter	
1.0	–	–	13.7	11.5	?	–
–	1.0	–	1.5	1.3	?	–
–	1.2	7.5	3.1	3.1	1.6	1.7
–	2.4	7.5	2.1	4.2	1.2	1.3
–	4.9	7.5	1.6	6.4	0.4	0.4
–	7.7	7.5	0.0	0.0	0.0	0.0
–	9.8	7.5	0.4	3.2	0.0	0.0

denaturation of the phospholipase A_2 during the prolonged incubations. When small aliquots of the mitochondria were removed from the incubation mixture at different times to determine the phospholipase A_2 activity with excess exogenous 1-acyl-2-[1-^{14}C]linoleoylphosphatidylethanolamine, the enzyme appeared to have remained fully active. Also, when the mitochondria at various times were delipidated by ammoniacal acetone as described previously [11], a constant amount of phospholipase A_2 activity could be extracted (Fig. 4).

To simplify the two-membrane system of mitochondria, the experiment of Fig. 3 was repeated for mitoplasts. The mitoplast preparation contained 63% of the succinate dehydrogenase and 8% of the monoamine oxidase activity of the original mitochondria, indicating an almost 8-fold enrichment of the inner membrane marker in comparison to outer membrane marker (Table III). In view of the earlier finding [21] that mitochondrial phospholipase A_2-exhibited two plateaux in the activity versus Ca^{2+} concentration curve, the mitoplasts were incubated at 0.25 mM Ca^{2+} to saturate only the high-affinity Ca^{2+}-binding site. As can be seen in Fig. 5, the time-course for hydrolysis of endogenous phospholipids is very similar to that observed with whole mitochondria, although the absolute numbers differ somewhat due to a different phospholipid composition. The plot of phospholipid decrease in 10 min intervals as a function of remaining phospholipid (Fig. 5B) shows the same characteristics as observed for mitochondria. Again, initially the rates are barely influenced by the decrease in the amounts of phospholipids, phosphatidylethanolamine is hydrolyzed fastest, and phospholipid hydrolysis arrests while still considerable amounts of substrate are potentially available.

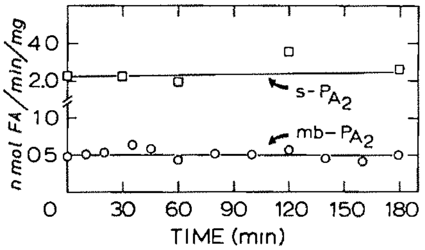

Fig. 4. Activity of mitochondrial phospholipase A_2 towards exogenous phosphatidylethanolamine as a function of mitochondrial incubation time. Mitochondria were incubated in the presence of 10 mM Ca^{2+} in an experiment identical to that of Fig. 3A At the indicated times, aliquots (0.2 mg protein) were withdrawn to assay for phospholipase A_2 activity with exogenous phosphatidylethanolamine (O–O, membrane-bound phospholipase A_2, mb-PA_2). Alternatively, the enzyme was solubilized by ammoniacal acetone treatment of 7.5 mg mitochondrial protein and extraction of the delipidated pellet with 0.5 M KCl [11]. Specific activity of the solubilized phospholipase A_2 was determined with 1-acyl-2-[1-^{14}C]linoleoylphosphatidylethanolamine as substrate (□-□, s-PA_2).

TABLE III

RECOVERY OF MARKER ENZYMES IN MITOPLASTS

Mean values of three experiments with a mean value for protein recovery of 46% are given.

Preparation	Succinate dehydrogenase			Monoamine oxidase		
	total (nmol/min)	spec act (nmol/min per mg)	%	total (ΔA_{360}/min)	spec act. (ΔA_{360}/min per mg)	%
Mitochondria	2055	23.4	100	2.39	0.0263	100
Mitoplasts	1298	33.8	63	0.19	0.0048	8

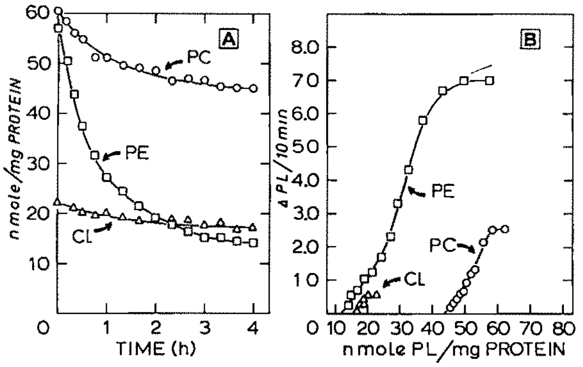

Fig. 5. Hydrolysis of endogenous phospholipids in mitoplasts The experimental conditions were identical to those of Fig 3, except that mitoplasts were used in the presence of 0 25 mM $CaCL_2$ Mean values of two experiments, varying by less than 15%, are given. Abbreviations as in Fig 3.

Discussion

In this paper we have shown that the hydrolysis of endogenous phospholipids by mitochondrial phospholipase A_2 proceeds nearly entirely by an intraorganelle action of the enzyme. As discussed in the Introduction, intermembrane enzyme action has been claimed to contribute significantly to the in vitro hydrolysis of membrane-bound substrates by diglyceride lipase from rat brain [5] and rat liver [8] microsomes, sphingomyelinase from chicken erythrocyte ghosts [6] and lysophospholipase from *M. gallisepticum* [7]. Although these contradictory findings may be due to the use of different systems, it should also be realized that a different methodology was applied in our experiments with mitochondria. To assess the contribution of intermembrane routes in the action of diglyceride lipase [5,8] or lysophospholipase [7] the membrane vesicles containing the radioactive substrates and inactivated enzymes were prepared by treatment of the membranes with lipolytic enzymes to generate substrate and by heat treatment to inactivate enzyme. The experiments with mitochondria used endogenous substrate and an active-site-directed inhibitor to inactivate enzyme. In addition, the finding of intermembrane enzyme action as reported [5,7,8] requires us to rule out the possibility that this is only apparent and in fact caused by membrane fusion or transport of substrate from the membrane containing the inactivated enzyme to the membrane having the active enzyme. When considerable amounts of membrane phospholipids are hydrolyzed by lipolytic enzymes to generate substrate, fusion and/or substrate transport is difficult to exclude. This holds especially when the pH optimum of the enzyme under investigation requires incubations at acidic pH values [5] known to cause membrane aggregation or when the substrate is a lysophospholipid [7] known to exchange rapidly between membranes [22].

The hydrolysis of endogenous mitochondrial phospholipids appears to be catalyzed completely by enzyme acting on substrate in the same organelle. The curves depicting the velocity of this process as a function of the amounts of remaining phospholipid show that some phospholipid may be hydrolyzed without appreciably affecting the rates. This suggests that the phospholipase A_2 in its natural environment with the given phospholipid composition is saturated with these substrates, and stresses the necessity for tight regulation of the membrane-associated phospholipase A_2 in order to prevent digestion of membrane phosphoglycerides.

It is an intriguing finding that the rate of phospholipid hydrolysis in both mitochondria and mitoplasts approaches zero (Figs. 3 and 5), while still considerable amounts of substrate are present and the enzyme does no appear to become denatured (Fig. 4). One possible explanation could be that the remaining phospholipids are firmly bound to membrane proteins and inaccessible to the enzyme. In the case of mitoplasts it is possible and necessary to consider the data in terms of sidedness of both phospholipids and enzyme, especially since at the end of the 4 h incubation 46% of the total phospholipids are degraded. It can be calculated from Fig. 5 and data not shown that 25% of phosphatidylcholine, 75% of phosphatidylethanolamine, 23% of cardiolipin, about 35% of phosphatidylinositol and about 80% of phosphatidylserine, are hydrolyzed at the end of the incubation of mitoplasts. Although these values might suggest the complete hydrolysis of phospholipids in one monolayer of the inner membrane with the percentages of the individual phospholipids hydrolyzed being present in that monolayer, the results cannot yet be interpreted in this simple way because of conflicting data in the literature concerning the localization of both phospholipase A_2 and phospholipids in the transverse plane of the inner mitochondrial membrane. Based on experiments with the Ca^{2+}-transport blocker, Ruthenium red, Severina and Evtodienko [23] concluded that all mitochondrial phospholipase A_2 activity is localized on the matrix side of the inner membrane. This conclusion contradicts earlier findings by Waite [3] and Nachbaur et al. [4] who reported that only about one-third of the total mitochondrial phospholipase A_2 was present in the inner membrane. In addition, Zurini et al. [24] stated that even of the total inner membrane phospholipase A_2, only about one-third is located at the matrix side.

De Kruijff et al. [25] have found that in the intact mitochondrial membranes phospholipids are largely present in a bilayer structure at 37°C. Conflicting data have been reported, however, concerning the asymmetric distribution of phospholipids over the two halves of the mitochondrial inner membrane. Whereas Crain and Marinetti [26] found that 30–40% of the inner membrane phosphatidylethanolamine is located on the outside surface, Nilsson and Dallner [27] reported about 90% of this phospholipid to be present in the outer leaflet. In view of these discrepancies it is obvious that further investigations are required before the exact localization of phospholipase A_2 and phospholipids in the transverse plane of the inner mitochondrial membrane can be stated with certainty. In the meantime there is a third argument to consider it unlikely that the arrest of phospholipid hydrolysis upon incubation of mitoplasts is caused by depletion of the phospholipids in one monolayer, i.e., the monolayer that contains a putatively asymmetric phospholipase A_2. This argument stems from ^{31}P-NMR spectra of the phospholipids in isolated inner mitochondrial membranes which indicated that part of the phospholipids underwent isotropic motion [28]. This, and the subsequent production during incubation of mitoplasts of large amounts of free fatty acids and lysophospholipids, would suggest so much disturbance of the bilayer that potentially all the phospholipids, even when they were asymmetrically present to begin with, could come into contact with the phospholipase A_2. Indeed, ^{31}P-NMR spectra of residual membranes during incubation of mitoplast ghosts with Ca^{2+} indicated that a considerable part of the phospholipids experienced isotropic motion (data not shown). However, isotropic signals were also present in mitoplast ghosts incubated in the presence of EDTA and the possibility could not be excluded that these signals were caused by rapid tumbling of small inner membrane fragments. In view of these considerations we feel that the fact that phospholipid hydrolysis nearly stops upon incubation of mitochondria and mitoplasts has to be ascribed to changes in the lipid environment of the enzyme that render the phospholipase A_2 inactive. Most likely, the production of unsaturated free fatty acids plays an important role in this process. We have previously shown [11] that hydrolysis of phosphatidylethanolamine by purified mitochondrial phospholipase A_2 is strongly inhibited by addition of linoleate, whereas lysophosphatidylethanolamine exerted no effect. Others have recently confirmed this phenomenon by showing that phospholipase A_2 activity in human platelet homogenates is markedly inhibited by unsaturated fatty acids present in the homogenate [29].

The conclusion from this paper that hydrolysis of endogenous phospholipids by mitochondrial phospholipase A_2 proceeds nearly entirely by intramembrane hydrolysis raises the question how exogenous substrates became hydrolyzed. This question is dealt with in the accompanying paper [30].

Acknowledgements

This study was carried out under the auspices of the Netherlands Foundation for Chemical Research (S.O.N.) with financial aid from the Netherlands Organization for the Advancement of Pure Research (Z.W.O.).

References

1 Bjørnstad, P. (1960) J Lipid Res. 7, 612–620

2 Scherphof, G.L. and Van Deenen, L L M (1965) Biochim Biophys. Acta 98, 204–206

3 Waite, M. (1969) Biochemistry 8, 2536–2542

4 Nachbaur, J , Colbeau, A. and Vignais, P M (1972) Biochim. Biophys. Acta 274, 426–446

5 Rousseau, A and Gatt, S. (1979) J. Biol. Chem. 254, 7741–7745

6 Record, M., Loyter, A. and Gatt, S. (1980) Biochem. J. 187, 115–121

7 Gatt, S , Morag, B. and Rottem, S (1982) J. Bacteriol. 151, 1095–1101

8 Rousseau, A. and Gatt, S (1984) FEBS Lett. 167, 42–46

9 Van Heusden, G.P H. and Van den Bosch, H. (1978) Eur. J. Biochem. 84, 405–412

10 Marggraf, W.D., Zertani, R., Anderer, F.A. and Kanfer, J.N. (1982) Biochim Biophys. Acta 710, 314–323

11 De Winter, J.M , Vianen, G.M. and Van den Bosch, H. (1982) Biochim Biophys Acta 712, 332–341

12 Parsons, D F and Williams, G.R (1967) Methods Enzymol 10, 443–448

13 Sottacasa, G L , Kuylenstierna, B., Ernster, L and Bergstrand, A (1967) Methods Enzymol. 10, 448–463

14 Bligh, E.G and Dyer, W.J (1959) Can J Biochem. Physiol. 37, 911–917

15 Rouser, G , Siakotos, A N. and Fleischer, S (1966) Lipids 1, 85–86

16 Lowry, O.H., Rosebrough, N J., Farr, A.L. and Randall, R.J. (1951) J. Biol Chem. 193, 265–275

17 Chen, P.S., Toribara, T Y. and Warner, H. (1956) Anal. Chem. 28, 1756–1758

18 Ames, B.N. and Dubin, D T (1960) J Biol Chem 235, 769–775

19 Weissbach, H., Smith, T.E., Daly, J.W , Witkop, B. and Udenfriend, S (1960) J. Biol Chem. 235, 1160–1163

20 Green, D E , Mii, S and Kohout, P M. (1955) J Biol. Chem. 217, 551–567

21 De Winter, J.M., Korpancova, J. and Van den Bosch, H. (1984) Arch. Biochem. Biophys. 234, 243–252

22 Van den Besselaar, A.M.H.P , Van den Bosch, H and Van Deenen, L.L.M. (1977) Biochim. Biophys. Acta 465, 454–465

23 Severina, E.P. and Evtodienko, Y.N (1981) Biochemistry U.S S R 46, 964–966

24 Zurini, M , Hugentobler, G. and Gazzotti, P. (1981) Eur J. Biochem. 119, 517–521

25 De Kruijff, B., Nayar, R. and Cullis, P.R (1982) Biochim Biophys. Acta 684, 47–52

26 Crain, R.C. and Marinetti, G V. (1979) Biochemistry 18, 2407–2414

27 Nilsson, O. and Dallner, G. (1977) Biochim. Biophys. Acta 464, 453–458

28 Cullis, P R., De Kruijff, B., Hope, M.J , Nayar, R., Rietveld, A. and Verkleij, A J. (1980) Biochim. Biophys Acta 600, 625–635

29 Ballou, L.R and Cheung, W.Y (1985) Proc. Natl. Acad. Sci. U S.A 82, 371–375

30 Lenting, H.B.M., Neys, F.W. and Van den Bosch, H. (1987) Biochim. Biophys Acta 917, 178–185

Biochimica et Biophysica Acta 917 (1987) 178–185
Elsevier

BBA 52326

Hydrolysis of exogenous substrates by mitochondrial phospholipase A_2

H.B.M. Lenting, F.W. Neys and H. van den Bosch

Laboratory of Biochemistry, State University of Utrecht, Utrecht (The Netherlands)

(Received 11 July 1986)

Key words. Phospholipase A_2; Phospholipid association; Phosphatidylethanolamine; (Rat liver mitochondrion)

Evidence is provided in this paper to indicate that hydrolysis of exogenously added phosphatidylethanolamine and phosphatidylcholine by the membrane-bound phospholipase A_2 from rat-liver mitochondria is preceded by association of the substrates with the membranes. Hydrolysis of phosphatidylethanolamine after preincubation of mitochondria and substrate is nearly independent of incubation volume, indicating that substrate and mitochondria are not independently diluted. The association is greatly enhanced in the presence of Ca^{2+}, especially for phosphatidylethanolamine. Association can be measured after sucrose-gradient centrifugation of mitochondria preincubated with phosphatidylethanolamine and can be visualized by freeze-fracture electronmicroscopy, showing substrate clusters fused with mitochondria. The association provides an explanation for the hydrolysis of exogenous substrates by a membrane-associated phospholipase A_2 as well as for the high preference for phosphatidylethanolamine degradation often observed in studies on membrane-bound phospholipases A. This preference is likely to result in part from the tendency of unsaturated phosphatidylethanolamines to adopt non-bilayer lipid phases allowing a more extensive association with biomembranes in the presence of Ca^{2+}, and does not reflect enzyme specificity per se. This phenomenon should be kept in mind when determining the substrate specificity of membrane-bound phospholipases A by the use of exogenous substrates.

Introduction

The membrane-associated phospholipase A_2 from rat liver mitochondria hydrolyzes endogenous mitochondrial phospholipids entirely via an intramembrane mode of enzyme action and does not appear able to hydrolyze phospholipids from other mitochondrial membranes [1]. Yet initial studies [2–7] with isolated mitochondria have shown that exogenously added phospholipids were degraded as well. In general, in this process phosphatidylethanolamine appeared to be a much better substrate than phosphatidylcholine. A possible explanation for this apparent discrepancy could be that the membrane-associated phospholipase A_2 acts in fact only on the exogenously added substrates after these become somehow associated with the mitochondrial membranes. If such an association of the added substrates with the membrane in the presence of Ca^{2+} (necessary to assay phospholipase A_2 activity) occurred more easily with hexagonal phosphatidylethanolamine than with lamellar phosphatidylcholine, this could also explain the large preference that membrane-associated phospholipases A_2 generally exhibit for phosphatidylethanolamine as exogenous substrate [2,3,8–14]. In this paper we describe experiments to validate these hypotheses by investigating the mode of exogenous substrate hydrolysis and the association of these substrates with mitochondria.

Correspondence: Dr. H. van den Bosch, Laboratory of Biochemistry, State University of Utrecht, Transitorium 3, Padualaan 8, NL-3584 CH Utrecht, The Netherlands

0005-2760/87/$03.50 © 1987 Elsevier Science Publishers B V (Biomedical Division)

Materials and Methods

Materials

[1-^{14}C]Linoleate was obtained from Amersham International, U.K. Phosphatidylethanolamine and phosphatidylcholine containing [1-^{14}C]linoleate at the *sn*-2-position, were prepared biosynthetically using rat-liver microsomes as previously described [15]. Phosphatidylethanolamine and phosphatidylcholine were extracted from rat liver according to Bligh and Dyer [16] and purified on silica columns according to standard procedures. Phosphatidylcholine-specific transfer protein from rat liver was kindly donated by Dr. D. van Loon from this laboratory.

Methods

Isolation of mitochondria. Mitochondria were isolated from 10% (w/v) rat liver homogenates in 0.25 M sucrose/1 mM EDTA/20 mM Tris-HCl (pH 7.4). The homogenates were prepared by use of a Potter-Elvehjem tube and centrifuged for 15 min at 700 × *g* to remove nuclei and debris and then for 10 min at 9000 × *g* to pellet the mitochondria. The pellet was washed twice by resuspending it in one-quarter with respect to the original homogenate volume of the sucrose/EDTA/Tris-HCl solution, and was finally resuspended in this solution.

Assay of mitochondrial phospholipase A_2. Phospholipase A_2 activity was measured under the standard conditions described earlier [7]. Substrates and other variables are indicated in the respective legends.

Other procedures. Protein was determined by the dye-binding method of Bradford [17] using bovine serum albumin as standard. Other procedures are described in the respective legends.

Results

The membrane-associated phospholipase A_2 from rat-liver mitochondria hydrolyzed endogenous phosphatidylethanolamine by an intramembrane mode of substrate recognition and apparently is not able to reach the *sn*-2-ester bond of substrates in adjacent biomembranes [1]. Yet, in agreement with literature data, the mitochondrial phospholipase A_2 hydrolyzed also exogenously added phosphatidylethanolamine sonicates (Fig. 1A). Two possible explanations for this observation come to mind. Either the enzyme is able to recognize the *sn*-2-ester bond in the phosphatidylethanolamine structures as present in the sonicate and acts by an intermembrane enzyme: substrate mode of recognition, or the substrate becomes associated with the membrane and becomes hydrolyzed in an intramembrane enzyme: substrate recognition process. In the latter case one would expect dilution to have less influence on the hydrolysis rate than in the former case. For such dilution experiments a substrate concentration of 0.2 mM was chosen from the data obtained in Fig. 1A. Mitochondria were preincubated for either 5 or 15 min with 0.2 mm phosphatidylethanolamine and the mixtures were diluted as indicated in Fig. 1B for the determination of substrate hydrolysis in a further incubation for 30 min. The expected influence of the dilution on the rate of hydrolysis

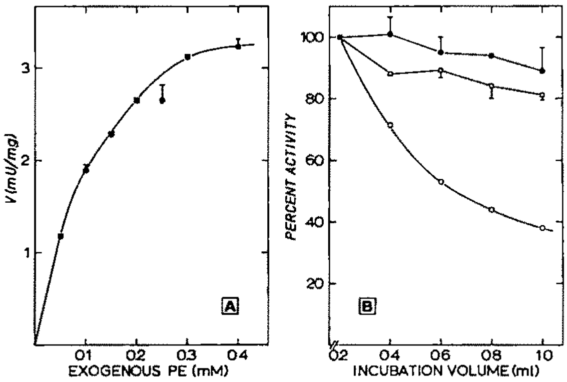

Fig. 1. Hydrolysis of exogenous phosphatidylethanolamine by rat liver mitochondria. (A) Influence of substrate concentration. Mixtures containing 0.1 mg mitochondrial protein in 0.5 ml 20 mM Tris-HCl buffer (pH 8.5) in 0.25 M sucrose/1 mM EDTA/10 mM $CaCl_2$ and the indicated concentations of 1-acyl-2-[1-^{14}C]linoleoylphosphatidylethanolamine (PE, 500 dpm·nmol^{-1}) were incubated for 30 min at 37°C. 1 mU = 1 nmol fatty acid released per min (B) Influence of dilution on hydrolysis Mitochondria (0.1 mg protein) were preincubated for 5 min (□) or 15 min (●) at 37°C with 0.2 mM phosphatidylethanolamine in 0.2 ml of the same buffer as used under (a). The mixtures were then diluted with this buffer as indicated and further incubated for 30 min at 37°C. Substrate hydrolysis during this period, after subtraction of hydrolysis in the preincubation period, was expressed as percent of the hydrolysis measured in the undiluted sample The expected percentage hydrolysis as calculated from the substrate concentration dependency (A) and the dilution is also indicated (○).

assuming intermembrane enzyme action was calculated from the data in Fig. 1A and is expressed as percentage of the rate obtained at 0.2 mM phosphatidylethanolamine. These data are plotted as a function of the incubation volume in Fig. 1B (open circles). As can be seen in Fig. 1B the actual hydrolyses measured hardly decreased upon dilution of the preincubation mixtures. Even upon 5-fold dilution, expected to result in less than 40% of the hydrolysis rate of the undiluted mixture if enzyme action was governed by the concentration of substrate particles (Fig. 1A), enzyme activity amounted to 81 or 89% of undiluted controls preincubated for 5 or 15 min, respectively. These results suggest that enzyme : substrate recognition proceeds within the membranes and is independent of the total incubation volume. The finding that hydrolysis is less dependent on incubation volume after a preincubation of 15 min as compared to a preincubation of 5 min and thus allowing more association of the substrate with the mitochondria is in line with this interpretation.

To gain more insight into the process of exogenous phospholipid hydrolysis, mitochondria were preincubated with labeled phosphatidylethanolamine or phosphatidylcholine. To facilitate uptake of lamellar phosphatidylcholine, these experiments were also done in the presence of a specific phosphatidylcholine transfer protein. Then either the mixtures were incubated directly with Ca^{2+} to measure total, inter- plus intramembrane, substrate hydrolysis or the mitochondria were first isolated prior to addition of Ca^{2+} to measure hydrolysis of mitochondrial associated substrate by intramembrane enzyme action. The results of those experiments (Table I) indicated that total hydrolysis of phosphatidylethanolamine was about 19-fold that of phosphatidylcholine. Whereas the total hydrolysis of phosphatidylethanonolamine was not influenced by addition of the specific transfer protein, phosphatidylcholine hydrolysis increased 2-fold. When the mitochondria were first isolated after the preincubation with exogenous substrate, about 6% of the added phosphatidylethanolamine was associated with the mitochondria and this amount was not influenced by the presence of the phosphatidylcholine-specific transfer protein. In contrast, only 2% of phosphatidylcholine appeared to be associated with the mitochondria, and this increased 6-fold in the presence of the specific transfer protein. Incubation of these isolated mitochondria with Ca^{2+} resulted in about 18% hydrolysis of the membrane-associated radioactive phosphatidylethanolamine, whereas the membrane-associated radioactive phosphatidylcholine was hydrolyzed for about 7%. This 2.5-fold

TABLE I

COMPARISON OF HYDROLYSIS OF TOTAL ADDED AND MITOCHONDRIA-ASSOCIATED SUBSTRATES

Mitochondria (0.22 mg protein) were preincubated for 30 min at 25°C with either 1-acyl-2-[1-^{14}C]linoleoylphosphatidylethanolamine (100 nmol; 308 dpm·nmol^{-1}) or 1-acyl-2-[1-^{14}C]linoleoylphosphatidylcholine (100 nmol; 1025 dpm·nmol^{-1}) in the absence or presence of 20 μg phosphatidylcholine-specific transfer protein in 0.25 M sucrose/1 mM EDTA/20 mM Tris-HCl buffer (pH 8.5). The radioactive phospholipids were sonicated in this medium for 15 min at 0°C at 60 W with a Branson sonifier and centrifuged for 20 min at 15000 × g before addition to the incubation medium. After the preincubation the mitochondrial suspension was either incubated directly with a final concentration of 10 mM Ca^{2+} for 30 min at 37°C to measure total hydrolysis or the mitochondria were isolated by centrifugation (15 min at 10000 × g), resuspended in the above medium and incubated for 30 min at 37°C in the presence of 10 mM Ca^{2+} to measure hydrolysis of mitochondria-associated radioactive substrates. Mean values of three experiments differing by less than 15% are given. Abbreviations: PE, phosphatidylethanolamine; PC, phosphatidylcholine, TP, PC-specific transfer protein.

Substrate	Total hydrolysis		Mitochondria-associated substrate		Hydrolysis of mitochondria-associated substrate	
	dpm	nmol	dpm	nmol	dpm	%hydrolysis
PE	5788	18.8	1972	6.4	344	17.4
PE+TP	6050	19.6	2040	6.6	372	18.2
PC	1076	1.0	1850	1.8	90	4.9
PC+TP	2310	2.3	12290	12.0	896	7.3

preference for hydrolysis of phosphatidylethanolamine, when compared with phosphatidylcholine, agrees well with the preference observed for hydrolysis of endogenous substrates [1] and suggests that similar enzyme : substrate recognition processes are involved in the hydrolysis of membrane-associated radioactive substrates and endogenous substrates. The fact that this preference is much less than the 19-fold difference observed when total hydrolysis of added substrates was measured (Table I) suggested that hydrolysis of exogenous phosphatidylethanolamine is strongly favored over that of phosphatidylcholine because of a more extensive association with the mitochondria. This was borne out already in the 3.5-fold better uptake of phosphatidylethanolamine in the preincubation with Ca^{2+} and transfer protein (Table I). In the presence of Ca^{2+} the preferential uptake of phosphatidylethanolamine becomes even more pronounced (vide infra). The effect of Ca^{2+} on the association of phosphatidylethanolamine with mitochondria was suggested by the observation (compare Table I) that total hydrolysis of radioactive phosphatidylethanolamine, measured after addition of Ca^{2+} to the preincubation mixture (about 19 nmol), is much higher than the amount of phosphatidylethanolamine associated with the mitochondria after preincubation without Ca^{2+} (about 6.5 nmol). This can be explained by assuming that either exogenous phosphatidylethanolamine was hydrolyzed by intermembrane action of the mitochondrial phospholipase A_2 (in contrast to the results of earlier experiments, which seemed to exclude this possibility), or that more phosphatidylethanolamine than the 6.5 nmol after the preincubation without Ca^{2+} become associated with mitochondria when Ca^{2+} was added to measure total hydrolysis. To investigate the latter possibility, association of added phosphatidylethanolamine and phosphatidylcholine with mitochondria was measured in the absence and presence of Ca^{2+}. The results of these experiments (Table II) indicated that the 1.3% of coprecipitation of phosphatidylcholine with mitochondria in the absence of Ca^{2+} increased to 7.4% in the presence of

TABLE II

INFLUENCE OF Ca^{2+} ON COPRECIPITATION OF SUBSTRATE WITH MITOCHONDRIA

Sonicated substrates, prepared as described in the legend of Table 1, in amounts of 200 nmol, were incubated for 15 min at 25°C with or without 10 mM Ca^{2+} either alone or with mitochondria (0.22 mg protein) in 0.5 ml of 0.25 M sucrose/1 mM EDTA/20 mM Tris-HCl (pH 8.5). After incubation the mixtures were centrifuged for 15 min at $10000 \times g$ to measure the amount of precipitated substrate. Mean values of three experiments differing by less than 10% are given.

Substrate	Precipitated substrate (nmol)			
	plus mitochondria		minus mitochondria	
	$-Ca^{2+}$	$+Ca^{2+}$	$-Ca^{2+}$	$+Ca^{2+}$
Phosphatidylethanolamine	6.8	194	0	199
Phosphatidylcholine	2,7	14.8	0	0

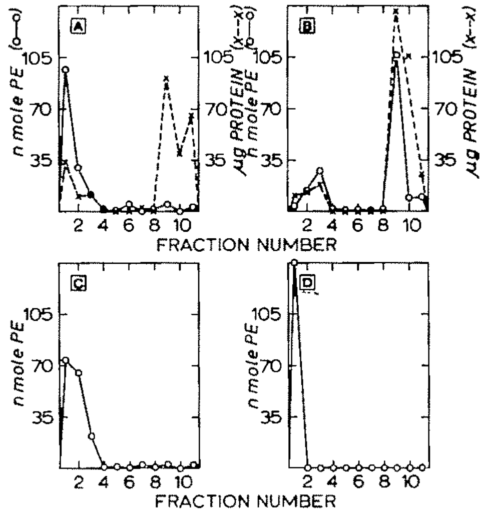

Fig. 2. Association of phospatidylethanolamine with mitochondria. Incubation of phosphatidylethanolamine with or without Ca^{2+} and mitochondria was carried out as described in the legend of Table II. The incubation mixtures were layered on top of a discontinuous sucrose gradient consisting of 2 ml 10%, 6.5 ml 25%, and 2 ml 65% sucrose in 20 mM Tris-HCl (pH 8.5). The tubes were centrifuged for 30 min at 25000 rpm in a SW 41 rotor of a Kontron TGA 50 centrifuge. Fractions (numbered 1–11 from top to bottom) were analyzed for mitochondrial protein and ^{14}C radioactivity. (A) phosphatidylethanolamine (PE) + mitochondria; (B) phosphatidylethanolamine + mitochondria + Ca^{2+}; (C) phosphatidylethanolamine; (D) phosphatidylethanolamine + Ca^{2+}. Recoveries ranged from 75% to 92% for mitochondrial protein and from 70% to 86% for ^{14}C radioactivity. ^{14}C radioactivity recovered was present for more than 99% in phosphatidylethanolamine in all peaks, except for in fractions 9–11 from experiment B, where 7–10% was present as free fatty acid. Results similar to those depicted in this figure were obtained in three independent experiments.

Ca^{2+}. Coprecipitation of phosphatidylethanolamine increased much more dramatically from 3.4% in the absence of Ca^{2+} to 97.0% in the presence of this metal ion. However, this experiment was not conclusive, in that addition of Ca^{2+} alone to phosphatidylethanolamine sonicates also caused precipitation of this substrate in the absence of mitochondria. Apparently this procedure caused clustering of phosphatidylethanolamine to larger structures which precipitated under the conditions used to spin-down mitochondria. This clustering was seen neither with phosphatidylethanolamine

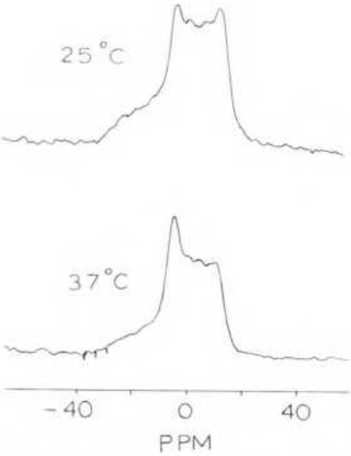

Fig. 3. ^{31}P-NMR proton-decoupled spectra of aqueous dispersions of rat liver phosphatidylethanolamine. The samples were prepared by dispersing 100 μmol phosphatidylethanolamine in 1.0 ml 30% ^2H_2O/40 mM KCl/10 mM Ca^{2+}/100 mM Tris-HCl buffer (pH 8.5). Spectra at 36.4 MHz at the indicated temperatures were recorded on a Bruker WH 90 Fourier transform spectrometer equipped with temperature-control and proton-decoupling facilities as described [19].

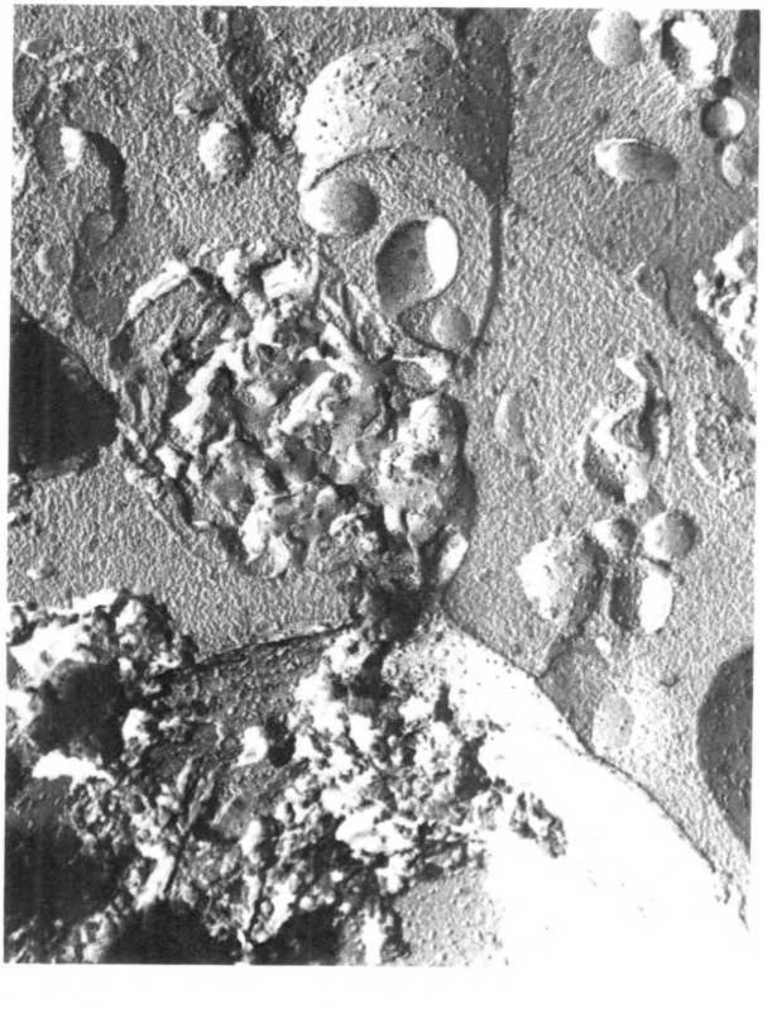

Fig. 4. Freeze-fracture electronmicrograph of mitochondria-associated phosphatidylethanolamine. Mitochondria were incubated with phosphatidylethanolamine in the presence of Ca^{2+} as described in the legend of Table II and isolated by centrifugation. Magnification: 60000-fold.

in the absence of Ca^{2+} nor with phosphatidylcholine in the absence or presence of Ca^{2+}. To determine whether the recovery of phosphatidylethanolamine in the presence of Ca^{2+} in the mitochondrial pellet resulted from coprecipitation or from association with mitochondria, the latter were reisolated by sucrose gradient centrifugation. As can be seen in Figs. 2C and D, phosphatidylethanolamine both in the presence and absence of Ca^{2+} remained at the top of the gradient. Fig. 2A shows that in the absence of Ca^{2+} only a few percent of the radioactive phosphatidylethanolamine became associated with mitochondria, in agreement with earlier experiments (Tables I and II). However, in the presence of Ca^{2+}, over 70% of the radioactive phosphatidylethanolamine was recovered in gradient fractions containing the mitochondria.

Two possible explanations for the additional association of phospholipids, especially phosphatidylethanolamine, with mitochondria in the presence of Ca^{2+} can be envisaged. Ca^{2+} initiates hydrolysis of endogenous phospholipids [1] and it could be that the formation of lysophospholipids and free fatty acids facilitates the association of the exogenously added substrates. However, this possibility was ruled out in experiments where mitochondria were preincubated with Ca^{2+} to generate lysophospholipids and free fatty acids. Association of phosphatidylethanolamine and phosphatidylcholine with the reisolated mitochondria was comparable for preincubated and control mitochondria (data not shown). The second possibility to explain the additional association of especially phosphatidylethanolamine with mitochondria in the presence of Ca^{2+} takes the structure of the exogenously added phospholipids, derived from rat liver, into consideration. Rat liver phosphatidylethanolamine showed the presence of hexagonal H_{II} phase in the ^{31}P-NMR spectra, even at the temperature of 25°C used in the preincubation (Fig. 3). As expected [18,19], this phase was more prominent at 37°C. It is well known that phosphatidylcholines remain organized in extended bilayers [20,21] and this was confirmed for rat liver phosphatidylcholine in the medium used (data not shown).

The nature of the association of phosphatidylethanolamine with mitochondria at the molecular level remains to be elucidated. Freeze-fracture electronmicrographs of the pellet obtained after incubation of mitochondria with phosphatidylethanolamine in the presence of Ca^{2+} revealed clusters of phosphatidylethanolamine fused with the mitochondrial membrane. The lipid clusters themselves consist of fused vesicles (Fig. 4).

Discussion

In the accompanying paper [1] we showed that hydrolysis of endogenous substrates by mitochondrial phospholipase A_2 proceeded with an intramembrane process of enzyme : substrate recognition. In this process phosphatidylethanolamine was hydrolyzed with 2- to 3-fold preference over phosphatidylcholine. Both conclusions, i.e., the intramembrane mode of action and the 2- to 3-fold preference for phosphatidylethanolamine, were in apparent contrast to the finding that exogenous phospholipids become degraded upon incubation with mitochondria and this with a much higher preference, up to almost 20-fold (Table I). In this paper we provide results to suggest that the apparent discrepancy can be explained by the association of the exogenous phospholipids with the mitochondrial membranes prior to hydrolysis. That this association must take place followed from the near independence of substrate hydrolysis when preincubated mixtures of mitochondria with phosphatidylethanolamine were diluted up to 5-fold (Fig. 1B). Recently, Scheel et al. [22,23] used similar techniques to prove that ganglioside degradation by a membrane-bound sialidase from calf brain proceeded only after the ganglioside micelles had been inserted into the membrane.

The more extenisve association of phosphatidylethanolamine contributes considerably to the large preference in exogenous substrate hydrolysis for phosphatidylethanolamine. When only the hydrolysis of associated radiolabeled substrates was measured (Table I) similar preferences for phosphatidylethanolamine as observed for endogenous substrates were found. The more extensive association of phosphatidylethanolamine in comparison to phosphatidylcholine, especially in the presence of Ca^{2+}, is most likely related to the structures of the hydrated phospholipids. In contrast to rat liver phosphatidylcholine, that formed extended bilayers at both 25 and 37°C, the phosphatidylethanolamine from this source exhibited lamellar and hexagonal H_{II} phases at pH 8.5 and 25°C. At 37°C the presence of the hexagonal phase had increased at the expense of the lamellar phase (Fig. 3). At 25°C about 60% of the phosphatidylethanolamine was still present in the lamella phase. This implies that in the case where more than 70% of the added phosphatidylethanolamine became associated with the mitochondrial membranes at 25°C (Fig. 2B) the association was not exclusively restricted to the non-bilayer phase. On the other hand, the association process may have been facilitated by the induction of non-bilayer lipid structures in the mitochondrial membranes in the presence of Ca^{2+} [24,25]. This could also explain why some association of lamellar phosphatidylcholine with mitochondria was consistently noticed (Tables I and II), especially in the presence of Ca^{2+} (Table II). Whatever the exact mechanism, in view of the potential involvement of non-bilayer lipid structures in membrane fusion events [21], it appears plausible that the preferential association with mitochondria of phosphatidylethanolamine when compared with phosphatidylcholine is related to the non-bilayer-forming tendencies of the former phospholipid. With regard to the nature of the association, it is clear from freeze-fracture electronmicrographs (Fig. 4) that most of the phosphatidylethanolamine is not taken up in the membranes, although some incorporation cannot be excluded. Rather, most of the substrate appears present in large clusters of fused substrate with a honeycomb structure that are locally fused with mitochondrial membranes. Presumably, these fusion points allow a flow of phosphatidylethanolamine from the substrate cluster to the membrane-associated phospholipase A_2. Such a mechanism remains in line with the previous conclusion [1] that the mitochondrial phospholipase A_2 preferably acts by intramembrane substrate hydrolysis. At the same time, the association provides an explanation for the higher preference for phosphatidylethanolamine hydrolysis when exogenous substrates are used than observed with endogenous substrates.

This phenomenon may not be specific for mitochondrial phospholipase A_2. Many membrane-bound phospholipases A have been reported to hydrolyze exogenous phosphatidylethanolamine in preference to phosphatidylcholine, at least when assayed without detergents [2,3,8–14]. Similar experiments as described in Table I for mitochondria have been done with rat liver microsomes (Lenting, unpublished data). This membrane contains mainly phospholipase A_1 activity [3,26] and hydrolyzed exogenous phosphatidylethanolamine with an 11-fold preference over phosphatidylcholine. However, with microsomal-associated substrates this preference was reduced to only 2- to 3-fold, in much the same way as found for mitochondrial phospholipase A_2. The high preference for exogenous phosphatidylethanolamine results in part from its physicochemical properties, allowing a better association with biomembranes, and does not reflect enzyme specificity per se. This phenomenon should be kept in mind when assessing the substrate specificity of membrane-associated phospholipases A by the use of exogenous substrates.

Acknowledgements

We thank Prof. dr. A.J. Verkleij, Institute of Molecular Biology of this University, for making freeze-fracture electronmicrographs and Dr. G. van Duijn for help with the NMR experiments. This study was carried out under the auspices of the Netherlands Foundation for Chemical Research (S.O.N.) with financial aid from the Netherlands Organization for the Advancement of Pure Research (Z.W.O.).

References

1 De Winter, J.M., Lenting, H.B.M, Neys, F.W. and Van den Bosch, H. (1987) Biochim. Biophys. Acta 917, 169–177
2 Scherphof, G.L. and Van Deenen, L.L.M. (1965) Biochim. Biophys. Acta 98, 204–206
3 Scherphof, G.L., Waite, M. and Van Deenen, L.L.M. (1966) Biochim. Biophys. Acta 125, 406–409
4 Bjørnstad, P. (1966) J. Lipid Res. 7, 612–620
5 Parsons, D.F. and Williams, G.R. (1967) Methods Enzymol. 10, 443–448
6 Nachbaur, J., Colbeau, A. and Vignais, P.M. (1972) Biochim. Biophys Acta 274, 426–446
7 De Winter, J.M., Vianen, G.M. and Van den Bosch, H. (1982) Biochim. Biophys Acta 712, 332–341
8 Victoria, E.J., Van Golde, L.M.G., Hostetler, K.Y., Scherphof, G.L and Van Deenen, L.L.M. (1971) Biochim. Biophys. Acta 239, 443–457

9 Newkirk, J.D. and Waite, M. (1973) Biochim. Biophys. Acta 298, 562–576

10 Kunze, H., Nahas, N. and Wurl, M. (1974) Biochim. Biophys Acta 348, 35–44

11 Kannagi, R. and Koizumi, K (1979) Arch. Biochem Biophys. 196, 534–542

12 Natori, Y., Nishijima, M., Nojima, S. and Satoh, H (1980) J. Biochem. 87, 959–967

13 Tam, S W., Man, R.Y.K. and Choy, P.C (1984) Can. J. Biochem Cell. Biol. 62, 1269–1274

14 Van den Bosch, H. (1980) Biochim Biophys. Acta 604, 191–246

15 Van den Bosch, H., Aarsman, A.J. and Van Deenen, L.L.M. (1974) Biochim Biophys Acta 348, 197–207

16 Bligh, E.G. and Dyer, W.J. (1959) Can. J. Biochem. Physiol 37 911–917

17 Bradford, M.M (1976) Anal. Biochem. 72, 248–254

18 Cullis, P.R and De Kruijff, B. (1978) Biochim. Biophys. Acta 513, 31–42

19 De Kruijff, B., Rietveld, A and Cullis, P R. (1980) Biochim. Biophys. Acta 600, 343–357

20 Cullis, P.R., De Kruijff, B and Richards, R.E (1976) Biochim Biophys Acta 426, 433–446

21 Cullis, P R and De Kruijff, B. (1979) Biochim Biophys Acta 559, 399–420

22 Scheel, G., Acevedo, E., Conzelmann, E., Nehrkorn, H. and Sandhoff, K. (1982) Eur. J. Biochem. 127, 245–253

23 Scheel, G., Schwarzmann, G , Hoffmann-Bleihauer, P and Sandhoff, K. (1985) Eur J. Biochem. 153, 29–35

24 Cullis, P.R , De Kruijff, B., Hope, M.J., Nayar, R., Rietveld, A. and Verkleij, A J (1980) Biochim. Biophys Acta 600, 625–635

25 De Kruijff, B., Nayar, R. and Cullis, P.R. (1982) Biochim Biophys. Acta 684, 47–52

26 Lumb, R.H and Allen, K.F. (1976) Biochim Biophys. Acta 450, 175–184

Biochimica et Biophysica Acta 917 (1987) 186–193
Elsevier

BBA 52442

Structural modulation of salt-resistant rat-liver lipase alters the relative phospholipase and triacylglycerol hydrolase activities

N.L.M. Persoon, W.C. Hülsmann and H. Jansen

Department of Biochemistry I, Medical Faculty, Erasmus University, Rotterdam (The Netherlands)

(Received 10 July 1986)

Key words: Liver lipase; Immunoinhibition; Proteolysis; Protein modification;
Phospholipase A_1, Triacylglycerol hydrolase

This paper demonstrates that structural modification of the heparin-releasable salt-resistant lipase of rat liver (liver lipase) alters its relative capacity to hydrolyze phospholipid and triacylglycerol emulsions. Enzymatic activities were modified by immunoinhibition and proteolysis and by selective amino acid agents. Binding of three different monoclonal antibodies resulted in a lower extent of inhibition of phospholipase than of triacylglycerol hydrolase activity. Degradation of the enzyme by trypsin under mild conditions led to a decrease of both enzyme activities in a different way. Triacylglycerol hydrolase activity was less affected than the phospholipase activity. Visualization of the proteolysis of the purified enzyme by immunoblotting revealed the actual breakdown of a 58 kDa protein into a 53 kDa protein band and subsequently in a 48 kDa one. Incubation of the purified enzyme by *N*-tosyl-L-phenylethylchloromethyl ketone (acting on cysteine or histidine) or *N*-ethylmaleimide (a sulfhydryl reagent) did not influence either enzyme activity. On the other hand, after the selective modification of lysine residue(s) by phenylisothiocyanate, the phospholipase A_1 activity was stimulated by 68%, whereas the triacylglycerol hydrolase activity was completely lost. The role of a lysine residue(s) in the activity of the enzyme towards phospholipid and triacylglycerol emulsions is discussed.

Introduction

The liver of many, if not all, vertebrates [1] contains a heparin-releasable lipase, commonly referred to as hepatic triglyceridase or liver lipase. Evidence has been presented for a role of this enzyme in lipoprotein metabolism. After the in vivo inhibition of the enzyme activity, for instance by using anti-liver lipase antibodies [2,3] or by the administration of estrogens [4,5], significant changes were observed in serum lipoprotein levels, suggesting a role of the enzyme in the conversion of HDL subfractions [4,6,7]. Since a similar enzyme [8,9] was reported in the adrenal gland and in the ovary, a mechanism was proposed [7] by which the hydrolytic action of the enzyme on HDL phospholipids would promote the flux of free cholesterol between the HDL particle and the underlying tissue in favor of the three organs mentioned. The extracellular localization of the enzyme in the liver [10] was recently also established in the corpus luteum [11,12] and in the zona fasciculata in the adrenal cortex [11], indicating a role of the enzyme in progesterone synthesis and

---

Abbreviations: TPCK, *N*-tosyl-L-phenylethylchloromethyl ketone; PMSF, phenylmethylsulfonyl fluoride; HDL, high-density lipoprotein.

Correspondence: Dr. N.L.M Persoon, Department of Biochemistry I, Medical Faculty, Erasmus University Rotterdam, P.O. Box 1738, 3000 DR Rotterdam, The Netherlands.

0005-2760/87/$03 50 © 1987 Elsevier Science Publishers B V. (Biomedical Division)

in glucocorticoid production. It is not clear whether the enzyme is also important for in vivo triacylglycerol hydrolysis. In vitro, the enzyme has a high K_m for the triacylglycerol substrate [13]. Collagenase treatment of rat liver lipase by Kuusi et al. [14] resulted in a drastic decrease in triacylglycerol hydrolase activity without effect on its monoacylglycerol hydrolase activity. Jensen et al. [15] and Shirai et al. [16] confirmed these results using monooleoylglycerol [15] and tributyroylglycerol [16], respectively. Jensen et al. [15] did not observe any change in the phospholipase activity after the proteolytic digestion, whereas Shirai et al. showed that the capability of the enzyme to bind to dipalmitoylphosphatidylcholine vesicles was lost. These results suggest the existence of a hydrophobic binding site on the molecule for triacylglycerol micelles apart from the catalytic centre. The aim of the present study is to investigate the effects of structural alteration of the enzyme on the hydrolysis of phosphatidylcholine and triacylglycerol emulsion by rat liver lipase. For this purpose, three different methods were used.

(i) Immunoinhibition of phospholipase A_1 activity and triacylglycerol hydrolase activity with monoclonal antibodies.

(ii) The effect of mild tryptic digestion on both enzyme activities.

(iii) Protein modification with amino acid reactive agents and the effect on enzyme activities. By the selective modification of a single amino acid, complete inactivation of some enzymes has been reported [17,18]. The influence of three protein modifiers was studied to elucidate the role of certain amino acids in both phospholipase A_1 and the triacylglycerol hydrolase activities: TPCK, which is known to react with either histidine [8] or cysteine [17,19], *N*-ethylmaleimide, a sulfhydryl reagent, specific for cysteine [19,20], and phenylisothiocyanate, which binds the ϵ amino group of lysine at an alkaline pH [21].

Materials and Methods

Monoclonal antibodies. A panel of five different monoclonal antibodies against salt-resistant rat liver lipase was used in this study. The characteristics of these antibodies that were indicated as A, B, C, D and E and a control (indicated as C_1) with respect to immunoprecipitation and immunoinhibition of triacylglycerol hydrolase activity of the enzyme was reported earlier [9].

Determination of triacylglycerol hydrolase activity. A mixture of 20 μCi tri[^{3}H]oleoylglycerol (Amersham, U.K.) (1.0 Ci/mmol) and 34 mg trioleoylglycerol was taken to dryness and emulsified by sonication in 2.5 ml 5% (w/v) gum acacia (BDH Chemicals, U.K.) containing 8 mM $NaHCO_3$. The emulsion was mixed with 3 ml 10% (w/v) defatted bovine serum albumin, 0.5 ml 1 M Tris-HCl (pH 8.5) and 1.5 ml 5 M NaCl. 150 μl of the mixture was incubated with 100 μl sample for 30 min at 30°C. The free fatty acids formed were extracted as described by Belfrage and Vaughan [22]. Triacylglycerol hydrolase activity was determined as mU/ml (1 mU represents 1 nmol free fatty acid released from the substrate in 1 min at 30°C).

Determination of phospholipase A_1 activity

Labeling of phosphatidylcholine was performed by incubation of rat liver microsomes with [9,10-^{3}H]oleic acid, ATP, $MgCl_2$ and coenzyme A as described by Van den Bosch et al. [23]. In a similar procedure, using phosphatidylethanolamine as a substrate, Groot et al. [24] showed that 98.6% of the acyl label was associated with position 1 of the lipid. Radioactive phosphatidylcholine was purified from rat liver microsomes according to established methods [24]. The lipid concentration was determined according to Steward [25].

A mixture of 0.4 μCi 1-[9,10-^{3}H]oleoylphosphatidylcholine and 250 nmol phosphatidylcholine (also from rat liver microsomal origin) was evaporated under N_2 and emulsified by sonication in 0.25 ml water. The emulsion was mixed with 50 μl 55 mM $CaCl_2$, 50 μl 1 M Tris (pH 8.50) and 150 μl water. 50 μl of the mixture was incubated with 100 μl sample for 15 min at 30°C. The reaction was terminated with 1 ml of a mixture of heptane, isopropanol and 10 N H_2SO_4 (40:40:0.1, v/v). After the addition of 200 μl water, vigorous stirring and centrifugation, the water phase was incubated with silicic acid to remove all phosphatidylcholine. After centrifugation, the radioactivity was determined in 200 μl of the sample by liquid scintillation counting. Phospholipase A_1 activity was determined in mU/ml.

Purification of rat liver lipase. Liver lipase was isolated from eight rats by means of in vitro perfusion of the liver at 6°C with a Tyrode buffer gassed with 95% O_2/5% CO_2 containing 30% (v/v) glycerol, 10 IU/ml heparin (Tromboliquine; Organon, Oss, The Netherlands) and 100 μM PMSF (Merck, Darmstadt, F.R.G.). To avoid proteolytic degradation of the enzyme during the isolation procedure, PMSF was included in all buffers. 100 μM PMSF during the isolation procedure does not have any effect on the relative triacylglycerol hydrolase/phospholipase A_1 activity of the purified enzyme (20 : 1). The perfusates were loaded on a Sepharose-heparin column and the enzyme was eluted with a linear salt gradient from 0.0 to 2.0 M NaCl as described by Jensen [26]. The enzyme was concentrated by $(NH_4)_2SO_4$ precipitation and dialysed against 5% (v/v) glycerol in 50 mM Tris buffer (pH 7.2) without PMSF (350 mU/ml triacylglycerol hydrolase activity, 17.5 mU/ml phospholipase A_1 activity). During the determination of the effect of pH on the hydrolysis of trioleoylglycerol and phosphatidylcholine by liver lipase, the enzyme was tested for both enzyme activities by using the following buffers: citrate-phosphate buffer (pH 3.95), Tris-maleate buffer (pH 5.20, 5.85, 6.85, 7.40, 8.05, 8.70) and glycine-NaOH buffer (pH 9.80 and 10.60).

Immunoprecipitation. A mixture of 5 μl purified liver lipase and an increasing amount of anti-liver lipase monoclonal antibodies A, B, C, D and E (0, 25, 50, 75 or 100 μl hybridoma supernatants) was incubated for 1 h on ice. Hybridoma supernatant is about 1.5 mg/ml. Whole rabbit anti-mouse immunoglobulins (Nordic Immunology, Tilburg, The Netherlands) were used as a second antibody (10 μl from a stock solution of 1 ml of lyophylized antibody (10 mg/ml) dissolved in phosphate-buffered saline were incubated for 30 min on ice). 50 μl of a 1 : 1 suspension of protein A-Sepharose 4B (Pharmacia, Uppsala, Sweden) in phosphate-buffered saline were used as the precipitant. Incubation was performed for 30 min with gentle rotation at 4°C. Samples were centrifuged and phospholipase A_1 activity was determined in 100 μl of the supernatants. As a control, mouse IgG_1 antibodies that do not bind with liver lipase (C_1) were used. Phospholipase A_1 activity is not inhibited by protein A-Sepharose 4B, the second antibody or the tissue culture medium.

Immunoinhibition. In the immunoinhibition assay, a mixture of 5 μl purified liver lipase and 75 μl (hybridoma supernatant) of monoclonal antibody A, B, C, D or E was incubated for 1 h on ice and subsequently tested for phospholipase A_1 activity. Again an identical incubation with 75 μl hybridoma supernatant C_1 served as a control.

Proteolytic degradation of liver lipase. An amount of 384 μl purified liver lipase and 100 μl 0.1% (w/v) trypsin were incubated at 37°C. The reaction was terminated after 0 s, 15 min, 45 min, 60 min and 75 min by mixing 78 μl of the reaction mixture with 50 μl 0.1% (w/v) trypsin inhibitor (trypsin/trypsin inhibitor = 1 : 3). The samples were kept on ice and tested for both triacylglycerol hydrolase activity and phospholipase A_1 activity. An identical experiment without trypsin but with trypsin inhibitor incubated for 75 min at 37°C served as a control.

A similar experiment was carried out and the samples were prepared for protein blotting. Liver lipase and trypsin were incubated on ice for 0 s, 20 s, 1.5 min, 3 min, 6 min and 10 min. Again, an identical inhibition of liver lipase without trypsin but with trypsin inhibitor for 10 min on ice served as a control. After SDS-polyacrylamide gel electrophoresis, the proteins were blotted onto nitrocellulose paper. Liver lipase was identified on the blot using a mixture of the anti-liver lipase monoclonal antibodies and ^{125}I-labelled anti-mouse whole antibodies [9].

Modification of liver lipase. 5 μl purified liver lipase and 75 μl 25 mM Tris-HCl (pH 7.6) were incubated with 20 μl TPCK or *N*-ethylmaleimide (BDH Chemicals, U.K.), dissolved in methanol at a final concentration of 50 μM, 100 μM, 200 μM or 300 μM (TPCK was a generous gift from Dr. B. Kraal, Department of Biochemistry, State University of Leiden). After 75 min on ice, the reaction was terminated by the addition of 25 μl 20 mM 2-mercaptoethanol and triacylglycerol hydrolase and phospholipase A_1 activities were measured. Identical incubations with 20 μl water or 20 μl methanol served as controls. Modification of liver lipase with phenylisothiocyanate (lot No. 26921, Pierce, Rockford, U.S.A.) was carried out with 5

μl purified enzyme, 85 μl glycine-NaOH buffer (pH 9.5) and 0 μl, 0.125 μl, 5 μl or 10 μl PITC in a total volume of 100 μl for 45 min at 22°C.

Results

pH-dependency of phospholipase A_1 and triacylglycerol hydrolase activity of purified rat liver lipase

The effect of pH on the hydrolysis of a phosphatidylcholine emulsion or a trioleoylglycerol emulsion is shown in Fig. 1. Both enzyme activities show a pH curve with a maximum at a pH of about 9.5. At a physiological pH, the phospholipase A_1 activity is about 80% of the maximal enzyme activity at pH 9.5, whereas more than 50% of the maximal triacylglycerolhydrolase activity is found.

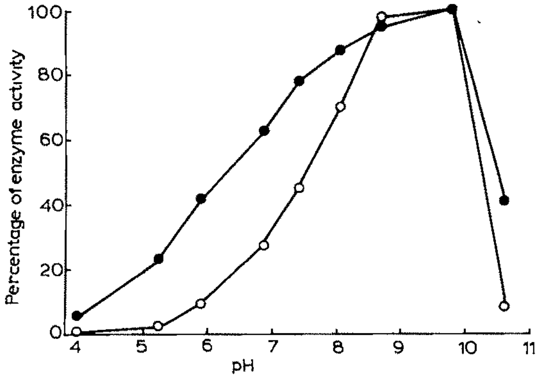

Fig. 1. A purified sample of rat liver lipase was tested for phospholipase A_1 activity (●) and triacylglycerol hydrolase activity (○) at different pH levels. 100% activity is 349 mU/ml triacylglycerol hydrolase and 16.5 mU/ml phospholipase A_1 activity. Measurements were carried out at least twice.

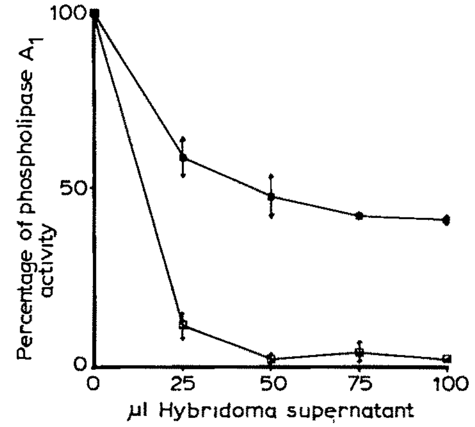

Fig 2 Immunoprecipitation of phospholipase A_1 activity of 5 μl purified rat liver lipase with an increasing amount of hybridoma supernatant A (□) and E (■). Hybridoma supernatant C_1 (100 μl) was used as a control (in the figure (○), at zero hybridoma supernatant). 100% represents 13 6 mU/ml phospholipase A_1 activity. Measurements were carried out at least twice.

Effect of monoclonal antibodies on phospholipase A_1 activity

To study the effect of five monoclonal antibodies on the phospholipase A_1 activity of purified rat liver lipase, it is important to know the binding capacity of the enzyme for the several antibody preparations. Fig. 2 shows the results of the immunoprecipitation of 5 μl purified rat liver lipase by an increasing amount of hybridoma supernatants A and E. The results with hybridoma supernatant B, C and D were identical with those obtained with A and are therefore not given in this figure. 50 μl hybridoma supernatant A, B, C or D is shown to be sufficient for 98% precipitation of the phospholipase A_1 activity of 5 μl purified liver lipase that was used in the assay. Monoclonal antibody E, on the other hand, surprisingly shows only 59% precipitation of the phospholipase A_1 activity with 75 μl hybridoma supernatant or more. In other words: 41% of the phospholipase A_1 activity of the purified enzyme is not recognized by monoclonal antibody E. An identical amount of the purified enzyme (5 μl) was tested for phospholipase A_1 activity in an immunoinhibition assay, using an excess amount (75 μl) of hybridoma supernatant A, B, C, D or E (Table I). It is shown in this table that all monoclonal antibodies inhibit phospholipase A_1 activity of the purified enzyme to a certain degree. Whereas monoclonal antibodies C and D inhibit both the phospholipase A_1 and triacylglycerol hydrolase activity (Table I, Ref. 9) in a similar way, antibodies A, B and E show different results. Immunoinhibition of phospholipase A_1 and triacylglycerol hydrolase activity was also tested with an emulsified mixture of both substrates (see Materials and Methods) to exclude the possibility that the differences in immunoinhibition obtained with both enzyme activities could be related to the

TABLE I

ENZYME INHIBITION OF PHOSPHOLIPASE A_1 ACTIVITY OF PURIFIED RAT LIVER LIPASE

5 μl of a purified sample of rat liver lipase was incubated for 1 h on ice with 75 μl hybridoma supernatants A, B, C, D, E and tested for phospholipase A_1 activity. C_1 served as control hybridoma supernatant. Results are given as means ± S.D of three separate experiments in triplicate Inhibitions are expressed as percentages

Antibody preparation	Enzyme activity (mU/ml)	Inhibition (%)
C_1 (control)	16.0±0.8	0
A	11.4±0.5	29± 3
B	12.2±0.5	24± 3
C	9.1±0.8	43± 5
D	11.4±1.8	29±11
E	10.6±2.1	34±13

different micellar substrates used. The results obtained were similar to those reported in Table I (not shown).

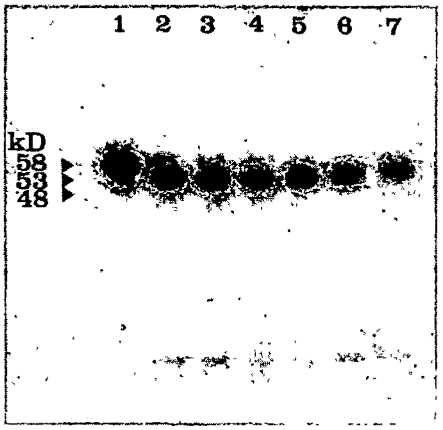

Fig. 4. Immunoblotting of trypsin digested purified rat liver lipase. The enzyme was detected using a mixture of the monoclonal antibodies (A–E) and a ^{125}I-labelled anti-mouse antibody (as the second antibody). Liver lipase and trypsin were incubated on ice for 0 s (lane 7), 20 s (lane 6), 1.5 min (lane 5), 3 min (lane 4), 6 min (lane 3) and 10 min (lane 2). An identical incubation for 10 min without trypsin (lane 1) served as a control

Proteolytic digestion of rat liver lipase

The results of the proteolytic degradation of liver lipase and its consequences for enzyme activity are presented in Figs. 3 and 4. Both the triacylglycerol hydrolase and the phospholipase A_1 activities of purified rat liver lipase are lowered by trypsin treatment of the enzyme (Fig. 3). However, the phospholipase A_1 activity is more sensitive to proteolysis than the triacylglycerol hydrolase activity. To study the actual breakdown of the molecule, the degradation by trypsin was followed by western blotting (Fig. 4). Immunoblotting of the enzyme revealed a 58 kDa enzyme form, as was reported earlier [9]. Fig. 4 shows that after a 1.5 min incubation of liver lipase with trypsin on ice, 100% of the enzyme is degraded into a smaller, 53 kDa, form (lane 5). After an incubation for 10 min on ice, the intensity of the 48 kDa band increased at the expense of a 53 kDa band (lane 2). Incubations for 15 min or longer at 37°C (not shown) result in a rapid decrease of both the 53 and the 48 kDa band, indicating a further breakdown of the enzyme which, however, cannot be detected any more by the monoclonal antibodies.

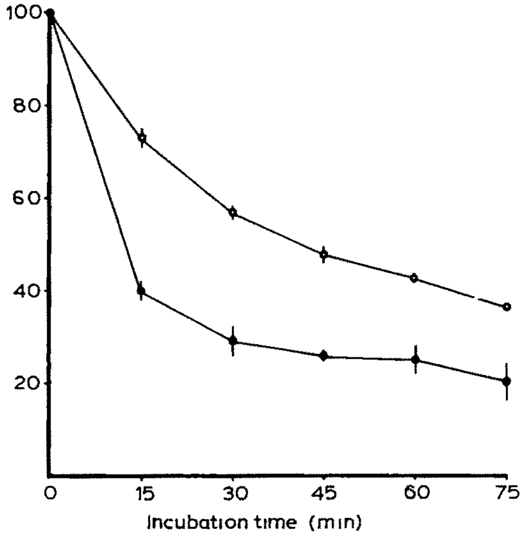

Fig 3. Proteolytic digestion of purified rat liver lipase by trypsin. The degradation was carried out at 37°C and was terminated by means of trypsin inhibitor at the time intervals indicated. 100% phospholipase A_1 activity (●) is about 0.17 mU/ml and triacylglycerol hydrolase activity (○) is 12.8 mU/ml. Measurements were carried out at least twice.

Modification of liver lipase

TPCK modification (Fig. 5) and *N*-ethylmaleimide modification (Fig. 6) of purified rat liver lipase did not have any effect on phospholi-

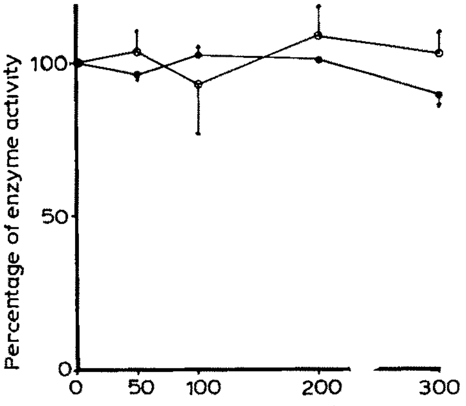

Fig 5. Modification of purified rat liver lipase by TPCK. 5 µl of the enzyme was incubated with 20 µl TPCK (in methanol) for 75 min on ice in a total volume of 100 µl The reaction was terminated with 25 µl 20 mM 2-mercaptoethanol The enzyme was tested for phospholipase A_1 (●)activity (100% = 9.6 mU/ml) and triacylglycerol hydrolase (○) activity (100% =195 mU/ml). Measurements were carried out in duplicate

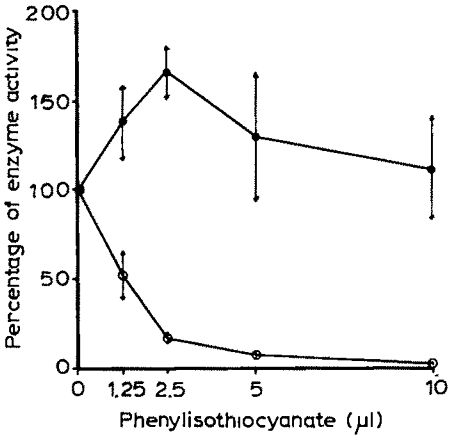

Fig 7 Modification of purified rat liver lipase by phenylisothiocyanate 5 µl of the enzyme was incubated with 0, 0.125, 5 or 10 µl phenylisothiocyanate in a glycine-NaOH buffer (pH 9.50) in a total volume of 100 µl for 45 min at 22°C. The enzyme was tested for phospholipase A_1 (●) activity and triacylglycerol hydrolase (○) activity. Measurements were carried out at least three times.

pase A_1 or triacylglycerol hydrolase activities. On the other hand, after modification of lysine residue(s) by phenylisothiocyanate, marked changes were observed in both enzyme activities tested (Fig. 7). Although this modification rapidly decreases the capability of the enzyme to hydrolyze a triolein emulsion, the phospholipase A_1 activity is even initially stimulated upto 168% of the control value.

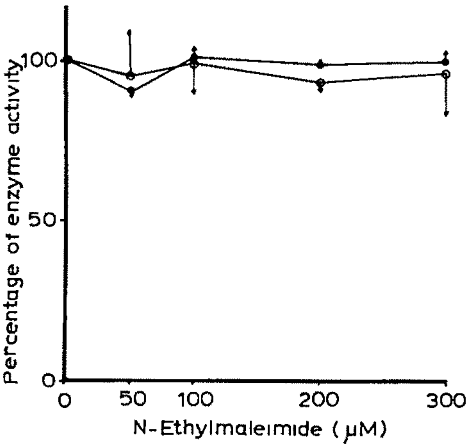

Fig. 6 Modification of purified rat liver lipase by N-ethylmaleimide. The reaction was carried out as described in the legend of Fig 5. The enzyme was tested for phospholipase A_1 (●) activity and triacylglycerol hydrolase (○) activity.

Discussion

In the study on the function of the salt-resistant heparin releasable liver lipase, evidence has been presented by several groups [2–5, 27, 28], along different lines, for the role of the enzyme in the metabolism of HDL. Besides these studies that support the hypothesis of the role of the enzyme in the degradation of HDL phospholipids, an effect on human HDL_2 triacylglycerol was also reported [27, 29, 30]. Goldberg et al. [31], on the other hand, presented data in the Cynomolgus monkey, suggesting a possible function of the enzyme in the metabolism of intermediate density lipoproteins. Nozaki et al. [32] demonstrated that in humans under pathological conditions intermediate density lipoprotein concentrations are inversely correlated with human liver lipase. From these studies the question arises, whether liver lipase is besides as a phospholipase also important as a triacylglycerol hydrolase in vivo. Information about the action of the enzyme on both phospholipid and triacylglycerol as the in vitro substrate might be helpful for a better understanding of the physiological action of liver lipase. The activity is in vitro most frequently tested at the optimal alkaline pH. It is shown in Fig. 1, however, that at a physiological pH, in spite of the higher triacylglycerol hydrolase activity (that is always observed in vitro), enzyme activity is changed in favor of the phospholipase A_1 activity (ratio triacylglycerol hydrolase/phospholipase A_1 = 10 vs. 20).

Based on the almost complete precipitation by the monoclonal antibodies A, B, C and D of both the triacylglycerolhydrolase activity (94%, Ref. 9) and the phospholipase A_1 activity (98%) in a purified sample of the enzyme, it is concluded that liver lipase as a single protein is capable in performing both activities. In the presence of an excess of monoclonal antibody E on the other hand, triacylglycerol hydrolase activity and phospholipase A_1 activity were precipitated for 88% [9] and 59% respectively (Fig. 2). This suggests the presence of a form of liver lipase that represents about 12% of the triacylglycerol hydrolase activity and about 41% of the phospholipase A_1 activity of the total precipitable amount of activity by the antibodies A, B, C and D. This heterogeneity is not reflected in different molecular weights studied by immunoblotting of the same purified sample using the different monoclonal antibodies. On the other hand, the complete precipitation of enzyme activity by the four different monoclonal antibodies, A, B, C and D, shows a strong homology that would suggest for just a minor difference(s) between the two forms described above. The nature of the enzyme form with a relatively higher phospholipase A_1 activity is not clear yet. Besides the effect of the antibodies on the triacylglycerol hydrolase activity [9], it is shown in this paper that all antibodies are also able to inhibit its phospholipase A_1 activity (Table I). It is important to note that, while monoclonal antibodies C and D inhibit both activities similarly, binding of antibody A, B or E results in pronounced differences. When using different enzyme preparations (the purified enzyme or the enzyme in postheparin plasma) or an emulsified mixture of both substrates, identical results were obtained. Inhibition of enzyme activities may be the result of the binding of a 160 kDa IgG_1 antibody to the enzyme, thereby interfering with the hydrolyzing action of the enzyme or with the interaction with the micellar substrate. These results strongly suggest a difference between the phospholipase A_1 activity and the triacylglycerol hydrolase activity, possibly related to structural differences in the enzyme molecule.

Proteolytic digestion of liver lipase by trypsin decreased both enzyme activities (Fig. 3). However, the phospholipase A_1 activity was more sensitive to tryptic digestion of the enzyme than the triacylglycerol hydrolase activity which again strongly suggests a difference between both enzyme activities, as was discussed above. The results obtained with the phospholipase A_1 activity disagree with a study of Jensen et al. [15] but support the finding of Shirai et al. [16] of a loss of the capability of the enzyme to bind dipalmitoylphosphatidylcholine vesicles after tryptic digestion. Tryptic digestion of the enzyme seems therefore to destroy the binding site(s) of the enzyme for both micellar substrates, thereby decreasing its activity. Immunoblotting of the trypsin-digested enzyme did reveal that the 53 kDa protein, which was also observed by others [9, 33, 34], results from proteolysis of a 58 kDa protein, which was suggested earlier [9] (Fig. 4). The use of proteolytic inhibitors during the isolation of the enzyme is therefore highly recommended. These results show that, when using the partially degraded enzyme in the study on the function of liver lipase, the phospholipase A_1 activity of the enzyme will be highly underestimated.

From the results obtained with the protein modification with TPCK and *N*-ethylmaleimide (Figs. 5 and 6), it can be concluded that neither cysteine nor histidine residue(s) are directly involved in the catalytic activity of the enzyme towards phospholipids or triacylglycerols. Neutralization of the positive charge on the ϵ-amino group of a lysine residue(s) and the introduction of the hydrophobic phenyl group by the modification with phenylisothiocyanate, on the other hand, did strongly influence both enzyme activities (Fig. 7). The organisation of neutral and charged amino acids in the binding site(s) of liver lipase will of course be very important for the appropriate interaction of the enzyme with phospholipid and triacylglycerol emulsions. The introduction of a phenyl group in a hydrophylic region might irreversibly disturb the correct interaction of the hydrophobic micelle with the enzyme, resulting in a complete loss of triacylglycerol hydrolase activity. The complexity of the interactions of the enzyme with the different substrates may be even larger if natural substrates (lipoproteins) containing possible cofactors (apolipoproteins) are involved. This will be studied in future experiments.

Acknowledgements

We thank Dr. B. Kraal for helpful discussions with respect to the protein modification and Miss Ina Kalkman for the isolation of phosphatidylcholine from rat liver microsomes. Miss Cecile Hanson and Miss Martha Wieriks are thanked for preparing the manuscript. This work was carried out under the auspices of the Netherlands Foundation for Chemical Research (S.O.N.) and with financial aid from the Netherlands Organization for the Advancement of Pure Scientific Research (Z.W.O.).

References

1 Jansen, H. and Hülsmann, W.C (1985) Biochem Soc. Trans 13(1), 24–27

2 Jansen, H., Van Tol, A. and Hülsmann, W.C. (1980) Biochem Biophys. Res Commun 92, 53–59

3 Kuusi, T, Kinnunen, P.K.J. and Nikkilä, E.A (1979) FEBS Lett 104, 384–388.

4 Nikkilä, E A, Kuusi, T., Harno, K., Tikkanen, M. and Taskinene, M.R (1980) in Atherosclerosis V. (Gotto, A M. Jr, Smith, L.C and Allen, B., eds), p. 387, Springer-Verlag, New York

5 Applebaum, D M, Goldberg, A P., Pykälistö, O J, Brunzell, J D. and Hazzard, W R (1977) J. Clin. Invest. 59, 601–608

6 Kuusi, T., Saarinen, P. and Nikkilä, E A. (1980) Atherosclerosis 36, 589–593

7 Jansen, H. and Hulsmann, W C. (1980) Trends Biochem. Sci 5, 265–268

8 Jansen, H. and De Greef, W J. (1981) Biochem. J 196, 739–745

9 Persoon, N.L.M., Sips, H.J., Hülsmann, W.C. and Jansen, H. (1986) Biochim. Biophys. Acta 875, 286–292.

10 Kuusi, T., Nikkilä, E A, Virtanen, I. and Kinnunen, P.K J (1979) Biochem. J. 181, 245–246.

11 Persoon, N.L.M., Hülsmann, W.C. and Jansen, H. (1986) Eur. J Cell Biol., 41, 134–137

12 Jansen, H., De Greef, W J. and Uilenbroek, J.Th J (1985) Mol Cell Endocrinol. 42, 253–258.

13 Jansen, H, Oerlemans, M C. and Hülsmann, W C. (1977) Biochem. Biophys Res. Commun. 77, 861–867

14 Kuusi, T, Bry, K, Nikkilä, E.A. and Kinnunen, P.K J. (1979) Med. Biol. 57, 192–195

15 Jensen, G.L., Daggy, B. and Bensadoun, A (1982) Biochim. Biophys Acta 710, 464–470

16 Shirai, K., Saito, Y. and Yoshida, S. (1984) Biochim. Biophys. Acta 795, 9–14

17 Whitaker, J R and Perez/Villasenor, J. (1968) Arch. Biochem Biophys. 124, 70–78

18 Schoellmann, G. and Shaw, E. (1963) Biochemistry 2, 252–255

19 Van Noort, J M., Duisterwinkel, F.J., Jonak, J., Sedlacek, J, Kraal, B and Bosch, L (1982) EMBO J. 1(10), 1199–1205

20 Colman, R F. and Chu, R. (1970) J. Biol. Chem. 245, 601–607

21 Boehnert, M. and Schlessinger, D.H. (1979) Anal. Biochem 96, 469–473

22 Belfrage, P. and Vaughan, M (1969) J. Lipid Res. 10, 341–344

23 Van den Bosch, H., Slotboom, A.J. and Van Deenen, L.L.M (1969) Biochim. Biophys. Acta 176, 632–634

24 Groot, P.H.E., Oerlemans, M C. and Scheek, L.M. (1978) Biochim. Biophys. Acta 530, 91–98

25 Stewart, J.C.M. (1980) Anal. Biochem. 104, 10–14

26 Jensen, G L. and Bensadoun, A (1981) Anal Biochem 113, 246–252

27 Shirai, K., Barnhart, R.L. and Jackson, R.L (1981) Biochem. Biophys. Res. Commun. 100, 591–599

28 Landin, B., Nilsson, A, Twu, J.-S and Schotz, M C (1984) J. Lipid Res 25, 559–563

29 Groot, P.H.E., Scheek, L.M and Jansen, H. (1983) Biochim. Biophys. Acta 751, 393–400

30 Patsch, J.R, Prasad, S., Gotto, A.M. and Bengtsson-Olivecrona, G (1984) J Clin. Invest. 74, 2017–2033

31 Goldberg, I.J., Le, N.-A., Paterniti, J R, Ginsberg, H.N., Lindgren, F.T and Brown, W.W (1982) J. Clin. Invest. 70, 1184–1192

32 Nozaki, S., Kubo, M., Sudo, H Matsuzawa, Y and Tarui, S (1986) Metabolism 35, 53–58

33 Cisar, L.A and Bensadoun, A. (1985) J Lipid Res. 26, 380–386

34 Twu, J S., Garfinkel, A.S. and Schotz, M.C (1984) Biochim Biophys. Acta 792, 330–337

Biochimica et Biophysica Acta 917 (1987) 194–202
Elsevier

BBA 52327

Structure determination of the polymorphism of acylgalactosylceramide in rat brain by gas chromatography / mass spectrometry and proton magnetic resonance

Nathalie Theret [a], Patrick Boulenguer [b], Jean-Michel Wieruszeski [b],
Bernard Fournet [b], Jean-Charles Fruchart [a], Jean-Marie Bourre [c]
and Christiane Delbart [a]

[a] *SERLIA, Institut Pasteur, Lille,* [b] *Université des Sciences et Techniques de Lille I and* [c] *INSERM U.26, Hôpital Fernand Vidal, Paris (France)*

(Received 8 August 1986)

Key words: Acylglycosylceramide, Mass spectrometry; NMR; (Rat brain)

This paper describes the structure of acylcerebrosides isolated from rat brains. Three fractions (acylglycosylceramides I, II, III) were resolved according to their decreasing R_F values on TLC. GLC analysis of acylglycosylceramides II and III indicates that their ester-linked fatty acids are short and rather unsaturated, while amide-linked fatty acids are longer and hydroxylated. Sugar GLC analysis indicates that acylglycosylceramides II and III contain only galactose. To determine the substitution position of the acyl group on the galactose moiety, the free hydroxyl groups of acylglycosylceramide were protected with dihydropyran, deacylated and subjected to permethylation. The methylated galactoside acetates obtained after hydrolysis and reduction were then analyzed by gas chromatography / mass spectrometry. Acylglycosylceramides II and III turned out to be complex mixtures of 2-*O*-acyl-, 3-*O*-acyl-, 4-*O*-acyl- and 6-*O*-acylgalactosylceramides. Moreover, the abundance of α-methylgalactoside reveals the existence of unsubstituted galactose, suggesting that some ester-linked fatty acids could be esterified to the hydroxyl group of hydroxy fatty acids linked to sphingosine. NMR spectrometry was used to confirm this ester linkage. The key spectral feature of the fatty acid-galactose linkage (4.45 ppm) did move to 4.15 ppm after saponification of acylglycosylceramide II; on the other hand, acylglycosylceramide III contained only the spectral feature 4.15 ppm, corresponding to a high percentage of unsubstituted galactose and consistent with the presence in the molecule of a fatty acid esterified by the ω-OH group of the hydroxy fatty acid (3.95 ppm).

Introduction

A glycolipid fraction of lower polarity than cerebrosides has been isolated from mammalian brains [1–5] and resolved mainly into four galactolipids. These glycolipids were demonstrated to be galactosylceramides combined with an additional fatty acid through an ester linkage. The acylcerebrosides isolated from human, whale and bovine brains are, in fact, a mixture of 2-*O*-acyl-, 3-*O*-acyl-, 4-*O*-acyl- and 6-*O*-acylgalactosylceramides [5].

The presence of ester cerebrosides has also been reported in hog stomach [6] and rat and pig epidermis [7–13].

In the latter, the acylcerebrosides were first identified as acylglucosylceramides [9], suggesting that esterification was via the sugar ring. However,

---

Correspondence: Dr. C. Delbart, SERLIA, Institut Pasteur, 3 rue du Professeur Calmette, 59019 Lille Cedex, France

0005-2760/87/$03.50 © 1987 Elsevier Science Publishers B.V. (Biomedical Division)

reinvestigation of the sphingolipid structure using high-field NMR spectroscopy has shown that, at least in pig epidermis, the ester-linked fatty acid is attached to the ω-hydroxyl group of the ceramide fatty acid and not to the sugar [11].

Here we present evidence that rat brain acylcerebrosides are a mixture of 2-*O*-acyl-, 3-*O*-acyl-, 4-*O*-acyl- and 6-*O*-acylgalactosylceramides and also contain a fraction in which fatty acids are esterified to the ω-hydroxyl group of the hydroxy acid.

Materials and Methods

Wistar rats were obtained from a commercial source (IFFA-Credo 69210 L'Arbresle, France). Florisil (60–100 mesh) and Silica gel 60 HPTLC plates were purchased from Merck. Sep Pak C_{18} was obtained from INC (Stillwater, U.S.A.). All organic solvents and other compounds were of analytical quality unless otherwise specified.

Isolation and purification of acylglycosylceramide

The brains of rats were carefully dissected free of blood vessels and extracted with $CHCl_3/CH_3OH$ (2:1, v/v) according to the procedure of Folch et al. [14]. The pooled lipid extracts were evaporated to dryness, dissolved in chloroform and applied to a 1 × 10 cm Florisil column. Cholesterol is eluted with $CHCl_3$ (50 ml), while more polar lipids appear following successive washes with 50 ml $CHCl_3/CH_3OH$ (97:3, v/v), 50 ml $CHCl_3/CH_3OH$ (96:4, v/v), 50 ml $CHCl_3/CH_3OH$ (94:6, v/v) and 50 ml CH_3OH. Purification of acylglycosylceramide was monitored by TLC. The acylglycosylceramide-rich fractions were further refined by preparative TLC, and three glycolipid esters were thus prepared and designated as fractions I, II and III (in order of decreasing R_F value).

Thin-layer chromatography

Analytical and preparative TLC was performed on Silicagel 60 HPTLC plates. Acylglycosylceramides were separated using $CHCl_3/CH_3OH/H_2O$ (40:10:1, v/v) as solvent system [12]. The non-hydroxy and hydroxy fatty acids were isolated with Hexane/ethyl ether/acetic acid (70:30:1, v/v) [9]. Visualization of compounds was achieved by spraying the plates with Rhodamine 6 G for all lipids and orcinol reagent for hexose-containing lipids.

Mild alkali treatment

Saponification of acylglycosylceramide was performed as described by Wertz et al. [9] with $CHCl_3/CH_3OH$/10 M aqueous NaOH (2:7:1, v/v). After acidification with HCl, the released free fatty acids were extracted with hexane and subjected to GLC analysis following methylation.

The deacylated acylglycosylceramide were further purified by preparative TLC using $CHCl_3/CH_3OH/H_2O$ (40:10:1, v/v) as solvent system.

GLC analysis of fatty acid methyl esters and monosaccharides

For GLC analysis of components, deacylated acylglycosylceramides were methanolysed in 1 M methanolic HCl [15]. After extraction with hexane, the amide-linked hydroxylated and non-hydroxylated fatty acid were separated from each other on Florisil columns [16]. The methanolic phase containing the methylglycosides was neutralized and trimethylsilylated before GLC analysis [17]. GLC analyses were performed with a Girdel 3000 or a Varian 6000 instrument equipped with a flame ionization detector.

The trimethylsilyl derivatives of methyl glycosides were analyzed with a Cp Sil 5 CB (Chrompack) using a program which increased the column temperature from 120 to 240°C at a rate of 2 Cdeg/min.

The methyl ester of amide- and ester-linked fatty acids and the trimethylsilyl and methyl derivatives of hydroxy fatty acid methyl esters were analysed on a CP Sil 5CB column (25 m × 0.25 mm) using a program which increased the column temperature from 100 to 240°C at the rate of 2 Cdeg/min. Identification of fatty acids derivatives was confirmed by GC-MS on a Ribermag 10-10 apparatus coupled to a Sidar 21 data processor with an electron impact energy of 70 eV and an ionizing current of 0.2 mA.

Determination of the position of the acyl group on acylglycosylceramide

Methylation of acylglycosylceramide was performed using the following modifications to the procedure described by Yasugi et al. [4] and Parente et al. [18]: acylglycosylceramide (500 μg) was dissolved in 500 μl of dimethylformamide and treated with dihydropyran (0.05 ml) and 1% *p*-toluenesulfonic acid (0.05 ml) in dimethylformamide for 15 h at room temperature.

The reaction mixture was concentrated to dryness, redissolved in 1 ml of diethyl ether, sonicated for 30 min and washed with 20 ml of 5% sodium bicarbonate to remove *p*-toluenesulfonic acid. The diethyl ether layer was then dried with sodium sulfate, evaporated to dryness, redissolved in 1 ml of CH_3OH/H_2O (8 : 2, v/v) and applied on a Sep-pak C_{18} cartridge as described previously [4] for purification. Deacylation of acylglycosylceramide was performed using 0.1 M methanolic sodium methoxide (40°C for 2 h), the products were then dried with sodium sulfate. Methylation was performed according to the method of Parente et al. [18]. The mixture of methyl mono-*o*-methylgalactoside peracetates and methylgalactoside peracetates obtained after methanolysis and peracetylation of permethyl galactosylceramide II and III were identified by GLC-MS on a Ribermag 10-10 apparatus coupled to a Sidar 21 data processor. The electron impact energy which was used was 70 eV, coupled with an ionizing current of 0.2 mA. Mass chromatograms of peracetylmethylmono-*o*-methylgalactosides were obtained at *m/e* 71 (4-mono-*o*-methyl-), 116 (2-mono-*o*-methyl-), 232 (3-mono-*o*-methyl-), 289 (6-mono-*o*-methyl-) and 303 (A_1 fragment for all monomethyls) [19].

NMR measurement

Approx. 1 mg of acylglycosylceramide was treated three times with 0.5 ml $C^2HCl_3/C^2H_3O^2H$ (2 : 1 by v/v) and then lyophilized. Proton NMR spectra of acylglycosylceramide, dissolved in 0.6 ml $C^2HCl_3/C^2H_3O^2H$ (2 : 1, v/v) were obtained on a Brucker AM-400-WB spectrometer, operating in the Fourier transform mode. The spectral width was 4 kHz. The operation was performed at 27°C. Chemical shifts (δ) are expressed in ppm downfield from internal reference of tetramethylsilane ($\delta = 0.000$ ppm) but were measured by reference to the residual proton signal from C^2HCl_3 ($\delta = 7.487$ ppm).

Results

Isolation of acylglycosylceramide from rat brain

Acylglycosylceramide largely free from other lipids were obtained by developing a Florisil column with $CHCl_3/CH_3OH$ mixtures (Fig. 1). In order to eliminate the small amounts of the contaminating ceramides, the pooled acylglycosylceramide fractions (96–4; 94–6) were purified by further preparative TLC using $CHCl_3/CH_3OH/H_2O$ (40 : 10 : 1, v/v) as solvent system.

The TLC pattern of acylglycosylceramide reveals the presence of three homogeneous bands named I, II, III, in order of decreasing R_F values; orcinol staining indicates that each contains hexose sugars.

After saponification with mild alkaline reagent, acylglycosylceramides are converted into cerebrosides and free fatty acids, suggesting the presence of ester-linked fatty acids in those lipids.

Composition analysis

Composition analysis has been performed only

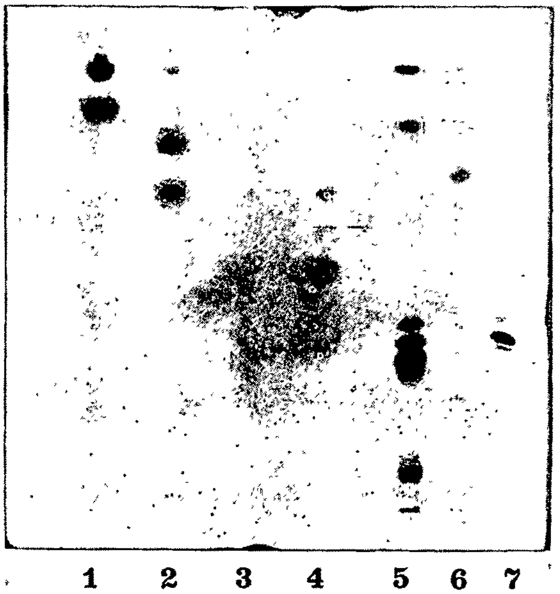

Fig. 1. Separation of total rat brain lipids on a Florisil column. Eluting solvents: (1) $CHCl_3$; (2) $CHCl_3/CH_3OH$ (97.3, v/v); (3) $CHCl_3/CH_3OH$ (96 : 4, v/v); (4) $CHCl_3/CH_3OH$ (94 : 6 v/v); (5) CH_3OH; (6) ceramide; (7) cerebroside.

on acylglycosylceramides II and III. Acylglycosylceramide I is characterized by an R_F value similar to that of ceramides, so further purification of this fraction will be necessary before compositional analysis is possible.

GLC of the trimethylsilylated methylglycosides formed from the carbohydrate portion of acylglycosylceramides II and III has established that galactose is the unique sugar component. Table I gives the fatty acid distribution of isolated acylglycosylceramides II and III. The ester-linked fatty acids were liberated by saponification, while the amide-linked fatty acid composition was achieved after methanolysis of the deacylated acylglycosylceramide. It is worth noting that the ester-linked fatty acids are short and unsaturated, while amide-linked fatty acids are longer. Moreover, composition analysis of both ester and amide-linked fatty acids was achieved by GLC-MS as described under experimental procedures. No hydroxy fatty acids were found in ester-linked fatty acids after saponification of either acylglycosylceramide II or III. On the other hand, hydroxy fatty acids are liberated by acid hydrolysis of the previously saponified acylglycosylceramides II and III. The unique hydroxy fatty acid encountered in acylglycosylceramide II is an ω-hydroxystearic acid

TABLE I

COMPOSITION OF ESTER-LINKED AND AMIDE-LINKED FATTY ACIDS OF ACYLGALACTOSYLCERAMIDE II AND III

Values are expressed as percent distributions.

Fatty acids	Ester-linked acids		Amide-linked acids	
	II	III	II	III
14:0	1.3	1.2	2.0	2.56
15:0	0.4	0.5	0.4	0.6
16:0	30.0	29.7	24.7	27.0
16.1	1.7	1.9	6.7	7.0
18:0	33.5	24.7	25.7	22.7
18:1	22.8	23.6	21.1	18.1
20:0	0.8	6.8	11.0	10.6
20:1	0.3	3.0	2.7	5.3
20:4(*n* − 6)	7.3	2.8	–	–
22:0	0.5	2.2	3.0	1.8
22:1	0.5	1.8	2.5	3.5
24:0	0.6	1.0	0.7	0.5
24:1	0.3	0.8	0.5	0.44

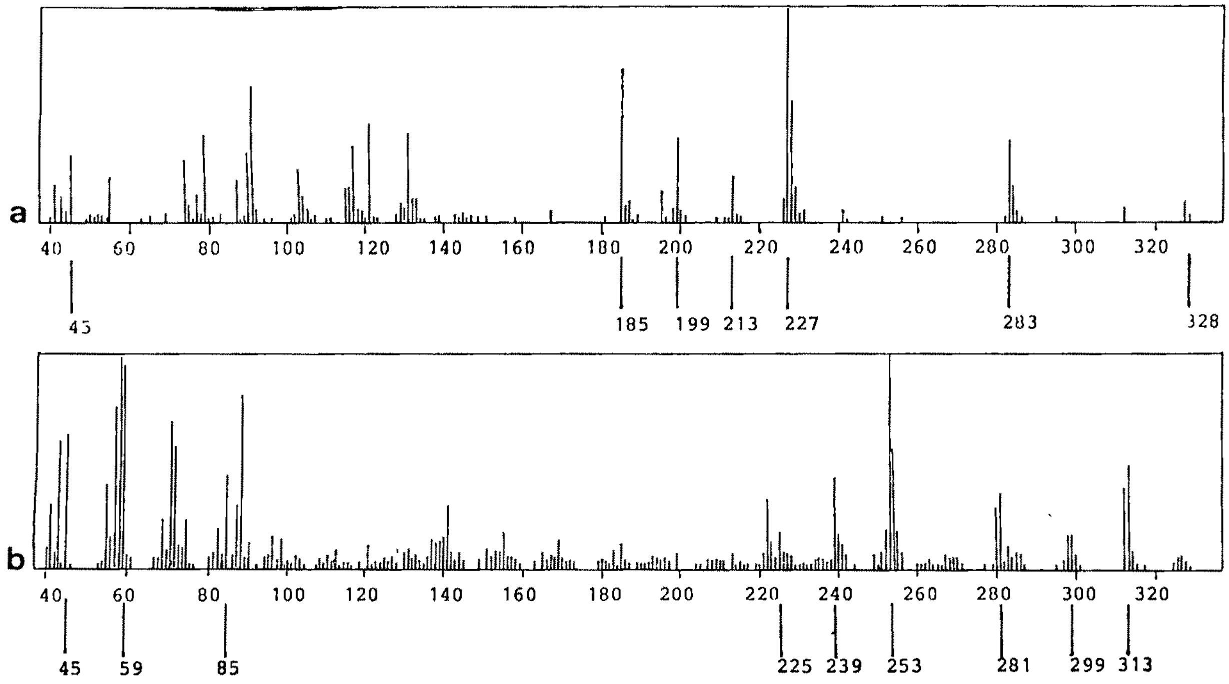

Fig. 2 Mass spectrometry of (a) ω-hydroxystearic acid in acylgalactosylceramide II; (b) α-ω-dihydroxystearic acid in acylgalactosylceramide III.

(18-OH-18:O), but acylglycosylceramide II is characterized by a minute amount of this 18-OH-18:O (18-OH-18:0/18:0 = 0.186). The presence of ω-hydroxystearic acid is attested on the basis of a molecular ion at *m/e* 328, peaks at *m/e* 283 $(M-45)^+$, 227, 213, 199 and 185. On the other hand, the carboxy part of the molecule gives rise to characteristic peaks at *m/e* 74 and 87 (Fig. 2a and Fig. 3a).

GLC-MS analysis of hydroxy fatty acids from acylglycosylceramide III reveals the presence of an α,ω dihydroxy fatty acid identified as an α,ω-dihydroxystearic acid (2,18-OH_2-18:0). Acylglycosylceramide III is very rich in this fatty acid (2,18-OH_2-18:0/ 18:0 = 0.698). The α,ω-dihydroxy fatty acid was demonstrated by the production of peaks at *m/e* 313 $(M-45)^+$, 229, 285 (Fig. 2b). The hydroxyl group in position α was demonstrated by comparison with a α-hydroxystearic acid by peaks at *m/e* 41, 44; 55, 57; 63, 71; 83, 85; 97, 99; 111, 113. The hydroxyl group in position ω was demonstrated by a peak at *m/e* 45. Moreover, the loss of 1 mol methanol (Fig. 3b) from the α-methonyl group gives characteristic ions at *m/e* 281, 253, 239, 225. On GC chromatograms, the α,ω-dihydroxy fatty acid is detected 9 min after the stearic fatty acid under experimental procedures described above.

The presence of a hydroxy fatty acid in the molecule of acylglycosylceramide is of particular importance and represents a potential ester linkage.

Methylation analysis

Previous investigations [4,11] indicated that the linkage position of the additional acyl group in the acylglycosylceramide can be situated either on galactose moieties, or on a hydroxy fatty acid linked to the sphingosine.

The position of the esterifing fatty acid was investigated by GLC-MS as described under Materials and Methods.

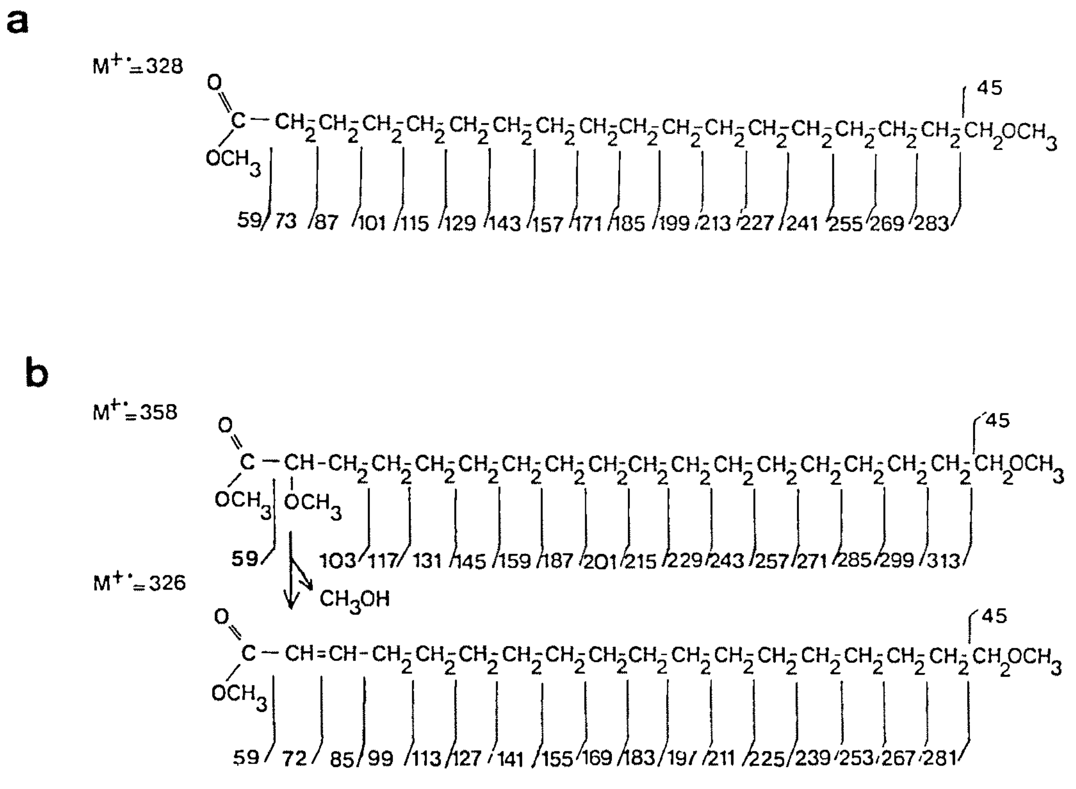

Fig. 3. Fragmentation diagram of (a) ω-hydroxystearic acid in acylgalactosylceramide II; (b) α,ω-dihydroxystearic acid in acylgalactosylceramide III.

GLC-MS analysis (Fig. 4) of partially methylated methylglycosides produced by the different acylglycosylceramides reveals the presence of a mixture of monomethyltri-*O*-acetylmethyl galactosides. In a chromatogram based on total ionizing current, some peaks have the retention time of the monomethyl sugar. With a specific ion *m/e* 303 current, only monomethyl galactosides appear and they have the heterogenous population distribution indicated in Table II.

The identification of monomethyl galactoside was performed according to Fournet [19]. The cerebroside esters are a mixture of 2-*O*-; 3-*O*-, 4-*O*- and 6-*O*-acylgalactosylceramide, which correspond to about 71% of fraction II and 35% of fraction III. The rest of the population consists of cerebroside esters in which the fatty acids are presumably linked to the ω-hydroxy fatty acid.

TABLE II

PERCENT DISTRIBUTION OF MONOMETHYLGALACTOSIDE ACETATE OBTAINED AFTER PERMETHYLATION, METHANOLYSIS AND PERACETYLATION FROM ACYLGALACTOSYLCERAMIDE II AND III

Position of substituent		Acylgalactosylceramide	
methyl	acetyl	II	III
2	3, 4, 6	40.0	19.3
3	2, 4, 6	17.4	30.7
4	2, 3, 6	26.0	39.7
6	2, 3, 4	16.6	10.3

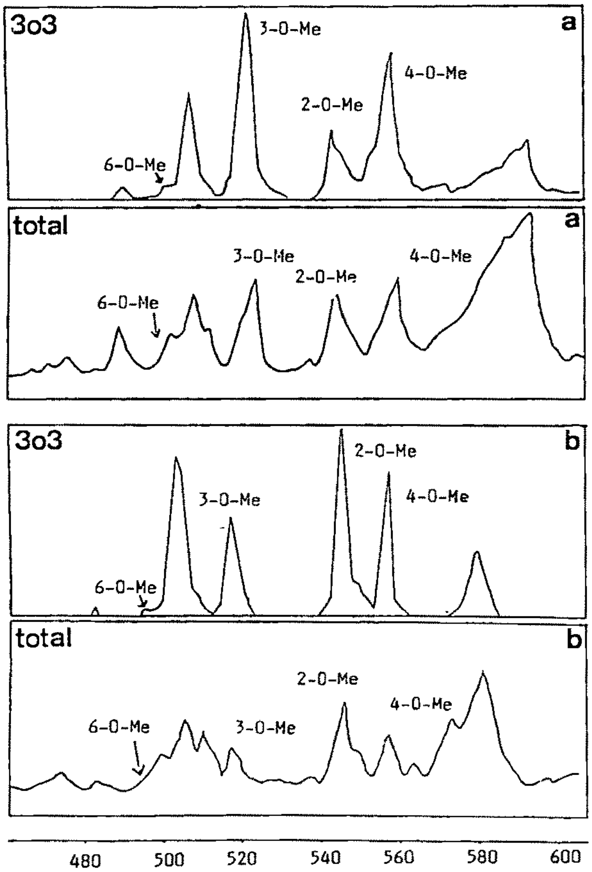

Fig. 4. GLC-MS analysis of partially methylated methyl glycoside: *m/e* 303 and total ionizing current (a) Acylglycosylceramide III. (b) Acylglycosylceramide II.

All the above results show that the additional fatty acid can esterify the galactose residue or the hydroxy fatty acid linked to the sphingosine.

The finding that the majority of acylglycosylceramide III was not an *O*-acylgalactosylceramide suggested the possibility that this lipid might be a galactosyl *N*-(ω-*O*-acyl)ceramide and raised questions about the nature of the acyl linkage.

NMR analysis

To determine whether the additional fatty acid was associated with the hydroxy fatty acid on the long-chain base, the NMR spectra of the different acylglycosylceramides were analysed.

The whole NMR spectrum is presented in Fig. 5; acylglycosylceramides III, II and II saponified.

The hydroxyl and the amide protons were deuterated by exchange with C^2HCl_3-$C^2H_3O^2H$ and assignment of all peaks is effected as previously described [11,20].

The heterogeneity in composition of both acylglycosylceramides II and III revealed previously by GLC-MS analysis is confirmed by NMR spectrum analysis. The acylglycosylceramide II fraction is characterized by a major H_1 peak which appears at 4.404 ppm, indicating the existence of an esterified galactose in the molecule. Saponification of acylglycosylceramide II induces a downfield shift of the sugar anomeric proton and the H_1 peak moves to 4.218 ppm. This H_1 peak at 4.218 ppm can be detected in native acylglycosylceramide II to a small extent. In acylglycosylceramide III, the major H_1 peak appears at 4.218 ppm, corresponding to an unesterified galactose

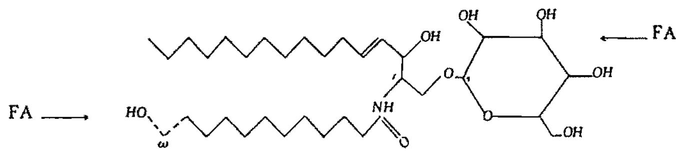

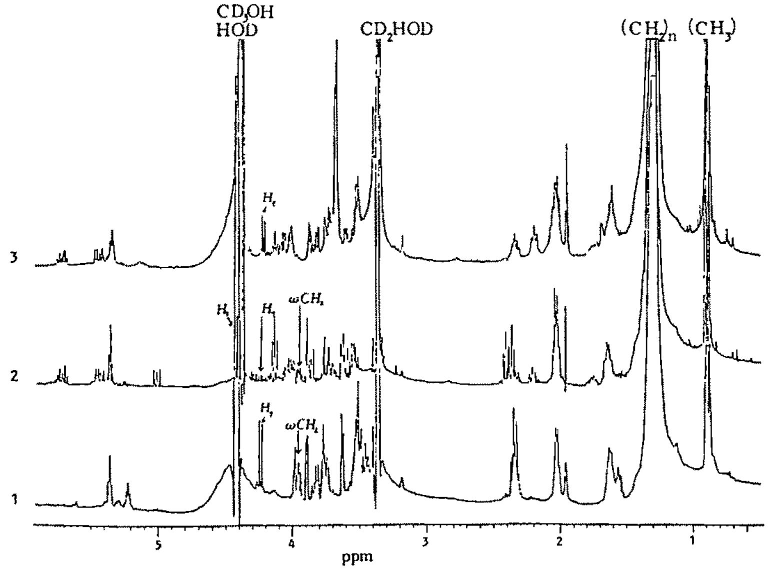

Fig 5 400 MHz proton magnetic resonance spectrum of the acylgalactosylceramide from rat brain. (1) Acylglycosylceramide III (2) Acylglycosylceramide II. (3) Acylglycosylceramide II saponified.

residue. Unfortunately, in the NMR spectrum of acylglycosylceramide III, the water peak (4.400 ppm) overlaps the H_1 doublet in less concentrated samples. Moreover, the acylglycosylceramide III spectrum is also characterized by a chemical shift value of 3.952 ppm, which is close to that reported for a methylene group bearing an esterified hydroxyl group and indicating esterification at the ω-OH position between linoleic and ω-hydroxytriacontanoic acids [11]. All these results (Table III) indicate that native acylglycosylceramide II characterized by a major peak at 4.404 ppm and two minor peaks at 4.218 ppm and 3.952 ppm mostly is represented by *O*-acylgalactosylceramides where the galactose residue is esterified (71%). On the other hand, native acylglycosylceramide III displays two major peaks at 4.218 ppm and 3.952 ppm, testifying to a high percentage (65%) of esterified hydroxy fatty acids as encountered in galactosyl(*N*-ω-*O*-acyl)ceramides.

These results are also supported by the fact that

TABLE III

CHEMICAL SHIFTS (IN ppm) AND COUPLING CONSTANTS (IN Hz)

	H_1 of Gal	CH_2 of ceramide
Acylgalactosylceramide III (0.5 mg)	4.237 ppm $J = 7.26$ Hz	3.952 ppm $J = 5\ 70$ Hz
Acylgalactosylceramide II (1 0 mg)	4.404 ppm $J = 8.00$ Hz	– –
Variation [a]	4.297 ppm $J = 5.70$ Hz 4.284 ppm $J = 7.42$ Hz 4 241 ppm $J = 6.85$ Hz	– – – – – –
Acylgalactosylceramide saponified (<1 mg)	4.218 ppm $J = 7.32$ Hz	– –

[a] Variation of H_1 chemical shift with position of fatty acid on galactose (minor peaks).

acylglycosylceramide II contains less ω-hydroxy fatty acids than acylglycosylceramide III.

Discussion

The present study demonstrates that acylgalactosyl ceramides of rat brain are resolved into three distinct galactolipids, and concentrates on the structure of the more polar lipids (i.e., acylglycosylceramides II and III).

Compositional analyses of acylglycosylceramides II and III are mostly similar when focusing on the identity of the monosaccharide or on the composition of the amide- or ester-linked non-hydroxy fatty acids. The main difference between the two acylglycosylceramides lies in the presence of hydroxy fatty acids that are linked to the sphingosine. The less polar acylglycosylceramide II contains only a minute amount of ω-hydroxy fatty acid, while the more polar acylglycosylceramide III is very rich in an α,ω-dihydoxy fatty acid. This characteristic feature of acylglycosylceramide III is in complete agreement with the high polarity of the lipid. It may also be noted that rat acylcerebrosides are complex mixture of 2-*O*-acyl-, 3-*O*-acyl-, 4-*O*-acyl- and 6-*O*-acylgalactosylceramides, but also contain galactosyl-*N*-(ω-*O*-acyl)ceramides, where a fatty acid is esterified to the ω-hydroxyl group of the fatty acid linked to the sphingosine. The existence of glucosyl-*N*-(ω-*O*-acyl)ceramide was reported previously for animal epidermis but nowhere else [11]. We report here evidence of the presence of galactosyl *N*-(ω-*O*-acyl)ceramide in rat brain.

On the basis of GLC-MS analysis, it seems that acylglycosylceramide III is mostly composed of galactosyl-*N* – (ω-*O*-acyl)ceramide, while the major component of acylglycosylceramide II is a 2-*O*-acylgalactosylceramide. Thus, the acylglycosylceramides of rat brain are remarkable when compared to other mammalian acylglycosylceramides which contain 6-*O*-acylgalactosylceramide as their major component [2,4,5]. Moreover, rat brain acylglycosylceramide is very different from those described in the various types of epidermis [8,10–13]. Their osidic and ceramide moieties are very different.

In both acylglycosylceramides, the ester-linked fatty acids proved to be mainly short and rather unsaturated, with high percentages of stearic and oleic acid. The amide-linked fatty acids were shown to consist of long-chain fatty acids (C_{20}), and of 18-OH-18:0 or 2,18-OH_2-18:0 as the hydroxy fatty acid. So it is quite clear (Table I) that in galactosyl *N*-(ω-*O*-acyl)ceramides of rat brain, acyl fatty acids linked to the sphingosine are not linoleoyltriacontanoic acids, as encountered in rat [8,12,13] or pig [10,11] epidermis.

It has been proposed that acylglycosylceramides may serve as transmembranal elements, and as such stabilize the lipid bilayers [21]. Within the context of this hypothesis, acylglycosylceramide II of rat brain could have a function in the stabilization of myelin structures. We are currently measuring the occurrence of acylglycosylceramide in purified myelin.

Acknowledgements

This work was supported by Grants (CRE 866 003) from the Institut National de la Santé et de la Recherche Médicale (INSERM). We are indebted to Dr. J. Shepherd for his help in preparing the manuscript.

References

1 Norton, W.T. and Brotz, M (1963) Biochem. Biophys. Res. Commun 12, 198–203

2 Kishimoto, Y., Wajda, M. and Radin, N S (1968) J. Lipid. Res 9, 27–33

3 Tamar, Y (1968) Japan J. Exp. Med. 38, 65–73

4 Yasugi, E, Saito, E, Kasama, T., Kojima, H and Yamakawa, T (1982) J. Biochem. 91, 1121–1127

5 Yasugi, E., Kasema, T, Kojima, H and Tamakawa, T (1983) J. Biochem. 93, 1595–1599

6 Slomiany, B.L , Slomiany, A. and Horowitz, M.I (1972) Biochim Biophys. Acta 280, 383–392

7 Gray, G.M., White, R.J. and Majer, J.R. (1978) Biochim. Biophys. Acta 528, 127–137

8 Hansen, H.S. and Jensen, B. (1985) Biochim. Biophys Acta 834, 357–363

9 Wertz, P.W and Downing, D.T (1983) J Lipid Res 24, 753–758

10 Bowser, P A., Nugteren, D.H., White, R.J., Houtsmuller, U.M.T. and Prottey, C. (1985) Biochim. Biophys Acta 834, 419–428

11 Abraham, W., Wertz, P W. and Downing, D.T. (1985) J Lipid Res. 26, 761–766

12 Wertz, P.W , Cho, E.S. and Downing, D.T. (1983) Biochim. Biophys. Acta 753, 350–355

13 Wertz, P.W., Downing, D.T., Freinkel, R K. and Traczyk, T.N (1984) J. Invest Dermatol 83, 193–195

14 Folch, J., Lees, M and Stanley, S. (1957) J. Biol Chem. 226, 497–509

15 Gaver, R.G. and Sweeley, C.C. (1985) J. Am. Oil. Chem. Soc 42, 294–298

16 Bouhours, J F and Guignard, H. (1979) J. Lipid Res 20, 897–907

17 Kamerling, J.P., Gerwig, G.J. and Vliegenthart, J.F G (1975) Biochem. J. 151, 491–495

18 Parente, J.P., Cardon, P, Leory, Y., Montreuil, J. and Fournet, B. (1985) Carbohydr. Res 141, 41–47

19 Fournet, J P., Strecker, G., Leroy, Y. and Montreuil, J (1981) Anal. Biochem 116, 489–502

20 Dabrowski, J., Egge, H. ad Handfland, P (1980) Chem. Phys. Lipids 26, 187–196

21 Landmann, L., Wertz, P.W and Downing, D T (1984) Biochim Biophys Acta 778, 412–418

Biochimica et Biophysica Acta 917 (1987) 203–210
Elsevier

BBA 52324

Role of α-glucosidase in fetal lung maturation

Jacques R. Bourbon, Edith Doucet and Michel Rieutort

Laboratoire de Physiologie du Développement, Collège de France, Paris (France)

(Received 28 July 1986)

Key words: α-Glucosidase; acid α-Glucosidase; Maturation; Surfactant; (Fetal rat lung)

The role of lysosomal enzyme acid α-glucosidase in fetal lung development was investigated with the aid of a specific inhibitor, the pseudosaccharide acarbose. The drug was added to a Waymouth culture medium of fetal rat lung explants cultivated for 48 h from gestational stage 19.5 days, an in vitro system previously shown to allow morphological and biochemical maturation of alveolar epithelium. Glycogenolysis was reduced by 40% as compared with tissue cultivated on control medium, which means that α-glucosidase could account for as much as 40% of fetal lung glycogenolysis, the remaining 60% being presumably achieved by cytosolic phosphorylase and by a microsomal neutral α-glucosidase. By the same time, the increase of phospholipids of surfactant fraction extracted from cultivated explants was partially inhibited: total and saturated phosphatidylcholine, phosphatidylethanolamine, phosphatidylglycerol and phosphatidylinositol were about 30–40% lower than in lungs cultivated on control medium. It should be emphasized that DNA concentration and increases in non-surfactant phospholipids were unchanged by the drug. α-Glucosidase activity was evidenced in the lysosomal fraction, in the microsomal fraction and, although in lower amounts, in the surfactant fraction extracted from term fetal lung. The results suggest that lysosomal α-glucosidase plays a major role in lung maturation and could facilitate glycogenolysis for the specific use of glycogen stores in providing substrates for surfactant phospholipid biosynthesis.

Introduction

Glycogen stored in fetal lung at earlier stages is utilized at the time when surfactant biosynthesis surges [1–4]. A precursor-product relationship between glycogen and lung lipids, more especially surfactant phospholipids, has been evidenced [5,6] and as much as 25% of glycogen stores could be used for providing carbon for the glycerol and fatty acid backbone during lipid synthesis by the maturing lung [6].

The lysosomal enzyme, acid α-glucosidase or amyloglucosidase, had previously been found in fetal rat lung [4,7] and its implication in maturational processes had been demonstrated [4]. However, the precise function of this enzyme in the developing lung and the respective roles of acid α-glucosidase and phosphorylase in lung glycogen breakdown remained unknown. The use of acarbose (BAY g 5421), an inhibitor of acid α-glucosidase which reproduces in rats a syndrome similar to type II glycogenosis [8,9], facilitates investigation of these questions. Because of the limited availability of acarbose, its effects on lung development were studied in vitro on rat fetal lung organ cultures, a system previously shown to allow type II pneumocyte differentiation and surfactant accumulation in various species [10–13].

Consequences of acarbose treatment were studied on the glycogenolytic rate and on accumu-

---

Correspondence: Dr. J.R Bourbon, Laboratoire de Physiologie du Développement, Collège de France, 11, place Marcelin Berthelot, 75231 Paris Cedex 05, France

0005-2760/87/$03.50 © 1987 Elsevier Science Publishers B V. (Biomedical Division)

lation of phospholipids, both in a surfactant fraction isolated by Frosolono's method [14] and in residual (non-surfactant) fraction. To analyze further the specificity of acarbose effects, the activity of acid α-glucosidase and of glycogen phosphorylase was determined in lung explants at the end of the cultivation period. Because of the lysosomal-related origin of lamellar bodies [2,15], acid α-glucosidase activity was sought in the lamellar-body-enriched surfactant fraction and was documented in subcellular fractions, including purified lysosomes.

The results presented argue for a proportionally important role of acid α-glucosidase in fetal lung glycogenolysis and for a specific role in glycogen utilization for surfactant-phospholipid biosynthesis.

Material and Methods

Explant culture preparation

Wistar rats obtained from Centre d'Elevage R. Janvier (St. Berthevin, Mayenne, France), were mated overnight and pregnancies were dated as described previously [4].

On day 19.5 of gestation, the stage when glycogen accumulation is maximum [3,4], rats were killed by a blow to the head, and fetuses rapidly delivered by cesarean section under aseptic conditions. Fetal lungs were immediately removed and pooled in ice-chilled Waymouth MB752/1 medium. Four or five litters were pooled for each culture experiment. Fetal lungs were then cut into 0.7 mm edge pieces with aid of a McIllwain tissue chopper (Mickle Lab. Eng. Co., Gomshall, U.K.). They were again transferred to ice-chilled medium until being plated on top of a semi-solid culture medium according to the method described for allowing optimal conditions for surfactant biosynthesis in vitro [16]. In brief, 3 vols. of Waymouth medium (Eurobio, Paris, France) containing 250 IU/ml penicillin and 10 ng/ml streptomycin were mixed with 1 vol. of heated agar solution (2% agar in Krebs-Ringer bicarbonate solution). When still warm, the mix was dispensed to Lindbro (Flow Laboratories Inc., Hamden, CT) multi-well plates and allowed to gel. Waymouth medium was chosen because it allows a glycogenolytic rate in vitro close to that in vivo (see Results). Acarbose was added to the culture medium at a final concentration of 1 mg/ml. Osmolarity was adjusted in the control medium by addition of 0.25 mg of glucose per ml, since the molecular weight of acarbose is approx. 4-fold that of glucose (this represented a 5% increase in glucose concentration). In a few experiments, the biologically inert mannitol was added in place of glucose; no difference was observed in glycogen breakdown or in phospholipid synthesis. At the end of culture initiation, remaining explants were frozen and kept for determination of initial state parameters.

Explants were cultivated for 48 h under 76% N_2,/19% O_2/5% CO_2 (Air Liquide Co, Vitry, France) at 37°C. They were then harvested and frozen in liquid nitrogen, and stored at −25°C pending biochemical analysis. Explants were taken at random in a same culture experiment for determining either glycogen or phospholipids.

Culture media were provided by Eurobio (Paris, France). Agar, glucose and mannitol were purchased from Sigma (St. Louis,MO). Acarbose was a gift of Dr. Puls (Bayer, Leverkusen, F.R.G.).

Subcellular fractionation techniques

The surfactant fraction was isolated by discontinuous sucrose density gradient centrifugations by the method initially described by Frosolono et al. [14], revised by Sanders and Longmore [17] and adapted to small-size biological samples [18]. The surfactant fraction was isolated from cultivated lung explants for phospholipid analyses and from the lung of 21.5-day-old fetuses for determination of acid α-glucosidase activity. Lysosomes were purified from the lung of 21.5-day-old fetuses according to Hook and Gilmore [19]. Mitochondria and microsomes were isolated according to Harding et al. [20].

Biochemical analyses

Glycogen was assayed on lung tissue homogenate by the amyloglucosidase method of Chan and Exton [21] using oyster glycogen (Sigma) as a standard and the GOD-Perid kit of Boehringer (Mannheim, F.R.G.) for glucose determination.

Lipids were extracted overnight from surfactant and residual fractions using the method of Bligh and Dyer [22]. ^{14}C-labelled dipalmitoylphosphatidylcholine (Amersham International, Les Ulis, France) was added in trace amount to determine recovery after processing. After drying and resolubilization in chloroform/ methanol (2 : 1, v/v), an aliquot was taken for total phospholipid determination, and the rest was plated on silica-gel-60 precoated plates (Merck, Darmstadt, F.R.G.) for phospholipids separation by two-dimensional thin-layer chromatography as previously described [5]. Phospholipid spots were scraped and eluted by the method of Bligh and Dyer [22]. Total phosphatidylcholine (PC) was divided into three aliquots for determination of phosphorus, radioactivity and disaturated PC by the osmium tetroxide method of Mason et al. [23]. Inorganic phosphate was determined on ashed phospholipid samples by the method of Ames and Dubin [24].

Acid amyloglucosidase (*P*-nitrophenylglucosidase, EC 3.2.1.20) activity was assayed according to Torres and Olavarría [25] by determining the speed of *P*-nitrophenyl α-glucoside (Sigma) hydrolysis at pH 4.8. This pH has been shown to be optimal for the purified hepatic enzyme [25]. *p*-Nitrophenylglucosidase activity was also determined in lung homogenates at pH 7.4. The reactive mix comprised 5 mM *P*-nitrophenylglucoside, 0.06% Triton X-100 and lung homogenate in distilled water, with the appropriate acetate or phosphate buffer, pH 4.8 or 7.4, respectively. Phosphorylase *a* activity (EC 2.4.1.1) was assayed by the method of Hue et al. [26], measuring the release of inorganic phosphate from glucose 1-phosphate. Proteins were determined by the method of Schacterle and Pollack [27] using bovine serum albumin (fraction V, Sigma) as a standard. DNA was assayed by the diphenylamine method of Burton [28] using calf thymus DNA (Sigma as a reference.

Statistical analyses

Mean ± S.E. values are presented throughout the report. Differences between mean values of culture-experiment series were analyzed for statistical significance using the unpaired Student's *t*-test.

Results

Acid α-glucosidase activity at different acarbose concentrations

α-Glucosidase activity was assayed in total lung homogenates of 21.5-day-old fetuses, in the presence of acarbose at a final concentration varying from 10^{-5} to 5 mg per ml reactive mix, at pH 4.8 and 7.4. *p*-Nitrophenyl α-glucoside hydrolytic activity measured at pH 7.4 in absence of acarbose was about 1.5-times higher than that determined at pH 4.8 (63.5 vs. 39.5 nmol/mg protein per h in homogenates used for this study). At pH 4.8, acarbose exerted a significant inhibition already at a concentration of 10^{-5} mg/ml; The percentage of inhibition increased slightly until 10^{-3} mg/ml, then increased abruptly to reach total inhibition between 10^{-2} and 10^{-1} mg/ml (Fig. 1). By contrast, acarbose exerted low inhibition on the activity measured at pH 7.4; no inhibition was detected below 10^{-2} mg/ml and it was only about 50% at 5 mg/ml. Obviously, the activities determined at pH 4.8 and 7.4 must correspond to distinct enzymes, presumably to the so-called 'acid' (lysosomal) and 'neutral' (microsomal) glucosidases previously evidenced in liver [25]. Effects of acarbose in culture experiments reported below (1 mg/ml culture medium) appear therefore as consequences of the inhibition of the acid form of the enzyme.

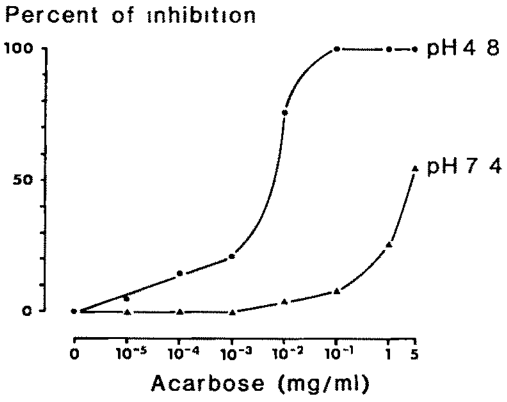

Fig. 1. Semi log plot of α-glucosidase (*p*-nitrophenyl α-glucosidase) inhibition by acarbose at various concentrations in reactive mix Assay conditions were as stated in Material and Methods. Lungs of 21.5-day-old fetuses were used The enzyme activity determined at pH 4 8 was about 1000-times more sensitive to acarbose inhibition than that determined at pH 7.4.

Choice of culture medium

In a preliminary set of experiments, glycogenolytic rate in-vitro was determined in five different commercial media (Waymouth MB 752/1, Dulbecco's modified minimum essential medium, CMRL 1066, Ham's F12K and RPMI 1640). Results are reported in Fig. 2. It should be recalled that the glycogen concentration in fetal rat lung peaks at 19.5 days, decreases slightly between this stage and 20.5 days, then sharply thereafter [3,4]. Ideally, a culture condition would reproduce that glycogenolytic rate occurring in vivo. In fact, glycogenolysis was faster in vitro than in vivo with all media. Waymouth medium was the one allowing the slowest glycogenolytic rate, the least different from the in vivo rate. Since Waymouth medium was shown in previous experiments [16] to support an in vitro accretion of surfactant phospholipids of the same order as that occurring in vivo during the same period, it was chosen for studying the effects of acarbose.

DNA in cultivated explants (Table I)

DNA concentration did not change significantly during culture, either in presence or absence of acarbose. This was in keeping with previous observations [16].

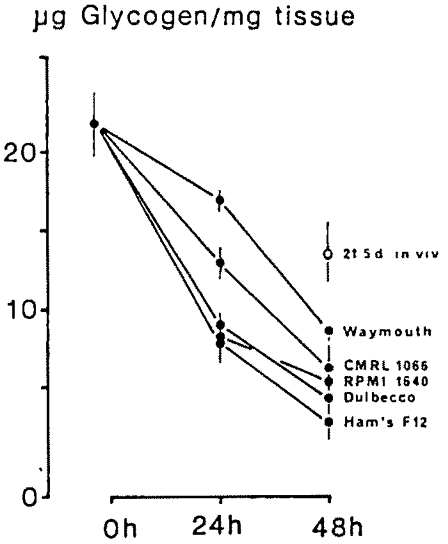

Fig. 2. Glycogenolytic rate in lung explants from 19 5-day-old rat fetuses cultivated for 48 h on five different culture media. The closest rate to that occurring in vivo (21.5 d) was observed with Waymouth medium. (Mean ± S E on six culture experiments.)

TABLE I

DNA AND GLYCOGEN CONTENT OF FETAL LUNG EXPLANTS CULTIVATED FOR 48 h ON CONTROL WAYMOUTH MEDIUM OR IN PRESENCE OF 1 mg/ml ACARBOSE

Mean ± S E. on the number of culture experiments indicated in brackets.

	DNA ($n = 10$) (μg/mg tissue)	Glycogen ($n = 8$) (μg/mg tissue)
Initial (19.5 d)	7.0 ± 0.2	25.7 ± 1.0
Final (48 h of culture)		
Control medium	7.2 ± 0.5	9.7 ± 0.6
Acarbose	7.2 ± 0.3	15.9 ± 0.4 [a]

[a] Significant difference with control medium for $P < 0.001$

Effects of acarbose upon glycogenolysis in vitro (Table I)

About 62% of the initial glycogen content of the explants was broken down during the 48 h of cultivation in control medium. In presence of acarbose, glycogenolysis was partly prevented, and only 38% of initial glycogen were utilized on the average. This effect was constant in the eight culture experiments performed, with very low deviation from the mean value. In other words, acarbose induced a 40% inhibition of glycogenolysis.

Effects of acarbose on phospholipids in surfactant and residual fractions

Table II describes changes which occurred in surfactant fraction phospholipids in culture, in control medium and in the presence of acarbose. Phospholipids of the surfactant fraction considerably increased in vitro, reaching about 10-times the initial level. The major phospholipid components (PC, disaturated PC, phosphatidylethanolamine, phosphatidylinositol and phosphatidylglycerol) increased in the same proportion as total phospholipids. Sphingomyelin and phosphatidylserine increased in lesser proportion, while lysoPC exhibited little change.

In presence of acarbose, the level achieved for total phospholipids, PC, disaturated PC and phosphatidylethanolamine was about 30% lower than in control medium. For phosphatidylinositol it was 35% lower and for phosphatidylglycerol 47%

TABLE II

CHANGES OCCURRING IN SURFACTANT FRACTION PHOSPHOLIPIDS OF FETAL LUNG EXPLANTS CULTIVATED FOR 48 h ON CONTROL WAYMOUTH MEDIUM OR IN PRESENCE OF 1 mg/ml ACARBOSE

Abbreviations: TPL, total phospholipids; PC, total phosphatidylcholine; DSPC, disaturated phosphatidylcholine; lyso-PC, lysophosphatidylcholine; PG, phosphatidylglycerol; PI, phosphatidylinositol; PE, phosphatidylethanolamine; PS, phosphatidylserine; Sm, sphingomyelin. Mean ± S.E. on ten culture experiments. Unit, nmol P_i per mg tissue.

	Initial (19.5 days)	Control medium	Acarbose
TPL	0.63 ±0.07	6.05±0.44	4.33 ±0.29 [a]
PC	0.35 ±0.04	3.91±0.36	2.76 ±0.23 [b]
DSPC	0.25 ±0.04	2.64±0.34	1.91 ±0.28 [c]
lyso PC	0.020±0.004	0.05±0.01	0.030±0.008
PG	0.010±0.004	0.17±0.03	0.09 ±0.01 [b]
PI	0.020±0.003	0.17±0.03	0.11 ±0.01 [c]
PE	0.05 ±0.01	0.63±0.07	0.42 ±0.02 [a]
PS	0.020±0.005	0.09±0.01	0.080±0.005
Sm	0.030±0.002	0.10±0.02	0.090±0.007

Significant difference between control medium and acarbose for. [a] $P < 0.005$; [b] $P < 0.025$; [c] $P < 0.05$.

lower. The concentrations of sphingomyelin, phosphatidylserine and lyso-PC appeared unaffected by acarbose.

Phospholipid concentration in the residual fraction also increased in cultivated explants, although to a lesser extent than in the surfactant fraction (Table III). Acarbose did not significantly modify changes occurring in the residual fraction total phospholipid content or PC content (Table III). Other specific phospholipids were not determined in the residual fraction.

TABLE III

CHANGES OCCURRING IN RESIDUAL FRACTION PHOSPHOLIPIDS OF FETAL LUNG EXPLANTS CULTIVATED FOR 48 h ON CONTROL WAYMOUTH MEDIUM OR IN PRESENCE OF 1 mg/ml ACARBOSE

Abbreviations as in Table II. Mean ± S.E. on ten culture experiments. Unit = nmol P_i per mg tissue. No difference is significant between control medium and acarbose

	TPL	PC
Initial (19.5 d)	9.5±0.7	4.1±0.6
Final (48 h of culture)		
Control medium	13.2±1.2	5.1±0.5
Acarbose	11.5±1.3	4.9±0.8

Acid α-glucosidase and glycogen phosphorylase activities in explants

Both enzyme activities were determined in explants grown for 48 h either on control medium or in presence of acarbose 1 mg/ml. Acid α-glucosidase activity was reduced by about 90% by acarbose (3.1 ± 0.2 nmol/mg protein per h vs. 29.0 ± 0.7 in control explants, $P < 0.001$). By contrast, no change was detected for phosphorylase activity (23.6 ± 0.7 nmol P_i/mg protein per min versus 23.8 ± 1.2 in control explants).

Acid α-glucosidase activity in different subcellular fractions (Table IV)

Acid α-glucosidase activity was found in all studied subcellular fractions prepared from 21.5-day-old fetal rat lungs. The specific activity of the enzyme was the same in the purified lysosomes and in the surfactant fraction as in the whole

TABLE IV

SPECIFIC ACTIVITY OF ACID α-GLUCOSIDASE AND PERCENTAGE OF TOTAL ACTIVITY RECOVERED IN VARIOUS SUBCELLULAR FRACTIONS PREPARED FROM THE LUNG OF 21.5-DAY-OLD RAT FETUSES

Mean ± S.E. on six individuals. Activity in cell debris and nuclei was subtracted from total activity before calculating the yield in fractions.

	Whole homogenate	Lysosomes	S fraction	Microsomes	Mitochondria
Specific activity (nmol/mg protein per h)	37.3+1.0	35.0+2.2	35.2+1.9	19.0±0.9	12.5±1.4
Percent of activity recovered	100	7.0±0.5	1.5±0.3	6.3±0.3	1.9±0.1

homogenate. It was lower in microsomes and still lower in mitochondria. The highest yield was in lysosomes and microsomes, although total activity was not recovered in subcellular fractions. Surfactant fraction activity accounted for 1.5% of total activity.

Discussion

The results reported here show that acarbose, a pseudosaccharide which was reported to inhibit the lysosomal enzyme acid α-glucosidase [9,29,30], inhibited glycogenolysis in fetal lung organ cultures by 40%. If the inhibition was specific, this means that acid α-glucosidase could account for no less than 40% of glycogen breakdown in the culture conditions which were used. It could even account for more, since the enzyme activity was probably not totally inhibited in fetal lung explants, as indicated by enzyme assays performed at the end of culture period. Indeed, a neutral microsomal α-glucosidase activity also exists in the lung as confirmed by the potent *p*-nitrophenylglucosidase activity evidenced at pH 7.4, but acarbose exerted a weak inhibiting effect on this activity when added to the reaction mixture, as compared to inhibition at pH 4.8. It was therefore probably the acid lysosomal enzyme which was primarily inhibited by acarbose in culture experiments at the concentration used. In addition, previous observations dealing with liver glycogen clearly indicated that acarbose slowed down degradation of glycogen within the lysosomal compartment, whereas mobilization of extra-lysosomal glycogen stores was accelerated [9]. It is remarkable that phosphorylase activity in lung explants was unchanged by acarbose. Phosphorylase, the activity of which was reported to increase in fetal rat lung near term [3,4], and possibly the neutral α-glucosidase would therefore account for the rest of the glycogenolysis. Taken together, these observations argue for the specificity of acarbose effects, and lysosomal α-glucosidase appears to play a major role from a quantitative point of view in lung glycogenolysis during lung maturation.

By the same time, acarbose inhibited the increase in surfactant phospholipids occurring in lung explants. This is consistent with the previously reported [5,6] utilization of glycogen stores as a precursor pool for biosynthesis of phospholipids in developing lung. It seems likely that surfactant phospholipid synthesis was decreased because of decreased availability of substrates resulting from impaired glycogenolysis. Nevertheless, other mechanisms could also be involved. Geddes and Taylor [9] indicated that acarbose somewhat decreased acid phosphatase activity in the liver. Taking into account the importance of protein phosphorylation in cell metabolism, this might influence lung maturational processes. The absence of change in the phosphorylase activity, however, argues against this assumption, since protein phosphatase activities are directly involved in regulatory processes of glycogen metabolism through the phosphorolytic pathway. The absence of significant changes in in vitro biosynthesis of non-surfactant phospholipids also argues against this mechanism and suggests that glycogen utilization mediated by α-glucosidase is specific to surfactant-phospholipid biosynthesis. The much higher rate of surfactant increase in vitro might, however, have apparently increased the inhibitory effect as compared with the residual fraction.

It should be underlined that the glucose in the culture medium, despite its high concentration (5 mg/ml) did not appear to compensate the deficit of glycogenolysis. This may appear surprising, since α-glucosidase releases free glucose, which as that taken up from medium, must first be phosphorylated to be metabolized further. This preferential use of glucose from glycogen had already been evidenced in culture experiments in which glycogenolysis had been prevented by high glucose concentration and insulin in the medium [5]. There is at present no explanation of this phenomenon, but compartmentalization of glucose inside the type II pneumonocyte is possible assuming that glucose issued from glycogen hydrolysis belongs to a pool different from that of glucose from the medium. From a teleological point of view, this could correspond to the necessity of access to a large precursor pool represented by glycogen stores inside the cell at a stage when the developing pneumonocyte is separated from capillary vessels by several layers of mesenchymal cells [31], a situation which could limit the accessibility to circulating substrates. In addition, it has been shown that from the 19th to the 21st day of gestation, i.e., at the stages when surfactant is accumulating, glucose incorporation into DSPC increases at a rate much lower than that of DSPC synthesis measured by choline incorporation in fetal rat lung slices [32]. Furthermore, exogenous glucose appears to be used 3–5-times more as an energy substrate than as a precursor substrate for lipogenesis by fetal rat lung [32]. This argues for a need for other precursor substrates, among which is glycogen.

On the whole, as far as the observations above can be extended to in vivo processes, one can assume that surfactant biosynthesis requires α-glucosidase action for providing precursors. Phosphorylase-mediated and neutral amyloglucosidase-mediated glycogenolysis could also provide precursors, but their alternative function would be to provide energy and reduced coenzymes for lipid biosynthesis through glycolysis [3].

The involvement of α-glucosidase in providing substrates for surfactant biosynthesis and a possible different role of phosphorylase are still suggested by morphological evidence. Lamellar bodies, the intracellular form of surfactant, have been shown to appear in close spatial relationship with glycogen patches in differentiating type II cell [2]. In fetal monkeys, glycogen has even been demonstrated inside lamellar bodies [33]. This is in keeping with the probable lysosomal origin of lamellar bodies and of their precursors, multivesicular bodies [2,15,34], with the presence of α-glucosidase activity in purified lamellar bodies [19,35] and with our finding of α-glucosidase activity in surfactant fraction. Other lysosomal enzyme activities have also been evidenced in lamellar bodies [19,34,35]. Two distinct α-glucosidase activities have been identified in human lung lamellar bodies [35]. It is likely that the activity determined here corresponds to the major specific acid α-glucosidase previously evidenced [35]. Taking into account the facts that the proportion of α-glucosidase activity present in the surfactant fraction is low, and that lamellar bodies do not seem to possess the complete enzyme equipment necessary for phospholipid biosynthesis [36,37], it seems unlikely that a major part of glycogen breakdown and utilization would occur in the lamellar bodies themselves. However, it should be emphasized that the surfactant fraction derives only from type II pneumonocytes, whereas other fractions represent all lung cell types. Considering the cellular heterogeneity of lung and the relatively small number of type II cells, amyloglucosidase activity in surfactant fraction could represent a larger proportion of total activity in type II pneumonocytes. Although total activity in each subcellular fraction was probably not recovered, the highest yield was in purified lysosomes and microsomes. This suggests the probable implication of secondary lysosomes, of endoplasmic reticulum, and possibly of multivesicular bodies in α-glucosidase-mediated glycogenolysis. A compartmentalization of glycogen stores depending on their fate therefore appears likely, which would explain the above presumed existence of different glucose pools.

In conclusion, the present work suggests that lysosomal α-glucosidase plays a major role in lung maturation in exploiting of glycogen stores at a local level specifically for providing precursor substrates for surfactant phospholipid biosynthesis.

Acknowledgments

The authors thank Dr. W. Puls for his generous supply of acarbose. This work was partly supported by an INSERM research grant PRC 135002 'Reproduction et Développement'.

References

1 Buckingham, S., Heinemann, H.O, Sommers, S.O. and McNarry, W.F (1966) Am. J. Pathol. 48, 1027–1041
2 Kikkawa, V, Motoyama, E K. and Gluck, L. (1968) Am J Pathol. 52, 177–192
3 Maniscalco, W.M., Wilson, C.M., Gross, I, Gobran, L, Rooney, S.A. and Warshaw, J.B. (1978) Biochim. Biophys Acta 530, 333–346
4 Bourbon, J. and Jost, A. (1982) Pediatr. Res. 16, 50–56
5 Bourbon, J.R., Rieutort, M., Engle, M.J and Farrell, P.M (1982) Biochim. Biophys. Acta 712, 382–389
6 Farrell, P.M. and Bourbon, J.R. (1986) Biochim. Biophys Acta 878, 159–167
7 Greengard, D., Cayanis, E. and Bodanszky, H (1980) J Devel Physiol. 2, 291–304
8 Lüllmann-Rauch, R. (1981) Virchows Arch. Cell Pathol. 38, 89–100
9 Geddes, R and Taylor, J.A. (1985) Biochem. J. 228, 319–324
10 Funkhouser, J.D and Hugues, E R (1978) Biochim. Biophys. Acta 530, 9–16
11 Gross, I., Walker-Smith, G.J., Maniscalco, W.M, Czajka,

M.R , Wilson, C.M. and Rooney, S A. (1978) J. Appl. Physiol. Respirat Environ. Exercise Physiol. 45, 355–362

12 Longmuir, K.J., Bleasdale, J.E., Quirk, J G and Johnston, J M. (1982) Biochim. Biophys. Acta 712, 356–364

13 Snyder, J.M., Johnston, J.M. and Mendelson, C.R. (1981) Cell Tissue Res. 220, 17–25

14 Frosolono, M.F., Charms, B.L , Pawlowski, R.P and Slivka, S. (1970) J. Lipid Res. 11, 439–457

15 Balis, J.U. and Conen, P E (1964) Lab Invest. 13, 1215–1229

16 Doucet, E., Bourbon, J., Rieutort, M., Marin, L. and Tordet, C. (1986) In Vitro, in the press

17 Sanders, R.L. and Longmore, W J. (1975) Biochemistry 14, 835–840

18 Rieutort, M., Farrell, P.M., Engle, M.J., Pignol, B. and Bourbon, J.R. (1986) Pediatr. Res. 20, 650–654

19 Hook, G.E.R. and Gilmore, L.B (1982) J Biol Chem. 257, 9211–9220

20 Harding, P.G.R., Chan, F., Casola, P.G , Fellows, G.F., Wong, T. and Possmayer, F. (1983) Biochim. Biophys. Acta 750, 373–382

21 Chan, T M. and Exton, J.M (1976) Anal. Biochem 71, 96–105

22 Bligh, E.G. and Dyer, W J. (1959) Can. J. Biochem. Physiol. 37, 911–917

23 Mason, R.J , Nellenbogen, J. and Clements, J.S (1976) J. Lipid Res 17, 281–284

24 Ames, B.N. and Dubin, D.T (1960) J Biol. Chem. 235, 769–775

25 Torres, H.N. and Olavarría, J.M. (1964) J. Biol. Chem 239, 2427–2434

26 Hue, L , Bontemps, F. and Hers, H G. (1975) Biochem J. 152, 105–114

27 Schacterle, G.R. and Pollack, R L. (1973) Anal. Biochem. 51, 654–655

28 Burton, K. (1956) Biochem. J 62, 315–323

29 Schmidt, D D., Frommer, W , Junge, B., Müller, L., Wingender, W., Truscheit, E. and Schäfer, D. (1977) Naturwissenschaften 64, 535–536

30 Puls, W , Keup, U , Krause, H.P., Schmidt, D.D , Thomas, G. and Truscheit, E. (1980) Front Hormone Res. 7, 235–247

31 Marin, L., Dameron, F. and Relier, J P. (1982) Biol. Neonate 41, 172–182

32 Patterson, C.E , Koniki, M.V., Selig, W.M., Owens, C.M and Rhoades, R.A (1986) Exp Lung. Res. 10, 71–86

33 Chi, E Y. (1985) Exp. Lung Res. 8, 275–289

34 Goldfischer, S., Kikkawa, Y. and Hoffman, L. (1968) J. Histochem. Cytochem. 16, 102–109

35 Devries, A.C.J., Schram, A.W., Tager, J.M., Batenburg, J.J. and Van Golde, L M G (1985) Biochim. Biophys. Acta 837, 230–238

36 Rooney, S.A., Page-Roberts, B.A. and Motoyama, E.K (1975) J Lipid Res. 16, 418–425

37 Garcia, A., Sener, S.F. and Mavis, R.D (1976) Lipids 11, 109–112

ANNOUNCEMENT

PREPARATION OF FIGURES

A few guidelines are presented which may be of assistance to authors. Detailed suggestions are to be found in 'Information for Contributors' (Biochim. Biophys. Acta 715 (1982) 1–23, also available as a booklet, free of charge, from the BBA Editorial Secretariat, P.O. Box 1345, 1000 BH Amsterdam, The Netherlands).

□ Note that figures are almost always reduced to fit within the breadth of one column (7.5 cm). You should arrange for letters and symbols to be at least 1.5 mm high *after* reduction.

□ Electron micrographs should always carry a bar denoting unit length, defined in the figure legend. A minimum essential area of the micrograph should be indicated to aid in reproduction.

□ For second and third copies of the article, good copies of the original figures are acceptable, but all photographs (gels, electron micrographs, etc.) should be submitted in triplicate.

□ Use tracing or good quality drawing paper no larger than the paper on which the article is typed. Please do not use heavy card as a mount for photographs. Use black, waterproof ink, or submit sharp, high-contrast, glossy prints. Typewriting and handwriting on figures should be avoided.

□ On graphs, each trace should be defined using a standard symbol selected from the following: ⌖ △ ⦶ ⬔ ◩ ⬕ ◪ ⬠ ⬡ ◧ ° * ◒ ⦵ ☆ ■ ⊠ □ ● ▲ ▼ ▶ ⊞ ⊟ ⊗ ⊙ ○ ◇ △ ▽ ▷ ◁ ⊕ ⊖ ★ ◉ Traces may also be labelled, but any abbreviations should be fully defined in the legend. Please avoid bar diagrams, unless they are true histograms. Tables of numerical values are more informative.

□ Please type the legend(s), using double or triple spacing, on sheets separate from the figures. The actual figure should not bear a title (use A, B, etc. for different panels within a figure). The first sentence of the figure legend should constitute a brief title. Please bear in mind the vertical space occupied by the figure legend, particularly in the case of full-page figures (where 1 cm per 50 words should be allowed). The total typesetting length is 20.5 cm.

INFORMATION FOR CONTRIBUTORS TO BIOCHIMICA ET BIOPHYSICA ACTA

Biochimica et Biophysica Acta publishes papers reporting advances in our knowledge or understanding of any field of biochemistry or biophysics. Descriptions of new methods valuable for biochemists or biophysicists are also acceptable if their application is made obvious or a new principle is introduced. Negative results will be accepted only when they can be considered to advance our knowledge significantly. Papers providing only confirmatory evidence or extending observations firmly established in one species to another will not normally be accepted.

Two types of paper are published, specified as Regular Papers and BBA Reports. As its name implies, a Regular Paper is the usual medium of publication.

BBA Reports will be restricted to papers describing short, complete studies. They should not exceed three printed pages, including figures and tables, and should be written in a continuous style, without subdivision into Introduction, Methods, Results, Discussion and Acknowledgements. They should always begin with a short summary. A BBA Report, although brief, should be a complete and final publication, and figures and tables should not be included in a later paper.

Papers should be written in English (either American or British spelling is permitted, but only one form should be used in the same paper).

Preparation of papers

Authors and their typists should consult a recent issue of the journal in order to make themselves familiar with the conventions and layout of articles, especially title pages and reference lists. In particular, typists should ensure that the beginning of each new paragraph is clearly indicated, preferably by indentation.

Four copies are required of all material submitted (including the submission letter, if it contains information of relevance to the editors). Legible carbon copies or photocopies are adequate for the second and subsequent copies, except for photographs of electrophoretic patterns, electron micrographs, etc., where high-quality prints must be provided in quadruplicate.

The entire text, including figure and table legends and reference list, should be typed with double or triple spacing on pages of uniform size, on one side of the paper, with a 5-cm margin. All pages should be numbered consecutively.

Title

A paper should be headed by a concise, informative title. Authors are reminded that titles are widely used in information-retrieval systems. The title should be followed by the names of the authors (with first or middle names in full) and by the name(s) and address(es) of the laboratory(ies) where the work was carried out. If the work has been done in more than one laboratory, the one in which each author has worked during the study should be indicated.

Summary

A paper should begin with a summary of 100–200 words for a Regular Paper and approx. 50 words for a BBA Report.

Tables

Tables and their legends should be typed with double or triple spacing.

Figures and illustrations

Legends to figures should not be typed or written on the illustrations but should be typewritten, with double or triple spacing, on separate sheets of paper. The legends should consist of a title followed by a brief description of the way the particular experiment was carried out, and any other necessary material describing the symbols or lines on the figure.

Biochimica et Biophysica Acta **Vol. 917, No. 1**
Lipids and Lipid Metabolism L82(1) January 13, 1987

Contents

Biochimica et Biophysica Acta: 40 years on *v*

Regular Papers

Effect of chloroquine on the activity of some lysosomal enzymes involved in ganglioside degradation (BBA 52299)
by P. Fredman, G.W. Klinghardt and L. Svennerholm (Sweden) 1
The uptake of the apoprotein and cholesteryl ester of high-density lipoproteins by the perfused rat liver (BBA 52315)
by C.M. Arbeeny, V.A. Rifici and H.A. Eder (U.S.A.) 9
Purinoceptor agonists stimulate phosphatidylcholine secretion in primary cultures of adult rat type II pneumocytes (BBA 52316)
by A.M. Gilfillan and S.A. Rooney (U.S.A.) 18
Some properties and subcellular distribution of acyl-coenzyme A: retinol acyltransferase activity in rat testes (BBA 52430)
by L.R. Chaudhary and E.C. Nelson (U.S.A.) 24
Metabolism of platelet-activating factor (alkylacetylphosphocholine) by type-II epithelial cells and fibroblasts from rat lungs (BBA 52432)
by R. Kumar, R.J. King, H.M. Martin and D.J. Hanahan (U.S.A.) 33
Metabolic activities in human skin fibroblasts preloaded with labeled G_{M2}-ganglioside (BBA 52434)
by S. Raghavan, T.A. Lyerla, A. Krusell and E.H. Kolodny (U.S.A.) 42
Incorporation of arachidonic acid into 1-acyl-2-lyso-*sn*-glycero-3-phosphocholine of the human neutrophil (BBA 52436)
by F.H. Chilton, J.S. Hadley and R.C. Murphy (U.S.A.) 48
Increased response to peroxisomal proliferators in starved rats (BBA 52322)
by R. Hertz and J. Bar-Tana (Israel) 57
Composition and properties of very low density lipoproteins secreted by the perfused rat liver and subfractionated by affinity chromatography (BBA 52441)
by F. Schroeder, A.B. Kier, D.A. Kinden, H.G. Wilcox and T.P. Mawhinney (U.S.A.) 62
Cell-density-dependent uptake of chylomicron remnants in rat hepatocyte monolayers. Effects of compactin and mevalonic acid (BBA 52300)
by E. Jensen, C.-H. Florén and Å. Nilsson (Sweden) 74
1,25-Dihydroxycholecalciferol stimulates renal phosphate transport by directly altering membrane phosphatidylcholine composition (BBA 52313)
by B.R.C. Kurnik, M. Huskey and K.A. Hruska (U.S.A.) 81
Use of the fluorescence activated cell sorter for studying uptake of fluorescent fatty acids into cultured cells (BBA 52321)
by N. Nahas, E. Fibach, H. Giloh and S. Gatt (Israel) 86
Increase in hepatic low-density lipoprotein receptor activity during pregnancy in Watanabe heritable hyperlipidemic rabbits; an animal model for familial hypercholesterolemia (BBA 52433)
by M. Shiomi, T. Ito and Y. Watanabe (Japan) 92
Partial purification and characterization of 7α-hydroxysteroid dehydrogenase from rat liver microsomes (BBA 52435)
by Y. Amuro, W. Yamade, T. Yamamoto, A. Maebo, T. Hada and K. Higashino (Japan) 101
Covalently bound ω-hydroxyacylsphingosine in the stratum corneum (BBA 52318)
by P.W. Wertz and D.T. Downing (U.S.A.) 108

continued

Age-dependent changes in the distribution and concentration of human lens cholesterol and phospholipids (BBA 52437)
by L.-K. Li, L. So and A. Spector (U.S.A.) 112

Glucocorticoid-induced elevation of serum high-density lipoprotein-cholesterol and its reversal by adrenocorticotropin in the rat (BBA 52438)
by T. Mitamura (Japan) 121

Isolation of protein components from rat lung lamellar bodies (BBA 52439)
by J.G. Nijssen, D. Hardeman, H.N.M.L. Luyckx, L.W. Promes, J.A. Post and H. Van den Bosch (The Netherlands) 131

Phospholipid-protein interactions in rat lung lamellar bodies (BBA 52440)
by J.G. Nijssen, L.W. Promes, D. Hardeman and H. Van den Bosch (The Netherlands) 140

Astrocytes synthesize apolipoprotein E and metabolize apolipoprotein E-containing lipoproteins (BBA 52317)
by R.E. Pitas, J.K. Boyles, S.H. Lee, D. Foss and R.W. Mahley (U.S.A.) 148

Enzyme immunoassay of a plant phospholipid transfer protein (BBA 52323)
by M. Grosbois, F. Guerbette, D. Douady and J.-C. Kader (France) 162

Hydrolysis of membrane-associated phosphoglycerides by mitochondrial phospholipase A_2 (BBA 52325)
by J.M. De Winter, H.B.M. Lenting, F.W. Neys and H. Van den Bosch (The Netherlands) 169

Hydrolysis of exogenous substrates by mitochondrial phospholipase A_2 (BBA 52326)
by H.B.M. Lenting, F.W. Neys and H. Van den Bosch (The Netherlands) 178

Structural modulation of salt-resistant rat-liver lipase alters the relative phospholipase and triacylglycerol hydrolase activities (BBA 52442)
by N.L.M. Persoon, W.C. Hülsmann and H. Jansen (The Netherlands) 186

Structure determination of the polymorphism of acylgalactosylceramide in rat brain by gas chromatography/mass spectrometry and proton magnetic resonance (BBA 52327)
by N. Theret, P. Boulenguer, J.-M. Wieruszeski, B. Fournet, J.-C. Fruchart, J.-M. Bourre and C. Delbart (France) 194

Role of α-glucosidase in fetal lung maturation (BBA 52324)
by J.R. Bourbon, E. Doucet and M. Rieutort (France) 203

Cited in: Current Contents Life Sciences - Biological Abstracts - Chemical Abstracts - Index Chemicus - Index Medicus - Excerpta Medica (EMBASE)

INFORMATION FOR CONTRIBUTORS TO BIOCHIMICA ET BIOPHYSICA ACTA

The 1982 edition of this booklet, offering detailed guidance to authors, is available free of charge from the BBA Editorial Secretariat, P.O. Box 1345, 1000 BH Amsterdam, The Netherlands. It is also published as Biochim. Biophys. Acta 715 (1982) 1–23.

BIOCHIMICA ET BIOPHYSICA ACTA
International Journal of Biochemistry and Biophysics
Founded in 1947 by H.G.K Westenbrink, Managing Editor 1947–1964

© 1987, Elsevier Science Publishers B.V (Biomedical Division)
Printed in The Netherlands

All rights reserved. No part of this publication may be reproduced, stored in a retrieval system, or transmitted, in any form or by any means, electronic, mechanical, photocopying, recording or otherwise, without the prior written permission of the publisher, Elsevier Science Publishers B V. (Biomedical Division), P O. Box 1527, 1000 BM Amsterdam, The Netherlands. Submission of a paper to this journal entails the author's irrevocable and exclusive authorization of the publisher to collect any sums or considerations for copying or reproduction payable by third parties (as mentioned in article 17 paragraph 2 of the Dutch Copyright Act of 1912 and in the Royal Decree of June 20, 1974 (S. 351) pursuant to article 16b of the Dutch Copyright Act of 1912) and/or to act in or out of Court in connection therewith.

Special regulations for readers in the U.S.A. This journal has been registered with the Copyright Clearance Center, Inc. Consent is given for copying of articles for personal or internal use, or for the personal use of specific clients. This consent is given on the condition that the copier pays through the Center the per-copy fee stated in the code on the first page of each article for copying beyond that permitted by Sections 107 or 108 of the U S Copyright Law The appropriate fee should be forwarded with a copy of the first page of the article to the Copyright Clearance Center, Inc., 27 Congress Street, Salem, MA 01970, U.S A. If no code appears in an article, the author has not given broad consent to copy and permission to copy must be obtained directly from the author. All articles published prior to 1980 may be copied for a per-copy fee of US$ 2.25, also payable through the Center. This consent does not extend to other kinds of copying, such as for general distribution, resale, advertising and promotion purposes, or for creating new collective works Special written permission must be obtained from the publisher for such copying.

Special regulations for authors Upon acceptance of an article by the journal, the author(s) will be asked to transfer copyright of the article to the publisher. This transfer will ensure the widest possible dissemination of information.

bioenergetics

SAMPLE COPY

for additional information contact:

ALLIED/ELSEVIER JOURNALS
MARKETING GROUP
30, WEST COTT ROAD, Ph: 82468
MADRAS - 600 014./
750, MOUNT ROAD,
MADRAS - 600 002.

BBA

Biochimica et Biophysica Acta (B)

Managing Editors: P Borst, P. Cohen,
K van Dam, L.L.M. van Deenen (Chairman),
E.P. Kennedy and G K. Radda

Honorary Managing Editor. E.C. Slater

Vol. 890, No. 1, pp. 1–116
January 16, 1987
Elsevier

ISSN 0006-3002
0005[illegible]728
BBACAQ 890 (1) 1–116 (1987)
BBBEB4 890 (1) 1–116 (1987)

40 YEARS OF BBA !

PUBLICATION SCHEDULE FOR 1987

BBA is published according to a volume-numbering scheme that embraces all sections of the journal In addition, each regular section has its own sequential volume-numbering system, running parallel to the overall BBA scheme, as set out below
Full subscription: 42 volumes plus Cumulative Index 1986

	BIO-ENERGETICS 6 volumes [a]	BIO-MEMBRANES 11 volumes [b]	GENE STRUCTURE AND EXPRESSION 3 volumes	PROTEIN STRUCTURE AND MOLECULAR ENZYMOLOGY 6 volumes	LIPIDS AND LIPID METABOLISM 6 volumes	GENERAL SUBJECTS 4 volumes	MOLECULAR CELL RESEARCH 5 volumes	BBA REVIEW SECTIONS 3 volumes
Jan	890-1 = B80-1	896-1 = M145-1 896-2 = M145-2		911-1 = P39-1 911-2 = P39-2	917-1 = L82-1 917-2 = L82-2	923-1 = G126-1	927-1 = C17-1	BBA REVIEWS ON BIOENERGETICS
Feb	890-2 = B80-2 890-3 = B80-3	897-1 = M146-1 897-2 = M146-2	908-1 = N17-1	911-3 = P39-3	917-3 = L82-3	923-2 = G126-2	927-2 = C17-2 927-3 = C17-3	895-1 = BR15-1
March	891-1 = B81-1	897-3 = M146-3 898-1 = M147-1	908-2 = N17-2	912-1 = P40-1 912-2 = P40-2	918-1 = L83-1 918-2 = L83-2	923-3 = G126-3	928-1 = C18-1	895-2 = BR15-2 895-3 = BR15-3
April	891-2 = B81-2	898-2 = M147-2 898-3 = M147-3	908-3 = N17-3	912-3 = P40-3	918-3 = L83-3	924-1 = G127-1	928-2 = C18-2	
May	891-3 = B81-3	899-1 = M148-1 899-2 = M148-2		913-1 = P41-1 913-2 = P41-2	919-1 = L84-1 919-2 = L84-2	924-2 = G127-2	928-3 = C18-3	BBA REVIEWS ON BIOMEMBRANES
June	892-1 = B82-1 892-2 = B82-2	900-1 = M149-1 900-2 = M149-2	909-1 = N18-1	913-3 = P41-3	919-3 = L84-3	924-3 = G127-3	929-1 = C19-1 929-2 = C19-2	906-1 = MR16-1 906-2 = MR16-2
July	892-3 = B82-3	901-1 = M150-1 901-2 = M150-2	909-2 = N18-2	914-1 = P42-1 914-2 = P42-2	920-1 = L85-1 920-2 = L85-2	925-1 = G128-1	929-3 = C19-3	906-3 = MR16-3
Aug	893-1 = B83-1	902-1 = M151-1 902-2 = M151-2	909-3 = N18-3	914-3 = P42-3	920-3 = L85-3	925-2 = G128-2	930-1 = C20-1	BBA REVIEWS ON CANCER
Sept	893-2 = B83-2	902-3 = M151-3 903-1 = M152-1	910-1 = N19-1	915-1 = P43-1 915-2 = P43-2	921-1 = L86-1 921-2 = L86-2	925-3 = G128-3	930-2 = C20-2	907-1 = CR14-1 907-2 = CR14-2
Oct	893-3 = B83-3	903-2 = M152-2 903-3 = M152-3	910-2 = N19-2	915-3 = P43-3	921-3 = L86-3	926-1 = G129-1	930-3 = C20-3	907-3 = CR14-3
Nov	894-1 = B84-1 894-2 = B84-2	904-1 = M153-1 904-2 = M153-2		916-1 = P44-1 916-2 = P44-2	922-1 = L87-1 922-2 = L87-2	926-2 = G129-2	931-1 = C21-1 931-2 = C21-2	
Dec	894-3 = B84-3	905-1 = M154-1 905-2 = M154-2	910-3 = N19-3	916-3 = P44-3	922-3 = L87-3	926-3 = G129-3	931-3 = C21-3	

[a] This includes BBA Reviews on Bioenergetics, Vol 895 [b] This includes BBA Reviews on Biomembranes, Vol 906

Authors should submit their manuscripts (four copies) for publication in BIOCHIMICA ET BIOPHYSICA ACTA by sending them to one of the Managing Editors

Dr P Borst, c/o BBA Editorial Secretariat, P O. Box 1345, 1000 BH Amsterdam, The Netherlands
Dr P Cohen, Department of Biochemistry, Medical Sciences Institute, University of Dundee, Dundee, DD1 4HN, U K
Dr. K van Dam, c/o BBA Editorial Secretariat, P.O Box 1345, 1000 BH Amsterdam, The Netherlands
Dr. L.L M. van Deenen, c/o BBA Editorial Secretariat, P.O Box 1345, 1000 BH Amsterdam, The Netherlands
Dr E P Kennedy, c/o BBA Editorial Secretariat (Boston), Box C 9123, Brookline, MA 02146, U S A
Dr. G K Radda, Department of Biochemistry, University of Oxford, South Parks Road, Oxford, OX1 3QU, U.K

Detailed information for contributors may be found in Biochim. Biophys. Acta 715 (1982) 1–23, also published as the 1982 edition of the booklet
INFORMATION FOR CONTRIBUTORS TO BIOCHIMICA ET BIOPHYSICA ACTA
which is available free of charge from the BBA Editorial Secretariat

---

Subscription information

1987 BBA Bioenergetics, Volumes 890–895 (including Reviews) (6 volumes in 18 issues), Dfl 1470 (US$ 653.25) + Dfl. 150 (US$ 66.75) postage, packaging and handling .Total price: Dfl 1620 (US$ 720 00)
1987 BBA full subscription, Volumes 890–931 (42 volumes in 120 issues), Dfl 7812 (US$ 3472.00) + Dfl. 1050 (US$ 467 00) postage, packaging and handling. Total price· Dfl 8862 (US$ 3939 00)
The Dutch guilder price is definitive The U S. dollar price is subject to exchange-rate fluctuations and is given only as a guide
Journals are sent by surface delivery to all countries, except the following countries where SAL air delivery (Surface Airlifted Mail) is ensured· U S A., Canada, Japan, Australia, New Zealand, P R.China, India, Israel, South Africa, Malaysia, Singapore, South Korea, Taiwan, Pakistan, Hong Kong, Brazil, Argentina, Mexico and Thailand Airmail rates for other countries are available on request
Subscription orders can be entered only by calendar year (Jan -Dec.) and should be sent to Elsevier Science Publishers, Journals Department, P.O. Box 211, 1000 AE Amsterdam, The Netherlands, Tel (020) 5803 642, Telex 18582 ESPA NL, or to your usual subscription agent Claims for missing issues should be made within 3 months of publication, otherwise they cannot be honoured free of charge
The Publisher reserves the right to issue additional volumes during the course of the year Such volumes will be invoiced before publication and delivered after receipt of payment
In the U S A. and Canada for further information contact Elsevier Science Publishers, Journal Information Center, 52 Vanderbilt Avenue, New York, NY 10017, U S.A., Tel (212) 370-5520

Biochimica et Biophysica Acta

BIOCHIMICA ET BIOPHYSICA ACTA

MANAGING EDITORS

L L M van Deenen (Utrecht)
(Chairman)
P Borst (Amsterdam)
P Cohen (Dundee)
E.P. Kennedy (Boston, MA)
G.K. Radda (Oxford)
K van Dam (Amsterdam)

HONORARY MANAGING EDITOR

E C. Slater (Southampton)

EDITORS

H.R V. Arnstein (London)
J Barber (London)
I Björkhem (Huddinge)
B. Borgström (Lund)
J. Brachet (Brussels)
J. Bremer (Oslo)
R Burgess (Madison, WI)
E Carafoli (Zürich)
J E Cleaver (San Francisco, CA)
C. Crane-Robinson (Portsmouth)
J.W. Daly (Bethesda, MD)
E A Dawidowicz (Boston, MA)
B de Kruijff (Utrecht)
J G Demaille (Montpellier)
J.J.H H.M. de Pont (Nijmegen)
B Deuticke (Aachen)
K.T Douglas (Colchester)
S Ebashi (Tokyo)
L. Ernster (Stockholm)
S. Ferguson (Birmingham)
I Fridovich (Durham)
F. Gibson (Canberra)
W B Gratzer (London)
M. Hamberg (Stockholm)
T.E Hardingham (London)
J.L. Harwood (Cardiff)
E Heinz (Dortmund)
E J.M. Helmreich (Würzburg)
F. Hofmann (Homburg)
M.D. Houslay (Glasgow)
R.C Hughes (London)
J B. Jackson (Birmingham)
P. Jollès (Paris)
P.L Jørgensen (Århus)
Y. Kagawa (Tochigi)
K.-A Karlsson (Gothenburg)
M. Kates (Ottawa)
J Kay (Cardiff)
Y. Kaziro (Tokyo)
R. Kinne (Dortmund)
C. Klee (Bethesda, MD)
A. Kleinzeller (Philadelphia, PA)
P. Läuger (Constance)
A.G Lee (Southampton)
D.M. Lee (Oklahoma City, OK)
F Maley (Albany, NY)
D. Marsh (Göttingen)
V Massey (Ann Arbor, MI)
D.J. Morré (West Lafayette, IN)
J F Morrison (Canberra)
L E Mortenson (Athens, GA)
G Nelsestuen (St Paul, MN)
D.G. Nicholls (Dundee)
Y. Nishizuka (Kobe)
R.C. Nordlie (Grand Forks, ND)
S Numa (Kyoto)
C. Pace-Asciak (Toronto)
P.G W Plagemann (Minneapolis, MN)
I Ragan (Harlow)
P Randle (Oxford)
A Razin (Jerusalem)
A.M Scanu (Chicago, IL)
H J Schatzmann (Bern)
G.L. Scherphof (Groningen)
J Seelig (Basel)
N Sharon (Rehovot)
G G Shipley (Boston, MA)
D. Shugar (Warsaw)
W.D Stein (Jerusalem)
J.M. Tager (Amsterdam)
T. Taniguchi (Tokyo)
J P Thornber (Los Angeles, CA)
I Tinoco (Berkeley, CA)
K.F Tipton (Dublin)
I.P. Trayer (Birmingham)
I. Trowbridge (San Diego, CA)
C.L Tsou (Beijing)
D.E. Vance (Edmonton)
H.J van Gorkom (Leiden)
B R. Velthuys (Gif-sur-Yvette)
T. Vänngård (Gothenburg)
A Watts (Oxford)
C. Weissmann (Zürich)
R.J.P Williams (Oxford)
R G Williamson (London)
C Wraight (Urbana, IL)
K Wüthrich (Zürich)
R.F.A Zwaal (Maastricht)

ELSEVIER SCIENCE PUBLISHERS B.V.
AMSTERDAM

BIOCHIMICA
ET BIOPHYSICA ACTA

INTERNATIONAL JOURNAL OF BIOCHEMISTRY AND BIOPHYSICS

bioenergetics

890 (1987)
(B80)

ELSEVIER SCIENCE PUBLISHERS B.V.
AMSTERDAM

PUBLICATION SCHEDULE FOR 1987

BBA is published according to a volume-numbering scheme that embraces all sections of the journal In addition, each regular section has its own sequential volume-numbering system, running parallel to the overall BBA scheme, as set out below

Full subscription 42 volumes plus Cumulative Index 1986

	BIO-ENERGETICS 6 volumes [a]	BIO-MEMBRANES 11 volumes [b]	GENE STRUCTURE AND EXPRESSION 3 volumes	PROTEIN STRUCTURE AND MOLECULAR ENZYMOLOGY 6 volumes	LIPIDS AND LIPID METABOLISM 6 volumes	GENERAL SUBJECTS 4 volumes	MOLECULAR CELL RESEARCH 5 volumes	BBA REVIEW SECTIONS 3 volumes
Jan	890-1 = B80-1	896-1 = M145-1 896-2 = M145-2		911-1 = P39-1 911-2 = P39-2	917-1 = L82-1 917-2 = L82-2	923-1 = G126-1	927-1 = C17-1	BBA REVIEWS ON BIOENERGETICS
Feb	890-2 = B80-2 890-3 = B80-3	897-1 = M146-1 897-2 = M146-2	908-1 = N17-1	911-3 = P39-3	917-3 = L82-3	923-2 = G126-2	927-2 = C17-2	895-1 = BR15-1
March	891-1 = B81-1	897-3 = M146-3 898-1 = M147-1	908-2 = N17-2	912-1 = P40-1 912-2 = P40-2	918-1 = L83-1 918-2 = L83-2	923-3 = G126-3	927-3 = C17-3 928-1 = C18-1	895-2 = BR15-2 895-3 = BR15-3
April	891-2 = B81-2	898-2 = M147-2 898-3 = M147-3	908-3 = N17-3	912-3 = P40-3	918-3 = L83-3	924-1 = G127-1	928-2 = C18-2	
May	891-3 = B81-3	899-1 = M148-1 899-2 = M148-2		913-1 = P41-1 913-2 = P41-2	919-1 = L84-1 919-2 = L84-2	924-2 = G127-2	928-3 = C18-3	BBA REVIEWS ON BIOMEMBRANES
June	892-1 = B82-1 892-2 = B82-2	900-1 = M149-1 900-2 = M149-2	909-1 = N18-1	913-3 = P41-3	919-3 = L84-3	924-3 = G127-3	929-1 = C19-1	906-1 = MR16-1 906-2 = MR16-2
July	892-3 = B82-3	901-1 = M150-1 901-2 = M150-2	909-2 = N18-2	914-1 = P42-1 914-2 = P42-2	920-1 = L85-1 920-2 = L85-2	925-1 = G128-1	929-2 = C19-2 929-3 = C19-3	906-3 = MR16-3
Aug	893-1 = B83-1	902-1 = M151-1 902-2 = M151-2	909-3 = N18-3	914-3 = P42-3	920-3 = L85-3	925-2 = G128-2	930-1 = C20-1	BBA REVIEWS ON CANCER
Sept	893-2 = B83-2	902-3 = M151-3 903-1 = M152-1	910-1 = N19-1	915-1 = P43-1 915-2 = P43-2	921-1 = L86-1 921-2 = L86-2	925-3 = G128-3	930-2 = C20-2	907-1 = CR14-1 907-2 = CR14-2
Oct	893-3 = B83-3 894-1 = B84-1	903-2 = M152-2 903-3 = M152-3	910-2 = N19-2	915-3 = P43-3	921-3 = L86-3	926-1 = G129-1	930-3 = C20-3 931-1 = C21-1	907-3 = CR14-3
Nov	894-2 = B84-2	904-1 = M153-1 904-2 = M153-2		916-1 = P44-1 916-2 = P44-2	922-1 = L87-1 922-2 = L87-2	926-2 = G129-2	931-2 = C21-2	
Dec	894-3 = B84-3	905-1 = M154-1 905-2 = M154-2	910-3 = N19-3	916-3 = P44-3	922-3 = L87-3	926-3 = G129-3	931-3 = C21-3	

[a] This includes BBA Reviews on Bioenergetics, Vol 895 [b] This includes BBA Reviews on Biomembranes, Vol 906

© 1987, Elsevier Science Publishers B V (Biomedical Division)

All rights reserved. No part of this publication may be reproduced, stored in a retrieval system, or transmitted, in any form or by any means, electronic, mechanical, photocopying, recording or otherwise without the prior written permission of the publisher, Elsevier Science Publishers B.V. (Biomedical Division), P O Box 1527, 1000 BM Amsterdam, The Netherlands. Submission of a paper to this journal entails the author's irrevocable and exclusive authorization of the publisher to collect any sums or considerations for copying or reproduction payable by third parties (as mentioned in article 17 paragraph 2 of the Dutch Copyright Act of 1912 and in the Royal Decree of June 20, 1974 (S. 351) pursuant to article 16b of the Dutch Copyright Act of 1912) and/or to act in or out of Court in connection therewith.

Special regulations for readers in the U S A. This journal has been registered with the Copyright Clearance Center, Inc Consent is given for copying of articles for personal or internal use, or for the personal use of specific clients This consent is given on the condition that the copier pays through the Center the per-copy fee stated in the code on the first page of each article for copying beyond that permitted by Sections 107 or 108 of the U S Copyright Law. The appropriate fee should be forwarded with a copy of the first page of the article to the Copyright Clearance Center, Inc , 27 Congress Street, Salem, MA 01970, U.S A. If no code appears in an article, the author has not given broad consent to copy and permission to copy must be obtained directly from the author. All articles published prior to 1980 may be copied for a per-copy fee of US$ 2.25, also payable through the Center. This consent does not extend to other kinds of copying, such as for general distribution, resale, advertising and promotion purposes, or for creating new collective works Special written permission must be obtained from the publisher for such copying.

Special regulations for authors. Upon acceptance of an article by the journal, the author(s) will be asked to transfer copyright of the article to the publisher. This transfer will ensure the widest possible dissemination of information

Printed in The Netherlands

Biochimica et Biophysica Acta: 40 years on

Professor H.G.K. Westenbrink

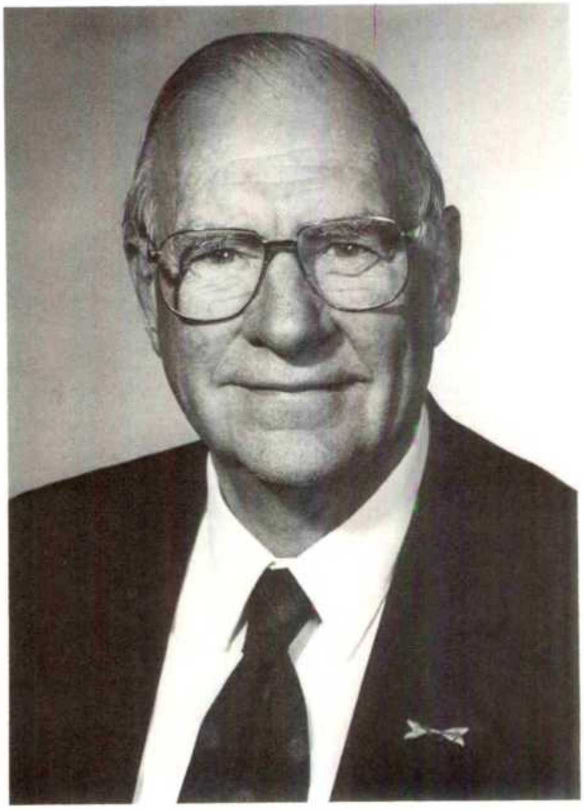

Professor E.C. Slater

Biochimica et Biophysica Acta, the first truly international journal in the field of biochemistry and biophysics, and now undoubtedly one of the largest, is celebrating its 40th anniversary with this issue.

The journal was founded in 1947 by Professor H.G.K. Westenbrink, who remained Managing Editor of the journal until 1964. He was succeeded by Professor E.C. Slater, who was able to fulfil this function until his recent retirement as Chairman of the Board of Managing Editors. Professor Slater was encouraged to write a history of BBA, recalling its remarkably rapid growth and some of the intricacies involved in the journal's birth and early development [1].

On the auspicious occasion of the journal's 40th birthday, the Publisher would like to take the opportunity of thanking all those who have played an active role in the journal's development, and looks forward to further stimulating developments over subsequent decades.

The photograph of E.C. Slater is reproduced by permission of Godfrey Argent, U.K., photographers.

[1] *Biochimica et Biophysica Acta: The Story of a Biochemical Journal* by E.C. Slater (1986) Elsevier Science Publishers, ISBN 0-444-80769-1; Price Dfl.75.00.

Biochimica et Biophysica Acta 890 (1987) 1–5
Elsevier

BBA 42067

The role of fixed and mobile buffers in the kinetics of proton movement

Wolfgang Junge and Stuart McLaughlin

Abteilung Biophysik, Fachbereich Biologie/Chemie, Universität Osnabrück, Postfach 4469, D-4500 Osnabrück (F.R.G.) and Department of Physiology and Biophysics, Health Sciences Center, State University of New York at Stony Brook, Stony Brook, NY 11794 (U.S.A.)

(Received 14 August 1986)

Key words. Proton diffusion, Mobile buffer

We derive a simple expression for the effective diffusion coefficient of protons in Fick's second law, D^{eff}, when both spatially fixed, HF, and mobile, HM, buffers are present. These buffers are present at moderately high concentrations ($[\text{F}^{\text{tot}}]$, $[\text{M}^{\text{tot}}] > 1$ mM) in most biological systems. We consider only the case where the protonation reactions remain at equilibrium during the diffusion process. When the pH is to the alkaline side of the pK values of the fixed and mobile buffers ($[\text{H}^+] < K_{\text{F}}, K_{\text{M}}$), the effective diffusion coefficient of protons in Ficks second law is:

$$D^{\text{eff}} = \frac{D_{\text{H}} + \dfrac{D_{\text{HM}}[\text{M}^{\text{tot}}]}{K_{\text{M}}}}{1 + \dfrac{[\text{M}^{\text{tot}}]}{K_{\text{M}}} + \dfrac{[\text{F}^{\text{tot}}]}{K_{\text{F}}}}$$

where D_{H} is the diffusion coefficient of the protons free in the aqueous phase and D_{HM} is the diffusion coefficient of the mobile buffer. The equation illustrates three features of diffusion in a buffered system. Firstly, the effective diffusion coefficient of protons is always lower than the diffusion coefficient of free protons. Secondly, increasing the concentration of fixed buffers always decreases D^{eff}. Thirdly, increasing the concentration of mobile buffer can increase D^{eff} when fixed buffers are present.

Introduction

Spatially fixed buffers decrease the effective diffusion coefficient of buffered ions: the effective diffusion coefficient in Fick's second law is $D^{\text{eff}} = D/(1+R)$, where D is the diffusion coefficient of the free ions in the aqueous phase and R is the ratio of bound-to-free ions (e.g., see page 327 of Ref. 1). The high concentration of fixed buffers for H^+ and OH^- in biological cells and organelles implies that R is large and that buffers should affect the kinetics of these ions' movement. For example, Polle and Junge [2] observed very slow relaxation of an alkalinization pulse in the narrow domain (width, 5 nm) between stacked thylakoid membranes; they [3] argued that fixed buffers in this narrow domain reduce the diffusion coefficient of OH^- by a factor of 10^4–10^5.

Mobile buffers, however, can counteract the effect of fixed buffers and enhance the effective diffusion coefficients of OH^- and H^+ when both types of buffer are present. Biological systems usually contain both fixed and mobile buffers. For example, the cytoplasm contains mobile buffers

---

Correspondence. Dr S. McLaughlin, Department of Physiology and Biophysics, Health Sciences Center, State University of New York at Stony Brook, Stony Brook, NY 11794, U S A

0005-2728/87/$03 50 © 1987 Elsevier Science Publishers B.V. (Biomedical Division)

such as phosphate ($D \approx 10^{-9}$ m^2/s), the plasma and intracellular membranes contain mobile buffers such as phosphatidic acid ($D \approx 10^{-11}$ m^2/s), and both the aqueous and membrane phases contain fixed buffers such as proteins. We derive here a simple expression for the effective diffusion coefficient in Fick's second law when both fixed and mobile buffers are present.

We discuss here only the effect of buffers on the kinetics of proton movement. Other investigators have clearly discussed how mobile buffers enhance the steady-state flux of protons through an aqueous unstirred layer adjacent to a membrane [4] and from a source to a sink in a system of enzymes [5].

Analysis

We consider the kinetics of the proton movement described by Fick's second law. To simplify our analysis we assume the system is homogeneous *, diffusion coefficients are independent of position, diffusion occurs in one dimension **, activity coefficients are unity, the diffusion of H^+ is electroneutral because there is a high concentration of indifferent electrolyte, and the diffusion of OH^- may be ignored *** with respect to H^+. In the absence of buffers, Fick's second law is:

$$\frac{\partial[H^+]}{\partial t} = \frac{D_H \partial^2 [H^+]}{\partial x^2} \tag{1}$$

where D_H is the diffusion coefficient of protons in water ($D_H \approx 10^{-8}$ m^2/s). In the presence of buffers, HB_i (where B_i can be either a fixed, F_i, or mobile, M_i, buffer), we express Fick's second law as

$$\frac{\partial([H^+] + \Sigma_i [HB_i])}{\partial t} = \frac{D_H \partial^2 [H^+]}{\partial x^2} + \frac{\Sigma_i D_i \partial^2 [HB_i]}{\partial x^2} \tag{2}$$

This equation follows from the conservation of mass and Fick's first law, which states that the flux of a solute is proportional to the gradient of its concentration. Eqn. 2 states that the rate of change in the concentration of free and bound protons in an infinitesimal volume is equal to the divergence of the flux of these molecules into the volume. Note that the time derivative on the left-hand side of the equation includes both fixed and mobile buffers, but the second-order spatial derivative ** on the right hand side includes only the mobile buffers, for which $D_i > 0$.

Fixed buffers

Single pK

We first consider the case of one species of fixed buffer with a single dissociable group:

$$H^+ + F^- \rightleftarrows HF$$

We assume this protonation reaction is rapid compared to diffusion and may be considered at equilibrium †:

$$[H^+][F^-] = K_F[HF] \tag{3}$$

where K_F is the equilibrium dissociation constant. If we define

$$[F^{tot}] = [F^-] + [HF] \tag{4}$$

---

* Our analysis may be extended simply to some inhomogeneous biological systems. For example, McLaughlin and Brown [11] considered the diffusion of an ion in an aqueous space between two membranes when the fixed buffer groups are bound to the membranes, and the membranes have a net negative charge. The surface concentration of a fixed buffer is divided by the width of the aqueous space to convert it into an effective three-dimensional buffer concentration and the value of the dissociation constant is divided by the Boltzmann term, $\exp(-zF\varphi(0)/RT)$, where z is the valence of the buffered ion and $\varphi(0)$ is the surface potential, to convert it from an intrinsic to an apparent dissociation constant The width of the aqueous space must be significantly smaller than the diffusion length for this treatment to be valid.

** When diffusion occurs in more than one dimension, the second-order spatial derivatives on the right-hand side of Eqns. 1, 2, 7, 10, 14 and 17 are replaced by the Laplacian, $\nabla^2 \equiv \nabla \cdot \nabla$.

*** We consider below an approximate expression that includes the effect of OH^- diffusion (Eqn. 19).

† The thickness of the 'reaction layer', the distance over which the equilibrium described by Eqn. 3 cannot be maintained, is about 1 nm when the buffer concentration is 0.1 M and about 10 nm when the buffer concentration is 0 001 M (e.g., Delahay [12], see pp. 87–95) Westerhof and Chen [13] have considered the diffusion of protons between a source and a sink separated by a distance less than the reaction layer.

then

$$[\mathrm{HF}] = \frac{[\mathrm{F}^{\mathrm{tot}}][\mathrm{H}^+]}{[\mathrm{H}^+] + \mathrm{K}_\mathrm{F}} \tag{5}$$

To simplify the algebra, we assume $[\mathrm{H}^+] \ll K_\mathrm{F}$. In other words, we assume the pH is to the alkaline side of the pK. Eqn. 5 reduces now to

$$[\mathrm{HF}] = \frac{[\mathrm{F}^{\mathrm{tot}}][\mathrm{H}^+]}{K_\mathrm{F}} \tag{6}$$

We insert Eqn. 6 into Eqn. 2 to obtain

$$\frac{\partial^2[\mathrm{H}^+]}{\partial t^2} = \frac{D_{1\mathrm{a}}\partial^2[\mathrm{H}^+]}{\partial x^2} \tag{7}$$

where $D_{1\mathrm{a}}$ is the effective diffusion coefficient of the protons:

$$D_{1\mathrm{a}} = \frac{\mathrm{D_H}}{1 + \dfrac{[\mathrm{F}^{\mathrm{tot}}]}{K_\mathrm{F}}} \tag{8}$$

This is the case considered by Crank [1], because $[\mathrm{F}^{\mathrm{tot}}]/K_\mathrm{F}$ is the ratio of bound-to-free protons, $[\mathrm{HF}]/[\mathrm{H}^+]$, as illustrated by Eqn. 6. For example, if we assume that groups with a pK of 6 ($K_\mathrm{F} = 10^{-6}$ M) are present at a concentration of $[\mathrm{F}^{\mathrm{tot}}] = 10^{-2}$ M on spatially fixed proteins, the effective diffusion coefficient is 10^4-fold lower than the diffusion coefficient of the free protons. According to the Einstein [6] relation, $x^2 = 2Dt$, it will take a proton $t = 100$ s rather than 10 ms to diffuse a distance $x = 10$ μm when the buffer is present.

Multiple pK values

Consider a more biologically relevant system in which the buffers are fixed proteins whose side chains have a broad spectrum of pK values. The slope of the titration curve, the buffer capacity β, is

$$\beta \equiv -\frac{\mathrm{d}([\mathrm{H}^+] + \Sigma_i[\mathrm{HF}_i])}{\mathrm{d(pH)}} \tag{9}$$

Inserting Eqn. 9 into Eqn. 2 we obtain

$$\frac{\partial[\mathrm{H}^+]}{\partial t} = D_{1\mathrm{b}}\frac{\partial^2[\mathrm{H}^+]}{\partial x^2} \tag{10}$$

where

$$D_{1\mathrm{b}} = D_\mathrm{H}\,\frac{2.3[\mathrm{H}^+]}{\beta} \tag{11}$$

Eqn. 11 is more general than Eqn. 8. The relationship between these two equations is illustrated by considering the limiting case where the buffers have only one dissociable group. The combination of Eqns. 5 and 9 yields

$$\beta = 2.3[\mathrm{H}^+]\left(1 + \frac{[\mathrm{F}^{\mathrm{tot}}]K_\mathrm{F}}{([\mathrm{H}^+] + K_\mathrm{F})^2}\right) \tag{12}$$

If we assume, as before, that $[\mathrm{H}^+] \ll K_\mathrm{F}$, then combining Eqns. 11 and 12 yields Eqn. 8.

Fixed and mobile buffers

Single pK

We first consider the case where fixed and mobile buffers are present and each buffer has a single dissociable group. Eqn. 5 characterizes the fixed buffer and Eqn. 13 describes the mobile buffer if, as before, we assume that the reactions are essentially at equilibrium:

$$\mathrm{H}^+ + \mathrm{M}^- \rightleftarrows \mathrm{HM}$$

$$[\mathrm{HM}] = \frac{[\mathrm{M}^{\mathrm{tot}}][\mathrm{H}^+]}{[\mathrm{H}^+] + \mathrm{K_M}} \tag{13}$$

where $[\mathrm{M}^{\mathrm{tot}}] = [\mathrm{M}^-] + [\mathrm{HM}]$. We assume that the pH is to the alkaline side of the pK values of both the mobile and fixed buffers, $[\mathrm{H}^+] \ll \mathrm{K_M}$, K_F, and insert Eqns. 5 and 13 into Eqn. 2 to obtain

$$\frac{\partial[\mathrm{H}^+]}{\partial t} = D_{2\mathrm{a}}\frac{\partial^2[\mathrm{H}^+]}{\partial x^2} \tag{14}$$

where

$$D_{2\mathrm{a}} = \frac{D_\mathrm{H} + \dfrac{D_{\mathrm{HM}}[\mathrm{M}^{\mathrm{tot}}]}{K_\mathrm{M}}}{1 + \dfrac{[\mathrm{M}^{\mathrm{tot}}]}{K_\mathrm{M}} + \dfrac{[\mathrm{F}^{\mathrm{tot}}]}{K_\mathrm{F}}} \tag{15}$$

Note that when $[\mathrm{M}^{\mathrm{tot}}] = [\mathrm{F}^{\mathrm{tot}}] = 0$, Eqns. 14 and 15 reduce to Eqn. 1 and when $[\mathrm{M}^{\mathrm{tot}}] = 0$, they reduce to Eqns. 7 and 8. Eqn. 15 illustrates that fixed buffers always decrease the effective diffusion coefficient, D_{2a}, but mobile buffers can either increase or decrease the value of D_{2a}. In the absence of fixed buffers, mobile buffers always decrease D_{2a}. For example, if $[M^{tot}]/K_M \gg 1$, then $D_{2a} \approx D_{HM}$. The maximum value of D_{HM} is about 10^{-9} m^2/s and is characteristic of a small molecule such as phosphate or bicarbonate. On the other hand, the value of D_H is about 10^{-8} m^2/s because protons diffuse by the Grotthus mechanism.

In the presence of fixed buffers, mobile buffers can partially compensate for the decrease in D_{2a} caused by the fixed molecules. Consider a numerical example: if pH = 7, $pK_F = pK_M = 6$, $[F^{tot}] = 10^{-2}$ M, $[M^{tot}] = 0$, then $D_{2a} = D_H/10^4$. However, if $[M^{tot}]$ is 10^{-3} M, D_{2a} increases to $D_{HM}/10 \approx D_H/10^2$.

Eqn. 15 can be simplified under certain conditions. If $pK_F = pK_M$, $[F^{tot}] > [M^{tot}]$ and $[F^{tot}]/K_F > 1$, then $D_{2a} \approx (D_{HM}/D_H)([M^{tot}]/[F^{tot}])D_H$. In other words, the effective diffusion coefficient is lower than the value in an unbuffered aqueous solution, D_H, by a factor $D_H/D_{HM} \approx 10$ because protons move mainly in the form of HM rather than free ions. It is reduced by a further factor $[F^{tot}]/[M^{tot}]$, which represents either the relative concentration of protons bound to fixed and mobile buffers or the relative time a single proton is bound to fixed and mobile buffers.

Multiple pK values

We now consider the case where both the mobile and fixed buffers have a distribution of pK values. We define a total buffer capacity:

$$\beta^{tot} = \Sigma_i \beta_i \tag{16}$$

where β_i is defined in analogy with Eqn. 9 for both the fixed and mobile buffers. It follows from Eqn. 2 that

$$\frac{\partial[H^+]}{\partial t} = \frac{D_{2b}\,\partial^2[H^+]}{\partial x^2} \tag{17}$$

where

$$D_{2b} = \frac{2.3[H^+]D_H}{\beta^{tot}} + \frac{\Sigma_i D_i \beta_i}{\beta^{tot}} \tag{18}$$

Eqn. 18 describes more generally than Eqn. 15 the effect of fixed and mobile buffers on the effective diffusion coefficient of protons. Both equations allow us to draw three conclusions. Firstly, when buffers are present, the effective diffusion coefficient, D_{2b} in Eqn. 18, is always less than the free diffusion coefficient of protons, D_H. Secondly, fixed buffers always decrease D_{2b}. Thirdly, mobile buffers blunt this decrease; the buffer with the largest product $D_i\beta_i$ has the largest effect.

In the stroma of chloroplasts or the matrix of mitochondria the pH is alkaline and we expect the relaxation of a pH profile to be dominated by OH^- rather than by H^+ [3]. Around neutral pH, where both H^+ and OH^- contribute to the relaxation, the analysis is complicated. However, if we assume a high curvature for the initial pH profile, i.e.,

$$\frac{\partial^2[H^+]}{\partial x^2} \gg \frac{1}{[H^+]}\left[\frac{\partial[H^+]}{\partial x}\right]^2$$

Eqn. 18 takes an approximate form:

$$D^{eff} \approx D_H\left[\frac{2.3[H^+]}{\beta^{tot}}\right] + D_{OH}\left[\frac{2.3\ 10^{-14}}{\beta^{tot}[H^+]}\right] + \frac{\Sigma_i D_i \beta_i}{\beta^{tot}} \tag{19}$$

where D_{OH} denotes the diffusion coefficient of free OH^- and the other parameters are defined above.

Discussion

The analysis above is simple, but we cannot find a similar quantitative discussion in the literature. Other investigators have recognized that mobile buffers can reduce equilibration times for protons when fixed buffers are present. Engasser and Horvath [5], for example, discussed this phenomenon when they considered qualitatively the results of Bishop and Richards [7]. These investigators found that the acid-base titration of crystalline β-lactoglobulin crosslinked with glutaraldehyde took several hours to reach the endpoint, but addition of a small amount of acetate to the mixture reduced the equilibration time to 2 or 3 min. Engasser and Horvath [5] concluded that "buffer-facilitated proton transport can have profound significance in reducing the time needed to achieve equilibrium when the rate of equilibration is limited by the diffusion of H^+". We agree.

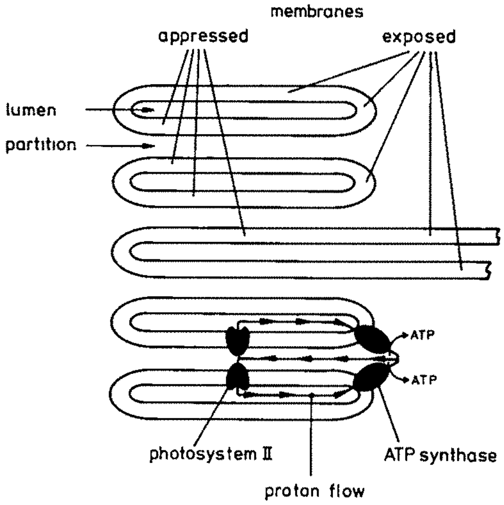

Fig. 1. Diagram illustrating the circulation of protons in thylakoids (see Ref 3).

We consider one biologically relevant example of the effect of fixed and mobile buffers on the kinetics of proton movement. As illustrated in Fig. 1, protons cycle between Photosystem II, a light-driven proton pump, and ATP synthases in thylakoids [3]. The alkaline partition region and the acidic lumen both contain high concentrations of buffers [3,8–10]. If we assume the pH of the partition region is about 8, it is apparent from Eqn. 19 that the diffusion of OH^- is about two orders of magnitude more important than the diffusion of H^+ in this region. The buffer capacity of the partition region is at least $2 \cdot 10^{-2}$ M per pH at pH = 8 [3]. It is determined mainly by large protein complexes, which we assume have a diffusion coefficient of $D_{\text{protein}} = 10^{-13}$ m^2/s. We assume that the pK of inorganic phosphate is 7, its diffusion coefficient is $D_{\text{phosphate}} = 10^{-9}$ m^2/s, and its concentration in the partition region is 10^{-3} M. Eqn. 12 indicates that phosphate contributes only about 1% of the total buffer capacity at pH 8. That is, $\beta_{\text{protein}} \approx 0.99\ \beta^{\text{tot}}$ and $\beta_{\text{phosphate}} \approx 0.01\ \beta^{\text{tot}}$. However, Eqn. 19 illustrates that this concentration of phosphate has a large influence on the effective diffusion coefficient:

$$D^{\text{eff}} \approx D_{\text{OH}}(2.3 \cdot 10^{-6}/2 \cdot 10^{-2})$$

$$+ D_{\text{phosphate}}(0.01) + D_{\text{protein}}(0.99)$$

$$\approx 10 \cdot 10^{-13} + 100 \cdot 10^{-13} + 10^{-13}\ \text{m}^2/\text{s}.$$

In the absence of phosphate ions the proteins are predicted to reduce the effective diffusion coefficient by at least four orders of magnitude from 10^{-8} to 10^{-12} m^2/s, because the term multiplying D_{OH} in Eqn. 19 is about 0.0001. This prediction agrees with the experimental results [3]. The addition of 10^{-3} M phosphate to the partition region should increase the effective diffusion coefficient by an order of magnitude even though it contributes only 1% to the buffer capacity of this region.

Acknowledgements

The work was supported by NSF grant BNS 85-01456 to S.McL. and by DFG grant B3-SFB171 to W.J. We thank Ira Cohen for helpful suggestions.

References

1 Crank, J. (1979) The Mathematics of Diffusion, p. 327, Clarendon, London
2 Polle, A. and Junge, W (1986) Biochim. Biophys Acta 848, 257–264
3 Junge, W. and Polle, A (1986) Biochim. Biophys. Acta 848, 265–273
4 Gutknecht, J. and Tosteson, D.C (1973) Science 182, 1258–1261
5 Engasser, J.-M. and Horvath, C (1974) Biochim. Biophys. Acta 358, 178–192
6 Einstein, A (1905) Ann Phys. 17, 549–560 (for English translation, see Einstein, A. (1956) Investigations on the Theory of the Brownian Movement (Furth, R , ed.) (Cowper, A D., transl.), p. 19, Dover Publishing, New York
7 Bishop, W H and Richards, F.M. (1968) J. Mol Biol. 33, 415–421
8 Walz, D , Goldstein, L. and Avron, M. (1974) Eur. J. Biochem. 47, 403–407
9 Junge, W , Auslander, W., McGeer, A.J. and Runge, T. (1979) Biochim. Biophys. Acta 546, 121–141
10 Junge, W. (1982) Curr. Top. Membr. Transp. 16, 431–465
11 McLaughlin, S. and Brown, J. (1981) J Gen Physiol. 77, 475–487
12 Delahay, P. (1954) New Instrumental Methods in Electrochemistry, Ch. 5, Interscience/Wiley & Sons, New York
13 Westerhoff, H v. and Chen, Y-D. (1985) Proc Natl. Acad Sci USA 82, 3222–3226

Biochimica et Biophysica Acta 890 (1987) 6–14
Elsevier

BBA 42065

Evidence for an association between a 33 kDa extrinsic membrane protein, manganese and photosynthetic oxygen evolution.
I. Correlation with the S_2 multiline EPR signal

D. Hunziker, D.A. Abramowicz *, R. Damoder ** and G.C. Dismukes

Princeton University, Department of Chemistry, Princeton, NJ 08544 (U.S.A.)

(Received 20 March 1986)

Key words. Photosynthesis; Oxygen evolution; Water oxidation; Manganese; Photosystem II; (EPR)

The removal of peripheral membrane proteins of a molecular mass of 17 and 23 kDa by washing of spinach Photosystem-II (PS II) membranes in 1 M salt between pH 4.5 and 6.5 produces a minimal loss of the $S_1 \rightarrow S_2$ reaction, as seen by the multiline EPR signal for the S_2 state of the water-oxidizing complex, while reversibly inhibiting O_2 evolution. The multiline EPR signal simplifies from a '19-line' spectrum to a '16-line' spectrum, suggestive of partial uncoupling of a cluster of 3 or 4 Mn ions to yield photo-oxidation of a binuclear Mn site. Alkaline salt washing progressively releases a 33 kDa peripheral protein between pH 6.5 and 9.5, in direct parallel with the loss of O_2 evolution and the S_2 multiline EPR signal. The 33 kDa protein can be partially removed (20%) at pH 8.0 prior to manganese release. Salt treatment releases four Mn ions between pH 8.0 and 9.5 with the first 2 or 3 Mn ions released cooperatively. A common binding site is thus suggested in agreement with earlier EPR spectroscopic data establishing a tetranuclear Mn site. At least two of these Mn ions bind directly at a site in the PS II complex for which photooxidation by the reaction center is controlled by the 33 kDa protein. The washing of PS II membranes with 1 M $CaCl_2$ to affect the release of the 33 kDa protein, while preserving Mn binding to the membrane (Ono, T.-A. and Inoue, Y. (1983) FEBS Lett. 164, 255–260), is found to leave some 33 kDa protein undissociated in proportion to the extent of O_2 evolution and S_2 multiline yield. These depleted membranes do not oxidize water or produce the normal S_2 state without the binding of the 33 kDa protein. A method for the accurate determination of relative concentrations of the peripheral membrane proteins using gel electrophoresis is presented.

Introduction

There is keen interest in, yet limited knowledge of, the organization of manganese within the complex responsible for the oxidation of water to O_2 in photosynthetic membranes. Manganese has been indirectly implicated as the site for water binding and direct observations of oxidation state changes have indicated a clear redox function (reviewed in Refs. 1 and 2).

Of the four Mn ions located within the smallest protein-membrane complexes capable of high O_2

---

* Present address: Research and Development Center, General Electric Co., Schenectady, NY 12301, U.S.A.

** Present address: Research and Development Division, Dow Chemical Company, Midland, MI, U.S.A.

Abbreviations: Chl, chlorophyll; PS II, Photosystem II; PPBQ, *p*-phenylbenzoquinone; LDS, lithium dodecylsulfate; Mes, 4-morpholineethanesulfonic acid; Hepes, 4-(2-hydroxyethyl)-1-piperazineethanesulfonic acid; Tricine, *N*-[2-hydroxy-1,1-bis(hydroxymethyl)ethyl]glycine; Ches, 2-[*N*-cyclohexylamino]-ethanesulfonic acid.

Correspondence: Dr G.C. Dismukes, Princeton University, Department of Chemistry, Princeton, NJ 08544, U.S.A.

evolution activity, there is evidence for their organization into two distinct types based upon their lability to denaturing conditions [3–7]. A close arrangement of at least two Mn ions separated by a shared ligand is well established [8] and this pair shows clear evidence for coupling to another paramagnetic center believed to comprise one or both of the other Mn ions [9,10,13].

Furthermore, there is evidence that two of the four ions can be replaced by divalent ions in the reactivation of electron donation from exogenous donors (but not significant O_2 evolution) [5,7]. It is not yet clear if this pair of cations must also be Mn in order to observe optimal O_2 evolution rates. There is some speculation that this labile pair may be required for a structural rather than redox function. In contrast, electronic spectroscopic data have been interpreted as evidence for a redox function for all four Mn ions in water oxidation [11,12]. Evaluation of these diverse lines of evidence on the function and organization of manganese has been interpreted in favor of a model in which the catalytic unit is comprised of two pairs of closely interacting Mn ions [9,13].

Three extrinsic membrane proteins associated with O_2 evolution can be dissociated from Photosystem-II (PS-II) membranes (reviewed in Ref. 19). Two of these subunits have apparent molecular masses of 16–18 kDa and 23–24 kDa and participate in the regulation of Cl^- affinity, a required physiological anion. The 23 kDa protein plays a more important role and can be replaced by Ca(II) [15–17] and by Cl^- at a 20–50-fold higher concentration than is physiologically optimal [17,18].

The third subunit has a mass of 33 kDa. Manganese can be released with this protein depending upon the conditions used for dissociation from the membrane. Alkaline Tris washing releases this protein and 2 Mn ions from membranes initially depleted of the 17- and 23-kDa proteins by salt washing [4]. Protein release by osmotic shock of membranes [20] or by extraction with acetone [3] or butanol [38] results in the partial binding of Mn to the protein. Enhanced binding of Mn to this protein is favored by inclusion of mild chemical oxidants during isolation, which apparently suppresses the reduction of Mn(III). The protein binds a maximum of 2 Mn(III) ions under these conditions [3,20].

No Mn is released initially from the membrane when these three proteins are dissociated by washing in 1 M $CaCl_2$ [21] or 2.5 M urea [22]. Loss of the 33 kDa protein is invariably accompanied by a complete loss or significant reduction of O_2 evolution activity, which can be partially reversed upon rebinding of the protein [3,23,24,42,43], additional Cl^- [22] or Ca^{2+} [25]. These results are at odds with the earlier data showing a direct correlation between O_2 evolution activity and the binding of the 33 kDa protein and Mn to the PS-II complex.

A possible answer to this contradiction has come in a recent study showing that the Mn binding site on PS-II membranes, following release of the 33 kDa protein and Ca^{2+} by washing in 1 mM $LaCl_3$, is structurally altered and not capable of photo-oxidation by the reaction center [37]. These observations have been interpreted to indicate the binding of a relatively labile pair of the four Mn ions at the interface between two protein domains, involving the amino acid residues of the peripheral 33 kDa protein and either the 47 kDa intrinsic membrane protein of the reaction center [19] or an intrinsic membrane protein of 34 kDa [39].

In an effort to resolve these seemingly contradictory results we have titrated the release of the three peripheral membrane proteins, and examined the release of manganese, the loss of O_2 rate and the loss of the S_2 multiline EPR signal. New insights on how manganese is organized within the water-oxidizing complex are revealed.

Materials and Methods

PS-II membranes were prepared as described previously [26]. They had a steady-state O_2 evolution rate (Clark type electrode) of 340 μmol per mg Chl per h. Salt-washing treatments were based on the original procedure by Kuwabara and Murata [4]. PS-II membranes retaining specific amounts of the extrinsic 33 kDa protein can be prepared by salt washing at various pH values. All salt-washing buffers contained 1 M NaCl, 0.2 M sucrose and an appropriate Good pH buffer. The buffers used were: acetate (pH 4.5); Mes (pH 5.5 and 6.5); Hepes, (pH 7.5); Tricine, (pH 8.0 and 8.5); and Ches (pH 9.0 and 9.5). All buffers were at a final concentration of 25 mM. PS-II particles were incubated in these salt buffers at a Chl concentration of 0.5 mg/ml for 30 min on ice while shaking. Supernatants and pellets were collected after centrifugation at 48 000 × *g* for 30 min. The resultant depleted membranes were prepared for EPR measurements at a single pH by equilibration at pH 6.5 by washing twice in a buffer containing 25 mM Mes, 0.2 M sucrose, 10 mM $CaCl_2$ and either 25 or 110 mM NaCl. This washing released small quantities of additional protein which did not dissociate on the initial salt washing. Prior to EPR sample freezing 2 mM PPBQ was added as an electron acceptor.

Dark-adapted EPR samples (> 20 min, 274 K) were illuminated with a quartz-halogen lamp (1 W/cm^2) at 200 K in a dry ice/methanol bath for 3 min to produce the S_2 multiline EPR signal, or at 300 K for 3 min while cooling to 200 K in the presence of 50 μM DCMU. Heating of the EPR samples during illumination was insignificant at less than 3 K temperatures rise as monitored by measurements of both the bath and sample. Control samples were washed the same way except using a non-denaturing sucrose buffer at ph 6.5.

Proteins released by salt washing were prepared for electrophoresis by precipitation in acetone. Supernatants were diluted to a final NaCl concentration of 0.5 M and diluted with cold acetone to a final concentration of 80%. The solution was centrifuged at 48 000 × *g* for 20 min at 2°C or with a table top centrifuge for 1 h. The resulting pellet was resuspended in an electrophoresis buffer. Proteins were electrophorised by the procedure of Laemmli in the presence of 4 M urea and 0.2% LDS at 4.0°C [33].

The amount of the 33 kDa protein remaining on the membranes after salt washing can be determined by its release into the supernatant upon heat shock of the depleted membranes [34]. We have found this method to be far more reliable than estimation of the amount of protein in the pellet in cases where overlapping bands cause interference, e.g. at 31–34 kDa. For these experiments the salt-washed membranes that were prepared for EPR measurements were heat shocked at 55°C for 5 min at 1 mg Chl/ml.

Relative protein concentrations were determined by absorbance of Coomassie stained slab gel electrophoresis chromatograms with a Hewlett Packard 8450 spectrophotometer and a densitometer of local design.

EPR spectra were recorded at 11 K as previousy described [8]. The intensity of the S_2 multiline signal was obtained by summing the amplitudes of the peaks labelled −5, −6, −7, 5, 6, and 7 given in Fig. 3 after baseline subtraction. This avoids interference with the signals from chrome *b*-559 and Q^-Fe^{2+} which overlap with peaks labelled −4/−3 and 4/3, respectively.

Manganese was determined by atomic absorption using a graphite furnace, Perkin-Elmer model 305B and HGA-2000 furnace. Error analysis was conducted on the manganese and chlorophyll data in order to establish the precision of successive determinations. The reported values of Mn/RC have associated with the standard deviations of 2% and 4% for Mn and Chl determinations respectively, for replicate runs of the same sample. Averaging of data sets from three independent runs was performed on the data reported in Fig. 5. The average standard deviation from the mean of these three sets was 10%.

Results

Protein release by salt washing

Determination of the identity and extent of proteins released from PS-II membranes by salt washing at different pH values was performed by densitometry of Coomassie-stained LDS polyacrylamide gels as summarized in Figs. 1 and 2. In Fig. 1, B-I, there is nearly complete release of two proteins at M_r 17 and 23 kDa upon salt washing between pH 6.5 and 9.5, confirming earlier reports. There is 60% 17 kDa and some 23 kDa protein which remains bound at pH 4.5 and these decrease at higher pH. Progressively greater release of a 33 kDa protein is observed above pH 7. Approx. 50% of the 33 kDa band remains after salt washing at pH 8.5 and complete loss is observed at pH 9.5. These are compared to control membranes washes in non-denaturing sucrose buffer at pH 6.5 (A), and with membranes washed in 1 M $CaCl_2$ at pH 6.5 (J), a treatment known to release all three proteins. Other prominent bands associated with the PS-II core proteins at 47, 43, 34, 32, 24, 21, 20, 10 and 9 kDa and the light

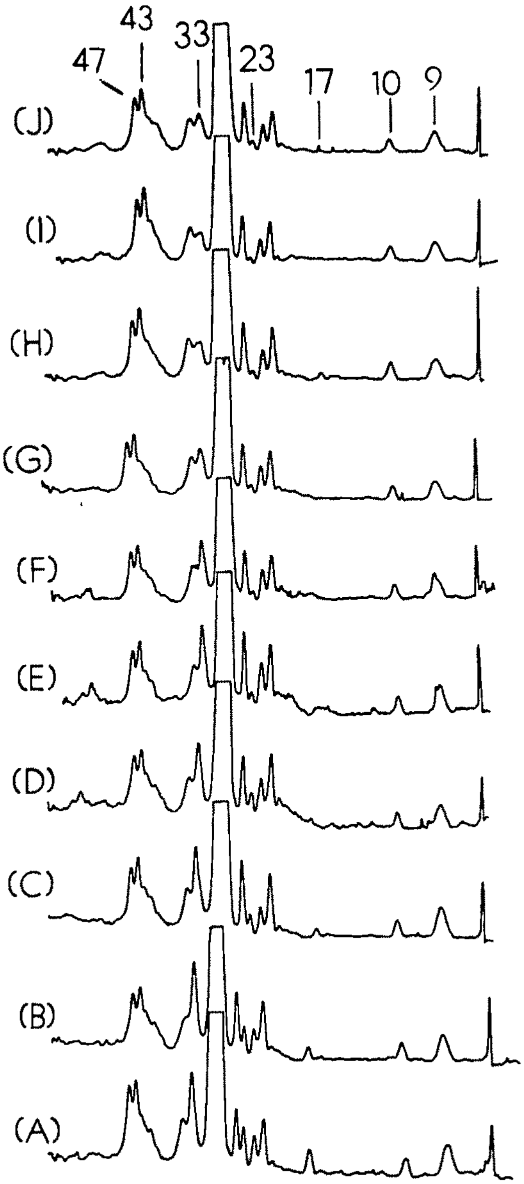

Fig. 1 LDS-PAGE densitometric traces of proteins remaining in PS II membranes following salt washing at various pHs. (A) Control, 25 mM NaCl (pH 6.5), (B) 1 M NaCl (pH 4 5); (C) 1 M NaCl, (pH 5.5); (D) 1 M NaCl, (pH 6.5), (E) 1 M NaCl, (pH 7.5); (F) 1 M NaCl (pH 8.0); (G) 1 M NaCl (pH 8.5); (H) 1 M NaCl (pH 9 0); (I) 1 M NaCl (pH 9.5); (J) 1 M $CaCl_2$ (pH 6.5)

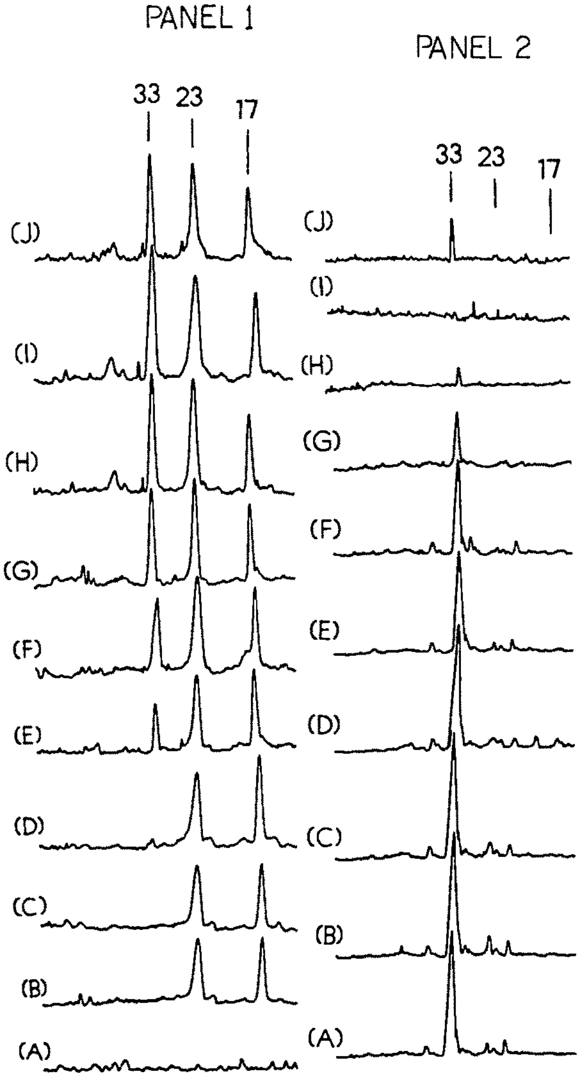

Fig. 2 Panel 1: LDS-polyacrylamide gel electrophoresis densitometric traces of proteins released from membranes by salt-washing at various pHs, as in Fig 1. Panel 2. LDS-polyacrylamide gel electrophoresis densitometric traces of proteins released by heat shock of salt-washed PS-II membranes from Fig. 1. After salt washing, membranes were washed and resuspended twice at pH 6 5 prior to heat shocking This removed the peripheral proteins of 23 and 17 kDa.

harvesting complex at 28–26 are resolved and are invariant under these treatments.

Quantitation of the amount of 33 kDa protein bound to the membrane is difficult using the data of Fig. 1 due to interference from neighboring bands at 32 and 34 kDa. This interference is resolved by determination of the relative amounts of protein released into the supernatants (as given in Fig. 2, panel 1). This confirms that there are only three proteins released by NaCl washing, with nearly uniform release of the 17- and 23-kDa proteins between pH 6.5 and 9.5, and an increasing amount of the 33 kDa protein released. The residual binding of the 33 kDa protein was assayed by release upon heat shock of the depleted membranes [34]. As shown in Fig. 2, panel 2, there is a progressive increase with pH in the release of the 33 kDa protein between pH 7 and 9.5. The residual 17 and 23 kDa proteins which are bound at pH 4.5–6.5 in Figs. 1 and 2 are not observed because these are lost during the washing treatment prior to heat shocking. No significant release of the other proteins seen in Fig. 1 was observed by these treatments. The fraction of 33 kDa protein which remains bound at each pH is plotted in Fig. 4. Protein analysis conducted in this manner proved to be reproducible, while analysis of the depleted membrane was not nearly as reliable. It is interesting to note that washing in 1 M $CaCl_2$, a treatment which is claimed to quantitatively release the 33 kDa protein [22,25] leaves about 1/3 of this protein on the membrane, as can be seen by release using heat shock (Fig. 2).

The salt-washed depleted membranes were examined further to determine the extent of the $S_1 \rightarrow S_2$ reaction from the yield of the manganese S_2 multiline EPR signal, produced by illumination at 200 K, as shown in Fig. 3 for a typical control sample. In Fig. 4 the yield of this signal following salt treatment is compared to the fraction of bound 33 kDa protein, to the amount of Mn released, as determined by atomic absorption of the supernatants and to the O_2 evolution rate. It shows that nearly complete release of the 17 and 23 kDa proteins by salt washing is accomplished by a 75% retention in the yield of the multiline signal relative to the control. This loss was smaller for incubation times less than 30 min and at higher Cl^- concentrations. The decrease of the multiline signal parallels the release of the 33 kDa, both approachng zero at pH 9.5. On the other hand, starting with membranes containing close to the minimal Mn content (4–5 Mn/PS II) capable of sustaining high activity, there is almost no Mn release, except above pH 7.5. At pH 5.5–7.5 there is no release of Mn, while at pH 4.5 and 8.0 there is less than 0.2–0.3 Mn released per PS-II. 90% of the Mn, about 4 Mn/PS II, is released by pH 9.5. This contrasts with about 20% release of the 33 kDa protein with increasing pH between pH 6.5 and 8.0 where no significant release of Mn occurs. This Mn is, however, not photo-oxidized as seen by the loss of the multiline signal. At pH 8.5 and above the release of Mn and protein parallel each other.

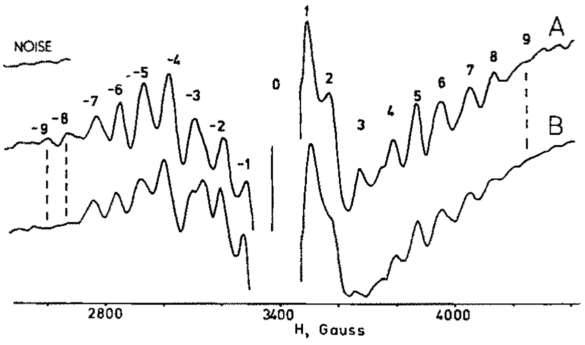

Fig 3 EPR spectra recorded in the dark illumination of dark adapted PS II membranes at pH 6.5. The multiline signal is formed by illumination at 200 K and observed at 11 K. (A) Control, prior to salt washing (B) after washing in 1 M NaCl (pH 7.5) buffer A numbering system for peaks is shown The relative peak-to-noise is 0.04.

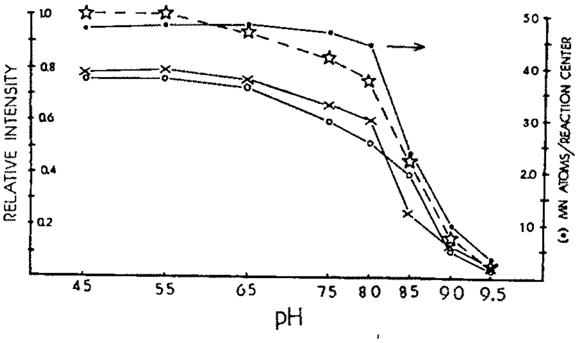

Fig. 4. Correlation between the loss of S_2 multiline EPR signal (O), binding the the 33 kDa protein (☆) (relative error, 0.04), O_2 evolution (×) [relative error, 0 07] and the amount of Mn per reaction center (●). Associated error of 0.5 atoms Mn reaction center in PS-II membranes upon salt washing at various pH values. Samples are identical to those in Figs 1 and 2. The measurements were conducted on samples adjusted to pH 6.5 after treatment. All measurements are relative to the control samples washed in sucrose buffer at pH 6.5 without salt The protein data are an average of three experiments involving quantiation by heat shock as in Fig. 3 The multiline intensities and manganese content are the average of two data sets Optimum O_2 evolution rates were assayed at pH 6 5 and 235 mM Cl^-/5 mM Ca^{+2}.

The losses in protein and multiline signal are accompanied by a parallel loss in the O_2 evolution rate. Three different Cl^-/Ca^{2+} concentrations were surveyed in the assay for O_2 rate in order to optimize activity (data not shown). As appreciably higher Cl^- requirement for O_2 evolution in membranes depleted of the 17- and 23-kDa proteins was confirmed [16–18,28,29]. About 80% restoration of the O_2-evolution rate was achieved with concentrations of 5 mM $CaCl_2$ and 235 mM NaCl. The data given in Fig. 4 indicate that electron transfer, as monitored by O_2 evolution, follows the content of 33 kDa protein rather than Mn content in salt washed membranes. This again supports the claim that the Mn which remains bound following release of the 33 kDa is not capable of oxidizing water to oxygen.

Table I gives the same results for samples washed in 1 M $CaCl_2$ at pH 6.5. Here we see that, as found previously by others, there is appreciable retention of Mn on the membrane, about 3.7 Mn/PS-II. However, the yield of the multiline signal parallels the amount of 33 kDa protein remaining on the membrane, about 1/3 of the control, and not the Mn content. The optional O_2 evolution rate which could be observed was also about 40% of the control. Apparently, the bound Mn without the 33 kDa protein is not photo-oxidizable. This is compared to a sample that is salt-washed at pH 8.5 and has comparable yields of the S_2 signal and 33 kDa protein, but only 2.2 Mn/PS II. We find no evidence that this protein can be replaced by Ca^{2+} or Cl^- in the formation of the S_2 multiline signal or O_2 evolution, in contrast to O_2 evolution [22,25].

We felt it was important to learn if the loss of the S_2 multiline signal upon salt washing might be due to a change in the conditions necessary for generation of the signal, rather than due to loss of an essential cofactor for the manganese site. We tested two parameters: the Cl^- concentration in the assay medium and the illumination temperature. We found little further improvement in the amplitude of the multiline signal, in membranes washed at pH 6.5 or above, upon increasing the concentration of Cl^- in the assay medium. The yield increased only from 75% to 80% of the control for the optimum samples (pH 6.5) upon increasing the salt concentration from 25 mM to 110 mM. Therefore, the loss of multiline signal above pH 6.5 cannot be accounted for by an unsatisfied Cl^- requirement. The yield of the multiline signal in membranes depleted below pH 6.5 actually decreased when the Cl^- concentration was increased from 25 mM to 110 mM, indicating an antagonistic influence of Cl^- below about pH 6.

The results on the temperature dependence of the formation of the multiline signal in salt-treated membranes by illumination at 200 K and 300 K (50 μM + DCMU) showed that a lower yield is observed at 300 K for all pH/salt extractions. Thus an increased activation energy is not the source of the reduction in the signal relative to control membranes (data not shown). It may be possible to reduce further the 20% loss of the S_2 multiline signal by using shorter times for salt incubation and centrifugation than the 30 min intervals we adopted for both.

TABLE I

CORRELATION OF RELATIVE S_2 MULTILINE SIGNAL YIELD, OXYGEN EVOLUTION, MANGANESE AND 33 kDa PROTEINS IN PS-II MEMBRANES TREATED WITH 1 M $CaCl_2$, pH 6.5 OR 1 M NaCl, pH = 8.5

Treatment	Relative S_2 yield	Relative 33 kDa bond	Relative Oxygen evolution	Manganese reaction center
$CaCl_2$ (pH 6.5)	0.37	0.35	0.39	3.7
NaCl (pH 8.5)	0.39	0.43	0.24	2.2
Control	1.0	1.0	1.0	4.7

The g = 4.1 signal

We also searched for the light-induced $g = 4.1$ EPR signal attributed to an oxidized donor, possibly Mn(IV) in PS II membranes [35,36]. This signal did not form in salt-treated samples illuminated at 200 K or in control samples (data not shown).

Discussion

Protein determination

The results in Figs. 1 and 2 illustrate that accurate determination of the relative extent of 33 kDa protein bound to the membrane is greatly aided by release of the protein from the membrane by the heat shock method [34]. Once in solution interference from non-soluble proteins is eliminated. When combined with a titration method for protein release this offers a quantitative assay for the presence of this protein.

Salt washing

The 20–25% reduction in the amplitude of the multiline signal which accompanies the release of the 23- and 17-kDa proteins at pH 4.5–5.5 (Fig. 4) suggests a role for these proteins in maintaining efficient photooxidation of the S_2 state of the O_2-evolving complex by the reaction center, but not an obligatory role. We cannot rule out the possibility that the loss of one or both of these proteins upon salt washing is unrelated to the reduced quantum yield for the S_2 multiline signal. In contrast, the large loss in O_2 evolution rate upon dissociation of the 23 kDa protein [28] when combined with the present results, indicate that it must be required for physiological activity involving the formation of S_3 or S_4. These results agree with the general findings in Ref. 30 showing that salt treatment to release the 17- and 23-kDa proteins abolishes the S_2 signal and O_2 evolution, but reversibly, upon dialysis to remove excess salt. An earlier report [41] has found that removal of the 17- and 23 kDa-proteins by salt washing blocks or greatly suppresses the advancement of the water oxidizing complex to the S_2 state, as seen by the multiline yield. This discrepancy is probably attributable to the absence of sufficient Cl^- (1 mM) and Ca(II) (none) in their assay medium. This underscores the ease with which this signal is lost if conditions are not optimized.

The spectrum of the S_2 multiline signal which forms in salt-washed membranes has fewer lines compared to the minimum of 19 lines which form in the control membranes at 200 K. Fig. 3 shows that the two low field peaks, -8 and -9, disappear upon salt washing at pH 7.5. This signal is referred to as the ‘16-line’ S_2 multiline signal. ‘16-line’ EPR spectra analogous to this signal are observed for synthetic binuclear manganese complexes in the mixed-valence state Mn_2 (III, IV) [14]. The S_2 multiline signal in untreated membranes converts also from a ‘19-line’ form, achieved by illumination at 200 K, to a ‘16-line’ form produced by multiple turn-overs at 300 K [1,14]. It has been attributed to an altered coupling between the manganese ions.

The results of Fig. 4 show that it is possible to dissociate about 20% of the 33 kDa protein without loss of Mn from the membrane between pH 6.5 and 8.0. Consequently, this protein is not essential for the binding of Mn to the membrane, but it is essential for photo-oxidation of Mn (S_2 multiline signal) and the evolution of O_2 (Fig. 4). These results are in agreement with previous results showing conditions under which the three peripheral proteins may be partially, dissociated prior to significant Mn release [21,22,30]. The multiline signal and O_2 evolution are restored upon rebinding of the 33 kDa protein, provided manganese has not been lost from the protein depleted membrane [42,43].

The Mn which remains on the membrane following partial dissociation of the 33 kDa protein is more susceptible to dissociation than in intact PS-II membranes, suggesting a direct influence of this protein on Mn binding [19,43,44]. Previous results [20] show binding of two Mn(III) ions to the 33 kDa protein in the presence of oxidants can be understood in terms of the current results. Manganese binding to PS-II membranes appears to occur at the interface between the 33 kDa protein and an integral membrane protein of the reaction center core, so that it may be carried with either the dissociated protein or with the depleted membrane depending upon the conditions used for extraction. Similar conclusions were reached in studies of Ca(II) exchange for La(III) [37]. This other protein has been suggested to be either the 47 kDa reaction center core protein [19], or possibly an intrinsic membrane protein of 34 kDa [39]. Another less likely possibility is that the 33 kDa protein, while stabilizing the binding of manganese, is not directly involved in manganese coordination; inferring that the observed isolation of a manganese protein complex by use of chemical oxidants [20,38] is a curious artifact. The capability of this manganese protein to restore lost O_2 evolution activity to depleted membranes [3] favors the former interpretation.

Manganese binding

A comparison of the observed binding of Mn to the membrane with theoretical predictions for cooperative binding is given in Fig. 5. The theoretical curves are generated using the Hill formulation for the fraction of bound sites, Y [40]:

$$\bar{Y}=\frac{\left(\frac{[\mathrm{OH}^-]}{K}\right)^{\alpha}}{1+\left(\frac{[\mathrm{OH}^-]}{K}\right)^{\alpha}} \tag{1}$$

Two curves are shown for Hill parameters of $\alpha=1$ and 2. The case of $\alpha=1$ corresponds to non-cooperative binding. The experimental data are clearly in better agreement with a cooperative release of the initial 2 or 3 Mn ions by alkaline salt washing. Therefore, at least 2 and possibly all 4 Mn ions may be grouped together into a common binding site. This conclusion was evident already from the spectroscopic interpretation of the S_2 multiline EPR signal which is best understood by models involving the electronic interaction of four Mn ions [1,9,13,14]. Combined with the present biochemical data these results indicate that these four Mn ions are organized into two groups comprised of 2 or 3 Mn ions that are cooperatively released and another 2 or 1 Mn ions that bind at a site which is characterized by release which is thermodynamically non-cooperative. These results do not preclude the possibility that all four Mn ions are bound to a common site.

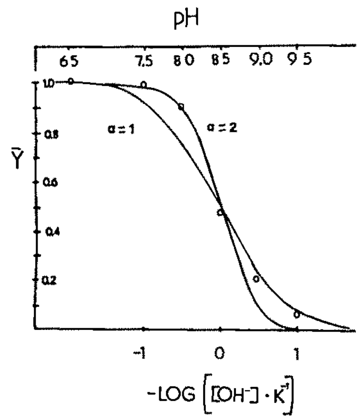

Fig. 5. Comparison of the Mn binding data taken from Fig. 4 with an empirical model for cooperative binding. see Eqn. 1 Curves are plotted for the Hill coefficients of $\alpha=1$ and $\alpha=2$. The data represent averages from three independent determinations each subject to a precision error of 0.04.

$CaCl_2$ washing

Previous studies have found that PS-II membranes which have been completely stripped of the 17-, 23- and 33-kDa proteins by washing in 1 M $CaCl_2$ retain Mn which is functional in the reconstitution of partial O_2 evolution activity by addition of Ca(II) [25] or excess Cl^- [22]. While we see retention of Mn binding, we have found no evidence supporting the claim that this Mn, without the 33 kDa protein, is functional in O_2 evolution or S_2 multiline formation with or without added Ca(II) or Cl^- (Fig. 4 and Table I). The answer to this difference may lie in the results in Table I, showing that this treatment actually leaves about 1/3 of the 33 kDa protein on the membrane. This is easily missed if protein determination by gel electrophoresis is conducted using the depleted membrane for which interference from bands at 34- and 32 kDa occurs (Fig. 1). Therefore, the partial O_2 rate recovery seen in previous work may reflect a Cl^- or Ca(II) dependent recoupling of undissociated 33 kDa protein to the O_2-evolving complex.

Osmotic release

Previously, we observed that release of the 33 kDa protein by osmotic shock also releases 2 or 3 Mn atoms from thylakoid membranes [20] and 2 Mn atoms from PS-II membranes [3]. Furthermore, a strict correlation was observed between the extent of release of the 33 kDa protein and the loss of the multiline signal and O_2 evolution from PS-II membranes by osmotic shock [3]. These results agree well with the results from alkaline salt washing, and confirm how general the results are with different methods for protein dissociation. The release of only 2 of the 4 Mn ions by the milder osmotic treatment indicates that the 33 kDa protein stabilizes preferentially 2 of the 4 Mn ions that can be released by alkaline salt washing.

Acknowledgements

This work was supported by grants from the National Science Foundation (GHE82-17920) and the Department of Energy Soleras Program DE-FG02-84CH10199.

References

1 Dismukes, G.C. (1986) Photochem. Photobiol. 43, 99–114
2 Govindjee, Kambara, T. and Coleman, W (1985) Photochem Photobiol 42, 187–210
3 Abramowicz, D A. (1984) Ph.D Dissertation, Princeton University, Princeton, NJ
4 Kuwabara, T and Murata, N. (1983) Plant Cell Physiol 24, 741–747
5 Packham, N.K and Barber, J. (1984) Biochim Biophys Acta 764, 17–23
6 Miller, M and Cox, R.P. (1983) FEBS Lett. 155, 331–333
7 Klimov, V.V., Allakhverdiev, V A, Shuvalov, V A and Krasnovsky, A A (1982) Biofizika 28, 357–363
8 Dismukes, G.C. and Siderer, Y. (1981) Proc Natl Acad Sci. USA 78, 274–278
9 De Paula, J. and Brudvig, G.W (1985) J Am Chem Soc 107, 2643
10 Damoder, R. and Dismukes, G.C. (1985) Biophys J 47, 166a
11 Saygin, O. and Witt, H.T., FEBS Lett 176, 83–87
12 Dekker, J P., Van Gorkom, H.J, Wensink, J. and Ouwehand, L (1984) Biochim. Biophys. Acta, 767, 1–9
13 Dismukes, G.C., Ferris, K and Watnick, P (1982) Photobiochem Photobiophys. 3, 243–256
14 Dismukes, G.C (1986) in Manganese in Metabolism and Enzyme Function (Schram, V.L and Wedler, F C., eds.), Academic Press, New York, in the press
15 Ghanotakis, D.F., Babcock, G.T. and Yocum, C.F. (1984) FEBS Lett 167, 127–130
16 Miyao, M and Murata, N. (1984) FEBS Lett. 168, 118–120
17 Nakatani, H.Y. (1984) Biochem Biophys Res. Commun 120, 299–304
18 Andersson, B, Critchley, C., Ryrie, I.H., Jansson, C, Larsson, C. and Anderson, J.M. (1984) FEBS Lett. 168, 230
19 Murata, N. and Miyao, M. (1985) Trends Biochem Sci., March, 122–124
20 Abramowicz, D A. and Dismukes, G.C., (1984) Biochim Biophys. Acta 765, 318–328
21 Ono, T. and Inoue, Y. (1983) FEBS Lett. 164, 255–260
22 Miyao, M. and Murata, N. (1984) FEBS Lett 170, 350–354
23 Ono, T and Inoue, Y (1984) FEBS Lett 166, 381–384
24 Miyao, M. and Murata, N (1983) FEBS Lett. 164, 375–378
25 Ono, T. and Inoue, Y. (1984) FEBS Lett 168, 281–286
26 Ford, R.C and Evans, M.C.W (1983), FEBS Lett. 160, 159–164
27 Homann, P (1968) Biochim Biophys Res Commun. 33, 229
28 Åkerlund, H.-E., Jansson, C. and Andersson, B. (1982) Biochim. Biophys. Acta 681, 1–10
29 Ghanotakis, D.F., Topper, J.N., Babcock, G.T. and Yocum, C.F. (1984) FEBS Lett. 170, 169–173
30 Blough, N.V and Sauer, K (1984) Biochim Biophys Acta 767, 377–381
31 Fukutaka, E., Imaoka, A, Akabori, K. and Toyoshima, Y (1983) FEBS Lett. 158, 217–221
32 Miyao, N and Murata, N. (1983) Biochim Biophys. Acta 725, 87–93
33 Laemmli, U K. (1970) Nature 227, 680–685
34 Franzen, L.-G and Andréasson, L -E. (1984) Biochim Biophys. Acta 765, 166–170
35 Casey, J. and Sauer, K. (1984) Biochim Biophys Acta 767, 21–28
36 Zimmerman, J.L. and Rutherford, A.W (1984) Biochim. Biophys Acta 767, 160–167
37 Ghanotakis, D F., Babcock, G.T, Yocum, C.F. (1985) Biochim. Biophys. Acta 809, 173–180
38 Yamamoto, Y, Shinkai, H, Isogai, K, Matsurra, K. and Nishimura, M. (1984) FEBS Lett. 175, 429–432
39 Bishop, N.I (1983) in The Oxygen Evolving System of Photosynthesis (Inoue, Y, Crofts, A.R., Govindjee, Murata, N., Renger, G. and Satoh, K., eds.), pp. 177–188, Academic Press Japan, Tokyo
40 Cantor, C.R. and Schimmel, P.R (1980) Biophysical Chemistry, Vol. III, p. 864, W H. Freeman, Publ, San Francisco
41 Franzén, L -G., Hansson, Ö. and Andréasson, L.-E. (1985) Biochim. Biophys. Acta 808, 171–179
42 Cole, J, Boska, M., Blough, N V. and Sauer, K (1986) Biochim Biophys. Acta 848, 41–47
43 Imaoka, A., Akabori, K., Yanagi, M., Izumi, K., Togoshima, Y., Kawamori, A., Nakayama, H and Sato, J. (1986) Biochim Biophys. Acta 848, 201–211
44 Seibert, M and Cotton, T.M (1985) FEBS Lett 182, 34–38

Biochimica et Biophysica Acta 890 (1987) 15–22
Elsevier

BBA 42078

Long-term delayed luminescence in *Scenedesmus obliquus*
I. Spectral and kinetic properties

Werner Schmidt and Horst Senger

Fachbereich Biologie und Botanik der Philipps-Universität Marburg, D-3550 Marburg an der Lahn, Lahnberge (F.R.G.)

(Received 11 September 1986)

Key words: Fluorescence; Long-term delayed luminescence; Chlorophyll spectrum; Spectrophotometry; (*S. obliquus*)

Long-term delayed luminescence varying from 0.3 s to several minutes has been investigated in wild-type cells of *Scenedesmus obliquus*. Complex decay kinetics as well as the comparison of excitation and emission spectra of long-term delayed luminescence with those of prompt fluorescence suggest the involvement of both Photosystem I and II in long-term delayed luminescence. A long-term intermediate showing maximal luminescence approx. 10 s after a 1 s excitation far-red light pulse is particularly attributed to the pigment system of Photosystem I. A mathematical model fitting the long-term delayed luminescence decay kinetics is presented.

Introduction

Delayed luminescence has been discovered in 1951 by Strehler and Arnold [1]. Detection of typical fluence rates smaller than 10^8 quanta/ml per s requires custom-made set-ups. As a valuable guide Lavorel [2] introduced the so-called 'τ-scale', which separates delayed luminescence in terms of three distinct regions of decay kinetics with half-lives ranging from 10^{-5} s up to several minutes. The domain larger than $t_{1/2} = 5$ s comprises very little data in the literature, even though valuable information may be extracted from this type of experiments [3,4].

The present continues an earlier investigation [5] of Long-term Delayed Luminescence (sometimes referred to as 'long-term delayed fluorescence'). Emission spectra and exciation spectra of short-term delayed luminescence often resemble those of prompt fluorescence [6,3]. Consequently, short-term delayed luminescence has been assumed to involve the same molecular species as prompt fluorescence: the lowest-excited singlet state of Chl *a* of PS II [7,8]. This has been claimed particularly for *Scenedesmus* by Haug et al. (Ref. 9; for further references, see Ref. 5). Various possible mechanisms for generating delayed luminescence have been suggested (for reviews, see Refs 10; 2 and 4). The most accepted explanation at present favors a thermally induced back-reaction of the transmembraneously accumulated charges as built up by the photosynthetic electron-transport chain. This, in turn, is taken to lead to a radiative charge recombination, giving rise either to delayed luminescence of "thermoluminescence" depending on the experimental conditions.

Nevertheless, there have been claims that some types of delayed luminescence originate from PS I (for reviews, see Refs. 4 and 11–13), even if the data are not as clear-cut as those supporting the

---

Abbreviations: PS I, Photosystem I; PS II, Photosystem II, Chl, chlorophyll

Correspondence: Dr W. Schmidt, Fachbereich Biologie und Botanik der Philipps-Universität Marburg, Lahnberge, D-3550 Marburg an der Lahn, F.R.G.

0005-2728/87/$03.50 © 1987 Elsevier Science Publishers B.V. (Biomedical Division)

involvement of PS II. A previous investigation [5] focussed on long-term delayed luminescence of tobacco leaves, and comparison of spectra of prompt fluorescence and long-term delayed luminescence also suggested processes different from a plain reversal of charge separation by PS II, postulating more complex molecular mechanisms.

Screening, selfabsorption and scattering as indispensable obstacles inherent in optical spectroscopy of opaque materials such as mature leaves of higher plants will truncate both spectra and kinetics in an uncontrolled manner. Therefore, in the present work we adopted the green alga *Scenedesmus obliquus*: suspensions of algae can be handled more conveniently and – due to strict standardization – allow a better control of various optical and physiological parameters such as extinction, temperature, uptake of exogeneous inhibitors or pH. In addition, there are several specific mutants available with well-defined defects which allow further analysis of the origin of long-term delayed luminescence.

Materials and Methods

Cultures of the unicellulr algae *Scenedesmus obliquus* strain D_3 were grown at a temperature of 30°C in liquid inorganic medium [14], aerated with 3% CO_2 in air. The cells were synchronized by a light-dark regime of 14 h white light of 15 $W \cdot m^{-2}$ and 10 h darkness. At the beginning of each light period the cultures were diluted automatically with a photoelectrically controlled dilution device [15] to a preset density. If not stated otherwise, cells were harvested for the experiments at the 16th hour of the life cycle.

The device for measuring long-term delayed luminescence has been described in detail previously [5] and was slightly modified for measuring algae suspensions: Petri dishes of 100 mm diameter and 18 mm height were filled with 10 ml suspension (corresponding to $A = 0.25$) and placed on top of a vertical, red-light sensitive end-on photomultiplier tube (EMI 9658 B, S20 photocathode, 1 inch diameter) with 'shutter 1' in between for protection of the photomultiplier tube during irradiation with exciting light. Prior to illumination, cell suspensions wer adjusted to a chlorophyll concentration of 5 $\mu g \cdot ml^{-1}$ by dilution with the culture medium. Measurements were usually performed at $20 \pm 1°C$ under dim green safelight (cf. action spectrum of long-term delayed luminescence in Fig. 6, bottom). Using a mechanically operated 'shutter 2' (Prontor Press) in series with a lens system, the suspension was uniformly illuminated from above for 1 s with monochromatic light of a given fluence rate. Light intensities were measured with a photometer/radiometer system (Ealing, Model 450). Excitation and Emission wavelengths were defined by interference filters (DIL, half-band widths of 8–10 nm, Schott, Mainz, F.R.G)

With a time lapse of approx. 0.3 s after terminating the exciting light the kinetics of long-term delayed luminescence were monitored typically for 1 min. The photomultiplier signal was amplified by a low-noise amplifier (Brookdeal, model 450) which was operated in the ratemeter mode, and fed either to a NIC 1174 special purpose microcomputer (and stored on magnetic tape for subsequent evaluation), or directly to a Hewlett-Packard strip chart recorder (7101 BM).

Absorption measurements and 4th-derivative analysis were performed with a self-made, computerized single-beam spectrophotometer described in detail previously [16]. Measurements of corrected excitation and emission fluorescence spectra were done with a Shimadzu correcting fluorimeter, model RF-502. The action spectrum for long-term delayed luminescence was measured according to Shropshire, Jr. [17].

Results and Discussion

In a previous study of long-term delayed luminescence in tobacco leaves [5] occasionally deviations from simple first-order kinetics of long-term delayed luminescence were observed, i.e., an initial, relatively fast decay, succeeded by a (smaller) optimum in long-term delayed luminescence, i.e., the build up of some kind of luminescing intermediate. Occurrence and conditions for its occurrence have been far from being clear. The same effect is observed in *Scenedesmus* as well, and was studied more thorougly in the present paper.

The dependency of the decay kinetics of long-term delayed luminescence of *Scenedesmus* as a function of fluence rate of the 1 s exciting light

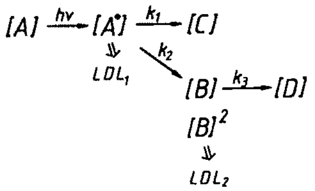

$$LDL_{tot} = LDL_1 + LDL_2$$

$$\frac{d[A^*]}{dt} = -(k_1 + k_2)[A^*]$$

and

$$\frac{d[B]}{dt} = k_2[A^*] - k_3[B]$$

with the solutions $k_1 \gg k_2$

$$[A^*] = [A^*]_0\, e^{-k_1 t} \approx LDL_1$$

$$[B] = [A^*]_0 \frac{k_2}{k_3 - k_1}(e^{-k_1 t} - e^{-k_3 t}) \approx \sqrt{LDL_2}$$

$$LDL_{tot} = [A^*]_0\left(e^{-k_1 t} + m[A^*]_0\left\{\frac{k_2}{k_3 - k_1}(e^{-k_1 t} - e^{-k_3 t})\right\}^2\right)$$

with m = relative luminescence quantum efficiency.

Scheme I. Minimum model which crudely explains the crude shape of the long-term delayed luminescence kinetics, including the luminescent intermediate (top). The only light reaction is the excitation of some component A to A* (for details, see text). The solution of the differential equation (bottom) is visualized in Fig. 4

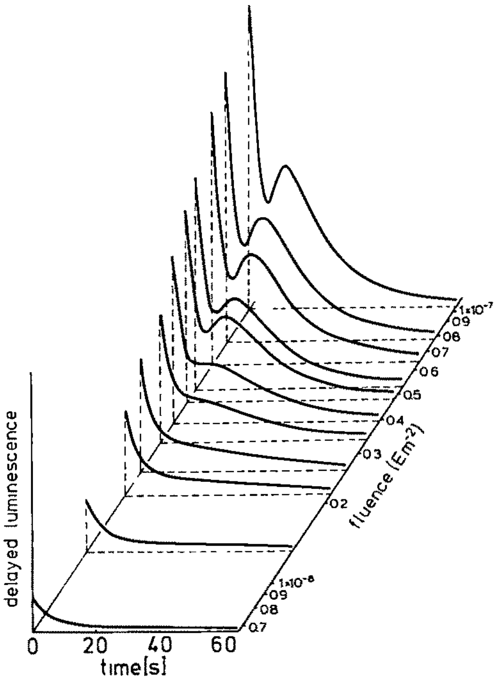

Fig 1 Kinetics of long-term delayed luminescence as function of the fluence of a 1 s exciting light pulse of 721 nm. Light emission was monitored at 712 nm. At increasing fluence rates a luminescing intermediate builds up after approx 10 s.

pulse is shown in Figs. 1 and 2. At defined 'medium' intensities, and with light emission monitored at 712 nm and excitation at 721 nm (Fig. 1) or 694 nm (Fig. 2), after about 10 s a long term luminescent intermediate is observed. When 694 nm exciting light is used, the intermediate appears to be less pronounced compared to 721 nm, and fades out at higher fluence rates (Fig. 2). Depending on the conditions used, the long-term delayed luminescence signal decays more or less rapidly to zero after a specific period of time.

In order to measure a crude 'action spectrum' for the generation of this intermediate, we adjusted the intensity of the exciting light at various wavelengths to generate the same initial height of the long-term delayed luminescence signal (corresponding to approx. 10^{-7} $E \cdot m^{-2}$; Fig. 3. Clearly – at the light intensities chosen – the intermediate only developes when long-term delayed luminescence is excited between 700 and 730 nm, with a maximum at 720 nm; blue light turned out to be inactive at any light intensity. At higher intensities of red light the intermediate can still be seen using exciting light from a slightly wider wavelength range (extension, approx. ±10 nm).

In Scheme I we propose the minimum model, which crudely explains the shape of the kinetics, including the intermediate. Some species 'A' are excited to 'A*', which emit LDL_1. A*, in turn, decays to a non-luminescing species 'C' with a reaction constant k_1, and to a species 'B' with a reaction constant k_2. Subsequently, 'B' undergoes a bimolecular reaction, thereby generating LDL_2, and finally decays with a reaction constant k_3 towards another, nonluminescent product 'D'. This bimolecular reaction turned out to be an indispensible part of the model, and cannot be re-

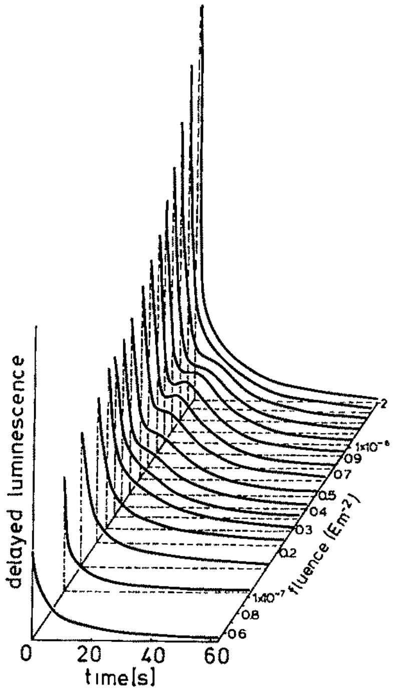

Fig 2. Kinetics of long-term delayed luminescence as function of the fluence of a 1 s exciting light pulse of 694 nm. Light emission was monitored at 712 m. Approx 10 s after the pulse medium fluence rates will generate some intermediate species. With higher fluence rates the intermediate fades away.

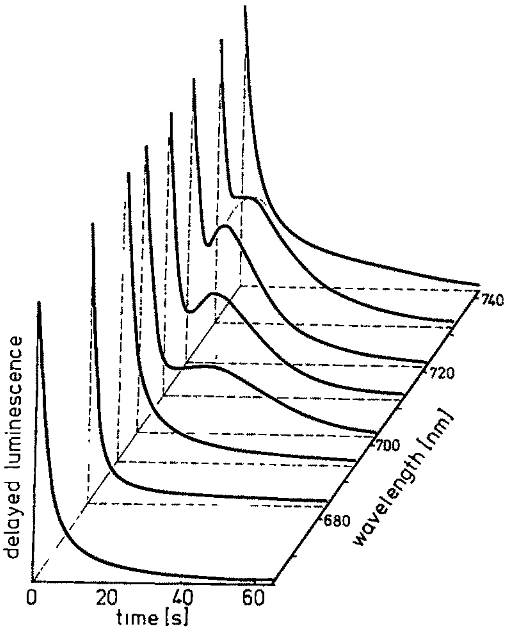

Fig. 3 Kinetics of long-term delayed luminescence as function of wavelength of the exciting light pulse of 1 s producing the same initial quantum emission (approx 10^{-7} E·m^{-2}). The dashed line indicates the crude action spectrum for the production of fluorescing intermediate with a maximum around 720 nm

placed by a monomolecular one. According to their small quantum efficiencies, long-term delayed luminescence reactions (empty arrows in Scheme I) do not significantly consume the substrates A* and B which simplifies the proposed scheme. Long-term delayed luminescence either originates in A* and B themselves, or is generated by energy transfer from these species towards pigment molecules with the proper spectral emission characteristics exhibited by Figs. 7 and 8.

The solution of the corresponding differential equation is given in Scheme I and visualized in Fig. 4. The parameter '*m*' defines the contribution of LDL_2 to the total signal LDL_{tot} and can be defined as the 'relative luminescence efficiency'. The course of the actual kinetics is essentially fitted by this model, as the comparison with the measurement shows (dotted line, taken from Fig. 1). In addition, the model explains the decrease of the intermediate long-term delayed luminescence species with decreasing fluence rates of the ex-

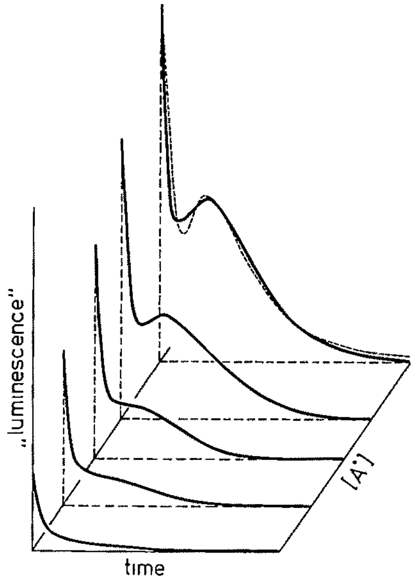

Fig. 4 Visualization of Scheme I: the minimum model which crudely explains the shape of the kinetics of long-term delayed luminescence. It also explains the fact that with lower 'intensities' of the exciting light, i e., with decreasing A_0^*, the intermediate fades out.

citing light; the fluence of the exciting light is mimicked by varying the concentration of 'A_0^*' (all other parameters are kept constant). The curve was fitted with the help of a microcomputer (Commodore, model 8032). For this calculation no attempt was made to develope an automatic parameter-search program, which probably would result in a more satisfying fit of the kinetics.

The semilogarithmic plot (not shown) of the long-term delayed luminescence kinetics of *Scenedesmus*, excited with 421 nm light where no intermediate is build up, is complex and does not allow any further interpretation. It can neither be fitted by a first- or second-order kinetic, nor by a composition of two individual first-order kinetics, indicative of the involvement of several pigments or pigment systems in long-term delayed luminescence. This implication was further clarified by determining a true action spectrum for long-term delayed luminescence.

Following standard procedure, we first measured a series of fluence-response curves (Fig. 5, covering more than five orders of fluence. They do not run in a strictly parallel manner, i.e., there are either several photoreceptors and/or screening pigments involved. The action spectra deduced for three different responses specified by the intersection of the fluence response curves with the horizontal lines 'a', 'b' or 'c' (Fig. 5) are given in Fig. 6, bottom; no essential differences are established. With the irradiation system utilized, no saturation of the signal was achieved at any wavelength. Due to these limitations at higher responses the spectra are incomplete (Fig. 6, bottom, b and c). For comparison, the absorption spectrum of *Scenedesmus* cells, including the 4th derivative in order to increase wavelength resolution, is depicted in Fig. 6, top, and the corresponding excitation spectrum of prompt fluorescence in Fig. 6, middle. Prompt fluorescence is essentially emitted by Photosystem II, in full agreement with the general assumption. Peaks in the blue and red part of this spectrum can readily identified by the 4th derivative of the absorption spectrum (Fig. 6, top), at least involving two Chl a species with Soret-bands at 444 and 479 nm.

The action spectrum of long-term delayed luminescence (Fig. 6, bottom) consists of a peak in the Soret-region between 400 and 430 nm (partly coincident with the peak at 413 nm in the fourth derivative of the absorption spectrum), a massive contribution by some ultraviolet-absorbing com-

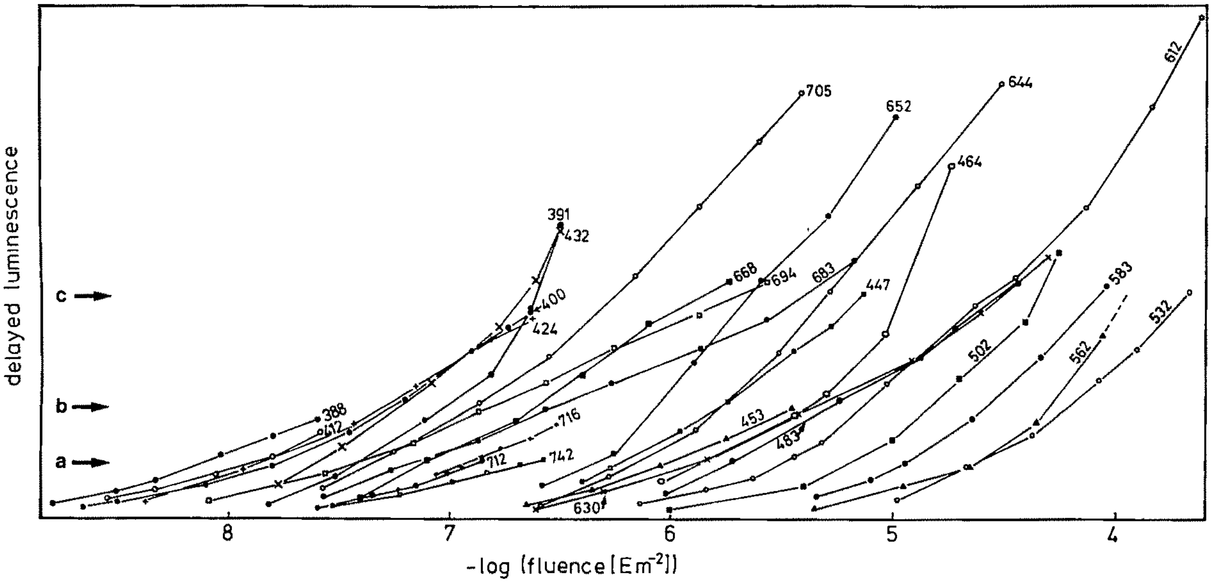

Fig. 5 Fluence-response curves of the initial quantum output of long-term delayed luminescence. More than five order of fluence are covered with the set-up used. Based on three different responses marked 'a', 'b' and 'c' true action spectra for the induction of long-term delayed luminescence are calculated and shown in Fig. 6, bottom

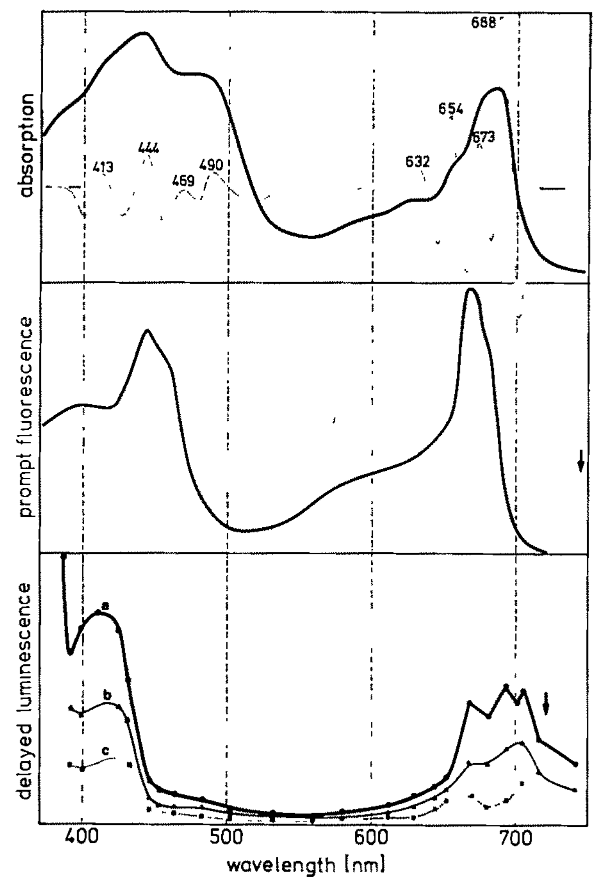

Fig 6. Top: absorption spectra of wild-type *Scenedesmus o.* Total extinction is approx. $A = 1$ The fourth derivative (dotted line) was taken with $dx = 3.0$, 3.1, 3.2, and 3.3 nm (Ref. 21); wavelengths indicated are based upon calibration with argon lines Middle: corrected excitation spectrum of prompt fluorescence The measurement has been performed under steady-state conditions. Excitation wavelength: slit width, 5 nm, emission wavelength, 750 nm; slit width, 15 nm. Bottom: action spectra derived from the fluence response curves in Fig. 5 as based upon three different responses ('a', 'b', 'c').

ponent(s), and a relatively broad peak in the far-red region. This, again, reflects the involvement of several pigments, particularly the 'long-wavelength antenna' of PS I (fluorescence emission at 725 nm; Ref. 20). To summarize, excitation spectra of prompt fluorescence and long-term delayed luminescence are significantly different, suggesting quite distinctive molecular species and mechanisms involved in these two processes. Based upon identical optical properties of the (macro) environment (range corresponding to the optical wavelength of approx. 700 nm) of the pigments or pigment-systems involved in these processes, trivial optical reasons such as scattering, screening or selfabsorption cannot account for the observed differences. This, again, suggests a different molecular origin of prompt fluorescence and long-term delayed luminescence: long-term delayed luminescence does not plainly represent the reversal of the initial steps of light-induced charge separation in Photosystem II. Kinetics and spectral extension of long-term delayed luminescence into the far-red region suggest the (additional) involvement of components generally attributed to PS I.

Experiments performed by other workers emphasize the diversity of pigments giving rise to prompt and delayed light emission: pronounced variations of fluorescence may occur without corresponding changes of delayed fluorescence [23]. Prompt fluorescence is quenched by carotenoids [18], whereas delayed fluorescence is not affected [19]. Since excitation produced by charge recombination always starts out from the reaction center(s), the transfer of excitation energy to the reaction center chlorophyll may be significantly faster – and therefore the predominant reaction to occur – than to the antenna chlorophylls. Thus, Amesz and Gorkom [3] hypothesized in their review "that delayed luminescence may originate largely from chlorophyll molecules in the vicinity of the reaction center" (of PS I and PS II, Ref. 4), whereas prompt fluorescence is known to originate in the bulk chlorophylls mainly associated with PS II. This would explain the distinct reactivities in response to various exogenous parameters, and long-term delayed luminescence might offer itself as a sensitive and specific probe of reaction-center activity.

The next experiments focussed on the emission spectrum of long-term delayed luminescence. We monitored the emission spectrum based upon the initial height (i.e., the rate of quantum emission) of the long-term delayed luminescence kinetics. As before, luminescence was excited for 1 s with 412 nm light of 10^{-8} $E \cdot m^{-2} \cdot s^{-1}$, where no luminescing intermediate developes. In order to select a particular emission wavelength, long-term delayed luminescence was monitored with the proper interference filter sandwiched between petridishsample and photomultiplier cathode. Taking into account the transmittance of the interference filter used, we obtained the corrected emission spectrum depicted in Fig. 7B (dots). In some consistency with the excitation spectrum in the red, its extraordinary width also suggests the involvement of diverse luminescing species.

We cannot necessarily expect a direct correlation of excitation and emission spectra of long-term delayed luminescence typical for prompt fluorescence (however, we cannot exclude it either). Excitation and emission spectra of long-term delayed luminescence might be due to different molecular species. In order to analyze the composition of the emission spectrum, we first investigated the emission spectrum of prompt fluorescence of *Scenedesmus* on the basis of individual Lorentz-shaped bands, adopting the known wavelengths of maximal fluorescence of Photosystem II and I (685 and 725 nm, Fig. 7A; the choice of free wavelength positions of all four individual components would introduce ambiguity; i.e., various different parameter sets would fit the measured emission spectrum of long-term delayed luminescence).

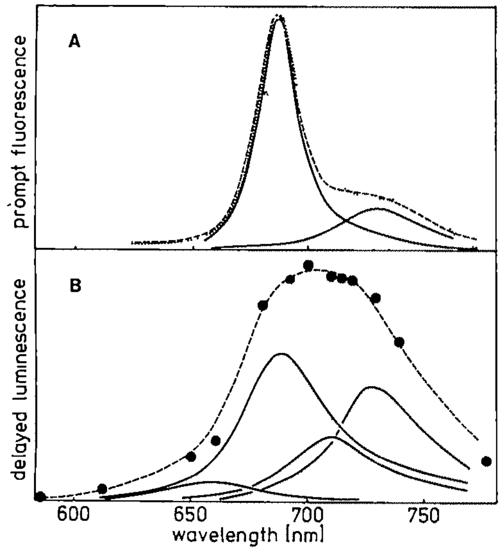

Fig 7. (A) Dotted line: measured emission spectrum of prompt fluorescence. Dashed line: Calculated spectrum composed of two individual Lorentz-shaped bands at 685 and 775 nm (solid lines) (B) Dots corrected emission spectrum of the initial components of delayed luminescence (LDL_1) This spectrum was fitted (dashed line) by superposition of varios Lorentz-shaped bands (solid lines)

Again, the calculations were performed with a CBM 8032 personal computer, utilizing a home-made parameter search program in this case. Two additional components with peaks occurring at 712 and 660 nm were introduced in order to explain the measured long-term delayed luminescence emission spectrum. After proper adjustment of all parameters defining width, height and wavelength of the individual components we obtained a reasonable good fit (Fig. 7B), comprising pigments of PS I and PS II.

As mentioned above, when measuring long-term delayed luminescence kinetics we noticed a significant change of the long-term delayed luminescence intermediate with the emission wavelength. Therefore, we measured the long-term delayed luminescence kinetics with respect to the intermediate long-term delayed luminescence component and obtained the spectrum depicted in Fig. 8. As a measure for the intermediate we utilized the ratio of sections a and b as indicated in Fig. 8. Based on known spectral properties, it appears to be chiefly related to the pigment system of PS I rather than PS II [20]. However, the molecular identity of the intermediate remains obscure, except that it undergoes a bimolecular reaction, as pointed out above. Under no circumstances we were able to observe the intermediate without the initial long-term delayed luminescence signal taking place. In consistency with Scheme I, a molecular species A* giving rise to emission of LDL_1, is the indispensable prerequisite for LDL_2 to occur. This interpretation is supported by experiments with the mutant C6E of *Scenedesmus*, which only contains active PS I: it does not show any long-term delayed luminescence signal. Only further experiments will allow a definite mutual assignment of spectra, pigments and mechanisms.

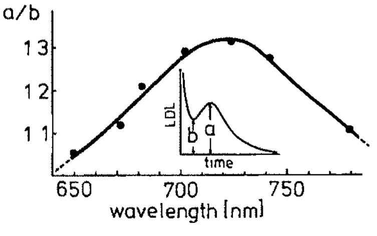

Fig. 8. Dependence of the intermediate (assayed by the *a/b* ratio as indicated) on the wavelength of emission. A maximal 'hump' is observed between 700 and 750 nm.

TABLE I

APPROXIMATE WAVELENGTHS OR WAVELENGTH RANGES OF EXCITATION AND EMISSION OF PROMPT FLUORESCENCE, AND OF THE FAST AND INTERMEDIATE COMPONENTS OF DELAYED LUMINESCENCE ($LDL_{1,2}$)

	Excitation	Emission
Prompt fluorescence	444, 665	685, 725
LDL_1	400–430, 650–740	665–750
LDL_2	690–740	675–770

The approximate wavelengths or wavelength ranges of both excitation and emission spectra of prompt fluorescence, and of the initial and intermediate components of long-term delayed luminescence are listed in Table I.

We are now investigating long-term delayed luminescence of *Scenedesmus* as a function of various parameters such as temperature, age during the diurnal life cycle, exogeneous pH, various herbicides, and deficiencies of essential trace elements and components. Preliminary results suggest that virtually all these parameters are capable of influencing shape and extent of long-term delayed luminescence kinetics. Particularly, so-called 'state transitions' of the photosystems appear to exhibit a strong impact. Utilizing different mutants of *Scenedesmus* with specific defects in their photosynthetic apparatus, we are studying the (light-dependent) development of the potency of exhibiting long-term delayed luminescence.

Acknowledgement

This work was supported by the Deutsche Forschungsgemeinschaft (SFB 305).

References

1 Strehler, B L. and Arnold, W. (1951) J Gen Physiol. 34, 809–820

2 Lavorel, J. (1975) in Bioenergetics of Photosynthesis (Govindjee, R ed.), pp 225–314, Academic Press, New York, San Francisco, London

3 Amesz, J. and Gorkom, H J. v. (1978) Ann. Rev. Plant Physiol. 29, 47–66

4 Malkin, S (1977) in Primary Processes of Photosynthesis., (Barber, J., ed.), pp. 351–430, North Holland Biomedical Press

5 Schmidt, W. (1985) Photobiochem Photobiophys. 9, 89–97

6 Inoue, Y and Shibata K. (1982) in Photosynthesis, Vol. 1 (Govindjee, ed), pp. 507–533, Academic Press, New York, San Francisco, London

7 Robinson, H H. and Crofts, A.R. (1983) FEBS Letters 153, 221–226

8 Rutherford, A W and Inoue, Y (1984) FEBS Letters 165, 163–170

9 Haug, A., Jaquet, D.D and Bell, H C. (1972) Biochim Biophys. Acta 283, 92–99

10 Clayton, R (1969) Biophys. J 9, 60–76

11 Björn, L.O. (1971) Photochem Photobiol 13, 5–20

12 Goedheer, J.C. (1963) Biochim. Biophys. Acta 66, 61–71

13 Sane, P.V., Desai, T.S. and Takake, V G. (1980) Z. Naturforsch 35c, 289–292

14 Senger, H. and Bishop, N.I (1972) Proc 2nd Int. Cong. on Photosynthesis Res , Vol. 1, (Forti G., Avron M , Melandri A., eds.), pp 678–687, W. Junk, The Hague

15 Senger, H., Pfau, J. and Werthmüller, K. (1972) in Methods of Cell Physiology, Vol V., (San Pietro, A., ed.), pp. 301–323, Academic Press, New York and London

16 Schmidt, W. (1982) Anal. Biochem. 125, 162–167

17 Shrophire, Jr., W. (1972) in Phytochrome (Mitrakos, K., Shrophire, Jr , W eds), pp. 161–181, Academic Press, London

18 Duysens, L N.M., Van der Schatte Olivier, T.E. and Den Haan G.A (1972) Int. Congr. Photobiol , 5th, Bochum, abstract 277

19 Van Best, J A. and Duysens, L.N.M (1977) Biochim Biophys. Acta 459: 187–206

20 Brinkmann, G. and Senger, H. (1981) in Photosynthesis, Vol. 3 (Akoyunoglou, G., ed.), pp. 337–346, Balaban Int Science Services, Philadelphia

21 Butler, W.L. and Hopkins, D.W. (1970) Photochem Photobiol. 12, 439–450

22 Velthuys, B.R. and J. Amesz (1973) Biochim Biophys. Acta 225, 126–137

23 Den Haan, G A. (1977) Ph.D thesis, University of Leiden

Biochimica et Biophysica Acta 890 (1987) 23–31
Elsevier

BBA 42159

pH dependence of oxygen evolution and reduction kinetics of photooxidized chlorophyll a_{II} (P-680) in Photosystem II particles from *Synechococcus* sp.

E. Schlodder and B. Meyer

Max-Volmer-Institut für Biophysikalische und Physikalische Chemie, Technische Universität Berlin, 1000 Berlin 12 (F R G.)

(Received 24 July 1986)

Key words: Oxygen evolution; Photosystem II, pH effect; P-680; (*Synechococcus*)

The oxygen flash yield and the kinetics of Chl a_{II}^{+} (P-680^{+}) reduction have been measured under repetitive excitation as a function of pH between pH 4.0 and pH 9.0 in oxygen-evolving PS II particles from *Synechococcus* sp. (i) The optimum of oxygen yield is observed between pH 6.5 and pH 7.5. The inhibition in the acidic pH region is reversible and can be described by a monoprotic binding site with a p*K* value of about 4.5. In the alkaline pH region the inhibition is half maximal at pH 8.3 and might be described by the titration of three binding sites or more. The loss of oxygen evolution at pH 9.0 is caused by reversible inhibition and irreversible inactivation. (ii) Between pH 4.0 and pH 7.5 the fraction of Chl a_{II}^{+} decaying in the nanosecond time range and the oxygen yield follow the same pH dependence. (iii) Both in Photosystem II centers reversibly inhibited at low pH and in Photosystem II centers inactivated at high pH, Chl a_{II}^{+} is reduced by a donor Z, different from the normal immediate donor D_1 or a modified state of D_1, and, in part, by back reaction. (iv) Below pH 5.0, the decay in the nanosecond range can be explained by the existence of two phases with $t_{1/2} \approx 42$ ns and $t_{1/2} \approx 300$ ns (ratio of amplitudes, 1.3:1). A reduction phase with $t_{1/2} = 20$ ns that is the major phase around the pH optimum is not observed below pH 5.0.

Introduction

Light-induced charge separation between a specialized chlorophyll *a* molecule, Chl a_{II} (P-680) [1,2] and the first stable acceptor, a special plastoquinone, Q_A (X-320) [3,4], starts the reaction sequence leading to water oxidation. In order to oxidize 2 H_2O into 1 O_2 and 4 H^+, the stepwise accumulation of four oxidizing equivalents in the O_2-evolving complex by four consecutive photooxidations of Chl a_{II} is required. Thereby the O_2-evolving complex passes through four different redox states (the so-called S-states, S_0–S_3) before oxygen is released during the transition $S_3 \rightarrow S_0$ [5–7]. Protons are released with a pattern (1, 0, 1, 2) during the transitions $S_0 \rightarrow S_1$, $S_1 \rightarrow S_2$, $S_2 \rightarrow S_3$ and $S_3 \rightarrow S_0$, respectively [8–11].

Chl a_{II}^{+} reduction kinetics depend on the oxidation state of the O_2-evolving complex [12]. The phase with $t_{1/2} \approx 20$ ns is associated with states S_0 and S_1, respectively. Slower biphasic reduction

---

Abbreviations: Q_A, primary quinone acceptor of Photosystem II; Chl, chlorophyll; Mes, 4-morpholineethanesulphonic acid; PS I, Photosystem I; PS II, Photosystem II; D_1, immediate electron donor to Chl a_{II}^{+}; D_2, electron carrier between D_1 and the oxygen-evolving complex; Tricine, *N*-[2-hydroxy-1,1-bis(hydroxymethyl)ethyl]glycine; Z, electron donor to Chl a_{II}^{+} after inhibition of O_2 evolution characterized by EPR Signal $\mathrm{II_f}$; SB 12, *N*-dodecyl-*N,N*-dimethyl-3-ammonio-1-propanesulfonate; Mops, 4-morpholinepropanesulphonic acid; Hepes, 4-(2-hydroxyethyl)-1-piperazineethanesulphonic acid.

Correspondence: E Schlodder, Max-Volmer-Institut für Biophysikalische und Physikalische Chemie, Technische Universität Berlin, Sekr. PC 14, Strasse des 17. Juni 135, D-1000 Berlin 12, F.R.G.

0005-2728/87/$03.50 © 1987 Elsevier Science Publishers B.V (Biomedical Division)

with half-life times of 50 and 260 ns occurs in state S_2 as well as S_3 [12]. The retardation of electron transfer to Chl a_{II}^+ in states S_2 and S_3 was explained by Coulomb attraction due to a positive excess charge located in the O_2-evolving complex in states S_2 and S_3 [12]. The formation of excess charges in S_2 and S_3 was also shown by electrochromic absorption changes [13]. In the nanosecond time range the multi-phasic reduction kinetics of Chl a_{II}^+ under repetitive excitation could be explained by a superposition of the S-state-dependent electron-transfer times. They were explained by the existence of three nanosecond phases with half-life times of 20, 50 and 260 ns (together about 85% of the total amplitude) [14,15]. Minor phases (about 15%) in the microsecond range were observed under repetitive excitation [15]. The amplitude of a 35-μs phase varies as a function of the S-states, being maximal in states S_2 and S_3 [15].

The experiments summarized so far were performed around the pH optimum of oxygen evolutin (pH 6–8). A pH dependence of the amplitude of microsecond decay phases has been observed in former measurements of the absorption changes in thylakoids around 690 nm [16].

Because of the biphasic nanosecond reduction kinetics of Chl a_{II}^+ in the S_2 and S_3 state we proposed the existence of two intermediate carriers, D_1 and D_2, between Chl a_{II} and the O_2-evolving complex [12]. The direct donor to Chl a_{II}^+, D_1, has not yet been identified. On the basis of EPR [17,18] and optical spectroscopy [19–21] D_2 has been proposed to be a plastoquinol. D_2^+ is reduced by manganese bound in the O_2-evolving complex. The kinetics of D_2^+ reduction [22] and manganese oxidation [23] are both dependent on the S-states and coincide as far as known.

After irreversible inhibition of oxygen evolution, Chl a_{II}^+ is reduced by a component giving rise to EPR Signal II_f in the oxidized form [24]. Since it is not clear if this component is a modified state of D_1 or D_2 or an alternative donor, we call it Z.

Several studies on the pH-dependence of oxygen evolution have been reported [16,25–28]. Some of these studies, however, may not be entirely convincing, since the measured O_2-evolving rate in continuous light may also be affected by pH effects on the acceptor side of PS II (see, e.g., Refs. 26 and 27). In other studies carried out with chloroplasts the internal thylakoid pH which controls the reactions on the donor side of PS II will be different from that of the external medium [16]. The analysis of the results requires therefore reliable determination of the internal pH. The pH-dependent inhibition of the oxygen evolution has also been investigated by fluorescence measurements [25,29–31], EPR studies [28,33–36], measurements of the release of both Mn^{2+} and peripheral proteins [28,33,34], and thermoluminescence studies [34]. It was found that the irreversible inactivation at alkaline pH (pH > 8) is accompanied by the loss of Mn^{2+} [32,33], the release of peripheral proteins (18, 24 and 33 kDa) [34–36], the appearance of EPR Signal II_f [28,33], and the loss of the light-induced multi-line and $g = 4.1$ EPR signal which were attributed to the S_2 state [28]. At acidic pH (pH < 5) release of Mn^{2+} and increase of the EPR Signal II_f amplitude have also been observed [29].

In this work we have measured the reduction kinetics of Chl a_{II}^+ under repetitive flash excitation as a function of pH in the nano- to millisecond time range. These measurements were carried out in connection with measurements of O_2 evolution under repetitive flash light. All experiments were performed with PS II particles from *Synechococcus* sp. [37].

Materials and Methods

Oxygen-evolving PS II particles were prepared from the thermophilic cyanobacterium *Synechococcus* sp. as described by Schatz and Witt [37]. The PS II particles were finally obtained in solution A (80% v/v), glycerol (20% v/v) and about 0.3% (w/w) of the detergent SB 12. Solution A contained $3 \cdot 10^{-3}$ M Mes-NaOH (pH 6)/$1 \cdot 10^{-2}$ M $MgCl_2$/$2 \cdot 10^{-3}$ M KH_2PO_4/0.5 M mannitol. The chlorophyll content was about 10^{-4} M in the stock suspension. It was stored at −80°C before further use. The PS II particles are characterized by a PS II/PS I ratio of about 50 and by an O_2-flash yield of $(2.5–3.6) \cdot 10^{-3}$ O_2 per Chl and flash corresponding to 70–100 Chl per Chl a_{II} active in O_2 evolution. Absorption changes at 824 nm were measured as described previously [12,15]. For measurements in the nanosecond range, the detection system (photodiode FND-100 from EG &G; amplifier TVV 123 from Telemeter; Transient recorder with 2 ns/point, Biomation 6500; signal averager, Nicolet 1170) had an electrical bandwidth of 100 Hz–100 MHz. In the microsecond and millisecond range, the measuring light was monitored by a photodiode (FND 100 from EG&G) loaded with 1 kΩ. The signals were further amplified (Tektronix AM 502) and digitized by a Nicolet 1170 with plug-in Model 174. The electrical bandwidth was 2 Hz to 1 MHz. The samples were excited by 3 ns (FWHM) laser flashes at 532 nm from a frequency-doubled Nd/YAG laser (YG 441 from Quantel). The energy per flash corresponds to approx. 80% saturation. Most signals were transmitted to an Apple II microcomputer and fitted by means of least-squares curve-fitting programs as described previously [12].

Flash-induced oxygen evolution was measured with a zirconia oxygen sensor (Programm-electronic AG, Dornach, Switzerland). Purified N_2 gas (50 ppb O_2) was used as a carrier gas. Oxygen produced in the reaction cuvette was swept out by the carrier gas and transported to the zirconium dioxide high-temperature oxygen electrode. The oxygen content of the gas stream was recorded with a microcomputer (Commodore 64) and the peak due to oxygen evolution was integrated to give the absolute amount of oxygen produced. Calibration of the apparatus was achieved by injecting 50 µl of air-saturated water. The samples were illuminated with saturating Xe flashes of approx. 20 µs (FWHM). The repetition rate was 1 Hz. For comparison, flash-induced oxygen evolution was measured with a Clark-type electrode (Bachofer).

The reaction medium contained solution B/approx. 2% (v/v) glycerol/approx. 0.03% (w/w) SB 12/$2 \cdot 10^{-4}$ M phenyl-*p*-benzoquinone/$2 \cdot 10^{-3}$ M $K_3Fe(CN)_6$/$1 \cdot 10^{-5}$ M chlorophyll. 3 ml of the reaction medium were divided into two parts for measurements of absorption changes and oxygen evolution. Solution B contained $5 \cdot 10^{-2}$ M buffer/10^{-2} M $MgCl_2$/$2 \cdot 10^{-3}$ M KH_2PO_4/0.5 M mannitol. The following buffers were used:

at pH 4.0 glycylglycine (p*K* 3.1)
at pH 4.0–5.0 succinic acid (pK_1 4.19, pK_2 5.57)
at pH 5.5–6.5 Mes (p*K* 6.15)
at pH 6.5–7.0 Mops (p*K* 7.2)
at pH 7.0–7.5 Hepes (p*K* 7.55)
at pH 7.5–9.0 Tricine (p*K* 8.15)

The buffers were adjusted to the appropriate pH by addition of NaOH or HCl.

Reversibility experiments were performed as follows: PS II particles were stored for 10 min in the dark at pH 4.0 or pH 9.0, respectively. Electron acceptors were added to the final concentrations of $2 \cdot 10^{-3}$ M $K_3Fe(CN)_6$ and $2 \cdot 10^{-4}$ M phenyl-*p*-benzoquinone. In some experiments the sample was additionally illuminated with 500 flashes. By addition of solution B (pH 8.5 or pH 6.0, respectively) the pH values of the samples were adjusted to pH 7.0. Final concnetrations of chlorophyll and electron acceptors were the same as in the reaction medium.

Results

Fig. 1 shows the time course of the 824 nm absorption changes in O_2-evolving PS II particles from *Synechococcus* sp. at different pH values. The absorption changes were attributed to photooxidation and re-reduction of Chl a_{II}. The small rapid transient ($t_{1/2} \leq 5$ ns corresponding to the instrumental response time) is probably caused by the phycobilin pigments which normally contaminate these preparations. The amplitude of Chl a_{II}^{+} decaying in the nanosecond time range ($t_{1/2} <$ 1 µs) gets significantly smaller when the pH is lowered (Fig. 1a). We analyzed the decay in the 10–1500 ns time range by two-exponential phases which are sufficient for a good fit. Although the decay in the nanosecond range is a superposition of three nanosecond phases as derived from single flash experiments already for a two-exponential fit the deviations between measured signal and fitting function are not well above the noise. The slow phases decaying in the micro- and millsecond range were taken into account by a slightly declining straight line. The results of the fits of the signals in Fig. 1a are given in Table I.

On the average (taking into account differences in preparations, reaction media and sets of experiments) an adaptation of the decay kinetics between pH 8.0 and pH 6.0 by two-exponential phases yielded the following parameters. $t_{1/2} = 23 \pm 7$ ns, $t_{1/2} = 220 \pm 50$ ns, $a_1/a_2 = 2.5 \pm 0.8$; $a_3 = 0.15$ to 0.4. Between pH 4.5 and pH 4.0 the

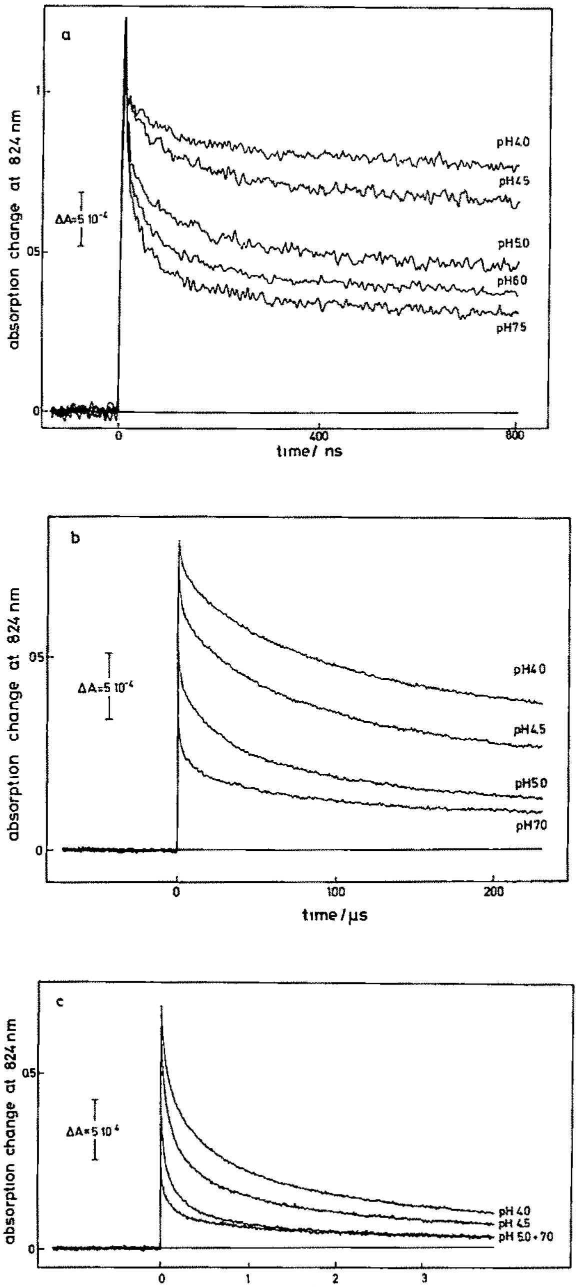

Fig 1. Time-course of the absorption changes at 824 nm in O_2-evolving PS II paticles from *Synechococcus* sp. at different pH values. Excitation by approx. 80% saturating laser flashes (3 ns FWHM; 532 nm; repetition rate, 1 Hz). 10^{-5} M Chl/$2\cdot10^{-3}$ M $K_3Fe(CN)_6$ and $2\cdot10^{-4}$ M phenyl-*p*-benzoquinone as electron acceptors. (a) Time-course digitized with 2 ns/point, electrical bandwidth 100 Hz–100 MHz, 1024 averages; (b) time-course digitized with 300 ns/point, electrical bandwidth 2 Hz–1 MHz, 256 averages; (c) time-course digitized with 5 μs/point, electrical bandwidth 2 Hz–1 MHz, 256 averages.

TABLE I

RESULTS OF THE TWO-EXPONENTIAL FITS FOR THE SIGNALS IN FIG. 1a

pH	$t_{1/2}$ (ns)	a_1	$t_{1/2}$ (ns)	a_2	a_3
7.5	17	0.53	180	0.16	0.31
6.0	20	0.45	200	0.16	0.39
5.0	19	0.35	210	0.20	0.45
4.5	42	0.20	250	0.14	0.66
4.0	44	0.13	340	0.10	0.77

$t_{1/2}$, half-life time, a_i (i = 1–3), relative amplitudes, a_3 is the initial amplitude of slow phases decaying in the micro- and millisecond range, which were taken into account by a slightly declining straight line.

result of the fit is significantly different: $t_{1/2} = 42 \pm 6$ ns, $t_{1/2} = 300 \pm 50$ ns and $a_1/a_2 = 1.3 \pm 0.5$.

The most striking feature is the decrease of the fraction of Chl a_{II}^+ decaying in the nanosecond time range ($a_1 + a_2$) by lowering of the pH from 6.0 to 4.0 (see Table I). The acidification slows down the reduction of an increasing fraction of Chl a_{II}^+ (a_3) into the micro- and millisecond range. Fig. 1b and c shows the time-course of the 824 nm absorption changes at different pH values on a microsecond (Fig. 1b) and millisecond (Fig. 1c) time scale. It is observed that the lower the pH, the slower Chl a_{II}^+ is reduced. For a rough analysis of the pH-dependent decay in the micro- to millisecond range, the fractions of Chl a_{II}^+ decaying between 1.5 μs and 200 μs and between 200 μs and 3 ms are depicted in Fig. 2 as a function of pH. The increase of the fraction decaying between 1.5 μs and 200 μs below pH 6 is mainly caused by a reduction phase with a half-life time of about 5 μs at pH 6 (not shown) of about 15 μs at pH 5 and of about 30–40 μs at pH 4.5 and 4.0 (see Fig. 1b). Below pH 5.0 the amplitudes of slower reduction phases with half-life times of about 200 μs, 500–700 μs and about 5 ms increase (see Fig. 1c).

In the following we ask for a correlation between the reduction kinetics of Chl a_{II}^+ and the oxygen-evolving activity. The dependence of the O_2-flash yield on the pH is shown in Fig. 3a. The optimum of the oxygen yield is observed between pH 6.5 and pH 7.5. The yield decreases sharply in the alkaline region and is at a half maximum at

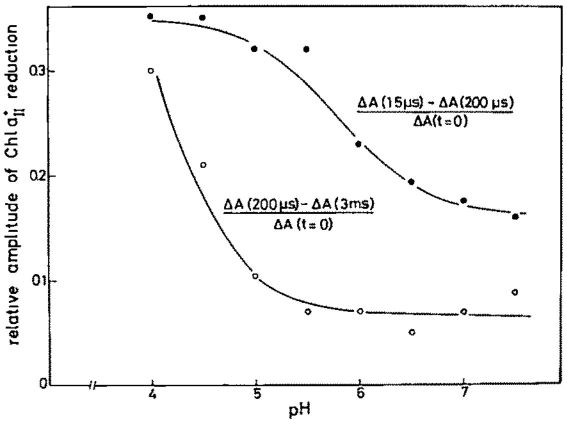

Fig 2. Difference between the relative absorption change at 1.5 μs and 200 μs (●) and between 200 μs and 3 ms (○) as a function of pH. For experimental details see Fig. 1.

pH 8.3. In the acid region, the inhibition is half maximal at pH 4.5. The fraction of Chl a_{II}^+ decaying in the nanosecond time range ($a_1 + a_2$) which was normalized to the result at pH 7.0 is depicted as a function of pH in Fig. 3b. Within the experimental error characterized by the scattering of data in different sets of experiments the O_2 yield and the amplitude of nanosecond decay components of Chl a_{II}^+ follow the same dependence on the pH (for a better comparison the curves drawn in Fig. 3a and b are the same).

At pH 9.0, where O_2 evolution is zero, Chl a_{II}^+ was mainly reduced with a half-life time of about 180 ns (Fig. 4a). It was found that the amplitude of this phase depends on the laser-flash frequency (not shown). With increasing repetition rate the amplitude of the 180-ns pahse decreases and a larger proportion of slower phases ($t_{1/2} \geqslant 200$ μs) was observed. This flash-frequency effect is characteristic of PS II particles in which oxygen evolution is inhibited [38]. Therefore, we measured the reduction of Chl a_{II}^+ in Tris-treated PS II particles from *Synechococcus* sp. At pH 9.0 the same half-life time of 180 ns was observed (Fig. 4b). This indicates that the half-life time of 180 ns observed in untreated PS II particles at pH 9.0 can be attributed to electron donation from donor Z to Chl a_{II}^+. The pH dependence of Chl a_{II}^+ reduction by the donor Z in Tris-treated PS II particles from *Synechococcus* sp. is given in Table II. Above pH 7.5 the nanosecond decay of Chl a_{II}^+ in untreated

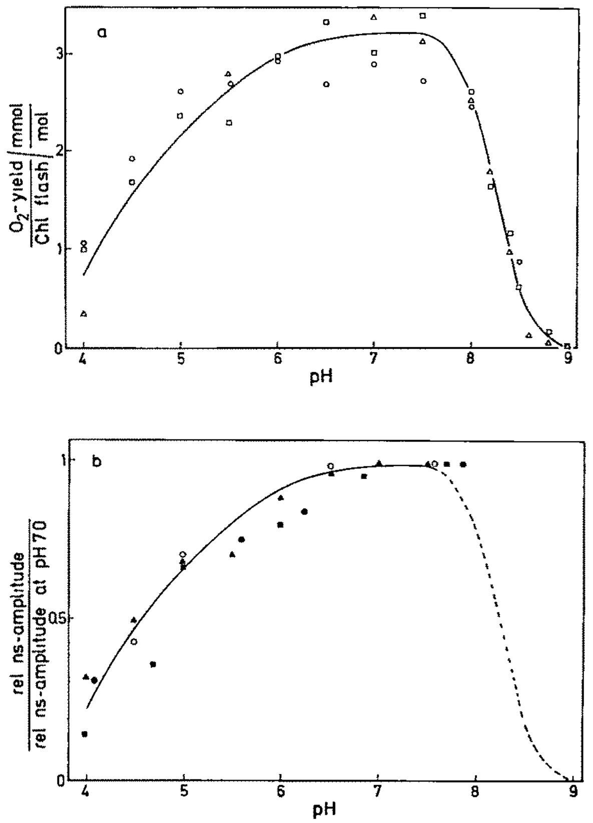

Fig 3. (a) O_2 yield per flash and chlorophyll in dependence on the pH value measured with a zirconia oxygen sensor (□, △, two different sets of experiments) and with a Clark-type electrode (○). Samples were excited by saturating xenon flashes (20 μs FWHM). (b) Fraction of Chl a_{II}^+ decaying with nanosecond half-life times as a function of pH. The data are normalized to the fraction maximum at pH 7.0. The different symbols represent different sets of experiments (conditions as in Fig. 1a). For further details, see text.

PS II particles is presumably a superposition of electron donation by the donor D_1 in centers still active in oxygen evolution and by the donor Z in centers which are inhibited. Therefore, in Fig. 3b data points are not marked in the alkaline pH region above pH 8.0 and the curve is shown as a broken line. Compared to data published for Tris-trated chloroplasts [38] the pH dependence found in PS II particles from *Synechococcus* (see Table II) is more pronounced. The change of the half-life time per pH unit is a factor of 3–3.5 rather than about 2 as observed in spinach chloroplasts [38]. It is remarkable that the half-life time

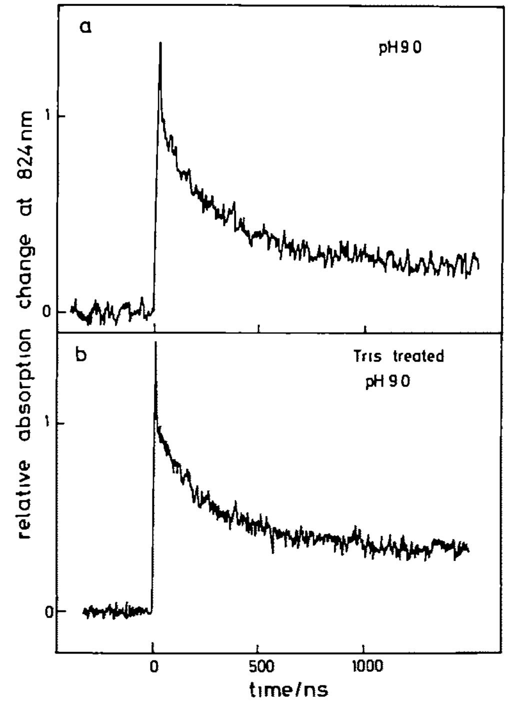

Fig. 4. Time-course of the relative absorption change at 824 nm (a) in untreated PS II particles at pH 9.0 and (b) in Tris-treated PS II particles at pH 9.0. Repetition rate. 0.5 Hz, other conditions as in Fig 1a.

at pH 9.0 is lower by a factor of about 6 in PS II particles from *Synechococcus*.

In the following we asked for the reversibility of the inhibition of oxygen evolution at extreme pH values (see Table III). After the indicated pre-treatment the activity was measured at the pH 7.0. Table III shows that the inhibition of oxygen evolution observed at low pH (Fig. 3a) is reversible. Reversibility of the retardation of Chl a_{II}^{+} reduction by low pH is demonstrated in Fig. 5. The reduction is strongly retarded at pH 4. Returning the sample to pH 7 after incubation at pH 4, the Chl a_{II}^{+} reduction kinetics (see curve b) is nearly the same as in the control experiment (see curve a), where Chl a_{II}^{+} reduction was measured at pH 7.0 without pretreatment.

After incubation at high pH (pH 9.0) in the dark, oxygen yield is restored to only about 65% returning the sample to pH 7.0. Irreversible inactivation is significantly increased if the sample is illuminated at the alkaline pH (see Table III).

TABLE II

PH DEPENDENCE OF THE HALF-LIFE TIME OF CHL a_{II}^{+} REDUCTION BY THE DONOR Z IN TRIS-TREATED PS II PARTICLES FROM *SYNECHOCOCCUS* sp

pH	half-life time
4.5	30 μs
5.5	10 μs
6.5	4 μs
7.5	650 ns
9.0	180 ns
10.0	180 ns

TABLE III

OXYGEN-FLASH YIELD AT pH 7.0 AFTER PRETREATMENT AT pH AS INDICATED

pH	Incubated for 10 min in the dark at pH indicated, measured at pH 7.0	Incubated for 10 min at pH indicated plus illumination with 500 flashes, measured at pH 7.0
7.0	100%	88%
4.0	92%	81%
9.0	65%	28%

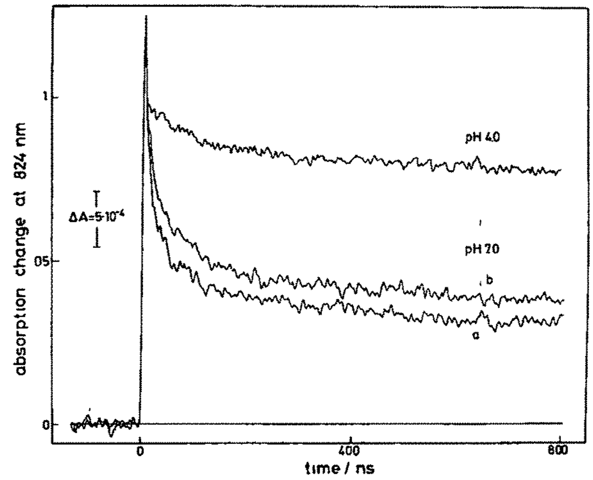

Fig. 5. Time-course of the 824 nm absorption change at pH 4.0, at pH 7.0 after incubation at pH 4.0 (trace b) and at pH 7.0 without pretreatment (trace a) Experimental conditions as in Fig. 1a.

Discussion

In this study the reduction kinetics of photooxidized Chl a_{II} were investigated parallel to the oxygen-flash yield as a function of pH under repetitive excitation. The experiments were performed with isolated O_2-evolving PS II particles from *Synechococcus* sp. in order to insure that the medium pH controls O_2 evoltuion and electron-transfer reactions in PS II directly.

Between pH 6.5 and pH 7.5 the oxygen-flash yield and the fraction of Chl a_{II}^+ decaying in the nanosecond time range is maximal and independent of pH. The inhibition of oxygen evolution observed at pH < 6.5 and pH > 7.5 is accompanied by a drastic change of the Chl a_{II}^+ reduction kientics (see Figs. 1 and 5).

In the acidic pH region the decrease of oxygen evolution is half maximal at pH 4.5. The pH dependence of the inhibition can be roughly described by a monoprotic binding site with a p*K* value of 4.5. Inhibition of oxygen evolution is accompanied by a retardation of Chl a_{II}^+ reduction into the microsecond and millisecond time range. Lowering the pH we observed at first an increase of the Chl a_{II}^+ fraction decaying between 1.5 μs and 200 μs (see Fig. 2). This increase is mainly caused by a reduction phase with a half-life time of about 5 μs at pH 6, of about 15 μs at pH 5, and of about 30–40 μs at pH 4.5 and 4.0. Since the electron donation from Z to Chl a_{II}^+ in Tris-treated PS II particles shows a similar pH dependence of the half-life time (see Table II), we assume that the increase of the fast microsecond phase reflects an increasing fraction of PS II centers, where Chl a_{II}^+ is reduced by Z after inhibition of oxygen evolution. This conclusion is supported by the observation that inhibition of oxygen evolution at low pH is correlated with an increase of the amplitude of EPR Signal II_f [29].

Below pH 5.0 the amplitudes of slower reduction phases with half-life times of about 200 μs, 500–700 μs and about 5 ms increase (see Figs. 2 and 1c). The Chl a_{II}^+ reduction phase with $t_{1/2} \approx$ 200 μs has been attributed to the Chl a_{II}^+ Q_A^- charge recombination [39,40]. In accordance with our results it has been reported that the amplitude of this phase increases significantly in thylakoids below pH_{in} 4.5 [16,39]. The 500–700 μs phase of Chl a_{II}^+ reduction which has also been observed in PS II particles from *Phormidium* [41,42] is presumably also caused by charge recombination. As proposed for PS II particles from chloroplasts, the different half-life times may represent back reactions from different states of inhibited PS II centers (e.g., a faster back reaction from the state Z^+Chl a_{II}^+ $Q_A^-Q_B^-$, a slower back reaction from the state Z Chl a_{II}^+ $Q_A^-Q_B^-$) [43]. The origin of the small reduction phase with a half-life time of about 5 ms (up to 10% at pH 4) is not yet clear.

An influence of acidic pH on the amplitude of decay phases of Chl a_{II}^+ in the microsecond time range has been reported for broken spinach chloroplasts [16]. The authors measured absorption changes at 690 nm with an instrumental response time of about 12 μs. The results were analyzed as a function of pH of the internal thylakoid phase which was estimated in consideration of the light-induced transmembrane pH gradient. The amplitude of a 35 μs phase increased from about 15% to about 50% of the total Chl a_{II}^+ reduction when the pH_{in} was lowered from 5.6 to 4.5 [16]. It has been shown [15] that at pH 7.0 the amplitude of a 35 μs reduction phase depends on the S-states of the oxygen-evolving complex. Therefore, it was suggested that this 35 μs phase (about 10% of the total Chl a_{II}^+ reduction) is connected to water oxidation [15]. Our finding that at low pH the normal electron transfer at the donor side is interrupted and electron donation from Z occurs, makes it probable that the large amplitude of Chl a_{II}^+ reduction with $t_{1/2} = 35$ μs (see Fig. 1b and Ref. 16) at pH 4.5 is mainly due to PS II centers which are inactive in oxygen evolution.

The remaining ns decay of Chl a_{II}^+ at low pH shows significantly different kinetics, compared to those around pH 7.0 (see Fig. 1 and Table I). Under repetitive excitation, the reduction kinetics in the nanosecond time range have been adapted by two phases with half-life times of 42 ns (≈ 20%) and 250 ns (≈ 14%) at pH 4.5 and 44 ns (≈ 13%) and 340 ns (≈ 10%) at pH 4.0. A 20 ns-phase that was associated with states S_0 and S_1 based on single flash experiments at pH 6.5 (12) is not observed. Instead, the kinetics under repetitive excitation at low pH (pH < 4.5) are similar to the slower biphasic kinetics ($t_{1/2} \approx 50$ ns and ≈ 300 ns) which have been linked to states S_2 and S_3

[12]. The retardation of the electron transfer in states S_2 and S_3 has been explained by Coulomb attraction due to a positive excess charge located in the oxygen-evolving complex in states S_2 and S_3 [12]. The absence of a 20 ns phase that is the major phase around the pH optimum indicates that below pH 5.0 a retardation of the electron donation to Chl a_{II}^{+} occurs. This retardation might be explained by the protonation of a binding site close to D_1 at low pH.

A retardation of the electron transfer from the oxygen-evolving complex to Chl a_{II}^{+} might also be caused by the increase of the standard free enthalpy, ΔG^{O}, of water oxidation lowering the pH. For example, lowering of the pH from 8 to 4 leads to a decrease of the redox potential difference between Chl a_{II}/Chl a_{II}^{+} and 2 H_2O_2/O_2, 4 H^+ by 240 mV.

Down to pH 4.0 the inhibition of oxygen evolution and the change of Chl a_{II}^{+} reduction kinetics were reversible (see Table III and Fig. 5). Performing single-flash experiments at pH 4.5 we found that the electron transfer to Chl a_{II}^{+} is already slowed down into the microsecond time range after the first flash given to a dark-adapted sample (not shown). This indicates that the inhibition occurs in the dark and may be caused by a reversible protonation of a functional group which regulates the electron transfer from D_1 to Chl a_{II}^{+}. Irreversible inactivation, which has been observed in spinach chloroplasts in connection with release of Mn^{2+} [29] below pH 5.0, is probably shifted to lower pH values in PS II particles from *Synechococcus*.

At alkaline pH the oxygen-flash yield decreases strongly between pH 8.0 and 9.0 with a half-maximum at pH 8.3 (see Fig. 3a). A Hill plot of

$$\log \frac{Y_{\mathrm{O}_2}^{\max} - Y_{\mathrm{O}_2}}{Y_{\mathrm{O}_2}} \text{ against pH } (Y_{\mathrm{O}_2} = \mathrm{O}_2 \text{ flash yield})$$

between pH 8.0 and 9.0 yields a straight line of slope $n = 2.6$ (not shown). The Hill coefficient n yields a minimum number of three binding sites for H^+ or OH^- involved in the inhibition of oxygen evolution caused by deprotonation or binding of OH^-. This inhibition is accompanied by a change of the Chl a_{II}^{+} reduction kinetics. Increasing the pH above pH 8.0, an increasing fraction of Chl a_{II}^{+} is reduced by the donor Z. Consistent with our results, the amplitude of EPR Signal II_{f} due to the oxidized form of Z increases under continuous illumination with increasing alkalinization [28,33]. At pH 9.0 the half-life time of electron donation by Z is 180 ns (see Fig. 4). Significantly slower Chl a_{II}^{+} reduction kinetics are probably due to charge recombination (see above).

Table III shows that at pH 9.0 reversible inhibition and irreversible inactivation of oxygen evolution are superimposed. As a possible mechanism of the reversible inhibition it has been proposed that bound Cl^- from the catalytic site of the oxygen-evolving complex is displaced by OH^- [44,45]. It has been shown that the irreversible inactivation is time-dependent and increases significantly by illumination (Refs. 32 and 33; see also Table III). This has been explained by specific sensitivity of the S_2 state to alkalinization [32]. The inactivation is accompanied by loss of Mn^{2+} and the release of the peripheral 33 kDa protein [33,34].

The results of this work show that the electron donation from the immediate donor, D_1, to Chl a_{II}^{+} is sensitive to both reversible inhibition at low pH and irreversible inactivation of oxygen evolution at high pH. We assume that under these conditions Chl a_{II}^{+} is reduced by the donor Z, which might be a modified state of D_1 and, in part, by charge recombination. Z^+ is ultimately reduced by an electron from the acceptor side. The nanosecond decay connected with water oxidation shows altered kinetics below pH 5.5. Single-flash experiments are in preparation in order to clarify (a) the pH dependence of the pattern of the positive excess charge located in the oxygen-evolving complex and (b) if the reversible inhibition of O_2 evolution at low pH can be explained by an increase of misses in all centers or by an increase of a fraction of centers which are completely blocked.

Acknowledgements

The authors thank Ms. Irene Geisenheimer for preparing the PS II particles from *Synechococcus* and for the measurements of flash-induced oxygen evolution with the Clark-type electrode. The participation of Dr. K. Brettel and Dipl.-Phys. S.

Gerken in the initial stage of this project is gratefully acknowledged. We wish to thank Prof. Dr. H.T. Witt and Dr. J.P. Dekker for reading the manuscript. This work was supported by grants from the Deutsche Forschungsgemeinschaft, Sonderforschungsbereich 312, Teilprojekt A3.

References

1 Döring, G , Stiehl, H.H. and Witt, H.T (1967) Z Naturforsch. 22b, 639–644
2 Döring, G., Renger, G , Vater, J. and Witt, H.T. (1969) Z. Naturforsch. 24b, 1139–1143
3 Stiehl, H H and Witt, H.T. (1968) Z. Naturforsch. 23b, 220–224
4 Stiehl, H H and Witt, H.T. (1969) Z. Naturforsch. 24b, 1588–1598
5 Joliot, P., Barbieri, G. and Chabaud, R. (1969) Photochem Photobiol. 10, 309–329
6 Kok, B., Forbush, B. and McGloin, M P (1970) Photochem. Photobiol. 11, 457–475
7 Forbush, B., Kok, B. and McGloin, M.P (1971) Photochem. Photobiol. 14, 307–321
8 Fowler, C.F. (1977) Biochim. Biophys Acta 462, 414–421
9 Saphon, S and Crofts, A.R. (1977) Z. Naturforsch 32c, 617–626
10 Velthuys, B R. (1980) FEBS Lett. 115, 167–170
11 Förster, V., Hong, Y.-Q. and Junge, W (1981) Biochim. Biophys. Acta 638, 141–152
12 Brettel, K., Schlodder, E and Witt, H.T. (1984) Biochim. Biophys Acta 766, 403–415
13 Saygin, Ö and Witt, H.T (1985) FEBS Lett. 187, 224–226
14 Schlodder, E., Brettel, K., Schatz, G.H and Witt, H.T. (1984) Biochim. Biophys. Acta 765, 178–185
15 Schlodder, E., Brettel, K. and Witt, H.T. (1985) Biochim Biophys Acta 808, 123–131
16 Renger, G., Gläser, M and Buchwald, H.E. (1976) Biochim. Biophys Acta 461, 392–402
17 O'Malley, P.J and Babcock, G T. (1984) Biochim Biophys. Acta 765, 370–379
18 O'Malley, P.J., Babcock, G.T and Prince, R. (1984) Biochim Biophys. Acta 766, 283–288
19 Diner, B A. and DeVitry, C. (1984) in Advances in Photosynthesis Research (Sybesma, C., ed.), Vol. I, pp 407–411, Martinus Nijhoff/Dr. W. Junk Publishers, Dordrecht, The Netherlands
20 Dekker, J.P., Van Gorkom, H.J., Brok, M and Ouwehand, L (1984) Biochim. Biophys. Acta 764, 301–309
21 Weiss, W and Renger, G (1984) FEBS Lett 169, 219–223
22 Babcock, G.T , Blankenship, R.E. and Sauer, K (1976) FEBS Lett. 61, 286–289
23 Dekker, J.P., Plijter, J J., Ouwehand, L and Van Gorkom, H.J. (1984) Biochim Biophys. Acta 767, 176–179
24 Babcock, G.T. and Sauer K. (1975) Biochim Biophys. Acta 376, 329–344
25 Wraight, C.A., Kraan, G.P.B and Gerrits, N.M (1972) Biochim Biophys. Acta 283, 259–267
26 Schatz, G H. and Witt, H T. (1984) Photobiochem Photobiophys 7, 77–89
27 Bowes, J.M., Stewart, A.C and Bendall, D.S. (1983) Biochim Biophys Acta 725, 210–219
28 Cole, J., Boska, M., Blough, N.V and Sauer, K (1986) Biochim. Biophys Acta 848, 41–47
29 Pulles, M.P.J., Van Gorkom, H J. and Verschoor, G A M (1976) Biochim. Biophys. Acta 440, 98–106
30 Van Gorkom, H J , Pulles, M P J., Haveman, J. and Den Haan, G.A (1976) Biochim. Biophys. Acta 423, 217–226
31 Bowes, J.M., Crofts, A.R. and Itoh, S (1979) Biochim Biophys. Acta 547, 336–346
32 Briantais, J.-M , Vernotte, C., Lavergne, J. and Arntzen, C J. (1977) Biochim Biphys. Acta 461, 61–74
33 Maison-Peteri, B , Vernotte, C and Briantais, J.-M. (1981) Biochim. Biophys. Acta 637, 202–208
34 Vass, I., Koike, H. and Inoue, Y. (1985) Biochim. Biophys Acta 810, 302–309
35 Kuwabara, T. and Murata, N. (1983) Plant Cell Physiol. 24, 741–747
36 Sandusky, P.O., Selvius Deroo, C.L., Hicks, D.B , Yocum, C.F., Ghanotakis, D.F. and Babcock, G.T. (1983) in The Oxygen Evolving System of Photosynthesis (Inoue, Y. et al., eds.), pp. 189–199, Acdemic Press Japan, Tokyo
37 Schatz, G H. and Witt, H T (1984) Photobiochem. Photobiophys 7, 1–14
38 Conjeaud, H and Mathis, P. (1980) Biochim. Biophys. Acta 590, 353–359
39 Haveman, J. and Mathis, P. (1976) Biochim. Biophys. Acta 440, 346–355
40 Renger, G. and Wolff, Ch. (1976) Biochim. Biophys. Acta 423, 610–614
41 Reinman, R , Mathis, P , Conjeaud, H. and Stewart, A (1981) Biochim. Biophys. Acta 635, 429–433
42 Brettel, K., Ford, R C., Schlodder, E., Atkinson, Y.E., Witt, H.T. and Evans, M C W (1985) FEBS Lett. 181, 88–94
43 Ford, R.C. and Evans, M.C W. (1985) Biochim. Biophys Act 807, 1–9
44 Sandusky, P.O and Yocum, C F (1983) FEBS Lett 162, 339–343
45 Critchley, C., Baianu, I C , Govindjee and Gutowski, H S. (1982) Biochim Biophys Acta 682, 436–445

Biochimica et Biophysica Acta 890 (1987) 32–38
Elsevier

BBA 42079

Formation and flash-dependent oscillation of the S_2-state multiline EPR signal in an oxygen-evolving Photosystem-II preparation lacking the three extrinsic proteins in the oxygen-evolving system

Stenbjörn Styring [a,b], Mitsue Miyao [c] and A. William Rutherford [b]

[a] *Service de Biophysique, Département de Biologie, Centre d'Etudes Nucleaires de Saclay, Saclay and* [b] *Laboratoire de Photosynthèse, CNRS, 91190 Gif-sur-Yvette (France) and* [c] *National Institute for Basic Biology, Myodaiji, Okazaki 444 (Japan)*

(Received 14 July 1986)

Key words: Photosystem II; ESR; S_2-state; Oxygen evolution, (Spinach chloroplast)

In PS-II-enriched membranes lacking the three extrinsic water-soluble proteins in the oxygen-evolving system (18, 24 and 33 kDa), but still evolving oxygen to some extent, the formation of the multiline EPR signal originating from the S_2-state is dependent on the concentration of Cl^-. In 200 mM Cl^- the multiline signal was observed after the first flash and oscillated with the flash number with a period of four. At 20 mM Cl^- no signal could be observed in this material. These results suggest that the extrinsic proteins are not necessary for multiline signal formation and that complete advancement through the S-states can occur in their absence when sufficient Cl^- is present.

Introduction

Photosystem II is a membrane-bound multicomponent enzyme that catalyzes the reduction of plastoquinone and the light-driven oxidation of H_2O to O_2 in plants, algae and cyanobacteria. The molecular organisation of the oxygen-evolving system has been extensively studied in recent years, and biochemical analysis has revealed the importance of four manganese atoms and three extrinsic water-soluble proteins (of 33, 24 and 18 kDa, respectively) in the oxygen evolution [1]. These extrinsic proteins can be selectively extracted from PS II by various treatments [1] and it has been suggested that they play an obligatory role in oxygen evolution [2,3]. However, it is now clear that, under optimal ionic conditions, oxygen evolution can still proceed (at least to some extent) in the absence of these proteins [4,5]. Instead, the role of the extrinsic proteins seems to be to increase the affinity for Cl^- and Ca^{2+}, and these ions are essential for oxygen evolution [1]. The presence of the 24 kDa protein provides a high-affinity site for Ca^{2+} [6]. The 18 and 24 kDa proteins lower the Cl^- requirement for optimal oxygen evolution from 30 mM in their absence to less than 1 mM in their presence [7], while removal of the 33 kDa protein drastically changes the Cl^- requirement of the system and, in its absence, as much as 200 mM Cl^- is necessary for maximal oxygen evolution [7,8].

Four successive charge separations in the PS II reaction center create the oxidizing equivalents which are necessary for the formation of one molecule of oxygen from two molecules of water (for a recent review, see Ref. 9). These positive

---

Abbreviations PS II, Photosystem II; Chl, chlorophyll; Mes, 4-morpholineethanesulfonic acid; PPBQ, phenylbenzoquinone.

Correspondence: S Styring, Laboratoire de Photosynthèse, CNRS, Boîte Postale 1, 91190 Gif-sur-Yvette, France.

0005-2728/87/$03.50 © 1987 Elsevier Science Publishers B.V. (Biomedical Division)

charges are stored, possibly on the manganese cluster in the oxygen-evolving system, which exists in five intermediary oxidation states: S_0–S_4 [10]. The chemistry of the S-states remains in many respects a matter of speculation. One probe to the structure of the S_2-state and to the S-state turnover is an unusual multiline EPR signal which originates from the S_2-state [11–14]. Power saturation studies [15], computer simulations of the signal shape [16] and comparisons to model systems [3] have provided evidence that the signal originates from a cluster of two or possibly four manganese atoms in a mixed-valent state. So far the multiline signal has been reported from all oxygen-producing materials that have been investigated, while many treatments that inhibit oxygen evolution also inhibit the formation of the multiline signal [3].

A number of studies have correlated the removal of the extrinsic proteins with inability to form the multiline signal from the S_2-state [3,17–20]. However, as with many studies of oxygen evolution it seems likely that these results are due to the use of nonoptimal concentrations of Cl^- and/or Ca^{2+}, since removal of the extrinsic proteins results in much lowered affinity for these ions (for a discussion, see Refs. 21 and 22). Despite this, it was claimed in a recent study of the role of Cl^- and the extrinsic proteins in the oxygen-evolving system that the 33 kDa protein was required for formation of the multiline signal [17].

In this communication we have attempted to resolve some of the anomalous EPR observations and to bring them in line with the current knowledge of the function of the extrinsic proteins and Cl^-. We demonstrate that in the absence of the three water-soluble proteins the S_2-state exhibits an essentially normal multiline EPR signal, which oscillates with a period of 4 with the maximum amplitude after the first flash. It is also shown that the absence of the multiline signal reported by Imaoka et al. [17] is due to insufficient Cl^- in their study.

Materials and Methods

PS-II-enriched membranes were prepared from spinach chloroplasts according to Kuwabara and Murata [23]. These membranes showed an oxygen-evolving activity in 10 mM Cl^- of 440 μmol O_2/mg Chl per h with 0.3 mM PPBQ as electron acceptor. These membranes (hereafter called 'intact material') were treated with either 1 M NaCl or 2.6 M urea in combination with 0.2 M NaCl. The treatment with 1 M NaCl specifically removes the 18 and 24 kDa proteins from PS II (the material is called 'NaCl-washed') [23], while the treatment with urea + NaCl removes all three extrinsic proteins while the Mn-atoms are still bound to the PS II centers (this material is called 'urea + NaCl-treated') [8]. Less than 5% of the 33 kDa protein remained bound to the membranes as judged from Coomassie brilliant blue staining of SDS-polyacrylamide gels using purified 33 kDa protein an as internal standard. These preparations showed oxygen-evolving activity of 350 μmol O_2/mg Chl per h for NaCl-washed membranes (measured in 10 mM Ca^{2+} and 20 mM Cl^-) and 170 μmol O_2/mg Chl per h for urea + NaCl-treated membranes (measured at 10 mM Ca^{2+} and 200 mM Cl^-). The urea + NaCl-treated membranes showed no oxygen evolution when measured in 20 mM Cl^-. Purification of the 33 kDa protein and reconstitution of the urea + NaCl-treated membranes with the purified protein was performed as described in Ref. 24. The activity of this material (called 'urea + NaCl-treated + 33 kDa') was 253 μmol O_2/mg Chl per h. The preparations were frozen in liquid nitrogen and could be stored for several months at −80°C. The buffer used throughout the study was 20 mM Mes-NaOH at pH 6.5 containing 300 mM sucrose, 10 mM $CaCl_2$, 30% ethylene glycol (v/v/v) and varied concentrations of Cl^- (added as NaCl). Ca^{2+} was present at 10 mM in all experiments to saturate the requirement for this ion [1].

EPR samples in calibrated quartz tubes were dark-adapted for 10 min at 20°C before being illuminated at 4°C with saturating flashes [14] from a Nd-YAG laser (15 ns, 100 mJ, 530 nm). The time between flashes in a flash-train was 1 s. In most experiments the samples were given a preflash, after which they were allowed to relax at 20°C in absolute darkness. After 10 min, 20 mM PPBQ in dimethylsulfoxide was added as an acceptor to a final concentration of 0.5 mM. After addition of PPBQ the sample was illuminated with the required number of flashes. The illuminated samples were rapidly frozen at 200 K and subsequently stored at 77 K. EPR spectra were recorded at liquid-helium temperatures with a Bruker ER-200t-X-band EPR spectrometer or a Bruker ER200D-SRC spectrometer, equipped with an Oxford Instruments cryostat. A Tracor-Northern 1710A apparatus was used for subtraction of spectra. All sample handling was performed in near darkness.

Results and Discussion

In Fig. 1A is shown the high-field part of the multiline signal obtained from the urea + NaCl-treated material illuminated with various numbers of flashes (for the complete spectrum, see Fig. 3C). The multiline signal was formed after the first flash. From the amplitude of the three well-defined lines at high field we estimate that the amplitude of the signal after one flash in the urea + NaCl-treated PS-II-centers was approx. 50% of the multiline signal formed after one flash in the intact material (Fig. 1B). The formation of the multiline signal was dependent on the flash number. The signal amplitude was maximal after the first and fifth flashes. Thus it oscillated with a period of 4 and reflects the S_2-state. The oscillation pattern (Fig. 1A, right) is similar to that observed in the intact material (Fig. 1B, right) and to that earlier observed in PS-II-enriched membranes [14,18] prepared according to Berthold et al. [25].

It was sometimes observed that in the urea + NaCl-treated membranes the first flash resulted in simultaneous formation of the multiline signal and an increased amount of EPR-Signal II_{slow} (S II_s). This signal is thought to be due to a cationic quinone radical on the donor side in PS II [26] which, when present in its reduced form, can donate an electron to the S_2-state [27], thus reducing the yield of any multiline signal formed. S II_s formation on the first flash indicates that it was present in the reduced form in the dark in this material. This is not normally the case in PS-II-enriched membranes. However, because of its sensitivity to light the urea + NaCl-treated material was prepared under very low light conditions [8] which might have allowed some decay of S II_s in

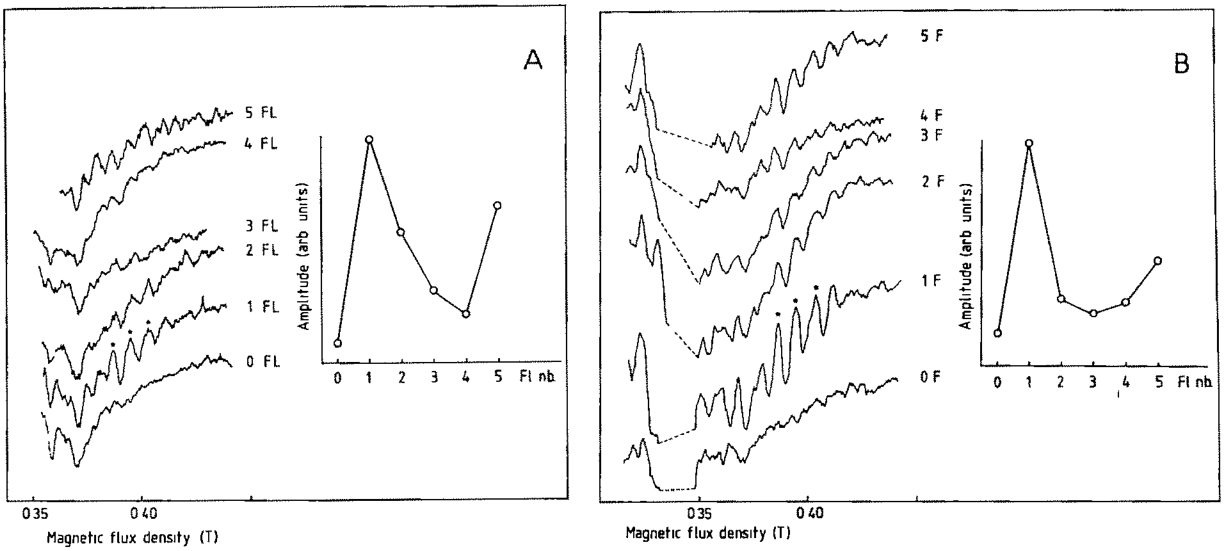

Fig 1. Flash-dependent oscillation of the multiline EPR signal from the S_2-state. (A) Urea + NaCl-treated membranes, (B) intact membranes The high-field part of the EPR spectra is shown for samples given a preflash and, 10 min thereafter, a different number of flashes as described in the text The concentration of the membranes was 2.9 mg Chl/ml and 2.7 mg Chl/ml in (A) and (B), respectively. The respective concentrations of Cl^- were 200 and 20 mM. The amplitude of the multiline signal as a function of the number of flashes given is shown at the right side. The amplitude was calculated from the added amplitudes of the three easily distinguished high-field peaks marked with asterisks in the figure Microwave frequency, 9.43 GHz, temperature, 8 K; modulation amplitude, 3.2 mT; microwave power, 32 mW; spectrometer gain, $4 \cdot 10^5$.

the dark. The simultaneous formation of the multiline signal and S II_s would result in strong damping of the flash-dependent oscillation of the multiline signal. To avoid this, we used one preflash to oxidise S II_s. This preflash also resulted in the formation of some multiline signal. It has recently been shown [28], that the S_2-state has a half-time for the deactivation of 2.5 min in the dark at 20 °C in the urea + NaCl-treated material, and thus 10 min dark adaptation after the preflash was needed to allow essentially complete deactivation of the S_2-state. S II_s remained oxidized during this time. The preflash treatment was used in all experiments. It should be noted that the Mn cluster in the urea + NaCl-treated membranes is more labile than in the intact membranes. This results in some loss of manganese from the membranes which gives an EPR-spectrum from nonfunctional Mn^{2+} which overlaps the multiline spectrum around $g = 2$. Lines originating from this Mn^{2+} are for example seen in the spectrum after zero flash in Fig. 1A. It seems likely that the loss of manganese atoms from the PS II centers in the urea + NaCl-treated membranes at least partly explains the lower amount of the multiline signal observed in this material.

Thus it is possible to obtain high yields of an oscillating multiline signal from a PS-II-preparation lacking the three water-soluble proteins. This result is clearly different from those obtained by Imaoka et al. [17] who were unable to observe the multiline signal from the S_2-state in PS-II-enriched membranes washed with 1 M $CaCl_2$. This material lacks the three extrinsic, water-soluble proteins of 33, 24 and 18 kDa and is known to evolve oxygen only at elevated concentrations of Cl^- [5]. It is thus very similar to the urea + NaCl-treated membranes used in our study [4]. However, their experiments were performed at 20 mM Cl^-, which is too low to allow oxygen evolution from PS-II centers lacking the three water-soluble proteins. This suggests that it was not the absence of the 33 kDa protein that was directly responsible for the inability to form the multiline signal (in contrast to the suggestion by Imaoka et al. [17]). Instead, this inability can probably be explained by the low concentration of Cl^- used.

To test this we performed an experiment under comparable conditions (20 mM Cl^-) (Fig. 2). Urea + NaCl-treated membranes, stored in 200 mM Cl^-, were diluted 10 times in a buffer containing 20 mM Cl^-, allowed to equilibrate on ice for 10 min and then pelleted by centrifugation. The membranes were resuspended in a buffer containing 20 mM Cl^- and divided into two samples. To one was added 2 M NaCl to a final concentration of 200 mM Cl^- and to the other a similar volume of 20 mM NaCl. EPR spectra were recorded after one saturating flash. From Fig. 2A and B it is clear that high yield of the multiline signal was observed in the sample containing 200 mM Cl^-, while no multiline signal was observed at 20 mM Cl^-. Thus it seems clear that it is the concentration of Cl^- that governs the formation of the multiline signal.

It was therefore tested whether the change in Cl^- requirement caused by the removal of the 33 kDa protein was reversible with regard to the

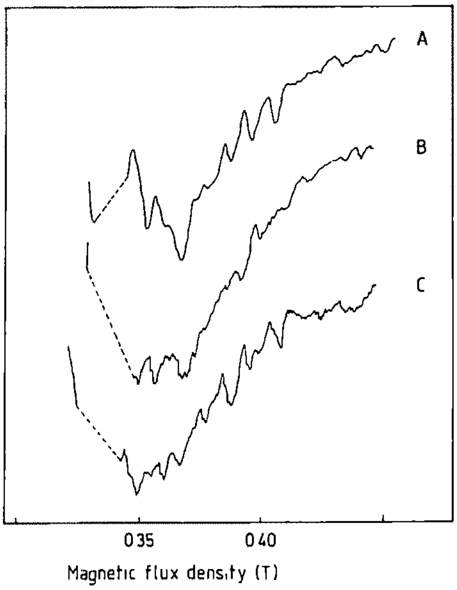

Fig. 2 Effect of the chloride concentration and the 33 kDa protein on the formation of the multiline EPR signal. (A, B) Samples of urea+NaCl-treated membranes prepared as described in the text and given one saturating flash in the presence of 200 mM Cl^- (A) and 20 mM Cl^- (B); the concentration of Chl was identical: 3.0 mg Chl/ml in either sample. (C) Urea+NaCl-treated membranes (3.0 mg Chl/ml) reconstituted with the 33 kDa protein and given one flash in the presence of 20 mM Cl^-. Instrumental settings; microwave frequency, 9.46 GHz; temperature, 8 K; microwave power, 32 mW; modulation amplitude, 2.2 mT; spectrometer gains; $2.5 \cdot 10^5$ (A), $4 \cdot 10^5$ (B) and $4 \cdot 10^5$ (C).

formation of the multiline signal. Such a reversibility has been shown for oxygen-evolution [4,17]. In Fig. 2C it is shown that urea + NaCl-treated membranes which were reconstituted with the 33 kDa protein exhibited appreciable amounts of the multiline signal after one flash. This experiment was performed at 20 mM Cl$^-$, which indicates that rebinding of the 33 kDa protein increased the Cl$^-$ affinity by more than 10-fold.

NaCl-washed PS-II-enriched membranes have a high oxygen-evolving activity at 20 mM Cl$^-$ [7] and a high yield of the multiline signal was obtained after one flash in this material at this concentration of Cl$^-$ (Fig. 3B). The formation of large amounts of the multiline signal in the absence of the 24 and 18 kDa proteins is in contrast to earlier experiments [18,20] which were performed in low (1 mM, Ref. 18) or nonsaturating (10 mM, Ref. 20) concentrations of Cl$^-$. However, the result is in agreement with the earlier observations of the multiline signal in this type of material in 20 mM Cl$^-$ [17,19]. Thus the formation of the multiline signal is dependent on the concentration of Cl$^-$ in the surrounding medium in a manner similar to the Cl$^-$ dependence of the oxygen evolution in this material also.

In Fig. 3 are shown the EPR spectra of the multiline signal formed after one flash in four different PS-II-enriched materials. The spectra from the intact material (Fig. 3A) and from the NaCl-washed material (lacking the 18 and 24 kDa proteins) (Fig. 3B) are essentially similar. The peaks are similarly situated and the relative amplitudes of the peaks are comparable. Thus the removal of the two smaller proteins does not lead to any major changes in the configuration of the Mn cluster in the S$_2$-state.

Removal of the 33 kDa protein by the urea + NaCl-treatment or by CaCl$_2$-washing renders the Mn cluster more labile and at low concentrations of Cl$^-$, two Mn atoms are easily released [5,8]. This suggests that the environment of the Mn cluster is changed when the 33 kDa protein is released. Alterations of the Mn cluster are also revealed by the multiline signal (Fig. 3C). Due to lower concentration of the multiline signal the spectrum from the urea + NaCl-treated membranes is weaker, and the presence of nonfunctional manganese complicates the subtraction of the dark-spectrum from the spectrum recorded after one flash. This is especially prominent on the low-field side near $g = 2$. Despite these problems it is clear that some peaks (marked with arrows in the spectra) are present in positions similar to those in the intact membranes (Fig. 3A) or in the reconstituted material (Fig. 3D), while in other regions (particularly at low-field values) there is little correspondance with the other spectra. The changes suggest that removal of the 33 kDa pro-

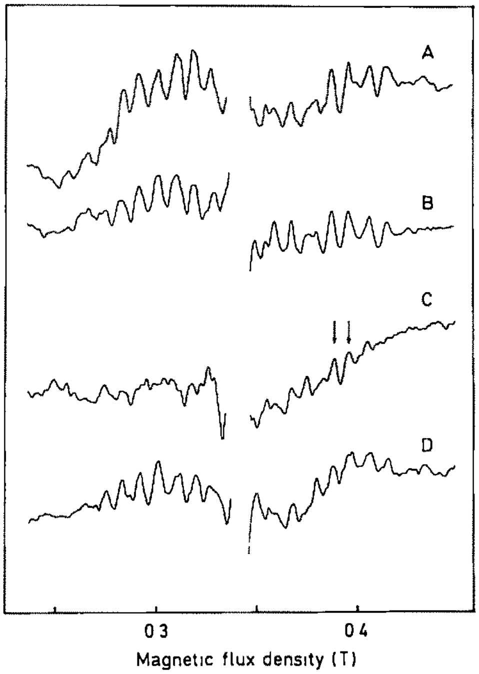

Fig. 3. Comparison of the multiline EPR signal originating from the S$_2$-state in PS-II-enriched membranes with different protein composition (A) Intact material (3 mg Chl/ml, 20 mM Cl$^-$), (B) NaCl-washed material (lacking the 18 and 24 kDa proteins) (3 mg Chl/ml; 20 mM Cl$^-$); (c) Urea+NaCl-treated material (lacking the 18, 24 and 33 kDa proteins) (3 mg Chl/ml, 200 mM Cl$^-$); (D) Urea+NaCl-treated material reconstituted with the 33 kDa protein (lacking the 18 and 24 kDa proteins) (3 mg Chl/ml; 20 mM Cl$^-$) The figure shows the spectra obtained after subtraction of the dark spectrum from the spectrum recorded after one flash in the same sample. First the spectrum was recorded after one flash, thereafter the sample was thawed and allowed to equilibrate at 20 °C in complete darkness After 10 min the sample was frozen and the dark spectrum was recorded. This procedure allowed near complete relaxation of the S$_2$-state, but also resulted in some release of manganese from the urea+NaCl-treated membranes (C). Instrumental settings. modulation amplitude, 1.25 mT; spectrometer gain, $2.5 \cdot 10^5$; other settings as in Fig. 2

tein results in a changed coupling between the Mn atoms giving rise to the multiline signal.

In Fig. 3D is shown the multiline signal obtained with the urea + NaCl-treated membranes reconstituted with the 33 kDa protein. This spectrum is different from the spectrum recorded in the absence of the 33 kDa protein (Fig. 3C). It is similar, but not identical, to that recorded for the NaCl-washed material (Fig. 3B), which has the same composition in terms of the extrinsic proteins. The slight differences between spectra 3D and 3B, if significant, could be due to incomplete restoration of the configuration of the Mn cluster, even though oxygen evolution was restored to 80%.

Summarizing we conclude that the 33 kDa protein can be replaced by Cl^- for both multiline-signal formation and oxygen evolution. However, the absence of this protein modifies the Mn cluster leading to an altered multiline signal from the S_2-state. Cl^- can also replace the 24 and 18 kDa proteins with respect to oxygen evolution [1] and multiline formation (Refs. 17 and 19; see also this work, Fig. 3B) when Ca^{2+} is present. Thus Cl^- is very important for the formation of the multiline signal from the S_2-state, and it seems clear that suboptimal concentrations of Cl^- results in inability to form the multiline signal in intact [21], NaCl-washed (Refs. 18 and 19; this work, Fig. 3B) and urea + NaCl-treated membranes (this work, Figs. 1A and 2). However, in contrast to earlier suggestions [17] it is not necessarily the S_1–S_2 transition that is inhibited at very low concentrations of Cl^-. Instead, it was reported recently that the S_1–S_2-state transition functions at low Cl^- concentrations forming an S_2-state not showing the multiline signal and that Cl^- depletion inhibits the S_2–S_3 transition [21].

Finally, from the observation in this report of the flash-dependent oscillation of the multiline signal (Fig. 1A) and from earlier activity measurements [5,8] it is clear that the water-soluble proteins are not necessary for oxygen evolution. Furthermore, the observation of the multiline signal in the absence of the extrinsic proteins (Fig. 3) suggests that their presence or absence does not cause major changes in the mechanism for oxygen evolution, provided sufficient Cl^- is present in the medium.

After the submission of this manuscript the formation of the multiline signal after illumination at 200 K was reported in $CaCl_2$-washed material lacking the three extrinsic proteins. The formation of the multiline signal in this material was dependent on the concentration of Ca^{2+}, provided sufficient Cl^- (200 mM) was present in the medium (Miller, A.-F., De Paula, J.C. and Brudvig, G.W. (1987) in Proceedings of the VIIth International Congress on Photosynthesis (Biggins, J., ed.), Martinus Nijhoff, Dordrecht, The Netherlands, in the press).

Acknowledgements

S.S. is grateful for a postdoctoral grant from the Knut and Alice Wallenbergs foundation. A.W.R. is supported by the CNRS. M.M. was supported by a Grant-in-Aid for Science Program for International Cooperative Research (60041101) from the Japanese Ministry of Education, Science and Culture.

References

1 Murata, N. and Miyao, M. (1985) Trends Biochem. Sci. 10, 122–124
2 Åkerlund, H.-E. (1983) in The oxygen evolving system of photosynthesis (Inoue, Y., Crofts, A.R., Govindjee, Murata, N., Renger, G. and Satoh, K., eds.), pp. 201–208, Academic Press Japan, Tokyo
3 Dismukes, G.C. (1986) Photochem. Photobiol. 43, 99–115
4 Kuwabara, T., Miyao, M., Murata, T and Murata, N. (1985) Biochim. Biophys. Acta 806, 283–289
5 Ono, T.A. and Inoue, Y (1984) FEBS Lett 168, 281–286
6 Ghanotakis, D F., Topper, J.N., Babcock, G.T. and Yocum, C F (1984) FEBS Lett 170, 169–173
7 Miyao, M. and Murata, N. (1985) FEBS Lett. 180, 303–308
8 Miyao, M. and Murata, N. (1984) FEBS Lett. 170, 350–354
9 Renger, G. and Govindjee (1985) Photosynth. Res 6, 33–55
10 Kok, B., Forbush, B. and McGloin, M (1970) Photochem. Photobiol. 11, 457–475
11 Dismukes, G.C and Siderer, Y. (1981) Proc. Natl. Acad Sci. USA 78, 274–278
12 Hansson, Ö. and Andréasson, L.-E (1982) Biochim. Biophys. Acta 679, 261–268
13 Brudvig, G.W, Casey, J.L. and Sauer, K. (1983) Biochim. Biophys Acta 723, 361–371
14 Zimmermann, J.L. and Rutherford, A.W. (1984) Biochim Biophys Acta 767, 160–167
15 De Paula, J.C. and Brudvig, G W. (1985) J Am. Chem. Soc 107, 2643–2648
16 Hansson, Ö., Andréasson, L -E and Vänngård, T. (1984) in Advances in Photosynthesis Research (Sybesma, C., ed.),

vol. I, pp. 307–310, Martinus Nijhoff/Dr. W Junk Publishers, Dordrecht, The Netherlands

17 Imaoka, A., Akabori, K., Yanagi, M , Izumi, K , Toyoshima, T., Kawamori, A , Nakayama, H and Sato, J. (1986) Biochim Biophys. Acta 848, 201–211

18 Franzén, L -G., Hansson, Ö. and Andréasson, L.-E (1985) Biochim Biophys. Acta 808, 171–179

19 Toyoshima, Y., Akabori, K , Imaoka, A., Nakayama, H , Ohkouchi, N and Kawamori, A. (1984) FEBS Lett. 176, 346–350

20 Blough, N.V. and Sauer, K. (1984) Biochim. Biophys. Acta 767, 377–381

21 Ono, T , Zimmermann, J L , Inoue, Y. and Rutherford, A.W. (1986) Biochim. Biophys Acta 851, 193–201

22 Zimmermann, J.L. and Rutherford, A W (1985) Physiol Vég. 23, 425–434

23 Kuwabara, T and Murata, N. (1982) Plant Cell Physiol 23, 533–539

24 Kuwabara, T., Murata, T., Miyao, M. and Murata, N (1986) Biochim. Biophys Acta, in the press

25 Berthold, D.A., Babcock, G.T and Yocum, C.F. (1981) FEBS Lett. 134, 231–234

26 O'Malley, P.J. and Babcock, G T. (1984) Biochim Biophys. Acta 765, 370–379

27 Velthuys, B.R. and Visser, J W M. (1975) FEBS Lett. 55, 109–112

28 Miyao, M., Murata, N., Lavorel, J., Maison-Peteri, B., Boussac, A. and Etienne, A -L. (1987) Biochim. Biophys Acta 890, issue 2, in the press

Biochimica et Biophysica Acta 890 (1987) 39–46
Elsevier

BBA 42157

Photoaffinity labeling of the mitochondrial phosphate carrier by 4-azido-2-nitrophenyl phosphate

M. Tommasino, G. Prezioso and F. Palmieri

Department of Pharmaco-Biology, Laboratory of Biochemistry, University of Bari and CNR Unit for the Study of Mitochondria and Bioenergetics, Via Amendola 165/A, 70126 Bari (Italy)

(Received 18 July 1986)

Key words: Phosphate carrier; Photoaffinity labeling; Phosphate transport; Mitochondria; (Pig heart)

The effect of 4-azido-2-nitrophenyl phosphate (ANPP), a photoreactive analogue of phosphate, on the phosphate carrier of pig-heart mitochondria has been investigated. In the dark, ANPP inhibits the transport of phosphate in a competitive manner with a K_i of 3.2 mM. Upon photoirradiation with visible light, [^{32}P]ANPP binds covalently to the phosphate carrier and the inhibition becomes irreversible. Both the inhibition of phosphate transport and the incorporation of [^{32}P]ANPP into the phosphate carrier depend on the concentration of the inhibitor and the pH of the medium. Incubation of the mitochondria with phosphate during illumination in the presence of ANPP protects the carrier against inactivation and decreases the amount of radioactivity which is found to be associated with the purified protein. By extrapolation it is calculated that at 100% inactivation of the phosphate carrier 0.35 mol of reagent are bound per mol of 33 kDa carrier protein. It is concluded that ANPP can be used for photoaffinity labeling of the mitochondrial phosphate carrier at the substrate-binding site.

Introduction

The synthesis of ATP during oxidative phosphorylation requires uptake of ADP and phosphate into the mitochondria. The translocation of phosphate across the inner mitochondrial membrane is catalyzed by a specific transport system known as the phosphate carrier (for a review, see Refs. 1–3). This protein has been purified from heart mitochondria and reconstituted in liposomes [4–6]. The amino-terminal part of the protein has been sequenced [7–8] and cysteine at position 42 has been identified as the binding site of the inhibitor *N*-ethylmaleimide [7].

Nothing, however, is known so far about the substrate-binding site of the phosphate carrier. Indeed, it has not even been established whether the particular −SH group responsible for the inhibition by *N*-ethylmaleimide is located at or near the substrate-binding site, although it has been reported that the presence of phosphate decreases to some extent the reactivity of SH-blocking reagents with the phosphate carrier [9–11].

In order to have a tool to characterize the phosphate-binding site, the reactivity of the phosphate carrier with the photoreactive substrate analogue ANPP has been investigated. ANPP had been introduced by Lauquin et al. [12] to label the phosphate-binding site of the F_1-ATPase. By photoirradiation of submitochondrial particles with [^{32}P]ANPP, these authors showed that also a 30

Abbreviations: ANPP, 4-azido-2-nitrophenylphosphate; ANP, 4-azido-2-nitrophenol; Hepes, 4-(2-hydroxyethyl)-1-piperazine-ethanesulphonic acid; SDS, sodium dodecyl sulphate.

Correspondence: Dr. F. Palmieri, Istituto di Biochimica, Università di Bari, Via Amendola, 165/A, 70126 Bari, Italy.

0005-2728/87/$03.50 © 1987 Elsevier Science Publishers B.V. (Biomedical Division)

kDa protein is labeled by ANPP. This was tentatively suggested to be the phosphate carrier. In this paper we show that ANPP inhibits the phosphate carrier. The inhibition becomes irreversible in the presence of light. Phosphate protects the carrier against inactivation and labeling by [^{32}P]ANPP. Complete inhibition of the phosphate carrier is accomplished when 0.35 mol ANPP are bound per mol of phosphate carrier.

Materials and Methods

Materials. ANP and ANPP were synthesized from 4-amino-2-nitrophenol (Aldrich) as described by Lauquin et al. [12]. [^{32}P]ANPP was synthetized by the same method using [^{32}P]phosphate. Hydroxyapatite (Bio-Gel HTP) and Dowex AG1-X8 were purchased from Bio-Rad. [^{32}P] phosphate was obtained from the Radiochemical Centre (Amersham, U.K.), egg yolk phospholipids from Fluka, cardiolipin from Avanti-Polar Lipids, Triton X-114 and *N*-ethylmaleimide from Serva. Mitochondrial phospholipids were isolated by the procedure described in Ref. 13. All the other reagents were of the highest purity commercially available.

Incubation with ANPP. Pig-heart mitochondria were prepared as described in Ref. 14 and stored at −70°C. For the incubation with ANPP, thawed mitochondria were washed twice in 250 mM sucrose/10 mM Tris-HCl (pH 6.8)/1 mM EGTA/1 mM NaF, resuspended in the same medium at a concentration of 10 mg protein/ml and then incubated with the indicated concentrations of ANPP at 0°C in the dark. After 30 min, aliquots were transferred into glass tubes and illuminated with a 250 W Osram Halogen lamp for 15 min at 0°C as described in Ref. 12, while the rest was kept in the dark. To prevent cleavage of ANPP, NaF was included in the incubation buffer to inhibit potential phosphatase activity [12,15]. In control experiments it was shown that NaF has no effect on the phosphate carrier activity. After the incubation, the mitochondria treated with ANPP with or without illumination were washed twice in 20 mM K H_2PO_4/20 mM KCl/2 mM EGTA (pH 6.5). In the experiments where the transport of phosphate was measured by the swelling technique, freshly prepared mitochondria were incubated with ANPP and ANPP-treated mitochondria were directly transferred into the assay mixture.

Isolation of the phosphate carrier. It was performed as described previously [6], except that the mitochondria were solubilized by 2% Triton X-114 at a final concentration of 15 mg protein/ml.

Incorporation of the phosphate carrier into liposomes. Liposomes were prepared as described previously [6] by sonication of a mixture of 80 mg/ml egg yolk phospholipids and 20 mg/ml mitochondrial phospholipids in a buffer containing 50 mM KCl/20 mM Hepes/1 mM EDTA (pH 6.5). In the experiments where the phosphate-phosphate exchange was measured, 20 mM phosphate was also included in the sonication buffer.

The phosphate carrier protein was incorporated into liposomes by the freeze-thaw-sonication procedure [16,17]. 1 ml liposomes was mixed with 50 μl mitochondrial extract or hydroxyapatite eluate. After 2 min at 0°C the mixture was frozen in liquid N_2, thawed in a water bath at 15°C and then pulse-sonicated (0.3 s sonication, 0.7 s intermission) for 6.0 s at 0°C.

Assay of phosphate transport. In mitochondria the transport of phosphate was assayed by monitoring the rate of mitochondrial swelling, i.e., by recording the decrease in absorbance at 546 nm of the mitochondrial suspension in 100 mM ammonium phosphate [18,19] with an Eppendorf photometer model 1101 M. Alternatively, phosphate transport in intact mitochondria was assayed by measuring the uptake of [^{32}P]phosphate by the inhibitor stop method [20]. Mitochondria (2 mg/ml) were incubated at 0°C in 100 mM KCl/20 mM Tris-HCl (pH 6.5)/1 mM EGTA/1 μg per ml rotenone/20 mM butylmalonate (to inhibit the dicarboxylate carrier which is also able to transport phosphate). The uptake was started by adding 0.5 mM [^{32}P]phosphate and stopped 5 s later with 1 mM mersalyl. After rapid centrifugation of the mitochondria, the radioactivity was counted and the amount of substrate incorporated into the matrix space was calculated as described [20].

In order to measure phosphate transport in proteoliposomes, proteoliposomes prepared in the presence or in the absence of 20 mM phosphate were distributed in Eppendorf cups (160 μl each) and equilibrated at 25°C. After 4 min they were used for exchange or uptake measurements, respectively, essentially as described previously [6]. Transport was initiated by adding carrier free [^{32}P]phosphate (exchange) or the indicated concentrations of [^{32}P]phosphate (uptake) and was stopped after 1 min by the addition of 2 mM *N*-ethylmaleimide. In control samples *N*-ethylmaleimide was added 30 s before the labeled substrate. To remove the external radioactivity each sample was applied to a Dowex AG1-X8 column, chloride-form (0.5 × 4 cm equilibrated with 170 mM sucrose). The liposomes, eluted with 1.2 ml 170 mM sucrose, were collected and counted. The activity of phosphate uptake or phosphate-phosphate exchange was calculated by subtracting the control values from the experimental samples.

SDS-gel electrophoresis. Polyacrylamide slab gel electrophoresis of acetone-precipitated samples was performed in the presence of 0.1% SDS according to Laemmli [21]. The stacking gel contained 5% polyacrylamide and the separation gel contained 17.5% acrylamide and an acrylamide-to-bisacrylamide ratio of 150. Staining with Coomassie blue R 250 and destaining were carried out according to Downer et al. [22]. Autoradiographies were performed making use of Kodak X-OMAT S films. Gel slices 1 mm thick were digested by 0.6 ml 15% H_2O_2 at 70°C for 8 h [23], were mixed with 4 ml of scintillation mixture (Maxifluor Baker, The Netherlands) and counted.

Other methods. Protein was determined by the Lowry method modified as described in Ref. 24 and adapted to the presence of Triton [25]. To measure the binding of [^{32}P]ANPP to the phosphate carrier, preparations of purified carrier obtained from [^{32}P]ANPP-treated mitochondria were delipidated [26] and assayed for radioactivity. Alternatively, the [^{32}P]ANPP binding was measured by dissolving [23] the protein bands, obtained from SDS gels, corresponding to the purified phosphate carrier and counting the radioactivity.

Results

Inhibition of the phosphate carrier by ANPP without illumination

In preliminary experiments the effect of ANPP on the transport of phosphate was tested in intact mitochondria without illumination. It was found that ANPP inhibits the uptake of [^{32}P]phosphate catalyzed by the phosphate carrier, causing 50% inhibition at a concentration of approx. 4 mM.

In order to analyze the inhibition of the phosphate carrier caused by ANPP in the dark, the influence of this inhibitor on the rate of phosphate transport must be determined. Since the rate of phosphate uptake in mitochondria is very high and cannot be measured accurately without the use of rather sophisticated apparatus [20,27], we have studied the effect of ANPP on phosphate transport in reconstituted liposomes. The reciprocal plot presented in Fig. 1 shows that ANPP inhibits the transport of phosphate in a competitive manner with respect to the substrate. The K_i can be determined to be 3.2 mM. In contrast, under the same experimental conditions, ANP, the non phosphorylated analogue of ANPP, shows no effect on phosphate transport in reconstituted liposomes (not shown).

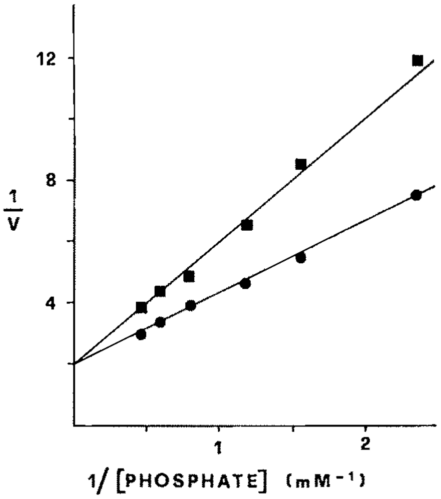

Fig 1. Competitive inhibition of phosphate transport by ANPP in the dark. The mitochondria were solubilized with Triton X-114 and the extract was incorporated into liposomes. The activity of phosphate transport was measured in reconstituted liposomes. The reaction mixture contained the indicated concentrations of [^{32}P]phosphate and, where indicated, 2.8 mM ANPP added together with the labeled substrate. Reaction time: 1 min; temperature: 25°C V is expressed in μmol/min per mg protein. ■, with ANPP; ●, without ANPP. ANPP has no effect on the radioactivity associated to control samples, i.e., with the stop inhibitor added before the labeled substrate.

Inhibition of the phosphate carrier by ANPP upon illumination

As an azido compound, ANPP can react with proteins after photoactivation and formation of a nitrene intermediate. Thus the effect of ANPP on the transport of phosphate in intact mitochondria was investigated upon illumination. As a control, ANP was also tested. Pig heart mitochondria were incubated in the dark at 0°C in the presence of 1.4 mM ANPP or ANP and in the absence of phosphate. After 30 min an aliquot of the incubation was subjected to photoirradiation for 15 min at 0°C, while the rest was kept in the dark. Both portions were then tested for phosphate-transport activity by the swelling technique, i.e., in the presence of a very high concentration of phosphate. The results illustrated in Fig. 2A show that both ANPP and ANP when used in the dark do not have any effect on the swelling of mitochondria in the presence of 100 mM ammonium phosphate. When, on the other hand, mitochondria were illuminated in the presence of the azido compounds, ANPP strongly inhibits the rate of swelling, whereas ANP still has no effect (Fig. 2B). The striking difference between the effect of ANPP on the mitochondrial swelling in 100 mM phosphate under illumination and its lack of effect in the dark demonstrates the formation of an irreversible modification of the phosphate carrier by ANPP during irradiation. Furthermore, the failure of ANP to inhibit the phosphate carrier even in the presence of light indicates that the phosphate group and not the hydrophobic part of ANPP is important for the interaction between the inhibitor molecule and the phosphate carrier.

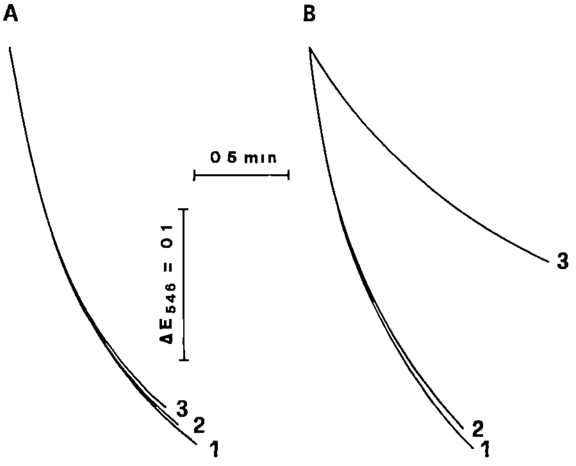

Fig. 2. The effect of ANPP and ANP, in the dark and upon illumination, on turbidity changes corresponding to swelling of mitochondria in ammonium phosphate. Freshly prepared mitochondria were incubated with 1.4 mM ANPP (curves 3) or ANP (curves 2) with and without illumination 0.5 mg mitochondrial protein were transferred to cuvettes containing 0 5 ml of 100 mM ammonium phosphate, 10 mM Tris-HCl, 1 μg rotenone (pH 7.4). Temperature: 25°C. (A) without illumination; (B) with illumination. Curves 1, controls without addition of ANPP or ANP.

Fig. 3 illustrates the dependence of the light-induced ANPP inhibition of the phosphate carrier on the concentration of the inhibitor. In these experiments mitochondria were illuminated in the presence of ANPP. After washing of the mitochondria in the presence of an excess of phosphate, the membranes were solubilized with Triton X-114 and the activity of the reconstituted phosphate transport was measured in liposomes. The results show that the inhibition of the phosphate-phosphate exchange activity increases with increasing concentrations of ANPP (Fig. 3), reaching a value of 76% at 1.6 mM ANPP. As a control, Fig. 3 shows that the activity of the phosphate carrier is not influenced by ANPP without photoirradiation, in agreement with the finding that the inhibition by ANPP in the dark is

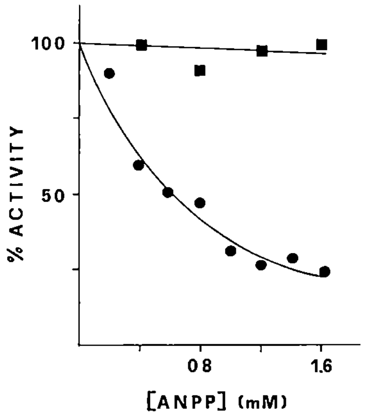

Fig 3 Concentration dependence of the inhibition of the phosphate-phosphate exchange activity by ANPP in the dark and upon illumination. Mitochondria incubated with the indicated concentrations of ANPP with (●) or without (■) illumination were washed in the presence of an excess of phosphate before solubilization. The activity was measured in liposomes reconstituted with Triton X-114 mitochondrial extracts.

reversible (Fig. 1 and 2A). It should also be pointed out that photoirradiation of the mitochondria alone, i.e., in the absence of ANPP, does not affect the phosphate carrier (not shown).

It is known that the binding affinity of phosphate for the phosphate carrier increases on lowering the pH [28]. It was therefore interesting to investigate also the pH dependence of the light-induced inhibition of the phosphate carrier by ANPP. For this purpose, mitochondria were illuminated in the presence of 0.3 mM ANPP at different pH values. After washing and solubilization of the mitochondria, phosphate-transport activity was measured at the same pH of 6.5 in liposomes reconstituted with the different mitochondrial extracts. It was found that the inhibition of the phosphate carrier by ANPP in the light increases substantially on lowering the pH from 7.4 to 6.4 (data not shown). In a typical experiment, the residual activity of the phosphate carrier treated with 0.3 mM ANPP was 73% at pH 7.0 and only 32% at pH 6.4. Correspondingly, the amount of [^{32}P]ANPP bound to the purified phosphate carrier was increased from 0.14 to 0.29 mol/mol of carrier protein.

Protein labeling by [^{32}P]ANPP

In order to identify the mitochondrial proteins labeled by ANPP, the SDS-extract, the Triton X-114 extract and the purified phosphate carrier obtained from [^{32}P]ANPP photolabeled mitochondria were subjected to SDS-polyacrylamide gel electrophoresis. The radioactive-labeled proteins were then identified by autoradiography. Lanes 4 of Fig. 4A and B show that [^{32}P]ANPP is bound to the purified phosphate carrier which corresponds to a single band of an apparent molecular weight of 33 kDa. Among the other protein bands present in the SDS or Triton X-114 extracts of mitochondria only two are substantially labeled (Fig. 4, lanes 2 and 3). On the basis of their staining intensity and their molecular weight, they can be identified as the ADP/ATP carrier (30 kDa) and the β-subunit of the F_1-ATPase complex (50 kDa). The labeling of the latter by [^{32}P]ANPP has been reported by Lauquin et al. [12].

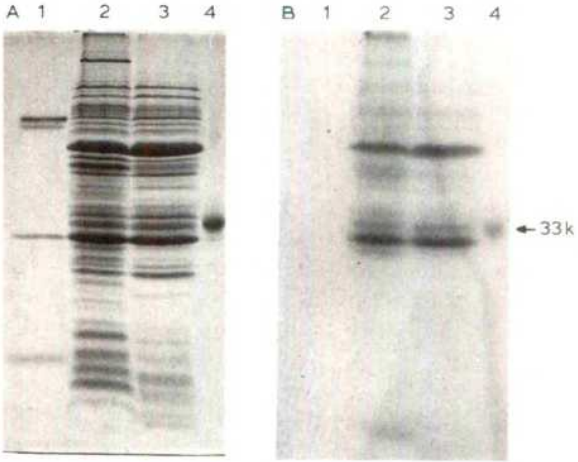

Fig. 4. Labeling of the phosphate carrier by [^{32}P]ANPP. SDS-polyacrylamide gel electrophoresis (A) and autoradiography (B) of the SDS extract (lanes 2), the Triton X-114 extract (lanes 3) and the purified phosphate carrier (lanes 4) obtained from 1 mM [^{32}P]ANPP photolabeled mitochondria. Lanes 1, marker proteins (bovine serum albumin, carbonic anhydrase, cytochrome *c*).

On the basis of the competition experiments it can be assumed that ANPP binds to the phosphate carrier at the substrate-binding site. Therefore, it was necessary to test whether phosphate correspondingly protects the phosphate carrier from inactivation and labeling by [^{32}P]ANPP. Fig. 5 shows that, in fact, the light-induced inhibition of the phosphate-transport activity by 0.8 mM ANPP is progressively suppressed by the presence of increasing concentrations of phosphate during photoirradiation. A nearly complete protection is achieved in the presence of 10 mM phosphate. The specificity of the protection of the phosphate carrier against ANPP inactivation was investigated by testing the effect of several anions. As shown in Fig. 5, sulphate up to 20 mM has no protective effect. Similarly ADP, malate, citrate and 2-oxoglutarate have virtually no effect on the inhibition of the phosphate carrier by ANPP (not shown). In contrast, arsenate, which is known to be a substrate of the phosphate carrier in mitochondria [29], exhibits a significant protection, although lower than that exerted by phosphate. Under the conditions of Fig. 5, the inhibition of the phosphate-transport activity caused by 0.8 mM ANPP is reduced to 23% by 20 mM arsenate.

The observed protection by phosphate against inhibition by ANPP is accompanied by a decreased

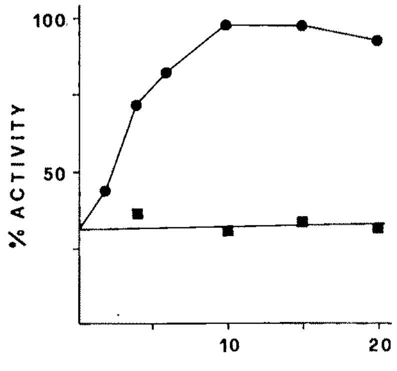

Fig. 5. Effect of phosphate and sulphate on the light-induced inhibition of the phosphate carrier by ANPP. The indicated concentrations of phosphate (●) or sulphate (■) were present during the incubation of the mitochondria with 0.8 mM ANPP in the light. The activity was measured as in Fig. 3.

labeling of the carrier. Thus the radioactivity associated with the phosphate carrier purified from [^{32}P]ANPP photolabeled mitochondria is much less in the presence of phosphate during photoirradiation than in its absence (Fig. 6).

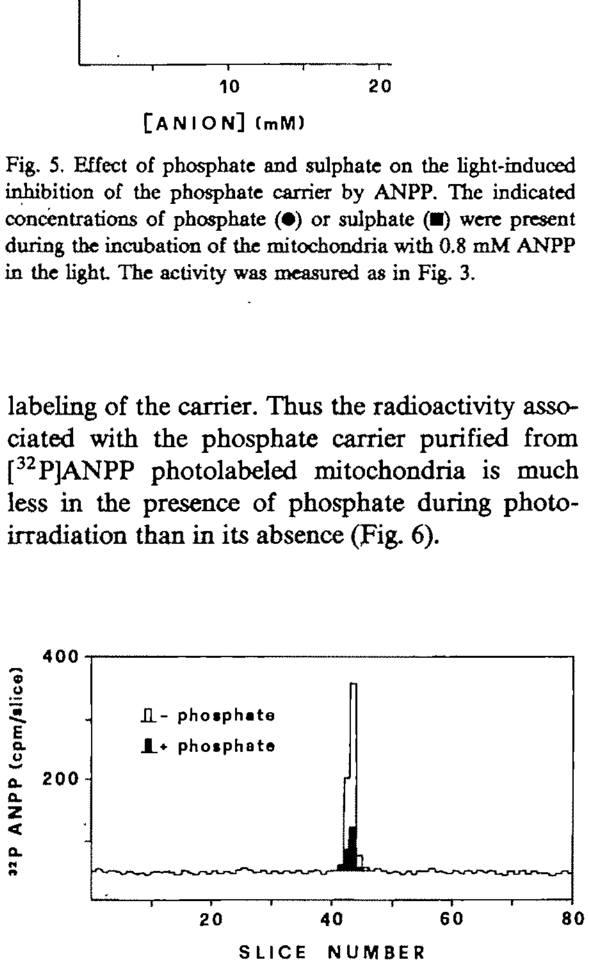

Fig. 6. [^{32}P]ANPP labeling of the phosphate carrier in the presence and absence of phosphate. The mitochondria were illuminated in the presence of 1 mM [^{32}P]ANPP with and without 20 mM phosphate. The phosphate carrier was purified and subjected to SDS gel electrophoresis. The distribution of radioactivity was determined after staining, destaining and slicing the gels. The histograms show [^{32}P]incorporation in the presence and absence of phosphate. For fractions 1–41 and 47–80 only the values of radioactivity obtained in the absence of phosphate are reported, since those in the presence of phosphate are not significantly different. Fractions 42–45 corresponding to an M_r of 33000 are the only ones which were stained by Coomassie blue.

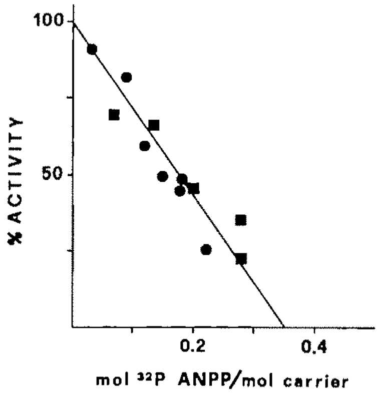

Fig. 7. Inhibition of the phosphate-phosphate exchange activity as a function of the amount of [^{32}P]ANPP bound to the phosphate carrier. Mitochondria were photolabeled by different concentrations of [^{32}P]ANPP. After purification of the phosphate carrier the activity was measured in proteoliposomes. The amount of [^{32}P]ANPP bound (mol/mol protein) was determined by counting the radioactivity of the purified carrier preparations after delipidation (●) or gel electrophoresis (■) and assuming a molecular weight of the carrier of 33 kDa.

Stoichiometry of [^{32}P]ANPP binding

The stoichiometry of ANPP binding to the phosphate carrier was investigated by incubating the mitochondria with increasing concentrations of [^{32}P]ANPP in the presence of light. After washing of the mitochondria, the phosphate carrier was solubilized and purified. Both the amount of [^{32}P]ANPP bound to the protein and the transport activity in the reconstituted system were determined. The results are reported in Fig. 7. If the data correlating binding and extent of inhibition are extrapolated to 100% inhibition a maximal binding of 0.35 mol of [^{32}P]ANPP per mol of 33 kDa phosphate carrier protein is obtained.

Discussion

It has been demonstrated in this paper that ANPP can be used as photoaffinity label for the phosphate carrier of mitochondria. When mitochondria are incubated with ANPP and then illuminated, the phosphate carrier is irreversibly modified. It is interesting to note that ANPP is able to inhibit the transport of phosphate in mitochondria and in proteoliposomes even without illumination. The inhibition is correlated with the amount of inhibitor used. Almost 80% inhibition is achieved when mitochondria are treated with 1.6 mM ANPP in the light (Fig. 3). Since azido derivatives show an unspecific reactivity towards aminoacid side-chains, it was important to see whether the observed inhibition was the result of a random modification of the carrier by the azido moiety of the label. The results obtained by incubating the mitochondria with ANP, the non-phosphorylated analogue of ANPP, both in the dark and in the light, clearly demonstrate that the presence of the phosphate group is an essential requirement for the label molecule to inhibit the transport of phosphate. Thus we can suggest that ANPP reacts at the phosphate-binding site of the phosphate carrier. This suggestion is supported by the kinetic data of Fig. 1. In fact when ANPP is incubated in the dark with the reconstituted phosphate carrier the label inhibits the transport of phosphate in a competitive manner. This can easily explain why ANPP, if used in the dark, shows no inhibition when the uptake of phosphate is measured by the swelling technique. Swelling of mitochondria is in fact measured in the presence of 100 mM phosphate, whose high concentration is able to remove ANPP inhibition. Since ANPP behaves as a competitive inhibitor, one should expect that phosphate is also able to protect the phosphate carrier against the inactivation caused by ANPP in the light. Indeed we have found that the transport of phosphate is not inhibited when the mitochondria are illuminated with ANPP in the presence of at least 10 mM phosphate (Fig. 5). The protective effect of phosphate shows again that ANPP reacts with the phosphate carrier at the phosphate-binding site. Moreover, among several other anions tested, only arsenate, which is also a substrate for the phosphate carrier [29], is able to prevent the inhibition of phosphate transport by ANPP. It is interesting to note that the inhibition of phosphate transport by ANPP is pH-dependent. At lower pH values the label shows a stronger inhibitory effect. This result could be explained by the increased affinity of the phosphate group at lower pH, since it has been shown that the K_m of phosphate for the phosphate carrier decreases on lowering the pH of the medium [28]. In this respect it is possible to suggest that positive charges are important for the recognition of the substrate at the substrate-binding site of the protein.

In order to ascertain how many molecules of the reagent become bound to the phosphate carrier at maximal inhibition of transport, ^{32}P-radioactive ANPP has been used. Incubation of the mitochondria with [^{32}P]ANPP in the presence of light results in the labeling of the phosphate carrier and, in addition, of the ADP/ATP translocator and the β-subunit of the F_1-ATPase complex (Fig. 4). The latter result is in agreement with the finding of Lauquin et al., who used ANPP to label the phosphate-binding site of the F_1-ATPase [12,30]. When the labeling is carried out in the presence of phosphate the amount of [^{32}P]ANPP bound to the phosphate carrier is drastically reduced (Fig. 6). Phosphate also protects the β-subunit of the ATPase and, less efficiently, the ADP/ATP translocator against labeling (results not shown). Conversely, ADP shows a protective effect on the ADP/ATP carrier and the F_1-ATPase complex, but not on the phosphate carrier. Correlation of the [^{32}P]ANPP incorporation into the purified phosphate carrier with the activity inhibition indicates that at 100% inhibition only 0.35 mol of ANPP are bound per mol of 33 kDa carrier protein. This result could be explained by assuming that the phosphate carrier exists in an oligomeric structure formed by two identical subunits. However, the amount of ANPP bound per protein may be underestimated for at least two reasons: (a) the phosphate group of the label may be partly hydrolyzed as reported by Lauquin et al. [12], and (b) some molecules of the carrier may not have reacted with ANPP. A stoichiometry of 1 : 1 can therefore not be excluded by the present results. In conclusion, we have shown that ANPP is a suitable label to characterize the phosphate-binding site of the mitochondrial phosphate carrier. We are currently investigating the location and the modified aminoacid(s) in the primary structure of the phosphate carrier.

References

1 Palmieri, F and Quagliariello, E. (1978) in Bioenergetics at Mitochondrial and Cellular Levels (Wojtczak, L , Lenartowicz, E. and Zborowski, J , eds.), pp. 5–38, Nencki Institute of Experimental Biology, Warsaw

2 LaNoue, K.F. and Schoolwerth, A.C. (1979) Annu. Rev. Biochem. 48, 871–922

3 Fonyó, A (1979) Pharmacol. Ther 7, 627–645

4 Wohlrab, H. (1980) J. Biol. Chem. 255, 8170–8173

5 Kolbe, H.V.J., Bottrich, J., Genchi, G., Palmieri, F. and Kadenbach, B. (1981) FEBS Lett 124, 265–269

6 Bisaccia, F and Palmieri, F. (1984) Biochim. Biophys Acta 766, 386–394

7 Kolbe, H.V.J and Wohlrab, H. (1985) J. Biol Chem. 260, 15899–15906

8 Palmieri, F., Bisaccia, F., Indiveri, C. and Izzo, A (1985) in Achievements and Perspectives in Mitochondrial Research, Vol I Bioenergetics (Quagliariello, E., Slater. E.C., Palmieri, F., Saccone, C. and Kroon, A.M., eds.), pp. 291–302, Elsevier, Amsterdam

9 Klingenberg, M., Durand, R. and Guérin, B (1974) Eur. J. Biochem. 42, 135–150

10 Fonyò, A. and Vignais, P.V. (1980) J Bioenerg. Biomembranes 12, 137–149

11 Ligeti, E and Fonyò, A (1984) Eur J Biochem 139, 279–285

12 Lauquin, G., Pougeois, R and Vignais, P.V. (1980) Biochemistry 19, 4620–4626

13 Rouse, G. and Fleischer, S (1967) Methods Enzymol. 10, 325–329

14 Smith, A.L. (1967) Methods Enzymol. 10, 81–86

15 Krisch, K. (1971) Enzymes 5, 43–69

16 Kasahara, M. and Hinkle, P.C. (1977) J. Biol. Chem. 252, 7384–7390

17 Kramer, R and Klingenberg, M. (1977) FEBS Lett. 82, 363–367

18 Chappell, J.B. and Crofts, A.R. (1966) in Regulation of Metabolic Processes in Mitochondria (Tager, J.M., Papa, S., Quagliariello, E. and Slater, E.C., eds.), p 293–316, Elsevier, Amsterdam

19 Palmieri, F and Klingenberg, M (1967) Eur. J. Biochem. 1, 439–446

20 Palmieri, F. and Klingenberg, M. (1979) Methods Enzymol. 56, 279–301

21 Laemmli, U.K (1970) Nature 227, 680–685

22 Downer, N.W., Robinson, N.C. and Capaldi, R.A. (1976) Biochemistry 15, 2930–2936

23 Tommasino, M. and Capaldi, R.A (1985) Biochemistry 24, 3972–3976

24 Bensadoun, A. and Weinstein, D. (1976) Anal. Biochem. 70, 241–250

25 Kusov, Y.Y. and Kalinchuck, N.A (1978) Anal Biochem 88, 256–262

26 Folch, J., Less, M., Stanley, S. and Stanley, G.H. (1957) J Biol. Chem. 226 497–553

27 Ligeti, E., Brandolin, G., Dupont, Y. and Vignais, P.V. (1985) Biochemistry 24, 4423–4428

28 Fonyò, A., Palmieri, F., Ritvay, J. and Quagliariello, E (1974) in Membrane Proteins in Transport and Phosphorylation (Azzone, G.F. et al., eds.), pp. 283–286, Elsevier/North-Holland, Amsterdam

29 Chappell, J.B (1968) Brit. Med. Bull. 24, 150–157

30 Pougeois, R. and Lauquin, G. (1985) Biochemistry 24, 1020–1024

Biochimica et Biophysica Acta 890 (1987) 47–54
Elsevier

BBA 42203

Subunit component and their roles in the sodium-transport NADH : quinone reductase of a marine bacterium, *Vibrio alginolyticus*

Maki Hayashi [a] and Tsutomu Unemoto [b]

Departments of [a] Enzymology and [b] Membrane Biochemistry, Research Institute for Chemobiodynamics,
Chiba University, 1-8-1 Inohana, Chiba 280 (Japan)

(Received 8 July 1986)

Key words Flavoprotein; NADH : quinone reductase; Respiratory chain; Subunit composition;
Sodium ion transport; (Marine bacterium, *V. alginolyticus*)

The sodium-transport respiratory chain NADH : quinone reductase of a marine bacterium, *Vibrio alginolyticus*, was purified by high-performance liquid chromatography. The purified quinone reductase, which catalyses the reduction of ubiquinone to ubiquinol, was composed of three subunits, α, β and γ, with apparent molecular weights of 52 000, 46 000 and 32 000, respectively. The subunit β contained one molecule of FAD per molecule and catalysed the reduction of ubiquinone to ubisemiquinone. The subunit α contained FMN as a prosthetic group. The quinone reductase was reconstituted from α and $\beta\gamma$, but not from α and β, and the maximum activity was obtained at the equimolar amounts of FAD(β) and FMN(α). The molecular weight of quinone reductase complex was estimated to be 254 000, which corresponded to a dimer of $\alpha\beta\gamma$ complex or $\alpha_2\beta_2\gamma_2$. The subunit γ increased the affinity of β for ubiquinone-1. The reaction catalysed by FMN-containing α-subunit was essential for the generation of membrane potential in proteoliposomes and the coupling site of sodium pump in the quinone reductase was localised to this reaction step.

Introduction

A marine bacterium, *Vibrio alginolyticus,* has a respiratory chain-coupled Na^+ extrusion system functioning at alkaline pH [1,2]. The respiratory chain NADH : quinone reductase of this bacterium requires Na^+ for the maximum activity [3,4] and the Na^+-dependent quinone reductase has been shown to be tightly coupled to the extrusion of Na^+ [5,6]. The quinone reductase was partially purified from the membrane of *V. alginolyticus* and the reduction of ubiquinone to ubiquinol was found to proceed via ubisemiquinone radicals [7]. The reduction of ubiquinone to ubisemiquinone was catalysed by a flavoprotein, NADH dehydrogenase. Very recently, we have shown that in addition to FAD-containing NADH dehydrogenase, another flavoprotein containing FMN is required for the quinone reductase activity [8]. In this paper, we report the subunit composition and the role of subunits in the sodium-transport quinone reductase of *V. alginolyticus.*

Materials and Methods

Chemicals. Liponox DCH, an alkyl polyoxyethylene ether detergent having average alkyl chain and polyoxyethylene chain lengths of 10 and 8, respectively, was kindly supplied by Lion Co.,

---

Abbreviations: Q-1, ubiquinone-1; HQNO, 2-*n*-heptyl-4-hydroxyquinoline *N*-oxide; oxonol VI, bis(3-propyl-5-oxoisoxazole-4-yl)pentamethineoxonol

Correspondence: T Unemoto, Department of Membrane Biochemistry, Research Institute for Chemobiodynamics, Chiba University, 1-8-1 Inohana, Chiba 280, Japan.

0005-2728/87/$03 50 © 1987 Elsevier Science Publishers B V (Biomedical Division)

Kanagawa, Japan. Ubiquinone-1 (Q-1) was kindly supplied by Eizai Co., Tokyo, Japan. 2-*n*-Heptyl-4-hydroxyquinoline *N*-oxide (HQNO) and L-α-phosphatidylcholine from soybean, Type IV-S, were obtained from Sigma. Bis(3-propyl-5-oxoisoxazole-4-yl)pentamethine-oxonol (oxonol VI) was obtained from Molecular Probes, Inc., OR.

Enzyme assays. NADH dehydrogenase was assayed at 30°C from the decrease in absorbance at 340 nm with menadione as an electron acceptor as described in Ref. 7. Quinone reductase was assayed at 30°C by following the formation of reduced Q-1 from the changes in absorption difference at the wavelength pair, 248–267 nm, as described [7]. Since the membrane and Liponox extract contain quinol oxidase activity, the quinone reductase of these fractions was assayed in the presence of 10 mM KCN.

One unit of activity is defined as the amount of enzyme catalysing the oxidation of 1 μmol NADH or the reduction of 1 μmol Q-1 per min.

High-performance liquid chromatography. Prepacked high-performance columns were obtained from Toyo Soda Manufacturing Co., Tokyo, Japan. Gel chromatography with a TSK-gel G3000SWG column (21.5 × 600 mm) and ion-exchange chromatography with a TSK-gel DEAE-5PW (21.5 × 150 mm) were performed as described previously [8].

Determination of molecular weight of quinone reductase complex. The molecular weight of the reductase complex was determined by means of a low-angle laser light scattering combined with high-performance gel chromatography as described by Maezawa and Takagi [9]. In this experiment, TSK-gel G4000SW (7.5 × 600 mm) and G3000SW (7.5 × 600 mm) columns were connected in series and it was equilibrated and developed with 20 mM Tris-HCl (pH 7.0)/0.1 M NaCl/5% glycerol/0.1 mM EDTA/0.1% Liponox. The eluate was monitored successively by an ultraviolet spectrophotometer UV-8000 (Toyo Soda), a precision differential refractometer RI-8000 (Toyo Soda) and by a low-angle laser light scattering photometer model LS-8000 (Toyo Soda). The molecular weight of protein moiety of the reductase complex was calculated according to Maezawa and Takagi [9]. The instrument constants were determined by use of monomer, dimer and trimer of bovine serum albumin as standards.

Preparation of proteoliposomes. Proteoliposomes containing quinone reductase were prepared by a cholate-deoxycholate dialysis procedure according to Sone et al. [10]. L-α-Phosphatidylcholine from soybean, Type IV-S, which contains about 40% of phosphatidylcholine, was used without further purification. The phospholipids were suspended in the medium containing 2% sodium cholate, 1% sodium deoxycholate, 10 mM Hepes-NaOH (pH 7.6) and 0.2 mM EDTA at the concentration of 50 mg/ml, and then it was subjected to sonic oscillation in a bath-type sonicator. The phospholipid solution (0.4 ml) and the enzyme solution (0.1 ml) were combined and the mixture was dialysed against 250 ml of solution containing 10 mM Hepes-KOH (pH 7.6)/2.5 mM $MgSO_4$/0.2 mM EDTA with stirring for 20 h at room temperature.

Measurement of membrane potential. The generation of membrane potential, positive inside, in proteoliposomes was monitored by an absorbance band shift of oxonol VI [11,12] at 625–587 nm with a Hitachi 557 two-wavelengths spectrophotometer.

Other methods. Flavins were identified by thin-layer chromatography on silica gel [8], and FAD and FMN contents were determined by the method of Faeder and Siegel [13]. SDS-polyacrylamide gel electrophoresis was performed by the method of Laemmli [14]. Gels were stained with Coomassie brilliant blue G-250 and then scanned by using a Shimazu dual-wavelegth chromato-scanner, CS-910, at 590–440 nm.

Kinetic constants and their standard errors were calculated as described previously [7].

Protein was determined by the method of Lowry et al. [15] with bovine albumin as a standard. The method of Bradford [16] was also employed for the determined of purified enzyme protein and the dye reagent was obtained from Bio-Rad Laboratories.

Results

Purification of quinone reductase

In our previous paper [7], we have shown that rechromatography of the quinone reductase on QAE-Sephadex leads to a partial dissociation of the reductase complex into subunits. Therefore, a high-performance liquid gel chromatography was employed to remove impurities as much as possible and then the reductase complex was applied to an ion-exchange column.

The purification procedure has been outlined in our recent paper [8]. Briefly, the quinone reductase was extracted from the membrane fraction of *V. alginolyticus* with 1% Liponox in the presence of 10% glycerol as described in Ref. 7. The Liponox extract was applied to DEAE-Sephacel column and the reductase was eluted with 0.3 M NaCl (DEAE-Sephacel fraction). This fraction was applied to a TSK-gel G3000SWG gel column as described in Ref. 8. This step may be repeated to increase the specific activity of quinone reductase. The peak fraction was collected (SWG fraction) and then it was applied to TSK-gel DEAE-5PW.

Fig. 1 is the result of DEAE-5PW chromatography. The quinone reductase, which catalyses the reduction of ubiquinone to ubiquinol [7], was eluted at 61.5 min and the NADH dehydrogenase, which catalyses the reduction of Q-1 to ubisemiquinone [7], was eluted at 65.5 min. The relative amounts of the two enzymes varied depending on preparations and a prolonged storage of the sample increased the amount of NADH dehydrogenase.

Table I is a typical result of purification. The purified quinone reductase with the specific activity of 112 units/mg protein showed a high NADH dehydrogenase activity (181 units/mg protein). On the other hand, the NADH dehydrogenase with the specific activity of 255 units/mg protein showed only a slight quinone reductase activity. Further purification of NADH dehydrogenase with Bio-Gel HTP as described in Ref. 7 gave a highly purified enzyme with the specific activity of 390 units/mg protein, which showed no quinone reductase activity. Apparently, the NADH dehydrogenase was a component of the quinone reductase and was separated from the reductase complex during purification.

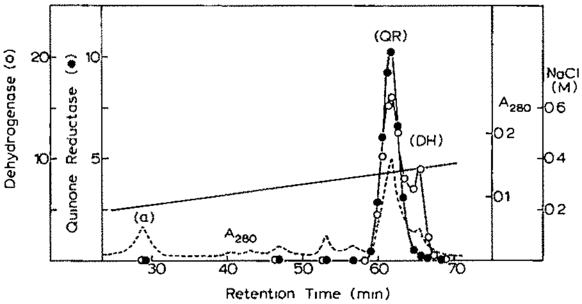

Fig. 1 TSK-gel DEAE-5PW chromatography. About 2.8 mg protein of second SWG fraction was applied to the column and it was eluted by a linear gradient from 0.1 to 0.55 M NaCl at the flow rate of 3 ml/min The enzyme activities of eluate were measured by the NADH dehydrogenase assay (○) and by the quinone reductase assay (●) as described under Materials and Methods The activity is expressed in units/ml. The dotted line denotes the absorbance of eluate at 280 nm QR, quinone reductase; DH, NADH dehydrogenase.

Subunit composition and flavin content of quinone reductase

Fig. 2 is the densitometric scans of stained bands of SDS-polyacrylamide gel electrophoresis. The three polypeptide components, designated as

TABLE I

PURIFICATION OF QUINONE REDUCTASE AND NADH DEHYDROGENASE FROM THE MEMBRANE OF *VIBRIO ALGINOLYTICUS*

Fraction	Protein (mg)	Quinone reductase assay		NADH dehydrogenase assay	
		(units)	(U/mg)	(units)	(U/mg)
1. Membrane	6440	8040	1.25	15485	2.40
2. Liponox extract	1054	3544	3.36	6038	5.73
3 DEAE-Sephacel	416	2958	7.11	5118	12.3
4. First SWG	35.5	1159	32.7	1983	55.9
5. Second SWG	14.0	753	53.8	1292	92.3
6 DEAE-5PW					
Quinone reductase	3.1	346	112	561	181
NADH dehydrogenase	1.2	14	11.7	306	255

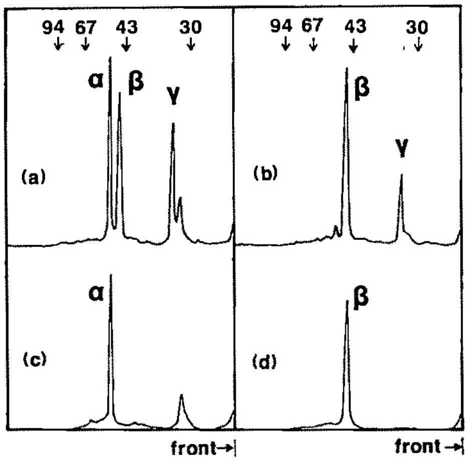

Fig. 2. Densitometer trace of SDS-polyacrylamide gel electrophoresis of purified enzyme on 10% acrylamide gel. The gel was stained and then scanned as described under Materials and Methods. The samples analysed, with specific activities in parentheses, were: (a) quinone reductase from DEAE-5PW (112); (b) NADH dehydrogenase from DEAE-5PW (255); (c) the α fraction from DEAE-5PW; (d) NADH dehydrogenase further purified by Bio-Gel HTP (390) The molecular weights of standard proteins are indicated in thousands

α, β and γ, were concentrated in the quinone reductase (Fig. 2a). The plots of log relative mobilities of these subunits versus gel concentrations, namely Ferguson plots, showed no anomalous behavior and the apparent molecular weights of α, β and γ were estimated to be 52 000, 46 000 and 32 000, respectively. The NADH dehydrogenase from DEAE-5PW (Fig. 2b) contained β and γ. However, the enzyme further purified by Bio-Gel HTP (Fig. 2d) contained a single polypeptide band β, indicating that the subunit β is NADH dehydrogenase.

The highly purified NADH dehydrogenase with the specific activity of 390 units/mg protein contained 21.3 nmol FAD/mg protein [8]. The molecular weight per FAD molecule was calculated to be 47 000, which was very similar to that of β (46 000). This means that β subunit contains one FAD molecule per molecule.

The subunit α was surveyed by means of the appearence of quinone reductase activity in combination with βγ as well as the detection of an α band on SDS-polyacrylamide gel electrophoresis. As shown in Fig. 1, the protein peak eluted at 29 min corresponded to α fraction. This fraction contained FMN as a prosthetic group at the concentration of 8.8–10.3 nmol/mg protein. As shown in Fig. 2c, this fraction still contained a broad polypeptide band as a contaminant, which appeared in front of γ.

Assuming that the color density of stained band is proportional to the amount of polypeptides, the weight ratio α : β : γ of the quinone reductase was calculated from the each peak area of Fig. 2a to be 1.25 : 1 : 0.84. If the quinone reductase was composed of equimolar quantities of α, β and γ, the weight ratio α : β : γ can be calculated to be 1.13 : 1 : 0.70 from their molecular weights. These values were very close to the estimated values. On the other hand, the NADH dehydrogenase from DEAE-5PW (Fig. 2b) contained β and γ in the ratio 1 : 0.46. The ratio of γ to β, however, varied from 0.24 to 0.54 depending on preparations, suggesting that γ was likely to be lost from the complex especially in the absence of α.

The purified quinone reductase contained FAD and FMN in equimolar quantities amounting to 6.6–7.2 nmol each flavin/mg protein. The flavin content corresponded to a minimum molecular weight of 150 000–140 000/each flavin molecule. Since the sum total of α + β + γ is 130 000, these results also strongly suggested that the quinone reductase contains α, β and γ in equimolar quantities.

Determination of molecular weight of quinone reductase complex

The molecular weight of purified quinone reductase complex in 0.1% Liponox solution was determined by means of a low-angle laser light scattering combined with high-performance gel chromatography as described under Materials and Methods. As shown in Fig. 3, the quinone reductase complex was eluted as a single peak at a retention time of 35.5 min. The first peak observed only for the tracing of light scattering photometer (LS) was due to contaminated large particles or small air-bubbles. No other active species were detected in the eluate. The extinction coefficient at 280 nm for quinone reductase was estimated to be 1.85 ml · mg^{-1} · cm^{-1}. From the values of output of each detector, the molecular weight of protein moiety of the complex was calculated to be 254 000. This value was twice that of α + β + γ, indicating

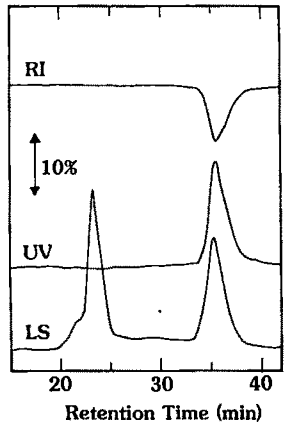

Fig. 3. Elution pattern of quinone reductase complex in 0.1% Liponox The quinone reductase (83 μg) in 300 μl of the elution buffer was applied to the column and it was eluted at the flow rate of 0.8 ml/min The eluate was monitored successively by the ultraviolet spectrophotometer at 280 nm (UV), the differential refractometer (RI) and by the laser light scattering photometer (LS). The tracings in the figure were adjusted so as to compensate time-lags among recordings of each monitor Gain setting: ultraviolet monitor, 0.64 full scale, RI monitor, $128 \cdot 10^{-6}$; LS monitor, ×32.

that the active reductase complex exists as a dimer of αβγ or $\alpha_2\beta_2\gamma_2$ in 0.1% Liponox solution.

Reconstitution of quinone reductase

The α fraction by itself showed no enzyme activity, but the combination of α with βγ manifested the quinone reductase activity. Fig. 4 shows the reconstitution of quinone reductase from α and βγ. In this experiment, the amount of subunit was expressed in flavin content and the reductase activity was expressed in units/nmol FAD. With the increase in α (FMN), the activity increased and reached the maximum value at the equimolar amounts of FAD and FMN. The optimum ratio was not affected by the amount of βγ(FAD) used for the reconstitution. These results further indicated that the quinone reductase complex is composed of equimolar amounts of FAD and FMN. As shown in fig. 4, the combination of β with α gave no significant reductase activity and the presence of γ subunits was essential for the reconstitution of quinone reductase.

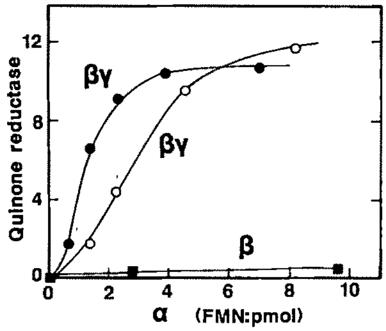

Fig. 4. Reconstitution of quinone reductase. βγ corresponding to 3.25 (●) or 6.5 (○) pmol FAD, or β corresponding to 3.6 pmol FAD (■), was preincubated with varied amounts of α for 30 min at 20°C in the medium containing 10 mM Tris-HCl (pH 7.9)/0.34 M NaCl/5% glycerol/0.1 mM EDTA/0.1% Liponox in a total volume of 20 μl. After that, 2 μl of the reaction mixture was used for the quinone reductase assay under the standard conditions. The activity is expressed in units/nmol FAD.

Effect of γ on the K_m value of β for Q-1

We have shown that Q-1 functions as the substrate of NADH dehydrogenase and quinone reductase and that the apparent K_m value for Q-1 of the former is considerably higher than that of the latter [7]. Therefore, the effect of γ on the K_m value of β for Q-1 was examined. In this experiment, preparations of βγ differing in the ratio γ : β were employed. As shown in Table II, the K_m value of β in the absence of γ was 11.7 μM, which decreased with the increase in the ratio γ : β. Although β and βγ used were prepared separately, the difference in the maximum velocity was small when expressed in units/nmol FAD. Apparently, γ subunit affected the affinity of β for Q-1. On the other hand, the K_m value of quinone reductase complex (αβγ) for Q-1 was very low amounting to about 0.2 μM. Due to the

TABLE II

EFFECT OF γ ON THE K_m VALUE OF β FOR Q-1

The reaction was carried out under the conditions of quinone reductase assay except for the variation of the concentration of Q-1. The initial velocity was determined from the rate of NADH consumption. The ratio γ : β was determined from the ratio of color density of stained SDS-polyacrylamide gel.

Subunit	Ratio (γ/β)	K_m value for Q-1 (μM)	Maximum velocity (U/nmol FAD)
β	0	11.7 ±1.0	4.2 ±0.2
βγ	0.25	5.31±0.46	6.73±0.20
βγ	0.46	2.70±0.37	6.27±0.25
αβγ	0.87	0.19±0.17	21.6 ±1.1

absence of purified γ at present, the saturation level of γ could not be determined. However, the increase of γ to the level of quinone reductase seemed to decrease the K_m value of β close to that of αβγ. In contrast to β and βγ, since the αβγ complex catalyses the reduction of Q-1 to ubiquinol, the maximum velocity obtained with αβγ could not be directly comparable to those of β and βγ.

Generation of membrane potential in proteoliposomes

Proteoliposomes containing quinone reductase complex were prepared by cholate-deoxycholate dialysis procedure and the generation of membrane potential, positive inside, was monitored by the absorbance band shift of oxonol VI. As shown in Fig. 5, the addition of NADH in the presence of Q-1 induced the oxonol response suggesting the generation of Δψ, positive inside. The Δψ was collapsed by the addition of 1 μM valinomycin or 10 mM SCN^-. In a separate experiment, the quinone reductase activity was monitored under the same conditions. As shown in Fig. 5, the initial rate of quinol formation was 2.56 μM/min which corresponded to 28.4 units/mg protein. The oxonol response was dissipated with the consumption of Q-1, where all of Q-1 (7 μM) was converted to ubiquinol (Fig. 5). Further addition of Q-1 to the reaction mixture re-generated the Δψ. Although not shown here, when the reaction was carried out in the K^+-medium containing 50 mM K_2SO_4/10 mM Hepes-KOH (pH 7.6), no Δψ was generated. Under those conditions, the addition of 50 mM Na^+ induced the oxonol response as well as the ubiquinol formation. These Na^+-dependent reactions were completely inhibited in the presence of 2.5 μM HQNO. When menadione that accepts electrons from β(FAD) was used as an electron acceptor, no significant Δψ was generated (Fig. 5). Apparently the Δψ was generated in response to uniquinol formation and the Na^+-dependent and HQNO-sensitive reaction catalysed by α(FMN) directly participated in the generation of Δψ.

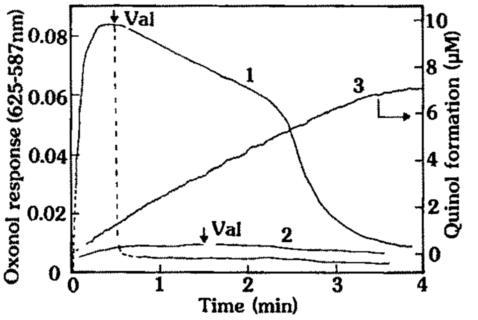

Fig 5. Oxonol VI response of proteoliposomes containing quinone reductase complex. Proteoliposomes were prepared as described under Materials and Methods, which contained about 5 mM K^+ inside the vesicles. The stock solution of proteoliposomes contained 40 mg phospholipids and 36 μg quinone reductase (54 units/mg protein) per ml. The reaction mixture contained 10 mM Hepes-NaOH (pH 7.6)/2 mM $MgSO_4$/50 mM Na_2SO_4/1 μM oxonol VI/7 μM Q-1/0.1 mM NADH/5 μl proteoliposomes in a total volume of 2.0 ml. The reaction was started by the addition of NADH and the oxonol response was monitored at 625–587 nm (curve 1). In the curve 2, 25 μM menadione was used in place of Q-1. In a separate experiment, the quinol formation was monitored under the experimental conditions of curve 1 by following the absorbance changes at 248–267 nm (curve 3). Valinomycin (Val) was used at the concentration of 1 μM.

Discussion

Earlier studies in this laboratory [7] have demonstrated that the Na^+-dependent respiratory chain NADH : quinone reductase of *V. alginolyticus* catalyses the reduction of ubiquinone to ubiquinol via ubisemiquinone radicals. The formation of ubisemiquinone is catalysed by NADH dehydrogenase which has no specific requirement for Na^+ and is insensitive to HQNO. On the other hand, the latter reaction catalysing the formation of ubiquinol specifically requires Na^+ and is very sensitive to HQNO, that is a specific inhibitor of Na^+ pump [5]. In the present work, the highly purified quinone reductase was found to be composed of three polypeptide subunits α, β and γ with apparent molecular weights of 52000, 46000 and 32000, respectively (Fig. 2). Among these subunits, β corresponds to NADH dehydrogenase and contains one molecule of FAD per molecule as a prosthetic group. Since βγ complex shows no quinone reductase activity, the FMN-containing subunit α apparently participates in the reaction catalysing the quinol formation. This reaction is Na^+-dependent and HQNO-sensitive [7] and is essential for the generation of membrane potential in proteoliposomes (Fig. 5). Although a direct measurement of Na^+ transport has not been made in this experiment, the coupling site of Na^+ pump in the quinone reductase may well be localized to the reaction catalysed by the α subunit from its Na^+-dependence and HQNO-sensitivity [5–7].

The attempt to isolate the γ-subunit in a pure state was unsuccessful at present and the molecular nature of γ remains to be established. However, it was apparent that γ is essential for the quinone reductase (Fig. 4). Since the presence of γ increases the affinity of β for Q-1 (Table II), γ seems to play an important role in the interaction of ubiquinone with the complex as well as the electron transfer from β(FAD) to α(FMN). King [17] has reported the participation of ubiquinone-binding proteins in the Complex I, II and III of mitochondrial respiratory chain. These proteins have been considered to stabilize ubisemiquinone and to dictate the location of Q sites in the redox reactions. Thus α is highly probable to be a kind of uniquinone-binding protein.

With respect to subunit composition, the quinone reductase contains α, β and γ in equimolar quantities. This conclusion was derived from the following findings: (1) the densitometric result of the stained SDS-polyacrylamide gel coincided with the presence of equimolar amounts of α, β and γ (Fig. 2); (2) the quinone reductase contained equimolar amounts of FAD and FMN, and the maximum activity was reconstituted at the equimolar amounts of FAD and FMN (Fig. 4); (3) the molecular weight of the complex per each flavin coincided with that of $\alpha+\beta+\gamma$ (130000). To estimate the molecular weight of active quinone reductase complex, a low-angle laser light scattering combined with high-performance gel chromatography was employed. This method was developed by Takagi and his coworkers and was successfully applied to membrane proteins [18]. The active quinone reductase is eluted as a single peak in the gel chromatography and the molecular weight of protein moiety is estimated to be 254000 (Fig. 3). Thus the active complex exists as a dimer of $\alpha\beta\gamma$ or as $\alpha_2\beta_2\gamma_2$ in 0.1% Liponox solution. Since no other active species are detected in the eluate, it is highly probable that this complex functions as a minimum active entity in the membrane also.

Ragan [19] proposed the electron-transfer pathways in Complex I of the mitochondrial respiratory chain, which cotnains FMN as a sole flavin and at least six iron-sulfur reaction centers. It has been postulated that the reduction-oxidation cycle of FMN via flavosemiquinone mediates the translocation of H^+ across the membrane in cooperation with iron-sulfur centers. On the other hand, Suzuki and King [20] reported that ubisemiquinone plays a central role in the translocation of H^+. Since the present enzyme system translocates Na^+ across the membrane [5,6], it is unlikely that either flavosemiquinone or ubisemiquinone directly functions as a carrier of Na^+. Thus an indirect-coupling redox pump mechanism as proposed for Complex III by Wikström and Krab [21] seems to be plausible to this enzyme system. Further studies are required to resolve these problems.

Acknowledgements

We are grateful to the technical assistance of Toyo Soda Manufacturing Co. in obtaining the result of Fig. 3. A part of this work was supported by a grant in aid from the Japanese Ministry of Education, Science and Culture.

References

1 Tokuda, H. and Unemoto, T. (1981) Biochem Biophys. Res. Commun. 120, 265–271
2 Tokuda, H and Unemoto, T (1982) J. Biol. Chem. 257, 10007–10014
3 Unemoto, T., Hayashi, M. and Hayashi, M (1977) J. Biochem 82, 1389–1395
4 Unemoto, T. and Hayashi, M. (1979) J. Biochem. 85, 1461–1467
5 Tokuda, H and Unemoto, T. (1984) J. Biol. Chem. 259, 7785–7790
6 Tokuda, H., Udagawa, T and Unemoto, T. (1985) FEBS Lett. 183, 95–98
7 Hayashi, M. and Unemoto, T (1984) Biochim. Biophys Acta 767, 470–478
8 Hayashi, M. and Unemoto, T. (1986) FEBS Lett 202, 327–330
9 Maezawa, S. and Takagi, T. (1983) J. Chromatogr 280, 124–130
10 Sone, N., Yoshida, M., Hirata, H and Kagawa, Y. (1977) J. Biochem 81, 519–528
11 Bashford, C.L. and Thayer, W.S. (1977) J Biol Chem. 252, 8459–8463
12 Russell, J.T. (1984) J. Biol. Chem. 259, 9496–9507
13 Faeder, E J. and Siegel, L.M. (1973) Anal. Biochem 53, 332–336

14 Laemmli, U.K. (1970) Nature 227, 680–685

15 Lowry, O.H., Rosebrough, N.J., Farr, A L. and Randall, R.J. (1951) J Biol Chem. 193, 265–275

16 Bradford, M M. (1976) Anal. Biochem 72, 248–254

17 King, T E. (1985) in Coenzyme Q (Lenaz, G , ed.), pp. 391–408, John Wiley & Sons, Chichester

18 Maezawa, S., Hayashi, Y., Nakae, T., Ishii, J., Kameyama, K. and Takagi, T (1983) Biochim. Biophys. Acta 747, 291–297

19 Ragan, C.I (1985) in Coenzyme Q (Lenaz, G., ed.), pp 315–336, John Wiley & Sons, Chichester

20 Suzuki, H. and King, T E (1983) J. Biol. Chem. 258, 352–358

21 Wikström, M. and Krab, K (1980) Curr. Top Bioenerg 10, 51–101

Biochimica et Biophysica Acta 890 (1987) 55–65
Elsevier

BBA 42077

Availability to monoclonal antibodies of antigenic sites of the α and β subunits in active, denatured or membrane-bound mitochondrial F_1-ATPase

Mahnaz Moradi-Améli and Catherine Godinot

Laboratoire de Biologie et Technologie des Membranes du CNRS, Université Claude Bernard de Lyon, F-69622 Villeurbanne (France)

(Received 1 September 1986)

Key words: Monoclonal antibody; Protein conformation; ATPase, F_1; (Pig heart mitochondria)

The binding of five monoclonal antibodies to mitochondrial F_1-ATPase has been studied. Competition experiments between monoclonal antibodies demonstrate that these antibodies recognize four different antigenic sites and provide information on the proximity of these sites. The accessibility of the epitopes has been compared for F_1 integrated in the mitochondrial membrane, for purified β-subunit and for purified F_1 maintained in its active form by the presence of nucleotides or inactivated either by dilution in the absence of ATP or by urea treatment. The three anti-β monoclonal antibodies bound more easily to the β-subunit than to active F_1, and recognized equally active F_1 and F_1 integrated in the membrane, indicating that their antigenic sites are partly buried similarly in purified or membrane-bound F_1 and better exposed in the isolated β-subunit. In addition, unfolding F_1 by urea strongly increased the binding of one anti-β monoclonal antibody (14 D_5) indicating that this domain is at least partly shielded inside the β-subunit. One anti-α monoclonal antibody (20 D_6) bound poorly to F_1 integrated in the membrane, while the other (7 B_3) had a higher affinity for F_1 integrated in the membrane than for soluble F_1. Therefore, 20 D_6 recognizes an epitope of the α-subunit buried inside F_1 integrated in the membrane, while 7 B_3 binds to a domain of the α-subunit well exposed at the surface of the inner face of the mitochondrial membrane.

Introduction

The ATPase-ATPsynthase (F_0-F_1) is essential for ATP synthesis in energy-transducing membranes, such as bacteria, chloroplasts and mitochondria. This complex contains two distinct parts: the F_0 part channelling the transfer of protons across the membrane, and the F_1 part containing the catalytic sites for ATP synthesis and ATP hydrolysis (for recent reviews, see Refs. 1–6).

F_1 can be solubilized and is made of five subunits organized according to a stoichiometry $\alpha_3\beta_3\gamma\delta\epsilon$. The mechanism of ATP synthesis, although studied extensively by many laboratories, is still controversial. A better understanding of the F_0-F_1 structure and of the fine changes of this structure occurring during catalysis is a requirement in order to elucidate this mechanism. Monoclonal antibodies (mAbs) may be powerful tools to reach this goal.

MAbs specific to the α- and β-subunits of F_1 were prepared for the first time in our laboratory for pig heart mitochondria [7,8]. These antibodies, as well as mAbs raised against the oligomycin-

---

Abbreviations: F_1, mitochondrial F_1-ATPase; mAb, monoclonal antibody; ELISA, enzyme-linked immunosorbent assay; RIA, radioimmunoassay.

Correspondence: C. Godinot, Laboratoire de Biologie et Technologie des Membranes du CNRS, Université Claude Bernard de Lyon, 43, Boulevard du 11 Novembre 1918, F-69622 Villeurbanne Cedex, France.

0005-2728/87/$03.50 © 1987 Elsevier Science Publishers (Biomedical Division)

sensitivity-conferring protein [9], have been used: (i) to determine an $\alpha_3\beta_3$ stoichiometry in F_1 [7] and a ratio of two oligomycin-sensitivity-conferring proteins per F_1 in mitochondria (10); (ii) to identify essential epitopes on the β-subunit by studying interspecies cross-reactivity [9]; and (iii) to analyze the topography of the oligomycin-sensitivity-conferring protein in the mitochondrial membrane [11]. Other mAbs have been raised against α, β and a peptide of 25 kDa of the yeast mitochondrial F_0-F_1 complex [12], against the α and β subunits of *Escherichia coli* F_1 [13], against the α [14], β and γ subunits [15] of chloroplast F_1, against the coupling factor B of mitochondria [16], and against all subunits of *E. coli* F_1 [17]. Stoichiometries of 3α and 3β subunits have also been found for all species with these mAbs. Moreover, a correlation between inhibitory effects of mAbs and conservation of epitopes along the phylogenic scale has been stressed [17].

In the present paper, the binding of anti-α and anti-β mAbs to F_1 is used as a probe of the availability of domains of α- and β-subunits of F_1. It is shown that the accessibility of four distinct antigenic determinants to mAbs can be modulated by unfolding the protein, by integration of F_1 in the membrane or by the addition of nucleotides to soluble F_1. In addition, the binding curves of anti-α mAbs to soluble or membrane-bound F_1 suggest an asymmetry of the α-subunits.

Materials and Methods

Materials

[^{125}I]NaI was obtained from the Commissariat à l'Energie Atomique, France. Specific chemicals were purchased from the following sources: protein A-Sepharose; Pharmacia; protein A: I.B.F.; horseradish-peroxidase conjugated antimouse immunoglobulin sheep antibody; Biosys; IODO-GEN; Pierce. All other chemicals were of the highest purity available.

Methods

Biological preparations. Previously described procedures were used to obtain: pig-heart mitochondria [18]; F_1 [19]; purified β-subunit [20]; and electron-transport particles prepared according to Penin et al. [21], which are essentially inverted submitochondrial particles as checked according to Ref. 22. MAbs prepared according to Kohler and Milstein [23] have been previously characterized: 14 D_5, 19 D_3 and 5 G_{11} were specific of the β-subunit and 20 D_6 of the α-subunit [7]; 7 B_3 obtained from another fusion was specific of the α-subunit [8]. The monoclonal antibodies were purified from ascitic or culture supernatant fluid by affinity chromatography on protein A-Sepharose [24]. Purified mAbs or protein A were iodinated with ^{125}I in the presence of IODO-GEN [25], as described previously [7]. Protein concentration was estimated by the method of Lowry et al. [26]. The ATPase activity was measured as in Ref. 19.

Coating of F_1 to microtitration plates. The wells of microtest plates were coated with 50 μl F_1 (80 μg/ml in 0.1 M sodium phosphate buffer, pH 7.5) and air dried. The 96-wells microtest plates used were either flexible (Falcon 3912) for RIA or rigid (Nunclon Delta) for ELISA. To improve the coating of F_1, 50 μl 80% acetone in water (v/v) was added to each well. After drying, the remaining non-specific binding sites were saturated with serum albumin: three successive washings were made by filling the wells with 10 mM sodium phosphate buffer/150 mM NaCl (pH 7.2) containing 1% bovine serum albumin, incubating the plates for 10 min and emptying the wells by flicking the plates. The plates containing solid phase F_1 could be kept at −20 °C for several weeks before use.

Competition among mAbs for binding to antigenic determinants of F_1. The ability of binding of one α- or β-specific mAb in the presence of a saturating concentration of another mAb was tested by radioimmunoassay. In preliminary experiments the saturating amount of mAbs was determined as follows: serial dilutions of mAb (purified or 50% ammonium sulfate precipitate of ascitic fluid) were incubated overnight with F_1 coated to the wells of flexible plates. After three washings with 10 mM sodium phosphate buffer/150 mM NaCl (pH 7.2) containing 1% bovine serum albumin, 50 μl sheep antibody to mouse immunoglobulin (diluted 1 : 300 in 10 mM sodium phosphate buffer/150 mM NaCl) were incubated in each well for 1 h at 37 °C. After three more washings, 50 μl of ^{125}I-labeled protein A

($2 \cdot 10^5$ cpm per well) were incubated for 1 h. The wells were washed six times, dried, cut out and counted in a γ-counter (Packard). The dilution of mAb giving the maximal binding to solid phase F_1 was used for subsequent competition studies. The competition between antibodies for binding to solid phase F_1 was then tested as described in Table I by first incubating one mAb at saturating concentration (protecting antibody) and then measuring the binding of another mAb labeled with ^{125}I (tested mAb).

Competitive ELISA. Competition between binding of soluble antigens (F_1, β-subunit, electron-transport particles) and solid phase F_1 (F_1 coated to microtitration plates) to a given mAb was made as follows: after preincubation of the studied antigen with the mAb, the mixture was added to microtitration wells containing solid phase F_1. Only the mAbs not bound to soluble antigen could react with coated F_1 and be titrated afterwards with the second antibody. For these experiments, limited concentrations of mAb corresponding to 60–80% of the maximal binding to coated F_1 were used. The mAbs were preincubated in the presence of various concentrations of competing antigens for 2 h at 30°C. For competitions with F_1 or β, the buffer A contained 30 mM Tris-base/192 mM glycin/0.5 mM EDTA (pH 8.0)/5% glycerol/0.02% Tween 20; when ATP + $MgCl_2$ were aded, EDTA was omitted. For competitions with electron-transport particles, the buffer B contained 0.25 M sucrose, 30 mM Tris-base, 192 mM glycin, 0.5 mM $MgSO_4$ (pH 8.0), 0.02% Tween 20. The mixture of mAb and competing antigen (50 μl) was transferred to the 96-wells rigid plate coated with F_1. After a 3 h-incubation at 37°C, the plates were washed three times with 10 mM sodium phosphate buffer/150 mM NaCl containing 0.05% Tween 20 and incubated for 1 h at 37°C with 50 μl of peroxidase conjugated-antimouse immunoglobulin sheep antibody (diluted 1/300 in sodium phosphate buffer/NaCl). The plates were washed three times with 10 mM sodium phosphate buffer/150 mM NaCl/0.05% Tween 20.

The peroxidase substrate (100 μl 0.25 mM 2,2′-azinobis (3-ethylbenzthiazolinesulfonic acid)/0.18 mM H_2O_2/0.1 mM sodium phosphate, pH 6.8) was then incubated for 30 min at room temperature with gentle shaking. The color intensity of the plates was measured with a Dynatech microplate reader at 410 nm.

When the competition was studied with denatured F_1, F_1 was pretreated with 8 M urea: the stock solution of F_1 (5 mg protein per ml 100 mM Tris-SO_4/5 mM EDTA/50% glycerol, pH 8.0) was diluted with an equal volume of 25 mM Tris-base/192 mM glycin (pH 8.0). Crystals of urea were added to obtain a final concentration of 8 M. The mixture was heated for 5 min at 100°C and diluted 4-fold in buffer A. Verification was made that the presence of 2 M urea (which corresponds to the highest concentration of solutions tested containing F_1 unfolded by urea) did not significantly modify the interaction between F_1 and the various mAbs.

Use of competitive binding curves to estimate the number of β-subunits of F_1 accessible to the monoclonal antibodies, using an isolated β-subunit as a standard. Berzofsky and Schechter [27] have proposed a mathematical analysis for the binding of a ligand to an homogeneous antibody in the presence of a competitor. For example, for the binding of a protein, they have shown that, in this type of competition curves, the total concentration of the soluble protein which reduces by 50% the binding of the antibody to the protein bound to the solid support, corresponds to a value

$$[X] = \frac{1}{K_X} + \frac{A}{2}$$

where A is the concentration of antibody binding sites and K_X the affinity of the antibody for the protein. In order to use this equation to compare the binding of one mAb to F_1 and to the isolated β-subunit, it is necessary to assume that K_X, the affinity of the mAb for the β-subunit, is the same when the β-subunit is isolated as when it is integrated in F_1. Under these conditions, the total soluble protein concentration ([β] or [F_1]), corresponding to 50% binding of the antibody, will be directly proportional to the concentration of antibody binding sites. When a log scale is used, the slope of the binding curve is proportional to the affinity of the competitor (here soluble protein vs. bound protein) [27,28]. Therefore, it is reasonable to assume that the affinity of one mAb for F_1 and for the β-subunit is identical when the curves are parallel. In such a case, the number of antibody binding sites on F_1 can be estimated by comparison of the midpoint of the curves obtained with the isolated β-subunit and with F_1.

Titration of F_1 present in the mitochondrial membrane. The total amount of F_1 present in submitochondrial particles was measured by quantitative immunotitration using monoclonal antibodies as described previously [10]. It was found that the electron-transport particles used in the present work contained 0.39 nmol F_1 per mg of mitochondrial protein [29]. Taking into account an M_r of 380 000 for F_1 [1], the electron-transport particles contain 15% of F_1.

Results

Analysis of the proximity between antigenic determinants of α and β in F_1. To determine whether the various mAbs recognize distinct or overlapping sites on F_1, the binding of each labeled mAb was tested in the presence of saturating amounts of each other mAb (protecting mAb). Table I shows that, when the labeled mAb is tested in the presence of the same unlabeled mAb, 11–18% of the binding observed in the absence of protecting mAb are measured. Therefore, a percentage of ^{125}I-labeled mAb binding lower than 20% cannot be considered as corresponding to a different antigenic determinant. Moreover, a percentage of binding higher than 60% can be considered as corresponding to a different antigenic determinant [30]. The results presented in Table I can be analyzed on the basis of these limits. The presence of 7 B_3 (anti-d), as the protecting mAb, does not significantly decrease the binding of any other labeled anti-α or anti-β mAbs (63 to 82%), suggesting that it recognizes a determinant distinct from the others. The presence of 20 D_6 (anti-α) slightly hinders the binding of both the anti-α 7 B_3 (50 %) and the anti-β 19 D_3 (56%), but it does not significantly decrease the binding of other anti-β mAbs 5 G_{11} and 14 D_5. The presence of 14 D_5 (anti-β) does not prevent the binding of anti-α mAbs (7 B_3, 69% and 20 D_6, 82%), while it slightly hinders the binding of anti-β mAbs 19 D_3 and 5 G_{11} (45% and 59% of binding, respectively). The presence of 19 D_3 (anti-β) does not significantly diminish the binding of anti-α mAbs and anti-β 14 D_5 (70–80% of binding), but it strongly decreases the binding of 5 G_{11} (only 7% of binding). The presence of 5 G_{11} (anti-β) does not prevent the

TABLE I

COMPETITION BETWEEN VARIOUS MONOCLONAL ANTIBODIES FOR BINDING TO ANTIGENIC SITES OF MITOCHONDRIAL F_1-ATPase

The wells of flat-bottom microtest flexible plates were coated with F_1 and saturated with bovine serum albumin as described in Materials and Methods. In preliminary experiments, the dilution of purified mAb necessary to saturate the wells was tested by measuring the maximal amount of antibody that could be retained by F_1 coated to the wells For competition experiments, each well received 50 μl of the saturating concentration of the protecting mAb estimated in the preliminary experiment. After overnight incubation, 50 μl of the ^{125}I-mAb under test were added to each well and incubated for 4 h at room temperature with gentle shaking Each well was then emptied, washed 6 times with 10 mM sodium phosphate buffer/150 mM NaCl containing 1% bovine serum albumin, cut out and counted. Five wells were run for each mAb combination Each value represents the average of at least two experiments. For each mAb, five wells were used to measure the maximal binding (i.e., without protecting mAb) and five wells to determine the background (i.e., without F_1). The counts corresponding to the maximal binding obtained for the various mAbs were respectively: 37700 for 7 B_3, 64600 for 20 D_6, 46130 for 14 D_5, 19800 for 19 D_3 and 4300 cpm for 5 G_{11} The average value of the backgrounds was 150 cpm. The Greek character in parenthesis indicates the F_1 subunit recognized by the corresponding mAb.

Protecting mAb	Tested ^{125}I-mAb Percentage of binding of tested labeled mAb in the presence of protecting mAb				
	7 B_3	20 D_6	14 D_5	19 D_3	5 G_{11}
7 B_3 (α)	12	72	82	63	68
20 D_6 (α)	50	18	62	56	70
14 D_5 (β)	69	82	11	45	59
19 D_3 (β)	70	80	70	16	7
5 G_{11} (β)	78	50	50	36	18

binding of 7 B_3, while it decreases the binding of other mAbs, barely for 20 D_6 and 14 D_5 (50%) and significantly for 19 D_3 (36%).

In conclusion, among the antibody pairs tested, a significant reciprocal inhibition is observed in only one case: 5 G_{11} and 19 D_3. This indicates common or overlapping epitopes. In addition, a reciprocal inhibition at the limit of the significance is observed between 14 D_5 and 5 G_{11}.

Competition studies

In the above experiments, the binding of mAbs was studied with F_1 immobilized on microtitration plates. In such a case, variations in the accessibility of the epitopes related to conformational changes of the antigen under different conditions were unlikely. In all further experiments, the binding of mAbs to F_1 was first carried out in solution

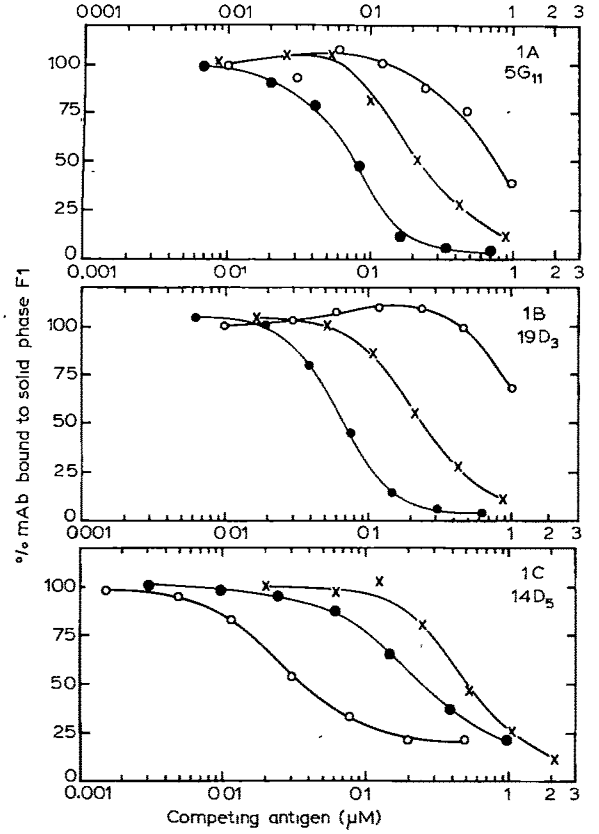

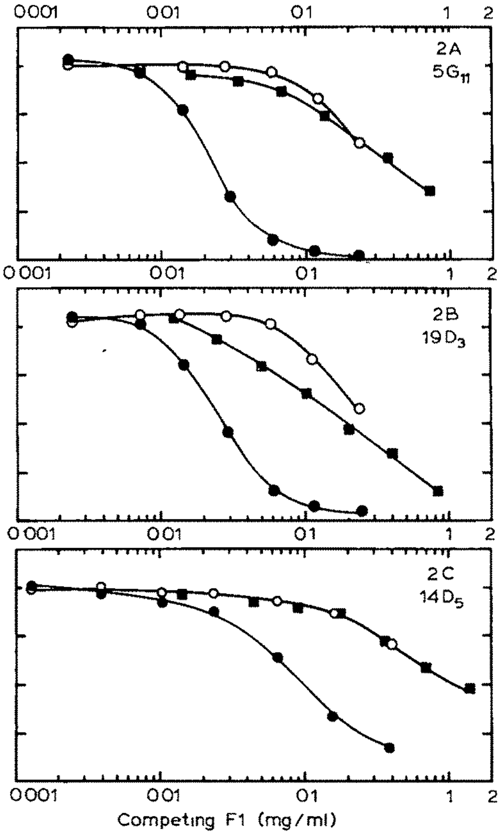

Fig. 1. Comparison of the binding of anti-β subunit mAbs to purified β-subunit, to soluble F_1 and to F_1 unfolded with urea Limiting concentrations of mAb were preincubated in solution with the indicated concentrations of soluble F_1 (●), urea-treated F_1 (○) or purified β-subunit (×). After a 2-h incubation at 30°C, 50 μl of each sample was added to the wells of microtitration plates coated with F_1 The amounts of mAb bound to solid phase F_1 was measured by ELISA as described in Materials and Methods The results are expressed as percentages of the maximal amount of mAb bound to solid phase F_1 measured simultaneously under the same conditions, except that the competing antigen was omitted from the preincubation medium The M_r of F_1 and β were taken as 380000 [1] and 51300 [37], respectively.

Fig. 2. Decrease of the binding of 3 anti-β subunit mAbs to F_1 upon addition of MgATP or insertion of F_1 in the membrane Limiting concentrations of mAb (adequately diluted, see Materials and Methods) were preincubated either with ETP (■) or with the indicated concentrations of F_1 in the absence (●) or presence (○) of 1 mM ATP+1 mM $MgCl_2$. The electron-transport particles contain the indicated concentration of F_1, as calculated from Penin et al. [29]. Other experimental conditions as described in Fig. 1.

to allow for the detection of eventual conformational changes of F_1. Then, the remaining free mAbs was titrated by their binding to an excess of F_1 coated to the plates (see Materials and Methods). The concentration of competing antigen in solution capable of reducing by 50% the binding of mAbs to coated F_1 is defined as $K_{1/2}$.

Anti-β mAbs

Influence of the treatment of F_1 with urea on the binding of mAbs. Fig. 1A shows that, when 5 G_{11} is preincubated with F_1, the value of $K_{1/2}$ is about 0.07 μM. If F_1 has been treated with 8 M urea before the preincubation with 5 G_{11}, the value of $K_{1/2}$ is increased to 0.8 μM. Similar results are observed with 19 D_3 (Fig. 1B). Therefore, urea treatment of F_1 decreases the binding of both 5 G_{11} and 19 D_3. On the contrary, the $K_{1/2}$ value for 14 D_5 is lower for urea-treated F_1 (0.034 μM) than for F_1 (0.24 μM), indicating that the unfolding of F_1 enhances the binding of 14 D_5 (Fig. 1C).

Binding of mAbs to F_1 and to an isolated β-subunit. Fig. 1A and B shows that both mAbs 5 G_{11} and 19 D_3 exhibit titration curves for the purified β-subunit parallel to that of F_1. The experiment was repeated four times with 5 G_{11}. The $K_{1/2}$ values obtained when soluble F_1 and β are used as competing antigen were 0.071 ± 0.002 μM and 0.201 ± 0.027 μM, respectively. The ratios of $K_{1/2}$ for β and F_1 were calculated in each experiment. The mean of these radios was 2.78 ± 0.33 mol of β accessible to 5 G_{11} in each mol of F_1 (four experiments) and 3.2 mol of β accessible to 19 D_3 in each mol in F_1 (two experiments).

When the binding of 14 D_5 to F_1 and to purified β-subunit are compared (Fig. 1C), the titration curves are not parallel. Under these conditions, the concentrations of antibody binding sites in F_1 cannot be directly calculated from the binding curve of 14 D_5 to β (see below in Discussion).

Changes in the binding of mAbs to F_1 in the presence of nucleotides. Correlation with changes of ATPase activity. Fig. 2 shows that the presence of the substrate MgATP (1 mM) during the preincubation of soluble F_1 with all anti-β mAbs drastically decreases their binding to soluble F_1. Indeed, a $K_{1/2}$ higher than 0.23 mg/ml is obtained for F_1 preincubated in the presence of MgATP in the case of either 5 G_{11} or 19 D_3 instead of 0.021 mg/ml and 0.024 mg/ml, respectively, for 5 G_{11} and 19 D_3 binding to F_1 in the absence of MgATP. The $K_{1/2}$ value for 14 D_5 binding to F_1 raises up to 1 mg/ml in the presence of MgATP instead of 0.1 mg/ml in the absence of MgATP. Therefore, the presence of 1 mM MgATP decreases the binding of all three anti-β-mAbs. Verification was made that the presence of 1 mM MgATP did not change the binding of these mAbs to solid phase F_1 in the absence of any competing F_1.

F_1 is notorious for progressively falling apart into subunits when diluted in the absence of nucleotides [31]. The experiments described here involve incubations of F_1 lasting up to 5 h. In order to determine the extent of inactivation of F_1 occurring during these incubations, the ATPase activity of F_1 has been measured under the conditions used for competition studies, except that the addition of mAb was omitted. In the absence of nucleotides, only about 6% of the initial ATPase activity of soluble F_1 was recovered at the end of the experiment. On the contrary, in the presence of MgATP about 80% of the initial ATPase activ-

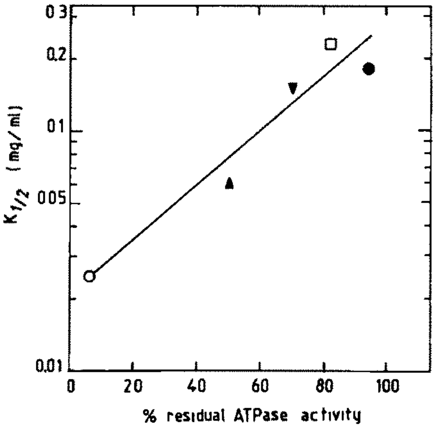

Fig 3. Variations of the $K_{1/2}$ values for 5 G_{11} binding to F_1 in the presence of different nucleotides as a function of residual ATPase activity after a 5-h incubation. $K_{1/2}$ values expressed as mg F_1 per ml preincubation medium was determined as described in fig 1A, except that 5 G_{11} was preincubated with F_1 either in the absence (○) or the presence of nucleotides: 1 mM GTP (▲), 5 mM GTP (▼), 1 mM ATP (●) or 1 mM ATP + 1 mM $MgCl_2$ (□). To measure the ATPase activity, F_1 was incubated at a concentration of F_1 of 0.037 mg per ml in buffer A (see Materials and Methods) supplemented with nucleotides. The residual activity was estimated by comparing the ATPase activity at the beginning and at the end of a 5-h incubation.

ity was remaining. These percentages were similar whatever F_1 concentration (within the range tested for competition experiments). The inactivation of F_1 could also be partly slowed down by the presence of either ATP in the absence of Mg^{2+}, or ADP or else GTP, although GTP was less efficient. Fig. 3 shows that the residual ATPase activity measured at the end of the incubation is roughly proportional to the $K_{1/2}$ value measured for the binding of 5 G_{11} to F_1, indicating that the value of $K_{1/2}$ increases with the percentage of active F_1.

Binding of mAbs to F_1 integrated in the membrane. When F_1 is integrated in the membrane (electron-transport particles), the total amount of membrane bound F_1 necessary to bind 50% of each anti-β mAb is the same as that observed with active F_1 preincubated with mgATP (Fig. 2A, B and C). This indicates that membrane-bound F_1 is as accessible to the three anti-β mAbs as active F_1. The ATPase activity of membrane-bound F_1 was also checked during the competition experiments, it was slightly increased from 3 to 4 μmol ATP hydrolyzed per min per mg protein.

Anti-α mAbs

Influence of the treatment of F_1 with urea on the binding of mAbs. Fig. 4A shows that the $K_{1/2}$ value of 7 B_3 is slightly higher for urea-treated F_1 (0.17 μM) than for untreated F_1 (0.076 μM), suggesting a diminution of the binding of 7 B_3 to urea treated F_1. On the contrary, for 20 D_6, the treatment of F_1 with urea decreases the value of $K_{1/2}$ by about 5-fold (0.0024 μM instead of 0.013 μM for untreated F_1) (Fig. 4B). This means that the unfolding of F_1 increases the binding of 20 D_6. Besides, when 20 D_6 is preincubated with untreated F_1, a plateau corresponding to about 25% of mAb bound to solid-phase F_1 is observed. In contrast, the binding of 20 D_6 to solid phase F_1 can be completely inhibited by urea-treated F_1 at concentrations as low as 0.02 μM.

Binding of mAbs to F_1 integrated in the membrane. Fig. 5B shows that the $K_{1/2}$ value for 20 D_6 binding of membrane bound F_1 (electron-transport particles) is about 50-times higher than the value observed with soluble F_1 (0.28 mg/ml instead of 0.006 mg/ml). On the contrary, this value

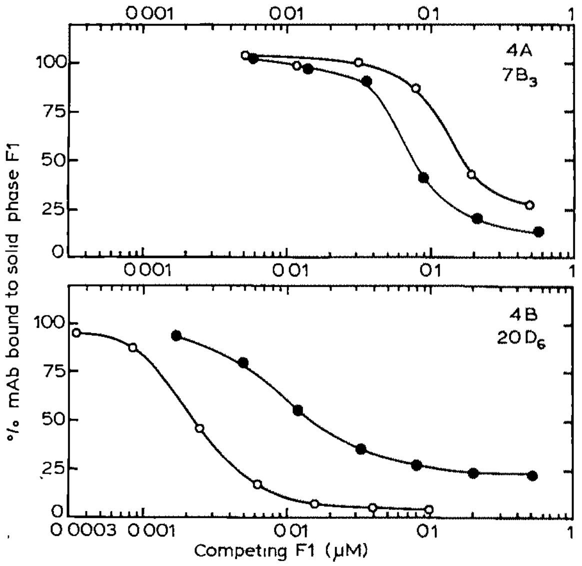

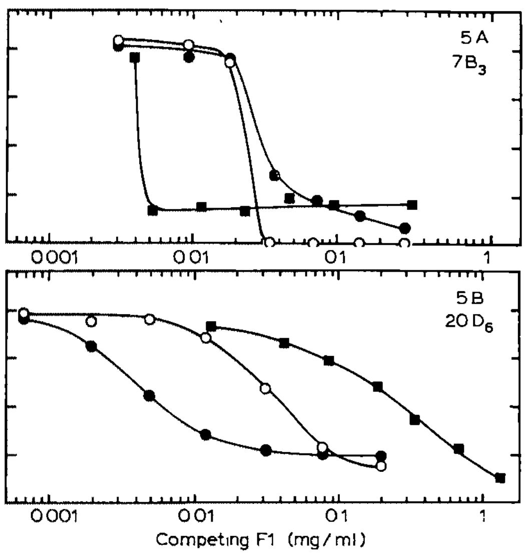

Fig. 4. Effects of unfolding of F_1 with urea on the binding of 2 anti-α subunit mAbs. Conditions as described in Fig. 1 Active F_1, ●; urea-treated F_1, ○

Fig. 5. Modifications of the binding of two anti-α subunit mAb to F_1 upon addition of MgATP or insertion of F_1 in the membrane. Conditions are the same as in Fig. 2. Electron-transport particles, ■; soluble F_1 preincubated in the absence (●) or presence (○) of 1 mM ATP + 1 mM $MgCl_2$.

for 7 B_3 binding to F_1 present in the electron-transport particles (0.004 mg/ml) is much lower than that observed for soluble F_1 (0.027 mg/ml), as shown in Fig. 5A. These results indicate that, while the epitope recognized by 20 D_6 is less accessible in the membrane than in soluble F_1, the epitope of 7 B_3 is better exposed in the membrane than in soluble F_1. However, in spite of the higher reactivity of 7 B_3 with the electron-transport particles, a plateau corresponding to about 20% of mAb bound to solid phase F_1 is observed even for very high concentrations of membrane bound F_1 as competing antigen (Fig. 5A).

Changes in the binding of mAbs to F_1 in the presence of MgATP. The presence of 1 mM MgATP decreases the binding of anti-α 20 D_6 to soluble F_1 as in the case of the anti-β mAbs: the $K_{1/2}$ value is about 0.045 mg/ml of active soluble F_1 in the presence of MgATP, while 0.006 mg/ml was sufficient in the absence of Mg ATP (Fig. 5B). In the case of 7 B_3 (Fig. 5A), the addition of 1 mM MgATP barely decreases the $K_{1/2}$ value of soluble F_1. However, the presence of MgATP completely inhibits the binding of 7 B_3 to solid phase F_1 at a F_1 concentration of 0.035 mg/ml, while in the absence of MgATP this total inhibition is not yet reached at 0.3 mg F_1/ml. The curve obtained with 7 B_3 in the absence of MgATP is biphasic.

Discussion

Proximity of antigenic sites

In experiments where the binding of two mAbs to a protein are compared pairwise, the antigenic determinants recognized by these mAbs can be considered as identical or overlapping when the presence of one of them prevents the binding of the other and vice-versa. The results presented here show that two anti-β mAbs (5 G_{11} and 19 D_3) recognize identical or overlapping epitopes on F_1. In addition, the other anti-β mAb (14 D_5) occupies a site different from the two others, but closer to the site of 5 G_{11} than that of 19 D_3. The sites of the two anti-α mAbs are not close to each other. Indeed, although 20 D_6 inhibits 50% of the binding of 7 B_3, there is no reciprocity.

In conclusion, at least four distinct antigenic determinants can be detected with these mAbs on F_1, two on α-subunits (20 D_6 and 7 B_3) and two on β-subunits (14 D_5 and 5 G_{11} or 19 D_3). The close proximity between the epitopes of 5 G_{11} and 19 D_3 demonstrated by the experiments made with immobilized F_1 is further supported by the experiments made with soluble F_1. Indeed, both mAbs behave in a similar manner in all experiments performed. This conclusion is further supported by recent studies on the localization of the antigenic sites of the anti-β mAbs on the β-subunit [32]. These experiments have shown that 14 D_5 recognizes the large N-terminal formic acid cleavage product of the β-subunit and the cyanogen bromide cleavage product corresponding to the sequence spanning Glu 168 to Met 200 in the bovine heart enzyme. On the contrary, both 5 G_{11} and 19 D_3 recognize a 12 kDa, C-terminal acid formic cleavage product of the β-subunit [32].

Availability of antigenic sites on the β-subunit and on F_1

The titration curves obtained for 5 G_{11} and 19 D_3 using F_1 as a competing antigen are parallel to those obtained with the β-subunit. According to Berzofsky and Schechter [27] allows this behavior us to calculate that about 2.8 and 3.2 mol of β-subunit per mol of F_1 are accessible to 5 G_{11} and 19 D_3, respectively. Since F_1 contains 3 β-subunits [1,7], it means that 5 G_{11} and 19 D_3 can bind as well to all three β-subunits of purified F_1 as to the isolated β-subunit. However, since these experiments were performed in the absence of MgATP, the ATPase activity of F_1 was drastically reduced during the incubation. This is very likely due to a dissociation of F_1 into subunits [31]. On the contrary, in the presence of MgATP, the ATPase activity of F_1 was essentially preserved and the availability of the epitopes was much lower as shown by the increase in $K_{1/2}$-values. This availability is inversely proportional to the percentage of F_1 maintained in an active conformation. All these results indicate that the epitope corresponding to 5 G_{11} and 19 D_3 is available at the surface of the β-subunit, but becomes at least partly buried when the β-subunits are complexed with the other subunits to form an active F_1.

In a previous work [9], we have shown that 5 G_{11} and 19 D_3 recognize the β-subunits of all tested species including bacteria, chloroplasts, yeast and mammalian mitochondria. In addition, both mAbs can, under specific conditions, inhibit ATP hydrolysis or ATP synthesis [9,33]. Dunn et al. [17] have suggested that the most conserved regions of the ATPase lie in the interior rather than on the surface of F_1. Our results show that at least one well-conserved epitope located on the C-terminal sequence of β and related to the enzyme activity lies on the surface of the β-subunit and becomes buried in active F_1.

The effects induced by unfolding of F_1 with urea provide other information on the topology of the antibody binding sites. Urea treatment increases by more than one order of magnitude the concentration of soluble F_1 necessary to bind 50% of the mAbs 5 G_{11} and 19 D_3. Similarly, it has been shown previously [7] that a treatment of F_1 with SDS decreased the reactivity of these two antibodies. This experiment suggested that 5 G_{11} and 19 D_3 were mainly conformational antibodies. Urea and/or SDS destroy the secondary and tertiary structure of F_1, which is necessary to observe an optimal binding of 5 G_{11} and 19 D_3. It can be concluded that these structures are sufficiently maintained in the isolated β-subunit to preserve the binding capacity of 5 G_{11} and 19 D_3. The higher affinity of 5 G_{11} and 19 D_3 for F_1 as compared to F_1 denatured by SDS and urea can be explained by a distortion of the linear sequence epitope by unfolding. If the epitopes comprise amino-acid residues very distant in the sequence, but juxtaposed only on the protein surface by folding, urea or SDS treatments would completely destroy the epitopes. Therefore, 5 G_{11} and 19 D_3 recognize a fragment of the primary sequence of β able to change its conformation by folding.

In the case of the anti-β mAb, 14 D_5, the binding curves of F_1 incubated in the absence of nucleotide and of the isolated β-subunit are not parallel, indicating that the epitopes are not exposed in the same way. This might indicate that F_1 incompletely dissociated is still interacting with some subunits, rendering the epitope less accessible to 14 D_5 than in the case of the isolated β-subunit. Contrary to what is observed for 19 D_3 and 5 G_{11}, urea treatment of F_1 increases the binding of 14 D_5. This means that the epitope recognized by 14 D_5 must be at least partially buried in the β-subunit.

Active F_1 in the presence of ATP and F_1 integrated in the membrane give similar binding curves for the 3 anti-β mAbs. This indicates that the epitopes exposed at the surface of F_1 in the presence of ATP and on the electron-transport particles have the same affinity for the anti-β mAbs. Therefore, the conformation of β in active electron-transport particles is similar to that of F_1 maintained in its active form by preincubation with MgATP.

Availability of the antigenic sites of the α-subunit in soluble or membrane-bound F_1

The epitope corresponding to the anti-α 20 D_6 is optimally exposed when F_1 is completely dissociated by urea treatment, less accessible in F_1 incubated in the absence of nucleotide and even less in active F_1. Therefore, this epitope must be at least partly located on the surface of α-subunit in an area interacting with other subunits. This area is not as easily accessible when F_1 is maintained in its active form by the presence of nucleotide as in inactive F_1.

When F_1 is integrated in the mitochondrial membrane the accessibility of the epitope recognized by 20 D_6 is further decreased by a factor of 6 in comparison to active F_1. This epitope either lies on the surface of F_1 which is in contact with the membrane, or is further masked inside F_1 due to a conformational change occurring when F_1 binds to the membrane.

The only mAb which binds to a very-well-exposed antigenic site of F_1 is the anti-α 7 B_3. Contrarily to all other mAbs tested, the affinity of this antibody becomes higher and higher when the conformation of F_1 becomes closer to the 'in situ' conformation, that is in membrane-bound F_1.

The behavior of these mAbs recognizing two distinct sites suggests a conformation of α different in electron-transport particles and in active F_1.

Apparent heterogeneity of the α-subunits in soluble or membrane-bound F_1

The binding curves of 20 D_6 to untreated F_1 in the presence or absence of ATP show plateau values at significantly less than 100% binding of these antibodies. The presence of such plateaus indicates a heterogeneity of either the antibody or the antigen [27,34]. Since the antibodies are monoclonal [8], the heterogeneity must be due to the antigen. After urea treatment of F_1, the plateau observed for 20 D_6 disappears. This result suggests that there is a heterogeneity between the three α-subunits of soluble F_1, and that, upon urea treatment, these three α-subunits become equivalent. However, it cannot be excluded that this heterogeneity might be induced by the binding of a first mAb to F_1 which might decrease the affinity of a second mAb to another α-subunit of the same F_1 molecule. For the anti-α 7 B_3, although very low concentrations of electron-transport particles can decrease by 50% the binding of the antibody, a complete inhibition of the binding is never reached (plateau at less than 100%) even when the electron-transport particles concentration is increased by more than 100 times. As discussed above, this type of behavior is characteristic of a heterogeneity in the molecular structure of the binding sites. This indicates that the α-subunits present at the surface of the electron-transport particles appear heterogeneous. On the contrary, the α-subunits accessible at the surface of active F_1 appear homogeneous for the binding of 7 B_3, since no plateau is observed.

The apparent heterogeneity of the α-subunits is in agreement with the conclusions of Amzel and Pedersen [1], who have shown by single crystal X-ray diffraction studies that the three α- and β-subunits are not structurally equivalent. The heterogeneous behavior of the α-subunits has also been recently proposed in the case of chloroplast F_1 [35] and of yeast F_1 [36] to explain heterogeneous modification of the α-subunits by chemical reagents. Our results suggest that the heterogeneity of the α-subunits also exist in membrane-bound F_1.

Acknowledgements

The authors wish to thank Professor D.C. Gautheron for stimulating discussions during the course of this study. This work would not have been possible without the expertise of François Penin in the preparation of F_1-ATPase. The authors are also indebted to Christian Van Herrewege for the art work. This work was supported by the Centre National de la Recherche Scientifique (ATP 950003 and UM 380024).

References

1 Amzel, L M. and Pedersen, P.L. (1983) Annu. Rev. Biochem. 52, 801–824
2 Futai, M and Kanazawa, H. (1983) Microbiol. Rev 47, 285–312
3 Hoppe, J. and Sebald, W (1984) Biochim. Biophys. Acta 768, 1–27
4 Vignais, P.V. and Satre, M (1984) Mol. Cell. Biochem. 60, 33–70
5 Hatefi, Y. (1985) Annu. Rev. Biochem. 54, 1015–1069
6 Godinot, C. and DiPietro, A. (1986) Biochimie 68, 367–374
7 Moradi-Améli, M. and Godinot, C. (1983) Proc. Natl. Acad. Sci. USA 80, 6167–6170
8 Godinot, C., Moradi-Améli, M. and Gautheron, D C. (1986) Methods Enzymol. 126, 761–769
9 Archinard, P, Moradi-Améli, M, Godinot, C. and Gautheron, D.C (1984) Biochem Biophys. Res. Commun. 123, 254–261
10 Penin, F., Archinard, P., Moradi-Améli, M. and Godinot, C (1985) Biochim. Biophys. Acta 810, 346–353
11 Archinard, P., Godinot, C., Comte, J. and Gautheron, D C. (1986) Biochemistry 25, 3397–3404
12 Hadikusumo, R G., Hertzog, P J. and Marzuki, S. (1984) Biochim. Biophys. Acta 765, 258–267
13 Lunsdorf, H., Ehrig, K, Friedl, P. and Schairer, H.U. (1984) J. Mol. Biol. 173, 131–136
14 Tiedge, H., Lunsdorf, H., Schafer, G. and Schairer, H.U. (1985) Proc. Natl. Acad. Sci. USA 82, 7874–7878
15 Spitsberg, V L, Pfeiffer, N.E., Partridge, B., Wylie, D.E. and Schuster, S M. (1985) Plant Physiol. 77, 339–345
16 Joshi, S., Kantham, L., Kaplay, S and Sanadi, D.R. (1985) FEBS Lett. 179, 143–147
17 Dunn, S.D., Tozer, R.G., Antczak, D.F. and Heppel, L A (1985) J. Biol. Chem. 260, 10418–10425
18 Godinot, C, Vial, C, Font, B. and Gautheron, D C. (1969) Eur. J. Biochem 8, 385–394
19 Penin, F., Godinot, C. and Gautheron, D.C. (1979) Biochim. Biophys. Acta 548, 63–71
20 Issartel, J.P., Klein, G., Satre, M. and Vignais, P.V. (1983) Biochemistry 22, 3492–3497
21 Penin, F., Godinot, C., Comte, J and Gautheron, D.C (1982) Biochim Biophys. Acta 679, 198–209
22 Godinot, C. and Gautheron, D C (1979) Methods Enzymol. 55, 112–114
23 Kohler, G. and Milstein, C (1975) Nature (London) 256, 495–497
24 Ey, P.L.M., Prowse, S.J. and Jenkin, C.R. (1978) Immunochemistry 15, 429–436
25 Fracker, P.J. and Speck, J.C. (1978) Biochem. Biophys. Res. Commun. 80, 842–857
26 Lowry, O.H., Rosebrough, N.J., Farr, A.L. and Randall, J (1951) J. Biol. Chem. 193, 265–275
27 Berzofsky, J.A. and Schechter, A.N. (1981) Mol Immunol 18, 751–763
28 Chard, T. (1978) in Laboratory Techniques in Biochemistry and Molecular Biology (Work, T.S. and Work, E., eds), Vol. 6, part II, an Introduction to Radioimmunoassay and

Related Techniques, pp. 463–478, Elsevier/North-Holland, Amsterdam

29 Penin, F., Deléage, G., Godinot, C. and Gautheron, D.C (1986) Biochim. Biophys. Acta 852, 55–67

30 Ray, K., Vockley, J. and Harris, H. (1984) FEBS Lett. 174, 294–299

31 Vambutas, V.K and Racker, E. (1965) J. Biol. Chem. 240, 2660–2664

32 Clerc, F., Julliard, J.H., Godinot, C. and Gautheron, D.C. (1986) EBEC short reports, 4, 240

33 Gautheron, D.C, DiPietro, A., Penin, F., Moradi-Améli, M., Fellous, G. and Godinot, C. (1984) in "H^+-ATPase (ATP-synthase) Structure, Function, Biogenesis. The F_0-F_1 complex of coupling membranes (Papa, S., Altendorf, K., Ernster, L., Packer, L, eds), pp. 219–228, ICSU Press-Adriatica Editrice, Bari, Italy

34 Berzofsky, J.A. and Berkower, I.J. (1984) in Fundamental Immynology, (Paul, W.E., ed.) pp. 595–644, Raven Press, New York

35 Nalin, C.M., Snyder, B and McCarty, R.E. (1985) Biochemistry 24, 2318–2324

36 Falson, P., DiPietro, A and Gautheron, D.C. (1986) J Biol Chem. 261, 7151–7159

37 Runswick, M J. and Walker, J E (1983) J. Biol Chem. 258, 3081–3089

Biochimica et Biophysica Acta 890 (1987) 66–76
Elsevier

BBA 42155

Effects of trypsin and bivalent cations on P-680$^+$-reduction, fluorescence induction and oxygen evolution in Photosystem II membrane fragments from spinach

M. Völker, H.-J. Eckert and G. Renger

Max-Volmer-Institut für Biophysikalische und Physikalische Chemie der Technischen Universität, D 1000 Berlin 12 (F.R.G.)

(Received 30 June 1986)

Key words: Oxygen evolution; P-680$^+$ reduction; Calcium ion effect; Proteolysis, Photosystem II, (Spinach)

Laser-flash-induced absorption changes at 830 nm, fluorescence-induction curves and the average oxygen yield per flash have been measured in spinach Photosystem II membrane fragments as a function of trypsin treatment and its modification by $CaCl_2$. The following was found. (i) The relative contribution of the nanosecond relaxation to the overall decay kinetics of 830 nm absorption changes reflecting the P-680$^+$-reduction decreases as a function of incubation time with trypsin. Simultaneously, mild treatment at pH = 6.0 markedly increases the extent of 200 μs kinetics that highly revert back to nanosecond kinetics by $CaCl_2$ addition. After harsher trypsin treatment (pH = 7.5) pH-dependent 2–20 μs kinetics appear that cannot be reverted to nanosecond kinetics by $CaCl_2$. (ii) The $CaCl_2$-induced restoration of nanosecond kinetics is mainly due to a Ca^{2+}-induced effect rather than to a functional role of Cl^-. Sr^{2+} can substantially substitute for Ca^{2+}, whereas Mg^{2+}, Mn^{2+} and monovalent ions are almost inefficient. (iii) A quantitative correlation between the extent of the nanosecond kinetics and the average oxygen yield per flash was not observed. (iv) If $CaCl_2$ is present in the assay medium for trypsin treatment the samples are markedly protected to proteolytic degradation. This effect mainly refers to the reaction pattern of the acceptor side. Other bivalent cations can substitute Ca^{2+} for its protective function. (v) The $CaCl_2$-induced protection to proteolytic attack is extremely sensitive to a very short trypsin pretreatment that does hardly affect the shape of the fluorescence induction curve. The results are discussed in relation to the functional and structural organization of Photosystem II.

Introduction

Photosynthetic water oxidation by visible light takes place in Photosystem II via a four-step univalent redox-reaction sequence initiated by photooxidation of a special chlorophyll *a*, referred to as P-680. Dioxygen formation is assumed to occur at a catalytic site which contains a binuclear manganese center (for a recent discussion, see Ref. 1).

The functional connection between the catalytic binuclear manganese cluster and P-680 implies at least one further redox component, referred to as Z [2]. In samples competent in oxygen evolution, P-680$^+$ reduction exhibits a multiphasic kinetics in the nano- and microsecond range [3–5], whereas the oxidation of the catalytic site was

---

Abbreviations: PS II, Photosystem II; Chl, chlorophyll; Cyt, cytochrome; Mes, 4-morpholineethanesulphonic acid.

Correspondence: G. Renger, Max-Volmer-Institut für Biophysikalische und Physikalische Chemie, Technische Universität Berlin, Sekr. PC 14, Strasse des 17 Juni 135, D-1000 Berlin 12, F R G.

0005-2728/87/$03 50 © 1987 Elsevier Science Publishers B.V. (Biomedical Division)

shown to occur within the range of 30 μs to 1 ms, depending on its redox state S_i [6–8]. If the oxygen-evolving capacity is completely eliminated by selective treatments (e.g., Tris-washing) the P-680$^+$-reduction kinetics markedly slow down: P-680$^+$ becomes reduced either via a pH-dependent electron flow from Z with half-life times of 2–20 μs [9] or via a back reaction ($t_{1/2} = 100$–200 μs) with the reduced primary plastoquinone acceptor Q_A^- [10,11]. This phenomenon raised the idea that any microsecond kinetics of P-680$^+$-reduction might be indicative of detrimental effects at the water-oxidizing enzyme system Y [12]. In this case the extent of nanosecond kinetics could be used as a measure of the percentage of PS II reaction centers that are functionally coupled with an intact catalytic site for water oxidation [12,13]. However, experiments with ADRY-agents [14] indicated that the extent of a 35 μs kinetics of 690 nm absorption changes depends upon the flash number of repetitive flash groups [15]. Therefore at least part of the microsecond kinetics are related to functionally intact systems Y. Furthermore, based on these data the P-680$^+$ reduction kinetics were inferred to depend on the redox state S_i of the water-oxidizing enzyme system Y [15]. Later much more refined measurements confirmed this basic conclusion [13].

In order to study possible correlations between P-680$^+$-reduction kinetics and the structural and functional integrity of the PS II donor side, experiments have to be performed in properly modified PS II membrane fragments. Mild trypsin treatment at pH = 6.5 leads to degradation of the surface exposed 18 kDa, 23 kDa and 33 kDa polypeptides [16] which act as regulatory subunits (decrease of Cl^- requirement, Ca^{2+} trapping and stabilizing of functional manganese) of the water-oxidizing enzyme system Y (for a recent review, see Ref. 17). Likewise, integral membrane proteins of the PS II reaction center and its associated core antenna (CP47, CP43, D1, D2 and Cyt *b* 559) are attacked by trypsin [16,18]. On the other hand, oxygen evolution with $K_3[Fe(CN)_6]$ as exogeneous electron acceptor remains highly active in trypsinized PS II membrane fragments [16] and inside-out vesicles [19]. Furthermore, under comparable conditions (trypsination at pH = 6.0), the low temperature EPR signals due to light-induced S_2 formation (multiline and $g = 4.1$ signal) and of donor D (signal II_s) are almost unaffected; whereas, the high potential Cyt *b*-559 is transformed into the low potential species [20]. Accordingly, limited proteolysis of PS II membrane fragments appears to be a proper tool for analyzing the functional and structural topography of PS II. Here we report the effect of trypsin treatment on 830 nm absorption changes that reflect the turnover of P-680 on oxygen evolution and on fluorescence induction. Furthermore, our attention was focused on the effect of Ca^{2+} as an essential cofactor for the function of system Y [21–23] because recent experiments revealed a marked stimulation of the oxygen evolution rate in trypsinized PS II membrane fragments [16].

Materials and Methods

PS-II particles with a high oxygen-evolving capacity were prepared from market spinach as described in Ref. 24 with the modifications described in Ref. 16, except that the applied Triton X-100/chlorophyll ratio was 20:1. Bovine pancreas trypsin was purchased from Boehringer (Mannheim). For comparitive measurements the proteolytic treatment for the measurements of the oxygen-evolving activity and of absorption changes at 830 nm was carried out under identical conditions, i.e., the PS-II particles (50 μg Chl/ml) were incubated in darkness with trypsin (trypsin/Chl = 2:1) at 20°C in the oxygen-measuring cuvette and after a certain time either illuminated directly for detecting the oxygen yield or transferred to the cuvette of the flash photometer for measuring absorption changes. In all other experiments trypsination was performed in the sample cuvette. In either experiment the dark time between the flashes was 600 ms and the samples were illuminated with the same number of flashes. The flash induced O_2-yield was measured as described earlier [14].

The measurements of the 830 nm absorption changes with nanosecond time resolution were performed with a single-beam flash photometer similar to the one described in Ref. 3. The measuring light was provided by a laser diode (TXF 8300 AEG-Telefunken, λ = 834 nm). By means of a microscope objective lens, the beam was focussed through the cuvette (4 cm pathlength) onto a 1 mm aperture, which was located in front of the photodetector (Photodiode preamplifier module RCA C 30952 E). In order to suppress a flash-induced fluorescence artefact, the distance between the cuvette and the aperture was approx. 1 m.

The photodiode was protected against fluorescence by a 830 nm interference filter and coupled via a 50 MHz amplifier (Pacific 2 A 50) to a Tektronix 7912 digitizer. 128 signals were averaged and stored on floppy disks.

In order to make sure that the total initial amplitude of the absorption change in the nanosecond time range could be detected with our time resolution an additional check was performed. NH_2OH (3 mM, 6 min dark incubation) was added to the sample after each experiment that leads to retardation of the relaxation kinetics at 830 nm, due to an inhibition of the water-oxidizing enzyme. The total amplitudes of the 830 nm absorption changes in the presence of NH_2OH are not limited by time resolution of our equipment. Accordingly, the extent of the nanosecond component related to the corresponding control value was calculated in two different ways: (1) the portion of the amplitude that decay within 1 μs related to the total amplitude at $t = 0$; and (2) the portion of the amplitude that decays within 1 μs related to the total amplitude in NH_2OH-treated samples at $t = 0$.

In experiments with microsecond time resolution, the photodetector was coupled to a 1 MHz amplifier (Tektronix AM 502) and the signals were transferred to a Nicolet 1170 averager.

Photosynthesis was excited by non saturating pulses from a Q-switched frequency-doubled NdYAG-laser (Spektrum GmbH, Berlin, $\lambda = 534$ nm; duration, 7 ns).

All experiments were carried out with a chlorophyll concentration of 50 μg/ml in a medium containing 10 mM NaCl and 20 mM Mes/NaOH (pH 6.0) with 1 mM $K_3[Fe(CN)_6]$ as an artificial electron acceptor. Other additions, as indicated in the figure legends. Fluorescence was monitored as described in Ref. 25. For these measurements the chlorophyll concentration was 5 μM.

Results

The P-680 turnover can be monitored by absorption changes peaking around 820 nm [3,11]. Typical traces of absorption changes at 830 nm induced by repetitive flashes in spinach PS II membrane fragments are depicted in Fig. 1. The relaxation kinetics that reflect the reduction of P-680$^+$ exhibits a multiphasic pattern. In oxygen-evolving control samples at pH = 6.0 the decay is dominated by nanosecond kinetics contributing approx. 65–70% to the overall relaxation. Addition of 10 mM $CaCl_2$ further increases the relative extent of the nanosecond kinetics up to 80%. Destruction of the oxygen-evolving capacity by incubation with 3 mM NH_2OH for 6 min is accompanied with complete elimination of the nanosecond kinetics. In these samples P-680$^+$ ex-

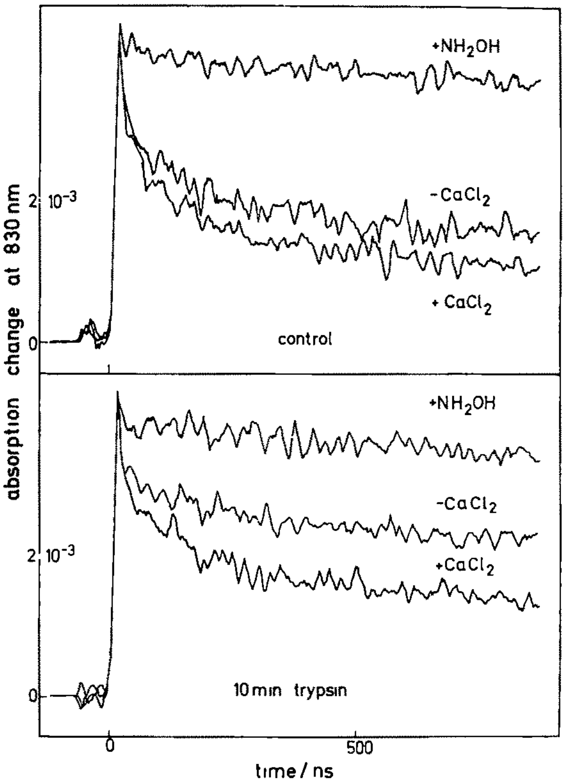

Fig. 1. Absorption changes at 830 nm induced by repetitive laser flashes in normal and trypsinized PS II membrane fragments at pH = 6.0 in the absence and after addition of 10 mM $CaCl_2$. Experimental conditions as described in Materials and Methods.

hibits half-life times in the microsecond range that depend upon illumination conditions [26]. The invariance of the initial amplitude to NH_2OH treatment indicates that the detection of the nanosecond kinetics of P-680^+ reduction is not limited by the time resolution of our equipment. After incubation of PS II membrane fragments with trypsin at pH = 6.0 the extent of microsecond relaxation kinetics increases (up to more than 50%) at the expense of nanosecond components. This effect appears to be interesting in the light of recent findings, indicating that oxygen evolution was hardly affected by mild trypsin treatment at pH = 6.0 in PS II-membrane fragments [16] and inside-out vesicles [19], whereas the polypeptide pattern became modified [16]. The relaxation kinetics of 830 nm absorption changes was analyzed as a function of trypsin treatment. A thorough analysis reveals that at least three different kinetics with half-life times of the order of 10 µs, 200 µs and more than 1 ms (these kinetics will be referred to as 10-µs, 200-µs and slow components, respectively) contribute to the decay in the micro- to millisecond time domain (data not shown).

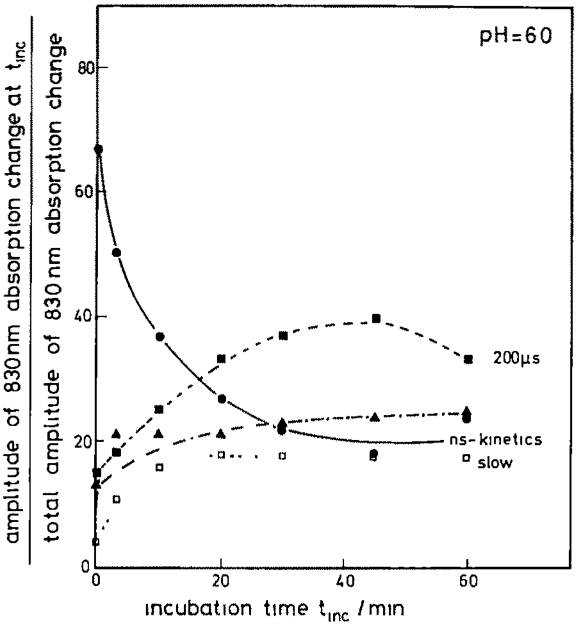

Fig. 2. Relative extent of different kinetics in the overall decay of 830 nm absorption changes in PS II membrane fragments as a function of incubation time with trypsin at pH = 6.0. Experimental conditions as described in Materials and Methods.

Fig. 2 shows the extent of the different kinetics related to the overall relaxation of 830 nm absorption changes as a function of incubation time with trypsin at pH = 6.0. The data reveal a marked decrease of the relative extent of nanosecond kinetics (for the sake of simplicity a separation into different nanosecond components was not performed) and a concomitant increase of contributions in the micro- to millisecond range. Recently, it was found that trypsin treatment at pH = 7.5 highly reduces oxygen evolution and elicits the pH-dependent 2–20 µs kinetics [17,26] which are characteristic for the electron transfer from Z to P-680^+ after destruction of the water-oxidizing enzyme system [9]. Accordingly, it seemed worthwhile to study the pattern of relaxation kinetics as a function of trypsin treatment at pH = 7.5. The results of Fig. 3 reveal an interesting phenomenon. At the beginning, the 200-µs component (also the slow component, data not shown) sharply rises and subsequently steeply declines, whereas the 10-µs component continues to increase with increasing incubation time. The most simple explanation for the appearance of 200-µs kinetics is the assumption that after elimination of the function of water to act as an electron donor Z^{ox} remains oxidized under repetitive flash excitation and therefore a back reaction arises between P-680^+ and Q_A^-. This interpretation would imply that progressing trypsination accelerates the regeneration of Z^{ox} (as shown for inside-out vesicles, see Ref. 19) so that under the same excitation conditions the extent of the 10-µs component increases. The P-680^+-reduction pattern in mildly trypsinized (pH = 6.0) PS II membrane fragments is markedly affected by addition of $CaCl_2$. In respect to the origin of the $CaCl_2$ reversible kinetics arising due to mild trypsin treatment, an interesting finding should be mentioned. The extent of the 200-µs relaxation kinetics is not affected by exogeneous PS II donors (data not shown) that are known to feed electrons efficiently to Z^{ox}, if the water-oxidizing enzyme system Y is destroyed (e.g., by Tris-washing), but do not compete with dioxygen evolution in functionally competent samples. This result indicates that the shielding effect exerted by polypeptides

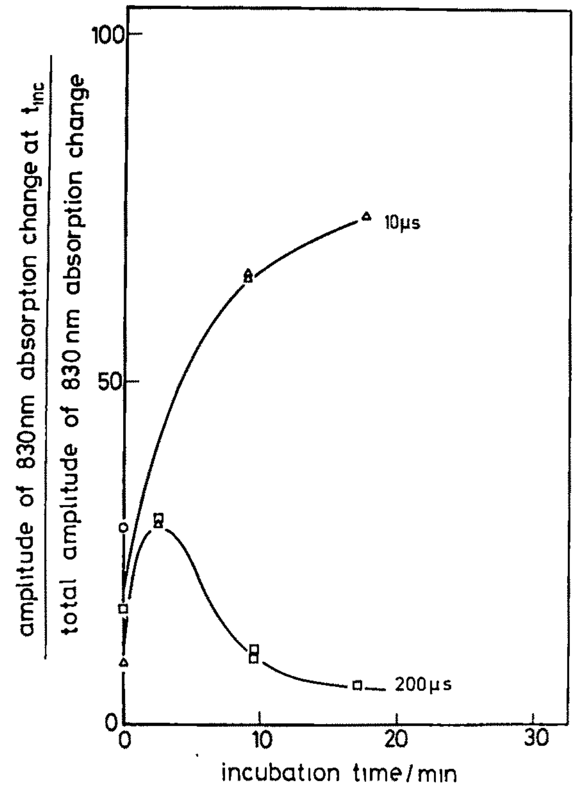

Fig. 3. Relative extent of the 10-μs and 200-μs kinetics in the overall decay of 830 nm absorption changes in PS II membrane fragments as a function of incubation time with trypsin at pH = 7.5 Experimental conditions as described in Materials and Methods.

which are probably related to the water-oxidizing enzyme system Y is not eliminated by the mild trypsin treatment. On the other hand, the pattern of P-680$^+$ reduction becomes significantly affected. Therefore, it appears reasonable to assume that a mild proteolytic attack causes structural changes which modify the functional connection between reaction center and water-oxidizing enzyme system Y without degrading the functional capacity of the latter operational unit. In Fig. 1 the extent of the nanosecond kinetics was shown to become increased by addition of $CaCl_2$. This effect is pronounced in PS-II membrane fragments trypsinized at pH = 6.0. Therefore, it was interesting to analyze the $CaCl_2$-induced transformation of the relaxation pattern. Fig. 4 depicts the relative extent of ns, 10-μs and 200-μs components as a function of incubation time with trypsin at pH = 6.0 and of its modification by addition of 10 mM $CaCl_2$ after the indicated time of proteolysis. The data reveal two characteristics: (a) $CaCl_2$-addition partly restores the contributions of nanosecond kinetics and (b) the 200-μs component is markedly reduced after $CaCl_2$ addition, whereas the 10-μs kinetics remains almost unaffected.

The partial restoration of the nanosecond kinetics by $CaCl_2$ could be related to specific effects of Ca^{2+} and/or Cl^- [21–23,27–29] or simply caused by structural effects due to nonspecific electrostatic interactions that are changed by salt addition. In order to test these alternatives experiments with different salts were performed in trypsinized PS II membrane fragments. A relative simple method was applied for the determination of the restoration degree. The results of Fig. 1 show that the extent of nanosecond kinetics can be easily determined as the difference of the am-

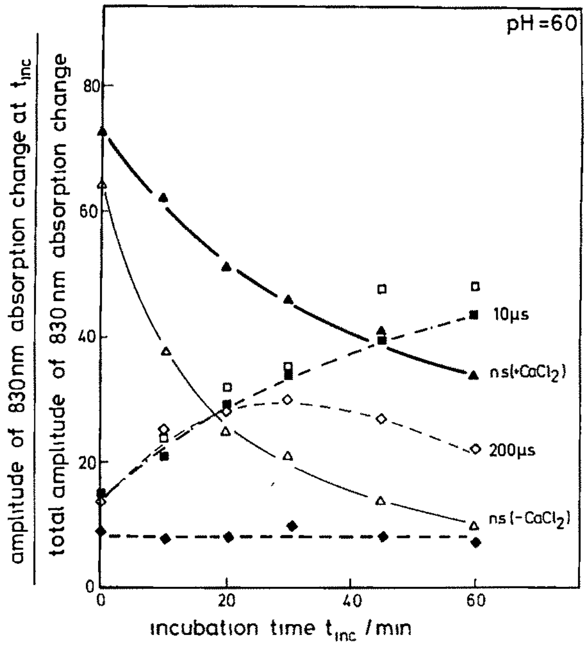

Fig. 4. Relative extent of the ns, 10-μs and 200-μs kinetics in the overall decay of 830 nm absorption changes in PS II membrane fragments as a function of incubation time with trypsin at pH = 6.0 in the absence and after addition of 10 mM $CaCl_2$. Experimental conditions as described in Materials and Methods Open symbols, experiments without $CaCl_2$; closed symbols, with $CaCl_2$.

plitudes at 1 μs, measured in the presence of 3 mM NH_2OH and its absence, respectively, i.e.

$$\Delta A_{830}^{ns} = \Delta A_{830}^{1\mu s}(+NH_2OH) - \Delta A_{830}^{1\mu s}(-NH_2OH)$$

This relation can be applied only if the 830 nm absorption changes remain invariant (in extent and kinetics up to 1 μs) to different salt additions. This was shown to be practically the case for all salts tested (data not shown). Taking into account $\Delta A_{830}^{1\mu s}(+NH_2OH) = \text{constant}$, the reconstitution factor related to the $CaCl_2$ effect can be expressed by Eqn. 1:

$$\Delta R_{salt}^{ns} = \left(\frac{\Delta A_{830}^{1\mu s}(\text{control}) - \Delta A_{830}^{1\mu s}(\text{salt})}{\Delta A_{830}^{1\mu s}(\text{control}) - \Delta A_{830}^{1\mu s}(10\ \text{mM}\ CaCl_2)} \right)_{\text{trypsin}} \quad (1)$$

where ΔR_{salt}^{ns} represents the normalized reconstitution factor of the extent of the nanosecond kinetics in PS II membrane fragments trypsinized at pH = 6.0. 10 mM $CaCl_2$ was used as reference, because at this concentration the restoration effect completely saturates [30].

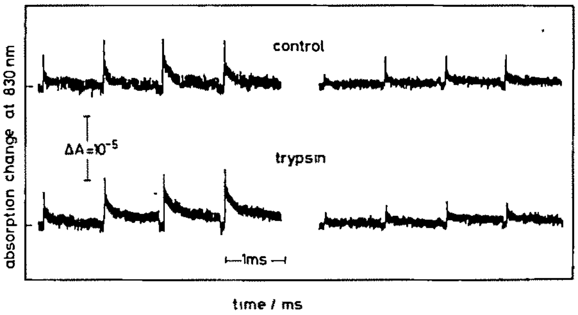

Fig. 5. Absorption changes at 830 nm induced by a train of four flashes in dark-adapted normal and trypsinized PS II membrane fragments at pH = 6.0 in the absence (left side) and presence (right side) of 10 mM $CaCl_2$. Experimental conditions as described in Materials and Methods.

The data obtained for different salts are summarized in Table I in terms of percentage reconstitution, i.e. $100 \times \Delta R_{salt}^{ns}$. The results clearly demonstrate that the restoration of the nanosecond kinetics is dominated by Ca^{2+} and that Cl^- plays only a marginal role. Ca^{2+} can be substituted to a marked extent by Sr^{2+} and partly by Ba^{2+}, whereas Mg^{2+}, Mn^{2+} and monovalent cations are almost inefficient. It should be mentioned that Ba^{2+} causes additionally a time-dependent inhibition. Therefore the data of Table I for Ba^{2+} refer only to the initial activity. The degree of the conversion of nanosecond kinetics of P-680$^+$-reduction in PS II membrane fragments into decay components in the microsecond range by mild trypsin treatment at pH = 6.0 as well as the extent of restoration by 10 mM $CaCl_2$ varied quantitatively for different preparations. The same qualitative behaviour, however, was observed in all samples that were used in this study. The above-mentioned results support the idea that a specific structural modification affects the reduction kinetics of P-680$^+$. Now the question arises about the functional site of the trypsin-induced effect and its partial reversal by Ca^{2+}. Fig. 5 depicts the absorption changes induced by a flash

TABLE I

Salt added	$\frac{\Delta A_{830}^{1\mu s}(\text{control}) - \Delta A_{830}^{1\mu s}(\text{salt})}{\Delta A_{830}^{1\mu s}(\text{control}) - \Delta A_{830}^{1\mu s}(10\ \text{mM}\ CaCl_2)} \cdot 100\%$
10 mM $CaCl_2$	100
10 mM $Ca(NO_3)_2$	92
10 mM $Ca(OAc)_2$	89
10 mM $Ca(OAc)_2$ (assay medium − Cl^-)	74
10 mM $SrCl_2$	85
10 mM $BaCl_2$*	43
10 mM $MgCl_2$	8
10 mM $MnCl_2$	29
10 mM NaCl	0
100 mM NaCl	15
10 mM KCl	0

train in dark-adapted PS II membrane fragments. The data indicate a progressive increase of the slow kinetics during the flash train (the steady state is reached only after 20–30 flashes, data not shown). This pattern is not indicative for a selective blockage of Z^{ox}-reduction at a specific redox state S_i (see Discussion). In order to test a possible correlation between the extent of the nanosecond kinetics and the oxygen evolving capacity, the average oxygen yield per flash was measured under comparable experimental conditions (see Materials and Methods). In most of our experiments oxygen was found to be less sensitive than the nanosecond kinetics to mild trypsin at pH = 6.0, as is shown in Fig. 6. Unfortunately, we observed for different preparations marked deviations from the pattern depicted in Fig. 6. Therefore unambiguous conclusions cannot be drawn at this point. However, the opposite effect, i.e., persistence of nanosecond kinetics to specific treatments that highly suppress oxygen evolution, was recently well established [31]. Therefore, the relative extent of the nanosecond kinetics of P-680$^+$ reduction cannot be used as an unambiguous quantitative measure for the percentage of functionally competent water-oxidizing enzyme systems. So far we have analyzed the modification of the P-680$^+$-reduction pattern by mild trypsin treatment at pH = 6.0 and the Ca^{2+}-induced partial restoration. Recently, it was shown that $CaCl_2$ in the assay medium affects also the susceptibility to trypsin of herbicide binding and the *p*-benzoquinone-mediated electron transport in PS II membrane fragments [32]. This protective effect to tryptic attack was further investigated by measurements of room temperature fluorescence induction curves in PS-II membrane fragments that were trypsinized at pH = 7.5 in the absence or presence of 10 mM $CaCl_2$. Fig. 7 shows the effect of increasing incubation time with trypsin. After a few minutes trypsination in the absence of $CaCl_2$ interruption takes place of electron transfer from Q_A^- to Q_B. This effect causes a fast fluorescence rise. The retardation of the subsequent slower-rising part probably reflects two effects: a fraction of the PS-II centers could remain connected with the total plastoquinone pool, and in addition the donor side activity degrades too. Further, the decrease of the maximum fluorescence reflects a trypsin-induced quenching, probably by effects of trypsin on the light-harvesting complex [33–35]. A markedly different pattern is observed, if trypsin treatment is performed in the presence of $CaCl_2$. Under these conditions, the acceptor side is highly protected against tryptic attack as shown by the invariance of the fast-rising part of variable fluorescence. This result is in perfect agreement with corresponding lines of evidence from herbicide binding studies and measurements of *p*-BQ-mediated electron transfer [32].

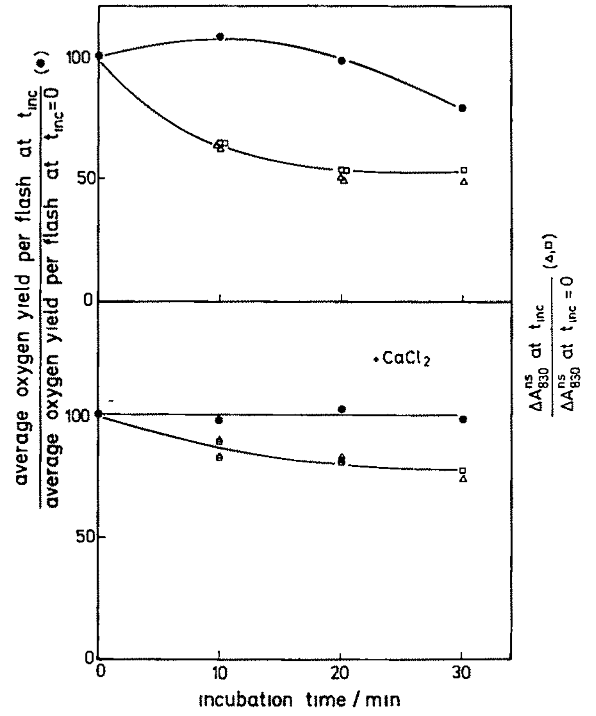

Fig 6 Average oxygen yield per flash and extent of the nanosecond kinetics in the overall decay of 830 nm absorption changes in PS II membrane fragments as a function of incubation time with trypsin at pH = 6.0 in the absence (top) and after additions of 10 mM $CaCl_2$ (bottom). Experimental conditions as described in Materials and Methods

In PS II membrane fragments trypsinized at pH = 7.5 in the absence of $CaCl_2$ the shape of the fluorescence induction curve becomes only slightly changed after addition of 3 mM NH_2OH (data not shown). This result indicates that the trypsin-induced blockage at the acceptor side involves a large fraction of the PS II reaction centers. A markedly different pattern is observed if 10 mM $CaCl_2$ is present during the 10 min trypsin treat-

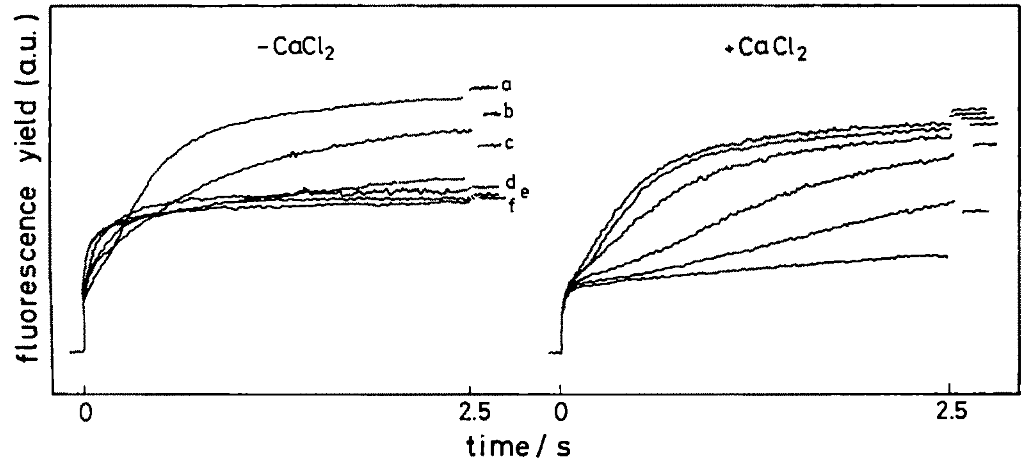

Fig. 7. Fluorescence yield as a function of actinic illumination in normal and trypsinized PS II membrane fragments: (a) control, (b) 1 min; (c) 3 min; (d) 5 min, (e) 10 min and (f) 20 min. PS II membrane fragments were trypsinized at $pH = 7.5$ in the absence or presence of 10 mM $CaCl_2$. The level indicated at the end of each induction curve was taken after 7 s Experimental conditions as described in Materials and Methods

ment. In this case, the acceptor side is highly protected against tryptic attack, whereas the donor-side capacity appears to be diminished due to degradation of the water-oxidizing enzyme system. Addition of 3 mM NH_2OH almost completely restores the inducation curve of the control samples (data not shown). Accordingly, in the presence of $CaCl_2$ the donor side is less resistant to tryptic attack than the acceptor side.

Fluorescence measurements also show [30] that the protective function of Ca^{2+} regarding further proteolytic degradation disappears after trypsin treatment of PS II membrane fragments. Two questions are of mechanistic relevance. (a) Does the loss of Ca^{2+} protection after trypsin treatment kinetically coincide with the proteolytic degradation of PS II? (b) Does the protective function exhibit the same specificity as the partial restoration effect of the nanosecond kinetics?

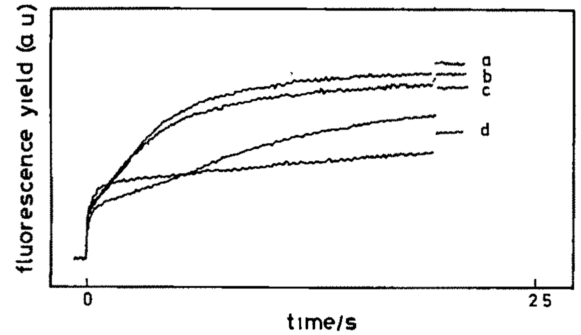

Fig. 8. Fluorescence yield as a function of actinic illumination time in PS II membrane fragments: (a) control; (b) trypsinized for 20 s at $pH = 7.5$ in the absence of $CaCl_2$; (c) trypsinized for 10 min in the presence of 10 mM $CaCl_2$, (d) trypsinized for 20 s, then addition of 10 mM $CaCl_2$ and further trypsination up to 10 min. Other experimental conditions as described in Material and Methods

The experimental data depicted in Fig. 8 show that a trypsin treatment of only 20 s is sufficient for preventing the protective action of added $CaCl_2$. On the other hand, the 20 s trypsination itself hardly affects the fluorescence curve. This interesting finding indicates that the potency of Ca^{2+} to act as protectant is lost after a rather short trypsin treatment which does not affect the general pattern of PS II electron transport. Specific surface modifications are assumed to be responsible for this phenomenon. Referring to the specificity of the Ca^{2+}-induced protection to trypsin experiments were performed with different salts. The protective effect was found to be much less specific than the restoration of the nanosecond kinetics. All bivalent ions tested exhibit similar effects.

Discussion

The present study shows that trypsin treatment at $pH = 6.0$ markedly affects the P-680$^+$ reduction by transforming part of the nanosecond kinetics into markedly slower kinetics. Taking into account the effect of trypsin on the polypeptide pattern [16,19] the data reflect a structural modification of the PSII donor side leading to a change of the electron-transport pattern. For the 200-μs kinetics this modification can be functionally compensated to a significant extent by the specific action of Ca^{2+} salts. This phenomenon implies different questions of mechanistic relevance for the functional and structural organization of the PS II donor side. (1) What is the origin of the trypsin-induced 200-μs reduction kinetics of P-680^+? (2) What is the nature of the Ca^{2+}-binding site? (3) What is the functional role of Ca^{2+}?

Two alternative interpretations can be proposed for the trypsin-induced 200-μs back reaction: (a) blockage of electron transport from the water-oxidizing enzyme system Y to Z^{ox} giving rise to a back reaction between P-680^+ and Q_A^-, or (b) retardation of the electron-transfer kinetics from Z to P-680^+. The former proposal could be in line with recent reports on NaCl-washed samples. Measurements of ultraviolet absorption changes (320 nm) and of the average oxygen yield per flash in inside-out vesicles indicated that after removal of the 23 kDa protein a back reaction between P-680^+ and Q_A^- probably arises under repetitive flash excitation at the expense of the oxygen-evolving capacity [36]. Based on delayed fluorescence and oxygen-yield measurements in dark-adapted NaCl-washed PS II membrane fragments deprived of their 18 and 23 kDa polypeptides the redox transition $S_3Z^{ox} \rightarrow S_0Z + O_2 + 2H^+$ was inferred to be blocked. The reaction can be restored by Ca^{2+} [37]. Likewise, under comparable conditions a partial loss of oxygen evolution and a concomitant increase of the EPR signal II_f have been observed that can be reversed by Ca^{2+}, but not by other cations [22,38]. Therefore, our present data could be analogously explained by a trypsin-induced degradation of the 18 and 23 kDa polypeptides which causes a Ca^{2+} reversible blockage of Z^{ox} reduction by S_3. This would lead to a P-680^+ Q_A^- back reaction under repetitive flash excitation. Measurements of 320 nm absorption changes (data not shown) are not in contradiction to this idea, but do not provide an unambiguous proof. However, other tests are available. If the appearance of the 200-μs kinetics at the expense of the nanosecond reduction of P-680^+ after mild trypsin treatment (pH = 6.0) is exclusively due to blockage of S_3 oxidation by Z^{ox}, then two effects should be observed: (a) stoichiometric correlation between the average oxygen yield per flash and the extent of the nanosecond kinetics; (b) excitation of dark-adapted trypsinized samples with a flash train should exhibit a rather small extent of the 200-μs kinetics after the first three flashes followed by a marked increase after the 4th flash due to formation of the state $S_3 \| Z^{ox}$P-680^+ Q_A^-. Both phenomena have not been observed at the expected degree (see Figs. 5 and 6). Therefore, we conclude that trypsin treatment affects the electron-transfer rate not only between the water-oxidizing enzyme system Y and Z^{ox}, but also between Z and P-680^+. The quantitative correlation of these effects remains to be clarified.

The trypsin-induced functional modification of the PS II donor side appears to be closely related to the site of Ca^{2+} action. It is now well established that the surface-exposed polypeptides of 18, 23 and 33 kDa do not contain the Ca^{2+}-binding site (for a recent review, see Ref. 17). Recently, it was shown that after removal of the 23 kDa polypeptide a light-induced conformational change takes place at a not yet identified intrinsic polypeptide that opens the Ca^{2+}-binding site to the outer aqueous medium [39]. Ca^{2+} release is assumed to cause blockage of oxygen evolution. Addition of sufficient exogenous Ca^{2+} saturates the binding site and restores oxygen evolution via an unknown mechanism. Based on thermoluminescence and oxygen-yield measurements in dark-adapted PS II membrane fragments, Ca^{2+} was inferred to be required for the functional integrity of system Y through an all-or-none-type mechanism [40]. Furthermore, it is interesting to note that after depletion of the surface-exposed polypeptides the Ca^{2+}-induced restoration of oxygen evolution exhibits a marked heterogeneity [40]. A similar heterogeneity of the Ca^{2+} effect has been also observed in PS II membrane fragments deprived of their 18 kDa and 23 kDa polyeptpides by NaCl washing. The existence of a high affinity (50–100 μM) and a low affinity (1–2 mM) binding site was reported [41]. A quantitative analysis of the restoration effect of P-680$^+$-reduction kinetics reported here as a function of $CaCl_2$ concentration led to the conclusion that the Ca^{2+} effect is a cooperative effect implying at least two binding sites with affinities of 60 μM and 1.3 mM [30]. These values are in close correspondence with the above-mentioned data [41] and latest findings in NaCl-washed wheat PS II-membrane fragments [42]. This suggests that the effect induced by mild trypsin treatment (pH = 6.0) is caused predominantly by microenvironmental changes of the same Ca^{2+}-binding site(s) that is (are) also affected by NaCl washing. Therefore, removal (NaCl washing) or desintegration (trypsin, pH = 6.0) of the surface-exposed polypeptides markedly affects the binding of Ca^{2+} that is functionally relevant to water oxidation. However, it remains to be clarified whether the regulatory function of Ca^{2+} implies only one binding site per PS II or two cooperatively interacting binding sites. As Ca^{2+} cannot act as a redox active group its function is assumed to be a tuning of the reaction coordinates at the donor site by structural 'calibration' of the polypeptide matrix and/or electrostatic affects. Our data confirm that the effect of Ca^{2+} is rather specific [22]. The mechanistic implications of this specificity have to be identified in future work. It is interesting to note that after harsher trypsin treatment (pH = 7.5), a pH-dependent 2–20 μs kinetics emerges for the P-680$^+$ reduction which cannot be reversed by Ca^{2+}. In this case the water-oxidizing enzyme system becomes irreversibly destroyed [16].

Beyond the Ca^{2+} restoration of functional defects at the donor side due to Ca^{2+} release after mild trypsin treatment (pH = 6.0) a marked protection effect against proteolytic degradation of the acceptor side is observed, if Ca^{2+} is present in the assay medium. This effect is very likely related to a tight membrane appression which hampers trypsin attack. The implications of this protection shall not be discussed extensively in this study.

Acknowledgements

The authors would like to thank S. Hohm-Veit for skillfull technical assistance and A. Bowe-Gräber for drawing the figures. The financial support by Deutsche Forschungsgemeinschaft (Sonderforschungsbereich 312) is gratefully acknowledged.

References

1 Renger, G and Govindjee (1985) Photosynth Res. 6, 33–55

2 Babcock, G.T. and Sauer, K. (1975) Biochim Biophys. Acta 376, 315–328

3 Van Best, J.A. and Mathis, P (1978) Biochim. Biophys Acta 408, 154–163

4 Brettel, K. and Witt, H.T (1983) Photobiochem Photobiophys. 6, 253–260

5 Eckert, H.J , Renger, G and Witt, H.T. (1984) FEBS Lett. 167, 316–320

6 Babcock, G.T , Blankenship, R.E and Sauer, K. (1976) FEBS Lett. 61, 286–289

7 Dekker, J P , Plijter, J.J., Ouwehand, L , Van Gorkom, H.J. (1984) Biochim. Biophys. Acta 767, 176–179

8 Renger, G. and Weiss (1985) Biochem Soc Trans 14, 17–20

9 Conjeaud, H. and Mathis, P. (1980) Biochim. Biophys. Acta 590, 353–359

10 Renger, G. and Wolff, C. (1976) Biochim. Biophys. Acta 423, 610–614

11 Havemann, J and Mathis, P. (1976) Biochim. Biophys. Acta 440, 346–355

12 Buttner, W.J. and Babcock, G.T. (1984) Biochim. Biophys. Acta 767, 272–287

13 Schlodder, E., Brettel, K and Witt, H T. (1985) Biochim Biophys. Acta 808, 123–131

14 Renger, G. (1972) Biochim Biophys. Acta 256, 428–439

15 Gläser, M., Wolff, C. and Renger, G. (1976) Z Naturforsch 31c, 712–721

16 Völker, M., Ono, T., Inoue, Y. and Renger, G (1985) Biochim. Biophys. Acta 806, 25–34

17 Murata, N and Miyao, M. (1987) in Proceedings of the VIIth International Congress on Photosynthesis (Biggins, J., ed.), Martinus Nijhoff, Dordrecht, The Netherlands, in the press

18 Irrgang, K.D., Renger, G. and Vater, J (1986) FEBS Lett. 204, 67–75

19 Renger, G., Volker, M. and Weiss, W. (1984) Biochim. Biophys Acta 766, 582–591

20 Völker, M., Renger, G. and Rutherford, A.W. (1986) Biochim. Biophys. Acta 851, 424–430

21 Ono, T. and Inoue, Y. (1983) in The Oxygen Evolving System of Photosynthesis (Inoue, Y., Crofts, A.R., Govindjee, Murata, N., Renger, G. and Satoh, K., eds.), pp. 337–344, Academic Press Japan, Tokyo

22 Ghanotakis, D.F , Babcock, G T. and Yocum, C.F (1984) FEBS Lett. 167, 127–130

23 Miyao, M and Murata, N. (1985) FEBS Lett. 168, 118–120

24 Berthold, D.A., Babcock, G.G and Yocum, C.F. (1981) FEBS Lett. 134, 231–234

25 Renger, G. and Schulze, A. (1985) Photobiochem. Photobiophys 9, 79–87

26 Weiss, W. and Renger, G (1986) Biochim. Biophys Acta 860, 173–183

27 Murata, N. and Miyao, M. (1985) Trends Biochem. Sci 122–124

28 Ono, T and Inoue, Y. (1983) FEBS Lett. 166, 381–384

29 Ghanotakis, Babcock, G.T. and Yocum, C.F. (1985) FEBS Lett. 192, 1–3

30 Völker, M., Eckert, H J. and Renger, G. (1987) in Proceedings of the VIIth International Congress on Photosynthesis (Biggins, J., ed.), Martinus Nijhoff, Dordrecht, The Netherlands, in the press

31 Eckert, H.J., Wydrzynski, T., Völker, M. and Renger, G (1986) Photochem. Photobiol 43, suppl, 1025

32 Renger, G, Hagemann, R and Fromme, R. (1986) FEBS Lett. 203, 210–214

33 Gerola, P., De Benedetti, E., Rizzi, S, Forti, G and Gerlaschi, F M. (1977) in Bioenergetics of Membrane (Packer, L., Papageorgiou, G.C. and Trebst, A., eds), pp 361–369, Elsevier, Amsterdam

34 Steinback, K.E, Burke, J J and Artzen, C.J. (1979) Arch. Biochem Biophys. 195, 546–557

35 Jennigs, R.C., Forti, R C, Gerola, P.D. and Gerlaschi, F.M. (1978) Plant Physiol 62, 879–884

36 Akerlund, H.E., Renger, G., Hagemann, R and Weiss, W. (1984) Biochim. Biophys. Acta 765, 1–6

37 Boussac, A, Maison-Peteri, B., Vernotte, C and Etienne, A.L. (1985) Biochim. Biophys. Acta 808, 25–230

38 Dekker, J.P, Ghanotakis, D F, Plijter, J.J., Van Gorkom, H J. and Babcock, G.T. (1984) Biochim Biophys. Acta 767, 515–523

39 Miyao, M. and Murata, N. (1986) Butler Memorial Volume (Govindjee et al., eds), Photosynth. Res., in the press

40 Ono, T. and Inoue, Y (1986) Biochim. Biophys. Acta 850, 380–389

41 Boussac, A, Maison-Peteri, B Etienne, A.L and Vernotte, C. (1985) Biochim. Biophys Acta 808, 231–234

42 Cammarata, K and Cheniae, G. (1987) in Proceedings of the VIIth International Congress on Photosynthesis (Biggins, J., ed.), Martinus Nijhoff, Dordrecht, The Netherlands, in the press

Biochimica et Biophysica Acta 890 (1987) 77–81
Elsevier

BBA 42156

Light modulation of serine and threonine phosphorylation in histone III by thylakoids

Héctor A. Lucero, Néstor Cortez and Rubén H. Vallejos

Centro de Estudios Fotosintéticos y Bioquímicos, CEFOBI (Consejo Nacional de Investigaciones Científicas y Técnicas, F.M. Lillo y Universidad Nacional de Rosario), Suipacha 531, 2000 Rosario (Argentina)

(Received 8 April 1986)
(Revised manuscript received 26 August 1986)

Key words: Protein phosphorylation; Histone phosphorylation; Light modulation; Protein kinase; (Spinach chloroplast)

Thylakoids from dark-adapted leaves phosphorylated histone III faster in the light than in the dark, such process being the resultant of a light activation of a threonine protein phosphorylation and a light inactivation of a serine protein phosphorylation. Phosphorylation of histone III by thylakoids from dark-adapted leaves showed an optimal pH of 7.1 in the light and of 8.5 in the dark. Storage of the thylakoids at −20°C for 3 weeks completely abolished threonine phosphorylation, but had minor effect on serine protein phosphorylation which was also inhibited by illumination during the protein kinase assay. Preillumination of the spinach leaves inactivated the serine protein phosphorylation catalyzed by thylakoids. These results are consistent with the presence of two distinguishable thylakoid-bound protein kinase activities in terms of their response to light, optimal pH and specificity for amino acid residue in the protein substrate.

Introduction

The energy distribution between the two photosystems in higher plant chloroplasts is regulated by the phosphorylation of the light-harvesting, chlorophyll-protein complex (LHCP) [1] by a thylakoid-bound protein kinase which is in turn activated by the reduced state of plastoquinone [2,3]. The LHCP protein kinase is specific for threonine residues in endogenous substrates [4]. It is consensus that thylakoids contain more than one protein kinase [5–9]. Chloroplast protein kinase 1 ($ChlPK_1$) and chloroplast protein kinase 2 ($ChlPK_2$) are thylakoid serine protein kinases which can be purified by extraction with detergents and phosphorylate a number of exogenous substrates [6,7]. From the existence of at least two thylakoid-bound serine protein kinases it might be predicted that these membranes should catalyze serine protein phosphorylation in endogenous and/or exogenous substrates. In this paper we show that using histone III as exogenous substrate it is possible to distinguish threonine protein kinase activity from serine protein kinase activity of the thylakoids in terms of their sensitivity to freezing and thawing of the membranes, modulation by light and optimal pH.

Materials and Methods

Materials

Phosphoserine, phosphothreonine, phosvitin,

Abbreviations: P_i, inorganic phosphate; Tricine, *N*-[2-hydroxy-1,1-bis-(hydroxymethyl)ethyl]glycine; Mes, 4-morpholineethanesulphonic acid, Mops, 4-morpholinepropanesulphonic acid

Correspondence: Dr. Rubén H Vallejos, CEFOBI, Suipacha 531, 2000 Rosario, Argentina

0005-2728/87/$03 50 © 1987 Elsevier Science Publishers B V. (Biomedical Division)

casein, histone II-AS and lysine rich histone IIIS were from Sigma Chemical Co. (U.S.A.). Carrier-free $^{32}P_i$ was from Dupont NR. P. Boston, MA. Salt-free, carrier-free [γ-^{32}P]ATP was prepared as in Ref. 10. Spinach (*Spinacia olearacea* L.) plants were grown under environmental-controlled conditions for 4 weeks at 21°C and 70% relative humidity with a 10–14 h light-dark periods at a photosynthetic light intensity of $7 \cdot 10^{15}$ quants $\cdot$ $m^{-2} \cdot s^{-1}$.

Chloroplast isolation

Spinach leaves (6 g), cut from the plants after 10–12 h of dark period, were left in the dark at room temperature of illuminated with a 150 W tungsten lamp through 2 cm of 1% $CuSO_4$ as a heat-absorbing filter for 30 s as described [11]. Chloroplasts were rapidly isolated in the dark as described [12], by homogenization of the leaves in 10 ml of a medium containing 250 mM sucrose/10 mM NaCl/10 mM $MgCl_2$/0.1 mM EDTA/20 mM Tricine-NaOH (pH 8). Isolated chloroplasts were washed twice in 10 mM NaCl/10 mM $MgCl_2$/0.1 mM EDTA/10 mM Tricine-NaOH (pH 7.3) and resuspended in the same medium to a final concentration of 1 mg chlorophyll per ml. Chlorophyll concentration was determined as described [13].

Protein kinase assay

Thylakoids (25 μg chlorophyll) were incubated at 25°C in the dark in a medium (120 μl) containing 75 mM Mes/Mops/Tricine buffer (25 mM each) adjusted to pH 7.3 unless otherwise stated/10 mM $MgCl_2$/100 μM [γ-^{32}P]ATP (500–1000 cpm per pmol)/50 μg histone III. The assay was terminated by addition of 5 μl 0.4 M ATP and 30 μl 1 M HCl. Histone was recovered in the supernatant after centrifugation for 2 min at 13000 rpm in an Eppendorf microcentrifuge. When casein or phosvitin was used as substrates, the kinase assay was terminated by addition of 5 μl 0.4 M ATP and centrifuged to sediment thylakoids. Aliquots (50 μl) from the supernatant were spotted on Whatman 3 mm paper (2 × 2 cm) and protein kinase assay was pursued as described [6].

Phosphoamino acid analysis

After termination of the protein kinase assay as indicated above, proteins in the supernatant (50 μl) were precipitated with 50 μl 50% trichloroacetic acid. Elimination of the excess of radioactive ATP, acid hydrolysis of the proteins, high-voltage paper electrophoresis to resolve the phosphoamino acid and detection of the phosphorylated amino acids were carried out as described [6]. Samples were hydrolyzed and processed under identical conditions to compare their relative amounts of phosphoamino acids [14]. The standard error for the determination of each phosphoamino acid in samples by triplicate was always lower than 5% of the mean value presented as 10^{-3} cpm.

Results

After phosphorylation of histone III, thylakoids were precipitated with hydrochloric acid and the phosphoamino acids present and the level of protein phosphorylation corresponding to histone III were determined in the supernatant. Therefore, the results reported here do not correspond to those of endogenous proteins of thylakoids. Phosphoserine was the only phosphoamino acid found in histone III when it was phosphorylated by fresh thylakoids in the dark (Fig. 1). The same result was observed when histone II, casein or phosvitin was used as a substrate (data not shown).

Light stimulates histone III phosphorylation by fresh thylakoids [15]. Analysis of phosphoamino acids showed that this light stimulation is the resultant of two opposite effects: a stimulation of threonine phosphorylation and an inhibition of serine phosphorylation (Fig. 1). DCMU prevented the light-dependent phosphorylation of histone III in threonine residues, but did not prevent the light inactivation of histone III phosphorylation in serine residues (Fig. 1). The radioactivity recovered in the phosphoamino acid spots is shown in Fig. 1B.

Storage of the thylakoids at −20°C for 3 weeks inhibited the light-activated protein kinase involved in the phosphorylation of LHCP (data not shown). However, these frozen-thawed membranes preserved most of the activity observed in fresh thylakoids that phosphorylated histone III in the dark. Illumination during the assay inhibited histone III phosphorylation by frozen-thawed

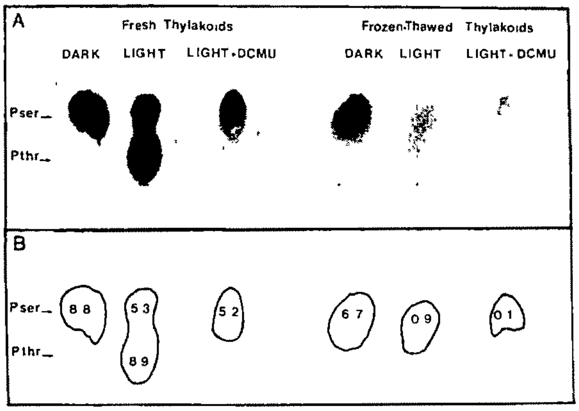

Fig 1 Phosphoamino acids in histone III phosphorylated by fresh or frozen-thawed thylakoids. Protein kinase assay and phosphoamino acid analysis were described under 'Experimental procedures' (A) Autoradiography of the phosphoamino acid analysis of histone III phosphorylated by thylakoids from dark-adapted leaves. The specific activities for the phosphorylation of histone III by fresh thylakoids were 1.8 and 6 nmol ^{32}P/min per mg chlorophyll in the dark and in the light, respectively; for frozen-thawed thylakoids the activities were 1.9 and 0.3 nmol ^{32}P/min per mg chlorophyll in the dark and in the light, respectively (B) 10^{-3} cpm counted in the phosphoamino acid spots.

thylakoids from 1.9 to 0.3 nmol ^{32}P/min per mg chlorophyll. Phosphoamino acid analysis indicated that only serine residues were phophorylated in the dark by frozen-thawed thylakoids (Fig. 1A), such phosphorylation being inhibited by light from 6700 cpm to 928 cpm (Fig. 1B). DCMU did not prevent the light inactivation of serine protein phosphorylation in histone III by frozen-thawed thylakoids.

Histone III was phosphorylated by fresh thylakoids from dark-adapted leaves at different pH values in the light and in the dark. The optimal pH values for histone phosphorylation were 7.1 and 8.5 in the light and in the dark, respectively (Fig. 2A). The phosphoamino acid analysis of histone III phosphorylated in the light and in the dark at pH 6.5, 7.3 and 8.5 is shown in Fig. 2B. In the light both phosphoserine and phosphothreonine were detected in all the pH values assayed, while phosphoserine was prevalent in the dark. The radioactivity recovered in the phosphoamino acid spots indicated that in the light histone III was preferentially phosphorylated in threonine residues at pH 6.5 and 7.3. At higher pH values the ratio phosphoserine/phosphothreonine was close to the unit (Fig. 2C). On the other hand, in the dark, histone III was mainly phosphorylated in serine residues with maximal incorporation at pH 8.5 (Fig. 2C). The optimal pH values determined by the radioactivity recovered in the phosphoamino acid spots (Fig. 2C) were consistent with the values determined by protein kinase assay (Fig. 2A).

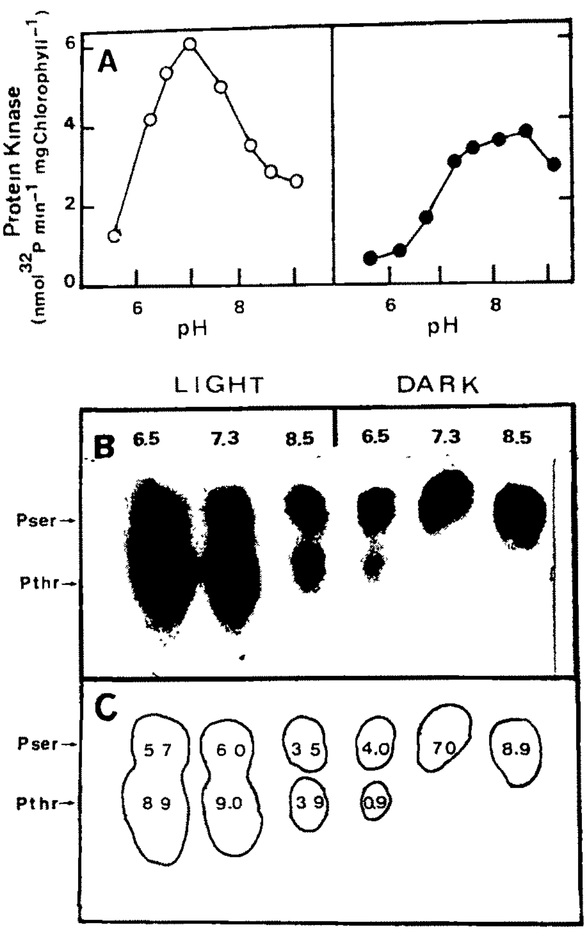

Fig 2 Effect of pH on histone III phosphorylation in the light and in the dark by fresh thylakoids Protein kinase activity of thylakoids from dark-adapted leaves and phosphoamino acid analysis were carried out as described in the text (A) pH titration of histone III phosphorylated in the light (○——○) or in the dark (●——●). (B) Autoradiography of the phosphoamino acid analysis of histone III (C) (10^{-3} cpm) in the phosphoamino acid spots corresponding to (B).

Thylakoids from dark-adapted leaves phos-

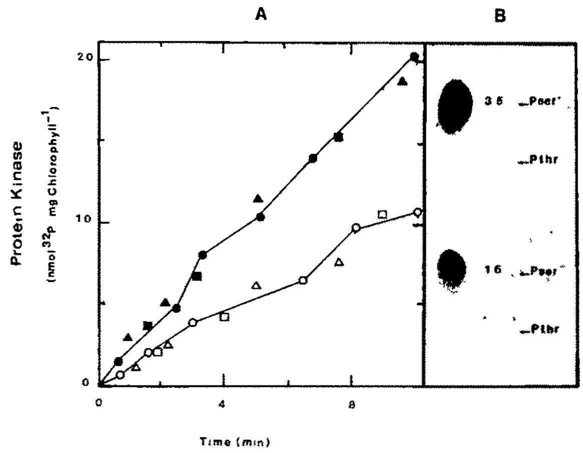

Fig 3 Phosphorylation of histone III by thylakoids from preilluminated or dark-adapted leaves (A) Histone III was phosphorylated in the dark by thylakoids from dark-adapted leaves (●———●) or by thylakoids from preilluminated leaves (○———○) in the presence of 60 μg/ml Dio-9 (△, ▲) or 100 nm gramicidin (□, ■) (B) Autoradiography of the phosphoamino acid detected in histone III phosphorylated for 10 min by thylakoids from dark-adapted leaves (upper) or by thylakoids from preilluminated leaves (lower) Numerals are 10^{-3} cpm.

phorylated histone III in the dark 1.9-folds faster than thylakoids from leaves that were preilluminated with incandescent light (Fig. 3A). The addition of Dio-9, an inhibitor [16] or gramicidin, a deactivator [12] of the thylakoid-bound proton ATPase to the protein kinase assay medium did not alter the control rates of histone phosphorylation (Fig. 3A), suggesting that the proton ATPase which is activated by preillumination of the leaves [12], does not interfere with the assay under our experimental conditions. The phosphoamino acid found in histone III, phosphorylated by thylakoids as in Fig. 3A was phosphoserine regardless the pretreatment of the leaves. Moreover, the level of radioactivity recovered as phosphoserine in histone III was lower when the substrate was phosphorylated by thylakoids from preilluminated leaves (1600 cpm) than when it was phosphorylated by thylakoids from dark-adapted leaves (3500 cpm) (Fig. 3B).

Discussion

LHCP protein kinase is specific for threonine residues in endogenous substrates [4] and its activation is linked to the reduced state of plastoquinone [2,3]. DCMU prevents the light activation of LHCP protein kinase by blocking the electron transport before the reduction site of platoquinone [2,3]. Histone III is phosphorylated by thylakoids in threonine residues only in the light and such phosphorylation is prevented by DCMU, which suggests that the reaction is catalyzed by LHCP protein kinase (Fig. 1). Histone III is also phosphorylated by thylakoids in serine residues but this phosphorylation is partially prevented by light (fig. 1). This light inactivation does not require reduced plastoquinone for it is not prevented by DCMU (Fig. 1). Neither is it the result of a competition of serine protein kinases with threonine protein kinase(s) for it is also observed with frozen-thawed thylakoids which lack threonine protein kinase activity (Fig. 1).

The inactivation by light of serine phosphorylation in histone III was also observed when intact leaves were illuminated prior to the isolation of thylakoids (Fig. 3) suggesting that the negative modulation by light of this serine protein kinase activity may also occur under physiological conditions.

The different optimal pH (Fig. 2A), the opposite response to the light (Fig. 1 and Fig. 3) and the different sensitivity to freezing and thawing of the membranes (Fig. 1) indicate that serine protein kinase and threonine protein kinase activities of thylakoids are distinguishable in functional terms. On one hand there is a light-activated protein kinase activity that phosphorylates LHCP and histone III in threonine residues which can be referred to as thylakoid threonine protein kinase. This activity may be composed of more than one enzyme [9] and it is physiologically involved in the regulation of the state transition [1,17]. On the other hand, there is a protein kinase activity phosphorylating histone III and endogenous proteins of thylakoids (unpublished data) in serine residues which can be referred to as thylakoid serine protein kinase. Since two serine kinases were purified from spinach thylakoids [6,7], at least one of them is likely to be inactivated by light. The mechanism of light inactivation, the identification of endogenous substrates and the physiological role of the intrinsic serine kinases of thylakoids are as yet unknown.

The use of histone as exogenous substrate has provided a non-physiological, albeit useful, means to trace intrinsic thylakoid protein kinases. Phosphoamino acid analysis of the phosphorylated substrate was essential not only to differentiate the protein kinases according to their amino acid specificity, but also to allow the detection of a negative modulation by light of an intrinsic thylakoid serine protein kinase otherwise masked in standard protein kinase assays.

Acknowledgements

This work has been supported by grants from Consejo Nacional de Investigaciones Científicas y Técnicas (Argentina). H.A.L. and R.H.V. are members of the Investigator Career and N.C. is a Fellow of the same Institution.

References

1 Bennett, J , Steinback, K E. and Arntzen, C.J (1980) Proc Natl. Acad Sci USA 77, 5253–5257
2 Allen, J.F., Bennett, J., Steinback, K E and Arntzen, C.J. (1981) Nature 291, 21–25
3 Alfonzo, R E (1981) Thesis, Cornell University, p. 101
4 Bennett, J (1977) Nature 269, 344–346
5 Markwell, J P., Baker, N R., Bradbury, M. and Thornber, J.P. (1984) Plant Physiol. 74, 348–354
6 Lin, Z.F., Lucero, H A. and Racker, E (1982) J Biol. Chem 257, 12153–12156
7 Lucero, H.A., Lin, Z.F. and Racker, E (1982) J. Biol. Chem 257, 12157–12160
8 Markwell, J.P., Baker, N R and Thornber, J P. (1983) Photobiochem. Photobiophys. 5, 201–205
9 Cnaani, O. (1985) FEBS Lett. 188, 281–285
10 Palme, J L. and Avruch, J. (1981) Anal Biochem 116, 372–373
11 Morita, S., Itoh, S and Nishimura, M. (1982) Biochim Biophys Acta 679, 125–130
12 Vallejos, R., Arana, J L. and Ravizzini, R A (1983) J Biol. Chem 258, 7317–7321
13 Arnon, D.I. (1949) Plant Physiol. 24, 1–15
14 Weller, M and Rodnight, R (1971) Biochem. J 124, 393–406
15 Alfonzo, R.E., Nelson, N and Racker, E. (1980) Plant Physiol 65, 730–734
16 McCarty, R.E , Guillory, R.J and Racker, E (1965) J Biol Chem 240, 4822–4823
17 Canaani, O., Barber, J and Malkin, S (1984) Proc. Natl Acad. Sci USA 81, 1614–1618

Biochimica et Biophysica Acta 890 (1987) 82–88
Elsevier

BBA 42158

Peroxidative injury of the mitochondrial respiratory chain during reperfusion of hypothermic rat liver

Toshirou Nishida [a], Hideo Shibata [b], Masato Koseki [a], Kazuyasu Nakao [a], Yasunaru Kawashima [a], Yukuo Yoshida [b] and Kunio Tagawa [b]

[a] *First Department of Surgery, Osaka University Medical School, 1-1-50 Fukushima, Fukushima-ku, Osaka 553, and*
[b] *Department of Physiological Chemistry, Osaka University Medical School, 4-3-57 Nakanoshima, Kita-ku, Osaka 530 (Japan)*

(Received 23 June 1986)

Key words: Ischemia; Oxidative phosphorylation, Lipid peroxidation; Electron transport, (Rat liver mitochondria)

Mitochondrial dysfunction in ischemic liver has been demonstrated to be due to decrease in the intramitochondrial level of ATP and the subsequent disruption of the proton barrier of the inner membrane (Watanabe, F., Hashimoto, T. and Tagawa, K. (1985) J. Biochem. 97, 1229–1234). In this study, another injury process, impairment of the electron-transfer system, which occurred during reoxygenation of ischemic liver, was studied during reperfusion of cold preserved liver and during cold incubation of isolated rat-liver mitochondria. The sites of the respirtory chain that were sensitive to peroxidative damage were ubiquinone-cytochrome *c* oxidoreductase and NADH-ubiquinone oxidoreductase. These enzymic activities decreased with increase in lipid peroxidation. Incubation of submitochondrial particles with *t*-butyl hydroperoxide or with an NADPH-dependent peroxidation system decreased the enzymic activities of the electron-transport system. These data strongly suggested that lipid peroxidation during reoxygenation of ischemic liver impaired the electron-transfer system. Thus, mitochondria of ischemic liver suffer from two different types of injury: increase in proton permeability during anoxia, and decrease in enzymic activities of the electron-transport system during reoxygenation.

Introduction

Prolonged ischemia causes functional and structural damage of cells, and finally leads to cell death. The biochemical mechanism of cell death is still not fully understood, but it has been widely accepted that irreversible damage in ischemia is due to loss of the oxidative phosphorylation capacity of mitochondria [1–3]. Previously, we demonstrated that mitochondrial dysfunction during ischemia was caused by increased proton permeability through the inner mitochondrial membrane [4], and that this increase in proton permeability was associated with decrease of the intramitochondrial ATP level, which triggered release of Ca^{2+} from mitochondria [5].

Another biochemical mechanism of ischemic damage has been reported by several workers [6–8]. This is called ‘reperfusion injury’, and is the damage caused by peroxidation of various cellular components during reperfusion of ischemic organs. This peroxidation is known to occur on intracellular production of activated oxygen [9], and to

---

Abbreviations: DCIP, 2,6-dichloro-indophenol; CCCP, carbonyl cyanide *m*-chlorophenylhydrazone.

Correspondence: K. Tagawa, Department of Physiological Chemistry, Osaka University Medical School, 4-3-57, Nakanoshima, Kita-ku, Osaka 530, Japan.

0005-2728/87/$03.50 © 1987 Elsevier Science Publishers B.V. (Biomedical Division)

cause mitochondrial dysfunction in many cases [6,10]. However, the precise mechanism of mitochondrial dysfunction by peroxidation during reperfusion is still unknown. With respect to peroxidative damage of mitochondria, NADPH-dependent peroxidation has been shown to decrease the electron-transfer activities of submitochondrial particles [11]. These findings strongly suggest that, in addition to increase in proton permeability, peroxidation during reperfusion causes serious damage of the mitochondrial respiratory chain, and that this type of injury is unavoidable on reperfusion of an ischemic organ. In this work, we studied the damage of mitochondria during reperfusion in relation with lipid peroxidation at the mitochondrial membrane. We found that reperfusion of ischemic liver directly suppressed mitochondrial electron-transfer activities, especially the enzymic activities of Complex I and III, as the result of lipid peroxidation.

Materials and Methods

Male Sprague-Dawley rats weighing about 200 g were used for liver perfusion studies, and those of about 350 g for isolation of mitochondria. The animals were starved for about 24 h and anesthetized by intraperitoneal injection of ketamine at 100 mg/kg body weight before use.

Perfusion of isolated rat livers. The perfusion system described by Sugano et al. [12] was used. Livers were perfused for 50 min with Krebs–Henseleit bicarbonate solution containing 5.6 mM glucose at 30°C. The flow rate was 3 ml/min per g liver, the perfusion pressure was about 10 cm H_2O, and the perfusate was saturated with 95% O_2/5% CO_2 gas mixture with a gas change device [13]. Then livers were flushed with Collins' solution [14] and incubated at 0°C for 6 h, 24 h or 48 h. They were then reperfused. The oxygen concentration in the perfusion fluid leaving the liver was measured with a Clark-type electrode and the activity of aspartate aminotransferase (EC 2.6.1.1) in the perfusate was measured to check that perfusion was appropriate.

Preparation of mitochondria and submitochondrial particles. Mitochondria were isolated from rat livers as described previously [15]. Submitochondrial particles were prepared by sonication of mitochondria by the method of Beyer [16], and were washed three times to remove superoxide dismutase and glutathione peroxidase.

Incubation of mitochondria and submitochondrial particels. Mitochondria (10 mg protein/ml) were incubated as described previously [5]. The incubation medium consisted of 0.3 M mannitol/10 mM Tris-HCl (pH 7.4)/5 mM potassium phosphate (pH 7.4)/0.1 mM EDTA/0.1% bovine serum albumin/1 mM $MgCl_2$. The mitochondrial suspension was divided in two: one half was incubated under aerobic conditions (room air), and the other under 95% N_2/5% CO_2. Under the aerobic conditions, the adequate oxygen concentration required to prevent increase in the rate of State-4 respiration [15] was maintained by shaking the mitochondrial suspension very slowly for 24 h, 48 h and 72 h at 4°C. For experiments on artificial peroxidation, submitochondrial particles, 5–10 mg protein/ml, were incubated in the incubation medium with *t*-butyl hydroperoxide at 25°C. NADPH-dependent peroxidation of submitochondrial particles were achieved in a medium containing 0.1 M mannitol/5 mM potassium phosphate (pH 7.4)/10 mM Tris-HCl (pH 7.4)/0.1 mM EDTA/1 mM ADP/0.3 mM $FeCl_3$ at 25°C. The reaction was started by the addition of NADPH (0.5 mM).

Assay methods. The rate of oxygen consumption by isolated mitochondria was measured with an oxygen electrode (PC-100, Sumitomo Electric Industries) at 25°C in reaction mixture as described previously [5]. Adenine nucleotides were determined by high-performance liquid chromatography (HPLC) as described by Watanabe et al. [4]. Malondialdehyde was measured by the method of Ohkawa et al. [17]. Cytochromes were determined from the reduced-minus-oxidized difference spectra as described [11]. Ubiquinones were extracted from mitochondria by the method of Takeda et al. [18] and measured by the method of Vadhanavikit et al. [19].

Enzymic activities were determined at 25°C: succinate oxidase and NADH oxidase were assayed polarographically with an oxygen electrode. Other enzymes were assayed spectrophotometrically: NADH-cytochrome *c* oxidoreductase from the decrease in A_{340} and increase in A_{550} [20], cytochrome *c* oxidase from thedecrease in A_{550} [21], NADH-ferricyanide oxidoreductase from the decrease in A_{340} [22], NADH-2,6-dichloro-indophenol (DCIP) oxidoreductase from the decrease in A_{600} [22], succinate-DCIP oxidoreductase from the decrease in A_{600} [23], NADH-ubiquinone-1-oxidoreductase from the decrease in A_{340} [24], succinate-ubiquinone-2-oxidoreductase from the decrease in A_{600} [25], and dehydro-ubiquinone-cytochrome *c* oxidoreductase from the increase in A_{550} [26]. Protein was determined by the method of Lowry et al. [27] with bovine serum albumin as a standard.

Chemicals. Ubiquinone-1, and ubiquinone-2 were kindly provided by Nisshin Seifun Co.

Results

Damage of mitochondrial respiratory chain on reoxygenation after hypothermic incubation of rat livers

There are several reports that preserved or ischemic organs show decreased rates of oxygen consumption on reoxygenation [28,29]. This was confirmed in this study: we found that the rate of hepatic oxygen consumption during reperfusion decreased to 92%, 78% and 63% of that initially after cold incubation periods of 6 h, 24 h and 48 h, respectively. Because the oxygen consumption is overwhelmingly due to mitochondrial respiration, this decrease seemed to be caused by dysfunction of mitochondria. Therefore, we examined the oxygen consumption rate of mitochondria isolated from these livers after their anoxic incubation and then reperfusion for 60 min. The rate of State-3 respiration decreased with that of total hepatic respiration and a similar decrease was also observed in uncoupler-released respiration. Unlike in the case of mitochondrial damage during warm anoxia, there was little increase in State-4 respiration in reperfused livers after prolonged cold incubation (Fig. 1). These results indicated that the mitochondrial electron-transfer system was preferentially damaged in reperfused livers after hypothermic incubation.

Damage of the mitochondrial respiration chain during hypothermic incubation of isolated mitochondria

Similar mitochondrial damage was observed when mitochondria isolated from normal rat liver were incubated under hypothermic aerobic conditions. Mitochondria incubated under aerobic conditions showed marked decrease in uncoupler-released respiration, in striking contrast to mitochondrial damage by anoxia, which showed no decrease in uncoupler-released respiration (Fig. 2A and B). Decrease of the State-3 respiration rate

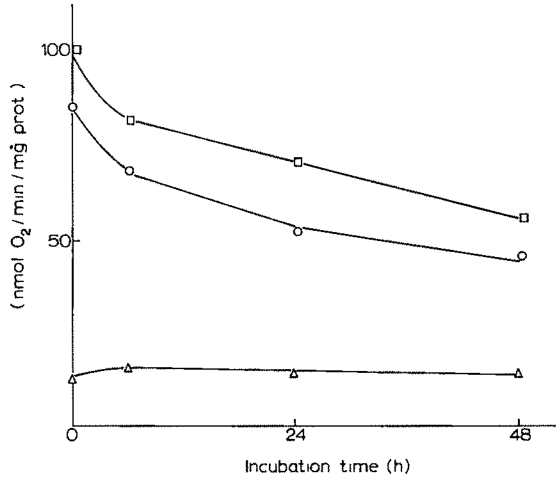

Fig. 1. Changes in mitochondrial respiration rate of reperfused livers after hypothermic incubation Perfusion of isolated rat livers and hypothermic incubation were performed as described in Materials and Methods Mitochondria were isolated from livers that had been reperfused for 60 min at 30°C. □, respiration rate in the presence of uncoupler (CCCP); O, rate of State-3 respiration; △, rate of State-4 respiration

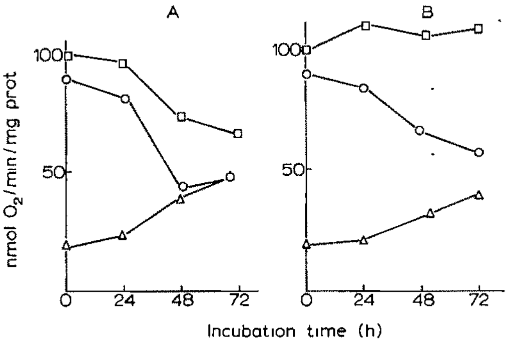

Fig. 2 Changes in mitochondrial respiration rate during aerobic and anaerobic incubations. Mitochondria were incubated as described in Materials and Methods At the times indicated, the respiration rate of mitochondria (oxidizing succinate; A and B) was measured. (A) showed the changes during aerobic incubation. (B) showed those during anaerobic incubation. □, respiration rate in the presence of CCCP; O, rate of State-3 respiration; △, rate of State-4 respiration.

and increase of the State-4 respiration rate were observed during both aerobic and anaerobic hypothermic incubations. The increase of the State-4 respiration rate during aerobic and anaerobic incubations was accounted for by decrease in the intramitochondrial ATP level, as described previously [4,5]. The decrease of State-3 respiration rate during anaerobic incubation has been shown to be caused by decrease of total adenine nucleotides in mitochondira [15]. In addition to decrease of total adenine nucleotides, the decrease of uncoupler-released respiration might be partly related to decrease of State-3 respiration during aerobic incubations. However, the mechanism of the repression of electron-transfer activity observed during aerobic incubation seemed to be completely different and to involve a toxic action of activated oxygen, because it did not occur under anaerobic conditions.

Changes in activities of enzyme complexes of the mitochondrial electron-transport system during hypothermic incubation

Similar decrease in respiratory activity were observed with succinate and NAD-linked substrates as respiratory substrates (data not shown). To determine the sites that were inhibited during aerobic incubation, we measured the activities of several enzymes involved in the mitochondrial electron-transport system. As shown in Fig. 3A and B, there was no remarkable change in the activity of succinate dehydrogenase (with DCIP as electron acceptor), NADH dehydrogenase (with ferricyanide or DCIP as electron acceptor), or cytochrome *c* oxidase, but NADH-cytochrome *c* oxidoreductase activity was reduced during aerobic incubation. Thus, the inhibitory site seemed to be in about the middle of the electron-transfer chain, and so the following three partial reactions involving oxidation-reduction of ubiquinone were examined. During aerobic incubation, there was no significant decrease in the activity of succinate-ubiquinone oxidoreductase, but moderate decrease in that of NADH-ubiquinone oxidoreductase, and marked decrease in that of dihydroubiquinone-cytochrome *c* oxidoreductase (Fig. 3C). In contrast to the decrease in enzymic activities, little change was observed in the contents of electron carriers, such as cytochromes and ubiquinones, during aerobic incubation (data not shown).

Increase of lipid peroxidation during aerobic incubation

Because the decreases of electron-transfer activ-

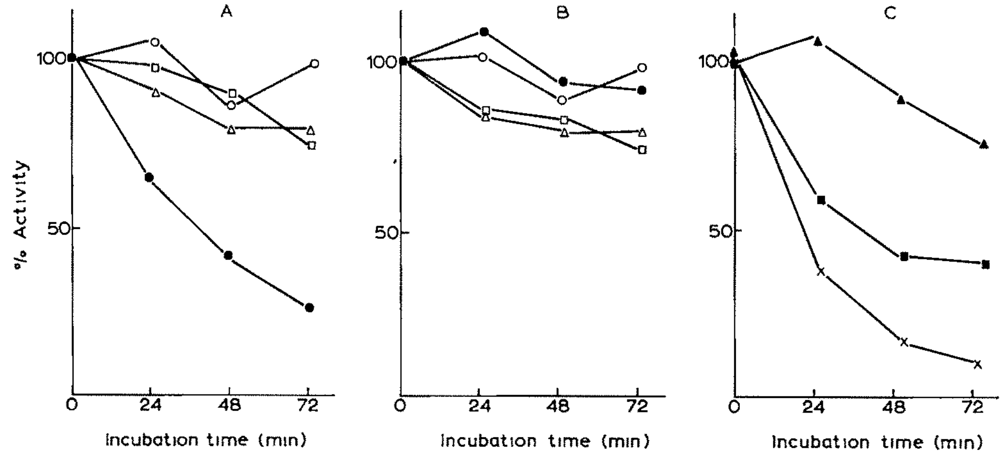

Fig 3 Changes in enzymic activities of mitochondria in aerobic and anaerobic conditions. Mitochondria were incubated as for Fig. 2, and then solubilized by 0.1% Triton X-100 or 0.2% deoxycholate in 50 mM potassium phosphate buffer (pH 7.4) or sonicated at the times indicated. (A) and (C) show changes during aerobic incubation (B) shows those during anaerobic incubation. Enzymic activities are expressed as percentages of the initial value (activities at zero time are given in parentheses in nmol/min per mg protein at 25°C) □, succinate dehydrogenase (93.7); ○, NADH dehydrogenase with DCIP as electron acceptor (194), ●, antimycin-sensitive activity of NADH cytochrome *c* oxidoreductase (102); △, cytochrome *c* oxidase (first order constant = 2.95/s per mg protein); ■, rotenone-sensitive activity of NADH-ubiquinone oxidoreductase (45); ▲, succinate-ubiquinone oxidoreductase (95); ×, activity of dihydroubiquinone-cytochrome *c* oxidoreductase (187).

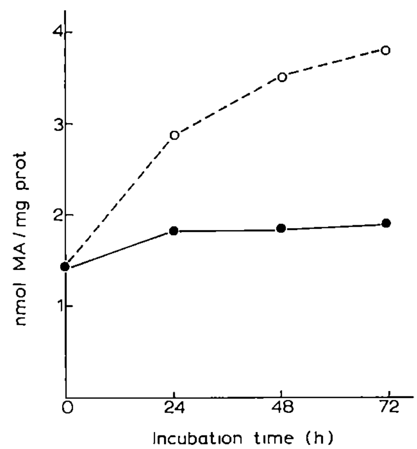

Fig. 4. Increase of lipid peroxidation during aerobic incubation Mitochondria were incubated as described in Materials and Methods. Lipid peroxidation was expressed as formation of malondialdehyde. Incubation: ○, aerobic conditions; ●, anaerobic conditions.

ities during aerobic incubation seemed to be caused by toxic effects of activated oxygen species, we measured changes in the content of lipid peroxides. As shown in Fig. 4, malondialdehyde formation increased with time during aerobic incubation, but not during anaerobic incubation. These changes together with the absence of change in the contents of electron carriers strongly suggested that the decrease of electron-transfer activities during aerobic incubation was caused by lipid peroxidation.

Damage to electron-transfer activities of rat-liver submitochondrial particles induced by lipid peroxidation

To verify that lipid peroxidation caused the damage of the electron-transport system, we examined the toxic effects of an artificial peroxide, *t*-butyl hydroperoxide, on the respiratory activity of submitochondrial particles of rat liver. When added to the incubation mixture, *t*-butyl hydroperoxide caused dose- and time-dependent decrease in the activity of succinate oxidase (Fig. 5A). NADH oxidase was more sensitive than succinate oxidase to *t*-butyl hydroperoxide (Fig. 5B). Concomitantly with the decreases of these enzymic activities, products of lipid peroxidation, measured as malondialdehyde formation, increased (Fig. 5C). An experimental peroxide forming system, composed of NADPH, ADP, $FeCl_3$ and O_2, also strongly inhibited the activities of succinate and NADH oxidases (Fig. 6). The activity of NADH oxidase was slightly more sensitive than that of succinate oxidase to this system as it was to *t*-butyl hydroperoxide. This was probably because NADH oxidase has one more site than

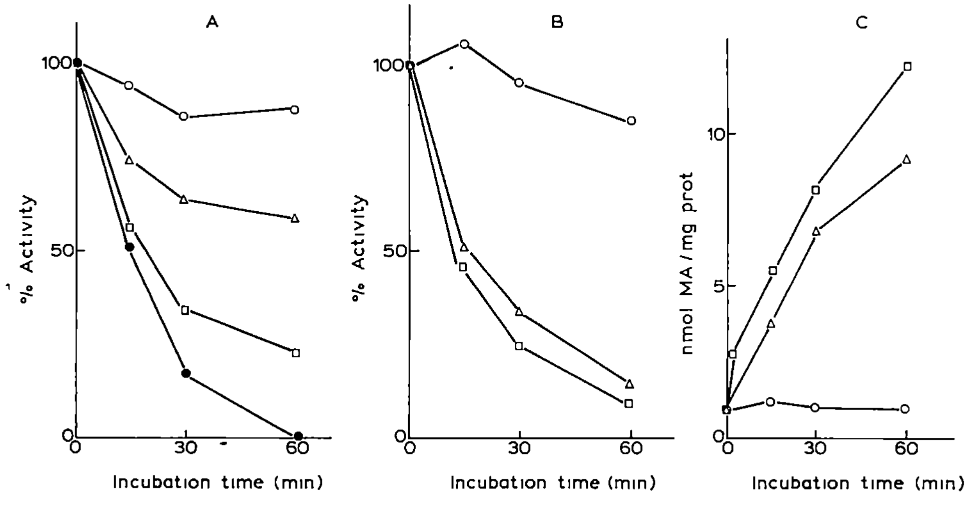

Fig. 5. *t*-Butyl hydroperoxide-induced damage of the mitochondrial respiratory chain. Submitochondrial particles were incubated as described in Materials and Methods At the times indicated, the activities of succinate oxidase (A), NADH oxidase (B), and lipid peroxidation (C) were measured. Enzymic activities are expressed as percentages of the initial value (activities of succinate oxidase and NADH oxidase at zero time are 47.0 ± 6.50 and 124 ± 6.24 nmol O_2/min per mg protein at 25°C, respectively) ○, no addition; △, 2 mM *t*-butyl hydroperoxide; □, 5 mM *t*-butyl hydroperoxide; ●, 10 mM *t*-butyl hydroperoxide.

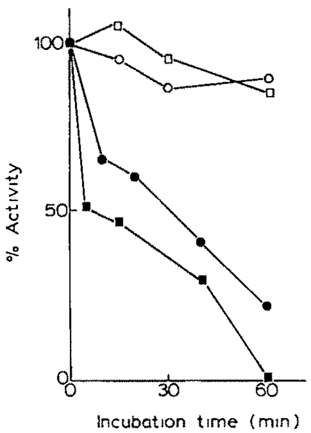

Fig 6. Effect of NADPH-dependent lipid peroxidation on the mitochondrial respiratory chain. Submitochondrial particles were incubated as described in Materials and Methods. At the times indicated, the activities of succinate oxidase (○, ●) and NADH oxidase (□, ■) were measured. Enzymic activities are expressed as percentages of the initial value as Fig. 5. ○ and □, control, ● and ■, NADPH-dependent lipid peroxidation.

succinate oxidase that is sensitive to the peroxidation (Fig. 3A and B). These data showed that lipid peroxidation caused decrease in the electron-transfer activities of mitochondria during reperfusion and during aerobic incubation.

Discussion

The present study together with a previous study on mitochondrial damage during anoxia [1,4,5,15] showed that two different biochemical mechanisms of mitochondrial dysfunction were involved in cellular injury of ischemic liver. One mechanism acts during anoxia, and the other on reoxygenation after anoxia. During anoxia, decrease in the intramitochondrial ATP level causes release of Ca^{2+} [5], which disrupts the barrier against proton diffusion of the mitochondrial inner membrane [4]. During reoxygenation, the cells recover from anoxic damage, but they are concomitantly injured by peroxidation. Lipid peroxides generated by oxygen radicals have been found to cause various morphological and functional disturbances [7,8,30]. The present study showed that when hypothermically preserved liver was reperfused, lipid peroxidation inhibited the activity of the mitochondrial electron-transport system.

In intact cells in mammalian liver, oxygen radicals are formed at a rate of 24 nmol O_2/min per g [31], but normally these radicals are not detectable, and do not cause injury because they are quickly scavenged by a battery of intracellular defence enzymes, such as superoxide dismutase, catalase and several peroxidases [9]. In mitochondria, about 2% of the State-4 respiration rate results in production of oxygen radicals [32]. The sites where superoxide anion is generated have been shown to be Complex I [33] and Complex III [34,35]. These sites are closely related to the sites that were shown in this study to be sensitive to and injured by peroxidation. Probably in vivo oxygen radicals are degraded so rapidly that they can only react with lipids close to the site of their production. The following reasons may explain why oxygen damages ischemic cells on reoxygenation, but does not damage normal cells.

(1) Reperfusion and reoxygenation result in a burst of free radical production because of the accumulation of reduced substrates during anoxia and ischemia [9]. Actually mitochondria produce much more H_2O_2 in State-4 respiration than in State-3 [32], and electron carriers in Complex III are capable of reducing O_2 to O_2^- only when they are reduced [34]. This is probably the main reason for reperfusion injury.

(2) Substrates such as hypoxanthine, which accumulate during anoxia, are oxidized by xanthine oxidase with production of superoxide anion. In this context it is noteworthy that pretreatment with allopurinol has a protective effect against reperfusion injury [7].

(3) The supply of endogenous scavengers may decrease during ischemia. This decrease may be partly related to the observations of decrease in the cellular level of NADPH in oxidative stress [36,37], and decrease of superoxide dismutase activity during ischemia [38].

Free radicals generated during reperfusion after ischemia cause lipid peroxidation. Unsaturated fatty acids are the most susceptible to peroxidation because of thermodynamic stabilization of a free radical adjacent to an olefinic group [39]. In mitochondria, 50% of all fatty acids are unsaturated and in particular cardiolipin consists of polyunsaturated fatty acids [40]. This, in turn, suggests that mitochondrial lipids, especially cardiolipin, are particularly susceptible to peroxidation. In fact, cardiolipin decreased rapidly in NADPH-dependent peroxidation in vitro [11]. In this connection, it is noteworthy that Fry and Green [41] have shown the absolute requirement of several mitochondrial enzymic activities for cardiolipin. The enzymic complex that requires cardiolipin involves dihydroubiquinone-cytochrome *c* oxidoreductase and NADH-ubiquinone oxidoreductase, but not NADH-ferricyanide reductase. This finding is consistent with our results. Thus we conclude that free radicals generated during reperfusion after ischemia and during aerobic incubation of mitochondria cause lipid peroxidation, probably peroxidation of cardiolipin, which leads to decreases of the enzymic activities of Complex I and III.

Acknowledgement

This work was supported in part by Grants for Scientific Research (B59480131 and B61480130) from the Ministry of Education, Science, and Culture of Japan.

References

1 Kamiike, W., Watanabe, F., Hashimoto, T., Tagawa, K., Ikeda, Y., Nakao, K. and Kawashima, Y. (1982) J Biochem. 91, 1349–1356

2 Mittnacht, S, Jr., Sherman, C. and Farber, J.L. (1979) J. Biol. Chem. 254, 9871–9878

3 Mittnacht, S., Jr. and Farber, J.L. (1981) J Biol Chem 256, 3199–3206

4 Watanabe, F., Hashimoto, T and Tagawa, K (1985) J Biochem 97, 1229–1234

5 Tagawa, K., Nishida, T, Watanabe, F. and Koseki, M. (1985) Mol Physiol 8, 515–524

6 Marubayashi, S., Dohi, K., Yamada, K. and Kawasaki, T (1984) Biochim. Biophys. Acta 797, 1–9

7 Peterson, D.A, Asinger, R.W., Elsperger, K.J., Homans, D.C. and Eaton, J.W. (1985) Biochem. Biophys. Res Commun. 127, 87–93

8 Paller, M.S., Hoidal, J R. and Ferris, T F. (1984) J. Clin. Invest 74, 1156–1164

9 Fridovich, I. (1983) Annu. Rev Pharmacol. Toxicol. 23, 239–57

10 Fuller, E.O., Goldberg, D.I., Starnes, J.W, Sacks, L M. and Delivoria-Papadopoulos, M. (1985) J. Mol. Cell Cardiol. 17, 71–81

11 Narabayashi, H, Takeshige, K. and Minakami, S (1982) Biochem. J. 202, 97–105

12 Sugano, T, Suda, K, Shimada, M. and Oshino, N. (1978) J. Biochem. 83, 995–1007

13 Hamilton, R.L., Berry, M.N., Williams, M.C and Severinghaus, E.M. (1974) J. Lipid Res. 15, 182–186

14 Collins, G.M., Petterson, T., Wichomb, W.N. and Halasz, N.A. (1984) J Surg. Res. 36, 1–8

15 Watanabe, F., Kamiike, W., Nishimura, T., Hashimoto, T. and Tagawa, K. (1983) J. Biochem. 94, 493–499

16 Beyer, R E (1967) Methods Enzymol 10, 184–194

17 Ohkawa, H., Ohishi, N. and Yagi, K. (1979) Anal. Biochem. 95, 351–358

18 Takeda, M., Ikenoya, S., Yuzuriha, T and Katayama, K. (1984) Methods Enzymol 105, 147–155

19 Vadhanavikit, S, Sakamoto, N., Ashida, N, Kishi, T. and Folkers, K. (1984) Anal Biochem 142, 155–158

20 Hatefi, Y. and Rieske, J.S. (1967) Methods Enzymol. 10, 225–231

21 Wharton, D.C. and Tzagoloff, A (1967) Methods Enzymol. 10, 245–250

22 Galante, Y M. and Hatefi, Y. (1978) Methods Enzymol. 53, 15–21

23 Ackrell, B A.C., Kearney, E B. and Singer, T.P (1978) Methods Enzymol 53, 466–483

24 Hatefi, Y (1978) Methods Enzymol. 53, 11–14

25 Hatefi, Y. and Stiggall, D.L (1978) Methods Enzymol 53, 21–27

26 Hatefi, Y (1978) Methods Enzymol. 53, 35–40

27 Lowry, O.H, Rosebrough, N J., Farr, A.L. and Randall, R.J. (1951) J. Biol. Chem 193, 265–275

28 Vladovic-Relja, T. (1984) Cryobiology 21, 511–520

29 Lannon, S.G., Tukaram, K T., Oliver, J A, McKinnon, K.J and Dossetor, J B. (1967) Surg. Gynecol. Obstet 124, 999–1004

30 Post, J A., Leunissen-Bijvelt, J., Ruigrok, T.J.C. and Verkleij, A.J. (1985) Biochim. Biophys. Acta 845, 119–123

31 Chance, B, Sies, H. and Boveris, A (1979) Physiol. Rev 59, 527–605

32 Boveris, A, Oshino, N. and Chance, B. (1972) Biochem. J 128, 617–630

33 Turrens, J.F. and Boveris, A. (1980) Biochem J 191, 421–427

34 Ksenzenko, M., Konstantinov, A.A., Khomutov, G.B., Tikhonov, A.N and Ruuge, E.K (1983) FEBS Lett. 155, 19–24

35 Turrens, J.F, Alexandre, A. and Lehninger, A.L. (1985) Arch. Biochem. Biophys. 237, 408–414

36 Eklow, L, Moldeus, P and Orrenius, S (1984) Eur J. Biochem. 138, 459–463

37 Sutherland, M.W, Nelson, J, Harrison, G. and Forman, H.J. (1985) Arch. Biochem. Biophys. 243, 325–331

38 Guarnieri, C., Flamigini, F and Cal, C M (1980) J. Mol. Cell. Cardiol. 12, 797–808

39 Sevanian, A and Hochstein, P. (1985) Annu. Rev. Nutr. 5, 365–390

40 Daum, G. (1985) Biochim. Biophys. Acta 822, 1–42

41 Fry, M. and Green, D.E. (1981) J Biol. Chem. 256, 1874–1880

Biochimica et Biophysica Acta 890 (1987) 89–96
Elsevier

BBA 42080

The high-affinity binding site for manganese on the oxidizing side of Photosystem II

Ban-Dar Hsu, Jee-Yau Lee and Rong-Long Pan

Institute of Radiation Biology, National Tsing Hua University, Hsin-Chu, Taiwan 30043 (Taiwan, China)

(Received 3 July 1986)

Key words: Photosystem II; Manganese; Oxygen evolution; Chloride ion effect

Electron donation to Photosystem II (PS II) by diphenylcarbazide (DPC) is interrupted by the presence of endogenous Mn in PS II particles. Removal of this Mn by Tris treatment greatly stimulates the electron transport with DPC as donor. Binding of low concentration of exogenous Mn(II) to Tris-treated PS II particles inhibits DPC photooxidation competitively with DPC. This phenomenon was used to locate a highly specific Mn(II) binding site on the oxidizing side of Photosystem II with dissociation constant about 0.15 μM. The binding of Mn(II) is electrostatic in nature. Its affinity depends not only on the ionic strength, but also on the anion species of the salt in the medium. The effectiveness in decreasing the affinity follows the order $F^- > SO_4^{2-} > CH_3COO^- > Cl^- > Br^- > NO_3^-$. This observation is interpreted as follows: smaller ions, like F^-, CH_3COO^-, and larger ions, like SO_4^{2-}, have inhibitory effects on Mn(II) binding, whereas ions with optimal size, like Cl^-, Br^- and NO_3^-, can stabilize the binding, resembling the anion requirement for reactivation of Cl^--depleted chloroplasts. We suggest that the binding site for Mn(II) we observed is the site for the endogenous Mn in the O_2-evolving complex of PS II. This site remains after Tris treatment, which removes all the endogenous Mn as well as the three extrinsic proteins, indicating that it is on the intrinsic component(s) of PS II reaction centers. Furthermore, the Cl^- requirement for O_2 evolution may be attributed, at least partly to its stabilizing effect on Mn binding.

Introduction

Although the role of Mn in photosynthetic O_2 evolution has been studied extensively, uncertainties about its mechanism still remain [1–3]. One of the complications is that there are at least three distinguishable pools of bound Mn in chloroplasts. One pool, termed weakly bound Mn, can be removed by EDTA washing or by incubation with a low concentration of divalent cations [4,5]. This pool of Mn is thought to be nonfunctional, because its removal does not affect O_2-evolution activity [6]. There are several treatments on chloroplasts, such as Tris [7,8], NH_2OH [4,9] and heat treatments [6,10], which release another pool of Mn concomitant with loss of O_2-evolving capacity. This pool, classified as strongly bound, is considered to be involved in water oxidation. The third pool, termed very strongly bound, is not removed by the treatments mentioned above. Its function is still not clear. However, it has been shown that O_2 evolution can be reactivated in Tris-treated 'inside-out thylakoid vesicles' [11], suggesting that the pool of very strongly bound Mn is associated with water oxidation.

Abbreviations: Chl, chlorophyll; DPC, diphenylcarbazide; DCIP, 2,6-dichlorophenylindophenol; Mes, 4-morpholineethanesulfonic acid; PS II, Photosystem II; P-680, the reaction center of Photosystem II; Z, the primary electron donor to P-680

Correspondence: B.D Hsu, Institute of Radiation Biology, National Tsing Hua University, Hsin-Chu, Taiwain 30043, Taiwan, China.

0005-2728/87/$03.50 © 1987 Elsevier Science Publishers B V. (Biomedical Division)

As for the Mn binding site(s), a 33 kDa extrinsic protein has been found to be closely related to the activity of water oxidation [12,13]. Furthermore, it has been shown that the protein binds Mn when released from thylakoids or PS II preparations by osmotic shock or by a method using butanol in the presence of mild chemical oxidants [14,15]. However, it has also been shown that the 33 kDa protein along with two other extrinsic proteins of sizes 24 and 18 kDa can be washed away (by 1 M $CaCl_2$) without affecting the Mn content of PS II particles [16]. Partial reactivation of O_2 evolution by high concentrations of Cl^- has been demonstrated in these PS II particles [17]. Thus, it appears that the binding site(s) for the functional Mn in PS II is not yet clear.

Cl^- has been shown to be an essential cofactor for O_2 evolution [18]. Its function, however, can be partially substituted by other anions, with effectiveness following the order $Cl^- > Br^- \gg NO_3^- > I^-$. Smaller ions, such as F^- and OH^-, act as competitive inhibitors, whereas larger ions, like SO_4^{2-}, ClO_4^- and PO_4^{3-}, have no effect [19]. It has been suggested that Cl^- participates in the reaction as a ligand bound to the functional Mn, and stabilizes the S-states of the O_2-evolving complex [20,21]. On the other hand, it has also been proposed that Cl^- neutralizes positive charges to produce an active conformation of the O_2-evolving complex [22,23].

Most commonly used electron donors cannot compete with H_2O, the natural donor, but they interact with Z, the primary electron donor to P-680, in Mn-depleted PS II [24]. In this study, we found that the endogenous Mn is the major barrier to electron donation by DPC. We also found that the photooxidiation of DPC by Tris-treated PS II particles which have been depleted of Mn was inhibited by adding low concentrations of exogenous Mn(II). This phenomenon was used to locate a highly specific Mn(II) binding site on the oxidizing side of PS II. The binding of Mn(II) is electrostatic in nature and is influenced by the species of anions present in the medium in a way similar to the anion requirement for reactivation of O_2 evolution in Cl^--depleted PS II. We suggest that the Mn(II) binding site we observed is likely to be the site occupied by the endogenous Mn in the O_2-evolving complex. It is located on the intrinsic component(s) of PS II and the Mn binding on this site is stabilized by the presence of anions like Cl^-.

Materials and Methods

PS II particles from local market spinach were prepared with Triton X-100 as in Ref. 25 and stored in liquid nitrogen. The typical electron-transport activity was about 200 μmol DCIP/mg Chl per h. The PS II particles were washed with 10 mM NaCl/20 mM Mes-NaOH (pH 6.1) before use. For salt treatments, the particles (400 μg Chl/ml) were incubated at room temperature for 15 min in a medium containing 20 mM Mes-NaOH (pH 6.1) and either 1 M NaCl or 1 M $CaCl_2$. For Tris treatment, the particles (400 μg Chl/ml) were incubated in 0.8 M Tris (pH 8.5) for 15 min at room temperature. The three types of treated PS II particle were then washed twice with and resuspended in 15 mM Mes-NaOH (pH 6.1). In some experiments, $CaCl_2$ washed PS II particles were further treated with EDTA. The particles (400 μg Chl/ml) were extracted twice with 15 mM EDTA followed by washing twice with and resuspension in 15 mM Mes-NaOH (pH 6.1). Chlorophyll concentration was estimated according to Ref. 26. All steps were carried out at 0–4°C.

The electron-transport activity of PS II was measured by DCIP reduction at room temperature using a homemade spectrophotometer as described in Ref. 27. The reaction cuvette routinely contained 3 ml medium of 15 mM Mes-NaOH (pH 6.1), 33 μM DCIP and a designated amount of DPC if desired. $MnCl_2$ or $MnSO_4$ was added as inhibitor when indicated. In some experiments, salts of various species were also added to investigate their effect on the inhibition by Mn(II). The pH effect experiments were performed in the same reaction medium, except that Mes-NaOH (pH 6.1) buffer was replaced by Tricine-NaOH (pH 7.7). The PS II particles were added at a chlorophyll concentration of 5 μg/ml. The reduction was monitored by absorbance change at 590 nm and an extinction coefficient of 14.5 $mM^{-1} \cdot cm^{-1}$ was used.

The assay for Mn content was done at room temperature with PS II particles (1 mg Chl/ml) pretreated with 0.5 M HCl. A Bruker ER-200D

EPR spectrometer at 9.74 GHz was used. Instrumental conditions: microwave power, 20 mW; modulation amplitude, 20 G; time constant, 0.5 s; gain, $4 \cdot 10^5$. To estimate the total number of Mn bound at various Mn(II) concentrations, Tris-treated PS II particles (5 µg/ml) were incubated at room temperature for 15 min in a medium containing a designated concentration of $MnCl_2$. The particles were then collected by centrifugation followed by acid treatment. The contribution from unbound Mn, under this condition, was estimated to be less than 1%.

Results

In Table I, it is shown that the isolated PS II particles contained about 6.8 Mn/400 Chl. NaCl wash, which removes two proteins of molecular masses 24 and 18 kDa from PS II particles [28], resulted in no loss of Mn. PS II particles washed by $CaCl_2$ lose an additional 33 kDa protein [16], but still retained almost all the Mn. EDTA extraction after $CaCl_2$ washing removed about 50% of Mn, whereas Tris treatment removed almost all the Mn from the PS II particles.

Since most commonly used reductants cannot compete with H_2O as electron donor to PS II, the small difference in the ability of PS II particles to photoreduce DCIP in the presence or absence of exogenous electron donor DPC indicates that DPC has no access to the reaction center of PS II. A similar phenomenon was observed in NaCl- and $CaCl_2$-washed PS II particles, which retain the normal amount of Mn. Somewhat higher activity of DCIP reduction supported by DPC (as compared with $H_2O \rightarrow$ DCIP) was obtained in $CaCl_2$/EDTA-treated PS II particles which have lost about 50% of Mn, and a dramatic stimulation in such an activity was observed in Tris-treated PS II particles which contain no Mn. It is believed that DPC interacts directly with Z in the absence of endogenous Mn [24]. The close relationship between the Mn content and the ability of DPC to act as an electron donor implies that the endogenous Mn is the obstruction between DPC and the reaction center of PS II. A similar observation was made in Ref. 29 with benzidine as donor.

If a low concentration of exogenous $MnCl_2$ was added to Tris-treated PS II particles, the electron-transport activity from DPC to DCIP decreased accordingly, whereas no inhibition was observed in untreated particles (Fig. 1). Similar results were obtained by using either $MnCl_2$ or $MnSO_4$, indicating the inhibition was due to Mn(II). This inhibition is specific for Mn(II). To achieve 50% inhibition, we found that, for Co(II) or Zn(II), a concentration higher than 20 µM was required, whereas for Mg(II) or Ca(II), hardly any inhibition was observed in the same concentration range. The inhibition was also found to be reversible. Reactivation of DPC to DCIP activity was observed upon decreasing the concentration of Mn(II), implying that the binding of Mn(II) is a reversible process (data not shown).

TABLE I

Mn CONTENTS AND ELECTRON-TRANSPORT ACTIVITY OF PS II PARTICLES SUBJECTED TO VARIOUS TREATMENTS

Treatments on PS II particles, Mn contents and assays for electron-transport activity (in µmol DCIP/mg Chl per h) were carried out as described in Materials and Methods Assay medium contained 5 µg Chl/ml PS II particles 15 mM Mes-NaOH (pH 6.1), 33 µM DCIP and 200 µM DPC if desired.

Treatments	Control	NaCl	$CaCl_2$	$CaCl_2$/EDTA	Tris
Mn/400 Chl	6.8	6.3	5.8	3.1	0.65
$H_2O \rightarrow$ DCIP	198	50	6	0	0
DPC $\rightarrow$ DCIP	205	66	29	68	273

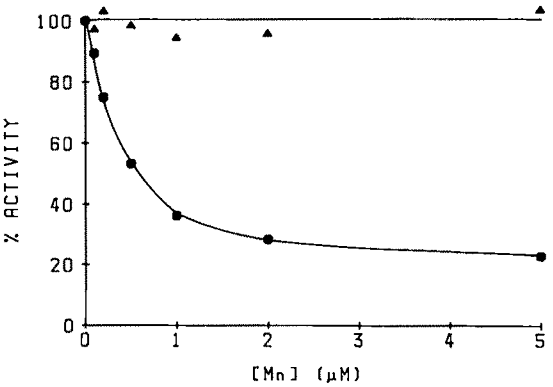

Fig. 1. The effect of Mn(II) on the electron-transport activity from DPC to DCIP of PS II particles. Assays were carried out using Tris-treated (●) or untreated (▲) PS II particles as described in Materials and Methods Assay medium contained 5 µg Chl/ml PS II particles, 15 mM Mes-NaOH (pH 6.1), 33 µM DCIP, 200 µM DPC and various amounts of $MnCl_2$.

In addition, we investigated the light-intensity dependence of the electron-transport activity (DPC → DCIP) of Mn(II)-inhibited (0.5 μM $MnCl_2$) and uninhibited Tris-treated PS II particles, respectively. As shown in Fig. 2, the activity of Mn(II)-inhibited PS II particles saturated at much lower light intensity than that of uninhibited particles. The result indicates that the inhibition by Mn(II) can be ascribed to a decreased rate at all PS II centers, rather than to complete inhibition in a fraction of the PS II population. Unfortunately, the number of Mn(II) binding at this specific site could not be determined by EPR spectrometer. It was found that addition of 0.5 μM $MnCl_2$, a concentration which will induce about 50% inhibition (see Fig. 1), to Tris-treated PS II particles resulted in a total binding of 7 Mn/400 Chl. The amount of Mn bound increased to 13 Mn/400 Chl when 1 μM $MnCl_2$ was added. The unrealistically large number of Mn(II) binding indicates the presence of other, non-specific Mn(II) binding on PS II particles [30].

In order to examine the mechanism of Mn(II) binding, we used steady-state kinetics to study the type of inhibition by Mn(II). The results are shown in Fig. 3. Fig. 3A is a Lineweaver–Burk plot which shows a competitive interaction between DPC and Mn(II). The Michaelis constant K_m for DPC in the absence of Mn(II) is about 150 μM, as estimated by the intersection of the no-Mn line

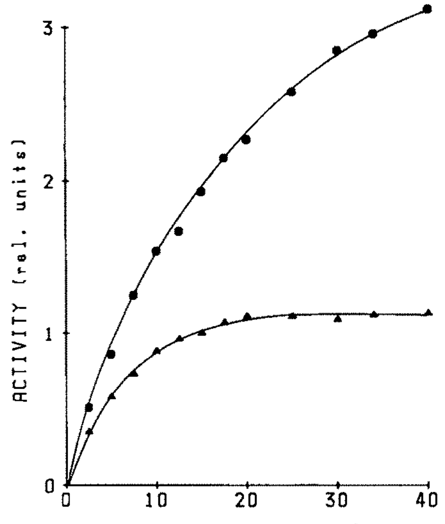

Fig. 2 Light-intensity dependence of the electron-transport activity (DPC → DCIP) of Mn(II) inhibited and uninhibited Tris-treated PS II particles. Activity assays were carried out in the presence (▲) or absence (●) of 0.5 μM $MnCl_2$, as described in Fig. 1.

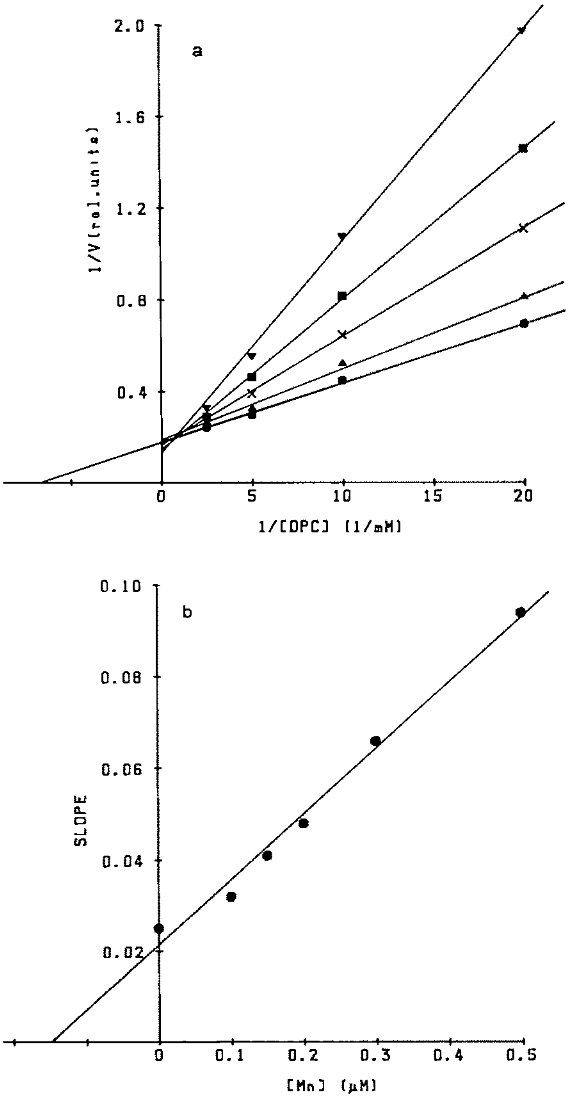

Fig. 3 (a) Lineweaver–Burk plot of Mn(II)-induced inhibition of the electron-transport activity from DPC to DCIP of Tris-treated PS II particles. ●, No $MnCl_2$; ▲, 0.1 μM $MnCl_2$; ×, 0.2 μM $MnCl_2$; ■, 0.3 μM $MnCl_2$, ▼, 0.5 μM $MnCl_2$. (b) Replot of the slope obtained from (a) vs. Mn(II) concentration. Assays were carried out as described in Materials and Methods. Assay medium contained 5 μg Chl/mg Tris-treated PS II particles, 15 mM Mes-NaOH (pH 6.1), 33 μM DCIP and various amounts of DPC and $MnCl_2$.

with the negative X-axis. The slope replot shown in Fig. 3B gives the dissociation constnat K_I of 0.15 μM for Mn(II). A straight line in Fig. 3B indicates that the competition between Mn(II) and DPC is linear, i.e., they compete for the same binding site [31].

The nature of Mn(II) binding was studied further by investigating the salt effect on the binding of Mn(II). We found that the inhibition declined with increasing concentration of NaCl. The weakening of the Mn(II) binding by NaCl was indicated by the increase of the K_I values for Mn(II) along with NaCl concentration as presented in Table II. We therefore conclude that the interaction between Mn(II) and its specific binding site is electrostatic in nature. However, the competitive relationship between Mn(II) and DPC (data not shown) as well as the K_m for DPC were not affected by NaCl (Table II) suggesting that DPC, although competing with Mn(II) for the same binding site, does not bind electrostatically. This is consistent with the non-polar nature of DPC.

Since it has been shown that Cl^- is a special cofactor for the O_2-evolving complex and its function can be partially substituted by several anions like Br^-, NO_3^- and inhibited by F^- [26], we also investigated the effects of various salts on the binding of Mn(II). As shown in Fig. 4, with the ionic strength kept at 50 mM, LiCl and KCl show the same inhibitory effect as NaCl, indicating that the effect is due to the Cl^- anion. Other sodium salts tested had various effects on preventing the binding of Mn(II). The order of effectiveness is $F^- > SO_4^{2-} > CH_3COO^- > Cl^- > Br > NO_3^-$. The K_I values for Mn(II) in the presence of the two most effective anions, F^- and SO_4^{2-}, as well as their corresponding K_m for DPC, are given in Table II. It was found that the competitive relationship between DPC and Mn(II) still remains (data not shown), but the K_I values increase significantly. The results indicate that, in addition to the ionic strength, the species of anions is also an important factor in determining the affinity for Mn(II) binding.

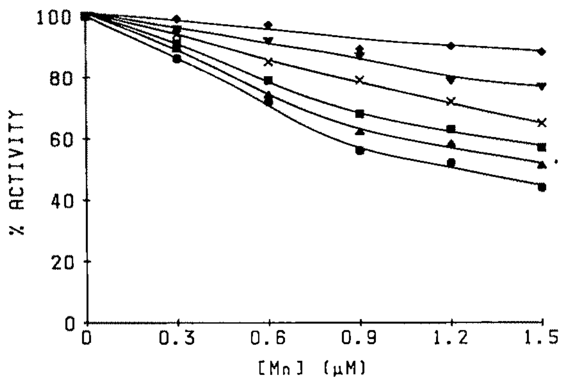

Fig 4. The effect of various salts on Mn(II)-induced inhibition of the electron-transport activity from DPC to DCIP of Tris-treated PS II particles. The ionic strength of added salts were kept at 50 mM. ●, 50 mM $NaNO_3$; ▲, 50 mM NaBr; ■, 50 mM NaCl or LiCl or KCl; ×, 50 mM CH_3COONa; ▼, 17 mM Na_2SO_4; ◆, 50 mM NaF Assays were performed as described in Fig. 1. Mn(II) was added as $MnSO_4$.

The pH effect on the Mn(II) binding was also studied. We found that, at pH 7.7, Mn(II) became a noncompetitive inhibitor to DPC electron donation (data not shown). Furthermore, the K_I value for Mn(II) (0.55 μ) was about 2.5-fold larger than the corresponding value obtained at pH 6.1, suggesting that high pH, besides altering the manner of inhibition, also weakens the binding of Mn(II).

TABLE II

THE EFFECT OF VARIOUS SALTS ON K_I VALUES FOR Mn(II) AND K_m VALUES FOR DPC DERIVED FROM STEADY-STATE KINETIC EXPERIMENTS

K_m, the Michaelis constants for DPC, and K_I, the dissociation constants for Mn(II), were obtained by using the plotting procedure as described in Fig. 3.

Salt concentration	0 mM NaCl	10 mM NaCl	50 mM NaCl	100 mM NaCl	50 mM NaF	17 mM Na_2SO_4
K_I for Mn (μM)	0.15	0 21	0.53	0.76	4.50	1 36
K_m for DPC (μM)	149	152	163	169	110	118

Discussion

The high-affinity binding site for Mn(II) we observed on the oxidizing side of PS II is very likely to be the binding site for the endogenous Mn in the O_2-evolving complex for the following four reasons.

(1) The binding site is very specific for Mn(II) and the affinity for Mn(II) is high (0.15 μM) at low salt concentration.

(2) Mn(II) at the binding site acts as a competitive inhibitor to DPC electron donation in Tris-treated PS II particles which have been depleted of the endogenous Mn. The competitive relationship can explain the interrupting effect of the endogenous Mn on DPC electron donation to PS II (see Table I), if we assume that the binding of Mn(II) is at the site for the endogenous Mn.

(3) The binding of Mn(II), although electrostatic, is highly dependent on the species of anions in the medium. At the same ionic strength, F^-, SO_4^{2-} and CH_3COO^- are very effective in preventing the binding of Mn(II). In contrast, NO_3^-, Br^- and Cl^- are able to stabilize the Mn(II) binding as compared to F^-, SO_4^{2-} and CH_3COO^-. Qualitatively, these are similar to the findings in the studies of anion requirement for reactivation of the O_2 evolution in Cl^--depleted PS II, where Br^- and NO_3^- can partially substitute for Cl^-; SO_4^{2-} and CH_3COO^- have no effect; and F^- is a strong inhibitor. Fig. 5 shows the percentage of inhibition by 1.5 μM Mn(II) of the electron-transport acativity of Tris-treated PS II particles with the presence of various anions vs. the ion volume. It resembles the plot of reactivation of O_2 evolution by various anions in Cl^--depleted thylakoids vs. the anion volume (Fig. 9, Ref. 19), except that the optimal volume is shifted from 0.25 nm^3 to 0.32 nm^3. Since the percentage of inhibition by Mn(II) in Fig. 5 is a function of the binding affinity for Mn(II), the similar effects of various anions on O_2 evolution and Mn(II) binding suggest that the Mn(II) binding site is likely to be the same for the endogenous Mn in the O_2-evolving complex. As for the shift of the optimal volume, it is probably due to the fact that chloroplasts were used in Ref. 19, whereas here PS II particles were studied.

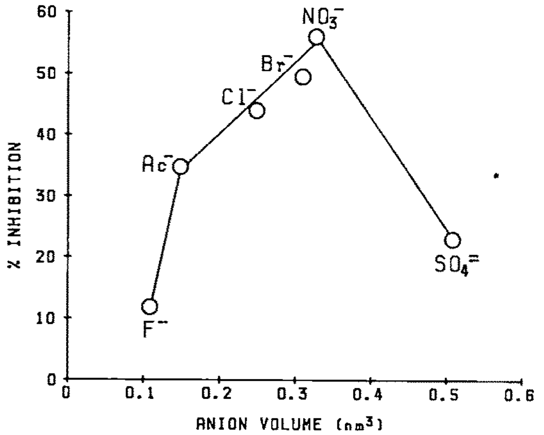

Fig 5. The percentages of inhibition by 1.5 μM Mn(II) of the electron-transport activity (DPC → DCIP) of Tris-treated PS II particles with the presence of various anions vs. the ion volume Data of percentage inhibition were taken from Fig. 4 The anion volumes were calculated for a spherical ion from the Pauling radius.

(4) When the pH was shifted from 6.1 to 7.7, we found that the affinity for Mn(II) was lowered. This is in accordance with the finding that washing PS II particles at high pH results in removal of Mn from the O_2-evolving complex, indicating that the binding of endogenous Mn is destabilized at high pH. In addition, if Cl^- plays a role in stabilizing the binding of Mn(II), then the lowering in Mn(II) affinity at high pH may be attributed to the removal of Cl^-, which is consistent with the finding that OH^- reversibly inhibits O_2 evolution competitively with Cl^- [19,23]. However, the competitive relationship between Mn(II) and DPC disappears upon raising the pH, indicating that high pH not only alters the affinity for Mn(II) but also changes the manner of interacation between Mn(II), DPC and PS II. The mechanism behind it is not yet clear.

If we identify the Mn(II)-binding site with the one for the endogenous Mn in the O_2-evolving complex, then the results of this report have two implications. The first is that the binding site for endogenous Mn is not located on any of the extrinsic proteins removable by Tris treatment, but on the intrinsic component(s) of PS II. This is inconsistent with the suggestion that the extrinsic 33 kDa protein is the Mn-binding protein [14,15]. The second is that the requirement of Cl^- in O_2 evolution probably involves a stabilizing effect of Cl^- on Mn binding. A similar conclusion was drawn from the observations that when PS II particles are washed with urea/NaCl or $CaCl_2$, the three extrinsic proteins but only a small portion of Mn are released [12,17]. Omission of NaCl during urea wash or incubating $CaCl_2$-washed PS II in low salt medium (10 mM NaCl) leads to the release of 2 Mn/PS II suggesting that Cl^- plays a role in stabilizing the binding of endogenous Mn.

The endogenous Mn bind very tightly to PS II centers with affinity greater than that to EDTA (K_A for Mn-EDTA is 10^{14}); they are classified as strongly and very strongly bound in the three pools of Mn associated with thylakoid membranes (see Introduction). Removal of the three extrinsic proteins (by $CaCl_2$ washing) lowers the affinity for (or increases the accessibility to) 50% of the Mn to a level that allows its extraction by EDTA (see Table I). This probably corresponds to the strongly bound Mn. The remaining 50% of the Mn in our PS II particles can be extracted by Tris washing. For the moment, we do not know whether the Mn(II) binding we observed belongs to the pool of strongly or very strongly bound.

Recently, Tamura and Cheniae [32] also demonstrated the ligation of Mn(II) into the O_2-evolving complex of PS II particles which have been depleted of their endogenous Mn and the three extrinsic proteins. The process, shown by reactivation of O_2 evolution, required light and Ca(II). Our observation on the binding of Mn(II) showed at least two differences from theirs: the first, no Ca(II) was needed and the second, the Mn(II) concentration required to achieve half-maximal effect was much lower (0.5 μM vs. 0.25 mM). The differences may be attributed to the different ways in inactivating the PS II particles (Tris treatment vs. $CaCl_2$ washing plus $DCIPH_2$) and/or in measuring the Mn(II) binding (inhibition on DPC to DCIP vs. reactivation of O_2 evolution).

Klimov et al. [33] also showed that their Tris-washed PS II preparations can be reactivated by adding $MnCl_2$, but at a very low concentration (0.1–0.2 μM in the absence of Mg^{2+} and 0.05–0.1 μM in the presence of Mg^{2+} or other divalent cation of metals). We could not observe any reactivation on our Tris-treated PS II particles. Nevertheless, the K_I for Mn(II) we found at low salt concentration agrees with their value in the absence of Mg^{2+}.

Acknowledgements

This study was supported by grants from National Science Council, Taiwan, China (NSC74-0201-B007-01) to B.D.H. and (NSC74-0201-B007-06) to R.L.P.

References

1 Amesz, J (1983) Biochim. Biophys. Acta 726, 1–12

2 Govindjee, Kambara, T. and Coleman, W. (1985) Photochem. Photobiol. 42, 187–210

3 Dismukes, G.C. (1986) Photochem. Photobiol. 43, 99–115

4 Yocum, C.F., Yerkes, C.T., Blankenship, R.E., Sharp, R.R. and Babcock, G.T (1981) Proc. Natl Acad Sci. USA 78, 7507–7511

5 Theg, S.M and Sayre, R.T (1979) Plant Sci. Lett 16, 319–326

6 Blankenship, R.E, Babcock, G T and Sauer, K. (1975) Biochim Biophys Acta 387, 165–175

7 Yamashita, T. and Butler, W.L. (1968) Plant Physiol. 43, 1978–1986

8 Cheniae, G.M. (1980) Methods Enzymol. 89, 349–363

9 Kuwabara, T. and Murata, N (1983) Plant Cell Physiol. 24, 741–747

10 Wydrzynski, T. and Sauer, K. (1980) Biochim. Biophys. Acta 589, 56–70

11 Mansfield, R. and Barber, J (1982) FEBS Lett. 140, 165–168

12 Miyao, M and Murata, N. (1984) Biochim. Biophys Acta 765, 253–257

13 Ono, T. and Inoue, Y. (1984) FEBS Lett. 166, 381–384

14 Abramowicz, D.A. and Dismukes, G.C. (1984) Biochim. Biophys. Acta 765, 318–328

15 Yamamoto, Y., Shinkai, H., Isogai, Y., Matsurra, K and Nishimura, M. (1984) FEBS Lett. 175, 429–432

16 Ono, T. and Inoue, Y (1983) FEBS Lett. 164, 255–260

17 Kuwabara, T., Miyao, M., Murata, T. and Murata, N. (1985) Biochim. Biophys. Acta 806, 283–289

18 Critchley, C. (1985) Biochim. Biophys. Acta 811, 33–46

19 Critchley, C., Baianu, I.C, Govindjee and Gutowsky, H.S (1982) Biochim. Biophys. Acta 682, 436–445

20 Sandusky, P.O. and Yocum, C.F. (1984) Biochim Biophys. Acta 766, 603–611

21 Sandusky, P.O. and Yocum, C F. (1986) Biochim. Biophys. Acta 849, 85–93

22 Johnson, J., Pfister, V and Homann, P.H. (1983) Biochim. Biophys. Acta 723, 256–265

23 Homann, P H. (1985) Biochim. Biophys Acta 809, 311–319

24 Yerkes, C.T. and Babcock, C.T. (1980) Biochim. Biophys. Acta 590, 360–372

25 Ford, R C. and Evans, M.C.W. (1983) FEBS Lett. 160, 159–164

26 Arnon, D.I. (1949) Plant Physiol. 24, 1–15

27 Lee, J Y., Hsu, B.-D and Pan, R -L. (1985) Biochem. Biophys. Res. Commun. 128, 464–469

28 Kuwabara, T and Murata, N. (1982) Plant Cell Physiol. 23, 533–539

29 Ghanotakis, D.F , Babcock, G.T. and Yocum, C.F. (1984) Biochim. Biophys. Acta 765, 388–398

30 Takahashi, M. and Asada, K. (1976) Eur J. Biochem 64, 445–455

31 Roberts, D.V. (1977) in Enzyme Kinetics, Ch 3, Cambridge University Press, Cambridge

32 Tamura, N. and Cheniae, G.M. (1986) FEBS Lett 200, 231–236

33 Klimov, V.V., Allakhverdiev, V A., Shuvalov, V.A. and Krasnovsky, A.A. (1982) FEBS Lett. 148, 307–312

Biochimica et Biophysica Acta 890 (1987) 97–105
Elsevier

BBA 42066

Escherichia coli F_1 ATPase is reversibly inhibited by intra- and intersubunit crosslinking: an approach to assess rotational catalysis

Rajendra P. Kandpal and Paul D. Boyer

Molecular Biology Institute and Department of Chemistry and Biochemistry, University of California, Los Angeles, CA 90024 (U.S.A.)

(Received 2 September 1986)

Key words: F_1-ATPase; ATPase crosslinking, Rotational catalysis; ATPase conformation; (*E. coli*)

Reaction of the multisubunit F_1 ATPase from *Escherichia coli* (EF_1) with a bifunctional cleavable crosslinker, 3,3′-dithiobis(succinimidylpropionate) (DSP), has been used to explore the possibility that during catalysis a rotational movement of catalytic subunits relative to noncatalytic subunits occurs. The premise is that such rotational catalysis is tenable if intersubunit crosslinking of a major subunit with one of the minor subunits inhibits the enzyme activity and if upon cleavage of the crosslinks, the enzyme regains activity. The results presented in this paper show that crosslinking of about 5–6 reactive groups on EF_1 with DSP is accompanied by a loss of 2/3 of the enzyme activity. Both intra- and intersubunit crosslinks are formed. The most prominent intersubunit crosslinks are those of γ and δ subunits with the α subunit. Nearly complete recovery of activity can be attained by cleaving the disulfide bond in the crosslinker with dithiothreitol. Because the chemical modification of enzyme groups remains after the crosslinker is cleaved, the loss in activity before cleavage can be ascribed to conformational restraints. The results show that catalysis by the EF_1 ATPase is highly sensitive to the restrictions of crosslinking, and are consistent with the view that catalysis is accompanied by appreciable movements of the major subunits with respect to the minor subunits, as suggested for rotational catalysis.

Introduction

The F_1 ATPases from bacteria, chloroplasts and mitochondria consist of five subunits with a stoichiometry of $\alpha_3\beta_3\gamma\delta\varepsilon$, with the catalytic site likely residing on the β subunit (see for reviews, Refs. 1 and 2). The binding change mechanism for ATP synthesis [3] has been proposed to involve sequential participation of the catalytic sites. All three β subunits are regarded as being functionally equivalent but as being in three different conformations at any one time. Recent papers from several laboratories [4–6] add to the evidence for structural asymmetry of the β subunits of the enzyme under conditions when it is not turning over.

Prominent interactions occur between the γ subunit and the α and β subunits as shown by the requirement of all three subunits for catalysis (see review, Ref. 7), and the demonstrations that modifications of –SH groups on the γ subunit of CF_1 ATPase markedly affect catalysis [8]. Measurements in this laboratory of the species of $[^{18}O]P_i$

Abbreviations: F_1, coupling factor one ATPase; EF_1 ATPase, F_1 ATPase from *Escherichia coli*; Mops, 4-morpholinepropanesulfonic acid; DSP, 3,3′-dithiobis(succinimidylpropionate); SDS, sodium dodecyl sulfate; DMSO, dimethylsulfoxide; P_i, inorganic phosphate; DTT, dithiothreitol.

Correspondence: Dr Paul D. Boyer, Department of Chemistry and Biochemistry, University of California, Los Angeles, CA 90024, U.S.A.

0005-2728/87/$03.50 © 1987 Elsevier Science Publishers B.V. (Biomedical Division)

formed from ^{18}O-labeled ATP during ATP hydrolysis [9], or of [^{18}O]ATP formed from [^{18}O]P_i during ATP synthesis [10] demonstrate that every participating catalytic site is performing catalysis in a closely similar or identical manner. The sequence data for the F_1 ATPases [11] show lack of any tripartite symmetry of the γ subunit. Thus, certain groups or regions on the γ subunit must interact with the β subunit, either directly or through the α subunit, to influence the catalytic behavior of the β subunits. For the three β subunits to pass through equivalent states during catalysis, the β subunits would need to sequentially change their positions in the enzyme complex in relation to the γ subunit.

Such considerations led to the suggestion in 1981 [12,13] of a "rotational catalysis" for the ATP synthase and F_1 ATPases involving a rotational change in the position of the β subunits relative to a core of the minor subunits. Subsequently, based on structural considerations, Cox et al. advanced a similar proposal [14], Oosawa and Hayashi have proposed a mechanism for a rotational model [15], and Mitchell has suggested a model in which α and β subunits spin in place [16]. The Boyer and the Cox proposals explain how the β subunits can maintain interactions with minor subunits, yet pass through identical conformations during catalysis.

Experimental approaches that have the potential for proving whether or not rotational catalysis occurs are difficult to formulate. The approach used for the present paper had the possibility of proving that rotational catalysis very likely did not occur or of adding to the findings consistent with such catalysis. The latter result was obtained.

If rotational catalysis occurs, a chemical crosslink between the β and γ subunits would be expected to stop catalysis. If catalysis continued with such a crosslink, rotational catalysis would be untenable. If the lost activity is regained when the crosslink is cleaved, then spatial restrictions and not chemical modification of groups could be regarded as the reason for loss of catalytic capacity. Such behavior would provide evidence consistent with rotational catalysis. Although a considerable number of crosslinking experiments have been performed with F_1 ATPases [17–23], and loss of catalytic activity has resulted [19,20,23], the use of cleavable crosslinkers in an approach that would test rotational catalysis has not to our knowledge been undertaken.

The studies reported here made use of a cleavable crosslinker, DSP. The inhibition of over 50% of the catalytic activity of EF_1 ATPase was found to be nearly completely reversible by cleavage of the crosslinker. The activity loss thus resulted from intersubunit and intrasubunit crosslinking and not from extensive derivatization of reactive groups, likely $-NH_2$ groups.

Experimental procedures

Materials

ATP, NADH, pyruvate kinase, lactate dehydrogenase, ε-amino caproic acid, *p*-aminobenzamidine, and dithiothreitol were supplied by the Sigma Chemical Co. Sepharose CL-6B and DEAE-Sepharose CL-6B were obtained from Pharmacia Fine Chemicals. DSP was a product of Pierce Chemical Co. *E. coli* strain AN 1460 was obtained from Dr. A.E. Senior of the University of Rochester.

Methods

Purification of EF_1 ATPase. E. coli strain AN 1460 was grown to mid-exponential phase and the cells were stored at −80°C.

The membrane preparation and enzyme purification were essentially carried out by the method of Senior et al. [24], except for minor changes in the F_1 purification procedure. The eluate from DEAE-Sepharose CL-6B was precipitated with 65% saturated ammonium sulfate. The precipitate was dissolved in 50 mM Tris buffer (pH 7.4), containing 10% (v/v) glycerol/2 mM EDTA/1 mM ATP/1 mM DTT/40 mM ε-amino caproic acid. The solution was then applied to a column of Sepharose CL-6B (2.5 cm × 90 cm), the eluted fractions containing highest specific activity were pooled, and the enzyme was stored as an ammonium sulfate suspension at 4°C.

ATPase assay. The enzyme activity was monitored by a coupling assay [25] after incubation in dilute solution. The specific activity of EF_1 increases as concentration is lowered as a result of dissociation of the ε subunit from the complex [26,27]. The enzyme was assayed at a concentration of around 0.1 μg/ml after preincubation at 30 °C for 20 min in a mixture consisting of 30 mM Tris-acetate (pH 7.6)/30 mM potassium acetate/3 mM ATP/40 μg per ml pyruvate kinase/20 μg per ml lactate dehydrogenase/0.2 mM NADH. The reaction was initiated by adding an aliquot of Mg-acetate (final concentration, 5 mM) and activity was measured by determining the decrease in the absorbance of NADH at 340 nm. The specific activity of the enzyme was expressed as μmol product formed/min per mg protein. Protein was determined by the method of Lowry et al. [28], using bovine serum albumin as standard.

Crosslinking with DSP. Two procedures were used for crosslinking the enzyme. In one, an aliquot of the ammonium sulfate suspension was pelleted, dissolved in 100 mM Mops-Tris buffer (pH 7.0) and passed through a centrifuge-Sephadex column [29] equilibrated with the same buffer. The desalted enzyme was crosslinked in a mixture containing 100 mM Mops-Tris (pH 7.0)/20 mM ATP. An aliquot of DSP (20–40 mM stock in dimethyl sulfoxide) was added such that the final DMSO concentration was less than 10% (v/v). The reaction was allowed to proceed for 5 min at room temperature (22–25 °C) or as indicated in various experiments and then passed through a centrifuge-Sephadex column. The eluate was used for the assay of ATPase activity and electrophoresis.

Alternatively, an aliquot of the ammonium sulfate suspension was pelleted, dissolved in 50 mM phosphate buffer (pH 7.0) and passed through a centrifuge-Sephadex column equilibrated with the same buffer. The crosslinking reaction was carried out in a reaction mixture containing 50 mM phosphate buffer (pH 7.0) and 20 mM ATP at 10 °C, as described in the preceding paragraph.

The control enzyme was similarly treated with only DMSO and processed as described for experimental samples.

Cleavage of crosslinks with DTT. The crosslinked enzyme was incubated with 33 mM DTT and 33 mM ATP at 37 °C for 30 min and then assayed for enzyme activity. Because of the high dilution for assay, the concentration of ATP and other constituents during assay were essentially those of the assay mix. The control (uncrosslinked) enzyme was treated in the same manner.

Gel electrophoresis. One-dimensional SDS-polyacrylamide gel electrophoresis was carried out with either a 12% or 15% uniform or 3–22% gradient gel by the method of Laemmli [30]. A stacking gel (5%) was used with the uniform polyacrylamide gels. The stacking gel was omitted for the gradient gel and a comb was inserted immediately after pouring gradients, and the gel was allowed to polymerize. The crosslinked samples were prepared in a sodium dodecyl sulfate sample buffer lacking 2-mercaptoethanol. 30–50 μg protein was applied to the wells and electrophoresis was carried out at 50 mA per slab for 3 h. The gel was stained with Coomassie Blue R overnight.

For the second dimension, the gel strip (1 cm wide) was cut out from the one-dimensional gel and placed horizontally over a 5% stacking gel of a 0.75 mm thick 15% acrylamide gel. The strip was surrounded by 1% agarose in 125 mM Tris-HCl buffer (pH 8.5) containing 0.1% (w/v) sodium dodecyl sulfate and 2% (v/v) 2-mercaptoethanol, and run at a current of 50 mA per slab.

Quantitation of subunits in the control and crosslinked enzyme. The relative amounts of different subunits were estimated by excising the bands corresponding to α, β, γ, δ and ε subunits, extracting the dye in 1 ml DMSO (100%) for over 12 h at room temperature and determining the absorbance in DMSO of the extract at 595 nm. The same procedure was used for quantitating the subunits in the second dimension gel, obtained after DTT cleavage.

To test the dye extraction method, various amounts of EF_1 were put through the separation and extraction procedure. The absorbance was found to increase linearly for individual subunits over a range of 6–50 μg of applied EF_1. All the extractions were carried out with duplicate samples.

Results

Time-course and buffer dependency of the reaction with DSP

The time-course of the reaction in 100 mM Mops-Tris buffer or 50 mM phosphate buffer at pH 7.0 is shown in Fig. 1. The results show that the reaction reached completion in about 5 min when carried out in Mops-Tris buffer at room

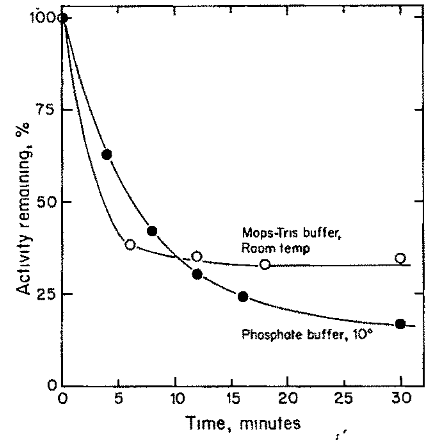

Fig. 1 Time-course for inactivation of EF_1 ATPase with DSP. ○——— ○, inactivation in Mops-Tris buffer To EF_1 ATPase (1.54 mg/ml) in 100 µl of a reaction mixture at room temperature containing 100 mM Mops-Tris buffer (pH 7.0) and 20 mM ATP was added 2 µl of DSP in DMSO (DSP concentration, 0.5 mM final). The reaction mixture was vortexed immediately and incubated at room temperature (22–25°C). ●———●, inactivation in phosphate buffer. EF_1 ATPase (1.01 mg/ml) in 100 µl of a reaction mixture at 10°C containing 50 mM phosphate buffer (pH 7.0) and 20 mM ATP was treated with DSP as indicated for the reaction with Mops-Tris buffer, except incubation was at 10°C. Aliquots were drawn at times indicated in the figure and assayed as described in Experimental procedures.

temperature. A slower reaction occurred in phosphate buffer at 10°C, however, the extent of inactivation was greater than in Mops-Tris buffer, suggesting that the DSP reacts with Tris, thereby reducing its effective concentration in the reaction mixture. More variability was encountered when Tris buffer was used. This could also be a reflection of a reaction of the reagent with the Tris buffer, if, for example, there are rapid competing reactions as the reagent added in DMSO is being diluted.

Effect of DSP concentration on activity loss

Fig. 2 shows the effect of a 5 min exposure to varying concentration of DSP on the activity of the enzyme. The crosslinking in these experiments was carried out in PO_4 buffer at 10°C. The activity loss approximated a first-order reaction course.

Reversible loss of enzyme activity by reaction with DSP

When the EF_1 ATPase was treated with DSP, subunit crosslinking similar to that reported by Bragg and Hou [20] was observed, but with less extensive crosslinking as anticipated by our use of lower DSP concentrations.

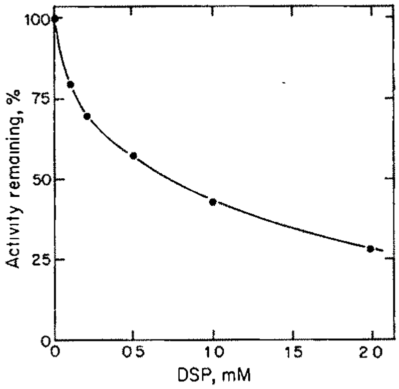

Fig. 2. Effect of DSP concentration on EF_1 ATPase activity To EF_1 ATPase (0.62 mg/ml) in 100 µl of a reaction mixture containing 50 mM phosphate buffer and 20 mM ATP at pH 7.0, was added 5 µl of DSP in DMSO (final concentration of DSP as indicated) The mixture was vortexed immediately and incubated at 10°C for 5 min. The reaction mixture was then passed through a centrifuge-Sephadex column and the eluate was used to assay enzyme activity as described in Experimental procedures.

Table I shows representative experiments showing loss of activity due to enzyme modification by DSP in 100 mM Mops-Tris buffer. The results

TABLE I

EFFECT OF CROSSLINKING AND CLEAVAGE OF CROSSLINKS ON THE ACTIVITY OF EF_1 ATPase

EF_1 ATPase (1.1–4.6 mg/ml) was modified with the indicated concentrations of DSP, in a reaction mixture containing 100 mM Mops-Tris and 20 mM ATP at pH 7.0 for 5 min at room temperature. The reaction was stopped by passing the mixture through a centrifuge-Sephadex column. The eluate was used for ATPase assay. The crosslinks were cleaved with dithiothreitol (DTT) in the presence of ATP at 37°C as described in the Experimental procedures section The results are means± standard deviation of four experiments. Each assay was carried out in duplicate

Concentration of DSP (mM)	Activity (%)	Activity after DTT treatment (%)
0	100	100± 5
2	29±12	85± 4
3.33	29± 3	70±12

indicate that as much as 70% activity was lost at a DSP concentration of 3.33 mM. A major portion of the lost activity could be recovered on cleaving the crosslinks with dithiothreitol in the presence of ATP. Other experiments showed that the presence of ATP in the modification mixture was essential for reversible inactivation. When modification was carried out in the absence of ATP, very little activity was regained after dithiothreitol cleavage of the crosslinks (data not shown). Also, the presence of ATP was required for optimal regain of activity upon cleavage of crosslinks with dithiothreitol.

Correlation of subunit crosslinking with enzyme inactivation

To find whether activity loss might be attributed to any particular intersubunit crosslinks, the subunits crosslinked were identified by gel electrophoresis. Intersubunit crosslinking was evident after DSP reaction as shown by the appearance of higher molecular-weight species (Fig. 3). The higher molecular-weight crosslinks were not attributable to intermolecular crosslinking because their appearance was independent of enzyme concentration. Also, the electrophoresis of the crosslinked enzyme on a nondissociating gel (no SDS) revealed the absence of intermolecular crosslinking. In this gel, the undissociated enzyme migrated as a single major band.

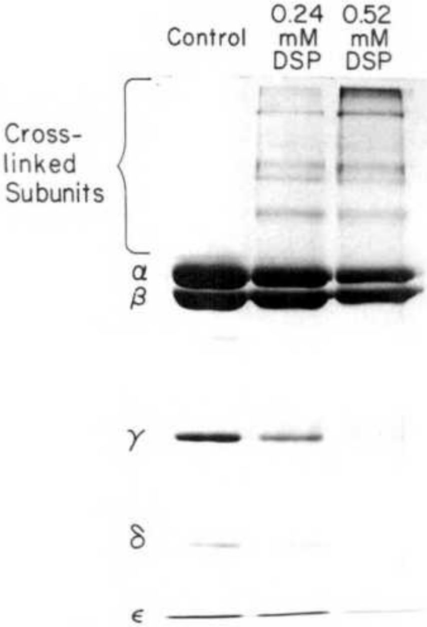

Fig. 3. Gel electrophoresis patterns after crosslinking. EF_1 ATPase (1.9 mg/ml) in a 100 μl volume was incubated with 0.24 or 0.52 mM DSP in 100 mM Mops-Tris buffer, containing 20 mM ATP at pH 7.0, and at room temperature for 5 min as described in Experimental procedures. The enzyme retained 69% and 29% activity, respectively, and regained 100% and 87% activity after dithiothreitol-cleavage. 42 μg (control), 38 μg (modified with 0.24 mM DSP) and 31 μg (modified with 0.52 mM DSP) of protein were applied as indicated to a 12% SDS-polyacrylamide gel, with 5% stacking gel, and electrophoresed at 50 mA for 3 h before staining.

Experimental results of crosslinking in Tris buffer are presented in Table II. The amount of noncrosslinked subunit remaining after reaction with DSP is expressed as the % of the total original amount of subunit present. The data show that the extent of crosslinking of γ and δ subunit was about equal to the loss of activity, while the extent of crosslinking of the α and β subunits was much less than the activity loss. The γ and δ subunits that were crosslinked were present in bands corresponding to greater apparent M_r than underivatized α and β subunits showing that they were crosslinked to the larger subunits.

In one of these experiments the amounts of all the five subunits remaining uncrosslinked were compared with native enzyme. The results are presented in part B of Table II. They show that crosslinking of 33% of the α subunit or 11% of the β subunit is accompanied by 71% loss of activity. The preferential crosslinking of the α subunit suggests that the principal crosslinks of the γ and δ subunits were to the α subunit. γ–δ subunit crosslinks were not observed. Actiivty loss was somewhat greater than the crosslinking of the γ or δ subunits to the larger subunits. There was little crosslinking of the ε subunit with any other subunit.

Experimental results of subunit crosslinking in phosphate buffer are presented in Table III. The loss of activity and extent of crosslinking were more pronounced relative to the reaction in Mops-Tris buffer. Crosslinking was 61%, 28%, 65%, 69%, 32% for α, β, γ, δ and ε subunits, respectively, when modification was carried out for 15 min (Table IIIA). Electrophoresis of the crosslinked species in a second dimension after di-

TABLE II

EFFECT OF DSP TREATMENT ON THE EXTENT OF INTERSUBUNIT CROSSLINKING AND EF_1 ATPase ACTIVITY

EF_1 ATPase (1.9–2.9 mg/ml) was modified with the indicated concentration of DSP. The reaction mixture containing 100 mM Mops-Tris/20 mM ATP at pH 7.0 and EF_1 ATPase was added to an aliquot (5 μl) of DSP in dimethylsulfoxide and vortexed immediately. Incubation was carried out for 5 min at room temperature. The control enzyme designated as unmodified was similarly treated with an aliquot of dimethylsulfoxide. The reaction was stopped by passing the mixture through a centrifuge-Sephadex column. The eluate was used for enzyme assay and electrophoresis. Electrophoresis and quantitation of individual subunits were carried out as described in the Experimental procedures section. The results are the mean of three experiments. All the determinations and assays for each experiment were carried out in duplicate. The results in part B of the table represent a typical experiment, where amounts of all the five subunits were determined. DTT, dithiothreitol.

IIA

Concentration of DSP (mM)	Activity (%)	Activity after DTT treatment (%)	Subunits not crosslinked (%)		
			α + β	γ	δ
0	100	118 ± 3.7	100	100	100
0.24	73.5 ± 7.2	114 ± 2.0	84 ± 3	60 ± 5	69 ± 8
0.52	33.6 ± 4.5	91 ± 12.0	71 ± 7	34 ± 8	41 ± 3

IIB

Enzyme	Activity (%)	Activity after DTT treatment (%)	Subunits not crosslinked (%)				
			α	β	γ	δ	ε
Unmodified	100	120	100	100	100	100	100
Modified	29	76	67	89	44	44	96

thiothreitol-cleavage showed that αβ, αα, αγ, αδ and β_γ crosslinks were formed.

Occurrence of intersubunit crosslinks

The first dimension electrophoresis and determination of uncrosslinked subunits by dye extraction revealed that a larger fraction of the α subunit than of the β subunit was crosslinked. To ascertain which subunits were crosslinked, the first dimension gel strip was run in a second dimension after DTT-cleavage. The bands corresponding to α, β, γ, δ and ε subunits in the uncrosslinked, as well as crosslinked species, were determined. The results are expressed as the percent of unmodified (native) enzyme subunits (Table IIIB). In the second dimension, the uncrosslinked subunits move along a diagonal path, while the subunits arising from cleavage of the crosslinked species move away from this diagonal. About equal amounts of native and modified enzyme preparations were applied to the gel whenever a comparison of the relative abundance of subunits was made. The results presented in part B of Table III confirm that the individual subunits indicated as lost in part A appear in the crosslinked species. The extent of crosslinking reported in part B agrees reasonably well with that presented in part A. A greater proportion of α subunits than of the β subunits was observed in the crosslinked species.

Although as much as 20–30% reduction in the amount of uncrosslinked ε subunit was observed in some experiments, no ε subunit was found in the cleavage products of the crosslinked species of mass greater than 55–60 kDa. Some intramolecular crosslinks in the ε subunit may have caused a change in its mobility, without crosslinking it to a major subunit, or it was dispersed in crosslinked products so that its abundance was too low to show up in the second dimension.

This left open the question whether the inhibition of activity upon crosslinking might result from binding of the ε subunit to the enzyme in a manner that retained the inhibitory effect of the subunit upon dilution of the enzyme to attain

TABLE III

EFFECT OF DSP TREATMENT ON THE EXTENT OF INTERSUBUNIT CROSSLINKING AND EF_1 ATPase ACTIVITY

To EF_1 ATPase (1.0–1.45 mg/ml) in a 400 μl volume containing 50 mM phosphate buffer and 20 mM ATP at pH 7.0, was added a 10 μl aliquot of DSP in dimethylsulfoxide (final concentration, 0.5 mM) and the reaction mixture vortexed immediately. Incubations were at 10°C. Aliquots were withdrawn at times indicated and passed through centrifuge-Sephadex columns. The eluate was used for enzyme assays and electrophoresis. The results are means of three experiments. The determinations for each experiment were carried out in duplicate. Part B of the table presents the percentages of the subunits in uncrosslinked and crosslinked fractions of the modified preparation. The enzyme modified with DSP for 15 min was run in SDS-polyacrylamide gel electrophoresis. This lane was then run in the second dimension after dithiothreitol (DTT) cleavage as described in the Experimental procedures section. The amounts of subunits are expressed as percent of unmodified preparation presented in the first row of part A. The results are mean of three experiments.

A. One-dimensional electrophoresis

Sample	Incubation time with DSP (min)	Activity (%)	Activity after DTT-treatment (%)	Fraction of subunit not crosslinked				
				α (%)	β (%)	γ (%)	δ (%)	ε (%)
1	0	100	106 ±6	100	100	100	100	100
2	5	67.5±4.9	94.5±2.5	69±3	89± 6	68±2	72±10	77±11
3	10	53.0±1.0	85.5±6.5	63±7	88± 5	54±1	70± 3	76± 5
4	15	41.6±2.5	83.3±4.5	39±8	72±11	35±9	31± 4	68± 8

B Second dimension of electrophoresis for sample 4

Subunit measurement	Subunit				
	α	β	γ	δ	ε
Recovered from uncross-linked portion of gel [a]	32±4	58±5	25±7	31±14	51±7
Recovered from cross-linked portion of gel [a]	44±6	17±4	42±7	33± 8	–
Total recovered from gel [a]	76	75	67	64	–
Fraction not crosslinked	0.42	0 77	0 37	0.48	–

[a] As % of subunits found in sample 1, part A, with no DSP treatment.

maximum specific activity. When the noncross-linked enzyme was assayed at a concentration of 1.5 μg/ml, no effect of subunit dissociation was apparent and the specific activity was about 1/3 of that observed when assayed at 0.1 μg/ml (where specific activity is maximal [26,27]). When the crosslinked enzyme was assayed at a concentration of 1.5 μg/ml, the inhibition produced was similar to that noted when assayed at 0.1 μg/ml. Hence, the inhibition upon crosslinking can be attributed to derivatization of other subunits and not to lack of ε subunit dissociation.

Extent of derivatization and possible intramolecular crosslinks

To assess the extent of derivatization and of possible intramolecular crosslinks in the major α and β subunits, samples were analyzed by 2-D gel electrophoresis. After cleavage of the –S–S bond by thiol, samples were exposed to isoelectric focusing in one dimension, then separated by SDS-polyacrylamide gel electrophoresis in a second dimension. Reaction with the DSP would be expected to remove a positive charge of an amino group, and thus the subunits that have reacted with one or more succinimidyl groups of the reagent will be revealed as one or more spots migrating separately from the unmodified subunit. After reaction with DSP under the conditions required to inhibit about 2/3 of the catalytic activity, the α subunit no longer migrated primarily as a single spot, but now displayed about equal amounts of five spots as expected for reaction with up to 5 or 6 NH_2 groups for the most derivatized spot. The β subunit showed migration patterns consistent with derivatization up to 3 or 4 NH_2 groups. It was estimated that an average of 4–6 groups, likely NH_2, on the α and β subunits of each enzyme had reacted. Reaction of less than one group per α or β subunit would suffice to account for the extent of intersubunit crosslinking reported in Table III. The balance of the reacted groups could be singly derivatized with the reagent, the other end of the reagent having reacted with water. The absence of any appreciable intrasubunit crosslinking is indicated by the migration in SDS-polyacrylamide gel electrophoresis of the α and β subunits that had not formed intersubunit crosslinks. Such subunits migrated identically with those of unreacted enzyme (Fig. 1). Intrasubunit crosslinks could readily retard protein unfolding and lessen SDS binding, resulting in changes in migration patterns. But the data do not rule out intrasubunit crosslinks. Each intrasubunit crosslink requires the reaction of two groups on the subunit, and the α subunits could have an average of about two and the β subunits an average of about one such crosslink.

Discussion

The results presented in this paper show the following points. (1) Treatment of EF_1 with DSP results in electrophoretically distinguishable intersubunit crosslinks accompanied by loss of catalytic activity. (2) The loss of activity of the modified enzyme results principally from conformational restraints of crosslinking and not from chemical modification of reactive groups. (3) The extent of crosslinking of α or β subunits is less than the loss of enzyme activity, but the extent of crosslinking of γ or δ subunits is about equivalent to or greater than the loss of enzyme activity.

The crosslinking by DSP likely involves reaction with lysine amino groups on nearby peptide chains. Only a few crosslinks need to be inserted to account for the intersubunit crosslinking observed when about 2/3 of the catalytic activity is lost. Such loss of activity is observed when about 0.7 of the γ and δ subunits are crosslinked to major subunits. A reaction of only 2.8 NH_2 groups per mol could give 1.4 crosslinks per mol. An additional 5–6 NH_2 groups appear to be derivatized in the noncrosslinked α and β subunits, and other NH_2 groups on the γ, δ and ε subunits could have reacted without crosslinking. The recovery of activity after cleavage of the cross-links shows that over 5–6 groups, likely NH_2, per mol can be derivatized without appreciable loss of catalytic activity. This, although of interest, is not an unusual finding. What appears unusual is that the tying together of only 2–4 of these nonessential groups in intersubunit crosslinks could be the cause of a pronounced loss in catalytic activity. The activity loss could result from additive effects of several crosslinks, or, alternatively, specific single intersubunit crosslinks might stop catalysis.

It must be emphasized, however, that the loss of catalytic capacity following reaction with DSP could also result from intrasubunit crosslinks. The isoelectric focusing dimension in 2-dimensional gel analysis showed that although intrasubunit crosslinks may have been lacking, it does not rule out that some intramolecular crosslinks might have been present in the inhibited enzyme, mostly in the α subunits. If α or β subunits undergo appreciable conformational changes during catalysis, then either intrasubunit or intersubunit crosslinks might stop catalytic events. In contrast, for rotational catalysis, it seems highly likely that intersubunit crosslinks between portions of subunits with relative motions in opposite directions would block catalysis.

If the intersubunit crosslinks are responsible for the loss in catalytic activity, then the activity loss is most readily attributable to the linking of the γ and δ subunits to major subunits, particularly the α subunit. Such crosslinks could readily inhibit catalysis by preventing essential conformational changes. If, in rotational catalysis, the β subunits moved around a core that included the α subunits, then crosslinking of 1/3 of the β subunits to α, γ or δ subunits would be expected to stop activity. In the experiment reported in Table IIB, insufficient β subunit was crosslinked to account for activity loss on this basis. If the α and β subunits moved together, the extent of crosslinking of the α subunit to minor subunits in all experiments was sufficient to account for the loss of activity. Even if β subunits moved independently of α subunits, both α and β subunits could have considerable conformational change during catalysis, and crosslinking of α subunits to single-copy subunits could stop ctalysis.

As mentioned in the Introduction, a finding that a crosslink between the γ subunit and the β subunit specifically inhibited catalysis would support the occurrence of a rotational catalysis as proposed by Boyer and by Cox. The present results are consistent with, but do not provide, a critical test of this possibility. We are currently attempting to devise a means of attaining specific β–γ subunit crosslinks as a further test of the feasibility of rotational catalysis.

The suggestion that the binding change mechanism proceeds with sequential participation of catalytic sites such that the β subunits have the same time-averaged conformations is by no means proven at this stage. The concept of rotational catalysis must be regarded as even more tenuous. However, the results presented here do give strong evidence that major conformational changes accompany catalysis by the F_1 ATPases, and add to the accumulating findings that are consistent with and perhaps best explained by rotational catalysis.

Acknowledgements

We wish to thank John Wise for many valuable suggestions and Z. Xue for performing isoelectric focusing. This study was supported in part by grant GM 11094 from the U.S. Public Health Service and Grant DMB81-00817 of the National Science Foundation.

References

1 Cross, R.L. (1981) Annu. Rev. Biochem. 50, 681–714

2 Senior, A.E. and Wise, J.G (1983) J. Membrane Biol 73, 105–124

3 Boyer, P.D. (1979) in Membrane Bioenergetics (Lee, C P., Schatz, G. and Ernster, L., eds.), pp. 461–479, Addison-Wesley, Reading, MA

4 Lotscher, H.R. and Capaldi, R.A. (1984) Biochem Biophys. Res. Comm. 121, 331–340

5 Stan-Lotter, H. and Bragg, P.D. (1986) Eur. J. Biochem. 154, 321–327

6 Melese, T. and Boyer, P.D. (1985) J. Biol Chem 260, 15398–15401

7 Futai, M. and Kanazawa, H (1983) Microbiol. Rev. 47, 285–312

8 Nalin, C.M., Beliveau, R. and McCarty, R E (1983) J Biol. Chem 258, 3376–3381

9 Hutton, R L. and Boyer, P.D. (1979) J. Biol. Chem. 254, 9990–9993

10 Hackney, D.D. and Boyer, P.D (1978) J. Biol. Chem. 253, 3164–3170

11 Walker, J.E., Saraste, M and Gay, N.J. (1984) Biochim. Biophys. Acta 768, 164–200

12 Boyer, P.D. and Kohlbrenner, W.E. (1981) in Energy Coupling in Photosynthesis (Selman, B.R. and Selman-Reimer, S., eds.), pp. 231–240, Elsevier/North-Holland, Amsterdam

13 Gresser, M, Myers, J A and Boyer, P D (1982) J Biol Chem. 257, 12030–12038

14 Cox, G.B., Jans, D.A., Fimel, A.L., Gibson, F. and Hatch, L. (1984) Biochim. Biophys. Acta 768, 201–208

15 Oosawa, F. and Hayashi, S (1984) J. Phys Soc. Japan 53, 1575–1579

16 Mitchell, P. (1985) FEBS Lett. 182, 1–7

17 Klein, G., Lunardi, J., Satre, M., Lauquin, G J.M. and Vignais, P.V. (1977) in Structure and Function of Energy Transducing Membranes (Van Dam, K. and Van Gelder, B.F., eds.), pp. 283–294, Elsevier/North-Holland Biomedical Press, Amsterdam

18 Baird, B.A. and Hammes, G.G. (1976) J. Biol. Chem. 251, 6953–6962

19 Baird, B.A. and Hammes, G.G. (1977) J Biol Chem. 252, 4743–4748

20 Bragg, P.D. and Hou, C. (1975) Arch. Biochem Biophys. 167, 311–321

21 Bragg, P D. and Hou, C (1980) Eur. J. Biochem 106, 495–503

22 Bragg, P.D. and Hou, C. (1986) Arch. Biochem. Biophys. 244, 361–372

23 Chernyak, B.V, Chernyak, Y Ya., Gladysheva, T.B., Kozhanova, Z E. and Kozlov, I A. (1981) Biochim. Biophys. Acta 635, 552–570

24 Senior, A.E., Downie, J.A., Cox, G.B., Gibson, F., Langman, L and Fayle, D.R.H. (1979) Biochem. J. 180, 103–109

25 Pullman, M.E., Penefsky, H.S., Datta, A. and Racker, E (1960) J Biol. Chem. 235, 3322–3329

26 Laget, P.P. and Smith, J.B. (1979) Arch Biochem. Biophys 197, 83–89

27 Sternweis, P.C. and Smith, J.B. (1980) Biochemistry 19, 526–531

28 Lowry, O.H., Rosebrough, N.J., Farr, A.L. and Randall, R J. (1951) J. Biol. Chem. 193, 265–275

29 Penefsky, H.S. (1977) J. Biol Chem. 252, 2891–2899

Biochimica et Biophysica Acta 890 (1987) 106–115
Elsevier

BBA 42068

Stoichiometries and energetics of proton translocation coupled to electron transport in chloroplasts

Roger P. Hangarter *, Robert W. Jones **, Donald R. Ort
and John Whitmarsh

Department of Plant Biology, USDA/ARS, University of Illinois, Urbana, IL 61801 (U.S.A.)

(Received 21 July 1986)

Key words: Proton translocation, Electron transport, Cytochrome *b/f* complex, Photosystem II; Thylakoid vesicle

We have investigated the stoichiometry of electron transport-driven proton uptake from the external medium and proton release into thylakoid vesicles of chloroplasts during single-turnover flash illumination. Proton uptake from the external medium was measured using a glass pH-electrode. For each electron originating from the oxidation of water by Photosystem II and ultimately forming H_2O_2 via the photoreduction of methyl viologen, approx. 2.7 protons were taken up from the external medium. For each electron originating from the oxidation of duroquinol by the cytochrome *b/f* complex and ultimately forming H_2O_2 via methyl viologen under conditions in which water oxidation was inhibited by diuron, approx. 1.7 protons were taken up from the external medium. It is presumed that for each electron involved in the formation of H_2O_2 that one proton is taken up. Therefore, these results indicate that the electron-transfer reaction from H_2O to Photosystem I involves the uptake of approx. 1.7 protons per electron, and that in the reaction from duroquinol to Photosystem I approx. 0.7 protons per electron are taken up. Proton release within the thylakoid vesicles was measured spectrophotometrically using the pH-sensitive dye neutral red. Flash-induced absorbance changes due to neutral red indicated that for each proton released within the thylakoid vesicle due to water oxidation approx. 1.9 protons appear inside the vesicle as a result of quinol oxidation. The flash-induced formation of ATP was determined by the incorporation of $^{32}P_i$ into ATP. The initiation of flash-induced ATP formation by Photosystem II operating alone required nearly twice as many flashes as were necessary when the Photosystem I-dependent turnover of the cytochrome *b/f* complex was responsible for proton accumulation, and nearly three times more than when Photosystem II and the cytochrome *b/f* complex operated together. This is taken to indicate that both of the reactions that result in proton accumulation within the vesicle contribute energetically to ATP synthesis and contribute in proportion to their measured H^+/e^- ratio. All of these flash-induced measurements, proton uptake from the external medium, proton release inside the vesicle, and the filling of the energetic threshold pool required for the

---

* Current address: Botany Department, The Ohio State University, 1725 Neil Avenue, Columbus, OH 43210, U.S.A.

** Current address: Center for Arid Studies, University College of North Wales, Bangor, Gwynedd LL57 2UW, Wales, U.K.

Abbreviations: Chl, chlorophyll; Cyt, cytochrome; DBMIB, 2,5-dibromo-3-methyl-6-isopropyl-*p*-benzoquinone; DCMU, 3-(3′,4′-dichlorophenyl)-1,1-dimethylurea; DMQ, 2,5-dimethylquinone; DQH_2, duroquinol; FCCP, carbonylcyanide *p*-trifluoromethoxyphenylhydrazone; FeCN, ferricyanide, Hepes, 4-(2-hydroxyethyl)-1-piperazineethanesulfonic acid; Mes, 4-morpholineethanesulfonic acid; P_i, inorganic phosphate, P-700, the primary donor of Photosystem I; PS I, Photosystem I; PS II, Photosystem II

Correspondence. Dr. J. Whitmarsh, Department of Plant Biology, USDA/ARS, 289 Morrill Hall, University of Illinois, 505 South Goodwin Avenue, Urbana, IL 61801, U.S.A.

0005-2728/87/$03.50 © 1987 Elsevier Science Publishers B.V. (Biomedical Division)

onset of ATP synthesis, demonstrate that for each electron transferred from water through the cytochrome *b/f* complex to Photosystem I nearly three protons are accumulated within the thylakoid membrane. Thus, these data indicate that oxidation of quinol by the cytochrome *b/f* complex is able to support the translocation of two protons per electron during flash energization.

Introduction

Proton accumulation within chloroplast thylakoid vesicles is the result of both proton release associated with the oxidation of water by Photosystem II and proton translocation associated with the oxidation of plastoquinol by the cytochrome *b/f* complex. The translocation of protons across the thylakoid membrane includes reactions involved in the uptake of protons from the external medium in addition to the reactions involved in the release of protons into the vesicle. It is clear that one of the reactions resulting in the uptake of protons from the external medium is the reduction and subsequent protonation of plastoquinone by the Photosystem II reaction center [1,2]. Patterned after the original proposals of a Q-cycle by Mitchell [3] and a *b*-cycle by Wikström [4] numerous models are being considered for the oxidation of plastoquinol that involve a proposed second reaction for proton uptake from the external medium during intersystem electron transfer (reviewed in Refs. 5 and 6). Thus, in addition to the proton taken up for each electron involved in plastoquinone reduction by Photosystem II and its subsequent release into the vesicle upon plastoquinol oxidation, these models provide for the uptake and release of an additional proton for each electron transferred through the Cyt *b/f* complex to Photosystem I. In either the Q-cycle or *b*-cycle mechanisms quinol oxidation is envisioned to occur near the inner surface of the membrane allowing for the release of one proton for each of the sequential single electron steps of the oxidation. The models have in common that one of the electrons originating from the quinol is transported to Photosystem I via the Rieske FeS center, cytochrome *f* and plastocyanin, whereas the other is directed through the *b*-cytochromes. Although the alternative mechanisms differ in how the reduced *b*-cytochrome leads to quinone reduction and the attendant uptake of protons from the external medium, they share the salient features that two sequential turnovers of a Cyt *b/f* complex result in the net oxidation of one quinol, the transfer of two electrons to Photosystem I, and the translocation of four protons across the membrane.

There are numerous lines of experimental evidence that support the operation, under certain conditions, of some form of proton translocation coupled to an electron cycling through the Cyt *b/f* complex. Among these is the demonstration of a slow electrogenic reaction occurring between the photosystems indicating transmembrane charge transfer associated with the Cyt *b/f* complex [7]. Electrogenic charge transfer by the Cyt *b/f* complex is evident not only from the existence of the slow phase of electrochromic band shift, but also from the slowing effect of a transmembrane electric potential on the turnover of the Cyt *b/f* complex [8,9]. The involvement of Cyt b_6 redox activity in transmembrane electron transfer is indicated by the kinetic correlation between the cytochrome's redox behavior and the formation of at least a significant portion of the slow electrochromic shift [10–12]. One of the most convincing tests for the operation of a proton-coupled electron cycle within the Cyt *b/f* complex, measurements of the number of protons taken up from the external media and the number of protons translocated into the thylakoid vesicle during quinol oxidation, has yielded equivocal results. This is due in part to experimental difficulties in determining proton-to-electron ratios, and in part to the complexity of the plastoquinol-cytochrome *b/f* interaction. While there are several reports of proton uptake from the external medium [9,10,14–16], and proton release into the thylakoid vesicle [17] indicating the operation of modified Q or *b*-cycle, there are other reports that have failed to detect any additional proton translocation associated with plastoquinol oxidation [18,19]. In the work presented here we examine the crucial issue of whether the protons disappearing from the external medium are accumulated within the thylakoid vesicle and whether they contribute proportionately to membrane energization. We show that flash-induced proton uptake is indeed greater than that predicted for a linear electron-transport scheme and, through two independent methods, we show that these protons are translocated into the thylakoid vesicles. We measured electron-transport-driven proton uptake from the external medium and, using neutral red, we measured pH changes in the internal space of thylakoid vesicles. We found that the protons taken up from the external medium appeared inside the thylakoids. Furthermore, the protons released into the inner aqueous phase were shown to contribute to the generation of the threshold transmembrane pH difference required for the onset of ATP synthesis.

Materials and Methods

Isolation of chloroplast thylakoid membranes

Thylakoid membranes were isolated from commercial spinach (*Spinacia oleracea* L.) as described elsewhere [20] with the exception of the final resuspension medium. For potentiometric and ATP formation measurements the thylakoid membranes were resuspended in a medium containing 100 mM sorbitol/2 mM $MgCl_2$/20 mM KCl/5 mM Mes-KOH (pH 6.5)/5 mM Hepes-KOH (pH 7.0 and 7.5)/5 mM Tricine-KOH (pH 8.0 and 8.5). For spectroscopic measurements the resuspension medium was the same as described above, except that the buffer used was 2 mM Hepes-KOH at pH 7.0, 7.5 and 8.0. The chlorophyll concentration was determined using the specific absorption coefficients for Chl *a* and *b* published by Ziegler and Egle [21].

Measurement of flash-induced electron transfer

The amount of electron transfer occurring per flash was measured using two different techniques. One method employed a glass pH-electrode to measure the irreversible flash-induced pH change resulting from proton release during water oxidation in the presence of nigericin (3 μM). In these experiments the terminal electron acceptor was ferricyanide (0.2 mM). In order to measure electron transfer through Photosystem II alone 2,5-dimethylquinone (0.2 mM) was added to mediate electron transfer from Photosystem II to ferricyanide and DBMIB (0.5 μM) was present to prevent electron flow from plastoquinone through Photosystem I. The alternate method used a Clark-type oxygen electrode to measure, depending on the electron mediator employed, either oxygen uptake or evolution [20]. In order to ensure an oxygen consumption to electron-transfer ratio of 2.0 for the duroquinol to methyl viologen reaction, excess superoxide dismutase was included to eliminate the oxidation of duroquinol by the superoxide radical anion that is produced as an intermediate in the aerobic oxidation of photoreduced methyl viologen. For technical reasons the oxygen flash yield measurements were made at 20°C, whereas proton flash yield measurements were made at 4°C. However, we demonstrated in an earlier study [20], and confirmed here, that flash-induced electron transfer measured at flash frequencies below 20 Hz was constant over the temperature range from 4 to 20°C. Assuming the predicted exponential saturation of the reaction centers as a function of increasing flash intensity, it was determined from light attenuation experiments with calibrated neutral density filters that the unattenuated xenon flashes (6 μs at half peak height) were greater than 98% saturating. Reaction mixtures and further details are given in the figure and table legends.

Measurement of flash-induced proton uptake from the external medium

The amount of proton uptake was determined by measuring the extent of the reversible pH change of the reaction medium induced by a series of single-turnover flashes. The pH changes were measured with a glass pH-electrode and calibrated by addition of a standard HCl solution. We were able to fit the proton efflux occurring after the flash series to a single component exponential decay using an iterative nonlinear least-squares program [23] to calculate the total extent of proton uptake as described previously [9]. The measurements were done at 4°C. Reaction mixtures and further details are given in the figure and table legends.

Measurement of flash-induced proton release into the thylakoid vesicle

The release of protons rapidly equilibrating with the internal aqueous space of the thylakoid membranes was measured by a modification of the procedure developed by Junge and co-workers [24–26] using the pH-indicating dye neutral red. Light-induced absorbance changes were measured using a laboratory-built spectrophotometer. The pathlength of the measuring beam was 1 cm. The neutral red-dependent response was measured as the absorbance change at 545 nm in the presence of neutral red minus the absorbance change at 545 nm in the absence of neutral red. We determined that the measuring beam resulted in an average reaction center turnover rate of less than once every 30 s. The actinic xenon flashes were filtered by a red (CS 2-58, Corning Glass Co. *, Rochester, NY) blocking filter. The photomultiplier tube was protected from scattered actinic light by a Corning CS 4-96 blocking filter and a Balzers Interference Filter (DT-Green). For technical reasons the absorbance changes due to neutral red reported were measured at 17°C. Measurements done at 4°C gave similar results. Reaction mixtures and further details are given in the figure and table legends.

Measurement of flash-induced ATP formation

The ATP synthesis resulting from a series of single-turnover flashes was measured as the incorporation of $^{32}P_i$ into ATP according to the method of Smith et al. [27] as described previously [20]. The threshold number of flashes required for the onset of ATP synthesis was taken to be the first flash resulting in more than 0.2 mmol ATP per mol Chl [20]. The measurements were done at 4°C. Reaction mixtures and further details are given in the figure and table legends.

Results

Flash-induced proton uptake from the external medium

The ratio of the number of protons taken up from the external medium to the number of electrons transferred from water through the Photosystem I acceptor Methyl viologen to O_2 was 2.7 ± 0.3 for single turnover flash excitation (Table I). Fig. 1 shows that this H^+/e^- value was maintained at turnover rates as high as 60 s^{-1}.

Fig. 2 shows the dependence of proton uptake and electron transfer on the number of saturating single turnover flashes absorbed by the sample at a flash frequency of 10 Hz. The amount of electron transfer per flash was determined from measurements of the irreversible, uncoupler-insensitive, proton release associated with water oxidation and is independent of flash number. However, the flash-yield of proton uptake per flash is decidedly flash number dependent, so the maximum H^+/e^- ratio of 2.6 is observed only during the first 20–30 saturating flashes. For example, if we calculate the H^+/e^- from the slope of the line between 50 and 80 flashes the apparent value drops to 1.6. While this decline in H^+ uptake most likely reflects an actual change in the H^+/e^- ratio during the later flashes, we believe the actual proton uptake is likely to be somewhat greater

TABLE I

THE RATIO OF PROTON UPTAKE FROM THE EXTERNAL MEDIUM TO ELECTRON TRANSFER FOR DIFFERENT ELECTRON-TRANSPORT REACTIONS

Flash-induced proton uptake was measured with a glass electrode in 4 ml of reaction medium consisting of 100 mM sorbitol/2 mM $MgCl_2$/20 mM KCl/0.5 mM Hepes-KOH (pH 7.5)/150 units per ml superoxide dismutase/0 5 μM nonactin/thylakoid membranes containing 140 nmol chlorophyll The concentration of methyl viologen was 100 μM when present When duroquinol (0.2 mM) was used as the electron donor, DCMU (5 μM) was present to prevent Photosystem II turnover When 2,5-dimethylquinone (0.2 mM) was used to intercept electrons directly from Photosystem II, DBMIB (0.5 μM) was present to prevent electron flow beyond plastoquinone. Flash-induced electron transfer through Photosystem II alone, or from H_2O through PS II + PS I, was measured using a glass pH-electrode as described in Materials and Methods. Flash-induced electron transfer from duroquinol through PS I was measured using a Clark-type oxygen electrode as described in Materials and Methods The values given are the average ± standard deviation

Electron-transfer reaction	H^+/e^-
$H_2O \rightarrow$ methyl viologen	2.7 ± 0 3
$DQH_2 \rightarrow$ methyl viologen	1.7 ± 0.2
$H_2O \rightarrow$ DMQ	1.0 ± 0.3

---

* Mention of a trademark, proprietary product, or vendor does not constitute a guarantee or warranty of the product by the U.S. Department of Agriculture or the University of Illinois and does not imply its approval to the exclusion of other products or vendors which may be suitable.

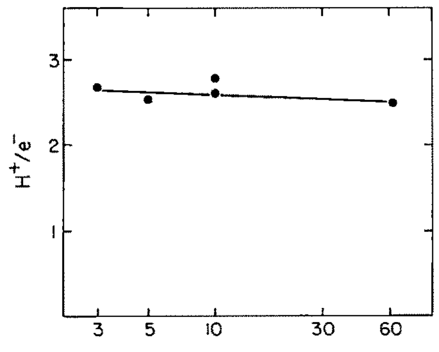

Fig. 1. Ratio of proton uptake from the external medium to electrons transferred from H_2O to methyl viologen as a function of flash frequency Proton uptake and electron transfer were measured with a glass pH-electrode as described in Table I.

than that estimated from the slope of the line from 50 to 80 flashes shown in Fig. 2. The reason for the underestimation of proton uptake arises from the fact that the system is beginning to enter a steady state, in which the rate of proton uptake is equal to the rate of proton efflux so that additional flashes result in no net proton uptake.

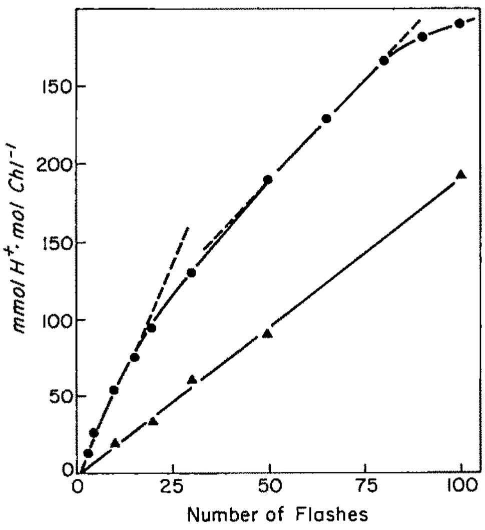

Fig. 2. The dependence of the efficiency of flash-induced proton uptake and electron transport on the number of flashes at a flash frequency of 10 Hz. Proton uptake (●) was measured in a 4 ml reaction mixture consisting of 100 mM sorbitol/2 mM $MgCl_2$/25 mM KCl/0.5 mM Tricine-KOH (pH 8.1)/100 μM methyl viologen/0.4 μM valinomycin/thylakoid membranes containing 175 nmol chlorophyll. Electron transport (▲) was determined as described in Table I using a glass pH electrode

The effects that nonactin- or valinomycin-catalyzed K^+ movements are apt to have on the membrane surface charge raise the possibility of flash-induced proton binding to the external surface of the thylakoid membrane (e.g., Ref. 28). The observation that the initially high H^+/e^- value observed in the presence of nonactin is unaffected by medium pH (Fig. 3) indicates that external proton binding is an unlikely possibility, as do the measurements of proton release into the inner thylakoid space that are presented below.

Since the aerobic oxidation of photoreduced methyl viologen involves the uptake of one proton from the external medium per electron to form H_2O_2, the data in Fig. 2 indicate that about 1.6 protons were taken up from the external medium by the thylakoid membrane for each electron transferred between the photosystems. Flash-induced proton uptake associated with Photosystem I-dependent oxidation of duroquinol by the Cyt *b/f* complex is consistent with this notion. We measured the uptake of 1.7 ± 0.2 protons for each electron transferred to O_2 via photoreduced methyl viologen (Table I). Since in this reaction, as for the one above, one proton is taken up from the external medium for each electron reducing

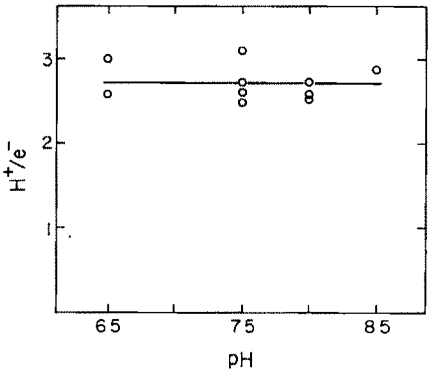

Fig 3. Ratio of proton uptake from the external medium to electron transferred from H_2O to methyl viologen per flash as a function of pH. Proton uptake was measured with a glass electrode and flashes were given at a frequency of 10 Hz The reaction conditions were the same as in Table I, except that the buffers used were 0.5 mM Mes-KOH (pH 6.5), Hepes-KOH (pH 7.5), and Tricine-KOH (pH 8.0 and 8.5).

oxygen, about 0.7 protons per electron are taken up by the thylakoid. With either water or duroquinol as the electron donor it is presumed that for each proton consumed in the external medium during H_2O_2 formation one proton is released and retained within the thylakoid vesicle.

Flash-induced proton uptake from the external medium dependent solely on Photosystem II can be measured when dimethylquinone is present to intercept electrons directly from Photosystem II and DBMIB is present to prevent any residual electron flow through Photosystem I [29]. We observed 1.0 ± 0.3 protons taken up from the external medium for each electron transferred from H_2O to dimethylquinone to form dimethylquinol (Table I). The flash-induced proton uptake was entirely reversible after the completion of the flash series indicating that, as with H_2O_2 formation discussed above, one proton is retained within the vesicle for each one consumed externally in dimethylquinone reduction.

Flash-induced proton release into the inner space of thylakoid vesicles

The flash-induced release of protons into the internal space of thylakoid vesicles was monitored using the pH-indicating dye neutral red. Despite the fact that interpreting the neutral red absorbance change is complicated and depends on several simplifying assumptions, Junge and coworkers [24–26] have shown that it can be a useful probe of internal proton release under carefully selected experimental conditions. In order to isolate the portion of the neutral-red signal indicative of this release of protons into the inner space of the thylakoid vesicle, all absorbance changes of neutral red due to proton uptake in the external medium were eliminated by stabilizing the external pH with membrane-impermeant buffers such as Hepes or Tricine. Flash-induced absorbance changes due to components other than neutral red, for example Cyt *f* redox changes, were accounted for by subtracting the absorbance change observed at 545 nm in the absence of neutral red from that measured in its presence. The remaining flash-induced absorbance change observed at 545 nm in the presence of neutral red was sensitive to buffers that penetrate into the thylakoid vesicle and thereby prevent, or substantially decrease, flash-induced pH changes. For example the presence of either 4-(2-hydroxyethyl)-morpholine (1 mM) or imidazole (10 mM) decreases the absorbance change greater than 90%. Furthermore, the neutral red signal was abolished by nigericin (0.33 μM), and diminished more than 85% by FCCP (0.5 μM). High concentrations of gramicidin (5 μM) failed to eliminate the neutral red signal (in some cases more than 30% of the signal remained); it should be noted that gramicidin has been reported to be less effective than other uncouplers in preventing the uptake of basic amines that are used to quantify the transmembrane ΔpH [30].

Recently, De Wolf et al. [28] have shown that under certain circumstances neutral red can undergo flash-induced reduction by Photosystem I, resulting in an absorbance decrease. Using Photosystem I vesicles and ferredoxin and NADP as the terminal electron acceptor De Wolf et al. show that neutral-red absorbance changes can be caused by the reduction of neutral red as well as by pH changes. In our study, using methyl viologen as an efficient Photosystem I electron acceptor, we find no evidence for a redox indicator function for neutral red. We base this conclusion on the following: (1) there is no rapid absorbance decrease indicative of neutral-red reduction; (2) the neutral-red signal is sensitive to the uncouplers nigericin and FCCP; and (3) the neutral-red signal is abolished by permeant buffers. Additional support for this conclusion is provided by the observation that the absorbance change due to neutral red in the electron-transfer reaction from duroquinol to methyl viologen (Fig. 4, trace E) is inhibited 90% by 1.5 μM DBMIB (data not shown). Under these conditions we have shown that at the low flash frequency of 0.2 Hz used, Photosystem I continues to turn over, even though the rapid oxidation of quinol by the Cyt *b*/*f* complex is inhibited. The sensitivity of a flash-induced neutral red absorbance change to DBMIB indicates that the signal is associated with quinol oxidation by the Cyt *b*/*f* complex and is not due to the Photosystem I reduction of neutral red under our experimental conditions.

The neutral red-dependent absorbance change associated with flash-induced water oxidation is shown in trace A of Fig. 4. In order to improve the precision of the measurements the results of 64 flashes given at a frequency of 0.2 Hz were summed for signal averaging. Even at this low repetition frequency the ΔpH does not entirely relax between successive flashes, and as a result the internal pH becomes progressively lower during the flash series. This is an important issue, since the differential absorption coefficient of the protonated and unprotonated forms of neutral red is a sensitive function of pH. The extent to which the internal pH is lowered during the series of 64 flashes will depend upon the number of protons released per electron transferred. In order to evaluate the effect that a lower internal pH brought on by higher H^+/e^- ratios has on the size of the neutral-red absorbance change, we mimicked, with Photosystem II turnovers, reactions of higher H^+/e^- ratios by delivering groups of two (Fig. 4, trace B) or three (Fig. 4, trace C) flashes spaced 100 ms apart at a flash group frequency of 0.2 Hz. The results show that there is an increase in the average absorbance per flash of about 20% for the 2- and 3-flash groups compared to the train of individual flashes. Thus, in making a quantitative comparison to the Photosystem II-dependent absorbance change with absorbance change dependent on Photosystem I turnover it is important that this feature of neutral-red behavior be accommodated. Additionally, any such comparison must be concerned with the relative abundance of Photosystem II centers relative to the Cyt *b/f* complex. We have shown previously [22] that the number of Photosystem II centers able to oxidize water in the presence of dimethylquinone is very nearly identical to the number of Photosystem I centers and Cyt *b/f* complexes (that is, each is present at about 1.7 mmol per mol Chl). There are numerous indications of Photosystem II centers that under normal conditions have negligible turnover rates [31–34]. While these normally inactive centers can be induced to oxidize water rapidly by the introduction of halogenated benzoquinones, they remain inactive with methyl-substituted benzoquinones such as 2,5-dimethylbenzoquinone used in these experiments at flash frequencies greater than 1 Hz [33].

A comparison of the number of protons released internally during electron transfer from H_2O to methyl viologen, and from duroquinol to methyl viologen is compiled in Table II. The extent of the neutral red absorbance increase due to a single flash given at 0.2 Hz for the reaction H_2O to methyl viologen (Fig. 4, trace D) is approximately the same as that observed for the group of three flashes given to Photosystem II (trace C); duroquinol to methyl viologen (trace E) is about the same as the two flash group (trace B). Thus, these measurements indicate that approx. twice as many protons are released internally for each electron transferred through the Cyt *b/f* complex than are released due to water oxidation. Using faster time resolution than shown here we found that the half-time for the absorbance rise for proton release associated with the Cyt *b/f* complex (approx. 15 ms) was much slower than for

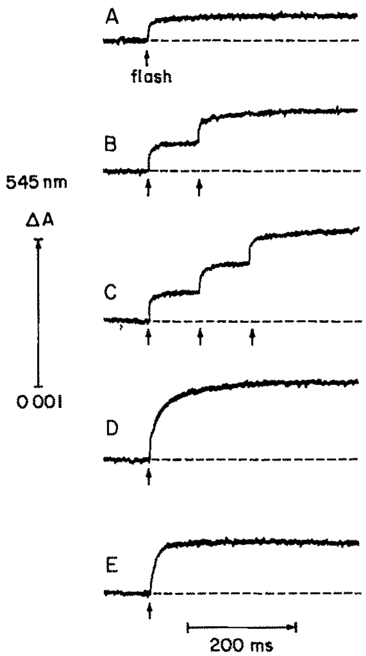

Fig 4. Flash-induced absorbance changes of neutral red measured at 545 nm. The traces shown are absorbance changes of thylakoids in the presence of 10 μM neutral red minus the absorbance change of thylakoids in the absence of neutral red. The 3 ml reaction mixture consisted of 100 mM sorbitol, 20 mM KCl, 2 mM $MgCl_2$, 2 mM Hepes-KOH (pH 7.5), 0.5 μM nonactin, 100 μM methyl viologen, thylakoid membranes containing to 90 nmol chlorophyll, and the following additions: (A–C) H_2O to dimethylquinone, 500 μM dimethylquinone and 0.5 μM DBMIB; (d) H_2O to methyl viologen; and (E) DQH_2 to methyl viologen, 250 μM duroquinol and 10 μM DCMU. The flashes are indicated by the arrows. The traces shown are the average of 64 flashes given at a frequency of 0.2 Hz.

TABLE II

A COMPARISON OF THE NUMBER OF PROTONS RELEASED INTO THE THYLAKOID VESICLE DURING ELECTRON TRANSPORT FROM WATER TO METHYL VIOLOGEN AND FROM DUROQUINOL TO METHYL VIOLOGEN

Flash-induced proton release into the inner space of thylakoid vesicles was estimated from absorbance changes observed in the presence of neutral red. Internal proton release due solely to Photosystem II-dependent water oxidation was measured using dimethylquinone (0.2 mM) to intercept electrons directly from Photosystem II and DBMIB (0.5 μM) to prevent any residual electron flow beyond plastoquinone. The reactions H_2O to methyl viologen, which includes PS II, Cyt *b/f* and PS I, and duroquinol to methyl viologen, which includes Cyt *b/f* and PS I, were measured as described in Fig. 4. Internal proton release due solely to PS II was assumed to be $1H^+$/PS II per flash.

pH	$H_2O \rightarrow$ methyl viologen	$DQH_2 \rightarrow$ methyl viologen
7.0	2.8±0.2	2.0±0.2
7.5	2.7±0.3	1.9±0 3
8.0	2.8±0.2	1.9±0.2

water oxidation (equal to or faster than 1 ms). Analysis of the proton release kinetics associated with quinol oxidation will be discussed elsewhere (Jones and Whitmarsh, unpublished results).

ATP synthesis associated with the flash-induced uptake and release of protons

We investigated the relationship between the threshold number of flashes necessary to initiate ATP synthesis and the amount of proton uptake from the external medium. In the absence of a transmembrane electric field about 80 mmol.H^+ per mol Chl need to be accumulated by thylakoid membrane vesicles for the initiation of net ATP synthesis [20]. This was found to be true even when the amount of H^+ uptake per flash was varied over a wide range and is documented again by the open circles in Fig. 5, where we measured the number of flashes required for the onset of ATP synthesis for flashes of different intensities. The solid line is the predicted relationship for a uniform threshold pool of protons that must be filled in order for net ATP synthesis to commence [20]. Based on the H^+/e^- ratios reported in Table I, it is anticipated that for the reaction DQH_2 to methyl viologen ($H^+/e^- = 1.7$) about 1.5-times more flashes should be required than for the reaction H_2O to methyl viologen ($H^+/e^- = 2.7$). Similarly, for the reaction H_2O to DMQ ($H^+/e^- = 1$) it is anticipated that about 3-times more flashes should be necessary to initiate net ATP synthesis than for H_2O to methyl viologen. In Fig. 5 the triangles represent the reaction DQH_2 to methyl viologen and the solid circles represent the reaction from H_2O to DMQ. About 22 flashes were required for the onset of ATP synthesis for the DQH_2 to methyl viologen reaction, about 50 for the H_2O to DMQ reaction and about 15 for the H_2O to methyl viologen reaction. Clearly these data points correspond closely to the predicted relationship (solid curve) indicating that the additional proton translocated by the Cyt *b/f* complex contributes in proportion to the measured

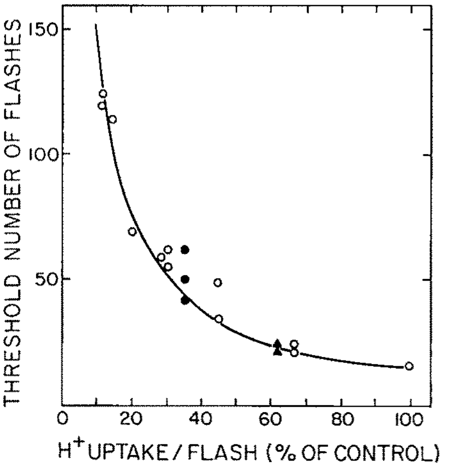

Fig 5. The relationship between the onset of ATP synthesis and the amount of proton uptake per flash. The threshold number of flashes required for the onset of ATP synthesis was determined as described under Materials and Methods Proton uptake per flash was varied in the H_2O to methyl viologen (open circles) by changing the intensity of the flashes with neutral density filters. The maximum H^+ uptake observed with saturating flash intensities was 5.4 mmol H^+ per mol Chl per flash. Proton uptake in PS II (solid circles) and PS I (triangles) reactions was measured using saturating flashes The electron donor and acceptor systems are the same as in Table I, except for the addition of 0.1 mM ADP and 0.5 mM $Na_2H^{32}PO_4$ (10 μCi) in the reaction mixture used to measure ATP synthesis The flash frequency was 10 Hz The solid line is the relationship predicted for the filling of a threshold proton pool by the translocated protons (details in the text and Ref 20).

H^+/e^- ratios to the energetic proton pool that drives ATP synthesis.

Discussion

The mechanism by which electron transfer from Photosystem II to Photosystem I transports protons across the thylakoid membrane has yet to be determined. A central element in efforts to understand this process is determining the number of protons that are translocated for each electron transferred through the Cyt *b/f* complex. While several previous studies support H^+/e^- values greater than 1 these have measured either proton uptake from the external medium [9,14,15] or release into the thylakoid vesicle [35], but not both. Thus, in these earlier studies the possibility that a fraction of the proton uptake or release was due to light-induced proton binding or debinding due to changes in the membrane surface charge could not be excluded. In the work presented here we measured proton uptake from the external medium and proton release into the internal aqueous phase under similar conditions. The data show that for each electron transferred through the Cyt *b/f* complex to Photosystem I that 1.7–1.8 protons are taken up by the thylakoid membrane, and that 1.7–2.0 protons are released into the inner aqueous space of the thylakoid membrane vesicle. These results demonstrate that, for each electron transferred through the Cyt *b/f* complex to Photosystem I an additional proton can be transferred across the thylakoid membrane. Moreover, these high H^+/e^- values for the flash-induced turnover of the Cyt *b/f* complex were not detectably affected by the pH of the external medium (Fig. 3 and Table II).

Independent evidence for the translocation of an extra proton by intersystem electron transfer is found in the onset behavior of ATP synthesis. In an earlier paper Hangarter and Ort [20] studied the filling of the threshold proton pool that drives ATP synthesis and found that the pool became sufficiently energized for ATP synthesis after about 80 mmol H^+ per mol Chl had been accumulated by the membrane vesicles regardless of the rate of accumulation. This was true when the rate of proton accumulation was varied by any of several different treatments that lowered the number of protons taken up per flash including the inhibition of either Photosystem II-dependent or Photosystem I-dependent proton uptake. Our data presented here (Fig. 5) show that Photosystem II-driven proton accumulation required approx. twice the number of flashes to fill the threshold pool as did the Photosystem I reaction from DQH_2 to methyl viologen that includes the Cyt *b/f* complex. The most straightforward explanation of these data is that intersystem electron transport translocates two protons for each proton released by PS II and that the additional proton translocation contributes to the electrochemical proton potential that drives the synthesis of ATP.

While the data shown here demonstrate that oxidation of quinol by the Cyt *b/f* complex results in the translocation of an additional proton, it must be emphasized that in electron transport under conditions of continuous high light intensity the question of additional proton translocation by the Cyt *b/f* complex remains unresolved. Several investigators support the suggestion that the extra proton translocation associated with the electrogenic steps of the Q- or *b*-cycle may be energetically feasible only when the transmembrane electrochemical potential is small [8,9,16]. In fact, our results indicate that even with single-turnover flashes given at relatively low frequency (10 Hz) and in the presence of an ionophore that prevents the formation of an electric potential, the extra proton translocation associated with the Cyt *b/f* complex is fully present during the first 20–30 turnovers after which the H^+/e^- probably declines gradually toward the steady-state value.

Acknowledgments

We thank Colin Wraight for his critical comments. This research was supported in part by grants from NSF (PCM 83-14461) (D.R.O.) and USDA/CRGO (AG82-CRCR-101044) (J.W.).

References

1 Crofts, A R and Wraight, C.A (1983) Biochim. Biophys Acta 726, 149–185
2 Polle, A. and Junge, W. (1986) Biochim. Biophys. Acta 840, 257–264
3 Mitchell, P. (1976) J Theor. Biol 62, 327–367

4 Wikström, M.K.F and Krab, K (1980) Curr Top. Bioenerg 10, 51–101
5 Cramer, W.A., Widger, W R., Black, M.T. and Girvin, M.E. (1986) Topics in Photosynthesis, Vol. 8: Electron Transfer Mechanisms and Oxygen Evolution (Barber, J., ed), in the press
6 Joliot, P. and Joliot, A. (1986) Photosynth Res. 9, 113–124
7 Joliot, P. and Delosme, R. (1974) Biochim Biophys Acta 357, 267–284
8 Bouges-Bocquet, B (1981) Biochim. Biophys. Acta 635, 327–340
9 Graan, T. and Ort, D R (1983) J Biol Chem. 258, 2831–2836
10 Velthuys, B R (1978) Proc. Natl. Acad Sci USA 75, 6031–6034
11 Jones, R.W. and Whitmarsh, J (1985) Photobiochem. Photobiophys. 9, 119–127
12 Jones, R.W. and Whitmarsh, J. (1987) in Proceedings of the VIIth International Congress on Photosynthesis (Biggins, J., ed.), Martinus Nijhoff/Dr. W. Junk Publishers, Dordrecht, in the press
13 Joliot, P and Joliot, A (1986) Biochim. Biophys. Acta 849, 211–222
14 Fowler, C.F and Kok, B. (1976) Biochim. Biophys Acta 423, 510–523
15 Olsen, L.F. and Cox, R. (1979) Eur. J. Biochem 95, 427–437
16 Rathenow, M. and Rumberg, B (1980) Ber Bunsenges. Phys. Chem. 84, 1059–1062
17 Velthuys, B.R. (1980) FEBS Lett. 115, 167–170
18 Olsen, L F.. Telfer, A and Barber, J. (1980) FEBS Lett 118, 11–17
19 Hope, A.B. and Matthews, D.B (1983) Aust. J. Plant Physiol. 10, 363–372
20 Hangarter, R. and Ort, D.R. (1985) Eur. J Biochem. 149, 503–510
21 Ziegler, R. and Egle, K (1965) Beitr. Biol Pflanz. 4, 11–37
22 Whitmarsh, J and Ort, D R (1984) Arch Biochem Biophys 231, 378–389
23 Bevington, P. (1969) in Data Reduction and Error Analysis for the Physical Sciences, pp 134–186, McGraw-Hill, New York
24 Junge, W., Ausländer, W , McGeer, A.J. and Runge, T (1979) Biochim. Biophys. Acta 546, 121–141
25 Hong, Y Q. and Junge, W (1983) Biochim Biophys. Acta 722, 197–208
26 Theg, S M. and Junge, W (1983) Biochim. Biophys. Acta 723, 294–307
27 Smith, D J , Stokes, B O and Boyer, P D (1976) J Biol Chem 251, 4165–4171
28 De Wolf, F A , Groen, B.H., Van Houte, L.P.A., Peters, F.A L J., Krab, K and Kraayenhof, R. (1985) Biochim Biophys Acta 809, 204–214
29 Flores, S and Ort, D.R. (1984) Biochim Biophys Acta 766, 289–302
30 Portis, A.R. and McCarty, R.E. (1976) J Biol. Chem. 251, 1610–1617
31 Lavergne, J. (1982) Photobiochem Photobiophys 3, 273–285
32 Melis, A. (1985) Biochim. Biophys. Acta 808, 174–180
33 Graan, T. and Ort, D.R. (1986) Biochim. Biophys. Acta 852, 320–330
34 Chylla, R , Garab, G and Whitmarsh, J. (1987) in Proceedings of the VIIth International Congress on Photosynthesis (Biggins, J., ed), Martinus Nijhoff/Dr W Junk Publishers, Dordrecht, in the press
35 Hope, A B., Handley, L. and Matthews, D B (1985) Aust. J. Plant Physiol. 12, 387–394

Biochimica et Biophysica Acta **Vol. 890, No. 1**
Bioenergetics B80(1) January 16, 1987

Contents

Biochimica et Biophysica Acta: 40 years on v

Regular Papers

The role of fixed and mobile buffers in the kinetics of proton movement (BBA 42067)
by W. Junge and S. McLaughlin (F.R.G., U.S.A.) 1

Evidence for an association between a 33 kDa extrinsic membrane protein, manganese and photosynthetic oxygen evolution. I. Correlation with the S_2 multiline EPR signal (BBA 42065)
by D. Hunziker, D.A. Abramowicz, R. Damoder and G.C. Dismukes (U.S.A.) 6

Long-term delayed luminescence in *Scenedesmus obliquus* I. Spectral and kinetic properties (BBA 42078)
by W. Schmidt and H. Senger (F.R.G.) 15

pH dependence of oxygen evolution and reduction kinetics of photooxidized chlorophyll a_{II} (P-680) in Photosystem II particles from *Synechococcus* sp (BBA 42159)
by E. Schlodder and B. Meyer (F.R.G.) 23

Formation and flash-dependent oscillation of the S_2-state multiline EPR signal in an oxygen-evolving Photosystem-II preparation lacking the three extrinsic proteins in the oxygen-evolving system (BBA 42079)
by S. Styring, M. Miyao and A.W. Rutherford (France, Japan) 32

Photoaffinity labeling of the mitochondrial phosphate carrier by 4-azido-2-nitrophenyl phosphate (BBA 42157)
by M. Tommasino, G. Prezioso and F. Palmieri (Italy) 39

Subunit component and their roles in the sodium-transport NADH: quinone reductase of a marine bacterium, *Vibrio alginolyticus* (BBA 42203)
by M. Hayashi and T. Unemoto (Japan) 47

Availability to monoclonal antibodies of antigenic sites of the α and β subunits in active, denatured or membrane-bound mitochondrial F_1-ATPase (BBA 42077)
by M. Moradi-Améli and C. Godinot (France) 55

Effects of trypsin and bivalent cations on P-680$^+$-reduction, fluorescence induction and oxygen evolution in Photosystem II membrane fragments from spinach (BBA 42155)
by M. Völker, H.-J. Eckert and G. Renger (F.R.G.) 66

Light modulation of serine and threonine phosphorylation in histone III by thylakoids (BBA 42156)
by H.A. Lucero, N. Cortez and R.H. Vallejos (Argentina) 77

Peroxidative injury of the mitochondrial respiratory chain during reperfusion of hypothermic rat liver (BBA 42158)
by T. Nishida, H. Shibata, M. Koseki, K. Nakao, Y. Kawashima, Y. Yoshida and K. Tagawa (Japan) 82

continued

Cited in: Current Contents Life Sciences - Biological Abstracts - Chemical Abstracts - Index Chemicus - Index Medicus - Excerpta Medica (EMBASE)

INFORMATION FOR CONTRIBUTORS TO BIOCHIMICA ET BIOPHYSICA ACTA

The 1982 edition of this booklet, offering detailed guidance to authors, is available free of charge from the BBA Editorial Secretariat, P.O. Box 1345, 1000 BH Amsterdam, The Netherlands. It is also published as Biochim. Biophys. Acta 715 (1982) 1–23.

The high-affinity binding site for manganese on the oxidizing side of Photosystem II (BBA 42080)
by B.-D. Hsu, J.-Y. Lee and R.-L. Pan (Taiwan, China) 89

Escherichia coli F_1 ATPase is reversibly inhibited by intra- and intersubunit cross-linking: an approach to assess rotational catalysis (BBA 42066)
by R.P. Kandpal and P.D. Boyer (U.S.A.) 97

Stoichiometries and energetics of proton translocation coupled to electron transport in chloroplasts (BBA 42068)
by R.P. Hangarter, R.W. Jones, D.R. Ort and J. Whitmarsh (U.S.A.) 106

BIOCHIMICA ET BIOPHYSICA ACTA
International Journal of Biochemistry and Biophysics
Founded in 1947 by H.G.K. Westenbrink, Managing Editor 1947–1964

© 1987, Elsevier Science Publishers B.V (Biomedical Division)
Printed in The Netherlands

All rights reserved. No part of this publication may be reproduced, stored in a retrieval system, or transmitted, in any form or by any means, electronic, mechanical, photocopying, recording or otherwise, without the prior written permission of the publisher, Elsevier Science Publishers B.V. (Biomedical Division), P.O. Box 1527, 1000 BM Amsterdam, The Netherlands. Submission of a paper to this journal entails the author's irrevocable and exclusive authorization of the publisher to collect any sums or considerations for copying or reproduction payable by third parties (as mentioned in article 17 paragraph 2 of the Dutch Copyright Act of 1912 and in the Royal Decree of June 20, 1974 (S. 351) pursuant to article 16b of the Dutch Copyright Act of 1912) and/or to act in or out of Court in connection therewith.

Special regulations for readers in the U.S.A. This journal has been registered with the Copyright Clearance Center, Inc. Consent is given for copying of articles for personal or internal use, or for the personal use of specific clients. This consent is given on the condition that the copier pays through the Center the per-copy fee stated in the code on the first page of each article for copying beyond that permitted by Sections 107 or 108 of the U.S. Copyright Law. The appropriate fee should be forwarded with a copy of the first page of the article to the Copyright Clearance Center, Inc., 27 Congress Street, Salem, MA 01970, U.S.A. If no code appears in an article, the author has not given broad consent to copy and permission to copy must be obtained directly from the author. All articles published prior to 1980 may be copied for a per-copy fee of US$ 2.25, also payable through the Center. This consent does not extend to other kinds of copying, such as for general distribution, resale, advertising and promotion purposes, or for creating new collective works. Special written permission must be obtained from the publisher for such copying.

Special regulations for authors. Upon acceptance of an article by the journal, the author(s) will be asked to transfer copyright of the article to the publisher. This transfer will ensure the widest possible dissemination of information.

general subjects

SAMPLE COPY

for additional information contact:

ALLIED/ELSEVIER JOURNALS
MARKETING GROUP
30, WEST COTT ROAD, Ph: 82468
MADRAS - 600 014./
750, MOUNT ROAD,
MADRAS - 600 002.

BBA

Biochimica et Biophysica Acta (G)

Managing Editors P Borst, P. Cohen,
K van Dam, L.L.M. van Deenen (Chairman),
E.P. Kennedy and G.K Radda

Honorary Managing Editor: E.C. Slater

Vol. 923, No. 1, pp. 1–166
January 20, 1987
Elsevier

ISSN 0006-3002
0304-4165
BBACAQ 923 (1) 1–166 (1987)
BBGSB3 923 (1) 1–166 (1987)

40 YEARS OF BBA!

PUBLICATION SCHEDULE FOR 1987

BBA is published according to a volume-numbering scheme that embraces all sections of the journal In addition, each regular section has its own sequential volume-numbering system, running parallel to the overall BBA scheme, as set out below.
Full subscription 42 volumes plus Cumulative Index 1986

	BIO-ENERGETICS	BIO-MEMBRANES	GENE STRUCTURE AND EXPRESSION	PROTEIN STRUCTURE AND MOLECULAR ENZYMOLOGY	LIPIDS AND LIPID METABOLISM	GENERAL SUBJECTS	MOLECULAR CELL RESEARCH	BBA REVIEW SECTIONS
	6 volumes [a]	11 volumes [b]	3 volumes	6 volumes	6 volumes	4 volumes	5 volumes	3 volumes
Jan	890-1 = B80-1	896-1 = M145-1 896-2 = M145-2	908-1 = N17-1	911-1 = P39-1 911-2 = P39-2	917-1 = L82-1 917-2 = L82-2	923-1 = G126-1	927-1 = C17-1	BBA REVIEWS ON BIOENERGETICS
Feb	890-2 = B80-2 890-3 = B80-3	897-1 = M146-1 897-2 = M146-2		911-3 = P39-3	917-3 = L82-3	923-2 = G126-2	927-2 = C17-2 927-3 = C17-3	895-1 = BR15-1
March	891-1 = B81-1	897-3 = M146-3 898-1 = M147-1	908-2 = N17-2	912-1 = P40-1 912-2 = P40-2	918-1 = L83-1 918-2 = L83-2	923-3 = G126-3	928-1 = C18-1	895-2 = BR15-2 895-3 = BR15-3
April	891-2 = B81-2	898-2 = M147-2 898-3 = M147-3	908-3 = N17-3	912-3 = P40-3	918-3 = L83-3	924-1 = G127-1	928-2 = C18-2	
May	891-3 = B81-3	899-1 = M148-1 899-2 = M148-2		913-1 = P41-1 913-2 = P41-2	919-1 = L84-1 919-2 = L84-2	924-2 = G127-2	928-3 = C18-3	BBA REVIEWS ON BIOMEMBRANES
June	892-1 = B82-1 892-2 = B82-2	900-1 = M149-1 900-2 = M149-2	909-1 = N18-1	913-3 = P41-3	919-3 = L84-3	924-3 = G127-3	929-1 = C19-1 929-2 = C19-2	906-1 = MR16-1 906-2 = MR16-2
July	892-3 = B82-3	901-1 = M150-1 901-2 = M150-2	909-2 = N18-2	914-1 = P42-1 914-2 = P42-2	920-1 = L85-1 920-2 = L85-2	925-1 = G128-1	929-3 = C19-3	906-3 = MR16-3
Aug	893-1 = B83-1	902-1 = M151-1 902-2 = M151-2	909-3 = N18-3	914-3 = P42-3	920-3 = L85-3	925-2 = G128-2	930-1 = C20-1	BBA REVIEWS ON CANCER
Sept	893-2 = B83-2	902-3 = M151-3 903-1 = M152-1	910-1 = N19-1	915-1 = P43-1 915-2 = P43-2	921-1 = L86-1 921-2 = L86-2	925-3 = G128-3	930-2 = C20-2	907-1 = CR14-1 907-2 = CR14-2
Oct	893-3 = B83-3	903-2 = M152-2 903-3 = M152-3	910-2 = N19-2	915-3 = P43-3	921-3 = L86-3	926-1 = G129-1	930-3 = C20-3	907-3 = CR14-3
Nov	894-1 = B84-1 894-2 = B84-2	904-1 = M153-1 904-2 = M153-2		916-1 = P44-1 916-2 = P44-2	922-1 = L87-1 922-2 = L87-2	926-2 = G129-2	931-1 = C21-1 931-2 = C21-2	
Dec	894-3 = B84-3	905-1 = M154-1 905-2 = M154-2	910-3 = N19-3	916-3 = P44-3	922-3 = L87-3	926-3 = G129-3	931-3 = C21-3	

[a] This includes BBA Reviews on Bioenergetics, Vol 895 [b] This includes BBA Reviews on Biomembranes, Vol 906

Authors should submit their manuscripts (four copies) for publication in BIOCHIMICA ET BIOPHYSICA ACTA by sending them to one of the Managing Editors.

Dr. P Borst, c/o BBA Editorial Secretariat, P O. Box 1345, 1000 BH Amsterdam, The Netherlands
Dr P Cohen, Department of Biochemistry, Medical Sciences Institute, University of Dundee, Dundee, DD1 4HN, U K
Dr K van Dam, c/o BBA Editorial Secretariat, P O Box 1345, 1000 BH Amsterdam, The Netherlands
Dr L L M van Deenen, c/o BBA Editorial Secretariat, P O Box 1345, 1000 BH Amsterdam, The Netherlands
Dr. E P Kennedy, c/o BBA Editorial Secretariat (Boston), Box C 9123, Brookline, MA 02146, U S A
Dr G K. Radda, Department of Biochemistry, University of Oxford, South Parks Road, Oxford, OX1 3QU, U K

Detailed information for contributors may be found in Biochim Biophys Acta 715 (1982) 1–23, also published as the 1982 edition of the booklet
INFORMATION FOR CONTRIBUTORS TO BIOCHIMICA ET BIOPHYSICA ACTA
which is available free of charge from the BBA Editorial Secretariat

---

Subscription information

1987 BBA General Subjects, Volumes 923–926 (4 volumes in 12 issues) Dfl. 980 (US$ 435 50) + Dfl 100 (US$ 44.50) postage, packaging and handling Total price Dfl. 1080 (US$ 480 00).
1987 BBA full subscription, Volumes 890–931 (42 volumes in 120 issues) Dfl 7812 (US$ 3472 00) + Dfl. 1050 (US$ 467 00) postage, packaging and handling Total price Dfl 8862 (US$ 3939.00)
The Dutch guilder price is definitive The U S dollar price is subject to exchange-rate fluctuations and is given only as a guide
Journals are sent by surface delivery to all countries, except the following countries where SAL air delivery (Surface Airlifted Mail) is ensured U.S.A , Canada, Japan, Australia, New Zealand, P R China, India, Israel, South Africa, Malaysia, Singapore, South Korea, Taiwan, Pakistan, Hong Kong, Brazil, Argentina, Mexico and Thailand Airmail rates for other countries are available on request
Subscription orders can be entered only by calendar year (Jan -Dec.) and should be sent to Elsevier Science Publishers, Journals Department, P.O Box 211, 1000 AE Amsterdam, The Netherlands, Telex 18582 ESPA NL, or to your usual subscription agent
Claims for missing issues should be made within 3 months of publication, otherwise they cannot be honoured free of charge. The Publisher reserves the right to issue additional volumes during the course of the year. Such volumes will be invoiced before publication and delivered after receipt of payment.
In the U S A and Canada for further information contact Elsevier Science Publishers, Journal Information Center, 52 Vanderbilt Avenue, New York, NY 10017, U.S.A., Tel (212) 370-5520

Biochimica
et Biophysica Acta

BIOCHIMICA
ET BIOPHYSICA ACTA

MANAGING EDITORS

L.L.M. van Deenen (Utrecht)
(Chairman)
P. Borst (Amsterdam)
P. Cohen (Dundee)
E.P. Kennedy (Boston, MA)
G.K. Radda (Oxford)
K. van Dam (Amsterdam)

HONORARY MANAGING EDITOR

E.C. Slater (Southampton)

EDITORS

H.R.V. Arnstein (London)
J. Barber (London)
I. Björkhem (Huddinge)
B. Borgström (Lund)
J. Brachet (Brussels)
J. Bremer (Oslo)
R. Burgess (Madison, WI)
E. Carafoli (Zürich)
J.E. Cleaver (San Francisco, CA)
C. Crane-Robinson (Portsmouth)
J.W. Daly (Bethesda, MD)
E.A. Dawidowicz (Boston, MA)
B. de Kruijff (Utrecht)
J.G. Demaille (Montpellier)
J.J.H.M. de Pont (Nijmegen)
B. Deuticke (Aachen)
K.T. Douglas (Colchester)
S. Ebashi (Tokyo)
L. Ernster (Stockholm)
S. Ferguson (Birmingham)
I. Fridovich (Durham)
F. Gibson (Canberra)
W.B. Gratzer (London)
M. Hamberg (Stockholm)
T.E. Hardingham (London)
J.L. Harwood (Cardiff)
E. Heinz (Dortmund)
E.J.M. Helmreich (Würzburg)
F. Hofmann (Homburg)
M.D. Houslay (Glasgow)
R.C. Hughes (London)
J.B. Jackson (Birmingham)
P. Jollès (Paris)
P.L. Jørgensen (Aarhus)
Y. Kagawa (Tochigi)
K.-A. Karlsson (Gothenburg)
M. Kates (Ottawa)
J. Kay (Cardiff)
Y. Kaziro (Tokyo)
R. Kinne (Dortmund)
C. Klee (Bethesda, MD)
A. Kleinzeller (Philadelphia, PA)
P. Läuger (Constance)
A.G. Lee (Southampton)
D.M. Lee (Oklahoma City, OK)
F. Maley (Albany, NY)
D. Marsh (Göttingen)
V. Massey (Ann Arbor, MI)
D.J. Morré (West Lafayette, IN)
J.F. Morrison (Canberra)
L.E. Mortenson (Athens, GA)
G. Nelsestuen (St. Paul, MN)
D.G. Nicholls (Dundee)
Y. Nishizuka (Kobe)
R.C. Nordlie (Grand Forks, ND)
S. Numa (Kyoto)
C. Pace-Asciak (Toronto)
P.G.W. Plagemann (Minneapolis, MN)
I. Ragan (Harlow)
P. Randle (Oxford)
A. Razin (Jerusalem)
A.M. Scanu (Chicago, IL)
H.J. Schatzmann (Bern)
G.L. Scherphof (Groningen)
J. Seelig (Basel)
N. Sharon (Rehovot)
G.G. Shipley (Boston, MA)
D. Shugar (Warsaw)
W.D. Stein (Jerusalem)
J.M. Tager (Amsterdam)
T. Taniguchi (Tokyo)
J.P. Thornber (Los Angeles, CA)
I. Tinoco (Berkeley, CA)
K.F. Tipton (Dublin)
I.P. Trayer (Birmingham)
I. Trowbridge (San Diego, CA)
C.L. Tsou (Beijing)
D.E. Vance (Edmonton)
H.J. van Gorkom (Leiden)
T. Vänngård (Gothenburg)
B.R. Velthuys (Gif-sur-Yvette)
A. Watts (Oxford)
C. Weissman (Zürich)
R.J.P. Williams (Oxford)
R.G. Williamson (London)
C. Wraight (Urbana, IL)
K. Wüthrich (Zürich)
R.F.A. Zwaal (Maastricht)

ELSEVIER SCIENCE PUBLISHERS B.V.
AMSTERDAM

BIOCHIMICA
ET BIOPHYSICA ACTA

INTERNATIONAL JOURNAL OF BIOCHEMISTRY AND BIOPHYSICS

general subjects

923 (1987)
(G126)

ELSEVIER SCIENCE PUBLISHERS B.V.
AMSTERDAM

PUBLICATION SCHEDULE FOR 1987

BBA is published according to a volume-numbering scheme that embraces all sections of the journal In addition, each regular section has its own sequential volume-numbering system, running parallel to the overall BBA scheme, as set out below
Full subscription 42 volumes plus Cumulative Index 1986

	BIO-ENERGETICS 6 volumes [a]	BIO-MEMBRANES 11 volumes [b]	GENE STRUCTURE AND EXPRESSION 3 volumes	PROTEIN STRUCTURE AND MOLECULAR ENZYMOLOGY 6 volumes	LIPIDS AND LIPID METABOLISM 6 volumes	GENERAL SUBJECTS 4 volumes	MOLECULAR CELL RESEARCH 5 volumes	BBA REVIEW SECTIONS 3 volumes
Jan	890-1 = B80-1 890-2 = B80-2	896-1 = M145-1 896-2 = M145-2	908-1 = N17-1	911-1 = P39-1 911-2 = P39-2	917-1 = L82-1 917-2 = L82-2	923-1 = G126-1	927-1 = C17-1	BBA REVIEWS ON BIOENERGETICS
Feb	890-3 = B80-3	897-1 = M146-1 897-2 = M146-2		911-3 = P39-3	917-3 = L82-3	923-2 = G126-2	927-2 = C17-2	895-1 = BR15-1
March	891-1 = B81-1	897-3 = M146-3 898-1 = M147-1	908-2 = N17-2	912-1 = P40-1 912-2 = P40-2	918-1 = L83-1 918-2 = L83-2	923-3 = G126-3	927-3 = C17-3 928-1 = C18-1	895-2 = BR15-2 895-3 = BR15-3
April	891-2 = B81-2	898-2 = M147-2 898-3 = M147-3	908-3 = N17-3	912-3 = P40-3	918-3 = L83-3	924-1 = G127-1	928-2 = C18-2	BBA REVIEWS ON BIOMEMBRANES
May	891-3 = B81-3	899-1 = M148-1 899-2 = M148-2		913-1 = P41-1 913-2 = P41-2	919-1 = L84-1 919-2 = L84-2	924-2 = G127-2	928-3 = C18-3	
June	892-1 = B82-1 892-2 = B82-2	900-1 = M149-1 900-2 = M149-2	909-1 = N18-1	913-3 = P41-3	919-3 = L84-3	924-3 = G127-3	929-1 = C19-1	906-1 = MR16-1 906-2 = MR16-2
July	892-3 = B82-3	901-1 = M150-1 901-2 = M150-2	909-2 = N18-2	914-1 = P42-1 914-2 = P42-2	920-1 = L85-1 920-2 = L85-2	925-1 = G128-1	929-2 = C19-2 929-3 = C19-3	906-3 = MR16-3
Aug	893-1 = B83-1	902-1 = M151-1 902-2 = M151-2	909-3 = N18-3	914-3 = P42-3	920-3 = L85-3	925-2 = G128-2	930-1 = C20-1	BBA REVIEWS ON CANCER
Sept	893-2 = B83-2	902-3 = M151-3 903-1 = M152-1	910-1 = N19-1	915-1 = P43-1 915-2 = P43-2	921-1 = L86-1 921-2 = L86-2	925-3 = G128-3	930-2 = C20-2	907-1 = CR14-1 907-2 = CR14-2
Oct	893-3 = B83-3 894-1 = B84-1	903-2 = M152-2 903-3 = M152-3	910-2 = N19-2	915-3 = P43-3	921-3 = L86-3	926-1 = G129-1	930-3 = C20-3	907-3 = CR14-3
Nov	894-2 = B84-2	904-1 = M153-1 904-2 = M153-2		916-1 = P44-1 916-2 = P44-2	922-1 = L87-1 922-2 = L87-2	926-2 = G129-2	931-1 = C21-1 931-2 = C21-2	
Dec	894-3 = B84-3	905-1 = M154-1 905-2 = M154-2	910-3 = N19-3	916-3 = P44-3	922-3 = L87-3	926-3 = G129-3	931-3 = C21-3	

[a] This includes BBA Reviews on Bioenergetics, Vol 895 [b] This includes BBA Reviews on Biomembranes, Vol 906

© 1987, Elsevier Science Publishers B.V (Biomedical Division)

All rights reserved. No part of this publication may be reproduced, stored in a retrieval system, or transmitted, in any form or by any means, electronic, mechanical, photocopying, recording or otherwise, without the prior written permission of the publisher, Elsevier Science Publishers B V (Biomedical Division), P O Box 1527, 1000 BM Amsterdam, The Netherlands. Submission of a paper to this journal entails the author's irrevocable and exclusive authorization of the publisher to collect any sums or considerations for copying or reproduction payable by third parties (as mentioned in article 17 paragraph 2 of the Dutch Copyright Act of 1912 and in the Royal Decree of June 20, 1974 (S. 351) pursuant to article 16b of the Dutch Copyright Act of 1912) and/or to act in or out of Court in connection therewith

Special regulations for readers in the U.S A This journal has been registered with the Copyright Clearance Center, Inc Consent is given for copying of articles for personal or internal use, or for the personal use of specific clients This consent is given on the condition that the copier pays through the Center the per-copy fee stated in the code on the first page of each article for copying beyond that permitted by Sections 107 or 108 of the U.S Copyright Law. The appropriate fee should be forwarded with a copy of the first page of the article to the Copyright Clearance Center, Inc., 27 Congress Street, Salem, MA 01970, U.S A If no code appears in an article, the author has not given broad consent to copy and permission to copy must be obtained directly from the author. All articles published prior to 1980 may be copied for a per-copy fee of US$ 2 25, also payable through the Center This consent does not extend to other kinds of copying, such as for general distribution, resale, advertising and promotion purposes, or for creating new collective works Special written permission must be obtained from the publisher for such copying.

Special regulations for authors Upon acceptance of an article by the journal, the author(s) will be asked to transfer copyright of the article to the publisher This transfer will ensure the widest possible dissemination of information.

Printed in The Netherlands

Biochimica et Biophysica Acta: 40 years on

Professor H.G.K. Westenbrink

Professor E.C. Slater

Biochimica et Biophysica Acta, the first truly international journal in the field of biochemistry and biophysics, and now undoubtedly one of the largest, is celebrating its 40th anniversary with this issue.

The journal was founded in 1947 by Professor H.G.K. Westenbrink, who remained Managing Editor of the journal until 1964. He was succeeded by Professor E.C. Slater, who was able to fulfil this function until his recent retirement as Chairman of the Board of Managing Editors. Professor Slater was encouraged to write a history of BBA, recalling its remarkably rapid growth and some of the intricacies involved in the journal's birth and early development [1].

On the auspicious occasion of the journal's 40th birthday, the Publisher would like to take the opportunity of thanking all those who have played an active role in the journal's development, and looks forward to further stimulating developments over subsequent decades.

The photograph of E.C. Slater is reproduced by permission of Godfrey Argent, U.K., photographers.

[1] *Biochimica et Biophysica Acta: The Story of a Biochemical Journal* by E.C. Slater (1986) Elsevier Science Publishers, ISBN 0-444-80769-1; Price Dfl.75.00.

Biochimica et Biophysica Acta 923 (1987) 1–7
Elsevier

BBA 22268

Evidence for the glycoprotein nature of vitamin K-dependent carboxylase from rat liver

Tom Brody * and John W. Suttie

Department of Biochemistry, College of Agricultural and Life Sciences, University of Wisconsin-Madison, Madison, WI 53706 (U.S.A.)

(Received 1 September 1986)

Key words: Lectin, Vitamin K-dependent carboxylase; Prothrombin; Glycoprotein

The ability of the rat liver microsomal vitamin K-dependent carboxylase and microsomal precursors of prothrombin and other vitamin K-dependent proteins to bind to lectin gels has been determined. Under denaturing conditions which dissociate precursor substrates from the carboxylase enzyme, prothrombin precursors and microsomal proteins labeled in γ-carboxyglutamate residues with [^{14}C]bicarbonate were nearly quantitatively bound to concanavalin A gels. When lentil lectin gels were used, only about one third of these proteins were bound, suggesting a heterogeneity of this glycoprotein pool. Under non-denaturing conditions, both precursor proteins and vitamin K-dependent carboxylase activity were retained on either concanavalin A or lentil lectin gels. These data are consistent with an increase in lectin binding determinants in the precursor-carboxyase complex and are evidence for the glycoprotein nature of this microsomal enzyme.

Introduction

The hepatic vitamin K-dependent carboxylase catalyzes the posttranslational carboxylation of specific glutamyl residues to form γ-carboxyglutamyl (Gla) residues. The enzyme is localized in the rough endoplasmic reticulum and appears to be an integral membrane protein [1]. The natural protein substrates for this enzyme are precursors of prothrombin and other vitamin K-dependent proteins, and a fraction of this precursor pool is tightly bound to the carboxylase. This association can be readily demonstrated by the ability of immobilized antibodies raised against prothrombin or Factor X to bind the carboxylase in an active form [2–5].

Precursors of vitamin K-dependent clotting factors accumulate when vitamin K function is blocked [2,6]. Both the membrane-associated fractions of the prothrombin precursor pools and a fraction that is readily released following membrane permeabilization have been shown to be glycoproteins [7]. A number of microsomal membrane proteins such as hydroxymethylglutaryl-CoA reductase [8,9], cytochrome *P*-450 [10], ribophorin [11], prostaglandin endoperoxide synthetase [12], and several separated but unidentified proteins [13,14] have been shown to be glycoproteins. Attempts to purify the vitamin K-dependent carboxylase have had limited success [2,5,15–17], and little is known of the properties of this pro-

---

* Present address: Medical University of South Carolina, Department of Anatomy, P.O. Box 12559, Charleston, SC 29412, U.S.A

Abbreviation: Gla, γ-carboxylglutamyl.

Correspondence: Prof. J.W Suttie, Department of Biochemistry, University of Wisconsin-Madison, Madison, WI 53706, U.S A.

0304-4165/87/$03 50 © 1987 Elsevier Science Publishers B V. (Biomedical Division)

tein. The nature of any carbohydrate attached to the carboxylase or its substrates has, therefore, been investigated by their association with immobilized lectins.

Materials and Methods

Chemicals. Triton X-100 was from RPI Research Products International (Elk Grove Village, IL). Concanavalin A-Sepharose 4B (Con A-Sepharose) and lentil lectin-Sepharose 4B were from Pharmacia Fine Chemicals (Uppsala, Sweden). The tripeptide substrate t-Boc-Glu-Glu-Leu-OMe was from Vega Fox Biochemicals (Tucson, AZ), and concanavalin A, methyl α-mannoside (grade III) and *E. carinatus* venom were from Sigma (St. Louis, MO). The chromogenic substrate S-2238 was from Kabi Diagnostics (Stockholm, Sweden). $NaH^{14}CO_3$ (60 mCi/mmol) and NCS tissue solubilizer were from Amersham/Searle (Arlington Heights, IL). Aquasol and Econofluor were from New England Nuclear (Boston, MA).

Microsomes. Male Holtzman rats (250–300 g) were given warfarin (5 mg/kg, i.p.), fasted overnight, and killed 18 h later. Livers were minced and homogenized in 2 vol. 0.25 M sucrose/25 mM imidazole-HCl (pH 7.0)/1 mM dithiothreitol at 2°C using a Teflon Potter-Elvehjem homogenizer. Microsomes were isolated as described previously [18], stored in liquid nitrogen, thawed, and resuspended with a Dounce homogenizer in a volume of added buffer identical to the original volume of post-mitochondrial supernatant.

Microsomes to be used as a source of solubilized vitamin K-dependent carboxylase were resuspended in 1 M KCl/1 mM dithiothreitol/25 mM imidazole-HCl (pH 7.0) at 2°C and repelleted by ultracentrifugation to remove contaminating proteins [19]. Pellets were solubilized in 0.5 M KCl/10% glycerol/1 mM dithiothreitol/25 mM imidazole-HCl (pH 7) (buffer A) containing 1% Triton X-100 for 30 min at 2°C and then centrifuged ($6.3 \cdot 10^6$ g · min) to remove a small pellet.

Microsomes were permeabilized by suspension in 80 mM KCl/0.25 M sucrose/1 mM dithiothreitol/25 mM imidazole-HCl (pH 7.0) (buffer B) containing 0.4% Triton X-100 for 20 min at 2°C followed by ultracentrifugation to separate the cisternal contents from the extracted membranes. The cisternal contents were then brought to 0.5 M NaCl and 2% Triton X-100 by adding salt crystals and a small volume of 25% Triton X-100. The extracted membranes were solubilized in 2% Triton/0.5 M NaCl/10% glycerol/1 mM dithiothreitol/25 mM imidazole-HCl (pH 7.0) (buffer C) at 2°C.

Intact microsomes were radiolabeled in Gla residues by suspending in buffer B and adding 0.18 mCi sodium [^{14}C]bicarbonate and 120 μg vitamin KH_2/ml of suspension. After incubation for 30 min at 17°C, the reaction mixture was cooled to 2°C and 0.1 M sodium bicarbonate was added. Microsomes were pelleted, washed again in bicarbonate, suspended in 20 mM dithiothreitol and 25 mM Tris-HCl (pH 8.0) containing 1% SDS at room temperature and placed in a boiling water bath for 5 min. An aliquot of the hot clear solubilized material was removed and mixed thoroughly with 5 vol. 0.5 M NaCl/10% glycerol/2 mM dithiothreitol/25 mM imidazole-HCl (pH 7.0) at room temperature containing 8% Triton X-100.

Radiolabeled microsomes were also solubilized under non-denaturing conditions using buffer C containing 1% Triton X-100. After clarification solutions were diluted in 5 vol. buffer C containing 8% Triton X-100.

Lectin-gel chromatography. Chromatography was carried out as describedi n the figure legends. Concanavalin A-gels were discarded after use. Lentil lectin gels were washed in 10% methyl α-mannoside, rinsed thoroughly with 0.25 M KCl/25 mM imidazole-HCl (pH 7)/1 mM $MnCl_2$/1 mM $CaCl_2$/0.2 mM merthiolate, stored wet at 4°C, and reused. Radioactivity in eluted fractions was determined by adding 2 mg albumin and 3 ml 10% trichloroacetic acid to a 1 ml aliquot and centrifuging for 2 h at 5000 × g. When the eluted fractions containing 2% Triton X-100 pellets were solubilized in 1 ml NCS solubilizer and 12 ml Econofluor and when 8 or 12% Triton was present, pellets were solubilized in 1 ml NCS and 12 ml Aquasol. These mixtures were stored at room temperature in the dark for a week in order to eliminate chemiluminescence before radioactivity was determined by liquid scintillation spectrometry.

Microsomal prothrombin precursors and vitamin K-dependent carboxylase assays. Microsomal prothrombin precursors were measured by incubating detergent-solubilized microsomes with *E. carinatus* venom followed by the addition of D-Phe-L-pipecolyl-L-Arg *p*-nitroanilide (S-2238). The product of the amidolytic reaction was measured by the absorbance at 405 nm. The procedure was that of Bertina et al. [20] as modified for use with microsomal protein by Shah et al. [21.22]. Amidolytic activity was shown to be linear over the period used for assay for both cisternal and membrane-bound precursor activity.

Vitamin K-dependent carboxylase activity was assayed in incubation mixtures containing 25–200 μl solubilized enzyme, 50 μl 10 mM tripeptide, 10 μl [^{14}C]-bicarbonate (20 μCi), 25 μl 0.2 M MnCl$_2$, 100 μl heat-denatured microsomes [23], 10 μl 15 mM vitamin KH$_2$ in ethanol, and supplementary buffer. The supplementary buffer was used to bring reaction mixtures to 0.5 M KCl/15% glycerol/1 mM dithiothreitol/25 mM imidazole-HCl (pH 7.0). The final volume was 0.5 ml and incubations were for 30 min at 17°C. Reactions were terminated with 2 ml 10% trichloroacetic acid. Radioactivity incorporated into tripeptide (peptide carboxylase) and into protein (protein carboxylase) was measured according to Suttie et al. [24].

Results

When Triton-solubilized microsomes were mixed with immobilized lectin gels, over 80% of the carboxylase activity was removed by concanavalin A and about 70% by lentil lectin Table I). This association was prevented when the buffer contained 10% methyl α-mannoside. The enzyme was active when bound to the immobilized lectins, and when concanavalin A gels were resuspended in the standard incubation mixture, about 80% of the original enzyme activity was bound to the gel, with remaining activity in the supernatant (Table II. Protein carboxylase activity was also bound in high yields, suggesting that nearly all carboxylatable precursors in solution are bound to the enzyme. Free precursors in the solubilized microsomal preparation would be expected to adhere to sites on the concanavalin A gel remote from sites binding carboxylase and would be unavailable to the glutamate substrate binding site of the enzyme. When soluble concanavalin A (2–6 mg/ml) was mixed with Triton-solubilized microsomal protein (6 mg/ml) prior to mixing with the concanavalin A-Sepharose 4B, enzyme binding was prevented (data not shown), indicating that the binding was specific for the affinity ligand rather than the column support.

TABLE I

BINDING OF VITAMIN K-DEPENDENT CARBOXYLASE TO IMMOBILIZED LECTIN GELS

Binding experiments were conducted by mixing 0.3 ml enzyme solubilized with 1% Triton in buffer A (glycerol) or in buffer A containing 10% methyl α-mannoside rather than glycerol with 0.3 cm^3 of concanavalin A gel, or 0.7 ml of enzyme with 1.0 cm^3 of lentil lectin gel Mixtures were agitated over the course of 15 min at 2°C, followed by centrifugation Results from vitamin K-dependent caboxylase assays of 100 μl supernatnats were used to express the binding data.

Expt.	Gel	Carboxylase activity (dpm×10^{-4})		Percent bound [a]
		methyl α-mannoside	glycerol	
A	Concanavalin A	5.9	1.02	83
B	Concanavalin A	5.2	0.66	87
C	Lentil lectin	1.6	0.53	67
D	Lentil lectin	1.3	0.35	73

[a] Amount of activity recovered in the presence of methyl α-mannoside that is removed when glycerol-containing buffer was used Recovery of enzyme in methyl α-mannoside incubations was 85–100%.

The Triton-solubilized preparation used in Ta-

TABLE II

VITAMIN K-DEPENDENT CARBOXYLASE ACTIVITY FOLLOWING CONCANAVALIN A GEL TREATMENT

Binding experiments were conducted by mixing 0.2 ml enzyme solubilized in buffer A containing 1% Triton X-100 with 2.0 of buffer A containing 0.5% Triton X-100 and 0.2 cm^3 of concanavalin A gel. Association was permitted for 1 h followed by centrifugation. Assays contained 100 μl unfractionated protein, 0.2 ml supernatants, or the 0.2 cm^3 concanavalin A gel in a total assay volume of 0.5 cm^3. Vitamin K-dependent carboxylation of Boc-Glu-Glu-Leu-OMe (peptide) or endogenous microsomal proteins (protein) was carried out

Expt.	Gel-bound activity, %		Non-bound activity, %	
	peptide	protein	peptide	protein
A	81.8	76.7	24.9	26.0
B	75.2	75.7	23.5	21.5

bles I and II contained complexes of precursor proteins and carboxylase [2,4,5], and lectin binding could have been due to association with either component. The ability of free precursor protein to bind to these gels was, therefore, assessed. Prothrombin precursors were derived from the cisternal contents of microsomes by extraction with buffer containing 0.4% Triton and 80 mM KCl [16]. This material contained only 3% of the total carboxylase activity of unextracted microsomes. When this precursor preparation was analyzed for glycoprotein content by fractionation on lentil lectin gel in the presence of 2% Triton, one third of the recovered activity was specifically bound (Fig. 1A). Where the non-binding material was reloaded on a concanavalin A gel, fully 70% of the material was specifically bound in the absence (Fig. 1B and C), but not in the presence of methyl α-mannoside. Thus, at least 90% of cisternal content prothrombin precursor acts as a glycoprotein, but the different lectin associations suggest that there are two pools.

In contrast to the low association of the cisternal content precursor activity to a lentil lectin gel, nearly 80% of the membrane-associated precursor activity bound to this gel and could be eluted with methyl α-mannoside (Fig. 1D). Again, about 75% of the material not bound to a lentil lectin gel could be bound to concanavalin A in the absence, but not in the presence, of methyl α-mannoside (Fig. 1E and 1F).

Similar results were obtained when microsomal precursors were labeled by incubation with vitamin K and $H^{14}CO_3^-$. When labeled material was solubilized in SDS and fractionated on a concanavalin A gel in the presence of buffer containing 10% glycerol, the recovery of radioactivity was only 14%, but where binding was prevented by 10% methyl α-mannoside the recovery was 80% (Fig. 2A and B). When this material was chromatographed on a lentil lectin gel, only 35% of the radioactivity bound to the gel in a manner that could be displaced by methyl α-mannoside (Fig. 2C). When the microsomes were solubilized with Triton only, which would leave precursor-carboxylase complexes intact, 65% of the radioactivity was specifically bound to he lentil lectin gel in the absence, but not in the presence, of methyl α-mannoside (Fig. 2C).

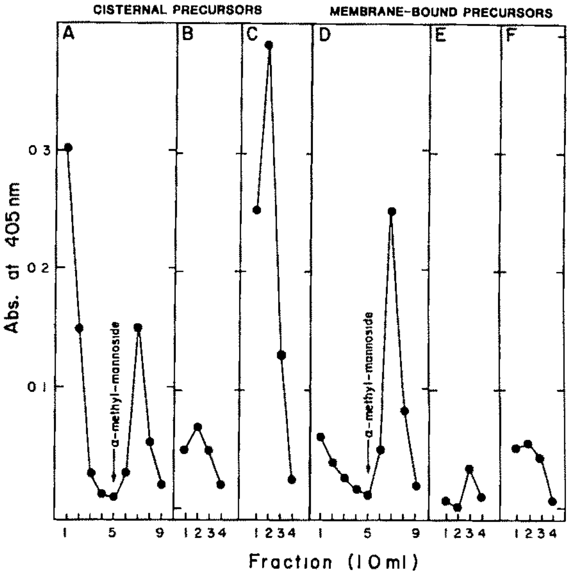

Fig. 1. Chromatography of cisternal content and membrane-bound prothrombin precursors on lectin gels. Cisternal (panel A) or memrbane-bound (panel D) prothrombin precursor extracts were prepared and 0.45 ml loaded on 1.25 cm^3 lentil lectin gels. The extract was washed with 0.55 ml buffer C, washed with 4×1.0 ml buffer C, and then developed with 4×1.0 ml buffer C containing 10% methyl α-mannoside rather than 10% glycerol. Total recovery of column A was 88%, and 128% of column D. Separations were conducted in quadruplicate to provide enough non-binding activity needed for rechromatography. The non-binding material (fraction 1, 1.5 ml) of column A was mixed with 150 mg sucrose, loaded on a 1.0 cm^3 concanavalin A column (B), and developed with buffer C, or mixed with 150 mg methyl α-mannoside, loaded on a concanavalin A column (C), and developed with buffer C containing 10% methyl α-mannoside. Recoveries were 21% for column B and 87% for column C. Fraction 1 of column D was fractionated in a similar manner on columns E and F with recoveries of 26% and 86%.

Further evidence that the prothrombin precursor was tightly complexed to the carboxylase under non-denaturing conditions was obtained by assessing the binding of ^{14}C-labeled precursors and vitamin K-dependent carboxylase activity to lentil lectin gels developed with different concentrations of methyl α-mannoside (Table III). Recovery of carboxylase activity from gels eluted with 0% methyl α-mannoside was only 23%, confirming the observation that the carboxylase enzyme binds well to lectin gels. Low concentrations of methyl α-mannoside increased the recovery. However, repeated attempts to develop these columns with a continuous gradient of methyl α-mannoside resulted in a progressive loss of carboxylase activity.

Specificity and reproducibility of the binding properties of the carboxylase and of prothrombin precursors were assessed by rechromatography (Fig. 3). When Triton solubilized ^{14}C-labeled precursors were applied to a lentil lectin gel, about 50% of the adsorbed radioactivity was eluted with 0.06% methyl α-mannoside and 50% with 10% of the sugar (Fig. 3A). When the material eluting with 0.06% methyl α-mannoside was dialyzed and reapplied to the column, less than 10% failed to adsorb and over 70% was again eluted with 0.06% methyl α-mannoside (Fig. 3A). Similar results were seen when the SDS-solubilized material was rechromatographed. A predominant elution at 10% methyl α-mannoside was also observed (data not shown) when the material eluting at 10% methyl α-mannoside was dialyzed and rechromatographed. Failure of a fraction of the ^{14}C-labeled material to bind was not due to saturation of binding sites on the lectin column, as material not

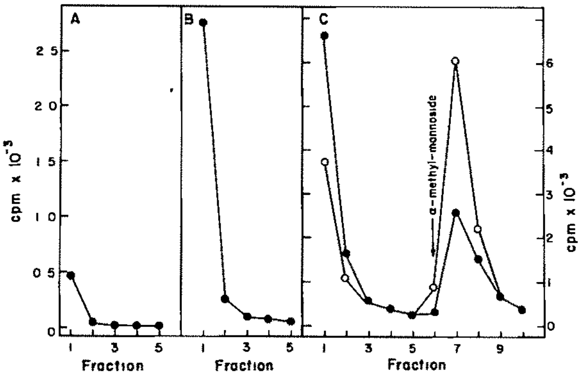

Fig. 2. Chromatography of ^{14}C-labeled precursors on lectin gels. Microsomal suspensions were labeled, dissolved in SDS, and diluted into a buffer containing 8% Triton X-100 Suspensions diluted in buffer containing 10% glycerol were loaded on concanavalin A column A, and suspensions diluted in buffer containing 10% methyl α-mannoside were loaded on concanavalin A column B. The columns were equilibrated and eluted with the same buffers. ^{14}C-labeled microsomes were also dissolved in the absence of SDS and the elutions of this material (○) and the SDS-denatured material (●) from a lentil lectin gel were compared in C. The columns were washed with buffer containing 10% glycerol and developed with buffer containing 10% methyl α-mannoside

TABLE III

CHROMATOGRPAHY OF VITAMIN K-DEPENDENT AND TRITON-SOLUBILIZED ^{14}C-LABELLED PRECURSORS ON LENTIL LECTIN GELS IN THE PRESENCE OF VARIOUS CONCENTRATIONS OF METHYL α-MANNOSIDE

Microsomes were solubilized in buffer A containing 1% Triton X-100 and 0.3 ml (1.8 mg) protein mixed with 3.0 ml of a column buffer consisting of 0.5 M KCl/0.4% Triton X-100/25 mM imidazole-HCl/1 0 mM MnCl$_2$/1 mM CaCl$_2$/1 mM dithiothreitol (pH 7.0)/10% glycerol. Columns (1 0 cm^3) were eluted with 6×0.6 ml of the same buffer containing the glycerol and methyl α-mannoside concentrations indicated. Carboxylase activity and recovery of radioactivity from proteins labeled with vitamin K and H^{14}CO$_3^-$ were determined. Recovery is calculated as the sum of all of the fractions collected compared to the activity added to the column.

Elution buffer		Recovery of carboxylase activity, %	Recovery of ^{14}C-labeled protein, %
methyl α-mannoside, %	glycerol, %		
0	10	23.3	32 2
0.03	10	32.6	44.2
0.06	10	41.9	53.2
0.12	10	50.8	64.0
10	0	64.1	75.6

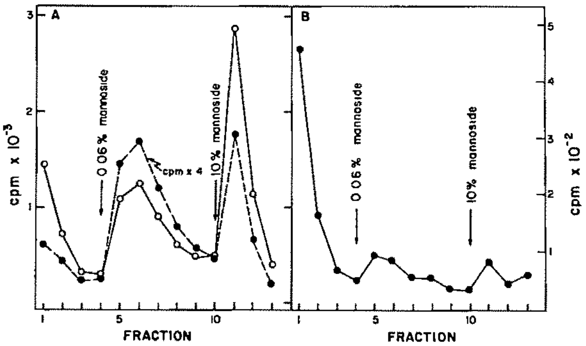

Fig. 3. Chromatography of Triton-solubilized ^{14}C-labeled precurosrs on lentil lectin gels Microsomal suspensions were labeled and solubilized in Triton X-100. (A) The sample (1.8 ml) was washed into the column with 1 ml buffer C containing 8% Triton and then developed with 8× 1.0 ml of this buffer with 0 06% mannoside added followed by 4×1 0 ml of a buffer where 10% methyl α-mannoside replaced the glycerol (○). Unfractionated proteins were chromatographed on lentil lectin gels in quadruplicate in order to accumulate enough separated material for rechromatography. Material eluting in fraction 6 (15% of total) was dialyzed overnight against buffer C containing 8% Triton at 4°C, reloaded on a fresh gel, and developed as before (●------●). (B) Non-binding ^{14}C-labeled protein recovered in fraction 1 (8% of total) was loaded on a fresh gel and the column developed as before.

adsorbed to the column passed through when loaded on a fresh gel (Fig. 3B).

Discussion

Prothrombin precursors accumulate in the crude liver microsomal fraction when vitamin K action is blocked, and can be separated into a membrane-bound pool which can be labeled by the vitamin K-dependent carboxylase in vitro and a lumenal pool which is a poor substrate for this enzyme. Studies with tunicamycin-treated rats [4] have demonstrated the glycoprotein nature of the prothrombin precursor pool, and the present lectin binding studies have confirmed and extended these studies to the entire ^{14}C-carboxylatable precursor pool. The membrane fraction of this pool could be followed by specific labeling with [^{14}C]bicarbonate, while the cisternal content prothrombin pool was detected by *E. carinatus*-generated thrombin. Although SDS-denatured ^{14}C-labelled precursors and cisternal content prothrombin precursors were shown to be glycoproteins by chromatography on concanavalin A gels, these precursors bound poorly to lentil lectin gels, indicating the absence of some oligosaccharide determinants needed to bind to this lectin. Concanavalin A binds oligosaccharide moieties of a variety of glycopeptides and glycoproteins [25–27], and lentil gels differ from concanavalin A gels in that their lectin protein density is less than that of concanavalin A gels and their oligosacchride binding specificity differs from that of concanavalin A gels [28].

Lentil lectin gel chromatography in the presence of Triton X-100 and varying methyl α-mannoside concentrations indicated that the microsomal vitamin K-dependent clotting factor precursors consist of a pool of heterogeneous glycoproteins. The basis of this heterogeneity may be related to the fact that certain clotting factors, such as bovine plasma prothrombin, contain three N-linked oligosaccharide chains, whereas others such as plasma Factor X contain only one chain [29].

In contrast to the decreased binding of precursors to lentil lectin as compared to concanavalin A gels, carboxylase-precursor complexes prepared under non-denaturing conditions bound with essentially equal affinity to the two lectins, suggesting that additional determinants are present in these preparations. The most consistent interpretation of these data is that the vitamin K-dependent carboxylase itself is a glycoprotein and furnishes the additional determinants. The nature of the oligosaccharide involved cannot be determined from these studies.

Proteins which bind to lentil lectin gels contain the N-linked core oligosaccharide, $\mathrm{Man_9Glc_3(GlcNAc)_2}$ [30]. It is unlikely that these oligosaccharides are modified by the presence of sialic acid, galactosamine, or fucose, as the appropriate monosaccharide transferases [31] and substrate transport systemes [32] are highly enriched in the Golgi. However, fucose linked to the *N*-acetylglucosamine at the protein terminus has been shown to be a determinant for binding of glycopeptides to lentil lectin gel [28], raising the possibility that the lentil lectin gel-binding proteins described here may contain fucose. Sialic acid and fucose [13,33] have been shown to be components of integral microsomal membrane proteins, and Boulan et al. [34] have claimed that lentil lectin binds to sites in the rough endoplasmic reticulum that are different from concanavalin A binding sites. A more detailed analysis of the nature of the carbohydrate composition of this microsomal enzyme will depend on purification, and the interactions with immobilized lectins demonstrated here should be useful in these efforts.

Acknowledgements

This work is supported by the College of Agricultural and Life Sciences of the University of Wisconsin-Madison and in part by grants AM-14881 and DE-07031 and postdoctoral fellowship HL-06554 from the National Institutes of Health, Bethesda, MD.

References

1 Suttie, J.W (1985) Annu. Rev. Biochem 54, 459–477

2 De Metz, M , Vermeer, C., Soute, B A.M., Van Scharrenburg, G J.M , Slotboom, A J. and Hemker, H.C. (1981) FEBS Lett. 123, 215–218

3 De Metz, M., Vermeer, C., Soute, B A.M. and Hemker, H.C (1981) J. Biol Chem 256, 10843–10846

4 Swanson, J.C. and Suttie, J.W. (1982) Biochemistry 21, 6011–6018

5 Olson, R.E., Hall, A L , Lee, F.C., Kappel, W.K , Meyer, R.G. and Bettger, W.J. (1983) in Vitamin K-dependent Carboxylase; A Heme Protein (Johnson, B C , ed), pp. 295–316, Academic Press, Inc , New York

6 Suttie, J.W. (1973) Science 179, 192–194

7 Swanson, J C and Suttie, J W. (1985) Biochemistry 24, 3890–3897

8 Liscum, L., Cummings, R.D , Anderson, R.G., Demartino, G N., Goldstein, J.L. and Brown, M.D. (1983) Proc Natl. Acad Sci. USA 80, 7165–7169

9 Brown, D.A. and Simoni, R.D. (1984) Proc. Natl Acad Sci. USA 81, 1674–1678

10 Haugen, D.A and Coon, M J. (1976) J Biol Chem. 251, 7929–7939

11 Boulan, E.R., Sabatini, D.D , Pereyra, B N and Kreibich, G. (1978) J. Cell Biol 78, 894–909

12 Van der Ouderaa, F.J., Buytenhek, M., Nugteren, D.H. and Van dorp, D.A. (1977) Biochim. Biophys Acta 487, 315–331

13 Blackburn, G.R. and Kasper, C.B. (1976) J. Biol. Chem 251, 7699–7708

14 Li, Y -T , Li, S.-C. and Shetlar, M R. (1968) J Biol Chem. 243, 656–665

15 Wallin, R and Suttie, J.W (1982) Arch Biochem. Biophys. 214, 155–163

16 Canfield, L.M., Sinsky, T.A. and Suttie, J.W. (1980) Arch. Biochem Biophys 202, 515–524

17 Girardot, J.-M. (1982) J. Biol. Chem. 257, 15008–15011

18 Esmon, C.T. and Suttie, J.W (1976) J Biol. Chem. 251, 6238–6243

19 Weining, R.R., Manganiello, V C., Chiu, R and Phillips, A.H (1972) Biochemistry 11, 3128–3135

20 Bertina, R.M., Van der Marel-van Nieuwkoop, W. and Loeliger, E A (1979) Thromb. Haemostasis (Stuttg) 42, 1296–1305

21 Shah, D.V., Suttie, J W. and Grant, G A (1973) Arch. Biochem. Biophys 159, 483–491

22 Shah, D V., Swanson, J.C. and Suttie, J W. (1984) Thrombos. Res. 35, 451–458

23 Brody, T. and Suttie, J.W. (1984) Methods Enzymol 107, 552–563

24 Suttie, J W., Hageman, J.M , Lehrman, S.R. and Rich, D H. (1976) J. Biol Chem. 251, 5827–5830

25 Kornfeld, R. and Ferris, C. (1975) J Biol. Chem 250, 2614–2619

26 Ogata, S.-I., Muramatsu, T. and Kobata, A. (1975) J Biochem. (Tokyo) 78, 687–696

27 Baenziger, J.U and Fiete, D (1979) J Biol. Chem. 254, 2400–2407

28 Kornfeld, K , Reitman, M.L. and Kornfeld, R. (1981) J. Biol. Chem. 256, 6633–6640

29 Jackson, C.M. and Nemerson, Y. (1980) Annu. Rev Biochem 49, 765–811

30 Hubbard, S.C. and Ivatt, R J. (1981) Annu. Rev. Biochem. 50, 555–583

31 Munro, J.R , Narashimhan, S., Wetmore, S., Riordan, J R and Schachter, H. (1975) Arch. Biochem Biophys. 169, 269–277

32 Sommers, L.W and Hirschberg, C.B. (1982) J Biol. Chem. 257, 10811–10817

33 Phillips, J.L. (1973) Arch. Biochem. Biophys 191, 571–577

34 Boulan, E R , Kreibich, G. and Sabatini, D D. (1978) J Cell Biol. 78, 874–893

Biochimica et Biophysica Acta 923 (1987) 8–21
Elsevier

BBA 22443

Purification and properties of a human plasma endogenous modulator for the platelet tricyclic binding/serotonin transport complex

Kakkudiyil I. Abraham, John R. Ieni and Laurence R. Meyerson

Department of Chemical Pharmacology, American Cyanamid Company, Medical Research Division, Ramapo College of New Jersey, 505 Ramapo Valley Road, Mahwah, NJ 07430 (U.S.A.)

(Received 18 April 1986)
(Revised manuscript received 30 September 1986)

Key words: Endogenous modulator; Imipramine binding site; α_1-Acid glycoprotein; Serotonin uptake; (Human)

An endogenous modulator for the site labeled by [^{3}H]imipramine which is putatively coupled to the serotonin transporter in human platelets was isolated and purified from plasma. Procedures included sequential chromatography on Cibacron blue-Sepharose 4B, concanavalin A-Sepharose 4B, Mono Q HR 10/10 anion exchange, DuPont GF-250 gel permeation and Mono S HR 5/5 cation exchange columns. The purified modulator is a protein of M_r 45000 with a very acidic pK (less than 3) and sensitive to various proteinases but heat- and acid-stable. This protein inhibited [^{3}H]imipramine binding to platelet membranes competitively (IC$_{50} \approx 6$ μM) and enhanced serotonin uptake in fresh human platelets (EC$_{50} \approx 7$ μM). Various physico-chemical properties, including chromatographic, electrophoretic and immunological as well as amino acid composition analysis revealed that the isolated protein is most probably the human α_1-acid glycoprotein.

Introduction

The mechanism of serotonin translocation in neurons and platelets has been the subject of numerous investigations [1–3]. Platelet serotonin uptake has been used as a model for the neuronal system, since both brain and platelet share many biochemical and pharmacological processes [4,5]. Many tricyclic antidepressive agents are potent inhibitors of serotonin uptake [1]. Using a radiolabeled form of the antidepressant imipramine, a specific high affinity binding site on platelets [6,7] as well as in neuronal membranes [8] has been identified. This recognition site labeled by [^{3}H]imipramine has been shown to be distinct but allosterically coupled to the serotonin transporter [9–13]. Clinical studies of depressed patients have demonstrated alterations in the density of [^{3}H]imipramine binding and reduced platelet [^{3}H]serotonin uptake [14–16] suggesting dysfunction of the serotonin system in depressive illness.

Serotonin possesses profound peripheral vasoconstrictive properties mediated through the vascular S$_2$ receptor [17,18]. Agents like ketanserin through blockade of the S$_2$ receptor have been shown to be effective antihypertensive agents [17,18]. It is possible that modulation of peripheral serotonin availability can ultimately affect vasomotor tone.

Abbreviations: TRH, thyrotropin-releasing hormone; 8-OH-DPAT, 8-hydroxy-2-(di-*n*-propylamino)tetralin; SDS, sodium dodecyl sulphate.

Correspondence: Dr. L.R. Meyerson, American Cyanamid Company, Medical Research Division, Ramapo College of New Jersey, 505 Ramapo Valley Rd., Mahwah, NJ 07430, U.S.A.

0304-4165/87/$03.50 © 1987 Elsevier Science Publishers B.V. (Biomedical Division)

Since the [^{3}H]imipramine binding site allosterically modulates serotonin transport, the presence of endogenous effectors of this site seems plausible. Recently, several laboratories have searched for endogenous serotonin transport modulators. A few low molecular weight materials have been detected or partially purified from either human plasma or from rat brain or plasma [19–24]. In addition, 5-methoxy-, 6-methoxy-, or 6-hydroxytryptolines have been suggested as potential endogenous modulators of [^{3}H]imipramine binding and serotonin uptake [25,26]. However, 5-methoxytryptoline's role as an endogenous ligand for the [^{3}H]imipramine site has been questioned [22]. The small molecular weight compounds [19–26] reported thus far inhibit both serotonin uptake and [^{3}H]imipramine binding. The results presented herein demonstrate the isolation, purification and some physico-chemical properties of a glycoprotein from human plasma which in human platelets enhances serotonin uptake while inhibiting [^{3}H]imipramine binding.

Materials and Methods

Chemicals and pharmaceuticals

All reagents were of the highest grade commercially available. The radiochemicals [^{3}H]imipramine (44.2 Ci/mmol), 2-[^{3}H]nitroimipramine (87 Ci/mmol), [^{3}H]serotonin binoxalate (21.4 Ci/mmol), [^{3}H]prazosin (19.3 Ci/mmol), ^{3}H-labelled thyrotropin-releasing hormone (TRH) (76.7 Ci/mmol), [^{3}H]quinuclidinyl benzilate (30.1 Ci/mmol), and [^{3}H]flunitrazepam (77.4 Ci/mmol) were purchased from DuPont/New England Nuclear Corp. 8-[^{3}H]Hydroxy-2-(di-*n*-propylamino)tetralin (8-[^{3}H]OH-DPAT) (187 Ci/mmol) was obtained from Amersham Corp. Nonradioactive TRH was obtained from Peninsula Laboratories and 8-OH-DPAT from Research Biochemicals, Inc. Human α_1-acid glycoprotein was purchased from Sigma Chemical Co. Rabbit antiserum to human α_1-acid glycoprotein was obtained from Calbiochem-Behring. The enzymes trypsin, chymotrypsin, pepsin, papain and neuraminidase were purchased from Worthington Biochemical Corp.

Pharmaceutical agents were obtained from the following sources: fluoxetine (E. Lilly), imipramine and phentolamine (Ciba-Geigy), clonazepam (Hoffman-La Roche), and atropine sulphate (Sigma).

Chromatographic materials

Affigel Blue (Cibacron blue-Sepharose 4B, 50–100 mesh, 150–300 μ, capacity: 11.56 mg albumin/ml gel) was obtained from Bio-Rad Laboratories. Concanavalin A-Sepharose 4B (10 mg concanavalin A/ml of gel), Mono Q HR 10/10 anion exchange, Mono S HR 5/5 cation exchange and Mono P 5/20 chromatofocusing columns were purchased from Pharmacia. Bio-series GF-250 preparative gel permeation column was purchased from DuPont Corp.

Receptor binding assays

[^{3}H]Imipramine binding to platelet membranes was performed according to established procedures in our laboratory [27]. Fluoxetine at 10 μM final concentration was used to determine non-specific binding. [^{3}H]Quinuclidinyl benzilate binding to rat cortical membrane preparations using atropine sulphate to assess non-specific binding was performed according to the method of Yamamura and Snyder [28]. [^{3}H]Flunitrazepam binding to rat cortical membranes was performed according to established procedures [29]. The assay for [^{3}H]methyl-TRH binding to rat amygdala membranes was performed according to previous reports [30,31] using unlabeled TRH for assessment of non-specific binding. The α_1-adrenergic receptor assay was performed on rat cardiac membranes according to the method of Hoffman and Lefkowitz [32] using [^{3}H]prazosin and phentolamine for determining non-specific binding. 8-[^{3}H]OH-DPAT binding assay for serotonin-1 receptors was conducted according to the method of Hall et al. [33]. All the binding assays were carried out in the presence and absence of the endogenous modulator at stated concentrations.

Protein determination

Protein concentrations were determined utilizing the method of Bradford [34] (Bio-Rad Laboratories) with bovine gamma globulin as the standard.

Definition of unit

One unit of endogenous plasma modulator is defined as the activity that displaces 1000 dpm (approx. 10.2 fmol) of specific [^{3}H]imipramine binding under the assay conditions described above. Control specific binding is typically 651 ± 21 fmol of [^{3}H]imipramine per mg of platelet membranes.

Uptake of [^{3}H]serotonin into intact human platelets

[^{3}H]Serotonin uptake in human platelets was carried out in the presence and absence of the endogenous modulator according to the protocol described elsewhere [35]. Serotonin was used at 1 μM final concentration.

Plasma and platelet preparation

Fresh human platelet-rich plasma from whole blood collected in citrate-dextrose anticoagulant was obtained from the New York Blood Center (New York, NY) and further manipulated 12 h later following normal human disease testing human T-cell lymphotropic virus III antibody and hepatitis, etc.). Platelet-rich plasma was centrifuged at 2500 × *g* for 15 min at 4°C and the plasma supernatant was stored at −70°C until use for the isolation of the endogenous modulator. Intact platelets were prepared for serotonin uptake studies or processed into membranes for [^{3}H]imipramine binding assays (stored at −70°C until use) [35].

Purification of the endogenous modulator

The following paragraphs describe the sequences for isolation and purification of a putative endogenous modulator for the serotonin transport system. Activity at each step in the purification process was determined by the ability of the fractions to inhibit [^{3}H]imipramine binding to human platelet membranes in vitro.

Affigel Blue chromatography

Platelet-free plasma (40 ml) in 50 mM Tris-HCl buffer (pH 7.5)/0.65 M NaCl, was loaded on an Affigel Blue column (2.3 × 40 cm, 200 ml gel) which was pre-equilibrated with 50 mM Tris-HCl (pH 7.5)/0.5 M NaCl (flow rate; 60 ml/h). The column was then washed with 500 ml of starting buffer. The combined effluent (550 ml) was tested for activity. The adsorbed protein was eluted with 0.25 M NaSCN in 50 mM Tris-HCl buffer (pH 7.5) and dialyzed against 50 mM Tris-HCl (pH 7.5) and tested for activity.

Concanavalin A-Sepharose 4B chromatography

The combined unadsorbed effluent (550 ml) from the previous step was loaded on a concanavalin A-sepharose 4B column (2.3 × 20 cm, 100 ml gel), pre-equilibrated with 50 mM Tris-HCl/0.5 M NaCl (pH 7.5) (flow rate; 60 ml/h). The column was then washed with 200 ml of starting buffer. Both the effluent and washings (750 ml) were collected and combined. The adsorbed protein was eluted with 0.25 M methyl mannopyranoside in 50 mM Tris-HCl buffer (pH 7.5). All fractions were tested for activity. The combined effluent and washings (containing the activity) was brought to 90% saturation with ammonium sulphate at 4°C and the precipitated protein was collected by centrifugation at 48 000 × *g* for 15 min, dissolved in 20 mM Tris-HCl buffer (pH 7.5) and dialyzed against the same buffer. This dialyzed solution was centrifuged at 30 000 × *g* for 15 min to remove trace amounts of denatured protein and the supernatant (16 ml) was further processed.

FPLC on Mono Q HR 10/10 anion exchanger

A Waters chromatographic system consisting of two pumps (Model 510) programmed with an automatic gradient controller (Model 680), a U6K injector with a loop of 4 ml loading capacity, a variable wavelength UV monitor (Lamda Max Model 480) coupled with a data module (Model 730) was used along with a FRAC 100 fraction collector (Pharmacia) for the following chromatography steps.

The sample from the concanavalin A-Sepharose 4B column was loaded (4 ml sample was processed each time) on a Mono Q HR 10/10 column (1 × 10 cm, ionic capacity 0.27–0.37 mmol/ml) pre-equilibrated with 20 mM Tris-HCl buffer (pH 7.5) and subsequently washed with the same buffer at a flow rate of 4 ml/min. The adsorbed protein was eluted with 0–0.75 M NaCl linear gradient in the starting buffer. Fractions of 4 ml each were collected and assayed for activity.

Size exclusion chromatography on Bio-series GF-250 column

Active fractions from the anion exchange column step were pooled and processed by gel permeation chromatography on a DuPont Bio-series GF-250 preparative column (2.12 × 25 cm), preequilibrated with 200 mM sodium phosphate buffer (pH 7.4). 2 ml samples were processed each time and fractions of 2 ml each were collected (flow rate; 2 ml/min). The active fractions were combined from each run, desalted and equilibrated with 25 mM sodium acetate buffer (pH 7.5) using Pharmacia PD 10 desalting columns.

FPLC on Mono S HR 5/5 cation exchanger

A Mono S HR 5/5 cation exchange column (0.5 × 5 cm, ionic capacity 0.13–0.18 mmol/column) was equilibrated with 25 mM sodium acetate buffer (pH 5.5) and 8 ml samples from the previous step were loaded by repeated injection. The column was washed with the same buffer (flow rate; 1 ml/min) and the adsorbed protein was eluted using a linear gradient of 0–0.75 M NaCl. The collected fractions (1 ml each) were equilibrated with 50 mM Tris-HCl buffer (pH 7.5) using a Pharmacia PD 10 column, prior to being assayed for activity. Active fractions were pooled and processed for further physico-chemical analysis.

Amino acid analysis

Amino acid analysis was carried out using a Beckman 121 MB amino acid analyser. Dried protein samples were hydrolyzed for 24, 48 and 72 h in a gaseous HCl atmosphere according to the procedure described for the PicoTag system (PicoTag work station, Operators Manual, 1984, Waters Associates, Milford, MA).

Immunofixation protocol

Immunofixation was performed according to the procedure supplied by the manufacturer (Technical bulletin 015-246A, Beckman Instruments, 1984). Rabbit antiserum to human α_1-acid glycoprotein (0.38 mg/ml) was used as the antibody source and human α_1-acid glycoprotein was used as the reference standard.

Electrophoretic, photoaffinity labeling and fluorographic techniques

SDS-polyacrylamide gel electrophoresis was performed with gels of 10 or 12.5% acrylamide (30 : 0.8 acrylamide/bisacrylamide, w/w) according to Laemmli [36]. Photoaffinity crosslinking experiments with 2-[^{3}H]nitroimipramine were carried out in the presence or absence of the purified endogenous human plasma modulator according to established procedures [35]. Gels were impregnated with Enlightening (New England Nuclear) for 30 min, dried and exposed to Kodak X-OMAT AR film at −80°C as described by Laskey and Mills [37].

Equilibrium binding of [^{3}H]imipramine to human plasma endogenous modulator

Equilibrium binding of [^{3}H]imipramine to human endogenous modulator was carried out at 4°C using two different techniques. Using equilibrium dialysis, human plasma modulator (300 μg protein) in 0.5 ml 50 mM Tris-HCl buffer (pH 7.5)/120 mM NaCl/5 mM KCl was mixed with an equal volume of 4 nM [^{3}H]imipramine solution and dialyzed against 1 ml of starting buffer at 4°C, using Spectrapor dialysis membranes (M_r cutoff: 12000–14000). Control experiments were devoid of any modulator protein. Aliquots of 100 μl were taken from both compartments at time intervals and measured for radioactivity using standard liquid scintillation counting techniques.

The second method employed gel filtration. In these experiments, human plasma modulator (300 μg protein) in 50 mM Tris-HCl buffer (pH 7.5)/120 mM NaCl/5 mM KCl was incubated with 2 nM [^{3}H]imipramine (total volume, 750 μl) at 4°C for 1.5 h and passed through a Pharmacia PD 10 gel filtration column preequilibrated with the starting buffer. The initial 2.5 ml effluent (void volume) were discarded and the next 3.5 ml were collected and counted for modulator bound radioactivity.

Results

Effect of human plasma on [^{3}H]imipramine binding and [^{3}H]serotonin uptake

Addition of platelet-free plasma to platelet membranes inhibited [^{3}H]imipramine binding in a dose-dependent manner (Fig. 1), indicating the presence of a plasma-derived inhibitor. In contrast, enhanced [^{3}H]serotonin uptake in intact human platelets was observed in the presence of

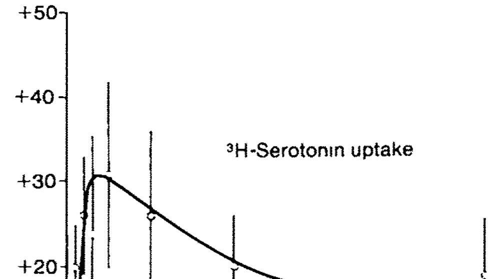

Fig 1 Effect of platelet-free plasma on [^{3}H]serotonin uptake in human platelets and [^{3}H]imipramine binding to human platelet membranes. Each data point represents mean ± S E values obtained from four separate experiments done in triplicate

small concentrations of platelet-free plasma (1–50 μl). The enhancement of [^{3}H]serotonin uptake at higher plasma concentrations (100–250 μl) was attenuated possibly due to the presence of endogenous plasma serotonin or another inhibitory modulator.

Chromatographic purification of the endogenous modulator

Cibacron blue-Sepharose 4B chromatography was adopted as the initial step since albumin, which represents approximately 50% of the total plasma proteins, is preferentially bound by this affinity gel matrix. The unadsorbed protein from this column, which contained 66% of the original activity, was not retained by a concanavalin A-Sepharose 4B column, even though this step removed some glycoproteins. Elution of the adsorbed protein from both the Cibacron blue-Sepharose 4B and concanavalin A-Sepharose 4B columns did not significantly inhibit platelet [^{3}H]imipramine binding. Removal of albumin and some glycoproteins in the first two chromatographic steps facilitated processing large amounts of the active protein on the subsequent Mono Q HR 10/10 column, even though there was loss of activity (Table I). This observed activity loss could have been due to removal of another plasma component which may inhibit or interfere with [^{3}H]imipramine binding. Alternatively, some modulator protein loss may have occurred during these purification steps.

Chromatography of the active fractions from the above step on a Mono Q HR 10/10 anion exchange column resulted in retention of all the active substance. The major amount of activity was eluted from this column at 0.25 M NaCl concentration (Fig. 2). The trailing of activity noticed throughout the chromatogram appears mainly due to interference of some proteins in the [^{3}H]imipramine binding assay.

Gel permeation chromatography of the above active fractions on a Bio-series GF-250 column resolved the proteins into two major species. All the imipramine binding inhibitory activity was associated with the second peak of $M_r \approx 46\,000$ (Fig. 3). The slight increase in total recovery units observed in this step (Table I) was most probably due to higher [^{3}H]imipramine binding in the presence of phosphate buffer.

The active fractions from the Bio-series GF-250 column were further chromatographed on a Mono S HR 5/5 cation exchange column, resulting in elution of a single active protein peak at 0.5 M NaCl concentration (Fig. 4). The trailing region of the 280 nm absorbance peak contained an inactive protein which was tenaciously bound to the column. This required prolonged washing with 0.75 M or 1.0 M NaCl for complete desorption.

An overall 115-fold purification of this modulator was achieved with 50% recovery by employing this purification scheme (Table I). This purified protein represents less than 1% of the total plasma proteins.

TABLE I

ISOLATION AND PURIFICATION OF A PLASMA ENDOGENOUS MODULATOR AND ITS EFFECTS ON IMIPRAMINE BINDING TO PLATELET MEMBRANES

One unit of endogenous plasma modulator is defined as the activity that displaces 1000 dpm (approx. 10.2 fmol) of specific [^{3}H]imipramine binding. See text for assay conditions Control specific binding is typically 651 ± 21 fmol of [^{3}H]imipramine per mg of platelet membranes. Each result represents one of several experiments done in an identical manner.

Step	Total activity (units)	Total protein (mg)	Percent recovery (units)	Specific activity (units/mg protein)	Purity (fold)
Platelet-free plasma	1781 6	2094 7	100.0	0 9	1.0
Cibacron blue-Sepharose 4B	1178 5	1042 2	66.2	1.1	1.3
Concanavalin A-Sepharose 4B	860.8	876.0	48.3	1 0	1 2
Mono Q HR 10/10	928 0	50 3	52.1	18.5	21.7
Bio-series GF-250	1196.0	23.5	67.1	50.9	59 8
Mono S HR 5/5	883.0	9 6	49.6	97 5	114.6

Purity

The purity of the active fractions at each stage of the chromatographic separations employed was assessed by SDS-polyacrylamide gel electrophoresis (Fig. 5). The purified modulator is a homogeneous band of $M_r \approx 42\,700$ according to this criterion. Rechromatography of this purified material resulted in a single symmetrical peak on the Bio-series GF-250 gel permeation column (Fig. 6A) and the Mono S HR 5/5 column (Fig. 6B).

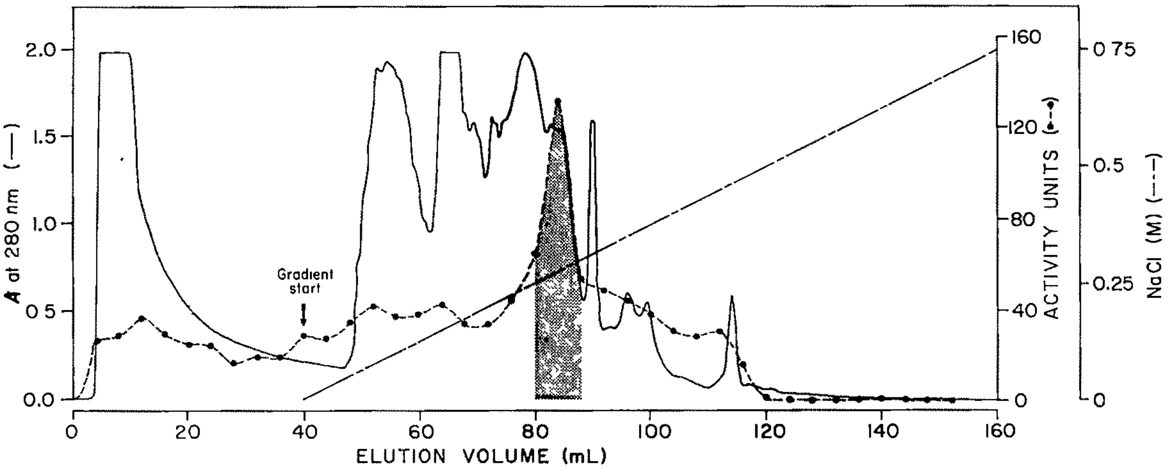

Fig. 2 Elution profile of human plasma endogenous modulator on FPLC anion exchange Mono Q HR 10/10 column. Active fraction from concanavalin A-Sepharose 4B step was loaded (4 ml) on a Mono Q HR 10/10 column (1 × 10 cm). The column was further washed with 36 ml 20 mM Tris-HCl buffer (pH 7.5), and then eluted with a gradient of 0–0.75 M NaCl in the starting buffer (4 ml fractions; flow rate, 4 ml/min). Protein was monitored at 280 nm and the activity (inhibition of [^{3}H]imipramine binding to platelet membranes) was measured for each fraction collected. Shaded area represents the active fractions pooled and processed for the next step. (———) protein; (●-----●) activity. This chromatographic profile represents one of several experiments done in an identical manner.

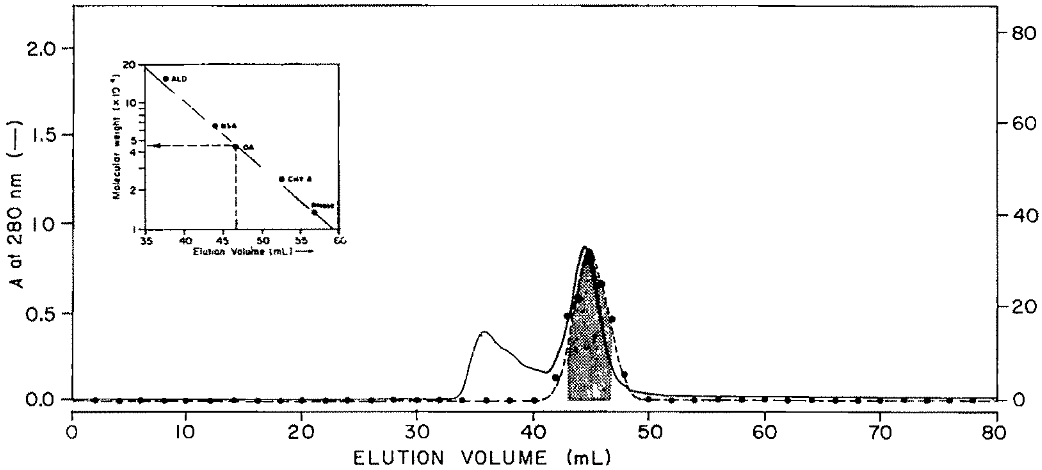

Fig 3. Gel permeation chromatograph of human plasma endogenous modulator on a Bio-series GF-250 column Active fractions of 2 ml each from the Mono Q HR 10/10 column were processed for gel permeation chromatography on a Bio-series GF-250 column (2 12×25 cm; 1 ml fractions; 2 ml/min) using 200 mM sodium phosphate buffer (pH 7.4) as an eluent Calibration of the columnn was accomplished using aldolase (ALD) (M_r 158000), bovine serum albumin (BSA) (M_r 68000), ovalbumin (OA) (M_r 45000), chymotrypsinogen-A (CHY-A) (M_r 25000), and ribonuclease (RNase) (M_r 13690) as standards. The relationship between log M_r vs elution volume is represented as an inset The endogenous modulator has a molecular mass of 46000 daltons. Shaded area represents the active fractions pooled and processed for the next step (———) protein; (●-----●) activity. This chromatographic profile represents one of several experiments done in an identical manner.

Physico-chemical properties

The purified modulator was sensitive to proteolytic enzyme digestion by chymotrypsin, papain

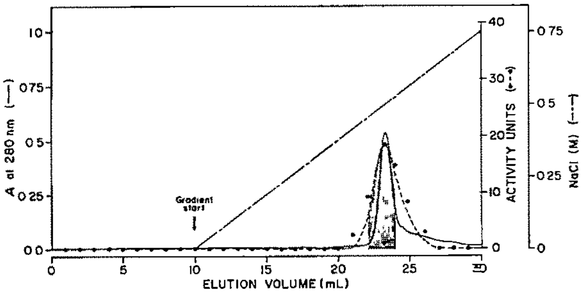

Fig. 4. Elution profile of human plasma endogenous modulator on FPLC cation exchange Mono S HR 5/5 column. Active fractions of 8 ml each from the gel permeation chromatography step were processed on a Mono S HR 5/5 column (0 5×5 cm; preequilibrated with 25 mM sodium acetate buffer, pH 5.5). The column was washed with 10 ml of starting buffer and the adsorbed protein was eluted using a linear gradient of 0–0.75 M NaCl (1 ml fractions; flow rate, 1 ml/min). Shaded area represents the active fractions pooled and processed for the physico-chemical studies. (———) protein; (●-----●) activity. This chromatographic profile represents one of several experiments done in an identical manner.

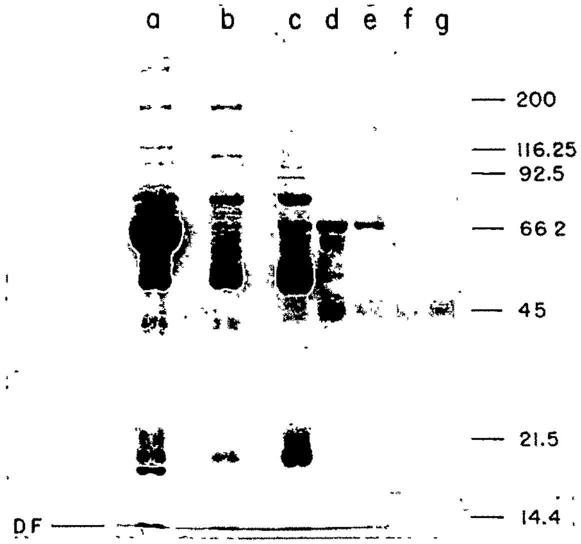

Fig 5. SDS-polyacrylamide gel electrophoresis pattern of human plasma endogenous modulator at various stages of purification. SDS-polyacrylamide gels (10%) were stained with Coomassie brilliant blue Each of the lanes represents the following. (a) platelet-free plasma; (b) Affigel Blue active fraction; (c) concanavalin A-Sepharose 4B active fraction; (d) pooled active fractions of Mono Q HR 10/10 column; (e) Bio-series GF-250 active fractions (pooled); (f,g) pooled active fractions of Mono S HR 5/5 column (5 and 10 µg each). Numbers on the right side represents relative positions of molecular mass standards in kilodaltons This electrophoretic pattern represents one of several experiments done in an identical manner.

TABLE II

EFFECTS OF SELECTED TREATMENTS OF THE PURIFIED PLASMA ENDOGENOUS MODULATOR ON ITS INHIBITION OF $[^3H]$IMIPRAMINE BINDING

Endogenous modulator treatment conditions ($n = 3$ experiments)	Percent displacement of specific $[^3H]$imipramine binding (mean ± S.E.)
Control [a]	57.7±3.9
Trypsin [b]	56.6±4.7
Chymotrypsin [b]	27.5±4.0
Papain [b]	0.0±5.1
Pepsin [b]	0.0±4.8
Neuraminidase [b]	2.8±4.4
25 mM H_2SO_4 (pH 1.8, 80°C, 1 h) [c]	35.3±3.2
Cyanogen bromide [d]	0.0±8.6
Heat stability (98°C, 10 min)	57.7±3.9
Acid stability (pH 1.0, 10 min) [c]	47.8±1.6

[a] Control $[^3H]$imipramine binding assay was done in the presence of untreated human plasma endogenous modulator. See text for assay conditions.

[b] The endogenous modulator was treated with these enzymes in a 25:1 w/w ratio for 4 h at 37°C. These enzymes were further inactivated by heating at 98°C for 10 min.

[c] After exposure to acid conditions the pH was adjusted to 7.5 using dilute NaOH.

[d] After treatment with CNBr, the acid and CNBr were removed by repeated lyophilization, and the residue was reconstituted in the binding buffer.

TABLE III

AMINO ACID ANALYSIS OF PURIFIED HUMAN PLASMA ENDOGENOUS MODULATOR

Cysteine and tryptophan contents were not estimated. Sample 1 represents purified human plasma endogenous modulator and sample 2 is authentic human α_1-acid glycoprotein obtained commercially.

Amino acid	Number of residues/mol protein [a]	
	sample 1	sample 2
Asp	43	45
Thr [b]	33	34
Ser [b]	15	16
Glu	68	66
Pro	11	13
Gly	16	16
Ala	18	18
Val	14	14
Met	2	2
Ile	19	19
Leu	32	31
Tyr	22	20
Phe	21	20
His	7	7
Lys	31	29
Arg	19	17

[a] Based on a molecular mass of 43000 daltons.

[b] Corrected for destruction during acid hydrolysis by extrapolating to zero time.

TABLE IV

EFFECT OF THE ENDOGENOUS MODULATOR ON DIFFERENT RECEPTOR SYSTEMS

Conditions for the the various receptor binding assays are detailed in the Materials and Methods section.

Receptor ligand	Control binding (fmol/mg protein)	Percent inhibition at different modulator concentration		
		5 μM	10 μM	20 μM
Imipramine (allosteric, serotonin transport)	651±21	46.2±1.1	70.4±1.1	82.0±0.4
Quinuclidinyl benzilate (muscarinic-cholinergic)	666±30	5.2±0.7	5.5±2.5	19.1±3.5
Flunitrazepam (benzodiazepine)	48± 1	0.0±0.8	0.0±0.9	0.0±1.1
8-OH-DPAT (serotonin-1)	255±15	8.8±3.4	17.3±0.4	24.8±0.5
Prazosin (α_1-adrenergic)	100±10	7.3±1.8	14.9±1.7	25.8±4.4
TRH (peptidergic)	96± 7	0.0±1.0	0.0±1.8	0.0±1.5

and pepsin, but insensitive to trypsin (Table II). In addition, the purified protein was stable to heat (98°C, 10 min) and exposure to acidic pH conditions (pH 1.0, 10 min). This protein was also sensitive to sialic acid removal by neuraminidase as well as cleavage at methionine residues by cyanogen bromide (Table II).

Analysis of total amino acid content of this

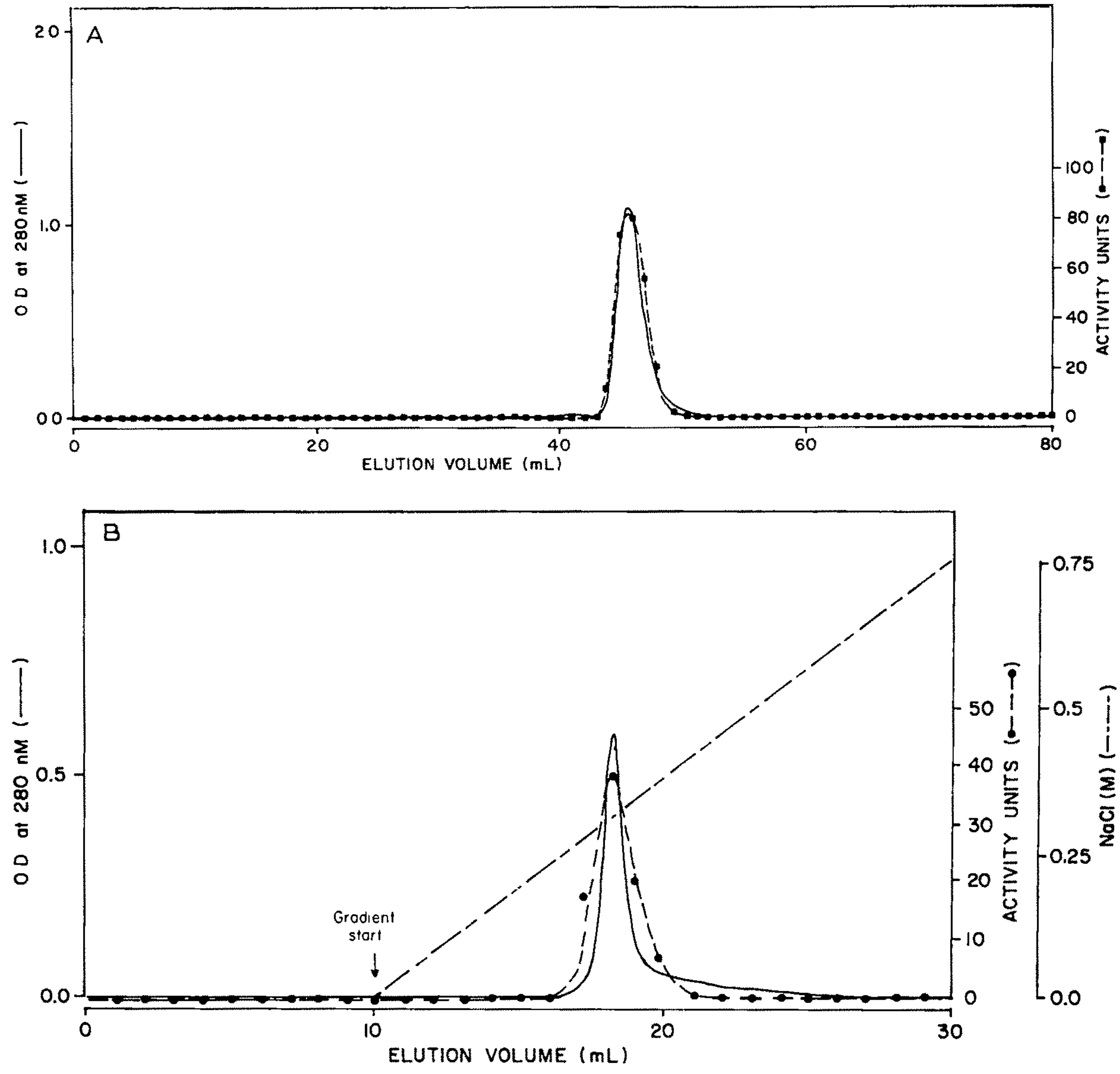

Fig 6 (A) Rechromatography of the purified human plasma endogenous modulator on a Bio-series GF-250 column. The purified fraction from the Mono S HR 5/5 column (approx. 230 units of activity) was processed for rechromatography on a Bio-series GF-250 column (2.12×25 cm, 1 ml fractions; flow rate, 2 ml/min) using 200 mM sodium phosphate buffer (pH 7.4) as an eluent. (———) protein; (●------●) activity. This chromatographic profile represents one of several experiments done in a similar manner (B) Rechromatography of the purified human plasma endogenous modulator on a Mono S HR 5/5 column. The purified fraction from a Mono S HR 5/5 column (approx. 90 units of activity) was processed for rechromatography on the same column under identical conditions (1 ml fractions; flow rate, 1 ml/min. (———) protein; (O------O) activity. This chromatographic profile represents one of several experiment done in a similar manner.

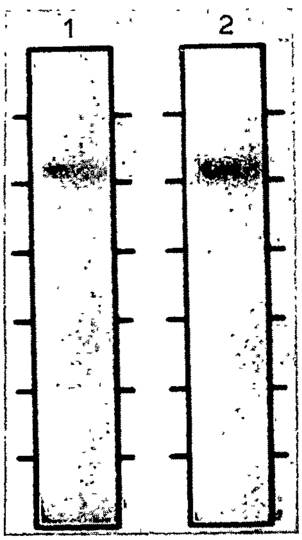

Fig. 7 Immunological cross-reactivity of human α_1-acid glycoprotein antibody to human endogenous modulator. Immunofixation gel of (1) purified human plasma endogenous modulator (approx. 0.4 μg) and (2) authentic human α_1-acid glycoprotein (approx 0 4 μg). This immunofixation gel represents one of several experiments done in an identical manner.

modulator protein and human α_1-acid glycoprotein is presented in Table III. Both the isolated protein and human α_1-acid glycoprotein show close similarity in the number of residues/mol of protein. Both these proteins contain a relatively high content of the acidic amino acids, aspartic acid and glutamic acid.

Examination of immunological cross-reactivity of rabbit α_1-acid glycoprotein antibody with the purified modulator and authentic human α_1-acid glycoprotien is represented in Fig. 7. Both proteins displayed a single reactive band of identical mobility in this immunofixation gel.

Equilibrium binding of [^{3}H]imipramine to the purified endogenous plasma modulator was performed using both equilibrium dialysis and gel filtration. Less than 6% (10–18 μmol [^{3}H]imipramine/mol protein) of the total ligand concentration in the standard assay mixture was observed to bind the endogenous protein at 4°C using both techniques (data not shown).

Photo-crosslinking 2-[^{3}H]nitroimipramine to human platelet membranes was found to label a protein of 30 000 daltons which was specifically displaced by excess cold fluoxetine, confirming our previous report [35]. Inclusion of the purified plasma modulator protein in the photo-crosslinking reaction mixture inhibited the crosslinking of 2-[^{3}H]nitroimipramine to the 30 000 dalton protein. In addition, 2-[^{3}H]nitroimipramine did not photo-crosslink with purified endogenous modulator protein (data not shown).

Effect of purified modulator on various receptor systems

The specificity of this purified protein was determined by observing its effects on various (receptor) binding sites (Table IV). Apart from imipramine binding or the serotonin uptake process, this purified protein had modest to minimal effects on other receptor systems tested. Scatchard analysis of platelet [^{3}H]imipramine saturation isotherms (Fig. 8) in the presence of 5.6 μM purified protien yielded a K_d of 7.5 ± 0.8 nM and B_{max} of 1258 ± 205 fmol/mg protein ($n = 3$). In contrast,

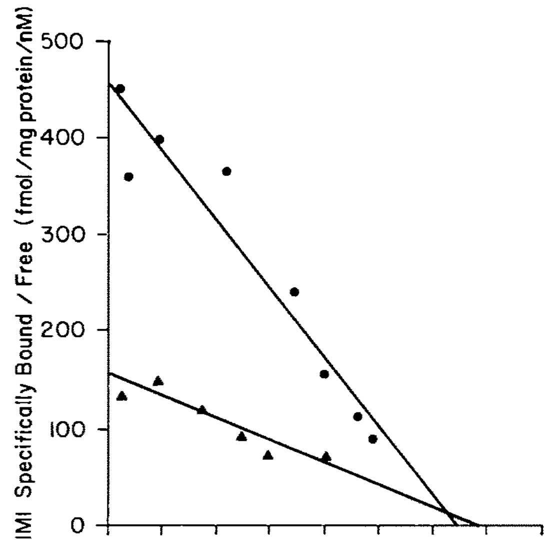

Fig. 8 Scatchard analysis of platelet [^{3}H]imipramine ([^{3}H]IMI) binding saturation isotherms in the presence of purified human plasma endogenous modulator. Each data point represents an average of triplicate determinations in a single experiment. (●——●) control: K_d 2.9 nM, B_{max} 1298 fmol/mg protein; (▲——▲) plus 5 6 μM purified human plasma endogenous modulator: K_d 8.8 nM, B_{max} 1362 fmol/mg protein. The mean ± S.E. values for K_d and B_{max} derived from three experiments are given in the result section

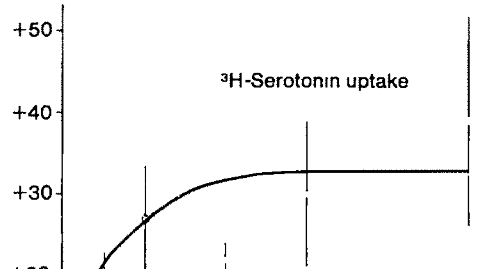

Fig. 9 Effects of increasing concentrations of endogenous modulator on human platelet [^{3}H]serotonin uptake and [^{3}H]imipramine binding Each data point represents the mean ± S.E. value of five separate experiments for [^{3}H]serotonin uptake and four separate experiments for [^{3}H]imipramine binding done in triplicate

control binding yielded a K_d of 2.2 ± 0.4 nM and B_{max} of 1226 ± 142 fmol/mg protein ($n = 3$). The observed 3-fold increase in K_d without alteration of the B_{max} value by the presence of the purified modulator protein suggests a competitive type of inhibition. An IC_{50} value of 5.8 μM and Hill coefficient of 1.4 were determined for the endogenous modulator by competition in the [^{3}H]imipramine binding assay. The Hill coefficient greater than unity may reflect positive cooperativity or allosterism.

The effects of the purified endogenous modulator on [^{3}H]imipramine binding and serotonin uptake are shown in Fig. 9. The binding of [^{3}H]imipramine to human platelets was almost completely inhibited by the isolated endogenous modulator protein at concentrations approaching 40–60 μM. In contrast, similar concentrations of the endogenous modulator increased the rate of [^{3}H]serotonin uptake into human platelets (EC_{50} ≈ 7 μM) with a maximum stimulation of about 30%. Unlike the effects of platelet-free plasma on [^{3}H]serotonin uptake, the purified modulator only enhanced the uptake process. Thus, in crude plasma, there probably is another component which inhibits [^{3}H]imipramine binding and reduces [^{3}H]serotonin uptake.

Discussion

The present report describes the isolation of an endogenous modulator from human plasma which inhibits imipramine binding to whole platelets or membranes and enhances serotonin uptake in platelets. Through a series of affinity, ion exchange and gel permeation chromatographic procedures, the protein was purified and appeared to be homogeneous by SDS-polyacrylamide gel electrophoresis and rechromatography on gel permeation and cation exchange columns. A molecular mass of 42 700 daltons obtained for this modulator under denaturing conditions of SDS-polyacrylamide gel electrophoresis is in close agreement with the value obtained by Bio-series GF-250 gel permeation chromatography (46 000 daltons), suggesting that this modulator is a single polypeptide.

Attempts to purify and/or determine the isoelectric point of this protein by chromatofocusing on a Mono P HR 5/20 column was unsuccessful due to its extreme acidic nature (pI < 3). The acidic nature may be partly due to sialic acid residues associated with this macromolecule. Treating this protein with neuraminidase or 0.025 N H_2SO_4 to desialate resulted in a slightly faster migration on SDS-polyacrylamide gel electrophoresis (M_r 38 000–40 000) (data not shown). Studies are under way to estimate the total sialic acid content of this protein.

The proteinaceous nature of this plasma modulator was established by its sensitivity to various proteinases (chymotrypsin, papain, pepsin) as well as by cleavage at methionine residues with cyanogen bromide. Since desialysation by neuraminidase or acid treatment abolished/reduced the inhibitory activity in the [^{3}H]imipramine binding assay, sialic acid residues probably play a key role in the maintenance of activity. Part of this protein's unique nature is its stability at elevated temperature (98°C). This effect may be due to stabilization by associated carbohydrates. Treatment of this protein with trypsin resulted in negligible loss of activity, which could be due either to its resistance to tryptic digestion or to generation of an active tryptic peptide. Analysis of such a situation has not yet been carried out.

Apart from the inhibition of [^{3}H]imipramine binding and stimulation of serotonin uptake in platelets, this modulator had modest to minimal effects on other receptor systems tested, suggesting a high degree of preference for the serotonin transporter complex. The presence of the endogenous modulator resulted in increased total serotonin uptake, without affecting non-specific serotonin uptake (determined in the presence of 10 μM fluoxetine, a specific serotonin uptake inhibitor). Therefore, the stimulation of serotonin uptake by this endogenous modulator does not appear to be a non-specific effect caused by alteration of the platelet membrane.

Scatchard analysis of [^{3}H]imipramine binding saturation isotherms in the presence of this endogenous modulator showed competitive kinetics. Hill analysis of displacement assays revealed an IC_{50} in the low micromolar range and Napp of 1.4 which suggests positive cooperativity or allosterism. The IC_{50} for the modulator is in the physiological concentration range of α_1-acid glycoprotein found in human plasma (0.5–1.2 mg/ml) [38]. Since previous reports have demonstrated that α_1-acid glycoprotein can bind [^{3}H]imipramine at 37°C [39,40], the question arose whether the inhibition of [^{3}H]imipramine binding observed in the present study was due to depletion or chelation of ligand during the binding assay incubation. Evaluation of this potential effect was performed using two different techniques, equilibrium dialysis and gel filtration chromatography. Negligible amounts of [^{3}H]imipramine (assayed at 2 nM [^{3}H]imipramine) were observed to bind to this modulator protein at 4°C. Photolabeling of the 30000 dalton protein of human platelet membranes by 2-[^{3}H]nitroimipramine was found to be inhibited by the presence of physiologically relevant levels of the purified human plasma endogenous modulator protein. These experiments in conjunction with kinetic analyses suggest a direct interaction of this modulator protein with platelet membrane site labeled by [^{3}H]imipramine.

Cross-reactivity to rabbit antibody raised against human α_1-acid glycoprotein revealed that this isolated protein shares antigenic determinants similar to authentic human α_1-acid glycoprotein. The amino acid content of this modulator protein was found to be quite similar to human α_1-acid glycoprotein. All other characteristics such as chromatographic behaviour, electrophoretic migration, and various physico-chemical properties were found to be quite similar for the modulator protein and human α_1-acid glycoprotein. Our initial attempts to determine the N-terminal amino acid sequence of this protein and α_1-acid glycoprotein using gas phase sequencing were unsuccessful since both proteins appear to have blocked N-terminal residues.

Several other investigators [19–24] have partially purified low molecular weight substances from rat brain, rat plasma or human plasma which inhibit [^{3}H]imipramine binding, and suggested their possible roles in modulating serotonin uptake. All these low molecular weight substances inhibit serotonin uptake [19–24], in contrast to the present report. This is particularly noteworthy since in previous reports, Wennogle and Meyerson [9,10], Meyerson et al. [13] and Briley et al. [12] presented evidence that the [^{3}H]imipramine binding site is allosterically coupled to the serotonin uptake site. This modulator most probably acts at the recognition site labeled by [^{3}H]imipramine. Occupation of the site by α_1-acid glycoprotein is likely to activate the serotonin uptake process allosterically.

Whether α_1-acid glycoprotein is a modulator of the central nervous system serotonin uptake process is currently unknown. Having a molecular mass of approximately 43000 daltons, this protein probably does not pass through the blood-brain barrier. Therefore, synthesis of α_1-acid glycoprotein within the brain would be essential for any modulatory activity on the brain serotonin uptake process. However, no demonstration of the existence of α_1-acid glycoprotein within the central nervous system has been reported. Thus, though α_1-acid glycoprotien has demonstrated modulatory effects on peripheral serotonin transport, its putative effects in the brain remain to be determined.

The physiological role of α_1-acid glycoprotein is unclear. Clinical data exist showing increased levels of this protein during stress, inflammation, malignancy and various hematologic conditions [41]. One function of α_1-acid glycoprotein may relate to the regulation of serum serotonin during its diurnal rhythm. It has been known for some time that serum serotonin levels display a diurnal variation [42]. In addition, circadian rhythms have also been observed in serotonin uptake activity, as well as [^{3}H]imipramine binding [43–45]. Interaction of the endogenous modulator with the site labeled by [^{3}H]imipramine may participate in the variation seen in serotonin levels by altering the rate of serotonin taken up into platelets. This mechanism may play an important role in blood pressure regulation. The significance of this modulator as it relates to serotonergic physiology awaits further investigation.

Acknowledgements

We wish to thank Dr. Steve Burkin of Columbia University College of Physicians and Surgeons for performing the amino acid composition analysis, Ms. Mary Wilfred for her graphic arts contribution and Ms. Carol Kalajian for her clerical assistance.

References

1 Ross, S.B. (1982) in Biology of serotonin transmission (Osborne, N.N., ed), pp 159–195, John Wiley and Sons Ltd., New York

2 Sneddon, J.M. (1973) Prog. Neurobiol. 1, 151–198

3 Lingjaerde, O. (1977) in Serotonin in Health and Disease (Essman, W.B., ed.), Vol 4, pp. 139–199, Spectrum Publications, Inc., New York

4 Rotman, A. (1983) Proc. Neuro-Psychopharmacol. Biol. Psychiatry 7, 135–151

5 Paul, S M., Rehavi, M., Skolnick, P. and Goodwin, F K. (1981) in Recent Advances in Neuropsychopharmacology (Angrist, B , Burrows, G.D , Lader, M., Lingjaerde, O , Sedall, G and Wheatley, P , eds.), pp. 187–193, Pergamon Press, New York

6 Briley, M.S., Raisman, R. and Langer, S.Z (1979) Eur. J. Pharmacol 58, 347–348

7 Paul, S.M., Rehavi, M., Skolnick, P and Goodwin, F.K. (1980) Life Sci. 26, 953–959

8 Raisman, R , Briley, M. and Langer, S.Z. (1979) Nature 281, 148–150

9 Wennogle, L.P. and Meyerson, L.R. (1983) Eur. J. Pharmacol 86, 303–307

10 Wennogle, L.P. and Meyerson, L.R (1985) Life Sci. 36, 1541–1550

11 Barbaccia, M.L , Brunello, N., Chaung, D.M. and Costa, E (1983) Neuropharmacology 22, 373–383

12 Briley, M., Langer, S Z. and Sette, M. (1981) Br J. Pharmacol. 74, 817P–818P

13 Meyerson, L.R., Ieni, J R. and Wennogle, L.P. (1987) J. Neurochem., in the press

14 Briley, M., Langer, S Z , Raisman, R , Sechter, D. and Zarifian, E. (1980) Science 209, 303–305

15 Paul, S.M., Rehavi, M., Skolnick, P , Ballenger, J.C. and Goodwin, F.K. (1981) Arch. Gen. Psychiatry 38, 1315–1317

16 Tuomisto, J and Tukiamen, E. (1976) Nature 262, 596–598

17 Peroutka, S.J. (1984) Biochem Pharmacol 33, 2349–2353

18 Vanhoutte, P.M. and Luscher, T.F. (1986) J. Hypertension (Suppl.) 4, s29–35

19 Angel, I. and Paul, S.M. (1984) FEBS Lett. 171, 280–284

20 Angel, I., Goldman, M.E., Skolnick, P., Pisano, J J and Paul, S M. (1985) in Progress in Clinical and Biological Research (ENDOCOIDS) (Lal, H , Labella, F. and Lane, J., eds.), Vol. 192, pp 457–464, Alan R Liss, Inc , New York

21 Barbaccia, M.L , Gandolfi, O., Chuang, D.M. and Costa, E. (1983) Proc. Natl. Acad Sci. USA 80, 5134–5138

22 Barbaccia, M.L , Melloni, P., Pozzi, O. and Costa, E. (1986) Eur. J. Pharmacol. 123, 45–52

23 Rehavi, M., Ventura, I. and Sarne, Y. (1985) Life Sci 36, 687–693

24 Rehavi, M., Ventura, I and Sarne, Y. (1985) in Progress in Clinical and Biological Research (ENDOCOIDS) (Lal, H , Labella, F. and Lane, J., eds), Vol 192, pp. 465–472, Alan R. Liss, Inc., New York

25 Segonzac, A., Schoemaker, H., Tateishi, T. and Langer, S.Z. (1985) J. Neurochem 45, 249–256

26 Langer, S.Z., Lee, C.R., Schoemaker, H., Segonzac, A. and Esnand, H. (1985) in Progess in Clincial and Biological Research (ENDOCOIDS) (Lal, H., Labella, F. and Lane, J., eds.), Vol. 192, pp. 441–455, Alan R Liss, Inc., New York

27 Wennogle, L.P , Beer, B. and Meyerson, L R. (1981) Pharmacol. Biochem Behav. 15, 975–982

28 Yamamura, H.I. and Snyder, S.H. (1974) Proc. Natl. Acad Sci. USA 71, 1725–1727

29 Lippa, A S., Garrett, K.M., Tabakoff, B , Beer, B., Wennogle, L.P. and Meyerson, L.R. (1985) Brain Res Bull. 14, 189–195

30 Taylor, R.L. and Burt, D.R. (1982) J. Neurochem 38, 1649–1656

31 Simasko, S.M and Horita, A. (1982) Life Sci. 30, 1793–1799

32 Hoffman, B.B and Lefkowitz, R.J. (1982) J. Cardiovasc. Pharmacol 4, S14–S18

33 Hall, M.D., El Mestikawy, S., Emerit, M B., Pichat, L., Hamon, M. and Gozlan, H (1985) J Neurochem 44, 1685–1696

34 Bradford, M.M. (1976) Anal. Biochem. 72, 248–254

35 Wennogle, L.P, Ashton, R A., Schuster, D.I., Murphy, R.B and Meyerson, L.R. (1985) EMBO J 4, 971–977

36 Laemmli, U.K. (1970) Nature 227, 680–685

37 Laskey, R.A. and Mills, A.P. (1975) Eur. J. Biochem 56, 335–341

38 Lyngbye, J. and Kroll, J. (1971) Clin Chem. 17, 495–500

39 Javaid, J I, Hendricks, K and Davis, J M (1983) Biochem Pharmacol. 32, 1149–1153

40 Sluijs, P. and Van der Meijer, D.K F (1985) J Pharmacol Exp. Ther 234, 703–707

41 Schmid, K. (1975) in The plasma proteins, Vol. 1 (Putnam, F.W., ed.), pp. 184–228, Academic Press, Inc., New York

42 Sarai, K. and Kayano, M (1968) Folia Psychiatr Neurol. Jap. 22, 271–281

43 Wirz-Justice, A (1974) Experientia 30, 1240–1241

44 Oxenkrug, G.H., Prakhje, I and Mikhalenko, I N (1978) Activ Nerv. Super 20, 66–67

45 Wirz-Justice, A, Krauchi, K., Morimasa, T, Willener, R and Feer, H. (1983) Eur. J. Pharmacol. 87, 331–333

Biochimica et Biophysica Acta 923 (1987) 22–28
Elsevier

BBA 22442

Topo-optical investigations of human erythrocyte glycocalyx conformational changes induced by dextran

Hans Bäumler [a], Karl-Jürgen Halbhuber [b], Dietger Stibenz [b]
and Dietmar Lerche [a]

[a] *Department of Hemorheology and Hemodynamics, Institute of Medical Physics and Biophysics, Medical School (Charité), Humboldt University, DDR-1040 Berlin and* [b] *Department of Histochemistry, Institute of Anatomy, Friedrich Schiller University, DDR-6900 Jena (G.D.R.)*

(Received 12 August 1986)

Key words: Cell surface, Erythrocyte aggregation; Glycocalyx, Dextran; Membrane anisotropy

Cell surface properties are involved in the aggregation process of red blood cells. Using the topo-optical toluidine blue reaction, conformational changes of the glycocalyx (main component glycophorin A) were found when red blood cells were incubated and fixed in the presence of dextran. Relative differences in optical path as a measure of red blood cell membrane anisotropy decreased in relation to dextran concentration during fixation. These conformational changes could not be detected by electrophoretic measurements. When incubating, fixing and staining red blood cells in the presence of dextran, anisotropy decreased only at low dextran concentrations and increased at rising dextran concentrations. This biphasic course of differences in optical path seems to be due to different effects of dextran superimposing upon each other: (i) a disturbing influence on the spatial order of sialic acid carrying oligosaccharide side chains due to H-bond interaction, and (ii) an increase in the size of dye aggregates and suppression of the thermal motion of macromolecules at higher dextran concentrations.

Introduction

The aggregation process of red blood cells is based on a balance of energies between the cells. This balance involves bonding energies resulting, e.g., from dextran adsorption, van-der-Waals electrodynamic energy, free energy from changes of viscoelastic energy, electrostatic energy resulting from negative charges on the red blood cell surface, and steric energy [1,2]. It was assumed that electrostatic forces are dominant in stabilizing red blood cells in suspensions [1,10–13]. Theoretical calculations of electrostatic repulsive forces [2,9] show that these forces are rather small. They cannot be responsible alone for the fact that the red blood cells do not aggregate in the absence of macromolecules under isotonic conditions [5,14]. The properties of the cell surface coat seem to play an important role in the interaction process of cells, since the glycocalyx responds very sensitively to variations of the suspension medium by changes of its structure [2–8].

In the presence of dextran, red blood cells show molecular weight and concentration-dependent aggregation [1,10] as well as an increase of the effective electrophoretic mobility $\eta\mu/\eta_0$ with rising dextran concentration (η and η_0, viscosity of suspending medium with and without dextran, respectively; μ, electrophoretic mobility). This

---

Correspondence address: Department of Hemorheology and Hemodynamics, Institute of Medical Physics and Biophysics, Medical School (Charité), Humboldt University, DDR-1040 Berlin, G.D.R.

0304-4165/87/$03.50 © 1987 Elsevier Science Publishers B.V. (Biomedical Division)

cannot be explained by volume exclusion effects alone [9]. Conformational changes of the glycocalyx should also be taken into consideration.

Quantitative calculations of the interaction energy between red blood cells presuppose knowledge of the structural arrangement of macromolecules on the cell surface. The extracellular segment of glycophorin A represents the major constituent of the glycocalyx [16] and carries about 70% of the sialic acid and 50% of the carbohydrates of the carbohydrates of the human erythrocyte glycocalyx [17].

By means of topo-optical toluidine blue reaction [18–20] information is available about the spatial order of the sialic acid residues. Cationic dye molecules are used to detect anionic groups in metachromotropic structures. In the case of the red blood cell membrane, the sialic-acaid residues of N-terminal hydrophilic domains of glycophorin A are the main target structures for toluidine blue reaction. Radial birefringence is caused by formation of staple-like dye aggregates, with a preference for ordered dye micelles [21,23]. Prerequisite to the formation of such uniformly ordered dye micelles is the existence of a corresponding degree of spatial order of toluidine blue binding sialic-acid residues. A structural model of the N-terminal, extracellular glycophorin A segment was deduced from determinations of the secondary structure of this glycopeptide segment [24]. This model includes experimental findings about the influence of pH and ionic strength of topo-optical reaction [8,17,24], electrophoretic mobility [3,9,25], artificial aggregation behaviour of red blood cells [5,26] and cell-glass surface-adhesion distance determined by interference-reflection microscopy [27]. The supposed spatial structure of the extracellular glycophorin A segment could be stabilized by H-bonds and Ca^{2+}/Mg^{2+}-bridges between the saccharide chains of glycophorins and interpenetrating minor glycoproteins and gangliosides [5,7,24].

Since dextran interacts mainly via H-bonds [28,29] with the red blood cell membrane, it should disturb the spatial order of carbohydrate side chains with their terminal sialic-acid residues of the extracellular glycophorin A segment. It is the aim of this paper to study possible structural changes of glycophorin A caused by dextran by means of the topo-optical toluidine blue reaction.

Material and Methods

Red blood cell preparation

Red blood cells from human citrate-dextrose-adenine-guanosine (ACD-AG) whole-blood preserves stored for 0–2 days at 4°C were washed three times with 9 vol. of 67 mM phosphate buffer (pH 7.4, 300 mosmol with NaCl; phosphate buffered saline) at 20°C, once in dextran-phosphate buffered saline (dextran concentrations 0.5, 1, 3, 6, 8, 10 g/dl and mean molecular weights 40000, 75000 (Serva dextran 32, dextran 75) and 500000 (Pharmacia dextran 500), and finally resuspended at a hematocrit of 30% in the same dextran-phosphate buffered saline solutions. 1 ml of the red blood cell suspension was mixed with 9 ml glutaraldehyde-phosphate buffer (1g/dl glutaraldehyde (Merck); 67 mM phosphate buffer (pH 7.4), 300 mosmol) and fixed for 30 min at 20°C. The glutaraldehyde solutions contained several concentrations and molecular weight fractions of dextran. After fixation the red blood cells were washed three times either in phosphate buffered saline to wash out the dextran or in dextran-phosphate buffered saline. Control cells were washed and fixed in the same way but without dextran in any solution.

Topo-optical staining procedure

Air-dried smears of fixed red blood cell specimens were stained with toluidine blue O (C.I. 52040, Merck) in (a) phosphate buffered saline or (b) dextran-phosphate buffered saline for 7 min. The toluidine blue-stained smears were rinsed with a solution containing 2 g/dl potassium ferricyanide and 2 g/dl potassium iodide (a) without and (b) with dextran, respectively. The smears were coated with thin films of gum arabic supplemented with 2 g/dl potassium ferricyanide and 2 g/dl potassium iodide. For cell birefringence analysis ($\lambda = 475$ nm) six different preserves containing 100 red blood cells each were included (microscope Amplival Pol-d, Carl Zeiss, Jena). In case (c), the red blood cells were washed and fixed like control cells but stained as in case (b). Table I gives details of the red blood cell preparations used for birefringence.

Electrophoretic investigations

Red blood cells were treated as described under 'Red blood cell preparation' and resuspended in

TABLE I

REGIME OF PREPARATION OF RED BLOOD CELLS WITH RESPECT TO THE USE OF DEXTRAN DURING FIXATION AND STAINING, RESPECTIVELY

Regime	Glutaraldehyde fixation	Toluidine blue staining
a	with dextran	without dextran
b	with dextran	with dextran
c	without dextran	with dextran
control	without dextran	without dextran

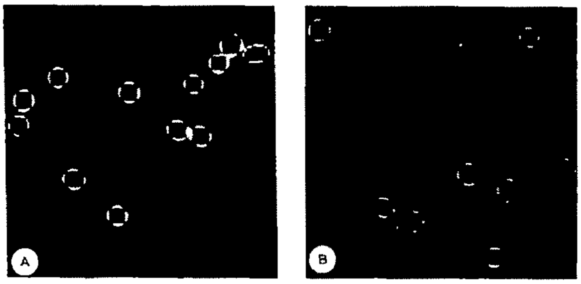

Fig 1. Topo-optical blue staining reaction of glutaraldehyde-fixed human red blood cells. Micrograph made between crossed polars (magnification ×300). (A) Control cells. (B) Red blood cells fixed in the presence of 10 g/dl dextran 75, and stained in the absence of dextran

phosphate buffered saline as well as in dextran-phosphate buffered saline at a hematocrit of 0.1% (for details see Table II). Electrophoretic mobility was determined with an Opton cytopherometer (Zeiss, Oberkochen). 25 cells per specimen were measured in both directions at 25°C in accordance with the procedure given by Donath and Lerche [3]. Glutaraldehyde-fixed red blood cells served as control cells, and non-fixed red blood cells as normal cells.

Spectrophotometric measurement

The influence of dextran on the formation of dye aggregates was investigated using a Specord double beam spectrophotometer (Carl Zeiss, Jena) in the range between 400 and 600 nm. Toluidine blue concentration was 1 mg/dl in phosphate buffered saline containing from 1 g/dl to 10 g/dl dextran 75. Reference solutions were corresponding dextran-phosphate buffered saline solutions without toluidine blue.

Results

In the absence of dextran, red blood cells exhibit intensive topo-optical toluidine blue staining. Polarization-optical analysis between crossed polars with linearly polarized light showed radial positive sphericities. The value of anisotropy (differences in optical path) was 19.7 ± 2.5 nm. Reduced intensities of birefringence patterns (differences in optical path) have been found upon fixing the red blood cells in the presence of dextran, but staining with dextran-free solution (Fig. 1). Differences in optical path of red blood cells, dependent on dextran concentration, during the incubation and fixation procedure relative to control cells is shown in Fig. 2 for dextran 32, dextran 75 and dextran 500. In the range from 0 to 1 g/dl dextran a pronounced decrease of the differences in optical path can be seen, but a further decrease of is much slower from 3 to 10 g/dl for all three dextran specimens investigated. There are no significant differences between the relative differences in optical path of dextran 32, dextran 75 and dextran 500, respectively, but compared with the control differences in optical path the reduction was always significant ($P = 0.001$).

In contrast with the results obtained by topo-optical staining with dextran-free toluidine blue solutions (Fig. 2), the induced toluidine blue anisotropy after staining red blood cells in the presence of dextran exhibits a less pronounced decrease for low dextran concentrations, reaching a minimum and increasing again at higher dextran concentrations (Fig. 3). The dependence of optical path differences on dextran concentration is similar for both dextran 32 and dextran 500, but there are quantitative differences. In the case of dextran 32, the change in the differences in optical path is not significant for 1 g/dl and 3 g/dl in comparison with control, but for concentrations higher than 3 g/dl it is significantly higher than for control cells. Staining red blood cells in the presence of dextran 500 leads to a significant decrease in the differences in optical path at low dextran concentrations compared with control. On increasing the dextran 500 concentration, the difference in optical path rises too, reaching the level of control cells at dextran concentrations of about about 8 g/dl.

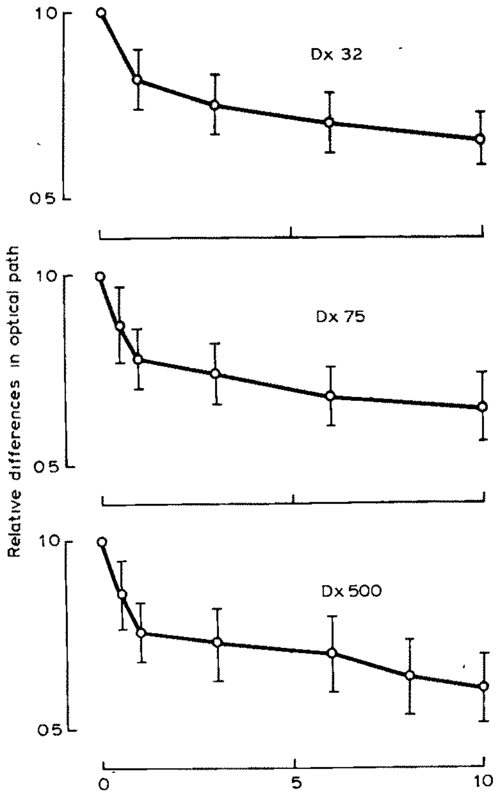

Fig. 2. Mean values and S.D. of differences in optical path relative to control cells in relation to dextran (Dx) concentration in the bulk phase during red blood cell fixation with glutaraldehyde Red blood cell staining in the absence of dextran.

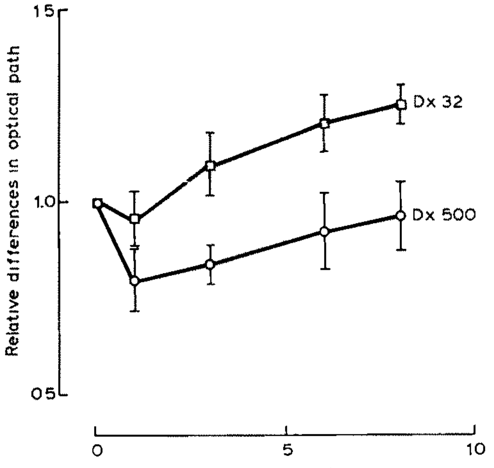

Fig. 3. Mean values and S.D of differences in optical path relative to control cells in relation to dextran (Dx) concentration. Fixation and toluidine blue staining of red blood cells in the presence of dextran.

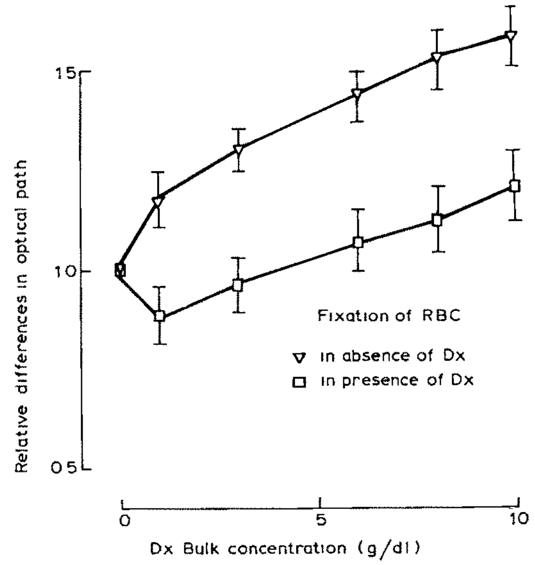

Fig 4. Mean values and S.D. of relative differences in optical path for different red blood cell preparations in relation to dextran 75 (Dx) concentration: ▽, fixation without dextran and toluidine blue staining of red blood cells with dextran, □, fixation and toluidine blue staining of red blood cells in the presence of dextran

The red blood cells fixed in glutaraldehyde-phosphate buffered saline (without dextran) show a steady increase of anisotropy after staining with toluidine blue solutions containing an increasing amount of dextran 75. The concentration-dependent course of the differences in optical path for red blood cell preparations fixed in either the presence or absence of dextran, and then stained with toluidine blue in the presence of dextran, are shown in Fig. 4.

The results of electrophoretic measurements are listed in Table II. The effective mobility of normal red blood cells is about 8% less than that of red blood cells after glutaraldehyde fixation (control). Control cells and red blood cells fixed in the presence of dextran 500 followed by several washings in phosphate buffered saline show no significant differences of mobility in phosphate buffered saline. In dextran-phosphate buffered saline (8 g/dl) the effective mobility of normal red blood cells is significantly higher than that of control cells. Differences between control red blood cells and dextran-treated red blood cells proved not to be significant.

For cases (b) and (c) (see Table I), the interac-

TABLE II

EFFECTIVE ELECTROPHORETIC MOBILITY, $\eta\mu/\eta_0$ (10^{-2} μm/s PER V/m) OF RED BLOOD CELL WITHOUT GLUTARALDEHYDE FIXATION AND AFTER FIXATION IN GLUTARALDEHYDE IN THE PRESENCE AND ABSENCE OF DEXTRAN 500 ($T = 25.0 \pm 0.1°$C)

Data represent mean values and S.D of six different samples containing 25 red blood cells each

	Phosphate buffered saline	Dextran (8 g/dl)
Normal red blood cells	0.98 ± 0.03	$3.51 \pm 0\ 07$
Glutaraldehyde-fixed red blood cells (control)	1.04 ± 0.04	3.25 ± 0.08
Glutaraldehyde fixation with 3 g/dl dextran	$1\ 06 \pm 0\ 02$ [a] $1\ 07 \pm 0\ 03$ [b]	
Glutaraldehyde fixation with 10 g/dl dextran	1.05 ± 0.03 [a] $1.05 \pm 0\ 03$ [b]	3.30 ± 0.10

[a] Washed three times in phosphate buffered saline

[b] Washed five times in phosphate buffered saline.

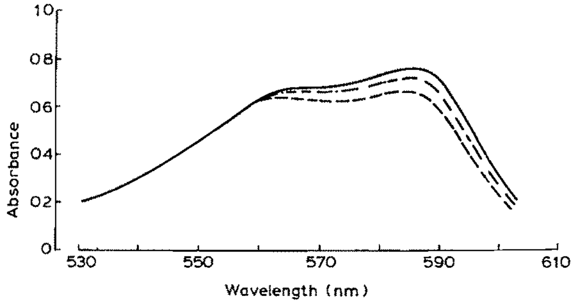

Fig. 5 Spectral absorbance of toluidine blue-dextran-phosphate buffered staining relative to dextran-phosphate buffered saline (1 mg/dl toluidine blue). — — —, 0 g/dl dextran 75, — · —, 6 g/dl dextran 75; ————, 10 g/dl dextran 75.

tion of dextran with the dye molecules must also be considered. Photometric investigations show (Fig. 5) that the absorbance of toluidine blue-dextran solutions increased with rising dextran concentration. This could be the result of stronger scattering effects due to larger dye aggregates. Particularly the fact that the maximum at 586 nm increases more than that at 566 nm is an indication of larger aggregates of dye molecules [23,32]. Since these effects are involved for both case (b) and case (c) of red blood cell staining, their relation to each other should not be influenced.

Discussion

The changes of measured values of induced toluidine blue anisotropy confirm the assumption that dextran disturbs the spatial order of the glycocalyx. Fig. 6A schematically shows the extracellular glycophorin A segment [24] with its carbohydrate side chains and their terminal sialic-acid residues. Under normal conditions (pH 7.4, 300 mosmol) the glycophorin A segment is parallel to the lipid bilayer of the red blood cell membrane. As shown by the experiments of Evans and Kukan [30] with liposomes and erythrocytes, dextran binds to the lipid membrane. Since dextran penetrates the glycocalyx, an expansion of glycophorin A should be possible [31]. This expansion seems to differ according to the fixation procedure used. If dextran is present during the fixation with glutaraldehyde the linking of glycophorin A is only partly possible, due to expansion and/or shielding of binding sites by dextran. After washing the cells in phosphate buffered saline dextran is removed (with no differences of electrophoretic mobility) and the extracellular glycophorin A segment remains movable. This means that less-oriented dye micelles can be formed and a reduction of the induced anisotropy (a decrease of differences in optical path) can be found.

If dextran is not removed by washing the cells with phosphate buffered saline, a biphasic course of anisotropy is obtained which is dependent on dextran concentration. For low dextran concentrations the shielding effect of dextran seems to be dominant with respect to its immobilizing effect. At high dextran concentrations glycophorin A could be stretched, allowing conformations which are favourable to the formation of oriented dye micelles (Fig. 6C). Additionally, dextran immobi-

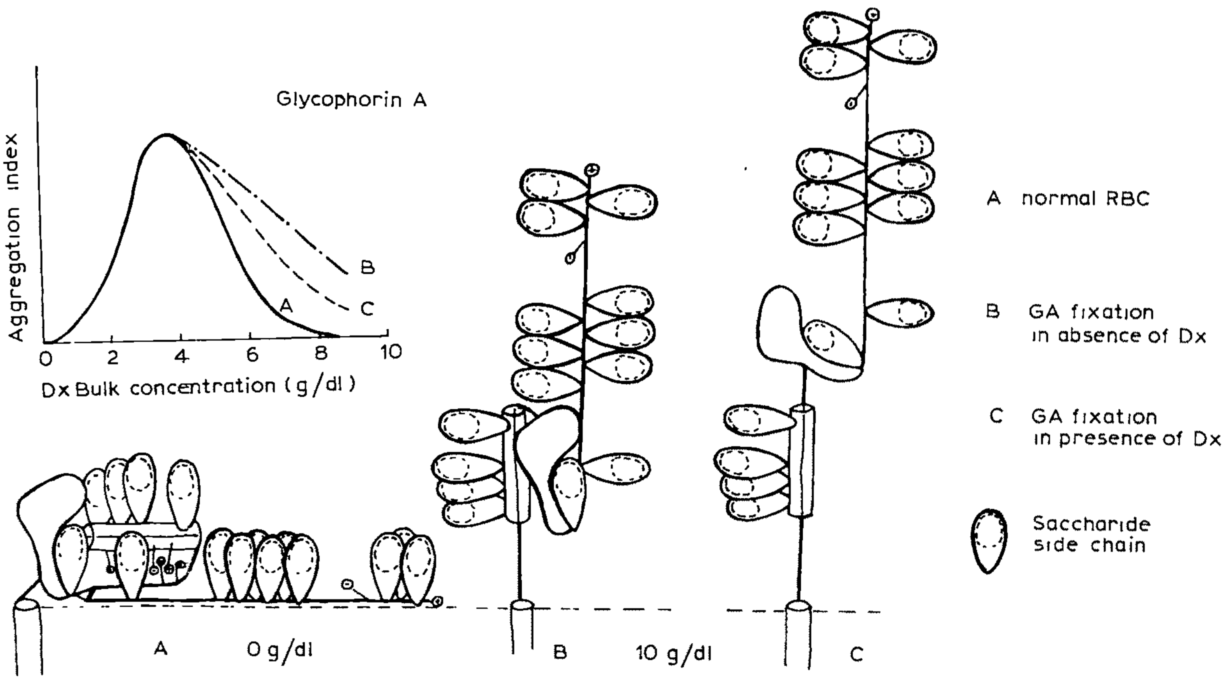
Glycophorin A
Aggregation index
B
C
A
0
2
4
6
8
10
Dx Bulk concentration (g/dl)
A normal RBC
B GA fixation in absence of Dx
C GA fixation in presence of Dx
Saccharide side chain
A
0 g/dl
B
10 g/dl
C

Fig. 6 Schematic presentation of the hypothetical structural model of the N-terminal hydrophilic segment of glycophorin A Disaggregation of red blood cells (RBC) occurs for dextran concentrations in the bulk phase A, normal red blood cells – 7 g/dl; B, fixation of red blood cells in the absence of dextran – more than 10 g/dl; C, fixation of red blood cells in the presence of 10 g/dl dextran – 8.5 g/dl. GA, glutaraldehyde.

lizes the glycophorin A segment resulting in an increase of the differences in optical path.

If the red blood cells were fixed in phosphate buffered saline and stained in dextran solutions (case (c), Table I), the differences in optical path steadily increased with rising dextran concentrations. In this case the immobilizing effect of dextran dominates. Since the conformation of the glycophorin A segment is widely preserved, the complete stretching due to dextran seems to be impossible (Fig. 6B). The density of dye micelles is greater than in the other cases, and therefore the difference in optical path is largest.

The unchanged effective electrophoretic mobility of red blood cells treated and fixed in the presence of different dextran 500 concentrations compared with cells washed and fixed in its absence indicates that glutaraldehyde fixation of the glycocalyx is obviously incomplete. The small number of possible reaction sites for glutaraldehyde, concerning especially glycophorin A subsegment 1–24 and low-grade secondary structuring, makes it probable that this subsegment should a priori be movable particularly after glutaraldehyde fixation. Assuming an interfacial rearrangement in the glycocalyx due to dextran interaction, there are two possibilities for electrophoertic mobility to remain unchanged under normal conditions: the glycophorin A segment is moved in the same plane forming new clusters, or deeper structures of glycophorin A are involved. In this connection it is important to remember that measurements of anisotropy after topo-optical toluidine blue staining (i) and of electrophoretic mobility (ii) of cells provide information about different properties of the red blood cell glycocalyx: spatial order of toluidine blue-binding sialic-acid residues (i) and spatial density of negative charges of the glycocalyx (ii). Thus, the disordering effect of dextran would change electrophoretic mobility only if space-charge density and/or porosity of the glycocalyx were altered at the same time.

The expansion of the glycocalyx at high dextran concentrations could also explain the disaggregation behaviour of red blood cells. At low dextran concentrations the distance between the red blood cell glycocalyces can be bridged by dextran molecules. This means that the red blood cells aggregate. At high dextran concentrations the glycocalyces of red blood cells would penetrate each other at the same distance as at low dextran concentration. This would lead to high values of steric repulsive forces, which cannot be compensated for by the bridging forces of dextran molecules. The result is the disaggregation of red blood cells.

Summing up, a basic structural change of the glycocalyx brought about by glycocalyx-dextran interaction can be inferred from this study.

Acknowledgements

We are grateful to Mrs. U. Möller, Mrs. M. Michalsky, Mr. M. Gliesing and Mr. Siegert for skillful technical assistance. H.B. thanks Prof. Dr. Scheuner for technical support and helpful discussions. The work was supported by the Ministry of Health of the GDR, 'HFR Artificial Organs and Biomaterials'.

References

1 Chien, S (1973) Bibl. Anat (Basel) 11, 303–309
2 Lerche, D (1983) Ann N Y Acad. Sci 416, 66–81
3 Donath, E and Lerche, D. (1980) J Electroanal. Chem 116, 41–53
4 Halbhuber, K-J, Stibenz, D., Müller, U.A, Fröber, R., Feuerstein, H, Meyer, H.W., Augsten, K. and Linss, W (1982) Acta Histochem. 70, 290–325
5 Lerche, D. (1982) Biorheology 19, 587–598
6 Lerche, D and Bäumler, H (1984) Biorheology 21, 393–403
7 Sharom, F J and Grant, C W.M. (1978) Biochim Biophys Acta 507, 280–293
8 Stibenz, D. and Geyer, G. (1980) Folia Haematol. 107, 787–792
9 Levine, S, Levine, M., Sharp, K A and Brooks, D.E. (1983) Biophys. J 42, 127–135
10 Brooks, D.E. (1973) J Colloid Interface Sci 43, 687–699
11 Brooks, D E. (1973) J. Colloid Interface Sci. 43, 700–713
12 Heard, D.H. and Seaman, G V.F. (1960) J. Gen Physiol 43, 635–653
13 Jan, K.M and Chien, S (1973) Bibl Anat (Basel) 11, 281–288
14 Lerche, D. (1981) Bioelectrochem. Bioenerg. 8, 293–299
15 Lerche, D. (1984) Biorheology 21, 477–492
16 Furtmayer, H. (1978) J. Supramol Struct. 9, 79–95
17 Stibenz, D (1984) Thesis, Dissertation B, Friedrich Schiller university, Jena
18 Romhanyi, G. (1963) Acta Histochem. 15, 201–233
19 Romhanyi, G., Molnar, L and Nemeth, A (1974) Histochemie 39, 261–276
20 Scheuner, G. and Hutschenreiter, J (1972) Polarisationsmikroskopie in der Histophysik, VEB Georg Thieme Verlag, Leipzig
21 Halbhuber, K-J., Gliesing, M., Stibenz, D. and Markovitzky, J (1984) Histochemie 81, 187–193
22 Chien, S., Simchon, S, Abbott, R E. and Jan, K M (1977) J. Colloid Interface Sci 62, 461–470
23 Scheuner, G. and Hutschenreiter, J (1975) in Prog. Histochem. Cytochem. 7(2)
24 Stibenz, D. and Geyer, G. (1982) Folia Haematol. 109, 251–254
25 Donath, E. and Pastushenko, V. (1979) Biolectrochem Bioenerg. 6, 543–554
26 Hessel, E. and Lerche, D. (1985) Vox Sang 49, 86–91
27 Donath, E. and Gingel, D (1983) J. Cell Sci. 63, 113–124
28 Brooks, D.E., Greig, R.G. and Janzen, J (1980) in Erythrocyte Mechanics and Blood Flow (Cokelet, G.R., Meiselman, H J. and Brooks, D E., eds.), pp 119–140, Alan R Liss, Inc., New York
29 Jan, K.M. (1979) J. Cell Physiol. 101, 49–56
30 Evans, E. and Kukan, B (1983) Biophys. J 44, 255–260
31 Snabre, P and Mills, P (1985) Colloid Polym. Sci. 263, 494–500
32 Scheibe, G. (1970) Palette 35, Sandoz AG, Basel

Biochimica et Biophysica Acta 923 (1987) 29–34
Elsevier

BBA 22444

The inhibitory effect of dithiothreitol on the assembly of the filamentous phage fd

Marilyn Vaccaro, Beverly Boehler-Kohler, Wolfram Müller and Ihab Rasched

Fakultät für Biologie der Universität Konstanz, D-7750 Constance (F.R G.)

(Received 16 June 1986)

Key words. Dithiothreitol; Gene 5 protein, ssDNA-protein complex; (Filamentous phage)

Assembly of the filamentous phage fd is preceded by the formation of a complex between the viral single-stranded (ss) DNA and the virally coded gene 5 protein (gene 5 protein-ssDNA complex). The presence of 5 mM dithiothreitol in the growth medium prevents phage production; however, phage infection, phage DNA replication and phage genome expression are still observed. In contrast, the gene 5 protein-ssDNA complex is not formed in the presence of dithiothreitol in vivo, although the complex is not affected by the disulfide reducing agent in vitro. Furthermore, host lipid composition is altered by growth in the presence of dithiothreitol. The zwitterionic lipid, phosphatidylethanolamine, increases while the cationic phospholipid content, cardiolipin and phosphatidylglycerol, decreases. This suggests a role for lipids or membranous structures in the process of gene 5 protein-ssDNA complex formation.

Introduction

Bacteriophage fd is a male-specific, single-stranded DNA phage closely related to phages M13 and f1. Their common hosts are *E. coli* strains harboring an F-factor. These phages are neither lytic nor lysogenic; infected cells multiply while continuing to release progeny phage through their membranes. The phage genome codes for ten genes [1]. The products of gene 2, gene X and gene 5 are involved in phage DNA replication [2]. After formation of a double-stranded circular superhelical DNA (RF I) by host enzymes, viral plus strand synthesis is initiated by gene 2 protein which nicks the RF I. Elongation at the 3′-end occurs via the rolling circle mechanism [3]. Gene 5 protein, a phage encoded DNA-binding protein, cooperatively associates with the nascent viral DNA-strand [4], thus initiating the first step in phage assembly. This nucleoprotein complex may be isolated from lysates of fd-infected cells [5] and appears to be associated with the cellular membrane [6]. During the final stages of assembly, gene 5 protein is displaced into the cytoplasm where it is recycled [5], and the DNA is covered with phage coat proteins 8, 3, 6, 7 and 9 before emerging outside the cell as a mature phage particle. In addition to the coat proteins, morphogenesis also requires the products of genes 1 and 4 and the presence of the host membrane protein thioredoxin [7].

Here we show that the disulfide reducing agent dithiothreitol inhibits phage morphogenesis at the level of DNA-protein complex formation. Our studies indicate that the target of dithiothreitol inhibition is not a phage component. Rather, growth of *E. coli* in the presence of dithiothreitol has an effect on the lipid composition of the host cell, suggesting that a particular membrane structure or component plays a role in the formation of the viral nucleoprotein complex in vivo.

Correspondence: Dr. I Rasched, Fakultät für Biologie der Universität Konstanz, D-7750 Constance, F.R G.

0304-4165/87/$03 50 © 1987 Elsevier Science Publishers B V (Biomedical Division)

Materials and Methods

Preparation of the gene 5 protein-DNA complex

Bacteriophage fd and *E. coli* strain K37 (*supD*) are from our collection. Fd-tet constructed by Zacher et al. [8] is a gift of these authors. L-[U-^{14}C]Arginine (> 300 mCi/mmol) and [*methyl*-^{3}H]thymidine (> 40 mCi/mmol) were purchased from Amersham Buchler, F.R.G. The isolation of the gene 5 protein-ssDNA complex from fd-infected *E. coli* cells proceeded according to Ref. 9, with the following modifications. Cells to be grown in the presence of dithiothreitol (Sigma) contained 5 mmol/l of the freshly dissolved powder in all cultivating media. The 10 ml culture containing infected cells in minimal medium [13] was doubly labeled with 100 μCi [^{14}C]arginine and 150 μCi [^{3}H]thymidine. Following an incubation of 90 min these cells were mixed with 200 ml of unlabeled infected bacteria, collected by centrifugation and washed twice to remove unincorporated label and phage. The cells were gently lysed with lysozyme, cleared, and the gene 5 protein-ssDNA complex was pelleted as described [9]. The resuspended sample was subsequently layered onto a linear 10–40% sucrose gradient in a 10 mM Tris-HCl buffer (pH 7.6) (1 mM in EDTA and 10 mM in NaCl; TEN buffer) and centrifuged at 34000 rpm in the Beckman SW40 rotor for 10 h. Fractions were collected from the bottom of the gradient and the location of the complex was inferred from the radioactivity profile. Fractions to be analysed were pooled accordingly, dialysed against TEN buffer followed by distilled water and lyophilized. In cases where the radioactivity did not show well separated peaks, the resuspended fractions were pooled and purified by sedimentation through a second 10–40% sucrose gradient.

Phospholipid analyses

Phospholipids from *E. coli* cells were extracted according to Ref. 10 and separated by ascending thin layer chromatography on acetone-activated silica gel G plates (Merck) in a chloroform/methanol/water (65:25:4, v/v) developing system. Phospholipids were visualized and identified with iodine vapor, phosphate spray reagent [11] and ninhydrin spray. Further identification was by chromatography with commercial standards and by mild alkaline hydrolysis [12]. The fractionated lipids were then extracted from the silica gel plate with chloroform/methanol (1:2). This extraction procedure was repeated two times. The relative quantities of each phospholipid were determined by measuring their inorganic phosphate content [13].

Results and Discussion

Growth of *E. coli* strain K37 is slightly affected by the presence of dithiothreitol up to a concentration of 5 mM. The generation time due to dithiothreitol was increased by approx. 10 min and the final concentration of cells after growth was reduced by one third. In contrast, the effect of dithiothreitol on the production of fd phage in the host is drastic. At a concentration of 5 mM, dithiothreitol completely inhibited the production of progeny phage as measured by the standard plaque assay in which case efficiency of plaque formation was less than 10^{-6}. In addition, no phage were precipitated from the culture medium with poly(ethylene glycol), ruling out the possibility that uninfectious particles are produced.

To investigate the possibility that dithiothreitol might interfere with phage infection, an fd-tet phage carrying the genes coding for tetracycline resistance [8] was used. *E. coli* cells grown in the presence of 5 mM dithiothreitol and infected with fd-tet were screened for their ability to grow on LB plates containing 10 μg/ml tetracycline and 5 mM dithiothreitol. Following a 10 min incubation, aliquots from the culture were washed twice and diluted with ice cold medium containing 5 mM dithiothreitol before spreading. The number of transduced colonies formed was the same as the number formed from parallel control cultures grown and infected with fd-tet in the absence of dithiothreitol. Thus, added dithiothreitol does not affect phage infection. Furthermore, the fact that colonies (containing approximately 20 generations of cells) grew on plates containing tetracycline and dithiothreitol indicates that the fd-genome must have been replicated.

Since dithiothreitol was shown to prevent phage production but not phage infection, we set out to determine at what point it interferes in the life cycle of fd. *E. coli* cells were cultured and infected with fd in the presence and absence of 5 mM dithiothreitol. Sucrose gradients were performed from lysates of both cultures in order to study the formation of the gene 5 protein-ssDNA complex. The sedimentation profiles shown in Fig. 1a clearly show the presence of gene 5 protein-ssDNA complex ($^{14}C/^{3}H$ double peak in fractions 6–10) in cells grown in the absence of dithiothreitol. However, this double peak is not observed in the profile obtained from cells grown in dithiothreitol (Fig. 1b).

The components of the sucrose gradients shown in Fig. 1 were further analysed by electrophoresis as described in the legends to Figs. 2 and 3. The double peak in radioactivity in the control sucrose gradient (Fig. 1a fractions 6–10) was shown to contain the gene 5 protein-ssDNA complex: analysis of the DNA content of these fractions by agarose gel electrophoresis showed that viral ssDNA was the major DNA species (Fig. 2, lane 4); and analysis of the protein content by SDS-polyacrylamide gel electrophoresis followed by immunoprecipitation showed that gene 5 protein was the major protein species present (Fig. 3, lane 2).

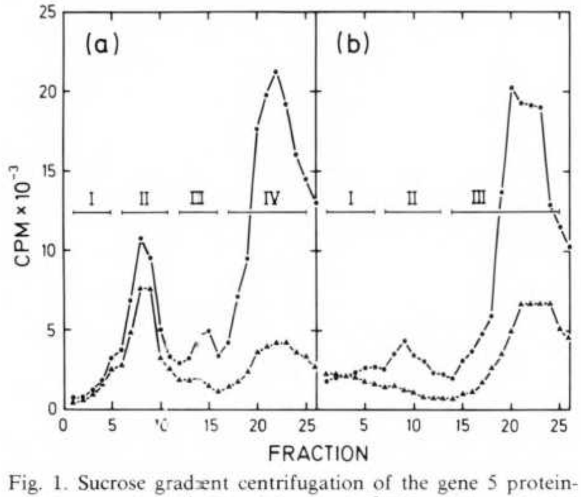

Fig. 1. Sucrose gradient centrifugation of the gene 5 protein-ssDNA complex. [^{14}C]Arginine and [^{3}H]thymidine labelled complex was isolated and purified from equal amounts of cells grown and infected in the absence (a) and presence (b) of 5 mM dithiothreitol as described in Materials and Methods. Fractions of 0.5 ml were collected from the bottom of the 10–40% (w/v) sucrose gradients. 20 μl aliquots of each fraction were analysed in a scintillation counter. (●) ^{14}C activity; (▲) ^{3}H activity. Roman numerals denote the pooling of fractions for further analysis in Figs. 2 and 3.

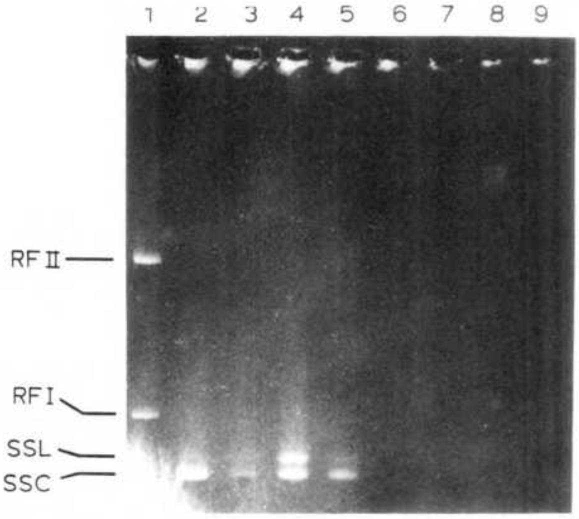

Fig. 2. Agarose gel electrophoresis of samples taken from sucrose gradients (Fig. 1). Fractions were pooled as indicated by roman numerals in Fig. 1, dialysed and concentrated as described in Materials and Methods and quantitatively resuspended in buffer containing 10 mM Tris-HCl (pH 8.1) and 1 mM EDTA. Aliquots to be analysed were made up to 1% SDS and incubated for 10 min at 60°C. After addition of 1/4 vol. 0.125% bromphenol blue and 20% glycerol, DNA samples were subjected to electrophoresis through 1% agarose gels in buffer containing 40 mM Tris-acetate (pH 8.2) 20 mM sodium acetate and 1 mM EDTA. DNA staining was done with 1 μg/ml ethidium bromide and visualized by ultraviolet light. Lanes: 1, fd RF I and II standards; 2, fd ss standard; 3–6, zones I–IV from the sucrose gradient in Fig. 1a; 7–9, peaks I–III from the sucrose gradient in Fig. 1b. RF I, supercoiled replicative form; RF II, nicked replicative form; SSC, single-stranded closed; SSL, single-stranded linear. Linearization was at least partly caused by lyophilization and storage.

Similar analysis of the cytoplasm from cells infected in the presence of dithiothreitol revealed that neither gene 5 protein nor fd ssDNA were contained in the equivalent fractions of the sucrose gradient. Gene 5 protein, however, was present in the uppermost fractions of the gradient (Fig. 3, lane 8) as well as in whole cell lysates of cells grown in dithiothreitol. This indicates that gene 5 protein is synthesized, however formation of the gene 5 protein-ssDNA complex is inhibited by the presence of dithiothreitol. While the smaller amounts of gene 5 protein observed in dithiothreitol-treated cultures could possibly account for the lack of complex formation, a substantial reduction in the total amount of gene 5 protein in

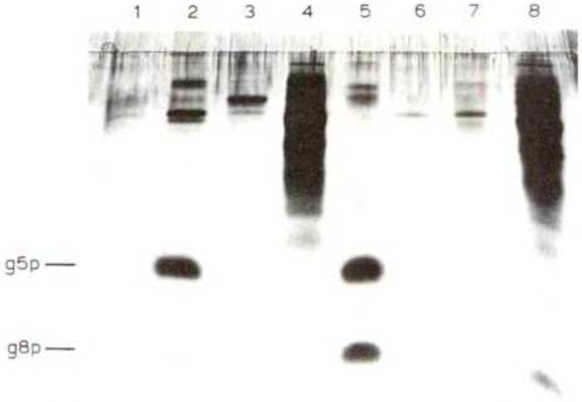

Fig. 3. SDS-polyacrylamide gel electrophoresis of samples from the sucrose gradients (Fig. 1). Fractions were pooled, dialysed, lyophilized and resuspended in 10 mM Tris-HCl (pH 8.5) to the volume of one fourth the original sucrose gradient fraction. One tenth of the resulting volume was applied and run on 12.5% acrylamide, 8 M urea gels as described in Ref. 22. The gel was subjected to western blotting according to Ref. 23 using antibodies directed against gene 8 and gene 5 proteins (g8p, g5p) before silver staining as in Ref. 24. Lanes 1–4, zones I–IV from the sucrose gradient in Fig. 1a; lane 5, isolated gene 5 and gene 8 proteins standards; lanes 6–8, zones I–III from Fig. 1b. All bands which migrated to the marked gene 5 and gene 8 protein position were verified to be these proteins through western blotting (nitrocellulose sheets not shown).

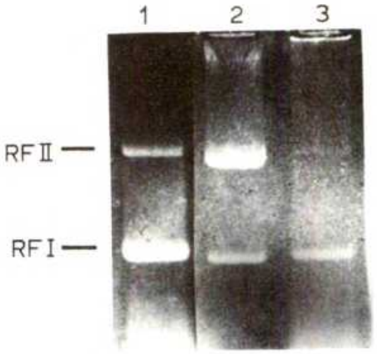

Fig. 4. Electrophoretic analysis of the RF DNA from infected whole cell lysates grown in the presence and absence of 5 mM dithiothreitol. Log phase cells were infected with phage fd (multiplicity of infection, 50) and grown (in the presence of 30 μg/ml chloramphenicol) under moderate aeration at 37°C for 90 min. Equal amounts of cells were harvested and their phage replication form DNA extracted according to the rapid alkaline extraction procedure described in Ref. 25. Lane 1: 10 μl from control lysates containing the DNA from approx. 10^7 cells; lane 2: 1.2 μg replicative form DNA purified through CsCl gradient; lane 3: as in lane 1, from dithiothreitol-treated cells.

dithiothreitol-treated cells is to be expected in light of the observation that no complex was formed in these cells. The pool of gene 5 protein is carefully regulated and only when it is bound to the viral DNA is it found in substantial amounts within the cell [14]. Furthermore, it should be emphasized that synthesis of single stranded DNA and therefore complex formation normally occurs in the cell shortly (4 min) after infection. At this time, the amount of accumulated gene 5 protein is also low [15]. Thus the cooperative nature of the bonding of ssDNA to gene 5 protein [4] enables complex formation even at low gene 5 protein concentrations. In addition to gene 5 protein, comparable amounts of gene 8 protein were obtained from both dithiothreitol-grown and control cultures, indicating that expression of phage proteins is not impaired by the reagent.

Analysis of the DNA content of whole cell lysates showed that the phage replicative form is indeed present within infected cells grown in the presence of dithiothreitol, although to a lesser degree than that found in control cultures (Fig. 4). On the other hand, only trace amounts of viral ssDNA were seen in cells infected and grown in dithiothreitol. This latter observation is to be expected since nascent viral strands are only stable when they are protected by the binding of gene 5 protein [2]. Likewise, the absence of complex formation can also explain the decreased amounts of replicative form DNA observed in dithiothreitol-treated cultures (which could be an additional cause for the decrease in viral strand synthesis). Gene 5 protein has been shown to repress the translation of the protein coded for by genes 2 and X [16]. In the case of dithiothreitol-grown cells, if the rapidly synthesized gene 5 protein is not bound to the emerging DNA, its accumulation would cause the repression of gene 2 (and gene X) proteins. This in turn would result in a decrease in phage DNA replication and hence fewer replicative form DNA copies per cell.

It is also improbable that gene 2 protein (containing five Cys residues) is the target of dithiothreitol's reducing activity, since experiments done in vitro demonstrating the endonuclease and ligating activities of this gene product (both functions being prerequisites for complex formation) have also been performed in the presence of mercaptoethanol [17]. Similarly, the morphogenesis proteins coded for by genes 1 and 4 are not likely targets for dithiothreitol's action, since gene 5 protein-ssDNA complex has been detected in cells infected with phage particles carrying mutations in these genes [9].

To ensure that dithiothreitol does not affect the stability of the complex itself, the following experiment was performed. Isolated, radioactively labeled complex was incubated with 5 mM dithiothreitol at 37°C for 1 h and subsequently sedimented through a sucrose gradient as described in the legend to Fig. 1. The radioactivity profile obtained was the same as seen in Fig. 1a.

The results presented thus far indicate that dithiothreitol does not prevent any essential process (i.e., phage DNA replication, genome expression, protein synthesis) required to occur prior to complex formation. In the presence of dithiothreitol the products of both genes 2 and 5 are present – the only viral proteins necessary for complex formation [9]. No other host component is mandatory for complex formation as ascertained from in vitro complex formation experiments [4]. However, it should be mentioned that several structural distinctions exist between complex found in vitro and in vivo [5], suggesting that the location of complex formation is important. In this regard, it has already been established that the products of genes 2 and 5 as well as the phage RF DNA and gene 5 protein-ssDNA complex itself have all been found associated with the cell envelope [6]. Therefore, we decided to study the effect of dithiothreitol on *E. coli* membrane lipid composition.

Table I shows the results obtained from experiments measuring the phospholipid content of cells grown and infected in the presence and absence of dithiothreitol. Infection caused a relative decrease in phosphatidylethanolamine content as compared to uninfected cultures, an observation previously reported by other laboratories [18,19]. In contrast, *E. coli* grown in the presence of dithiothreitol had a significantly higher phosphatidylethanolamine content. Cells containing this dithiothreitol-altered lipid composition did not show the phage-mediated decrease in phosphatidylethanolamine content but rather the higher dithiothreitol-related phosphatidylethanolamine content. This dithiothreitol-related increase in phosphatidylethanolamine at the expense of the anionic lipids phosphatidylglycerol and cardiolipin in the *E. coli* membrane would lead to a difference in the ratio of zwitterionic phosphatidylethanolamine to anionic phosphatidylglycerol and cardiolipin lipid content. The reason for putting the emphasis on anionic or zwitterionic content stems from a report [20] in which it was demonstrated that the surface and consequently binding properties of the *E. coli* membrane are not dependent on the exact chemical structure of the phospholipid polar head group, but rather on its physical properties. More specifi-

TABLE I

PHOSPHOLIPID COMPOSITION OF *E. COLI* GROWN IN THE PRESENCE AND ABSENCE OF DITHIOTHREITOL AND PHAGE fd

Results are expressed as percentage of total phospholipids. Values represent an average of 12 individual inorganic phosphate determinations from three different preparations. PE = phosphatidylethanolamine; PG = phosphatidylglycerol; CL = cardiolipin.

	Percent zwitterionic (PE)	Percent anionic (PG + CL)	Percent other	Zwitterionic/ anionic lipids
Control				
uninfected	75.6	22.3	2.1	3.4
infected	71.8	26.8	1.4	2.7
+ dithiothreitol				
uninfected	80.6	17.9	1.5	4.5
infected	81.4	16.7	1.9	4.9

cally it shows that the ratio of anionic to zwitterionic phospholipids is more relevant than the concentration of any particular phospholipid in the insertion of fd gene products into the cellular membrane. Because the effect of dithiothreitol on host cell lipids is seen in both infected and uninfected cells, the possibility that inhibition of phage assembly causes the observed membrane alteration can be ruled out.

In conclusion, the disulfide reducing agent has been shown to specifically inhibit fd phage assembly, probably by causing changes in the host membrane lipid composition. Whether the inhibitory effect of dithiothreitol is due exclusively to disturbances in the membrane, which in vivo probably serves as an organizing surface on which the necessary phage and host components are brought together, or whether dithiothreitol exerts an additional effect on some other components, is currently being studied in this laboratory. Other potential candidates are the protein necessary for producing the proton gradient across the cell membrane which has been shown to be necessary for fd phage assembly [21] or the redox enzyme thioredoxin which also plays a role in assembly [7]. In any case, dithiothreitol should prove to be helpful in elucidating the mechanism of fd phage assembly and perhaps also other membrane-involved assembly processes.

References

1 Horiuchi, K., Vovis, G.F. and Model, P. (1978) in The single-stranded DNA phages (Denhardt, D., Dressler, D. and Ray, D.S., eds.), pp. 113–137, Cold Spring Harbor Laboratory, Cold Spring Harbor, New York

2 Ray, D.S. (1977) Comp. Virol. 7, 105–177

3 Baas, P.D. (1985) Biochim. Biophys. Acta 825, 111–139

4 Alberts, B., Frey, L. and Delius, H. (1972) J. Mol. Biol. 68, 139–152

5 Pratt, D., Laws, P. and Griffith, J. (1974) J. Mol. Biol. 82, 425–439

6 Webster, R. and Cashman, J. (1973) Virology 55, 20–38

7 Russel, M. and Model, P. (1985) Proc. Natl. Acad. Sci. USA 82, 29–33

8 Zacher, A., Stock, C., Golden, J. and Smith, G. (1980) Gene 9, 127–140

9 Grant, R. and Webster, R. (1984) Virology 133, 315–328

10 Bligh, E.G. and Dyer, W.J. (1959) Can. J. Biochem. Phys. 37, 911–917

11 Dittmer, J.C. and Lester, R.L. (1964) J. Lipid Res. 5, 126–127

12 Dittmer, J.C. and Wells, M.A. (1969) Methods Enzymol. 14, 482–530

13 Ames, B.N. (1966) Methods Enzymol. 8, 115–118

14 Mazur, B. and Zinder, N. (1975) Virology 68, 490–502

15 Mazur, B. and Model, P. (1973) J. Mol. Biol. 78, 285–300

16 Model, P., McGill, C., Mazur, B. and Fulford, W. (1982) Cell 29, 329–335

17 Meyer, Th. and Geider, K. (1979) J. Biol. Chem. 254, 12636–12641 and 12642–12646

18 Ohnishi, J. (1971) J. Bacteriol. 107, 918–925

19 Woolford, J., Cashman, J. and Webster, J. (1974) Virology 58, 544–560

20 Plusche, G., Hirota, Y. and Overath, P. (1978) J. Biol. Chem. 253, 5048–5055

21 Ng, Y. and Dunker, A. (1980) in Bacteriophage Assembly (DuBow, M., ed.), Progress in Clinical and Biological Research, Vol. 64, pp. 467–474, Alan R. Liss, Inc., New York

22 Burr, F.A. and Burr, B. (1983) Methods Enzymol. 96, 239–244

23 Towbin, H., Staehelin, T. and Gordon, J. (1979) Proc. Natl. Acad. Sci. USA 76, 4350–4359

24 Morrisey, J.H. (1981) Anal. Biochem. 117, 307–310

25 Birnboim, H.C. and Doly, J. (1979) Nucleic Acid Res. 7, 1513–1523

Biochimica et Biophysica Acta 923 (1987) 35–41
Elsevier

BBA 22440

Metabolism of opioid peptides by cerebral microvascular aminopeptidase M

Laurie Churchill, Hester H. Bausback, Mary E. Gerritsen and Patrick E. Ward

Departments of Pharmacology and Physiology, New York Medical College, Valhalla, NY 10595 (U.S.A.)

(Received 26 June 1986)

Key words: Opioid peptide; Peptide metabolism; Aminopeptidase M; (Cerebral vasculature)

Aminopeptidase M (EC 3.4.11.2), which can degrade low molecular weight opioid peptides, has been reported in both peripheral vasculature and in the CNS. Thus, we have studied the metabolism of opioid peptides by membrane-bound aminopeptidase M derived from cerebral microvessels of hog and rabbit. Both hog and rabbit microvessels were found to contain membrane-bound aminopeptidase M. At neutral pH, microvessels preferentially degraded low molecular weight opioid peptides by hydrolysis of the N-terminal Tyr^1-Gly^2 bond. Degradation was inhibited by amastatin ($I_{50} = 0.2$ μM) and bestatin (10 μM), but not by a number of other peptidase inhibitors including captopril and phosphoramidon. Rates of degradation were highest for the shorter peptides (Met^5- and Leu^5-enkephalin) whereas β-endorphin was nearly completely resistant to N-terminal hydrolysis. K_m values for the microvascular aminopeptidase also decreased significantly with increasing peptide length ($K_m = 91.3 \pm 4.9$ and 28.9 ± 3.5 μM for Met^5-enkephalin and Met^5-enkephalin-Arg^6-Phe^7, respectively). Peptides known to be present within or in close proximity to cerebral vessels (e.g., neurotensin and substance P) competitively inhibited enkephalin degradation ($K_i = 20.4 \pm 2.5$ and 7.9 ± 1.6 μM, respectively). These data suggest that cerebral microvascular aminopeptidase M may play a role in vivo in modulating peptide-mediated local cerebral blood flow, and in preventing circulating enkephalins from crossing the blood-brain barrier.

Introduction

Opioid peptides may be involved in peripheral regulation of cardiovascular function [1]. Although capable of affecting vascular tone directly [2], they probably act more commonly through indirect mechanisms such as reducing transmitter release from sympathetic nerve terminals in the vessel wall [3]. Thus, the capacity of vasculature to degrade opioid peptides could have important physiologic significance [4].

We have previously found that a surface membrane fraction purified from large porcine blood vessels contains aminopeptidase M (EC 3.4.11.2) [5]. Although aminopeptidase M can metabolize low molecular weight opioid peptides [6], it is not known whether such metabolism occurs in microvasculature. Since membrane-bound aminopeptidase M is present in the CNS [7], and opioid peptides can alter cerebral vascular tone [2,8,9], we examined opioid peptide metabolism by isolated hog and rabbit cerebral microvessels.

Materials and Methods

Materials

All opioid and neurotensin peptides, leucyl-7-amido-4-methylcoumarin, leucyl-4-methoxy-2-naphthylamide, γ-glutamyl-2-naphthylamide, *o*-phenanthroline, bestatin, amastatin, puromycin and phosphoramidon (*N*-(α-rhamnopyranosyloxy-hydroxyphosphinyl)-L-leucyl-L-tryptophan) were obtained from Sigma Chemical Co (St. Louis,

---

Correspondence: Dr. P.E. Ward, Department of Pharmacology, New York Medical College, Valhalla, NY 10595, U.S.A.

0304-4165/87/$03.50 © 1987 Elsevier Science Publishers B.V. (Biomedical Division)

MO). Substance P, tetra(1–4)substance P and hepta(5–11)substance P were obtained from Peninsula Labs (San Carlos, CA). The angiotensin I-converting enzyme (EC 3.4.15.1) substrate ([^{3}H]benzoyl-Phe-Ala-Pro) and inhibitor (captopril) were obtained from Ventrex (Portland, ME) and Squibb (Princeton, NJ), respectively. The caboxypeptidase N (EC 3.4.17.3) inhibitor MERGETPA (DL-mercaptomethyl-3-guanidinoethylthiopropanoic acid) was obtained from Calbiochem-Behring (San Diego, CA). The nylon sieves used for microvessel isolation were from Tetko, Inc. (Elmsford, NY). Antibody to hog and rabbit renal brush border aminopeptidase M, obtained as previously described [5], precipitate aminopeptidase M but do not cross-react with other renal peptidases including aminopeptidase A (EC 3.4.11.7), dipeptidyl (amino)peptidase IV (EC 3.4.14.5), neutral endopeptidase (EC 3.4.24.11), carboxypeptidase P (EC 3.4.12.-) or angiotensin I-converting enzyme. All TLC and HPLC reagents were obtained as previously described [6].

Cerebral microvessel isolation

Tissues were obtained both frozen (Pel-Freeze; Rogers, AR) and from freshly slaughtered hogs and rabbits. Whole brains were immersed in cold phosphate-buffered saline (rabbit) or in Earle's buffer (pH 7.4) containing 0.1% (w/v) bovine serum albumin (hog). Microvessels were prepared according to Brendel et al. [10] as modified by Selivonchick and Roots [11]. Cortical grey matter was minced and homogenized (30 s) in 3 vol. of buffer using a Waring blender. The extract was then homogenized (Dounce, four strokes), poured through 1000 and 300-micron mesh nylon sieves and homogenized a second time. Vessels were collected on a 44-micron mesh sieve, centrifuged (4000 × g, 10 min) and resuspended (0.25 M sucrose). After centrifugation (21 000 × g, 45 min) on a discontinuous sucrose gradient (1.0 and 1.5 M), the pellet was freeze-powdered [12], sonicated and pelleted (20 000 × g, 15 min). Activity was measured either directly or after solubilization with 2% (v/v) Triton X-100. Microvessel purity was determined by phase contrast microscopy and assay of γ-glutamyltransferase (EC 2.3.2.2) [12].

Immunoelectrophoresis

Rocket and fused-rocket immunoelectrophoresis of the above detergent-solubilized membrane were carried out as described previously [5].

Enzyme assays

γ-Glutamyltransferase, aminopeptidase M and angiotensin I-converting enzyme activities were assayed as previously described [5]. Specific activities are expressed as units/mg protein where one unit equals the hydrolysis of one nmol substrate per min (γ-glutamyltransferase, enkephalin hydrolysis), 1% substrate hydrolyzed per min (converting enzyme) or change in relative fluorescence per min (aminopeptidase). Protein was determined using bovine serum albumin as a standard [13].

Opioid peptide metabolism

Qualitative analysis of opioid peptide metabolism was carried out by TLC on MN 300 cellulose plates [6]. Quantitative analysis was carried out by HPLC as previously described [6]. Where appropriate, inhibitors were preincubated with enzyme and buffer (20 min; 37°C) before addition of substrate. For pH experiments, a 100 mM sodium acetate buffer (pH 4.0–6.0) or a 100 mM sodium phosphate buffer (pH 6.5–8.0) were used. For K_m determinations, initial velocity was determined at six substrate concentrations (12.5–250 μM). Data were plotted according to the Lineweaver-Burk method ($1/V$ vs. $1/S$) and fit to the best straight line. For K_i determinations, initial velocity was determined at three substrate (Met^5-enkephalin) concentrations (50, 125 and 250 μM) in the presence of varying concentrations of peptide inhibitors added simultaneously. Data were plotted as $1/V$ vs. [I] and the K_i was determined graphically.

Results

Isolated microvessels

Phase contrast microscopy of isolated hog and rabbit cerebral microvessel preparations revealed intact vessels devoid of non-vascular contamination (Fig. 1). Vessels ranged in size from 7 to 70 microns in diameter and appeared as tangled masses exhibiting extensive dichotomous branching and numerous bifurcations. At higher magnifi-

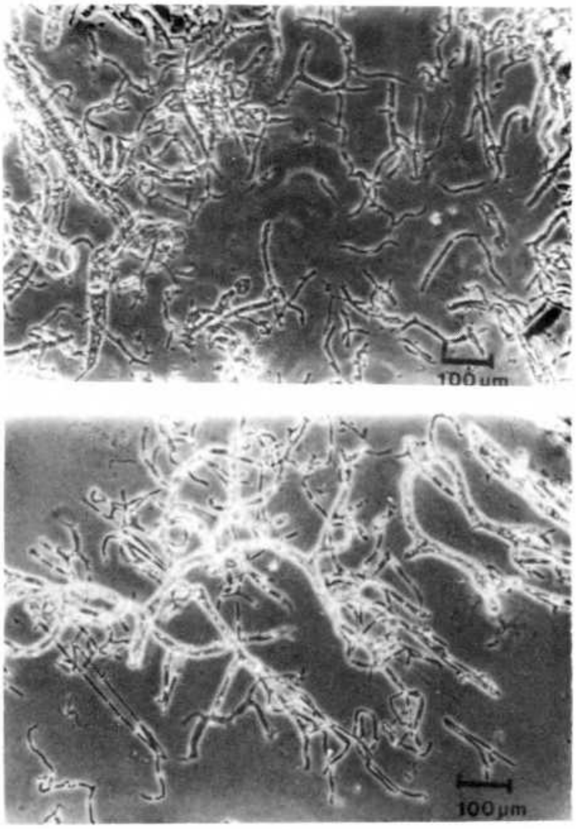

Fig. 1. Phase contrast micrographs of isolated hog (A) and rabbit (B) cerebral microvessels.

TABLE I

DISTRIBUTION OF γ-GLUTAMYLTRANSFERASE, ANGIOTENSIN I-CONVERTING ENZYME AND AMINOPEPTIDASE IN WHOLE BRAIN HOMOGENATE AND ISOLATED CEREBRAL MICROVESSELS

Specific activities are calculated as units/mg protein where one unit equals the hydrolysis of one nmol substrate per min (γ-glutamyltransferase), 1% substrate hydrolyzed per min (angiotensin I-converting enzyme) or change in relative fluorescence per min (aminopeptidase). Values given are the means ± S.E. from three experiments. Enrichment is calculated as (mean specific activity of microvessels fraction)/(mean specific activity of brain homogenate).

Enzyme	Brain homogenate	Cerebral microvessels	Enrichment
γ-Glutamyl transferase	0.15 ± 0.1	1.9 ± 0.5	12.7
Angiotensin I-converting enzyme	139 ± 10	2251 ± 450	16.2
Aminopeptidase	1.7 ± 0.3	9.8 ± 0.7	5.8

cations, endothelial cell nuclei could be visualized.

Microvessel purification was determined by marker enzyme enrichment (i.e., γ-glutamyltransferase and angiotensin I-converting enzyme). As seen in Table I hog cerebral microvessel γ-glutamyltransferase activity (1.9 ± 0.5 nmol/min per mg protein) was enriched 12.7-fold over the original homogenate (0.15 ± 0.1 units/mg). Similarly, microvessel angiotensin I-converting enzyme activity (2251 ± 450 units/mg) was 16.2-fold higher than original homogenate activity (139 ± 10 units/mg). Isolated microvessels also contained significant aminopeptidase activity (leucyl-7-amido-4-methylcoumarin hydrolysis). Homogenate and microvessel activities were 1.7 ± 0.3 and 9.8 ± 0.7 units/mg, respectively (Table I). Thus, microvessel aminopeptidase activity was enriched, although the extent of enrichment (5.8-fold) was somewhat less than that seen for γ-glutamyltransferase and angiotensin I-converting enzyme. Nevertheless, comparable increases were also found in rabbit cerebral microvessels (not shown). After centrifugation (20 000 × g, 15 min) of the freeze-powdered microvessels, more than 80% of the aminopeptidase activity was detected in the pelleted membrane fraction.

Immunologic analysis

Purified (Sigma) hog renal aminopeptidase M (H-AmM) and solubilized (2% v/v Triton X-100) membrane pellet of hog cerebral microvessels (H-CMV) were analyzed by fused-rocket immunoelectrophoresis. As shown in Fig. 2A, fused, rocket-shaped precipitates were visualized with no evidence of spurring. Shadowing of the precipitin lines resulted from overstaining in an effort to detect even minimal spurring. Thus, hog cerebral microvessel membrane (but not cytosol; not shown) contained an enzyme immunologically indistinguishable from renal aminopeptidase M. Similar experiments with antibody to rabbit brush border aminopeptidase M established that the rabbit cerebral microvessels (R-CMV) also contained an aminopeptidase immunologically indistinguishable from rabbit aminopeptidase M

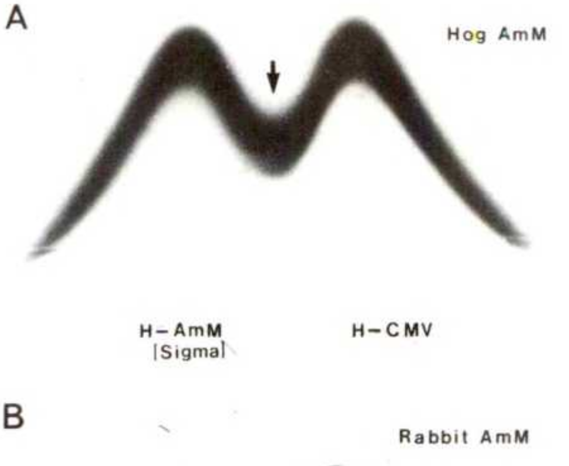

Fig. 2. Fused-rocket immunoelectrophoresis of detergent-solubilized hog aminopeptidase M (H-AmM/Sigma) (A) and rabbit kidney brush border aminopeptidase M (R-AmM/KBB) (B) with detergent-solubilized hog and rabbit cerebral microvessel membrane (CMV). After 1 h for diffusion, samples were vertically electrophoresed into gel containing anti-hog or anti-rabbit aminopeptidase M immunoglobulin at 2 V/cm for 18 h. Precipitin lines were visualized by staining for enzyme activity. Vertical arrows indicate areas of fusion.

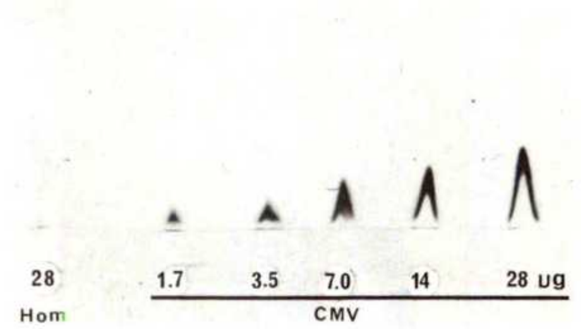

Fig. 3. Rocket immunoelectrophoresis of solubilized hog cerebral homogenate (Hom; 28 μg) and microvessel membrane (CMV; 1.7–28 μg). Samples were vertically electrophoresed into gel containing anti-hog aminopeptidase M immunoglobulin at 20 V/cm for 2 h. Precipitin lines were visualized by staining for enzyme activity.

solubilized from kidney brush border (R-AmM/KBB) (Fig. 2B).

Rocket-immunoelectrophoretic studies were carried out to quantify hog cerebral aminopeptidase M. Solubilized brain homogenate protein (28 μg) produced only a marginally detectable aminopeptidase M preciptin peak (Fig. 3; left side). However, the same amount of solubilized hog cerebral microvessel protein produced a strong, rocket-shaped precipitate (Fig. 3; right side), and sequential dilutions produced peak areas proportional to the amounts of microvessel protein used. As little as 1.7 μg of microvessel protein produced a peak approximately twice as large as the 28 μg of brain homogenate protein, indicative of approximately a 30-fold enrichment of immunoreactive aminopeptidase M in purified microvessels, The relatively small amount of immunoreactive aminopeptidase M in brain homogenate (compared to the rate of synthetic substrate hydrolysis shown in Table I) indicates that the majority of brain homogenate activity may be due to aminopeptidases other than aminopeptidase M, and is consistent with the variety of aminopeptidases found within the CNS [14].

Enkephalin metabolism-TLC

Incubation of Met^5-enkephalin with the above hog (Fig. 4A) or rabbit (Fig. 4B) cerebral microvessel protein and subsequent separation of metabolites by TLC revealed that the peptide was rapidly metabolized, producing the N-terminal Tyr metabolite within 10–15 min. With longer incubation, a second metabolite also appeared (Gly; not shown), demonstrating sequential N-terminal hydrolysis. Comparable results were obtained with all other opioid peptides tested except for [D-Ala^2]-Met^5-enkephalin, which was resistant to N-terminal hydrolysis even during extended incubations. Rather, slow carboxyl hydrolysis was observed (Phe/Met products) which was inhibited by the angiotensin I-converting enzyme inhibitor captopril (10 μM). Thus, despite the co-localization of converting enzyme, enkephalins were preferentially degraded by hydrolysis of the N-terminal Tyr^1-Gly^2 bond. Further, these observations with extracted microvessel membrane were con-

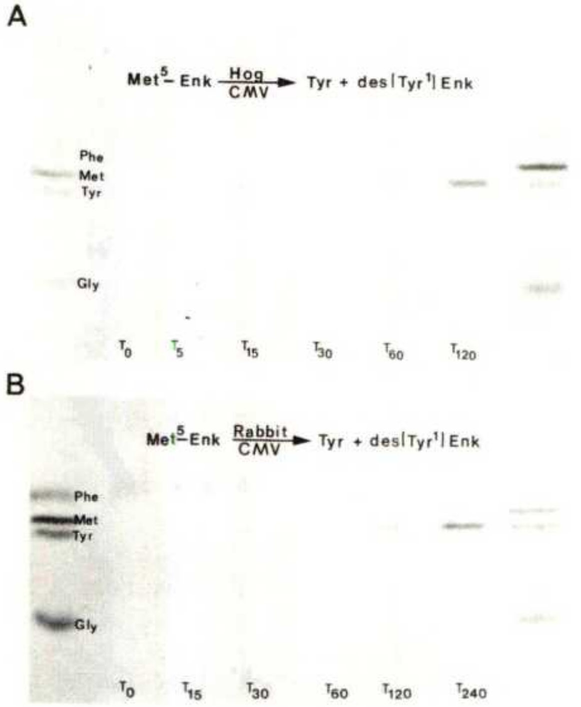
A
Met^5-Enk $\xrightarrow[CMV]{Hog}$ Tyr + des[Tyr^1]Enk
Phe
Met
Tyr
Gly
T_0
T_5
T_{15}
T_{30}
T_{60}
T_{120}
B
Met^5-Enk $\xrightarrow[CMV]{Rabbit}$ Tyr + des[Tyr^1]Enk
Phe
Met
Tyr
Gly
T_0
T_{15}
T_{30}
T_{60}
T_{120}
T_{240}

Fig. 4. Metabolism of Met^5-enkephalin by hog (A) and rabbit (B) cerebral microvessels (CMV) during 120 or 240-min incubations. Standards include phenylalanine (Phe), methionine (Met), tyrosine (Tyr) and glycine (Gly). Reaction metabolites and standards were spotted and developed in butanol/acetic acid/water (4:1:5) and stained for protein with 0.4% (w/v) ninhydrin in acetone.

firmed even when incubations were carried out with freshly prepared intact microvessels.

Enkephalin metabolism-HPLC

Cerebral microvessel membrane Met^5-enkephalin hydrolysis was directly proportional to both time of incubation and amount of microvessel protein used. Activity was optimal at pH 7.0 and was unaffected by $CaCl_2$ (1 mM). Both amastatin and bestatin were potent inhibitors with I_{50} values of 0.2 and 10 μM, respectively. Puromycin was significantly less effective ($I_{50} = 90$ μM). Enkephalin degradation was also inhibited by both 1 mM EDTA (85%) and 1 mM *o*-phenanthroline (100%). However, inhibitors of angiotensin-converting enzyme (captopril), carboxypeptidase N (MERGETPA) and neutral endopeptidase (phosphoramidon) had no significant effect (less than 5% inhibition at 10 μM final concentration).

Since aminopeptidase M was previously found to hydrolyze opioid peptides at different rates [6], the metabolism of larger opioid peptides were examined. As seen in Fig. 5, a clear relationship between rate of N-terminal hydrolysis and peptide length was apparent. Met^5- and Leu^5-enkephalin were hydrolyzed at comparable rates, whereas Met^5-enkephalin-Arg^6-Phe^7 and Met^5-enkephalin-Arg^6-Gly^7-Leu^8 were hydrolyzed more slowly. Hydrolysis of dynorphin (1–10) and dynorphin (1–13) was only 20 and 10%, respectively, as fast as that of Met^5-enkephalin. No significant degradation of β-endorphin was detected.

This progressive decrease in rat of degradation with increasing peptide length was also seen when velocities were calculated over a range of substrate concentrations of Met^5-enkephalin and Met^5-enkephalin-Arg^6-Phe^7. Maximal velocity decreased from 65.8 ± 1.8 nmol/min per ml for Met^5-enkephalin to 39.3 ± 0.6 units/ml for Met^5-enkephalin-Arg^6-Phe^7 (Table II). Similarly, the K_m of Met^5-enkephalin-Arg^6-Phe^7 (28.9 ± 3.5 μM) for the microvascular aminopeptidase was significantly lower than that of Met^5-enkephalin (91.3 ± 4.9 μM). Nevertheless, as previously found [6], further increases in chain length (i.e., dynorphin(1–10) and dynorphin(1–13)) were not associated with further changes in K_m (not shown).

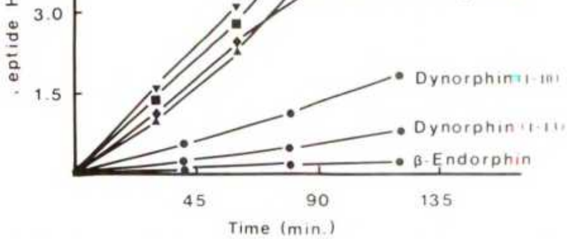

Fig. 5. N-terminal hydrolysis of low molecular weight opioid peptides (200 μM) by hog cerebral microvessels.

TABLE II

KINETICS OF N-TERMINAL HYDROLYSIS OF OPIOID PEPTIDES BY HOG CEREBRAL MICROVESSEL AMINOPEPTIDASE M AND ITS INHIBITION BY ENDOGENOUS PEPTIDES

Assays were performed at six substrate concentrations (12.5–250 μM). Values given are the means ± S.E. or averages of two determinations. Neurotensin: pGlu^1-Leu^2-Tyr^3-Glu^4-Asn^5-Lys^6-Pro^7-Arg^8-Arg^9-Pro^{10}-Tyr^{11}-Ile^{12}-Leu^{13}. Substance P: Arg^1-Pro^2-Lys^3-Pro^4-Gln^5-Gln^6-Phe^7-Phe^8-Gly^9-Leu^{10}-Met^{11}(NH_2).

Peptide	K_m (μM)	V_{max} (nmol/min per ml)	K_i (μM)
Met^5-enkephalin (n = 3)	91.3 ± 4.9 (n = 3)	65.8 ± 1.8	–
Met^5-enkephalin-Arg^6-Phe^7	28.9 ± 3.5 (n = 3)	39.3 ± 0.6 (n = 3)	–
Neurotensin	–	–	20.4 ± 2.5 (n = 5)
Neurotensin (8–13)	–	–	14.1 ± 1.6 (n = 4)
Substance P	–	–	7.9 ± 1.6 (n = 4)
Substance P (5–11)	–	–	25.3 ± 3.5 (n = 3)
Substance P (1–4)	–	–	56 (48, 64)

Neurotensin and neurotensin(8–13) were effective competitive inhibitors of Met^5-enkephalin degradation, with K_i values of 20.4 ± 2.5 and 14.1 ± 1.6 μM, respectively (Table II). Similarly, several tachykinin sequences were effective inhibitors, with the intact undecapeptide substance P being the most potent ($K_i = 7.9 \pm 1.6$ μM). Conversely, angiotensin II was relatively ineffective ($K_i = 200$ μM; not shown).

Discussion

In addition to plasma [1], enkephalins have been identified in pial, arachnoid and cerebral arteries [15]. Although Wahl [16] observed no significant changes in pial arterial dimensions by direct application of Leu^5-enkephalin, other studies have reported both constrictor [8,17] and dilator [9,18] effects. Enkephalins may also modulate vascular tone by affecting substance P-mediated neurogenic vasodilatation [19].

We have previously demonstrated that a plasma membrane fraction purified from large porcine blood vessels contained aminopeptidase M [5], and that specificity and kinetic data (changes in maximal velocity and K_m relative to peptide length) were consistent with a capacity for differential metabolism of opioid peptides in the microenvironment of vascular cell surface receptors [6]. However, whether such metabolism occurred in more physiologically significant systemic and/or specialized microvasculature was unknown.

Cerebral microvessels contain membrane-bound aminopeptidase M. Despite the presence of converting enzyme, enkephalins were preferentially hydrolyzed at their N-termini. Although contamination by other aminopeptidase cannot be ruled out, the characteristics of microvascular enkephalin hydrolysis are comparable to those reported for vascular plasma membrane aminopeptidase M [6], renal aminopeptidase M [20] and cerebral membrane aminopeptidase M [7]. These similarities include hydrolysis of N-terminal neutral and basic amino acids, sensitivity to inhibition by amastatin and bestatin, a relative insensitivity to inhibition by puromycin, and decreased rates of hydrolysis and K_m for larger opioid peptides. Further, some of these same characteristics rule out other peptidases such as cytosolic leucine aminopeptidase (EC 3.4.11.2) and aminopeptidase B (EC 3.4.11.6), and aminopeptidase A (EC 3.4.11.7), which is specific for N-terminal acidic amino acids and is activated by $CaCl_2$. Collectively, these data support the identification of aminopeptidase M as the principal enzyme responsible for microvascular enkephalin degradation. Indeed, considering the small amount of brain homogenate immunoreactive aminopeptidase M found in the present study, and the fact that the puromycin-insensitive aminopeptidase M characterized by Gros et al. [7] represented a small fraction of total cerebral membrane aminopeptidase activity, it is tempting to speculate that the majority of CNS aminopeptidase M may be localized to the vasculature.

The cellular localization of cerebral microvascular aminopeptidase M remains to be determined. If present on endothelium, aminopeptidase M could modulate the effects of circulating enkephalins on local blood flow. Endothelial aminopeptidase M could also function as a component of the blood-brain barrier to prevent peripheral opioids from entering the central nervous system [21]. Indeed, an endothelial localization would seem likely considering the epithelial (brush border) localization of renal aminopeptidase M and the epithelial properties of cerebral capillary endothelium [22]. Nevertheless, as in aortic smooth muscle cells [23], aminopeptidase M may also be present within the cerebral vascular wall. Such a localization would facilitate metabolism of locally released enkephalins and/or other perivascular peptides.

Vasoactive peptides such as substance P and neurotensin are present in both plasma and perivascular (e.g., cerebral) nerve terminals [24–26]. In addition to the modulating effects these peptides may have on one another [19], the results obtained in the present study demonstrate that they have the capacity to potentiate enkephalin levels by inhibition of aminopeptidase M-mediated enkephalin degradation. For instance, if local levels of substance P or its metabolites reach low micromolar concentrations in vivo, potentiation of circulating and/or local enkephalin levels could serve to attenuate further release of substance P [19].

Acknowledgements

This work was supported by grants R01 AM 28184 and R01 HL 34814/P01 HL 34300. We would like to thank the Karl Ehmer Co. for supplying fresh hog tissues.

References

1 Pfeiffer, N. and Illes, P. (1984) Trends Pharmacol. Sci. 5, 414–415

2 Hanko, J.H. and Hardebo, J.E. (1978) Eur. J. Pharmacol. 51, 295–297

3 Illes, P., Pfeiffer, N., Limberger, N. and Starke, K. (1983) Life Sci. 33 (Suppl. I), 307–310

4 Hughes, J. (1983) Br. Med. Bull. 39, 17–24

5 Ward, P.E. (1984) Biochem. Pharmacol. 33, 3183–3193

6 Bausback, H.H. and Ward, P.E. (1986) Biochim. Biophys. Acta 882, 437–444

7 Gross, C., Giros, B. and Schwartz, J.C. (1985) Biochemistry 24, 2179–2185

8 Sandor, P., Demchenko, I.T., Morgalyov, Y.N., Moskalenko, Y.E. and Kovach, A.G.B. (1983) Acta Physiol. Acad. Sci. Hung. 61, 155–161

9 Kobari, M., Gotoh, F., Fukuuchi, Y., Amano, T., Suzuki, N., Uematsu, D., Obara, K., Gogolak, I. and Sandor, P. (1985) J. Cereb. Blood Flow Metab. 5, 34–39

10 Brendel, K., Meezan, E. and Carlson, E.C. (1974) Science 185, 953–955

11 Selivonchick, D.P. and Roots, B.I. (1977) Lipids 12, 165–169

12 Gerritsen, M.E. and Printz, M.P. (1981) Circ. Res. 49, 1152–1163

13 Bradford, M.M. (1976) Anal. Biochem. 72, 248–254

14 Schwartz, J.-C., Malfroy, B. and DeLaBaume, S. (1981) Life Sci. 29, 1715–1740

15 Moskowitz, M.A., Liu-Chen, L.-Y., Mayberg, M.R., Norregaard, T.V., Weatherwax, R.C. and Gillespie, S. (1983) in Substance P (Skrabanek, P. and Bowell, D., eds.), pp. 217–218, Boole Press, Dublin

16 Wahl, M. (1982) in Cerebral Blood Flow: Effects of Nerves and Neurotransmitters (Heistad, D.D. and Marcus, M.L., eds.), pp. 235–241, Elsevier/North Holland, New York

17 Waters, A. and Harders, D.R. (1983) Neurosurgery 13, 676–679

18 Harder, D.R. and Madden, J.A. (1984) Eur. J. Pharmacol. 102, 411–416

19 Lembeck, F., Donnerer, J. and Bartho, L. (1982) Eur. J. Pharmacol. 85, 171–176

20 Austen, B.M. and Smyth, D.G. (1977) Biochem. Biophys. Res. Commun. 76, 477–482

21 Pardridge, W.M. and Mietus, L.J. (1981) Endocrinology 109, 1138–1143

22 Betz, A.L. (1985) Fed. Proc. 44, 2614–2615

23 Palmieri, F.E., Luckett, P.M., Stalcup, S.A. and Ward, P.E. (1984) Fed. Proc. 43, 651

24 Chan-Paley, V. (1977) in Neurogenic Control of the Brain Circulation (Owman, C. and Edvinsson, L., eds.), pp. 39–53, Pergamon press, Oxford

25 Said, S.I. (1983) Hypertension 5 (Suppl. I), I17–I26

26 Edvinsson, L. (1985) Trends Neurosci. 8, 126–131

Biochimica et Biophysica Acta 923 (1987) 42–45
Elsevier

BBA 22476

Lipids associated with tissue transglutaminase

Jolan Harsfalvi, Gabriella Arato and Laszlo Fesus

2nd Department of Medicine, 3rd Department of Medicine and Department of Biophysics, University School of Medicine, H-4012 Debrecen (Hungary)

(Received 28 July 1986)

Key words: Transglutaminase; Neutral lipid; Phospholipid; Covalent modification; Lauric acid; Membrane association

A substantial amount of lipids (cholesterol and its esters, mono-, di- and triacylglycerols, free fatty acids and the phospholipids phosphatidylethanolamine and phosphatidylinositol) was found associated with tissue transglutaminase purified to apparent homogeneity from guinea pig liver. Removal of lipids results in an increased tendency of the enzyme for self-association and a decreased stability. Lauric acid was detected following hydroxylamine treatment of the enzyme, suggesting the occurrence of a fatty acid-type, covalent, posttranslational modification of transglutaminase. The results provide support for the idea that part of tissue transglutaminase may be localized in the cell membrane.

Introduction

Transglutaminases are Ca^{2+}-dependent enzymes catalyzing an acyl transfer reaction between peptide-bound glutamine and the primary amino group of various amines including the ε-amino group of properly positioned lysine in substrate proteins [1]. Five isoenzyme forms of transglutaminase have been described so far, namely blood coagulation factor XIII in plasma, the epidermal, prostatic and hair follicle transglutaminases, and the ubiquitous tissue ('liver') type in cells [1–3]. Varying portions of the cellular transglutaminase have been found associated with the membrane fraction following tissue or cell homogenization [3–8], suggesting that under certain conditions this enzyme is localized in or associated with the cell membrane in living cells and tissues. There are no biochemical data, however, to explain the mechanism of the membrane localization of transglutaminases. We have recently found that a specific interaction occurs between purified liver transglutaminase and small unilamellar phospholipid vesicles at the lipid phase transition [9]. Now we present data showing that a substantial amount of lipid material, including covalently bound fatty acid, is associated with purified, guinea pig liver transglutaminase.

Materials and Methods

Transglutaminase. Guinea pig liver transglutaminase was purified according to Connellan et al. [10]. Its activity was assayed by measuring ammonia released during the transfer reaction between benzyloxycarbonyl-L-glutamylglycine and methylamine [9]. Electrophoretic behavior was studied using alkaline urea and sodium dodecyl sulfate-polyacrylamide gel electrophoresis [11,12].

Lipid extraction and analysis. Lipids were extracted from transglutaminase protein solution by chloroform/methanol (2 : 1, v/v; [13]). Mild extraction was carried out at 4°C by light petroleum/*n*-butanol (7 : 3, v/v; [14]). Organic solvents

---

Correspondence: Dr. L. Fesus, Department of Biophysics, University Medical School of Debrecen, H-4012 Debrecen, Hungary.

0304-4165/87/$03.50 © 1987 Elsevier Science Publishers B.V. (Biomedical Division)

were evaporated, the dry lipid was dissolved in chloroform and stored under nitrogen at $-30\,^\circ$C until the analysis. Aliquots were used for quantitation of total lipids and phospholipids [15,16], then a portion was spotted on a high performance thin layer plate (HPTLC plates silicagel 60 MERCK) to determine lipid pattern. The plate was developed in light petroleum/diethyl ether/acetic acid (82 : 18 : 1, v/v). Phospholipids which remained in the origin were scraped from the previous plate, resolved, applied to another plate and separated in chloroform/methanol/isopropanol/0.25% aqueous potassium chloride/acetic acid (60 : 18 : 50 : 12 : 36, v/v). Lipids were detected by conventional staining procedures [17] and identified comparing them to standards. Cholesterol and its esters, tri-, di- and monoacylglycerols, and fatty acids were obtained from Sigma; phosphatidylethanolamine, phosphatidylserine and phosphatidylinositol from Applied Science. All materials were reagent grade, and the organic solvents were destilled before use.

Protein-bound fatty acid. Transglutaminase, which had been extracted by light petroleum/*n*-butanol, was treated with hydroxylamine (1 mol/l, pH 7.0, for 6 h) then the protein-free aqueous solution obtained by centrifree Micropartition (Amicon) separation was extracted with eleven parts of chloroform/methanol (2 : 1, v/v) and analyzed by gas chromatography. Samples treated with diazomethane/diethyl ether solution to transform fatty acid hydrroxamates to fatty acid methyl esters, were injected into the gas chromatograph (Hewlett Packard, 5840 A) equipped with flame ionization detector ($300\,^\circ$C), and analyzed at 105–$300\,^\circ$C (heating rate 5 Cdeg/min) on a column packed with 10% OV-1 on Gaschrom Q 80–100 mesh.

Results and Discussion

A substantial amount of lipids could be extracted from the purified transglutaminase solution by chloroform/methanol; varying from batch to batch it was in the range of 13–120 μg/mg transglutaminase protein. Qualitative analysis of the extracted material showed mono-, di- and triacylglycerols, cholesterol and its esters, free fatty acids and phospholipids (Fig. 1a). The latter constituted about 2–5% of the total lipid by weight and was mainly phosphatidylethanolamine and phosphatidylinositol (Fig. 1b). The procedures for the purification of the guinea pig liver transglutaminase involves (following homogenization of liver in sucrose and ultracentrifugation) three ion exchange chromatography steps and one gel filtration step, a precipitation with ammonium sulfate and another with protamine sulfate [10]. The fact that the purified protein still carries lipids suggests a strong association between them and the possibility that some of the enzyme molecules may be originally localized in a lipid environment and then released during homogenization. The extraction and analytical procedures were repeated using different batches of transglutaminase preparations including one which was a kind gift of Dr. S.I. Chung (Enzyme Chemistry Section, NIDR, NIH, Bethesda, MD); the results were essentially the same, differing only in the quantity of total lipids associated with the enzyme. As shown in Fig. 2, the electrophoretic behavior of transglutaminase did not change following the extraction of lipids and their storage at $+4\,^\circ$C in the presence of EGTA and dithiothreitol. An increased tendency for self-association was observed during incubation of the enzyme at $37\,^\circ$C following lipid extraction (Fig. 2a). Specific activity of the enzyme decreased about 50% following

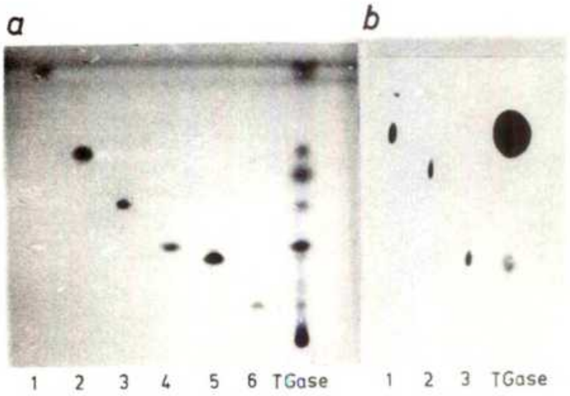

Fig. 1. Thin layer chromatography of lipids extracted from transglutaminase (Tgase). Panel a: neutral lipids; cholesterol ester (1), triacylglycerol (2), free fatty acid (3), cholesterol (4), diacylglycerol (5), monoacylglycerol (6) are standards. Panel b: phospholipids, obtained from origin of the previous plate; phosphatidylethanolamine (1), phosphatidylserine (2), phosphatidylinositol (3) are standards. 200 μg extracted lipid was applied onto the first plate.

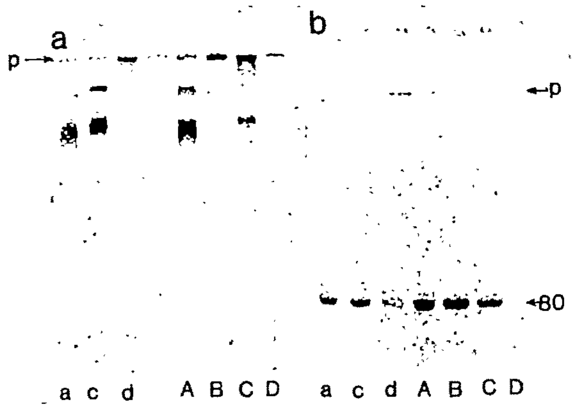

Fig. 2. Polyacrylamide gel electrophoresis of transglutaminase. Panel a: alkaline urea gel (10% acrylamide); a, c, d columns before, and A, B, C, D columns after delipidation and incubation at 37°C in the absence of Ca^{2+} for 0 (a, A), 20 (B), 60 (c, C) min or in the presence of 10 mM Ca^{2+} for 60 min (d, D). Panel b: sodium dodecyl sulfate gel (4% acrylamide): a, c, d, A, B, C, D samples were prepared parallel to those for alkaline urea polyacrylamide gel electrophoresis. p indicates high molecular weight polymers not entering separating gels. 80 shows the position of 80 kDa protein (molecular mass of transglutaminase) as determined by molecular weight standards.

the removal of lipids (data not shown). Enzymatic self cross-linkage [18] of the intact transglutaminase as well as the enzyme treated with organic solvent occurred when incubations were carried out at 37°C in the presence of Ca^{2+}.

Following the treatment of lipid-depleted transglutaminase protein with hydroxylamine (a method generally used to uncouple ester-linked fatty acids from proteins [19]), a fatty acid could be detected in the chloroform/methanol extract of the protein-free solution. Using appropriate standards the fatty acid was identified as lauric acid (Fig. 3). This was 0.5–1.4 mol per mol transglutaminase (using 80000 Da as the molecular mass of the enzyme in the calculation). It was not found without the addition of hydroxylamine. Recently, fatty acid modification of several viral and cellular proteins (including oncogen coded membrane proteins) have been observed [20–24] and these data have been convincingly used to explain the membrane localization of these proteins. Protein-bound fatty acids may serve as signals for membrane targeting and contribute to either an anchorage to the inner surface of the cell membrane or to a tight binding of integral membrane proteins to specific lipid structures in the bilayer of the membrane. In the case of transglutaminases, several investigators have demonstrated varying degrees of association of this enzyme with the membrane fraction prepared from cells and tissues [3–8,25, 26]. Although the tissue (liver) type of transglutaminase seems to be mostly cytoplasmic in cultured cells [27], quite a high proportion of it was found in the membrane fraction prepared from tissues such as liver [4,25] and lung [8]. The localization of epidermal transglutaminase is almost exclusively the cell membrane [3,5,26]. Since we used a tissue to purify the enzyme it is not possible to decide what cell type was the source of the enzyme-lipid complex. However, our transglutaminase preparation is antigenically homogeneous: it does not cross-react with antibodies raised against epidermal, hair follicle and blood coagulation factor XIII transglutaminases (data not shown). Therefore, the most likely explanation

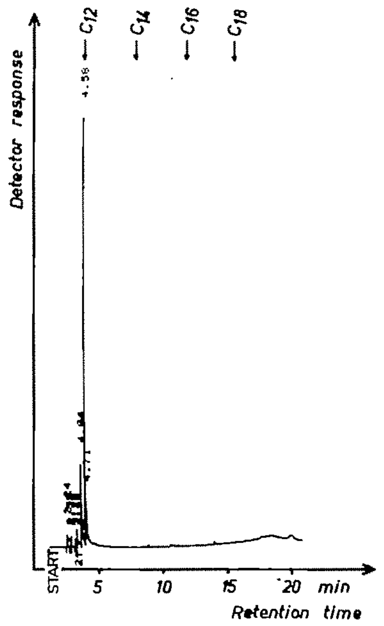

Fig. 3. Gas chromatography profile of the chloroform/methanol extract prepared from the protein-free aqueous solution of hydroxylamine-treated transglutaminase (300 μg protein). Before hydroxylamine treatment the enzyme was extracted with light petroleum/n-butanol (7:3, v/v) at 4°C). ↓ with number represents the retention time of saturated fatty acid standards with given carbon atoms as determined in a separate run.

of our finding is that tissue transglutaminase in liver is partially membrane-associated [4,25], because of fatty acylation and the observation that a portion of the membrane-localized transglutaminase is released during the homogenization procedure carrying some of the lipids with which it was associated in the bilayer.

We have previously shown that an interaction takes place between purified liver transglutaminase and small unilamellar phospholipid vesicles at the lipid phase transition [9]. The activity of transglutaminase inserted into the lipid layer is greatly reduced [9]. Interestingly, an increased transglutaminase activity can be measured in lysates of several kinds of cells shortly following their stimulation; e.g., in lymphocytes treated with mitogens [28], in macrophages during the process of immune-complex-induced phagocytosis [29], in mast cells upon immunologic and non-immunologic stimuli to release histamine [30], in isoproterenol-stimulated glioma cells [31], in sympathetic ganglion after axotomy [32], and in liver following hepatectomy [33]. Since the inhibition of protein synthesis did not prevent the increased activities, it is possible that enzyme molecules are released from the lipid environment related to cell activation. As a consequence, more catalytically active transglutaminase molecules are available, the measurable activity is higher and an increased amount of transglutaminase product (like protein bound γ-glutamylhistamine in mast cells [30]) can be detected. In such an interpretation, membrane-bound transglutaminase may represent a properly positioned inactive ('cryptic') enzyme pool which is readily activated by its release from the membrane and the increasing Ca^{2+} concentration [34] during the biochemical process of transmembrane signaling.

Acknowledgement

We gratefully acknowledge the help of J. Harangi (Biochemical Department of L. Kossuth University) in performing the gas chromatographic analysis.

References

1 Folk, J.E. (1980) Annu. Rev. Biochem 49, 517–531

2 Chung, S.I (1975) in Isoenzymes, Vol 1 (Market, C L, ed.), pp 259–272, Academic Press, New York

3 Thacher, S M and Rice, R.H. (1985) Cell 40, 685–695

4 Slife, C.W., Dorsett, M D, Bouquett, G T, Register, A, Taylor, E and Conroy, S (1985) Arch. Biochem. Biophys. 241, 329–336

5 Lichti, U., Ben, T and Yuspa, S H. (1985) J Biol. Chem. 260, 1422–1426

6 Schmidt, R, Reichert, U., Michael, S., Shroot, B. and Boucher, M. (1985) FEBS Lett. 186, 201–204

7 Bures, M.D., Goldsmith, L.A and Stone, K.R (1980) Invest. Urol 17, 298–304

8 Chang, S K. and Chung, S.I. (1986) J Biol Chem 261, 8112–8121

9 Fesus, L, Horvath, A. and Harsfalvi, J (1983) FEBS Lett 155, 1–5

10 Connellan, J.M., Chung, S.I., Whetzel, N K., Bradley, L M and Folk, J.E. (1970) J Biol. Chem. 246, 1093–1096

11 Head, J.F. and Perry, S V. (1974) Biochem. J. 137, 145–153

12 Laemmli, U K. (1970) Nature 277, 680–685

13 Bowyer, D.E and King, J.P (1977) J. Chromatogr. 143, 473–490

14 Emmelot, T P. and Bos, C.J. (1968) Biochim. Biophys. Acta 150, 341–353

15 Bragdon, J.H (1951) J Biol Chem. 190, 513–517

16 Itaya, K. and Ui, M (1966) Clin. Chim. Acta 14, 361–366

17 Kates, M. (1972) in Techniques of lipidology (Work, T.S. and Burden, R., eds.), pp 335–441, North-Holland, Amsterdam

18 Birckbichler, P J., Orr, G.R., Carter, H.A and Patterson, M.F., Jr. (1977) Biochim Biophys Res. Commun 78, 1–5

19 Schlesinger, M.J and Magee, A I. (1982) Biophys J. 37, 126–127

20 Schlesinger, M.J. (1981) Annu. Rev. Biochem 50, 193–206

21 Dahl, C.E, Dahl, J.S and Bloch, K. (1983) J Biol Chem 258, 11814–11818

22 Henderson, L E, Krutzsch, H.C. and Oroszlan, S (1983) Proc Natl Acad. Sci. USA 80, 339–343

23 Berger, M. and Schmidt, M.F.G (1984) J. Biol Chem. 259, 5364–5367

24 Kaufman, J.F, Krangel, M.S. and Strominger, J L (1984) J. Biol. Chem. 259, 7230–7238

25 Barnes, R N, Bungay, P J., Elliott, B.M., Walton, P.L and Griffin, M. (1985) Carcinogenesis 6, 459–463

26 Simon, M. and Green, H. (1985) Cell 40, 677–683

27 Davies, P J.A., Cornwell, M.M, Johnson, J D., Reggiom, A., Myer, M. and Murtaugh, M.P. (1984) Diab. Care 7, Suppl. 1, 35–41

28 Novogrodsky, A., Quittener, S., Rubin, A L. and Stenzel, K.H. (1978) Proc. Natl. Acad Sci. USA 75, 1157–1161

29 Fesus, L., Sandor, M., Horvath, A., Bagyinka, C., Erdei, A. and Gergely, A. (1981) Mol. Immunol 18, 633–638

30 Fesus, L, Szucs, E.F, Barrett, K., Metcalfe, D.E. and Folk, J.E (1985) J. Biol. Chem. 260, 13771–13779

31 Komer, G. and Bachrach, U (1985) J Cell Physiol. 124, 379–385

32 Gilad, G.M., Varon, L.E. and Gilad, V.H. (1985) J Neurochem 44, 1385–1390

33 Haddox, M.K. and Russel, D.H. (1981) Proc. Natl. Acad Sci USA 78, 1712–1716

34 Fesus, L, Harsfalvi, J, Horvath, A. and Sandor, M. (1984) Mol Immunol. 21, 1161–1165

Biochimica et Biophysica Acta 923 (1987) 46–51
Elsevier

BBA 22559

Effect of Ca^{2+} and Mg^{2+} on the uptake of Fe^{3+} by mouse intestinal mucosa

Kishor B. Raja, Robert J. Simpson and Timothy J. Peters

Division of Clinical Cell Biology, MRC Clinical Research Centre, Harrow, HA1 3UJ (U.K.)

(Received 5 May 1986)

Key words: Ferric ion absorption; Hypoxia; Calcium ion; Magnesium ion; (Mouse intestinal mucosa)

Initial Fe^{3+} uptake rates by mouse intestinal fragments were determined in vitro. Uptake was dependent primarily on the Fe^{3+}-nitrilotriacetate complex concentration. Addition of Ca^{2+} and Mg^{2+} to the incubation medium had only small effects on the Fe^{3+} uptake rate. Duodenal fragments from hypoxic animals showed enhanced uptake of Fe^{3+}; this increase was more pronounced with a divalent cation-free medium. Ca^{2+} markedly diminished the Fe^{3+} uptake by mucosa from hypoxic mice; Mg^{2+} had no appreciable effect. Distal ileal fragments exhibited lower uptake rates compared to the duodenum, but were more sensitive to the effects of added Ca^{2+}. The ileal fragments did not show an adaptive response of Fe^{3+} uptake to hypoxia. These results suggest the existence of more than one pathway for mucosal Fe^{3+} uptake. One pathway, sensitive to Ca^{2+} and not stimulated by hypoxia, may be present in the duodenum and ileum. A second pathway, inhibited by Ca^{2+} and exhibiting an adaptive response to hypoxia, occurs only in the duodenum. This latter pathway is more sensitive to the effects of metabolic inhibitors.

Introduction

Iron homeostasis is controlled primarily by the regulation of proximal intestinal absorption. Iron in food is mainly present as complexes or chelates and its availability for absorption is dependent on the effective stability of these complexes. Thus, the nature of the ligands forming chelate compounds with iron and the ionic composition of the luminal contents are important in determining the rate of iron absorption.

An in vitro method has previously been described by Cox and Peters [1] for determining the initial rates of iron uptake by human intestinal biopsy specimens. This technique has also been applied to study iron uptake by intestinal fragments from rabbits [2] and more recently mice [3]. The incubation medium used by these workers contains Ca^{2+} and Mg^{2+}, both of which may affect the rate of iron uptake. Indeed, Simpson and Peters [4] have previously shown that the rate of uptake of Fe^{3+} by brush-border membrane vesicles is enhanced by divalent cations. This enhancement may be due to the competition of these cations with iron for the chelating ligand, nitrilotriacetate [5]. In contrast, most nutritional studies have demonstrated that calcium reduces the absorption of iron from the diet [6–9].

In this paper we have investigated the effect of Ca^{2+} and Mg^{2+} on the rate of Fe^{3+} uptake by mouse intestinal fragments. In addition, similar studies were performed with hypoxic mice, as these provide a convenient model of enhanced iron absorption [3].

Abbreviation: Hepes, 4-(2-hydroxyethyl)-1-piperazineethanesulphonic acid.

Correspondence: Mr K.B Raja, Division of Clinical Cell Biology, MRC Clinical Research Centre, Watford Road, Harrow, HA1 3UJ, U K.

0304-4165/87/$03.50 © 1987 Elsevier Science Publishers B V (Biomedical Division)

Materials and Methods

Reagents. Biochemicals were purchased from BDH Chemicals (Poole, Dorset, U.K.) and were of Analar Grade. Hepes, nitrilotriacetic acid (trisodium salt) and 2,4-dinitrophenol were purchased from Sigma Chemical Company Ltd., Poole, Dorset, U.K. Radioisotopes were purchased from Amersham International, Amersham, U.K.

Animals. Male mice, To strain, 6–8 weeks of age, were fed a standard rodent diet (K & K, Greeff Chemicals Ltd, Croydon, U.K.).

Hypoxia. Animals were subjected to a simulated altitude of 15000–16000 feet by placing them in a hypobaric chamber maintained at 53.3 kPa (0.5 atm) for 3 days. Food and water were provided ad libitum during this period.

Fe^{3+} uptake studies. An in vitro technique, previously described [1,3], was used for determining initial rates of iron uptake by intestinal mucosal fragments. The method satisfies the criteria set by Sallee et al. [10] for the valid measurement of rates of unidirectional uptake into intestinal tissue. The incubation medium contained no Ca^{2+} or Mg^{2+} unless specifically indicated. Mice were killed by cervical dislocation and pieces of intestinal tissue were removed from the appropriate region of the gastro-intestinal tract. Duodenal tissue was obtained from the first 5 cm, and ileal tissue up to 10 cm proximal to the ileocaecal valve. The tissue pieces were cut longitudinally and sectioned into tissue fragments (2–10 mg wet weight). After rinsing in oxygenated buffer, the fragments were incubated in a medium containing 125 mM NaCl, 3.5 mM KCl, 10 mM D-glucose, 16 mM Na-Hepes (pH 7.4) and $^{59}Fe^{3+}$-nitrilotriacetate with cyano[^{57}Co]cobalamin, as an extracellular fluid marker. The uptakes obtained in vitro have been shown to be similar to the in vivo total mucosal iron uptake over the same time period [11]. α-Glucosidase was assayed as in Ref. 4.

Results and Discussion

Fe^{3+} uptake studies

Fig. 1 shows the uptake of $^{59}Fe^{3+}$ by mouse duodenal fragments, as a function of time at two different concentrations of iron. Since uptake was linear for at least 5 min at both concentrations, this incubation time was used throughout. This short period of incubation was adequate for equilibration of the extracellular fluid marker, cyano[^{57}Co]cobalamin. Previous experiments [3] have suggested that iron is transferred to the mucosa from the chelate complex at the cell surface whilst the intact chelate is excluded from cell entry.

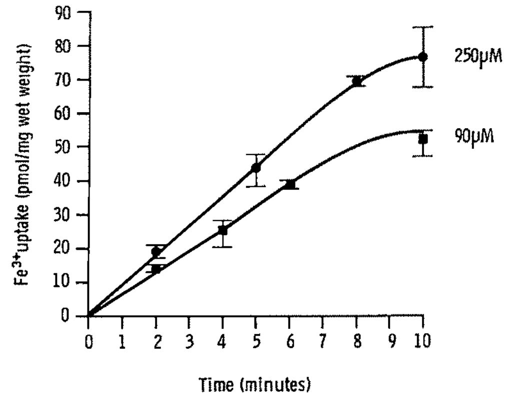

Fig. 1. Time course for $^{59}Fe^{3+}$ uptake by mouse duodenal fragments at two different medium iron concentrations. The iron in the medium was presented as a ferric chelate of nitrilotriacetic acid (Fe^{3+}/chelate ratio, 1:2) Results are shown as means ± S.E. for four determinations at each time point

Table I shows the effect of varying the Fe^{3+}/nitrilotriacetic acid ratio at constant Fe^{3+} concentration on the rate of $^{59}Fe^{3+}$ uptake. De-

TABLE I

EFFECT OF VARYING CHELATE/IRON RATIO ON THE RATE OF Fe^{3+} UPTAKE BY MOUSE DUODENAL FRAGMENTS

Mouse duodenal fragments were incubated for 5 min at 37°C in a physiological medium as described in the Materials and Methods section. The medium lacked divalent cations. Medium Fe^{3+} concentration was 90 μM and the concentration of nitrilotriacetic acid was varied. Results are shown as means ± S.E. for (n) determinations. Statistical analysis by one-way analysis of variance: * $P < 0.03$; ** $P < 0.001$, compared to uptake values at Fe^{3+}/chelate ratio 1.0:1.6

Fe^{3+}/nitrilotriacetic acid ratio	Fe^{3+} uptake (pmol/min per mg tissue)
1.0:1.6	6.0±0.6 (8)
1.0:2.0	5.3±0.8 (8)
1.0:4.0	4.2±0.4 (8) *
1.0:10.0	2.6±0.2 (8) **

creasing the Fe^{3+}/nitrilotriacetic acid ratio results in a gradual decline in uptake rate. The decline in uptake rate is much less than the changes in unchelated Fe^{3+} concentrations which would be anticipated in such experiments [5]. Experiments performed in the presence of 1 mM Ca^{2+} and 10 mM Mg^{2+} have also shown a similar decline in Fe^{3+} uptake with increasing chelate/iron ratios [3].

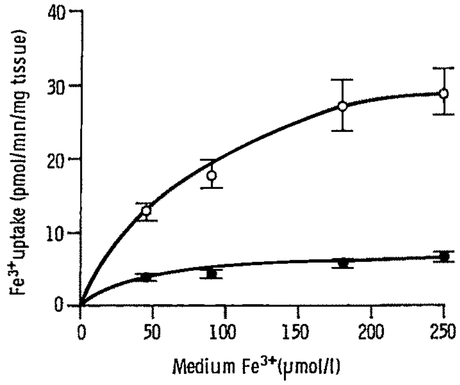

Fig. 2. $^{59}Fe^{3+}$ uptake by mouse duodenum from control animals (●) or those exposed to hypoxia for 3 days (○). Results are shown as means ± S.E. for three experiments Medium Fe^{3+}/chelate, 1 : 2. The lines were obtained by fitting the data points to the Michaelis-Menten curve [12] and are characterised by K_m^{app} value = 70.0 μmol/l, $V_{max}^{app} = 8.4$ pmol/mg per min for control mice, and $K_m^{app} = 102$, $V_{max}^{app} =$ 41 8 for 3 day hypoxic mice

Fig. 2 shows Fe^{3+} uptake by duodenal fragments over a range of medium iron concentrations. Uptake by both control animals and those exposed to hypoxia for 3 days is hyperbolic with respect to medium Fe^{3+}-nitrilotriacetate. A similar dependence was obtained with inclusion of Ca^{2+} and Mg^{2+} in the medium. The data were further processed in order to calculate the kinetic parameters for Fe^{3+} influx, by the direct linear plot method of Eisenthal and Cornish-Bowden [12]. The values for the apparent kinetic parameters for Fe^{3+} uptake are shown in Table II. The uptake rate for fragments from controls, with the Ca^{2+} and Mg^{2+}-free medium, was not significantly different from the rate obtained with the cation-containing medium. In contrast, uptake by duodenal fragments from hypoxic animals was found to be stimulated 4-fold compared to appropriate controls; this increase is significantly greater than that seen with the cation-containing medium, and implies that Ca^{2+} and Mg^{2+} have an inhibitory effect on the rate of iron uptake by hypoxic animals. These findings contradict the report of Sheehan [13] employing everted sacs of rat intestine in vitro, that mucosal iron uptake is mediated by passive diffusion and is not subject to adaptive regulation. He used ^{125}I-polyvinylpyr-

TABLE II

KINETIC CONSTANTS FOR Fe^{3+} UPTAKE BY MOUSE DUODENUM FROM CONTROL AND HYPOXIC ANIMALS

Uptake studies were performed at various medium Fe^{3+} concentrations with constant nitrilotriacetic acid/Fe^{3+} ratio. Incubation time 5 min. The incubation medium was either divalent cation-free or contained 1 mM Ca^{2+} and 10 mM Mg^{2+} K_t^{app} = apparent affinity constant and V_{max}^{app} = maximal uptake capacity for Fe^{3+} uptake. Results are shown as means ± S.E for (n) animals. Statistical analysis by 't' test $^{+}$ $P < 0.05$, compared to hypoxic animals with a Ca^{2+} and Mg^{2+}-containing medium * $P < 0.01$, compared to normal controls, with a divalent cation-free medium ** $P < 0$ 001, compared to normal controls, with a Ca^{2+} and Mg^{2+}-containing medium

Animals	Incubation medium	n	Kinetic parameters	
			K_t^{app} (μmol/l)	V_{max}^{app} (pmol/min per mg tissue)
Controls	Ca^{2+} and Mg^{2+}-containing	9	103 ± 20	10.5 ± 0.9
Controls	cation-free	5	65 7 ± 9 0	9.4 ± 1.0
Hypoxia (3-day)	Ca^{2+} and Mg^{2+}-containing	8	103 ± 17 0	22 7 ± 2.5 **
Hypoxia (3-day)	cation-free	5	90.0 ± 20 5	35 6 ± 6.1 *,+

rolidone as the extracellular fluid marker and found iron uptake to be only 1–2-fold greater than the uptake of this marker. Our uptake rates were at least 2–3-fold greater than the entry of the extracellular fluid markers (cyano[^{57}Co]cobalamin or ^{51}Cr-EDTA) in normal tissue and more than 10-times greater in tissue from hypoxic mice. We employed a 2:1 nitrilotriacetic acid/Fe^{3+} ratio, as we find that the 1:1 ratio gives variable uptake rates, especially in the presence of Ca^{2+} and Mg^{2+}, which further destabilises the Fe^{3+}-nitrilotriacetate complex [5]. Sheehan [13] employed a 1:1 nitrilotriacetic acid/Fe^{3+} ratio in the presence of 0.1 mM Ca^{2+} and 1.1 mM Mg^{2+}.

The data presented above demonstrate clearly that mucosal uptake of Fe^{3+} from Fe^{3+}-nitrilotriacetate depends on the medium Fe-nitrilotriacetate concentration, rather than the concentration of unchelated Fe^{3+}. This contrasts with observations made with isolated brush border membrane [4].

Effect of divalent cations on Fe^{3+} uptake in vitro

The effect of various concentrations of Ca^{2+} and Mg^{2+} on the rate of iron uptake by duodenal fragments is shown in Fig. 3. Ca^{2+} had little effect on Fe^{3+} uptake by duodenal fragments from normal controls, whilst Mg^{2+} was inhibitory. In contrast, the rate of iron uptake by duodenal fragments from hypoxic animals was markedly inhibited by 1 mM Ca^{2+}. Mg^{2+}, at all concentrations used, had no marked effects on the rate of iron uptake by duodenal fragments from hypoxic animals. These observations could therefore account for the lower V_{max}^{app} values for duodenal fragments from hypoxic animals (Table II) when the incubation medium containing 1 mM Ca^{2+} and 10 mM Mg^{2+} was used.

Effect of metabolic inhibitors on $^{59}Fe^{3+}$ uptake by duodenal fragments

Table III shows the effect of sodium fluoride, NaF (an inhibitor of glycolysis) and dinitrophenol (an inhibitor of oxidative phosphorylation) on Fe^{3+} uptake by duodenal fragments from control and hypoxic animals. Uptake in the presence of NaF and dinitrophenol was reduced by approximately 45%. NaF or dinitrophenol alone inhibited uptake of Fe^{3+} by 19–27%. A greater degree of

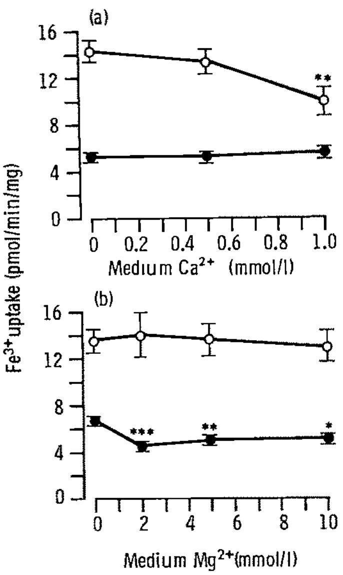

Fig 3 Effect of various concentrations of (a) Ca^{2+} and (b) Mg^{2+} on the rate of $^{59}Fe^{3+}$ uptake by mouse duodenal fragments from control (●) and hypoxic (○) animals. Medium Fe^{3+} concentration was 90 μM Fe^{3+}/chelate ratio, 1:2. Results shown as means ± S.E. for three separate experiments Statistical analysis by students 't' test· * $P < 0.05$; ** $P < 0.02$; *** $P < 0.001$, compared to uptake rate observed in divalent cation-free medium

TABLE III

EFFECT OF METABOLIC INHIBITORS ON RATE OF DUODENAL Fe^{3+} UPTAKE

Uptakes were performed in the presence of 10 mM NaF, 0.1 mM dinitrophenol or a combination of both with either cation-containing or cation-free media Results are shown as mean percentage inhibition of uptake rate ± S E for (n) experiments compared to control values obtained in the absence of inhibitors. Several pieces of fragments were used for each experiment Fe^{3+} concentration = 250 μM Fe^{3+}/chelate = 1:2

Animal group	Inhibition (%)		
	NaF	dinitrophenol	NaF + dinitrophenol
Cation-containing medium			
controls	19.4 ± 5.1 (2)	26.8 ± 4.2 (3)	43.4 ± 2.9 (4)
hypoxia (3-day)	17.2 ± 1.2 (2)	35.1 ± 5.0 (2)	56.9 ± 7.3 (4)
Cation-free medium			
controls	18.9 ± 3.7 (2)	24.9 ± 5.3 (2)	45.0 ± 5.9 (2)
hypoxia (3-day)	35.4 ± 3.2 (2)	47.0 ± 5.4 (2)	74.2 ± 4.3 (2)

inhibition was found with tissue from hypoxic animals, particularly with cation-free incubation medium, in which uptake was maximal.

Fe^{3+} uptake by fragments from the distal ileum

The characteristics for Fe^{3+} uptake by distal ileum differ from that of the duodenum (Table IV). Using the divalent cation-free medium, uptake by fragments from the duodenum was significantly greater than ileum. Furthermore, 1 mM Ca^{2+} significantly increased the initial rate of uptake of Fe^{3+} by the distal ileal fragments. Mg^{2+}, on the other hand, had no significant effect on the uptake rate. The V_{max}^{app} for uptake by ileal fragments was 6.5 ± 0.2 pmol/min per mg (mean ± S.E., $n = 5$) in divalent cation-free medium. This value is significantly lower ($P < 0.05$) than that observed in the duodenum (9.4 ± 1.0 pmol/min per mg), confirming the reduced uptake noted above. The apparent distribution volume of the extracellular fluid marker, cyano[^{57}Co]cobalamin, associated with the ileal tissue was similar to that for duodenal fragments. Exposure of animals to 3-day hypoxia did not affect the distal ileal uptake rate (uptakes performed at Fe^{3+} concentration, 250 μM; control = 4.7 ± 0.4 [12] pmol/min per mg; hypoxic = 5.1 ± 0.7 [11]). This is in marked contrast to the response in the duodenum.

Effects of Ca^{2+} on Fe^{3+} uptake by duodenum and ileum

The major effects of Ca^{2+} on Fe^{3+} uptake are stimulation in normal ileum, no significant effect in normal duodenum and inhibition in hypoxic duodenum. The simplest model which can explain these observations is a two-pathway model. One pathway of Fe^{3+} uptake is present in both duodenum and ileum and is stimulated by Ca^{2+} and not greatly altered in hypoxia. The second pathway, present in the duodenum but not ileum, is enhanced in hypoxia and inhibited by Ca^{2+}. Fig. 4 shows the interrelationship of these proposed uptake pathways in duodenum.

In a series of experiments the reversibility of the effect of Ca^{2+} was investigated in normal and hypoxic animals. Fragments of intestinal tissue were pre-incubated for 5 min in either cation-free medium or medium containing 1 mM Ca^{2+} and washed in cation-free medium. Fe^{3+} uptake studies were performed in cation-free medium containing 90 μM Fe^{3+} and 180 μM nitrilotriacetic acid. The results showed that pre-incubation in Ca^{2+}-containing medium, compared with control medium, had no significant effect on the subsequent rate of uptake of Fe^{3+} by duodenal and ileal fragments from controls or duodenal fragments from hypoxic animals. These observations indicate that the effect of Ca^{2+} reported above is reversible.

TABLE IV

EFFECT OF Ca^{2+} AND Mg^{2+} ON THE RATE OF UPTAKE OF Fe^{3+} BY MOUSE DUODENAL AND DISTAL ILEAL FRAGMENTS

Uptakes by duodenal and distal ileal fragments were performed with a medium containing or lacking 1 mM Ca^{2+} or 10 mM Mg^{2+} Results are shown as mean uptake rates ± S.E for two or three experiments with four or five tissue samples per experiment. Incubation time = 5 min. Medium Fe^{3+} concentration = 90 μM. Fe^{3+}/chelate ratio = 1 : 2 Statistical analysis by students 't' test: * $P < 0.01$, ** $P < 0.001$; compared to uptake by ileal fragments in a divalent cation-free medium.

Incubation medium	Uptake rates (pmol/mg per min)	
	duodenal	ileal
Cation-free	6.0±0.3 **	1.9±0.2
+1 mM Ca^{2+}	6.1±0.6	5.6±1.5 *
+10 mM Mg^{2+}	4.8±0.6	1.8±0.2

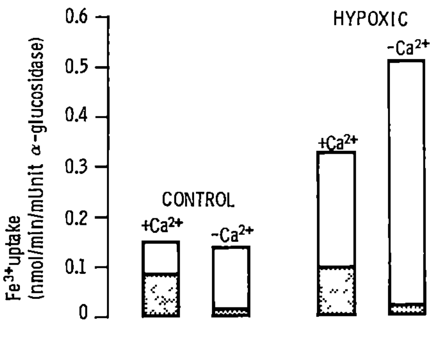

Fig. 4. Relative contributions of two postulated pathways to overall Fe^{3+} uptake by Ca^{2+}-stimulated (hatched area; pathway one) and Ca^{2+}-inhibited (open area; pathway two) mechanisms in normal and hypoxic mouse duodenum. The $^{59}Fe^{3+}$ uptake rates have been expressed relative to the activity of α-glucosidase, a brush-border membrane marker enzyme.

This two-pathway model also accounts for recent observations of Fe^{3+} transport by isolated mouse intestine brush-border membrane vesicles and intact intestine in vivo. The studies [4,14] of Fe^{3+} transport across isolated brush border membrane have demonstrated Ca^{2+}-stimulated Fe^{3+} transport in both duodenal and ileal brush-border membrane vesicles. Uptake was only slightly increased in duodenal vesicles from hypoxic mice [14]. This Fe^{3+} transport by brush-border vesicles could account quantitatively and qualitatively for the specific uptake of $^{59}Fe^{3+}$ by distal ileal mucosa in vivo. In contrast, the uptake in vivo with normal duodenal mucosa cannot be wholly explained by the isolated membrane transport [15].

In order to explain the lack of effect of Ca^{2+} on duodenal uptake by normal tissue, our two-pathway model requires that the Ca^{2+} stimulation of duodenal Fe^{3+} uptake by pathway one be greater than the stimulation of this pathway in ileum. We have found that transport by duodenal brush-border membrane vesicles is stimulated greater than 7-fold by 1 mM Ca^{2+} [4] whilst ileal vesicle uptake is stimulated only 4-fold [14,15], consistent with this requirement. We therefore propose that pathway one represents the transport mechanism expressed by isolated brush-border membrane vesicles. Pathway two, which appears to be quantitatively more important under our incubation conditions, especially in hypoxia, is not demonstrable by brush-border membrane vesicles and appears to require intact, metabolically active, cells in order to function.

Conclusions

Fe^{3+} uptake by intact intestinal mucosa exhibits Ca^{2+} sensitivity which is consistent with two distinct Fe^{3+} uptake mechanisms operating in duodenum but only one in ileum. One of these mechanisms may be that expressed by isolated brush-border membrane. The other mechanism is particularly sensitive to metabolic inhibitors and Ca^{2+} inhibition.

Acknowledgements

We thank Mrs. Teresa Barrett for typing the manuscript. R.J. S. is an MRC Training Fellow.

References

1 Cox, T.M and Peters, T J. (1979) J. Physiol. 289, 469–478
2 Cox, T.M. and O'Donnell, M.W. (1982) Br J. Nutr 47, 251–258
3 Raja, K.B., Bjarnason, I., Simpson, R.J. and Peters, T J. (1987) Cell. Biochem Function, in the press
4 Simpson, R J. and Peters, T.J (1984) Biochim. Biophys. Acta 772, 220–226
5 Sillen, L.G. and Martell, A.E. (1971) Special Publication No. 25, The Chemical Society, Burlington House, London
6 Greig, W.A. (1952) Br. J. Nutr. 6, 280–294
7 Dunn, J.A. (1968) S. Afr J. Med Sci 33, 65–70
8 Amine, E K. and Hegsted, D.M. (1971) J. Nutr. 101, 927–936
9 Barton, J C., Conrad, M.E and Parmley, R.T. (1983) Gastroenterology 84, 90–101
10 Sallee, V.L., Wilson, F.A. and Dietschy, J.M. (1972) J. Lipid Res. 13, 184–192
11 Peters, T J , Raja, K.B. and Simpson, R.J. (1984) J Physiol. 354, 36P
12 Eisenthal, R. and Cornish-Bowden, A. (1974) Biochem. J. 139, 715–720
13 Sheehan, R.G. (1976) Am J. Physiol. 231, 1438–1444
14 Simpson, R.J., Raja, K.B. and Peters, T.J (1985) Biochim. Biophys. Acta 814, 8–12
15 Simpson, R.J. and Peters, T J. (1986) Biochim Biophys. Acta 856, 115–122

Biochimica et Biophysica Acta 923 (1987) 52–58
Elsevier

BBA 22441

Partial purification and characterization of an aldohexose 1-*P* phosphatase from pig skeletal muscle

R. Cussó, A.M. Bassols and J. Carreras

Departamento de Bioquímica, Facultad de Medicina, Universidad de Barcelona, Casanova 143, 08036 Barcelona (Spain)

(Received 11 July 1986)

Key words: Aldohexose-1-phosphate phosphatase; Glucose-1-phosphate phosphatase; Galactose 1-phosphate; Mannose 1-phosphate; (Skeletal muscle)

An enzyme with a molecular weight of 54 000 which possesses phosphatase activity acting on glucose 1-*P*, galactose 1-*P* and mannose 1-*P* has been partially purified and characterized from pig skeletal muscle. The enzyme is free of phosphoglucomutase and galactokinase activities, and it possesses a neutral optimum pH. P_i acts as an inhibitor; glucose, galactose and mannose do not produce any effect. Divalent cations are required for activity, Mg^{2+} being the most effective activator. Micromolar levels of fluoride and millimolar levels of chloride act as inhibitors; however, vanadate does not produce any effect. The enzyme may have an important role when galactose accumulates in tissues; for example, in galactosemic patients and in young animals ingesting high-galactose diets.

Introduction

The enzymes involved in glucose 1-*P* and galactose 1-*P* breakdown in vertebrates are not well known. Purified preparations of alkaline phosphatase (EC 3.1.3.1), acid phosphatase (EC 3.1.3.2) and glucose 6-*P* phosphatase (EC 3.1.3.9) can hydrolyze glucose 1-*P* to a certain extent [1–3]. However, it has been shown that the main route of glucose 1-*P* hydrolysis is through a preliminary conversion into glucose 6-*P* via phosphoglucomutase [4]. A galactose 1-*P* phosphatase has been detected in chick brain [5] and in fibroblasts of galactosemic patients [6].

This paper reports the partial purification and characterization from pig skeletal muscle of a phosphatase acting on glucose 1-*P*, galactose 1-*P* and mannose 1-*P*. The enzyme is active at neutral pH and is free of phosphoglucomutase activity. It differs in several properties from a phosphatase also specific for glucose 1-*P* and galactose 1-*P* detected in silkworm blood [7], and from the less specific glucose monophosphate phosphatase detected in pea seeds [8].

Materials and Methods

Materials

Enzymes, substrates, chemicals and chromatography products were purchased from the sources previously indicated [25]. Fructose 2,6-P_2 was a generous gift of Dr. R. Bartrons. Sepharose 4B was coupled with glucosamine 6-*P* as described by Jett and Soderling [9].

Enzyme and protein assays

The phosphatase activity was measured by incubating, at 37°C, 100 μl of a mixture containing: 8 mM glucose 1-*P* or any other phosphorylated substrate assayed, 4 mM $MgCl_2$, 40 mM Tris-acetate buffer (pH 7.4), and the sample tested. The reaction was stopped by the addition of 200

Correspondence: Dr. R. Cussó, Department of Biochemistry, University of Barcelona, Casanova 143, 08036 Barcelona, Spain.

0304-4165/87/$03.50 © 1987 Elsevier Science Publishers B.V. (Biomedical Division)

μl of 10% (v/v) $HClO_4$ and the protein precipitate was removed by centrifugation. The inorganic phosphate released was measured using malachite green in acid-molybdate medium [11]. One unit (U) of enzyme is defined as the amount which releases 1 μmol of P_i per min under the conditions described.

Alternatively, glucose 1-*P* phosphatase was determined by measuring the disappearance of glucose 1-*P*. The incubating medium was as described above. The glucose 1-*P* remaining in the supernatant was measured spectrophotometrically by conversion to glucose 6-*P* with phosphoglucomutase and oxidation of glucose 6-*P* by NADP and glucose 6-*P* dehydrogenase [12].

To determine the influence of pH on the initial rate, the following buffers (40 mM) were used: acetic-acetate (pH 5.0–5.5); imidazole-acetic (pH 5.5–7.5); Tris-acetate (pH 7.0–9.0), and glycine-NaOH (pH 8.0–9.0).

Phosphoglucomutase was measured by a spectrophotometric method [13]. Glucose 1,6-P_2 synthase was assayed as previously described [10]. Protein phosphatase activity was measured using, as substrates, purified glycogen phosphorylase *a* and glycogen synthase D from rabbit muscle [14,15], and purified hydroxymethylglutaryl-CoA reductase from rat liver [16]. The phosphatase activity was determined by measuring the activation of glycogen synthase [17] and hydroxymethylglutaryl-CoA reductase [18], and the inactivation of glycogen phosphorylase [19]. Galactokinase activity was determined measuring the decrease in galactose after incubation with ATP. The galactose concentration was measured with galactose dehydrogenase [20].

Protein was measured according to the method of Lowry et al. [21] or spectrophotometrically by reading the absorbance at 280 nm.

Determination of the molecular weight

The molecular weight of the purified enzyme was estimated by gel filtration on Sephadex G-75. Bovine serum albumin (M_r: 67000), ovalbumin (M_r: 44000) and myoglobin (M_r: 17200) were used as standards. Samples (10 mg) of each standard protein and 90 mU of enzyme in 2 ml 20 mM Tris-acetate, 100 mM NaCl, 5% glycerol, 2 mM β-mercaptoethanol were applied to the column (1.5 × 150 cm) and eluted with the same buffer. At a flow rate of 5 ml/h, 2 ml fractions were collected and assayed for enzymatic activity and A_{280}. The molecular weight was determined using the standard curve of log M_r versus elution volume.

Electrophoresis

Electrophoresis in 12% polyacrylamide gels containing SDS was performed [22] at 20°C for 4 h at a constant current of 40 mA per gel. Protein bands were detected by silver staining [23].

Tissue extraction

Pig skeletal muscle (back muscle) was obtained fresh from a slaughterhouse. The cleaned muscle was minced and homogenized in 3 vol. (w/v) of 20 mM Tris-acetate buffer (pH 7.4) containing 2 mM β-mercaptoethanol, with a Sorvall-Omnimixer (4000 rpm, 2–3 min). After centrifugation at 35000 × *g* for 45 min, the supernatant was precipitated with ammonium sulfate (80% saturation, 120 min), resuspended and dialyzed overnight against the homogenization buffer (fraction I).

Results

Aldohexose 1-P phosphatase activity in muscle extract

Glucose 1-*P*, galactose 1-*P* and mannose 1-*P* phosphatase activities were determined in pig muscle extract, in the presence of 10 mM vanadate to abolish phosphoglucomutase activity [24] and to avoid the conversion of glucose 1-*P* into glucose 6-*P*. Control experiments with purified aldohexose 1-*P* phosphatase showed that its activity was not affected by vanadate. The activities found were 110 mU, 73 mU and 33 mU per g of tissue, respectively. The phosphoglucomutase and the glucose 6-*P* phosphatase activities of the extract were 85 U and 20 U/g tissue, respectively.

Purification of aldohexose 1-P phosphatase

All steps were carried out at 0–4°C.

DE-cellulose chromatography. Fraction I was applied to a column of DE-cellulose equilibrated with extraction buffer. After washing with the same buffer, the column was eluted first with 100 mM Tris-acetate containing 2 mM β-mercaptoethanol (pH 7.4), and then with a linear gradient (100–300 mM) of the same buffer (Fig. 1). The peak with glucose 1-*P* phosphatase activity was pooled, concentrated by precipitation with ammonium sulfate (80% saturation, 60 min), resuspended and dialyzed against extraction buffer. This preparation (fraction II) was free of phosphoglucomutase activity.

Sephadex G-150 chromatography. One sample of fraction II was concentrated by ultrafiltration and applied (2 ml, 70 mg protein/ml) to a Sephadex G-150 column (1.5 × 143 cm), equilibrated with 20 mM Tris-acetate buffer, containing 100 mM NaCl and 2 mM β-mercaptoethanol. The column was eluted with the same buffer at a flow rate of 10 ml/h, 2 ml fractions being collected. Glucose 1-*P* phosphatase emerged as a single symmetrical peak (not shown). Fractions with activity were pooled and concentrated by ultrafiltration to give fraction III.

Sepharose 4B-glucosamine 6-P chromatography. Fraction III was dialyzed against extraction buffer and loaded (2.5 ml, 18 mg protein/ml) into a column (1.5 × 6 cm) of Sepharose 4B coupled with glucosamine 6-*P* equilibrated with extraction buffer. The column was eluted, at a flow rate of 20 ml/h, with a discontinuous gradient of Tris-acetate buffer containing 2 mM β-mercaptoethanol (pH 7.4) (20 mM, 100 mM and 300 mM Tris). The peak with glucose 1-*P* phosphatase activity was eluted at 100 mM Tris-acetate. It was concentrated by ultrafiltration and dialyzed against extraction buffer to give fraction IV.

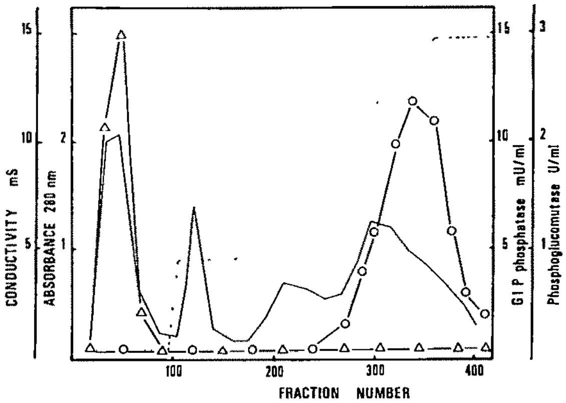

Fig. 1. Separation of aldohexose 1-*P* phosphatase from phosphoglucomutase by DE-cellulose chromatography. Fraction I (110 ml, 25 mg protein/ml) was applied to the column (3×13 cm) at a flow rate of 40 ml/h, and 3 ml fractions were collected and assayed for glucose 1-*P* phosphatase (O) and phosphoglucomutase (△). Absorbance at 280 nm (———) Salt conductivity (------).

Fraction IV was stored at −40°C with glycerol and 5 mM β-mercaptoethanol. Under storing conditions, the activity was lost within 15 days. The enzyme was purified about 400-fold, although the preparation was not homogeneous. Gel electrophoresis in polyacrylamide containing SDS showed four bands (not shown). The overall yield was about 40%. Table I summarizes the results of the purification procedure.

Molecular weight

When chromatographed on Sephadex G-75 the enzyme emerged between bovine serum albumin and ovalbumin. The apparent molecular weight was found to be 54000 ± 1000.

Substrate specificity of the enzyme preparation

The substrate specificity of the purified preparation was studied with several mono- and bisphosphorylated sugars, phosphorylated triose derivatives, nucleotides and *p*-nitrophenyl phosphate. As summarized in Table II, under standard assay conditions, the enzyme preferentially hydrolyzes galactose 1-*P*, glucose 1-*P* and mannose 1-*P*. Fructose 1-*P*, the C_6 phosphorylated and the bisphosphorylated hexoses are not significantly hydrolyzed. The specific activity (mU/mg) was found to be approximately 1014, 1100 and 507 for glucose 1-*P*, galactose 1-*P* and mannose 1-*P*, respectively.

To discard the phosphatase activity as a collateral reaction of galactokinase or glycogen phosphorylase, the enzyme preparation was tested for these activities. The results were negative (not shown). The preparation was found to be free of protein phosphatase activity when glycogen phosphorylase *a*, glycogen synthase D and hydroxymethylglutaryl-CoA reductase were used as substrates. It was also free of phosphoglucomutase and glucose 1,6-P_2 synthase activities.

Functional properties

Effect of substrate concentration. The activity patterns obtained varying glucose 1-*P*, galactose

TABLE I

SUMMARY OF ALDOHEXOSE 1-*P* PHOSPHATASE PURIFICATION

Purification step	Activity [a] (mU/ml)	Total activity [a] (mU)	Protein concentration (mg/ml)	Specific activity (mU/mg)	Yield (%)	Purification factor
Extract [b]	43.5	72862	15	2.9	100	1
DE-cellulose	234	70130	6.1	38.3	96	13
Ammonium sulfate	1800	84640	17.8	100.0	116	34
Sephadex G-150	4045	52810	18.0	224.0	72	77
Glucosamine 6*P*-Sepharose	75	30549	0.067	1119.0	42	386

[a] Glucose 1-*P* was used as substrate.

[b] The activity was assayed in the presence of 10 mM vanadate

TABLE II

SUBSTRATE SPECIFICITY OF ALDOHEXOSE 1-*P* PHOSPHATASE

Substrate	Activity (%)
Glucose 1-*P*	100
Glucose 6-*P*	3
Glucose 1,6-P_2	10–20
Galactose 1-*P*	68–112
Galactose 6-*P*	0
Fructose 1-*P*	3
Fructose 6-*P*	9
Fructose 1,6-P_2	0
Fructose 2,6-P_2	0
Mannose 6-*P*	0
Mannose 1-*P*	40–73
Ribose 5-*P*	10
Ribulose 5-*P*	31–40
Glycerate 2-*P*	0
Glycerate 3-*P*	0
Glycerate 2,3-*P*	0
Glycerol 1-*P*	11
Glycerol 2-*P*	32–42
Phospho*enol*pyruvate	1
Glycolate 2-*P*	15–27
Glyceraldehyde 3-*P*	5
p-Nitrophenyl phosphate pH 4.8	3
7.5	2
10.5	10
ATP	9
ADP	9
AMP	11–15
IMP	3
NADP	0
UDPG	0
Serine-*P*	0
Threonine-*P*	0
Tyrosine-*P*	0

1-*P* and mannose 1-*P* concentrations followed hyperbolic kinetics with the three substrates. The K_m values, calculated from the intercepts at the abscissa, were estimated to be 0.78 mM, 0.9 mM and 1.25 mM for glucose 1-*P*, galactose 1-*P* and mannose 1-*P*, respectively.

Effect of pH. The optimum pH was found to be 7.0–7.2 for both glucose 1-*P* and galactose 1-*P*, and 7.2–7.4 for mannose 1-*P* (not shown).

Effect of the reaction products. As shown in Fig. 2, inorganic phosphate inhibited competitively the glucose 1-*P* phosphatase activity. The K_i was calculated to be about 1.5 mM. Glucose, galactose and mannose up to 50 mM concentration did not produce any effect (not shown).

Effect of divalent cations. Divalent cations were found to be required for glucose 1-*P*, galactose 1-*P* and mannose 1-*P* activities. Mg^{2+} was the most effective activator, showing a maximum effect at 3–6 mM concentration. Mn^{2+} showed a maximum effect at 1–2 mM, being inhibitory at higher concentration (Fig. 3). Co^{2+} and Zn^{2+} showed a much lower activatory effect. No enzymatic activity was observed in the presence of Ca^{2-} up to 20 mM. Addition of EGTA up to 1 mM to the standard assay mixture did not produce any effect. Mg^{2+} and Mn^{2+} did not show synergistic or antagonistic effects (not shown).

Effect of inhibitors. The effects of several compounds known to be inhibitors or activators of some phosphatases were tested. As shown in Table III, glucose 1-*P* phosphatase activity was inhibited by fluoride at micromolar concentration, and by

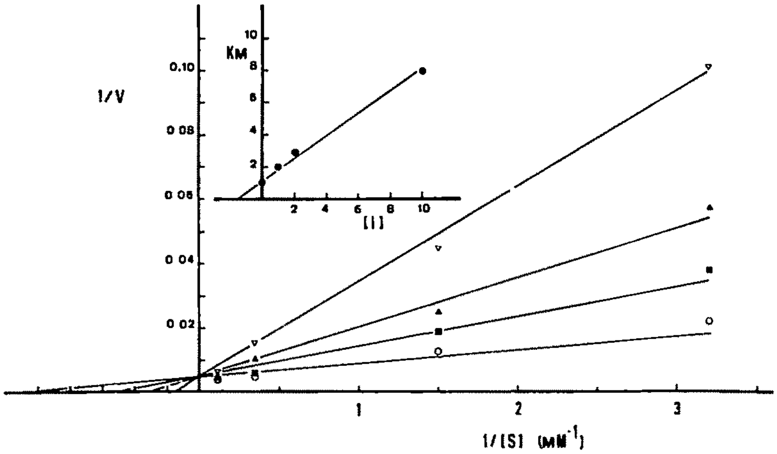

Fig 2. Inhibition of inorganic phosphate on aldohexose 1-*P* phosphatase activity. The phosphatase activity was measured spectrophotometrically using glucose 1-*P* as substrate in the presence of different concentrations of P_i (○) control, (■) 1 mM P_i, (▲) 2 mM P_i and (▽) 10 mM P_i. The insert shows the replot of the K_m and the concentration of the inhibitor.

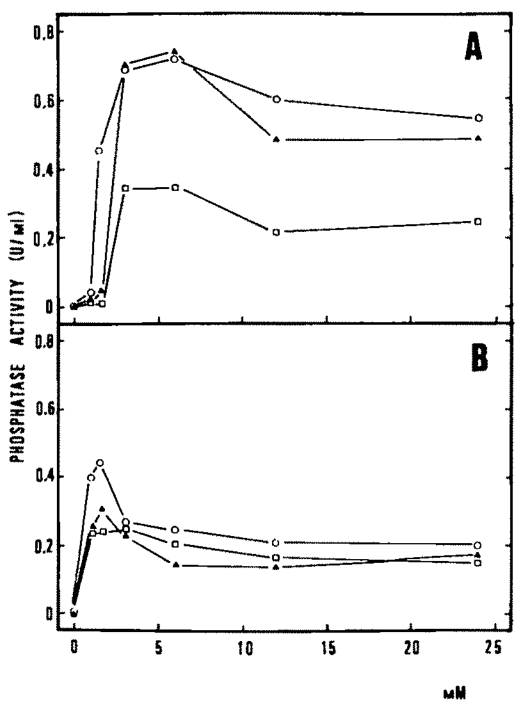

Fig. 3. Effect of Mg^{2+} and Mn^{2+} on aldohexose 1-*P* phosphatase activity. The phosphatase activity was measured with glucose 1-*P* (▲), galactose 1-*P* (○) and mannose 1-*P* (□) as substrates, in the presence of different concentrations of magnesium acetate (panel A) and manganese acetate (panel B).

chloride at millimolar concentration. Tartrate (0.5 mM) and vanadate (up to 10 mM) were not inhibitory. α- and β-glycerophosphate, IMP, AMP, ADP and ATP did not produce any effect.

TABLE III

EFFECT OF SOME INHIBITORS ON GLUCOSE 1-*P* PHOSPHATASE

The assay was initiated by addition of the enzyme to the reaction mixture containing the inhibitor. To test for the effect of vanadate the enzyme was preincubated with it for 30 min

Addition	Concentration (mM)	Activity (%)
None	–	100
F^-	0.125	70
	0.250	39
	0.500	26
	1	16
	2	9
	5	5
	10	3
Cl^-	100	89
	200	86
	500	44
Tartrate	0.5	100
Vanadate	10	97

Discussion

In a previous report [25], it was found that most of the glucose 1-*P* phosphatase activity from pig skeletal muscle eluted associated with the main peak of glucose 1,6-P_2 phosphatase activity when the muscle extract was subjected to ion-exchange chromatography. The procedure described here allows the separation of the activities and a highly purified preparation of hexose 1-*P* phosphatase. The enzyme is specific for aldohexose 1-*P*; in addition to glucose 1-*P*, it hydrolyzes galactose 1-*P* and, less efficiently, mannose 1-*P*. It is not a collateral activity of phosphoglucomutase, galactokinase, glycogen phosphorylase or protein phosphatase, since the enzymatic preparation is free of these activities.

This aldohexose 1-*P* phosphatase has some properties in common with the glucose 1-*P* phosphatase found in silkworm blood [7]. Like the insect phosphatase, the pig enzyme shows a high substrate specificity; of the naturally occurring phosphate esters, only glucose 1-*P* and galactose 1-*P* are hydrolyzed to any considerable degree. Both the pig and the silkworm phosphatases are inhibited by fluoride and they are similarly affected by the reaction products; they are strongly inhibited by P_i but not affected by glucose and galactose. However, the two enzymes differ in their optimum pH and in the requirement for divalent cations. Whereas the pig muscle enzyme has a neutral optimum pH, the insect phosphatase shows maximal activity at acid pH (4.0–4.5). In addition, whereas the pig phosphatase requires Mg^{2+} for activity, the silkworm enzyme is not affected by this cation.

The aldohexose 1-*P* phosphatase also differs from glucose 6-*P* phosphatase and the acid phosphatases. In contrast with the aldohexose 1-*P* phosphatase, glucose 6-*P* phosphatase is inhibited by divalent cations, including Mg^{2+}, Zn^{2+} and Ca^{2+} and by nucleoside di- and triphosphate [3]. The acid phosphatases do not require Mg^{2+} and are inhibited by Ca^{2+}, tartrate and adenine nucleotides [2].

The physiological role of the aldohexose 1-*P* phosphatase is uncertain. Its K_m for glucose 1-*P* (0.78 mM) is much higher than the concentration of glucose 1-*P* in muscle (50 μM) [26]. Furthermore, phosphoglucomutase, which is present in pig muscle in much higher concentration than aldohexose 1-*P* phosphatase, possesses a much lower K_m for the phosphorylated sugar than the phosphatase (10 μM) [26]. Glucose 6-*P* phosphatase activity is of the same order of magnitude as glucose 1-*P* phosphatase activity. Therefore, in a normal situation, glucose 1-*P* is probably dephosphorylated before it can be converted to glucose 6-*P* by phosphoglucomutase.

Aldohexose 1-*P* phosphatase may have an important role when galactose 1-*P* accumulates in tissues, for example, in young animals ingesting high-galactose diets [5] and in galactosemic patients [27]. It has been shown that in such circumstances, in muscle, galactose 1-*P* is converted to galactitol through an alternative route which involves free galactose and the action of an aldose reductase [28]. Galactose 1-*P* levels have been found to be elevated in red cells, lens, liver and kidney of galactosemic patients [29,30]. In addition, high concentrations of galactitol were found in the brain and muscle of such patients [31,32]. Therefore, in the muscle, aldohexose 1-*P* phosphatase could have a central role in initiating the route leading to the synthesis of galactitol. Although the value of the K_m of aldohexose 1-*P* phosphatase is high (0.9 mM), it is much lower than the K_m of the aldose : NADP oxidoreductase for galactose (12–20 mM) [33,34]. Galactose 1-*P* could be the substrate for the phosphoglucomutase [35]; however, the K_m of phosphoglucomutase for galactose 1-*P* is not lower than that of aldohexose 1-*P* phosphatase [26].

Acknowledgements

We wish to thank Miss Victoria Esser for the determinations of protein phosphatase activities and Mr. Joaquin Ariño for synthesizing the Sepharose 4B-glucosamine 6-*P*. This work was supported by research grants from CAICYT, FIS and CIRIT.

References

1 Fernley, H.N (1971) in The Enzymes (Boyer, P D., eds), Vol. 4, pp. 417–447, Academic Press, New York
2 Hollander, V.P. (1971) in The Enzymes (Boyer ,P D., eds.), Vol. 4, pp 449–497, Academic Press, New York

3 Nordlie, R.C. (1971) in The Enzymes (Boyer, P.D., ed), Vol 4, pp 543–609, Academic Press, New York

4 Goodlad, G.A.J. and Mills, G T. (1957) Biochem. J 66, 354–357

5 Kozak, L.P. and Wells, W.W. (1971) J Neurochem 18, 2217–2228

6 Mayes, J.S. and Miller, L.R. (1973) Biochim. Biophys. Acta 313, 9–16

7 Faulkner, P. (1955) Biochem. J. 60, 590–596

8 Turner, D.H. and Turner, J.F. (1960) Biochem. J. 74, 486–491

9 Jett, H.F. and Soderling, T.R. (1979) J. Biol Chem. 254, 6739–6745

10 Climent, F , Carreras, M. and Carreras, J (1985) Comp Biochem Physiol 81B, 737–742

11 Itaya, K. and Ui, M (1966) Clin. Chim. Acta 14, 361–366

12 Ray, W.J , Jr. and Roscelli, G.A. (1966) J. Biol. Chem. 241, 2596–2602

13 Dawson, D.M and Mitchell, A (1969) Biochemistry 8, 609–614

14 Fischer, E.H. and Krebs, E.G. (1958) J Biol. Chem. 231, 65–71

15 Takeda, Y. and Larner, J. (1975) J Biol. Chem. 250, 8951–8956

16 Gil, G , Sitges, M. and Hegardt, F G. (1981) Arch. Biochem. Biophys. 210, 224–229

17 Thomas, J A., Schlender, K.K. and Larner, J (1968) Anal. Biochem. 47, 20–27

18 Philipp, B.W. and Shapiro, D.J (1979) J Lipid Res. 20, 588–593

19 Gilboe, D.P., Larson, K.L. and Nutall, F Q. (1972) Anal Biochem. 47, 20–27

20 Fujimura, J. (1984) in Methods of Enzymatic Analysis (Bergmeyer, H.V., ed.), Vol. VI, pp 288–296, Verlag Chemie, Basel

21 Lowry, O.H., Rosebrough, N.J., Farr, A L. and Randall, R J. (1951) J Biol. Chem. 193, 265–275

22 Laemmli, U.K. (1970) Nature 227, 680–685

23 Wray, W., Boulikas, T , Wray, V. and Hancock, R. (1981) Anal. Biochem. 118, 197–203

24 Climent, F., Bartrons, R , Pons, G. and Carreras, J. (1981) Biochem. Biophys Res. Commun. 101, 570–576

25 Bassols, A , Cussó, R. and Carreras, J. (1985) Comp. Biochem. Physiol. 81B, 981–987

26 Lowry, O.H. and Passonneau, J.V. (1969) J. Biol. Chem 244, 910–916

27 Komrower, G.M , Schwarz, V., Holzel, A and Golberg, L. (1956) Arch. Dis. Child, 31, 254–258

28 Hers, H G. (1960) Biochim. Biophys. Acta 37, 120–126

29 Schwarz, V (1960) Arch. Dis. Child. 35, 428–432

30 Schwarz, V., Golberg, L., Komrower, G.M. and Holzel, A (1956) Biochem. J. 62, 34–40

31 Wells, W.W , Pitman, T A., Wells, H.J. and Egan, T.J. (1964) J. Biol Chem. 240, 1002–1004

32 Quan-Ma, R., Wells, H J., Wells, W.W., Sherman, F.E and Egan, T.J. (1966) Am. J. Dis. Child. 112, 477–478

33 Hayman, S. and Kinoshita, J.H. (1965) J. Biol. Chem. 240, 877–882

34 Moonsammy, G. and Stewart, M. (1967) J. Neurochem. 14, 1187–1192

35 Posternak, Th and Rosselet, J.P. (1954) Helv. Chim. Acta 37, 246–251

Biochimica et Biophysica Acta 923 (1987) 59–65
Elsevier

BBA 22460

The preparation of deglycosylated ricin by recombination of glycosidase-treated A- and B-chains: effects of deglycosylation on toxicity and in vivo distribution

Brian M.J. Foxwell, David C. Blakey, Alex N.F. Brown, Tom A. Donovan
and Philip E. Thorpe

Cellular Pharmacology and Drug Targeting Laboratories, Imperial Cancer Research Fund, London, WC2A 3PX (U.K.)

(Received 12 June 1986)

Key words: Ricin; Deglycosylation; Glycosidase

Deglycosylation of ricin may be necessary to prevent the entrapment of antibody-ricin conjugates in vivo by cells of the reticuloendothelial system which have receptors that recognise the oligosaccharide side chains on the A- and B-chains of the toxin. Carbohydrate-deficient ricin was therefore prepared by recombining the A-chain, which had been treated with α-mannosidase, with the B-chain, which had been treated with endoglycosidase H or α-mannosidase or both. By recombining treated and untreated chains, a series of ricin preparations was made having different carbohydrate moieties. The removal of carbohydrate from the B-chain did not affect the ability of the toxin to agglutinate erythrocytes, and α-mannosidase treatment of the A-chain did not affect its ability to inactivate ribosomes. The toxicity of ricin to cells in culture was only reduced in those preparations containing B-chain that had been treated with α-mannosidase, when a 75% decrease in toxicity was observed. The toxicity of the combined ricin preparation to mice varied from double to half that of native ricin, depending on the chain(s) treated and the enzymes used. Removal of carbohydrate greatly reduced the hepatic clearance of the toxin and the levels of toxin in the blood were correspondingly higher. These results suggest that antibody-ricin conjugates prepared from deglycosylated ricin would be cleared more slowly by the liver, inflict less liver damage, and have greater opportunity to reach their target.

Introduction

In recent years many attempts have been made to direct ricin to designated cell types in animals by linking it to specific antibodies [1–4]. Ricin, the toxic lectin from the castor bean (*Ricinus communis*), is a glycoprotein consisting of two polypeptide chains, A and B, linked by a disulphide bond. The B-chain has galactose recognition sites by which the toxin binds to glycoproteins and glycolipids on cell surfaces and the A-chain then enters the cytosol (probably from an endocytic vesicle) and kills the cell by catalytically inactivating 60 S ribosomal subunits [5–7].

When ricin is injected intravenously into mice or rats, it rapidly accumulates in the liver causing damage to the non-parenchymal cells, mainly Kupffer and sinusoidal endothelial cells [8,9]. The uptake of the ricin by the non-parenchymal cells appears to be due principally to recognition of mannose-containing carbohydrate side chains in the toxin [10–12]. The B-chain contains two high mannose-type oligosaccharide units whereas the A-chain mainly contains a single complex oligosaccharide unit of composition $(GlcNAc)_2$-Fuc-Xyl-$(Man)_{4-6}$. Approximately one third of the

---

Correspondence (present address): Dr. B.M J. Foxwell, Preclinical Research, Sandoz Ltd , Basle, CH-4002, Switzerland.

0304-4165/87/$03.50 © 1987 Elsevier Science Publishers B V (Biomedical Division)

A-chains also contain a mannose-rich oligosaccharide similar to that found on the B-chain [12,13]. Recently, Bourrie et al. [14] showed that an antibody-ricin A-chain conjugate was rapidly removed from the bloodstream of animals, the major site of clearance being the liver. The blood clearance of the conjugate could be slowed by coinjection of yeast mannan. These findings suggest that antibody-ricin conjugates would be rapidly cleared from the bloodstream by the reticuloendothelial cells of the liver, thus reducing their therapeutic value. This prompted us to seek ways of removing the carbohydrate from ricin before linking it to the antibody.

In an earlier report [13] we described a procedure for the removal of carbohydrate from ricin using α-mannosidase and endoglycosidase H. Since intact native ricin was resistant to enzymic deglycosylation the toxin first had to be split into its A- and B-chains by reduction. The terminal mannose residues could be removed from the isolated native A- or B-chains by α-mannosidase treatment and one of the high mannose oligosaccharide chains present on the B-chain could be removed by treatment with endoglycosidase H.

In the present report we describe the preparation of carbohydrate-depleted ricin by separating the A- and B-chains, treating them with glycosidases, and then recombining them to form intact ricin. The modified toxin showed no loss of haemagglutinating activity or of inhibitory activity on cell-free protein synthesis, and its toxicity to cells in vitro was only reduced in those preparations containing B-chain that had been treated with α-mannosidase. The most highly deglycosylated preparation of ricin had a much reduced tendency to home to the liver after intravenous injection into rats.

Materials and Methods

Materials

Ricin (electrofocusing at pH 7.2) was kindly supplied by Dr. J.A. Forrester, Chester Beatty Research Institute, Fulham Road, London. The toxin was purified from an aqueous extract of untoasted Chinese castor bean cake by $(NH_4)_2SO_4$ precipitation, affinity chromatography on Sepharose 4B (Pharmacia Ltd., Milton Keynes, U.K.) and gel filtration on Sephacryl S-200 (Pharmacia), essentially as described by Nicolson and Blaustein [15].

$Na^{125}I$ (IMS 30) for protein iodination and L-[4,5-^{3}H]leucine (TRK 170) were obtained from Amersham International, Amersham, U.K.

Endoglycosidase H (*Streptomyces griseus*) was obtained from Miles Laboratories Ltd., Slough, U.K. and α-mannosidase EC 3.2.1.24 (jack bean) from Sigma, Poole, Dorset, U.K.

Concanavalin A (Con A) was purchased from Pharmacia Ltd. It was linked to CNBr-Sepharose (Pharmacia) in the presence of 0.2 M methyl α-mannoside (Sigma Chemical Co., Poole, Dorset, U.K.) using the manufacturer's instructions. The concentration of concanavalin A bound was 3 mg protein per ml of swollen gel.

1,10-Phenanthroline hydrate (*o*-phenanthroline), Analar grade, was obtained from Hopkin and Williams Ltd., Chadwell Heath, Essex, U.K. Phenylmethylsulphonyl fluoride (PMSF) was from Sigma. Tissue culture medium RPMI 1640 and fetal calf serum were obtained from Gibco-Biocult Ltd.

The mouse lymphoma cell line, AKR-A, was kindly provided by Professor I. MacLennon, Department of Experimental Pathology, Birmingham University, U.K.

Methods

Isolation of A- and B-chains

Ricin was split into its constituent chains by reduction with 2-mercaptoethanol followed by ion-exchange chromatography on DEAE-Sepharose (Pharmacia). The A-chain was further purified by passage through asiolofetuin-Sepharose and the B-chain was further purified by ion-exchange chromatography on CM-Sepharose (Pharmacia) [13]. Ricin A-chain was fractionated on a Con A-Sepharose column into a non-binding component, A-chain Con A(−), and a binding component, A-chain Con A(+), which was eluted from the column with methyl α-mannoside as described previously [13]. Concanavalin A has a high affinity for trimannosidic core structures [16] and preferentially binds the A-chains which contain the high mannose type oligosaccharide [13].

Deglycosylation of A- and B-chains

A-chain or A-chain Con A(−) was treated with α-mannosidase as follows: 3 ml of A-chain at 0.685 mg/ml in 0.2 M sodium citrate buffer (pH 5.5) were treated with 0.75 U of α-mannosidase in the presence of 1 mM PMSF and left at room temperature for 2 days. B-chain at 2 mg/ml in 0.1 M sodium citrate (pH 5.5) containing 0.2 M galactose, 0.25% 2-mercaptoethanol and 1 mM PMSF was deglycosylated using one of the following methods: (a) incubation with 10 mU/ml endoglycosidase H for 3 days, (b) incubation with 0.5 U/ml α-mannosidase for 3 days, (c) incubation with 10 mU/ml endoglycosidase H for 2 days after which 0.18 U/ml of α-mannosidase (treated with 1 mM PMSF) was added and the incubation continued for a further 24 h. All incubations were performed at room temperature. After treatment, 2 mg of B-chain was filtered at a flow rate of 0.5 ml/min through a 1.5 ml Con A-Sepharose column equilibrated with phosphate-buffered saline containing 0.1 M galactose. Bound material was eluted from the column with phosphate-buffered saline containing 0.2 M methyl α-mannoside and 0.1 M galactose. The total protein recovered from the column was always greater than 90% unless stated otherwise.

Recombination of A- and B-chains

Ricin A-chain and B-chain (deglycosylated or untreated) were recombined to form the holotoxin using the method of Uchida et al. [17], with slight modification. 1 mg each of A- and B-chain were mixed. The concentration of galactose in the mixture was maintained at 0.05 M or more by the addition of solid galactose. The concentration of protein was then adjusted to 400 μg/ml with phosphate-buffered saline containing 0.1 M galactose. Dithiothreitol (final concentration 25 mM) was added, after which the solution was dialysed extensively in 5 l of 10 mM sodium phosphate (pH 6.2) containing 50 mM galactose. The solution was then dialysed, 3 × 2 h, in the above buffer containing 50 μM 1,10-phenanthroline hydrate and 10 μM $CuSO_4$, two agents which promote oxidation-induced disulphide bond formation [18,19]. The solution was dialysed overnight in 10 mM sodium phosphate buffer (pH 6.2) containing 50 mM galactose and, thereafter, the solution was dialysed extensively in phosphate-buffered saline. The dialysed solution was passed through a 0.22 μm filter (Millipore) to remove any precipitated B-chain and was then applied to a 2 ml acid-treated Sepharose 4B column (Pharmacia). The majority of the material bound to the column and was eluted with phosphate-buffered saline containing 0.1 M galactose. The amount of protein that eluted from the column was measured by ultraviolet absorption at 280 nm and was always greater than 70%. Analysis by sodium dodecyl sulphate (SDS) -polyacrylamide gel electrophoresis [20] showed that the recombined ricin migrated with a molecular weight similar to that of native ricin (Fig. 3). The protein solutions were sterilised by filtration through a 0.22 μm filter and were stored at 4°C in the dark.

Haemagglutination

Haemagglutination assays on serial doubling dilutions of deglycosylated ricin were performed using neuraminidase-treated rabbit erythrocytes as has been previously described [21].

Inhibition of protein synthesis in reticulocyte lysate

The concentration of A-chain (α-mannosidase treated or untreated) that caused a 50% reduction in [^{14}C]leucine incorporation into trichloroacetic acid-precipitable material in a rabbit reticulocyte lysate system was measured of the method by Saragiacomo et al. [22].

Toxicity to cells in tissue culture

AKR-A cells were incubated for 24 h with different preparations of toxin and their ability to incorporate [^{3}H]leucine was measured 24 h later was previously described [23]. The concentration of toxin that produced 50% reduction in [^{3}H]leucine incorporation (IC_{50}) was calculated. The standard deviation of each triplicate determination was always less than 5% of the geometric mean value.

Toxicity to mice

Ricin solutions in phosphate-buffered saline containing 2 mg/ml bovine serum albumin were injected intravenously into groups of three to five male CBA mice aged 12–16 weeks. The volume injected was 0.25 ml per 25 g body weight. The LD$_{50}$ was calculated according to Weil [24].

In vivo distribution

Deglycosylated and untreated ricin solutions were labelled with ^{125}I using the Iodo-Gen reagent (Pierce, Rockford, IL, U.S.A.) to a specific activity of $4 \cdot 10^6$ dpm/μg according to the manufacturer's recommended instructions. The radiolabelled ricin solutions were adjusted to 20 μg/ml in phosphate-buffered saline containing 5 mg/ml bovine serum albumin and to $4 \cdot 10^6$ dpm/ml by adding unlabelled homologue. Groups of three male Wistar rats, aged 10–14 weeks, were anaesthetised and injected via the tail vein with radiolabelled toxin solutions. The volume of solution injected into each rat was 0.25 ml/250 g body weight. After 15 min the animals were re-anaesthetised and bled by cardiac puncture, the blood being collected into heparinized tubes. The animals were killed and various organs were removed, weighed and their radioactivity measured using a United Technologies Packard γ-counter. Results were expressed as the percentage of the injected dose localising to the tissues and all results were corrected for the blood volumes of the tissues which had been determined previously [25]. The blood volume of the rats was taken as 12.8 ml/200 g body weight [26]. Samples of blood, washed erythrocytes, plasma and washed 20% trichloroacetic acid-precipitated plasma proteins were also measured for their radioactivity.

Results

Reconstitution of A- and B-chains

Native and glycosidase-treated A- and B-chains were recombined in different combinations to produce intact ricin that was deficient in carbohydrate in the A-chain, the B-chain or in both. The treatment of the individual chains used to form the toxins is listed in Table I. The enzyme-treated A- and B-chains recombined to form intact ricin with an intact interchain disulphide bond (Fig. 1). The variation in mobility of the different toxin products relates to the level of carbohydrate removal. The yield of intact toxin from each recombination mixture was 70% or more.

TABLE I

THE EFFECT OF ENZYMIC DEGLYCOSYLATION OF RICIN ON ITS TOXICITY

Ricin	Treatment		Toxicity	
	A-chain	B-chain	in vitro (%) [a]	in vivo (LD$_{50}$, ng)
I [b]	n.t. [c]	n.t.	100	110
II	Con A(−) [d]	n.t.	100	90
III	Con A(−), α-mannosidase	n.t.	100	90
IV	Con A(−)	α-mannosidase, Con A(+)	25	180
V	Con A(−)	α-mannosidase, Con A(−)	25	180
VI	Con A(−)	endoglycosidase H, Con A(+)	100	56
VII	Con A(−)	endoglycosidase H, α-mannosidase, Con A(−)	25	90
VIII	Con A(−), α-mannosidase	endoglycosidase H, α-mannosidase, Con A(−)	16	90

[a] Toxicity expressed as a percentage of that of ricin I (IC$_{50}$ = $2.82 \cdot 10^{-6}$ mg/ml) to AKR-A lymphoma cells in tissue culture.

[b] The results for ricin I were the same as those for native untreated ricin

[c] n.t = not treated.

[d] Separation on Con A: (−) = not bound; (+) = bound and eluted.

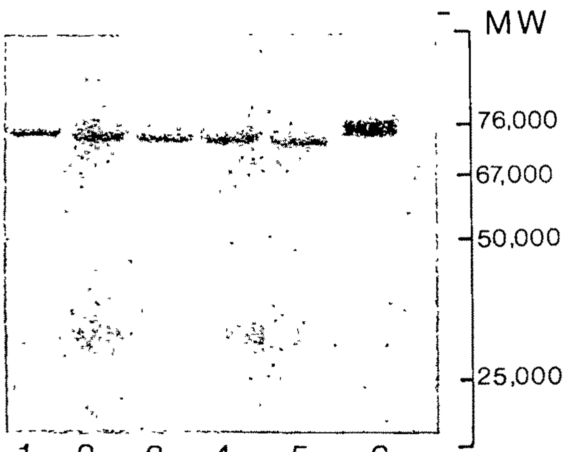

Fig. 1. Recombination of deglycosylated A- and B-chains Samples containing 10–12 μg of the mixture of A- and B-chains were electrophoresed in the following order: lane 1, ricin III; lane 2, ricin IV; lane 3, ricin V; lane 4, ricin VI, lane 5, ricin VII; lane 6, ricin I. The treatments of the A- and B-chains that were recombined to form ricin are listed in Table I Native ricin had the same mobility as ricin I under these conditions

Biological activity of deglycosylated ricin

Haemagglutination assays showed that all the deglycosylated ricin preparations fully retained their ability to bind to galactose-containing oligosaccharides on erythrocytes. Similarly reticulocyte lysate assays showed that the ribosome-damaging property of ricin A-chain was unimpaired after α-mannosidase or endoglycosidase H treatment (results not shown).

Table I summarises the results of the toxicity tests on the different preparations of glycosidase-treated ricin. Neither α-mannosidase treatment of the A-chain nor endoglycosidase H treatment of the B-chain affected the toxicity of the recombined ricin to AKR-A cells in tissue culture. Fractionation of either A- or B-chains on a concanavalin A column to remove material recognised by this lectin did not significantly affect the toxicity of the recombined toxins in vitro or in vivo (compare ricins I and II or IV and V).

However, α-mannosidase treatment of the B-chain reduced the toxicity of the recombined ricin (preparations IV, V, VII and VIII) to a quarter of that of ricin that had been recombined from the untreated chains.

The least toxicity to mice was exhibited by ricins IV and V, which were approximately half as toxic as native ricin or ricin that had been formed from the untreated chains (ricin I). The greatest toxicity was exhibited by ricin VI, which was twice as toxic as ricin I. The most extensively deglycosylated preparations, ricins VII and VIII, had unaltered toxicity to mice.

In vivo distribution of deglycosylated ricin

Ricin I, which had been formed from untreated chains, was rapidly cleared from the bloodstream by the liver after intravenous injection into rats (Table II). 15 min after injection 26% of the injected radioactivity had accumulated in the liver and only 24% remained in the blood. Deglycosylated ricin (ricin VIII) was cleared from the bloodstream by the liver more slowly than native ricin. Approximately 40% of the deglycosylated toxin remained in the blood 15 min after injection and only 10% was present in the liver (Table II). Little or no difference was seen in the accumulation of the deglycosylated ricin compared to the native toxin in other organs. Of the radioactivity in the blood, 92.3 (±0.4)% was in the plasma, 89.3 (±2.1)% of which was precipitable with trichloroacetic acid.

TABLE II

TISSUE DISTRIBUTION OF NATIVE AND DEGLYCOSYLATED ^{125}I-RICIN IN RATS

Groups of three rats were injected intravenously with 5 μg ^{125}I-ricin I or with 5 μg ^{125}I-ricin VIII and the percentage of the injected radioactivity in the tissues shown was measured 15 min later. Results represent one standard deviation about the arithmetic mean of triplicate determinations

Organ or tissue	Distribution (% of injected dose)	
	ricin I	ricin VIII
Liver	26.2±2.4	10.1±0.1
Spleen	6.2±0.6	6.4±0.5
Kidney [a]	2.4±0.1	3.1±0.1
Heart	0.4±0.3	0.4±0.4
Lung	3.0±0.1	3.2±0.4
Blood	24.3±0.8	38.6±3.1

[a] Both organs taken

Discussion

The major finding in the present study is that the enzymic removal of carbohydrates from ricin causes a decrease in cytotoxicity to cells in tissue culture, an increase in toxicity to mice and reduced clearance by the liver.

α-Mannosidase treatment of B-chain reduced the cytotoxic activity of the recombined ricin preparations (ricins IV, V, VII and VIII) whereas the removal of one complete oligosaccharide with endoglycosidase H treatment did not. None of the preparations showed any reduction in haemagglutinating activity, suggesting that the terminal mannose residues on the endoglycosidase H-resistant oligosaccharide on the B-chain play a role in toxicity which is unrelated to cell binding. One possibility is that the mannose residues are needed to maintain the conformation of the B-chain or of the toxin itself so that their removal reduces the ability of the B-chain to assist the passage of the A-chain across the cell membrane to the cytosol. Alternatively, changes in conformation of the B-chain after mannose removal could render the toxin more susceptible to cleavage by cellular thiols or proteolytic enzymes.

The in vivo toxicity of the various ricin preparations did not parallel their in vitro toxicity. In particular, the most highly deglycosylated toxin preparations (ricins VII and VIII), which were 4–5-fold less toxic than native ricin in vitro, did not show decreased toxicity to mice. Ricin VI, which had unaltered toxicity in vitro, was twice as toxic to mice. It is possible that the tissue or organ that is the target for ricin in the mouse does not have the same reduced sensitivity to deglycosylated ricin as AKR-A cells. Alternatively, the slower in vivo clearance of deglycosylated ricin could allow more of the toxin to reach the target organs and thus counteract the loss in cytotoxicity of the toxin resulting from deglycosylation.

Ricin that had been formed from the most extensively deglycosylated A- and B-chains showed reduced hepatic uptake after injection into rats and the blood levels of the deglycosylated toxin were correspondingly higher. This result accords with our earlier findings with chemically deglycosylated ricin [12]. The reduced hepatic entrapment of the deglycosylated toxin probably relfects the fact that the removal of carbohydrate from the toxin would prevent its recognition by the mannose receptors present on the non-parenchymal cells. In support of this, we have previously shown that α-mannosidase-treated A- and B-chains are taken up more slowly than native ricin A- and B-chains by hepatic non-parenchymal cells in vitro [27].

In conclusion, the enzymic removal of oligosaccharides from ricin retards its hepatic clearance from the bloodstream. Immunotoxins prepared from deglycosylated ricin should thus have a greater change of reaching their target cells in vivo. This may offset the slightly (2–5-fold) reduced toxicity to target cells in vitro that was observed by Vitetta and Thorpe [28] with immunotoxins prepared from chemically deglycosylated A- and B-chains and which, from the present results, is to be expected with immunotoxins made from enzymically deglycosylated chains.

Acknowledgements

We are very grateful for the help of Dr. A. Creighton and Dr. M. Owen of the ICRF and Dr. E. Vitetta of the University of Texas in giving their valuable comments on the manuscript. Ms. S.I. Detre and Mr. G. Watson are thanked for their technical assistance, and Mrs. A. Becket for typing the manuscript.

References

1 Olsnes, S. and Pihl, A. (1982) Pharmacol. Ther. 15, 355–381

2 Thorpe, P.E, Edwards, D.C., Ross, W C.J. and Davies, A.J.S. (1982) in Monoclonal Antibodies in Clinical Medicine (Fabre, S. and McMichael, A., eds.), pp 167–201, Academic Press, London

3 Thorpe, P.E. (1985) in Monoclonal Antibodies 84; Biological and Clinical Applications (Pinchera, A., Doria, G., Dammacco, F. and Bargellesi, A., eds.), pp. 475–512, Editrice Kurtis, S.R L , Milan, Italy

4 Vitetta, E S., Cushley, W. and Uhr, J. (1984) Science 219, 644–650

5 Olsnes, S. and Pihl, A. (1976) in Receptors and Recognition, Series B, Vol. 1 (Cuatrecasas, P , ed.), pp. 127–173, Chapman and Hall, London

6 Olsnes, S. and Pihl, A. (1982) in Molecular Action of Toxins and Viruses (Cohen, P and Van Heyningen, S., eds.), pp. 51–105, Elsevier Biomedical Press, New York

7 Olsnes, S. and Sandvig, K. (1983) in Receptors and Recognition, Series B, Vol. 15 (Cuatrecasas, P. and Roth, T., eds.), pp 189–236, Chapman and Hall, London

8 Fodstad, O.. Olsnes, S and Pihl, A. (1976) Br. J. Cancer 34, 418–425

9 Derenzini, M, Bonetti, E., Marinozzi, V. and Stirpe, F (1976) Virchow Arch. B. Cell Pathol 20, 15–28

10 Skilleter, D.N., Paine, A.J. and Stirpe, F. (1981) Biochim Biophys Acta 677, 495–500

11 Skilleter, D.N., Price, R.J. and Thorpe, P E. (1985) Biochim. Biophys. Acta 842, 12–21

12 Thorpe, P.E., Detre, S.I., Foxwell, B M.J., Brown, A.N.F , Skilleter, D.N., Wilson, G., Forrester, A.J. and Stirpe, F (1985) Eur J. Biochem. 147, 197–206

13 Foxwell, B.M.J., Donovan, T A , Thorpe, P.E. and Wilson, G. (1985) Biochim Biophys. Acta 840, 193–203

14 Bourne, B J.P., Casellas, P., Blythman, H.E. and Jansen, F K. (1986) Eur. J. Biochem 155, 1–10

15 Nicolson, G.L. and Blaustein, J. (1972) Biochim. Biophys Acta 266, 543–547

16 Baenziger, J.U and Fiete, D (1979) J Biol. Chem 254, 2400–2407

17 Uchida, T., Yamaizumi, M., Mekada, E , Okada, Y , Tsuda, M., Kurukawa, T and Sugino, Y (1978) J Biol. Chem. 253, 6307–6310

18 Kobashi, K and Horecker, B.L (1967) Arch. Biochem Biophys 121, 178–186

19 Steck, T.L. (1972) J Mol. Biol 66, 295–305

20 Laemmli, U.K. (1970) Nature 227, 680–685

21 Foxwell, B M.J., Detre, S I., Donovan, T A and Thorpe, P.E. (1985) Toxicology 34, 79–88

22 Saragiacomo, M., Barbieri, L., Stirpe, F and Tomasi, M. (1983) FEBS Lett. 157, 150–159

23 Thorpe, P.E , Brown, A.N.F., Ross, W.C.J , Cumber, A J , Detre, S I., Edwards, D.C., Davis, A J S and Stirpe, F. (1981) Eur. J. Biochem 116, 447–45

24 Weil, C. (1952) Biometrics 8, 249–254

25 Stirpe, F , Derenzini, M., Barbieri, L., Farabegoli, F., Brown, A.N.F , Knowles, P.K. and Thorpe, P E , Lab. Invest., in the press

26 Wang, L (1959) Am. J Physiol. 196, 188–203

27 Skilleter, D.N. and Foxwell, B.M.J (1986) FEBS Lett. 196, 344–348

28 Vitetta, E.S. and Thorpe, P.E (1985) Cancer Drug Delivery 2, 191–198

Biochimica et Biophysica Acta 923 (1987) 66–73
Elsevier

BBA 22461

Organothallium(III) reagents for modification of biomacromolecules: interaction of thallium derivatives with transfer RNA

Swati R. Baindur and Kenneth T. Douglas

Department of Chemistry, University of Essex, Colchester, Essex, CO4 34SQ (U.K.)

(Received 22 July 1986)

Key words: tRNA derivative; Thallium; RNA–metal interaction

As an extension of work on the inhibition of enzymes by arylthallium(III) reagents, the thallium analogues of the organomercurials, we have studied the interactions of these molecules with transfer RNA. In contrast to thallous acetate, thallium(III) derivatives (thallic trifluoroacetate, *p*-methylphenylthallium(III) bis-trifluoroacetate (MPT) and *o*-carboxyphenylthallium(III) bis-trifluoroacetate) bound to *Escherichia coli* tRNA. The interaction was fully reversible upon Sephadex G-25 gel filtration, and binding constants and stoichiometries were evaluated by a number of procedures. The likely site of interaction was shown to be the thiouridine residue (s^4U_8) based on changes induced by MPT on the absorbance around 330 nm. No changes in stacking interactions could be detected from the absorption or circular dichroic spectra. The detailed structure of the groups on thallium(III) affected the interaction with tRNA. Thalliation at s^4U_8 affects the absorbance at 335 nm and the amino-acid uptake capacity of *E. coli* $tRNA^{Phe}$ in parallel, the latter being progressively inhibited by increasing amounts of MPT. In a model nucleoside system, uridine disulphide is probably formed from reduced thiouridine by the oxidative action of the Tl(III) reagents. No evidence of cross-linking of *E. coli* tRNA molecules under gel electrophoretic conditions was obtained in contrast to the model nucleoside. The easily reversible interaction of MPT with sulphur sites in *E. coli* tRNA contrasts with the stable (to gel filtration) bonds formed between MPT and (thiol) sites in enzymes.

Introduction

We have recently introduced organothallium(III) reagents (**1**, $ArTlL_2$) as a new approach to label proteins specifically and inactivate enzymes [1]. Thallium reagents offer a number of potential advantages in biological studies. By analogy with the common organomercurials, we reasoned that organothallium(III) derivatives might be expected to prefer 'softer' sites in biomolecules (e.g. sulphur, nitrogen). However, in contrast to the traditional organomercurials these new reagents have a number of important properties. Firstly, the stable isotope ^{205}Tl (spin $\frac{1}{2}$, 70.48% natural abundance) is an NMR-active nucleus with a chemical shift range over approx. 2000 ppm. It is 19.2% as sensitive in NMR as the ^1H nucleus, and Tl-H coupling constants are extremely large [2]. There have been a few cases of the use of Tl NMR to obtain structural information in protein chemistry but, with the exception of a recent study on transferrin with the Tl^{3+} ion [3], these have simply used Tl^+ as a substitute for K^+ ions [4–6]. Secondly, $ArTlL_2$ species have two displaceable

---

Abbreviations: CD, circular dichroism; $tRNA^{Phe}$, transfer ribonucleic acid, phenylalanine-specific; MPT, *p*-tolylthallium(III) bis-trifluoroacetate; CPT, *o*-carboxyphenylthallium(III) bis-trifluoroacetate; USH, 4-thiouridine, reduced form; USSU, 4-thiouridine disulphide

Correspondence: Dr. K.T. Douglas, Department of Chemistry, University of Essex, Colchester, Essex, CO4 34SQ, U.K.

0304-4165/87/$03.50 © 1987 Elsevier Science Publishers B.V. (Biomedical Division)

ligands (L is usually $CF_3CO_2^-$) making them potential cross-linking reagents (cf. ArHgCl which is monofunctional at mercury). Further, the Tl(III)/Tl(I) redox change is accessible and pH dependent and one may anticipate redox modifications at biological sites under some appropriate circumstances.

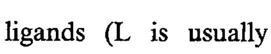

1: (a) X = *p*CH_3 (MPT)
(b) X = *o*CO_2H (CPT)

The nature of the pendant groups (aryl for **1a** and **1b**, $CF_3CO_2^-$ for $Tl(O_2CCF_3)_3$) affects the specificity of these reagents for enzymes, e.g., lactate dehydrogenase from various species [1], phosphoglycerate phosphokinase [7], glyceraldehyde-3-phosphate dehydrogenase [7].

There are reports of efficient interactions of Tl^+ (as a K^+ replacement) with ribosomes and of effects on aminoacyl-tRNA binding and peptidyl transferase activity [8,9]. Poly(U)-directed binding of $tRNA^{Phe}$ to mammalian ribosomes is stimulated effectively by Tl^+ [9,10]. We now report on the selective modification of *Escherichia coli* tRNA with arylthallium(III) reagents (**1**), indicating that these reagents may serve as potential probes not only of proteins but also of these nucleic acids.

Materials and Methods

Chemicals

The following were purchased from Sigma Chemical Co. (St. Louis, MO): trifluoroacetic acid; transfer RNA (Baker's yeast type X; *E. coli* strain W, type XXI; *E. coli* tRNA, type XXI); transfer RNA, phenylalanine-specific from *E. coli* type XXI; uridine disulphide; thallous acetate, Sephadex G-25. Thallic trifluoroacetate was purchased from Aldrich Chemical Co. (Dorset, U.K.). Buffers were prepared from Analar quality materials using glass-distilled water. Dimethyl sulphoxide (DMSO) was purified by drying overnight over $CaSO_4$ and fractional distillation from CaH_2 and was stored over a molecular sieve (type 4A) under nitrogen. Radiolabelled toluene was from Amersham International PLC. Crude tRNA amino-acid synthetase was prepared by the method described in Refs. [11 and 12].

Synthesis of p-methylphenylthallium(III) bis-trifluoroacetate (MPT)

This was prepared by a modification of the method of McKillop et al. [13]. Thallium trifluoroacetate (5.1 g, 9.4 mmol) in redistilled trifluoroacetic acid (18 ml) was added dropwise to toluene (1.0 ml, 0.867 g, 9.4 mmol) in trifluoroacetic acid (18 ml) and the mixture was allowed to stand at room temperature overnight. The resulting white crystals of product were isolated after washing with cold carbon tetrachloride and dried by suction to give the product, 1.5 g, m.p. 169–185°C (in Ref. 13, 174–190°C). The proton and ^{205}Tl NMR spectra were in agreement with the proposed structure. MPT is now commercially available (Sigma Chemical Co., St. Louis, MO).

A similar procedure was adopted for the preparation of ^{14}C-labelled MPT (^{14}C-MPT). To [*methyl*-^{14}C]toluene (5.2 μmol, 250 μCi), in the ampoule in which it was received under vacuum, was added redistilled trifluoroacetic acid (10.08 ml), and the solution was transferred to a small flask. Non-radioactive toluene (0.56 ml) was added. Thallic trifluoroacetate solution (2.86 g in 10.08 ml trifluoroacetic acid) was added dropwise and the resulting mixture was left at room temperature overnight. Product was isolated, purified and characterised as previously. The specific radioactivity was determined to be $7.86 \cdot 10^4$ cpm/μmol.

Concentrations of MPT solutions were estimated from the absorption coefficient of $1.08 \cdot 10^4$ $M^{-1} \cdot cm^{-1}$ at 230 nm which had been determined for a carefully purified cold sample.

Methods

Ultraviolet-visible spectrophotometry was carried out using a Carlo Erba Spectracomp 601. NMR spectra were obtained using a Bruker WP80 SY instrument, fitted with a thallium probe when necessary. Scintillation counting was effected by means of a three channel Betaszint BF5000 counter. Studies by Sephadex G-25 gel filtration were carried out using a Pharmacia FRAC 100 fraction collector and UV (254 nm) monitor system. An Amicon MPS1 micropartition system with YM10 ultrafilters was used in combination with an MSE High Speed 25 Centrifuge for some binding assays using ^{14}C-MPT.

Atomic absorption measurements of the thallium contents of samples were performed using a Varian Atomic Absorption Instrument, with a thallium lamp, according to the supplier's instructions (with thallic trifluoroacetate as standard).

tRNA aminoacylation assay

The method used was a combination of procedures described in the literature [11,12,14,15]. *E. coli* tRNA^{Phe} (100 μl of 10^{-5} M) was incubated in a small tube with 100 μl of an 'incubation mix' which was made up of the following: Tris 40 μmol, $MgCl_2$ 4 μmol, EDTA 0.5 μmol, ATP 1 μmol and KCl 40 μmol, and to which had been added 50 μl/ml L-[U-^{14}C]phenylalanine and 100 μl/ml of crude tRNA amino-acid synthetase. After incubation (5 min) in the tube, 100 μl of the mixture (tRNA^{Phe} plus 'incubation mix') was put onto a filter-paper disc (3 MM Whatman, 30 mm diameter), which was then plunged into cold 10% trichloroacetic acid/0.1 M KCl to precipitate the tRNA. This disc was then washed with 10% trichloroacetic acid followed by 0.5 M NaCl, 10% and 5% trichloroacetic acid in turn. The discs were air-dried and counted in a scintillant (4% BBOT in toluene).

Results

Thallium reagents were added to *E. coli* tRNA in 0.1 M Tris buffer at pH 7.50 (containing 0.1 M NaCl and 10 mM $MgCl_2$) at 25.0°C. In some cases changes in the absorption spectra were observed. Thus, in Fig. 1 the spectra in the region of the 335 nm band of tRNA in the presence and absence of MPT ($1.7 \cdot 10^{-4}$ M) are shown. It is clear that the addition of this organothallium(III) derivative causes a significant diminution of this spectral characteristic, which is ascribed to the thiouridine, s^4U_8 [16]. In contrast, for this same system there was no detectable change in the absorption at 260 nm, a spectral band which reflects the environment of the bases.

Similar effects were observed with *E. coli* tRNA and CPT at the same concentrations and under the above conditions. However, the addition of an approx. 10^4-fold molar excess of thallous acetate (Tl^+) to *E. coli* tRNA had no detectable spectral effects at 260 nm or at 335 nm (see Fig. 2). There is clearly no significant change in the 335 nm band (see inset) and the spectrum marked 'mixture' (main body) was the accurate summation of the component spectra of tRNA and thallous acetate, which were recorded digitally in separate experiments.

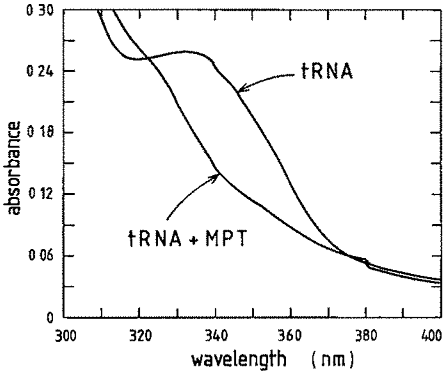

Fig. 1. Spectral effects of MPT on *E. coli* transfer RNA. Spectra of *E. coli* tRNA (6.6 μM) in 0.1 M Tris buffer (pH 7.50, 0.1 M NaCl, 0.01 M $MgCl_2$) alone and with added MPT (1.7 10^{-4} M) at 25°C

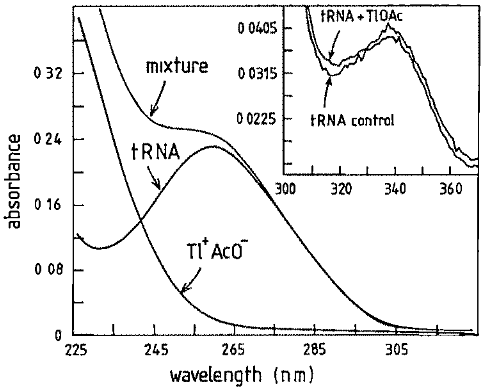

Fig. 2. Spectral studies of *E. coli* transfer RNA with thallous acetate. Spectra of thallous acetate (Tl^+AcO^-, 4.8 mM), *E. coli* tRNA (0.57 μM) and a mixture of them ($Tl^+ OAc^-$ = 4.8 mM, tRNA = 0.57 μM) in pH 7.50 Tris buffer (0.1 M Tris containing 0.1 M NaCl and 0.01 M $MgCl_2$) at 25°C. A digital recording of wavelength/absorbance was also taken (200 points) over the wavelength range indicated in the diagram to allow summation of tRNA plus TlOAc spectra at each wavelength for comparison with the (digital) spectrum of the mixture. The inset shows the expanded region of the 335 nm band under the above conditions

Reversibility of tRNA thalliation

The reversibility of the interaction of MPT with *E. coli* tRNA was studied by incubation tRNA (3.0 ml, $A_{260} = 2.05$) with ^{14}C-MPT ($8.3 \cdot 10^{-5}$ M, $7.86 \cdot 10^4$ cpm/μmol), in 0.1 M Tris buffer (pH 7.50, 0.1 M NaCl, 0.01 M $MgCl_2$) for 1 hour at ambient temperature. This mixture was studied spectrophotometrically to ascertain that reaction of the thallium reagent with the thiouridine was complete, with maximal change in the 335 nm band, as described above (cf. Fig. 1). The product mixture was loaded onto a Sephadex G-25 column (30 × 2 cm) preequilibrated with 0.1 M Tris buffer (pH 7.50, 0.1 M NaCl, 0.01 M $MgCl_2$) and subjected to gel filtration with the same buffer for elution. The fractions were monitored both using the absorbance at 254 nm and by removing aliquots (0.1 ml) for scintillation counting in a mixture of ethanol (1.5 ml) and toluene (3.5 ml, 0.6% w/v BBOT). The elution profile is shown in Fig. 3. It is clear that there is no significant level of radioactivity associated with the tRNA fraction which eluted first and that unbound labelled thallium reagent is well resolved from the nucleic acid peak.

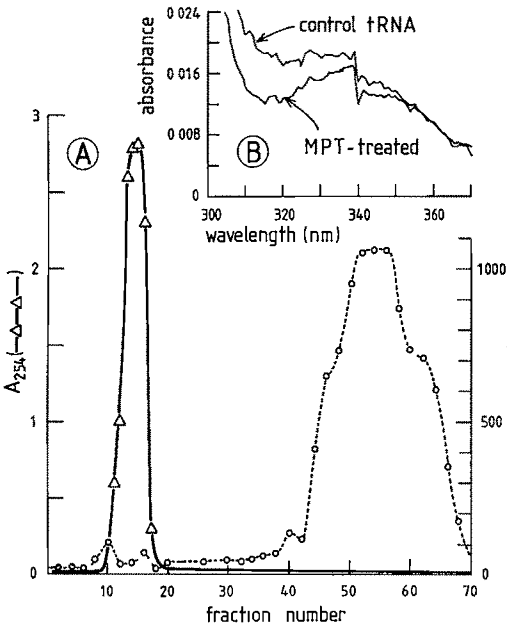

Fig. 3. Chromatography of MPT-treated *E. coli* transfer RNA. Elution profile (G-25) of ^{14}C-MPT-treated *E. coli* tRNA in pH 7.50 Tris buffer (0.1 M NaCl, 0.01 M $MgCl_2$), O------O refers to the results of scintillation counting (cpm) of aliquots of the fractions and Δ———Δ shows the absorbance at 254 nm of the fractions. The inset shows the spectra in the 335 nm region of the tRNA fraction obtained by this procedure compared with that of a control tRNA sample, at the same concentration and treated similarly (i.e., incubation, gel filtration, etc.) but without ^{14}C-MPT treatment.

In the inset to Fig. 3 are shown the spectra in the 335 nm region of the control tRNA (treated similarly to the above but with no ^{14}C-MPT added) and the MPT-treated tRNA after Sephadex G-25 reisolation. Passage over this gel filtration column restored the absorption band at 335 nm effectively quantitatively (the slight difference in the spectra is likely to be artefactual given the small absorbance changes involved). There was no significant change in the 260 nm spectral band after ^{14}C-MPT treatment and gel filtration. These observations indicate that the thalliation of tRNA by MPT is fully reversible by this criterion under these conditions.

Measurements of binding constants

The extent of change in the 335 nm band intensity relative to free tRNA depended on the ratio of added arylthallium(III) reagent (ligand) to the free tRNA present. This was analysed in a number of ways.

A Job plot was constructed by varying the ligand/tRNA ratio at a constant total concentration of $3 \cdot 10^{-5}$ ([MPT] plus [tRNA]). The change in absorbance at 335 nm (ΔA_{335}) was plotted against the mole fraction of MPT present (Fig. 4, inset) and indicated a 1:1 complex as the maximal change in absorbance was at 0.5 mole fraction of MPT.

The same system was studied to obtain data for a Scatchard plot using Eqn. 1:

$$\frac{r}{[\mathrm{MPT}]_{\mathrm{free}}} = \frac{n}{K_{\mathrm{d}}} - \frac{r}{K_{\mathrm{d}}} \qquad (1)$$

where K_{d} is the dissociation constant of the MPT-tRNA complex ($1/K_{\mathrm{d}} = K$, the equilibrium constant), n is the number of binding sites and r is the ratio of $[\mathrm{MPT}]_{\mathrm{bound}}$ to $[\mathrm{tRNA}]_{\mathrm{total}}$. Linear regression analysis of the data gave $K = 7.25 \pm 0.19 \cdot 10^4$ M^{-1}, i.e., $K_{\mathrm{d}} = 1.37 \pm 0.04 \cdot 10^{-5}$ M (for $[\mathrm{tRNA}]_{\mathrm{total}} = 3.50 \cdot 10^{-5}$ M and $[\mathrm{MPT}]_{\mathrm{total}}$ in the range $5.00 \cdot 10^{-5}$ M to $1.37 \cdot 10^{-4}$ M). From the

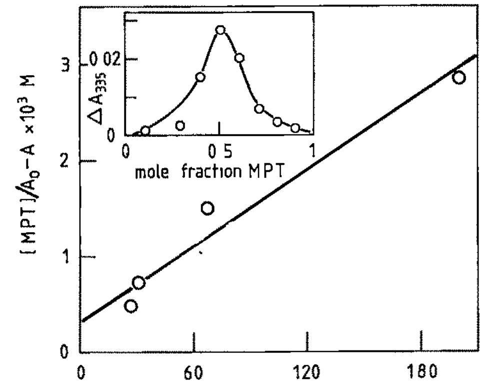

Fig 4. Binding of MPT to *E coli* transfer RNA. Plot of spectrophotometric data for the interaction of *E coli* tRNA with MPT at 25°C in pH 7.50 Tris buffer (0.1 M NaCl, 0.01 M $MgCl_2$) using Eqn. 1. Measurements were made at 335 nm at a tRNA concentration of $5.8 \cdot 10^{-6}$ M with varying levels of MPT, ranging from $6.25 \cdot 10^{-5}$ M to $1.3 \cdot 10^{-4}$ M Points are experimental, and the line was obtained by least-squares linear regression analysis.

Scatchard analysis it appears that under these conditions there is only one class of binding site and that the number of binding sites per tRNA molecule is one ($n = 1.05 \pm 0.04$).

We also measured the binding by an independent technique following the procedure of Armor and Haim [17]. This has been used previously to measure the binding of arylmercury derivatives to thioguanines [18]. The spectral changes of the tRNA at 335 nm for 1:1 binding (see Job and Scatchard analyses) can be written [17] in the form of Eqn. 2:

$$\frac{[\mathrm{MPT}]}{(A_0 - A)} = \frac{1}{K} \cdot \frac{1}{(A - A_\infty)} - \frac{1}{(\varepsilon_1 - \varepsilon_2)} \qquad (2)$$

for 1 cm pathlength, where [MPT] is the total MPT concentration, A is the absorbance of tRNA/MPT mixtures (corrected for absorbance of the blank), A_0 and A_∞ are the absorbances of tRNA and the tRNA-MPT complex (formed according to eqn. (3)), respectively, at the same tRNA concentrations. The absorption coefficients of tRNA and the complex are ε_1 and ε_2 respectively.

$$\mathrm{MPT} + \mathrm{tRNA} \overset{K}{\rightleftharpoons} \mathrm{MPT}\cdot\mathrm{tRNA} \qquad (3)$$

The equilibrium constant for binding is K. The value of A_∞ was obtained by extrapolation to $1/[\mathrm{MPT}] = 0$ on a plot of ΔA_{335}^{-1} versus $[\mathrm{MPT}]^{-1}$. A plot of the data obtained at 25°C is shown in Fig. 4, from which the slope of the graph obtained by least-squares linear regression analysis allowed calculation of $K = 7.69 \pm 1.02 \cdot 10^4$ M^{-1}.

Aminoacylation of MPT-treated E. coli tRNA^{Phe}

E. coli $tRNA^{Phe}$ ($1.36 \cdot 10^{-5}$ M) was incubated with MPT ($1.20 \cdot 10^{-5}$ M) for 1 h at 25°C in pH 7.50 buffer at 25°C and an aliquot (100 μl) was taken for assay. Controls of $tRNA^{Phe}$ with enzyme or ethanol (the solvent in which MPT was dissolved) were compared. The following results were obtained and are quoted as the system used with observed counts per min of assay disc in parentheses: enzyme alone (145); $tRNA^{Phe}$ with ethanol and enzyme present (5235); $tRNA^{Phe}$ with MPT and enzyme (2618). Clearly MPT causes a decrease in amino-acid uptake in this assay. The experiment was repeated using a range of concentrations of MPT with *E. coli* $tRNA^{Phe}$ ($1 \cdot 10^{-5}$ m), also recording the change in intensity of the 335 nm band of tRNA on MPT treatment. The data are shown in Fig. 5 as plots of assay activity (cpm, amino-acid uptake by tRNA) and A_{334} vs. the concentration of tRNA present.

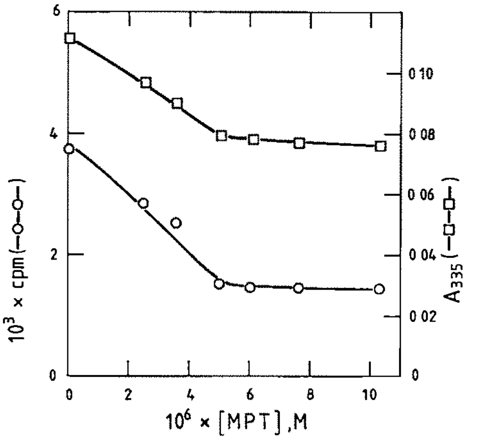

Fig. 5. Effect of MPT on amino-acid uptake by *E coli* transfer RNA. Plot of the changes in the absorbance at 335 nm (A_{335}) of *E. coli* $tRNA^{Phe}$ ($1 \cdot 10^{-5}$) (□) and amino-acid uptake in cpm (○) in pH 7.50 buffer at 25°C concentration of MPT

Model reactions of MPT with thiouridine

The interaction of arylthallium(III) derivatives was suspected to involve thio-bases and consequently a simplified system was studied to confirm this. Thiouridine (USH) was prepared in situ (in a spectrophotometer cuvette) by reduction of thiouridine disulphide (USSU, $1.2 \cdot 10^{-5}$ M) by sodium dithionite ($6.7 \cdot 10^{-5}$ M) in pH 7.50 Tris buffer, 0.1 M NaCl, 0.01 M $MgCl_2$. On addition of the sodium dithionite to USSU the spectrum of thiouridine disulphide (Fig. 6), with $\lambda_{max} = 310 \pm 1$ nm; $\varepsilon_{max} = 2.8 \cdot 10^4\ M^{-1} \cdot cm^{-1}$, was replaced by that of thiouridine with $\lambda_{max} = 331$ nm, $\varepsilon_{max} = 20000\ M^{-1} \cdot cm^{-1}$. Addition of MPT (final concentration $1.67 \cdot 10^{-4}$ M by addition of 50 μl of 0.01 M stock in dimethyl sulphoxide to 3.0 ml of USH in buffer) led to an immediate spectral change. The peak at 331 nm characteristic of USH was replaced by a peak at 312 nm similar in shape to that from USSU but of intensity greater by some 30% at λ_{max}. This increased intensity probably indicates the formation of absorbing thallium products but the shape of the peak from USH plus MPT is closely comparable in gross features to that of the parent USSU, perhaps indicating that this is formed also.

Discussion

Site of attack

Arylthallium(III) reagents are efficient and selective reagents in protein modification, having been used to modify a number of enzymes including lactate dehydrogenase [1] and phosphoglycerate phosphokinase (Ref. 7 and M.A. Bunni et al., unpublished data). In these systems, treatment with **1** led to inactivation of the enzyme activity and there was an attendant loss in thiol titre. This is in line with the concept of 'hard' and 'soft' acids and bases [19] – Tl(III) would be anticipated to have an affinity for softer sites, e.g., S and N.

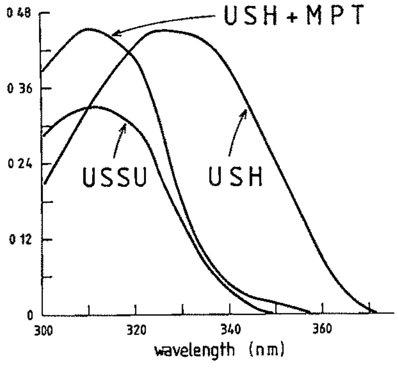

Fig. 6. Spectral studies of MPT with thiouridine. Spectra of USSU ($1.2 \cdot 10^{-5}$ M), of USH ($2.3 \cdot 10^{-5}$ M) and a mixture of USH ($2.3\ 10^{-5}$ M) with MPT ($1.67 \cdot 10^{-4}$ M) in pH 7.5 tris buffer, 0.1 M NaCl, 0.01 M $MgCl_2$ at 25°C.

There are a number of pieces of evidence which point to an apparently similar mode of attack for these arylthallium(III) species with *E. coli* tRNA. The absorbance band around 335 nm of *E. coli* tRNA has been ascribed firmly to the thiouridine base [16,20,21]. Treatment with MPT or CPT selectively diminishes this absorption in a concentration-dependent manner. Organomercurials also react with the thiouridine, although the tRNA must be denatured first to achieve reaction. Mercuric chloride reacts with thiouridine in *E. coli* $tRNA^{Val}$ (native) but this tRNA must have its tertiary structure labilised to allow reaction with *p*-hydroxymercuribenzoate (PHMB) [18]. In contrast, Pal et al. [21] reported that PHMB reacted with native *E. coli* tRNA to diminish the 330 nm absorbance, but that dialysis in the presence of Mg^{2+} led to regeneration of the spectrum. Pentafluorophenylmercuric chloride reacts with $tRNA^{Tyr}$ to give a stable derivative [20]. The thallium(III) derivative reacts with native tRNA to give a reasonably strong complex, which is dissociated on G-25 gel filtration in the presence of Mg^{2+} ions, in line with the results of Pal et al. [21] for organomercurials. Yeast tRNA with no thiouridine base (U_8 instead of s^4U_8) is unaffected by MPT or CPT.

In the model system, treatment of reduced thiouridine by addition of MPT leads to loss of the reduced USH band around 331 nm, probably, from the spectral results, with formation of USSU. Clearly, for the free nucleoside Tl(III) can not only react at the sulphur site, but also exert its well-established [22] oxidising power, a simple scheme being given in Eqn. 4.

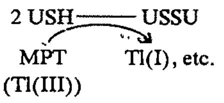 (4)

$$\underset{\substack{\text{MPT}\\(\text{Tl(III)})}}{2\ \text{USH}} \longrightarrow \underset{\text{Tl(I), etc.}}{\text{USSU}} \qquad (4)$$

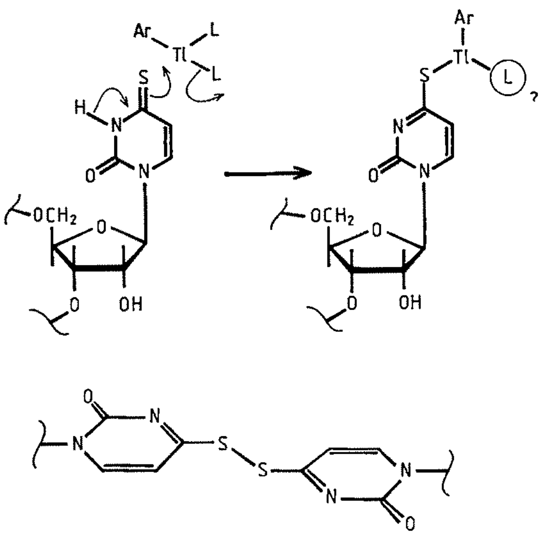

Scheme I

Nature of the thalliation of tRNA

The behaviour of MPT with tRNA contrasts with protein systems. For example, enzymic activity is lost irreversibly and thalliation of the protein is stable to gel filtration over G-25 (ref. 7, and M.A. Bunni et al., unpublished data). However, the interaction of *E. coli* tRNA with MPT is clearly reversed by passage over G-25. This is noteworthy in view of the behaviour of the model (isolated thiouridine) system. We found no electrophoretic evidence for significant amounts of tRNA dimers (cross-linked through s^4U_8) after treatment with MPT. This, along with the reversibility of binding and 1 : 1 stoichiometry, suggests a monofunctional modification by Tl(III) at s^4U_8 (Scheme I) as a minimal mechanism. The mechanism is indicated as a nucleophilic displacement at Tl(III), but as the aqueous solution structure of these Tl(III) species is not yet established one cannot safely define it as S_N2 (synchronous, as written) or S_N1 (with $ArTlL^+$ or $ArTl^{2+}$ or their aquo forms reacting). It is possible that the second trifluoroacetoxy ligand is also displaced by another group on the tRNA (e.g., a nitrogen atom of a base or a CO_2^- or $-PO_3^{2-}$ group) site to give a chelate.

Crude *E. coli* tRNA also reacts (with decrease in A_{335}) when there is an ortho-carboxy on the aryl residue (CPT) instead of the methyl group (MPT). The reactivity of CPT was found to be somewhat less than that of MPT in preliminary experiments. There were also significant precipitation problems with CPT.

Thallic trifluoroacetate (TTFA) was found to react with crude *E. coli* tRNA with a different stoichiometry ([tRNA]/[TTFA] = 3).

In contrast to these thallium(III) reagents *E. coli* tRNA seems to have no reactivity (as reflected by changes in A_{335} or A_{260}) with the thallous ion (thallous acetate was used). The spectra obtained were identical to those of controls even in the presence of 0.1 M thallous acetate.

The effect of thalliation appears to be a local, reversible modification at s^4U_8 and limited to thallium(III) reagents. Circular dichroism spectra of tRNA in the presence and absence of MPT indicated that the modification of s^4U_8 had no major effect on stacking interactions (S. Baindur, A.F. Drake and K.T. Douglas, unpublished observations), borne out by the lack of change in the absorbance at 260 nm in the spectrum. The parallel behaviour towards MPT concentration of the amino-acid uptake and ΔA_{335} studies (Fig. 5) indicates that modification of s^4U_8 in this way probably affects amino-acyl uptake, although with the use of a crude tRNA amino-acid synthetase preparation further study is clearly required in this aspect. Chemical or photo s^4U_8 modifications have been reported in the literature to leave amino-acid uptake unaffected [16,23] or to diminish [25] or abolish it [20,24]. Given the (usually) irreversible reaction of MPT with enzymes (Refs. 1, 7 and M.A. Bunni et al., unpublished data) it is possible that MPT might be useful in cross-linking studies of tRNA with enzymes (e.g., tRNA amino-acid synthetase) or ribosomal proteins, with the link to the tRNA being formed reversibly in contrast to that with the protein. In this context it is noteworthy that it has been suggested [24,26] that there is a transient covalent interaction between tRNA synthetase and the 5,6 double bond of the U_8 or s^4U_8 residue.

Acknowledgements

We are grateful to the Committee of Vice-Chancellors for an O.R.S. Award (to S.R.B.).

References

1 Bunni, M.A. and Douglas, K.T. (1984) Biochem J. 217, 383–390

2 Hinton, J.F., Metz, K.R. and Briggs, R.W (1982) Ann Rep. NMR Spectrom. 13, 211–311

3 Bertini, I., Luchinat, C. and Messori, L. (1983) J. Am. Chem. Soc. 105, 1347–1350

4 Grisham, C.M., Gupta, R.K, Barnett, R.E. and Mildvan, A.S. (1974) J Biol. Chem. 249, 6738–6744

5 Reuben, J and Kayne, F.J. (1971) J Biol Chem. 246, 6227–6234

6 Kayne, F.J. and Reuben, J. (1970) J. Am. Chem. Soc. 92, 220–223

7 Bunni, M.A. (1984) Ph D. Thesis, University of Essex

8 Hutlin, T. and Näslund, P.H. (1974) Acta Biol. Med. Germ. 33, 753–760

9 Hutlin, T. and Näslund, P.H. (1974) Chem. Biol Interact 8, 315–328

10 Hutlin, T. and Näslund, P.H. (1978) Eur. J Biochem. 88, 143–148

11 Zak, R., Prior, G and Rabinowitz, M. (1979) Methods Enzymol 59, 314–315

12 Zubay, G (1962) J. Mol. Biol. 4, 347–356

13 McKillop, A., Hunt, J.D., Zelesko, M J., Fowler, J S., Taylor, E.C., McGillivray, G. and Kienzle, F. (1971) J. Am Chem Soc. 93, 4841–4844

14 Gillam, I., Millward, S., Blaw, D., Von-Tigerstorm, M., Wimmer, E and Tener, G.M. (1967) Biochemistry 6, 3043–3056

15 Ayad, A.R. and Blamire, J. (1972) Techniques in Nucleic Acid Fractionation, pp. 28–30, Wiley, London

16 Wong, K.L. and Kearns, D.R. (1975) Biochim. Biophys Acta 395, 381–387

17 Armor, J N. and Haim, A. (1971) J. Am Chem Soc. 93, 867–873

18 Heitner, H I., Lippard, S.J. and Sunshine, H R. (1972) J Am. Chem. Soc. 94, 8936–8937

19 Pearson, R.G (1963) J. Am Chem. Soc 85, 3533–3537

20 Jones, A.S., Walker, R.T. and Youngs, V (1973) Biochim Biophys. Acta 299, 293–299

21 Pal, B.C., Shugart, L.R., Sham, K R. and Stulberg, M P. (1972) Arch. Biochem. Biophys. 150, 86–90

22 Lee, A.G. (1971) The Chemistry of Thallium, Elsevier, Amsterdam

23 Hara, H. and Horiuchi, T. (1970) Biochem. Biophys. Res. Commun 38, 305–311

24 Starzyk, R., Schoemaker, H.J.P. and Schimmel, P (1985) Proc Natl Acad. Sci. USA 82, 339–342

25 Carré, D S, Thomas, G. and Favre, A. (1974) Biochimie 56, 1089–1101

26 Schimmel, P R. (1979) Adv. Enzymol. 49, 187–223

Biochimica et Biophysica Acta 923 (1987) 74–82
Elsevier

BBA 22390

Nucleoside-triphosphatase and hydrolysis of thiamin triphosphate in *Escherichia coli*

Takahiro Nishimune [a], Shin-ichi Ito [a], Mitsuko Abe [a], Mitsuaki Kimoto [a]
and Ryoji Hayashi [b]

[a] *Department of Microbiology, Yamaguchi University School of Medicine, Ube*
and [b] *Medical College of Oita, Oita (Japan)*

(Received 17 October 1986)

Key words: Thiamin triphosphate; Thiamin-triphosphatase; Thiamin-diphosphate kinase, Nucleoside-triphosphatase

A membrane-bound nonspecific triphosphatase of *E. coli* was solubilized and purified to a homogeneous SDS-acrylamide gel electrophoresis band. It was found to be a single polypeptide of 16 kDa requiring no Mg^{2+}, with an optimal pH at 6.5. The substrate specificity was broad and a nonspecific Mg^{2+}-independent ribonucleoside-triphosphatase (NTPase) activity was expressed together with thiamin-triphosphatase activity. The molecular size and characteristics were clearly different from the known NTPases (EC 3.6.1.15). Using the purified thiamin-triphosphatase II, ATP : thiamin-diphosphate phosphoryl transferase (EC 2.7.4.15) activity was demonstrated with an optimal pH of approx. 5.3. Considering its kinetic parameters and other characteristics, however, the thiamin triphosphate synthesizing activity was not thought to take part in cellular thiamin triphosphate synthesis. The possibility that thiamin-triphosphatase II plays a part in the hydrolysis of thiamin triphosphate to control its cellular level is suggested.

Introduction

In a preliminary study, we found thiamin-triphosphatases of *Escherichia coli*. Mg^{2+}-dependent thiamin-triphosphatase I was mainly in the soluble fraction and thiamin-triphosphatase II was solubilized from the membrane. Thiamin-triphosphatase II had a smaller K_m for thiamin triphosphate, and it seemed likely that this enzyme had some role in the control of cellular thiamin triphosphate at relatively low concentrations. We have tried to purify thiamin-triphosphatase II and then to examine the relation between its thiamin-triphosphatase and nucleoside-triphosphatase (NTPase) activities. There appears to be no close relationship between the two enzyme activities in the rat [1,2]. It has also been reported that thiamin-diphosphatase and nucleoside-diphosphatase (NDPase) in bovine liver and rat brain are two activities expressed by one enzyme [3,4]. The results of our studies showed that thiamin-triphosphatase II of *E. coli* displays a novel nonspecific NTPase activity.

An earlier report [5] explored biosynthesis of thiamin triphosphate and suggested the presence of a thiamin triphosphate synthesizing activity in a subcellular fraction of *Mycobacterium*. We tried to detect it in *E. coli* and found that, among several subcellular fractions which showed the activity, the same fraction as thiamin-triphosphatase II was included. However, characterization of apparent thiamin triphosphate synthesizing activity revealed

---

Correspondence: Dr. T. Nishimune, Osaka Prefectural Institute of Public Health, Nakamichi, Higashinari, Osaka, 537, Japan

0304-4165/87/$03.50 © 1987 Elsevier Science Publishers B.V. (Biomedical Division)

that optimum conditions for this activity differed from the physiological state of bacterial cells both kinetically and in other characteristics. The apparent reversible character of the thiamin-triphosphatase II reaction was shown by detecting both thiamin-triphosphatase and thiamin-diphosphate kinase activities in the purified enzyme preparation.

Materials and Methods

Strain, medium, and culture conditions. Thiamin-triphosphatase II was prepared from cells of *Escherichia coli* W70-23 (thiamin$^-$) grown in a synthetic minimal medium [6] at double strength supplemented with $1 \cdot 10^{-8}$ M thiamin. Cells were grown for approx. 12 h at 37°C under aerobic conditions to early stationary phase.

Assay of thiamin-triphosphatase II and NTPase. The reaction mixture contained enzyme, 0.1 M Tris-maleate buffer (pH 6.5), 40 mM KCl, 0.2 mM 2-mercaptoethanol, 0.05% Lubrol PX and 0.5 mM thiamin triphosphate or nucleoside triphosphate in 50 μl. The mixture was incubated for 2 h at 37°C and the P_i liberated was determined by the method of Concustell et al. [7], or by the method of Baginski et al. [8] for pre-gel filtration samples. Since thiamin-triphosphatase II expressed acidic NTPase activity, both thiamin triphosphate and ATP were used as substrate where indicated. The inhibitory effect of thiamin triphosphate against NTPase was studied using [^{32}P]ATP as substrate, and approx. 0.26 μmol KH_2PO_4 was added as carrier before developing a 10 μl aliquot of the reaction mixture on a cellulose MN300G thin layer plate (Macherey-Nagel), using *tert*-pentanol/formic acid/water (3:2:1, v/v) [9]. The P_i spot was detected by spraying with Concustell's reagents (urea-albumin-phosphate solution followed by malachite green solution) and developing at 37°C for 15 min. The green spot was removed, added to a scintillation vial with a toluene based scintillator and counted in a liquid scintillation counter.

Assay of thiamin-diphosphate kinase and NDP kinase. The assay mixture contained enzyme, 0.1 M potassium acetate buffer (pH 5.5), 40 mM KCl, 2 mM 2-mercaptoethanol, 0.06% Lubrol PX, 0.27 M thiamin diphosphate or CDP and 0.5 M [γ-^{32}P]ATP (2.5 mCi/mmol) in 25 μl. The reaction was carried out for 1 or 2 h at 37°C, and 5 μl 25 mM thiamin triphosphate or CTP was added as carrier. The reaction proceeded linearly for at least 3 h, and the rate was also linearly dependent on the amount of enzyme. For the Mg^{2+}-NDP kinase assay, the buffer was Tris-HCl (pH 8.0), and 10 mM $MgCl_2$ was added with 4 mM CDP and 6 mM ATP [10]. The reaction was carried out for 10 min and carrier was added as above. 10 μl was analyzed via high voltage paper electrophoresis at pH 6.0 (0.1 M sodium phosphate buffer), and at 1. kV and 100–300 mA for approx. 3 h in *n*-hexane maintained at below 10°C using Toyo No. 50 paper (60 cm length). After drying, thiamin triphosphate and other components were detected under ultraviolet light. The areas were cut out of the paper, added to a vial containing toluene based scintillator and counted in a liquid scintillation counter (efficiency, approx. 70%). A control, which had not received the substrate, was also assayed and the count level was subtracted from that of test assays. For assay of [^{32}P]P_i liberated during thiamin [^{32}P]triphosphate synthesis (Fig. 3b), the assay mixture was developed on a cellulose MN300G thin-layer plate as above.

Solubilization of thiamin-triphosphatase II. E. coli W70-23 cells were grown as above, pelleted, washed with cold 0.01 M Tris-HCl (pH 7.4) containing 0.03 M KCl at 4°C and shocked osmotically. The shocked cell was dispersed in 10 mM Tris-HCl (pH 7.4) containing 0.5 mM 2-mercaptoethanol (40 ml/liter culture) and disrupted in a milder manner by sonication. The undisrupted cells were spun down and washed with 30 ml/liter culture of the same buffer. From the supernatant and the washing combined, membrane fraction was collected by 150 000 × *g* centrifugation at 4°C for 120 min and washed with the same buffer. To the membrane fraction, 5 M $NaClO_4$ (in 0.1 M Tris-HCl (pH 7.4), 0.5 mM 2-mercaptoethanol and 1 mM EDTA) was added to give 0.5 M $NaClO_4$ and shaken gently for 20 min at 30°C. The solubilized thiamin-triphosphatase was obtained in the supernatant from the 150 000 × *g* centrifugation at 4°C and dialyzed immediately as described below.

Column chromatographic purification of thiamin-triphosphatase II. Procedures were carried out at 4°C. Sample for Sephacryl S-300 gel filtration was obtained after $NaClO_4$ solubilization, as described above, of the membrane fraction of *E. coli* W70-23, which had been cultured in three batches of 15 l medium. The solubilized preparation was dialyzed immediately against 50 mM Tris-HCl (pH 7.4) containing 1 mM 2-mercaptoethanol, 1 mM EDTA and 0.05% Lubrol PX (buffer 1) added with 0.1 M KCl, and concentrated by ultrafiltration before applying to the Sephacryl column. The sample for phosphocellulose chromatography was dialyzed against buffer 2 (10 mM Tris-maleate (pH 6.5), 1 mM EDTA, 1 mM 2-mercaptoethanol, 0.05% Lubrol PX, and 0.17 M KCl). The column was pre-equilibrated and washed after sample application with the same buffer, and developed with a linear KCl gradient of 0.17–1.2 M (buffer 2). The sample for phenyl-Sepharose chromatography was passed, just before application, through a Sephadex G-25 column to equilibrate with 10 mM Tris-maleate (pH 6.5) containing 1 mM EDTA and 1 mM 2-mercaptoethanol (buffer 3) supplemented with 4 M NaCl. Elution from a phenyl-Sepharose column (approx. 10 ml gel) was carried out by a linear gradient of NaCl and nonionic detergent starting from buffer 3 containing 4 M NaCl to the final buffer 3 containing 0.4% Lubrol PX. Each fraction from phenyl-Sepharose was processed immediately through columns of Sephadex G-25 (2 × 8 cm) to re-equilibrate the buffer into buffer 1 containing 0.1 M KCl. The sample of Blue Sepharose was dialyzed against 10 mM Tris-HCl, 0.5 mM 2-mercaptoethanol, 0.5 mM EDTA, 0.04 M KCl and 0.05% Lubrol PX (pH 6.5) (buffer 4). Thiamin-triphosphatase II was eluted by a linear gradient of ATP and pH from 2 mM ATP in buffer 4 (pH 6.5) to 18 mM ATP in buffer 4 (pH 7.4).

Analytical methods and reagents. Molecular weight estimation by Sephadex G-200 chromatography (2.5 × 90 cm) was carried out in buffer 1 containing 0.1 M KCl. Standard proteins used were ribonuclease A 13.7 kDa, chymotrypsinogen A 25 kDa, ovalbumin 43 kDa, and bovine serum albumin 67 kDa. Polyacrylamide gel electrophoresis was carried out at pH 4.5 [11] with 7% acrylamide. The sample for the detection of activity was overlaid on the stacking gel with 15% sucrose and approx. 50 mM 2-mercaptoethylamine [12]. After running the gel at 4°C, the gel was cut into 2 mm lengths, the pieces were ground and extracted with 0.2 M Tris-maleate buffer (pH 6.5) containing 0.5 mM 2-mercaptoethanol and 0.1 mg/ml bovine serum albumin. The recovery was around 10% for thiamin-triphosphatase II and even lower for thiamin-diphosphate kinase activity. In polyacrylamide gel at pH 8.9 (7.5% gel), the activity did not penetrate into the gel toward the anode. SDS-acrylamide gel was run following the method of Laemmli [13] with 15% acrylamide. Protein was measured, depending on the stage of purification, by the Biuret method [14], or the method of Lowry et al. [15], or Bradford [16]. The N-terminal amino acid was determined by a gas phase amino acid sequencer (Applied Biosystems, type 470A). Isoelectric focusing was carried out using Ampholines (pH 7–9) in a flat bed equipment (LKB) for 18 h at 4°C. The sample (450 μmol/g per h) was from the Sephacryl S-300 eluate. After electrofocusing, each fraction was eluted with 0.4 M Tris-maleate buffer (pH 6.5), dialyzed against the same buffer of 0.1 M, and a sample of it was developed by polyacrylamide gel electrophoresis (pH 4.5) at 4°C. The gel was fractionated and extracted as above to measure thiamin-triphosphatase II. Thiamin triphosphate was a generous gift of Dr. M. Yamazaki of Sankyo Co., Tokyo. β,γ-Methylene-ATP (miles Laboratories), phosphocellulose P11 (Whatman), phenyl-Sepharose CL-4B and Blue Sepharose CL-6B (Pharmacia Fine Chemicals), and Lubrol PX (Sigma) were commercially obtained.

Results

Co-purification of thiamin-triphosphatase II and NTPase

Thiamin-triphosphatase II was solubilized from the membrane fraction of *E. coli* W70-23 as described in Materials and Methods and purified further by gel filtration, ion exchange and group specific affinity chromatography (Table I and see below). Throughout these steps, thiamin-triphosphatase II co-purified with Mg^{2+}-independent, acid optimum ATPase activity (activity ratio of NTPase/thiamin-triphosphatase was approx. 1). Substrate specificity among nucleoside phosphates and thiamin phosphates was measured (Table II).

TABLE I

PURIFICATION OF NTPase (THIAMIN-TRIPHOSPHATASE) AND THIAMIN-DIPHOSPHATE KINASE

n.d , not determined.

	Protein (μg) [a]	NTPase (thiamin-triphosphatase)		Thiamin-diphosphate kinase		Thiamin-diphosphate kinase/ ThTPase [b]	NTPase [c]/ ThTPase
		μmol/h [a]	μmol/g per h	μmol/h [a]	μmol/g per h		
Sephacryl eluate	364000	39.9	$0.11 \cdot 10^3$	1 58	4.34	0.040	1.09
Phosphocellulose eluate	18800	16.2	$0.86 \cdot 10^3$	1.08	57 4	0 067	1.00
Sephadex G-100 eluate	280	11.7	$41.8 \cdot 10^3$	0.95	$3.4 \cdot 10^3$	0.081	n d.
Phenyl-Sepharose eluate	25	9.34	$359 \cdot 10^3$	0.91	$35 \cdot 10^3$	0 097	n d
Blue Sepharose eluate	2	7 35	$3\ 7\ 10^6$	0.61	$0.31 \cdot 10^6$	0 83	1.06

[a] Total protein and total activity (measured as thiamin-triphosphatase) for 45 liter culture

[b] Thiamin-triphosphatase II.

[c] Measured as ATPase at pH 6.5 without Mg^{2+}

The results indicate that this phosphatase was a nonspecific NTPase exhibiting more activity towards thiamin triphosphate and ribose-NTPs than the deoxy-form and the diphosphates. These two activities of thiamin-triphosphatase II and ribose-NTPase were found to be catalyzed by a single protein since they were mutually inhibited, as shown in Fig. 1a and b. To determine whether the amount of thiamin diphosphate decreased by the addition of ATP through the mechanism of NDPase activation [3], thiamin monophosphate and free thiamin were measured in all samples of Fig. 1a, but the results were nearly equal to zero. Thus, participation of NDPase was excluded.

TABLE II

SUBSTRATE SPECIFICITY OF THIAMIN-TRIPHOSPHATASE II

Substrate	Activity (%)
Thiamin triphosphate	100 [a]
Thiamin diphosphate	13
Thiamin monophosphate	0
Glucose-6-*P*	0
p-Nitrophenyl phosphate	8
β-γ-Methylene-ATP	0
ATP	103
GTP	102
CTP	105
UTP	80
dATP	89
dGTP	83
dCTP	79
dUTP	85
dTTP	82
ADP	35
GDP	36
CDP	17
UDP	11
AMP	0
dAMP	3
dGMP	2
dCMP	0
dTMP	0

[a] 100% corresponded to 440 μmol/g per h.

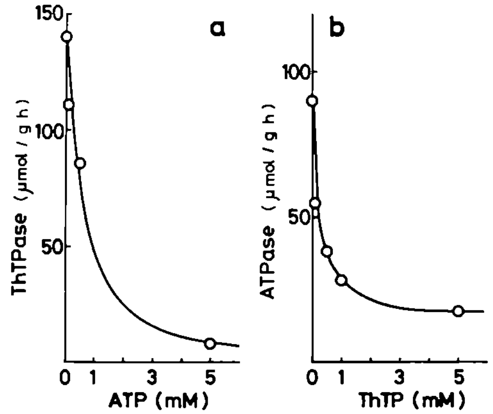

Fig 1 Apparent inhibition of thiamin-triphosphatase II by the two substrates ATP and thiamin triphosphate. (a) Thiamin-triphosphatase II (ThTPase) assay was carried out as in Materials and Methods but at 5-times the scale (250 μl) for approx. 15 h and the thiamin phosphates were analyzed by a gel filtration method [24]. Activity was calculated from the amount of thiamin diphosphate formed (b) NTPase was assayed as in Materials and Methods by developing on a thin layer of MN300G cellulose and the activity was expressed as the amount of $[^{32}P]P_i$ formed.

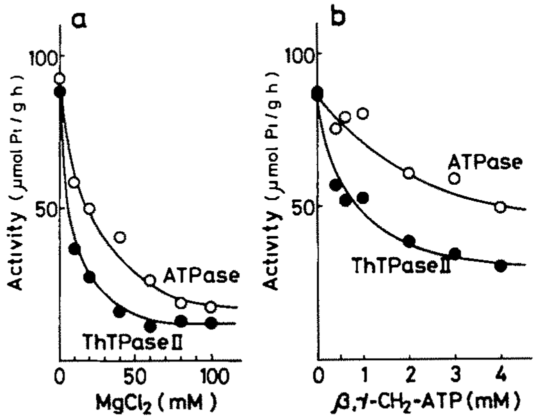

Fig. 2. Parallel inhibition by Mg^{2+} and β,γ-methylene-ATP of thiamin-triphosphatase II and acid NTPase. Thiamin-triphosphatase II (ThTPase) (Sephacryl S-300 eluate) was assayed according to Materials and Methods except for the absence of detergent from the reaction mixture and the addition of Mg^{2+} (a) or β,γ-methylene-ATP (b).

Thiamin-triphosphatase II shows Mg^{2+} inhibition (data not shown). The effect of Mg^{2+} on ribose-NTPase was similar (Fig. 2a). β,γ-Methylene-ATP, an inhibitor of NTPase, inhibited thiamin-triphosphatase II as if it was an analogue of thiamin triphosphate (Fig. 2b). Those results indicated that the activities of thiamin-triphosphatase II and ribose-NTPase were expressed by the same enzyme. Further, both activities were recovered at exactly the same position on polyacrylamide gel electrophoresis (data not shown). Hence, we concluded that thiamin-triphosphatase II was a kind of nonspecific ribose-NTPase. Considering the high activity shown on thiamin triphosphate and the rareness of an enzyme active on both nucleoside phosphates and thiamin phosphates, we called this enzyme thiamin-triphosphatase II. This enzyme showed differences from the known NTPases (EC 3.6.1.15) as described below.

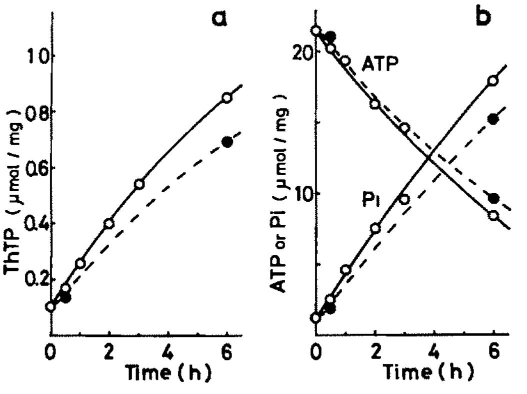

Fig. 3. Thiamin-diphosphate kinase activity detected in a thiamin-triphosphatase II preparation. A thiamin-triphosphatase II preparation (1.9 mmol/g per h) was used for the detection of thiamin-diphosphate kinase activity. The assay mixture contained 2.5 mM $MgCl_2$ in the case of hatched circle data. (a) Time-dependent accumulation of thiamin [^{32}P]triphosphate. (b) The same sample as in (a) was analyzed for the remaining [^{32}P]ATP and [^{32}P]P_i released. ThTP, thiamin triphosphate.

Thiamin diphosphate kinase activity of thiamin-triphosphatase II

When *E. coli* was loaded with thiamin diphosphate, cellular thiamin triphosphate increased (data not shown). One of these thiamin triphosphate synthesizing activities (ATP : thiamin-diphosphate phosphotransferase, EC 2.7.4.15) was assigned to the same fraction as thiamin-triphosphatase II when surveyed in a preliminary experiment. This reaction proceeded linearly for more than 3 h (Fig. 3a), with the simultaneous hydrolysis of approx. 20-times the number of moles of ATP (Fig. 3b) (see Table I for purified preparations; the ratio thiamin-diphosphate kinase/ thiamin-triphosphatase II). The enzyme used (Fig. 3) was free from known Mg^{2+}-dependent, alkaline optimum NDP kinase (EC 2.7.4.6) (see Fig. 5). The substrate specificity of thiamin-diphosphate kinase activity was relatively broad, exhibiting comparable activities on some other nucleoside diphosphates (Table III). A parallel effect on pH on thiamin-diphosphate kinase and on the P_i liberation from [γ-^{32}P]ATP (observed with the kinase reaction) was seen (data not shown). Further, the two activities were recovered from exactly the same position on polyacrylamide gel electrophoresis (data not shown).

Co-purification of thiamin triphosphatase II and thiamin-diphosphate kinase

To confirm that thiamin-triphosphatase II expresses a thiamin-diphosphate kinase activity, we purified thiamin-triphosphatase II from *E. coli* W70-23. The solubilized thiamin-triphosphatase II was developed on a Sephacryl S-300 column (Fig. 4). The profile showed that the major fraction of Mg^{2+}-ATPase (EC 3.6.1.3) eluted differently from

TABLE III

SOME CHARACTERISTICS OF THE TWO ACTIVITIES OF THIAMIN-TRIPHOSPHATASE II

Substrate	Thiamin-diphosphate kinase activity (%)		Additives	Thiamin-triphosphatase II activity (%)
	expt. 1	expt. 2		
Thiamin diphosphate	100 [a]	100 [a]	control	100 [b]
Thiamin monophosphate	17	0	1 mM thioglycollic acid	99
dTDP	107	87	1 mM dithiothreitol	103
CDP	49	68	1 mM EDTA	101
UDP	38	60	1 mM metal mixture (Cu, Zn, Mn, Ca)	72
Thiamin diphosphate + 10 mM EDTA	83		5 mM pyrithiamin	84
Thiamin diphosphate + 10 mM dithiothreitol	85			

[a] 100% corresponded to 60 μmol/g per h

[b] 100% corresponded to 2.5 mmol/g per h.

thiamin-triphosphatase II, and that thiamin-diphosphate kinase paralleled thiamin-triphosphatase II. Active fractions were pooled and applied on a phosphocellulose column. Thiamin-diphosphate kinase activity showed affinity for the phosphocellulose, whereas Mg^{2+}-dependent, alkaline optimum, NDP kinase (EC 2.7.4.6) did not bind at pH 6.5 and eluted in the flow-through fractions (Fig. 5). This activity (flow-through fractions) was not active on thiamin diphosphate at pH 6.5 (Fig. 5) or at pH 8.0 with Mg^{2+} added (data not shown). Thiamin-triphosphatase II was eluted in two peaks by KCl concentrations higher than 0.5 M, accompanied by thiamin-diphosphate kinase activity. The amount of former peak varied from experiment to experiment and was usually minor. The latter peak was pooled and applied on Sephadex G-100 column. Thiamin-triphosphatase II was eluted at the fractions which corresponded

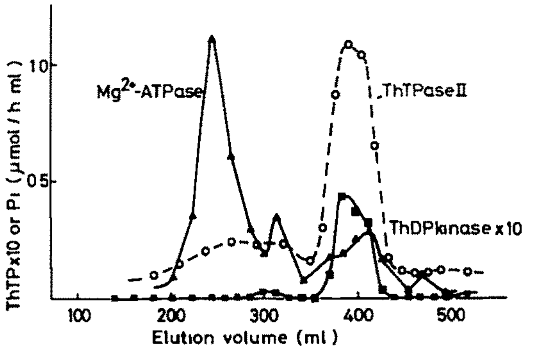

Fig. 4 Gel filtration chromatography of thiamin-triphosphatase II (ThTPase II) A membrane fraction (60.8 g protein) of *E. coli* W70-23 (45 l culture) was solubilized giving 1.61 g of solubilized protein and applied on a Sephacryl S-300 superfine (2.5×95 cm) column and developed with 'buffer 1' containing 0.1 M KCl. Thiamin-triphosphatase II (ThTPase II) activity was assayed using ATP as substrate at pH 6.5 Mg^{2+}-ATPase was assayed at pH approx 8.0 using [^{32}P]ATP as the substrate and the activity was expressed by the amount of [^{32}P]ATP degraded. Thiamin-diphosphate (ThDP) kinase was assayed as in Materials and Methods. ThTP, thiamin triphosphate.

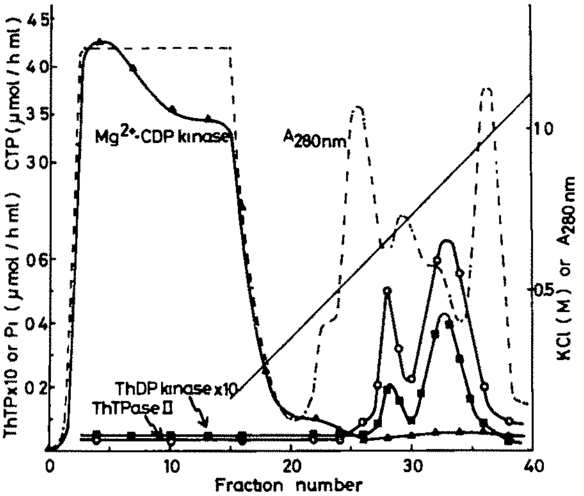

Fig. 5. Separation of thiamin-diphosphate (ThDP) kinase from Mg^{2+}-NDP kinase by phosphocellulose chromatography. The column (22 ml wet volume) was eluated with a linear gradient of KCl Eluate was fractionated into 10 g in fractions Nos. 1–15, or into 4.5 g in subsequent fractions ThTP, thiamin triphosphate

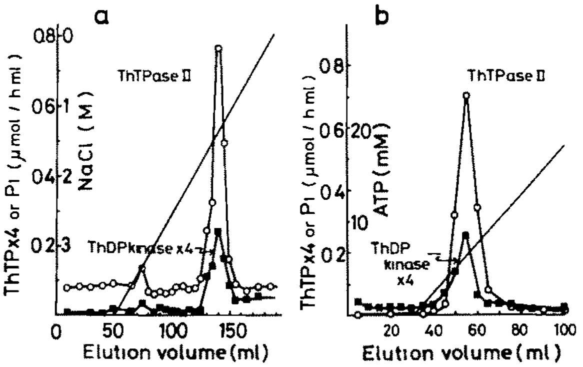

Fig 6. Co-purification of thiamin-triphosphatase II with thiamin-diphosphate (ThDP) kinase and acidic NTPase. (a) Phenyl-Sepharose CL-4B column chromatography. Elution was accomplished by a linear gradient of NaCl and Lubrol PX, but only the NaCl is plotted Each eluate fraction was applied on Sephadex G-25 column to re-equilibrate the buffer into 'buffer 1' containing 0.1 M KCl. Enzyme activities were assayed for this eluate Thiamin-triphosphatase (ThTPase) II activity was assayed with ATP as the substrate at pH 6.5. (b) Blue Sepharose CL-6B column chromatography. To 2.5 ml wet volume of Blue Sepharose CL-6B, the sample eluted from phenyl-Sepharose was applied after dialysis against 'buffer 4' The column was washed with 'buffer 4 containing 2 mM ATP and eluted with a gradient of ATP and pH (only ATP concentration is shown) with a flow rate of 2 ml/h. ThTP, thiamin triphosphate; ThDP, thiamin diphosphate.

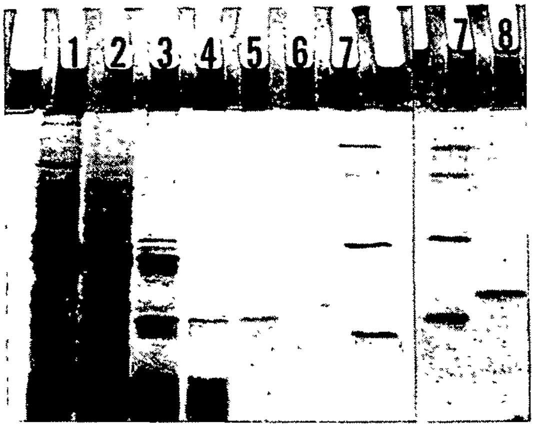

Fig. 7. SDS-polyacrylamide gel electrophoresis analysis of thiamin-triphosphatase II in each step of purification. Samples were analyzed with 15% gel and detected by silver staining 1, $NaClO_4$-solubilized sample; 2, Sephacryl S-300 eluate; 3, phosphocellulose eluate; 4, Sephadex G-100 eluate; 5, phenyl-Sepharose eluate; 6 and 8, Blue Sepharose eluate; 7, molecular weight standards (67 kDa, 43 kDa, 25 kDa and 13 7 kDa; 100 ng each was applied).

to a molecular weight of approx. 16 000 (data not shown, see below for the molecular weight). The fractions containing activity were concentrated with a membrane filter (Diafilter G05T), and the buffer was changed to a detergent-free high-salt one and applied on a column of phenyl-Sepharose. Thiamin-diphosphate kinase activity and thiamin-triphosphatase II were eluted at approx. 1.5 M NaCl plus 0.25% Lubrol PX (Fig. 6a). The pooled fractions containing the activity exhibited contaminating bands on the SDS-polyacrylamide gel electrophoresis (Fig. 7), and were purified further by Blue Sepharose CL-6B (Fig. 6b). In contrast to the known examples, thiamin-triphosphatase II was adsorbed firmly at acidic pH, and eluted at alkaline pH or when ATP was added. A combined linear gradient of 5.0–6.0 mM ATP and pH of 5.3–7.6 gave a better purification. Each step was analyzed with SDS-polyacrylamide gel electrophoresis (Fig. 7), as summarized in Table I.

Characteristics of thiamin-triphosphatase II

In the assay of thiamin-diphosphate kinase, approx. 10-times the number of moles of ATP was hydrolyzed in the purified enzyme (Table I, thiamin-diphosphate kinase/ thiamin-triphosphatase II). A saturating concentration of thiamin diphosphate was used in these assays (K_m for thiamin diphosphate was 56 mM and for ATP was 10 mM, data not shown). The optimum pH of thiamin-diphosphate kinase activity was approx. 5.3 (data not shown). The effect of temperature was studied and the optimum was approx. 50°C (data not shown). The effect of Mg^{2+} was inhibitory and a curve very similar to Fig. 2a was obtained (data not shown).

The molecular weight of thiamin-triphosphatase II was estimated by SDS-acrylamide gel electrophoresis (Fig. 7), giving a value of 15 900, and also by gel filtration chromatography with Sephadex G-200, with the value of 15 100. Thus, thiamin-triphosphatase II was shown to be a single polypeptide of molecular weight approx. 16 000. Using an eluate of Blue Sepharose, the N-terminal amino acid was determined to be glutamic acid. In experiments to determine the isoelectric point of thiamin-triphosphatase II, activity peaks were found at pH 8.54 (main peak), 8.30, 8.0, 7.6, and 7.00 (graph not shown).

Discussion

A bacterial thiamin-triphosphatase of *E. coli* was evidenced for the first time in a purified form. Purified enzyme was found to be accompanied by acid NTPase activity. Another example of an enzyme which shows reactivity on both thiamin phosphate and nucleoside phosphate is thiamin-diphosphatase of bovine liver and rat tissue [3,4]. In rat NDPase, two types of enzymes with clear differences in the pattern of isoelectric focusing have been observed [4]. Thiamin-triphosphatase II in this paper showed the typical pattern of a multi-isoelectric point enzyme and resembled more the brain-type thiamin diphosphatase of rat. These enzymes also resembled each other in that both thiamin phosphate and nucleoside phosphate could act as substrate at neutral pH.

We concluded that thiamin-triphosphatase II showed the activity of a nonspecific NTPase on the basis of the following observations. (i) The two activities were co-purified throughout the steps. (ii) Both activities were detected at the same position on acrylamide gel electrophoresis. (iii) The two activities were inhibited similarly by Mg^{2+} and β,γ-methylene-ATP. (iv) Thiamin-triphosphatase II was inhibited by ATP, and the Mg^{2+}-independent ATPase activity was inhibited by thiamin triphosphate. (v) Ribonucleoside triphosphates other than ATP were hydrolyzed at nearly the same rate. As the substrate, deoxyNTPs were 80–90% active, nucleoside diphosphates were approx. 30% active, and monophosphates were almost inactive. However, NTPase (EC 3.6.1.15) already reported [17–21] are all clearly different from thiamin-triphosphatase II. Their molecular sizes are between 100 kDa [20] and 260 kDa [17], and some of them [19] require dithiol for activation. Thus, thiamin-triphosphatase II is a novel NTPase of *E. coli.*

On the other hand, the well known Mg^{2+}-dependent, alkaline optimum NDP kinase (EC 2.7.4.6) showed no activity on thiamin diphosphate (Fig. 5). Enzymes for nucleoside metabolism seem to be strictly differentiated from thiamin metabolism in vivo, and there should be some particular function(s) for those enzymes which can act on both types of substrates. Besides the activity of thiamin-triphosphatase II, the purified enzyme catalyzed the reverse directed reaction. However, the kinetic parameters and characteristics of the reverse reaction (K_m for thiamin diphosphate of 56 mM, for ATP of 10 mM, optimum pH of 5.3, hydrolysis of approx. 10-times the number of moles of ATP) indicated that the thiamin-triphosphatase II activity was relatively favoured in the physiological state of the bacterial cell. Incidentally, the alkaline optimum NDP kinase of *E. coli* detected in Fig. 5 were recovered in the fractions which corresponded to an approximate molecular size of 16 kDa (Fig. 4). Thus *E. coli* Mg^{2+}-NDP kinase did not agree in size with the reported NDP kinase of *Salmonella typhimurium* (85 kDa) [22] or of *Bacillus subtilis* (100 kDa) [23].

On the basis of the data obtained, we deduce that some other enzyme than thiamin-triphosphatase II is responsible for the cellular thiamin triphosphate synthesis, and thiamin-triphosphatase I is now under investigation.

Acknowledgements

The authors express their gratitude to Dr. M. Yamazaki of Sankyo Co., Tokyo for his generous gift of thiamin triphosphate.

References

1 Barchi, R.L and Braun, P E (1972) J. Biol. Chem. 247, 7668–7673

2 Barchi, R.L (1976) in Thiamine (Gubler, C.J., Fujiwara, M and Dreyfus, P.M., eds.), pp. 195–225, John Wiley & Sons, New York

3 Yamazaki, M. and Hayaishi, O. (1968) J Biol Chem. 243, 2934–2942

4 Sano, S., Matsuda, Y , Miyamoto, S. and Nakagawa, H (1984) Biochem. Biophys. Res. Commun. 118, 292–298

5 FossiFanelli, A , Ipata, P.L. and Fasella, P (1961) Biochem Biophys. Res. Commun. 4, 23–27

6 Davis, B D. and Mingioli, E S (1950) J Bacteriol 60, 17–23

7 Concustell, E., Cortes, M., Ferragut, A and Gener, J (1977) Clin. Chim Acta 81, 267–272

8 Baginski, E.S , Foa, P.P and Zak, B. (1967) Clin Chim Acta 15, 155–158

9 Randerath, K (1962) Biochem Biophys Res Commun 6, 452–457

10 Ingraham, J. and Ginther, C.L. (1978) Methods Enzymol 51, 371–375

11 Reisfeld, R A., Lewis, U J. and Williams, D E (1962) Nature 195, 281–283

12 Brewer, J M. (1967) Science 156, 256–257
13 Laemmli, U.K. (1970) Nature 277, 680–685
14 Gornall, A.G., Bordawill, C.J. and Maxima, M.D (1949) J Biol. Chem. 177, 751–766
15 Lowry, O H., Rosebrough, N.J., Farr, A L and Randall, R J. (1951) J. Biol Chem. 193, 265–275
16 Bradford, M.M. (1976) Anal. Biochem. 72, 248–254
17 Lanka, E., Mikolajczyk, M., Schlicht, M and Schuster, H. (1978) J. Biol. Chem. 253, 4746–4753
18 Raacke, I.D. and Fiala, J. (1964) Proc. Natl. Acad. Sci. USA 51, 323–329
19 Asai, T., O'Sullivan, W J and Tatibana, M (1983) J. Biol. Chem 258, 6816–6822
20 Brightwell, R. and Tappel, A.L. (1968) Arch Biochem Biophys. 124, 333–343
21 Lewis, M. and Weissman, S. (1965) Arch. Biochem. Biophys 109, 490–498
22 Ginther, C.L and Ingraham, J L. (1974) J. Biol. Chem. 249, 3406–3411
23 Sedmak, J and Ramaley, R (1971) J. Biol. Chem 246, 5365–5372
24 Nishimune, T. and Hayashi, R (1980) Experientia 36, 916–918

Biochimica et Biophysica Acta 923 (1987) 83–87
Elsevier

BBA 22462

The binding of fluorescent 4,6,8(14)-triene-3-one steroids to cyclodextrins as a model for steroid–protein interactions *

M.A. Kempfle [a], R.F. Müller [a], R. Palluk [a] and H.A. Winkler [b]

[a] *Institute for Physiological Chemistry, University of Bonn, Nussallee 11, D-5300 Bonn, and* [b] *Max-Planck-Institute for Biophysical Chemistry Göttingen, Am Fassberg, D-3400 Göttingen-Nikolausberg (F.R.G.)*

(Received 28 July 1986)

Key words: Steroid binding; Cyclodextrin; Protein-steroid interaction; Fluorescence

The 4,6,8(14)-triene-3-one steroids, highly fluorescent in aqueous solutions, lose their fluorescence power when binding occurs to hydrophobic regions of other molecules, such as the hydrophobic cavity in the ring system of cyclodextrins. The fluorescence intensity decreases almost completely when β- and γ-cyclodextrins are present in the solution. Scatchard plots derived from fluorescence titrations show that one or two molecules of steroid bind to one cyclodextrin molecule with $K_{D,F}$-values of about 10^{-4}–10^{-5} mol/liter. Temperature-jump experiments show a single relaxation process, with rate constants for the decay of the β-cyclodextrin-steroid complexes of about 10^4–10^5 per s. For α- and γ-cyclodextrins such relaxation processes are not observed.

Introduction

The 4,6,8(14)-triene-3-one steroids – highly fluorescent in aqueous solutions and showing practically no fluorescence in aprotic solvents – differ from the naturally occurring androgens and gestagens – generally not fluorescent in both aqueous and non-aqueous solutions – by only two or three additional conjugated double bonds in the A-, B- and C-ring of the steroid skeleton (Fig. 1). When these double bonds are introduced into the steroid the energy of the fluorescent π-π^*-state is so greatly reduced that this state is shifted near to the non-fluorescent n-π^*-state resulting in a system with two states of approximately the same energy. Henceforward only small perturbations (such as interactions with solvents or micelle formation) will determine whether this system shows fluorescence (π-π^*-state lowest) or not (n-π^*-state lowest) [1]. In addition, the fluorescence intensity

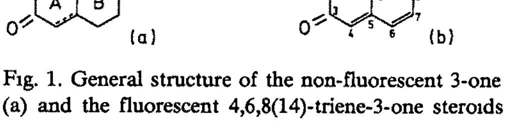

Fig. 1. General structure of the non-fluorescent 3-one steroids (a) and the fluorescent 4,6,8(14)-triene-3-one steroids investigated here (b). (a) Testosterone: R_1 = -OH, R_2 = -H; 17α-hydroxyprogesterone: R_1 = -CO-CH$_3$, R_2 = –OH. (b) Bisdehydrotestosterone: R_1 = -OH, R_2 = -H; bisdehydrohydroxyprogesterone: R_1 = -CO-CH$_3$, R_2 = -OH.

---

* Dedicated to Prof Dr M. Eigen on the occasion of his 60th birthday.

Abbreviations. 6,8(14)-bisdehydrotestosterone, 17β-hydroxy-4,6,8(14)-androstatriene-3-one; testosterone, 17β-hydroxy-4-androstene-3-one; 6,8(14)-bisdehydro-17α-hydroxyprogesterone, 17α-hydroxy-4,6,8(14)-pregnatriene-3,20-dione; 17α-hydroxyprogesterone, 17α-hydroxy-4-pregnene-3,20-dione; R 1881, 17α-methyl-17β-hydroxy-4,9,11-estratriene-3-one; $K_{D,F}$, dissociation constant of the cyclodextrin complex with fluorescent steroids.

Correspondence: Dr. M.A. Kempfle, Institute for Physiological Chemistry, University of Bonn, Nussallee 11, D-5300 Bonn, F.R.G.

0304-4165/87/$03.50 © 1987 Elsevier Science Publishers B.V. (Biomedical Division)

disappears almost completely when the fluorescent steroids bind to proteins, thus making these steroids useful probes for steroid–protein interactions. This quenching is explained by a decrease in the energy of the n-π^*-state compared to the nearby-situated π-π^*-state due to hydrophobic interactions, which are known to occur between proteins and steroids [2].

Since steroid-binding proteins are not always available in large quantities, we try to study the interactions of steroids with molecules having hydrophobic regions too. The cyclodextrins, due to the hydrophobic cavity in their ring system [3], prove to be such a model; thus we can expect that any interaction with the steroid will lead to measurable changes in the fluorescence intensity. These changes are in fact observed and enable us to study the binding process very easily by simple titration, or its kinetics by relaxation techniques.

Part of this paper was presented at the "First International Symposium on Binding Proteins: Steroid Hormones" in Lyon, France, April 28th–30th, 1986.

Materials and Methods

The fluorescent 4,6,8(14)-triene-3-one steroids were generous gifts from Schering and Searle, and the R1881 (characterized as a 4,9,11-triene-3-one) from Roussel-Uclaf. A single peak was observed with all substances after purification with repeated 'reversed phase' HPLC.

The cyclodextrins (α-, β- and γ-cyclodextrin, consisting of 6, 7 and 8 cyclically arranged glucose molecules) were purchased from Sigma and used without purification. All solutions were deoxygenated by flushing for 20 min with dry nitrogen and then degassed by a rotary vacuum pump.

Fluorescence measurements were performed with a Perkin-Elmer MPF 4 spectrofluorometer at 20.0°C. The excitation wavelength was 365 nm; the fluorescence emission spectra were recorded between 400 nm and 600 nm and the maximum value at 475 nm was taken as a measure of the fluorescence intensity.

Temperature-jump relaxation studies were performed with a fluorescence temperature-jump apparatus described previously [4]. The excitation wavelength was 365 nm and the emitted light was measured at right angles by two photomultipliers after passage through Kodak KV 418 cutoff filters to eliminate light of wavelengths below 400 nm. The temperature before the perturbation was 16.2°C and a temperature jump of 3.8°C brought the final temperature to 20.0°C. The heating time was less than 10 μs.

The recorded signal was primarily stored in a transient recorder (Datalab 905) and then transferred to a Univac 1108 for further processing. The relaxation times and their amplitudes were analyzed with the 'Discrete Program' of Provencher [5]. The reciprocal relaxation times given in Fig. 6 are mean values of 4 to 10 temperature jumps. Time intervals between two temperature jumps were 5 min, thus allowing a proper temperature equilibration.

Results and Discussion

(1)α-Cyclodextrin

This cyclodextrin exhibits no interaction with

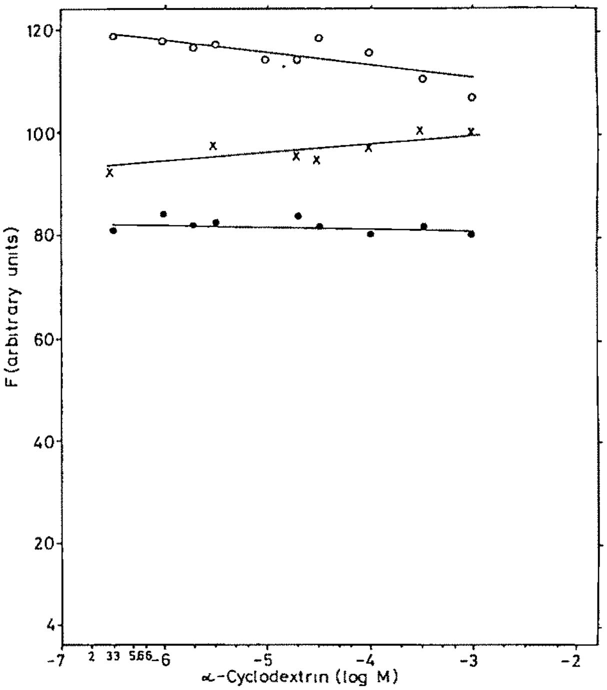

Fig 2. Fluorescence intensity of the triene-3-one steroids as a function of the α-cyclodextrin concentration in a logarithmic scale. $T = 20.0$°C. ● = 6,8(14)-bisdehydrotestosterone, 50 ng/ml; x = 6,8(14)-bisdehydro-17α-hydroxyprogesterone, 50 ng/ml; ○ = R 1881, 1 μg/ml.

any one of the steroids investigated here. Fig. 2 shows no significant fluorescence change over the concentration range of α-cyclodextrin taken here. Obviously the diameter of the α-cyclodextrin cavity (0.52 nm) is too small to allow binding of the steroid into it. Stopped-flow and temperature-jump experiments showed no measurable effects.

(2) β-Cyclodextrin

Binding studies. Titration of different steroid solutions with β-cyclodextrin leads to a drastic decrease in fluorescence intensity which becomes almost complete at high β-cyclodextrin concentrations (Fig. 3). Thus we can assume that the steroid is bound into the cavity of the β-cyclodextrin molecule.

Titration of a β-cyclodextrin solution with different steroid concentrations demonstrates the binding process too, as there is a considerable lag-phase in the intensity of the steroid fluorescence with cyclodextrin (Fig. 4a), whereas the fluorescence intensity of the steroid alone increases linearly with steroid concentration (Fig. 4b). From these two curves we can calculate the amount of bound steroid very easily (c_{bound} in Fig. 4). These results are shown in Fig. 5a. Scatchard plots (Fig. 5b) show that 6,8(14)bisdehydrotestosterone has the highest affinity to

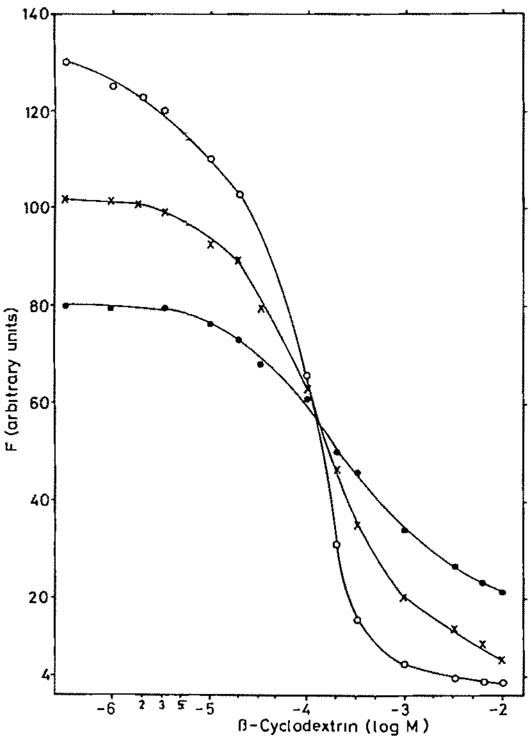

Fig. 3. Fluorescence intensity of the triene-3-one steroids as a function of β-cyclodextrin concentration (in mol/liter) in a logarithmic scale For symbols and concentrations see Fig 2.

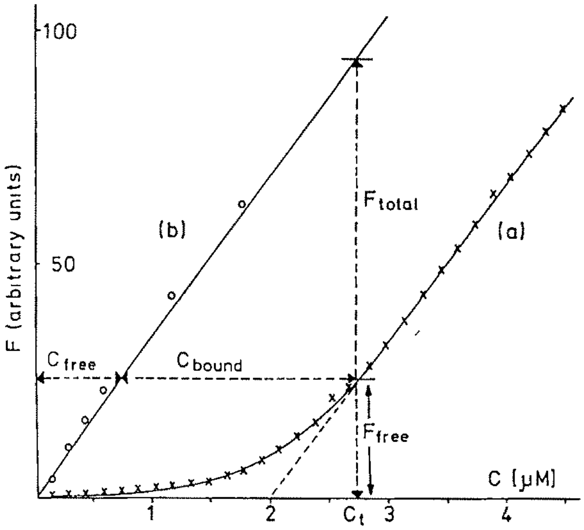

Fig 4. Titration curve (a) of the cyclodextrin-binding sites (β-cyclodextrin = $5 \cdot 10^{-4}$ M) with 6,8(14)-bisdehydrotestosterone (×); (b) fluorescence signal of 6,8(14)-bisdehydrotestosterone in H_2O (○) From the difference of the fluorescence intensity between (a) and (b) we calculate c_{free} and c_{bound} as shown on the abscissa.

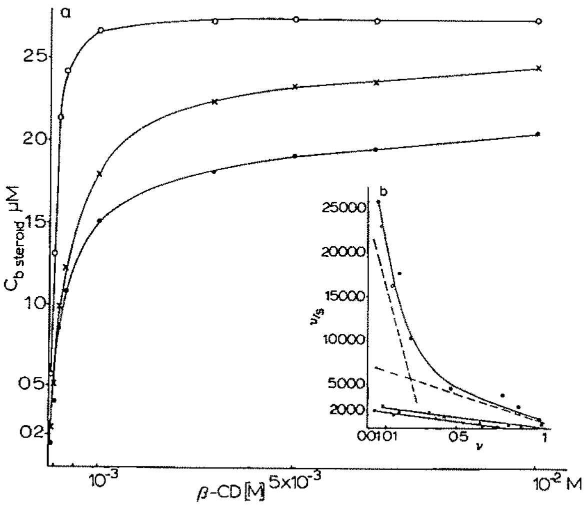

Fig. 5. (a) Binding of the triene-3-one steroids to β-cyclodextrin as a function of β-cyclodextrin concentration. For symbols see Fig. 2. (b) Corresponding Scatchard plot: ν = bound, S = free β-cyclodextrin. The $K_{D,F}$ values are given in Table I.

β-cyclodextrin. From the biphasic behaviour of this plot we have to assume some negative cooperativity for this molecule, and the data result in two dissociation constants. This is consistent with the data of Lach and Pauli [6] who proposed a 2:1 stoichiometry for testosterone binding to the β-cyclodextrin molecule. Obviously the binding of the second 6,8(14)-bisdehydrotestosterone molecule is somewhat hindered if the first one is already bound into the cavity. For the other steroid molecules investigated here we have to assume a 1:1 binding.

Table I shows the dissocation constants for some steroid-β-cyclodextrin complexes, presenting evidence that the affinity becomes somewhat lowered with an increasing side chain at the C-17 position.

Displacement studies. Titration of the steroid-cyclodextrin complex with a non-fluorescent steroid (i.e., testosterone) shows an increase in fluorescence intensity caused by the displaced steroid molecules.

From this type of experiment we are able to calculate the dissociation constants for non-fluorescent steroid-cyclodextrin complexes, as there is a simple relation between the dissociation constant $K_{D,F}$ of the fluorescent steroid-cyclodextrin complex and the dissociation constant $K_{D,NF}$ of the non-fluorescent steroid-cyclodextrin complex: $K_{D,NF} = K \times K_{D,F}$, where K is the so-called 'displacement constant'. K is determined by titration of the fluorescent steroid-cyclodextrin complex with the non-fluorescent steroid (or any other compound) [7].

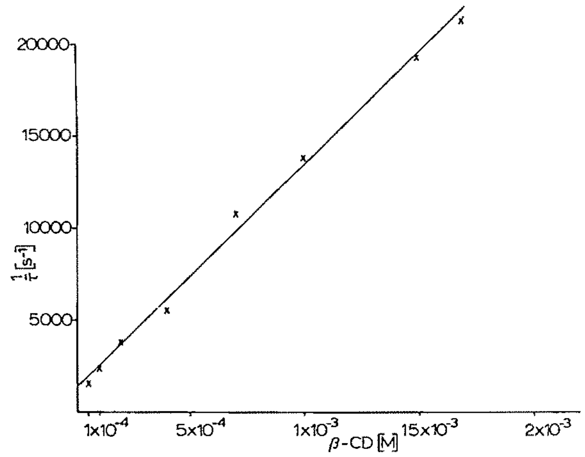

Fig. 6. Reciprocal relaxation times for the binding process of 6,8(14)-bisdehydrotestosterone to cyclodextrin as a function of β-cyclodextrin (β-CD) concentration. $T = 20\ 0\,°C$ 1 μl/ml = 3.4 μM 6,8(14)-bisdehydrotestosterone; the results are given in the text.

Kinetics of steroid binding to β-cyclodextrin. The remarkable fluorescence properties of the 4,6,8(14)-triene-3-one steroids allow the performance of kinetic studies upon their binding to macromolecules (i.e., cyclodextrin) which are not performable with non-fluorescent or radioactively labelled compounds. Fig. 6 shows the results of such kinetic experiments with β-cyclodextrin and 6,8(14)-bisdehydrotestosterone in the temperature-jump apparatus. From the concentration dependence of the reciprocal relaxation times we can calculate the rate constants for the dissociation process: $k_{off} = 1400$ sec^{-1}, and for the association process: $k_{on} = 12.3 \cdot 10^6$ liter $\cdot$ mol$^{-1} \cdot$ s^{-1}. The value $K_{D,F} = k_{off}/k_{on}$ is in good agreement with the results of the fluorescence titrations given in the table. One has to emphasize that the two dissociation constants from the table are so close together that they apparently cannot be resolved by the temperature-jump techniques; thus $K_{D,F}$

TABLE I

DISSOCIATION CONSTANTS FOR SOME STEROID-CYCLODEXTRIN COMPLEXES

$T = 20.0\,°C$. BDT, bisdehydrotestosterone; BD17αOHP, bisdehydro-17α-hydroxyprogesterone

Cyclodextrin	Diameter of the cavity (nm) [3]	Dissociation constant $K_{D,F}$ (mol/l)		
		6,8(14)-BDT	6,8(14)-BD17αOHP	R1881
α	0.52	no interactions observed		
β	0.62	$0.7 \cdot 10^{-4}$ $1.5 \cdot 10^{-4}$	$4 \cdot 10^{-4}$	$4.4 \cdot 10^{-4}$
γ	0 7	$1.5 \cdot 10^{-4}$	$2 \cdot 10^{-4}$	$2.6 \cdot 10^{-4}$

obtained by the kinetic method represents the mean of these two dissociation constants.

γ-*Cyclodextrin*

Table I demonstrates that the interactions of γ-cyclodextrin with different steroids are qualitatively the same (Fig. 7a) as in the case of the β-cyclodextrin (Fig. 5a) but with somewhat increased affinities. Scatchard plots (Fig. 7b) show straight lines, indicating only a simple type of interaction. The rate constants for the binding process, however, are apparently different from those of the β-cyclodextrin, as no detectable relaxation process appeared within the time limits of our temperature-jump apparatus. Therefore we have to assume that the greater cavity of the γ-cyclodextrin (diameter 0.7 nm) compared to the β-cyclodextrin cavity results in an increase of the rate constants, so that we are not able to observe any relaxation process.

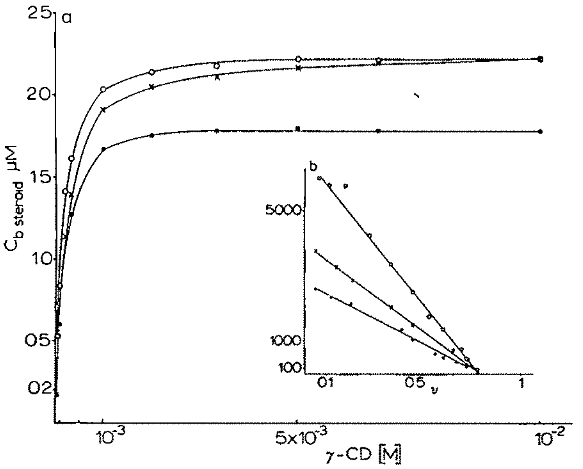

Fig 7. (a) Binding of the triene-3-one steroids to γ-cyclodextrin (γ-CD) as a function of γ-cyclodextrin concentration. (b) Corresponding Scatchard plot. For symbols see Figs. 2 and 5. The $K_{D,F}$ values are given in Table I.

The results presented here clearly state that the fluorescent 4,6,8(14)-triene-3-one steroids together with the cyclodextrins are powerful tools for simulating steroid–macromolecule interactions. As reported recently [8], their catalytic behaviour differs from that of the naturally occurring steroids only by a factor of two. Furthermore, the steroid-binding proteins exhibit almost the same binding properties with the fluorescent steroids as with non-fluorescent (relative affinity of the 6,8(14)-bisdehydrotestosterone = 0.8 related to testosterone with sex hormone binding globulin [9]), but due to the lack of large amounts of these proteins we have to take model substances which qualitatively simulate the binding properties of these proteins. The results of the experiments described above demonstrate that the cyclodextrins can serve as such model substances.

Acknowledgement

We thank Mrs. H. Haberstroh for her excellent and skilful technical assistance.

References

1 Kempfle, M., Müller, R., Palluk, R. and Zachariasse, K. (1983) Hoppe-Seyler's Z. Physiol Chem. 364, 1151–1152
2 Westphal, U. (1978) Hoppe-Seyler's Z Physiol. Chem. 359, 431–447
3 Sänger, W. (1980) Angew. Chem. 92, 343–361
4 Rigler, R, Rabl, C.R. and Jovin, T.M (1974) Rev Sci Instrum. 45, 580–588
5 Provencher, S W. (1976) Biophys J. 16, 37–41
6 Lach, J.L and Pauli, W A. (1966) J. Pharm. Sci. 55, 32–38
7 Kempfle, M, Müller, R., Sonnenberg, A. and Winkler, H (1977) Z. Anal Chem. 285, 237–243
8 Kempfle, M., Breuer, H., Müller, R. and Palluk, R (1985) Acta Endocrinol Suppl. 108, 112–113
9 Müller, R., Palluk, R. and Kempfle, M. (1985) Stud. Biophys. 109, 77–86

Biochimica et Biophysica Acta 923 (1987) 88–97
Elsevier

BBA 22457

Subunits and chromophores of a type I phycoerythrin from a *Chroomonas* sp. (Cryptophyceae)

Carol D. Martin and Roger G. Hiller

School of Biological Sciences, Macquarie University, North Ryde, 2113, N.S.W (Australia)

(Received 9 April 1986)

Key words: Phycoerythrin; Phycoerythrobilin, Cryptoviolin; Fluorescence; Polypeptide; (*Chroomonas* sp. CS24)

Phycoerythrin from a *Chroomonas* sp. CS24 has been characterised with respect to relative molecular mass, subunit composition and spectral properties (absorbance and fluorescence). The native protein has a typical type I absorbance spectrum, except for a shoulder at 644 nm. The proposed structure for the phycoerythrin is $\alpha_2\beta_2$ with a relative molecular mass of 63.5 kDa. The β subunit of relative molecular mass 20.5 kDa contains the chromophore phycoerythrobilin. There are four α subunits which differ in charge. Two of these are blue with absorbance and fluorescence maxima in 8 M urea (pH 5.1) that are similar to those of phycocyanin, suggesting the presence of a phycocyanobilin-like chromophore. These two subunits differ in relative molecular mass (11 and 12 kDa). The remaining two α subunits are purple at pH 5.1 in 8 M urea and possess a chromophore similar to the unidentified chromophore in the α subunit of phycoerythrocyanin (PXB). These subunits also differ in relative molecular mass (11 and 12 kDa). Titration of the α subunits with HCl and NaOH results in a reversible change between the phycocyanobilin-like and PXB-like forms. It is proposed that a single novel chromophore is present on the α subunits that mimics phycocyanobilin and PXB according to its environment and is probably identical with cryptoviolin (McColl, R., Guard-Friar, D. and Csatorday, K. (1983) Arch. Microbiol. 135, 194–198).

Introduction

In the blue-green and red algae, a pathway of energy transfer has been elucidated within the phycobilisome from phycoerythrin to chlorophyll *a* via phycocyanin and allophycocyanin with almost 100% efficiency [1]. Proposed models of phycobilisome structure accommodate such an energy transfer pathway [2,3]. The Cryptophyceae also have, as their major accessory light harvesting pigments, phycoerythrin and phycocyanin, but the intermediates in energy transfer to chlorophyll *a* are unknown. It is thought that energy is transferred directly to chlorophyll *a* from phycoerythrin or phycocyanin or via chlorophyll c_2 [4]. Lichtlé et al. [5] propose that *Cryptomonas rufescens* contains a phycoerythrin complex located within the intrathylakoid lumen that transfers light energy directly to chlorophyll *a* in Photosystem II, without mediation by chlorophyll c_2. It is widely accepted that in any one cryptophyte species either phycoerythrin or phycocyanin is present [6], and allophycocyanin absent. Detectable amounts of phycocyanin have, however, been reported in several species of cryptophytes, grown at low light intensities, which contain phycoerythrin as their

---

Abbreviations: PXB, unidentified chromophore in the α subunit of phycoerythrocyanin; SDS, sodium dodecyl sulphate; TEMED, N,N,N',N'-tetraethylmethylenediamine; Tris, tris-(hydroxymethyl)aminomethane.

Correspondence: Dr. R.G. Hiller, School of Biological Sciences, Macquarie University, North Ryde, 2113, N.S.W, Australia.

0304-4165/87/$03.50 © 1987 Elsevier Science Publishers B.V. (Biomedical Division)

major accessory light harvesting pigment [7]. In view of this we reinvestigated the phycobilins of *Chroomonas* CS24, which also contains a type I phycoerythrin, and for which data are already available on the chlorophyll protein complexes [8].

Cryptophyte phycoerythrins have been classified into three groups according to their absorbance maxima. Type I has an absorbance maximum near 545 nm, type II at about 555 nm and type III at about 565–568 nm [9]. They are composed of two polypeptide chains (α and β) of unequal size. Covalently bound to these chains are open tetrapyrrole prosthetic groups (chromophores). The number and type of chromophore present determines the absorbance properties of the protein [4]. Phycoerythrobilin is reportedly the only chromophore found in cryptophyte phycoerythrins [4,10]. However, MacColl et al. [11] have described an α subunit of *Rhodomonas lens* phycoerythrin containing two PXB-like chromophores (cryptoviolin) and one phycoerythrobilin chromophore.

This paper outlines the finding of an unusual type I phycoerythrin of form $\alpha_2\beta_2$ in which the α subunits can be of four different types. The α subunits possess chromophores of the cryptoviolin type [11]. Evidence is presented for a phycoerythrin protein that has subunits with the ability to absorb light from 540 nm to 644 nm and emit fluorescence at wavelengths from 574 to 652 nm. It is suggested that one or more of the α subunits of this phycoerythrin may provide the intermediate components necessary for energy transfer to chlorophyll *a*. After this work was completed, Guard-Friar and MacColl [12] reported the separation of two α subunits of phycoerythrin from *Rhodomonas*. The subunits possessed identical chromophores but differed in amino-acid composition and molecular weight.

Materials and Methods

Culture methods

Algal cells of an unidentified *Chroomonas* species (C.S.I.R.O. Division of Fisheries No. CS24; Hobart, Australia, 7000) were cultivated in a modified 'fe' medium [13] at 18°C under constant illumination of 20 μmol $\cdot$ m^{-2} $\cdot$ s^{-1} (Mazda universal white fluorescent tubes). The 'fe' medium was further modified by substantially increasing the amount of nutrients and vitamins. 2 ml of each nutrient stock solution and 0.4 ml of vitamin stock (2000 μg $\cdot$ ml^{-1} thiamin, 160 μg $\cdot$ ml^{-1} B-12, 80 μg $\cdot$ ml^{-1} biotin), were added to 1 litre of sea water. After 3 weeks growth, the algae were harvested for determination of phycobiliproteins.

Harvesting and extraction of phycobiliproteins

The unialgal cultures were harvested by centrifugation at 4°C. (10 min at 3000 × *g*). The cells were resuspended in 0.5 M potassium phosphate, 0.3 M potassium citrate buffer (pH 7.2) and homogenized in a glass homogenizer. The cell suspension was then subjected to a single passage through a French press at 82.75 MPa. The resultant solution was centrifuged for 30 min at 27000 × *g*, giving a pellet of cell debris and thylakoid membranes and a supernatant containing phycoerythrin. The pellet was rehomogenized in buffer and centrifuged as before. All supernatants were combined and stored at −22°C until required.

Purification of phycoerythrin

The crude extract of phycobiliproteins was dialysed against 50 mM Tris-HCl buffer (pH 7.0), (4 × 5 litre) for 24 h at 4°C. The dialysate was centrifuged for 30 min at 27000 × *g* and the resultant supernatant was subjected to ammonium sulphate fractionation at 4°C. Three fractions were separated (0–40%, 40–70% and 70–90%). At each stage, the solution was left to stand for 1 h. Phycoerythrin was present in both the 40–70% and 70–90% fractions. Based on the absorbance spectrum and the A_{545}/A_{280} ratio, the 70–90% fraction was selected for further purification.

The 70–90% precipitate was resuspended in a small volume of 50 mM Tris-HCl buffer (pH 7.0) and dialysed against the same buffer for 24 h (6 × 5 litre). The dialysed extract was then centrifuged and the supernatant concentrated using membrane cones (Amicon type CF 25).

The phycoerythrin was further purified by gel filtration (Ultrogel AcA54, L.K.B.) at 4°C on a column 90 × 1.5 cm, with a flow rate of 20 ml $\cdot$ h^{-1}. Fractions were collected and their A_{545}/A_{280} ratios monitored. Fractions with an A_{545}/A_{280} ratio > 10.0 were pooled for further study. Exposure to light was avoided during all stages of purification, by covering the column and collector with back cloth. Preparations were stored at −22°C in the dark to prevent photodegradation.

Molecular weight determination

The molecular weight of purified phycoerythrin was determined by gel filtration on Sephadex G-100 (90 × 1.5 cm column, flow rate 6 $\mathrm{ml \cdot h^{-1}}$) which had been calibrated with proteins of known molecular weight: haemoglobin (64 000), ovalbumin (43 000), chymotrypsin (25 000) and myoglobin (17 200). The void volume of the column was determined using Blue dextran (2 000 000).

Spectroscopic measurements

Fluorescence (excitation and emission spectra) was recorded using a Perkin-Elmer MPF-44B spectrophotofluorimeter. Excitation spectra were obtained in the ratio mode and not otherwise corrected. All samples used had an absorbance value of less than 0.05 at the absorbance maximum for phycoerythrin (i.e., 545 nm) and were diluted in buffer for room temperature measurements. The absorbance spectra were obtained on a Pye Unicam SP8-200 spectrophotometer, at room temperature.

Separation of phycoerythrin subunits

Phycoerythrin in 8 M urea, 50 mM Tris-HCl (pH 7.0) was applied to an Ultrogel AcA54 column (column 45 × 1.5 cm, flow rate 12 $\mathrm{ml \cdot h^{-1}}$) equilibrated in the same buffer. Two coloured bands eluted from the column, a pink followed by a blue fraction. The peaks of these fractions were selected for further analysis and the shoulders discarded.

Purified phycoerythrin and subunits obtained by gel filtration were further separated by ion exchange chromatography. The samples in 8 M urea, 5 mM ammonium acetate (pH 5.1) were applied to a column of carboxymethyl cellulose (Whatman CM32), which had been equilibrated in the same buffer and then developed with an increasing ammonium acetate gradient (5–150 mM ammonium acetate, column 15 × 1.0 cm, flow rate 28 $\mathrm{ml \cdot h^{-1}}$).

Pink, blue and purple bands developed on the column. 2 ml fractions were collected and absorbance spectra recorded. Fractions at the centre of each band were combined and stored at −22°C until required.

Polyacrylamide gel electrophoresis

Protein samples were denatured for electrophoresis by reconstituting lyophylized samples in 0.1 M dithiothreitol, 3% SDS and 20% sucrose, followed by boiling for 2 min. Polyacrylamide gel electrophoresis in the presence of sodium dodecyl sulphate was performed at 22°C using a modified Laemmli type gel 0.6 mm thick, with an acrylamide-to-*N*,*N*′-methylenebisacrylamide ratio of 50 : 1 [14]. The separating gel was made up of a linear gradient from 15–20% acrylamide accompanied by a 5–12.5% sucrose gradient and contained 0.2% SDS, 6% urea, 0.05% TEMED, 0.025% ammonium persulphate, and 0.375 M Tris-HCl (pH 8.5). The stacking gel contained 6% acrylamide, 0.1% SDS, 4% urea, 0.05% TEMED, 0.07% ammonium persulphate and 0.125 M Tris-HCl (pH 6.8) [15].

The running buffer was 50 mM Tris, 380 mM glycine and 0.1% SDS (pH 8.5). Gels were run at a constant current of 9 mA for 16 h. Molecular weights were determined by using the following protein markers: phosphorylase *b* (94 kDa), bovine serum albumin (67 kDa), ovalbumin (43 kDa), carbonic anhydrase (30 kDa); soybean trypsin inhibitor (20.1 kDa), and α-lactalbumin (14.4 kDa).

Gels were stained in Coomassie brilliant blue R and destained in 7% acetic acid/30% methanol before photographing.

Results

Isolation and purification

Phycoerythrin was purified to an A_{545}/A_{280} ratio of greater than 10 by ammonium sulphate fractionation and gel filtration. It was free of chlorophylls *a* and c_2 and carotenoid (Fig. 1). 32% of the phycoerythrin was recovered from the crude extract with an 18.7-fold increase in purity based on the changes in ratio of $A_{545\ \mathrm{nm}}/A_{280\ \mathrm{nm}}$ (Table I). It had a typical type I visible absorbance spectrum with a peak at 545 nm and a shoulder at 564 nm. However, a small absorbance peak was also observed at 644 nm (Fig. 1). Excita-

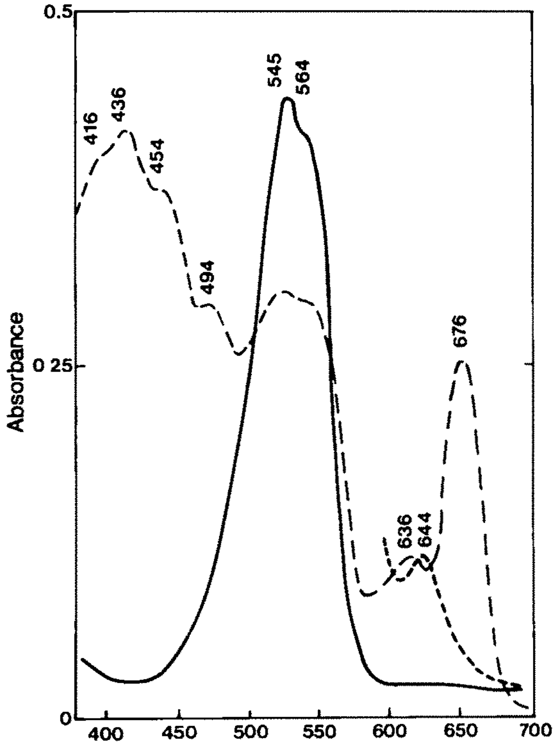

Fig. 1. Absorbance spectra of *Chroomonas* sp. whole cells, and purified phycoerythrin. — — —, Whole cells; ———, purified phycoerythrin; - - - - - -, purified phycoerythrin (×10).

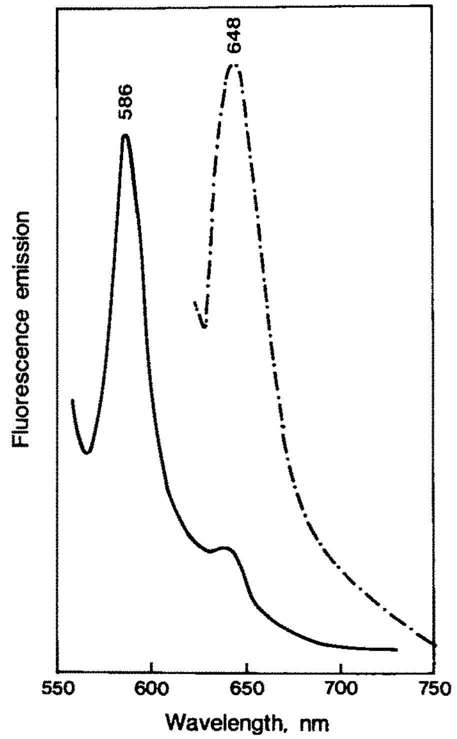

Fig. 2. Fluorescence emission spectrum of purified phycoerythrin excited at 535 nm (———) and at 625 nm (–·–)

tion of the native protein at 535 nm resulted in a large fluorescence emission band peaking at 586 nm with a minor maximum at 648 nm. Excitation at 625 nm resulted in a single emission peak at 648 nm (Fig. 2). The excitation spectrum for 715 nm emission from phycoerythrin has a large 545 nm peak with a shoulder at 564 nm and another peak at 640 nm (Fig. 3).

Molecular weight determination

The molecular weight of the native protein as determined by gel filtration was 63 500. This value is larger than other cryptophyte phycoerythrins and is consistent with an $\alpha_2\beta_2$ structure.

Separation of subunits in 8 M urea (pH 7.0)

Purified phycoerythrin was separated into two coloured fractions by gel filtration in 8 M urea. The first fraction was pink and had absorbance

TABLE I

PURIFICATION OF PHYCOERYTHRIN FROM *CHROOMONAS* CS24

	Protein $A_{280\text{ nm}}$	Phycoerythrin $A_{545\text{ nm}}$	A_{545}/A_{280}	Phycoerythrin recovery (%)
Initial crude extract	210	139	0.66	100
70–90% ammonium sulphate precipitation	13.1	77	5 88	55.4
Gel filtration (AcA54)	3.6	44.5	12.39	32.0

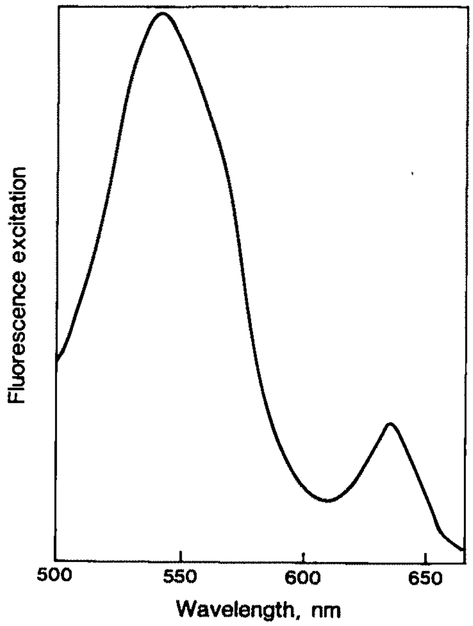

Fig 3 Fluorescence excitation spectrum of purified phycoerythrin recorded at 715 nm emission.

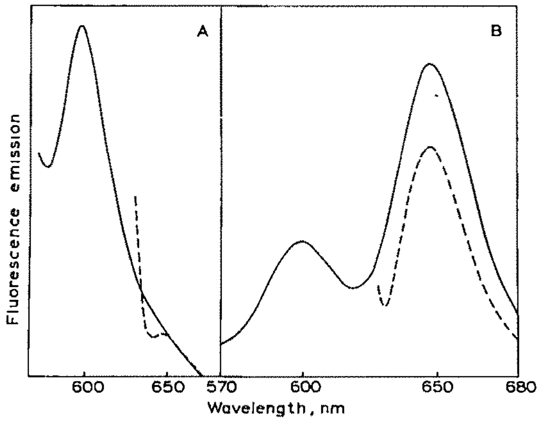

Fig. 5. Fluorescence emission of the pink (A) and blue (B) fractions isolated in 8 M urea (pH 7.0): ———, excited at 535 nm, — — —, excited at 625 nm.

peaks at 532 nm, 585 nm and a small shoulder at 644 nm (Fig. 4). Fluorescence emission at 600 nm was observed when this fraction was excited at 535 nm. Excitation at 625 nm resulted in a small shoulder in the 650 nm region (Fig. 5A).

The second fraction was blue, with absorbance peaks at 344, 590 and 644 nm. (Fig. 4). This fraction had fluorescence emission peaks at 600 and 648 nm when excited at 535 nm and a single peak at 648 nm when excited at 625 nm (Fig. 5B).

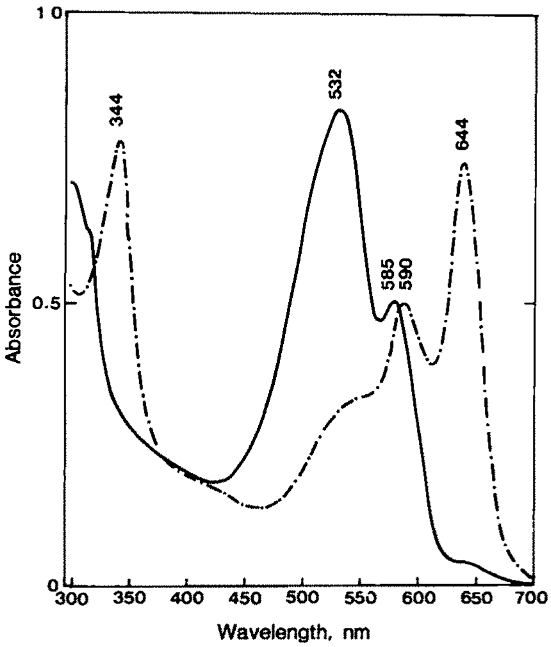

Fig. 4. Absorbance spectra of the pink and blue subunit fractions of phycoerythrin isolated in 8 M urea (pH 7.0) by gel filtration. ———, pink fraction (β subunit); –·–·–; blue fraction (α subunit complex)

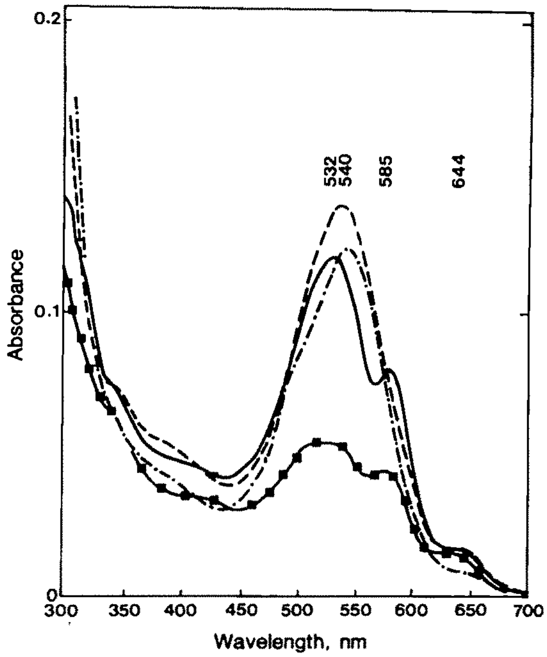

Fig. 6. Absorbance spectra of the pink fraction (β subunit) isolated at pH 7.0 (8 M urea), following titration with HCl to pH 1.9 and then to 8.5. ■———■, pH 8.5; ———, pH 7.0; –·–·–, pH 4.9; — — —, pH 1.9, 3.0.

The two fractions isolated were titrated with HCl to pH 1.9 and with NaOH back up to pH 10.0. The pink fraction, at low pH, lost its 585 nm absorbance peak and the principal absorbance peak shifted from 532 to 540 nm. When the pH was increased to 6.5 the absorbance maximum shifted back to 532 nm and the peak became broader. At higher pH (8.5, 10.0) the absorbance spectrum changed with reduced absorbance at 532 nm and the re-appearance of peaks at 585 nm and 644 nm (Fig. 6).

The colour of the blue fraction on titration to low pH (1.9, 3.0) undergoes a complete change to purple, which is reversed by titration back to pH 8.5 and above. Associated with this colour change from blue to purple is the disappearance of the 644 nm absorbance and the appearance of a major peak at 560 nm. The peak which is present at 344 nm at high pH shows a shift to 330 nm at pH 1.9 (Fig. 7).

The fluorescence properties of the pink β and blue α subunit complexes isolated in 8 M urea at pH 7.0 showed the same reversible changes upon titration to high and low pH that are seen in the absorbance spectra. The pink subunits showed no change in fluorescence at pH 1.9 and 3.0, but at pH 8.5 and 11.0 a small fluorescence peak was seen at 648 nm as well as an emission maximum at 600 nm. The blue fraction, containing the α subunits, showed a complete loss of 648 nm fluorescence emission at pH 1.9. At pH 7.0 and above the major fluorescence peak at 648 nm was evident; at pH 1.9 the major fluorescence peak was at 590 nm (results not shown).

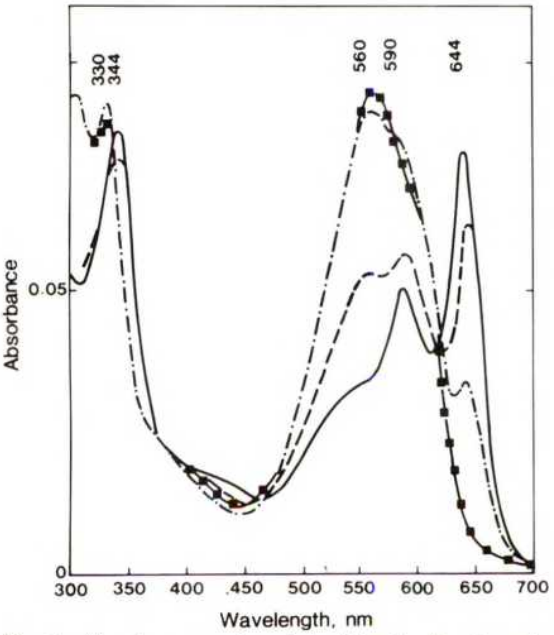

Fig. 7. Absorbance spectra of the blue fraction (α subunit complex) isolated at pH 7.0 (8 M urea) following titration with HCl to pH 1.9 and titration with NaOH back to pH > 7.0. ——, pH > 7.0; — — —, pH 4.9; –·–·–; pH 3.0; ■——■, pH 1.9.

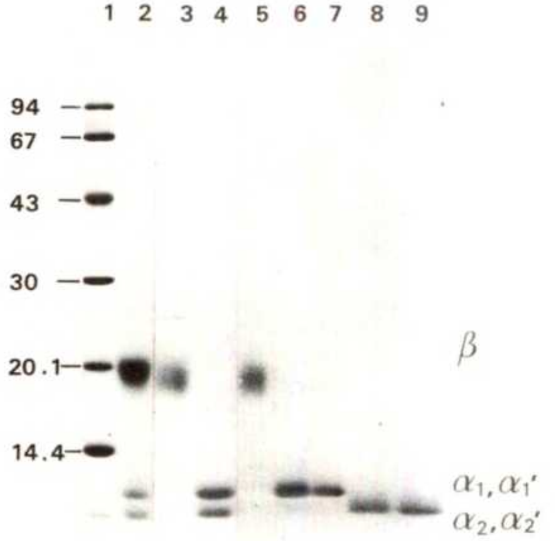

Fig. 8. SDS-polyacrylamide gel electrophoresis of phycoerythrin and its subunits. 1, marker proteins; 2, purified phycoerythrin; 3, pink fraction, β subunit; 4, blue fraction, α subunit complex; 5, β subunit; 6, α_1 subunit; 7, α_1' subunit; 8, α_2 subunit; 9, α_2' subunit.

Analysis of the polypeptides by SDS-polyacrylamide gel electrophoresis on these two fractions showed that the pink fraction contained a single band at 20.5 kDa whereas the blue fraction contained two bands, one at 12.0 kDa and the other at 11.0 kDa (Fig. 8). The harvesting, isolation and purification of phycoerythrin was repeated in the presence of the proteolytic inhibitor phenylmethylsulphonyl fluoride (final concentration 1 mM). Identical results to the above were obtained.

Subunit separation in 8 M urea-ammonium acetate (pH 5.1)

Ion exchange chromatography of purified phycoerythrin gave rise to five coloured fractions.

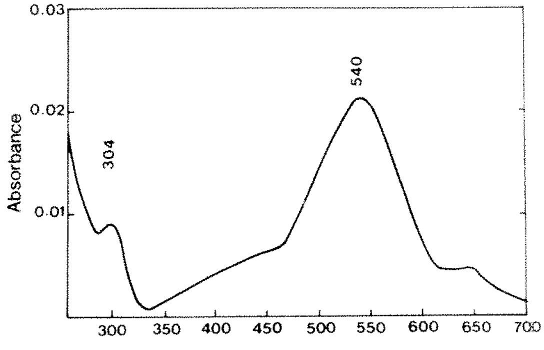

Fig. 9. Absorbance spectrum of β subunit isolated by ion exchange chromatography in 8 M urea (pH 5.1).

These fractions in order of elution from the CM32 column were designated as the β (pink), α_1(blue), α_1'(purple), α_2(blue), α_2'(purple) subunits of phycoerythrin. This terminology is based on that of Mörschel and Wehrmeyer [16] in which the larger polypeptide is designated β and the smaller polypeptide subunits which differ from each other by approx. 1 kDa are designated α_1 and α_2 respectively. The β subunit isolated at pH 5.1 had an absorbance peak at 540 nm and a fluorescence emission peak at 574 nm (Figs. 9 and 10).

The α_1 and α_2 subunits both had absorbance maxima at 344, 594 and 644 nm and fluorescence emission at 578 and 652 nm when excited at 535 nm (Figs. 10 and 11). The α_1' and α_2' subunits had major absorbance peaks at 330 and 560 nm with a small peak at 644 nm and a shoulder at 594 nm (Fig. 11). Fluorescence emission at 586 nm was observed when the two α' subunits were excited at 535 nm (Fig. 10). The two blue α subunits were found to be sensitive to pH change, reversibly showing change in spectral properties between the 644 nm absorbance spectrum and the 560 nm spectrum at high and low pH, respectively. The two α' subunits were found to alter on prolonged standing overnight, from 560 nm absorbance to the 644 nm absorbance. Associated with this change in spectral properties was a complete loss of the purple colour.

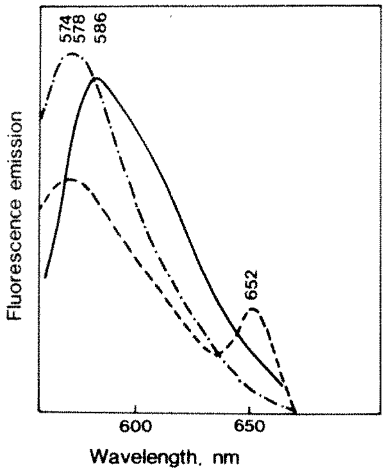

Fig. 10. Fluorescence emission spectra of α and β subunits in 8 M urea (pH 5.1). Excitation wavelength 535 nm. –·–·–, β subunit; — — —, α_1 and α_2 subunit, ———, α_1' and α_2' subunit.

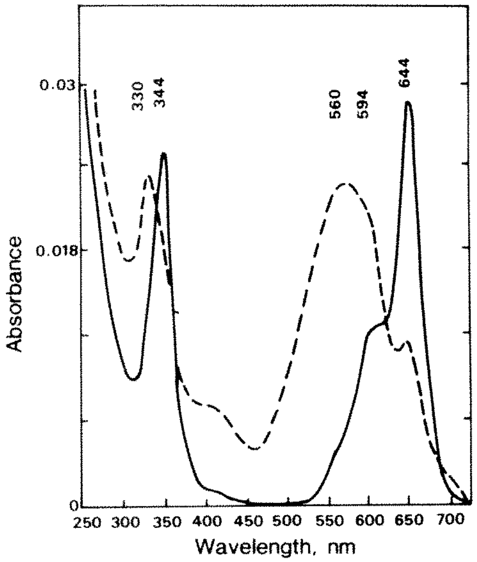

Fig. 11. Absorbance spectra of α_1, α_2, α_1', α_2', subunits isolated in 8 M urea, (pH 5.1). ———, α_1 and α_2 subunits; — — —, α_1' and α_2' subunits.

SDS-polyacrylamide gel electrophoresis of these fractions from the ion exchange column revealed that the pink fraction (β) contained a single polypeptide with relative molecular mass of 20.5 kDa. The first blue and purple fractions (α_1 and α_1') contained a single polypeptide of 12.0 kDa whereas the second blue and purple fractions (α_2 and α_2') also had a single polypeptide but of relative molecular mass 11.0 kDa (Fig. 8). The pink and blue subunit fractions separated from phycoerythrin by gel exclusion chromatography in 8 M urea (pH 7.0), as described above, were further analysed by elution with an ammonium acetate gradient from the CM32 ion exchange column. The blue fraction gave rise to four α subunits which were identical to those obtained from the native phycoerythrin. The pink fraction, however, gave variable results with one or more bands being resolved. These all possessed a single polypeptide of 20.5 kDa and had identical absorbance and fluorescence properties. This result suggests the possibility of charge heterogeneity in the β subunit as well as in the α subunit.

Discussion

The spectral properties of phycoerythrin isolated from *Chroomonas* CS24 are superficially those of a type I phycoerythrin, which is characterized by an absorbance peak at 544 nm and a shoulder at 564 nm [17,18]. The presence of a small absorbance peak at 644 nm is not characteristic of a type I phycoerythrin and has not been described previously. This absorbance cannot be attributed to chlorophyll c_2, which has an absorbance in the Soret region which is 5-times more intense than that in the red region of the spectrum. No evidence was obtained for a peak or shoulder in the region of 460 nm in any preparation of purified pycoerythrin.

The high A_{545}/A_{280} ratio of the purified phycoerythrin compares favourably with others previously [17,19] reported which range from greater than 6.0 to 8.5 and 12.5. The presence of an absorbance peak at 644 nm and fluorescence emission at 648 nm distinguishes this phycoerythrin from others. O'hEocha and Raftery [7] reported a slight absorbance at 620–630 nm in aqueous extracts of the cryptophyte *Sennia* sp. No. 9, which contained a type I phycoerythrin as its major accessory light harvesting pigment. They attributed this absorbance to phycocyanin. In our work, attempts to separate the 644 nm absorbance from phycoerythrin were unsuccessful. Methods such as ion exchange chromatography on DEAE-Sephacel using an increasing salt gradient, hydrophobic interaction chromatography using phenyl-Sepharose, and sucrose density gradients were employed. The absorbance at 644 nm was always associated with the 545 and 564 nm absorbance, suggesting that a single protein was being isolated. Furthermore the 644 nm absorbance was associated with two phycoerythrin (α_1 and α_2) subunits of unequal size and different charge. The other two subunits (α_1' and α_2') are also different with respect to size and charge and at pH 5.1 have little absorbance at 644 nm. Our results provide an explanation for those of O'hEocha and Raftery [7] and suggest that their 'phycocyanin' was also phycoerythrin containing an unusual chromophore. The nature of this chromophore is unknown but it is probably identical with 'cryptoviolin' on the α subunit of phycoerythrin from *Rhodomonas lens* [11] and PXB of phycoerythrocyanin [20]. Although in our study the absorbance spectra of the various α subunits in 8 M urea varies greatly with pH, we interpret these results in terms of a single chromophore in which one absorbance predominates over the other according to its protonation and the conformation of the polypeptide. However, there is a precedent [21] for multiple uncharacterized chromophores in the cryptomonads.

The β subunit has an absorbance spectrum that is consistent with the presence of the chromophore phycoerythrobilin with an absorbance peak at 540 nm in acid urea. Absorbance maxima for phycoerythrobilin range from 538 to 567 nm [23]. O'hEocha [10,22] reports that in aqueous acid solutions phycoerythrobilin has absorbance peaks at 307 and 556 nm. No peak at 307 nm was observed in this study, but a peak was evident at 304 nm. The β subunit also shows evidence of 644 nm absorbance, which is enhanced when titrated to high pH (Fig. 6). In addition, fluorescence emission is seen at 648 nm (excitation at 625 nm) under these conditions. This suggests that the chromophore of the α subunit may also be present on the β subunit, but that there are significantly fewer of this type of chromophore than the phycoerythrobilin type.

The molecular mass of 63.5 kDa determined here by gel filtration correlates well with the structure $\alpha_2\beta_2$. It is proposed that the α component is composed of various combinations of the four α subunits described. The β subunits are all 20.5 kDa, the α_1 and α_1' subunits are 12.0 kDa and the α_2 and α_2' subunits are 11.0 kDa as determined by the mobilities on SDS-polyacrylamide gel electrophoresis. Therefore the structure $\alpha_2\beta_2$ always results in a molecular mass within the range 63.0–65.0 kDa. Our value of 63.5 kDa is significantly higher than other type I cryptophyte phycoerythrins which range from 30.8 kDa [18] to 44.5 kDa [17]. Mörschel and Wehrmeyer [17] proposed an $\alpha_2\beta_2$ structure for type I phycoerythrin where the α subunit is 9.9 kDa and the β subunit is 15.7 kDa. There is also a report [18] of a monomeric type I phycoerythrin with an $\alpha\beta$ composition, with an α subunit of 11.0 kDa and a β subunit of 17.7 kDa. Although considerable variation may be expected in relative molecular masses determined in different laboratories by SDS-polyacrylamide gel electrophoresis, much less variation is expected in values obtained by gel filtration. The present work suggests a greater degree of complexity than previously reported for cryptophyte phycoerythrins and indicates strong structural similarities with cryptophyte phycocyanins [16,24].

In view of the colour changes obtained on separation of the phycoerythrin subunits, it is surprising that the unusual subunit chromophores (if typical of a type I cryptophyte phycoerythrin) have not been previously described. Brooks and Gantt [18] noted that the small subunit of types I and III phycoerythrin was blue when separated by SDS-polyacrylamide gel electrophoresis, but did not comment further. MacColl and Berns [25], using sucrose density gradients, found that the α subunit of phycoerythrin from *R. lens* was blue and had a molecular mass of 10 kDa. Most previous workers [17,21] have separated the phycoerythrin subunits by ion exchange chromatography or by sucrose density gradient centrifugation at pH 3.0. At this pH the 644 nm component was decreased in our study and may be completely missing in other species. We were unable to repeat the subunit separation at pH 3.0 due to the insolubility of our phycoerythrin at this pH. The spectrum of the aggregated α subunits of *R. lens* at pH 3.0 showed absorbance maxima at 333 nm and 560 nm [11] and are identical to those reported here for the α subunits at this pH. MacColl et al. [11] interpret their results in terms of two cryptoviolin chromophores per one phycoerythrobilin on the α subunit, although stressing the unreliable basis of the calculation. Our results suggest that most of, if not all, the chromophores on the α subunit are not phycoerythrobilin but some other novel chromophore with affinities to both PXB and phycocyanobilin. However, it appears that the phycoerythrin of *R. lens* [11] is identical to that of *Chroomonas* CS24. However, the published spectra for the α subunit (Fig. 4 of Ref. 12) show no evidence of a shoulder at 304 nm due to phycoerythrobilin. Our own data (Fig. 10) for the α_1 and α_2 subunits isolated by ion exchange chromatography at pH 5.1 indicate only a very small shoulder at 550 nm, far less than would be expected for a 1:2 ratio of phycoerythrobilin/cryptoviolin.

The phycobiliproteins of the cryptomonads are confined to the intrathylakoid spaces and since little is known of their organization and aggregation [26], charge heterogeneity of a single protein may provide a system for molecular organization [17]. This, coupled with the presence of the novel chromophores described, may provide a model whereby protein molecules can align themselves in an energy transfer chain that is similar to that of the phycobilisome in the cyanophytes and red algae. Such a proposal has also been made for 'pigment 697' as a final energy trap in *Chroomonas* phycocyanin 645 [27]. Additionally, a chromophore that reversibly alters with pH may have implications in the control and optimization of light absorption and energy transfer within the whole cell. However, we have not been able to demonstrate, in our extracts, significant energy transfer from phycoerythrobilin chromophores to the phycocyanobilin-like chromophores of the α subunits.

Acknowledgements

This work was supported by research grants from Macquarie University and by the Australian Research Grants Commission (No. D27915708).

References

1 Porter, G., Tredwell, C.J., Searle, G.F.W. and Barber, J. (1978) Biochim. Biophys. Acta 501, 232–245
2 Glazer, A.N. (1984) Biochim. Biophys. Acta 768, 29–51
3 Gantt, E. (1981) Annu. Rev. Plant Physiol. 32, 27–47
4 Glazer, A.N. (1981) in The Biochemistry of Plants (Hatch, M.D and Boardman, N.K., eds.), Vol. 8, pp. 51–96, Academic Press, New York.

5 Lichtlé, C., Jupin, H. and Duval, J.C. (1980) Biochim. Biophys. Acta 591, 104–112

6 Gantt, E. (1979). in Biochemistry and Physiology of Protozoa (2nd Edn.) (Levandowsky, M and Hunter, S.H., eds), Vol. II, pp. 121–137, Academic Press, New York

7 O'hEocha, C. and Raftery, M. (1959) Nature 184, 1049–1051

8 Ingram, K and Hiller, R G. (1983). Biochim Biophys. Acta 722, 310–319

9 O'hEocha, C., O'Carra, P. and Mitchell, D (1964). Proc R Ir. Acad Sect. B63, 191–200

10 O'hEocha, C. (1986) in Biochemistry of Chloroplasts (Goodwin, T.W, ed.), Vol I, pp 407–421, Academic Press, New York

11 MacColl, R., Guard-Friar, D. and Csatorday, D. (1983) Arch. Microbiol 135, 194–198

12 Guard-Friar, D and MacColl, R. (1986). Photochem. Photobiol. 43, 81–85

13 Guillard, R.L. and Ryther, J.H. (1962) Can. J. Microbiol. 8, 229–239

14 Laemmli, U.K. (1970). Nature 227, 680–685

15 Spiers, J. and Brady, C.J. (1981). Aust. J. Plant Physiol. 8, 603–618

16 Mörschel, E. and Wehrmeyer, W. (1975). Arch. Microbiol. 105, 153–158

17 Mörschel, E. and Wehrmeyer, W. (1977). Arch Microbiol 113, 83–89

18 Brooks, C. and Gantt, E. (1973). Arch. Microbiol. 88, 193–204

19 MacColl, R., Berns, D.S. and Gibbons, O (1976). Arch. Biochem. Biophys. 177, 265–275

20 Bryant, D A , Glazer, A.N. and Eiserling, F.A. (1976) Arch. Microbiol 110, 61–75

21 Glazer, A.N. and Cohen-Bazire, G. (1975) Arch. Microbiol. 104, 29–32

22 O'hEocha, C. (1965) in Chemistry and Biochemistry of Plant Pigments (Goodwin, T.W., ed.), Vol. 1, pp. 175–196, Academic Press, New York

23 Glazer, A.N (1977) Mol. Cell. Biochem 18, 125–139

24 Sidler, W., Kumpf, B , Fran, G., Suter, F., Morisset, W , Wehrmeyer, W. and Züber, H. (1985). Hoppe-Seylers Z Physiol. Chem. 366, 233–244

25 MacColl, R. and Berns, D.S. (1979). Biochem. Biophys. Res. Commun. 90, 849–855

26 Gantt, E., Edwards, M.R and Provasoli, L (1971). J Cell Biol. 48, 280–290

27 Zuber, H. (1985). in Antennas and Reaction Centres of Photosynthetic Bacteria (Michel-Beyerle, M.E., ed), pp. 2–14, Springer-Verlag, Berlin

Biochimica et Biophysica Acta 923 (1987) 98–102
Elsevier

BBA 22458

Multiple forms of a type I phycoerythrin from a *Chroomonas* sp. (Cryptophyceae) varying in subunit composition

Roger G. Hiller and Carol D. Martin

School of Biological Sciences, Macquarie University, North Ryde, 2113, N.S W. (Australia)

(Received 9 April 1986)

Key words: Phycoerythrin; Fluorescence, Isoelectric focusing; Energy transfer; (*Chroomonas* sp. CS24)

Four forms of phycoerythrin have been isolated by chromatofocusing, with isoelectric points of 7.16, 6.24, 5.46 and 4.98. Each isoprotein has a type I absorbance maximum at 545 nm and a shoulder at 564 nm with a small shoulder at 644 nm. Polyacrylamide gel electrophoresis in the presence of sodium dodecyl sulphate and urea revealed that the four isoprotein fractions contain a β-subunit of 20.5 kDa but are different with respect to the α subunits. The p*I* 7.16 isoprotein lacked the α polypeptide at 12.0 kDa, whereas the p*I* 4.98 and p*I* 5.46 forms contained predominantly the 12.0 kDa α polypeptide. The predominant p*I* 6.24 isoprotein contained α subunits of both 11 kDa and 12 kDa. Ion exchange chromatography of the α subunits showed that both existed as two differently charged species. Isoelectric focusing confirmed the existence of multiple forms of phycoerythrin. Eight or nine species of phycoerythrin were separated, consistent with the previously postulated $\alpha_2\beta_2$ structure (Martin, C.D. and Hiller, R.G. (1987) Biochim. Biophys. Acta 923, 88–97). None of the multiple forms isolated appears to be a specific intermediate in energy transfer between bulk phycoerythrin and chlorophyll *a*.

Introduction

Although the Cryptophyceae possess phycobiliproteins they lack phycobilisomes and the phycobiliproteins are confined to the thylakoid lumen. Little is known of the mechanism whereby energy is transferred from them to chlorophylls *a* or c_2, as allophycocyanin is always absent, as is phycocyanin, from those species which have phycoerythrin as accessory light harvesting pigment proteins [1]. As almost all cryptomonad phycobiliproteins characterized show multiple components [2–7], their occurrence, with isoelectric points ranging from slightly acidic to slightly basic, seems to be of significance in the cryptophytes. The multiple forms of crytomonad biliproteins may be built up into an energy transfer chain similar to that of the phycobilisome in the blue-green and red algae [7].

Martin and Hiller [8] have found four α subunits in a cryptophyte (*Chroomonas* CS24) phycoerythrin. These α subunits show differences in spectral properties, relative molecular mass and charge. Since it is proposed that the phycoerythrin has an $\alpha_2\beta_2$ structure, the number of possible combinations is ten, if the β subunit is invariant and if the α component can be composed of two identical polypeptides as well as varying pair combinations of the four α polypeptides. If only two forms of α subunit exist, the number of isoproteins reduces to three. However the number of

---

Abbreviations: PBE, Polybuffer exchanger (Pharmacia); SDS, sodium dodecyl sulphate; TEMED, *N*,*N*,*N'*,*N'*-tetraethylmethylenediamine; Tris, tris(hydroxymethyl)aminomethane

Correspondence: Dr. R.G Hiller, School of Biological Sciences, Macquarie University, North Ryde, 2113, N S.W., Australia

0304-4165/87/$03.50 © 1987 Elsevier Science Publishers B V (Biomedical Division)

possible isoproteins could be much greater than ten if the β subunits also showed charge variation. This study was undertaken to see whether the holoproteins showed any or all of the potential variation arising from the subunit analysis and whether any variant has properties of an intermediate carrier in energy transfer between bulk phycoerythrin and chlorophyll.

Materials and Methods

Chroomonas CS24 cells were grown and harvested as described previously [8]. Phycoerythrin was released from the cells by a single passage through a French press at 82.75 MPa and the resultant solution was centrifuged. The supernatant was subject to extensive dialysis in 50 mM Tris-HCl buffer (pH 7.0) and ammonium sulphate fractionation (70–90% saturation level). The precipitate was dissolved in Tris-HCl buffer (pH 7.0) and dialysed for 24 h against the same buffer.

After dialysis, the sample was centrifuged and dialysed against 0.025 M imidazole (pH 7.4) for several hours. All procedures were carried out at 4°C.

Chromatofocusing

The multiple pigment forms of phycoerythrin were separated using a chromatofocusing technique (Pharmacia) at 4°C. The column (30 × 1.5 cm) of PBE exchanger was equilibrated in 0.025 M imidazole (pH 7.4) and the proteins eluted with polybuffer 74. Polybuffer 74 was titrated to an initial pH of 4.0 with HCl. As the pH gradient developed in the column the proteins eluted at their isoelectric points (flow rate 15 $\mathrm{ml \cdot h^{-1}}$). Fractions were collected, and their A_{545}/A_{280} ratio, pH, absorbance and fluorescence emission spectra were recorded. Polybuffer was removed from the samples by precipitating the proteins with 80–100% saturated ammonium sulphate. The samples were left for 1–2 h before collecting the protein precipitate by centrifugation. The proteins were resuspended in 50 mM Tris-HCl (pH 7.0), dialysed overnight, lyophilized and stored at −22°C until required.

Isoelectric focusing

Isoelectric focusing was performed at 10°C using a 6% acrylamide, 1.8% N,N'-methylene-bisacrylamide gel, 0.6 mm thick incorporating 8% of LKB standard preparation of ampholines covering a pH range from 3.5 to 9.5. The gels contained 16% glycerol, 0.02% TEMED and 0.016% ammonium persulphate. The gels were run for 1 h with a limiting voltage of 2000 V. They were photographed under ultraviolet light, prior to staining with Coomassie brilliant blue R. The gels were destained in 7% acetic acid/30% methanol and photographed. Standard proteins were the Pharmacia wide range p*I* calibration kit.

Spectroscopic measurements

Fluorescence measurements (excitation and emission) were recorded using a Perkin-Elmer MPF-44B spectrophotofluorimeter. Excitation spectra were obtained in the ratio mode and not otherwise corrected. All samples used had an absorbance value of less than 0.05 at the absorbance maximum for phycoerythrin (i.e., 545 nm) and were diluted in buffer for room temperature measurements. The absorbance spectra were obtained on a Pye Unicam SP8-200 spectrophotometer.

Subunit separation

Subunit separation by ion exchange chromatography and SDS-polyacrylamide gel electrophoresis was performed as described in the previous paper [8].

Results

Isolation of multiple forms and spectral properties

Phycoerythrin was purified to an A_{545}/A_{280}

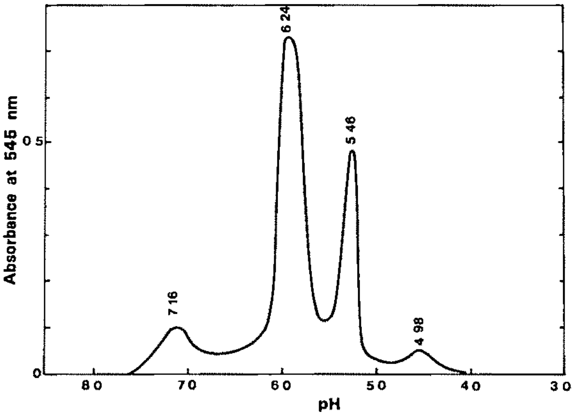

Fig. 1. Elution profile of phycoerythrin isoproteins isolated by chromatofocusing

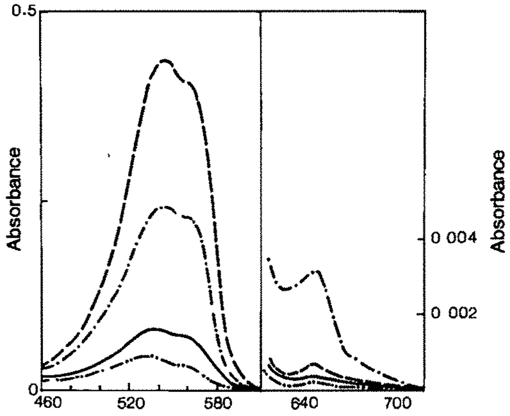

Fig 2. Absorbance spectra of multiple forms of phycoerythrin isolated by chromatofocusing ———, pI 7 16; — — —, pI 6.24; – – –·, pI 5.46; –··–··, pI 4 98.

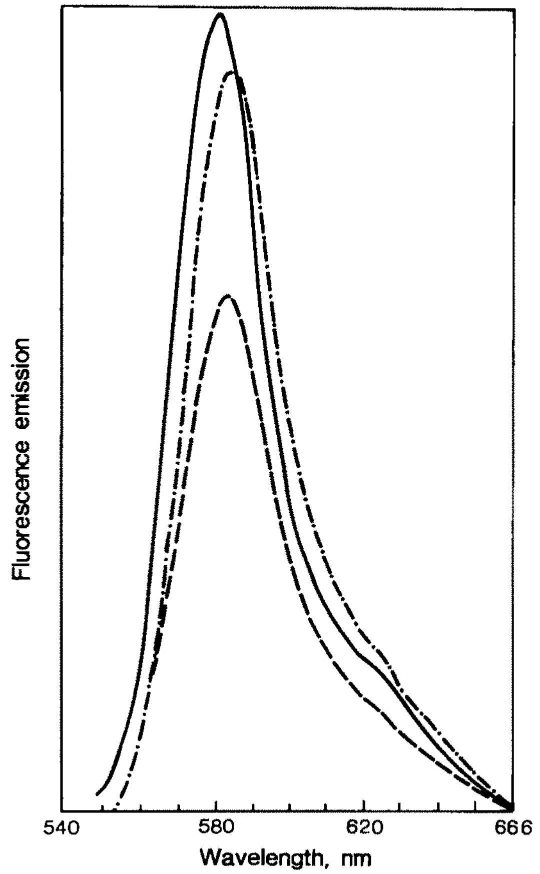

Fig. 3. Fluorescence emission spectra of multiple forms of phycoerythrin isolated by chromatofocusing. ———, pI 7.16; –·–·–, pI 6.24; –·–·–, pI 5.46; — — —, pI 4 98.

ratio of 7.0 by dialysis and ammonium sulphate precipitation. Chromatofocusing of phycoerythrin reproducibly resolved four isoproteins with isoelectric points at 7.16, 6.24, 5.46 and 4.98. Fig. 1 shows a typical elution profile of the phycoerythrin obtained from the PBE column. The relative amounts of each form calculated from the elution profile were 2.3 : 13 : 5 : 1 for the pI 7.16, pI 6.24, pI 5.46 and pI 4.98 isoproteins, respectively. All four proteins have absorbance maxima at 545 nm and a shoulder at 564 nm (Fig. 2), which is typical of a type I cryptophyte phycoerythrin [9], except that each protein has a small absorbance peak at 644 nm. There is a difference in the amount of absorbance at 644 nm, with the pI 5.46 isoprotein having the greatest absorbance at this wavelength and the highest A_{644}/A_{545} ratio. Difference spectra between the pI 6.24 and pI 5.46 forms confirmed this finding. The A_{545}/A_{280} ratios of the four proteins were 7.4, 10, 8.5 and 5.8, respectively. Fluorescence emission spectra (excitation at 535 nm) of the four proteins are shown in Fig. 3. The protein with pI 7.16 differs slightly from the other three having an emission peak at 581 nm and a shoulder at 625 nm. The other three proteins have similar asymmetrical spectra, but the peak is at 583 nm.

Isoelectric focusing

The two most abundant forms (pI 6.24 and pI 5.46) of phycoerythrin collectively resolved into six different bands, three present in each form and all showing bright orange fluorescence under ultraviolet light. The pI 6.24 isoprotein resolved bands with pI values of 5.85, 6.0 and 6.3, respectively. The pI 5.46 fraction resolved three bands with pI values of 5.15, 5.35 and 5.5, respectively (Fig. 4A and B).

The pI 7.16 isoprotein fraction contained two weakly fluorescent bands (white arrows in Fig. 4A and B) and these had isoelectric points at pH 6.55 and 6.85. The pI 4.98 isoprotein was shown to contain a band at pI 5.1, which was fluorescent under ultraviolet light, and an additional band focusing at pI 5.75, which was non-fluorescent, but stained with Coomassie brilliant blue R. The fluorescent band (pI 5.1) isolated from this fraction was only marginally different in position to the pI 5.15 band isolated from the pI 5.46 frac-

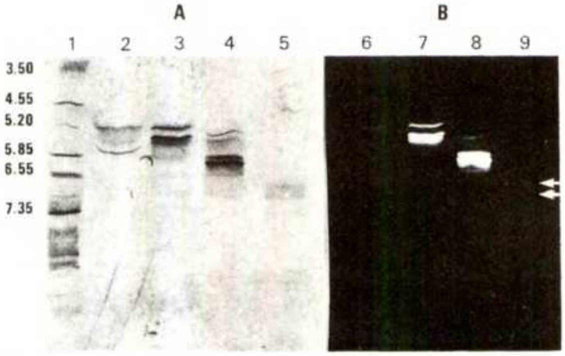

Fig. 4. Multiple forms of phycoerythrin separated by isoelectrofocusing. (A) Stained with Coomassie brilliant blue R. (B) Fluorescent forms under ultraviolet light. (A) 1, standard marker proteins; 2–5, phycoerythrin p*I* 7.16, 6.24, 5.46, 4.98. (B) 6–9, phycoerythrin p*I* 7.16, 6.24, 5.46, 4.98. Arrows indicate positions of bands clearly visible by visual inspection.

tion and it is possible that these represent the same phycoerythrin. If, however, these are different, then the total number of fluorescent phycoerythrin proteins detected by isoelectric focusing is nine, with isoelectric points, 5.1, 5.15, 5.35, 5.5, 5.85, 6.0, 6.3, 6.55 and 6.85.

SDS-polyacrylamide gel electrophoresis

The electrophoretic separation of the native phycoerythrin into subunits by SDS-polyacrylamide gel electrophoresis is shown in Fig. 5. The p*I* 6.24 protein has a heavy band at 20.5 kDa (β subunit) and two other bands at 12.0 kDa and 11.0 kDa (α subunits), whereas the p*I* 7.16 protein does not contain the α band of 12.0 kDa. The two proteins with the lowest p*I* values (5.46 and 4.98) appear to contain bands of both 12.0 kDa and 11.0 kDa but there is a quantitative difference, the 12 kDa polypeptide predominating.

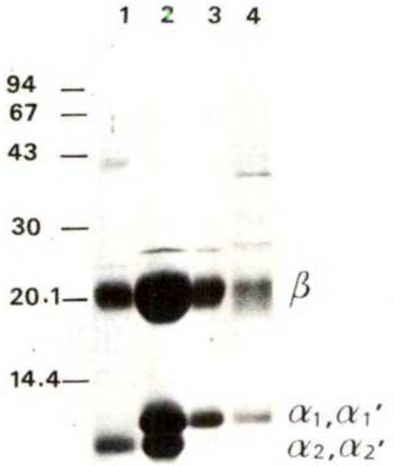

Fig. 5. SDS-polyacrylamide gel electrophoresis (15–20% polyacrylamide gradient). Lanes 1–4, phycoerythrin p*I* 7.16, 6.24, 5.46, 4.98.

Subunit analysis

Ion exchange chromatography of the p*I* 6.24 protein in 8 M urea at pH 5.1 resolved five subunits, a β subunit and four α subunits. Molecular masses of these subunits calculated from their mobilities on SDS gels were 20.5 kDa (β), 12.0 kDa (α_1, α_1'), and 11.0 kDa (α_2, α_2'). The subunits isolated from the p*I* 6.24 protein did not differ in absorbance and fluorescence properties from those previously isolated [8] from the total phycoerythrin.

Discussion

Four forms of a type 1 phycoerythrin have been isolated by chromatofocusing, purified and partially characterized. The four proteins differ in their isoelectric points and subunit composition. All have the same absorbance spectrum, and very similar fluorescence emission spectra. Isoelectric focusing on these four protein fractions resolved at least eight and possibly nine phycoerythrin isoproteins, ranging from p*I* 5.1 to p*I* 6.85. Others [2–7] have reported charge heterogeneity and multiple components within cryptomonad biliproteins both in phycoerythrin and phycocyanin. Mörschel and Wehrmeyer [7] found three charge isomers of phycoerythrin in *Cryptomonas maculata* with isoelectric points at 7.83, 5.05 and 4.84. These differed slightly in absorbance spectra, fluorescence emission spectra and molecular structure. The electrophoretic differences were attributed to the α subunits which show charge heterogeneity. Mörschel and Wehrmeyer [6], using sucrose density gradient electrofocusing, also isolated five isoproteins from a cryptophyte phycocyanin 645 with isoelectric points ranging from 7.03 to 4.88. They determined by SDS gel electrophoresis that phycocyanin 645 contained three subunits, a large β subunit (15.5 kDa) and two lighter subunits (α_1 and α_2), with molecular masses of 9.2 and 10.4 kDa, respectively, and suggest for this particular biliprotein the quaternary structure $(\alpha_1\beta)(\alpha_2\beta)$. Our analysis of the peptides from the phycoerythrin forms separated by chromatofocusing demonstrates, in addition, that the α component can be composed of the same or different polypeptides of identical molecular mass, since the p*I* 4.98 isoprotein contains only the 12 kDa α_1 peptides and the p*I* 7.16 isoprotein the α_2 polypeptides.

Multiple forms of phycoerythrin and phycocyanin in the Cryptophyceae are usual; phycocyanin from *Hemiselmis virescens* Plymouth 157 is exceptional [5]. It seems unlikely that they arise from artifacts. Although Glazer et al. [2] suggested that the different components were products of photodegradation, MacColl et al. [4] demonstrated by re-electrofocusing experiments that the occurrence of multiple forms was not artifactual. Mörschel and Wehrmeyer [7] also found that re-electrofocusing did not produce any new bands and gave consistently reproducibly results. In this study all stages were kept in the dark and where possible were performed at 4°C. In addition SDS gel electrophoresis of samples 11 days old (stored at −22°C in the dark) gave no additional bands when compared to fresh material.

The modification to several isoproteins which is typical for biliproteins might be important for molecule organization and alignment as well as light harvesting and energy transfer. However, in this and all previous studies, the spectral properties of the various isoproteins are so similar that none bridges the energy gap between the biliprotein fluorescence and the principal red absorbance band of chlorophyll *a*. This is in marked contrast to the situation in the phycobilisome [10,11], where not only are different phycobiliproteins present, but their individual spectral properties are modified by colourless spacer proteins ensuring small, directed, energy transfer steps between the chromophores. If charge isomers of cryptomonad phycobiliproteins are of significance in energy transfer to the intrinsic chlorophyll-proteins of the thylakoids, then this can only be in conjunction with as yet unknown colourless soluble proteins, interaction with thylakoid proteins adjoining the lumen, or perhaps simply as a result of concentration effects. We calculate that the concentration of phycoerythrin within the thylakoid lumen in *Chroomonas* CS24 is 100-times greater than that used for obtaining absorbance spectra and 1000-times greater than that for fluorescence measurements [12].

Acknowledgements

This work was supported by research grants from Macquarie University and by the Australian Research Grants Commission (No. D27915708). We gratefully acknowledge the assistance of Jon Jenkins with isoelectric focusing.

References

1 Gantt, E. (1979) in Biochemistry and Physiology of Protozoa (2nd Edn.) (Levandowsky, M. and Hunter, S.H., eds.), Vol. 1, pp. 121–137, Academic Press, New York

2 Glazer, A.N., Cohen-Bazire, G. and Stanier, R.Y. (1971) Arch. Microbiol. 80, 1–18

3 Brooks, C. and Gantt, E. (1973) Arch. Microbiol. 88, 193–204

4 MacColl, R., Habig, W. and Berns, D.S. (1973) J. Biol. Chem. 248, 7080–7086

5 Glazer, A.N. and Cohen-Bazire, G. (1975) Arch. Microbiol. 104, 29–32

6 Mörschel, E. and Wehrmeyer, W. (1975) Arch. Microbiol. 105, 153–158

7 Mörschel, E. and Wehrmeyer, W. (1977) Arch. Microbiol. 113, 83–89

8 Martin, C.D. and Hiller, R.G. (1987) Biochim. Biophys. Acta 923, 88–97

9 O'hEocha, C., O'Carra, P. and Mitchell, D. (1964) Proc. R. Ir. Acad. Sect. B63, 191–200

10 Gantt, E. (1981) Annu. Rev. Plant Physiol. 32, 27–47

11 Glazer, A.N. (1984) Biochim. Biophys. Acta 768, 29–51

12 Martin, C.D. (1985) M.Sc. thesis, Macquarie University, N.S.W., Australia

Biochimica et Biophysica Acta 923 (1987) 103–108
Elsevier

BBA 22479

The metabolism of deoxyguanosine in mitochondria: a characterization of the phosphorylation process which occurs in intact mitochondria

Linda F. Watkins and Roger A. Lewis

Department of Biochemistry, University of Nevada, Reno, NV 89557 (U.S.A.)

(Received 18 July 1986)

Key words: Deoxyguanosine, Mitochondrion; Deoxynucleoside metabolism

Isolated, intact mitochondria were evaluated for their ability to phosphorylate deoxyguanosine. This activity was stimulated by exogenous ATP, substrates for oxidative phosphorylation or added inorganic phosphate. Inhibitors of oxidative phosphorylation lowered the levels of deoxyguanosine phosphorylation. From a Hanes plot, an apparent K_m of 0.83 μM deoxyguanosine was calculated for the phosphorylation activity in intact mitochondria. In the presence of a 20-fold excess of added deoxynucleosides, none of those tested were strongly inhibitory. However, added UDP and dTDP were stimulatory and dGTP and dGDP were inhibitory to the phosphorylation of deoxyguanosine. These data show that mitochondria phosphorylate deoxyguanosine and that the process is regulated by other events which take place within the organelle.

Introduction

It is now well established that the mitochondrion is the locus for the biosynthesis of its DNA. Furthermore, this organelle has been shown to contain a variety of enzymes important for the biosynthesis of the dNTPs which serve as immediate precursors to the mitochondrial genome [1–4]. Mitochondrial pools of dTTP and dGTP have been shown to be distinct from those of the cytoplasm [5,6], suggesting that the organelle possesses the ability to provide precursors for its own DNA synthesis and may not rely on cytoplasmic sources.

Exogenous dNTPs serve in vitro as mitochondrial DNA precursors [7,8]. The mechanism by which these metabolites are incorporated into the mitochondria has not been reported; thus, it is not known whether these molecules are transported as the triphosphate derivative or whether they are metabolized to another chemical form prior to the transport process. We have reported that at least one deoxynucleoside, deoxyguanosine, is transported across the mitochondrial membrane barrier by a carrier-mediated process [9].

Fabianowska-Majewska and Greger [3] showed that rat liver mitochondria have the ability to phosphorylate the four common deoxynucleosides, including deoxyguanosine. Deoxyguanosine kinase activity was inhibited by thymidine, deoxycytidine and deoxyadenosine and was stimulated by dTDP, dTTP and dATP. dGTP was a potent inhibitor. Calf thymus mitochondrial deoxyguanosine kinase isolated by Gower et al. [4] was strongly inhibited by dGTP, dGDP and dITP and activated by dCDP, dTDP, dTTP, UDP and UTP. Thus, mitochondrial deoxyguanosine metabolism appears to be a highly regulated process.

Abbreviations. Hepes, 4-(2-hydroxyethyl)-1-piperazineethanesulfonic acid; Mops, 4-morpholinepropanesulfonic acid; DNP, 2,4-dinitrophenol.

Correspondence: Dr R A Lewis, Department of Biochemistry, University of Nevada, Reno, NV 89557, U.S.A

0304-4165/87/$03.50 © 1987 Elsevier Science Publishers B.V. (Biomedical Division)

Our laboratory is interested in the metabolism of deoxyguanosine in intact mitochondria. In previous reports [9,10] it was shown that mitochondria take up deoxyguanosine by a carrier-mediated process which requires the hydrolysis of ATP and a functional electron transport chain. The process appears to be controlled by other nucleotides, particularly ADP. The present study extends our understanding of mitochondrial deoxyguanosine metabolism by characterizing the phosphorylation of deoxyguanosine in intact rat liver mitochondria.

Materials and Methods

Mitochondria isolation

The differential centrifugation method of Chappell and Hansford [11] was used to isolate mitochondria from Long Evans rat liver. Homogenization buffer contained 250 mM sucrose, 30 mM Hepes (pH 7.4), 0.5% defatted bovine serum albumin, 1 mM EGTA; isolation buffer contained 250 mM sucrose, 5 mM Hepes (pH 7.4), 0.1 mM EGTA; final rinse buffer contained 150 mM KCl, 5 mM Hepes (pH 7.4), 0.1 mM EGTA. Each step of the isolation was conducted at 4°C. The tissue was minced in isolation buffer and after rinsing the tissue once with homogenization buffer the tissue was homogenized with a Dounce homogenizer. The supernatant produced by centrifugation at 700 × *g* for 10 min was recentrifuged at 12000 × *g* for 10 min. The resulting pellet was resuspended in the same buffer and the process was repeated one time. This pellet was mixed with a small amount of the final KCl buffer and centrifuged at 18700 × *g* for 10 min. The pellet was suspended in a volume of approximately 3 ml of the KCl final rinse buffer. Respiratory control ratios for glutamate, malate and ADP were routinely measured to be 5–7.

Phosphorylation assay

Phosphorylation of deoxyguanosine was assayed in a buffer that contained 100 mM KCl, 75 mM sucrose, 5 mM KH_2PO_4, 5 mM Hepes (pH 7.0). When Mops and Tris were substituted for Hepes the uptake activity was essentially the same. The concentration of deoxyguanosine (typically 5–60 μM [^{3}H]dG) and other additions are indicated in the figure legends. Assay mixture (100 μl) was warmed to 37°C and the assay was started by the addition of 25 μl of mitochondria (final concentration equals 0.3–0.5 mg protein/125 μl assay volume). Mitochondria were incubated at 37°C for various time periods as noted. The rate of phosphorylation was linear for at least 10 min and over the range of mitochondrial protein used. The phosphorylation reactions were stopped by the addition of 150 μl of cold ethanol and the assay tubes were immediately placed on ice prior to spotting on strips of PEI cellulose TLC plates. To remove unreacted substrate, the plates were rinsed with 0.1 mM ammonium acetate and then with water. After three washes of each solvent, the strips were dried and the sample spots were put into scintillation vials containing toluene-based scintillation fluor and quantified by standard scintillation techniques. Reported data are the average of four to six replicates per experiment and each experiment was repeated at least three times.

Results

Initial experiments were designed to test the influence of inorganic phosphate on deoxyguanosine phosphorylation. Rates of phosphorylation were measured in two separate buffers and as a function of added phosphate. It is seen in Table I that exogenous phosphate stimulated the phosphorylation process approximately 100%. As a result of these data, all further reactions were carried out in the presence of phosphate.

TABLE I

THE EFFECT OF PHOSPHATE ON DEOXYGUANOSINE PHOSPHORYLATION ACTIVITY IN MITOCHONDRIA

The concentration of deoxyguanosine was 60 μM and samples were incubated for 10 min.

Buffer (pH 7 0)	Specific activity (pmol product formed/ min per mg protein)
150 mM KCl, 75 mM Tris	210
150 mM KCl, 75 mM Tris, 10 mM KH_2PO_4	395
250 mM sucrose, 75 mM Tris	134
250 mM sucrose, 75 mM Tris, 10 mM KH_2PO_4	393

TABLE II

THE EFFECT OF EXOGENOUS ATP ON DEOXYGUANOSINE PHOSPHORYLATION

The activity was assayed with 10 μM deoxyguanosine. Incubation was for 8 min.

Substrate	Specific activity (pmol product formed/min per mg protein)	Activity (%)
None	72.97±2.73	100
1 mM ATP	94.23±0.90	129
10 mM ATP	101.90±3.77	140
1 mM ATP, 0.01 mM Mg^{2+}	97.94±0.74	134
10 mM ATP, 0.01 mM Mg^{2+}	110.56±3.09	152

Since phosphorylation of deoxyguanosine is known to require ATP, either in a direct or indirect manner, the influence of this compound was tested. Table II shows that added ATP significantly enhanced the phosphorylation of deoxyguanosine, either with or without added Mg^{2+}. Stimulation commonly varied between 115% and 150% of the control. The reason for this range of activities is not known, but it may be due to factors which influence deoxyguanosine metabolism but which vary in concentration as mitochondria are isolated at differing times. Possible factors include endogenous ATP, ADP, inorganic phosphate or precursors to the electron transport chain.

Table III compares the influence of exogenous MgATP, MgADP and MgADP/succinate/malate on the phosphorylating activity. In the presence of added phosphate, these additions made only small changes in the phosphorylation of deoxyguanosine. However, in the absence of exogenous phosphate, all three additions greatly stimulated the response. The stimulation appears to be one in which a diminished value in the absence of phosphate was restored to values measured in the presence of phosphate. These data show the importance of phosphate and/or a high energy nucleotide in the phosphorylation process and suggest that oxidative phosphorylation or its products are important for the phosphorylation of deoxyguanosine.

To support that concept, the phosphorylation of deoxyguanosine was measured in the presence and absence of inhibitors of oxidative phosphorylation (Table IV). In all cases, DNP and antimycin A inhibited dG phosphorylation, indicating that electron transport is important for the phosphorylation of deoxyguanosine. KCN was also inhibitory, but its effect in the presence of ADP/succinate/malate were less than that in the absence of these substrates. Oligomycin and atractyloside were inhibitory in all cases except when both phosphate was present and ADP/succinate/malate were absent. Atractyloside inhibition was more intense in the presence of ADP/succinate/malate, suggesting the importance of the transport

TABLE III

THE EFFECT OF EXOGENOUS ENERGY SOURCES IN THE ABSENCE AND PRESENCE OF P_i ON PHOSPHORYLATION ACTIVITY

Phosphorylation activity was assayed for 10 min with 50 μM deoxyguanosine. When present, phosphate (P_i) was added at a concentration of 10 mM.

Substrate	Specific activity (pmol product formed/min per mg protein)		Activity (%)		
	$+P_i$	$-P_i$	$+P_i$	$-P_i$	$+P_i/-P_i$ [a]
None	8.57±0.47	3.16±0.32	100	100	271
10 mM MgATP	9.73±0.09	8.96±1.69	114	284	109
10 mM MgADP	6.86±0.59	7.05±0.29	80	223	97
10 mM MgADP/ 5 mM succinate/ 1 mM malate	7.27±1.28	6.08±0.38	85	192	120

[a] $+P_i/-P_i$ represents the ratio of the activity measured in the presence of phosphate to that measured in the absence of phosphate, times 100.

TABLE IV

THE EFFECT OF INHIBITORS OF OXIDATIVE PHOSPHORYLATION ON DEOXYGUANOSINE PHOSPHORYLATION IN THE PRESENCE AND ABSENCE OF PHOSPHATE

The incubation buffers contained 50 μM deoxyguanosine and phosphorylation activity was assayed for 10 min

Additions	Activity (%)			
	no oxidative phosphorylation substrates		plus oxidative phosphorylation substrates	
	$-P_i$	$+P_i$	$-P_i$	$+P_i$
None	100 [a]	100 [b]	100 [c]	100 [d]
10 mM KCN	24	67	89	73
5 mM DNP	13	10	4	13
0.7 μg oligomycin	65	108	21	61
1 μg antimycin A	19	30	25	18
3 μM atractyloside	63	95	36	22

[a] 150 mM KCl, 75 mM Tris (pH 7.0).

[b] 150 mM KCl, 75 mM Tris (pH 7.0), 10 mM KH_2PO_4

[c] 150 mM KCl, 75 mM Tris (pH 7.0), 10 mM MgADP, 5 mM succinate, 1 mM malate.

[d] 150 mM KCl, 75 mM Tris (pH 7.0), 10 mM MgADP, 5 mM succinate, 1 mM malate, 10 mM KH_2PO_4

of ADP/ATP across the mitochondrial membrane. Collectively, these data show that inhibitors of oxidative phosphorylation block the phosphorylation of deoxyguanosine.

Kinetic data for phosphorylation activity are shown in Fig. 1 as a substrate saturation curve. From a Hanes plot of these data the following kinetic constants were calculated: K_m (apparent) = 0.83 μM deoxyguanosine, V_{max} = 91 pmol product formed/min per mg protein.

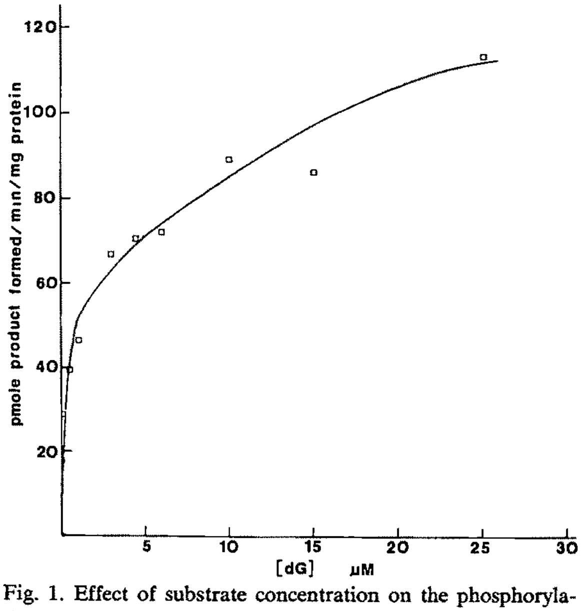

Fig. 1. Effect of substrate concentration on the phosphorylation of deoxyguanosine. Assay buffer contained 100 mM KCl, 75 mM sucrose, 10 mM Hepes (pH 7.0), 5 mM KH_2PO_4, 1 mM ATP, 1 mM malate and 5 mM glutamate. Incubation was for 10 min at 37°C

In order to test the influence of other nucleosides on deoxyguanosine phosphorylation, their competition with deoxyguanosine was measured under a variety of reaction conditions. Table V shows that under all conditions tested, there was very little inhibition of deoxyguanosine phosphorylation caused by a 20-fold excess of added nucleosides. In the presence of added ATP, deoxyadenosine and deoxycytidine were weakly inhibitory. However, in the presence of ADP/succinate/malate, deoxyadenosine and deoxycytidine slightly stimulated, but deoxyinosine and guanosine weakly inhibited the phosphorylation of deoxyguanosine.

Deoxyguanosine kinase activity has been reported to be affected by several nucleotides including dGTP and dGDP, which are known inhibitors of the isolated enzyme. Conversely, dTTP, dTDP and UDP are known to be stimulatory to this catalytic activity [4]. Table VI shows the response of added nucleotides on the phosphorylation of deoxyguanosine in intact mitochondria. Since the ratio of ATP/added nucleotide is 18/1, the influence of added nucleotide is probably not due to simple competition with ATP as a phos-

TABLE V

THE EFFECT OF NUCLEOSIDES ON DEOXYGUANOSINE PHOSPHORYLATION

Phosphorylation was assayed for 10 min in a buffer containing 10 μM deoxyguanosine. All nucleosides were added at a concentration of 200 μM.

Nucleoside	Specific activity (pmol product formed/ min per mg protein)	Activity (%)
A. No addition		
no added dN	18.24±2.83	100
dA	20.66±0.73	113
dI	14.65±5.40	80
dC	18.60±2.03	102
dT	16.48±0.37	90
guanosine	18.31±5.18	100
B. 1 mM ATP		
no added dN	25.85±2.25	100
dA	17.27±0.91	67
dI	19.15±5.28	74
dC	17.68±0.37	68
dT	19.05±2.51	74
guanosine	21.78±0.16	84
C. 1 mM ADP		
no added dN	16.43±0.06	100
dA	15.21±0.67	93
dI	17.51±0.45	107
dC	20.60±1.24	125
dT	15.52±0.78	94
guanosine	14.84±3.42	90
D. 1 mM ADP, 5 mM succinate, 1 mM malate		
no added dN	18.72±0.88	100
dA	24.54±0.33	131
dI	14.01±2.27	75
dC	23.00±2.44	123
dT	17.95±1.40	96
guanosine	13.96±2.47	75

phate donor. The data show that UDP and dTDP were stimulatory, but dGTP and dGDP were inhibitory. These data correlate well with that observed with the isolated deoxyguanosine kinase activity.

Discussion

Phosphorylation of deoxyguanosine in rat liver mitochondria appears to be a process which is interrelated with other functions of the organelle. This conclusion is supported by a variety of experimental observations, including: (i) inorganic phosphate or ATP stimulates the reaction, (ii) inhibitors of oxidative phosphorylation block the phosphorylation of deoxyguanosine, and (iii) the addition of various nucleotides modifies the phosphorylation activity.

TABLE VI

THE EFFECT OF NUCLEOTIDES ON DEOXYGUANOSINE PHOSPHORYLATION IN INTACT MITOCHONDRIA

The phosphorylation of deoxyguanosine was assayed in a buffer containing 12.5 mM MgATP, 22 μM deoxyguanosine, and 0.7 mM of added nucleotide. Incubation was for 10 min

Nucleotide	Specific activity (pmol product formed /min per mg protein)	Activity (%)
None	21.47±2.76	100
dTTP	22.49±2.67	105
dTDP	37.12±2.37	173
dATP	18.65±1.77	87
dCTP	19.89±0.67	93
dGTP	15.22±0.63	71
dGDP	13.69±1.73	64
UDP	35.73±2.44	166

A wide variety of inhibitors of oxidative phosphorylation also inhibited deoxyguanosine phosphorylation. Inhibition of deoxyguanosine phosphorylation was strongest in the absence of added substrates for electron transport, especially without exogenous P_i. With the additions of substrates of oxidative phosphorylation, some of the inhibitors of oxidative phosphorylation became less potent as agents against deoxyguanosine phosphorylation. Only DNP and antimycin A showed a consistent degree of inhibition. Neither of these two compounds block the phosphorylation of deoxyguanosine when assayed with protein extracts prepared from mitochondria, so their action can not be attributed directly to the blocking of the deoxyguanosine phosphorylating enzymes (data not shown).

With frozen mitochondria, ADP serves well as a source of energy for the phosphorylation of deoxyguanosine (data not shown). Presumably, mitochondrial deoxyguanosine kinase uses ATP formed from the action of mitochondrial adenylate kinase on the added ADP. When the influence of atractyloside was tested with intact mitochondria which were supplemented with ADP, the drug blocked deoxyguanosine phosphorylation. Since atractyloside is known to block the transport of ADP into and ATP out of the mitochondria, these data reveal that the phosphorylation activity for deoxyguanosine is located within the matrix. Further indication of the matrix location of deoxyguanosine phosphorylating activity was shown by the observation that ADP was inhibitory to the phosphorylation of deoxyguanosine when intact mitochondria were used, whereas with fractured organelles, ADP supported deoxyguanosine phosphorylation. If the phosphorylating activity was in the inner membrane space, ATP formed by adenylate kinase would have supported deoxyguanosine kinase activity, as it did in fractured mitochondria. This latter conclusion is consistent with a separate report [9] in which it was shown that deoxyguanosine is taken up and sequestered by mitochondria.

UDP and dTDP were observed to stimulate the phosphorylation of deoxyguanosine. It was previously reported that these two nucleotides stimulate mitochondrial deoxyguanosine kinase activity when assayed in partially purified preparations [4]. Likewise, there is a correlation between the inhibition observed by dGTP and dGDP as documented in this study and that seen with isolated deoxyguanosine kinase [4]. These data suggest that the phosporylation of deoxyguanosine in mitochondria is a process regulated by other pathways of nucleotide metabolism.

When intact mitochondria were used in the absence of added ATP or other sources of energy, little inhibition was observed when competing nucleotides were added at a 20 : 1 ratio. Thus, the phosphorylation of deoxyguanosine in the intact organelle appears to be relatively specific for that substrate. However, approximately 30% inhibition was measured for deoxyadenosine, deoxycytidine and deoxythymidine, when ATP was added as an energy source. About the same degree of inhibition was observed for deoxyinosine and guanosine when ADP/succinate/malate were added as energy sources. Given the concentration of added nucleoside this degree of inhibition may not be highly significant; however, it is possible that any one of a variety of phosphorylated products of these nucleosides may be causing the slightly inhibitory effects.

Acknowledgement

This research is a contribution of the Nevada Agricultural Experimental Station.

References

1 Cheng, Y , Domin, B and Lee, L (1977) Biochim. Biophys. Acta 481, 481–492

2 Leung, W., Dubbs, D R , Trukula, D. and Kit, S. (1975) J. Virol. 16, 486–497

3 Fabianowska-Majewska, K. and Gregor, J. (1982) Enzyme 27, 124–129

4 Gower, W.R., Jr., Carr, M C. and Ives, D H. (1979) J. Biol. Chem. 254, 2180–2183

5 Berk, A J. and Clayton, D.A (1973) J Biol. Chem. 248, 2722–2729

6 Bestwick, R.K., Moffet, G L. and Mathews, C.I.C. (1982) J. Biol. Chem. 257, 9300–9304

7 Parsons, P. ad Simpson, M.V (1973) J Biol. Chem. 248, 1912–1919

8 Mitra, R S. and Bernstein, I.A. (1970) J. Biol Chem. 245, 1255–1260

9 Watkins, L.F. and Lewis, R.A. (1985) Pediatr Res. 19, 781

10 Watkins, L.F. and Lewis, R.A. (1985) Fed. Proc. 44, 1598

11 Chappell, J.B. ad Hansford, R.G. (1972) in Subcellular Components: Preparations and Fractionation (Birnie, G.D , ed), 2nd Edn., Butterworth and Co., London.

Biochimica et Biophysica Acta 923 (1987) 109–115
Elsevier

BBA 22445

Stabilization of phosphofructokinase with sugars during freeze-drying: characterization of enhanced protection in the presence of divalent cations

John F. Carpenter, Lois M. Crowe and John H. Crowe

Department of Zoology, University of California, Davis, CA 95616 (U.S.A.)

(Received 22 August 1986)

Key words: Freeze-drying; Phosphofructokinase; Enzyme stabilization; Divalent cation; Disaccharide, (Sugar/transition metal synergism)

Phosphofructokinase purified from rabbit skeletal muscle is fully inactivated after freeze-drying and dissolution. The addition of trehalose or maltose to the enzyme solution prior to freeze-drying results in a recovery of up to 80% of the original activity. Slightly less stabilization is imparted by sucrose, whereas glucose and galactose at concentrations up to 500 mM are relatively ineffective at protecting phosphofructokinase. Addition of ionic zinc to enzyme-sugar mixtures prior to freeze-drying greatly enhances the stabilization imparted by the above sugars. This effect is not simply due to the summation of the individual protective capacities of zinc and the sugar. Zinc alone affords no protection, but a high degree of stabilization is achieved when zinc is added to a sugar solution, even when the sugar is at a concentration at which, by itself, it is totally ineffective. In the presence of a constant sugar concentration (100 mM), freeze-dry stabilization of phosphofructokinase is increased as the concentration of zinc is increased. When the zinc concentration is held constant (0.9 mM) and the sugar concentration varied, the maximum stabilization is noted with less than 200 mM sugar. At higher solute concentrations the degree of enhancement decreases such that with 500 mM sugar the addition of zinc results in only a slight increase in protection. Several other organic solutes (proline, 4-hydroxyproline, glycine, trimethylamine *N*-oxide, glycerol and *myo*-inositol) that afford cryoprotection to phosphofructokinase, an effect enhanced by the addition of zinc, do not stabilize the enzyme during freeze-drying, even if zinc is present. The addition of ionic copper, cadmium, nickel, cobalt, calcium and manganese to trehalose-phosphofructokinase solutions prior to freeze-drying also increases the percentage of activity recovered after dissolution. Magnesium is ineffective in this respect.

Introduction

In the few instances in which the effects of freeze-drying on enzyme activity have been compared to those of freeze-thawing, it has been noted that the former treatment results in a greater degree of inactivation. For example, Hanafusa [1] found that freeze-thawing of catalase resulted in at most a 60% inactivation of the enzyme, while after freeze-drying and rehydration, only 13% of the original activity remained. An even more extreme situation exists with L-asparaginase, which is fully active after freeze-thawing, but which can be inactivated by over 80% during freeze-drying [2,3]. This loss of activity can be fully blocked by the addition of organic solutes such as glucose, mannose, sorbitol or ribose [3]. Similarly, catalase is stabilized during freeze-drying in the presence of sucrose, inositol, glycine or glutamate [1]. Al-

---

Abbreviation. Tricine, *N*-[2-hydroxy-1,1-bis(hydroxymethyl)-ethyl]glycine

Correspondence: Dr. John F Carpenter, Department of Zoology, University of California, Davis, CA 95616, U.S.A.

0304-4165/87/$03.50 © 1987 Elsevier Science Publishers B.V. (Biomedical Division)

though many of these compounds have been found to be effective cryoprotectants for enzymes [4–7], the only evidence that an organic solute could stabilize the same enzyme during both freeze-thawing and freeeze-drying is that noted for the effects of sucrose on catalase [1,4]. In order to determine whether protective agents are effective during both of these treatments, we initiated a study on the stabilization of phosphofructokinase (EC 2.7.1.11) during freeze-drying, using organic solutes that we have previously shown to be effective at protecting this enzyme during freeze-thawing [7]. Phosphofructokinase, purified from rabbit skeletal muscle, provides an excellent model system for these comparisons because it is fully and irreversibly inactivated during both of the perturbations noted above.

During our earlier study on cryoprotection of phosphofructokinase, we discovered that the presence of divalent cations (e.g., less than 1 mM Zn^{2+}) greatly enhanced the stabilization afforded by a diverse group of organic solutes, including sugars, polyhydroxyl alcohols, and free amino acids [7]. This synergistic stabilization was not due to the summation of the individual effects of the cation and organic solute because in many instances essentially all of the prefreezing activity was recovered after thawing, even though each component was at a concentration at which, by itself, it was completely ineffective. We were also interested in determining whether a similar cation-dependent enhancement of phosphofructokinase stabilization would be operative during freeze-drying. Therefore, in addition to our characterization of the stabilization of phosphofructokinase by organic solutes during freeze-drying, in the present paper we present results of our studies on the influence of divalent cations on this process.

Materials and Methods

Materials. Glycerol-3-phosphate dehydrogenase (rabbit muscle) and triose-phosphate isomerase (rabbit muscle) were products of Boehringer Mannheim. Phosphofructokinase (type II), aldolase (type I), 4-hydroxyproline, trimethylamine *N*-oxide, glycine and galactose were purchased from Sigma Chemical Co. Trehalose and maltose were obtained from Pfanstiehl Laboratories. Glycerol and sucrose were purchased from Mallinckrodt, and proline was supplied by Fluka AG.

Purification and assay of phosphofructokinase. Rabbit skeletal muscle phosphofructokinase, obtained commercially as a crystalline suspension in ammonium sulfate, was purified following the procedure described by Carpenter et al. [7]. Purified phosphofructokinase was concentrated by dialysis (4°C) in 70% ammonium sulfate prepared in 0.1 M sodium phosphate buffer (pH 8.0, 5 mM dithiothreitol, 1 mM EDTA), and was stored as a crystalline suspension at 4°C. The enzyme was used within 12 weeks following purification.

Phosphofructokinase activity was assayed at 25°C using the fructose 1,6-bisphosphate-coupled assay described by Bock and Frieden [8]. The 2.0 ml reaction mixture contained 42 mM Tris-acetate buffer (pH 8.0), 2 mM magnesium acetate, 2 mM ATP, 2 mM fructose 6-phosphate, 51 mM KCl, 5.1 mM NH_4Cl, 0.16 mM NADH, 400 μg aldolase, 20 μg triose-phosphate isomerase and 50 μg glycerol-3-phosphate dehydrogenase. Protein was assayed according to the method of Peterson [9].

Freeze-dry experiments. Prior to each experiment, phosphofructokinase was dialyzed (4°C) for several hours against 1 mM sodium borate buffer (pH 7.8 at 23°C) containing 25 mM K_2SO_4, 2 mM $(NH_4)_2SO_4$ and 5 mM dithiothreitol. To avoid complications due to enzyme adsorption to glass, all phases of the freeze-dry experiments were performed in polypropylene Eppendorf test tubes. A 7 μl aliquot of the enzyme stock was added to 80.5 μl of the appropriate solution of organic solute and divalent cation (prepared in the above buffer) to give a final phosphofructokinase concentration of 40 μg/ml and the desired solute and cation concentration. Samples were kept on ice (approx. 1–2 h) from the time they were prepared until catalytic activity was measured. After these determinations, all samples in a given experiment were frozen simultaneously by immersion in liquid nitrogen for 90 s. The frozen samples were then lyophilized for at least 20 h on a VirTis lyophilizer.

Dried samples were rehydrated in 5 mM dithiothreitol (pH 7.8 at 23°C), the volume was determined, and residual phosphofructokinase activity was assayed. The results are expressed as the percentage of prefreeze-dry activity recovered after dissolution, corrected for any differences between the volumes of rehydrated and pretreated samples.

Results

We initially characterized the influence of divalent cations on the stabilization afforded by organic solutes during freeze-drying by determining the percentage of phosphofructokinase activity recovered after the enzyme was freeze-dried in the presence of 100 mM trehalose and variable concentrations of $ZnSO_4$. The effect noted is attributed to zinc because the buffer already contains 27 mM sulfate. As seen in Fig. 1, with trehalose alone less than 13% of the original activity is recovered. The addition of $ZnSO_4$ to the trehalose solution results in a marked increase in enzyme stabilization such that with 0.4 mM and higher concentrations of $ZnSO_4$, more than 80% of the initial activity is retained after rehydration. In contrast, phosphofructokinase is completely inactivated when freeze-dried in the presence of up to 0.6 mM $ZnSO_4$ and no organic solute, and less than 2% of the prefreeze-dry activity remains when 1 mM $ZnSO_4$ is employed (Fig. 1). It should be noted that the acute sensitivity of phosphofructokinase to freeze-drying is not simply reflective of the buffer system chosen for this study because no activity is detected after freeze-drying in 10 mM sodium phosphate (pH 8.0, 5 mM dithiothreitol), and less than 5% of the original activity is recovered when 20 mM Tricine (pH 7.9, 5 mM dithiothreitol) or 100 mM sodium phosphate (pH 8.0, 5 mM dithiothreitol) buffers are used (data not shown).

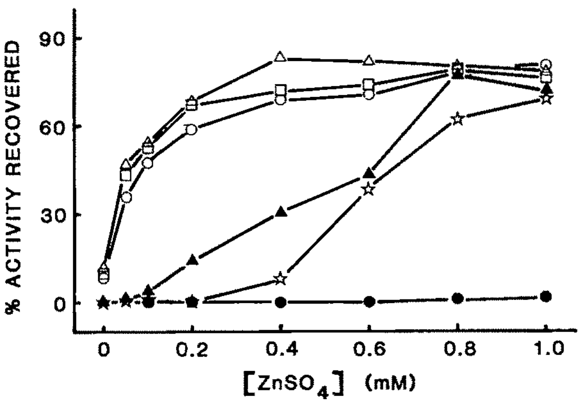

Fig. 1 The effect of $ZnSO_4$ on phosphofructokinase stabilization during freeze-drying. Percent activity recovered in 100 mM trehalose (△), maltose (□), sucrose (○), glucose (☆), galactose (▲), and with no organic solute present (●)

The synergistic enhancement of enzyme stabilization by zinc is not limited to trehalose. For example, strikingly similar results are seen when $ZnSO_4$ is added to solutions of maltose or sucrose (Fig. 1). In the presence of either disaccharide alone (100 mM), less than 10% of the original activity remains after freeze-drying. With the addition of 1 mM $ZnSO_4$, greater than 75% is recovered. In contrast, the two monosaccharides, galactose and glucose, at a concentration of 100 mM provide no stabilization without the addition of $ZnSO_4$, and higher concentrations of zinc are needed to achieve the same degree of enhanced enzyme preservation noted with the disaccharides. Finally, several other organic solutes (glycine, proline, 4-hydroxyproline, trimethylamine *N*-oxide, glycerol and *myo*-inositol), which afford a high degree of cryoprotection to phosphofructokinase in the presence of zinc [7], are essentially ineffective at preserving the enzyme during freeze-drying with or without added zinc (Table I).

In the next series of experiments, we determined the percentage of activity recovered as a function of sugar concentration both with and without $ZnSO_4$. With the disaccharides alone, there is generally an increased stabilization of phosphofructokinase as the sugar concentration is increased up to 500 mM (Fig. 2). The graphs for

TABLE I

PHOSPHOFRUCTOKINASE STABILIZATION DURING FREEZE-DRYING IN THE PRESENCE OF ORGANIC SOLUTES AND 0.9 mM $ZnSO_4$

Organic solute (100 mM)	Percent activity recovered [a]
Proline	2
4-Hydroxyproline	2
Glycine	5
Trimethylamine *N*-oxide	0
Glycerol	0
myo-Inositol	1

[a] When no $ZnSO_4$ was added, no activity was measurable

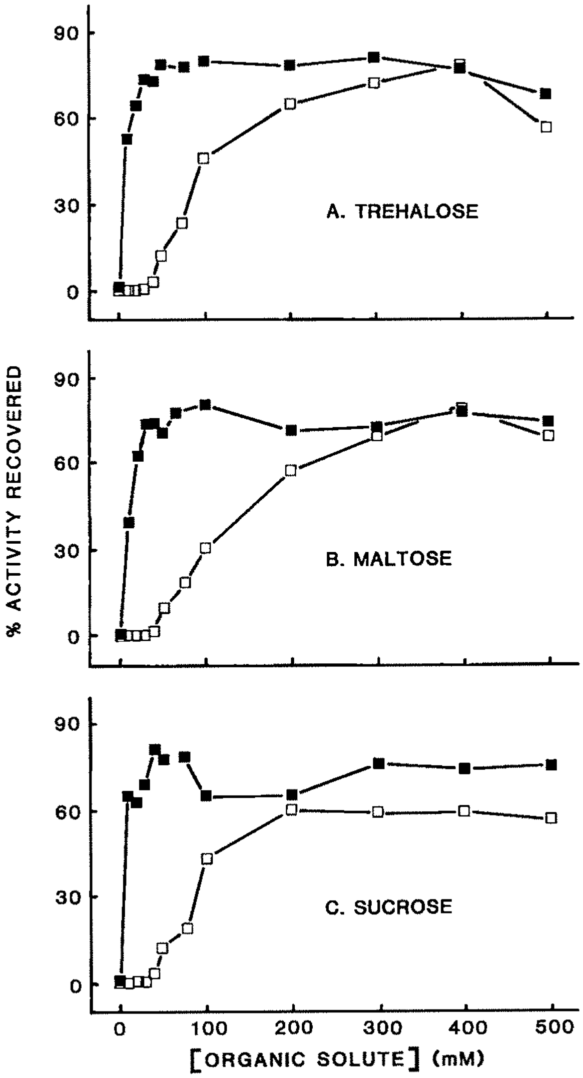

Fig. 2. Comparison of percentage of phosphofructokinase activity recovered after freeze-drying and dissolution in the presence of trehalose (A), maltose (B) and sucrose (C) alone (□) and with the addition of 0 9 mM $ZnSO_4$ (■)

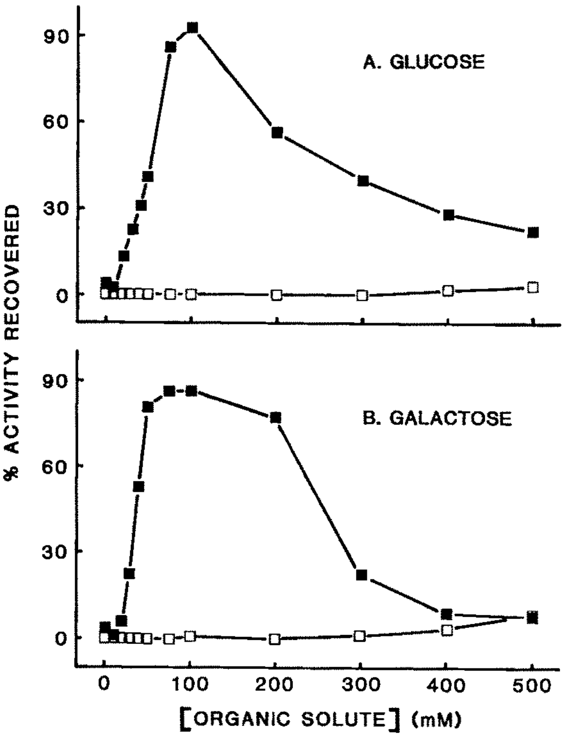

Fig. 3. Comparison of percentage of phosphofructokinase activity recovered after freeze-drying and dissolution in the presence of glucose (A) and galactose (B) alone (□) and with the addition of 0.9 mM $ZnSO_4$ (■).

trehalose and maltose are essentially superimposable, with greater than 70% of the prefreeze-dry activity remaining in 400 mM solutions (Fig. 2A, B). Similar results are seen for sucrose except that at most 60% is recovered and the stabilizing influence of the sugar reaches a maximum at a concentration of 200 mM (Fig. 2C). The monosaccharides, in contrast, were essentially ineffective at preserving phosphofructokinase (Fig. 3). No activity is recovered after freeze-drying in the presence of up to 300 mM glucose or galactose, and less than 5 and 10%, respectively, of the original activity is obtained with 500 mM solutions of these sugars.

When the above experiments are repeated with 0.9 mM $ZnSO_4$ present, a greater percentage of the initial activity is recovered (Figs. 2 and 3). With the disaccharides, the maximum degree of stabilization is seen at sugar concentrations of 100 mM or less (Fig. 2). At higher concentrations of trehalose and maltose, there is no further increase in activity recovered, and the values are similar to those obtained with the sugars alone (Fig. 2A, B). With sucrose, there is some enhancement of protection at concentrations above 200 mM, but it is not nearly as marked as that noted at lower concentrations (Fig. 2C). The most dramatic increase in stabilization in the presence of zinc is seen with the monosaccharides. At a 100 mM sugar concentration, greater than 85% and 90% of activity is recovered with galactose and glucose, respectively,

TABLE II

INFLUENCE OF DIVALENT CATIONS ON STABILIZATION OF PHOSPHOFRUCTOKINASE DURING FREEZE-DRYING IN THE PRESENCE OF 100 mM TREHALOSE

Salt added (0.9 mM)	Percent activity recovered [b]
None	13
$ZnSO_4$	75
$CuSO_4$	68
$NiCl_2$ [a]	51
$CoCl_2$ [a]	57
$MnSO_4$	21
$CaCl_2$	22
$MgSO_4$	16
$CdCl_2$ [a]	48

[a] Precipitate formed when the salt was added to the borate buffer

[b] In the absence of trehalose no activity was measurable except in the case of $CuSO_4$ (1% activity recovered).

even though the sugars alone afford no protection at this concentration (Fig. 3). As is seen with the disaccharides, there is a decreased degree of zinc-dependent enhancement at higher monosaccharide concentrations, which in this case results in a steep drop in recovered activity.

Finally, to ascertain whether the enhancement of enzyme preservation during freeze-drying was unique to zinc, the influence of other divalent cations on the stabilization afforded by 100 mM trehalose was tested. As shown in Table II, the addition of Cu^{2+}, Ni^{2+}, Co^{2+} and Cd^{2+} results in a substantial increase in the recovery of prefreeze-dry activity, whereas addition of Mn^{2+} and Ca^{2+} results in only a minimal increase in recovery, and Mg^{2+} has essentially no effect on enzyme stabilization. As is the case with Zn^{2+}, the above cations by themselves are ineffective at stabilizing phosphofructokinase against inactivation during freeze-drying.

Discussion

Rabbit muscle phosphofructokinase is completely inactivated after freeze-drying and dissolution, a characateristic that makes this enzyme especially suited for use in testing stabilizing compounds. Of the organic solutes that we compared in this role, disaccharides are the most effective at protecting phosphofructokinase against freeze-dry inactivation. Trehalose and maltose confer almost identical stability to phosphofructokinase and are somewhat better than sucrose in this respect. The similar effects of trehalose and maltose are not surprising because the only structural difference between these sugars is that the two α-D-glucose units are joined by a 1,1-glycosidic bond in trehalose and a 1,4-glycosidic bond in maltose. However, one might expect that a reducing sugar such as maltose would actually be detrimental to an enzyme's catalytic stability due to the propensity of reducing sugars to participate in protein browning via the Maillard reaction [10,11]. Since maltose is an effective stabilizer, it appears that in the short term experiments employed in the present study, protein browning does not contribute to alterations in phosphofructokinase catalytic activity.

This proposition is supported by the finding that at the highest concentrations tested, galactose and glucose, both of which are reducing sugars, do confer a slight degree of stabilization to phosphofructokinase. However, the protection afforded by glucose is much less than that noted for maltose and trehalose, even if the data are considered on the basis of equimolar amounts of glucose. These results indicate, as was the case with cryoprotection [7], that it is not just the type of sugar moiety present that is important for enzyme stabilization during freeze-drying, but that subunit orientation is also critical.

It is interesting that sugars, which are effective at stabilizing enzymes during freeze-thawing [7] or freeze-drying, are also known to stabilize the native structure of globular proteins in aqueous solution. For example, in the presence of 50% (w/w) sucrose or maltose the temperature of maximum rate of denaturation for ovalbumin is increased from 77°C to over 87°C [12]. Timasheff and colleagues [13–15] have determined that such stabilization is due to the preferential exclusion of the structure-stabilizing compounds from contact with the protein surface. That is, the protein is preferentially hydrated. Thus, as these authors explain, the addition of these compounds to an aqueous protein solution is thermodynamically unfavorable since it would serve to increase the chemical potentials of both protein and the additive. Protein structure is stabilized because denaturation of the protein molecule would lead to a greater contact surface between protein and solvent, and, therefore, augment this unfavorable effect.

Of course, it is not known whether the stabilization imparted by sugars in solution is translated by the same mechanism into stability during freeze-drying. If this were the case, then one would expect that glycerol would protect phosphofructokinase, since this compound has been shown to impart structural stability to proteins in solution by the same mechanism described above for sugars [16,17]. Also, it seems unlikely that the thermodynamic arguments presented above would be applicable to lyophilized proteins since water is removed from the system and 'concentrations' of nonvolatile solutes increase, essentially, to infinity.

Under these conditions, initial molarities would appear to have no meaning. However, the pre-freeze-dry concentration of sugar seems to be important in terms of the degree of stabilization imparted to dried phosphofructokinase since there is an increase in the amount of activity recovered when the enzyme is prepared in increasing concentrations of sugar. These results could imply that the final mole or mass ratio of sugar to protein in the dried sample is the limiting factor determining the degree of stabilization; we have found this to be the case for preservation of dried biological membranes and artificial lipid bilayers by sugars [18–20]. However, when the amount of protein in a sample is decreased to 25 μg/ml and the sugar concentration is held constant (a situation which increases the ratio of sugar to protein), less enzyme activity is recovered than when the enzyme is present at 40 μg/ml. For example, after freeze-drying in 200 mM trehalose 34 and 64% activity is recovered, respectively, with 25 and 40 μg/ml phosphofructokinase (unpublished observations).

The finding that other organic solutes (e.g., trimethylamine *N*-oxide) that stabilize active protein conformations in solution [21], as well as protect phosphofructokinase during freeze-thawing [7], also are ineffective at preserving phosphofructokinase activity during freeze-drying supports the contention that removal of water from a protein preparation can be more disruptive to enzyme function than freeze-thawing or thermally induced perturbations [1,2]. Further support for this position comes from our results on the influence of transition metals on phosphofructokinase preservation. We have previously shown that certain organic solutes (e.g., glycerol, inositol and glycine), which offer minimal cryoprotection even at concentrations as high as 0.5 M, when combined with Zn^{2+} almost fully preserve phosphofructokinase during freeze-thawing [7]. Although similar results were noted during our freeze-drying experiments with glucose and galactose (Fig. 3), even with the addition of Zn^{2+}, glycerol, inositol and glycine afforded virtually no protection to lyophilized phosphofructokinase.

As was the case with freeze-thawing, the increased preservation noted with zinc ion during freeze-drying is clearly not due to the summation of the individual effects of the sugars and zinc; zinc alone (0.9 mM) affords no protection to phosphofructokinase during freeze-drying, but when this cation is added to a sugar solution, at a concentration that is also ineffective at preserving phosphofructokinase, a great degree of stbilization is seen (Figs. 2 and 3). It might be suggested that this influence of zinc is specific to kinases because of the role that divalent cations play in catalysis by this category of enzymes. This appears not to be the case because Mg^{2+}, which is a cofactor and a potent activator of phosphofructokinase [22], does not provide any enhancement of stabilization of phosphofructokinase during freeze-drying (Table II).

However, several other cations tested are effective at increasing the phosphofructokinase activity recovered when the enzyme is frozen and dried in the presence of trehalose. These results can only be used to discern whether or not a given cation enhances stabilization. It is not possible to rank the cations according to their relative effectiveness because of their different solubilities in borate buffer (Table II). Even solutions of zinc and copper, in which no precipitate is visible, contain very low concentrations of free cation at pH 7.8. The maximum solubility of Zn^{2+} at pH 7.8 is less than 40 μM, and Cu^{2+} is almost four orders of magnitude less soluble [23]. It is presently not known which ionic species is responsible for the enhancement of the stabilization provided by sugars. Speculatively, it would seem that the free divalent ion is not critical because increased protection is seen as the $ZnSO_4$ concentration is increased up to 1 mM, a concentration that far exceeds the solubility of Zn^{2+}.

However, testing this suggestion is dependent on determining the mechanism by which cations alter the capacity of sugars to stabilize proteins during freeze-drying. Another perplexing question raised by the phenomenological results of the present study is: why are so many organic solutes, either alone or in concert with zinc, that afford cryoprotection to phosphofructokinase [7] virtually ineffective at preserving the enzyme during freeze-drying? Mechanistic studies are currently under way in our laboratory to address these sorts of question in an attempt to determine the manner in which cations influence the stabilization of enzymes under dehydration and freezing stresses and also to further understand the means by which organic solutes in general are effective as protein stabilizers during these treatments.

In closing, we point out that previous studies from this laboratory on preservation of freeze-dried membranes [18] and of phosholipid bilayers [19,20] by sugars, particularly trehalose, were conducted in the absence of Zn^{2+}. Thus, unlike the case for proteins, preservation of membranes does not require Zn^{2+}. Further, preservation of phospholipid bilayers has considerably greater specificity for the sugars tested [19,20] than that seen with proteins, which suggests that the mechanisms by which proteins and membranes are preserved by sugars is dissimilar.

Acknowledgment

We thank the National Science Foundation for support through grant DMB 85-18194.

References

1 Hanafusa, N. (1969) in Freezing and Drying of Microorganisms (Nei, T., ed), pp. 117–129, University Park Press, Baltimore

2 Marborough, D.I., Miller, D.S. and Cammack, K.A. (1975) Biochim. Biophys. Acta 386, 576–589

3 Hellman, K., Miller, D.S. and Cammack, K.A. (1983) Biochim. Biophys. Acta 749, 133–142

4 Shikama, K. and Yamazaki, I. (1961) Nature 190, 83–84

5 Chilson, O.P, Costello, L.A. and Kaplan, N.O. (1965) Fed. Proc. 24, S55–65

6 Brands, J.F, Fu, J. and Nordin, J.H. (1970) in The Frozen Cell (Wolstenholme, G.E.W. and O'Conner, M., eds), pp 189–212, J & A Churchill, London

7 Carpenter, J.F., Hand, S.C., Crowe, L.M and Crowe, J.H. (1986) Arch. Biochem. Biophys. 250, 505–512

8 Bock, P.E and Frieden, C. (1974) Biochemistry 13, 4191–4196

9 Peterson, G.L. (1977) Anal. Biochem 83, 346–356

10 Feeney, R.E., Blankehorn, G. and Dixon, H B.F. (1975) Adv. Protein Chem. 29, 135–203

11 Loomis, S.H, O'Dell, S.J. and Crowe, J H (1979) J. Exp. Zool. 208, 355–360

12 Back, J F, Oakenfull, D. and Smith, M.B. (1979) Biochemistry 18, 5191–5196

13 Timasheff, S.N., Lee, J.C., Pittz, E P. and Tweedy, N. (1976) J Colloid Interface Sci 55, 658–663

14 Arakawa, T. and Timasheff, S.N. (1982) Biochemistry 21, 6536–6544

15 Timasheff, S.N. (1982) in Biophysics of Water (Franks, F. and Mathias, S.F., eds.), pp. 70–72, Wiley, New York

16 Gekko, K. and Timasheff, S.N. (1981) Biochemistry 20, 4667–4676

17 Gekko, K and Timasheff, S.N. (1981) Biochemistry 20, 4677–4686

18 Crowe, J.H., Crowe, L.M. and Jackson, S.A. (1983) Arch Biochem. Biophys. 220, 477–484

19 Womersley, C., Uster, P S, Rudolph, A.S and Crowe, J.H. (1986) Cryobiology 23, 245–255

20 Crowe, L.M., Womersley, C., Crowe, J.H, Reid, D., Appel, L and Rudolph, A. (1986) Biochim. Biophys. Acta 861, 131–140

21 Hand, S.C. and Somero, G.N. (1982) J. Biol Chem. 257, 734–741

22 Hofer, H.W. and Pette, D. (1968) Hoppe-Seyler, Z. Physiol. Chem. 349, 1378–1392

23 Sillen, L.G. and Martell, A.E. (1964) Stability Constants of Metal-Ion Complexes, Special Publ No. 17, The Chemical Society, London

Biochimica et Biophysica Acta 923 (1987) 116–124
Elsevier

BBA 22385

Purification and partial characterization of cellular retinoic acid-binding protein from human placenta

Masataka Okuno [a], Michimasa Kato [b], Hisataka Moriwaki [a],
Masamitsu Kanai [c] and Yasutoshi Muto [a]

[a] *First Department of Internal Medicine, Gifu University School of Medicine, 40 Tsukasa-machi, Gifu 500,*
[b] *Department of Legal Medicine and*
[c] *Department of Laboratory Medicine, Shinshu University School of Medicine, 3 Asahi-machi, Matsumoto 390 (Japan)*

(Received 26 September 1986)

Key words: Cellular retinoic acid-binding protein; Cellular retinol-binding protein,
Retinoic acid; Retinol; (Human placenta)

Cellular retinoic acid-binding protein (CRABP) has been purified to homogeneity from human placenta by a series of procedures, including acetone powder extraction, gel filtration on Sephadex G-50, and ion-exchange chromatography on DEAE-cellulose and on SP-Sephadex. Cellular retinol-binding protein (CRBP) was isolated concurrently. CRABP was purified 75400-fold, based on total soluble acetone powder extract of placenta. The protein is a single polypeptide chain with a molecular mass of 14600 Da, estimated by sodium dodecyl sulfate (SDS) gel electrophoresis or gel filtration, and has an isoelectric point of 4.78 (apo-CRABP, 4.82). On analysis of absorption and fluorescence spectra, the protein was seen to exhibit an absorption peak at 350 nm, fluorescence excitation maxima at 350 and 370 nm, and a fluorescence emission maximum at 475 nm. Human CRABP was immunologically distinct from human CRBP and serum retinol-binding protein.

Introduction

Retinoic acid is a naturally occurring metabolite of vitamin A (retinol) that can maintain the growth and regulate the differentiation of normal and transformed cells [1,2]. It is well documented that specific binding proteins for retinol and/or for retinoic acid exist in the intracellular compartment in a number of tissues. One is cellular retinol-binding protein (CRBP) which binds retinol with high affinity and specificity; the other is cellular retinoic acid-binding protein (CRABP) which binds retinoic acid and its analogs. These binding proteins have been purified from several animal tissues [3–8] and recently CRBP has been also purified from human liver [9,10]. However, no information is available about human CRABP.

Of interest is the finding that CRABP occurs or increases its concentration in several neoplastic tumors and is not detected in histologically normal tissue adjacent to the tumor [11], in contrast to a decrease of CRBP in such neoplasms. In addition, cellular retinoid-binding proteins are considered to play an important role in the function and metabolism of retinoids. Recently, much attention has been paid to chemoprevention of cancer with acidic retinoids [12–15].

Abbreviations: CRABP, cellular retinoic acid-binding protein; CRBP, cellular retinol-binding protein, RBP, serum retinol-binding protein; SDS, sodium dodecyl sulfate.

Correspondence Dr Y. Muto, First Department of Internal Medicine, Gifu University School of Medicine, 40 Tsukasa-machi, Gifu 500, Japan.

0304-4165/87/$03.50 © 1987 Elsevier Science Publishers B.V (Biomedical Division)

We now report the purification and partial characterization of CRABP from human placenta, so as to extend our understanding of human CRABP. This report will provide fundamental information for the future studies that may reveal the mode of action of human CRABP.

Materials and Methods

Materials

Sephadex G-50, SP-Sephadex (C-50) and protein standards for isoelectric point analysis were purchased from Pharmacia Fine Chemicals (Uppsala, Sweden). DEAE-cellulose (DE-52) was obtained from Whatman, Inc. (Clifton, U.S.A.). All-*trans* retinol, monothioglycerol and thimerosal were purchased from Sigma Chemcial Co. (St. Louis, U.S.A.). The Bolton-Hunter reagent and all-*trans* [15-^{14}C]retinoic acid (28 μCi/mg) were obtained from Amersham Co. (Buckinghamshire, U.K.). Protein standards for molecular weight analysis were purchased from BDH Chemicals Ltd. (London, U.K.). Gabexate mesilate (FOY®) was supplied by Ono Pharmaceutical Co., Ltd. (Osaka, Japan). The human placenta samples from mothers with normal parturition were kindly supplied by Dr. K. Tomita, Department of Gynecology and Obstetrics, Shinshu University Hospital, and were stored at −80°C until used.

Preparation of placenta extract and fractionation steps in purification

The procedure described by Kato et al. [16] was employed with some modifications. Human placenta samples (total 2000 g) were lyophilized to dryness, and were homogenized with 4 liters of ice-cold acetone, using a Yamato LK-21 ultradisperser. The dried powder was homogenized with 4 liters of buffer A (50 mM Tris-HCl buffer (pH 8.4) containing 4 mM EDTA and 0.004% NaN_3) containing 12 mM monothioglycerol. The homogenate was centrifuged at 20000 × *g* for 60 min to remove cell debris. The resulting supernatant was filtered through glass fiber filters paper (pore size; 10 μm). To this soluble acetone powder extract was added all-*trans* retinol and all-*trans* [15-^{14}C]retinoic acid (8.5 μCi/μmol) to give a final concentration of 15 μM each, and incubated at 4°C for 16 h.

Fractionation procedures were carried out at 4°C. The fractions from each chromatography were assayed for protein-bound retinol by measuring fluorescence with excitation at 350 nm and emission at 475 nm and for protein-bound [^{14}C]retinoic acid by determination of radioactivity to identify the elution portions containing the binding proteins. Except in the final purification procedure, CRBP and CRABP eluted together and were not separated from each other during fractionation procedures.

The placenta extract was submitted to gel chromatography on a Sephadex G-50 (medium) column (10 × 125 cm) in buffer A containing 25 mM NaCl. Fractions of 18 ml each were collected at a flow rate of 240 ml/h. Eight column runs were repeated to process the whole preparation. Fractions containing both CRBP and CRABP were combined and concentrated by ultrafiltration using a YM 5 membrane in an Amicon cell. The solution was then reapplied to the same column and eluted exactly as described above.

The sample from the second gel filtration was dialyzed against buffer B (15 mM imidazole-acetate buffer (pH 6.4) containing 0.004% NaN_3), and was applied to a column (3.2 × 40 cm) of DEAE-cellulose equilibrated with buffer B. The column was eluted with a linear gradient of imidazole-acetate buffer from 15 to 200 mM at pH 6.4 (total volume, 1600 ml). Fractions of 15 ml each were collected at a flow rate of 40 ml/h.

Pooled and concentrated fractions containing both CRBP and CRABP were then dialyzed against buffer A, and applied to a column (1.5 × 15 cm) of DEAE-cellulose equilibrated with buffer A, and eluted with a linear gradient of NaCl from 0 to 150 mM in the same buffer (total volume, 200 ml). Fractions of 3 ml each were collected at a flow rate of 10 ml/h.

The resulting sample from above preparation was then submitted to gel chromatography on a small column (2 × 95 cm) of Sephadex G-50 (superfine) equilibrated and eluted with buffer A containing 25 mM NaCl. Fractions containing the binding proteins (each 3 ml at a flow rate of 6 ml/h) were concentrated and dialyzed against buffer C (10 mM sodium acetate buffer (pH 4.9)).

The final step of column chromatography was ion-exchange chromatography on a column (1.5 ×

30 cm) of SP-Sephadex. The dialyzed material was applied to the column previously equilibrated with buffer C, and eluted with a linear gradient of sodium acetate from 10 to 130 mM at pH 4.9 (total volume, 200 ml). The two peaks, representing CRBP and CRABP, were pooled separately, dialyzed against distilled water and lyophilized. The materials were used for later analyses.

Contamination of serum retinol-binding protein (RBP) or of albumin in the sample through the purification procedure was tested immunologically by means of the Ouchterlony double-immunodiffusion technique using agar plate. Rabbit antisera against RBP and albumin were freshly prepared in this laboratory [17].

Gel electrophoresis

Polyacrylamide gel electrophoresis in 0.1% sodium dodecyl sulfate (SDS) was performed according to the method of Weber and Osborn [18], using a 13% separating gel and 5.5% stacking gel at pH 8.8. The molecular weights of CRBP and CRABP were calculated based on a comparison of their migration rate through the gel with those of protein standards: ovotransferrin (M_r 76000–77000), bovine serum albumin (M_r 66200), ovalbumin (M_r 45000), bovine chymotrypsinogen A (M_r 25700), horse myoglobin (M_r 17200) and horse cytochrome *c* (M_r 12300).

Polyacrylamide gel electrophoresis without SDS was also run according to the method of Davis [19], using a 10% separating gel and 5.5% stacking gel at pH 8.8.

Analytical isoelectric focusing electrophoresis was performed on an LKB Ampholine® polyacrylamide gel electrophoresis plate, pH 3.5–9.5, LKB Sweden AB, Isoelectric point of the proteins was calculated based on a comparison of their migration rates with those of protein standards: human carbonic anhydrase B (p*I* 6.55), bovine carbonic anhydrase B (p*I* 5.85), β-lactoglobulin A (p*I* 5.20), soybean trypsin inhibitor (p*I* 4.55) and glucose oxidase (p*I* 4.15).

Gels were stained according to the method of Reisner et al. [20].

Radioimmunoassay system

An effective radioimmunoassay for human liver CRBP has been developed in our laboratory (Okuno, M. et al., unpublished data).

The anti-human CRBP antibodies were raised in three turkeys (approximately 8 kg body weight) by subcutaneous injections of 0.8 mg of purified CRBP with complete Freund's adjuvant, followed by booster injections of 0.3 mg and 0.2 mg of CRBP 1 week and 4 weeks after initial immunization, respectively. Purified monospecific antibody against CRBP was obtained by immunosorbent affinity chromatography on a CRBP-coupled Sepharose column. Antibody for immunoprecipitation of turkey IgG in the radioimmunoassay was prepared in a goat.

For labeling of CRBP with ^{125}I, CRBP was acylated with ^{125}I-labeled Bolton-Hunter reagent (4000 Ci/mmol) according to the original method [21]. The labeled CRBP was separated from non-protein-bound ^{125}I by Sephadex G-50 column chromatography. The specific radioactivity of the acylated CRBP preparation was 35 mCi/mg CRBP.

The buffer solution for the radioimmunoassay (RIA buffer) consists of 50 mM imidazole buffer (pH 7.4), 0.79% NaCl, 0.03% bovine serum albumin, 0.1% thimerosal, 0.01% gabexate mesilate and 1% Triton X-100. The concentrations of pure CRBP in the standard solutions were estimated by absorbance using an $A_{1\,\mathrm{cm}}^{1\%}$ of 14 [4]. The following steps were carried out at 4°C. Reagents were diluted in RIA buffer, and added to a polystyrene tube in the following sequence: (1) 100 μl of sample to be assayed or standard solution of liver CRBP; (2) 100 μl of diluted anti-CRBP IgG solution (containing 5 μg of purified specific IgG); (3) 250 μl of RIA buffer, incubated for 24 h; (4) 100 μl of ^{125}I-CRBP (approximately 20000 cpm), incubated for 72 h; (5) 100 μl of goat anti-turkey IgG antibody (containing 50 μg of IgG), incubated overnight. Samples were then centrifuged at 2000 × *g* for 30 min, and the supernatants were removed by aspiration. The radioactivity of the precipitates were measured in a Packard auto-Gamma 5650 counter.

HPLC system

CRABP and CRBP were estimated by a gel filtration binding assay as described previously [22], with some modifications. The HPLC system described here was based on the procedure of Allegretto et al. [23].

Aliquots from each purification step were analyzed by an HPLC system consisting of a TSK G 3000SW column (Toyo Soda Kogyo Co., Tokyo, Japan), a CCPM pump (Toyo Soda Kogyo Co.), a Toyo Soda UV-8000 HPLC detector (Toyo Soda Kogyo Co.) set at 280 nm and a Chromatocorder 11 integrator (System Instruments Co., Tokyo, Japan). Elution was performed with 200 mM phosphate buffer (pH 7.2) at a flow rate of 1 ml/min. Sixty fractions were collected for a total period of 30 min, and radioactivity in each fractions was measured with a Beckman LS-7500 liquid scintillation counter.

The molecular weights of the binding proteins were also estimated by gel filtration on the same HPLC column which was calibrated using the protein standards described above.

Other procedures

Absorbance measurements and absorption spectra were determined with a Hitachi 124 spectrophotometer. Fluorescence measurements and spectra were determined with a Hitachi 204 fluorescence spectrophotometer. The radioactivity of [^{14}C]retinoic acid was determined by a Beckman LS-7500 liquid scintillation counter.

Protein concentration was determined according to the method of Lowry et al. [24], using bovine serum albumin as a calibration standard.

Results

Purification of CRABP

CRBP and CRABP were purified by procedures similar to the method described by Kato et al. [16], with some modifications. Table I presents a sequence of six steps including: (1) gel chromatography on Sephadex G-50 (medium); (2) rechromatography on Sephadex G-50 (medium); (3) ion-exchange chromatography on DEAE-cellulose, pH 6.4; (4) ion-exchange chromatography on DEAE-cellulose, pH 8.4; (5) gel chromatography on Sephadex G-50 (superfine); and (6) ion-exchange chromatography on SP-Sephadex, pH 4.9. The overall purificiation procedure resulted in yields of 320 μg of CRABP and 2.7 mg of CRBP from 2.0 kg of human placenta.

As the first step, a soluble acetone powder extract was prepared and all-*trans* retinol and all-*trans* [15-^{14}C]retinoic acid were added to saturate the binding proteins. This solution was chromatographed on Sephadex G-50. Monitoring the fluorescence of protein-bound retinol and the radioactivity of protein-bound [^{14}C]retinoic acid, a prominent peak centered at 5094 ml (fraction 283) was observed (total bed volume, 9800 ml). Fractions containing this peak were combined and reapplied to the same Sephadex G-50 column (Fig. 1). The sample containing the binding proteins was applied to a DEAE-cellulose column at pH 6.4. On this column, three prominent peaks of fluorescence and/or ^{14}C radioactivity were observed (Fig. 2). The first peak was centered at 1005 ml (fraction 168), the second peak was at 1185 ml (fraction 186), and the third peak was at 1335 ml (fraction 201). When the fluorescence spectrum was examined, the excitation spectrum of the first peak had a peak at 350 nm, and the spectrum of the second peak had a peak at 330 nm. Moreover, the aliquots of the second and the third peak gave a single precipitated line on

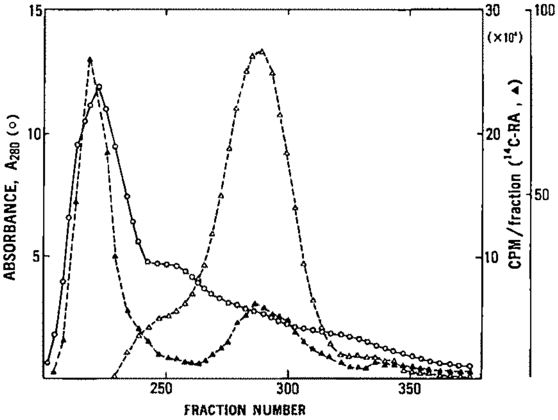

Fig. 1. Second chromatography on Sephadex G-50 of the combined binding protein – containing fractions obtained by eight runs of the first chromatography on Sephadex G-50. Fractions 250–320 containing both CRABP and CRBP were pooled Absorbance was monitored at 280 nm (O). CRABP was monitored by radioactivity of protein-bound [^{14}C]retinoic acid (^{14}C-RA; ▲). CRBP was monitored by fluorescence of protein-bound retinol (△; excitation at 350 nm and emission at 475 nm).

TABLE I

STEPS IN THE PURIFICATION OF CRABP FROM HUMAN PLACENTA

Procedure	Protein (mg) [a]	CRABP (mg)	CRBP (mg)	Purification (-fold)		Recovery (%)	
				CRABP	CRBP	CRABP	CRBP
Soluble acetone powder extract	181000	2.40 [b]	8.72 [b]				
Sephadex G-50, (I)	6000	2.06 [b]	7.12 [b]	26	25	86	82
Sephadex G-50, (II)	975	1.59 [b]	6.73 [b]	123	143	66	77
DEAE-cellulose, pH 6.4	111	1.09 [b]	5.01 [b]	740	940	45	57
DEAE-cellulose, pH 8.4	22.4	0.46 [b]	4.04 [b]	1550	3740	19	46
Sephadex G-50 (III)	9.9	0.41 [b]	3.59 [b]	3120	7530	17	41
SP-Sephadex, pH 4.9	0.32 (CRABP) 2.7 (CRBP)	0.32 [c]	2.70 [c]	75400	20700	13	31

[a] Estimated according to the method of Lowry et al [24].

[b] Estimated by a gel filtration binding assay (see text).

[c] Assumed since no protein other than CRABP or CRBP was demonstrable

Ouchterlony double-immunodiffusion using rabbit antibody against human RBP, while the aliquot of the first peak gave no line. The tests using rabbit anti-human albumin gave a negative response against all fractions from the three peaks. From these results, fractions comprising the first peak were assumed to contain CRBP and CRABP, and to be free from contamination by RBP or albumin. The fractions were combined and submitted to a DEAE-cellulose column at pH 8.4. On this column, CRBP annd CRABP eluted in a single peak of fluorescence and ^{14}C radioactivity, centered at 40 ml of a 200-ml gradient (data not shown). Fractions containing this peak were combined and applied to a smaller Sephadex G-50 (superfine) column. All three peaks of fluorescence, radioactivity and absorbance at 350 nm shared the same elution volume centered at 134 ml (total bed volume, 298 ml, data not shown). Absorbance at 350 nm of this peak was somewhat higher than that at 280 nm. The final step of chromatography was the ion-exchange chromatography on SP-Sephadex at pH 4.9 (Fig. 3). When a linear gradient of sodium acetate buffer was applied, two peaks of absorbance at 350 nm were observed in an elution volume centered at 69 ml (fraction 23) and at 120 ml (fraction 40) of a 200-ml gradient. The first peak corresponded to the peak of fluorescence of protein-bound retinol, and the second one was the peak of radioactivity of bound [^{14}C]retinoic acid, indicating the complete separation of CRABP from CRBP.

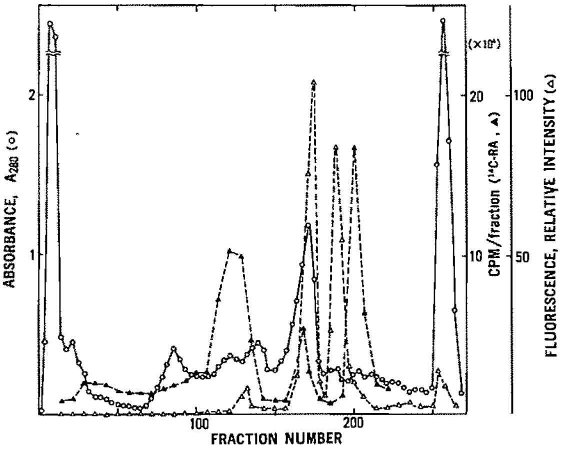

Fig 2. Chromatography on DEAE-cellulose of the sample from the second chromatography on Sephadex G-50 (Fig 1) The column was eluted with a linear gradient of imidazole-acetate buffer from 15 to 200 mM, pH 6.4 (total volume, 1600 ml). Three prominent peaks of fluorescence and/or radioactivity were observed on this column. Following analyses of fluorescence spectra and immunological reactivities, the first peak (fraction 157–179), containing CRABP and CRBP, was pooled The second (fraction 180–192) and the third (fraction 193–210) peaks were attributed to the retinoids bound to RBP (see Results). Absorbance was monitored at 280 nm (O). CRABP was monitored by radioactivity (^{14}C-RA; ▲) and CRBP was monitored by fluorescence (△).

The purity of the binding proteins was assessed by gel electrophoresis in three systems. In a disc gel electrophoresis system, CRABP was detected as a single protein band which had a distinctly different mobility than CRBP (Fig. 4A). By il-

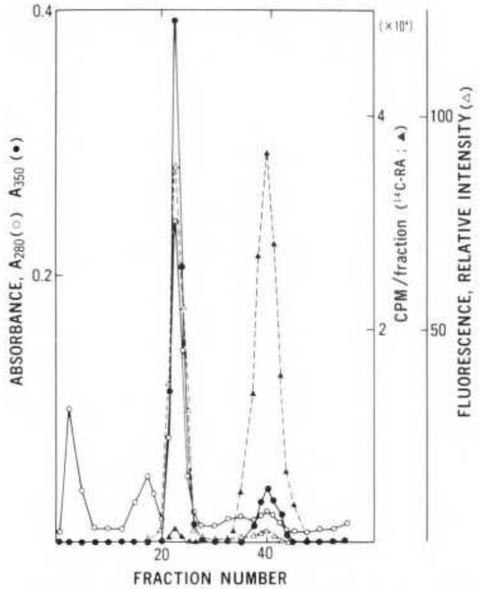

Fig. 3. Final chromatography on SP-Sephadex resulting in pure CRABP and CRBP. The column was eluted with a linear gradient of a sodium acetate buffer from 10 to 130 mM, pH 4.9 (total volume, 200 ml). Fractions 20–25 were pooled and contained pure CRBP; fractions 38–42 were pooled to yield pure CRABP. Absorbance was monitored at 280 nm (○) and 350 nm (●). CRABP was monitored by radioactivity (^{14}C-RA; ▲) and CRBP was monitored by fluorescence (△).

luminating the gel with long-wave ultraviolet light in the dark, a single yellow-green band was observed, which corresponded exactly to the single protein-staining band of CRBP. When the samples were also examined by SDS-polyacrylamide electrophoresis (Fig. 4B(2)), a single protein band was observed, demonstrating that both binding proteins were single polypeptide chains. CRABP gave a single band on the isoelectric focusing electrophoresis when the protein was saturated with retinoic acid (see below).

Molecular weight determination

The molecular weights of human CRABP and CRBP were estimated by two methods. By SDS-polyacrylamide gel electrophoresis by the method of Laemmli [25], the molecular weight of CRABP was calculated to be 14600, and that of CRBP was 14900, based on their migration through the gel (Fig. 4B(2)).

Samples were also submitted to gel filtration on

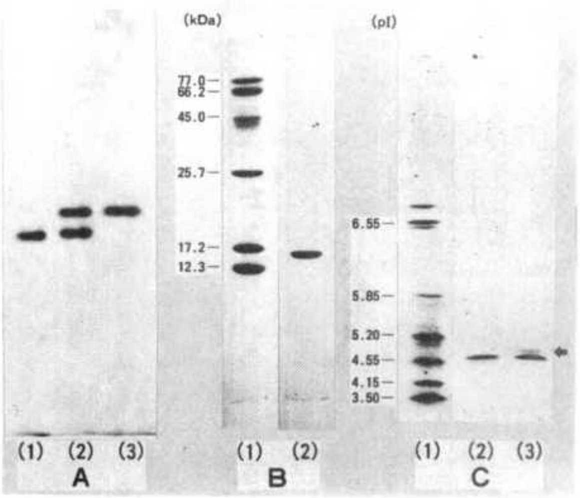

Fig. 4. Electrophoretic analyses of purified CRABP by different systems. Anode to the bottom. 10 μg of purified protein were analysed in each gel. (A) Polyacrylamide gel electrophoresis of CRBP (gels 1 and 2) and CRABP (gels 2 and 3) showing clear separation from each other. (B) SDS-polyacrylamide gel electrophoresis of molecular weight markers (gel 1) and CRABP (gel 2) suggesting size homogeneity (approximately 14.6 kDa). (C) Analytical isoelectric focusing in the pH interval of 3.5 to 9.5 performed on pI markers (gel 1) and on CRABP (gels 2 and 3) in the presence (gel 2) or absence (gel 3) of excess retinoic acid (see Materials and Methods). Note the disappearance of faint band (arrow in gel 3) by a preincubation of sample with excess retinoic acid (gel 2).

a calibrated TSK G 3000 SW column. The elution positions were monitored by absorbance and those of both binding proteins were equivalent to the same molecular weight of 14500.

Isoelectric point

The isoelectric point of human CRABP and CRBP were estimated by analytical isoelectric focusing electrophoresis in a pH range of 3.5–9.5. CRABP showed two bands with isoelectric pH values of 4.78 and 4.82 (Fig. 4C(3)). When preincubated with excess retinoic acid, a single band was observed with an isoelectric pH value of 4.78 (Fig. 4C(2)). CRBP showed one fluorescent and protein-staining band with an isoelectric pH value of 4.90 (data not shown).

Absorption spectra

The absorption spectra of purified CRABP and

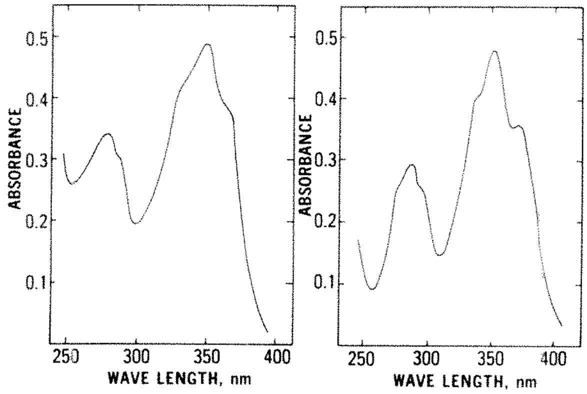

Fig. 5. Absorption spectra of CRABP bound with retinoic acid (left) and CRBP bound with retinol (right), at a protein concentration of 10^{-5} M in 20 mM Tris-HCl buffer (pH 8.4).

CRBP, shown in Fig. 5, clearly indicate the presence of the respective bound ligands with the absorption characterisitcs of retinoic acid (left) and retinol (right). CRABP displayed two absorption peaks, with maxima at 283 nm and 350 nm, respectively (Fig. 5, left). The first peak represented protein absorbance and the second peak was due to protein-bound retinoic acid. The ratio of A_{350} to A_{280} was 1.62. The first peak had a shoulder at 292 nm and the second peak showed shoulders at 334 and 367 nm. CRBP also displayed two absorption peaks, with maxima at 283 nm and 350 nm, which resembled CRABP (Fig. 5, right).

Fluorescence spectra

The fluorescence excitation and emission spectra of retinoic acid bound to CRABP and retinol bound to CRBP are shown in Fig. 6. The excitation spectrum of CRABP showed major peak at 350 nm, a second peak at 370 nm and a small peak at 290 nm. The emission spectrum of CRABP showed a single peak at 475 nm (Fig. 6A). Both the excitation and emission spectra of CRBP were very similar to those of CRABP (Fig. 6B).

Immunological properties

Fig. 7 shows the displacement of ^{125}I-CRBP from anti-liver CRBP antibodies by increasing amounts of pure unlabeled liver CRBP. This figure also shows the displacement curves for purified placenta CRBP, placenta CRABP, and serum RBP. Unlabeled placenta CRBP yielded a displacement curve that was identical with the curve for liver CRBP. However, neither placenta CRABP nor serum RBP displaced ^{125}I-CRBP from the

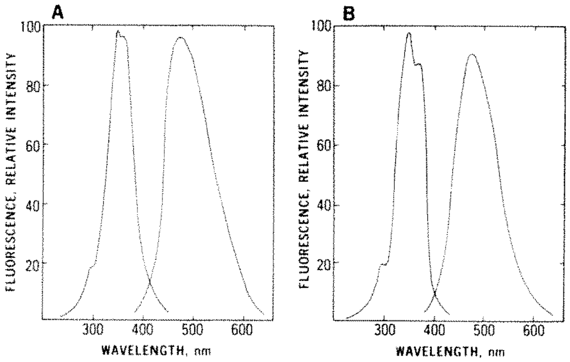

Fig. 6. Uncorrected fluorescence spectra of retinoic acid bound to CRABP (A) and retinol bound to CRBP (B), $5 \cdot 10^{-6}$ M in 20 mM Tris-HCl buffer (pH 8.4). The excitation spectra of CRABP (A, left) and CRBP (B, left) were determined measuring emission at 475 nm; the emission spectra of CRABP (A, right) and CRBP (B, right) were determined with excitation at 350 nm.

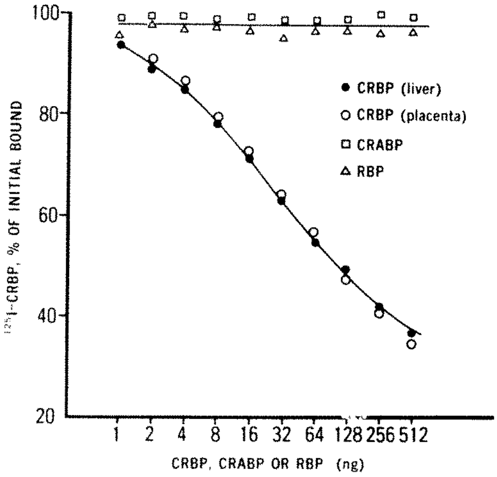

Fig. 7. Immunological cross-reactivity between human liver CRBP and placenta CRBP, and a lack of cross-reactivity of CRBP with either human placenta CRABP or human serum RBP. Procedures and conditions for the radioimmunoassay are as described under Materials and Methods. Unlabeled placenta CRBP, as much as liver CRBP, displaced antibody-bound ^{125}I-labelled liver CRBP. Absolutely no displacement was observed when placenta CRABP and serum RBP were included in the assay.

antibodies, in the range of protein concentrations added. Thus, two CRBP samples from placenta and liver appeared to be identical on the basis of immunoreactive behavior, whereas no cross-reactivity was observed between CRBP and CRABP.

Discussion

Recently, CRBP has been purified from human liver [9,10], and a radioimmunoassay system for human CRBP has been developed and the levels of CRBP in various human tissues have been given [26]. In our laboratory, we have also purified human CRBP and developed a radioimmunoassay system for human CRBP. However, no information is available about human CRABP. It has been reported that CRABP occurs in several tumors, but not in adjacent normal tissue [11]. Hence, much more interest has been focused on CRABP than CRBP in neoplastic tumors.

The present purification procedure resulted in high purity judging from the results of electrophoresis in several systems (Fig. 4).

As the first step, an acetone powder was prepared to remove most of lipids from placenta tissue, because Sklan et al. [27] reported that most of CRBP in rat liver homogenate (without preparation of an acetone powder) was eluted in the void volume on Sepharose 4B column chromatography, demonstrating that CRBP formed a high-molecular-weight, lipid-protein aggregate, whereas we had found that most of CRBP in the homogenate with preparation of an acetone powder existed in the free form by chromatography on Sephadex G-75 (data not shown). It seems likely that preparation of an acetone powder contributes to a higher yield of the binding proteins.

On the ion-exchange chromatography on DEAE-cellulose at pH 6.4, the third step of the fractionation procedure, three prominent peaks of fluorescence and/or radioactivity were observed (see Results). On analysis of fluorescence spectra and immunological reactivities, the second and third peaks of fluorescence and/or radioactivity were clearly attributed to the retinoids bound to RBP. RBP circulates in plasma as a protein-protein complex with transthyretin, and very little RBP is normally present in the free state [28]. The RBP-transthyretin complex is not altered by an acetone powder extraction (Kato, M. et al., unpublished data) and has been completely excluded from the free RBP pool by gel filtration of the present purification procedure. This indicates that a significant amount of RBP is not complexed to transthyretin in the human placenta. In a recent study in human, Sklan et al. reported that a significant amount of free RBP is present in the maternal and fetal circulation [29]. Their results may be relevant to our observation and suggest that free RBP originates in the maternal and fetal blood within the placenta samples, that were not perfused in this study. Since the molecular weight of RBP (M_r 21 000) is similar to that of CRBP and CRABP, these retinoid-binding proteins were not completely separated from each other on a Sephadex G-50 chromatography. RBP binds with not only retinol but also retinoic acid when excess retinoic acid is added in vitro, and a conformational change of RBP occurs [30].

The molecular weight of CRABP is similar to that determined for rat CRABP [3,5], and that of CRBP is similar to that previously reported for human CRBP [9,10]. Very recently, Sundelin et al. reported the primary structures of bovine CRABP [31] and rat liver CRBP [32]. The molecular weights calculated from the sequences were 15 460 (CRABP) and 15 700 (CRBP). Molecular weight values described here were estimated by SDS-polyacrylamide gel electrophoresis and by gel filtration, and may be underestimates of the true molecular weights.

On analytical isoelectric focusing, CRABP showed one major protein-staining band at pH 4.78 when preincubated with excess retinoic acid, and when not preincubated with retinoic acid, one major band at pH 4.78 and a faint band at pH 4.82 were observed (Fig. 4(3)). This result indicates that the faint band is apo-CRABP, and that the binding of retinoic acid to the binding protein may alter the charge of CRABP. A similar change of charge occurs on human CRBP as described by Fex and Johennesson [10]. This isoelectric point of holo-CRABP is similar to the value of rat CRABP [5]. CRBP showed one fluorescent and protein-staining band at pH 4.90. This value is similar to the result of rat CRBP purified by Ross et al. [5], but somewhat higher than the result of human CRBP purified by Fex and Johannesson [10].

Absorption and fluorescence spectra were identical with those of CRABP purified from animal tissues [3,5,6]; however, the ratio of A_{350} to A_{280} was somewhat lower than the ratio reported by Ong and Chytil [3]. This discrepancy can be explained by the presence of apo-CRABP, which has been detected on isoelectric focusing electrophoresis.

CRBP purified from human placenta was antigenically identical with CRBP from human liver, when examined by radioimmunoassay using a specific anti-liver CRBP antibody prepared in this laboratory, as shown in Fig. 7. In contrast, CRABP was antigenically distinct from CRBP.

Since CRABP occurs or markedly increases in several neoplastic tumors, for the future use of acidic retinoids in cancer treatment of chemoprevention it is of great importance to know the correct concentrations of CRABP in such tumors in order to judge an effective retinoid theorapy, in much the same way as determinations of estrogen receptor are used in the treatment of mammary cancer [26]. Several radioimmunoassay systems for rat CRABP have been developed and the CRABP levels in various rat tissues have been determined [33–35]. However, the immunoassay for human CRABP is not yet available.

We are now attempting to develop a sensitive radioimmunoassay system for human CRABP, when sufficient amounts of the antigen are available.

Acknowledgement

This work was supported in part by Grants-in-Aid (61480443) from the Ministry of Education, Science and Culture of Japan.

References

1 Roberts, A.B. and Spron, M.B. (1984) in The Retinoids (Sporn, M.B., Roberts, A.B. and Goodman, D.S., eds.), Vol. 2, pp. 209–286, Academic Press, New York

2 Moon, R.C. and Itri, L.M. (1984) in The Retinoids (Sporn, M.B., Roberts, A.B. and Goodman, D.S., eds.), Vol. 2, pp 327–371, Academic Press, New York

3 Ong, D.E. and Chytil, F. (1978) J Biol. Chem 253, 4551–4554

4 Ross, A.C., Takahashi, Y.I. and Goodman, D.S (1978) J Biol Chem 253, 6591–6598

5 Ross, A.C, Adachi, N.A and Goodman, D.S (1980) J. Lipid Res. 21, 100–109

6 Saari, J.C., Futterman, S. and Bredberg, L (1978) J. Biol. Chem 253, 6432–6436

7 Ong, D.E. and Chytil, F. (1978) J. Biol. Chem. 253, 828–832

8 Liou, G.I., Fong, S.L. and Bridges, C.D.E. (1981) J. Biol Chem. 256, 3153–3155

9 Ong, D.E (1982) Cancer Res. 42, 1033–1037

10 Fex, G and Johannesson, G. (1982) Biochim. Biophys Acta 714, 536–542

11 Ong, D.E., Page, D.L. and Chytil, F. (1975) Science 190, 60–61

12 Bollag, W. (1979) Cancer Chemother. Pharmacol. 3, 207–215

13 Sporn, M.B. and Newton, D.L. (1979) Fed Proc Fed. Am. Soc. Exp. Biol. 38, 2528–2534

14 Ong, D.E and Chytil, F (1983) Vitam. Horm. (N.Y.) 40, 105–144

15 Muto, Y. and Moriwaki, H. (1984) J Natl. Cancer Inst 73, 1389–1393

16 Kato, M., Kato, K and Goodman, D.S (1984) J. Cell Biol 98, 1696–1704

17 Kato, M., Kanai, M., Kameko, S., Ohno, Y., Fujii, Y and Nagata, T. (1982) Acta Histochem. Cytochem. 15, 68–75

18 Weber, K and Osborn, M. (1969) J Biol Chem. 244, 4406–4412

19 Davis, B.J. (1964) Ann. N.Y. Acad. Sci. 121, 404–427

20 Reisner, A.H, Names, P. and Bucholtz, C. (1975) Anal. Biochem. 64, 509–516

21 Bolton, A.E and Hunter, W.M. (1973) Biochem. J 133, 529–539

22 Muto, Y., Omori, M. and Sugawara, K. (1979) Gann 70, 215–222

23 Allegretto, E.A., Kelly, M.A., Donaldson, C.A., Levine, N, Pike, J.W. and Haussler, M.R. (1983) Biochem Biophys. Res. Commun. 116, 75–81

24 Lowry, O.H., Rosebrough, N.J., Farr, A.L. and Randall, R.J. (1951) J Biol. Chem. 193, 265–275

25 Laemmli, U.K. (1970) Nature (Lond.) 227, 680–685

26 Fex, G and Johannesson, G (1984) Cancer Res. 44, 3029–3032

27 Sklan, D., Blaner, W.S., Adachi, N., Smith, J.E and Goodman, D.S. (1982) Arch. Biochem Biophys 214, 35–44

28 Goodman, D.S. (1984) in The Retinoids (Sporn, M.B., Roberts, A.B. and Goodman, D.S., eds), Vol. 2, pp. 41–88, Academic Press, New York

29 Sklan, D., Shalit, I., Lasebnik, N., Spirer, Z and Weisman, Y (1985) Br. J. Nutr. 54, 577–583

30 Heller, J. and Horwitz, J. (1973) J Biol. Chem. 248, 6308–6316

31 Sundelin, J., Das, S.R, Eriksson, U, Rask, L and Peterson, P.A. (1985) J. Biol Chem. 260, 6494–6499

32 Sundelin, J., Anundi, H, Tragardh, L., Eriksson, U., Lind, P., Ronne, H., Peterson, P.A and Rask, L. (1985) J. Biol Chem. 260, 6488–6493

33 Ong, D.E, Crow, J.A. and Chytil, F (1982) J Biol. Chem 257, 13385–13389

34 Eriksson, U., Das, K., Busch, C., Nordlinder, H., Rask, L., Sundelin, J., Sallstrom, J and Peterson, P.A. (1984) J. Biol Chem. 259, 13464–13570

35 Kato, M., Blaner, W.S., Mertz, J.R., Das, K., Kato, K. and Goodman, D.S. (1985) J. Biol. Chem 260, 4832–4838

Biochimica et Biophysica Acta 923 (1987) 125–135
Elsevier

BBA 22478

The role of polyamine reutilization in depletion of cellular stores of polyamines in non-proliferating tissues

F.N. Bolkenius and N. Seiler

Merrell Dow Research Institute, 16, rue d'Ankara, 67084 Strasbourg-Cedex (France)

(Received 25 August 1986)

Key words. Putrescine; Spermidine; Ornithine decarboxylase; Polyamine oxidase; Polyamine reutilization

It was known from previous work that specific inhibition of neither ornithine decarboxylase activity nor polyamine oxidase activity produces spermidine depletion by more than 20% in non-growing organs, which are in a steady state with regard to polyamine metabolism. Combined treatment with inactivators of both ornithine decarboxylase and polyamine oxidase for a prolonged time caused, however, a gradual decrease of spermidine levels in liver, kidney and brain of mice by 50% and more. The method is in accordance with the previously suggested role of polyamine interconversion. Inhibition of polyamine oxidase prevents the reutilization for de novo polyamine biosynthesis of putrescine and spermidine, which are formed by oxidative splitting of N^1-acetylspermine and N^1-acetylspermidine, respectively, and the ornithine decarboxylase inhibitor prevents the compensatory increase of putrescine from ornithine. The findings are further evidence for the physiological significance of polyamine reutilization.

Introduction

It is well established that inhibition of ornithine decarboxylase activity in proliferating cells produces a gradual decrease of putrescine and spermidine concentrations [1]. One may observe at the same time an increase of spermine concentration, owing to the fact that *S*-adenosylmethionine decarboxylase is induced [2]. Since under these conditions no putrescine is available as substrate for spermidine synthase, spermine is formed preferentially as long as spermidine is available as substrate of spermine synthase. These changes can be especially well observed in closed metabolic systems, for example in the fertilized chicken egg [3]; if 5 mmol/kg of DL-α-difluoromethylornithine (Ornidyl^{TM}), the well known inactivator of ornithine decarboxylase [4], is injected into the yolk sac on day 4 of incubation, putrescine formation is completely blocked. The total polyamine content per chick embryo remains constant, but one observes the above-mentioned decrease of putrescine and spermidine concentrations and a concomitant increase of the spermine content per embryo. The embryo is capable of growing for a few additional days by using up the polyamine pool that is available at the time of difluoromethylornithine administration. This example demonstrates that difluoromethylornithine does not cause a depletion of the polyamines per se, but prevents putrescine formation, which makes de novo polyamine synthesis impossible. The cellular polyamine content is decreased by distribution of the pool among the daughter cells. This happens as long as the available polyamines enable cell division. If the polyamine pool is too small, cells stop dividing.

Taking these considerations into account it is not surprising that in contrast with tumors [5] and

---

Correspondence: Dr. N. Seiler, Merrell Dow Research Institute, 16, rue d'Ankara, 67084 Strasbourg-Cedex, France.

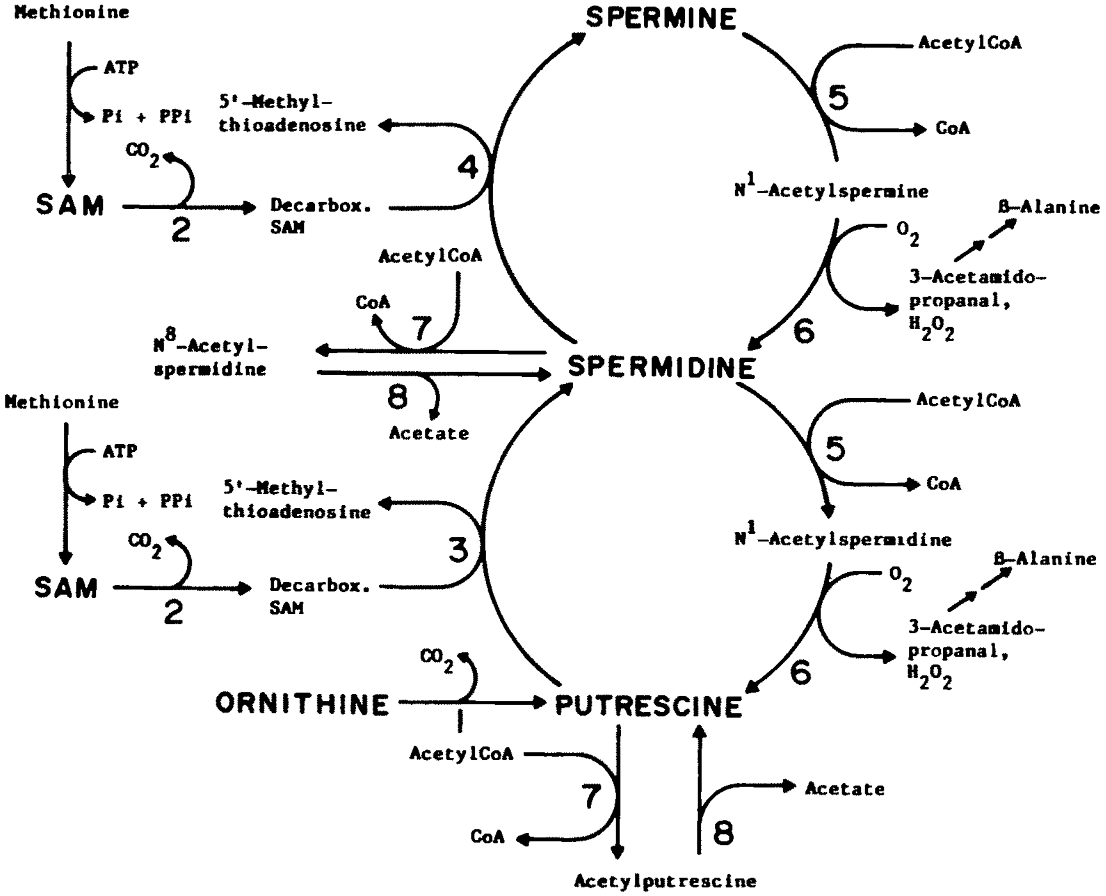

Fig 1 The interconversion pathway of the polyamines 1, Ornithine decarboxylase (EC 4.1.1.17), 2, S-adenosylmethionine (SAM) decarboxylase (EC 4.1.1 50); 3, spermidine synthase; 4, spermine synthase; 5, acetyl-CoA: spermidine/spermine N^1-acetyltransferase (cytosolic); 6, polyamine oxidase; 7, acetyl-CoA: spermidine N^8-acetyltransferase; 8, N^8-acetylspermidine acetylhydrolase.

some selected organs which are not in a steady state, as far as polyamines are concerned, such as prostate [6], treatment of animals with difluoromethylornithine even over an extended period of time had only a relatively small effect on the polyamine content of non-growing organs [6]; one observed only a very marked reduction of urinary polyamine excretion [5], i.e., of those polyamines that are normally either formed in excess and/or result from dead cells, whose content was emptied.

Another method of depleting cellular polyamine contents is theoretically based on the inhibition of polyamine interconversion: from the scheme (Fig. 1) it appears that the spermidine and putrescine, which are formed along the catabolic pathway [7,8], may be reutilized for polyamine biosynthesis. Evidence for putrescine reutilization has indeed been found for brain [9–12] and for the whole rat [13]. By inactivating polyamine oxidase, the enzyme which is oxidatively splitting N^1-acetylspermine and N^1-acetylspermidine (Fig. 1), formation of spermidine and putrescine by catabolism is prevented. Under these conditions, one should not only expect the urinary excretion of the amount of those polyamines, which is normally reutilized [13], but also a decrease of tissue putrescine and spermidine concentrations. However, the treatment of mice even for 6 weeks with a daily dose of 20 mg/kg N^1,N^4-bis-(2,3-butadienyl)-1,4-butanediamine (MDL 72527), a potent and specific inactivator of polyamine oxidase [14], produced less than 20% depletion of the spermidine content of various organs of mice [15], instead of a gradual decrease according to the rate of polyamine turnover. As a tentative explanation for the discrepancy between expectance and observations, a small compensatory increase of ornithine decarboxylase activity was postulated, although ornithine decarboxylase activity did not exceed measurably the low basal activity of tissues of untreated controls [15].

In order to allow one to study polyamine functions in normal vertebrate tissues by methods analogous to those used in cultured eukaryotic cells [16], it would be necessary to deplete tissue polyamine levels without impairment of other metabolic reactions by the inhibitors used. Relying on the above-described theoretical basis, and the specificity of difluoromethylornithine and MDL 72527 for ornithine decarboxylase and polyamine oxidase, respectively, we studied the effects of combined treatment with these two compounds on tissue polyamine levels.

Materials and Methods

Chemicals

Usual laboratory chemicals were from Merck (Darmstadt, F.R.G.). *o*-Phthalaldehyde was from Roth (Karlsruhe, F.R.G.), 1-octane sulfonate was a product of Eastman Kodak (Rochester, NY, U.S.A.); putrescine dihydrochloride, spermidine phosphate and spermine phosphate were from Fluka (Buchs, Switzerland).

N^1-Acetylspermidine dihydrochloride [17], N^1-acetylspermine trihydrochloride [18], (E)-2-(fluoromethyl)dehydroornithine methyl ester (MDL 72403) [19], N^1-methyl,N^4-(2,3-butadienyl)-1,4-butanediamine dihydrochoride (MDL 72521), and N^1,N^4-bis-(2,3-butadienyl)-1,4-butanediamine dihydrochloride (MDL 72527) [14] were synthesized in our institute according to published methods. α-Difluoromethylornithine (Ornidyl™) is a product of Merrell Dow Pharmaceutical Company.

Animals

Adult male CD1 albino mice (weighing 30–35 g) were purchased from Charles River (St. Aubin-les-Elbeuf, France). They were housed in groups of five under standardized conditions (22°C, 60% relative humidity; 12 h light, 12 h dark cycle; free access to standard diet and drinking solution). The drinking solutions were exchanged every 3 days and the amounts consumed per cage and day were noted.

Assay of polyamines

The animals were decapitated and the organs removed as quickly as possible, frozen in liquid nitrogen and stored at −80°C. The frozen organs were homogenized in 9 vol. of ice-cold 0.2 N perchloric acid. After centrifugation the perchloric acid extracts were stored at 2°C until analysis. Polyamines were determined in two- (brain) or five- (liver and kidney) times diluted extracts by separation of their ion pairs with 1-octane sulfonate on a reversed phase column (Ultrasphere-IP, Beckman), reaction with *o*-phthalaldehyde/2-mercaptoethanol reagent, and recording of fluorescence intensity at 455 nm (excitation wavelength 345 nm) [20].

Assay of decarboxylated S-adenosylmethionine

200 μl aliquots of undiluted perchloric acid tissue extracts were separated on an Ultrasphere IP-column using a mixture of buffer B and buffer A, 70:30, which contained 10 mM 1-octane sulfonate; (buffer A: 0.1 M sodium acetate (pH 4.5); buffer B: 0.2 M sodium acetate plus acetronitrile, 70:30). Absorbance at 254 nm was continuously recorded.

Assay of amino acids

The tissue extracts were diluted with 19 vol. of 0.2 N perchloric acid and separated on an Ultrasphere IP-column by isocratic elution using a buffer containing 630 ml 0.2 M phosphoric acid, 270 ml 0.1 M sodium acetate (pH 4.5), 100 ml methanol and 9 mM sodium dodecyl sulfate. Fluorescence intensity was recorded after reaction with *o*-phthalaldehyde/2-mercaptoethanol reagent [21].

Behavioral test

Free-moving mice were obserevd in a device described by Weischer [22]. Locomotor activity and exploratory behavior were recorded during a 5-min period.

TABLE I

POLYAMINE CONCENTRATIONS IN MOUSE ORGANS AFTER ADMINISTRATION OF SOLUTION OF 3% DIFLUOROMETHYLORNITHINE, OR 0 05% MDL 72527 OR THE COMBINATION OF THE TWO DRUGS INSTEAD OF DRINKING WATER

All difluoromethylornithine-treated animals received 3 h before death an additional 200 mg/kg i.p. dose of the drug. (Mean values ± S.D ; $N = 5-10$). n.d , not determined.

Treatment	Duration of treatment (days)	Polyamine (nmol per g tissue)					
		putrescine	N^1-acetyl-spermidine	N^1-acetyl-spermine	spermidine	spermine	decarboxylated S-adenosylmethionine
a) Brain							
none	–	11 ± 2	<1	<1	401 ± 28	363 ± 18	<1
difluoromethylornithine + MDL 72527	4	<1 *	41 ± 7 *	1.7 ± 0 4 *	283 ± 22 *	360 ± 14	n.d.
	10	<1 *	46 ± 6 *	2.4 ± 1 0 *	240 ± 17 *	370 ± 11	3 ± 1 *
	14	<1 *	31 ± 5 *	2.1 ± 0 4 *	197 ± 20 *	367 ± 22	4 ± 1 *
	21	<1 *	31 ± 3 *	3 ± 1	182 ± 22 *	425 ± 15 *	6 ± 1 *
difluoromethylornithine	4	3 4 ± 0.7 *	<1	<1	348 ± 11 *	345 ± 13	n d
	21	1 1 ± 0 4 *	<1	<1	322 ± 16 *	356 ± 19	<1
MDL 72527	4	2.7 ± 0 8 *	49 ± 7 *	2.5 ± 0.5 *	283 ± 16 *	367 ± 20	n.d.
	21	3.2 ± 0.8 *	57 ± 11 *	5.2 ± 0.9 *	283 ± 20 *	425 ± 13 *	n d
b) Kidney							
none	–	61 ± 11	<1	<1	397 ± 47	928 ± 50	2 ± 0.5
difluoromethylornithine + MDL 72527	10	2.1 ± 0.4 *	10 ± 4 *	11 ± 4 *	183 ± 43 *	964 ± 21	9 ± 6 *
	14	2.1 ± 0.3 *	7 ± 2 *	10 ± 3 *	152 ± 22 *	990 ± 45	14 ± 7
	21	1 7 ± 0.2 *	6 ± 3 *	13 ± 6 *	118 ± 31 *	1005 ± 69	12 ± 5 *
difluoromethylornithine	21	3 3 ± 0 6 *	<1	<1	291 ± 31 *	955 ± 52	5 ± 2 *
c) Liver							
none	–	11 ± 2	2 0 ± 0 5	<1	944 ± 82	1202 ± 56	<1
difluoromethylornithine + MDL 72527	10	1.9 ± 0.2 *	7 3 ± 3.0 *	7 ± 3 *	497 ± 94 *	1400 ± 106 *	<1
	14	1.6 ± 0.3 *	5 4 ± 0 3 *	7 ± 1 *	453 ± 95 *	1338 ± 119 *	<1
	21	1 5 ± 0 2 *	6.3 ± 1.1 *	12 ± 4 *	472 ± 77 *	1375 ± 95 *	<1
difluoromethylornithine	21	5 ± 1 *	1.4 ± 0.3	<1	785 ± 75 *	1357 ± 97 *	<1

* Statistically significant ($P \leqslant 0 05$) difference between treated and controls

Calculations

Results of polyamine and amino acid determinations were analyzed by single-factor analysis of variance [23]. For the evaluation of the behavioral test the non-parametric Kruskal-Wallis one-way analysis of variance was used with multiple comparisons [24,25].

Results

Effect of treatment with difluoromethylornithine and MDL 72527 on polyamine and amino acid levels in mouse organs

Groups of 5 to 10 mice received either a 3% solution of difluoromethylornithine, or a 0.05% solution of MDL 72527, or a solution containing both compounds as sole drinking fluid. At an average fluid intake of about 5 ml per day the drug intake corresponded to 4.3–5.0 g difluoromethylornithine per kg body weight, and 70–80 mg MDL 72527 per kg body weight per day. The average increase of body weight during a 21 day treatment period was: 5–3 g (controls), 4 ± 2 g (MDL 72527) and 2 ± 2 g difluoromethylornithine alone or in combination with MDL 72527), in agreement with the previously published fact that administration of difluoromethylornithine [26] but not of MDL 72527 [15] produces a slight retardation of growth.

In Table I the results of the polyamine analyses in brain, liver and kidney are summarized. Combined treatment with difluoromethylornithine and the polyamine oxidase inhibitor MDL 72527 is in all organs more effective in depleting putrescine levels than administration of difluoromethylornithine alone. In agreement with previous results [11,15], elevation of N^1-acetylspermidine and N^1-acetylspermine concentrations was greater in brain than in other organs. Prolonged treatment with the polyamine oxidase inhibitor alone did not enhance N^1-acetylspermidine concentratins above the initially observed value, but prolonged treatment with difluoromethylornithine and MDL 72527 caused a decrease of N^1-acetylspermidine concentrations. Administration of difluoromethylornithine alone had no effect on acetylpolyamines.

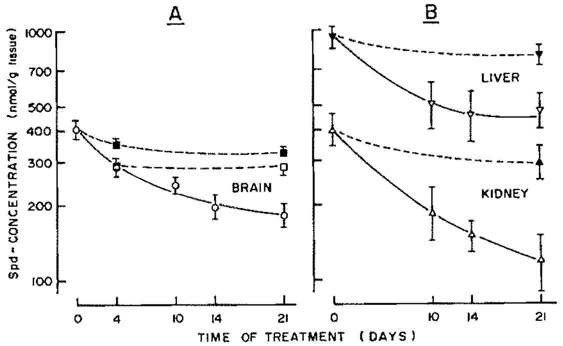

Fig. 2 Time-dependent decrease of spermidine (Spd) concentrations in brain (A) and liver and kidney (B) of mice receiving a 3% solution of difluoromethylornithine (ornithine decarboxylase inhibitor) (------), or a combination of 3% difluromethylornithine and 0.05% MDL 72527 (polyamine oxidase inhibitor) (———) as sole drinking fluid □------□, animals receiving only 0.05% MDL 72527 as drinking fluid Values are means ± S.D (indicated by the vertical bars).

Spermidine showed in all organs a time-dependent decrease, if the mice were treated with both difluoromethylornithine and MDL 72527. After 21 days of oral administration of the two inhibitors spermidine levels in brain were decreased by 55%, in liver by 50%, and in kidney even by 70%. The semilogarithmic plots (Fig. 2) demonstrate that the rate of spermidine depletion is decreasing with time.

The average rates of spermidine depletion are summarized in Table II. The value obtained for brain during the first 4 days of treatment is the same as was previously determined from the rate of N^1-acetylspermidine accumulation in mouse brain [11]. With increasing length of treatment the

TABLE II

AVERAGE RATE OF SPERMIDINE DEPLETION IN ORGANS OF MICE AFTER ORAL ADMINISTRATION OF DIFLUOROMETHYLORNITHINE AND MDL 72527

The values in this table were calculated from the data presented in Table I (mean values, range in parentheses)

Experimental period (days)	Spermidine depletion (nmol/g tissue per h)		
	brain	liver	kidney
1–4	1.2 (0 7–1.7)	–	–
1–10	0.7 (0.5–0.9)	1.9 (1.1–2 6)	0.9 (0.5–1.3)
14–21	0 1 (0 –0.3)	0 (0 –0 9)	0.2 (0 –0.5)
1–21	0.4 (0 3–0.5)	0.9 (0 6–1 3)	0 6 (0 4–0.7)

TABLE III

EFFECT OF ADMINISTRATION OF A SOLUTION CONTAINING 3% DIFLUOROMETHYLORNITHINE AND 0.05% MDL 72527 INSTEAD OF DRINKING WATER ON THE CONCENTRATION OF THE NON-ESSENTIAL AMINO ACIDS IN MOUSE BRAIN

Values are given as means ± S.D.; $N = 5$. The animals of this experiment were the same as those of Table I

Treatment	Duration of treatment (days)	Amino acid (μmol/g brain)									
		Gln	Ser	Asp	Glu	Glutathione	Thr	Gly	β-Ala	GABA	Ala
None	–	3.9±0.5	0.55±0.03	2.3±0.2	9.6±0.6	2.3±0.2	0.3 ±0.4	1.02±0.05	0.06±0.005	2.1±0.07	0.5±0.1
Difluoromethylornithine + MDL 72527	21	4.1±0.3	0.63±0.08 *	2.6±0.5	10.5±0.7	2.7±0.2 *	0.33±0.03	1.11±0.05 *	0.06±0.005	2.4±0.1 *	0.6±0.03

* Statistically significant difference ($P \leqslant 0.05$) between controls and treated.

rate of spermidine depletion is lowered to insignificant values.

In agreement with what has been previously observed in cultured rat hepatoma cells [2], spermine concentration was increasing in all tissues concomitantly with the loss of spermidine, and measurable concentrations of decarboxylated *S*-adenosylmethionine appeared at the same time in kidney and brain, but remained in liver below the detection limit of our method.

The determination of the non-essential amino acids (Table III) in the brains of mice after 21 days of treatment with difluoromethylornithine and MDL 72527 revealed small increases of serine, glycine, glutathione and GABA.

In order to achieve as complete an inhibition of ornithine decarboxylase as is practically possible, groups of four mice received not only a 3% solution of difluoromethylornithine as drinking fluid, but in addition daily three intraperitoneal injections of 200 mg/kg during the light period. MDL 72527 was given, as before, as 0.05% solution orally. Furthermore, another very potent inhibitor of ornithine decarboxylase, (*E*)-2-(fluoromethyl) dehydroornithine [19], was administered in the form of its methyl ester (MDL 72403) in order to compare it with difluoromethylornithine. The latter compound was given twice daily in a dose of 100 mg/kg i.p. Polyamine analyses were carried out after 6 days of treatment, 3 h after the last dose of ornithine decarboxylase inhibitor. The comparison of the results in Table IV with those in Table I reveals the following:

(a) the higher dose of difluoromethylornithine did not enhance spermidine depletion;
(b) MDL 72403 given in two daily doses of 100 mg/kg alone or in combination with MDL 72527 produced comparable changes in brain polyamines, as were observed after administration of a 3% solution of difluoromethylornithine in drinking water, and the combination of difluoromethylornithine/MDL 72527, respectively.

Experiments analogous to those described above have also been carried out with combinations of difluoromethylornithine (administered as 2% solution; i.e. 2.9–3.3 g/kg body weight per day) and N^1-methyl, N^4-allenylputrescine (MDL 72521) (given as 0.05% solution).

Since the 2% solution of difluoromethylornithine had about the same effect on tissue spermidine levels (Table V) as were observed after administration of a 3% solution (Table I), the less complete depletion of spermidine levels obtained after administration of the drug combination is obviously due to the lower potency of MDL 72521, as compared with MDL 72527. It was known that MDL 72521 penetrates the blood brain barrier less well [15], and therefore incomplete inhibition of polyamine oxidase in brain could be expected.

TABLE IV

COMPARISON OF THE EFFECTS OF THE ORNITHINE DECARBOXYLASE INHIBITORS DIFLUOROMETHYLORNITHINE AND *E*-2-(FLUOROMETHYL)DEHYDROORNITHINE (MDL 72403) ON BRAIN POLYAMINE CONCENTRATIONS

Difluoromethylornithine was given as 3% solution instead of drinking fluid, and the animals received in addition daily three 200 mg/kg i.p. doses of difluoromethylornithine. MDL 72403 was administered twice daily by i.p. injection of 100 mg/kg The polyamine oxidase inhibitor MDL 72527 was given as 0.05% solution as drinking fluid. Duration of treatment: 6 days; killing 3 h after the last dose of the ornithine decarboxylase inhibitors Values are given as means ± S.D., $N = 4$.

Treatment	Polyamine (nmol/g brain)				
	putrescine	N^1-acetyl spermidine	N^1-acetyl-spermine	spermidine	spermine
Physiological saline	12 ± 2	<1	<1	408 ± 16	363 ± 45
Difluoromethylornithine	4 ± 1 *	<1	<1	372 ± 22 *	339 ± 20
Difluoromethylornithine + MDL 72527	1.4 ± 0.1 *	47 ± 4 *	2.0 ± 0.6 *	280 ± 10 *	385 ± 33
MDL 72403	4 ± 1 *	<1	<1	381 ± 22	347 ± 13
MDL 72403 + MDL 72527	1.1 ± 0.3 *	42 ± 8 *	2.5 ± 0.2 *	288 ± 16 *	392 ± 18

* Statistically significant ($P \leqslant 0.05$) difference between treated and controls

TABLE V

POLYAMINE CONCENTRATIONS IN MOUSE ORGANS AFTER TREATMENT WITH SOLUTION OF 2% DIFLUOROMETHYLORNITHINE, OR 0.05% MDL 72521 OR THE COMBINATION OF THE TWO DRUGS INSTEAD OF DRINKING WATER

All difluoromethylornithine-treated animals received 3 h before death an additional 200 mg/kg i.p. dose of the drug Values are means ± S.D ; $N = 3$–6.

Treatment	Duration of treatment (days)	Polyamine (nmol/g tissue)				
		putrescine	N^1-acetyl-spermidine	N^1-acetyl-spermine	spermidine	spermine
a) Brain						
none	–	13 ± 2 *	<1	<1	408 ± 20	289 ± 17
difluoromethylornithine	7	4 ± 1 *	<1	<1	363 ± 27	303 ± 17
	14	3 4 ± 0.4 *	<1	<1	362 ± 21	311 ± 3
	21	1.9 ± 0.4 *	<1	<1	320 ± 33 *	286 ± 24
	28	1.9 ± 0.3 *	<1	<1	341 ± 27 *	308 ± 4
MDL 72521	7	7.8 ± 0.4 *	32 ± 6	<1	382 ± 22	301 ± 14
	14	8 ± 2 *	33 ± 11	<1	378 ± 60	275 ± 46
	21	9 ± 1 *	35 ± 5	<1	420 ± 36	299 ± 11
	28	9 ± 2 *	28 ± 2	<1	399 ± 30	297 ± 7
difluoromethylornithine + MDL 72521	7	1.3 ± 0.1 *	17 ± 3	<1	317 ± 7 *	293 ± 35
	14	1.0 ± 0.5 *	13 ± 1	<1	309 ± 13 *	312 ± 7
	21	1.3 ± 0.5 *	12 ± 4	<1	300 ± 11 *	308 ± 15
	28	1 1 ± 0.2 *	11 ± 1	<1	290 ± 3 *	301 ± 4
b) Kidney						
none	–	57 ± 15	<1	<1	465 ± 48	888 ± 51
difluoromethylornithine	7	6 ± 1 *	<1	<1	333 ± 12 *	898 ± 58
	14	6.9 ± 0.5 *	<1	<1	288 ± 44 *	860 ± 45
	21	6 7 ± 0.2 *	<1	<1	344 ± 86 *	963 ± 37
	28	7 ± 1 *	<1	<1	310 ± 13 *	892 ± 33
MDL 72521	7	29 ± 18	10 ± 2 *	18 ± 3 *	338 ± 12 *	860 ± 68
	14	53 ± 8	10 ± 2 *	16 ± 4 *	388 ± 34	956 ± 75
	21	42 ± 34	12 ± 1 *	16 ± 5 *	346 ± 51 *	914 ± 176
	28	43 ± 9	10 ± 2 *	15 ± 1 *	398 ± 24	953 ± 92
difluoromethylornithine + MDL 72521	7	3 ± 1 *	13 ± 1 *	26 ± 6 *	279 ± 21 *	1045 ± 43
	14	4 ± 2 *	9 ± 1 *	18 ± 6 *	213 ± 22 *	967 ± 15
	21	4 ± 2 *	11 ± 1 *	15 ± 4 *	270 ± 64 *	1062 ± 46
	28	5 ± 2 *	11 ± 3 *	22 ± 4 *	294 ± 47 *	1034 ± 58
c) Liver						
none	–	10 ± 1	<1	<1	1159 ± 145	1482 ± 190
difluoromethylornithine	7	8 ± 3	<1	<1	1084 ± 173	1369 ± 149
	14	13 ± 4	<1	<1	1058 ± 126	1635 ± 102
	21	7 ± 1	<1	<1	824 ± 16	1587 ± 18
	28	7 ± 2	<1	<1	913 ± 142	1588 ± 221
MDL 72521	7	7 ± 1	16 ± 2 *	15 ± 5 *	1254 ± 54	1624 ± 146
	14	6.1 ± 0.3	24 ± 14 *	15 ± 5 *	1105 ± 71	1659 ± 216
	21	10 ± 5	16 ± 4 *	18 ± 5 *	1025 ± 254	1411 ± 121
	28	6.0 ± 0.2	12 ± 2 *	14 ± 3 *	1119 ± 179	1538 ± 109
difluoromethylornithine + MDL 72521	7	5 ± 2	16 ± 9 *	21 ± 9 *	919 ± 284	1708 ± 115
	14	3 ± 2 *	11 ± 2 *	21 ± 2 *	793 ± 150 *	1506 ± 96
	21	2 ± 1 *	11 ± 3 *	17 ± 3 *	796 ± 170 *	1889 ± 85 *
	28	1.4 ± 0.1 *	8 ± 2 *	20 ± 3 *	784 ± 141 *	1794 ± 367

* Statistically significant ($P \leqslant 0.05$) difference between treated and controls

TABLE VI

EFFECT OF ADMINISTRATION OF A 3% SOLUTION OF DIFLUOROMETHYLORNITHINE, OR A 0.05% SOLUTION OF MDL 72527 OR A COMBINATION OF THE TWO DRUGS INSTEAD OF DRINKING WATER ON LOCOMOTION AND EXPLORATORY BEHAVIOR OF MICE

The difluoromethylornithine-treated animals received, 3 h before the behavioral test, an additional 200 mg/kg i.p dose of the drug Values are means; $n = 5$–10

Treatment	Duration of treatment (days)	Locomotion (scores)	Exploratory behaviour (scores)	Body weight gain during treatment (g)
None	–	86	94	5±3
Difluoromethylornithine + MDL 72527	21	72	64 *	2±2
Difluoromethylornithine	21	90	77	2±2
MDL 72527	21	88	81	4±2

* Statistically significant difference ($P < 0.05$) between treated and controls

However, the fact that this compound is also less effective than MDL 72527 in peripheral organs was a surprise.

In all experiments N^1-acetylspermidine concentrations in brain were somewhat higher, if the polyamine oxidase inhibitor was given alone, than after administration of the drug combination. This is in agreement with the reduced spermidine turnover rate after ornithine decarboxylase inhibition [11].

Toxicological and behavioral considerations

Treatment of mice with a 3% solution of difluoromethylornithine alone or in combination with MDL 72527 did not produce any apparent toxicity. Those animals which received difluoromethylornithine gained, however, about 50% less weight than the controls or the MDL 72527-treated groups. The absence of toxic effects of MDL 72527 has been previously reported [15]. Not only did we not observe toxic effects, but also there were not even any gross behavioral changes. As a first step to more detailed pharmacological studies, locomotor activity and exploratory behavior of the long-term treated mice were explored using the method of Weischer [22]. As appears from the results in Table VI, locomotor activity was not significantly affected by any of the treatments; however, a diminution of the exploratory behavior was noted.

Discussion

Profound depletion of spermidine in a non-growing tissue has previously only been demonstrated in the liver of starving mice [27]. Later on it was demonstrated that induction of the cytosolic acetyl-CoA : spermidine/spermine N^1-acetyltransferase [28] was important for the initiation of polyamine depletion [29].

Under the experimental conditions of the present work we found no evidence for the induction of acetyl-CoA : spermidine/spermine N^1-acetyltransferase. Our results can be easily explained as logical consequences of the existence of the interconversion pathway, if we postulate that putrescine (and spermidine) reutilization is not only important in brain, as has been previously shown [9–12], but also in liver and kidney. According to this scheme (Fig. 1) the polyamine oxidase inhibitor prevents the formation of spermidine and putrescine from spermine and spermidine, respectively, and thus their reentry into the synthetic pathway. Since the ornithine decarboxylase inhibitor prevents at the same time the compensatory formation of putrescine from ornithine, spermidine levels are decreasing (initially) at a rate which is equivalent to the basal turnover rate. The closely similar numbers obtained for the rate of spermidine depletion during the first days of treatment, and the previously determined degradation rate of spermidine in mouse brain [9–11] are suggestive in this regard.

Treatment with the polyamine oxidase inhibitors is apparently not affecting N^8-acetylation of spermidine by the nuclear acetyltransferase or the N^8-acetylspermidine acetylhydrolase (Fig. 1), as appears from the fact that neither tissue concentrations, nor, as has been shown previously [13], urinary excretion of N^8-acetylspermidine was changed by treatment with the polyamine oxidase inhibitors. Although acetylputrescine excretion has not been measured, one has to assume that its metabolism is also unaffected, because putrescine and spermidine N^8-acetylation is catalyzed by the same acetyltransferase [30] and hydrolysis of these acetyl derivatives by the same deacetylase [31].

The increase of spermine concentrations after a certain depletion of spermidine in various tissues obviously occurs due to the same reason, as was discussed in the introduction section; in the absence of putrescine, spermidine is the only substrate which can react with the excessively available decarboxylated *S*-adenosylmethionine. However, even in spite of the fact that in later phases of treatment spermidine depletion is not only caused by prevention of putrescine reutilization, but also by enhanced spermine formation, the rate of spermidine depletion is considerably slowed down after prolonged treatment with the two inhibitors. One potential explanation is that acetyl-CoA : spermidine/spermine N^1-acetyltransferase is down-regulated. The limited sensitivity of the present methods do not allow us to test this hypothesis. A more likely explanation is, however, the following. Owing to their cationic nature, we have to assume that only a small fraction of the total tissue spermidine and spermine is 'free' [32], and thus accessible to the cytosolic enzyme. With progressing depletion of spermidine, the equilibrium concentration of free (cytosolic) spermidine is gradually decreasing, since initially the pools with loosely bound spermidine are emptied. By analogy, its considerably higher affinity for anionic binding sites [33] is the reason for the slow degradation rate of spermine [11].

The relative inefficiency of ornithine decarboxylase inhibitors to deplete polyamine levels in non-growing tissues [6,19,26] has usually been ascribed to incomplete inactivation of ornithine decarboxylase in vivo, owing to the high turnover rate of this enzyme, the accumulation of the enzyme [34] and the difficulty to maintain continuously a high level of the ornithine decarboxylase inhibitors. The fact that administration of 2% or 3% solutions of difluoromethylornithine, or the additional injection of three times 200 mg/kg doses of this compound, did not produce greatly differing effects on brain polyamine levels, argues in favor of the assumption that the extent of ornithine decarboxylase inhibition may not be the only reason for the observed small polyamine depletion. A better explanation seems to be offered by the observation that only a small proportion of putrescine is formed under steady-state conditions by decarboxylation of ornithine. In mouse brain only 20–30% of the total putrescine formed seems to originate directly from ornithine, whereas 70–80% are formed by spermidine degradation [11,12]. Moreover, the possibility cannot be excluded that small amounts of polyamines are imported from the circulation. In fact we had assumed that uptake from the circulation would be a major polyamine source of peripheral organs, in contrast with brain, which is protected by the blood-brain barrier. The latter is known not to be penetrated effectively by the polyamines [35]. To our surprise, however, spermidine depletion by combined treatment with an ornithine decarboxylase and a polyamine oxidase inhibitor was in liver and kidney as efficient as in brain. This findings seems to exclude circulatory polyamines as a major source of non-growing organs in a steady-state situation. However, under our experimental conditions, tissue levels of N^1-acetylspermidine and N^1-acetylspermine are elevated. We cannot exclude at present that these intermediary metabolites of polyamine catabolism serve as signals, indicating enhanced polyamine catabolism, and thus prevent cellular polyamine uptake from the environment.

Conclusions

Combined treatment of laboratory animals with inhibitors of ornithine decarboxylase and polyamine oxidase is a means of depleting tissue levels of spermidine by about 50%. The method relies on the prevention of the reutilization of those portions of spermidine and putrescine which are formed along the interconversion pathway by oxidative splitting of N^1-acetylspermine and N^1-acetylspermidine, respectively. These substrates of polyamine oxidase are eliminated from the organs and are either excreted or further metabolized [36,37]. Complete depletion of tissue spermidine stores by this method seems infeasible due to the decrease of the turnover rate with progressing diminution of spermidine concentration. In order to enhance the rate of spermidine depletion above the turnover rate, it will be necessary to induce polyamine acetylation.

In spite of the fact that difluoromethylornithine and the polyamine oxidase inhibitor MDL 72527 have been administered over an extended period of time, no toxic effects have been observed. This underlines the specificity of these two enzyme-activated irreversible inhibitors. We therefore consider the method useful for in vivo studies of the physiological consequences of putrescine and spermidine depletion.

References

1 Heby, O. and Jänne, J. (1981) in Polyamines in Biology and Medicine (Morris, D.R. and Marton, L.J., eds.), pp. 243–310, Marcel Dekker, New York, Basal

2 Mamont, P.S, Danzin, C., Wagner, J., Siat, M., Joder-Ohlenbusch, A.-M. and Claverie, N (1982) Eur. J. Biochem. 123, 499–504

3 Seiler, N. and Sarharn, S. (1983) Neurochem. Int 5, 625–633

4 Bey, P. (1978) in Enzyme-Activated Irreversible Inhibitors (Seiler, N., Jung, M J. and Koch-Weser, J., eds.), pp. 27–41, Elsevier/North-Holland Biomedical Press, Amsterdam

5 Seiler, N., Knödgen B. and Bartholeyns, J. (1985) Anticancer Res. 5, 371–378

6 Danzin, C., Jung, M J., Grove, J and Bey, P. (1979) Life Sci. 24, 519–524

7 Seiler, N., Bolkenius, F.N and Rennert, O.M (1981) Med. Biol 59, 334–346

8 Seiler, N., Bolkenius, F.N, Bey, P., Mamont, P.S and Danzin, C. (1985) in Recent Progress in Polyamine Research (Selmeci, L., Brosnan, M.E. and Seiler, N, eds.), pp 305–319, Akademiai Kiado, Budapest

9 Antrup, H. and Seiler, N. (1980) Neurochem. Res. 5, 123–143

10 Seiler, N (1981) in Polyamines in Biology and Medicine (Morris, D.R. and Marton, L J., eds.), pp. 169–180, Marcel Dekker, New York, Basel

11 Seiler, N. and Bolkenius, F N. (1985) Neurochem. Res 10, 529–544

12 Bolkenius, F.N and Seiler, N. (1986) Int. J. Dev Neurosci. 4, 217–224

13 Seiler, N, Bolkenius, F.N. and Knödgen, B. (1985) Biochem. J. 225, 219–226

14 Bey, P., Bolkenius, F.N, Seiler, N. and Casara, P. (1985) Med. Chem. 28, 1–2

15 Bolkenius, F.N., Bey, P. and Seiler, N (1985) Biochim. Biophys. Acta 838, 69–76

16 Rudkin, B B, Mamont, P S. and Seiler, N. (1984) Biochem. J. 217, 731–741

17 Tabor, H., Tabor, C.W and De Meis, L. (1971) Methods Enzymol 17b, 829–833

18 Bolkenius, F N. and Seiler, N (1981) Int J Biochem. 13, 287–292

19 Mamont, P., Danzin, C, Kolb, M., Gerhard, F., Bey, P and Sjoerdsma, A. (1986) Biochem. Pharmacol 35, 159–165

20 Seiler, N. and Knödgen, B. (1985) J Chromatogr. 339, 45–57

21 Seiler, N and Knödgen, B. (1985) J. Chromatogr 341, 11–21

22 Weischer, M.L. (1976) Psychopharmacology 50, 275–279

23 Winer, B.J. (1971) Statistical principles in experimental design, McGraw-Hill, New York

24 Siegel, S. (1956) Non-parametric statistics for the behavioral sciences, pp. 184, McGraw-Hill, New York

25 Hollander, M. and Douglas, A. (1973) Nonparametric statistical methods, pp 124, John Wiley, New York

26 Seiler, N., Danzin, C, Prakash, N.J. and Koch-Weser, J. (1978) in Enzyme-Activated Irreversible Inhibitors (Seiler, N., Jung, M.J. and Koch-Weser, J., eds.), pp. 55–71, Elsevier/North-Holland Biomedical Press, Amsterdam

27 Seiler, N., Wener, G., Fischer, H.A., Knödgen, B. and Hinz, H. (1969) Hoppe-Seyler's Z. Physiol. Chem. 350, 676–682

28 Matsui, I., Wiegand, L. and Pegg, A E (1981) J. Biol Chem 256, 2454–2459

29 Seiler, N., Bolkenius, F N and Sarhan, S. (1981) Int J Biochem. 13, 1205–1214

30 Blankenship, J and Walle, T (1977) Arch. Biochem. Biophys 179, 235–242

31 Seiler, N. (1981) in Polyamines in Biology and Medicine (Morris, D.R and Marton, L.J., eds.), pp. 127–149, Marcel Dekker, New York, Basel

32 Brosnan, M.E. and Hu, Y.-W. (1985) in Recent Progress in Polyamine Research (Selmeci, L., Brosnan, M E and Seiler, N., eds.), pp. 169–180, Akademiai Kiado, Budapest

33 Bloomfield, V.A. and Wilson, R W. (1981) in Polyamines in Biology and Medicine (Morris, D R. and Marton, L J, eds.), pp. 183–206, Marcel Dekker, New York, Basel

34 Persson, L., Oredsson, S.M, Anehus, S and Heby, O. (1985) Biochem. Biophys. Res. Commun. 131, 239–245

35 Shin, W.W., Fong, W.-F. and Wong, P.C.-L. (1985) J. Neurochem. 44, 1056–1059

36 Seiler, N., Koch-Weser, J., Knödgen, B., Richards, W., Tardif, C., Bolkenius, F.N, Schechter, P., Tell, G., Mamont, P., Fozard, J., Bachrach, U. and Grosshans, E. (1981) Adv. Polyamine Res 3, 197–211

37 Seiler, N. (1985) in Structure and Functions of Amine Oxidases (Mondovi, B., ed), pp 21–35, CRC Press, Baton Rouge

Biochimica et Biophysica Acta 923 (1987) 136–142
Elsevier

BBA 22446

UDPgalactose:glucosylceramide $\beta1 \rightarrow 4$-galactosyltransferase activity in human proximal tubular cells from normal and familial hypercholesterolemic homozygotes

Subroto Chatterjee and Elizabeth Castiglione

Department of Pediatrics, Johns Hopkins University, Baltimore, MD 21205 (U.S.A.)

(Received 12 May 1986)
(Revised manuscript received 27 August 1986)

Key words: UDPgalactose; Glucosylceramide, Lactosylceramide, Galactosyltransferase; (Proximal tubular cell)

The activity of a galactosyltransferase (GalT-2) that catalyzes the transfer of galactose from uridinediphosphogalactose to glucosylceramide in cultured normal human proximal tubular (PT) cells was characterized with respect to substrate saturation and metal ion requirements. Using a membrane-bound enzyme source, optimum activity was obtained in the presence of 1.0 mM Mn^{2+}/Mg^{2+} (1:1) and a detergent mixture, Triton X-100/Cutscum (1:2, v/v), 0.1 mg/ml. The apparent K_m values for glucosylceramide and UDP[^{14}C]galactose were 3 μM and 0.5 μM, respectively. The V_{max} values for glucosylceramide and UDP[U-^{14}C]galactose were 0.12 nmol/mg protein per 2 h and 173 nmol/mg protein per 2 h, respectively. The purified ^{14}C-labelled product comigrated with authentic lactosylceramide (LacCer) on TLC and HPLC analysis. The presence of a terminal β-[^{14}C]galactosyl group in the enzymatic product was proved by its cleavage (79%) by β-galactosidase. Following the development of optimal assay conditions in normal PT cells, GalT-2 activity was next measured in urinary PT cells from homozygous familial hypercholesterolemic (FH) patients previously shown to accumulate large amounts of lactosylceramide. Urinary PT cells from familial hypercholesterolemic homozygous patients contained 35% higher GalT-2 activity as compared to control cells. We speculate that elevated GalT-2 activity may contribute to the storage of LacCer in FH-PT cells.

Introduction

Glycosphingolipids are integral components of cell membranes and human plasma lipoproteins [1–3]. Glycosphingolipids have been accorded numerous cell-surface functions [1]. The biosynthesis of glycosphingolipids occurs via a sequential transfer of sugars from nucleotide sugar donors to acceptor lipids such as ceramide for glucosylceramide synthesis and glucosylceramide for lactosylceramide synthesis [4–6]. These reactions are catalyzed by glycosphingolipid glycosyltransferases which are localized on the plasma membrane and Golgi apparatus [4,7]. The biosynthesis of LacCer is carried out by UDP-Gal: GlcCer $\beta1 \rightarrow 4$-galactosyltransferase (β-GalT-2) [5,8]. This is a key enzymatic reaction, since LacCer is a precursor for the synthesis of at least three different classes of glycosphingolipid. These are:

Abbreviations: GlcCer, glucosylceramide; LacCer, lactosylceramide; GbOse$_3$Cer, globotriosylceramide (trihexosylceramide); GbOse$_4$Cer, globotetraosylceramide (tetraglycosylceramide); PT, proximal tubular; FH, familial hypercholesterolemic; LDL, low density lipoprotein.

Correspondence: Dr. S. Chatterjee, Department of Pediatrics, Johns Hopkins University, 600 North Wolfe Street, Baltimore, MD 21205, U.S.A.

0304-4165/87/$03.50 © 1987 Elsevier Science Publishers B.V. (Biomedical Division)

gangliosides, sulfatides and $GbOse_3Cer$ [1]. Previously, membrane-bound enriched sources were used to characterize specific glycosphingolipid glycosyltransferase [5–10]. Because of the use of tissue culture systems to study various aspects of regulation of glycosphingolipid metabolism, the characterization studies in tissue extracts have been extended to these systems recently [8,10,12–14].

The present studies were undertaken to characterize UDP-Gal:GlcCer galactosyltransferase activity in normal human proximal tubular (PT) cells and to measure the activity of this enzyme in urinary PT cells from low density lipoprotein (LDL) receptor negative familial hypercholesterolemic (FH) homozygous patients. These studies are of particular interest to us because, first, LacCer, the product of this reaction, serves as a precursor for the biosynthesis of lactosylsulfatide, $GbOse_3Cer$, and G_{M3} present in these cells. Secondly, conditions developed in normal cells can be applied to test whether or not the accumulation of LacCer in urinary proximal tubular cells reported previously in FH patients is due to increased β-GalT-2 activity [3,15].

Materials and Methods

Materials

Uridine diphosphate-D-[U-^{14}C]galactose (UDP-Gal) (327 mCi/μmol) was purchased from New England Nuclear (Boston, MA). Unlabeled UDPgalactose, cacodylic acid, sodium cacodylate, Triton X-100 and Hepes buffer were purchased from Sigma Chemical Co. (St. Louis, MO). Cutscum was purchased from Fisher Chemical Co. (Fairlawn, NJ).

Other chemicals were purchased from commercial sources. Octyl-pentoxyethylene was a gift from Dr. Saul Roseman, Department of Biology of our institution. Glucosylceramide was purified from Gaucher (β-glucosidase deficiency) spleen and characterized by TLC, HPLC [16] techniques. Human kidney glycosphingolipids were prepared as described previously [17]. Minimum essential medium and heat-inactivated, dialyzed fetal calf serum were purchased from Gibco (Grand Island, NY) and Microbiological Associates, (Walkersville, MD), respectively. β-Galactosidase was purchased from Seikagaku Kogyo Co., Ltd. (2-9 Nihonbashihoncho, Chuo-Ka, Tokyo).

Cell culture

Human PT cells were prepared from autopsy kidney [18]. Cells (approximately $5 \cdot 10^5$) were grown in 75 cm^2 Corning plastic tissue culture flasks in Eagle's minimum essential medium and 10% fetal calf serum without antibiotics, since the latter compounds were found to give rise to 'myeloid bodies' [18]. Medium was replenished on day 1 and day 5 of cell growth. On day of cell growth, cell monolayers were washed and harvested in medium without fetal calf serum and centrifuged (500 × g, 10 min, 10 °C). Next, the cell pellet was suspended in 1 mM cacodylate buffer (pH 6.5) containing 0.32 M sucrose, 0.1% β-mercaptoethanol, 1 mM EDTA, 0.1% poly(ethylene glycol) (M_r 1000), and centrifuged. The cell pellets were frozen at −20 °C until further use. Freshly voided urine was collected under sterile conditions from two FH receptor-negative homozygotes (V.P., K.B.) [19]. Urinary sediments were prepared and PT cells isolated by Ficoll density gradient centrifugation, washed with phosphate-buffered saline and centrifuged [20]. The cell pellet was resuspended in the cacodylate buffer described above, centrifuged and stored frozen.

Preparation of cell homogenates

Cell pellets were suspended in the above-mentioned cacodylate buffer and transferred to 'Dounce' glass homogenizing tube and homogenized with a tight fitting glass pestle. Approximately ten strokes were applied. Homogenization was stopped when no intact cells were observed upon light microscopy. Suitable aliquots of the cell homogenate were solubilized in 1.0 M NaOH for protein assay [21].

UDPgalactose:glucosylceramide galactosyltransferase assay

The assay used is a modification of the method of Basu et al. [5]. Assay mixtures (in a total volume of 100 μl) contained the following components unless otherwise specified in the text: 100 μg crude homogenate protein; 10 μg Cutscum/Triton X-100, 2:1 (v/v); 5 μmol Mg^{2+}/Mn^{2+}, 1:1 (v/v); 20 mmol sodium cacodylate buffer (pH 6.8); 3.0 μmol glucosylceramide; and 0.1 mmol UDPgalactose.

Assay mixtures were incubated for 2 h at 37°C and reactions were stopped by the addition of 25 μmol EDTA plus 2.5 μmol KCl. Chloroform/methanol 2:1 (v/v) and 5 μg of human kidney glycosphingolipid were added and the products were isolated. The products were separated on 'Whatman' SG-81 paper chromatography (VWRScientific, San Francisco, CA). Chloroform/methanol/water 60:17:2 (w/v) was used as a solvent. Authentic lactosylceramide was cochromatographed. Following chromatography, the chromatogram was dried in cool air, and glycosphingolipids were identified by exposure to iodine vapors. The following R_F values were obtained: LacCer, either radiolabelled or unlabelled 0.68; Cer, 0.98; GlcCer, 0.91; GbOSe$_3$Cer, 0.49; and GbOse$_4$Cer, 0.27. Chromatogram areas corresponding in migration with authentic LacCer were cut and radioactivity was measured in a Beckman LS-3800 scintillation spectrometer using the background subtract setting and automatic quench setting as well as a 2.00 setting for the 2sigma statistical error. Assays without exogenous GlcCer served as blanks and were subtracted from all data points.

Protein assay

Protein content in cell homogenates was determined by the method of Lowry et al. [21] using crystalline bovine serum albumin as a standard.

Product identification

Product identification was carried out following modifications of the method of Lockney and Sweeley as described below [13]. In order to identify the glycosphingolipid product, a reaction mixture was prepared in which the specific activity of the UDPgalactose was increased 30-fold and the quantities of the rest of the reaction mixture were increased 30-fold. Following incubation, the reaction mixture was partitioned by adding chloroform/methanol/water (100:50:1.5, v/v) and centrifugation (500 × g, 5 min, 4°C). The lower phase was removed and the upper phase was extracted again with chloroform/methanol/water (87:14:1, v/v) and centrifuged. The lower phases were pooled and taken to dryness in a speed vac (Savant Instruments, Inc., Farmingdale, NY). The sample was resuspended in chloroform/methanol (2:1, v/v) and suitable aliquots were spotted on silica gel G plates and high performance thin layer chromatography (HPTLC) plates (E. Merck) employing chloroform/methanol/water (100:42:6, v/v) and chloroform/methanol/water/15 M NH_4OH (280:70:6:1, v/v) [11], respectively, and developed. The gel areas corresponding in chromatographic migration with authentic LacCer were scraped and eluted with chloroform/methanol/water (100:50:10, v/v) and centrifuged. The solvent layer was evaporated and the radioactivity was measured in a suitable aliquot.

β-Galactosidase treatment

The product of GalT-2 reaction purified by TLC as described above was dried in screw-cap tubes, and 100 μmol of carrier LacCer, β-galactosidase (0.1 units) and 7.5 μmol of sodium citrate buffer (pH 4.5) were added. One set of sample was immediately immersed in boiling water. The latter served as a boiled enzyme blank sample. The reaction mixture was incubated for 16 h at 37°C. The reaction was terminated with chloroform/methanol (2:1, v/v). 100 μg of unlabeled galactose and a suitable volume of 0.5 M KCl were added. The samples were mixed and centrifuged (500 × g, 10 min, 10°C). The upper phase was collected, washed with theoretical upper phase, centrifuged again, and radioactivity associated with free galactose was measured in 'Aquasol' (New England Nuclear, Boston, MA).

Results and Discussion

Lactosylceramide plays a pivotal role in glycosphingolipid biosynthesis since it serves as a precursor for complex neutral glycosphingolipids, sulfatides and gangliosides. Lactosylceramide synthesis occurs via the transfer of galactose from UDPgalactose to GlcCer. Employing polyclonal and monoclonal antibody against LacCer, the localization of LacCer has been shown to be cytoplasmic [22,23].

The effect of increasing concentrations of PT cell homogenate protein on GalT-2 activity is shown in Fig. 1A. Galactosyltransferase activity increased linearly with increasing concentrations

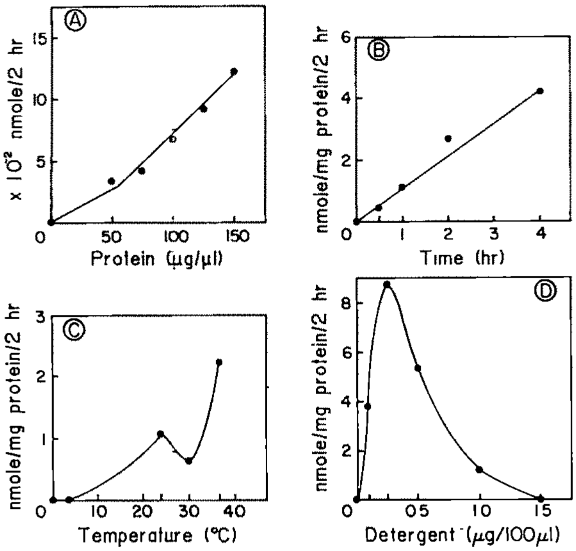

Fig 1. Effects of protein concentration, time, temperature of incubation, and detergent concentration on galactosyltransferase (GalT-2) activity in PT cell homogenates. The experimental conditions for GalT-2 assay in PT cell homogenates were varied as described in Materials and Methods. The product of the enzyme assay was purified by SG-81 'Whatman' paper chromatography employing chloroform/methanol/water (120:34:4, v/v). Radioactive spots which comigrated with LacCer were cut and radioactivity was measured employing scintillation spectrometry (A) Effects of protein concentration on GalT-2 activity in PT cell homogenates. (B) Effects of time of incubation on GalT-2 activity in PT cell homogenates (C) Effects of temperature of incubation on GalT-2 activity in PT cell homogenates (D) Effects of detergent concentration on GalT-2 activity in PT cell homogenates.

of homogenate protein from 50 to 150 µg/100 µl of assay mixture. GalT-2 activity increased linearly with time from 30 min to 4 h (Fig. 1B). 2 h of incubation was used routinely to measure GalT-2 activity on exogenously provided GlcCer. The effect of incubation temperature on GalT-2 activity is shown in Fig. 1C. No activity was observed at 4°C. However, GalT-2 activity increased with increasing temperature. Maximum GalT-2 activity was observed when the incubation temperature was set at 37°C. In contrast, GalT-2 activity was lowered when the incubation temperature was 30°C compared to 37°C. Therefore, subsequent studies were pursued by setting the incubation temperature to 37°C.

The effects of detergent concentration on GalT-2 activity is shown in Fig. 1D. GalT-2 activity rose linearly with the concentration of detergent mixture Cutscum/Triton 1 : 1 (v/v). Optimal GalT-2 activity was observed with 0.25 µg detergent mixture/100 µl assay. Further, increasing the detergent mixture concentration to 1.5 µg/100 µl assay rapidly decreased GalT-2 activity in PT cell homogenates. Cutscum and Triton X-100 used alone, or when used in various other ratios in the assay mixture, did not stimulate GalT-2 activity. Furthermore, other detergents tested, e.g., octylpentaoxyethylene, Triton X-100 only and cutscum only, were also without effect on GalT-2 activity in PT cell homogenates.

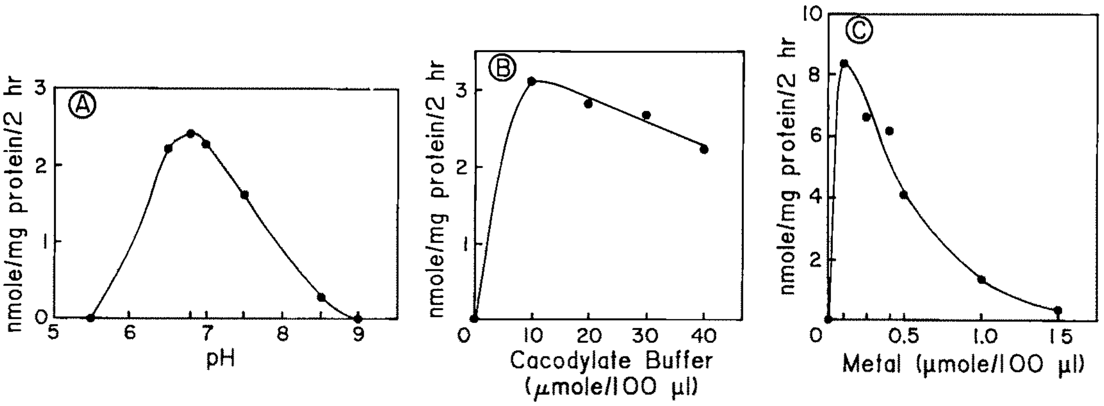

Fig. 2 Effects of pH, buffer concentration, and metal ion concentration on GalT-2 activity in PT cell homogenates. The experimental conditions for GalT-2 assay in PT cell homogenates were varied as described in Materials and Methods. The product was separated and radioactivity was measured as described in the legend to Fig 1. (A) Effect of pH on GalT-2 activity in PT cell homogenates (B) Effect of cacodylate buffer concentration on GalT-2 activity in PT cell homogenates. (C) Effect of divalent metal ion concentration on GalT-2 activity in PT cell homogenates.

The effect of buffer pH on GalT-2 activity in PT cell homogenates is shown in Fig. 2A. The enzyme was inactive at pH 5.5. Maximum GalT-2 activity was observed when the pH of the buffer was 6.8. GalT-2 activity decreased when the buffer pH was adjusted to 7.5 and 8.5. The enzyme was inactive at pH 9.0. The effects of cacodylate buffer concentration on GalT-2 activity in PT cell homogenates are shown in Fig. 2B. GalT-2 activity was inactive without the inclusion of cacodylate buffer in the enzyme assay mixture. Cacodylate gave a maximum activation of GalT-2 activity at 10 μmol/100 μl assay mixture. Further increase in cacodylate concentration (20–40 μmol/100 μl) in the enzyme assay mixture moderately decreased GalT-2 activity.

Fig. 2C shows the effect of Mn^{2+} plus Mg^{2+} (1 : 1 v/v) concentration on GalT-2 activity in PT cell homogenates. Without added metal ions, GalT-2 was inactive. Maximum GalT-2 activity was observed when 0.1 μmol of Mg^{2+} plus Mn^{2+} was added to 100 μl of the assay mixture. This translates to approximately 10.0 mM of Mg^{2+} plus Mn^{2+} and is within the range of metal ion requirements for the attainment of maximum glycosyltransferase activity [13]. Further increase in metal ion concentrations from 0.25 μmol to 1.5 μmol/100 μl assay mixture decreased GalT-2 activity in PT cell homogenates. Mg^{2+} and Mn^{2+} alone did not increase the activity significantly.

The effects of substrate (GlcCer) concentration and donor (UDP-Gal) concentration on GalT-2 activity in PT cell homogenates is shown in Fig. 3A and B, respectively. The data was plotted as $1/V$ and $1/S$ and the $K_{m,app}$ and V_{max} were calculated. The $K_{m,app}$ values for GlcCer and UDPgalactose were 3 μM and 0.5 μM, respectively. These values are approximately 4-times lower than those described for other glycosphingolipid glycosyltransferases in cultured cells [8,13,14]. Moreover, the V_{max} of the enzyme was 0.12 nmol/mg protein per 2 h and 173 nmol/4-mg protein per 2 h for GlcCer and UDP-Gal, respectively. This value is clearly higher than previously reported values of other glycosphingolipid glycosyltransferases and suggests that UDP-Gal was the rate-limiting step in the synthesis in vitro of LacCer.

Product identification was carried out employing TLC and scintillation spectrometry before and after digestion with β-galactosidase. We found that the majority (79%) of the radiolabeled product comigrated with authentic LacCer on TLC analysis (Table I). Radioactivity incorporated into GlcCer, GalCer, sulfatide, $GbOse_3Cer$ and G_{M3} were insignificant. However, a compound which

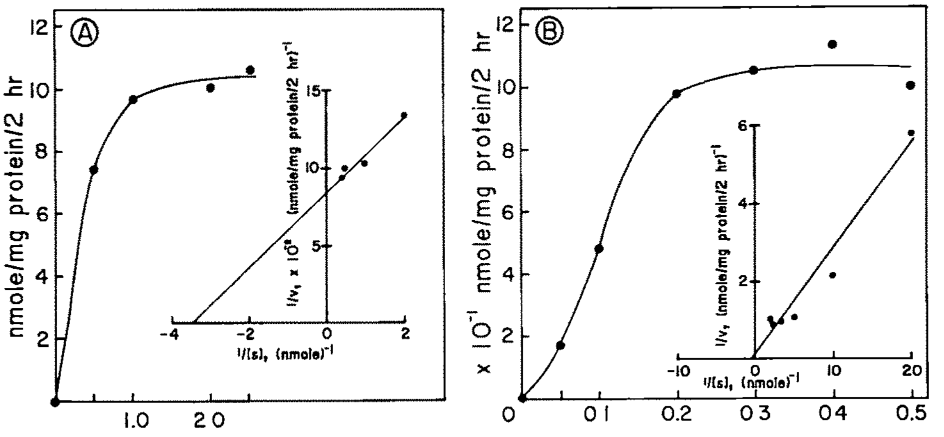

Fig. 3. Effect of glucosylceramide (GlcCer) concentration and UDP[^{14}C]galactose concentration on GalT-2 activity in PT cell homogenates Varying amounts of exogenous GlcCer acceptor and galactose donor, UDP[^{14}C]galactose was added and GalT-2 activity was measured. $K_{m,app}$ and $V_{max,app}$ were calculated by plotting the $1/V$ over $1/S$ data (shown in inset). (A) Effect of glucosylceramide concentration on GalT-2 activity in PT cell homogenates. (B) Effect of UDP[^{14}C]galactose concentrations on GalT-2 activity in PT cell homogenates.

TABLE I

DISTRIBUTION OF RADIOACTIVITY AMONG VARIOUS GLYCOSPHINGOLIPIDS IN PT CELL HOMOGENATE FOLLOWING GalT-2 ASSAY

Human PT cells were grown as described in Materials and Methods. A large-scale galactosyltransferase assay was pursued using PT cell homogenate, using GlcCer as acceptor and UDP[^{14}C]galactose as galactose donor. The product of the assay mixture was isolated by extraction with organic solvents as described in Materials and Methods, purified by silicic acid column chromatography [17] and separated on high performance thin layer chromatography (HPTLC) plates pre-sprayed with 1.5% sodium borate. The chromatogram was developed in chloroform/methanol/water/15 M NH_4OH (280:70:6:1, v/v) [11]. Gel areas corresponding to authentic glycosphingolipid were scraped and eluted with chloroform/methanol/water (100 · 50 . 10, v/v). Suitable aliquots of glycosphingolipid were subjected to radioactivity measurements employing scintillation spectrometry.

Product	dpm	Percent distribution of radioactivity
GlcCer	20	0.12
GalCer	20	0.12
LacCer	12288	79.09
Sulfatide	15	0.09
GbOse$_3$Cer	28	0.18
LcOse$_4$Cer	3088	19.87
G_{M3}	77	0.49
Total	15536	99.96

comigrated with GbOse$_4$Cer upon TLC incorporated large amounts of radioactivity. We believe that this radiolabeled compound is most probably lactotetraglycosylceramide (nLcOse$_4$Cer) because, first, nLcOse$_4$Cer has been shown to have the following structure (Galβ1 → 4GlcNAcβ1 → 3Galβ1 → 4Glcβ1 → 1′Cer) and has comigrated with GbOse$_4$Cer upon TLC. Second, using lactotriglycosylceramide (LcOse$_3$Cer, GlcNAcβ1 → 3Galcβ1 → 4Glcβ1 → 1′Cer) as substrate, we have found significant UDP-Gal:LcOse$_3$Cer galactosyltransferase (β-GalT-4) activity in PT cells (Chatterjee, S., unpublished information). Activity of this enzyme has been detected previously by Basu and his co-workers in rabbit bone marrow [24] and embryonic chicken brains [25]. We are in the process of characterizing this product employing various glycosphingolipid glycosidases.

Upon galactosidase digestion of the radiolabeled glycosphingolipid coimigrating with authentic LacCer, the majority (79%) of [^{14}C]-galactose was released, indicating that the major product formed due to GalT-2 activity in PT cells was LacCer. Moreover, upon HPLC analysis of the β-galactosidase-treated product, significant amounts of GlcCer could be detected in addition to undigested LacCer.

Using optimal conditions for the assay of GalT-2 in cultured normal human PT cells, we measured the activity of this enzyme in freshly isolated urinary PT cells from FH patients. The activity of GalT-2 in normal PT cells was 8.7 ± 0.50 nmol/mg protein per 2 h (these values were obtained from four separate batches of PT cells), whereas the activity of GalT-2 in FH-PT cells was 11.69 ± 0.50. The latter values were obtained from triplicate analysis of one homozygous FH subject (K.B.) and from another homozygous FH subject (V.P.) on one occasion. Thus, PT cells from homozygous FH patients contained 35% higher GalT-2 activity as compared to normal PT cells. We have previously shown that the levels of LacCer are elevated 15-fold in urinary PT cells from FH homozygous patients [15]. Based upon these data, we can now speculate that the increase in the cellular levels of LacCer in FH-PT cells may be due to an increase in GalT-2 activity. Previously, we have shown that cultured fibroblasts from homozygous FH subjects also have higher UDP-Gal:LacCer galactosyltransferase activity [26]. Taken together, these studies suggest that alterations in glycosyltransferase activities may regulate the cellular levels of certain glycosphingolipids.

Acknowledgements

We are grateful to Drs. Subash Basu and Manju Basu, Department of Chemistry, University of Notre Dame, for giving us fundamental instructions for the assay of glycosphingolipid glycosyltransferases and many valuable suggestions throughout the course of this study. This work was supported through an NIH grant RO-1-AM-31722.

References

1 Desnick, R.J and Sweeley, C.C. (1983) in The Metabolic Basis of Inherited Disease (Stanbury, J.B., Wyngaarden,

J B and Frederickson, D.S., eds.), pp. 906–944, McGraw-Hill, New York
2 Hakomori, S. (1981) Annu. Rev. Biochem 50, 733–764
3 Chatterjee, S. and Kwiterovich, P.O. (1984) Can J. Biochem Cell Biol. 62, 385–397
4 Roseman, S. (1970) Chem. Phys. Lipids 5, 270–297
5 Basu, S., Kaufman, B. and Roseman, S. (1968) J. Biol. Chem 243, 5802–5807
6 Hildebrand, J. and Hauser, G. (1960) J. Biol Chem. 244, 5170–5180
7 Keenan, T.W., Moore, D.J. and Basu, S (1974) J. Biol. Chem. 249, 310–315
8 Basu, S. and Basu, M. (1982) in The Glycoconjugates (Ginsburg, V, ed.), pp 265–285, Academic Press, New York
9 Coles, L. and Gray, G.M. (1970) Biochem. Biophys Res Commun 38, 520–526
10 Stoffyn, A., Stoffyn, P. and Hauser, G (1974) Biochim. Biophys Acta 360, 174–178
11 Saito, M, Saito, M and Rosenberg, A. (1985) Biochemistry 24, 3054–3059
12 Macher, B.A., Lockney, M., Moskal, J.R., Fung, Y.K. and Sweeley, C.C. Exp. Cell Res. 117, 95–102
13 Lockney, M W. and Sweeley, C.C. (1982) Biochim. Biophys. Acta 712, 234–241
14 Burczak, J.D., Fairley, J.L. and Sweeley, C.C. (1984) Biochim. Biophys. Acta 804, 662–669
15 Chatterjee, S., Sekerke, C.S. and Kwiterovich, P O. (1982) J. Lipid Res. 23, 513–522
16 Ullman, M.D. and Mcclure, R.H. (1977) J Lipid. Res. 18, 371–378
17 Esselman, W.J., Laine, R.A. and Sweeley, C C (1972) Methods Enzymol. 28, 140–156
18 Trifillis, A., Regec, A.L. and Trump, B.F (1985) J Urol. 133, 326–329
19 Sprecher, D.L., Hoeg, J.M., Schaefer, E.J., Zech, L.A, Gregg, R.T., Lakatos, E. and Brewer, H.B., Jr (1985) Metabolism 34, 294–310
20 Chatterjee, S., Gupta, P.K. and Kwiterovich, P.O (1984) Virchows Arch. Cell Pathol. 45, 365–376
21 Lowry, O.H., Rosebrough, N.J., Farr, A.L and Randall, R.J. (1951) J Biol Chem. 193, 265–275
22 Chatterjee, S, Kwiterovich, P.O., Gupta, P K., Erozan, Y.S., Alving, C.R. and Richards, R.L. (1983) Proc. Natl. Acad. Sci. USA 80, 131–1317
23 Symington, F.W. and Hakomori, S. (1985) in Glycoconjugates Proceedings of the VIIIth International Symposium, 2, 582
24 Basu, S. and Basu, M. (1972) J. Biol. Chem. 247, 1489–1495
25 Basu, S., Basu, M., Kyle, J.W. and Chon, H.C. (1984) in Gangliosides Structure and Functions (Ledeen, R., ed.), pp. 249–261, Plenum Press, New York
26 Chatterjee, S., Kwiterovich, P.O. and Sekerke, C.S (1980) in Cell Surface Glycolipids (Sweeley, C.C., ed.), pp. 265–302, American Chemical Society Symposium series, No. 128

Biochimica et Biophysica Acta 923 (1987) 143–149
Elsevier

BBA 22481

Affinity chromatography and some properties of the angiotensin-converting enzyme from human heart

Ivan Y. Sakharov, Sergei M. Danilov and Elena A. Dukhanina

Institute of Experimental Cardiology, USSR Cardiology Research Center, Moscow 121552 (U.S.S.R.)

(Received 17 April 1986)
(Revised manuscript received 6 August 1986)

Key words: Angiotensin-converting enzyme; Affinity chromatography; Anion activation; (Human heart)

Human heart angiotensin-converting enzyme has been purified by affinity chromatography on immobilized *N*-[1(*S*)-carboxy-5-aminopentyl]-Gly-Gly. The isolation procedure permitted a 1650-fold-purified enzyme to be obtained. The specific activity of angiotensin-converting enzyme was 38 units per mg protein. The molecular weight of enzyme determined by polyacrylamide gel electrophoresis in denaturing conditions was 150000. The isoelectric point (5.3) of the enzyme was determined by chromatofocusing. The K_m values of the enzyme for Bz-Gly-His-Leu and angiotensin I are 1.2 mM and 10 μM, respectively. Substrate inhibition of heart angiotensin-converting enzyme with a K_s' of 14 mM has been shown. The human heart enzyme is inhibited by SQ 20881 ($IC_{50} = 40$ nM). It was shown that NaCl, $CaCl_2$ as well as Na_2SO_4 in the absence of Cl^- are activators of the heart angiotensin-converting enzyme, whereas CH_3COONa and $NaNO_3$ have no effect on a catalytic activity of the enzyme.

Introduction

Angiotensin-converting enzyme (dipeptidyl carboxyhydrolase, EC 3.4.15.1), a zinc-metalloproteinase, plays an important role both in the renin-angiotensin and kallikrein-kinin systems by releasing hypertensive angiotensin II and by inactivating hypotensive kinins [1]. Besides, angiotensin-converting enzyme catalyses the hydrolysis of other physiologically active peptides, such as Met- and Leu-enkephalins and related compounds [2,3], substances P and K [4,5] and hydra head activator [6]. At present, homogeneous enzyme has been isolated from different animal [7–9] and human [10–13] tissues. Purification of human angiotensin-converting enzyme presents a more complicated problem, since the human enzyme appears to be more hydrophobic than the animal counterpart [13]. There are data testifying to the organ specificity of angiotensin-converting enzyme [5,8,14,15,16]. In this paper we describe the purification of angiotensin-converting enzyme from human heart with the use of affinity chromatography on the immobilized inhibitor, *N*-[1(*S*)-carboxy-5-aminopentyl]-Gly-Gly. The physico-chemical properties of the enzyme are discussed and compared with those of angiotensin-converting enzyme from other sources.

Materials and Methods

Chemicals. Hippuryl-L-histidyl-L-leucine (Bz-Gly-His-Leu), bradykinin-potentiating factor (SQ 20881) and ethanolamine were purchased from Serva; *N*-[1(*S*)-carboxy-5-aminopentyl]-Gly-Gly was a gift of Dr. J.F. Riordan (Harvard Medical School, Boston, MA, U.S.A.). Nonidet P-40, tryp-

---

Abbreviation: Mes, 4-morpholineethanesulfonic acid.

Correspondence: Dr. I.Y. Sakharov, Institute of Experimental Cardiology, USSR Cardiology Research Center, Moscow 121552, U.S.S.R.

0304-4165/87/$03.50 © 1987 Elsevier Science Publishers B.V. (Biomedical Division)

sin, soybean trypsin inhibitor, *N*-hydroxysuccinimide, *N,N*-dicyclohexylcarbodiimide and Mes were obtained from Sigma; *o*-phthalaldehyde was from Fluka; DEAE-cellulose (DE-52) was the product of Whatman; epoxy-activated Sepharose 6B, ion-exchanger PBE 94 and polybuffer 74 were obtained from Pharmacia Fine Chemicals.

Synthesis of a solid phase affinity adsorbent. *N*-[1(*S*)-carboxy-5-aminopentyl]-Gly-Gly-Sepharose was prepared by the method of Pantoliano et al. [7] with our modification. Similarly, 450 mg 6-[*N*-(*p*-aminobenzene)amino]caproic acid in 18 ml 0.1 M carbonate buffer (pH 11) were added to 3 g epoxy-activated Sepharose 6B and incubated for 17 h at 45°C. The unreacted epoxide groups were then blocked by making the suspension 1 M in ethanolamine (pH 9.0) and rotating it for 4 h at 25°C. The resulting gel was washed with 0.1 M sodium acetate/0.5 M NaCl (pH 4.0), then with 0.1 M sodium borate/0.5 M NaCl (pH 8.0), and with water and dioxane. To activate the carboxylic groups, 230 mg *N*-hydroxysuccinimide, and after 10 min, 500 mg dicyclohexylcarbodiimide were added to 20 ml of gel suspension in dioxane upon stirring. The reaction was run for 70 min at 25°C. The activated gel was washed with dioxane, methanol and again dioxane and dried on a glass filter. Then 60 mg *N*-[1(*S*)-cabroxy-5-aminopentyl]-Gly-Gly dissolved in 11 ml 0.1 M $NaHCO_3$ (pH 8.5) was added to the gel and incubated for 20 h at 4°C. The affinity adsorbent was consecutively washed with 0.1 M acetate buffer/0.5 M NaCl (pH 4.0), with 0.1 M borate buffer/0.5 M NaCl (pH 8.0) and with 20 mM Mes (pH 6.0) and stored at 4°C.

Isolation of the angiotensin-converting enzyme. The isolation procedures were done at 4°C. The purification included the following steps.

Extraction. The cardiac muscle (67 g) was withdrawn 2–4 h after death and stored before use at −70°C. The tissue was cut into small pieces and homogenized in 470 ml 50 mM K_2HPO_4 (pH 8.3) in a Waring blender at 'low speed' (1 min) and 'high speed' (1 min). The homogenate was centrifuged at 1000 × *g* for 10 min. The membrane fraction was obtained by centrifugation of the supernatant at 21 000 × *g* for 60 min. The pellet was resuspended in an equal volume of 50 mM K_2HPO_4 (pH 8.3) and recentrifuged in the same manner.

The membrane-bound enzyme was solubilized by trypsin treatment. The pellet was suspended in an equal volume of 2 mM $CaCl_2$ and mixed with 30 mg trypsin with stirring. After proteolysis for 1 h at 37°C, 30 mg soybean trypsin inhibitor was added, and the mixture was centrifuged at 21 000 × *g* for 80 min. The supernatant was dialysed against distilled water.

Ion-exchange chromatography on DEAE-cellulose. Angiotensin-converting enzyme was subjected to batch chromatography on DEAE-cellulose equilibrated with 10 mM phosphate buffer (pH 7.8). The protein/adsorbent ratio was maintained equal to 1 : 50 (g/g), which was shown to be optimal [10]. The enzyme was eluted with a starting buffer, containing 200 mM NaCl. The eluate having the enzyme activity was dialysed against 20 mM Mes (pH 6.0)/0.5 M NaCl/0.1 mM $ZnCl_2$/0.1% Nonidet P-40.

Affinity chromatography. Further purification of angiotensin-converting enzyme was performed on an affinity adsorbent with immobilized *N*-[1(*S*)-carboxy-5-aminopentyl]-Gly-Gly (Fig. 1). The enzyme solution was clarified by passage through a 0.45 μm filter and applied at room temperature to an affinity gel column (9 × 85 mm) equilibrated with 20 mM Mes (pH 6.0)/0.5 M NaCl/0.1 mM zinc acetate/0.1% Nonidet P-40, at a flow rate of 8 ml/h. To prevent nonspecific adsorption, the gel was washed with 150 ml of the starting buffer, and then with 80 ml of the same buffer without the detergent. A subsequent buffer change to 50 mM sodium borate (pH 8.9) caused the elution of bound angiotensin-conversion enzyme. The enzyme was stored at −40°C.

Enzyme assay. The activity of angiotensin-converting enzyme was measured in 100 mM Tris-HCl/400 mM NaCl/2.5 mM Bz-Gly-His-Leu at pH 7.8, except in pH dependence experiments (pH 7–9), or in 100 mM Tris-HCl/200 mM NaCl/0.2 mM angiotensin I (pH 7.4). The dipeptide formed was analyzed fluorimetrically using *o*-phthalaldehyde [17]. Incubation was carried out for 15 min at 37°C. Effect of various ions on the enzyme activity were studied in 100 mM Tris-H_2SO_4 (pH 7.8)/2.5 mM Bz-Gly-His-Leu, taking into account the effects of salts on the fluorescence of His-Leu.

One unit of enzyme activity is defined as the amount of angiotensin-converting enzyme that hydrolyses 1 μmol Bz-Gly-His-Leu per min under standard assay conditions. The specific activity is expressed as the number of units per mg protein.

Inhibition studies. The angiotensin-converting enzyme activity towards Bz-Gly-His-Leu was measured under standard conditions after preincubation of the enzyme with various concentrations of SQ 20881 ($1 \cdot 10^{-6}$–$1 \cdot 10^{-9}$ M) for 60 min at 37°C.

Analytical methods. Protein was determined by the Lowry method [18]. SDS electrophoresis was performed in 7.5% polyacrylamide gel as described by Laemmli [19]. The molecular weight of enzyme was determined using calibration proteins: myosin (205000), vinculin (130000), L-actinin (100000) and bovine serum albumin (67000). The chromatofocusing of the enzyme was carried out on ion-exchanger PBE 94 within the pH range of 6 to 4.

Results and Discussion

There are still no data about angiotensin converting enzyme from human cardiac tissue. Only partial purification of dipeptidyl carboxyhydrolase from bovine atrium has been described in a recent publication [20]. This event has given impetus to our investigation aimed at the isolation of angiotensin-converting enzyme from human heart.

The procedure of isolation of human heart angiotensin-converting enzyme is summarized in Table I. The enzyme, being a membrane-bound glycoprotein, is localized on the endothelial cell surface of human heart (unpublished data). To solubilize angiotensin-converting enzyme, we used limited proteolysis by trypsin treatment. This procedure resulted in a split-off of a hydrophobic anchor peptide inserted into the lipid bilayer of the plasma membrane [13]. A removal of this fragment does not in any way affect the activity, as shown for lung and kidney angiotensin-converting enzyme and atrium dipeptidyl carboxyhydrolase [20,21], which makes trypsinization a highly valuable and widespread methodological approach. One disadvantage of this method is the heterogeneity of angiotensin-converting enzyme preparations [10].

The earlier described, partially purified dipeptidyl carboxyhydrolase from bovine atrium [20] has a specific activity of 1.12 units per mg protein. The ventricular tissue homogenate possesses no enzyme activity. In contrast to data from an earlier study [20], we have demonstrated that human detergent-solubilized homogenates of both atrium (0.41 units per g tissue) and ventriculum (0.24 units per g tissue) exhibit the enzyme activity.

Attempts to achieve a greater purification of the bovine atrium enzyme by affinity chromatography on immobilized D-Cys-L-Pro were unsuccessful [20]. We isolated the human heart angiotensin-converting enzyme by affinity chromatography on *N*-[1(*S*)-carboxy-5-aminopentyl]-Gly-Gly coupled to Sepharose 6B (Fig. 1). The affinity resin binds up to 0.9 mg enzyme per g gel. A higher capacity of this adsorbent in relation to earlier described affinity resins [12,22,23] seems to be due to the use of an elongated spacer. The immobilized ligand was covalently linked to agarose via the spacer at a distance of 2.8 nm, which is thought to be optimal [7]. Another advantage of the affinity adsorbent is that it allows for quantitative elution of the angiotensin-converting enzyme activity under mild conditions. In addition, the affinity gel is highly stable. A 6-ml column of *N*-[1(*S*)-carboxy-5-aminopentyl]-Gly-

TABLE I

PURIFICATION OF HUMAN HEART ANGIOTENSIN-CONVERTING ENZYME

Procedure	Volume (ml)	Protein (mg)	Specific activity (units/mg)	Total activity (units)	Purification (*x*-fold)	Yield (%)
Homogenate	560	3250	0.023	74.8	1	100
Trypsinization	50	135	0.328	44.3	17	59
DEAE-cellulose	40	7.6	3.46	25.8	150	34
Affinity chromatography	10	0.57	38.0	21.7	1650	29

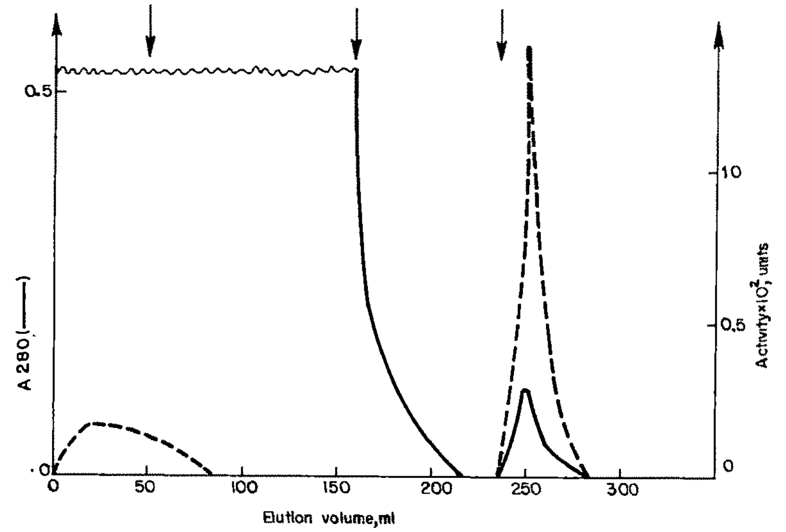

Fig. 1. Affinity chromatography of human heart angiotensin-converting enzyme on immobilized N-[1(S)-carboxy-5-aminopentyl]-Gly-Gly.

Gly-Sepharose was used 15 times over the course of 6 months for the large-scale isolation of heart enzyme. The binding capacity does not seem to diminish with use.

The use of affinity chromatography has culminated in a highly active preparation of human heart angiotensin-converting enzyme purified 1650-fold and having a specific activity of 38 units per mg protein (Table I). All steps of the isolation procedure are completed within 5 days. In this way, the use of affinity chromatography permits simplication of the purification procedure.

The purity of enzyme preparations was controlled by electrophoresis in 7.5% polyacrylamide gel slabs in the presence of SDS and 2-mercaptoethanol; the enzyme was found to migrate as single band of M_r 150000. This value is close to that for lung and kidney enzymes [10,24], but differs essentially from the M_r for aorta and testicular angiotensin-converting enzymes equal to 120000 and 100000, respectively, as well as from the M_r of 240000 for bovine atrium dipeptidyl carboxyhydrolase [20,25,26]. The isoelectric point for heart angiotensin-converting enzyme upon chromatofocusing was 5.3. This value differs from those of human angiotensin-converting enzyme from lung, kidney and blood (pI 4.45–4.55) [21,27].

The enzyme exhibited a bell-shaped pH dependence for the hydrolysis of Bz-Gly-His-Leu. a C-terminal analog of angiotensin I, with a maximum at 7.8. The pH optimum for human heart angiotensin-converting enzyme was shifted towards more acidic values as compared to corresponding values for lung and serum enzyme (8.3) [10,28]. For bovine atrium dipeptidyl carboxyhydrolase the pH optimum was at 7.3 [20]. Despite certain differences, the pH dependencies of the bovine and human cardiac enzymes are very similar. Both dependencies are narrow, which also makes heart angiotensin-converting enzyme different from its lung counterpart [29].

The value of K_m for hydrolysis of Bz-Gly-His-Leu by heart angiotensin-converting enzyme is not easily assigned because there is a pronounced substrate inhibition apparent at $[S]_0 > 4.1$ mM (Fig. 2). However, using the Michaelis-Menten equation as an empirical equation for calculating v at $[S]_0 < [S]_{opt}$, we can calculate an effective K_m. Extrapolation of the right branch of the curve gave the apparent K_m of 1.2 mM. Similar values were reported earlier for angiotensin-converting enzyme from other organs [30,31].

The observed decrease of the initial velocity of hydrolysis at high substrate concentrations has led us to consider the possibility of the formation of a ternary complex, ES_2. The symmetrical shape of the dependence of the reaction velocity (v) replotted against log $[S]_0$ is reflective of the lack of

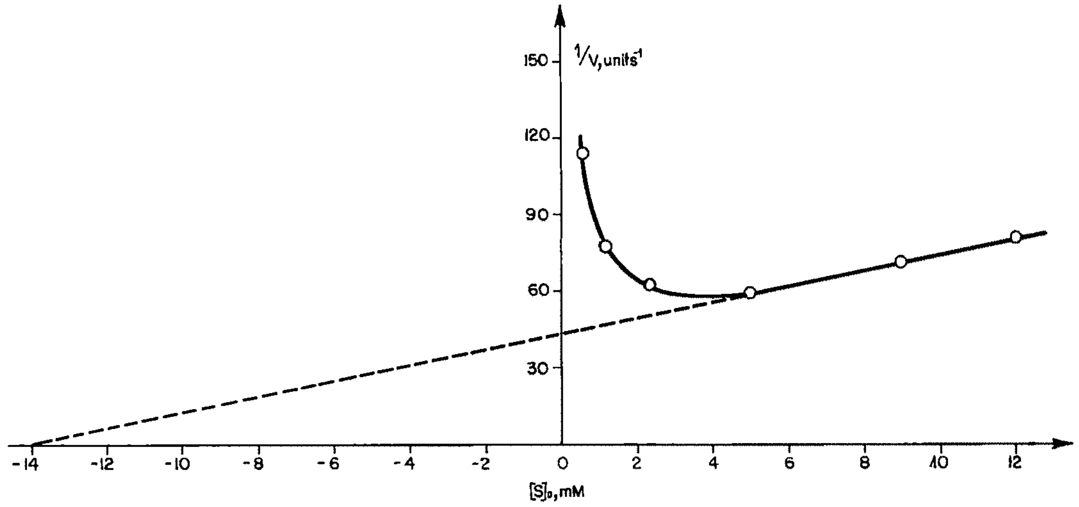

Fig. 2. Determination of inhibition constant of the heart angiotensin-converting enzyme by Bz-Gly-His-Leu.

enzymatic activity in the ES_2 complex [32]. The value of the inhibition constant K_s' (14 mM) was determined from the replots of $1/v$ versus $[S]_0$ (Fig. 2). Substrate inhibition was also observed for lung and atrium enzymes [20,33]. The coincidence of V_{max} values determined from different plots ($1/V$ versus $1/[S]_0$ and $1/V$ versus $[S]_0$) suggests that this scheme is fit for the description of enzyme reaction kinetics.

As a typical feature of angiotensin-converting enzyme is the ability of the enzyme to synthesize angiotensin II from angiotensin I [34], we have studied the hydrolysis of angiotensin I catalysed by human heart angiotensin-converting enzyme. The apparent K_m value was 10 μM. Earlier, K_m values were determined for human serum and kidney enzymes (71 and 4 μM, respectively) [13,22], which are close to the K_m obtained for the heart enzyme. The value of k_{cat} for the heart enzyme is 250 s^{-1}. Hence, the k_{cat}/K_m value for heart angiotensin-converting enzyme is 25 $M^{-1} \cdot s^{-1}$, whereas that for the lung enzyme is 20 $M^{-1} \cdot s^{-1}$ [24]. Data obtained have permitted us to define human heart dipeptidyl carboxyhydrolase as angiotensin-converting enzyme.

The angiotensin-converting enzyme showed a requirement for monovalent anions, notably chloride, for the hydrolysis of angiotensin I and related compounds [30]. The effects of various anions on the activity of human heart angiotensin-converting enzyme are shown in Fig. 3. At low salt concentrations, the increase of Cl^- results in the enzyme activation, the maximal activity being 7-fold the activity in the absence of Cl^- at 0.3–0.5 M NaCl. This value is lower than that obtained for human lung and serum counterparts (0.6 M)

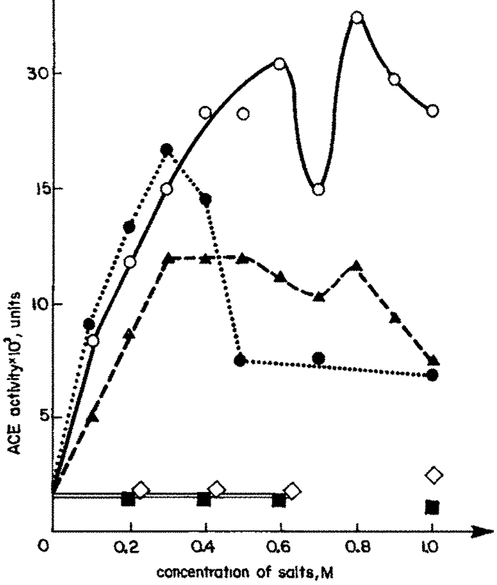

Fig. 3 Effect of different salts on the hydrolysis of Bz-Gly-His-Leu by the human heart angiotensin-converting enzyme (ACE). ▲— — —▲, NaCl; ○———○, Na_2SO_4; ●······●, $CaCl_2$; ■———■, $NaNO_3$; ◇———◇, CH_3COONa.

[10,35]. At higher NaCl concentrations, the activity of the heart enzyme sharply decreases in contrast to that of serum and lung angiotensin-converting enzymes, which is nonspecifically activated at high ionic strength [10,27].

Harris and Wilson [20] found that the activation of dipeptidyl carboxyhydrolase from bovine atrium is not controlled by Cl^-, but depends only on the ionic strength. However, this assumption is incorrect for human heart angiotensin-converting enzyme, because various salts affect differently the enzyme activity (Fig. 3). Thus, acetate and nitrate ions have no effect on the human enzyme activity. In contrast, the angiotensin-converting enzyme activity is increased 14-fold by sulfate ion in the absence of Cl^-. This fact is very important since sodium sulfate activates angiotensin-converting enzyme from other organs only in the presence of Cl^- and at high concentrations of the salt [27].

In the case of $CaCl_2$, the maximal enzyme activity is at 0.3 M salt. At higher concentrations the activity falls abruptly; at 0.5 M $CaCl_2$ the enzyme preserves only 50% of its maximal activity. The observed phenomenon can probably be explained by partial substitution of Zn^{2+} in the active site of angiotensin-converting enzyme [36] for Ca^{2+} at high concentrations of $CaCl_2$.

Human heart angiotensin-converting enzyme is effectively inhibited by SQ 20881 with an IC_{50} of 40 nM. This value of IC_{50} points to the high efficiency of the enzyme inhibition. The latter circumstance could play some role in the treatment of congestive heart failure by converting enzyme inhibitors [37]. Similar values of IC_{50} were obtained for human lung and kidney angiotensin-converting enzymes [10,11].

Thus, using affinity chromatography on *N*-[1(*S*)-carboxy-5-aminopentyl]-Gly-Gly immobilized on Sepharose, we have succeeded in isolating angiotensin-converting enzyme from human heart. It has been demonstrated that although the dipeptidyl carboxyhydrolase isolated in our laboratory may be related to angiotensin-converting enzyme, some of its physico-chemical properties differ markedly from those of converting enzyme from other organs. Analysis of immunological differences of angiotensin-converting enzyme from various human tissues with the use of monoclonal antibodies will be the subject of further studies.

Acknowledgements

We thank Dr. J.F. Riordan and Dr. B. Holmquist (Harvard Medical School, Boston, MA, U.S.A.) for their generous gift of the ligand and Dr. Zh.D. Bespalova (USSR Cardiology Research Center, Moscow, U.S.S.R.) for her help in the synthesis of the affinity resin.

References

1 Bunning, P. and Riordan, J.F (1981) in Metabolic Interconversion of Enzymes International Titisee Conference (Holzer, H., ed.), pp. 248–256, Springer, Berlin
2 Benuck, M. and Marks, N. (1979) Biochem. Biophys. Res Commun. 88, 215–221
3 Malfroy, B. and Schwartz, J.-C. (1985) Biochem Biophys. Res. Commun. 130, 372–378
4 Yokosawa, H., Endo, S., Ogura, Y and Ishii, S.-i. (1983) Biochem. Biophys Res Commun. 116, 735–742
5 Thiele, E.A., Strittmatter, S.M. and Snyder, S H (1985) Biochem. Biophys. Res. Commun. 128, 317–324
6 Roberge, M., Escher, E., Schaller, H C. and Bodenmuller, H. (1984) FEBS Lett. 173, 307–313
7 Pantoliano, M.W., Holmquist, B. and Riordan, J.F. (1984) Biochemistry 23, 1037–1042
8 Vellerti, P.A. (1985) Life Sci. 36, 1597–1608
9 Yokosawa, H, Ogura, Y. and Ishii, S -i. (1983) J Neurochem. 41, 403–410
10 Sakharov, I.Yu., Dukhanina, E.A. and Danilov, S.M. (1986) Biokhimiya 51, 946–951 (in Russian)
11 Weare, J.A , Gafford, J.T , Lu, H.S. and Erdos, E.G (1982) Anal. Biochem 123, 310–319
12 Taira, H., Mizutani, S., Kurauchi, O , Narita, O. and Tomoda, Y. (1985) J. Chromatogr. 339, 339–403
13 Erdos, E.G. and Skidgel, R.A. (1985) Biochem. Soc. Trans. 13, 42–44
14 Moore, M G., Chrzanowski, R.R., Mc Cormick, J.R., Cieplinski, W. and Schwink, A. (1984) Clin. Immunol. Immunopathol 33, 301–312
15 Van Sande, M., Sharpe, S.L. and Neels, H M (1985) J Clin Chem Clin. Biochem. 23, 381–386
16 Strittmatter, S.M., Thiele, E A., Kapiloff, M S. and Snyder, S.H (1985) J. Biol. Chem 260, 9825–9832
17 Piquilloud, Y., Reinharz, A and Roth, M (1970) Biochim. Biophys. Acta 206, 136–142
18 Lowry, O.H., Rosebrough, N.J., Farr, A L and Randall, R J. (1951) J. Biol. Chem. 193, 265–275
19 Laemmli, U.K. (1970) Nature 227, 680–685
20 Harris, R.B. and Wilson, I.B. (1984) Arch. Biochem. Biophys 233, 667–675
21 Lanzillo, J J , Stevens, J., Dasarathy, Y , Yotsumoto, H. and Fanburg, B L. (1985) J. Biol Chem 260, 14938–14944
22 Harris, R B., Ohlsson, S.T. and Wilson, I.B. (1981) Anal. Biochem 111, 227–234
23 El-Dorry, H.A., Bull, H.B., Iwata, K., Thornberry, N.A.,

Cordes, E.H. and Soffer, R.L (1982) J. Biol. Chem. 257, 14128–14133

24 Stewart, T.A., Weare, J.A. and Erdos, E G. (1981) Peptides 2, 145–152

25 Mizuno, K , Fukuchi, S and Kimura, A. (1984) Jap. Heart J. 25, 387–396

26 Soffer, R.L. and El-Dorry, H.A. (1983) Fed Proc. 42, 2735–2739

27 Ondetti, M.A. and Cushman, D.W. (1982) Annu. Rev. Biochem. 51, 283–308

28 Cushman, D.W. and Cheung, H S. (1971) Biochem Pharmacol. 20, 1637–1648

29 Neels, H.M., Scharpe, S.L., Van Sande, M E., Verkerk, R.M. and Van Asker, K.J (1982) Clin. Chem. 28, 1352–1355

30 Cushman, D.W. and Ondetti, M.A. (1980) Prog. Med Chem. 17, 42–104

31 Harris, R.B. and Wilson, I.B. (1985) Int. J. Peptide Protein Res 26, 78–82

32 Beresin, I.V. and Klyosov, A.A. (1976) Practice course of chemical and enzyme kinetics Moscow University, Moscow, 320 p

33 Rohrbach, M.S., Williams, E B. and Rolstadt, R.A. (1981) J. Biol. Chem. 256, 225–230

34 Skeggs, L.T., Marsh, W.H., Kahn, J R and Shumway, N.P (1954) J. Exp Med. 99, 275–282

35 Miyazaki, M., Okinishi, H., Nishimura, K. and Toda, N (1984) Clin. Sci 66, 39–45

36 Bunning, P. and Riordan, J.F. (1981) Isr. J. Chem 21, 43–47

37 Ferguson, R.K., Vlasses, P.H. and Rotmensch, H.H. (1984) Am. J Med. 77, 690–698

Biochimica et Biophysica Acta 923 (1987) 150–155
Elsevier

BBA 22477

Lysosomal and cytosolic sialidases in rabbit alveolar macrophages: demonstration of increased lysosomal activity after in vivo activation with bacillus Calmette-Guerin

Yannick Pilatte, Jean Bignon and Claude R. Lambré

Groupe d'immunopathologie pulmonaire, INSERM U 139, Hôpital H Mondor, 94010 Créteil (France)

(Received 18 July 1986)

Key words: Sialidase; Enzyme activation; Bacillus Calmette-Guerin; (Rabbit macrophage)

Sialidase activity was assayed in homogenized rabbit alveolar macrophages using a fluorogenic substrate: sodium 4-methylumbelliferyl-α-D-neuraminate. After differential centrifugation one acid-active enzyme (optimum pH 4.2) was detected in the 16000 × *g* pellet that contained lysosomes, mitochondria and peroxisomes. A second activity, with an optimum pH of 5.4, was found in the cytosolic fraction. The acid-active sialidase accounted for more than 95% of the total sialidase activity in crude homogenate. When alveolar macrophages were collected from rabbits stimulated with bacillus Calmette-Guerin (BCG), the acid-active sialidase specific activity was increased 2.5-fold whereas other lysosomal enzymes such as *N*-acetylglucosaminidase and β-galactosidase were stable. The cytosolic sialidase activity did not change.

Introduction

Alveolar macrophages play an important role in the inflammatory process as well as in the immune response. These mechanisms involve numerous interactions between cells and between cells and soluble effectors such as antibodies, lectins, toxins and cytokines. It was assumed that the carbohydrate moieties of membrane glycoproteins and glycolipids played a key role in these recognition phenomena [1,2]. In this context, sialic acids, essential components of most glycoconjugates, are frequently associated with numerous biological functions [3]. Thus, sialidase (EC 3.2.1.18), which hydrolyses alpha-ketosidic binding between sialic acids and glycoconjugates, could be considered as being a modulatory enzyme [3]. Mammalian sialidases are mainly lysosomal [4]. This is an important feature since phagocytic cells (including alveolar macrophages) indeed release lysosomal enzymes during endocytosis [5] or following activation by C5a [6]. It is possible that, once released into the medium, sialidases will modify membrane carbohydrates of the surrounding cells and thus alter their reactivity. A sialidase activity has been shown in immunocompetent cells such as lymphocytes and polymorphonuclear leukocytes [7]. To our knowledge, there is no available information on the presence of a sialidase activity in alveolar macrophages. Consequently, we looked for the possible presence of such an activity in these cells. Subsequently we studied the subcellular localization of this enzyme and characterized some of its kinetic parameters.

It has been shown that sialidase activity could be stimulated in activated T lymphocytes [8]. As BCG-treated rabbits are known to have activated alveolar macrophages [9], we examined the modifications of the sialidase activity in these cells collected from rabbits that had been injected with

---

Correspondence: Dr. Claude R. Lambré, INSERM U 139, Hôpital H. Mondor, 94010 Créteil Cedex, France.

0304-4165/87/$03.50 © 1987 Elsevier Science Publishers B.V. (Biomedical Division)

bacillus Calmette-Guerin (BCG). Comparatively, other enzymes such as *N*-acetylglucosaminidase (EC 3.2.1.30) and β-galactosidase (EC 3.2.1.23) have also been assayed in this model.

Materials and Methods

Cell types

Alveolar macrophages from normal rabbits. The lungs from normal male rabbits (albinos HyCr; 3 kg, Charles Rivers) were washed five times with 50 ml 154 mM NaCl maintained at 37°C. The returns were pooled (bronchoalveolar lavage) into a siliconized flask at +4°C. The number of cells obtained per rabbit ranged from $50 \cdot 10^6$ to $80 \cdot 10^6$. The bronchoalveolar lavage was centrifuged at 300 × *g* for 20 min at +4°C. The cell pellet was resuspended in Hanks' saline solution [10] at a concentration of $0.5 \cdot 10^6$ cells/ml, then 30 ml of the suspension was transferred into 110 mm (Falcon) petri dishes. After a 2 h incubation in a 5% CO_2 humid atmosphere, the non-adherent cells were removed and the petri dishes were washed three times with phosphate-buffered saline/Dulbecco buffer [11], pH 7.2 (without Ca^{2+} and Mg^{2+}). Adherent cells were harvested with a teflon scraper, resuspended in 3 ml cold phosphate-buffered saline and pelleted by centrifuging at 1000 × *g* for 20 min at +4°C. 94–98% of the cells had adhered and were macrophages as assessed by differential cell counts on smears stained with May-Grünwald Giemsa. The trypan blue dye exclusion test revealed a vitality of greater than 98%.

Alveolar macrophages from BCG-stimulated rabbits. The BCG activation was performed as according to Thomas et al. [12] with slight modifications. The rabbits were injected subcutaneously with 15 mg sonicated BCG (Institut Pasteur) in mineral oil. 14 days later the rabbits were re-injected in the marginal vein of the ear with 5 mg of sonicated BCG in saline. The lungs were washed 4 days later. The total number of cells from one rabbit ranged from 10^8 to $4 \cdot 10^8$. The cell population was heterogeneous, comprising macrophages, monocytes, lymphocytes and polymorphonuclear leukocytes. Macrophages were purified by differential adherence as described above. More than 95% of adherent cells were macrophages and the vitality exceeded 95%.

Subcellular fractionation

Alveolar macrophages were resuspended at a concentration of 10^7 cells/ml in 3 mM imidazole buffer (pH 7.2) containing 250 mM sucrose and 1 mM EDTA. The suspension was homogenized using a glass teflon homogenizer with ten strokes. The homogenate was centrifuged at 1000 × *g* for 10 min. The 'post nuclear' supernatant was then centrifuged at 16000 × *g* for 30 min. The resulting lysosome-enriched pellet was re-homogenized in distilled water (1 ml per 10^7 cells). The 16000 × *g* supernatant was centrifuged at 105000 × *g* for 1 h. The pellet was discarded and the supernatant corresponded to the soluble cytoplasmic (cytosolic) fraction. This process was performed at +4°C. The sialidase activity was assayed either immediately or after storage at −80°C.

Enzymatic assays

The sialidase activity was assayed by using a fluorogenic substrate [13]: sodium 4-methylumbelliferyl-α-D-neuraminate (Sigma, U.S.A.). In short, cell homogenates or subcellular fractions were incubated in a 100 mM sodium acetate-acetic acid buffer at various pH values for 1–4 h (at 37°C) with 250 μM substrate. The reaction (25 μl final volume) was stopped with 1 ml absolute ethanol. Sialidase activity was determined after adding 100 μl 1 M NaOH, then measuring the fluorescence intensity of released 4-methylumbelliferone. Fluorescence emission was red at 450 nm after excitation at 365 nm on a Turner fluorometer. Pure 4-methylumbelliferone was used as standard.

N-acetylglucosaminidase and β-galactosidase activities were assayed at their respective optimum pH using appropriate nitrophenolic substrates [14].

All the enzymatic assays were done in duplicate. One enzymatic unit was defined as the amount of enzyme which hydrolyses 1 nmol substrate per h at 37°C.

Protein concentration was determined using Bradford's method [15] with bovine serum albumin as standard.

Statistical evaluations

The difference between two groups was established by using analysis of variance (*F* test).

Results

Normal alveolar macrophages

Mammalian sialidases have been reported to be inhibited by Triton X-100 [7,16] and by mechanical disruption [16]. Thus, various homogenization methods were compared; namely: (a) mechanical disruption either with glass teflon homogenizer (in either 3 mM imidazole-sucrose buffer or distilled water), or by successive slow passages through a syringe needle (16 × 0.5 mm bore); and (b) detergent action (Triton X-100 0.1%). It was established that homogenization with a glass teflon homogenizer in 3 mM imidazole-sucrose buffer was the most suitable method since it allowed us to perform both subcellular-fractionation and enzymatic assays. Moreover as 3 mM imidazole buffer is weak compared to a 100 mM sodium acetate-acetic acid buffer, it allowed us to perform the enzymatic assays without prior dialysis of the homogenates or of the subcellular fractions. As plotted in Fig. 1, a sialidase showing an optimum activity at pH 4.4 was detected in the crude homogenate of normal rabbit alveolar macrophages. Its specific activity was 5 ± 2.55 U/mg of protein ($n = 5$ rabbits). The enzymatic activity was linear up to 4 h of incubation. Substrate hydrolysis was linear for an amount of protein ranging from 4.5 to 290 μg in the assay.

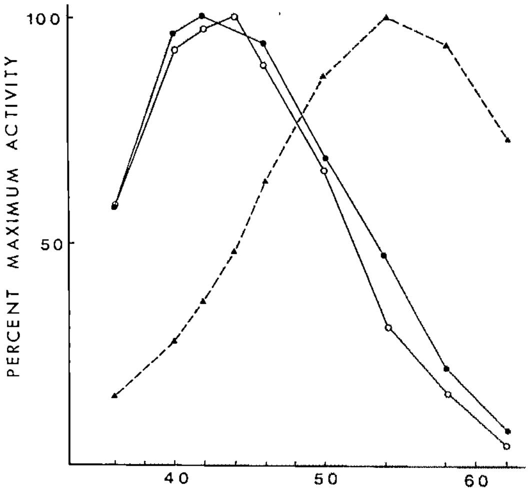

Fig. 1. pH activity curve of alveolar macrophages sialidases in the crude homogenate (○——○), in the lysosome-enriched fraction (●——●), and in the cytosolic fraction (▲— — —▲). Maximal activities are: 5±2.55 U/mg for the crude homogenate; 19.5±4.2 U/mg for the lysosome-enriched fraction; and 0.014±0.004 U/mg for the cytosolic fraction. Maximal activities are expressed in nmol substrate hydrolysed per h per mg protein.

Sialidase detected in the 16000 × g pellet had a pH activity curve very similar to that of the crude homogenate with an optimum pH at 4.2 (Fig. 1). More than 70% of the β-galactosidase activity that had been found in the crude homogenate was recovered in the 16000 × g pellet.

No sialidase activity could be detected in the 105000 × g supernatant (cytosol), unless it had been 20-fold concentrated on a DIAFLO PM 10 ultrafiltration membrane (Amicon, U.S.A.). The cytosolic sialidase then detected had an optimum activity at pH 5.4 (Fig. 1). This activity was very weak in comparison with that of the lysosome-enriched fraction. It accounted for no more than 5% of the total activity of the crude homogenate at pH 4.4. In the lysosome-enriched fraction, sialidase had an apparent K_m of 0.11 ± 0.014 mM ($n = 5$) at pH 4.2 whereas, in the cytosolic fraction, the apparent K_m was 0.28 ± 0.042 mM ($n = 4$) at pH 5.4. Some characteristics of these activities are summarized in Table I. It should be noticed that the cytosolic sialidase was more stable than the one associated with the lysosome-enriched fraction. After 1 week of storage at −80°C,

TABLE I

PROPERTIES OF SIALIDASES IN THE LYSOSOME-ENRICHED (LYSOSOMAL) AND CYTOSOLIC FRACTIONS FROM NORMAL RABBIT ALVEOLAR MACROPHAGES

Mu-NANA = sodium 4-methylumbelliferyl-α-D-neuraminate; NANA = N-acetylneuraminic acid.

	Lysosomal	Cytosolic
Optimum pH	4.2	5.4
Apparent K_m for Mu-NANA	0.11 ±0.014 mM	0.28 ±0.042 mM
Inhibition by 100 μM 2,3-dehydro-2-deoxy-NANA	90%	100%
Inhibition by 8 mM NANA	43%	76%
Inhibition by 10 mM EDTA	9%	0%
Activation by 20 mM $CaCl_2$	4%	19%
Residual activity after 1 week of storage at −80°C	57%	90%

the residual activity was respectively 57% and 90% in the lysosome-enriched and the cytosolic fractions.

BCG-stimulated alveolar macrophages

We have observed a 2.5-fold increase in the specific sialidase activity in the crude homogenate of alveolar macrophages collected from BCG-activated rabbits compared to normal rabbits (Table II). This increase seemed to be specific for sialidase since the specific activities of two lysosomal glycosidases (β-galactosidase and *N*-acetylglucosaminidase) were not significantly changed in the same animals (Table II). In alveolar macrophages from BCG-stimulated rabbits, the sialidase kinetic parameters were not modified. The pH activity curves and apparent K_m values were identical to those obtained from normal alveolar macrophages for both 'lysosomal' and cytosolic activities.

Effect of adherence to plastic on the enzymatic activities

The question arose as to what extent adherence of the cells, by itself, could modify the sialidase activity. In order to examine this possibility, the alveolar macrophages from normal rabbits were separated into two batches. The cells from the first batch were pelleted, then frozen at once, whereas the cells from the second one were pelleted, then frozen after an adherence step. The two pellets were homogenized and the crude homogenates were tested for sialidase, *N*-acetylglucosaminidase and β-galactosidase activities. Cells that had adhered to plastic showed a slight decrease in the specific sialidase activity (−30%). The activities of the two other glycosidases were not modified (Table III).

TABLE II

SPECIFIC ENZYMATIC ACTIVITIES IN ALVEOLAR MACROPHAGES FROM NORMAL AND BCG-STIMULATED RABBITS

^{ns} No significant difference, * significantly different ($P \leq 0.03$).

	Specific enzymic activities (nM substrate hydrolysed per h per mg protein)		
	sialidase	*N*-acetylglucosaminidase	β-galactosidase
Normal ($n = 5$)	5.02 ± 2.55	6547.2 ± 691.4	1551 ± 433.2
BCG-activated ($n = 5$)	13.03 ± 4.88 *	7277 ± 2701 ^{ns}	1612.8 ± 328 ^{ns}

TABLE III

EFFECT OF CELL ADHERENCE TO PLASTIC ON THE SPECIFIC ACTIVITY OF SIALIDASE, *N*-ACETYLGLUCOSAMINIDASE AND β-GALACTOSIDASE FROM NORMAL RABBIT ALVEOLAR MACROPHAGES

	Specific activity (nM substrate hydrolysed per h per mg protein)		
	sialidase	β-galactosidase	N-acetylglucosaminidase
Expt. No. 1			
without adherence	3.8	1304	6954
with adherence	2.6	1097	6618
Expt No. 2			
without adherence	4.4	2172	6870
with adherence	3.0	2268	6848

Discussion

This report provides evidence for the presence of sialidase activities in alveolar macrophages from normal rabbits. During differential subcellular fractionation a first activity was detected in the 16000 × *g* pellet with an acid optimum activity at pH 4.2. This pellet corresponded to the lysosome-enriched subcellular fraction as assessed by the presence of more than 70% of the β-galactosidase activity initially found in the crude homogenate. The presence of a lysosome-associated sialidase with an acidic optimum activity pH has been previously demonstrated in other cell types of the immune system such as lymphocytes and granulocytes [17–19]. A second activity was found in the soluble fraction of the cytoplasm. Its optimum activity pH was more neutral (pH 5.4). It seems that this is the first demonstration of a cytosolic sialidase in immunocompetent cells. This could be due to the fact that this very weak cytosolic sialidase activity has previously gone undetected, the activity being detectable only after concentration of the cytosolic fraction. However, a cytosolic sialidase with an optimum activity at a similar pH has been detected in extracts from pig brains [20] and rat liver [21].

It was also observed that alveolar macrophages that had adhered on petri dishes had a depressed acid-active sialidase (−30%). However, as no sialidase activity was detected in the cell-free medium, the origin of this observation remains unclear. Since membrane sialic acids influence cell adherence [3], it could be hypothesized that adherence may be facilitated by a decreased sialidase activity.

In alveolar macrophages harvested from BCG-stimulated rabbits, the acid-active sialidase activity (in the lysosome-enriched fraction) was significantly increased (2.5-fold) whereas the cytosolic sialidase activity did not change. By contrast, lysosomal enzymes such as *N*-acetylglucosaminidase and *β*-galactosidase were not stimulated. Therefore BCG seemed to induce a specific increase in the acid-active sialidase activity. This observation seems of interest to us in relation to the following results. In vivo BCG treatment induces plasma membrane glycoprotein alterations and cell fusion of these activated macrophages in culture [12]. Moreover, it has been demonstrated that protein-bound carbohydrates have higher molecular weights and more branched structures in BCG-activated peritoneal macrophages than in resting cells [22]. It is quite conceivable that sialidase may be involved in these modifications by allowing partial or total desialylation, possibly followed by reglycosylation of plasma membrane glycoproteins. This hypothesis is strenghthened by recent reports demonstrating that mouse concanavalin A-activated T lymphocytes expressed hyposialylated MHC class I glycoproteins [23] and had an increased level of endogenous sialidase activity [8]. Although several authors [8,24] have advocated that a direct correlation may exist between the level of membrane glycoprotein sialylation and the amount of intracellular sialidase activity, the responsiblity of the endogenous sialidase in membrane glycoprotein hyposialylation is not yet definitively assessed.

Sialidase-induced membrane desialylation may occur through two different pathways. Membrane glycoproteins may be desialylated by sialidase that could be released in the medium with other lysosomal enzymes following cell activation by different stimuli, for instance by C5a [6]. Alternatively, membrane glycoproteins may be desialylated during a recycling process in the course of which lysosomes could fuse with vesicles endocytosed from the cell surface [25]. Although the sialidase activity of alveolar macrophage sialidases was assayed with only one substrate (sodium 4-methylumbelliferyl-α-D-neuraminate), the efficiency of the enzyme on membrane glycoproteins seems likely. Thus, it has been shown that this substrate was relevant to assess the activity of sialidase on glycoproteins [26–28].

Furthermore, sialidases, through desialylation of cell membrane, have a potential pathogenic effect. It has been demonstrated that cell membrane desialylation is efficiently induced by either soluble (*Vibrio cholerae*) or particle-bound (influenza virus) sialidases. In these cases, desialylation result in complement-mediated cell lysis through an antibody-independent [29] or -dependent [30] mechanism. Thus, an increased and sustained release of lysosomal sialidase by activated cells could have a similar effect.

Further studies on the properties (substrate specificities, molecular weight) and on the functional role of alveolar macrophage sialidases, as well as on the pathological consequences following BCG activation, are now in progress.

Acknowledgment

The authors thank Laure Magne and Catherine Vaslin for skilled assistance.

References

1 Sharon, N. (1984) Trends Biochem. Sci. 9, 198–202

2 Baenziger, J.U. (1985) Am. J. Pathol 121, 382–391

3 Schauer, R. (1982) Adv Carbohydr. Chem Biochem 40, 131–234

4 Corfield, A.P., Michalski, J.-C. and Schauer, R (1981) in Prospectives in inherited metabolic diseases (Tettamanti, G., Durand, P. and Di Donato, S, eds.), Vol. 4, pp. 3–70, Edi Ermes, Milano

5 Schnyder, J and Baggioli, M (1980) in Mononuclear Phagocytes (Van Furth, R., ed.), pp. 1369–1381, Martinus Nihoff Publishers, The Hague

6 Hartung, H.P. and Hadding, U. (1983) Agents Actions 13, 415–428

7 Nguyen Hong, V., Beauregard, G, Potier, M., Bélisle, M., Mamelli, L., Gatti, R. and Durand, P. (1980) Biochim. Biophys Acta 616, 259–270

8 Landolfi, N.F., Leone, J., Womack, J.E. and Cook, R.G. (1985) Immunogenetics 22, 159–167

9 Thompson, B. and Myrvik, Q.N. (1985) Exp. Lung Res. 9, 237–253

10 Hanks, J H and Wallace, R.E. (1949) Proc. Soc Exp. Biol Med. 71, 196–200

11 Dulbecco, R. and Vogt, M. (1954) J. Exp. Med. 99, 167–182

12 Thomas, J.A., Hollande, E. and Vilain, C. (1971) C R. Acad. Sci. Paris 273, 2564–2567

13 Potier, M., Mamelli, L , Dallaire, L. and Melançon, S.B. (1979) Anal. Biochem 94, 287–296

14 Conchie, J., Finlay, J. and Levvy, G.A. (1959) Biochem J. 71, 318–325

15 Bradford, M.M. (1976) Anal. Biochem. 72, 248–254

16 Warner, T G. and O'Brien, J S. (1979) Biochemistry 18, 2783–2787

17 Yeh, A.K., Tulsiani, D R.P. and Carubelli, R. (1971) J. Lab. Clin. Med. 78, 771–778

18 Marchesini, S., Cestaro, B , Lombardo, A., Sciorelli, G. and Preti, A. (1984) Biochem Int. 8, 151–158

19 Schauer, R., Wember, M. and Tschesche, H. (1984) Hoppe-Seyler's Z. Physiol. Chem. 365, 419–426

20 Venerando, B , Tettamanti, G , Cestaro, B. and Zambotti, V. (1975) Biochim Biophys Acta 403, 461–472

21 Miyagi, T. and Tsuiki, S. (1985) J. Biol Chem. 260, 6710–6716

22 Mercurio, A.M and Robbins, P.W. (1985) J. Immunol. 135, 1305–1312

23 Landolfi, N.F. and Cook, R.G. (1986) Mol. Immunol 23, 297–309

24 Sohdi, A. and Prasab S B. (1985) Experientia 41, 93–95

25 Tsé, O.B. and Pernis, B. (1984) J Exp Med. 159, 193–207

26 Yamada, T., Tsuji, S., Ariga, T and Miyakate, T. (1983) Biochim Biophys. Acta 755, 106–111

27 Miyagi, T. and Tsuiki, S. (1984) Eur J. Biochem. 141, 75–81

28 Michalski, J C., Corfield, A.P. and Schauer, R (1986) Hoppe-Seyler's Z. Biol Chem. 367, 715–722

29 Lambré, C.R , Kazatchkine, M.D., Maillet, F. and Thibon, M. (1982) J. Immunol. 128, 629–634

30 Lambré, C.R., Pilatte, Y , Le Maho, S. and Blanc, C (1985) Mol Immunol. 22, 1123–1129

Biochimica et Biophysica Acta 923 (1987) 156–165
Elsevier

BBA 22483

Partial purification and characterisation of S-adenosylmethionine:protein-histidine N-methyltransferase from rabbit skeletal muscle

C. Vijayasarathy and B.S. Narasinga Rao

Department of Biophysics, National Institute of Nutrition, Indian Council of Medical Research, Jamai Osmania P.O., Hyderabad - 500 007 (India)

(Received 6 August 1986)

Key words: Protein-histidine methylase; 3-N-Methylhistidine; Actin; Myosin; (Skeletal muscle)

A new class of protein methylase (S-adenosylmethionine:protein-histidine N-methyltransferase) which methylates histidine residues of protein substrates using S-adenosylmethionine as the methyl donor has been partially purified from rabbit skeletal muscle, 22-fold with a yield of 56%. The enzyme activity was monitored using denatured myofibrils from young rabbit skeletal muscle as the methyl acceptor protein substrate. The enzyme was localised in the myofibrillar fraction and myofibrils isolated in pure form represented the enzyme-substrate complex. The enzyme was solubilised in 0.275 M KCl. The methylase showed no requirement for any metal ion and has a pH optimum of 8.0. It was shown to require a reducing agent like mercaptoethanol for its activity. It was also shown that cardiac and skeletal muscle forms of actins obtained from different species serve as the efficient methyl acceptor protein substrates. Since the enzyme was found to methylate specifically the histidine residues of actin we propose to designate this new methylase as protein methylase IV, to distinguish it from the already known protein methylases I, II and III.

Introduction

The methylated amino acids such as methyllysines, methylarginines and carboxymethyl esters of aspartic/glutamic acids occur widely in nature. They have been shown to arise from post-translational enzymatic methylation of side chains of amino acids in proteins wherein S-adenosylmethionine is the methyl donor [1,2]. So far three classes of protein methylases involved in the methylation of guanidino groups of arginine, protein carboxyl groups of aspartic/glutamic acids and ε-amino groups of lysine have been identified, characterised and have been designated as protein methylases I, II and III, respectively [2–6].

3-N-Methylhistidine (3-MeHis), yet another methylated amino acid, is unique to the contractile proteins actin and myosin. Methylation of contractile proteins of muscle has been studied under a variety of conditions and the existence of an enzyme which methylates protein histidine residues has been proposed [7–11]. However, the enzymes involved in muscle protein histidine methylation have been neither characterised (solubilised) nor purified. The present study describes the isolation, identification and partial purification of S-adenosylmethionine:protein-histidine N-methyltransferase (protein-histidine methylase) from rabbit skeletal muscle.

Abbreviations: AdoMet, S-adenosylmethionine; Me, methyl; 3-MeHis, 3-N-methylhistidine; SDS, sodium dodecyl sulfate; Tris, 2-amino-2-hydroxymethylpropane-1,3-diol.

Correspondence: Dr. B.S. Narasinga Rao, National Institute of Nutrition, Jamai Osmania P.O., Hyderabad-500 007, India.

0304-4165/87/$03.50 © 1987 Elsevier Science Publishers B V (Biomedical Division)

Materials and Methods

Animals

Young (less than 18 days old) and adult (2–3 months old) New Zealand albino rabbits were obtained from the Laboratory Animals Information Service Centre of the Institute. The animals were fed on a stock diet till killed. Bovine hearts were obtained fresh from a slaughter house in the city.

Chemicals

L-Methionine, L-histidine, 1-*N*-methylhistidine, 3-*N*-methylhistidine, *S*-adenosylhomocysteine, ATP, glutathione, nicotinamide, *N*′-methylnicotinamide, acrylamide, bisacrylamide, 2-mercaptoethanol, *N*-ethylmaleimide, Trizma base, histone type IIA, Dowex 50-X2 (100–200), Dowex 50-X8 (100–200), Sephadex G-200 and DEAE-Sephadex A-50 were purchased from Sigma Chemical Company, St. Louis, U.S.A.

L-[*methyl*-^{14}C]Methionine (specific activity 60.4 μCi/μmol) was obtained from the Radiochemical Centre, Amersham, U.K. Other chemicals used were of high purity analar grade.

Preparation of S-[methyl-^{14}C]adenosylmethionine ([Me-^{14}C]AdoMet)

[*Me*-^{14}C]AdoMet was synthesised using ATP:L-methionine *S*-adenosyltransferase (EC 2.5.1.6) isolated from rabbit liver [12]. The biological purity of [*Me*-^{14}C]AdoMet was determined by the rate of formation of *N*′-methylnicotinamide from AdoMet and nicotinamide catalysed by the enzyme *S*-adenosylmethionine:nicotinamide *N*-methyltransferase (EC 2.1.1.1) isolated from rat liver [13]. [*Me*-^{14}C]AdoMet was found to be biologically and radiochemically pure.

In vitro methylation of rabbit hind limb skeletal muscle proteins

Young and adult rabbits were killed by decapitation and hind limb muscles were quickly removed and placed on crushed ice. The muscle tissues were freed of fat and connective tissue and then cut into small pieces. They were then homogenised for 90 s in a polytron homogeniser (Type FT 10-35, Kinematica GmbH, CH 6010, KMiens/Luzern) with 3 vol. of 0.25 M sucrose/0.01 M Tris-HCl buffer (pH 7.6). All the above operations were carried out at 4–6 °C in a cold room. The skeletal muscle homogenates were then spun at 105 000 × *g* for 1 h (Beckman L 8-70 Ultra centrifuge) to separate into myofibrillar and sarcoplasmic fractions.

The whole skeletal muscle homogenates (3 ml) and the myofibrillar fraction with and without sarcoplasmic fractions were incubated for 5 h at 37 °C with 8 μM [*Me*-^{14}C]AdoMet in a total volume of 5 ml. The medium contained 0.2 M Tris-HCl (pH 7.6), 0.1 M KCl, 0.4 mM MgCl$_2$ and 0.8 mM mercaptoethanol. The fractions which were heated at 100 °C for 10 min served as blanks. The reaction was terminated by the addition of an equal volume of 25% trichloroacetic acid (w/v).

Methyl acceptor protein substrates

Myofibrils were isolated in 0.1 M KCl/0.039 M borate medium (pH 7.1) essentially as described earlier [14] from young (less than 18 days old) rabbit skeletal muscle. They were heated at 75 °C for 15 min and used as methyl acceptor protein substrate. The protein content of an aqueous suspension of the myofibrillar preparation was around 20–25 mg/ml.

The methyl acceptor contractile proteins myosin and actin were isolated from bovine heart and also from cardiac and skeletal muscle of rats and rabbits. Actin was prepared from acetone powder essentially as described by Seraydarian et al. [15] and purified by two polymerisation cycles [16]. Myosin was purified by column chromatography on a DEAE-Sephadex A-50 column [17].

Protein determination

Protein concentration was determined by the method of Lowry et al. [18] with bovine serum albumin as standard or by determination of absorbance at 280 nm.

Polyacrylamide gel electrophoresis

The purity of the protein preparations was determined using SDS-polyacrylamide gel electrophoresis according to the method of Weber and Osborn [19]. A single band was seen both on 5% and 7.5% polyacrylamide gels (Fig. 1A).

Solubilisation and partial purification of the protein-histidine methylase from rabbit skeletal muscle

All the operations were performed in a cold room at 4–6°C. To identify optimum conditions for isolating protein-histidine methylating enzyme the following preliminary experiment was carried out. Rabbit hind limb skeletal muscle was homogenised in a Waring Blendor at top speed for 2 min in different media. The media tested were: 0.25 M sucrose/0.01 M Tris-HCl (pH 7.6); 0.1 M KCl/0.039 M borate (pH 7.1) and 0.275 M KCl/0.039 M borate (pH 7.1). The total homogenate was subjected to differential centrifugation and the enzyme activity was determined in various fractions. Based on these initial trials the folowing scheme to isolate the partially purified protein-histidine methylase was developed.

The muscle from hind limbs of rabbits was freed of fat and connective tissue and cut into small pieces. It was then homogenised in a Waring Blendor at maximum speed for 2 min in 3 vol. of 0.25 M sucrose/0.01 M Tris-HCl (pH 7.4). The suspension was centrifuged for 10 min at 8000 × *g*. The supernatant was discarded and the pellet was extracted with 5 vol. of 0.275 M KCl/0.039 M borate medium (pH 7.1) for 1 h. The suspension was centrifuged for 10 min at 8000 × *g*. The supernatant was filtered through glass wool to remove fat particles. Then solid ammonium sulphate was added with constant stirring to give 40% saturation. The mixture was allowed to stand for 2 h in the cold and then centrifuged at 10000 rpm for 10 min. To the supernatant fluid additional ammonium sulphate was added to 60% saturation as described above. After 2 h on ice, the precipitate was collected by centrifugation and dissolved in ice-cold 0.275 M KCl/0.039 M borate medium (pH 7.1). Finally this was dialysed twice for 4 h against 100 vol. of glass-distilled water till it was free of ammonium sulphate and KCl.

Further purification of the methylase was attempted by chromatography on a Sephadex G-200 column (45 × 1 cm). The column was equilibrated with 0.275 M KCl/0.039 M borate medium (pH 7.1). The ammonium sulphate fraction which was dialysed against water was dissolved in 0.275 M KCl/0.039 M borate medium before loading on the column. A volume of 5 ml, equivalent to 98 mg protein, was applied on to the column. The column was eluted with 0.275 M KCl/0.039 M borate buffer at a flow rate of 20 ml/h and 5 ml fractions were collected. The fractions were dialysed against water before testing them for the enzyme activity.

An alternative chromatographic system using DEAE-Sephadex A-50 with 0.15 M phosphate/0.01 M EDTA buffer (pH 7.5) with a linear KCl gradient to 0.5 M KCl was employed to resolve the methylase from the myofibrillar protein aggregates. The ammonium sulphate fraction following dialysis first against water and then later against 0.15 M phosphate/0.01 M EDTA (pH 7.5) was applied on to a DEAE-Sephadex A-50 column (20 × 3 cm). A sample volume of 26 ml, equivalent to 148 mg protein, was loaded on the column. The column was eluted with equilibrating buffer at a flow rate of 30 ml/h and 15 ml fractions were collected. The gradient was started at 130 ml (250 ml equilibrating buffer plus 250 ml of the same made in 0.5 M KCl).

Enzyme assay

The general properties of the enzyme were studied using ammonium sulphate fraction (40–60% saturation) as the enzyme source. Enzyme preparation (2 mg protein) and methyl acceptor protein (heated myofibrils, 60 mg) were incubated for 1.5 h at 37°C in a 5 ml reaction medium containing 0.2 M Tris-HCl (pH 8.0), 4 mM mercaptoethanol and 4 μM [*Me*-^{14}C]AdoMet. Though in the initial studies the assay medium contained KCl and $MgCl_2$ based on the studies of Krzysik et al. [8], these were excluded in the latter experiments since they were found to inhibit the enzyme activity. The reaction was started by the addition of [*Me*-^{14}C]AdoMet and terminated with an equal volume of trichloroacetic acid 25% (w/v). A control with all the ingredients except the protein-histidine methylase was also also assayed.

Identification and quantitation of the reaction product 3-N-methylhistidine

The reaction products of three classes of protein methylases – the methylated arginines (protein methylase I), carboxymethyl esters of glutamic and aspartic acids (protein methylase II), and ϵ-*N*-methyllysines (protein methylase III) – have been selectively quantitated by employing the differences in pH optima for these three classes of protein methylases as well as the differences in the chemical properties of the methylated amino acids [2]. Both 3-MeHis and methyllysines being resistant to acid or alkali hydrolysis, their quantitation by selective destruction of either of them is not possible. Further, as shown in Table I, the ^{14}C-Me radioactivity in the substrate (denatured myofibrils) both in the control and in the presence of enzyme preparation was localised not only in 3-MeHis and methyllysine fractions but also in the acidic and neutral amino acid fractions, although the ^{14}C radioactivity in the 3-MeHis fraction progressively increased during the purification of rabbit skeletal muscle protein-histidine methylase. However, the nonspecific ^{14}C radioactivity in other amino acid fractions remained the same or decreased during the purification of the enzyme, indicating the specificity of the enzyme towards histidine methylation.

In all the assays of the protein-histidine methylase reported in these studies, the product of the enzyme 3-[*Me*-^{14}C]MeHis was routinely analysed following the selective isolation and quantitation of 3-[*Me*-^{14}C]MeHis from protein hydrolysates on Dowex 50-X8 columns.

The enzymatically methylated proteins were freed from the acid-soluble [*Me*-^{14}C]AdoMet, nucleic acid and phospholipids by successive washings with 10% hot and cold trichloroacetic acid, alcohol and diethyl ether as described by Krzysik et al. [8]. ^{14}C-Me-labelled proteins were hydrolysed in 6 M HCl under vacuum at 105°C for 18 h. 3-[*Me*-^{14}C]MeHis was quantitatively isolated from protein hydrolysates employing ion exchange chromatography on Dowex 50-X8 columns as described by Haverberg et al. [20]. Briefly, the protein hydrolysates in 0.2 M pyridine (1–10 mg protein/ml of packed column volume) were placed on the column and the neutral and acidic amino acids were eluted with 12 column vol. of 0.2 M pyridine. This was followed by elution with 5 column vol. of 1 M pyridine when 3-MeHis with some histidine combination was eluted out. The 3-MeHis fraction was dried by rotary evaporation

TABLE I

DISTRIBUTION OF ^{14}C RADIOACTIVITY OF METHYLATED DENATURED MYOFIBRILS IN VARIOUS AMINO ACID FRACTIONS DURING THE PURIFICATION OF RABBIT SKELETAL MUSCLE PROTEIN-HISTIDINE METHYLASE

The enzyme activity was assayed with denatured myofibrils (60 mg) from young rabbit skeletal muscle as methyl acceptor protein substrate. The reaction medium contained enzyme preparation (2 mg protein), 0.2 M Tris-HCl (pH 7.6), 0.1 M KCl, 0.4 mM $MgCl_2$, 0.8 mM mercaptoethanol and 8 μM [*Me*-^{14}C]AdoMet in a total volume of 5 ml. A control with all the ingredients except the enzyme preparation was also tested. The methylated proteins were freed from acid-soluble [*Me*-^{14}C]AdoMet, nucleic acids and phospholipids by successive washings with 10% hot and cold trichloroacetic acid, ethyl alcohol and diethyl ether The ^{14}C-Me-labelled proteins were hydrolysed and the protein hydrolysates in 0.2 M pyridine were loaded on a Dowex 50-X8 column (10 mg protein/ml of packed column volume). The acidic and neutral amino acids were eluted with 12 column vol of 0.2 M pyridine, 3-MeHis with 5 column vol of 1.0 M pyridine and basic amino acids with 3 column vol. of 3 M NH_4OH. The fractions were dried by rotary evaporation and dissolved in 1 ml water The ^{14}C radioactivity was determined in a liquid scintillation spectrometer using Brays mixture The ^{14}C radioactivity in the control tube was 9200 dpm in acidic and neutral amino acid; 504 dpm in 3-MeHis and 2320 dpm in basic amino acid fractions. This was taken as unity while expressing the activities in the presence of enzyme preparation.

Enzyme source	Amino acid fractions		
	acidic and neutral amino acids (0.2 M pyridine)	3-MeHis (1.0 M pyridine)	basic amino acids (3 M NH_4OH)
Nil (control)	1.0	1.0	1.0
Crude supernatant	2.8	12.7	5.0
40–60% ammonium sulphate fraction	1.8	60.0	1.8
DEAE-Sephadex A-50 chromatography fraction	1.3	526.0	1.5

and dissolved in 1 ml water. To this aqueous solution 20 ml Brays mixture was added and the ^{14}C radioactivity was determined in a liquid scintillation spectrometer (Packard 3255).

The identity and the recovery of 3-MeHis was checked in an automatic amino acid analyser (Beckman Model 119 CL). The chromatography was carried out on a column of W3P resin with a buffer flow rate of 44 ml/h. The starting buffer was 0.2 M lithium citrate (pH 2.83) followed by 0.2 M lithium citrate (pH 3.7) and 1 M lithium citrate (pH 3.75).

Enzyme activity

Enzyme activity was expressed as ^{14}C-Me incorporation in pmol/h per mg enzyme protein.

Results

All the data presented in this study are representative of three experiments.

Localisation of the enzyme and selection of myofibrils as methyl acceptor protein substrate

Incorporation of ^{14}C-Me groups into histidine residues of crude myofibrillar protein preparation of young animals was higher than that in adult animals (Table II). Further ^{14}C-Me incorporation into histidine residues of myofibrillar proteins essentially remained the same both in the presence and absence of sarcoplasmic fraction, indicating that the muscle protein-histidine methylase is associated with a myofibrillar fraction (Table II).

Myofibrils isolated in pure form, per se, incorporated ^{14}C-Me groups into their histidine residues. The rates of ^{14}C-Me incorporation which exhibited saturation kinetics ranged from 2.2 to 23.2 pmol/h per 70 mg myofibrillar protein over the [*Me*-^{14}C]AdoMet concentration range of 1–8 μM. Myofibrils heated at 75°C for 15 min to destroy the endogenous methylase exhibited negligible rates of ^{14}C-Me incorporation (less than 1 pmol/h per 70 mg myofibrillar protein at 8 μM AdoMet concentration) into their histidine residues. As will be shown later, the heated myofibrils can serve as an efficient methyl acceptor protein substrate.

Isolation of the enzyme

Since the enzyme, protein-histidine methylase, was found to be associated with myofibrils, the myofibrils were also processed to solubilise the enzyme. The data presented in Table III reveal the following facts: (a) the enzyme is not sucrose extractable; (b) 0.1 M KCl extracted around 38% of the enzyme activity; while (c) 0.275 M KCl extracted around 82% of the enzyme activity from the rabbit skeletal muscle homogenates. The data also confirm that the protein-histidine methylase is solubilised in 0.275 M KCl, the criterion for solubility being the presence of the enzyme in 105 000 × g supernatant fraction.

Ammonium sulphate fractionation precipitated out most of the enzyme between 40 and 60% saturation with an enrichment of 22-fold (Table IV). The protein pattern of partially purified en-

TABLE II

^{14}C-ME INCORPORATION INTO HISTIDINE RESIDUES OF SKELETAL MUSCLE PROTEINS OF YOUNG AND ADULT RABBITS

Values for 3 ml total homogenates (80 mg protein). 105 000 × g pellet made to original 3 ml volume with buffer. The reaction medium contained 0.2 M Tris-HCl (pH 7.6), 0.1 M KCl, 0.4 mM $MgCl_2$, 0.8 mM mercaptoethanol and 8 μM [*Me*-^{14}C]AdoMet in a total volume of 5 ml

	^{14}C-Me incorporation (pmol/h per reaction vessel)		
	total homogenate	105 000 × g pellet	105 000 × g pellet plus 105 000 × g supernatant
Young rabbits	21.2	19.8	22.0
(< 18 days old)	35.0	32.6	34.0
Adult rabbits	5.8	5.2	5.6
(2–3 months old)	7.0	6.8	7.4

TABLE III

SOLUBILISATION OF RABBIT SKELETAL MUSCLE PROTEIN-HISTIDINE METHYLASE

Activity in total volume of homogenate in each buffer is taken as 100%, which is equivalent to ^{14}C-Me incorporation of 3200 pmol/h. Enzyme activity was assayed as described in Table I with denatured myofibrils (60 mg) from young rabbit skeletal muscle as methyl acceptor protein substrate. All the preparations were dialysed against water before testing them for enzyme activity.

Homogenization buffer	Percent activity	
	total homogenate	activity in 105000 × *g* supernatant
0.25 M sucrose/0.01 M Tris-HCl (pH 7.4)	100.0	1 1
0.100 M KCl/0.039 M borate (pH 7 1)	100.0	38.0
0.275 M KCl/0.039 M borate (pH 7.1)	100.0	82.0

zyme on polyacrylamide gel electrophoresis in the presence and absence of SDS showed it to be a constituent of high molecular weight myofibrillar protein aggregate (Fig. 1B and C). A 40-fold purification was achieved by Sephadex G-200 chromatography and the enzyme was still found to be associated with myofibrillar protein aggregate. Though it was not retained on the DEAE-Sephadex A-50 column, the partially purified enzyme was freed of the bulk of the myofibrillar proteins (Fig. 1B and C).

General properties of the enzyme

An optimum pH of 8 was observed in Tris-HCl buffer for protein-histidine methylase (Fig. 2A) activity with heated myofibrils as methyl acceptor protein substrate. The half-maximum activity was at pH 6.8 and 9.0. The kind of buffer (either PO_4^{2-} or Tris-HCl) did not seem to have any effect. The relationship between enzyme activity and incubation time is shown in Fig. 2B. Proportionality exists only during the first 1.5 h. Hence, 1.5 h was chosen as the incubation time in the routine assay of the enzyme activity. The effect of addition of heated myofibrils and *S*-adenosylmethionine on the methylase activity is shown in Figs. 3A and 4A. Both the substrates, the myofibrils and *S*-adenosylmethionine, exhibited saturation kinetics. Linearity of enzyme activity with respect to varying protein concentration was observed up to a 2 mg protein level (Fig. 3B). *S*-Adenosylhomocysteine, a demethylated product of AdoMet and a well-known inhibitor of AdoMet-dependent methyltransferases, inhibited the rabbit skeletal muscle protein-histidine methylase (Fig. 4B).

TABLE IV

PURIFICATION OF RABBIT SKELETAL MUSCLE PROTEIN-HISTIDINE METHYLASE

Enzyme activities were measured with denatured myofibrils from young rabbit skeletal muscle as methyl acceptor protein substrate Assay conditions are as described in Table I.

	Volume (ml)	Protein (mg)	^{14}C-Me incorporation		Purification (fold)	Percent yield
			total activity (pmol/h)	specific activity (pmol/h per mg)		
0.275 M KCl extract	304	5746.0	3995	0.70	1.00	100 0
8000 × *g* supernatant	250	1000.0	3641	3.64	5.20	91 0
Ammonium sulphate range (percent)						
0– 20	25	42.5	32	0.75	1.07	0.8
21– 40	25	225.0	1236	5 50	7 85	30.9
41– 60	25	145.0	2229	15.40	22 00	55.8
61– 80	25	120.0	144	1.20	1.71	3.6
81–100	350	100.0	4	0.04	0.06	0 1

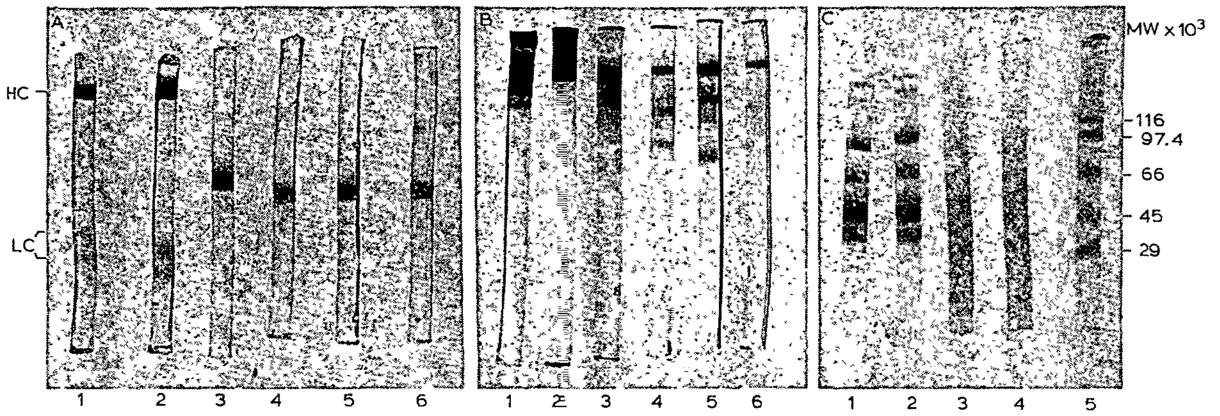

Fig. 1 (A) SDS-polyacrylamide gel electrophoretic pattern of muscle proteins (5% polyacrylamide 0.25% crosslinker) stained with Coomassie brilliant blue. 50–100 μg protein Heavy chains (HC), light chains (LC) Rabbit skeletal muscle myosin (lane 1) and actin (lane 3); rabbit cardiac muscle myosin (lane 2) and actin (lane 4); rat skeletal muscle actin (lane 5), bovine cardiac actin (lane 6). (B) Polyacrylamide gel electrophoretic pattern of rabbit skeletal muscle protein-histidine methylase during its purification. Rabbit skeletal muscle was homogenised in 3 vol. 0.25 M sucrose/0.01 M Tris-HCl (pH 7.4) and the 8000 × g pellet was extracted with 5 vol of 0.275 M KCl/0.039 M borate medium (pH 7.1). The 8000 × g supernatant of 0.275 M KCl extract was collected and the enzyme activity precipitated between 40–60% $(NH_4)_2SO_4$ saturation The $(NH_4)_2SO_4$ fraction 26 ml (148 mg protein) following dialysis against 0.15 M PO_4^{2-}/0.01 M EDTA (pH 7.5) was applied on to a DEAE-Sephadex A-50 column (20×3 cm) and eluted with PO_4^{2-} buffer at a flow rate of 30 ml/h and 15 ml fractions of a total volume of 680 ml were collected. The gradient was started at 130 ml (250 ml PO_4^{2-} buffer plus 250 ml of the same made in 0.5 M KCl). The bulk of methylase activity was eluted at 190–250 ml before the start of KCl gradient elution at 300 ml. 80 μg protein in each lane. Lane 1, $(NH_4)_2SO_4$ fraction; lanes 2–6, DEAE-Sephadex A-50 fractions. Lanes 2, 3 (70–130 ml), lanes 4, 5 (190–250 ml), showing peak methylase activity), lane 6 (250–280 ml) (C) SDS-polyacrylamide gel electrophoretic pattern of enzyme during purification (80 μg protein in each lane) Lane 1, $(NH_4)_2SO_4$ fraction; lanes 2–4, DEAE-Sephadex A-50 fractions. Lane 2 (70–130 ml), lanes 3, 4 (190–250 ml, showing peak methylase activity), lane 5 molecular weight markers (Sigma Chemicals). β-galactosidase (116 kDa), phosphorylase (97.4 kDa), bovine plasma albumin (66 kDa) egg ovalbumin (45 kDa), carbonic anhydrase (29 kDa)

Substrate specificity of the enzyme

Tables V and VI list the effects of various added proteins on the protein-histidine methylase activity. It is seen that the enzyme is specific only for myofibrils. Myofibrils heated at 75°C for 15 min to selectively destroy the endogenous methylase served as efficient methyl acceptor protein. Further, the partially purified methylase effectively catalysed the methylation of histidine residues of actins isolated from various sources. The

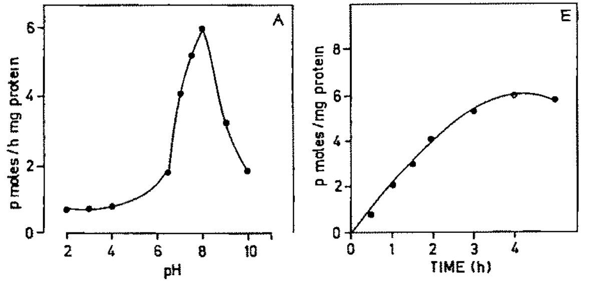

Fig. 2. (A) Effect of pH on the activity of protein-histidine methylase. The buffers used were glycine-HCl (pH 2 and 10), citrate-PO_4^{2-} (pH 3–6), PO_4^{2-} (pH 6–8) and Tris-HCl (pH 7–9). (B) Relationship between period of incubation and protein-histidine methylase activity. Assay conditions are as described in Table V.

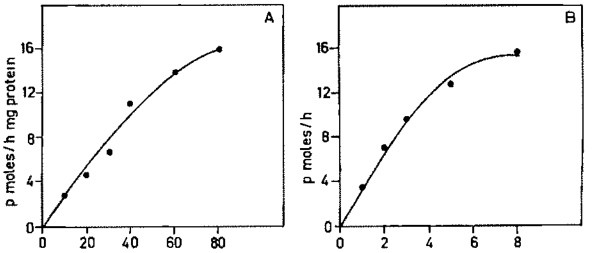

Fig. 3 (A) Effect of increasing concentrations of denatured myofibrillar protein on enzyme activity. (B) Relationship between enzyme protein concentration and the rate of histidine methylation Assay conditions as described in Table V.

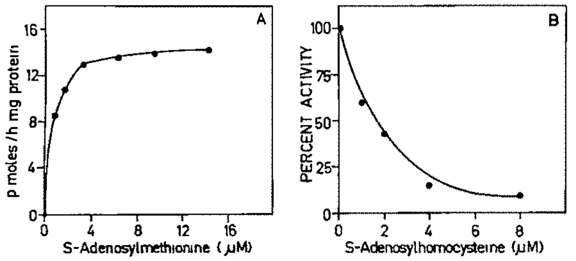

Fig. 4. (A) Effect of increasing concentrations of [Me-^{14}C]AdoMet on protein-histidine methylase activity. (B) Effect of S-adenosylhomocysteine on protein-histidine methylase activity. Assay conditions as described in Table V.

rates of myosin methylation were found to be negligible.

Effect of metal ions and reducing agent

The enzyme showed no absolute requirement for any metal ion. 2-Mercaptoethanol, which stimulated the enzyme activity 4-fold, indicated the requirement for a reducing agent. This was further supported by N-ethylmaleimide inhibition of methylase (Table VII). The methylase was inhibited by numerous salts (Table VII). Divalent ions were found to be more inhibitory than monovalent ions. Triton X-100 at 1% stimulated the enzyme activity by 150%.

TABLE V

RELATIVE SUBSTRATE SPECIFICITY OF PROTEIN-HISTIDINE METHYLASE ISOLATED FROM RABBIT SKELETAL MUSCLE

100% activity corresponds to ^{14}C-Me incorporation of 6.2 pmol/h per mg enzyme protein using denatured myofibrils as substrate. Enzyme preparation (40–60% $(NH_4)_2SO_4$ fraction, 2 mg protein) methyl acceptor protein (heated myofibrils, 60 mg) were incubated for 1.5 h at 37°C in a 5 ml reaction medium containing 0.2 M Tris-HCl (pH 8.0), 4 mM mercaptoethanol and 4 μM [Me-^{14}C]AdoMet. The other substrates were also tested for methyl acceptor capacity at 60 mg protein level.

Substrate protein	Percent activity	
	native	denatured
Myofibrils	71.0	100.0
Bovine serum albumin	0.1	0.5
Fibrinogen	0.9	0.9
Casein	1.2	1.5
Histone type IIA	0.1	0.4
Gluten	23.7	5.2
Gelatin	2.0	6.0
Human γ-globulin	0.8	1.4

TABLE VI

SPECIFICITY OF PARTIALLY PURIFIED RABBIT SKELETAL MUSCLE PROTEIN-HISTIDINE METHYLASE TOWARDS SKELETAL AND CARDIAC MUSCLE FORMS OF ACTIN AND MYOSIN

Assay conditions are as described in Table V.

Protein	(mg)	^{14}C-Me incorporation (pmol/h per mg enzyme protein)
1. Young rabbit skeletal muscle		
a) myofibrils	10.0	2.40
	20.0	5.00
b) actin	7.5	6.00
	15.0	9.00
	30.0	24.00
c) myosin	23.5	0.13
	47.0	0.26
2. Rabbit heart		
a) actin	4.0	6.00
	6.00	10.00
b) myosin	18.0	0.12
	36.0	0.21
3. Bovine heart		
a) actin	6.0	2.20
	12.0	5.00
	18.0	8.00
b) myosin	25.0	0.18
	50.0	0.25
4. Rat skeletal muscle		
a) actin	5.3	20.00
	10.6	36.00
	15.9	68.00

Stability of the enzyme

The enzyme was found to be highly thermolabile. While a brief exposure of the enzyme for 10 min at 50°C completely destroyed the enzyme activity, at 40°C 75% of the activity was found to be destroyed. Also the enzyme activity decreased by 75% when maintained for 4 days at 2°C. Neither mercaptoethanol nor glycerol stabilised the enzyme activity over this period. Once purified, the enzyme was found to be stable at −20°C.

TABLE VII

INFLUENCE OF VARIOUS SALTS AND REDUCING AGENT 2-MERCAPTOETHANOL ON RABBIT SKELETAL MUSCLE PROTEIN-HISTIDINE METHYLASE ACTIVITY

100% activity corresponds to ^{14}C-Me incorporation rate of 11.2 pmol/h per mg enzyme protein. Assay conditions are as described in Table V

Reagent	Concentration (mM)	Relative activity
2-Mercapto-ethanol	0.0	25.0
	2.0	100.0
N-Ethylmaleimide	2.0	72.0
	4.0	30.0
KCl	100.0	36.0
	200.0	18.0
NaCl	100.0	14.0
	200.0	5.0
$MgCl_2$	4.0	66.0
	8.0	40.0
$CaCl_2$	0.2	90.0
	0.4	70.0
ATP	0.2	75.0
	0.4	53.0
Borate	40.0	89.0
	80.0	80.0
EDTA	5.0	71.0
	10.0	64.0
Triton X-100	1%	155.0

Discussion

This is the first study to identify, isolate and partially purify the *S*-adenosylmethionine:protein-histidine *N*-methyltransferase from rabbit skeletal muscle. Unlike cardiac muscle, the skeletal muscle is known to contain both the actin-specific and myosin-specific histidine methylases [21,22]. Myofibrils isolated from young rabbit skeletal muscle served as an efficient methyl acceptor protein substrate for the enzyme. This may be because myofibrils from young animals offer more methyl acceptor histidine sites due to higher steady-state protein synthesis rates in them as compared to the adult ones. This is in line with the earlier observations of Bates et al. who reported higher steady-state synthesis rates of 3-MeHis in young rats as compared to adult rats as well as a developmental fall in myofibrillar protein synthesis rates with age [23,24]. Further, it was thought that the use of myofibrils as a methyl acceptor protein will provide both actin and myosin substrates.

The protein-histidine methylase activity was localised in the myofibrillar fraction. The isolated myofibrils represented the enzyme-substrate complex. Thus, while using myofibrils as methyl acceptor protein substrate the high rates of ^{14}C-Me incorporation by myofibrils per se due to the endogenous methylase hampered the sensitivity of the assay while determining the methylation rates due to the exogenously added enzyme. Myofibrils heated at 75°C for 15 min so as to destroy the contaminant methylase served as an efficient methyl acceptor protein.

During the isolation of myofibrils by the method described by Perry and Grey [14], 0.025 M KCl is used in the initial homogenisation of the skeletal muscle to reduce the contraction striation reversals. This is followed by a second homogenisation of minced muscle in 0.1 M KCl medium. It was during this later step that we observed a significant amount of histidine methylase activity being solubilised in 0.1 M KCl. The optimal solubilisation was achieved at 0.275 M KCl concentration. It was also during this step that the inhibitory effects of KCl on the activity of the enzyme were observed, which falsely gave the impression that the enzyme is inactivated during purification.

The ammonium sulphate (40–60% saturation) precipitation step achieved a 22-fold purification of the enzyme with a yield of 55.8%. The partially purified enzyme was found to be associated with myofibrillar proteins. Highly purified preparations of either actin or myosin exhibited no protein-histidine methylase activity. Though the enzyme was not retained on a DEAE-Sephadex A-50 column, this step achieved a 95-fold purification with a yield of 15.6%. Further, the partially purified enzyme had a tendency to be inactivated. The reason for this is not clear. So far none of the mammalian protein methylases except protein methylase II have been purified to homogenity [5].

Like other protein methylases, the protein-histidine methylase showed no absolute requirement for any metal ion. However, it showed a requirement for reducing agent. Many of the salts used in the extraction and isolation of contractile proteins inhibited the enzyme activity to varying extents. The data indicate that the ion or ion substrate interaction sites on the enzyme are both anionic and cationic [25]. The enzyme was found to be highly thermosensitive.

The enzyme exhibited a high degree of substrate specificity towards young rabbit skeletal muscle myofibrils and muscle forms of actins isolated from different species. This indicates that the enzyme is in fact an actin-specific histidine methylase. Since the enzyme was shown to specifically methylate the histidine residues of actins, we propose to designate the newly identified methylase as protein methylase IV, to distinguish it from the already known protein methylases, I, II and III. It will be interesting to test whether the same enzyme can methylate the non-muscle forms of actins also.

Although the tissue-specific occurrence and developmental regulation of 3-MeHis has long been known [21,22,26,27], the biological significance of protein histidine methylation has remained elusive so far. Recently it has also been shown that chemically methylated proteins differ in some of their properties from enzymatically methylated proteins [28]. Studies on further purification of actin-specific histidine methylase and identification of myosin-specific methylase will enable one to use these enzymes as biological tools to investigate the significance of protein histidine methylation.

Acknowledgement

The authors thank Mrs. G. Shakuntala for skillful technical assistance.

References

1 Paik, W.K. and Kim, S (1975) Adv. Enzymol. 42, 227–228
2 Paik, W.K. and Kim, S (1980) in Protein Methylation, John Wiley & Sons, New York
3 Tuck, M. and Paik, W.K. (1984) Methods Enzymol. 106, 268–274
4 Paik, W.K. and Di Maria, P (1984) Methods Enzymol 106, 274–287
5 Kim, S. (1984) Methods Enzymol. 106, 295–309
6 Stock, J.B , Clarke, S. and Koshland, D.E , Jr. (1984) Methods Enzymol. 106, 310–321
7 Hardy, M.F. and Perry, S.V. (1969) Nature 223, 300–302
8 Krzysik, B., Vergnes, J.P. and McManus, I.R. (1971) Arch. Biochem. Biophys. 146, 34–45
9 Laki, K. and Wilson, E. (1969) Physiol. Chem. Phys. 1, 536–540
10 Reporter, M. (1973) Arch. Biochem. Biophys 158, 577–585
11 Huszar, G (1975) J. Mol. Biol. 94, 311–326
12 Cantoni, G.L. and Durell, J (1957) J Biol Chem. 225, 1033–1048
13 Cantoni, G.L. (1955) Methods Enzymol. 2, 257–260
14 Perry, S.V. and Grey, T C. (1956) Biochem. J. 64, 184–192
15 Seraydarian, K., Briskey, E.J. and Mommaerts, W.F.H.M. (1967) Biochim Biophys Acta 133, 399–411
16 Spudich, J.A and Watt, S. (1971) J. Biol. Chem. 246, 4866–4871
17 Godfrey, J.E. and Harrington, W.F (1970) Biochemistry 9, 894–908
18 Lowry, O.H., Rosebrough, N.J., Farr, A L. and Randall, R.J. (1951) J. Biol. Chem 193, 265–275
19 Weber, K. and Osborn, M (1969) J. Biol. Chem. 244, 4406–4412
20 Haverberg, L.N , Munro, H.N. and Young, V.R. (1974) Biochim Biophys. Acta 371, 226–237
21 Huszar, G. and Elzinga, M. (1972) J. Biol. Chem. 247, 745–753
22 Huszar, G. (1972) Nature New Biol. 240, 260–264
23 Bates, P.C., Grimble, G.K., Sparrow, M.P. and Millward, D.J (1983) Biochem. J. 214, 593–605
24 Bates, P.C. and Millward, D.J. (1983) Biochem. J. 214, 587–592
25 Wong, L.J. and Patton, W F (1985) Int. J. Biochem. 17, 123–126
26 Trayer, I.P., Harris, C I. and Perry, S V (1968) Nature, 217, 452–453
27 Kuehl, W.M. and Adelstein, R.S. (1970) Biochem. Biophys. Res. Commun. 39, 956–964
28 Paik, W.K , Farooqui, J., Gupta, A., Smith, H.T. and Millett, F. (1983) Eur. J. Biochem. 135, 259–262

INFORMATION FOR CONTRIBUTORS TO BIOCHIMICA ET BIOPHYSICA ACTA

Biochimica et Biophysica Acta publishes papers reporting advances in our knowledge or understanding of any field of biochemistry or biophysics. Descriptions of new methods valuable for biochemists or biophysicists are also acceptable if their application is made obvious or a new principle is introduced. Negative results will be accepted only when they can be considered to advance our knowledge significantly. Papers providing only confirmatory evidence or extending observations firmly established in one species to another will not normally be accepted.

Two types of paper are published, specified as Regular Papers and BBA Reports. As its name implies, a Regular Paper is the usual medium of publication.

BBA Reports will be restricted to papers describing short, complete studies. They should not exceed three printed pages, including figures and tables, and should be written in a continuous style, without subdivision into Introduction, Methods, Results, Discussion and Acknowledgements. They should always begin with a short summary. A BBA Report, although brief, should be a complete and final publication, and figures and tables should not be included in a later paper.

Papers should be written in English (either American or British spelling is permitted, but only one form should be used in the same paper).

Preparation of papers

Authors and their typists should consult a recent issue of the journal in order to make themselves familiar with the conventions and layout of articles, especially title pages and reference lists. In particular, typists should ensure that the beginning of each new paragraph is clearly indicated, preferably by indentation.

Four copies are required of all material submitted (including the submission letter, if it contains information of relevance to the editors). Legible carbon copies or photocopies are adequate for the second and subsequent copies, except for photographs of electrophoretic patterns, electron micrographs, etc., where high-quality prints must be provided in quadruplicate.

The entire text, including figure and table legends and reference list, should be typed with double or triple spacing on pages of uniform size, on one side of the paper, with a 5-cm margin. All pages should be numbered consecutively.

Title

A paper should be headed by a concise, informative title. Authors are reminded that titles are widely used in information-retrieval systems. The title should be followed by the names of the authors (with first or middle names in full) and by the name(s) and address(es) of the laboratory(ies) where the work was carried out. If the work has been done in more than one laboratory, the one in which each author has worked during the study should be indicated.

Summary

A paper should begin with a summary of 100–200 words for a Regular Paper and approx. 50 words for a BBA Report.

Tables

Tables and their legends should be typed with double or triple spacing.

Figures and illustrations

Legends to figures should not be typed or written on the illustrations but should be typewritten, with double or triple spacing, on separate sheets of paper. The legends should consist of a title followed by a brief description of the way the particular experiment was carried out, and any other necessary material describing the symbols or lines on the figure.

Biochimica et Biophysica Acta **Vol. 923, No. 1**
General Subjects G126(1) January 20, 1987

Contents

Biochimica et Biophysica Acta. 40 years on v

Regular papers

Evidence for the glycoprotein nature of vitamin K-dependent carboxylase from rat liver (BBA 22268)
by T. Brody and J.W. Suttie (U.S.A.) 1

Purification and properties of a human plasma endogenous modulator for the platelet tricyclic binding/serotonin transport complex (BBA 22443)
by K.I. Abraham, J.R. Ieni and L.R. Meyerson (U.S.A.) 8

Topo-optical investigations of human erythrocyte glycocalyx conformational changes induced by dextran (BBA 22442)
by H. Bäumler, K.-J. Halbhuber, D. Stibenz and D. Lerche (G.D.R.) 22

The inhibitory effect of dithiothreitol on the assembly of the filamentous phage fd (BBA 22444)
by M. Vaccaro, B. Boehler-Kohler, W. Müller and I. Rasched (F.R.G.) 29

Metabolism of opioid peptides by cerebral microvascular aminopeptidase M (BBA 22440)
by L. Churchill, H.H. Bausback, M.E. Gerritsen and P.E. Ward (U.S.A.) 35

Lipids associated with tissue transglutaminase (BBA 22476)
by J. Harsfalvi, G. Arató and L. Fesus (Hungary) 42

Effect of Ca^{2+} and Mg^{2+} on the uptake of Fe^{3+} by mouse intestinal mucosa (BBA 22559)
by K.B. Raja, R.J. Simpson and T.J. Peters (U.K.) 46

Partial purification and characterization of an aldohexose 1-*P* phosphatase from pig skeletal muscle (BBA 22441)
by R. Cussó, A.M. Bassols and J. Carreras (Spain) 52

The preparation of deglycosylated ricin by recombination of glycosidase-treated A- and B-chains: effects of deglycosylation on toxicity and in vivo distribution (BBA 22460)
by B.M.J. Foxwell, D.C. Blakey, A.N.F. Brown, T.A. Donovan and P.E. Thorpe (U.K.) 59

Organothallium(III) reagents for modification of biomacromolecules: interaction of thallium derivatives with transfer RNA (BBA 22461)
by S.R. Baindur and K.T. Douglas (U.K.) 66

Nucleoside-triphosphatase and hydrolysis of thiamin triphosphate in *Escherichia coli* (BBA 22390)
by T. Nishimune, S.-i. Ito, M. Abe, M. Kimoto and R. Hayashi (Japan) 74

The binding of fluorescent 4,6,8(14)-triene-3-one steroids to cyclodextrins as a model for steroid–protein interactions (BBA 22462)
by M.A. Kempfle, R.F. Müller, R. Palluk and H.A. Winkler (F.R.G.) 83

Subunits and chromophores of a type I phycoerythrin from a *Chroomonas* sp. (Cryptophyceae) (BBA 22457)
by C.D. Martin and R.G. Hiller (Australia) 88

continued

Cited in: Current Contents Life Sciences - Biological Abstracts - Chemical Abstracts - Index Chemicus - Index Medicus - Excerpta Medica (EMBASE)

INFORMATION FOR CONTRIBUTORS TO BIOCHIMICA ET BIOPHYSICA ACTA

The 1982 edition of this booklet, offering detailed guidance to authors, is available free of charge from the BBA Editorial Secretariat, P.O. Box 1345, 1000 BH Amsterdam, The Netherlands. It is also published as Biochim. Biophys. Acta 715 (1982) 1–23.

Multiple forms of a type I phycoerythrin from a *Chroomonas* sp. (Cryptophyceae) varying in subunit composition (BBA 22458)
by R.G. Hiller and C.D Martin (Australia) 98

The metabolism of deoxyguanosine in mitochondria a characterization of the phosphorylation process which occurs in intact mitochondria (BBA 22479)
by L.F. Watkins and R.A Lewis (U.S.A) 103

Stabilization of phosphofructokinase with sugars during freeze-drying characterization of enhanced protection in the presence of divalent cations (BBA 22445)
by J.F. Carpenter, L M. Crowe and J H. Crowe (U.S.A.) 109

Purification and partial characterization of cellular retinoic acid-binding protein from human placenta (BBA 22385)
by M Okuno, M Kato, H. Moriwaki, M. Kanai and Y Muto (Japan) 116

The role of polyamine reutilization in depletion of cellular stores of polyamines in non-proliferating tissues (BBA 22478)
by F.N. Bolkenius and N. Seiler (France) 125

UDPgalactose:glucosylceramide $\beta 1 \rightarrow 4$-galactosyltransferase activity in human proximal tubular cells from normal and familial hypercholesterolemic homozygotes (BBA 22446)
by S Chatterjee and E. Castiglione (U.S A.) 136

Affinity chromatography and some properties of the angiotensin-converting enzyme from human heart (BBA 22481)
by I.Y Sakharov, S M Danilov and E.A. Dukhanina (U.S.S R) 143

Lysosomal and cytosolic sialidases in rabbit alveolar macrophages: demonstration of increased lysosomal activity after in vivo activation with bacillus Calmette-Guerin (BBA 22477)
by Y. Pilatte, J Bignon and C.R. Lambré (France) 150

Partial purification and characterisation of *S*-adenosylmethionine protein-histidine *N*-methyltransferase from rabbit skeletal muscle (BBA 22483)
by C. Vijayasarathy and B S. Narasinga Rao (India) 156

BIOCHIMICA ET BIOPHYSICA ACTA
International Journal of Biochemistry and Biophysics
Founded in 1947 by H G.K. Westenbrink, Managing Editor 1947–1964

© 1987, Elsevier Science Publishers B V. (Biomedical Division)
Printed in The Netherlands

All rights reserved No part of this publication may be reproduced, stored in a retrieval system, or transmitted, in any form or by any means, electronic, mechanical, photocopying, recording or otherwise, without the prior written permission of the publisher, Elsevier Science Publishers B.V. (Biomedical Division), P.O Box 1527, 1000 BM Amsterdam, The Netherlands Submission of a paper to this journal entails the author's irrevocable and exclusive authorization of the publisher to collect any sums or considerations for copying or reproduction payable by third parties (as mentioned in article 17 paragraph 2 of the Dutch Copyright Act of 1912 and in the Royal Decree of June 20, 1974 (S 351) pursuant to article 16b of the Dutch Copyright Act of 1912) and/or to act in or out of Court in connection therewith

Special regulations for readers in the U.S.A. This journal has been registered with the Copyright Clearance Center, Inc Consent is given for copying of articles for personal or internal use, or for the personal use of specific clients. This consent is given on the condition that the copier pays through the Center the per-copy fee stated in the code on the first page of each article for copying beyond that permitted by Sections 107 or 108 of the U S Copyright Law The appropriate fee should be forwarded with a copy of the first page of the article to the Copyright Clearance Center, Inc , 27 Congress Street, Salem, MA 01970, U S.A. If no code appears in an article, the author has not given broad consent to copy and permission to copy must be obtained directly from the author. All articles published prior to 1980 may be copied for a per-copy fee of US$ 2.25, also payable through the Center. This consent does not extend to other kinds of copying, such as for general distribution, resale, advertising and promotion purposes, or for creating new collective works Special written permission must be obtained from the publisher for such copying.

Special regulations for authors. Upon acceptance [illegible] article by the journal, the author(s) will be asked to transfer copyright of the article to the publisher. This [illegible] will ensure the widest possible dissemination of information